



**West
European
Graduate
Education
Marine
Technology**

SEVENTH GRADUATE SCHOOL

SHIPS AND STRUCTURES

IN ICE

**LABORATORY OF NAVAL ARCHITECTURE
AND MARINE ENGINEERING**

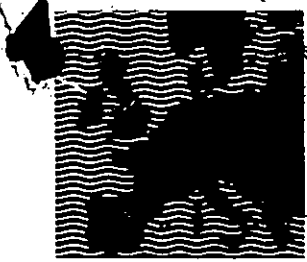
**HELSINKI UNIVERSITY OF TECHNOLOGY
ESPOO - FINLAND**

March 21-31, 1983



HUT

**HELSINKI UNIVERSITY OF
TECHNOLOGY**



West
European
Graduate
Education
Marine
Technology

SEVENTH GRADUATE SCHOOL
SHIPS AND STRUCTURES
IN ICE

LABORATORY OF NAVAL ARCHITECTURE
AND MARINE ENGINEERING

HELSINKI UNIVERSITY OF TECHNOLOGY
ESPOO - FINLAND

March 21-31, 1983



HUT
HELSINKI UNIVERSITY OF
TECHNOLOGY

FRIDAY 25th March 1983

8.15-10.00
MODELING TECHNIQUES IN VARIOUS
ICE MODEL BASINS
Dr. Joachim Schwarz
(HSVA GmbH, Hamburg)

10.15-11.45
LEVEL ICE RESISTANCE
Prof. Ernst Enkvist
Wärtsilä Arctic Design and
Marketing, Helsinki)

11.45-13.15 LUNCHEON

13.15-14.45
PROPULSION COEFFICIENTS AND
PROPELLER DESIGN FOR ICE-
BREAKING SHIPS
Dr. Jack W. Lewis
(Arctec Inc., Columbia, USA)

14.45-15.15 COFFEE

15.15-16.45
RECENT DEVELOPMENTS IN THE
PREDICTION OF LEVEL ICE RESISTANCE
Dr. J. W. Lewis

16.45-18.45 ~~17.30~~
CASE STUDIES: Ice Resistance
Prof. Ernst Enkvist

SATURDAY/SUNDAY 26-27th March 1983

ICEBREAKER TOUR

FRIDAY 28th March 1983

8.15- 9.45
SHIP PERFORMANCE AND RESISTANCE
IN ICE RIDGES
Dr. Arno Keinonen

10.00-11.30
PROPULSION IN ICE
Mr. Kimmo Juurmaa, MSc
(Wärtsilä Arctic Design and
Marketing, Helsinki)

11.30-13.00 LUNCHEON

13.00-14.00
ICE LOAD RESPONSE IN SHAFTING
Mr. Erik Sandberg, MSc
(Det Norske Veritas, Høvik, Norge)

14.15-14.45 COFFEE

14.45-15.45
MODELLING OF SHIP PERFORMANCE IN OLD
ICE-CLOGGED CHANNELS
Prof. Valter Kostilainen
(Helsinki University of Technology)

16.00-17.30
CASE STUDIES: Propulsion
Mr. Kimmo Juurmaa, MSc

TUESDAY 29th March 1983

8.15-10.00
PROPULSION MACHINERY SELECTION IN
ICEBREAKERS
Mr. Jarmo Laakso, MSc
(Wärtsilä Arctic Design and
Marketing, Helsinki)

10.15-11.00
MACHINERY DAMAGES
Mr. Lasse Norhamo, Senior Surveyor
(Det Norske Veritas, Høvik, Norge)

11.00-12.30 LUNCHEON

12.30-13.15
CPP IN ICE
Mr. Sven-Ola Andersson, MSc
(KaMeWa, Kristinehamn, Sweden)

13.30-14.15
RUDDERS AND STEERING
Mr. Peter Noble
(Arctec Canada Ltd, Calgary, Canada)

14.15-14.45 COFFEE

14.45-16.15
AUXILIARY SYSTEMS FOR ICEBREAKING
Mr. Göran Wilkman, MSc
(Wärtsilä Arctic Design and
Marketing, Helsinki)

16.15-18.15
CASE STUDIES: Progressive strength
Mr. Jarmo Laakso, MSc

WEDNESDAY 30th March 1983

8.15- 9.45
ICEBREAKERS
Mr. Jouko Virtanen
(Wärtsilä Arctic Design and
Marketing, Helsinki)

10.00-11.30
ICEBREAKING CARGO SHIPS
Mr. Markku Kanerva
(Wärtsilä Turku Shipyards)

11.30-13.00 LUNCHEON

13.00-14.30

SPECIAL SHIPS TO SUPPORT ARCTIC
EXPLORATION

Mr. M Edgecombe & Mr. B Johansson
(Dome Petroleum Ltd, Calgary, Canada)

14.30-15.00

COFFEE

15.00-15.45

ACV-ICEBREAKING

Mr. Peter Noble

16.00-17.00

VISIT TO SHIPYARD BUILDING ICE-
BREAKERS (WADAM)

20.00-

DINNER

TRANSPORTATION TO HOTELS

THURSDAY 31st March 1983

8.30-10.30

ICE LOAD ON CYLINDAR AND CONICAL
OFFSHORE STRUCTURES

Mr. Egon Wessels
(HSVA GmbH, Hamburg)

10.45-12.15

LUNCHEON

12.15-13.45

ICE ACTION ON ARTIFICIAL ISLANDS
AND WIDE STRUCTURES

Mr. Kenneth Croasdale
(Petro-Canada, Calgary, Canada)

13.45-14.15

COFFEE

14.15-15.00

OTHER (MOVABLE) STRUCTURES

Mr. Peter Noble

15.00-(16.00)

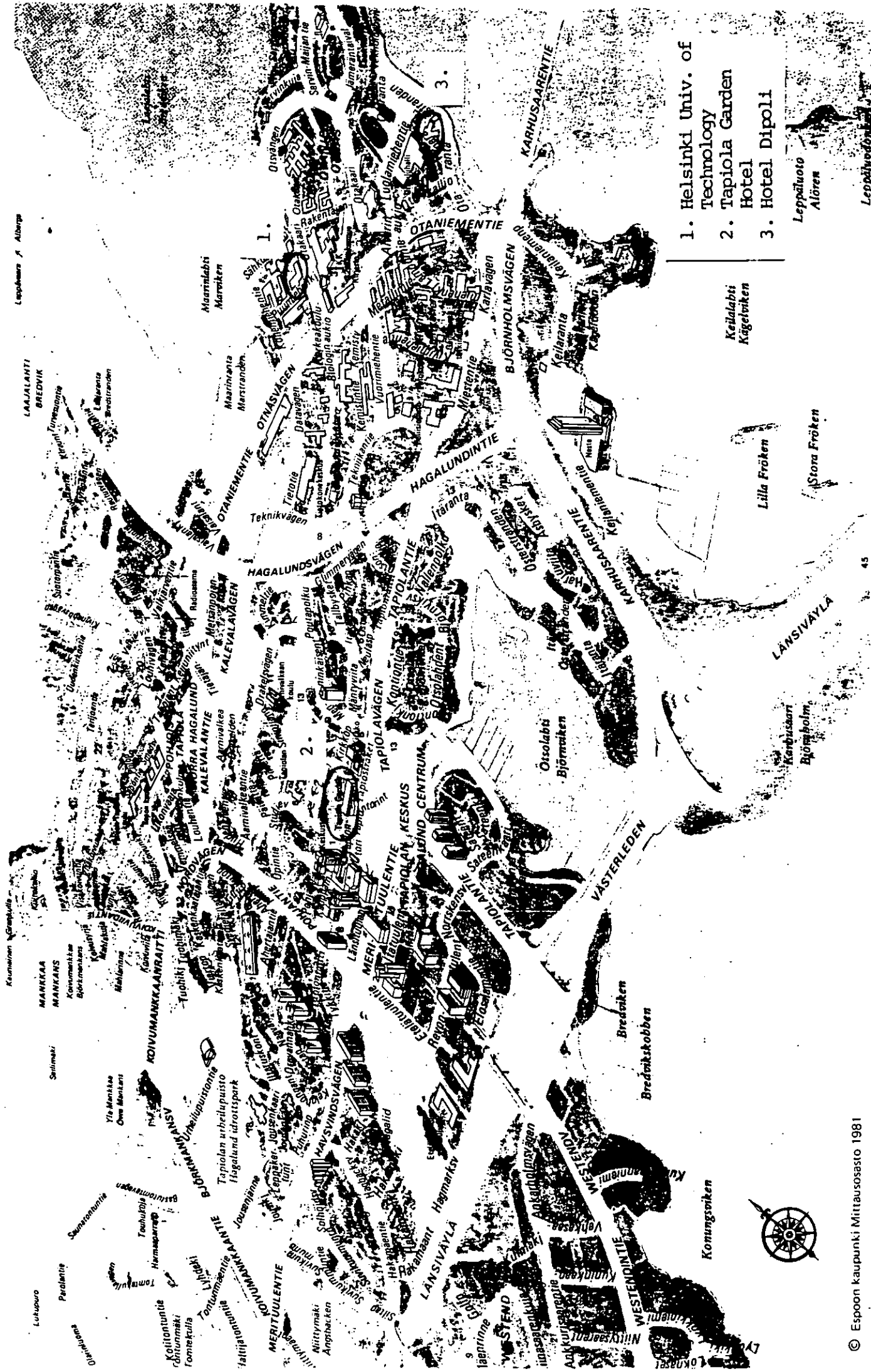
GENERAL DISCUSSION

L U N C H E O N

Mo. 21.3.1983 *Vegetable Stew*
Tu. 22.3.1983 *Meat balls*
We. 23.3.1983 *Carrot Pancakes*
Fri. 25.3.1983 *Fish in oven with almonds*
Mo. 28.3.1983 *Meat Casserole Caucasian Style*
To. 29.3.1983 *Escalope of veal with cheese*
We. 30.3.1983 *Fried Cod*
Thu. 31.3.1983 *Swiss Escalope of Veal*

*Meals include grated vegetables, white bread,
a bottle of beer or mineral water/person.*

Leppävaara / Alberg



1. Helsinki Univ. of Technology
2. Tapiola Garden
3. Hotel Dipoli

Kellalahti
Kägelviken

Leppävaara
Alören

Leppävaara



PLEASE NOTICE

THE REPRESENTANTS OF FINNAIR ARE AVAILABLE
AT THE SCHOOL FOR POSSIBLE REQUESTS
ON MARCH 25, 1983 FROM 8 AM TO 7 PM
AND
ON MARCH 28, 1983 FROM 8 AM TO 6 PM

WEGEMT VII GRADUATE SCHOOL 21st - 31st March 1983 SHIPS AND STRUCTURES IN ICE FINLAND

NAME	COMPANY/INSTITUT	COUNTRY	ARRIV/DEPART	HOTEL DIPOLJ/GARDEN	ICE- BREAK PARTY 21.3	TOWN HALL 22.3	WARC 24.3	ms ms APU/URJO 26.-27.3	WADAM 30.3	DINNER 30.3
<u>LECTURERS</u>										
Mr. S-O Andersson, MSc	KaMeWa	SWE	28.-30.3	X						
Prof. H. Benford	University of Michigan	USA	20.-24.3	X	X					
Mr. K. Croasdale	Petro-Canada	CAN	26.3-4.4	X						X
Mr. M. Edgcombe & Mr. B. Johansson	Dome Petroleum Ltd	CAN	26.3-10.4	X						X
Dr. E. Enkvist	Wärtsilä	FIN		X	X	X	X	X	X	X
Mr. F.U. Häusler	HSVA GmbH	DEU	21.-23.3	X	X	X				
Dr. J-E Jansson	Board of Navigation	FIN			X					
Mr. K. Juurmaa, MSc	Wärtsilä	FIN								
Mr. M. Kanerva	Wärtsilä	FIN	28.-30.3	X						
Dr. A. Keinonen	Dome Petroleum Ltd	CAN	22.3-10.4			X				X
Prof. V. Kostilainen	Helsinki University of Technology	FIN								
Mr. J. Laakso, MSc	Wärtsilä	FIN								
Dr. J.W. Lewis	Arctec Inc.	USA	24.-26.3	X						
Dr. A.A. Meyerhoff	Arctec Inc.	USA	20.-22.3	X						

WEGEMT VII GRADUATE SCHOOL 21st - 31st March 1983 SHIPS AND STRUCTURES IN ICE FINLAND

NAME	COMPANY/INSTITUTE	COUNTRY	ARRIV/DEPART	HOTEL DIPOLI/GARDEN	ICE- BREAK PARTY 21.3	TOWN HALL 22.3	WARG 24.3	ms APU/URHO 26.1-27.3	WADAM	DINNER
Mr. E. Mäkinen, MSC	Wärtsilä	FIN			X					
Mr. C. Mürer, Principal Surveyor	Det Norske Veritas	NOR	20.-24.3	X	X					
Mr. P. Noble	Arctec Canada Ltd	CAN	28.3-9.4	X						X
Mr. L. Norhamo, Senior Surveyor	Det Norske Veritas	NOR	26.-30.3	X						
Mr. K. Riska & Prof. P. Varsta	Technical Research Centre of Finland	FIN								
Mr. E. Sandberg, MSC	Det Norske Veritas	NOR	27.-30.3	X						
Dr. J. Schwarz	HSVA GmbH	DEU	21.-25.3	X	X					
Prof. T. Søreide	Norwegian Institute of Technology	NOR	20.-24.3	X	X					
Mr. T. Thompson	SMHI	SWE	21.-23.3	X	X					
Mr. J. Virtanen	Wärtsilä	FIN								
Dr. W.F. Weeks	GRREL	USA	20.3-10.4	X	X					X
Mr. E. Wessels	HSVA GmbH	DEU	30.3-1.4	X						X
Mr. G. Wilkman, MSC	Wärtsilä	FIN								
<u>STAFF</u>										
Mr. L. Grönfeldt, MSC	INSKO	FIN	20.-31.3		X	X			X	X
Ms. S. Ruotsalainen	INSKO	FIN	20.-31.3		X	X			X	X
Ms. S. Tuovonen	INSKO	FIN	20.-31.3		X	X			X	X

NAME	COMPANY/INSTITUT	COUNTRY	ARRIV/DEPART	HOTEL DIPOLI/GARDEN	ICE- BREAK PARTY	TOWN HALL	WARC	ms APU/URHO	WADAM	DINNER
					21.3	22.3	24.3	26.-27.3	30.3	30.3
<u>PARTICIPANTS</u>										
Mr. Davidson	1. German & Milne Inc.	CAN	19.3-1.4	X	X	X	X		X	X
Mr. Gosling	2. Gulf Canada Resources Inc.	CAN			X	X	X	X	X	X
Mr. Muhlert	3. Robert Allan Ltd	CAN	20.3-5.4		X	X	X		X	X
Mr. Rossi	4. College of Fisheries	CAN	19.-31.3	X	X	X	X		X	X
Mr. Blendermann	5. Institut fur Schiffbau der Univ. Hamburg	DEU			X	X	X	X	X	X
Mr. Jastram	6. Jastram Werke GmbH & Co	DEU	20.-22.3, 28.-31.3	X	X	X			X	X
Mr. Neuendorf	7. Bremer Vulkan AG	DEU	20.3-1.4		X	X	X		X	X
Mr. Pipples	8. Escher-Wyss GmbH	DEU			X	X	X		X	X
Mr. Schäfer	9. Lohman & Stolterfoht GmbH	DEU	25.-30.3						X	X
Mr. Alanko	10. Rauma-Repola Oy	FIN	21.-31.3	X	X	X	X	X	X	X
Mr. Arpiainen	11. Oy Wärtsilä Ab	FIN			X	X	X	X	X	X
Mr. Gräsbeck	12. Oy Wärtsilä Ab	FIN	22.-23.3, 29.-30.3	X	X	X	X	X	X	X
Mr. Immonen	13. Oy Laivateollisuus Ab	FIN	21.-25.3, 28.-31.3	X	X	X	X	X	X	X
Mr. Jalkanen	14. Oy Wärtsilä Ab	FIN		X	X	X	X	X	X	X

WEGEMT VII GRADUATE SCHOOL 21st - 31st March 1983 SHIPS AND STRUCTURES IN ICE FINLAND

NAME	COMPANY/INSTITUT	COUNTRY	ARRIV/DEPART	HOTEL/GARDEN	ICE-BREAK PARTY	TOWN HALL	WARC	ms APU/URHO	WADAM	DINNER
					21.3	22.3	24.3	26.-27.3	30.3	30.3
Mr. Joensuu	Oy Wärtsilä Ab	FIN	21.-25.3,		X	X	X	X	X	X
Mr. Kannari	Oy Wärtsilä Ab	FIN	28.-31.3		X	X	X	X	X	X
Mr. Kivi	Elomatic Oy	FIN	21.-31.3	X	X	X	X		X	X
Mr. Korri	Rauma-Repola Oy	FIN		X	X	X	X		X	X
Mr. Kujala	Techn. Research Centre of Finland	FIN			X	X	X		X	X
Mr. Kuutti	Oy Wärtsilä Ab	FIN	21.-25.3, 28.-29.3	X	X	X	X		X	X
Mr. Lehtonen	Hollming-yhtymä Oy	FIN			X	X	X		X	X
Mr. Lietepohja	Hollming-yhtymä Oy	FIN			X	X	X		X	X
Mr. Lybeck	Oy Brennership Ab	FIN			X	X	X		X	X
Mr. Mach	Oy Wärtsilä Ab	FIN	21.-22.3, 28.-30.3	X	X	X	X		X	X
Mr. Marttila	Oy Wärtsilä Ab	FIN			X	X	X		X	X
Mr. Matikainen	Techn. Research Centre of Finland	FIN			X	X	X		X	X
Mr. Matinlauri	Rauma-Repola Oy	FIN	21.-31.3	X	X	X	X	X	X	X
Mr. Miettinen	Rauma-Repola Oy	FIN			X	X	X		X	X
Mr. Mökkönen	Oy Wärtsilä Ab	FIN	21.-25.3, 27.-31.3	X	X	X	X		X	X

WEGEMT VII GRADUATE SCHOOL 21st - 31st March 1983 SHIPS AND STRUCTURES IN ICE FINLAND

NAME	COMPANY/INSTITUT	COUNTRY	ARRIV/DEPART	HOTEL DIPOLJ/GARDEN	ICE- BREAK PARTY	TOWN HALL	WARC	ms APU/URHO	WADAM	DINNER
					21.3	22.3	24.3	26.-27.3	30.3	30.3
Mr. Nyman	Hollming-yhtymä Oy	FIN			X	X	X		X	X
Mr. Pulli	Hollming-yhtymä Oy	FIN			X	X	X		X	X
Mr. Saari	Oy Wärtsilä Ab	FIN	21.-22.3, 29.-30.3	X	X	X			X	X
Mr. Salminen	Rauma-Repola Oy	FIN			X	X	X		X	X
Mr. Savikurki	Hollming-yhtymä Oy	FIN			X	X	X		X	X
Mr. Sihvola	Valmet Oy	FIN			X	X	X		X	X
Mr. Skytte	Oy Wärtsilä Ab	FIN	29.-30.3	X					X	X
Ms. Tikka	Oy Wärtsilä Ab	FIN	21.-25.3, 30.-31.3	X					X	X
Mr. Waselius	Finnlines Oy Ltd	FIN			X	X	X		X	X
Mr. Östring	Oy Laivateollisuus Ab	FIN	21.-31.3	X	X	X	X		X	X
Mr. Baumans	Bureau Veritas	FRA	21.-31.3		X	X	X		X	X
Mr. Duremberg	Gaz de France	FRA	20.-31.3	X	X	X	X		X	X
Mr. Huther	Bureau Veritas	FRA	20.-27.3, 27.-31.3	X	X	X	X		X	X
Mr. Ville	Bureau Veritas	FRA		X	X	X	X		X	X
Mr. Cusiter	Shell International Marine Ltd	GBR			X	X	X		X	X
Mr. Fulford	British Shipbuilders	GBR	20.3-1.4	X	X	X	X		X	X

WEGEMT VII GRADUATE SCHOOL 21st - 31st March 1983 SHIPS AND STRUCTURES IN ICE FINLAND

NAME	COMPANY/INSTITUT	COUNTRY	ARRIV/DEPART	HOTEL DIPOLJ/GARDEN	ICE- BREAK PARTY 21.3	TOWN HALL 22.3	WARC 24.3	ms ms APU/URHO 26.-27.3	WADAM 30.3	DINNER 30.3
Mr. McHenry	59. A. S. Computas	NOR	20.-31.3	X	X	X	X	X	X	X
Mr. Trosby	60. Det Norske Veritas	NOR	20.-31.3	X	X	X		X	X	X
Mr. Bergdahl	61. Chalmers University of Technology	SWE	21.-31.3		X	X	X		X	X
Mr. Forsman	62. The Swedish Maritime Research Centre	SWE	20.-31.3		X	X	X	X	X	X
Mr. Jansson	63. Götaverken Arendal	SWE	20.3-1.4	X	X	X	X		X	X
Mr. Sölve	64. Trollhätte Canal Administration	SWE	21.-24.3, 27.-31.3	X	X	X	X		X	X
Mr. Trägårdh	65. Götaverken Arendal	SWE	21.-25.3, 27.-31.3	X	X	X	X		X	X
Mr. Boban	66. Exxon International Co.	USA	20.-31.3	X	X	X	X	X	X	X
Mr. Bulow	67. Mobil Shipping & Transportation Co.	USA			X	X	X		X	X
Mr. Fiebrandt	68. U.S. Coast Guard	USA	20.3-1.4	X	X	X	X	X	X	X
Mr. Ralston	69. Exxon Production Research Co.	USA	20.-31.3	X	X	X	X	X	X	X
Mr. Slyker	70. Bethlehem Steel Corp.	USA	20.3-1.4	X	X	X	X	X	X	X

WEGEMT 1983

VII GRADUATE SCHOOL

SHIPS AND STRUCTURES IN ICE

- I ARCTIC RESOURCES
Dr. Arthur A. Meyerhoff
- II ARCTIC OPERATIONS
MSc Eero Mäkinen
- III SUB-ARCTIC WINTER NAVIGATION
Dr. Jan-Erik Jansson
- IV ASSESSING THE ECONOMICS OF ICE NAVIGATION - THE GREAT
LAKES AS A CASE STUDY
Prof. Harry Benford
- V SEA ICE AND THE ENVIRONMENT
Dr. Wilford F. Weeks
- VI THE MICROSTRUCTURE AND PHYSICAL PROPERTIES OF SEA ICE
Dr. W. F. Weeks
- VII MECHANICAL PROPERTIES OF SEA ICE
Mr. Franz U. Häusler
- VIII ICE SURVEILLANCE TECHNIQUES
Mr. Thomas Thompson
- IX STRUCTURAL ICE LOAD IN THE BALTIC
Mr. Kaj Riska & Dr. Petri Varsta
- X ICE LOADS ON SHIPS IN CANADIAN ARCTIC
Dr. Arno Keinonen
- XI COLLAPSE ANALYSIS OF SHIP SHELL PANELS
Prof. Tore Søreide
- XII STRENGTHENING OF HULL STRUCTURES IN ICE
Principal Surveyor Christian Mürer
- XIII CASE STUDIES: Ice load
Mr. Kaj Riska
- XIV MODELING TECHNIQUES IN VARIOUS ICE MODEL BASINS
Dr. Joachim Schwarz
- XV LEVEL ICE RESISTANCE
Dr. Ernst Enkvist
- XVI PROPULSION COEFFICIENTS AND PROPELLER DESIGN FOR
ICEBREAKING SHIPS

- XVII RECENT DEVELOPMENTS IN THE PREDICTION OF LEVEL
ICE RESISTANCE
Dr. J. Lewis
- XVIII CASE STUDIES: ICE RESISTANCE
Prof. Ernst Enkvist
- XIX PERFORMANCE AND ICE RESISTANCE OF SHIPS IN
RIDGES
Dr. Arno Keinonen
- XX PROPULSION IN ICE
MSc Kimmo Juurmaa
- XXI ICE LOAD RESPONSE IN SHAFTING
MSc Erik Sandberg
- XXII MODELLING OF SHIP PERFORMANCE IN OLD
ICE-CLOGGED CHANNELS
Prof. Valter Kostilainen
- XXIII CASE STUDIES: PROPULSION
MSc Kimmo Juurmaa
- XXIV PROPULSION MACHINERY SELECTION IN
ICEBREAKERS
MSc Jarmo Laakso
- XXV MACHINERY DAMAGES
Senior Surveyor Lasse Norhamo
- XXVI CP PROPELLERS FOR ICEGOING SHIP
MSc Sven-Ola Andersson
- XXVII RUDDERS AND STEERING
Mr Peter Noble
- XXVIII AUXILIARY SYSTEM FOR ICEBREAKING
MSc Göran Wilkman
- XXIX CASE STUDIES: PROGRESSIVE STRENGTH
MSc Jarmo Laakso
- XXX ICEBREAKERS
Mr Jouko Virtanen
- XXXI ICEBREAKING CARGO SHIPS
Mr Markku Kanerva
- XXXII SPECIAL SHIPS TO SUPPORT ARCTIC EXPLORATION
Mr Bengt Johansson
- XXXIII ACV-ICEBREAKING
Mr Peter Noble

- XXXIV ICE LOAD ON CYLINDRICAL AND CONICAL
OFFSHORE STRUCTURES
Mr Egon Wessels
- XXXV ARTIFICIAL ISLANDS AND WIDE STRUCTURES
Mr Kenneth Croasdale
- XXXVI OTHER (MOVABLE) STRUCTURES
Mr Peter Noble

REPRODUCE

Insinööritieto Oy 1983
Edition 150

ISBN 951-793-901-9
ISSN 0357-3451

MINERAL RESOURCES OF THE ARCTIC

by

Arthur A. Meyerhoff

Associated Resource Consultants, Inc.

P. O. Box 4602

Tulsa, OK 74159 USA

March 1983

MINERAL RESOURCES OF THE ARCTIC

CONTENTS

	<u>Page</u>
<u>INTRODUCTION</u> -----	1
<u>PETROLEUM</u> -----	3
<u>SUMMARY</u> -----	3
<u>BALTIC SYNECLISE</u> -----	6
Introduction-----	6
Regional Geologic Framework-----	7
Stratigraphy-----	8
Petroleum Geology-----	9
<u>TIMAN-PECHORA BASIN</u> -----	12
Introduction-----	12
Regional Geologic Framework-----	12
Stratigraphy-----	13
Petroleum Geology-----	14
<u>WESTERN NORWEGIAN SHELF</u> -----	15
<u>BARENTS SEA BASINS NORTH OF NORWAY</u> -----	16
Introduction-----	16
Regional Geologic Framework-----	20
Geology of Bear Island (Bjørnøya)-----	21
Geology of Svalbard and the Svalbard Platform-----	22
Petroleum Geology between Norway and the Svalbard Plat- form-----	25
Petroleum Geology of Svalbard-----	29
<u>BARENTS SEA BASINS NORTH OF THE USSR</u> -----	30
<u>WEST SIBERIAN BASIN</u> -----	32
Introduction-----	32
Regional Geologic Framework-----	33
Stratigraphy-----	34
Petroleum Geology-----	38
<u>NYUROL'KA BASIN</u> -----	43
Introduction-----	43
Regional Geologic Framework-----	43
Stratigraphy-----	44
Petroleum Geology-----	45
<u>LENA-TUNGUSKA PETROLEUM PROVINCE</u> -----	45
Introduction-----	45
Regional Geologic Framework-----	47
Stratigraphy-----	49
Petroleum Geology-----	51
<u>VILYUY BASIN (SYNECLISE)</u> -----	54
Introduction-----	54
Regional Geologic Framework-----	56
Stratigraphy-----	57
Petroleum Geology-----	58
Factors Bearing on Global Tectonic Problems-----	60

LENA-ANABAR, KHATANGA, AND YENISEY TROUGHS----- 61

 Introduction----- 61

 Regional Geologic Framework----- 62

 Stratigraphy----- 62

 Petroleum Geology----- 63

ASIATIC USSR--OFFSHORE BASINS OF THE ARCTIC----- 65

 North Kara Sea Basin----- 65

 Laptev Sea Basin----- 67

 Stolbovoy Basin----- 68

 North Laptev Basin----- 69

 Oloy Basin----- 70

 Faddeyevskiy Basin----- 71

 Northern East Siberian Basin (North Wrangel Basin)----- 71

 Southern East Siberian Basin (South Wrangel Basin)----- 72

BASINS OF THE NORTHEAST USSR (PACIFIC MOBILE BELT)----- 73

 Indigirka-Zyryanka and Homa Basins ----- 73

 Kolyma Basin----- 74

 Aynakhkurgun, Umkuveyen, and Ulyagan Basins----- 74

 Basins of the Amur and Ussuri Rivers Area----- 75

OKHOTSK AND JAPAN SEA BASINS (PACIFIC MOBILE BELT)----- 75

 East Sakhalin Basin----- 75

 Introduction----- 75

 Regional Geologic Framework----- 76

 Stratigraphy----- 77

 Petroleum Geology----- 78

 Terpeniya Gulf Basin----- 80

 Aniva Gulf Basin----- 80

 Tatar Strait Basin----- 81

 Priokhotsk and Parapol'-Palana Basins----- 82

 Severny Basin----- 83

 Penzhina Basin----- 84

 Central Kamchatka-Olyutor Trough----- 85

 East Kamchatka Basin----- 85

BERING SEA BASINS (PACIFIC MOBILE BELT)----- 87

 Khatyrka Basin----- 87

 Introduction----- 87

 Regional Geologic Framework----- 87

 Stratigraphy----- 88

 Petroleum Geology----- 88

 Anadyr Basin----- 89

 Introduction----- 89

 Regional Geologic Framework----- 89

 Stratigraphy----- 90

 Petroleum Geology----- 91

 Basins of the Offshore Bering Sea----- 93

 General----- 93

 Navarin Basin----- 94

 Walrus, Otter, and Inner Basins----- 94

 Zhemchug, Dalnoi, Garden, and Pribilof Basins----- 96

	<u>Page</u>
St. George Basin-----	97
Bristol (Bay) Basin-----	97
South Bethel Basin-----	99
Kresta Basin-----	99
Hall and St. Matthew Basins-----	99
Norton Basin-----	100
BASINS OF INTERIOR ALASKA (PACIFIC MOBILE BELT)-----	101
Bethel Basin-----	101
Koyukuk Basin-----	101
Yukon Flats-Porcupine-Kandik Basin-----	102
Middle Tanana Basin-----	102
DE LONG (HOPE) BASIN-----	103
NORTH CHUKCHI BASIN-----	104
THE NORTH SLOPE (COLVILLE TROUGH-BARROW ARCH)-----	105
Introduction-----	105
Regional Geologic Framework-----	108
Stratigraphy-----	109
Franklinian-----	110
Ellesmerian-----	110
Brookian-----	111
Petroleum Geology-----	111
ALASKAN ARCTIC (WESTERN BEAUFORT) SHELF-----	113
DEMARICATION BASIN-----	114
BEAUFORT-MACKENZIE BASIN-----	116
Introduction-----	116
Regional Geologic Framework-----	117
Stratigraphy-----	118
Petroleum Geology-----	120
BANKS AND ARCTIC COASTAL PLAIN BASINS-----	122
OLD CROW BASIN-----	124
EAGLE PLAIN BASIN-----	125
PEEL PLATEAU BASIN-----	126
MACKENZIE PLAIN BASIN-----	127
GREAT BEAR BASIN (INCLUDING ANDERSON SUBBASIN)-----	129
BANKS ISLAND AND EGLINTON ISLAND GRABENS-----	132
FRANKLINIAN GEOSYNCLINE-SVERDRUP BASIN-----	133
Introduction-----	133
Regional Geologic Framework-----	134
Stratigraphy-----	135
Origin of Sverdrup Basin-----	140
Petroleum Geology-----	142
WANDEL SEA BASIN-----	143
FOX E BASIN-----	145
HUDSON PLATFORM-----	145
HUDSON STRAIT-UNGAVA BAY BASIN-----	147
JONES BASIN-----	147
LANCASTER BASIN-----	148
NARES STRAIT (KANE) BASIN-----	149
BAFFIN SHELF-DAVIS STRAIT-----	151

	<u>Page</u>
LABRADOR SHELF-----	154
Introduction-----	154
Regional Geologic Framework-----	155
Stratigraphy-----	155
Petroleum Geology-----	157
EAST NEWFOUNDLAND SHELF-----	158
Introduction-----	158
Regional Geologic Framework-----	159
Stratigraphy-----	160
Petroleum Geology-----	161
WEST GREENLAND SHELF-----	163
Introduction-----	163
Regional Geologic Framework-----	164
Stratigraphy-----	164
Petroleum Geology-----	166
EAST GREENLAND SHELF-----	167
PLATE TECTONICS IN NORTHEASTERN NORTH AMERICA-----	168
CONCLUSIONS-----	168
<u>COAL</u> -----	169
INTRODUCTION-----	169
NORWAY-----	170
SWEDEN-----	172
BEAR ISLAND (BJÖRNÖYA)-----	172
SVALBARD-----	173
SOVIET UNION-----	174
General-----	174
Timan-Pechora Basin-----	175
Introduction-----	175
Geology-----	175
Resources-----	176
Eastern Urals-----	176
Taymyr Peninsula-----	177
Ekibastuz-----	178
Kuznetsk Basin (Kuzbas)-----	178
Kansk-Achinsk Basin-----	179
Tunguska Basin-Lena Trough-----	179
South Yakutia Coal Basin-----	181
Miscellaneous-----	181
ALASKA-----	183
General-----	183
Northern Alaska (North Slope)-----	184
Remainder of Alaska-----	184
CANADA-----	185
GREENLAND-----	186
West Greenland-----	186
East Greenland-----	187
Northeast Greenland-----	187
ICELAND-----	187
<u>OTHER HYDROCARBONS</u> -----	188
PEAT-----	188

OIL SHALE-----	189
Norway and Sweden-----	189
Northwestern USSR-----	190
Remainder of USSR-----	192
Alaska-----	192
Canada and Greenland-----	193
<u>TAR SANDS AND HEAVY OIL-----</u>	193
SOVIET UNION-----	193
Franz Josef Land-----	193
Timan-Pechora Basin-----	194
West Siberia Basin-----	194
Lena-Tunguska Petroleum Province and Lena-Anabar Trough---	195
ALASKA-----	200
CANADA-----	200
Western Canada Basin-----	200
Melville Island-----	201
<u>URANIUM-----</u>	201
GENERAL-----	201
NORWAY-----	203
SWEDEN-----	203
FINLAND-----	205
SOVIET UNION-----	206
General-----	206
Uranium Deposits-----	208
Kola Peninsula-----	208
Northern European USSR-----	209
Siberian Platform and Surrounding Areas-----	210
Soviet Far East-----	210
ALASKA-----	211
CANADA-----	212
General-----	212
District of Mackenzie, Northwest Territories-----	213
Northern Saskatchewan-----	214
Keewatin District, Northwest Territories-----	216
Labrador-----	216
GREENLAND-----	217
<u>GEOHERMAL ENERGY-----</u>	218
SOVIET UNION-----	218
ALASKA-----	220
ICELAND-----	220
<u>HYDROPOWER AND NUCLEAR POWER ELECTRIC PLANTS-----</u>	222
<u>WATER-DIVERSION PLANS IN THE USSR-----</u>	222
<u>FERROUS METALS-----</u>	224
GENERAL-----	224
IRON AND KINDRED METALS-----	226
Norway-----	227
Sweden-----	231

REFERENCES CITED -----
FIGURE CAPTIONS -----

MINERAL RESOURCES OF THE ARCTIC

Arthur A. Meyerhoff

Associated Resource Consultants, Inc.

P. O. Box 4602

Tulsa, Oklahoma 74159 USA

INTRODUCTION

For the purposes of this paper, I define the Arctic and Subarctic as the region which generally is north of lat 60°N . I have included the Baltic syncline because of the ice conditions that prevail in parts of this sea during the winter. Moreover, surprisingly little has been published in Western countries—with the obvious exceptions of Sweden and Finland—about the geology and mineral prospects of the Baltic syncline. The British Isles, Ireland, and North Sea south of 60° are not included because of the large and growing literature that deals with these regions. The entire West Siberian basin is included because it is a single geologic unit, extending from 54°N to 76°N (including the offshore Kara Sea). Sakhalin Island is included because it lies in the Arctic's "iceberg alley" of the Northern Pacific and therefore is analogous with the "iceberg alleys" east of Labrador and Greenland. All of the Lena-Tunguska province is included because the southern part is an area where major gas and oil reserves are being discovered in Proterozoic rocks, and to a lesser extent, in Lower Cambrian strata. Moreover, there are some similarities between the Lena-Tunguska province and the Great Bear basin and Minto arch of Canada, between Norman Wells and the northeastern coast of Victoria Island. Finally, I have included the Labrador Sea and the Grand Banks because of climatic and geologic conditions which are similar to those of other Arctic regions.

The region under consideration is enormous. It contains 36.4 million sq km, plus an additional 5 to 10 million sq km south of 60°N. About one tenth of the land area is covered by glaciers, a fact which can make operating conditions difficult. The known and suspected reserves of petroleum, coal, and other minerals are huge. The largest single concentration of gas in any one place in the world is in the West Siberian basin, and possibly the world's largest coal field underlies the Lena-Tunguska province.

The largest shelf areas on earth also are in the Arctic, mainly off the USSR. In terms of frontage along the Arctic coast, the USSR has 52 percent; Canada, 24 percent; Norway, 9 percent; Denmark's Greenland, 8 percent; and the United States, 7 percent. Other Arctic nations include Finland, Sweden, and Iceland. Therefore, the facts that (1) large petroleum and other mineral reserves have been found and (2) a huge resource basis remains for the future, make this an extremely important region, not only for economic reasons, but also for political (or geopolitical) reasons. The geopolitics of this area were discussed in some detail by Meyerhoff and Meyerhoff (1973) and by Meyerhoff (1982a).

Geologically, the Arctic region includes a wide variety of geologic settings, ranging from continental shelves to intracratonic basins, geosynclinal forelands, small ocean basins, marginal seas, and successor basins on island arcs, or relict island arcs. This wide diversity of geologic settings enhances the resource potential of the Arctic, because highly diverse geologic conditions make it possible to have a highly diverse mineral resource base.

So that there will be no doubt as to what I mean about the volumes of any particular mineral, I use the terms "resource" and "reserve." A reserve is a quantity of mineral, whether it be coal, petroleum, gold, or whatever, which has been measured in detail, usually on the basis of surface or borehole control points separated laterally by 500 m or less. Everything else is a resource--i.e., something believed or inferred to be present, but not actually measured or proved. (Probable reserves or identified reserves are terms which I use in some places.

These refer to a deposit in which detailed measurements are 500 to 1,000 m apart.)

To compile this summary, I have relied on nearly 2,000 publications and numerous unpublished reports, as well as on my own field and subsurface work in the USSR, Canada, and Iceland. I also consulted with scores of specialists from various countries, who supplied data, publications, and advice.

PETROLEUM

SUMMARY

I have included among Arctic and Subarctic petroleum-bearing, or potentially petroleum-bearing areas, such basins as the Baltic syncline, the southern part of the West Siberian basin, the Labrador Sea, and the Grand Banks of Newfoundland. The Northern North Sea basin, the basins west of Scotland and the Shetlands, and the Scotia shelf of eastern Canada are not considered.

The Baltic syncline is a Cambrian through Middle Devonian basin, with mainly Cambrian oil. Reserves probably are somewhat less than 100 million bbl. Most of the resources—possibly 500 million bbl or more—are expected to be in the Cambrian with lesser amounts in the Ordovician through Devonian. The Timan-Pechora basin of the northwestern USSR has production from the Silurian through the Triassic. Source rocks are mainly in the Devonian through Permian section. This basin bifurcates offshore, with the southwestern part of the basin appearing to join basins north of Norway on the west, and the eastern part of the basin continuing northward along the western side of Novaya Zemlya. Reserves in the Timan-Pechora basin are about 5.1 billion bbl of liquids and 19.4 Tcf of gas, all of it onshore. Although the onshore has important resource potential (4 billion bbl and 50 Tcf), the offshore has the greater potential (16 billion bbl and 100 Tcf). The Atlantic shelf west of Norway is little explored, but the best-known potential to date is in the Jurassic and Triassic sections. Two discoveries have been made.

In the Barents Sea north of Norway, the Triassic and Jurassic also have considerable resource potential, as does the Paleozoic section beneath.

East of the Urals and Novaya Zemlya, the West Siberian basin (including the Kara Sea) occupies an area of 2,376,000 sq km. The northern onshore part of the basin contains the world's largest concentration of gas reserves, most of it Cenomanian biogenic gas. Smaller amounts of gas are in the Neocomian and Upper Jurassic. The principal source of the biogenic gas is Aptian-Albian coal. The oil and gas of the remainder of the basin have a mainly Upper Jurassic source, although some source beds are in the Lower Cretaceous. Oil reserves are about 18 billion bbl; gas reserves are 545 Tcf. The resource potential is 54 billion bbl and at least 948 Tcf.

Several basins are known in East Siberia and the Soviet Far East. The largest are offshore and have major resource potential. Of the onshore basins, the Vilyuy has Tcf of gas reserves in Jurassic, Triassic, and Permian rocks; the resource potential is an additional 19 Tcf or more. The volume of liquids found to date is small. The gas sources appear to be Permian or older strata. East of the Vilyuy basin, the Lena-Tunguska province contains about 225 million bbl of oil and condensate and 18 Tcf of gas in rocks of Proterozoic and Early Cambrian ages. Sources are of the same ages. Resource potential is at least 2 billion bbl and 83 Tcf. On Sakhalin Island, along the Pacific coast, oil and gas are present in Miocene and lower Pliocene sandstones. Reserves are 24 million bbl of liquids and 2 Tcf of gas, with resource potentials of about 1 billion bbl and 5 Tcf.

The Okhotsk, Bering, Chukchi, East Siberian, and Laptev Seas have huge potential--27 billion bbl and 172 Tcf. Yet these areas are insufficiently explored; some hardly at all. Production from the first two areas should be mainly Tertiary; from the others, Mesozoic and lower Tertiary. In Alaska, including the Chukchi Sea, the North Slope contains at least 26 Tcf and 10 billion bbl. The

remainder of Alaska has about 2 Tcf and less than 300 million bbl. The resource potential is good, especially in the Beaufort Sea. The Beaufort Sea-Mackenzie delta region has reserves of at least 7 Tcf and 500 million bbl, but the potential for much greater volumes of oil and gas is considered to be good--perhaps 4 billion bbl in two offshore structures alone. Farther east, in the Franklinian fold belt and Sverdrup basin, the gas reserves are 20 to 25 Tcf; liquid reserves may be large but are unproved. Additional resource potential exists in the Lower Cambrian and Proterozoic of the Great Bear basin and Minto arch between Norman Wells and the northeastern side of Victoria Island, in Lancaster Sound, and Nares Strait. The Hudson Bay and Foxe basins are not very attractive. The western side of Baffin Bay has potential petroleum resources, as does the East Greenland shelf, and possibly some areas of northern Greenland. The presence of hydrocarbons has been established in the lower Tertiary, Aptian-Albian, and fractured Paleozoic carbonates of the Labrador shelf, and in Jurassic and Cretaceous rocks of the Grand Banks.

Ages of production differ significantly from area to area, with indigenous hydrocarbons in rocks of nearly every age from the Proterozoic through the early Pliocene. The geology of this complex region defies all tectonic models so far proposed for it--whether to explain a part of the region or the region as a whole. Perhaps the single most striking fact about the region as a whole is the very large volume of discovered hydrocarbons and hydrocarbon resource potential in rocks of Triassic, Jurassic, and Cretaceous ages. When the basins of Canada and Greenland are explored more thoroughly, the same statement probably will be true for rocks of most of the Paleozoic systems and very likely for the Proterozoic. Another striking feature is the great abundance of source rocks in Proterozoic and Cambrian sections, in the Devonian through Permian and in the Triassic-Cretaceous. Nor is this statement about source rocks confined only to Arctic regions. Whatever the answers are, they are complex. They are not answered in this paper, but I do attempt to synthesize some of the key points in the last part of the paper in the hope that the synthesis will contribute toward a solution to the problems encountered in the area.

For the benefit of those who wonder how I arrived at certain resource values, I have used the following methods. (1) In areas similar geologically to those where subsurface control is good and reserve estimates are reliable, I have assumed that the analogous basin will produce about the same number of barrels of oil or cubic feet of gas per cubic kilometer of sedimentary rock. (2) In areas where no petroleum has been found away from structures, I have used the volume of sedimentary rock beneath each structure, compared it directly with one whose reserves are known, and have added 10 percent for stratigraphic traps. (3) In unknown areas, I have used the Weeks (1975) method of a first approximation, but have reduced his recovery factor by 25 percent. For all three methods, my figures average approximately 40,000 bbl per cu km, which is possibly too high. However, it is conservative if areas such as the Viking graben in the North Sea are considered.

In all, the hydrocarbon resource potential of Arctic regions is extremely good. The principal problems--other than political--involve the very high costs of exploration and development, especially in areas covered by ice and permafrost.

BALTIC SYNECLISE

Introduction

The Baltic syncline (basin) occupies at least 180,000 sq km in Latvia, Lithuania, the Kaliningrad district of the RSFSR, northern Poland, the central Baltic Sea, and the Öland-Götland Islands area of coastal Sweden (Geodekyan, 1976; Dikenshteyn, 1977; Geodekyan et al., 1978; see Fig. 2). Of this amount, 100,000 sq km belongs to the USSR. Exploratory work began here in 1949. In 1960 and 1963, two small noncommercial oil discoveries were made in the USSR. Swedish exploration began with stratigraphic tests in 1967, and the first discovery was made on Gotland Island in 1974 (Dahl, 1982). In the USSR, the first two commercial fields

were found in 1968 and, by 1980, 16 commercial fields (38-45° API) had been discovered in USSR territory, in addition to 6 noncommercial fields. Five non-commercial finds had been made on Gotland Island, Sweden, and one in coastal Poland. Sixteen offshore wells had been drilled by the end of 1981--all dry, and 150 shallow wells had been drilled on Gotland Island, where small Ordovician reefs produce 2,000 bbl/d of 40° API oil from 200 to 300 m depths; 25 wells still were productive on January 1, 1982 (Anonymous, 1981a). In Polish waters, the first offshore discovery was made near Gdansk (Fig. 2) during 1981; one offset well was dry. The rig was moved to a new location 76 km north of Leba, and gas was found. A fourth well currently has been drilled in Soviet waters. These four wells are a joint venture of the Petro-Baltik Trest, the members of which are Poland, East Germany, and the USSR. Farther west, in West German waters, an American company in 1978 discovered an offshore field in the upper Paleozoic rocks of the Northwest German basin, at a depth of 1,500 m. Two production platforms for 14 development wells are being installed. The first, Schwedeneck See, is north of Kiel, and is an extension of an onshore field.

In late 1981, a fixed platform was built just offshore from Kaliningrad in the USSR, and the Soviet Union's first offshore drilling in the Baltic Sea commenced during 1982. The mobile rig that found oil offshore from Gdansk later moved to the USSR to drill one of the several structures known there (Fig. 2). Until 1982, the deepest well drilled in the basin was 2,984 m (onshore, near Kaliningrad), near the basin center (Fig. 2). The offshore test drilled in 1981 near Gdansk reached 2,520 m.

Regional Geologic Framework

The total sedimentary rock thickness is shown on Figure 2, which is a structural contour map of the base of the Cambrian. The stratigraphic sequence appears on Figures 3 and 4. The three figures illustrate that the Baltic syncline is a supracratonic depression of Early Cambrian through Middle Devonian ages. The

basin was overlapped from the south by Carboniferous and younger sediments of the Northwest German basin.

Stratigraphy

The Cambrian consists of up to 478 m (the thickest section known, northwest of Gdansk) of arkosic conglomerate which grades upward into increasingly finer grained terrigenous rocks. Some argillaceous and organogenic phosphatic limestone is present in the Middle and Upper Cambrian, together with quartzose sandstone, siltstone, and black shale. Marine fossils are abundant. The principal production is from quartz sandstone in the Middle Cambrian. The Cambrian becomes very fine grained offshore and siliceous in a southerly direction.

The Ordovician is 40 to 200 m of marine shallow-water and biostromal carbonates, conformable above the Cambrian. Argillaceous limestone, minor sandstone, and some glauconite are present. Approximately 100 km west of Gdansk near Slupsk, the Ordovician thickens abruptly to more than 1,400 m of deep-water black shale (Geodekyan, 1976).

The Silurian ranges in thickness from 500 to 2,200 m, and is complete in the central part of the syncline. It is conformable on the Ordovician. Around the flanks of the basin, the Silurian was eroded before deposition of the Devonian. It is a sequence of organic-rich bituminous and organic shales with beds of siltstone, sandstone, and carbonate rocks, including bioherms and biostromal limestone. Deep-water conditions prevailed in the central part of the basin and in the west.

Devonian time records a shallowing of the sea and its eventual retreat from the basin. The Lower Devonian, 50 to 400 m thick, overlies the Silurian unconformably, particularly along the basin flanks. The basin center shifted from near Gdansk to near Klaipeda (Fig. 2). The strata are lagoonal, marginal marine, and nonmarine sandstone, siltstone, shale, and marl. Colors range from gray to red and red violet. The lithology and depositional environment indicate the onset of the Caledonian tectogenesis.



MSc Eero Mäkinen

ARCTIC OPERATIONS

Lecture at WEGEMT in Helsinki on March 21, 1983 by Eero Mäkinen

1 INTRODUCTION

This lecture deals with marine operations in the arctic area. The term "arctic area" refers in this connection to the northern seas that are ice-covered all the year round or part of the year. It does not, however, include so-called subarctic areas, which are discussed in another paper. Such subarctic areas are, for example, the Baltic Sea, the Sea of Okhotsk, the American Great Lakes and Gulf of St. Lawrence, and rivers and lakes on the American and the Eurasian continents. All seas north of those listed above are regarded as arctic, and they include the northernmost waters in Canada, the United States, the Soviet Union, Norway, Iceland and Denmark (Greenland).

The term "operations" in this connection covers marine transportation (i.e. shipping), offshore activities, fishing, dredging, etc., and also naval operations.

The history of marine operations in the Arctic will not be dealt with, but this lecture sets out to give a summary of environmental conditions and general activities in the arctic areas, which form the basis for all marine activities, and will then go on to discuss the marine operations today and the tonnage used in those operations.

2 ENVIRONMENTAL CONDITIONS

From the point of view of developing, designing and constructing ships and marine structures for the Arctic, the sea ice is the dominant environmental factor. Other factors characterizing the arctic environment, such as air temperature, winds, precipitation and darkness, will not be discussed here.

The greater part of the Arctic Ocean is covered by pack ice throughout the year. Fig. 2.1. However, the areas close to the coast are ice-free at least a couple of months every year. The first-year ice reaches a maximum thickness of almost 3 metres, but in most arctic areas where marine operations take place today, the maximum thickness of first-year ice varies between 1 and 2 metres. Multi-year ice forms a much more difficult obstacle to marine operations than the first-year ice. The proportion of multi-year ice varies greatly, from very low, often non-existent, in southern areas, to very high, sometimes up to 80 per cent, in certain areas. In the areas of current operations, the proportion of multi-year ice is relatively low. In most of the areas the sea ice is covered by pack ice, which is in almost continuous slow movement and which contains cracks and leads. Only in coastal areas, inside archipelagoes and in very shallow areas, is the ice land-fast and in this case often has a smooth surface without ridging. Outside these areas the ice is more or less ridged. The degree of ridging varies not only from place to place, but very much also from year to year. Icebergs are another type of ice formation. Being of land origin and not so-called sea ice, they are massive and generally not penetrable by ships. Icebergs are concentrated in very limited areas only.

The ice conditions in the Soviet Arctic and North-American Arctic are very much alike, although there are certain differences. The North-American Arctic contains a large area covered by land-fast ice in the middle of the winter, while such areas are not found in the Soviet Arctic. Especially in the western part of the North-American Arctic, multi-year ice is found very close to the coast due to the neighbourhood of the polar pack. A very heavy concentration of icebergs exists in the area between Greenland and the Canadian islands, while in the Soviet Arctic there are practically no icebergs.

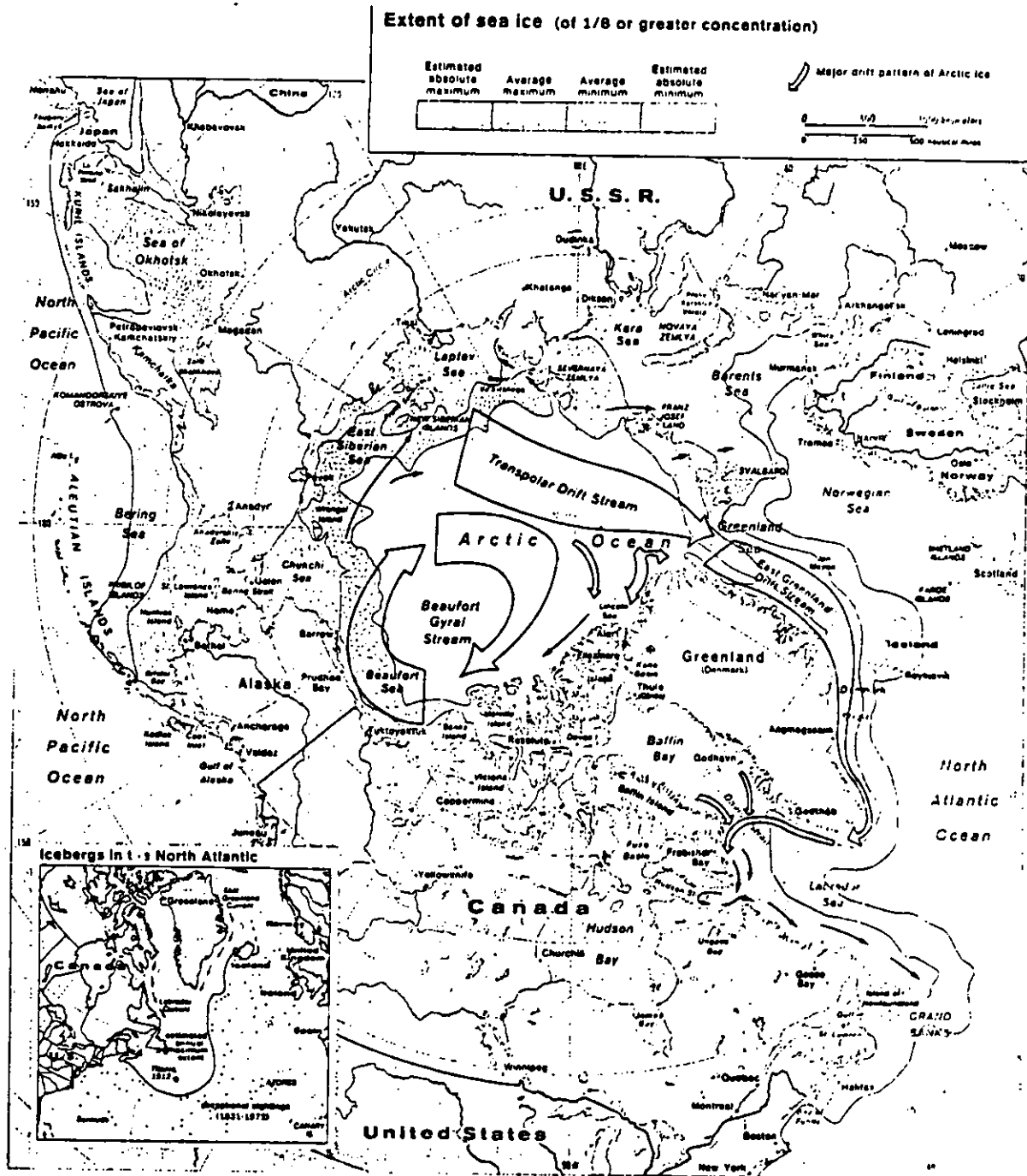


Fig. 2.1.

GENERAL ACTIVITIES IN THE ARCTIC AREA

We will have a quick look at general activities in the Arctic, because these form the basis for all marine operations.

Fig. 3.1 shows the population in certain parts of the Arctic. Generally the arctic areas are very sparsely populated, but comparing the population in the Soviet and the North-American Arctic we can see that the Soviet Arctic is much more densely populated. In the Soviet Arctic there are permanent settlements designed to have a normal southern-type infrastructure, while the life and activities in the North-American Arctic have a temporary nature.

Fig. 3.2 shows the urban population and economic activity. Apart from southern Alaska, this figure supports the previous conclusion.

Fig. 3.3 shows the extent of mining activities. Mining is today one of the major ways of utilizing the natural resources of the Arctic. In Fig. 3.4 the present oil and gas exploration/production activities are visualized. Oil and gas will become another important field of exploitation in the Arctic.

The dependence of industrial activities on marine operations is different in the Soviet and in the North-American Arctic. The development in North America will be primarily dependent on marine connections and offshore operation, while in the Soviet Arctic there are natural land connections. Despite the land connections, marine transportation will, however, predominate in certain areas due to economic reasons.

Fig. 3.5 shows the volume of waterway transportation in the Arctic. The volume is very small in comparison with the volume of transportation in the major sea routes of the world. The figure also shows that the activities are much higher in the Soviet Arctic than in the North-American Arctic.

Population growth since 1940

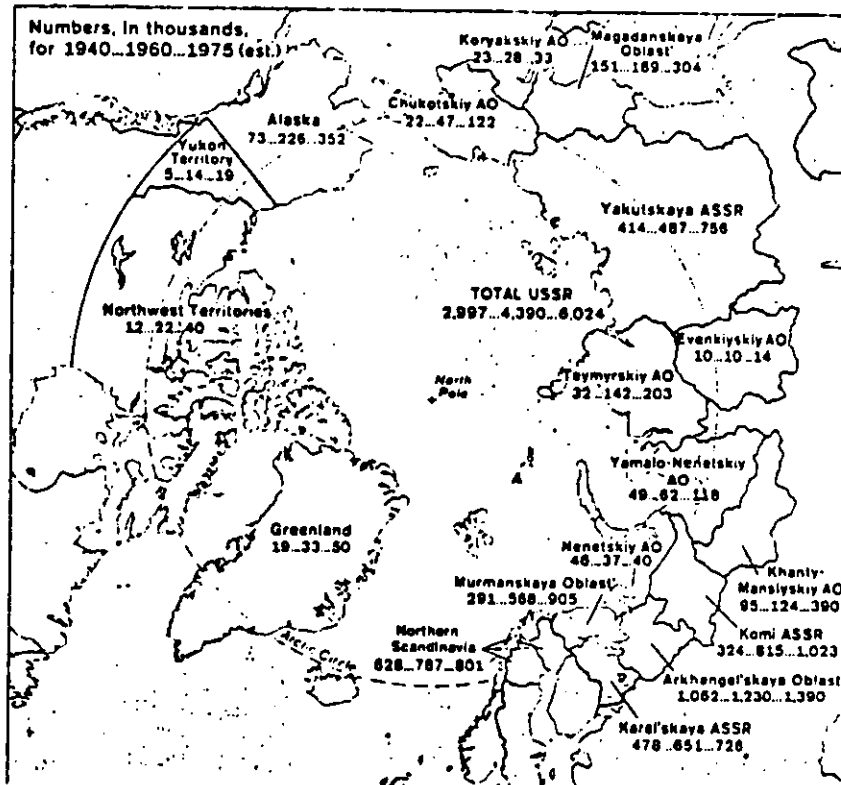


Fig. 3.1.

Urban population and economic activity

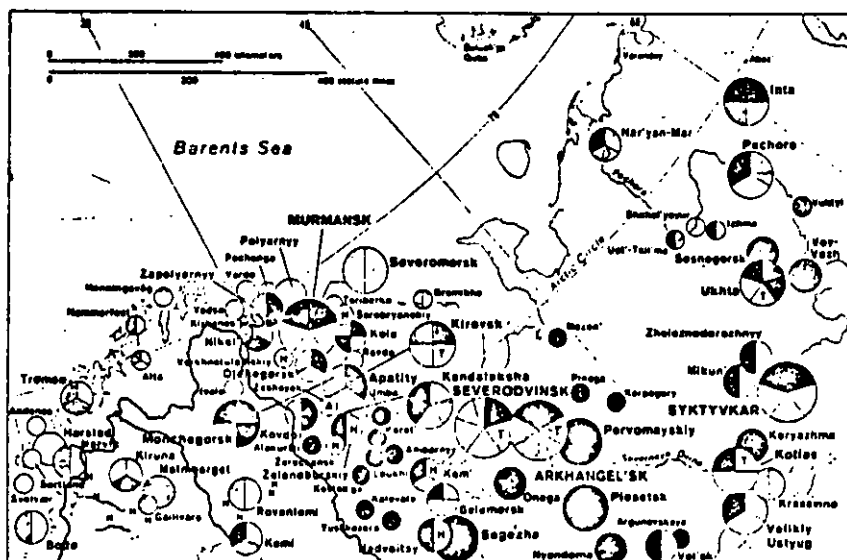
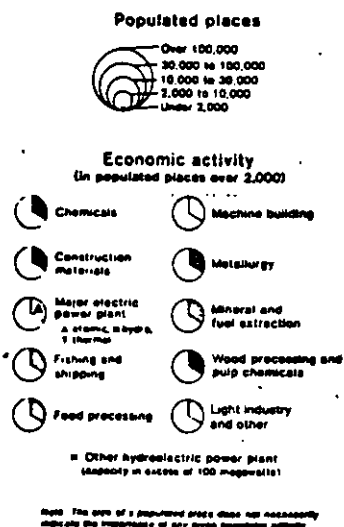
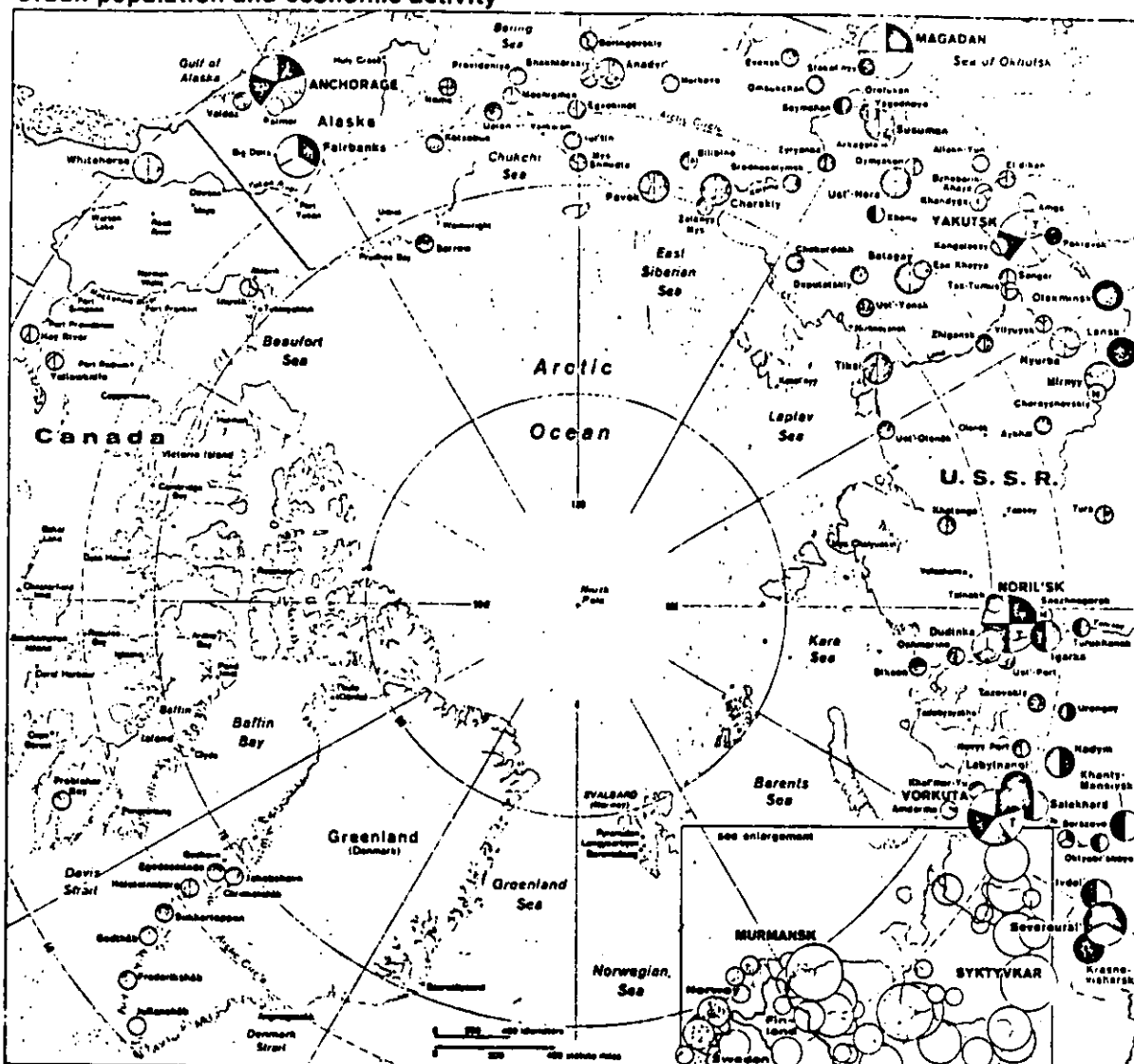


Fig. 3.2.

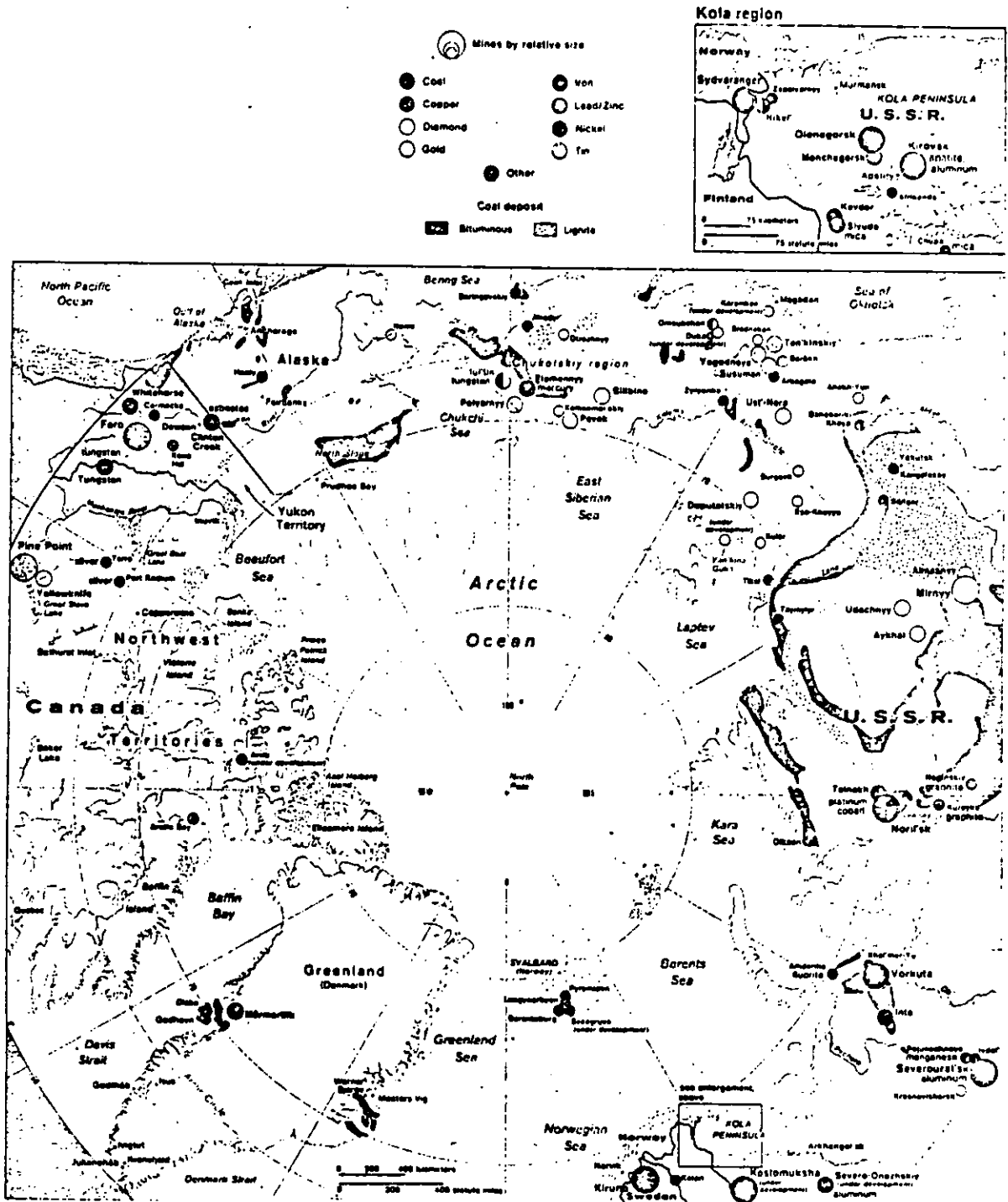
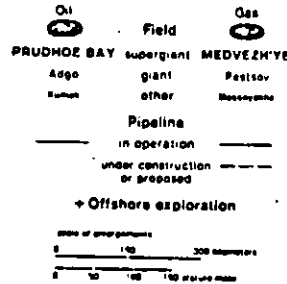
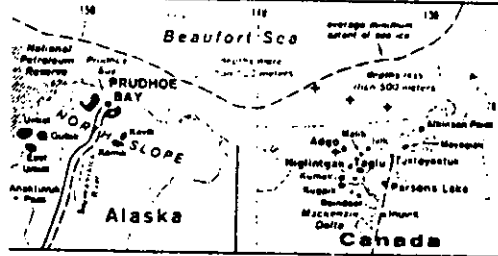
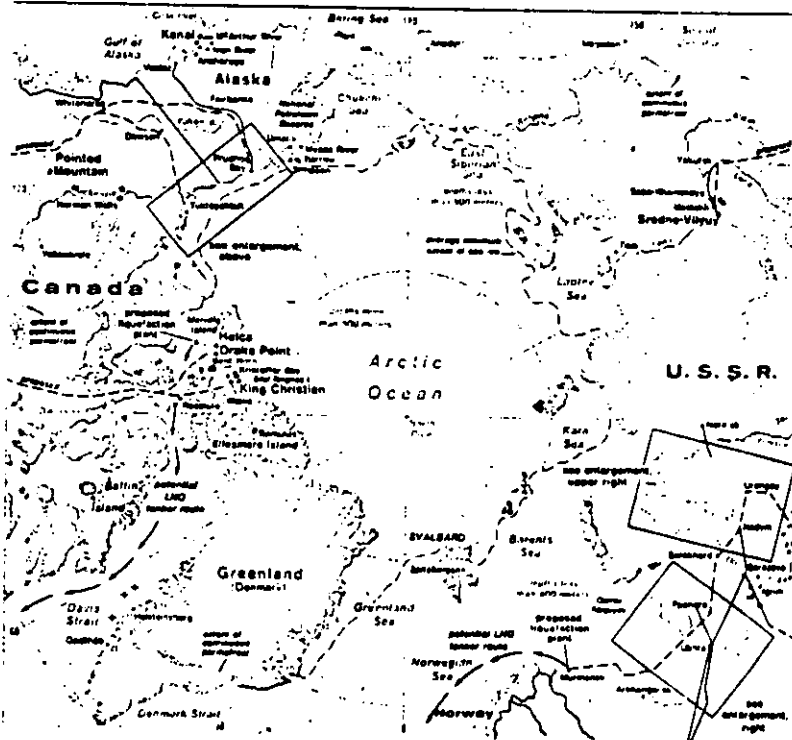
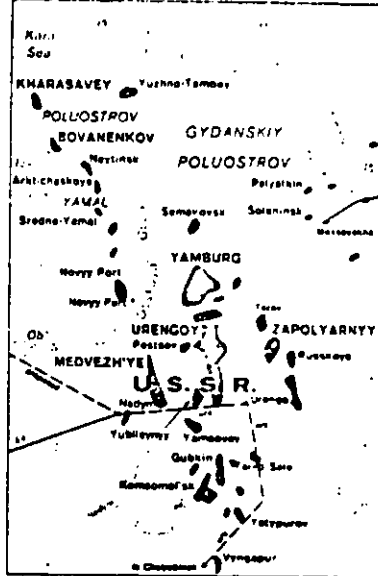


Fig. 3.3.

Mackenzie Delta/Beaufort Sea



Lower Ob' basin



Pechora basin

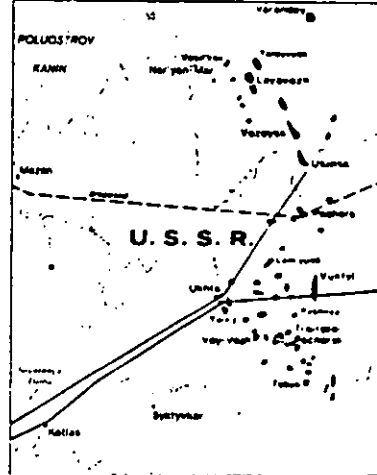


Fig. 3.4.

Waterway transportation: annual tonnage

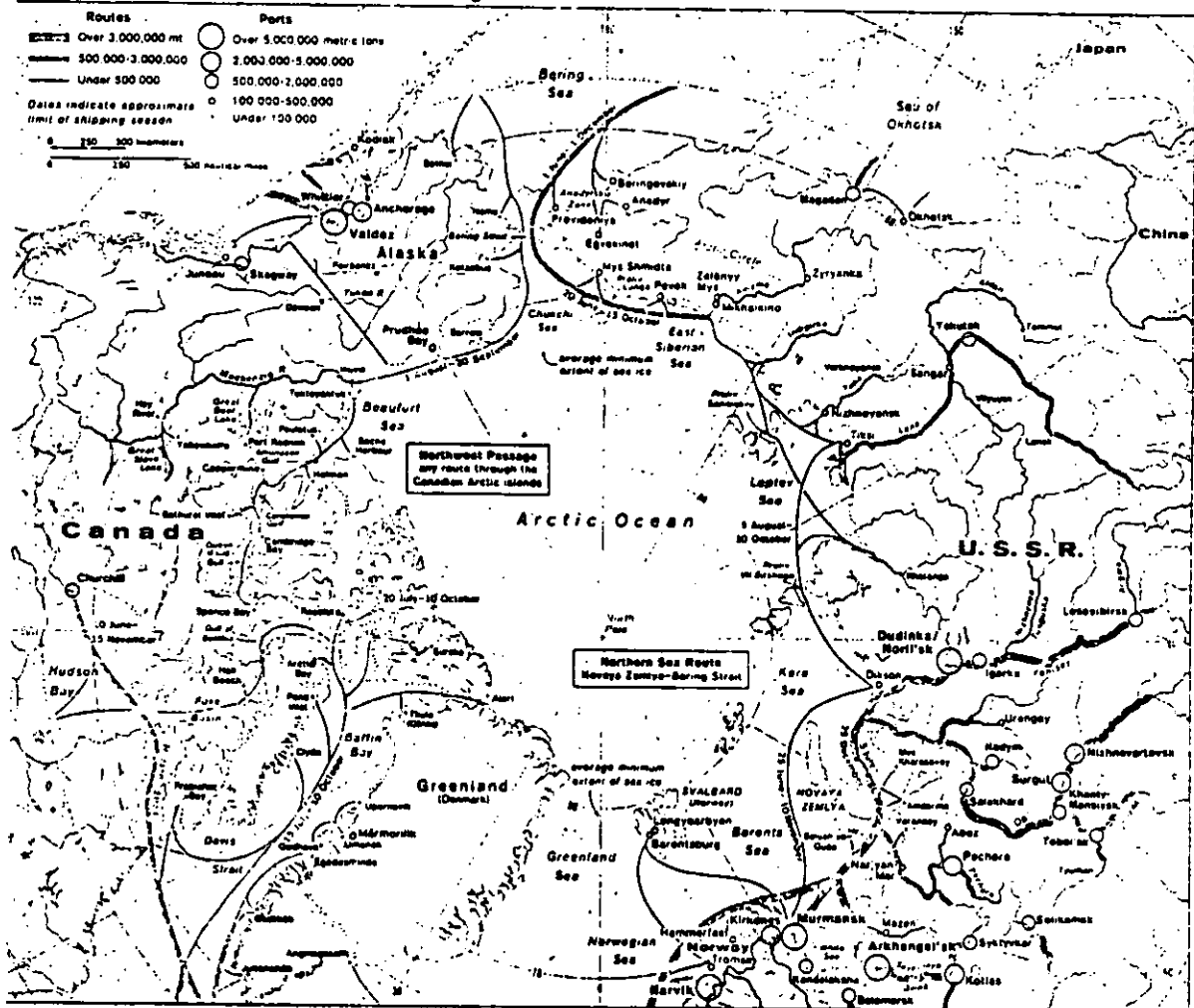


Fig. 3.5.

In the following, the operations in the Soviet Arctic and in the North-American Arctic are dealt with to some extent separately.

The main activities are shipping and offshore exploration/production, whereas, for example, fishing and naval operations are today of minor importance. Such activities as dredging, pipe-laying, etc., usually serve offshore work and are regarded here as part of that category.

4

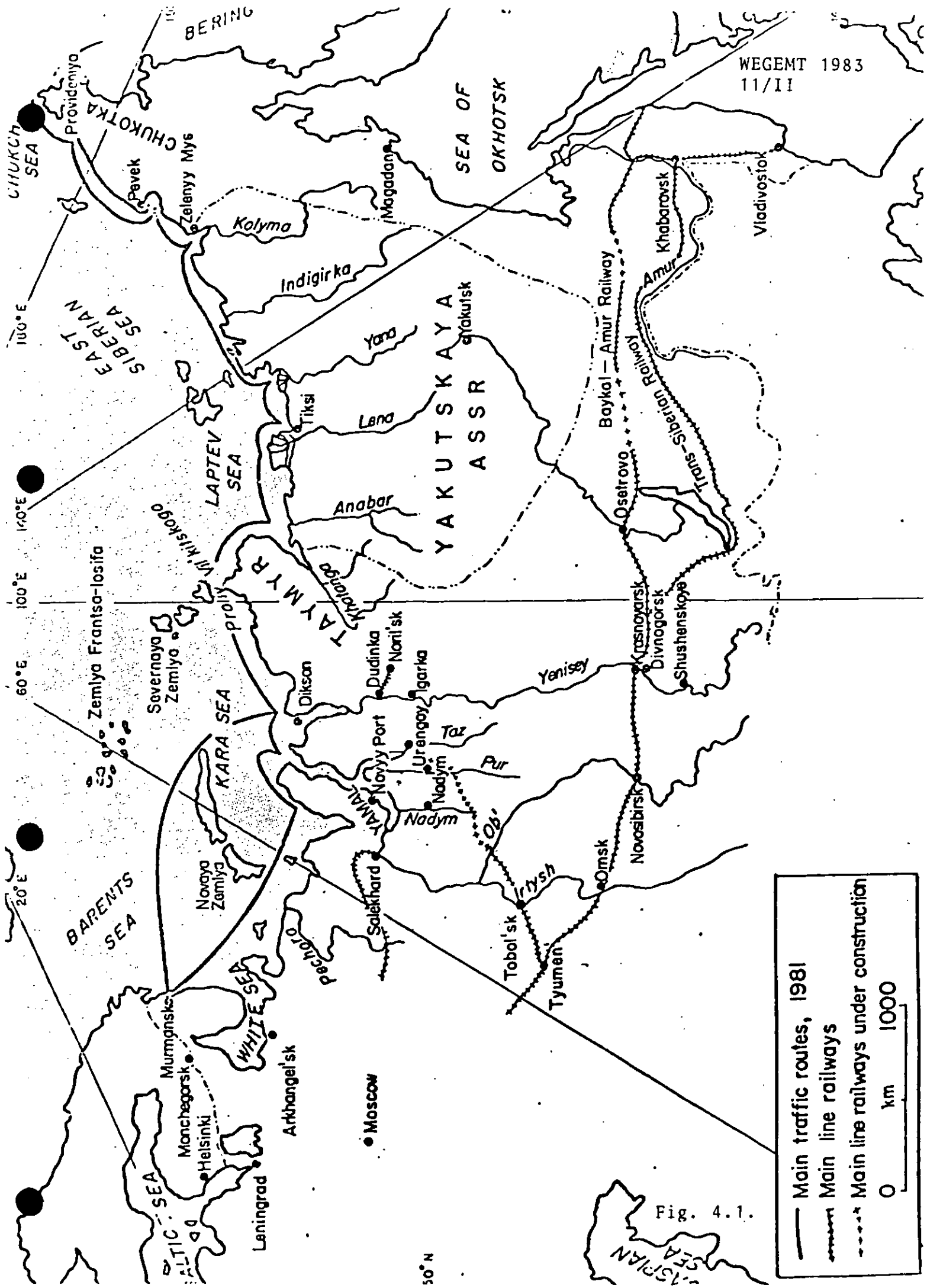
OPERATIONS TODAY

The Soviet Arctic

The marine transportation in the Soviet Arctic has been practised for a long time. More or less regular traffic, at least in the western part, began already several decades ago. The area with the major routes and cities is shown in Fig. 4.1. Earlier, the shipping served primarily to transport goods to the Arctic communities, but today there is also a great deal of bulk material transportation from the Arctic. The North-east Passage has no regular through-traffic, but is navigated on an experimental basis in summertime only. The length of the shipping season in the western part has been extended radically during the last five years, Fig. 4.2. Today there is year-round traffic up to the city of Dudinka on the Yenisei River. The only interruption is at the time of the break-up of the ice. The development of the shipping volumes can be seen in Fig. 4.3.

In the western part of the Soviet Arctic the year-round navigation is today a matter of routine, although the traffic flows extremely slowly in mid-winter and is certainly very costly.

The two experimental trips, one by the icebreaker Arktika to the North Pole in 1977 and the other by the icebreaker Sibir and a cargo ship through the Northwest Passage, show without doubt that the Soviets are able to operate everywhere in their arctic regions and can do this in some areas all the year round.



— Main traffic routes, 1981
- - - Main line railways
- · - · Main line railways under construction

0 km 1000

Fig. 4.1.

50° N

THE DURATION OF THE NAVIGATION
PERIOD IN THE SOVIET ARCTIC

1920 - 1981

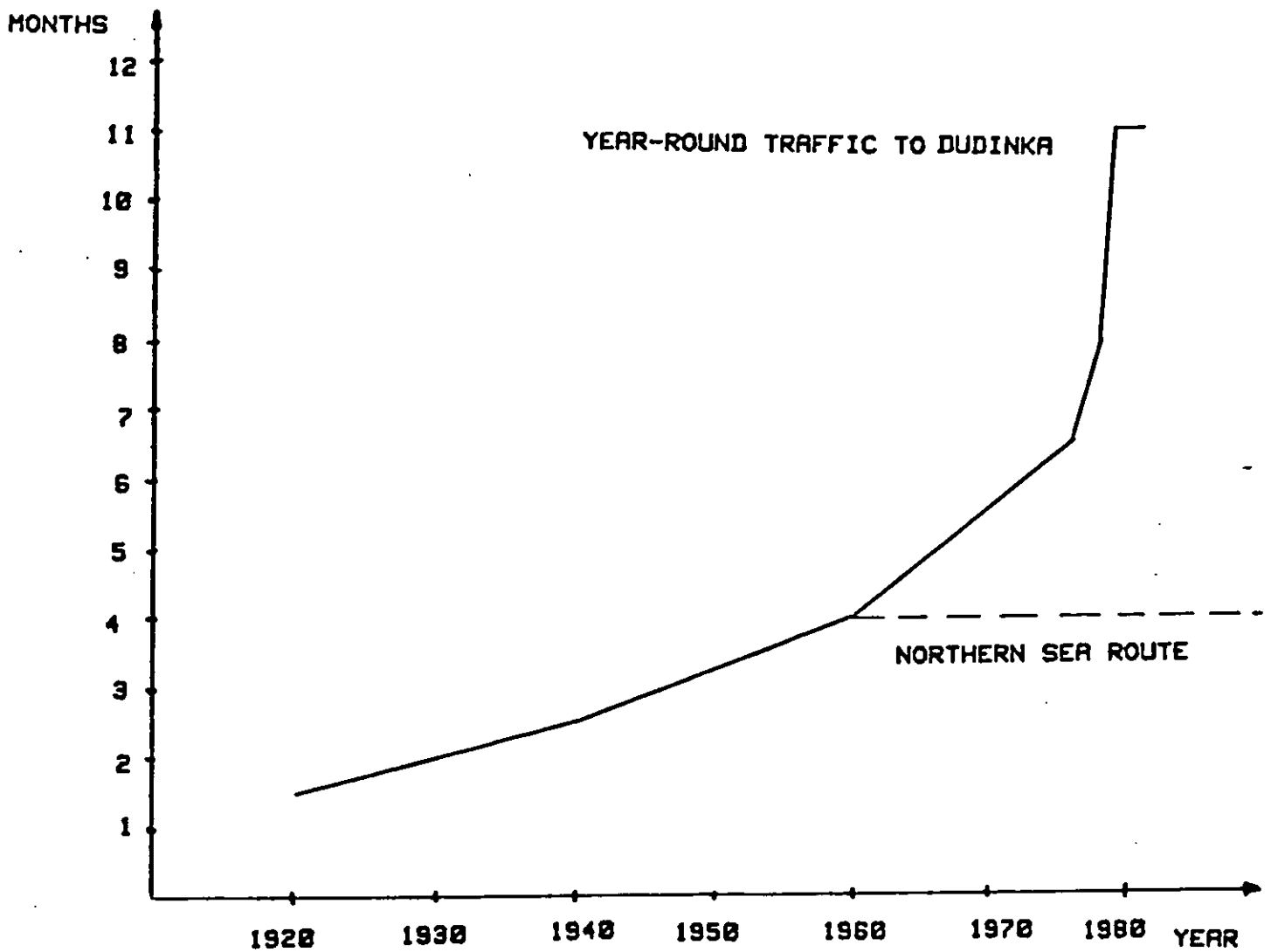


Fig. 4.2.

GOODS TRANSPORT THROUGH THE
HARBOUR OF DUDINKA

1978 - 1981

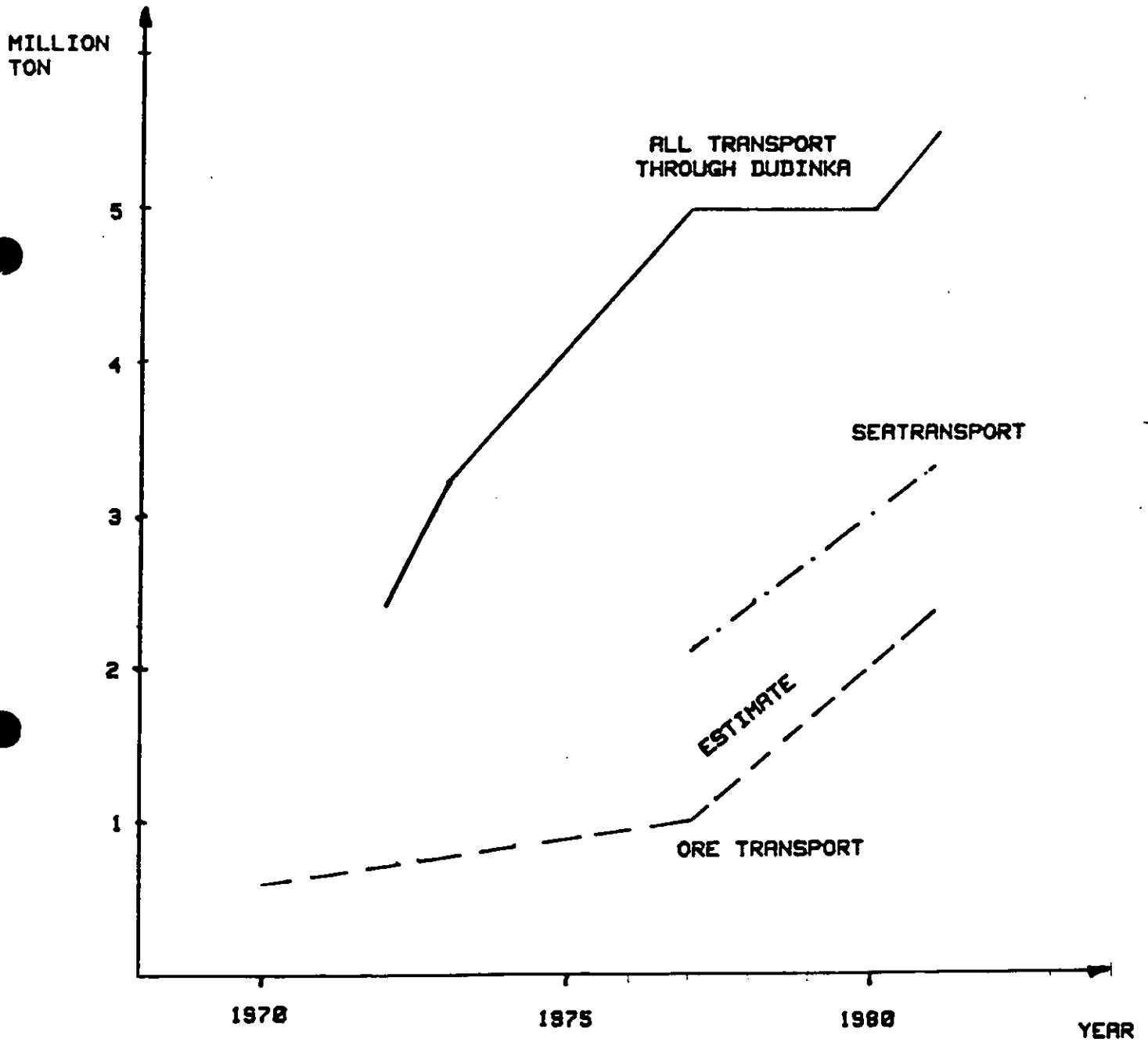


Fig. 4.3.

The mode of ice navigation is traditional: icebreakers lead convoys, which consist of one or several commercial vessels. These commercial vessels are usually ice-strengthened but are not able to do icebreaking by themselves. An indication of the development of the volume of the tonnage used in the Arctic is seen in Fig. 4.4. This list covers all ice-strengthened ships of the USSR and not only the ships built for arctic conditions. The number of ice class ships has been reduced, but the individual ships in service in 1977 are much more capable of ice navigation than those operating in 1970.

There is a clear trend towards ships with sufficient icebreaking capability to allow them to operate independently of icebreaker assistance in certain parts of the routes. For example, in the years 1982 to 1984 Finnish shipyards will deliver 14 arctic multipurpose cargo carriers, which have a deadweight of 20,000 tons and a machinery power of 21,000 hp. These ships are able to operate independently of icebreakers in ice up to one metre thick.

The list of icebreakers employed in Soviet arctic operation is given in Fig. 4.5. The number of icebreakers is very high in comparison with the cargo volume, which bespeaks the difficulty of the ice conditions. Some of these icebreakers are used in wintertime in subarctic waters. The Soviet Union now operates three nuclear icebreakers and has another under construction. Also, one arctic LASH/container vessel is being built. It seems that the Soviets have found a nuclear propulsion plant feasible for arctic operations, with the vessels operating far from populated areas and being able to utilize the greatest advantage of nuclear propulsion, i.e. high endurance.

Offshore oil and gas exploration in the Soviet Arctic has been very limited. Offshore activities have taken place only in the western part of the Soviet Arctic, as is shown in Fig. 4.6. According to it there are three drill ships working in the Barents Sea and two platforms in the Pechora Sea. In addition, there is probably some offshore exploration work going on in a shallow water area off the coast of Yamal Peninsula.

ICE-STRENGTHENED VESSELS

Type of vessel	<u>1970</u>		<u>1977</u>		Change in number
	Size dwt	Number	Size dwt	Number	
Icebreakers	873-5609	23	354-6147	30	+ 7
ULA Class freight carriers	6560-9573	12	310-9280	21	+ 9
Timber carriers	3300-6500	188	4454-6780	26	- 162
Tankers	1340-11680	31	17200	10	- 21
Fish processing vessels	1330-11086	48	790-1139	29	- 19
Passenger vessels	1350-1400	17	2427	5	- 12
Tugs	46-570	157	71-605	143	- 14
Others	100-9000	<u>266</u>	190-7430	<u>23</u>	<u>- 243</u>
		737		287	- 450

Fig. 4.4.

ICEBREAKERS OF 10,000 SHP OR MORE KNOWN TO OPERATE
ON THE NORTHERN SEA ROUTE

<u>Name</u>	<u>Where built</u>	<u>Power, shp</u>	<u>Displacement, tonnes</u>	<u>Entered service</u>	<u>Remarks</u>
Kapitan Belousov	Finland	10,500	5,360	1954	
Kapitan Voronin	Finland	10,500	5,360	1955	
Kapitan Melekhov	Finland	10,500	5,360	1956	
Lenin	USSR	44,000	16,000	1959	nuclear
Moskva	Finland	22,000	13,290	1960	
Leningrad	Finland	22,000	13,290	1961	
Kiyev	Finland	22,000	13,290	1965	
Murmansk	Finland	22,000	13,290	1968	
Vladivostok	Finland	22,000	13,290	1969	
Yermak	Finland	36,000	20,240	1974	
Admiral Makarov	Finland	36,000	20,240	1975	
Arktika	USSR	75,000	23,400	1975	nuclear
Krasin	Finland	36,000	20,240	1976	
Sibir	USSR	75,000	23,400	1977	nuclear
Kapitan Sorokin	Finland	22,000	14,900	1977	shallow-draught
Kapitan Nikolayev	Finland	22,000	14,900	1978	" "
Kapitan Dranitsyn	Finland	22,000	14,900	1980	" "
Kapitan Khlebnikov	Finland	22,000	14,900	1981	" "
Dikson	Finland	10,000		1982-83	not primarily for the North- ern Sea Route
Magadan	Finland	10,000		1982-83	" "
Mudyug	Finland	10,000		1982-83	" "
Under construction					
Rossiya	USSR	75,000		1985-86?	nuclear to be launched by Nov. 1983

Fig. 4.5.

The reason for the relatively limited offshore activities is of course that the Soviet Arctic has abundant onshore resources, which will be exploited first. Thus we can conclude that the development of arctic operations in the Soviet Union is bound to involve an increase in marine transportation first, and offshore exploration and production will come after that.

In addition to marine transportation and offshore work, extensive scientific research is going on in the Soviet arctic regions.

The North-American Arctic

There is no year-round marine transportation in the North-American Arctic, but shipping is limited to three or four summer months. Traditionally, shipping has served the local aboriginal communities and oil and gas exploration work, so that goods have chiefly been transported northwards. Since the late 70s, however, there have been two mines in operation in the Canadian Arctic. These are the Polaris mine on Little Cornwallis Island and the Nanisivik mine south of Lancaster Sound. The products of these mines have been transported southwards by ships, but only during the summer months. The mines are in operation all the year round, but the products are stored for transportation in summer. In addition to these two mines, there is a third one on the west coast of Greenland called Marmorilik. It seems today that no rapid expansion of the mining industry is to be expected within the next decade. Thus the future development of marine transportation is dependent on the results of oil and gas exploration. There will be a steep increase in marine transportation after the production of oil or gas starts in commercial volumes, unless the products are transported by pipeline, which is not likely to be the case.

Canada has a couple of government-owned icebreakers, which assist ice-strengthened cargo vessels. One bulk carrier, the MV Arctic with a deadweight of 28,000 tons, was specifically designed and built for transportation of ore from the Arctic. She has, however, rather limited ice-

breaking capability, about 60 cm thick ice in the continuous mode, and serves arctic traffic in summertime only. Again, no large icebreaking cargo carriers are to be expected, or even large icebreakers, before oil or gas production starts on a commercial scale.

In the Alaskan Arctic the marine transportation is limited to one convoy of barges sailing north of Alaska once a year. In this operation a government-owned icebreaker usually assists a convoy of several ice-strengthened or non-ice-strengthened barges loaded with commodities. This operation is scheduled to take place during the mildest season, namely in August, and the present tonnage would not be able to manage it at other times of the year.

Marine-based scientific and naval operations have been very modest both in the Canadian Arctic and in the Alaskan Arctic, being limited primarily to the summer season. However, the US Polar Class icebreakers have been used for experimental scientific trips in wintertime.

The development of marine operations in Canada and the United States is focused on offshore exploration and production. The activity has been very intense during the last six years especially on the Canadian side of the Beaufort Sea. A great number of second-hand drill ships and other vessels are being used, and, in addition, a large fleet of supply vessels with some icebreaking capability has been taken into service. The latter ships were specifically designed and built to operate in this area. However, the season today is far from year-round, being limited to about four months, and only some research work has been done at other periods of the year. In the Canadian Beaufort Sea, the technology of artificial islands is being applied, using both pure gravel islands and concrete/steel structures laid on a gravel berth. This development seems very promising and we can foresee that in the future there will be more and more structures the technology of which is based on a combination of civil engineering and naval architecture.

Development in the MacKenzie delta area has been very fast during the recent years, but is not expected to maintain this rate in the immediate future. This is primarily due to the overall economic depression and the development of oil prices, but it is also a consequence of too heavy investments without a sound background. However, we can say that great advances have been made in the Barents Sea in the technology of offshore operations and the marine activities supporting the exploration work. The results achieved there will certainly be useful for similar operations throughout the arctic regions. Fig. 4.7 shows the production from Canadian shipyards predicted up to the year 2000 on the basis of a forecast of the development of the Beaufort Sea and other Canadian areas. This prediction was found to be completely unrealistic, and looking at the year 1983, when a rapid expansion was expected to start, we can see that the situation is quite the opposite. The Canadian shipbuilding industry is suffering from a serious shortage of orders today.

Some offshore exploration has been carried out in the Canadian High Arctic in the areas around Melville Island and King Christian Island and in the adjacent waters. The offshore work done so far has taken place solely on the ice and does not fall within the scope of this lecture.

On the Canadian east coast, from Newfoundland up to the mouth of Lancaster Sound, some exploration work has been carried out. Compared with the Beaufort Sea, these areas are relatively deep and only floating structures have been used. The operations have been limited to the summer season and therefore it has been possible to employ tonnage designed and built for ice-free operation after only minor modifications. In this area, however, there are ice problems even in the middle of the summer, namely icebergs. Attempts have been made to solve this problem either by changing the direction of the movement of the iceberg or by installing a quick-release system on the platforms. In these areas too the development is primarily dependent on the need for exploiting new oil reserves irrespective of the higher cost. We can conclude that while in the Beaufort Sea civil engineering technology can be utilized to a great extent, in the eastern areas the floating mode will be dominant and the technology developed in, for example, the North Sea will be carried further in eastern Canada.

CANADIAN SHIP STEEL REQUIREMENTS 1981-2000
ADDITIONAL SHIPYARD EXPANSION SCENARIO

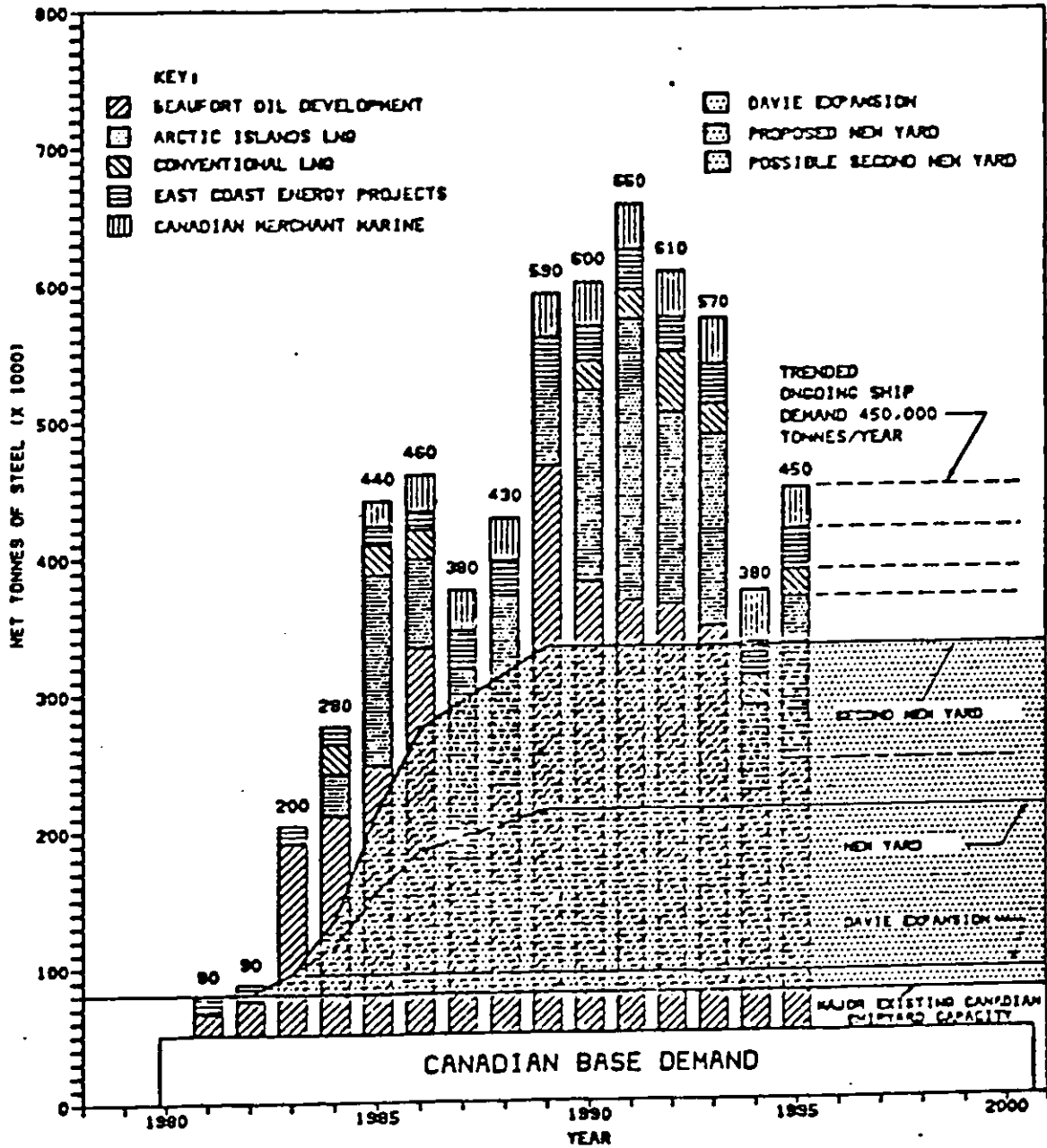


Fig. 4.7.

Some exploration has taken place in the areas north of the Alaskan coast. As regards the extent of the work, the development seems to be about five years behind that in Canada. As the depth conditions are similar, the technology developed for the Canadian Arctic can be utilized on the US side as well. However, the ice problems are more severe here, because the polar pack sometimes comes very near the coast. The Alaskan west coast area has only first-year ice and a relatively long ice-free season. It is foreseen that exploration, which will primarily be done during the ice-free season, will not necessarily require any special tonnage, while suitable technology will have to be developed for the production phase.

To summarize the differences between the Soviet and the North-American Arctic, we can conclude that development on the Soviet side is focused on marine transportation, while offshore exploration and production work take second place, whereas in the North-American Arctic the main emphasis is laid on offshore work, and marine transportation has a subordinate role. In the offshore exploration and production work new technical solutions are needed, while the technology for marine transportation has been developed to the level guaranteeing safe and reliable operation. The development in these two areas also differs in the respect that in the east marine operation serves populated areas with almost normal southern-like industrial activity and infrastructures and with a permanent population, while in the North-American Arctic the operations have so far had a temporary character, with temporary residents responsible for the work.

The arctic areas outside the Soviet Union, Canada and the United States, i.e. those in Norway, Greenland and Iceland, have very limited activities, which so far have related primarily to scientific research.

5 FUTURE

In the 70s huge steps were made both in the field of marine transportation in the Soviet Arctic and in the field of offshore exploration in the North-American Arctic. We have now proven technology for marine transportation and to some extent for offshore work, but new ideas and solutions are called for especially in the offshore work.

In the field of marine transportation the next ten years will see larger cargo ships, which will become increasingly independent of icebreaker assistance. The role of icebreakers will change. Assistance over long distances, as is the present practice, will be given only to convoys of ice-strengthened cargo ships, and local icebreaking service will be provided only in the critical areas for icebreaking cargo vessels. The speed of the cargo ships and the reliability and punctuality of the operations will increase. Economic optimization of marine transportation in the Arctic is becoming routine.

Steady but slow development can be expected in the offshore work in the Canadian and Alaskan Arctic. Only a drastic rise in the price of energy may speed up the development and justify high investment for faster utilization of the arctic resources. As regards platforms for offshore operation, the technology will be a combination of civil engineering and naval architecture. A great number of different kinds of auxiliary vessels are needed in the offshore exploration and production. In addition to their primary function, many of these will act as icebreakers. Successful exploration work will be followed by transportation of goods in large volumes .

The arctic areas are not free from political difficulties, although the areas where most activities take place today are not the subject of conflict. Fig. 5.1 shows the division of the Arctic according to certain philosophies. The only conflict of interest which has been apparent recently is that in the Barents Sea between the Soviet Union and Norway. The special status of Spitzbergen complicates the situation.

I have discussed here primarily marine transportation and offshore operations. In addition we will see fishing in the future in the arctic seas, and quite certainly also naval operations as soon as the icebreaking technology becomes readily applicable to naval craft. Although the latter are of no real use to anybody, I cannot foresee the arctic seas with heavy commercial activities without the existence of naval fleets.

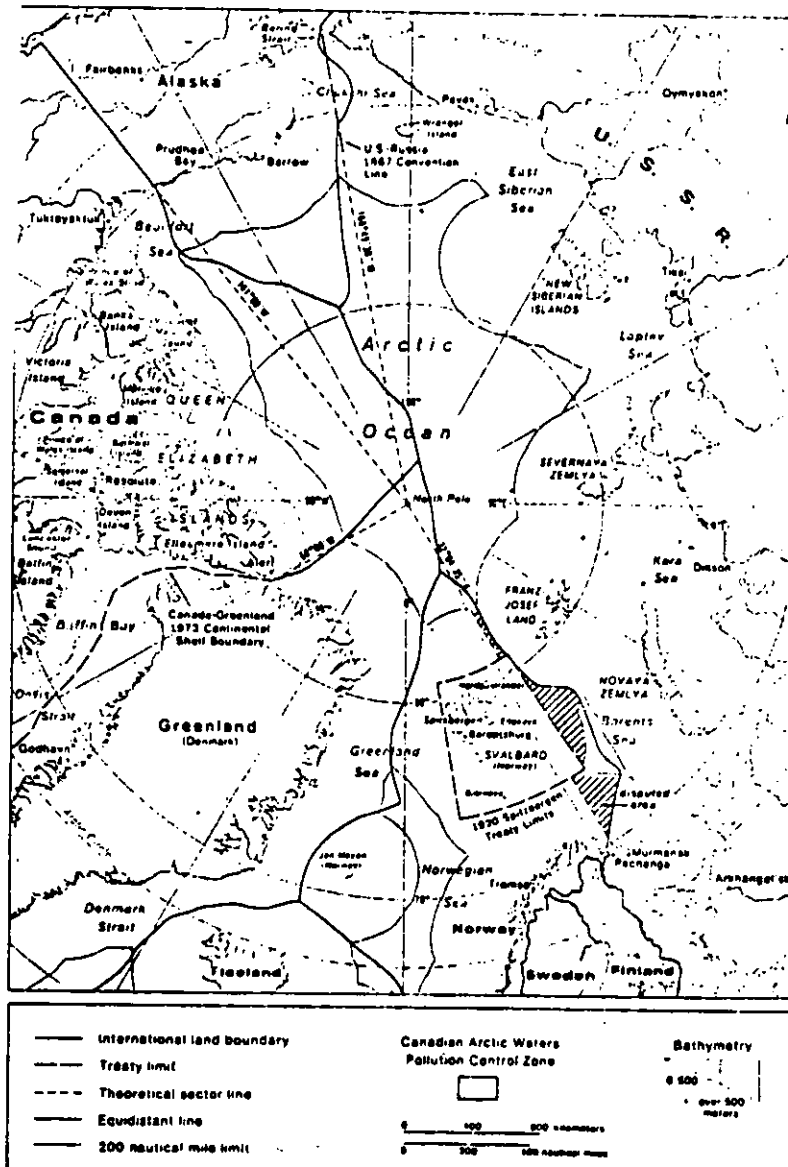


Fig. 5.1.



Dr. Jan-Erik Jansson

SUB-ARCTIC WINTER NAVIGATION

Climatological background

The climatological conditions for winter navigation present large seemingly unpredictable variations from year to year. However in very long perspective continuous changes are evident. According to Alan D. Hecht, director of the Climate Dynamics Program of the U.S. National Science Foundation (ref. 1) several ice ages have occurred during the history of the earth. The last ice period of the Northern Hemisphere dates back roughly 18 000 years ago when vast areas were covered by ice sheets several hundred meters thick. Each time an ice age developed, large amounts of water were transferred from ocean to the land where they were stored as ice and snow. When the ice melted the sea level rose again and the chemistry of the ocean water returned to what could be defined as normal.

From about 1550 to 1850 European and North American glaciers advanced further than they had at any time since the last ice age. This period is called the Little Ice Age and the weather conditions then were in sharp contrast to the climate of the previous centuries. For example between 1400 and 1550 mild weather permitted the cultivation in England of southern fruits. But only a century later the Baltic Sea froze strong enough to permit Swedish armies to cross it during the war 1618 - 1648. Between 1690 and 1700 the weather was particu-

larly cold and in 1693 one third of the Finnish population died from disease and starvation. I have permitted me to record these scientifically established facts in order to try to dramatically emphasize the importance of sub-arctic winter navigation, which no longer is questioned.

Turning now to the immediate past century it is evident that the mean annual temperature in the Northern Hemisphere from 1880 to the 1940s exhibited a general rising trend. After that there was a slight cooling and since 1965 the temperatures have been nearly constant. Scientists have expressed different opinions regarding future developments of the climate. A new little ice age could develop during the next millennium, but there could also be a warming, resulting from the insulating effect of the increased CO₂-content in the atmosphere.

Figure 1 shows the area of the total ice cover in the Baltic and its gulfs during every winter from 1720 up to last year. This statistical picture is very irregular and shows that there may be periods of relatively mild winters, on the other hand as during World War II successive winters may occur when the Baltic is almost completely frozen. The data in fig. 1 up to 1979 are taken from ref. 2 and the authors P. Alenius and L. Makkonen of the Institute of Marine Research in Helsinki, have made an attempt to find some periodicity in this statistics using spectral analysis. The result was not been very successful, but some regularity exhibiting mainly 8 year and 5,2 year periods may be suggested.

Summing up, my opinion is that it is impossible to base winter traffic decisions on predicated climatological developments. Even if predictions would materialize the time scale is many times longer than a few generations of ice strengthened ships or icebreakers.

Sub-arctic regions

In arctic regions - as is well known - multi-year hard ice may present great difficulties and hazards to all kind of shipping and off-shore operations. The subject of this paper however is sub-arctic operations. This I define as operation in temperate zones, where the age of the ice never exceeds one year. Consequently compared to arctic conditions the ice is generally softer and thinner. Maximum thickness of the solid ice in these regions may be anything up to about one meter not including snow layers. The most difficult conditions arise when wind pressure against ice supported horizontally by boundaries such as the coast, islands or grounded ice pack the ice into ridges and wall formations. These sometimes grotesque formations may be several times thicker and higher than the solid "raw material", and present great difficulties to navigation. Wall thicknesses in excess of 20 meters have been recorded in the Bay of Bothnia.

The most important sub-arctic region traffic-wise is the Baltic Sea and its gulfs including the Danish Straits and in cold winters Kattegat/Skagerrak between Denmark, Sweden and southern Norway. Another very important sub-arctic region is the St. Lawrence Seaway including Gulf of St. Lawrence area and the Great Lakes. Some other navigable lakes and fjords,

the White Sea and some areas north of the European coastline of the Soviet Union are sub-arctic regions with similar winter operational conditions. Sub-arctic is also the Finnish inland lake district, connected to the Finnish Gulf by the Saima Canal via Soviet territory. Winter traffic in this area is however very limited.

History of sub-arctic icebreaking

As pointed out in my 1956-paper "Icebreakers and their design", ref. 3 the history of ice operations is short in comparison with the several thousand year history of winter navigation. A pre-requisite for active icebreaking was the development of the reciprocating steam engine. The first breaking of channels in frozen harbours and river estuaries was performed in the U.S. with steamdriven side-wheelers. According to H. Ramsay, ref. 4 a well known pioneer was CITY ICE BOAT of Philadelphia breaking ice - when needed - with 500 ihp on Delaware river from 1837 to 1917!

Apparently these American harbour icebreakers did not influence European icebreaker design. The first icebreaker in modern sense was screw propelled and built in Hamburg in 1871. The name was EISBRECHER I with 570 t displacement and 600 ihp power. She - if feminine designation can be used for an icebreaker - worked between Hamburg and Cuxhaven. The next real icebreakers were the MJÖLNER in 1876 for Oslo-fjord, ISBRYTAREN 1882 for Gothenburg and the Danish BRYDEREN 1884 as well

as STAERKODDER 1885. Finnish icebreaker history is recorded in fig. 2 up to present days. It started with the MURTAJA built in Stockholm in 1890. This ship with 825 t normal displacement, 10.77 m waterline beam and a 1200 ihp steam engine represented at that time the greatest advance of the European type icebreaker characterized by a spoon formed forebody. The MURTAJA proved able to break comparatively thick solid ice - 47 cm has been reported - without snow cover. However icebreakers of this form were rather helpless in slush ice and snow covered ice. The full lined bow pushed the snow slush or snow forward and this accumulation frequently stopped the icebreaker. Towards the end of the last century development in icebreaking proceeded along new lines on the Great Lakes. There masters of ship in difficulties in ridges learned the technique of forcing their way out by backing into the ice. A logical development of this was to build icebreakers with an additional bow propeller. The first bowpropelled icebreaking ship was the ferry ST. IGNAC built in 1888 with a 2000 ihp stern and a 1000 ihp bow screw. The bow propeller washes away water and broken ice from the fore end of the ship and this lubrication reduces the frictional ice resistance considerably. In addition, by operating the bow propeller alternately backwards and forward it is possible gradually to reduce the strength of ice walls. However the wash of a single bow propeller is always unsymmetrical due to the rotational components. Therefore it will produce side forces resulting in manouvering difficulties.

Based on the American experience just referred to the first two bow screw equipped European icebreakers were built almost

simultaneously at the end of last century in Newcastle-on-Tyne. They were the Finnish SAMPO (1898), 3000 ihp and the huge Russian JERMAK, displacement 7875 t and originally total power 10 000 ihp with three propellers aft in addition to the bow propeller. JERMAK however was used against polar ice with resulting damage to the forward engine and propeller, which were removed. This decision by the famous Russian admiral S. Makarov may be the original reason why bow propellers apparently very rarely later have been used for extended periods in conditions where hard multi-year ice can be expected.

Developments proceeded and in 1926 the Finnish icebreaker JÄÄKARHU, 2 + 1 propellers, maximum power 9 200 ihp, was equipped with oilfired boilers increasing the radius of action considerably as compared with coal burning. In this ship heeling tanks were also introduced allowing it to be heeled a few degrees to either side by pumping water between tanks. This motion, which in modern icebreakers generates a vertical speed in the order of 1 cm/sec produces dynamic friction between the shell and the ice, thus reducing ice resistance.

The next step forward was introduced when the Swedish icebreaker YMER was equipped with DC diesel-electric propulsion plant. The YMER, delivered by Kockums in 1932 was almost identical in main dimensions and hull form with the JÄÄKARHU, but maximum dieselpower was 9 900 hp (Propeller power 3 x 2 700 hp = 8 100 hp).

Using the YMER as a pattern 8 dieselelectric icebreakers with 10 000 php were built in the U.S. during and immediately after

the world war. Seven of these formed the WIND class while the eighth was somewhat shallower beamier and longer. The latter built in 1944 in Cheboygan, Michigan is the MACKINAW still operating in the Great Lakes. All these were originally triple screw ships. For Arctic and Antarctic operation however the bow propeller of the WIND class ships was removed and the two propellers aft operated at 5 000 php each.

Finnish icebreaker development

The first SISU, delivered in 1939 by the forerunners of the present Wärtsilä Helsinki Shipyard represented the start of a long diesel-electric era still continuing in Finnish icebreaker design and construction. This ship still incorporated the unsymmetrical propulsive arrangement with one bow propeller and two aft propellers. The first Baltic icebreaker ordered after the world war is the quadruple screw VOIMA, completed by Wärtsilä in 1954. This icebreaker, absorbing at that time 10 500 php (metric) is a pioneering ship, because it incorporates the fully symmetrical arrangement of two inward turning bow propellers and two outward turning propellers aft. The original power distributing arrangement allowed 2/3 of the power to be absorbed by the aft propellers and 1/3 by the bow screws. If needed e.g. in penetrating heavy ridges the opposite power distribution, 1/3 aft and 2/3 in the bow or a 50/50 arrangement was also possible. This propeller arrangement represented a tremendous advance in ice operation not only considering wall penetration but also manoeuvrability and ability to assist and accurately circumnavigate other ships.

By distributing power and combining rotation direction properly of the four propellers translation in any direction of the icebreaker combined with rotation around a vertical axis is possible.

As evident from fig. 2 and also tables 1, 2 and 3 the VOIMA was kind of a lead ship for a long series gradually improved sub-arctic and arctic icebreakers all built by Wärtsilä. (Its Helsinki Shipyard has incidentally delivered more than 60 % of the present world icebreaker fleet in excess of 10 000 shp). Four sister ship of the VOIMA were built, three for the U.S.S.R. and one for Sweden. They were followed by mainly larger but also smaller icebreakers built for five countries. As evident from table 1 the Finnish National Board of Navigation presently operates nine own icebreakers. In addition a tenth, the HANSE owned by the Federal Republic of Germany is manned by Finnish crew and operated in Finnish waters, when not needed in the southern parts of the Baltic.

All these ten sub-arctic icebreakers are quadruple screw propelled with a similar flexible power distribution as in the original VOIMA. They were all built with separate diesel-electric propulsion system and auxiliary electrical system. However in modernizing the power plant of the VOIMA in 1979 (increase to 13 900 php) a power station system was introduced combining the diesel-electric propulsion and the auxiliary system. This power plant system reducing capital costs and fuel bill is incorporated in all diesel-electric icebreakers presently in design or construction in Finland.

Figures 3...10 show photographs and general arrangements of some representative icebreakers operated by the Finnish National Board of Navigation. The board is now proposing to replace the three KARHU class 7 500 php icebreakers, which are about 25 years old, with new more powerful ships intermediate in power between the TARMO class (12 000 php) and the URHO class (22 000 php). An artists impression of one of the two first ships is shown in fig. 11 and the preliminary general arrangement in fig. 12.

In these icebreakers the bow propellers are replaced by a very powerful airbubbling system (Wärtsilä patented WABS arrangement). This system includes a series of orifices on both sides of the ship approximately in the bilge area all the way between the bow and the midbody of the hull. By emitting compressed air through the orifices on both sides a friction reducing washing effect around the hull is created by the resulting two phase flow, which is more effective than that of bow propellers. Also the bow propeller bossing resistance is eliminated.

By using the airbubbling system unsymmetrically, for example concentrating all the compressor power to one side and closing the nozzles on the other side, a side force comparable to - or actually in excess of - that of a normal bow thruster is achieved.

The airbubbling system has been successfully used for more than ten years in a.o. Finnish cargo ships (first ship the FINN-CARRIER, $L_{WL} = 130$ m, in 1969) and also in arctic icebreakers delivered to the U.S.S.R. Airbubbling systems have been so far installed in more than fifty ships, about half of them icebreakers.

A description of the Wärtsilä Air Bubbling and its performance system has been published in a paper by K. Juurmaa, ref. 5, presented at a symposium "Ice, Ships and Winter Navigation" organized by the Finnish National Board of Navigation celebrating 100 years of Finnish Winter Navigation in 1977.

Winter and ice conditions in the Baltic

In order to facilitate decision making regarding winter navigation and icebreaker assistance the Swedish/Finnish Winter Navigation Research Foundation has sponsored the recently published CLIMATOLOGICAL ICE ATLAS for the Baltic Sea, Kattegat, Skagerrak and Lake Vänern, ref. 6. Since prior to the 1960s the amount of ice data from the open sea were limited, it was decided to establish a data bank containing ice information for the winters 1963...1979 from which the Atlas was developed. Comparisons with earlier ice data show that these 16 ice seasons (the year defined by the spring period) are fairly well representative for a longer succession of winters with the exception that during the 16 years the total Baltic area was never completely frozen.

Analysing the maximum annual ice extent in the Baltic and its gulfs during the century 1881...1980 a 0.6...1.0 relative ice cover (1.0 = maximum 420 000 km²) appeared during 26 % of all winters a 0.4...0.6 relative ice cover during 20 % and less than 0.4 cover during with 54 % frequency. Fig. 13 shows the probability of ice occurrence in the area analysed in the Atlas. From this it is evident that the Bothnian Bay and the

eastern part of the Gulf of Finland always are frozen, but Skagerrak and the central parts of southern Baltic very seldom. Fig. 14 shows maximum ice extent for the severest winter and fig. 15 the corresponding situation during the mildest winter of the 16 years analysed.

In the northernmost parts of the Bothnian Bay ice formation normally starts in late October or early November and continues to grow southward. The Bothnian Bay is on the average completely frozen by mid-January and the Bothnian Sea by mid-February. These dates are however very variable from year to year, and during a mild winter such as this middle parts of the Bothnian Bay freezes as late as mid-February. In the southern waters freezing starts from east about one month later than in northern waters and proceeds westwards. The ice break-up starts in the southern parts of the average in late February or early March and continues northward. During the first part of June all the area is free. Because the break-up process is two three times quicker (sun radiation!) than the freezing, variation in break-up dates are smaller than in ice formation start dates.

The average length of the ice season varies from more than six months at the northern coast of the Bothnian Bay to less than a month in the Baltic proper, Kattegat and Skagerrak.

Analysing further the data it is evident that the ice formation is rather slow in November and December due to the heat stored in the water. In January and February freezing rate is at its maximum and after that ice cover retardation is nearly linear

until the disappearance of ice at the end of the season. Only in late January is it possible to give an approximate prediction whether the ice winter can be classified as mild, normal or severe.

In planning winter navigation operation it is necessary to distinguish between the fast ice and moving ice. The fast level ice is attached to archipelago areas and the coasts. It often appears inside the depth contour of 5...15 meters. It develops rapidly during the freezing period and remains rather stationary for most of the season. In spring melting starts from the land bounded side. The rest of the ice cover is unfortunately of dynamic nature. Winds and currents cause it to move and deform. This process may result in slush belts, rafted ice or ice ridges. Both Swedish and Finnish administrations produce an ice (and water surface temperature) chart every day based on a variety of information including satellite pictures and ice reconnaissance flights with helicopters and fixed wing aircraft. This is transmitted to icebreakers and other "consumers" by radio ("telefax"). In Finland the chart is published twice a week, on Mondays and Thursdays. Figures 16...19 are examples of these showing the development and decline of the relatively cold ice winter 1979. Fig. 20 shows as example a satellite picture of the ice conditions in the Bothnian Bay and the northern part of the Bothnian Sea

1982-04-06-10.40.

In the open sea the ice thickness varies very much both in space and time due to the coupling of thermal and dynamical deformation processes. The maximum annual solid level ice thickness is on the average more than 70 cm in the north, close to 30 cm in the southwest parts of Finnish waters and about 10 cm in the southern Baltic. The largest value reported is 120 cm (1941). In areas with rafting the thickness is about double that of the surrounding ice sheets. Ice ridges usually visible portions (the "sail") 0.3...2 m high and the depth of the portions beneath the water may be 5...7 times as much. "Keel" depths down to 28 m have been reported in the Bothnian Bay. Recent observations in this region show that, considering areas on tens of square kilometers, the mass of ridges ice is usually 25...75 % of the mass of the level ice. As pointed out in the early part of this paper these conditions must carry a heavy weight as design parameters for ice traversing ships.

Naturally development and decline of ice conditions in other sub-arctic regions can be and are described and analysed in a way similar to that just described.

Baltic winter traffic

Baltic winter navigation from its start during the last century up to 1947 has been described eminently by H. Ramsay in his book, ref. 4. As pointed out earlier in this paper developments

since then in icebreaker design both qualitatively and quantitatively has been tremendous. This is also the case in the design of ice traversing merchant ships and shipping. In the old times shipping volume during the winter period to and from Finnish and northern Baltic ports was very limited. It was necessary to build up stores both of import and export commodities before the winter. With present day economic conditions this is no longer acceptable or even possible, partially with exception of crude oil import to Finland. Therefore the flow of goods must go on almost at the same rate around the year. Also time table requirements no longer permit any significant delays in the operation of merchant ships. In the old times average speed of icebreaker assisted ships was only a few knots. At present this may be 10...12 knots even in difficult ice conditions. In the last year the flow of goods carried to and from Finland by shipping form about 85 % of our foreign trade volume. Total shipping volume to and from Finland has been 46...48 million tons and this volume can be expected to remain constant or increase slightly during the next years (to this domestic shipping, about 8 million tons has to be added). About one third of this volume is shipped through ice conditions normally assisted by icebreakers. Of the Finnish ports the 22 most important have been officially classified as winter ports by the Board of Navigation. All these ports are generally blocked by ice for some time every winter, and Finland is the only country in the world, where all the ports are frozen each year. However using the icebreaker fleet the Board of Navigation has been able to keep all these ports open for navigation (except during a strike)

every winter since 1971. At this time the Board of Navigation normally operates 10 icebreakers each winter. Since 22 ports are kept navigable each icebreaker serves on the average about two ports. Since about 100 ships at any time are approaching or leaving Finnish ports this means that each icebreaker is rendering assistance to an average of ten ships.

In order to receive ice assistance each cargo ship has to be ice strengthened according to the Finnish/Swedish Ice Class Rules. This is because an unstrengthened ship in some situations would be unable to stand the pressure of especially moving ice and also the loads created when in tow behind an icebreaker. In such a case icebreaker assistance could be comparable to rescue operations. In order to maintain the capacity of its icebreaker fleet and guarantee safe winter navigation of all merchant ship the Board of Navigation is forced to issue restrictions regarding size and ice class as defined by the Finnish Ice Class Rules (IA Super, IA, IB, IC or II). For example in difficult conditions only ships larger than 3000 tdw and strengthened to Ice Class IA may be assisted to the northern ports. (Sometimes also minimum cargo amounts are required here). For the southern port smaller ships with lower class are usually accepted. Similar procedures and rules are maintained by the Swedish authorities rendering icebreaker assistance to merchant shipping. However all the Swedish ports are never blocked by ice simultaneously. The ice situation is also generally less severe in the northernmost Swedish ports as compared with corresponding Finnish ports.

The reason for this is the shallower waters on the Finnish coast and the large frequency of westerly winds creating more ice ridges and walls on the Finnish side of the Bothnian Bay.

It is not proposed here to discuss design of ice strengthened merchant ships. However in figures 21... 25 photographs and drawings of some very ice worthy merchant ships, all strengthened to ice class IA Super are shown. These ships are powerful enough to traverse medium ice conditions without icebreaker assistance.

Finnish icebreaker assistance

As mentioned earlier there are along the - approximately 1100 km long - Finnish coast 22 winter harbours. All the ports are municipal and most of them possess own harbour icebreakers or at least powerful tugs. It is therefore normal, that the government icebreakers assist merchant shipping to and from the municipality borders. However icebreaker assistance all the way into and out of the port is frequently undertaken. Thus delays are minimized and scheduling of winter shipping operations resemble as closely as possible those of summer shipping.

The traffic department of the Board of Navigation is managing the winter shipping and icebreaker operation. Each working day morning a meeting is held in the board, where based on latest meteorological, ice and shipping information decisions are taken regarding icebreaker operation, merchant ship assistance, possible changes of navigation restrictions etc. In

this way an optimal utilisation of the icebreaker service is achieved. Information on the ice situation and icebreaker movements are broadcast regularly every day in connection with weather reports.

There are two principally different icebreaker assistance situations, archipelago assistance and high-sea assistance. In the inner sheltered fairways the ice is almost stationary because of island supporting effect. A channel broken by the icebreaker may therefore remain comparatively easily trafficable by merchant ships for some time. Movements of icebreakers and merchant shipping are therefore timewise relatively independent of each other. However each time an opened channel is traversed by a ship, new free water surfaces form, which soon refreeze, thus creating larger ice mass. Also when a ship traverses a broken channel part of the broken ice pieces are pushed sidewise near or sometimes under the solid ice edge. These two effects gradually increase motion resistance in the broken channel. Therefore at a certain stage, if space permits, a new fresh parallel channel is broken and the clogging process can be started from scratch again.

Operating on the high sea outside the archipelago similar conditions seldom occur, because they would require no wind and no current. The channel behind the icebreaker almost always closes a short distance behind the icebreaker. Therefore the assisted ship should follow the icebreaker as closely as

possible. However an optimal distance of a few hundred meters exists in order to prevent the merchant ship to collide from the rear with the icebreaker in case the icebreaker for some reason stops. For capacity reasons of course always several ships should form a convoy in line behind the icebreaker the weakest ships leading and the distances optimized for reasons just explained. Usually the convoys are formed by only a few ships, but extreme cases of a long chain of ships assisted by the icebreaker (maximum known to the writer is 52 ships) have occurred. If a ship is unable to follow the icebreaker a difficult time consuming situation develops. Then the icebreaker has to return to the stopped ship and start a loose cutting manoeuvre before advancing again is possible. Similar icebreaker circumnavigating procedures at very short distance are sometimes necessary to perform quickly if horizontal ice pressure developed by e.g. increasing wind present structural dangers to icebound cargo ships. Cases are known, where ice pressure have sunk ("screwed down") medium size helpless ships in the Baltic. Assisting long convoys long distances in difficult ice conditions the best result are achieved using two icebreakers - if available - the stronger leading the convoy and the other giving "loose cutting service" to ships unable to maintain the speed of the convoy. More elaborate situations are possible for example when two convoys meet. Examples of a series of difficult and complicated situations occurred in 1979 in the Finnish Gulf west of Helsinki when we for about a couple of weeks had 40...50 ships with different destinations continuously assisted within a limited area by 4...5 icebreakers.

Returning now to the normal case of one icebreaker assisting one or a few cargo ships and loose cutting no longer helps, it is necessary to take the assisted ships one in turn in tow and pull them through the ice bridges or the clogged channel. For this reason all Finnish icebreakers are equipped with high capacity towing winches adjustable for either constant cable length or constant towing force. Towing is preferably carried out with long cable - approximately one ship length - which gives fairly good manoeuvrability. However in varying conditions and fast ice notch towage is necessary. The bow of the assisted ship is then fixed in the padded towing notch of the icebreaker stern and kept there with tight cable. The icebreaker and the assisted ship then move almost like a fixed system. The wash of the icebreaker propellers lubricates the bow and the middle body of the assisted ship thus decreasing total resistance. The towed ship is usually operating its own propeller at fractional power pushing ice masses backwards. However in very difficult conditions full power of the assisted ship is ordered, and as a last resort the heeling tank system of the icebreaker is activated. This of course adds to the always somewhat critical loading between the cargo ship bow and the icebreaker notch. If the assisted ship is powerful and heavy in comparison to the icebreaker the double propulsion method just described may, if the ice resistance of the icebreaker suddenly increases, lead to the icebreaker being pushed out of the original course.

In this connection it is important to mention the problems in ice of the bulbous bow. This is of course used in order to achieve low open water resistance. However the solid and ridged ice resistance of bulbous bow ships is larger compared with normal forms. Therefore in designing ships for regular opera-

tion in ice a weighed compromise hull form considering the probable length of the winter period makes sense from the ship-owning point of view. However although we still grant ice class to bulbous bow ships the Finnish Board of Navigation discourages operation of such ships in ice. Firstly they are slower in ice than other ships thus causing unjust assisting situations. Secondly notch towing is almost impossible both in loaded and ballast condition because of incompatibility between the form of most of the bulbs and the notch of the icebreaker stern. A solution of this problem would require at least detail design modification of the bulbous bow or icebreaker notch geometry and structural design. So far this has not been possible. If no solution is found the Board of Navigation may be forced to issue special navigational restrictions for bulbous bow ships at certain times and in certain areas such as the Bothnian Bay.

For icebreaking assisting service to Finnish ports an addition to the navigation fee is charged, which covers only a fraction of the total cost. If however a ship is towed by the icebreaker a special fee has to be paid corresponding approximately to the real costs.

Summing up on icebreaker assistance to Finnish ports the importance of information has to be stressed. Since it usually is economical to circumnavigate heavily ridged areas and of course utilize open or recently frozen leads their exact location has to be known by the icebreaker masters. Therefore in addition to general information used in making the ice charts such as information from ships, pilots, aircraft, satellite pictures etc. local reconnaissance flights with helicopters fitted with Decca position finders are frequently carried

out usually by icebreaker masters and navigation officers. The cost of this activity is small compared to savings in ice assistance, fuel costs etc. achieved.

Developments in icebreaking mechanics

Icebreaking mechanics is a very complicated area of naval architecture because of the large number of variables and the difficulty of defining and determining them accurately. Therefore before the world wars mainly unrealistic inventions were made and some patents issued. Attempts of serious analysis were very few and actually only one early publication is worth mentioning namely that of the Finnish engineer R. Runeberg, presented before The Institution of Civil Engineers in London 1888, ref. 7. However only during the last 15...30 years some theoretical analysis has formed basis for practical improvement of ice-breaking capability of ships.

The natural starting point was the least difficult problem of breaking homogenous solid ice with the ship moving at continuous speed. The understanding of the phenomenon developed well at the end of the 1960s and many parts of icebreaking resistance of ships were indentified. (Perhaps a maximum was reached in a diploma thesis realized under the guidance of the present writer, where no less than 13 components were defined!) The apparently most important contribution to our knowledge in this field at that time was the dissertation by professor (later) Ernst Enkvist in 1972, ref. 8. In this was conclusively shown the small contribution to the total ice resistance of the pure breaking process and the very large importance of friction, which usually is 50...70 % of the resistance.

According to the present theory and full scale observations the ice edge is first partly crushed and sheared in its first contact with the icebreaker bow. Then radial and peripheral cracks develop in front of the stem. The rather large broken floes are pushed down along the forebody shell and further broken in arc shaped cusps. Initially water is not admitted above the pieces. Therefore they are pushed down against hydrostatic pressure. The floes are frequently turned and in turning they push already broken pieces down along the icebreaker hull. At the end of this process usually the snowy top parts of the pieces slide along the hull and submerge at the afterbody sometimes touching the propeller.

At small speed a large part of the resistance is due to submerging the ice floes. At higher speed however turning of the broken pieces and accelerating them at this stage consumes more energy. In all stages of the process described large friction forces dependent on the smoothness of the shell plating appear. Actually the icebreaker slides over the broken ice and obviously a smooth hull surface especially in the forebody is important. As is well known this also contributes to low viscous resistance. A similar parallel is also evident regarding the hull form resistance of a ship breaking ice downwards.

The effect of snow cover on ice resistance was eminently discussed by Vanja Bulat at the SNAME STAR Symposium "Ice Tech 81" in Ottawa, ref. 9 and recently in ref. 10. Mr. Bulat has analysed full scale trials of the Canadian Coast Guard icebreakers PIERRE RADISSON in 1979, FRANKLIN in 1980, the U.S. Coast Guard icebreaker MACKINAW in 1971 as well as two other

ships. The conclusions are that the relative resistance increase due to snow cover increases with decrease of speed and also with an increase of the ratio between snow cover thickness and solid ice thickness. The snow cover directly increases the effective friction coefficient between the hull and the ice/snow combination beyond the pure friction coefficient between hull steel and ice alone. Also the snow acts as a damper in the dynamic process and consumes an amount of energy otherwise utilized in overcoming the different pure ice resistance components.

In his publications Bulat plots the relative increase (y) in ice resistance due to snow as function the nondimensional snow cover coefficient $\frac{V}{\sqrt{g \cdot h_i}} \cdot \frac{h_i}{h_s}$, where V is speed (in m/s) h_i solid ice thickness and h_s average snow cover thickness (in meters).

If we put total ice and snow resistance $R_{si} = R_i(1 + y)$ it is possible from the Bulat presentation to express this analytically in the following way: $y = \frac{C_{snow}}{\frac{V}{\sqrt{g \cdot h_i}} \cdot \frac{h_i}{h_s}}$, where C_{snow}

is apparently depending only weakly on ship type and form.

Analysing the data of Bulat all points are within $C_{snow} = 0.6 \dots 1.4$. Considering the complicated physical phenomenon it describes this variation must be considered modest. A good average appears to be $C_{snow} = 1.0$ giving simply the relative ice increase $y = \frac{1}{\frac{V}{\sqrt{g \cdot h_i}} \cdot \frac{h_i}{h_s}}$ as a first approximation.

Summing up, putting in realistic values for ice and snow thicknesses as well as the speed shows that increase in ice resis-

tance due to snow cover is very large, frequently 20...50 % at low speed.

During the last years the volume of studies regarding ice resistance to ship hulls in homogenous solid ice has increased considerably. I would like here to mention the dissertation of J.N. Naegle at the University of Michigan, ref. 11. Naegle, who compares model and full scale data with theoretical analysis and divides the pure ice resistance into three groups, those related to ice fracture, those to turning of ice floes and those to ice submergence. In each group both normal and frictional forces are treated thus giving totally six components. The relative contribution of these depends on the ice thickness and strength, ship speed and friction between the hull and ice.

A very good contribution to our knowledge in this field by Lewis, DeBord and Bulat, all of Arctec was discussed at the recent annual meeting of the SNAME in New York, ref. 12. On icebreaking hull resistance the authors quite correctly - in the opinion of this writer - state that there are so many hull, ice, water and motion variables which could influence hull resistance that it is currently impossible to explain the effect on everyone on resistance. Then they list no less than 14 independent variables, but later in the paper show how this number can be reduced considerably. After a stepwise multiple regression analysis using 196 data points they end up with an ice resistance equation with the excellent multiple correlation coefficient of 0.99 valid however only within certain ranges of the independent variables, for example $C_B = 0.500...0.625$.

More important from the operational point of view in temperate zones is the analysis of ridge resistance. Here our theoretical knowledge is still very limited and we are in the early period of rational analysis. The start of this was made by Arno Keinonen 1979 in his dissertation at the Helsinki University of Technology, ref. 13. He showed that the ice mass in ridges does not break in bending, but in shear along oblique planes. Using methods from soil mechanics "upside down" he was able to analyse the ice ridge resistance. From this work the importance of friction is obvious, and a preliminary conclusion is that low resistance hull forms breaking solid ice also are good - but not necessarily optimal - in ridges and ice walls. Dr. Keinonen continued his research on operation in ridges by analysing in ref. 14 the nonstationary phenomena of icebreaker penetration, extraction, reversing and acceleration in ridges where constant speed operation is impossible.

It is the hope of the writer that the newly improved winter navigation research institutions shall have sufficiently motivation and resources to carry the ice ridge resistance analysis further. If so, this may lead to a similar exposition of a large number of resistance components and parameters as in studying solid icebreaking. In anticipation of this the writer would like to save from being completely forgotten a very simple but interesting formula for icebreaking ability derived from a book published in 1946 in Moscow by Vinogradov, ref. 15. In this icebreaking ability is defined as the maximum ice ridge thickness h_{ir} , which may be penetrated by the icebreaker in charging. This is $h_{ir} = C_{ir} \cdot (\Delta \cdot P)^{\frac{1}{4}}$, where Δ is displacement and P total propulsion engine power. C_{ir} is a constant depending on icebreaker hull form, propellers and

their arrangement etc.

Miscellaneous icebreaking methods

Propeller design and icebreaking are two parts of Naval Architecture fascinating inventors. Through the years in both fields a large number of innovations have been proposed and even patented, most of which have proved useless or of only limited value. Some auxiliary icebreaking systems were already referred to here earlier such as heeling tanks and air hubbling systems, which are very useful indeed and in difficult conditions do considerably decrease the maximum propulsive power required.

Other special systems which work are water jets (uneconomical?) used in the Canadian CANMAR KIGORIAK and the experimental version of the MAX WALDECK, owned by the FRG. Further, dynamic icebreaking has been performed in European inland waterways using vibrators. There usually consist of two excentric masses rotating at the same speed on the same axis but in opposite derrections. By phasing the rotation correctly a large pulsating vertical force in the forebody is created. This is very unpleasant for the personnel onboard, but it has been demonstrated that equipped with this system even a small icebreaker advances in almost any ice condition "inch by inch".

A special and surprisingly efficient icebreaking effect in homogenous ice is achieved with air cushion vehicles. Two techniques are possible, one is high speed operation near critical waves in the ice surface, which is broken in relatively large pieces. The other possibility is slow speed motion utilizing under- and overpressure at the ice edge.

Icebreaking and flood control has been achieved by explosive charges and machining by saws etc. These methods are not however suitable for continuous operation. Melting ice by hot water or heated shell plating has been proposed, but it is obvious that these methods are uneconomical energywise even using atomic reactors.

Icebreaking with the purpose of clearing ice clogged channels and flood control are important tasks in certain sub-arctic areas such as the St. Lawrence River system. It is however not possible to deal with these problems within the frame of this lecture. Therefore only reference is made to a research project performed on this subject for the U.S. Coast Guard Research and Development Center in Connecticut, ref. 16.

Developments in icebreaker design

In developing and designing hull forms of new icebreakers their operating profiles time- and spacewise (average ice conditions) has to be considered. Even with a sophisticated hull form optimisation based on model tests in different conditions, full scale data etc. very large economical gains compared to icebreakers designed during the last years cannot be expected. The saving potential may be equally large in reducing frictional resistance by arranging in all conditions for a very smooth shell plating especially in the forebody. Innovative hull forms have been proposed as for example a bulb like forebody breaking the ice from the underside upwards. This has some appeal in certain conditions - a.o. low frictional resistance at the bow - but operation in ridges is problematical.

Another radical departure from conventional thinking in hull

form design is the novel concept originated by Dr. H. Waas, FRG, and fitted experimentally outside the forebody of the 2280 kW small icebreaker MAX WALDECK. This ship has been running experiments in Finnish waters near Vaasa in the winters of 1981 and 1982 as reported on by J. Schwarz, H. Wilckens and A. Freitas at the last annual meeting of the Schiffbautechnische Gesellschaft, ref. 17. The Waas icebreaker hull has basically a square bow with a flat sloping bottom and vertical sides parallel to the center line. The width of the bow is greater than the beam of the ship so that a gap exists between the edges of the channel broken and the ship's sides. The flat bottom is provided with runners which act as shearing edges. The bottom of the bow gradually fairs into the main body of the ship. The writer had opportunity to witness some tests of the MAX WALDECK during both winters. The channel left behind the icebreaker in homogenous ice was very sharply cut, and due to the air/water jets used most of the broken ice pieces were pushed under the fast ice edge leaving an almost ice free channel behind. Dynamic icebreaking using the excentric vibrating mechanism was successfully performed. It is therefore somewhat surprising that this is not mentioned in ref. 17. The Waas "landing craft" concept aims at arctic bulk transport, and the present writer does not see any possibilities of its use in icebreakers performing assisting duties in ridged sub-arctic areas.

The extremely important complex of icebreaker propulsion machinery and propellers is outside the scope of this presentation. However the writer would like to stress that propulsion systems for icebreaking ships have developed well during the

last ten years. Conventional diesel electric machinery has been replaced in some cases by diesel motors and/or turbines driving reduction gears and controllable pitch propellers. These installations are sometimes combined so that diesel engines are used under normal conditions and turbines in severe conditions. Mechanical troubles have been encountered in some cases especially in CP propellers. It is however believed that sufficient knowledge now exists to overcome these difficulties.

Detailed discussion of the various auxiliary icebreaking systems such as heeling and trimming tanks, air bubbling and thrusters are also outside this lecture. A difficult problem to remember here is the superposition of the action of the various auxiliary systems. This is not necessarily linear and has to be carefully studied.

Regarding structural design of sub-arctic icebreakers the writer must limit himself to pointing out only the following. In order to determine the ice loads to be expected, probable data on ice in the operating area are essential as well as on the human operating technique. Further the probable requirements and characteristics of the assisted ships and the freedom of the master in choosing his route is important to know. If this as well as the main dimensions and propulsive characteristics are known, then structural design of the hull can be performed starting from the outer shell loadings and continuing inwards via frames to stringers, webs, bulkheads etc. Consideration of various shock loads including small collisions is of course very important.

Finally in comparing different general or detail design alter-

natives a primitive but good procedure is listing all the capabilities and requirements on a weighted point basis. By adding these points a total picture is obtained as a sum of principally incompatible factors.

R E F E R E N C E S

1. Hecht, Alan D., "Clues to yesterday". World Paper, Boston USA. March 1982.
2. Alenius, P. & Makkonen, L. Institute of Marine Research, Helsinki, Finland. "Variability of the Annual Maximum Ice Extent of the Baltic Sea".

Arch. Met. Geoph. Biokl., Ser. B 29, p. 393-398.
Springer-Verlag, Austria 1981.
3. Jansson, Jan-Erik, "Icebreakers and their design". Paper at the NSTM in Oslo 1956. English version in European Shipbuilding, No 5-6, Selvigs Forlag, Oslo 1956.
4. Ramsay, Henrik, "I kamp med Östersjöns isar". 415 p. Holger Schildts förlag. Helsingfors 1947.
5. Juurmaa, Kimmo, "WABS" - a Method for Improving the Icebreaking Performance of Ships. Its Efficiency in Different Ice Conditions. Symposium Ice, Ships and Winter Navigation in Oulu University 1977-12-16...17. The Finnish Board of Navigation, Helsinki 1979.
6. CLIMATOLOGICAL ICE ATLAS for the Baltic Sea, Kattegat, Skagerrak and Lake Vänern (1963-1979). Swedish Meteorological and Hydrological Institute/Institute of Marine Research, Helsinki, Finland. Norrköping, Sweden 1982.
7. Runeberg, R., "On Steamers for Winter Navigation and Ice-breaking", Minutes of Proceedings of the Institution of Civil Engineers, London. Vol. XCVII, session 1888-1889, part III.
8. Enkvist, E., "On the Ice Resistance Encountered by Ships Operating in the Continous Mode of Icebreaking". Dissertation. The Swedish Academy of Engineering Sciences in Finland, Report Nr 24, Helsinki 1972.

9. Bulat, V., Discussion to Paper no 24, "Performance of CCGS FRANKLIN in Lake Melville, 1980 by M. Michailidis and D.C. Murdey. STAR Symposium "Ice Tech 81" The Society of Naval Architects and Marine Engineers, New York 1981.
10. Bulat, V., "The effect of snow cover on ice resistance", The Naval Architect, The Royal Institution of Naval Architects, London November 1982.
11. Naegle, J.N., "Ice-Resistance Prediction and Motion Simulation for Ships Operating in the Continuous Mode of Icebreaking", Ph. D. Dissertation, University of Michigan, Ann Arbor 1980.
12. Lewis, J.W., DeBord, F.W., Bulat, V.A., "Resistance and Propulsion of Ice-Worthy Ships", Annual Meeting. The Society of Naval Architects and Marine Engineers, New York November 1982.
13. Keinonen, A., "An Analytical Method for Calculating the Pure Ridge Resistance Encountered by Ships in First Year Ice Ridges". Dissertation. Helsinki University of Technology. Ship Hydrodynamics Laboratory Report No 17. Otaniemi. Finland 1979.
14. Keinonen, A., "The Phases of Navigating Through Ridges with a Ship". Helsinki University of Technology. Ship Hydrodynamics Laboratory Report No 18. Otaniemi. Finland 1979.
15. Vinogradov, I.V., "Suda Ledovogo Plavanija" (Ship for Ice Traversing). Moscow 1946.
16. St. John, J.W., Coburn, J.L., Kotras, T.V., "Study of Ice Clogged Channel Clearing Problems". Report No CG-D-34-81. U.S. Department of Transportation. U.S. Coast Guard, Washington D.C., May 1981.
17. Schwarz, J., Wilckens, H., Freitas, A., "Entwicklungsarbeiten an dem Thyssen-Waas Eisbrecherkonzept in Modell und Grossausführung". Schiffbautechnische Gesellschaft. Hauptversammlung. 17...20.11.1982. Berlin.

ICEBREAKERS USED BY THE FINNISH BOARD OF NAVIGATION

NAME	PROPELLER POWER hp DIESEL- ELECTRIC	NUMBER OF PROPELLERS	BUILT	PLACE OF BUILD	DISPLACE- MENT/t	GROSS TONS	LENGTH, PP/m	BREADTH, WATER- LINE/m	DRAFT/m
VOIMA	13900	4	1954/1979	HELSINKI	5209	3783,30	79,80	19,40	7,00
KARHU	7500	4	1958	"	3540	2720,72	69,10	17,40	6,80
MURTAJA	7500	4	1959	"	3540	2720,10	69,10	17,40	6,80
SAMPO	7500	4	1960	"	3540	2730,45	69,10	17,40	6,80
TARMO	12000	4	1963	"	4890	3954,82	78,50	21,20	7,30
VARMA	12000	4	1968	"	4890	3889,99	80,75	21,26	7,30
APU	12000	4	1970	"	4890	3895,08	80,75	21,26	7,30
URHO	22000	4	1975	"	9660	7010,82	95,80	23,85	8,30
SISU	22000	4	1976	"	9660	7094,97	95,80	23,85	8,30
OWNED BY FEDERAL REPUBLIC OF GERMANY:									
HANSE	7500	4	1966	HELSINKI	3676	2771,05	69,10	17,40	6,80

Table 1. Icebreaker presently used by the Finnish National Board of Navigation.

NAME	Nationality	Propeller power hp	Number of propellers	Built	Place of Build	Displacement/t	Length, PP/m	Breadth/m	Draft/m
THULE	Swedish	5600	1 + 2	1953	Karlskrona	1930	57,0	16,1	4,8
ODEN	"	10500	4	1957	Wärtsilä/ Helsinki	5180	77,5	19,4	7,0
TOR	"	12000	4	1964	"	4950	79,5	21,2	7,3
NJORD	"	12000	4	1969	"	4950	79,5	21,2	7,3
ATLE	"	22000	4	1974	"	9660	95,8	23,85	8,3
FREJ	"	22000	4	1975	"	9660	95,8	23,85	8,3
YMER	"	22000	4	1977	"	9660	95,8	23,85	8,3
DANBJÖRN	Danish	10700	4	1964	Odense	3685	68,0	17,3	6,0
ISBJÖRN	"	10700	4	1965	"	3685	68,0	17,3	6,0
THORBJÖRN	"	6400	2 (aft)	1980	Svendborg	2345	60,0	15,3	4,7
KAPITAN VATONIN	USSR	7720	4	1955	Wärtsilä/ Helsinki	5360	80,8	19,4	7,0
KAPITAN IZMAYLOV	"	2500	2 (aft)	1976	"	2048	53,9	15,5	4,2
PERKUN	Polish	2460	2 (aft)	1962	UK	1760	52,6	14,0	5,0

Table 2. Icebreakers presently operating in the Baltic. (In addition the U.S.S.R. operates Polar icebreakers.)
All listed icebreakers are diesel-electric except the direct diesel driven THORBJÖRN equipped with air bubbling.

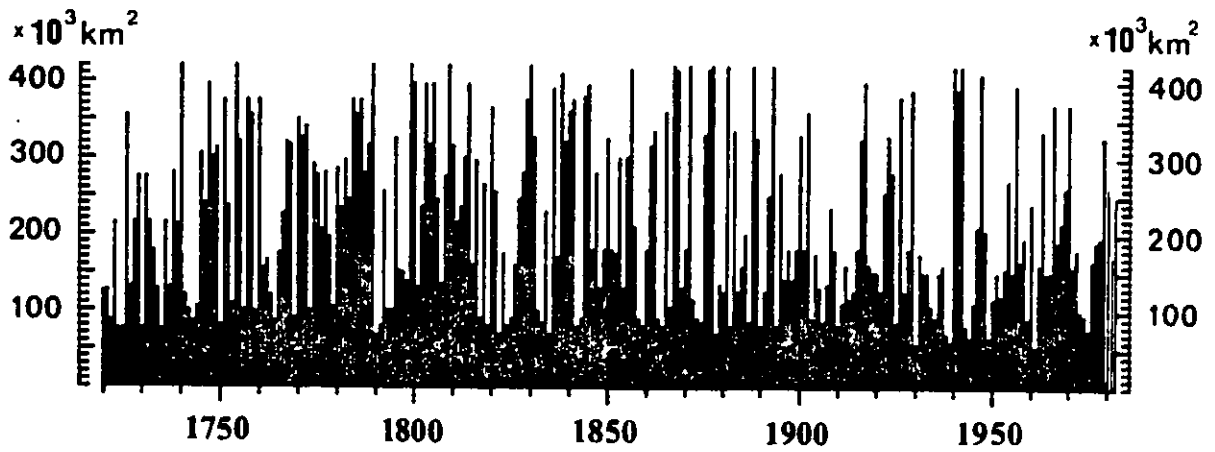


Fig. 1. Total ice covered area in km^2 of the Baltic and its gulfs. Maximum = 420.000 km^2 .

SUOMEN VALTION JÄÄNMURTAJAT • FINSKA STATENS ISBRYTARE
THE FINNISH STATE-OWNED ICEBREAKERS

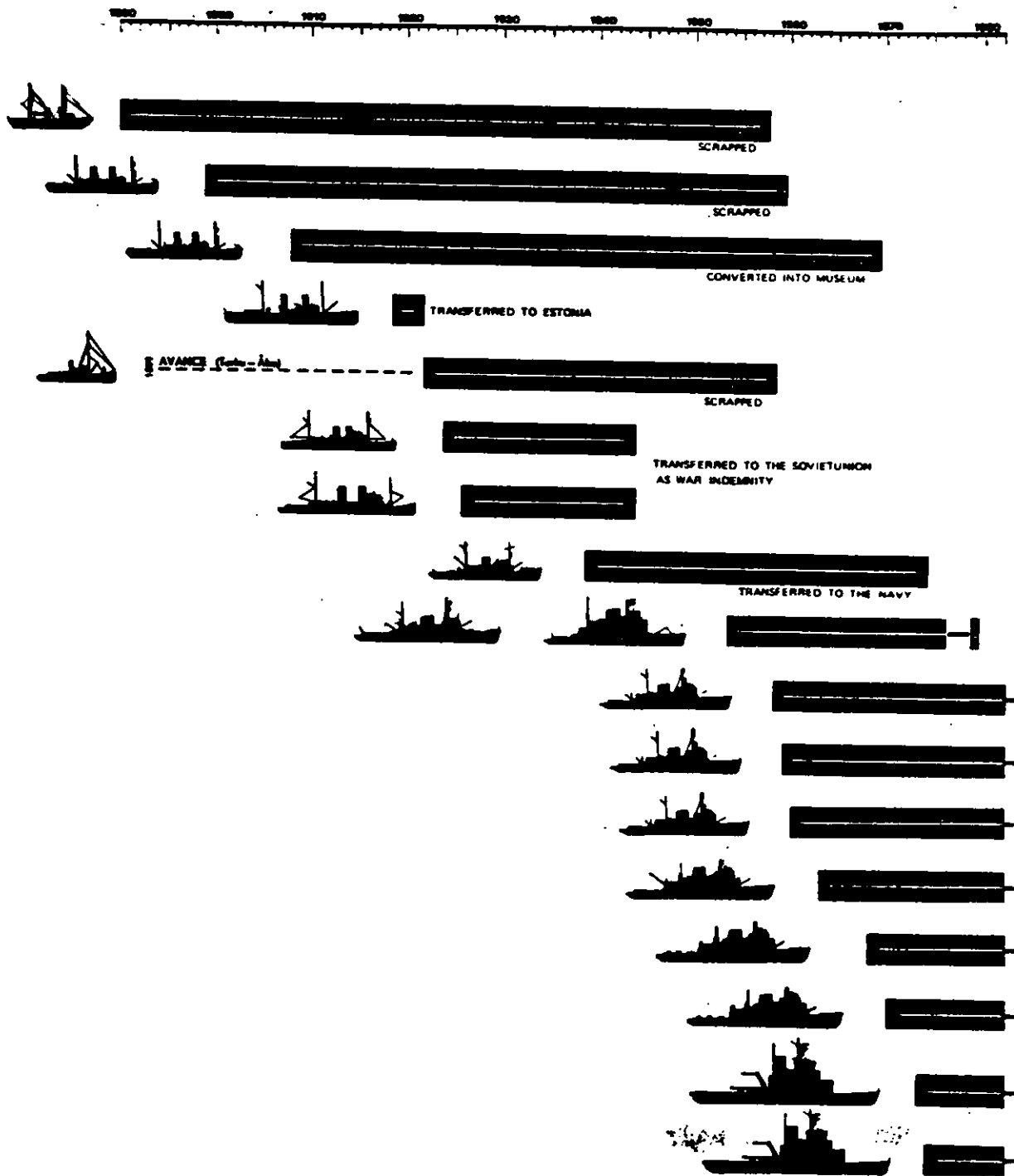


Fig. 2. History of Finnish icebreakers. (Machinery and accomodation of the VOIMA were renewed in 1979).

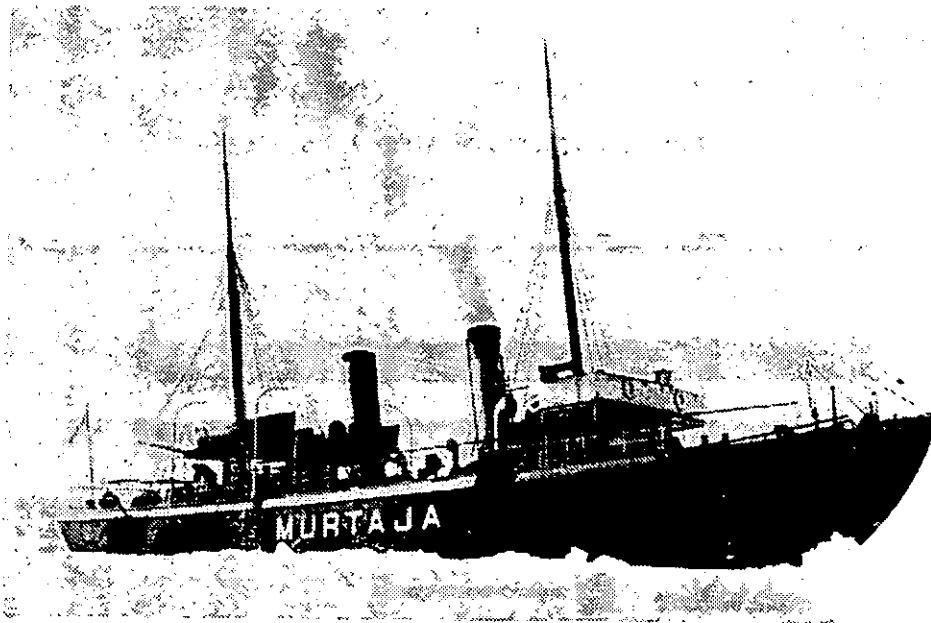


Fig. 3. 1200 ihp Finnish icebreaker MURTAJA built in 1890.

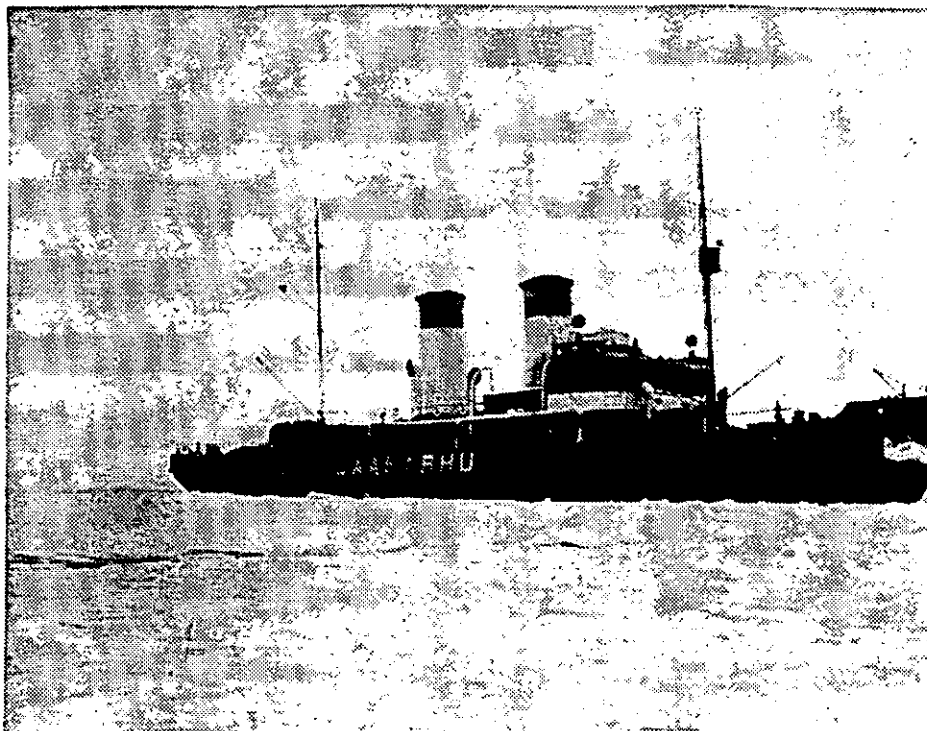


Fig. 4. Finnish triple screw 9.200 ihp icebreaker JÄÄKARHU.
Built in 1926.

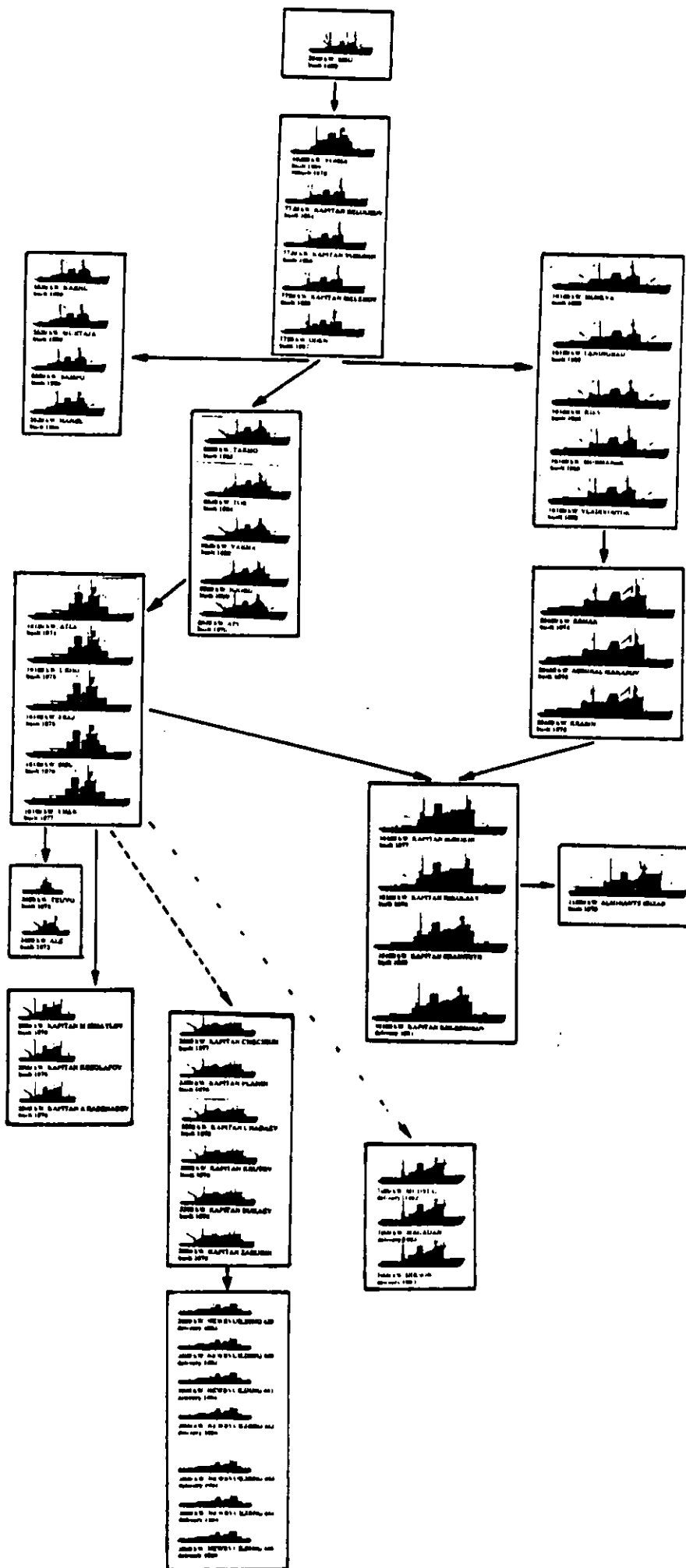
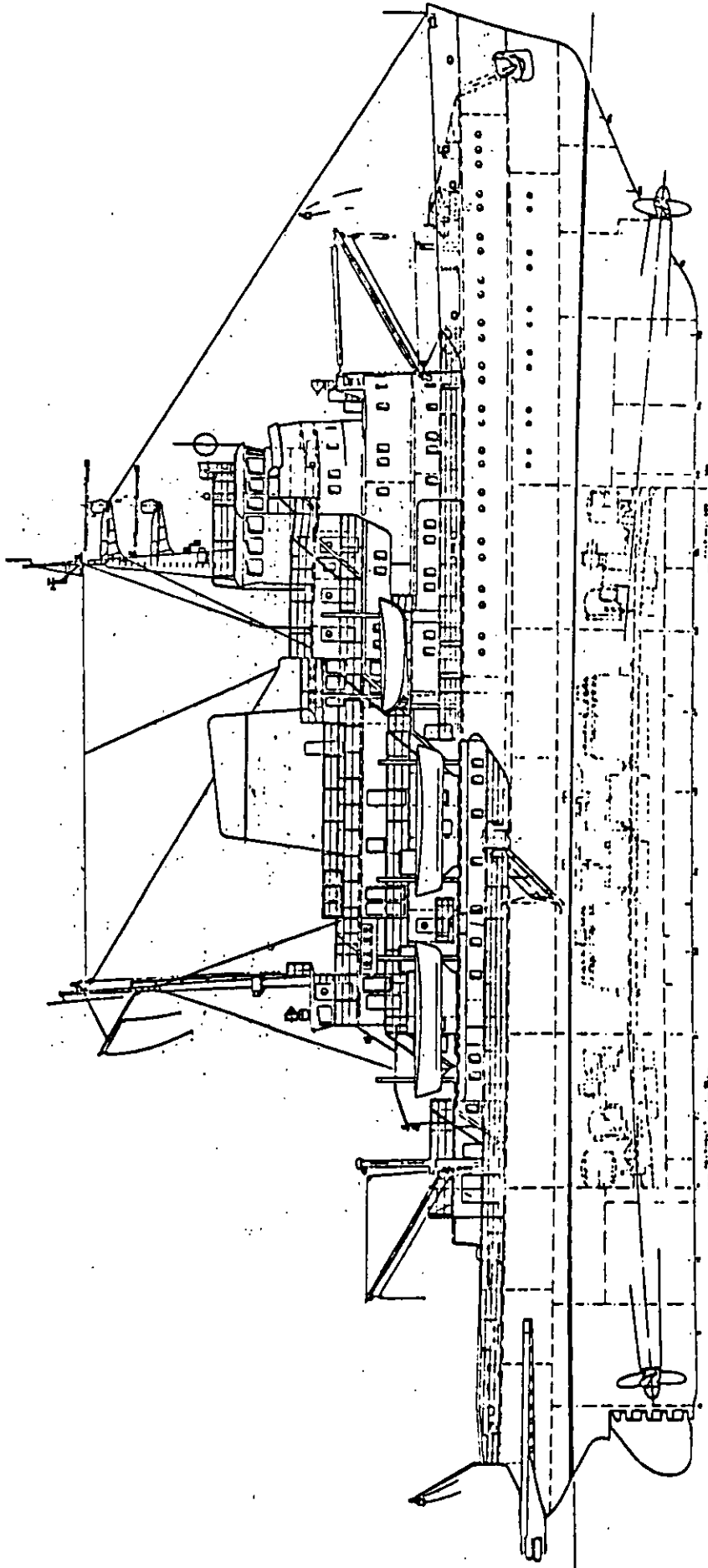


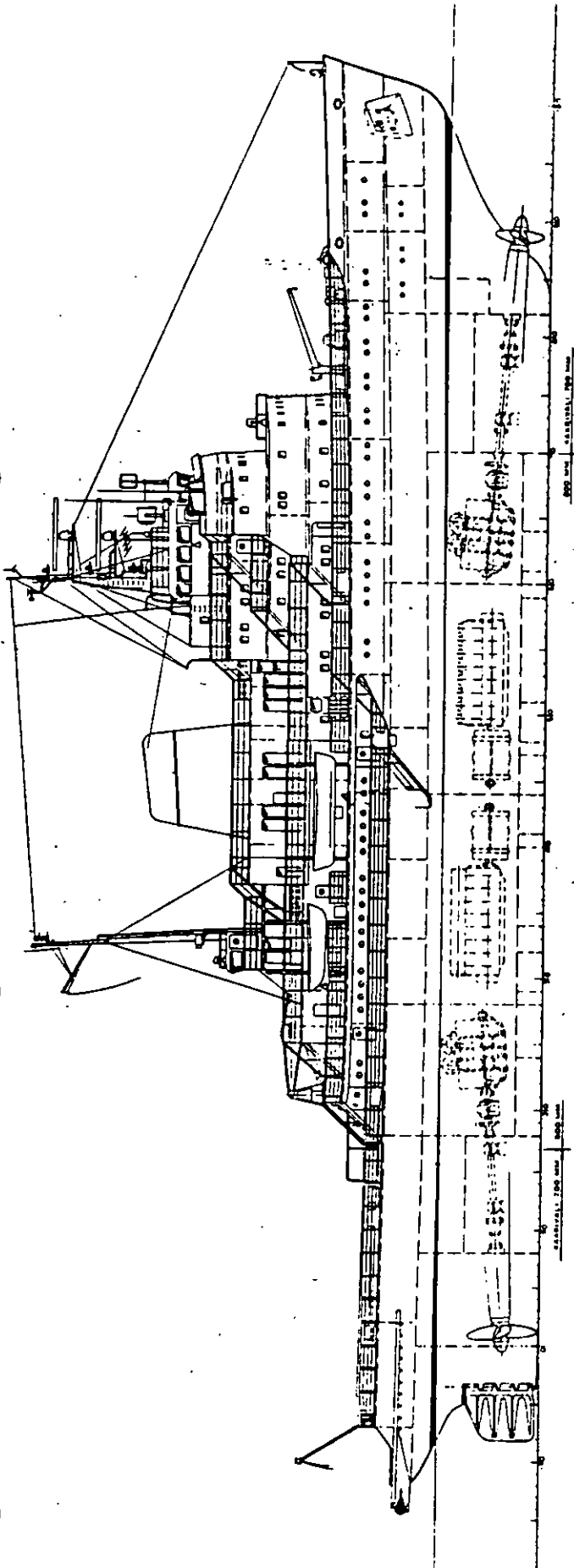
Fig. 5. Icebreakers delivered by Wärtsilä Company Helsinki Shipyard.



5520 kW ICEBREAKER

LENGTH	O.A (Without towing fork)	74.7 M
LENGTH	DWL	68.3 M
BREADTH	MAX	17.4 M
BREADTH	DWL	16.7 M
DRAUGHT	DWL	5.8 M
HEIGHT	TO UPPER DECK	8.8 M

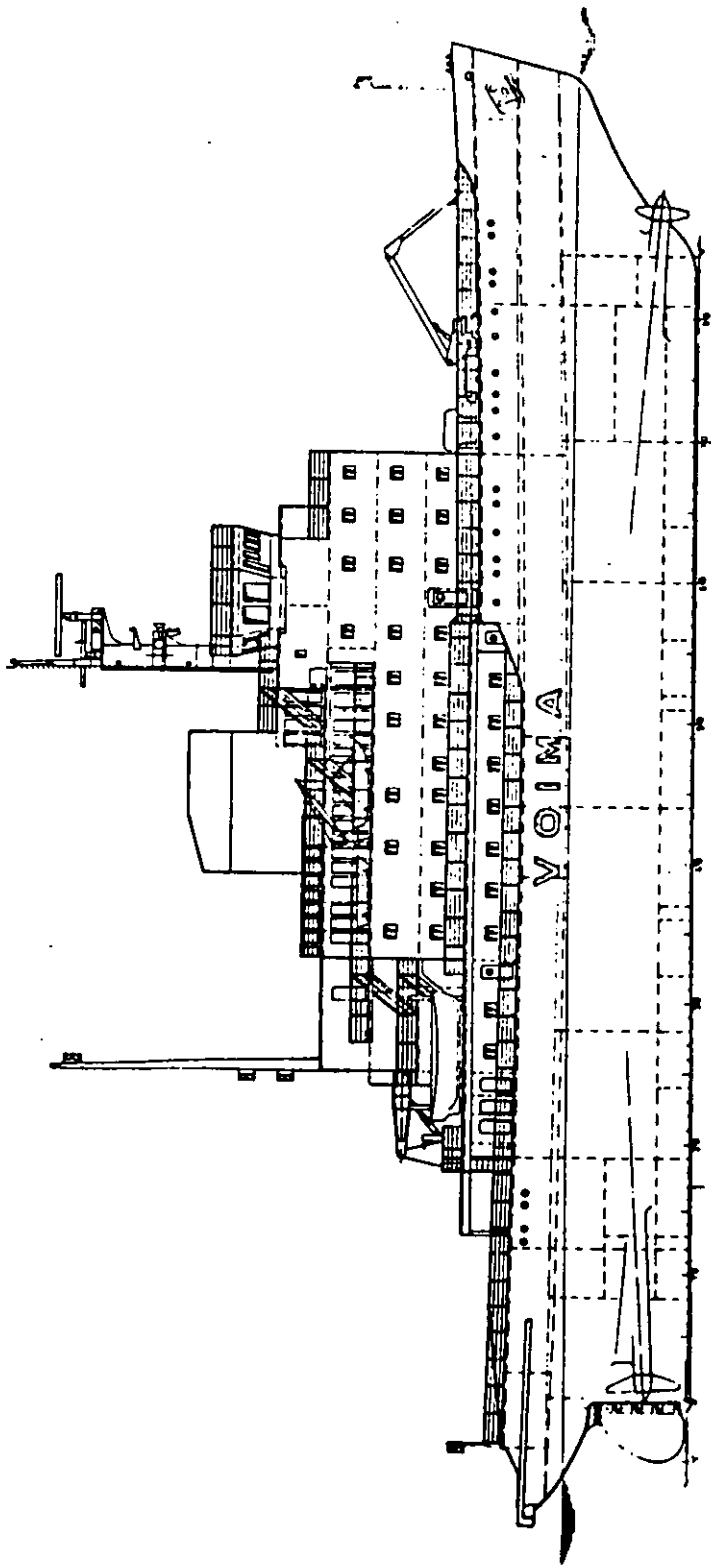
Fig. 6. Hanse.



8830 kW ICEBREAKER

LENGTH	O.A (Without towing fork)	86.5 M
LENGTH	DWL	79.5 M
BREADTH	MAX	21.2 M
BREADTH	DWL	20.5 M
DRAUGHT	DWL	6.2 M
HEIGHT	TO UPPER DECK	9.5 M

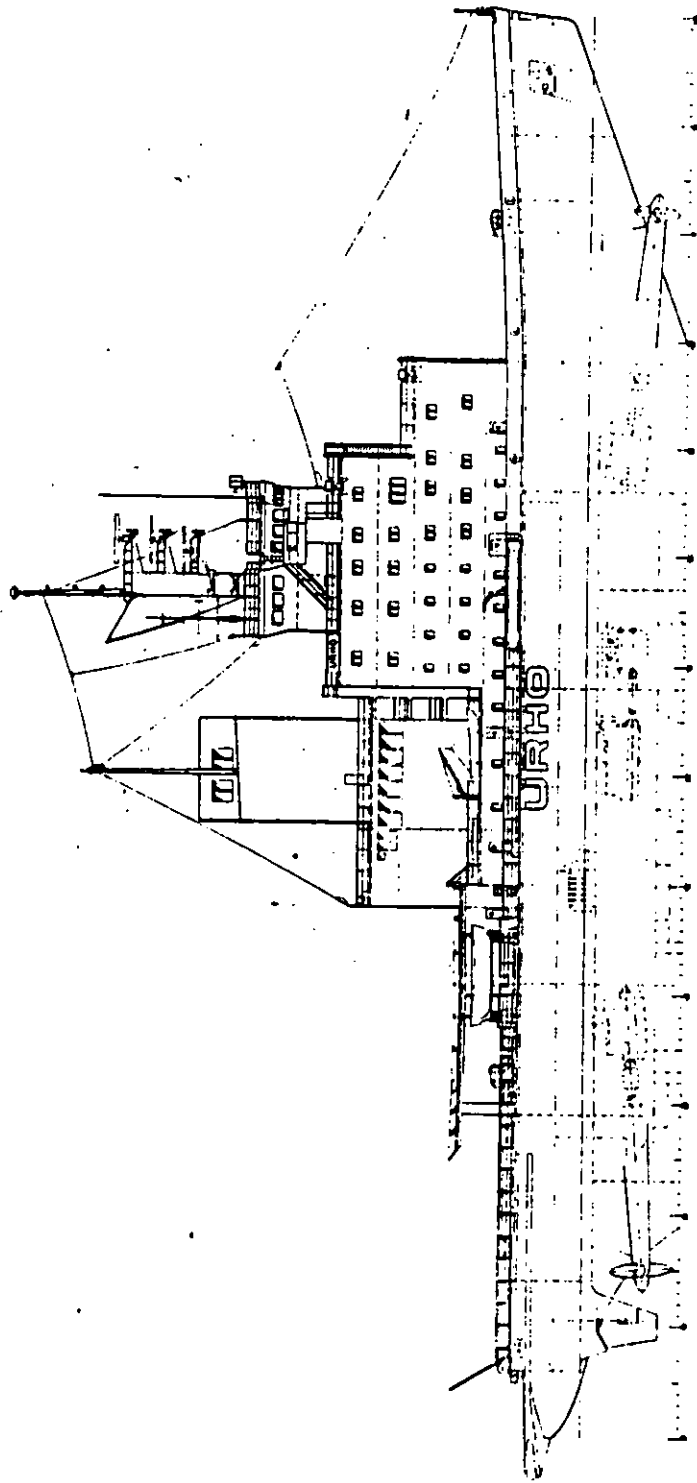
Fig. 7. Apu



10300 kW ICEBREAKER

LENGTH	O.A (Without towing fork)	83.5 M
LENGTH	DWL	79.8 M
BREADTH	MAX	19.4 M
BREADTH	DWL	19.0 M
DRAUGHT	DWL	6.0 M

Fig. 8. Voima.



16180 kW ICEBREAKER

LENGTH	O.R. (Without towing fork)	104.6 M
LENGTH	DWL	96.0 M
BREADTH	MAX	23.8 M
BREADTH	DWL	22.5 M
DRAUGHT	MAX	8.3 M
DRAUGHT	DWL	7.3 M
HEIGHT	TO UPPER DECK	12.1 M

Fig. 9. Urho.

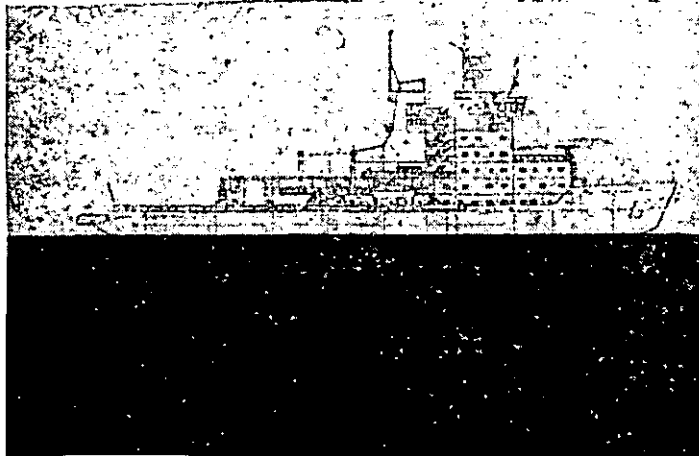


Fig. 10. Planned new icebreaker type for the Finnish Board of Navigation.

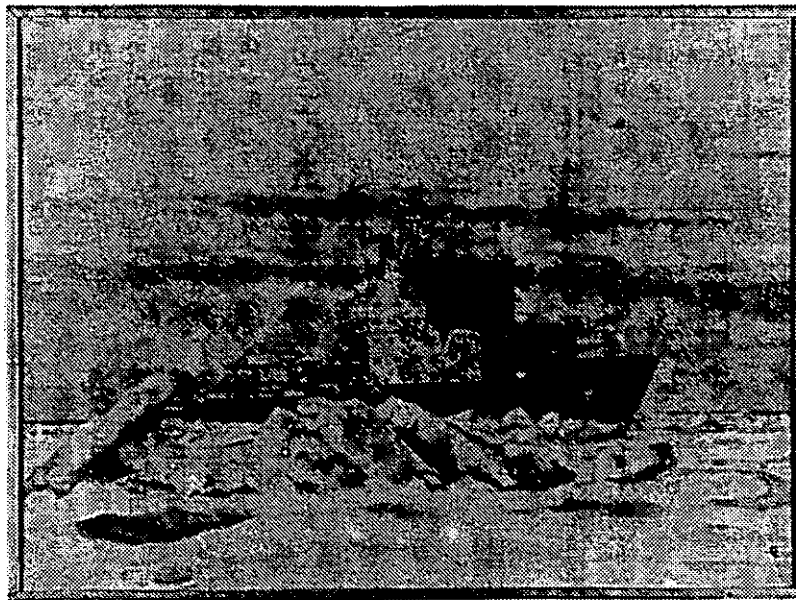


Fig. 11. Artist impression of new Finnish icebreaker.

Probability of ice occurrence, in percent
Sannolikhet för isförekomst, i procent
Jään esiintymistodennäköisyys, (%)

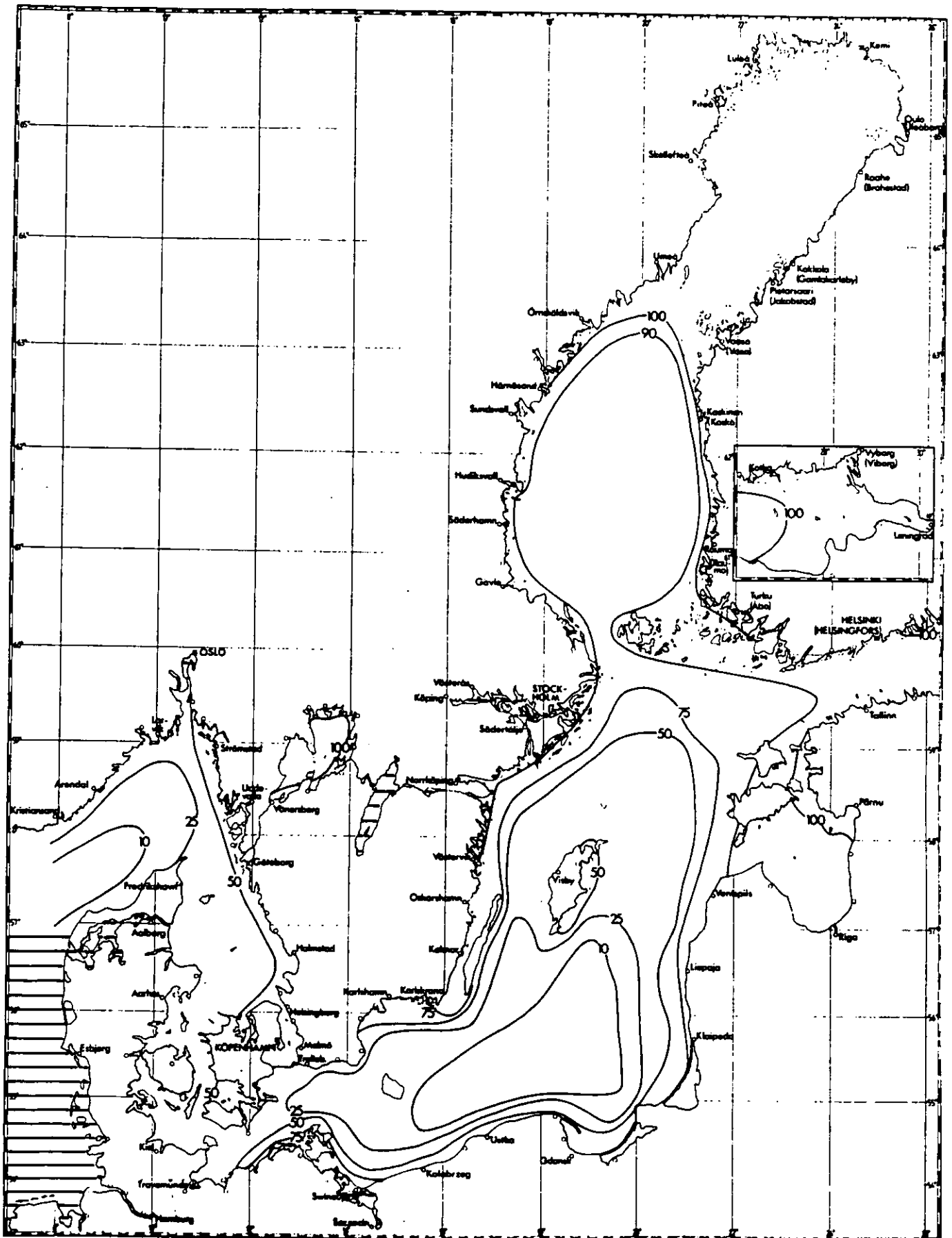


Fig. 12. Probability of ice occurrence in the Baltic in percent.

Routine chart for maximum ice extent in a severe winter
 Rutiniskarta med maximal isutbredning under en svår vinter
 Rutiinikartta suurimman jään laajuuden ajankohdalta kovana talvena

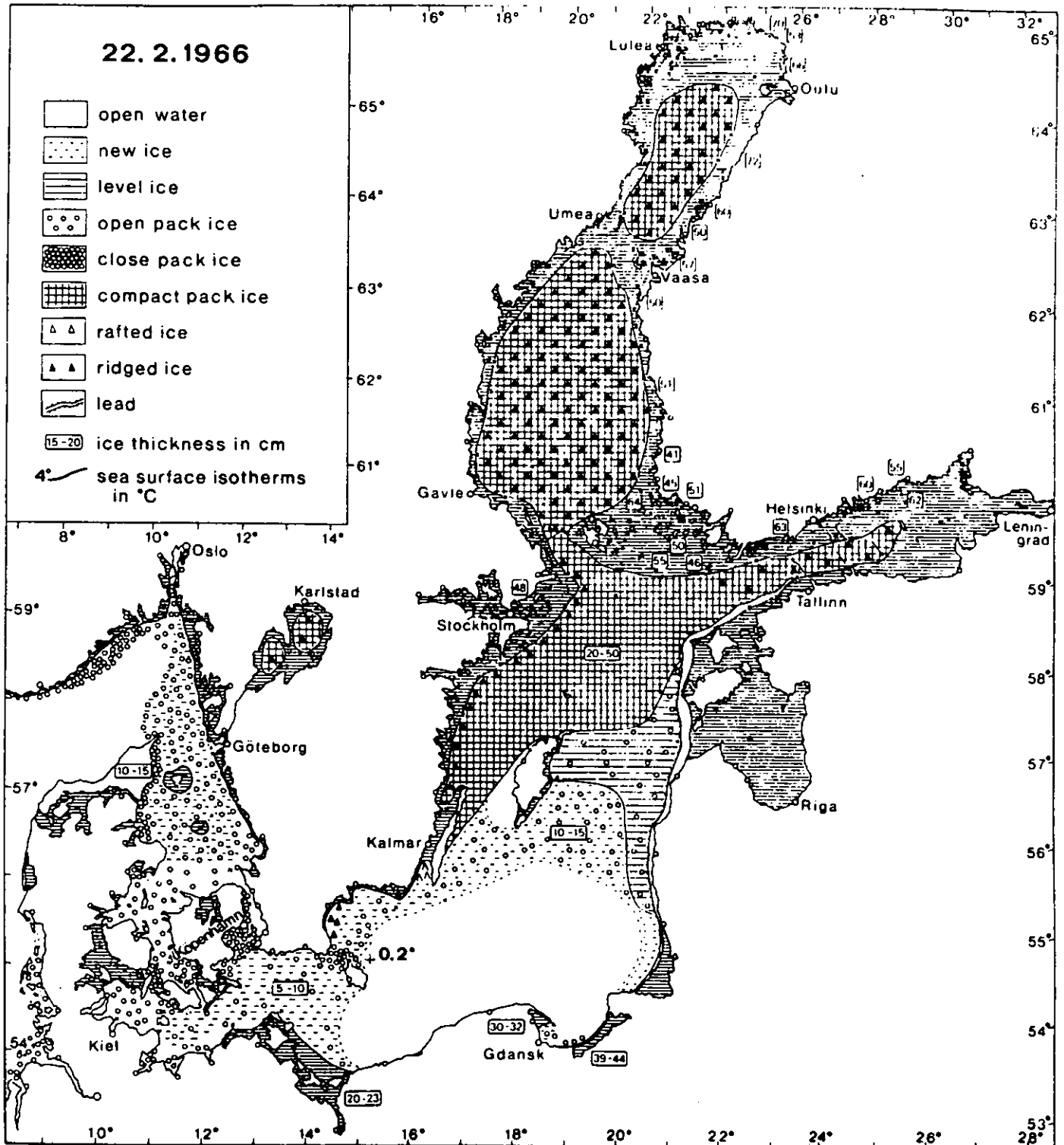


Fig. 13. Maximum ice extent in the Baltic in severe winter.

Routine chart for maximum ice extent in a mild winter
 Rutiniskarta med maximal isutbredning under en mild vinter
 Rutiinikartta suurimman jään laajuuden ajankohdalta leutona talvena

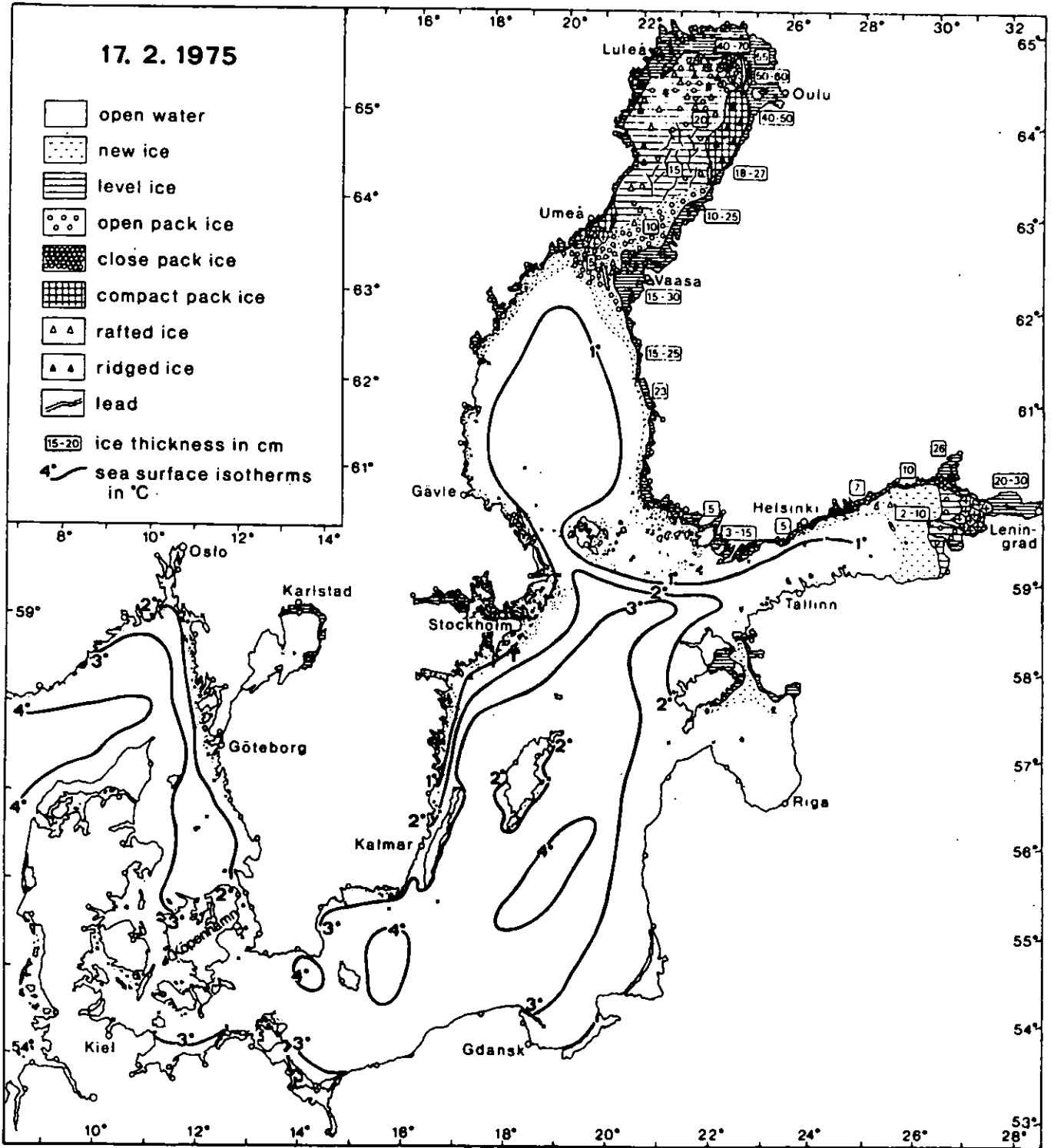


Fig. 14. Maximum ice extent in the Baltic in a very mild winter.

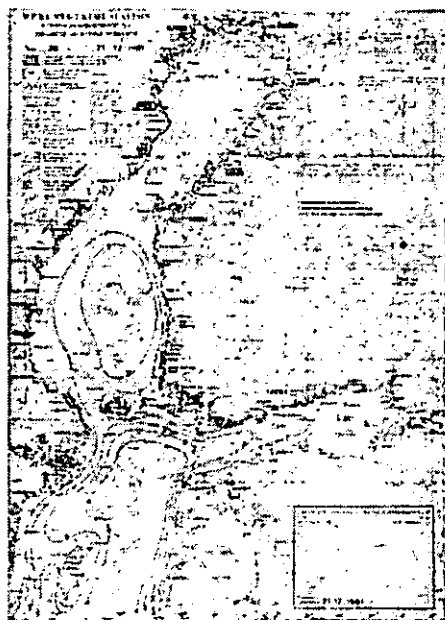


Fig. 15. Baltic ice situation 21.12.1981.



Fig. 16. Baltic ice situation 11.02.1982.



Fig. 17. Baltic ice situation 22.04.1983.

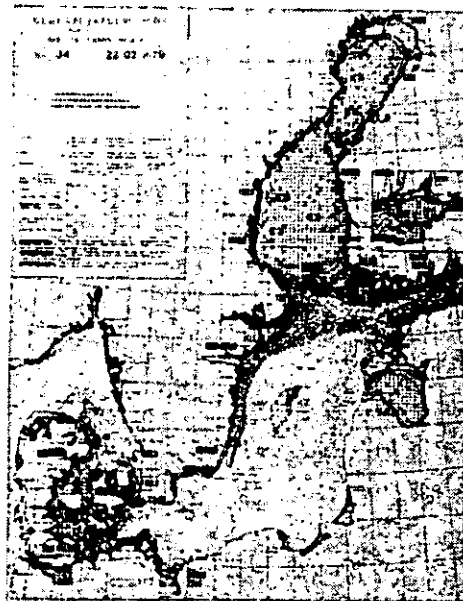


Fig. 18. Southern Baltic frozen 22.02.1979.

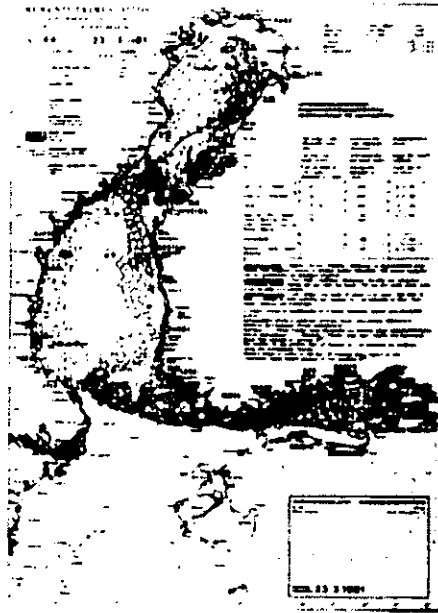


Fig. 19. Ice pressur from south 23.03.1981.



Fig. 20. Satellite picture of ice conditions in the Bothnian.
(06.04.1983. 10,40.)

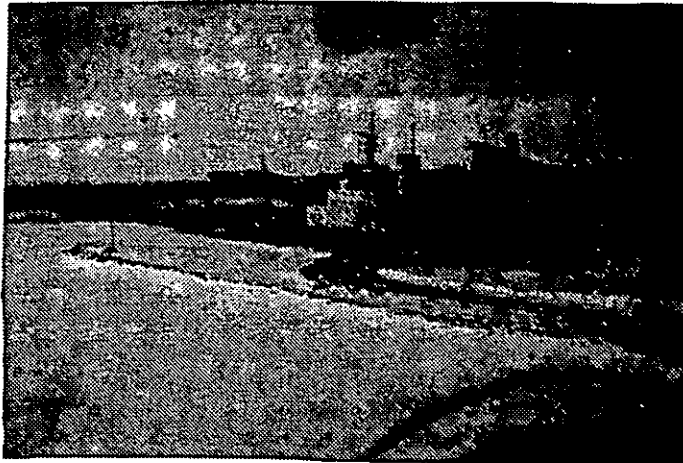


Fig. 21. Icebreaker and IA Super strengthened tanker in the Bothnien.

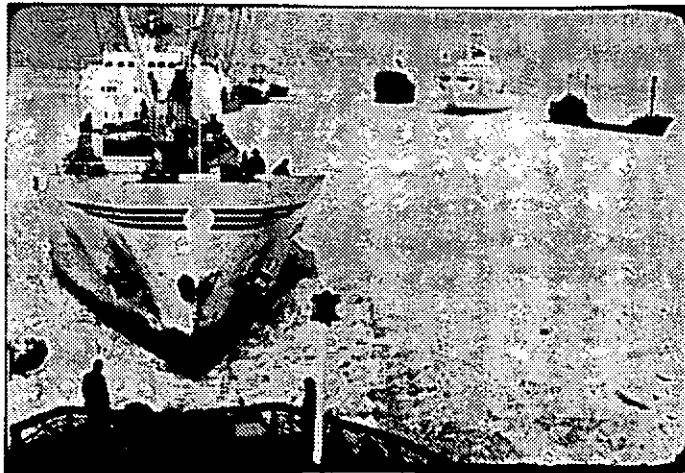


Fig. 22. Convoy assembling behind icebreaker.

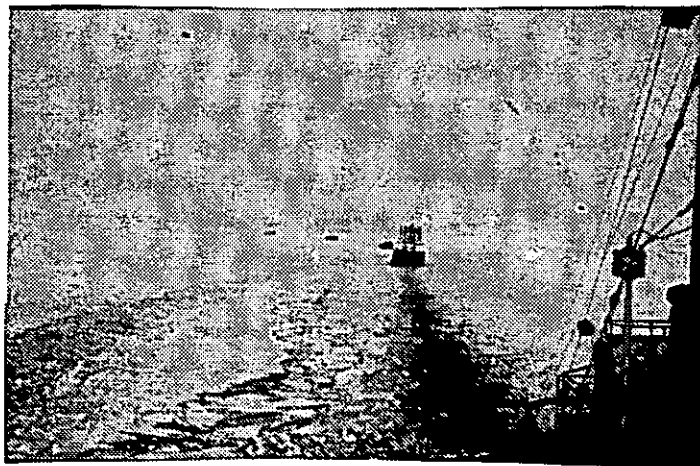


Fig. 23. Channel closes behind icebreaker.

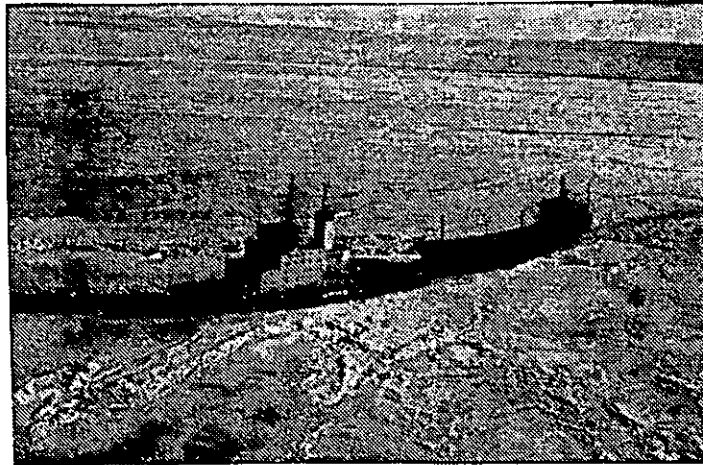


Fig. 24. Notch towing in ice ridges.

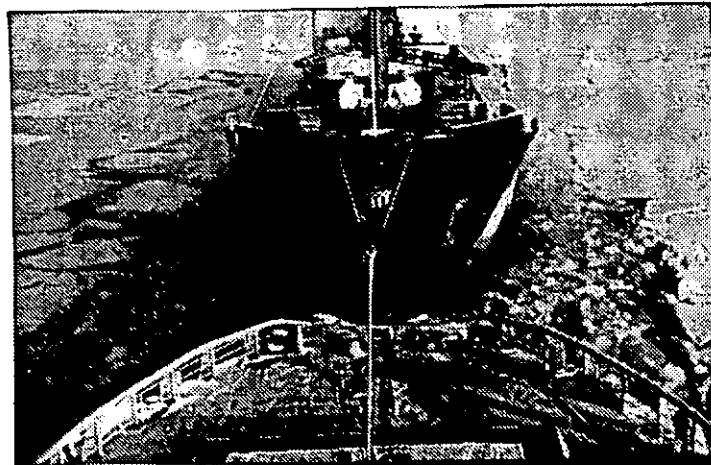


Fig. 25. Close up of notch towing.



WESTERN EUROPEAN GRADUATE EDUCATION
IN MARINE TECHNOLOGY

SEVENTH SCHOOL

March 21-31, 1983

in Helsinki

SHIPS AND STRUCTURES IN ICE

ASSESSING THE ECONOMICS OF
ICE NAVIGATION -- THE GREAT
LAKES AS A CASE STUDY

by

Harry Benford

Delivered

Date March 22, 1983

ASSESSING THE ECONOMICS OF ICE NAVIGATION --
THE GREAT LAKES AS A CASE STUDY

ABSTRACT

Shipowners contemplating navigation in ice-covered waters need answers to many questions pertaining to the economics of such operations. Great Lakes studies carried out a decade ago at The University of Michigan may provide some of the answers, or at least suggest methods of analysis.

These notes outline the analytical procedures used in those studies. They also provide detailed estimating data that, properly modified, may be gainfully employed in studies involving other kinds of ships in other parts of the world.

ABBREVIATIONS

A':	Uniform annual cash flow after tax, dollars per year
B:	Ship's beam, feet
BHP:	Brake horsepower, maximum continuous rating
C:	Annual transport capacity on a given trade route, long tons per year
C _B :	Block coefficient
CN:	Cubic number (product of length between perpendiculars, beam, and depth, all in feet, divided by 100)
CP:	Controllable pitch
CR:	Capital recovery factor, used to convert an initial investment into a uniform annual cost in which is recognized both profits and tax
D:	Ship's depth, feet
DW:	Ship's deadweight, long tons
H&M:	Hull and machinery insurance cost, dollars per year
i:	Annual interest rate
K:	Number in crew
L:	Ship's length between perpendiculars, feet
L.O.:	Lubricating oil
LT:	Long tons
M:	Months of operation per year
N:	Ship's economic life, years
NPV:	Net present value, discounting future cash flows at owner's minimum acceptable rate of return
P:	Initial investment, dollars
P&I:	Protection and indemnity insurance cost, dollars per year
RFR:	Required freight rate (rate owner must charge his customer if owner is to earn a reasonable after-tax return on his investment), dollars per ton
SHP:	Shaft horsepower, maximum continuous rating
SPW:	Series present worth factor for a uniform cash flow
W _C :	Weight of conveyor system, long tons
W _M :	Weight of propulsion plant, long tons
W _O :	Weight of outfit and hull engineering exclusive of self-unloading gear, long tons
W _S :	Weight of hull structure, long tons
Y:	Annual operating costs, dollars

Roman Numerals

IAS	} Finnish ice classes, of which IC is the lowest. Class II means no ice reinforcement.
IA	
IB	
IC	
II	

Note

Other abbreviations are explained where used.

INTRODUCTION

A shipowner who is considering operating his ships through ice will find himself faced with questions about the economics of alternative decisions. If his thinking involves new construction, or major modification to existing ships, his questions become more numerous and more complex. His fundamental question is this: Engaging in ice navigation can bring extra income; is it worth the extra costs? Related questions include:

- *What is a fair freight rate to charge if ice navigation is required?
- *What degree of ice strengthening (i.e., what ice class) is optimum, given the available freight income and graduated fee schedules such as those applied in Finnish waters?
- *How bad should ice conditions become before diverting the ship to less strenuous trades?
- *Given a fleet of mixed ice capability, how can each ship best be deployed?

I am not going to try to answer all those questions. My intent is more modest; it is to explain the procedure -- both general and detailed -- that a group of us at The University of Michigan developed about a decade ago. This work applies to the Great Lakes of North America and was done under contract with the Maritime Administration, then a part of the U.S. Department of Commerce.

The Great Lakes have their own peculiar kind of ships and their own ice conditions. Nevertheless, what I present here may serve as a useful starting point for assessing ice navigation in other parts of the world.

The basic aim of our work was to find the best ice class (hull and machinery) for any assumed trade route on the Lakes. This involved, secondarily, the need to find the proper length of operating season under mild, normal, or severe winter weather conditions. Our work was aimed primarily at ships in the design stage and that phase of our work is what I shall report on here.

The first task was to predict the ice conditions on many discrete parts of the Lakes at two-week intervals during mild, normal, or severe winters. That was a major undertaking, but one that need not be spelled out here.

Then, looking at one proposed design at a time, we tried to predict the economic benefits of operating the ship for various lengths of season under mild, normal, or severe winters. The procedure involved these steps:

1. Estimate light ship weight.
2. Estimate building costs.
3. Predict speed through open water and ice of various characteristics.
4. Predict roundtrip times (for an assumed voyage) and cargo deadweights during open water seasons, and biweekly during the winter. Derive annual transport capacity based on various lengths of season.
5. Predict annual operating costs for each of the various lengths of season.
6. From the above, derive required freight rate, net present value, and other measures of merit.

You may be tempted to analyze ice navigation simply by looking at the added costs and added benefits that occur during the winter months. It is not that simple. The impact of greater hull weight, for example, is with you year-round. So is the loss in cargo deadweight if an icebreaker bow is used. You must, in short, examine year-round economics starting with the economics of confining operations to the normal, ice-free season.

SINGLE SHIP ANALYSIS

What follows next is a series of expansions of each of the six steps mentioned above, followed by a presentation of some typical results.

I must point out that in all of this we are looking only at the economics of winter navigation as seen by the shipowners. Public costs, such as icebreaker assistance, are specifically excluded. The same is true of benefits to the users, such as reduced inventory costs.

I must also point out that I am omitting many details. Interested readers should acquire References 8 and 9 for further information.

1. Weights

Steel weight is based on a modification of Krappinger's formula (Reference 6):

$$W_S = 668 \left(\frac{CN}{1000} \right)^{0.75} \left(\frac{L}{D} + 2 \right) \left(0.565 + \frac{C_B}{2} \right) \quad (1)$$

where

W_S = net steel weight in long tons

CN = cubic number = $\frac{LBD}{100}$

L = length between perpendiculars, feet

B = beam, feet

D = depth, feet

C_B = block coefficient

Equation (1) is for a standard Great Lakes bulk carrier without added ice reinforcement. (The structural reinforcement found necessary for frequent contact with lock walls and docks is roughly equivalent to ice class IC). Figure 1 shows approximate additional steel weights required for higher ice classes.

If the ship is a self-unloader with A-frame and boom, add two percent to W_S .

Outfitting and hull engineering weight in long tons, exclusive of any conveyor system, is taken as:

$$W_0 = 233 \left(\frac{CN}{1000} \right)^{0.3} \quad (2)$$

Outfitting weight is but little affected by the demands of winter navigation.

The weight of the conveyor system, exclusive of A-frame and hoppers, is taken as:

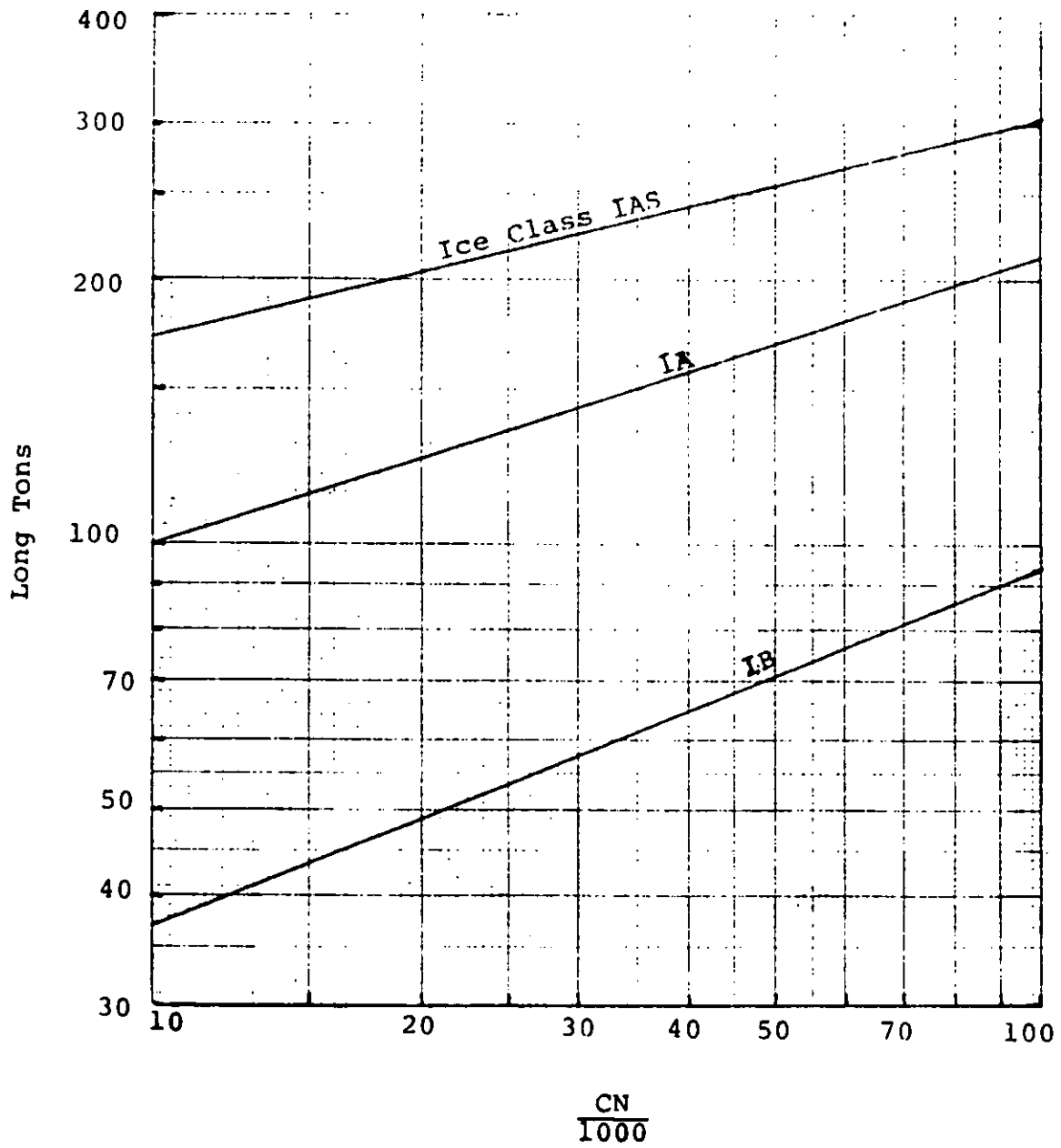


Figure 1. Net Added Steel Weight for Various Degrees of Ice Reinforcement

$$W_C = a \left(\frac{CN}{1000} \right)^b \quad (3)$$

where a and b have the following values for a boom conveyor system:

capacity, 1000 long tons per hr:	4	6	8	10
a	104	147	202	252
b	0.46	0.42	0.38	0.35

The weight of the entire propulsion machinery plant, in long tons, is taken as

$$W_M = a \left(\frac{SHP}{1000} \right)^{0.5} \quad (4)$$

where a equals

- 200 for single screw steam turbine plants
- 267 for twin screw steam turbine plants
- 180 for single screw medium speed diesel plants, and
- 200 for twin screw medium speed diesel plants.

The ice rules dictate minimum requirements for propeller blade thickness, shaft diameters, etc. The resulting increase in weight is negligible, however.

The light ship weight is the sum of the weights of structure, outfit, conveyor (if a self-unloader), and propulsion plant. Seventy tons are subtracted for the weight and lost displacement of a typical bow thruster system.

Weights of fuel, stores, etc. are taken up in Step 4.

2. Building Costs

Warning: These building cost estimates are based on 1971 cost levels in U.S. Great Lakes shipyards.

Table 1 summarizes the cost estimating relationships applying to non-self-unloaders with single screw and fixed propeller blades. Miscellaneous costs such as engineering, staging, temporary lights, launching, and trials are all recognized in the coefficients shown. The following assumptions apply:

- Overhead: 75 percent of labor cost
- Average hourly rate: \$4.10
- Profit: 5 percent of total cost to shipyard.

Table 1
COST ESTIMATING RELATIONSHIPS

		Cost Component	
		Material (\$)	Labor (man hours)
Ship Component	Structure	$\$236 W_S$	$130,000 \left(\frac{W_S}{1000} \right)^{0.85}$
	Outfit	$\$2400 W_O$	$280 W_O$
Machinery	Steam Turbine	$\overbrace{\$900,000 \left(\frac{SHP}{1000} \right)^{0.60}}$ Material, Labor, Overhead add 3% if 70% backing power is specified	
	Intermediate-Speed Diesel	$\$550,000 \left(\frac{BHP}{1000} \right)^{0.70}$	

The hull cost (structure plus outfitting) can be taken as the sum of the two material costs plus $(1.75 \times \$4.10)$ times the total man-hours. Adding the cost of machinery gives the total cost to the shipyard. For twin screw plants, increase figures shown in table by 33 percent for steam plants, 12.5 percent for diesels. The shipyard bill would be 5 percent greater than the sum of all those costs. You may want to toss in another few percent for additional owner's costs.

There is no need to append anything for costs of ice strengthening. The added steel weight and horsepower are already factored into the cost equations shown in Table 1. In the outfitting category, however, there should be a modest increase for strengthened rudder and steering gear. We used the following:

$$C = a \frac{LB}{100} \quad (5)$$

where

C = added cost to owner for winter outfitting

a = 0 for class II or IC

= \$15 for class IB

= \$30 for class IA

= \$45 for class IA Super

L = length between perpendiculars, feet

B = beam, feet

If the ship is to be a self-unloader with boom, the conveyor system cost plus profit would be:

$$C = a \left(\frac{CN}{1000} \right)^b \quad (6)$$

where a and b have these values:

capacity in 1000 long tons per hr:	4	6	8	10
a in \$1000:	442	597	794	922
b in \$1000:	0.23	0.22	0.19	0.19

The installed cost plus profit of a typical 800 BHP diesel bow thruster was estimated at \$150,000.

For controllable pitch propellers, the added cost plus profit would be:

$$C = a \left(\frac{SHP}{1000} \right)^{0.60} \quad (7)$$

where

a = \$20,000 for steam plants

a = \$13,500 for geared diesel plants.

3. Predicted Speed

Open water speeds were derived from empirical residuary resistance coefficients taken from Reference 11. These figures are applicable to the unique hull forms used on the Lakes and need not be repeated here. The frictional resistance coefficients were estimated from the ITTC line with a correlation allowance of 0.0002.

Wake fraction, thrust deduction, etc. were based on conventional estimating methods.

A considerable part of a typical Great Lakes voyage is in rivers where speeds have statutory limits. These limits have to be recognized in estimating voyage times and fuel consumption.

Speed in sheet ice was derived from data from Wärtsilä, Reference 5, using our own methods of interpolation and extrapolation. But, operating in sheet ice is the smaller part of the problem. More often we find the Great Lakes ship pushing its way through narrow channels clogged with broken ice (often refrozen) -- the debris of previous passages. Here our estimating methods combined Bronnikov's analytical technique (Reference 2) with pertinent data from ARCTEC (Reference 7).

4. Roundtrip Times and Transport Capacity

Given the speed and power estimating methods described above, we were able to establish a computer program that would predict the time required to complete each of many segments of the voyage during any time of the year. In this we assumed that when ice conditions slowed the speed below 5 miles per hour (4.3 knots) the engines would be stopped awaiting icebreaker assistance. Logical assumptions as to waiting time were incorporated into the program as was an assumed convoy speed of 5 miles per hour. To all of this, of course, we added standard times for port turnaround and reasonable delays for lockage, queuing, etc. Where appropriate, these were increased for winter conditions. We were gratified to learn that our resulting predictions for round-trip times agreed well with actual times experienced by the United States Steel Corporation's Great Lakes Fleet, which has led the way in winter navigation on the Lakes.

The transport capacity per round trip is affected by the allowable freeboard (which changes during each of four or five seasons of the year) as well as by the weight of fuel, water, and stores.

We estimated the fuel consumption per one way trip and added a 50 percent margin during the regular (i.e., essentially ice-free) season, and a 100 percent margin during the extended season.

Fuel use during delays or time in port was based on this expression:

$$f_s = 224 \frac{DW}{10,000} C_1 \quad (8)$$

where

f_s = pounds of fuel per hour
 DW = deadweight in long tons
 C_1 = 1.0 for steam plants
 = 0.7 for diesel plants

The other miscellaneous deadweight items were lumped into a single 150-ton allowance that we assumed constant.

Fuel weight was derived from each voyage's steaming profile, plus the margins mentioned above. For steam plants with 1450psi-950F reheat cycles, the daily fuel consumption at full power was estimated to be $4(\text{SHP}/1000)+8$. The corresponding figure for medium speed, geared diesels was $3.8(\text{RHP}/1000)+4$. When operating at reduced powers the daily rates were assumed to go up as follows:

Percent of Max. Power	Relative Fuel Rate	
	Steam	Diesel
100	1.000	1.000
90	1.007	1.014

(cont).

80	1.025	1.028
70	1.051	1.042
60	1.089	1.056
50	1.143	1.070

The computer program is arranged to work with all of the above weight and time data and project the annual transport capacity on any given trade route for any length of season. It can do that for mild, normal, and severe winters.

5. Annual Operating Costs

In those innocent days bunker oil was selling for \$32 per long ton (vs about \$150 per long ton today). A blended oil suited for medium speed diesels was more like \$36 per long ton.

During the regular 8-month operating season, the daily cost for crew wages and benefits was taken as \$380+\$46 per crew member. (A 26-man crew is typical.) We assumed that extended season operations would add 15 percent to those daily costs.

Subsistence costs were estimated to be \$2.70 per man-day.

We estimated P&I insurance costs as:

$$\text{P\&I per month} = \$11\text{K} + \$8.4 \frac{\text{CN}}{1000} \quad (9)$$

where

K = number in crew
CN = cubic number

During the extended season, however, we assigned a 25 percent penalty to the above.

Estimating H&M insurance was one of our more difficult tasks. The underwriters, in their admitted ignorance, were quoting completely unrealistic rates. (The U.S. Steel fleet managers were not put off by that, however, because they had confidence in what they were doing and their fleet was self-insured.) We proposed what we still think is a reasonable basis for H&M insurance on the Lakes:

$$\text{H\&M per year} = f\left(\$1000 + \frac{P}{1000}\right) \quad (10)$$

where

P = the ship's initial cost
f = a season-related factor equal to M for M values up to and including 9, M being the months of operation per year beginning April 16, the start of the normal operating season on the Lakes. After 9 months (i.e., after January 16):

$$f = M(a)^{M-9} \quad (11)$$

where

a = 1.184 for ice class IC a = 1.068 for ice class IA
a = 1.129 for ice class IB a = 1.039 for ice class IA Super

Figure 2 helps clarify this proposed approach to H&M insurance.

For annual maintenance and repair costs we proposed this for a normal, 8-month operating season:

$$M\&R = \$5000 \left(\frac{CN}{1000} \right)^{2/3} + f_1 \left(\frac{SHP}{1000} \right)^{2/3} + Z \quad (12)$$

where

- CN = cubic number
- SHP = shaft horsepower
- f_1 = \$5000 for steam plants
= \$6600 for diesel plants
- Z = \$50,000 special increment for self-unloaders.

If winter operations are involved, our expression for annual costs of M&R became:

$$M\&R = \frac{M}{8} \left\{ (a)^{M-9} \left[\$5000 \left(\frac{CN}{1000} \right)^{2/3} + f_1 \left(\frac{SHP}{1000} \right)^{2/3} \right] + Z \right\} \quad (13)$$

where a has the same values as those given for Equation (11).

Figures 3 and 4 show M&R costs for 8-month (ice-free) operations. Figure 5 shows correction factors (f) for extended season operations.

Towing costs per round trip during the normal season were taken as:

$$TCPRT = a \frac{LB}{1000} \quad (14)$$

where

- a = \$4 for ships with bow thrusters
- = \$13.50 for ships without bow thrusters

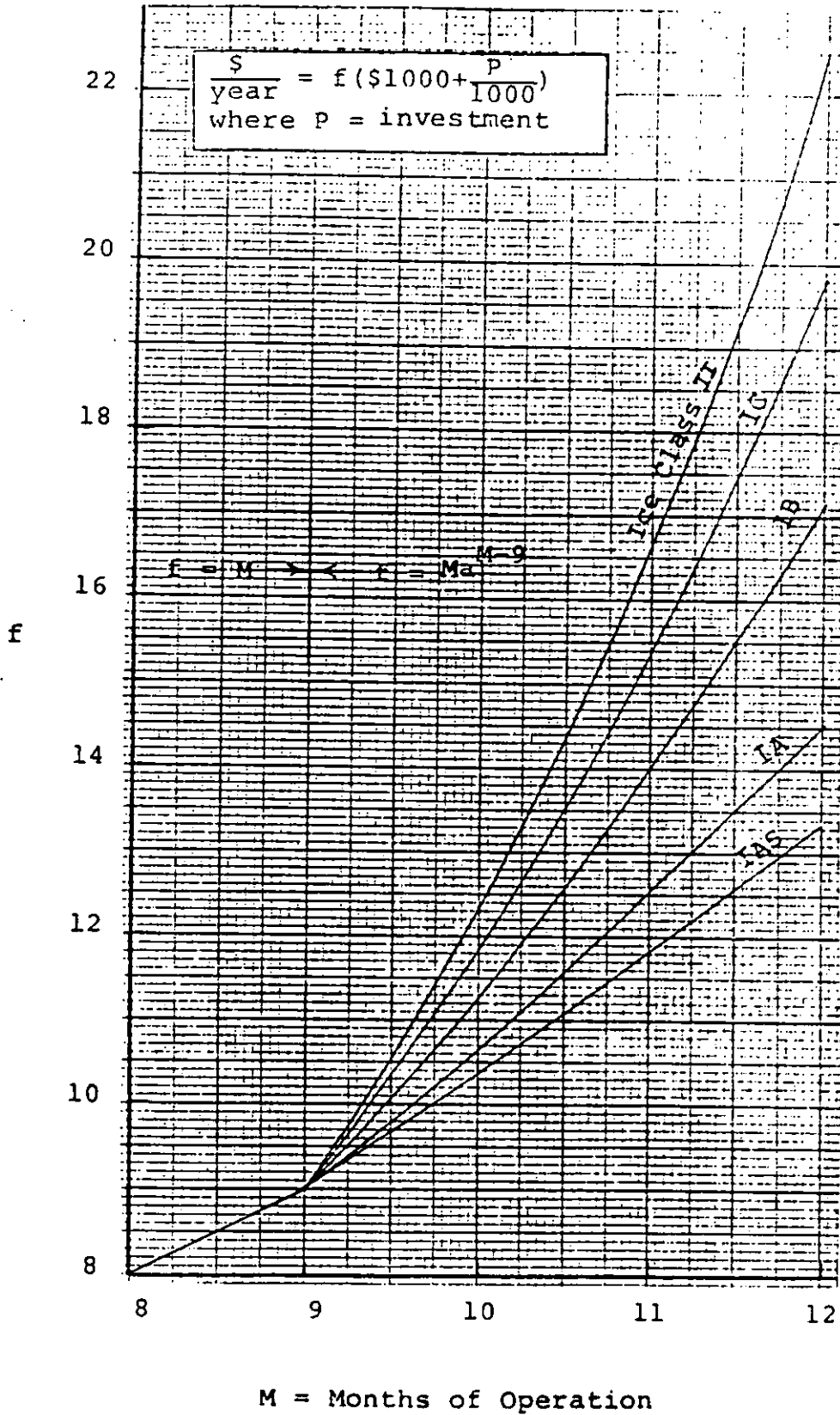


Figure 2. Cost Factors for Hull and Machinery Insurance

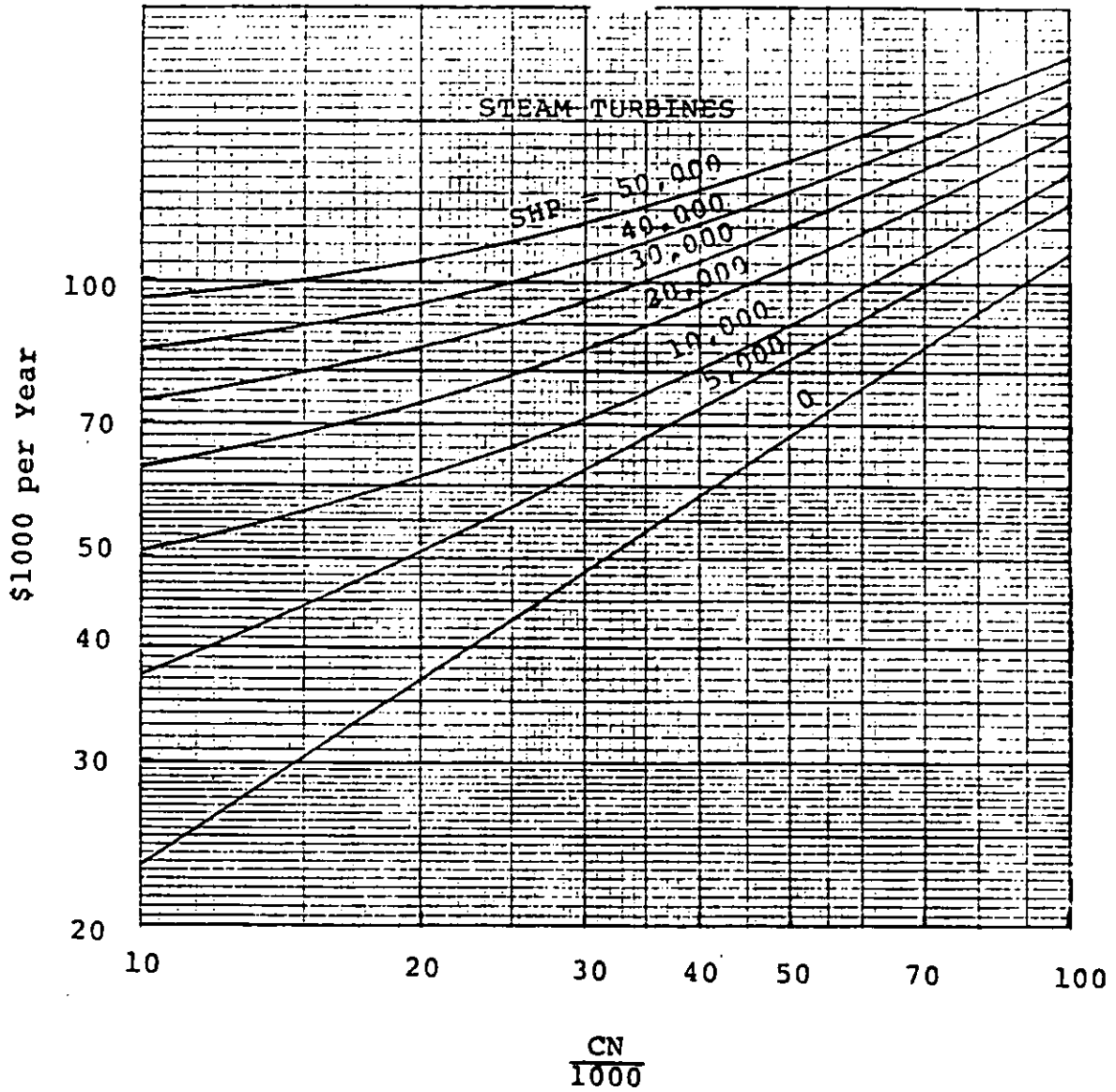


Figure 3. Annual Costs of Maintenance and Repair for 8-Month Season, Steam Turbine Machinery. Add \$50,000 for Self-Unloaders.

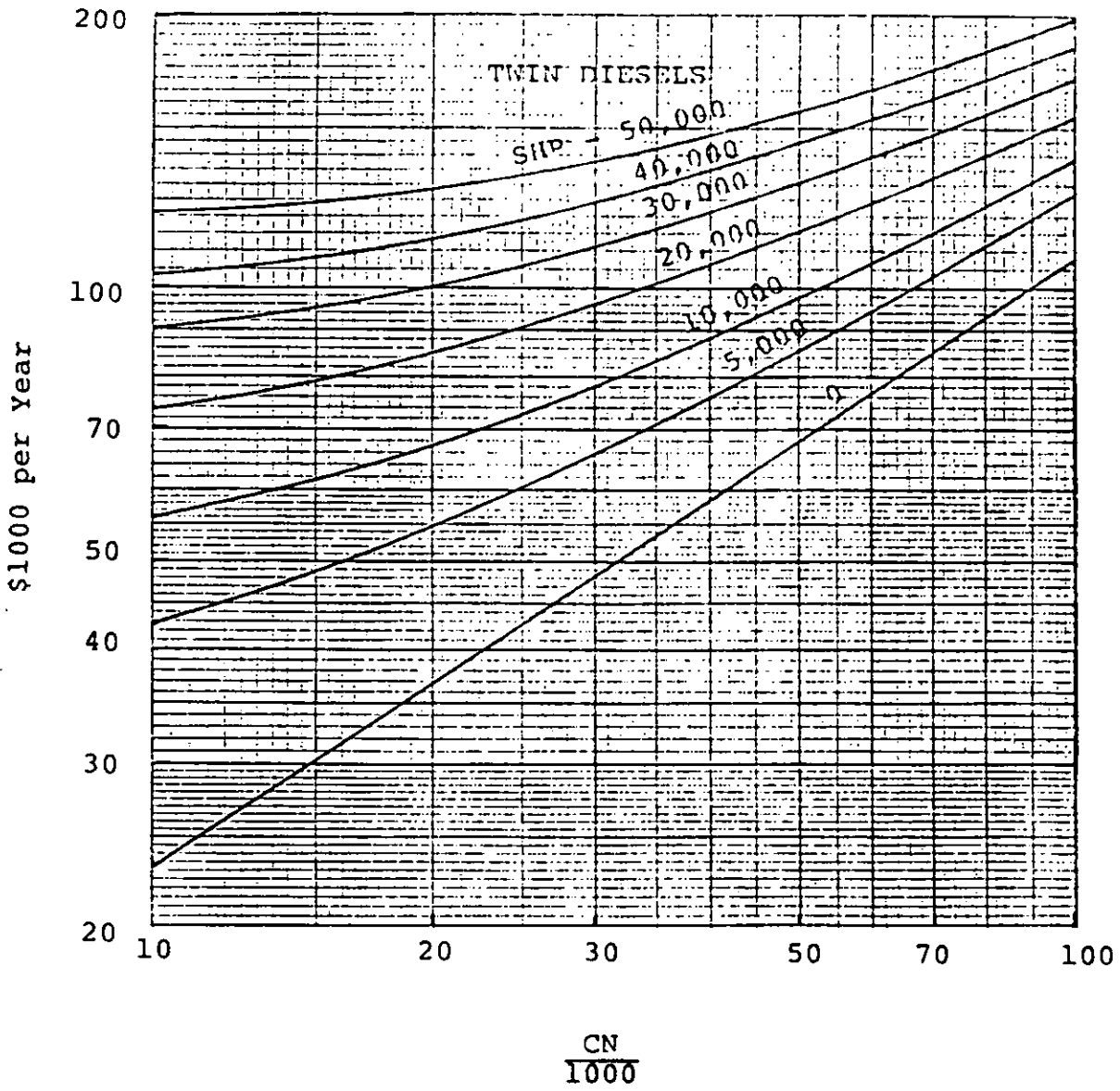


Figure 4. Annual Costs of Maintenance and Repair for 8-Month Season, Twin Diesel Machinery. Add \$50,000 for Self-Unloaders.

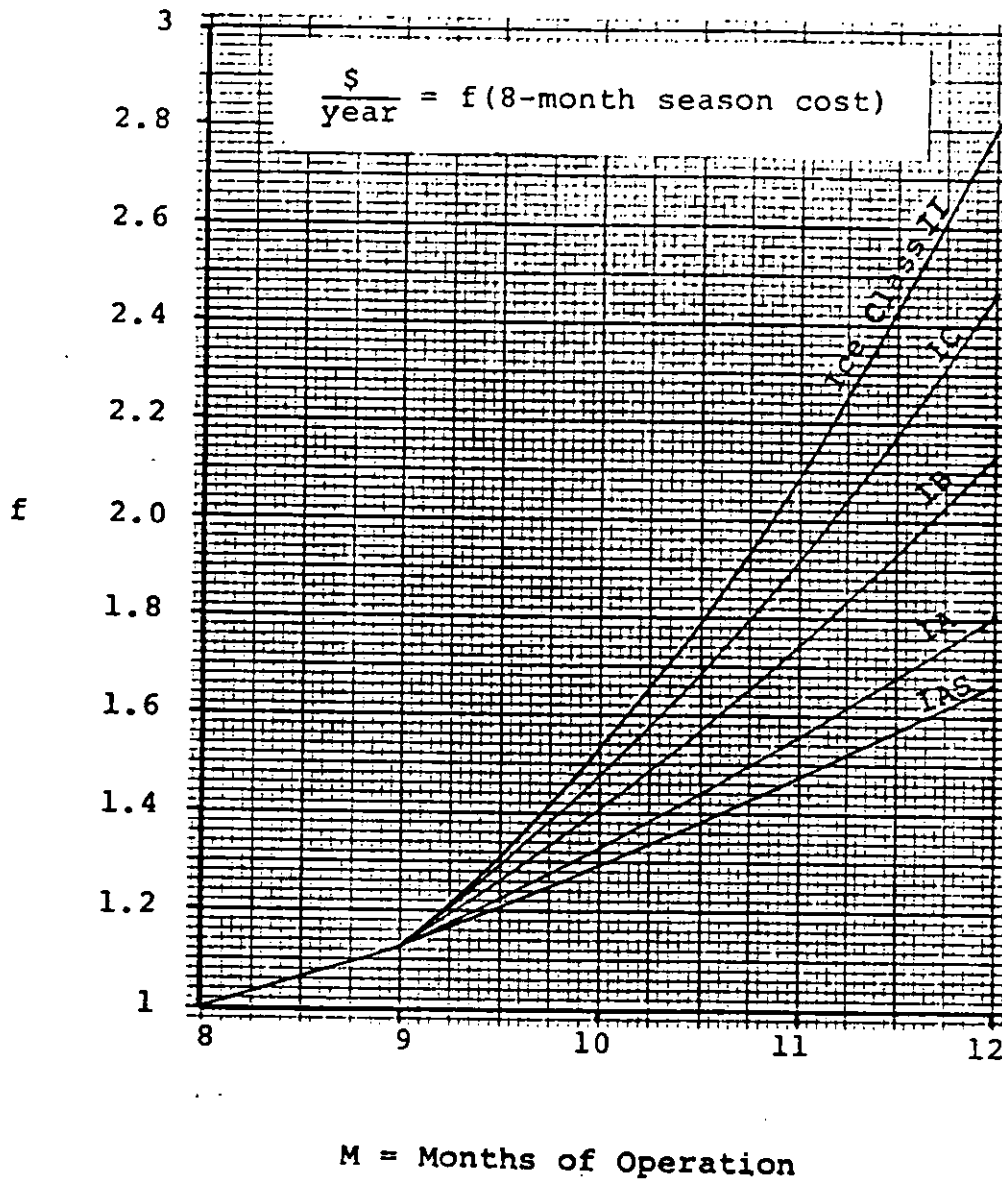


Figure 5. Factors for Increasing Annual Costs of Maintenance and Repair with Extended Season. Add \$6250 per month of extended season for self-unloaders.

During winter operations we increased the towing costs per voyage by 50 percent.

Whether winter or summer, we took the monthly cost of stores and supplies as:

$$S\&S = \$50\left(\frac{CN}{1000}\right) + \$37(K-10) \quad (15)$$

where

K = number in crew.

These figures were high enough to cover the cost of lubricating oil for steam plants. For diesel plants we assumed a L.O. consumption of 0.5 percent of fuel burned and a cost of 12¢ per pound (\$269 per ton).

A special expense on the Great Lakes is concerned with winter lay-up. As year-round operation is approached the lay-up work will involve a live ship rather than a dead one. Wharfage charges will be less, but a skeleton crew will be needed. We used this scale of costs:

<u>Months of Operation</u>	<u>Lay-up Cost</u>
up to 10	\$75,000
11	\$25,000
11.5	\$10,000

Our final operating cost was for overhead and miscellaneous expenses. On an annual basis we used:

$$OH = \$50,000 + \$200M + \$1250\left(\frac{CN}{1000}\right) \quad (16)$$

where

M = operating months per year.

The ten cost categories explained above constitute the entire annual operating cost for the proposed ship in service over any given number of months. These costs would vary somewhat between mild, normal, and severe winters.

6. Economic Summary

Armed with the above estimates of building cost, operating cost, and annual transport capacity, we are ready to derive several measure of economic merit. Typical of these is the required freight rate:

$$RFR = \frac{CR(P)+Y}{C} \quad (17)$$

where

- CR = a capital recovery factor set by owner's stipulated level of profitability, tax structure, and economic life of the ship
- P = initial investment, dollars
- Y = annual operating costs, dollars
- C = annual transport capacity, tons

Another typical measure of merit is the net present value:

$$NPV = (SPW-i-N)A' - P \quad (18)$$

where

(SPW-i-N) = series present worth factor for an annual interest rate, i , and ship's economic life in years, N .
A' = after-tax returns per year
= annual revenue minus operating costs minus tax.

If you are not already familiar with these measures of merit see References 1, 3, or 4.

The appendix shows a typical economic evaluation in summary form.

As you may by now suspect, our computer program is rather elaborate.

TYPICAL RESULTS

Having educated our computer in the intricate logic of winter navigation economics, we were in a position to study the relative merits of alternative design decisions. These were reported by Nowacki in Reference 8. A few typical results are shown here.

Figure 6, for example, shows projected net present value versus closing date of operations for a proposed self-unloader under different assumptions as to degree of hull reinforcement. The identifying letters refer to hull and machinery ice classes respectively. For this particular case we can conclude that there is no great benefit to be obtained from special ice reinforcement unless you intend to operate beyond the end of February -- and there is little to be gained by so doing in any event. Remember, however, that we are looking only at the shipowner's economics and are ignoring such benefits as reduced inventory costs and such costs as icebreaker service.

Figure 7 shows the results of some unsuccessful attempts to improve operations through the use of ice-breaking bows.

Figure 8 shows the effects of severity of weather upon roundtrip times, while Figure 9 shows how weather conditions may affect economic results.

Would today's higher fuel prices affect any of the above results? Net present values would presumably stay about where they are because the freight rates would be adjusted to offset the higher operating costs. The optimum length of operating season would probably be shortened somewhat. The rankings of the alternative designs would probably remain unchanged.

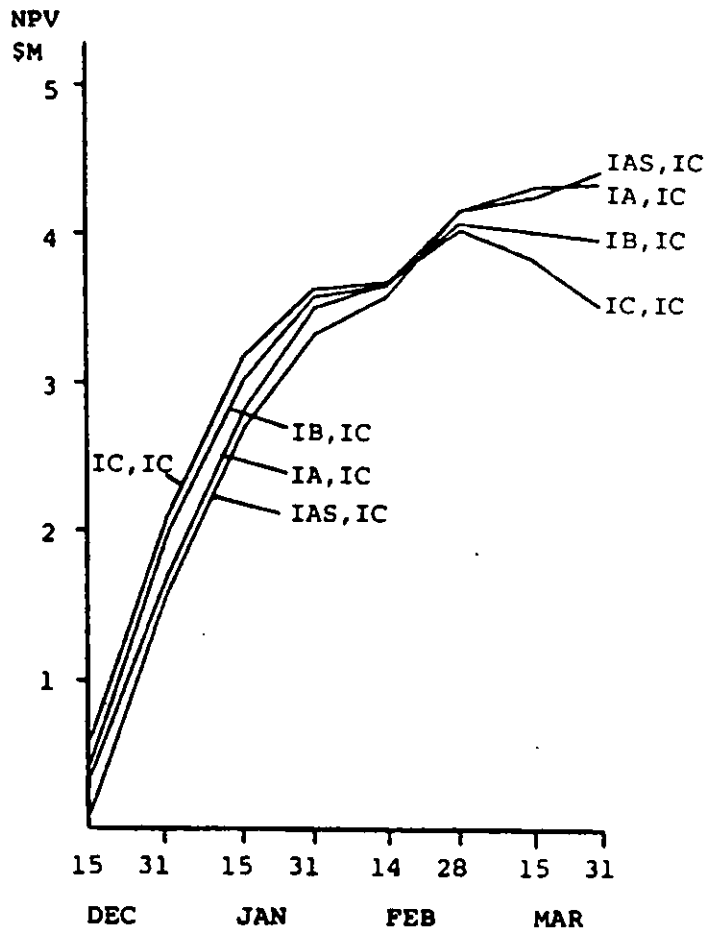


Figure 6. Effect upon NPV of Variations in Hull Ice Class for Proposed 988 Ft. Self-Unloader.

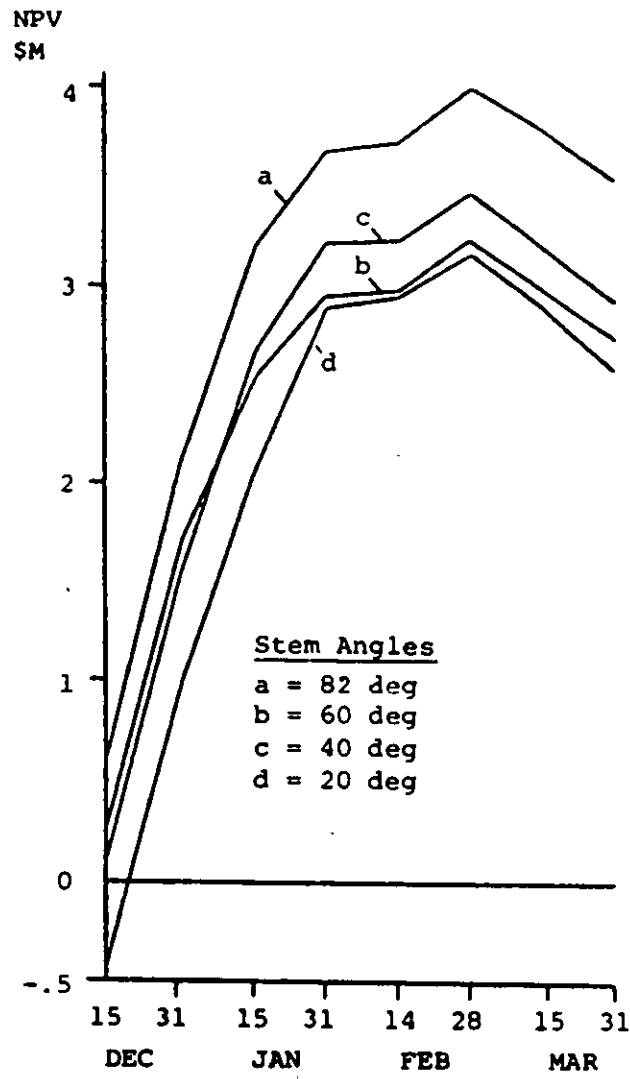


Figure 7. Effect upon NPV of Variation in Bow Shape in Proposed 988 Ft. Self-Unloader.

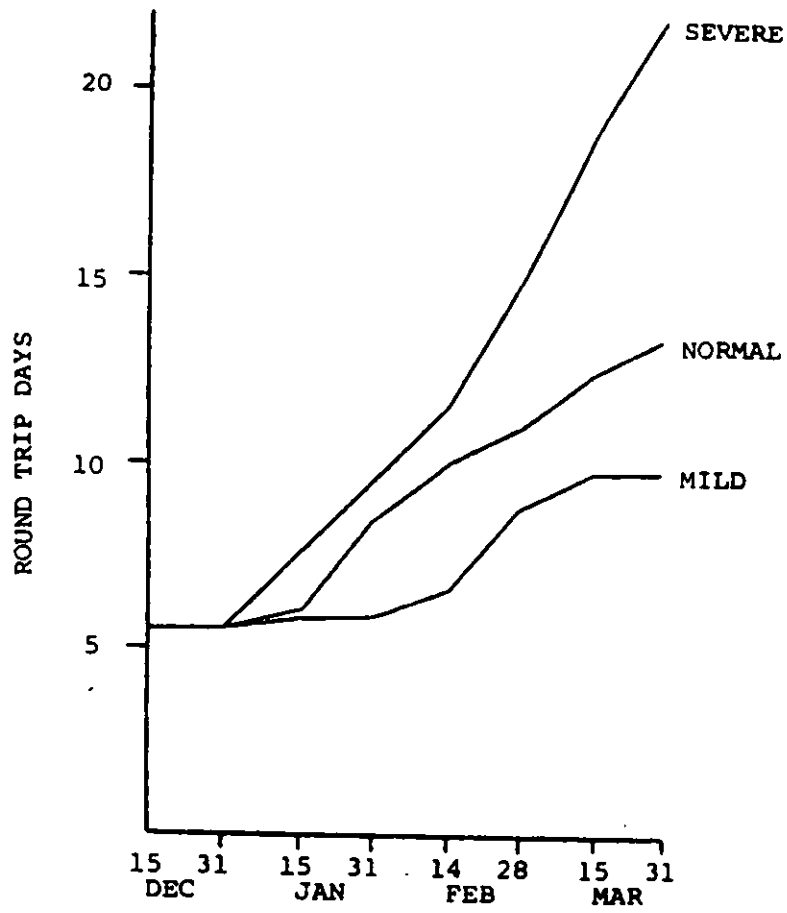


Figure 8. Effect of Winter Weather upon Round Trip Time for Proposed 988 Ft. Self-Unloader.

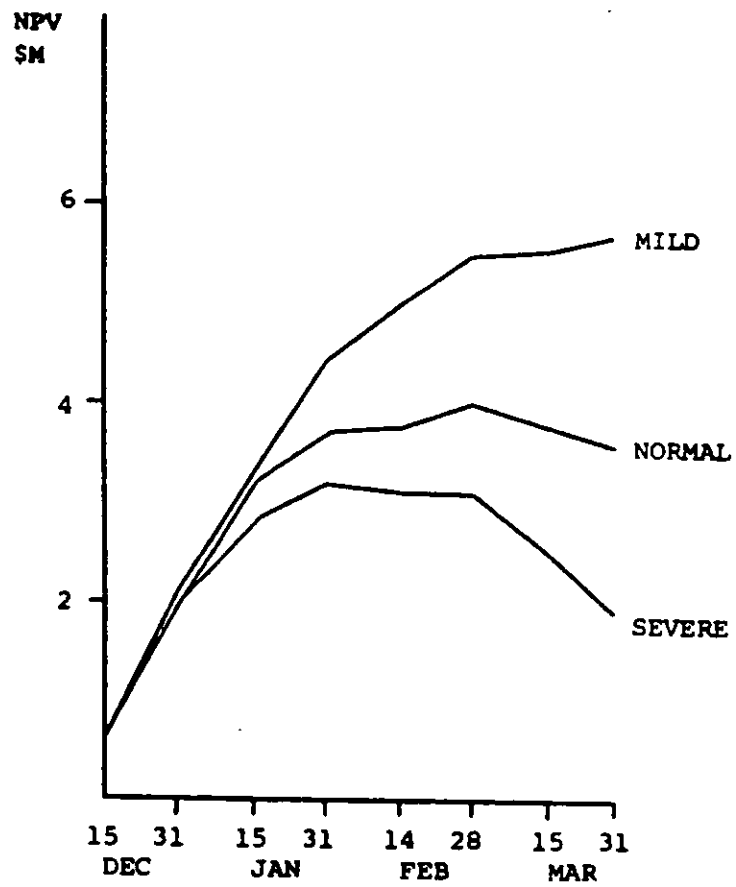


Figure 9. Effect of Winter Weather upon NPV for Proposed 988 Ft. Self-Unloader.

CONCLUSIONS

Some of the conclusions reported by Nowacki in Reference 8 may be of interest to this audience:

- 1) As a rule of thumb, one should not continue operating when roundtrip times in ice exceed twice normal open water times.
- 2) Conversions of existing vessels to higher hull and machinery ice classes are expensive and do not pay off on economic grounds. The higher speed gained due to the stronger engine throughout the shipping season does not offset the substantial investment cost for the stronger engine. This does not speak against minor hull reinforcement for purposes of greater safety or reliability.
- 3) The economics of bulk shipping are sensitive to delays of any sort, even delays of only a few hours per round trip. However, the general level of such delays does not materially affect the best length of operating season. Nonetheless, every effort must be made to avoid or reduce delays in summer and winter operations to save transport cost.
- 4) In newly proposed ships a higher class of hull ice strength may well pay off if the season is lengthened enough. The extra strength will either save insurance or repair costs, whereas the cost and weight penalties for higher hull ice classes in new construction do not appear to be too discouraging.
- 5) Special bow shapes with fine, icebreaking bow lines do not appear economically attractive in Great Lakes bulk carriers of the proposed size and configuration. The loss of payload throughout the shipping season in the finer shapes cannot be offset by gains in ice performance, although the ice resistance is substantially reduced in the finest bows. However, at the level of powering chosen and justified in this trade, even the vessels with the finest bow lines cannot avoid getting beset in ice, and, therefore, cannot prevent delays in waiting for icebreaker assistance.
- 6) Convoy speeds in icebreaker escorting practice must be kept at reasonable levels to ensure competitive operations during the winter season. Average speeds above 5 MPH would act as an incentive to extend the season beyond February, speeds below 5 MPH would suggest a shorter season extension.
- 7) Variations in icebreaking ability as predicted by different estimating methods do not materially affect the economic results of season extension. This conclusion might be reversed if a bulk carrier had such superior ice performance that it would become independent of icebreaker service.

ADDITIONAL FACTORS

In the foregoing we have alluded to costs of icebreaker assistance and the benefits of reduced inventory costs. Many other pertinent factors need also be considered. These include:

- 1) Crew attitudes and the need for crew rotation arrangements.
- 2) Need for new kinds of navigational aids.
- 3) Ice-clearing problems at locks and docks.
- 4) Potential for shore damage and other environmental considerations.

and

- 5) Reduced reliance on least efficient ships.

CLOSURE

The study I have reported on above was for a special kind of ship in an atypical physical environment. Nevertheless, the method of analysis should be applicable in many other parts of the world. Cost figures must of course be adjusted, and common sense applied throughout.

The micro-economics discussed here can be expanded into the macro-economics of fleet management. From these one can go into the economics of physical distribution. That would include the entire transport system: shore facilities, ships, icebreakers, and inventory cost of the goods in transit and in storage. My personal recommendation is that naval architects should develop at least some degree of competence in analyzing the economics of all of those components of the total transport picture.

REFERENCES

1. Benford, Harry: Fundamentals of Ship Design Economics, University of Michigan, Department of Naval Architecture and Marine Engineering, Report 086, 1979.
2. Bronnikov, A.V.: "Analysis of Resistance of Cargo Ships Going Through Pack Ice," Transactions Leningrad Shipbuilding Institute, 1959.
3. Buxton, I.L.: "Engineering Economics Applied to Ship Design," Transactions RINA, 1972.
4. Goss, Richard: "Economic Criteria for Optimal Ship Designs," Transactions RINA, 1965.
5. Johansson, B.V.; Mäkinen, E.: "Systematic Variation of Bow Lines and Main Dimensions of Hull Forms Suitable for the Great Lakes," SNAME Great Lakes and Great Rivers Section, January 1973.
6. Krappinger, O.: Great Lakes Ore Carrier Economics and Preliminary Design, University of Michigan, Department of Naval Architecture and Marine Engineering, Report 068, 1966.
7. Levine, G.H.; et al: Resistance Tests of Great Lakes Bulk Carriers in Ice Clogged Channels, ARTEC report to Maritime Administration, 1972.
8. Nowacki, Horst: Great Lakes Winter Navigation -- Technical and Economic Analyses Vol. III: Parametric Studies. Report to Maritime Administration. University of Michigan, Department of Naval Architecture and Marine Engineering, Report 153, 1974.
9. Nowacki, Horst; Benford, Harry; and Atkins, Anthony: Great Lakes Winter Navigation -- Technical and Economic Analyses Vol. I: Methods of Analysis. Report to Maritime Administration. University of Michigan, Department of Naval Architecture and Marine Engineering, Report 151, 1973.
10. Swift, Peter M. and Benford, Harry: "Economics of Winter Navigation in the Great Lakes and St. Lawrence Seaway," Transactions SNAME, 1975.
11. Swift, P.M.; Nowacki, H.; Fischer, J.: "Estimation of Great Lakes Bulk Carrier Resistance Based on Model Test Data Regression," Marine Technology, SNAME, October 1973.

APPENDIX

Table 2 develops the relative economics of a standard Great Lakes ship operating over a normal (8-month) season with those of a comparable ice reinforced ship operating over extended seasons of 10 or 11-1/2 months. The table serves to illustrate how all of the pertinent components are put together in order to produce predicted values of several measures of merit.

Table 2 also shows the energy efficiency measured as ton-miles of cargo carried per gallon of fuel burned. As you will note, winter navigation is of no benefit in this regard. That conclusion will be misleading if the alternative is to ship goods by rail in the winter.

The table is taken from Reference 10 and is used with permission of the Society of Naval Architects and Marine Engineers.

Table 2
COMPARATIVE ECONOMICS OF WINTER NAVIGATION: A TYPICAL CASE

COMMON FACTORS			
Voyage:	Sept.-Iles to Cleveland		
Cargo:	Ore		
Winter weather:	Normal		
Voyage length:	1146 statute miles		
LBP:	715 ft (217.93 m)		
Summer draft:	25.5 ft (7.77 m)		
Beam:	75.0 ft (22.86 m)		
Depth:	37.5 ft (11.43 m)		
Block coefficient:	0.845		
Displacement, fresh water:	32,185 LT (32,701 MT)		
Cargo gear:	Shuttle-type self-unloader		
Loading speed:	4000 LT/hr, avg		
Unloading speed:	3000 LT/hr, avg		
Machinery:	Single-screw steam turbine, fixed-blade propeller		
Crew:	26		
Cost levels:	1972		
Freight rate (for NPV and yield):	\$4.25		
Specified yield (for RFR):	10% after tax		
Discount rate (for NPV):	8%		
Corporate tax rate:	48%		
Economic life & tax life:	35 years		
COMPARATIVE FACTORS			
	Ship I	Ship II	
	IC	IB	
Shaft horsepower	5,708	10,156	
Service speed, mph	15.5	17.8	
Invested cost	\$13,161,000	\$14,351,000	
<i>Weights</i>			
Steel weight, LT	6,664	6,713	
Outfitting weight, LT	573	573	
Conveyor weight, LT	339	339	
Bow thruster weight, LT	70	70	
Machinery weight, LT	478	638	
Light ship, LT	8,124	8,333	
Dwt @ 25.5-ft draft, LT	24,062	23,853	
Summer payload, ^a LT	23,789	23,539	
Ice season payload, ^a LT		20,688	
<i>Building costs (including profit)</i>			
Steel hull cost	\$ 6,468,000	\$ 6,508,000	
Outfitting cost	\$ 3,079,000	\$ 3,087,000	
Conveyor cost	\$ 700,000	\$ 700,000	
Bow thruster cost	\$ 150,000	\$ 150,000	
Machinery cost	\$ 2,764,000	\$ 3,906,000	
Total cost	\$13,161,000	\$14,351,000	
	Ship I	Ship II	
Operating season, months	8	10	11½
<i>Transport capacity & revenue</i>			
Round trips per season	32	39	44
Tons carried per season	686,000	885,000	980,000
Ann. rev. @ \$4.25 per LT	\$2,915,000	\$3,761,000	\$4,165,000
<i>Operating costs per year</i>			
Crew wages	\$ 401,000	\$ 516,000	\$ 603,000
Stores and supplies	\$ 13,000	\$ 16,000	\$ 18,000
Maintenance and repair	\$ 103,000	\$ 141,000	\$ 169,000
Insurance	\$ 117,000	\$ 178,000	\$ 245,000
Overhead	\$ 91,000	\$ 95,000	\$ 98,000
Towing	\$ 6,000	\$ 9,000	\$ 11,000
Layup	\$ 75,000	\$ 75,000	\$ 10,000
Fuel	\$ 374,000	\$ 736,000	\$ 874,000
Total operating costs	\$1,180,000	\$1,766,000	\$2,028,000
Annual cost of capital recovery ^b	\$1,765,000	\$1,925,000	\$1,925,000
Average annual cost	\$2,945,000	\$3,691,000	\$3,953,000
<i>Measures of merit</i>			
RFR, \$/LT	4.30	4.17	4.00
Net present value ^b	\$1,949,000	\$2,832,000	\$3,777,000
Yield	9.8%	10.4%	11.2%
<i>Energy utilization</i>			
Ton-miles per gallon	577	379	363

^a Other season payloads omitted here.

^b With tax-deferral privilege; see reference [6], section 2.9.

Note: RFR does not include tolls.



MECHANICAL PROPERTIES OF ICE
IN THE ARCTIC SEAS

W.F. Weeks and M. Mellor

SUMMARY

The mechanical properties are reviewed for the main types of ice in arctic seas (glacial (icebergs), shelf (ice islands), sea ice) and representative values are given. Each ice type possesses a characteristic range of structures and compositions that differentiate it from other varieties of ice and to a considerable extent, these produce large variations in mechanical properties. Factors affecting mechanical properties (temperature, brine and gas volume, crystal orientation and size, strain rate) are discussed, as are gaps, contradictions, and inadequacies in available data.

1. INTRODUCTION

Even pure ice displays complicated mechanical properties, largely because it exists in nature at high homologous temperatures, commonly above 0.95 and almost always above 0.90. When deformed at high strain rates or loaded for brief periods, it behaves elastically. By contrast, when strained slowly or when subjected to sustained loadings ice is ductile, and it can creep to large strains without breaking. At any given stage in such a creep process, the relation between strain-rate and stress is strongly nonlinear, i.e. ice is visco-plastic rather than linearly viscous. Because ice properties are highly sensitive to strain rate and temperature, strength can vary greatly. Furthermore, the general effects of multiaxial stress states, as represented by failure criteria, also change drastically with changes in temperature and strain-rate.

It is not our purpose to discuss the idealized properties of bubble-free, fine-grained, randomly oriented, pure ice in this paper. Instead we shall discuss the more complicated ice that occurs naturally in the sea. The sources of these materials are highly varied, ranging from ice sheets and valley glaciers (icebergs), ice shelves (ice islands), rivers and lakes (freshwater ice), and from the freezing of the sea itself (sea ice). This last material is the predominant ice type in the seas of the Arctic and it comes in a variety of types, each with its own characteristic association of grain sizes, crystal orientations, and gas and brine inclusions. We shall discuss briefly how each type develops, its internal structure and its associated mechanical properties. To do this fully is a task far beyond the present limitations of time and space. Here we simply attempt to provide a balanced, general feel for the current state of this subject

and a listing of some of the more useful references. In doing this we draw heavily on more exhaustive reviews that have already been published [1-7].

Current interest in the properties of ice in the sea is neither the result of such ice being an ideal material for study, nor of the desire of materials engineers to spend their spare moments visiting the arctic ice pack, with its mobile scenery and delightful climate. Ice in the sea is the primary obstacle to effective and safe removal of the presumed large oil and gas reserves of the continental shelves of the Arctic, as well as a barrier to development of new sea routes across the Pole that would result in great changes in current patterns of marine commerce. To overcome this barrier, it is essential that engineers understand both the behavior of ice in the sea as well as its pertinent properties.

2. STRUCTURE AND COMPOSITION OF ICE IN THE SEA

To understand the mechanical behavior of the varieties of ice that occur in arctic seas, one should first understand something about the structure and composition of these materials and also of pure ice. We now briefly review this subject, starting with pure ice, then glacier (iceberg) ice, then sea ice, and finally shelf (ice island) ice thereby moving from simple to complex structures and compositions. Most attention will be given to sea ice, in that it is the most important ice type in the majority of arctic marine areas. River and lake ice will not be discussed as they are not of major importance in most marine areas.

2.1 Ice Ih

Although there are several polymorphs of ice [8], ice Ih (so-called ordinary ice) is the only one of these that exists in significant quantities under the physical conditions encountered at the earth's surface. In fact, ice Ih (which will be referred to simply as ice) is the stable polymorph even at the bottom of the world's thickest ice sheets. Ice is unusual in comparison to most materials in that the solid phase is less dense than the liquid phase. Therefore, ice floats, forming a cover over the seas, lakes, and rivers of the Arctic, causing a variety of engineering and operational problems that have largely inspired this meeting.

The general atomic structure of ice is well understood as ice Ih was one of the first substances to have its structure determined [9]. Each oxygen atom is located at the center of a tetrahedron with four other oxygen atoms located at each of the apices

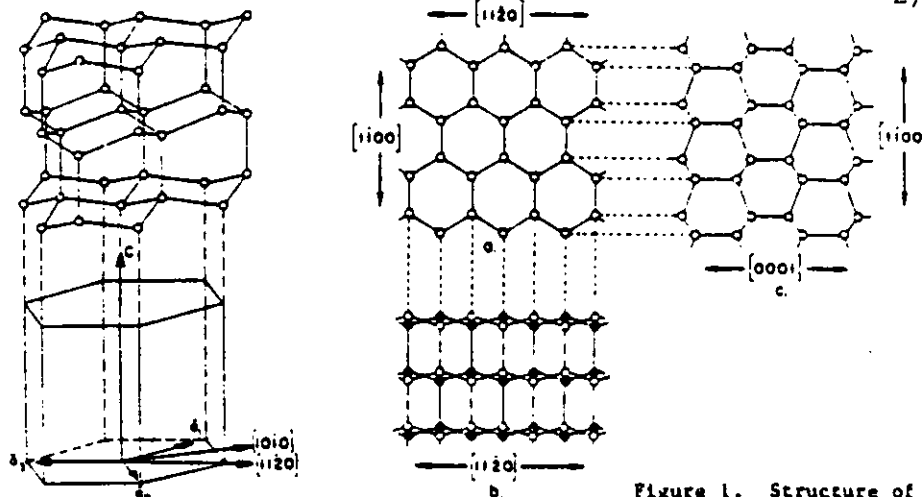


Figure 1. Structure of ice I.

(Figure 1). The tetrahedral coordination of the oxygen atoms produces an open, low density crystal structure with hexagonal symmetry. One important feature of this structure is that the oxygen atoms are concentrated close to a series of parallel planes, referred to as the basal planes. The direction perpendicular to these planes is the principal hexagonal axis, or c -axis. The arrangement is such that, in any unit cell which contains four oxygen atoms, fracture along the basal or (0001) plane involves the rupture of only two bonds, while fracture along any plane normal to this plane requires the rupture of at least four bonds. Therefore the observation that ice glides and cleaves readily on the basal plane can easily be explained in terms of its atomic arrangement. When the positions of the oxygen atoms are projected parallel to the c -axis, the resulting hexagonal array (Figure 1a) can be seen to be composed of three close-packed rows of atoms with each row paralleling the $\langle 11\bar{2}0 \rangle$ or a -axis directions. These directions, which are all equivalent, correspond to the directions of the arms of a) snow flakes growing from the vapor, b) dendritic sea ice crystals growing from the melt and c) internal melt features (Tyndall figures) that form inside ice crystals as the result of absorbed solar radiation. All are macroscopic manifestations of the atomic structure.

The structure of ice provides reasons for its characteristically low impurity content. For an impurity atom to occupy lattice sites in the atomic structure of an ice crystal, the impurity atom must be of a similar size and charge, and must form a similar type of chemical bond as the atom it is replacing. Impurities meeting these requirements for substitution into ice are rare. Possibilities are F^- , HF , NH_4^+ and NH_3 , NH_4OH , NH_4F and the hydrohalogen acids and, in fact, all of these substances do substitute in the ice structure in very small amounts (mole fractions of 1 in 5000 or less). However, such materials are not present in significant amounts in natural water bodies. The amount of other more common solutes that go into solid-solution in ice crystals is so small that ice formed by freezing even concentrated solutions can be considered pure. Therefore, the phase diagrams that govern the freezing of aqueous solutions are invariably of the simple eutectic type where the pure ice that forms initially is at equilibrium with increasingly concentrated solutions of brine as the temperature decreases.

2.2 Icebergs

In the Arctic, the primary source of icebergs is

the Greenland Ice Sheet, which contains $2.4 \times 10^6 \text{ km}^3$ of water, has a maximum thickness of 3300 m, and annually calves about 240 km^3 of ice into the surrounding seas. If all the other permanent ice fields located in the Canadian and Soviet Arctic and in Svalbard are taken together, they contain eight times less ice than Greenland. The iceberg production from these latter regions, although not well known, is certainly small and primarily of local importance (good examples are the small icebergs produced by the glaciers on Svalbard and the Soviet arctic islands [10]). Because of the distribution of iceberg sources, icebergs are not much of a problem in the North Pacific, the Bering Sea or most parts of the Arctic Ocean.

Estimates of the total number of icebergs spawned annually by the Greenland Ice Sheet vary from 20 to 34 thousand, with most being produced by west coast glaciers. The iceberg drift pattern is such that icebergs formed along the east coast usually drift around the southern tip of Greenland and then move north, joining the drift of the icebergs produced by the large outlet glaciers located along the west coast. This northern drift continues up to Baffin Bay, where the icebergs swing around and start moving south along the coasts of Baffin Island, Labrador and Newfoundland. They finally reach the Banks and ultimately melt in the North Atlantic. Although the southern limit of iceberg drift is in general defined by the northern edge of the warm ($>12^\circ\text{C}$) North Atlantic Current, icebergs have been known to transit this current in cold water eddies and have been sighted as far south as Bermuda and as far east as the Azores [11]. At present, concern about the drift and properties of icebergs is focused on the regions off the Baffin and Labrador coasts, on the Grand Banks, and to a lesser extent off the coast of West Greenland, especially in areas where exploration for offshore oil and gas is currently underway.

Few studies have been made of the characteristics of the ice in actual icebergs [11]. In the Antarctic this is not a major problem as the properties of most of the icebergs can, with some confidence, be inferred from the properties of the parent ice shelves which have been well studied [4]. Similar inferences cannot be made as readily in the case of Greenland icebergs, even though the Greenland Ice Sheet itself has been reasonably well studied. The reason for this difference is that in Greenland the inland ice invariably passes through the coastal mountains in outlet glaciers before forming icebergs. This usually produces strong deformation with resulting recrystallization changing both the crystal orientation and the grain size. The ice is then

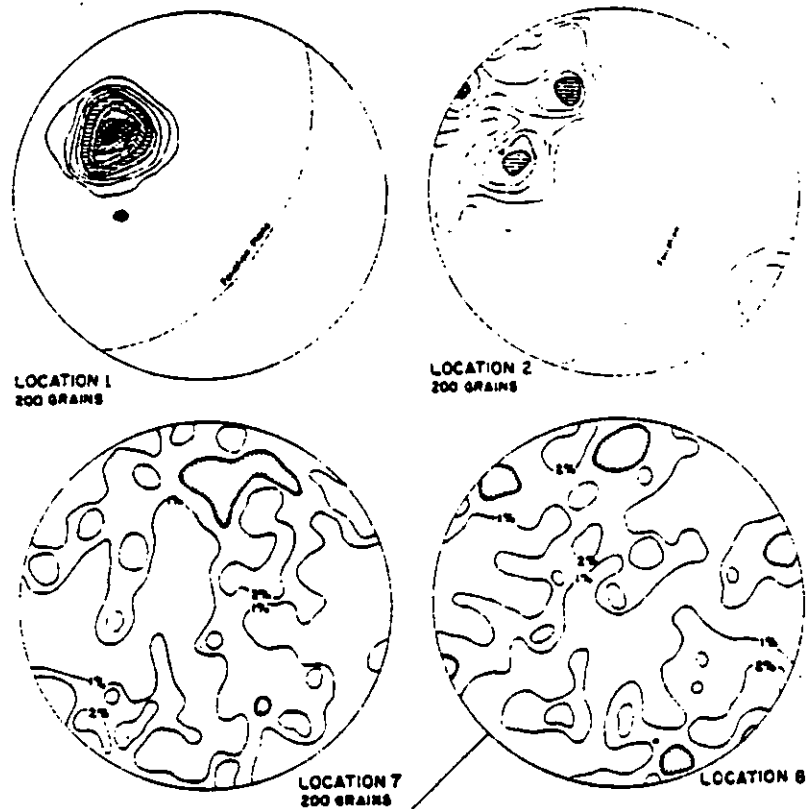


Figure 2. Four fabric diagrams of c-axis orientations in glacier ice from sites along the margin of the Greenland Ice Sheet [12].

comparable to a metamorphic rock. Figure 2 shows four fabric diagrams for ice from the margins of the Greenland Ice Sheet [12]. Two diagrams (locations 7 and 8) show a random pattern, indicating the absence of recrystallization in a strongly anisotropic stress field. Such fabrics are commonly observed in ice from the upper portions of large ice sheets, where representative crystal cross-sectional areas are 2 to 5 mm^2 . The third diagram (location 1) shows an extremely strong c-axis alignment normal to the foliation (i.e. normal to the plane of implied shear). Such strong single-pole alignments are usually found in fine-grained ice that is undergoing rapid shear deformation in either temperate or polar glaciers. The fourth diagram (location 2) is of the multimaximum type, in which the individual maxima are invariably within 45° of the center of fabric symmetry. Such multimaximum fabrics are believed to develop by recrystallization in strongly deformed ice that is at or near the pressure melting point [13]. Such fabrics would be expected to be common in Greenland icebergs, as the majority of Greenland outlet glaciers are believed to be temperate. For instance, fabrics from the Moltke Glacier, a major iceberg producer in NW Greenland, are of this type [12]. Associated with this recrystallization there is characteristically a pronounced increase in grain size with cross-sectional areas ranging between 100 and 1000 mm^2 . In contrast to the roughly equidimensional crystals commonly associated with the first two fabric types, the crystals showing the multimaximum fabric type are not only large, but show extremely complex interlocking shapes that makes their characterization by simple thin section analysis both difficult and time-consuming [14].

Changes in crystal alignment are usually associated with changes in characteristics of the air

bubbles present in the icebergs. Ice with random c-axis orientations generally has rounded bubbles up to about 2 mm in diameter. In anisotropic ice, air bubbles tend to be tubular, with diameters between 0.02 and 0.18 mm and lengths up to 4 mm [15]. As gas pressures in bubbles in glacier ice are commonly equal to the hydrostatic pressure at a specific depth, the gas pressures in bubbles in icebergs would be expected to vary from 20 bars (roughly equal to the maximum tensile strength of ice) to some lower value, depending upon ice relaxation and gas leakage. In fact, gas pressures ranging from 2 to 20 bars have been observed [11].

As the firn limit (snowline) in Greenland is at roughly 1400 m, little or no snow or permeable ice is found in Greenland icebergs, and the ice density is presumably reasonably uniform in the range of 880-910 Mg/m^3 [16]. This means that between 86 and 89% of these icebergs are submerged (as compared to about 83% submergence for Antarctic shelf icebergs which contain snow in their upper levels).

2.3 Sea Ice

Sea ice, formed by the freezing of sea water, is different from glacier ice in both structure and composition. In contrast to glacier ice, where chemical impurities are commonly at concentrations of parts per million or lower, sea ice salt concentrations (salinities) are invariably in the parts per thousand range. The ice structure is also quite different, exhibiting a characteristic defect structure within each sea ice crystal associated with the entrapment of impurities, and also strong, distinctive crystal alignments caused by directional growth. In the Arctic, there are pronounced changes

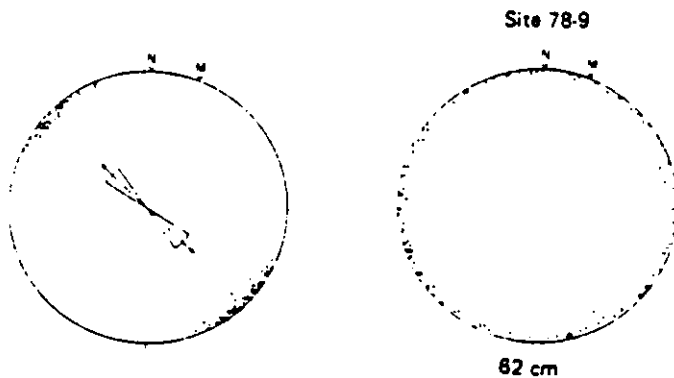


Figure 3. Representative fabric diagrams for sea ice collected along the coastline of arctic Alaska: a) random c-axis distribution in the horizontal plane, Cape Thompson, b) preferred c-axis alignment in the horizontal plane, Kotzebue Sound [20].

In the properties of the sea ice that has survived one or more summer melt seasons (so-called multi-year ice). We therefore discuss the structure and composition of several different types of first year ice, of multi-year ice and of the highly deformed ice that composes pressure ridges.

Structurally, first-year sea ice is similar to a cast ingot. There is an initial skim, then a transition zone where rapid changes in crystal orientation occur, and a columnar zone formed of long crystals oriented vertically (parallel to the direction of the heat flow). Although the structure of the initial skim and the transition zone are interesting from the point of view of crystal growth, these layers are quite thin (the base of the transition layer is usually less than 30 cm below the upper surface of the ice sheet). For present purposes we only consider the properties of ice in the columnar zone. In fact, there have been no specific studies made of the mechanical properties of the ice above the columnar zone.

The structure of ice in the columnar zone is fairly uniform, with essentially all the crystals having pronounced elongation in the direction of growth. The crystal orientation is invariably c-axis horizontal, as crystals in this orientation have a growth advantage over crystals oriented in other directions (their direction of maximum thermal conductivity is oriented parallel to the direction of heat flow [1, 17]). For years it was believed that the c-axis orientations in the columnar zone were always random in the horizontal plane [6] as a number of such fabrics had been observed. Such a material would be transversely isotropic; it would show property variations in the vertical direction associated with changes in grain size, crystal substructure, and salt content, but at any given level all directions in the horizontal plane would be identical. However, recent studies [18-21] have shown that most of the fast ice occurring over the continental shelves of the Arctic shows strong c-axis alignments within the horizontal plane. Theory, field observations and experiment [19, 22] suggest that these alignment directions are controlled by the direction of the current at the ice-sea water interface. Figure 3 shows two representative fabric diagrams for sea ice, the first showing a random c-axis orientation in the horizontal plane, the second a strong c-axis alignment. In a recent study of c-axis orientations along the Alaskan coast, over 95% of the sites sampled showed strong crystal alignments [20]. At first sight it might appear that such alignments would only develop in fast ice areas. However, observations

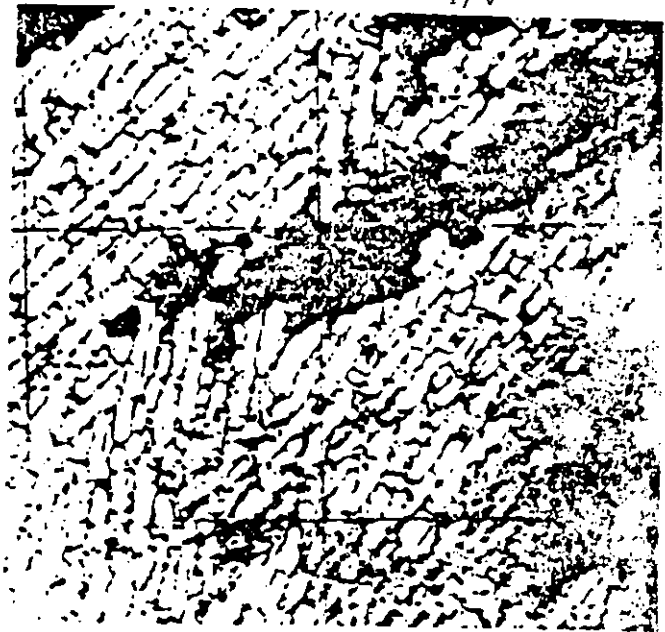


Figure 4. Photomicrograph of a thin section of sea ice showing its characteristic substructure. Grid spacing equals 1 cm.

suggest that strong alignments can develop in the pack [18, 23] if there is little rotation of the floes relative to the current direction. Such conditions do exist well offshore in the Arctic Ocean. Sea ice with such alignments is orthotropic, showing property differences along three orthogonal axes.

Associated with selective grain growth in the upper portion of the columnar zone is a marked increase in grain size with depth [1, 24]. Limited data suggest that mean grain diameter is proportional to depth in sea ice less than 50 cm thick. Mean diameters range from 0.5 to over 2 cm [6]. In thicker ice the linear increase in grain diameter with depth becomes less clear, and some decreases with depth have been observed [25]. In ice that has developed a strong c-axis alignment, it becomes difficult to distinguish one crystal from another orientation differences are less than 5 degrees.

The most distinctive feature of sea ice, in addition to its high salt content, is the substructure within the ice crystals. In the columnar zone each sea ice crystal is composed of a number of ice platelets that are joined together to produce a quasi-hexagonal network in the horizontal plane. This substructure, shown in Figure 4, results from crystal growth with a non-planar solid-liquid interface. Similar substructures are commonly produced during the solidification of impure melts. In fact, it is the entrapment of brine between the ice plates at the non-planar interface that causes sea ice to be salty. The spacing (measured parallel to the c-axis) between the brine pocket arrays (a_0) is commonly referred to either as the brine layer spacing or as the plate spacing, and it varies inversely with growth velocity [1, 26]. Typical a_0 variations range from 0.4 mm near the upper surface of the ice sheet to 1.0 mm at the base of the 2 m ice sheet. The best available study of these variations [27] was made recently at Eclipse Sound in the Northwest Territories. The results are shown in Figure 5. The inverse relation between a_0 and growth velocity is clear. In thick multi-year sea ice, which presumably grows very slowly, a_0 values of 1.5 mm have been observed. In the sea ice forming on the bottom of the Ross Ice Shelf at a location where the shelf is

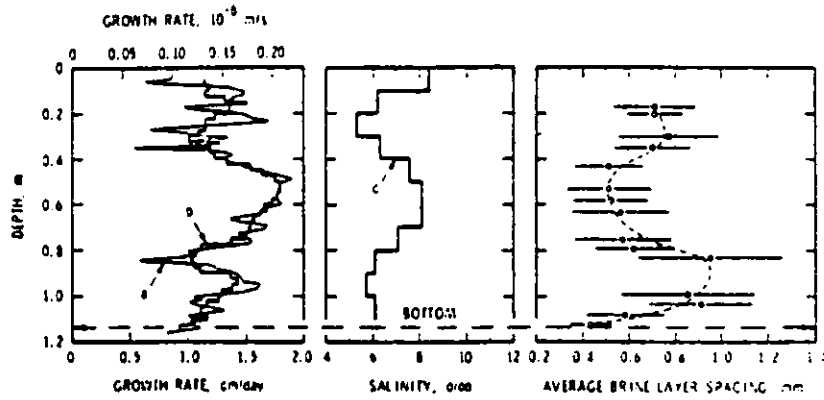


Figure 5. Profiles of growth rate, salinity and brine layer spacing. Curve b represents the mean of the calculated growth rate, curve a, for an interval of ± 50 mm for every 25 mm [27].

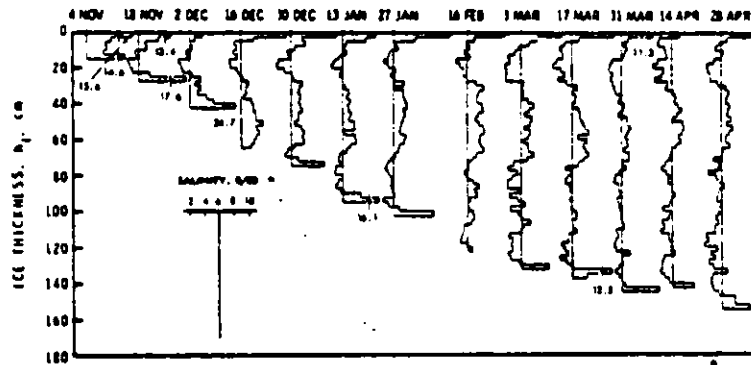


Figure 6. Salinity profiles of ice of Eclipse Sound made at two week intervals during the winter of 1977-78. Scale for salinity is shown in insert. Vertical solid lines represent a value of 6 ‰ and are given as reference [31].

416 m thick and the ice only grows about 2 cm/year, a_0 values of 5 mm have been noted [28]. Brine layer spacing is believed to affect the strength of sea ice [29].

As mentioned earlier, the salt in the sea ice is not the result of solid solution, but is caused by the entrapment of brine between the platelets of pure ice that compose individual crystals of sea ice. The amount of salt entrapped is not constant, but varies systematically with the salinity of the water being frozen and with the ice growth velocity. Very slow growth results in near-total rejection of salt from the ice, while very rapid freezing causes near total entrapment [1, 30]. The effect of changes in growth rate on ice salinity can also be seen clearly in Figure 5. A series of representative salinity profiles for first year sea ice is shown in Figure 6 [31]. Note that the upper and lower portions of the ice characteristically have higher salinities than the ice in between, and there is a gradual decrease in the mean salinity of the ice with time.

The drainage of brine from saline ice appears to be a complicated process and several different mechanisms are believed to be involved [1]. In the present context, the most important results of brine drainage are changes in the porosity and the development of brine drainage channels. These structural features, one of which is shown schematically in Figure 7, can be considered as tubular "river"

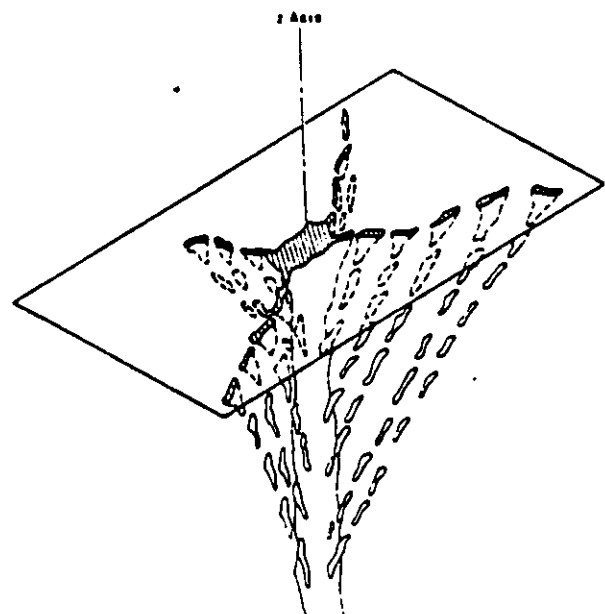


Figure 7. Schematic drawing of a cut through a brine drainage channel [32].

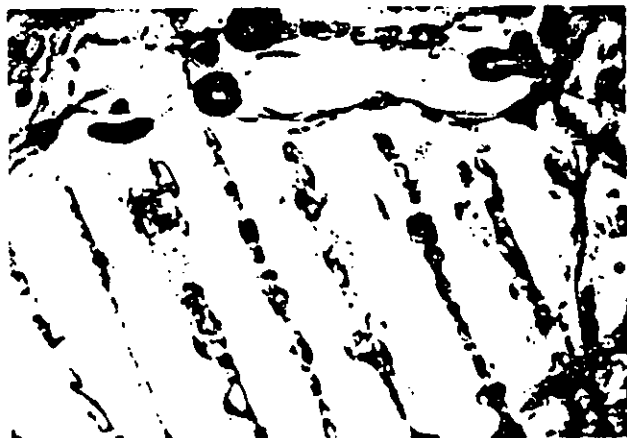


Figure 8. Shapes of brine pockets: a) horizontal view (brine layer spacing is approximately 0.5 mm), b) vertical view. Ice is from Thule, Greenland.



Figure 9. Scanning electron micrograph of a vertical section of a brine pocket at -30°C [35].

shapes of a series of brine pockets; they commonly are rather complex. The dark circles are gas bubbles. At lower temperatures there also are several different solid salts that precipitate in the ice (-8.7 , $\text{Na}_2\text{SO}_4 \cdot 10\text{H}_2\text{O}$; -22.9 , $\text{NaCl} \cdot 2\text{H}_2\text{O}$; -36.8 KCl ; etc). Figure 9 is a scanning electron micrograph of a vertical section of a brine pocket at -30°C showing the solid salt crystals [35]. The effect of these solid salts on the mechanical properties of sea ice has been studied surprisingly little.

In addition to columnar sea ice, there is one other type of first-year undeformed sea ice that should be mentioned. This is frazil ice, produced by accumulation of individual discs and spicules of ice that form in the water. It has commonly been thought that, although frazil ice is frequently observed during the formation of the initial ice cover, once this cover stabilized frazil ice generation would greatly decrease. Exceptions to this would be areas near the ice edge or in large polynyas where substantial regions of open water are found. However, recent work in the Weddell Sea to the east of the Antarctic Peninsula has indicated that, at least in that region, frazil ice generation is a very important ice producing mechanism [1, 36]. For instance, of the ice sampled, over 50% was frazil and the thicker the floe, the higher the percentage of frazil ice it contained. Whether such large amounts of frazil also occur in the Arctic is not known but there is no strong evidence against such a possibility. If major quantities of frazil ice form in the Arctic, there are interesting implications. First, because frazil ice forms by a completely different mechanism than columnar ice, present estimates of the amount of ice being generated in the Arctic might have to be revised. Secondly, frazil ice has a completely different crystal structure than does columnar ice. Structurally, frazil ice is commonly fine-grained, with crystal sizes of 1 mm or less, it has a crystal orientation which is presumed to be random, and there are brine pockets located mainly between the ice crystals, as opposed to within crystals. Although there have not yet been any systematic studies of the physical properties of frazil ice, they clearly would be expected to be different from those of columnar sea ice.

When sea ice goes through a summer melt period it undergoes a pronounced change in salinity produced by the percolation of relatively fresh surface melt-water down through the ice. The result is an ice sheet with very low salinities (<1 ‰) in the portion above water level and salinities of between 2 and 3.5 ‰ in the portion below water level.

systems in which the tributaries are arranged with cylindrical symmetry around each main channel [32-33]. Representative channel diameter at the bottom of a 1.55-m-thick ice sheet is 0.4 cm and there is, on the average, one channel every 180 cm^2 . Channel diameters as large as 10 cm have been noted, though most diameters range between 0.1 and 1 cm. Although these large "flaws" presumably have an effect on the mechanical properties of sea ice, no studies have been made of the matter.

Given a sample of sea ice with a specified salt content, the amount of liquid brine (the brine volume) present in the ice is a function of temperature only, because at each temperature the composition of brine in equilibrium with the ice is specified by the phase diagram [34]. Changes in the volume of brine in the sea ice are most pronounced near the melting point, where small changes in temperature cause large changes in brine volume. As most first-year sea ice has salinities in the range of 4 to 12 ‰ and temperatures between -2 and -30°C , the brine volume v can be expected to vary between 30 and 300 ‰. Figure 8 shows detailed

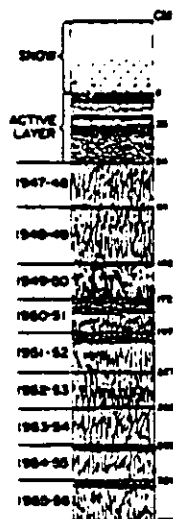


Figure 10. Cross-section of a multi-year floe [37].

Once the brine has drained from the upper portion, the ice is quite porous and it may recrystallize. Ice that has survived several summers ultimately becomes a layercake of the annual layers formed during successive winter periods of growth [37-38]. A cross-section of such a floe is shown in Figure 10. In fact, much multi-year ice was probably deformed at some time in its past and would show a much more complex cross-section. Confident statements concerning the relative percentages of multi-year ice that are undeformed, deformed, columnar or frazil will have to await more adequate sampling. In general, undeformed multi-year ice in the Arctic Basin is believed to reach a steady-state thickness of 3 to 5 m, at which time the thickness abated during the summer equals the thickness grown during the winter [39]. Although deformed sea ice can grow to greater thicknesses, rather atypical conditions are required and such ice, although known, would appear to be rare [40].

Ice thicker than 5 m is, however, rather common in the Arctic Basin. For instance, in a recent study of submarine sonar profiles of the underside of sea ice, over 40% was thicker than 5 m [41]. This thicker ice is generally believed to be pressure ridges and rubble fields that are produced by the deformation of thinner ice. Pressure ridges and deformed ice in general are common in all areas of pack ice, and are particularly common in the land-locked Arctic Ocean. Although data are limited, it currently appears that the most highly deformed, and also the thickest, ice in the Arctic occurs in a broad band starting off the NE corner of Greenland and stretching to the West, north of Ellesmere Land and then veering toward the SW down the coast of the Archipelago to the coast of Northern Alaska. The largest free-floating ridges that have been observed have sails up to 13 m high and keels up to 47 m deep. In near-coastal areas where pressure ridge keels can ground, ridge sails can be particularly high (heights in excess of 30 m have been noted [41]).

Considering the importance of ridges, there has been surprisingly little work done on them. As first-year ridges are composed of blocks, it would be interesting to have quantitative information on block block sizes and orientations from a variety of different locations and on the degree of bonding between the blocks. A limited amount of information is available for the first of these [42] but there is nothing on the latter. However it should be possible to obtain useful information on this subject from ramming tests with an icebreaker. In contrast to



Figure 11. Thin section of ice from a multi-year ridge in the Beaufort Sea showing a block of columnar ice "cemented" by fine grained granular ice. Core is 10.5 cm in diameter [43].

first-year ridges, multi-year ridges are commonly composed of massive ice, in that all the voids present in newly formed ridges have now been filled with ice. Figure 11 shows thin sections of ice from a multi-year ridge. The ice is quite complex, showing fragments of the initial ice cover that was crushed to form the ridge, plus a large amount of fine grained ice (presumably similar to frazil) that formed in the voids between the blocks [43].

2.4 Ice Islands

So called ice islands are, in fact, tabular icebergs from a relict Pleistocene ice shelf that still exists along the north coast of Ellesmere Island, the northern-most island in the Canadian Archipelago. Strictly speaking, ice islands are just a specific type of shelf iceberg, but we will discuss them in a separate category as they are unique to the Arctic Ocean and are composed of a rather complex mix of ice types. They are a particular hazard along the coasts of Northern Greenland, the Canadian Archipelago, and off the North Slope of Alaska. Ice islands can have long lifetimes. For instance, the best known ice island T-3 has been drifting around the Beaufort Gyre (the large clockwise circulation in the Beaufort Sea) for over 30 years. If current predictions of its trajectory are correct, T-3 may "die" within the next year by leaving the Arctic Ocean via the East Greenland Drift Stream and melting in the North Atlantic. Ice islands also have been known to leave the Arctic Ocean via Robeson channel (between Greenland and Ellesmere Island) and also through the Canadian Archipelago into Viscount Melville Sound. It is only after they leave the Arctic Ocean that they drift through regions where ordinary icebergs produced by glaciers are common.

As their origin is an ice shelf, ice islands are tabular with thicknesses of several tens of meters (T-3 had an initial thickness of approximately 70 m). Lateral dimensions are highly variable ranging from more than 10 kilometers to a few tens of meters for ice island fragments. There is no adequate census of the number of ice islands currently drifting in the Arctic Ocean. The numbers "sighted" at specific locations are highly variable. For instance in 1972, 433 ice islands were sighted along the Beaufort Coast. Of these 117 had lateral dimensions greater than 30 m and 1 had dimensions of over 1600 m. In 1975 there were no sightings along the same stretch of coast. It is generally believed that the large number of fragments seen in 1972 was the result of the breakup of a very large ice island

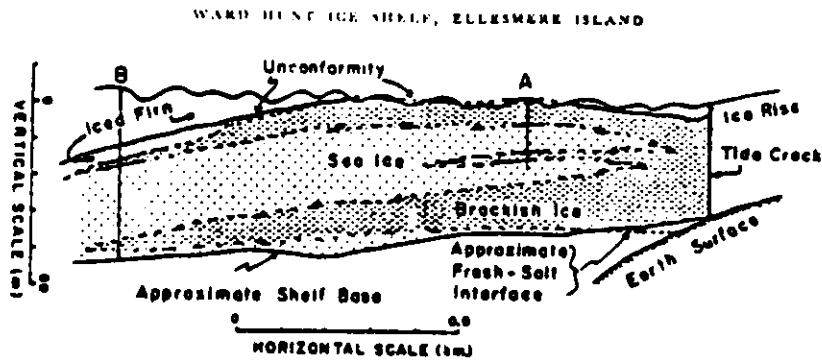


Figure 12. Interpretation of stratigraphy of part of Ward Hunt Ice Shelf, based on drill-core and laboratory studies [50].

that grounded north of Barter Island. The current interest in ice islands results from the threat they pose to offshore structures in the deeper waters of the Beaufort Shelf. The ice island problem is similar to that posed by large hurricanes in the Gulf of Mexico in that although the probability of a given structure being impacted by an ice island is small, the probability of the structure sustaining damage if a collision does occur is high.

Although the ice in ice islands has not been extensively studied, enough is known to be able to give a general description of the several different types involved [44-50]. The complex structures encountered in some ice islands can best be appreciated by referring to Figure 10 in Smith's study of Arlis II [47] and to Figure 12 which is presented here and which summarizes the Lyons et al. [50] picture of the structure of the ice in part of the Ward Hunt Ice Shelf. There are at least four different types of ice present. These are as follows:

Lake ice - The lake ice is the result of the freezing of elongated bodies of water that form on the surface of ice islands during the melt season. The ice can be easily recognized by its medium to very coarse grained texture, the long columnar crystals with straight grain boundaries and the long, linear, well oriented bubbles. Typical grain diameters are larger than 3 cm.

Snow ice - This ice type, which composes much of the upper part of the Ellesmere Shelf, is produced by the densification and recrystallization of snow. The crystals are equant and euhedral showing a typical mosaic texture. Crystal orientations are random and grain sizes characteristically range from 0.5 to 1.5 cm.

Sea ice - Sea ice usually occurs in the lower portion of the ice shelf. This material has the characteristics of multi-year sea ice, although the salinities are somewhat lower ($< 2 \text{ ‰}$). The crystals show the characteristic elongation of columnar zone sea ice and the substructure within each crystal is still evident. Some fine grained frazil ice has also been reported. In two cases [47, 49] strong preferred c-axis alignments have been noted.

Brackish ice - This ice shows a well developed stratification, which is a reflection of cyclic variations in the amount of entrapped gas and the average grain size. Typical layer thicknesses are between 20 and 25 cm, and the strata may locally be warped into a series of folds. Very large crystals are common, with some as large as 120 cm. C-axis orientations commonly are vertical and salinities are usually very low. Although several different explanations have been advanced to account for such unusual ice, the most likely explanation is that this material developed is a series of annual growth

layers that formed from the freezing of a layer of brackish melt water that is known to be present beneath the ice shelf at some locations [50]. This explanation can account for both the complex inter-stratification of this ice with normal sea ice, and for the measured oxygen isotope ratios.

3. MECHANICAL PROPERTIES

3.1 General behaviour

Systematic knowledge of the mechanical properties of ice derives mainly from studies of non-saline polycrystalline ice which is not strongly anisotropic. The principal motivations for study have been glaciology, where the chief concern is with flow under small deviatoric stresses ($< 0.2 \text{ MPa}$), and engineering, where the emphasis is on strength at relatively high strain rates ($> 10^{-6} \text{ s}^{-1}$). It is now possible to unify the findings from these areas of study [51], especially since it has been demonstrated that the favoured test of glaciology, the constant load creep test, can give essentially the same information as the favoured test of ice engineering, the constant strain rate strength test [52,53].

In simple terms, ice had the following characteristics.

1. Under moderate hydrostatic pressure and moderately low temperature, ice compresses elastically with a bulk modulus of about 9 GPa. Any bubbles in the ice compress so as to equilibrate in accordance with the gas laws, and they may eventually disappear to form a clathrate. Under sufficiently high pressure, ice Ih transforms into high density polymorphs (including water), as described by the phase diagram for isothermal compression. Under intense adiabatic compression (e.g. explosive loading), discrete phase transitions are not detected, but the Rankine-Hugoniot characteristic gives a pressure-volume relation that is not much different from a "smeared-out" version of the Bridgman isotherm.

2. Under deviatoric stress, ice deforms as a non-linear viscous solid, changing its fabric and structure in the process. Under constant stress, a complete creep curve shows deceleration followed by acceleration to a final rate in the usual way, although there are possible complications. Under constant strain rate, a complete stress/strain curve shows stress rising to a peak before falling and tending asymptotically to a limit, again with a possible complication in the form of an initial yield point. For any given stage of deformation, the stress/strain-rate relation is non-linear. It is usually given as a simple power relation, although the exponent changes over the complete range of

stresses and strain rates. Below about -10°C the effect of temperature can be described by an Arrhenius relation with an activation energy of about 70 kJ/mole. However, closer to the melting point, temperature sensitivity is greater than such an equation would predict.

3. High sensitivity to strain rate and temperature causes ice to display a broad range of rheological properties. With high rates and low temperature, elastic behaviour dominates, and deviatoric straining culminates in brittle fracture. With low rates and high temperatures, ductility is predominant, and large creep deformations can occur. Very often both elasticity and non-linear viscosity make significant contributions to deformation and rupture processes.

4. In multiaxial stress states, compressive bulk stress (isotropic component of stress tensor) has little effect on the deviatoric stress/strain-rate relation when stress deviators are very low and temperature is well below 0°C . By contrast, moderate pressure suppresses internal microcracks at high strain rates, and it increases deformation resistance and "strength." Extreme pressure at typical temperatures pushes ice towards the phase transformation to water, and consequently deformation resistance and "strength" decrease with increasing pressure, almost irrespective of the magnitude of deviatoric stress or strain rate.

Strength and deformation resistance are influenced by strain rate, temperature, porosity and grain size in the following way.

Strain rate. Deformation resistance and "strength" increase with increase of imposed strain rate. Conversely, strain rate $\dot{\epsilon}$ increases with increase of imposed stress σ . In either case, $\dot{\epsilon} = \sigma^n$, where n might range from 2 at very low stress (< 0.01 MPa) to 4 at high strain rates ($> 10^{-3}\text{s}^{-1}$).

Temperature. When ice is truly "solid" (below -10°C for non-saline ice, or below the eutectics of dissolved impurities), strain rate $\dot{\epsilon}$ for a given stress σ can be described by a relation of the form $\dot{\epsilon} = \exp(-Q/RT)$, where T is absolute temperature, R is the gas constant, and Q is an activation energy for the controlling deformation process, say 70 kJ/mole for diffusional creep. The corresponding relation for σ is obtained from the $\dot{\epsilon}$ - σ relation (the power law). At temperatures close to 0°C , all polycrystalline ice has liquid, or liquid-like transitional layers, at the grain boundaries. Thus there are additional thermally activated processes influencing strength and deformation, and the simple Arrhenius relation does not apply.

Porosity. In simple terms, strength and deformation resistance decrease with increasing porosity. For the complete range of material properties from dense, impermeable ice to highly compressible, permeable snow, there is a continuous decrease in strength and in deformation resistance. In saline ice, porosity is created by both air bubbles and brine cells. The effect of variations in the size and shape of pores has not received much experimental attention, although it is a tempting topic for theoretical speculation.

Grain size. Where elastic deformation and brittle fracture are significant contributors, strength σ decreases with increasing grain size d , and there is support for the idea that $\sigma = d^{-1/2}$. There are indications that coarse-grained ice may fracture and yield at strains smaller than the yield strains for fine-grained ice. In the range where ductility dominates, there is not yet any convincing evidence that strength and deformation are much affected by grain size.

Another factor to be considered is the size of the stressed volume, since non-metallic brittle solids typically get weaker as volume increases (increasing the probability of encountering bigger flaws). Published data for ice on this topic cover only a narrow range of volumes, but it is to be expected that fracture strength will decrease with increasing volume at high strain rates (where cracks and similar flaws control the failure). The deformation resistance is not expected to be much affected by size at very low strain rates (where the controlling flaws are thought to be dislocations).

Perhaps the most difficult variables to deal with are anisotropy and inhomogeneity. Studies of anisotropy are not very far advanced, so it is dangerous to venture generalizations. However, there is not much doubt that ice with preferred crystal orientation flows most easily when the resolved stress is parallel to the basal planes of the crystals. With high strain rates and multiaxial stress, the "strength" of columnar ice varies depending on whether the stress field is tending to push the columns together or apart.

Ice testing and experimental data. Under the best of circumstances, most mechanical tests are much more complicated than their textbook idealizations. When typical tests are applied to ice, the problems are magnified by thermal instability of the material (melting, evaporation, brine drainage, vapour and surface diffusion) and by high sensitivity to rate and temperature (changing the balance of elasticity and plasticity).

An international group has been trying for the last decade to bring some order to ice testing, but the standards of experimental work are still highly variable. For the present we have to use results from some test programs that are obviously flawed, and it is necessary to be aware of common sources of error and misunderstanding. The following points might be kept in mind when considering the data given in the remainder of this paper.

1. For tests near 0°C , lax temperature control can introduce large errors.
2. For high rate/low temperature tests (elastic/brittle), great care and very precise technique are needed to avoid errors.
3. For tests to large strains, special procedures are needed to produce representative results.
4. Most of the indirect tests, in which some material properties must be assumed, cannot be used to investigate rate and temperature effects. For example, the assumption of elasticity in beam flexure or disc compression is hard to justify when rates are low or temperatures high.
5. Blind application of test procedures from other technical fields can give misleading results (e.g. use of quasi-static tests to measure Young's modulus).
6. Large-scale field tests (e.g. on floating beams or cantilevers) can involve material which is inhomogeneous, anisotropic, and subject to appreciable temperature gradients.

There have been no truly comprehensive test programs covering all the variables in a systematic way, and so a certain amount of intelligent guesswork is needed in order to extrapolate and interpolate from the existing data. However, the broad picture is now starting to emerge, and any given set of data can be checked for consistency and plausibility against a variety of independent data sets.

3.2 Iceberg Ice

There are virtually no published data on mech-

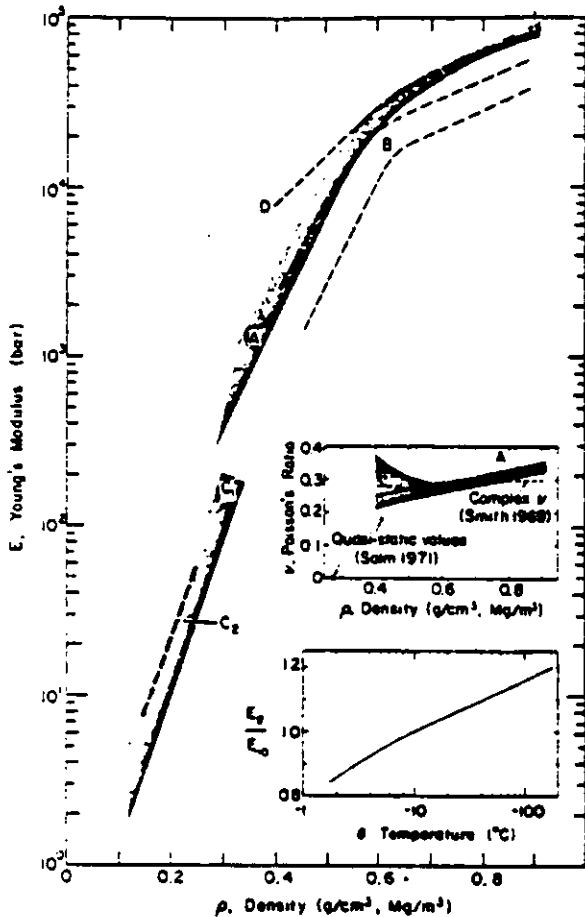


Figure 13. Summary of Young's modulus data for non-saline ice and snow (for data sources see [63]).

anical properties of ice that has been collected from icebergs, but there is plenty of information about glacier ice, which is what icebergs consist of. Over the interior areas of Greenland and Antarctica, glacier ice forms by a sedimentation process involving visco-plastic compaction of dry snow. The resulting material is fine-grained and almost isotropic, with included air which forms closed bubbles when the bulk density reaches about 0.8 Mg/m³. Only in the layers very close to the glacier bed is there significant shearing, with consequent development of preferred crystal orientation, but when ice from the interior is funneled out to the sea through ice streams and valley glaciers there is more general shearing, and some inclusion of rock debris. Therefore, in lieu of data on ice from actual icebergs we have to be content with a summary of the properties of glacier ice, of artificial ice which simulates isotropic polar glacier ice, and of some other types of non-saline ice.

Elastic moduli. For polycrystalline ice of low porosity (density $\rho = 0.917 \text{ Mg/m}^3$), high frequency dynamic measurements of Young's modulus E give values of approximately 9.0 to 9.5 GPa in the temperature range -5 to -10°C . Careful measurements of the initial tangent modulus for quasi-static uniaxial compression tests give quite similar values [54-57]. As temperature decreases, E increases nonlinearly (Fig. 13), but the effect is small for "true" Young's modulus (as opposed to "effective" values of E which include creep effects). Porosity α , which can be expressed alternatively as bulk density ρ , has a significant influence on E (Fig. 13), and it is interesting to note that E drops sharply below the density which represents close-packing of equant grains ($\rho = 0.55 \text{ Mg/m}^3$).

Poisson's ratio ν , as measured by dynamic tests, has values close to 0.3 for non-saline ice of low porosity (Fig. 13), and there is not much variation with porosity over the range where the material is regarded as "ice" rather than "snow" ($\rho > 0.8 \text{ Mg/m}^3$). Bulk modulus K is

$$K = E/3(1-2\nu) = E$$

and the shear modulus G is

$$G = E/2(1+\nu) = 0.38E$$

In ice engineering it is frequently necessary to apply elastic analyses in situations where the ice deformation is not purely elastic. In such cases, it may be appropriate to use "effective" moduli derived from relatively slow quasi-static tests. Because these effective moduli (E') represent the combined effects of elasticity, recoverable "delayed elasticity," and irrecoverable creep, they are appreciably more sensitive to temperature, strain rate and vibrational frequency than is Young's modulus E . At low temperatures and/or high strain rates, $E' = E$, but at low strain rates ($\sim 10^{-2} \text{ s}^{-1}$) or relatively high temperatures ($\sim -10^\circ\text{C}$), E' may be as low as 25% to 30% of E . When low strain rates are combined with temperatures approaching 0°C , E' can have very low values, and the elastic approximation may cease to be useful. In comparison with the effects of temperature and strain rate on E' , porosity variations over the typical range are not very significant, but there is a slight decrease of E' with increase of α (decrease of ρ).

"Effective" values of Young's modulus E' should be paired with "effective" values of Poisson's ratio, ν' . Although ν' does not receive explicit treatment in the literature, some deductions can be made [2]. As ductility increases it is reasonable to expect $\nu' \rightarrow 1/2$, representing incompressible flow, with $E'/K \rightarrow 0$. For ice which has low porosity (or water-filled pores) the bulk modulus K should not vary much with porosity, temperature, or strain rate, and for a first approximation it can be assumed equal to the true Young's modulus for zero porosity, E_0 . Thus ν' can be expressed as

$$\nu' = \frac{1}{2} - \frac{1}{6} \frac{E'}{E_0}$$

which gives a systematic variation between the limits $1/3$ and $1/2$.

Strength and deformation resistance. Strength for any specified state of stress can be defined as the maximum stress, or deformation resistance, for a given strain rate. For ductile yielding of fine-grained ice, constant strain rate strength tests give essentially the same information as constant stress creep tests, so that "strength" can be obtained from either the peak of a conventional stress/strain curve or the inflection point of a conventional creep curve [52, 53].

The most common test is uniaxial compression. Uniaxial compressive strength σ_c for non-saline ice at -5° to -10°C varies by three orders of magnitude (0.01 to 10 MPa) as strain rate varies from about 10^{-11} to 10^{-2} s^{-1} . At high strain rates, σ_c is not highly sensitive to temperature, and at very high rates the temperature effect is expected to be comparable to that for Young's modulus (Fig. 14). At very low strain rates, the variation of σ_c with temperature (Fig. 14) can be deduced from the dependence of minimum creep rate on temperature (Fig. 15). Because the stress/strain rate relation is the same for constant strain rate and constant stress (Fig. 16), the stress/strain-rate relations developed by

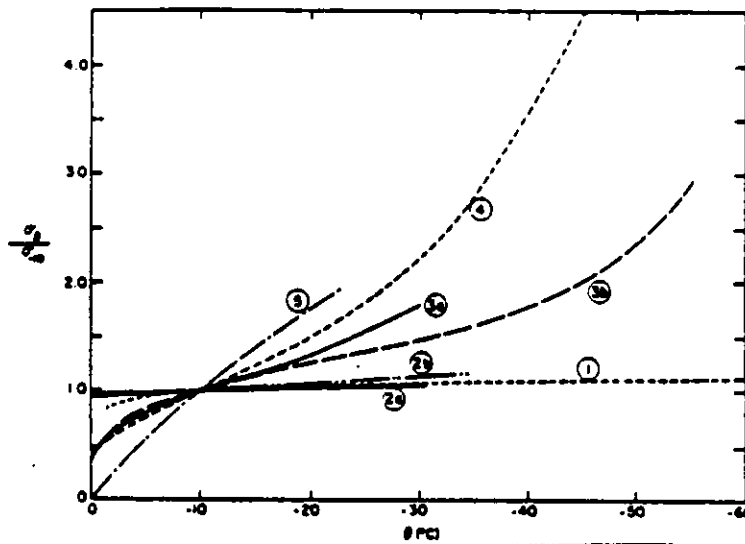


Figure 14. Compilation of temperature relationships [2]. All stress values are normalized with respect to the value for -10°C . 1) Variation of Young's modulus with temperature. 2a) Uniaxial tensile strength - data from [58]. 2b) Uniaxial tensile strength - data from [59]. 3a) Uniaxial compressive strength - data from [58]. 4) Ductile yield stress - data from [60]. 5) Pressure for phase transition from Ice Ih to water under isothermal hydrostatic compression.

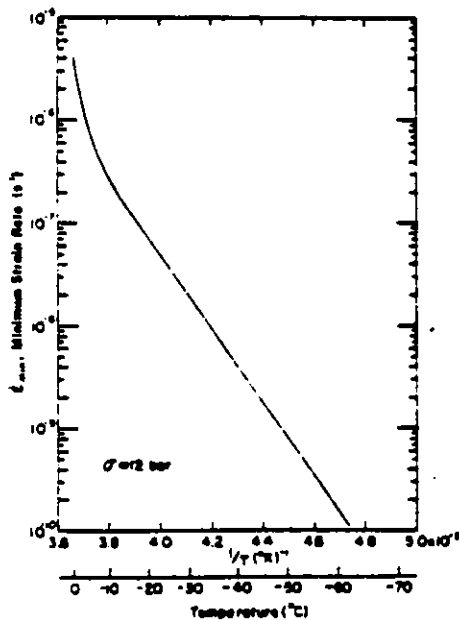


Figure 15. Empirical relation between minimum strain rate and temperature for high-stress creep [60].

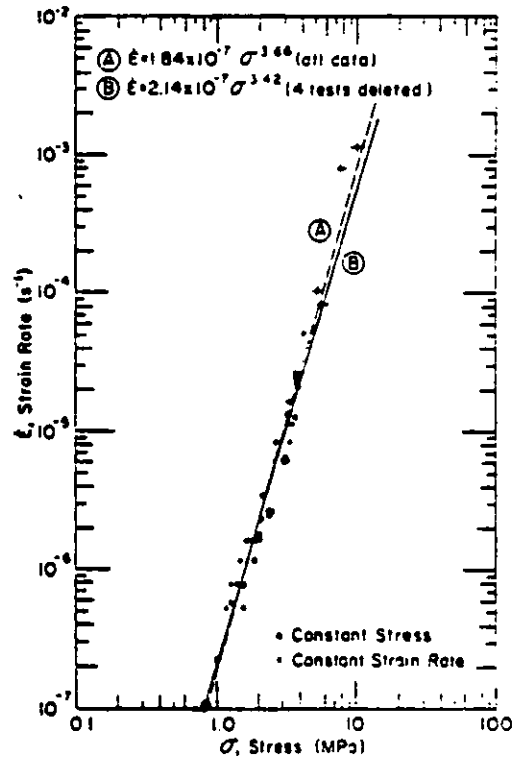


Figure 16. Data from tests under constant load and constant displacement rate. Lines A and B are regression lines, as indicated on the figure [53].

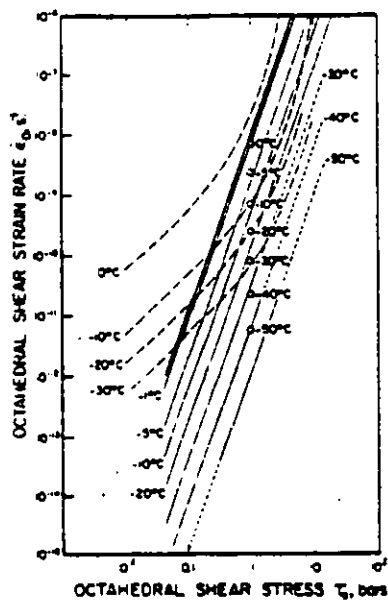


Figure 17. Stress/strain rate relations for creep of glacier ice [61]. Broken lines indicate relations derived from earlier studies [62].

glaciologists [61] for minimum creep rate (Fig. 17) can be interpreted as strength/strain-rate relations for low-rate ductile yield. It might be noted that glaciologists commonly represent axial stress σ_1 in terms of octahedral shear stress τ_{oct} ($\tau_{oct} = \sqrt{2} \sigma_1/3$) and axial strain rate $\dot{\epsilon}_1$ in terms of octahedral strain rate $\dot{\epsilon}_{oct}$ ($\dot{\epsilon}_{oct} = \dot{\epsilon}_1/\sqrt{2}$).

It is sometimes useful to know the "time-to-failure" t_f , defined as the time taken to reach the peak of a stress/strain curve or the inflection point of a creep curve. Figure 18 shows how t_f for fine-grained ice is inversely proportional to both strain rate and a power of stress.

At high strain rates, σ_c decreases as porosity increases (ρ decreases), as shown in Figure 19. For low strain rates, the effect of porosity on the σ_c - $\dot{\epsilon}$ relation has to be deduced indirectly (Fig. 20).

Grain size d does not appear to affect σ_c systematically at low strain rates ($< 10^{-4} \text{ s}^{-1}$). At high strain rates, σ_c is expected to decrease as d increases, perhaps with $\sigma_c = d^{-1/2}$, but adequate data are not yet available.

In cases where ice undergoes ductile yield without fracture or rupture, it is sometimes useful to know the "residual strength" at relatively large strains. The relation between residual strength and strain rate is much the same as the relation between creep rate and applied stress for large strains, and relevant data for both constant strain rate and constant stress are given in Figure 21.

Defining uniaxial tensile strength σ_T in the same way that σ_c was defined, there is little difference between σ_T and σ_c for isotropic ice at low strain rates ($< 10^{-4} \text{ s}^{-1}$). In both cases the ice yields by shearing, and the difference of normal stress does not seem to have much effect. Above some critical strain rate (10^{-5} s^{-1} at -7°C — see Fig. 22) there is a bifurcation in the stress/strain-rate curves for tension and compression, presumably because internal microcracks can form and influence the failure at high rates. At high rates ($> 10^{-5} \text{ s}^{-1}$), σ_T tends to a limiting value, while σ_c continues to increase. For fine-grained ice at -7°C , the high

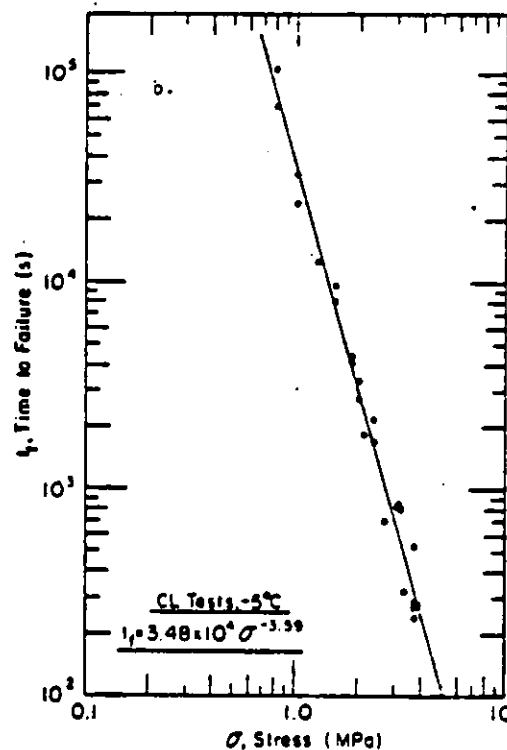
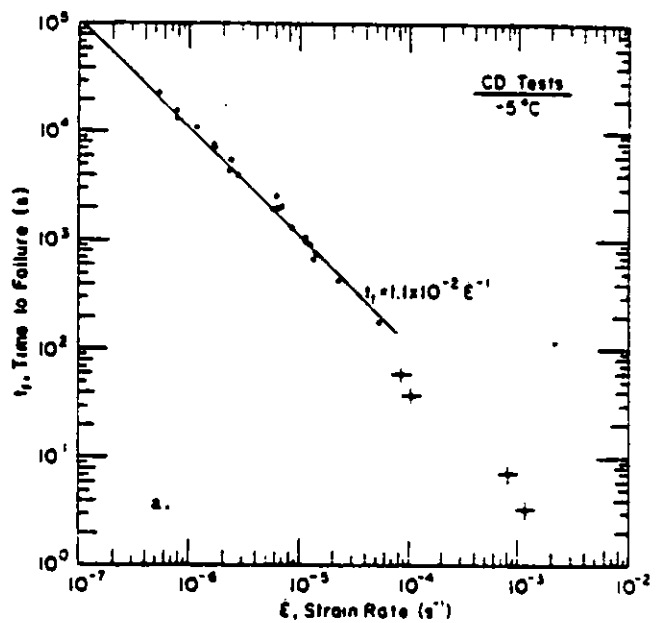


Figure 18. Time-to-failure t_f for fine grained non-saline ice. t_f is given as a function of strain rate (Fig. 18a), and as a function of stress (Fig. 18b).

rate limit of σ_T is about 2 MPa, with σ_c around 10 MPa. This gives a ratio of σ_c/σ_T well below the theoretical values of 8 or more that are predicted by Griffith theory and its derivatives (another reason why diametral compression of a disc or cylinder cannot be used to measure σ_T in ice).

The effect of temperature on σ_T is the same as its effect on σ_c at low strain rates. By contrast, the lack of sensitivity to strain rate at very high rates leads to the expectation that there will be a corresponding insensitivity to temperature in that

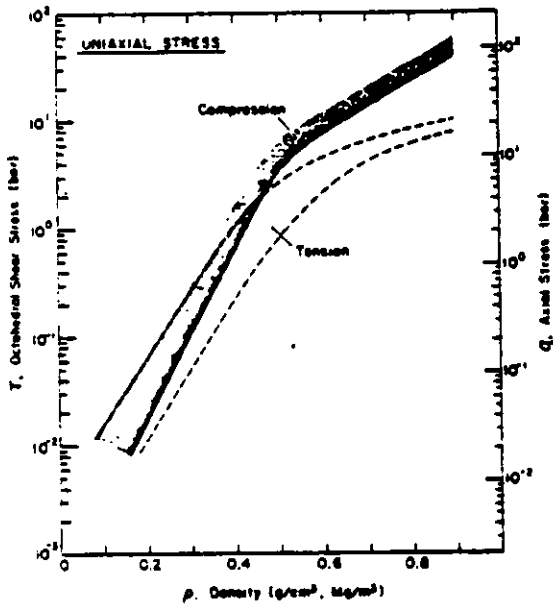


Figure 19. Summary of data on the strength of non-saline ice and snow (for details on data sources see [63]).

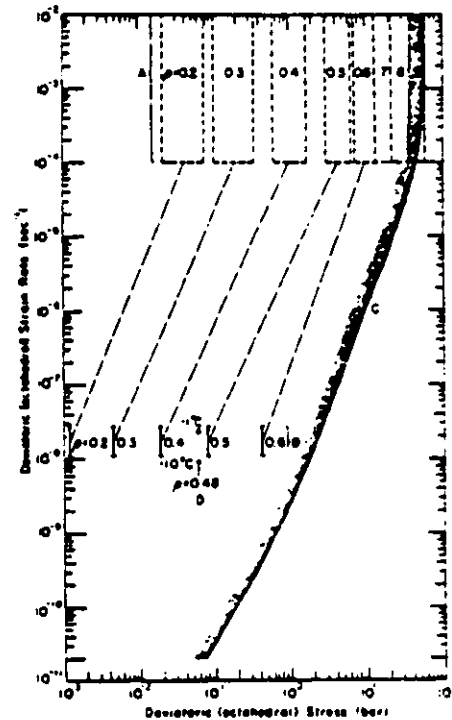


Figure 20. Deviatoric stress/strain-rate relations deduced indirectly from various data sources [63]. (A) Snow, -10°C . (B) Snow, 0° to -7°C . (C) Ice, 0.9 Mg/m^3 , -2°C to -10°C . (D) Snow, 0.49 Mg/m^3 , -1°C to -10°C .

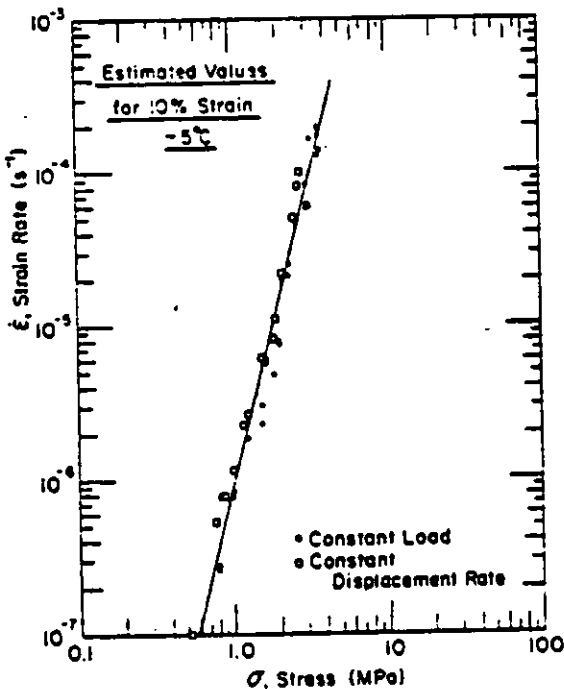


Figure 21. Stress/strain-rate data for 10% axial strain, obtained from extrapolation of constant load and constant displacement rate tests at -5°C . The regression line represents the combined data set [53].

range. The limited experimental data support this idea (Figs. 14 and 21).

At high strain rates, σ_T decreases with increasing porosity (decreasing density), as indicated in Figure 19. At low strain rates, the trend is expected to follow that for σ_c (Fig. 20).

The grain size d has a considerable influence on σ_T at moderate strain rates (10^{-6} s^{-1}). The effect can be described by the Hall-Petch relation

$$\sigma_T = a + b d^{-1/2}$$

where a and b are constants [64]. This type of behaviour is expected to prevail at strain rates higher than 10^{-6} s^{-1} , but at very low strain rates d may not have much effect. For practical purposes the value $\sigma_T = 2 \text{ MPa}$ for fine-grained ice can be regarded as an upper limit. More coarse-grained non-saline material that is encountered in glacier ice, lake ice, and old sea ice will usually have tensile strength much lower than 2 MPa (typically 1 MPa or less).

Failure strains and yield strains. Traditionally there has been rather little interest in absolute value of the strains at which fracture and ductile yielding occur in ice, and yield criteria have always been formulated in terms of stress. However, while yield stresses for ice vary by orders of magnitude, the strains for fracture and ductile yield stay within much more limited ranges.

When fine-grained ice is strained in uniaxial compression at rates less than about 10^{-4} s^{-1} , under either constant strain-rate or constant stress (Fig. 24), there is a well-defined ductile yield at axial strains of approximately 1% [52]. This shows up either as a peak stress on a stress/strain curve, or

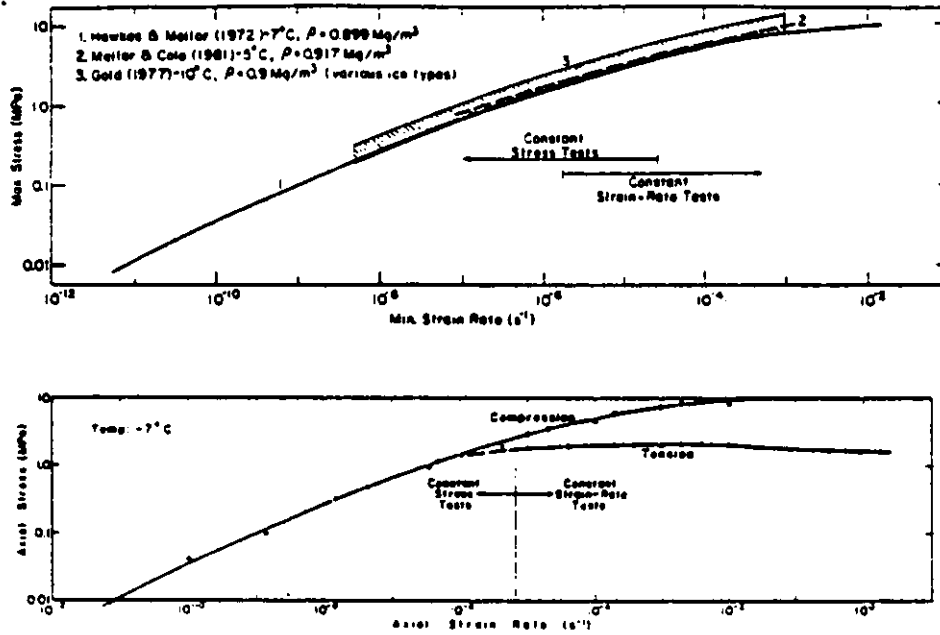


Figure 22. Effect of strain rate on σ_c and σ_T for non-saline ice. Figure 22a indicates σ_c values from various sources and for various ice types. Figure 22b compares σ_c and σ_T for fine-grained non-saline ice [55].

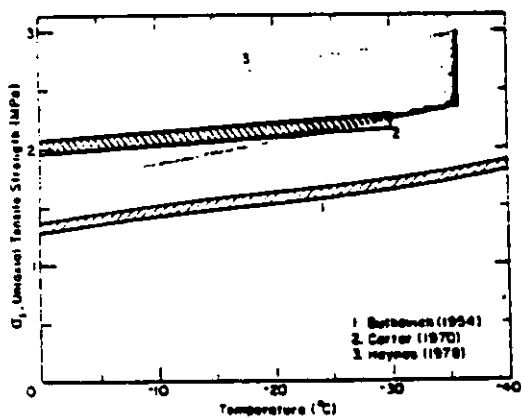


Figure 23. Variation of σ_T with temperature for non-saline ice. Data from [58, 59, 71].

as a strain-rate minimum on a creep curve. Even when the compressive stress is cycled at varying frequencies (Fig. 25), the mean creep curve still shows minimum creep rate at about 1% axial strain [65]. With strain rates in the range 10^{-7} to 10^{-6} s⁻¹, the same ice has an initial yield point which occurs at smaller strains (0.03 to 0.5%). This initial yield is associated with the onset of internal cracking. At very high strain rates ($> 10^{-2}$ s⁻¹) the initial yield becomes the sole yield, i.e. onset of internal

cracking is followed immediately by fracture of the entire specimen.

Comparable data for coarse-grained ice are not yet available, but current work on coarse-grained old sea ice of low salinity suggests that there may be only one identifiable yield point, with strains at that point always well below 1%.

Multiaxial stress states. For multiaxial stress states, strength is best specified by a formal failure criterion, such as an equation or graph describing the failure envelope in principal stress space. A general criterion is hard to formulate even for isotropic ice (none of the classical criteria are broadly applicable), and for anisotropic ice there are very great difficulties. Consequently, engineers often have to get by with the most primitive of assumptions, e.g. failure occurring when the major principal stress reaches σ_T or σ_c , depending on the nature of the problem.

There have been speculations about the qualitative forms of failure criteria for isotropic ice [66], drawing on the observed facts that: (i) hydrostatic pressure has little effect on shearing at very low creep rates, (ii) moderate pressure increases strength and deformation resistance at high strain rates, (iii) high pressure lowers the deformation resistance at all rates, (iv) the envelope intersects the principal stress axis at σ_T and σ_c , and intersects the hydrostat at the pressure for the phase transition from ice Ih to water.

In addition to data for σ_T and σ_c , and for phase transition pressures, there are a few data sets from triaxial tests ($\sigma_2 = \sigma_3$) in the compression-tension quadrants [67], and in the tension-tension quadrants [68]. There are also some data from biaxial tests ($\sigma_3 = 0$) [69]. However, when the number and range of potential variables are considered, these results are too fragmentary to provide a clear picture for this review.

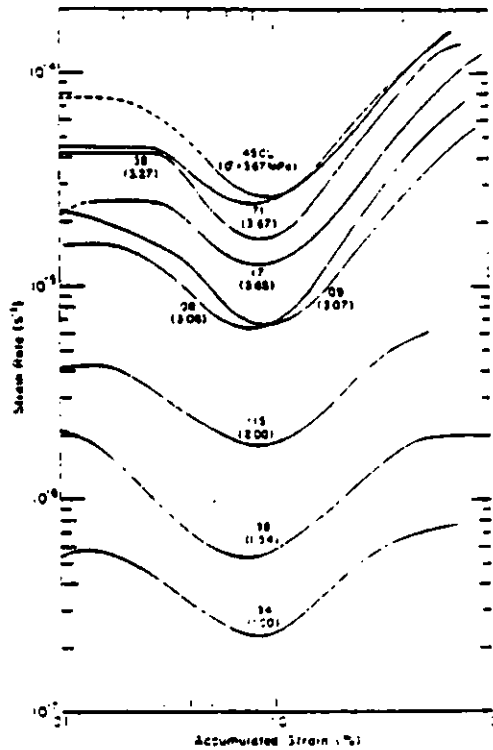
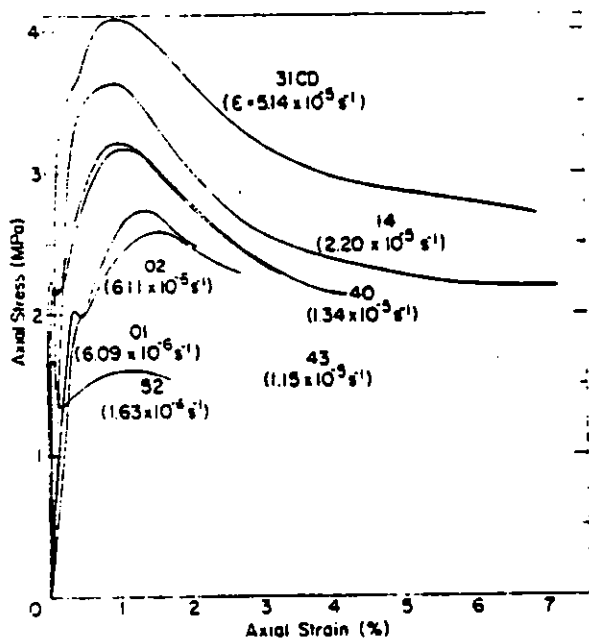


Figure 24. Example of (a) stress/strain curves and (b) creep curves for fine-grained non-saline ice at -5°C [52].

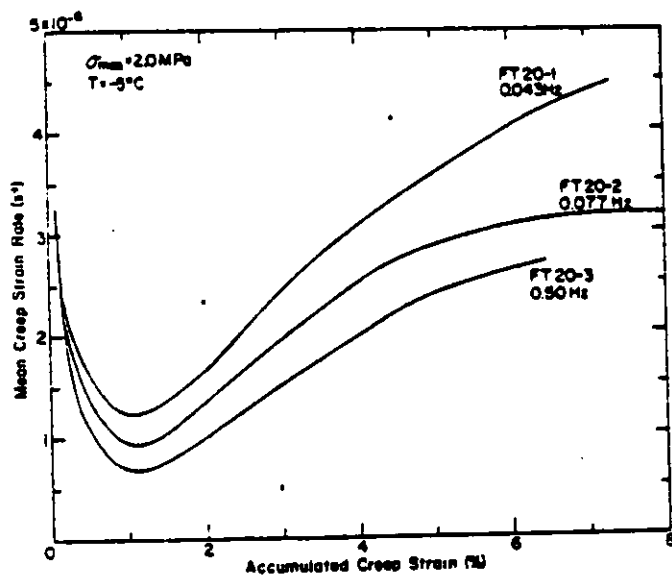


Figure 25. Examples of mean creep curves for tests on fine-grained ice in which compressive stress cycles between 0 and 2 MPa at the frequencies indicated [65].

Fracture toughness. The fracture toughness of ice has attracted considerable interest in recent years, but published data have to be approached with caution. The general concept is clearly applicable to ice under elastic/brittle conditions, but it is irrelevant when rates and temperatures are such that ice yields by flow and recrystallization rather than

by the nucleation and propagation of cracks. The flexural tests typically used to measure K_{IC} , the critical stress intensity factor for "Mode I" crack extension, can be interpreted by elastic theory at high rates and low temperature, but the elastic assumptions become progressively worse as rates and temperatures produce greater ductility.

Where ice is elastic and brittle, K_{IC} should be predictable from Young's modulus E (≈ 10 GPa) and the specific surface energy γ (≈ 0.1 J/m²). For plane stress,

$$K_{IC} = (2E\gamma)^{1/2} = 45 \text{ kN-m}^{-3/2}$$

Measured values of K_{IC} do appear to have a lower limit close to this value. More typical measured values are around $100 \text{ kN-m}^{-3/2}$, implying that γ_p , the specific energy for plastic working of Orowan/Irwin theory, is about 5γ . With this prima facie evidence that simple Griffith theory might be applicable for the elastic/brittle condition, one is tempted to calculate σ_T from E , γ and the controlling crack length $2c$. For plane stress,

$$\sigma_T = \left(\frac{2}{\pi}\right)^{1/2} \left(\frac{E\gamma}{c}\right)^{1/2} = \frac{2.52 \times 10^6}{\sqrt{c}} \text{ Pa}$$

where c is in metres. If we make a guess that $2c$ is equal to the grain size of the ice, calculated values of σ_T are as shown in Figure 26, which also gives measured values of σ_T .

When conditions are such that ice has some ductility, it might be expected that "toughness" would increase with increasing temperature and decreasing strain rate. With the exception of one data set, the

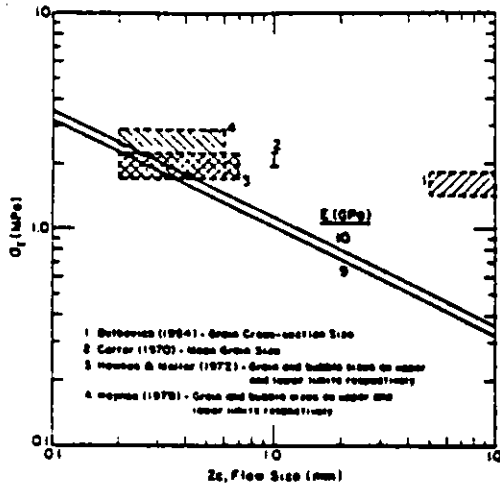


Figure 26. Comparison of theoretical tensile strength with measured values, assuming that flaw size equals grain size [70].

experimental evidence supports this expectation for rate effects (Fig. 27). However, test data show that K_{IC} increases as temperature decreases (Fig. 28), contradicting the simple expectation. Looking at things another way, K_{IC} can be expressed as

$$K_{IC} = \sigma_T(\tau_c)^{1/2}$$

and this suggests that K_{IC} might vary with rate and temperature in the same way as σ_T . The expectation would then be for K_{IC} to be insensitive to rate, and for K_{IC} to increase slowly with decreasing temperature. The latter appears to be borne out when testing rates are high (Fig. 28). However, another possibility is that the existence of liquid films or liquid-like layers in the grain boundaries might lead to a Rahnlander, or Joffe, effect [2]. Since the liquid/solid value of γ is about 30% of the vapour/solid value, K_{IC} could be halved by intrusion of a liquid film into a growing crack. Such intrusion would probably not occur where rates are very high, irrespective of temperature, but it could occur with a combination of high temperature and low test rate.

A more complete discussion of the fracture toughness of ice, and the underlying theory, is given elsewhere [2].

3.3 Sea Ice

Precise measurements of the basic mechanical properties of sea ice are not plentiful, partly because the material is difficult to work with (brine mobility, complex structure), and partly because of practical demands for relatively crude field data. Consequently we have to draw upon experimental results for non-saline ice for a background picture of how sea ice might behave in a general sense. In assessing the sea ice data, it may be helpful to regard salinity as a major new variable, with freshwater ice of zero salinity representing a reference state.

Salinity has a direct influence on porosity, since salts rejected by the ice crystals during freezing form concentrated brine, which is distributed through the ice mass in pores. At any given temperature, the volume of brine-filled pores ("brine porosity") increases with increase of overall salinity. However, the brine-filled pores are not the only pores in sea ice; there are also gas bubbles, and the total porosity is the "gas porosity" plus the "brine porosity." In the past, the "gas porosity" was usually unknown, and brine porosity was substituted for total porosity. There is now a simple method for overcoming this problem [74]. As temperature decreases in ice of a given salinity, brine volume decreases, since equilibrium concentration has to be maintained. This means that temperature has a dual effect on the mechanical properties of saline ice — it affects the ice matrix, such as it does in non-saline ice, but it also changes the porosity. Because increasing temperature and increasing porosity both tend to lower the stiffness, the deformation resistance and the strength of ice, it might be expected that temperature effects in sea ice would be stronger than those in non-saline ice.

Mechanical properties of sea ice are often plotted against porosity and against temperature. When examining such plots, it should be understood that these two variables are not normally independent of each other. Temperature is usually an implicit variable in porosity effects (porosity is varied by changing the temperature in ice of given salinity). Similarly, porosity is often an implicit variable in temperature effects.

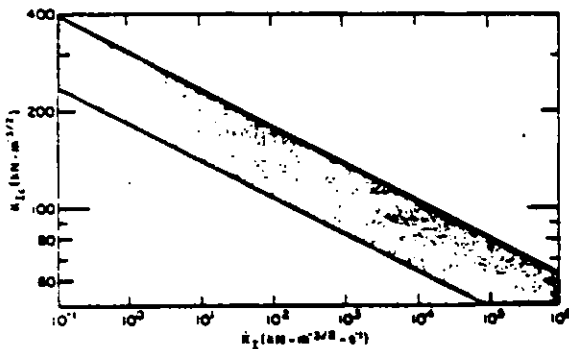


Figure 27. Effect of loading rate on K_{IC} for non-saline ice [70, 72].

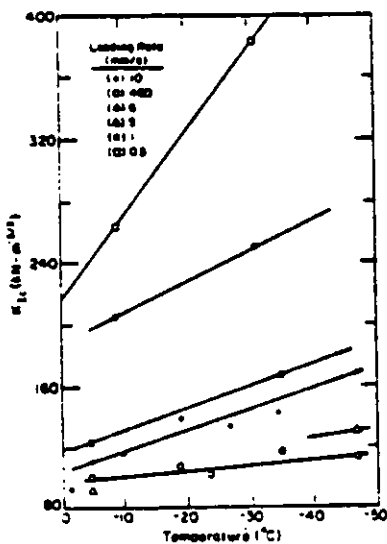


Figure 28. Variation of K_{IC} with temperature and loading rate [73].

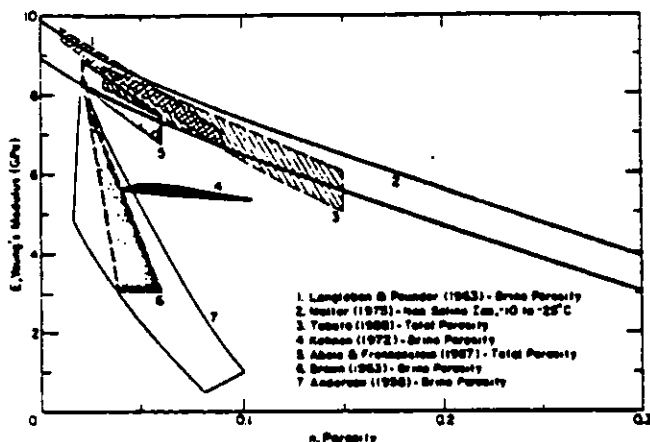


Figure 29. Young's modulus as a function of porosity [2, 63, 75, 76, 77, 78, 79, 80].

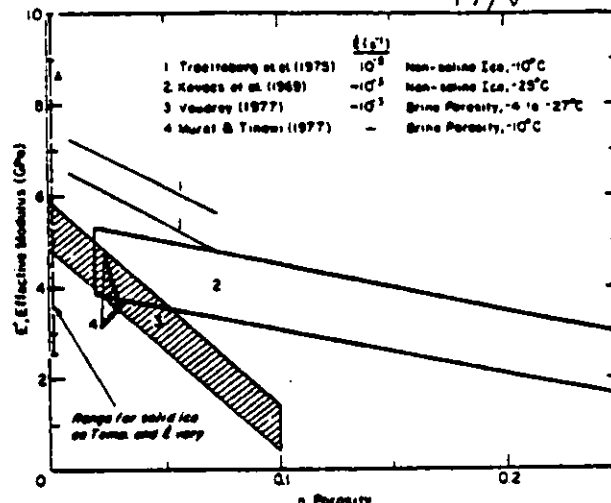


Figure 30. Summary of data for effective modulus E' plotted against porosity [2, 81, 82, 83, 84].

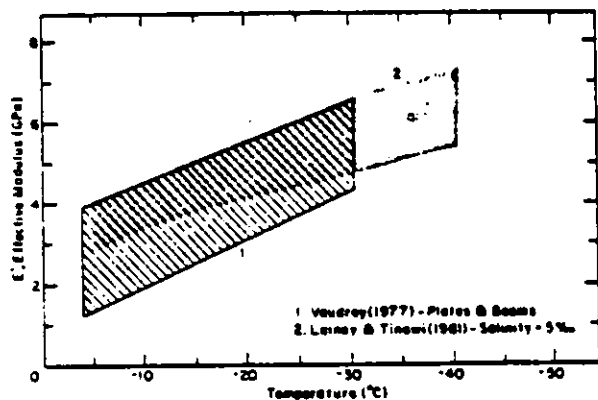


Figure 31. Summary of values for effective modulus E' plotted against temperature [2, 83, 85].

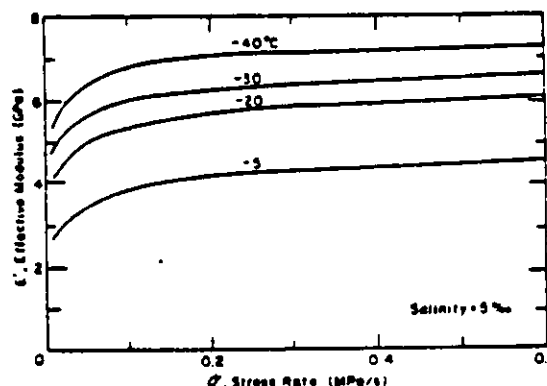


Figure 32. Variation of effective modulus E' with stress rate and temperature [85].

Elastic moduli. Measurements of Young's modulus E have been made by methods depending on high frequency waves, pulses or vibrations. Effective moduli E' have been measured by quasi-static tests (typically beam flexure), both in the laboratory and in the field.

Figure 29 gives a general impression of E values for sea ice over a range of porosity. It also provides a comparison with non-saline ice. The results for small-scale samples (data bands 1, 3, 5) show good agreement with non-saline ice (data band 2). The values obtained from seismic tests and flexural waves over wide areas are mostly much lower than E for non-saline ice, but this is not too surprising when all of the complications of the ice sheet are considered.

Values of E' are indicated in Figure 30, and are compared with E' values for non-saline ice. There is close agreement between sea ice and non-saline ice at low porosity, and the low values for sea ice at higher porosities can probably be attributed to the combined effects of porosity and temperature. Data band 3 for E' in Figure 30 agrees well with data bands 6 and 7 for E in Figure 29.

The effect of temperature on E' is indicated in Figure 31. The slightly steeper trend in data band 1 is probably due to the fact that all tests were made at a single value of salinity. Figure 32 shows how E' varies with stress rate and temperature at a fixed

value of salinity. At very low temperature and high stress (or strain) rate, E' approaches E .

Effective values of Poisson's ratio ν' for sea ice were measured in beam flexure experiments by Murat and Lainey [86]. For very low stress rates, ν' tended to the expected limit value of 0.5 (see page ___). For the highest test rates (0.6 MPa/s, and up to $1.6 \times 10^{-3} \text{ s}^{-1}$), ν' had values between 0.35 and 0.4. The mean value for high rate decreased with decreasing temperature, from about 0.40 at -5°C , to 0.37 at -30°C and -40°C . This observed temperature trend supports a speculation made much earlier by Weeks and Assur [6] on the basis of Soviet seismic data. Such a trend is opposite to what would be expected with air-filled pores, but it can be explained by expressing ν in terms of E and the bulk modulus K [2]:

$$\nu = (3K - E) / 6K = (3 - E/K) / 6$$

Since K is about the same for ice and water, a small increase in the volume of water-filled pores should have little effect on the overall value of K . Thus the variation of ν with porosity will be controlled largely by variations in E , which decreases as porosity increases. The equation therefore predicts an increase of ν with increase of porosity. Because porosity increases with increasing temperature in saline ice, ν should increase with increasing temperature.

In columnar sea ice, anisotropy may have a

greater influence on ν than do temperature or porosity. Wang [88] found that sea ice was much stiffer in a direction parallel to the long axes of columns (vertical) than in the perpendicular direction (horizontal), giving ν' in the range 0 to 0.2 vertically and 0.8 to 1.2 horizontally.

Bulk modulus K and shear modulus G are not commonly measured as such in sea ice, but given pairs of values for E and ν they are easily calculated (see page ___).

Strength and deformation resistance. Uniaxial stress tests provide clear and unambiguous data if they are done well. Uniaxial compression tests have been applied to sea ice by many investigators, but uniaxial tension has rarely been attempted. The most common strength tests have involved flexure of beams or cantilevers. For laboratory experiments small beams are cut from an ice sheet, or saline ice is produced artificially. For large scale field tests, beams or cantilevers are sawn in the ice sheet, with the "fixed" ends still attached to the sheet (limited flexure at the beam root is still possible). For the reasons mentioned earlier (page ___), beam tests can give misleading results, and beam data for non-saline ice have been ignored in this review. However, in the absence of adequate uniaxial data for sea ice, we have to make use of beam data, which do have special value when beam tests are regarded as analogue tests for plate flexure. To distinguish the "modulus of

rupture" or "flexural strength" from uniaxial tensile strength σ_T , we use the symbol σ_{FT} . We have completely disregarded results from once-popular Brazil tests and ring tests (diametral compression of discs and annuli), since these tests have proved unsuitable for ice [89].

The uniaxial compressive strength of sea ice is expected to vary with strain rate, temperature and porosity in a manner qualitatively similar to non-saline ice. Figure 33 represents some data by Wang [90] which conform to a power relation between strain rate and stress, with an exponent of about 4. Some other data, selected from results by Schwarz [91], are shown against strain rate in Figure 34. In Figure 35, the effect of temperature on σ_C is shown for sea ice and for some roughly comparable fresh-water ice (lake and river ice).

The effect of porosity on σ_C and other mechanical properties has traditionally been displayed by plotting the property against the square root of brine volume. For reasons discussed elsewhere [2], this practice is not followed here; brine volume is represented simply as brine porosity. Variation of σ_C with brine porosity at high strain rates ($\approx 10^{-3} \text{ s}^{-1}$) is shown in Figure 36, which also brings out the well established fact that σ_C is strongly dependent on the direction of loading in columnar ice. Further evidence is given

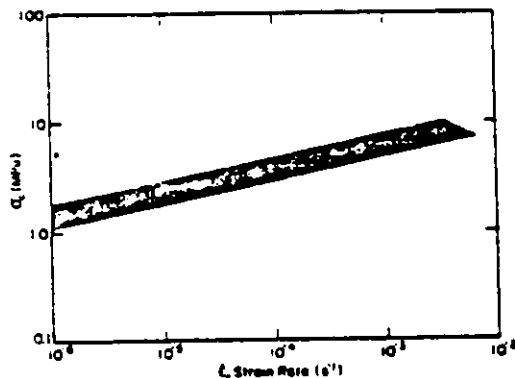


Figure 33. Uniaxial compressive strength of sea ice as a function of strain rate (data selected from [38]).

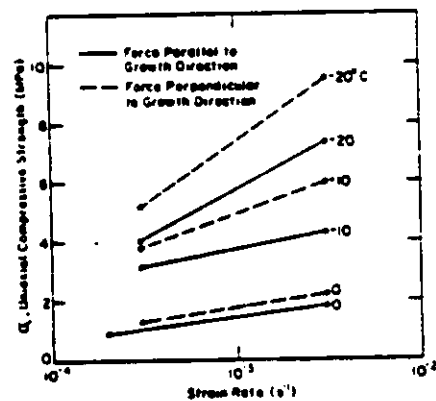


Figure 34. Variation of σ_C with strain rate, temperature and grain orientation (data selected from [91]).

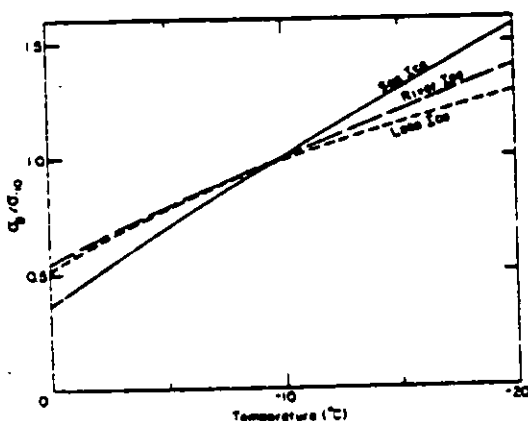


Figure 35. Variation of σ_C with temperature for three ice types (data from [91]).

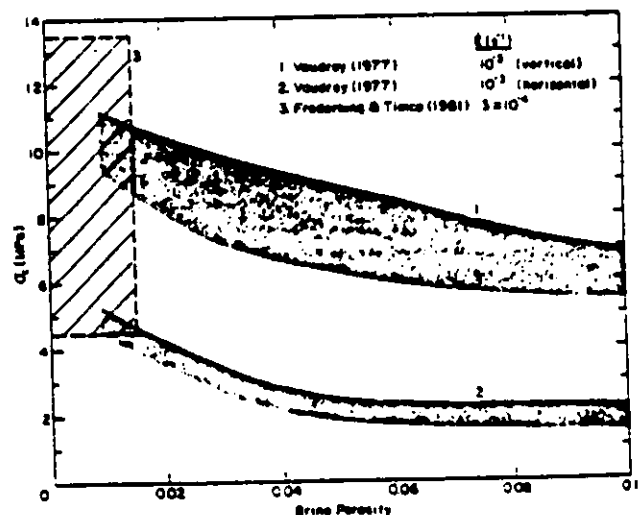


Figure 36. Summary of data for σ_C as a function of brine porosity [83, 92].

by Figure 37, which shows the ice to be weakest when major principal stress is at 45° to the direction of the c-axis (i.e., at 45° to the horizontal plane).

Figure 38 provides confirmation that σ_c decreases with increase of grain size at fairly high strain rates ($> 10^{-3} \text{ s}^{-1}$).

Uniaxial tensile tests on sea ice have been rare because of the difficulty in maintaining perfect specimen axiality and in avoiding perturbations of the stress field. These difficulties are now being overcome, but new data have not yet appeared. The only useable published data seem to be those represented in Figure 39, where σ_T is plotted against temperature for two salinities and two loading

directions. As might be expected, σ_T increases with decreasing temperature and decreasing salinity. It is greater for vertical specimens of columnar ice (Fig. 39a) than for horizontal specimens (Fig. 39b). The temperature effect implies a porosity effect, which is illustrated by a re-plot of mean values from Figure 39 in Figure 40.

Flexural strength σ_{FT} has been measured in many test programs involving both laboratory work and field work. The variability of results is somewhat daunting, as can be seen from the summary in Figure 41, where σ_{FT} is shown against brine porosity. Figure 42 summarizes some data on the variation of σ_{FT} with temperature, but the results should be

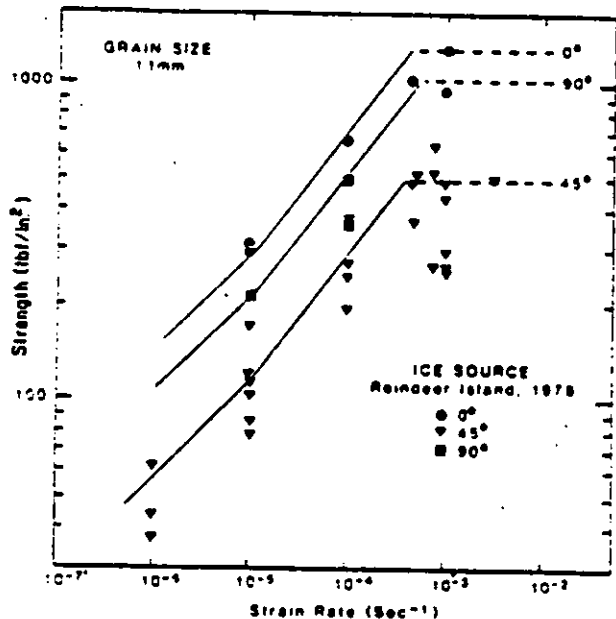


Figure 37. Variation of σ_c with strain rate in columnar sea ice at -10°C . The three data sets show the effect of crystal orientation [93].

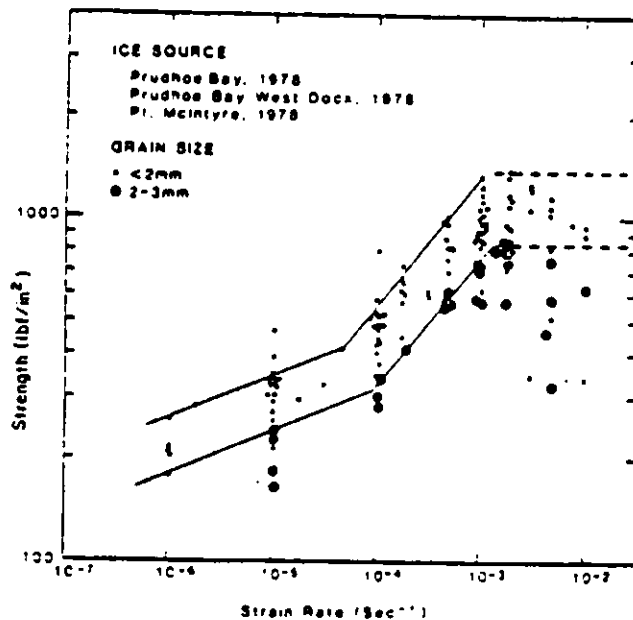


Figure 38. Variation of σ_c with strain rate in granular sea ice at -10°C . The effect of grain size is also indicated [93].

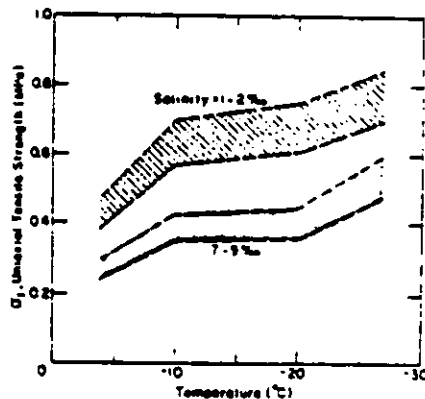
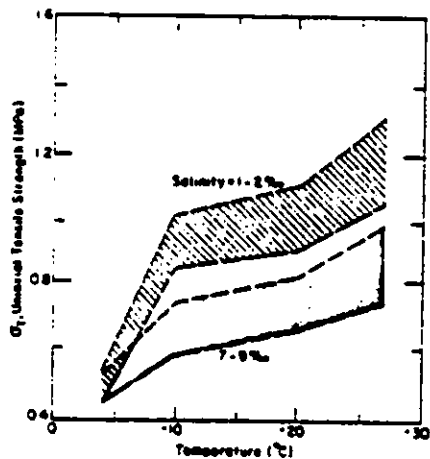


Figure 39. Variation of uniaxial tensile strength with temperature and salinity for sea ice: (a) vertical specimens, (b) horizontal specimens [94].

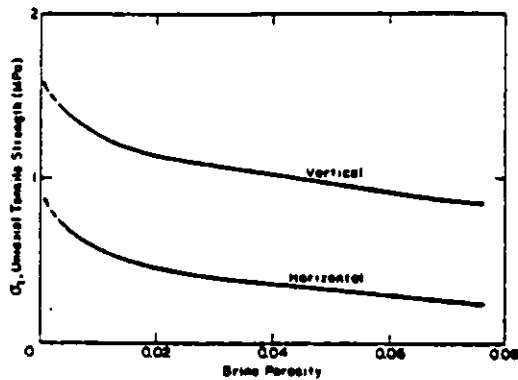


Figure 40. σ_T as a function of brine porosity [94].

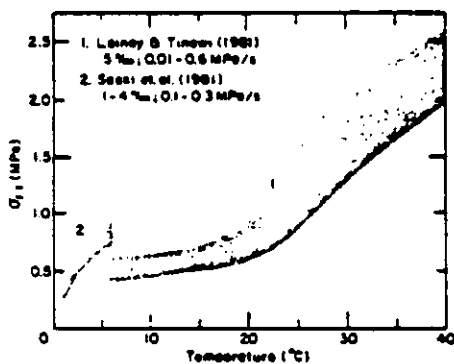


Figure 42. Variation of flexural strength with temperature [85, 98].

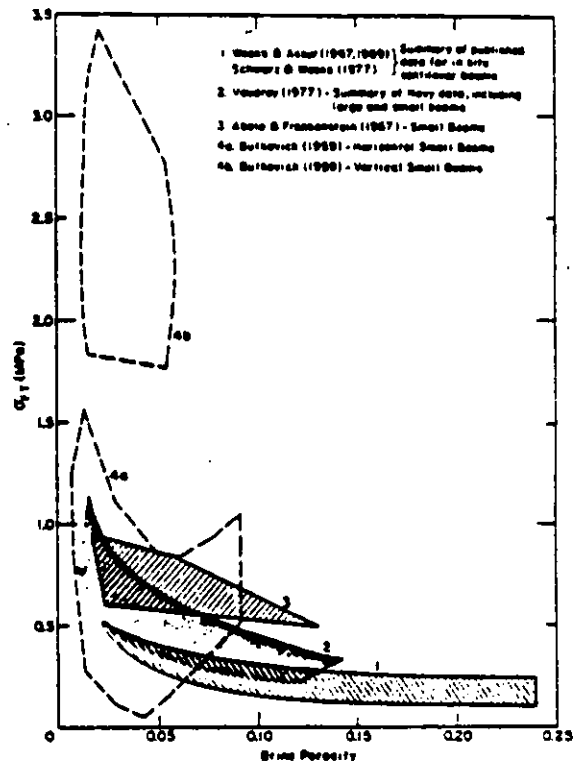


Figure 41. Summary of data for σ_T as a function of brine porosity [2, 6, 7, 78, 83, 96].

treated with caution because of probable departure from ideal elasticity at high temperatures. A discussion of rate effects, temperature effects and other complications is given elsewhere [2], but it might be worth mentioning here that *in situ* beams are subject to large variations in grain structure, steep temperature gradients, beam-root stress concentrations, scale effects and, at high rates, inertial effects in the underlying water.

Fracture toughness measurements on sea ice have been reported from several studies [72, 83, 99, 100, 102]. The effect of loading rate on K_{IC} is shown in Figures 43 and 44, and it can be seen that, for high loading rates, K_{IC} tends to values that are close to the theoretical "Griffith" value for non-saline ice (see page). In Figure 43, temperature seems to have very little effect on K_{IC} , in contrast to the trend shown earlier in Figure 28 for comparable deflection rates. One study [102] has given some evidence of a decrease in K_{IC} with increase of brine porosity; another study [83] purports to show the same trend, but the data points have no significant correlation. In both Figure 43 and Figure 44, it seems that K_{IC} increases with increase grain size.

Some conventional triaxial tests ($\sigma_1 \neq \sigma_2 = \sigma_3$) have been made on sea ice at moderately high rates. Soviet tests [103] on artificial and natural sea ice show the major principal stress σ_1 increasing with σ_2 , σ_3 , and the maximum shear stress, $(\sigma_1 - \sigma_2)/2$, increasing nonlinearly with the normal stress on the plane of maximum shear. The failure value of σ_1 was an order of magnitude higher than σ_c with σ_2 around 4 MPa. Under confining pressure, the failure stress decreased with increasing salinity and increasing temperature, just as it does in the uniaxial stress

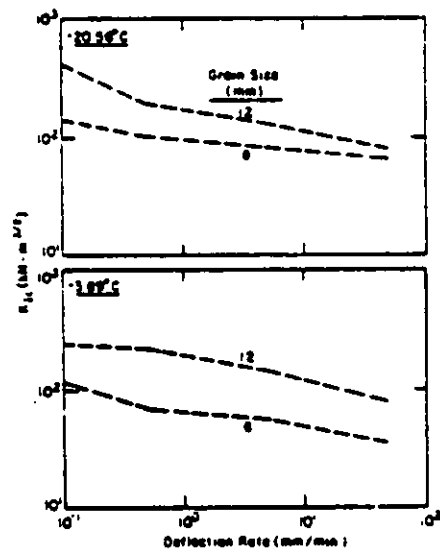


Figure 43. Variation of K_{IC} with loading rate, grain size and temperature [109] for columnar fresh water ice.

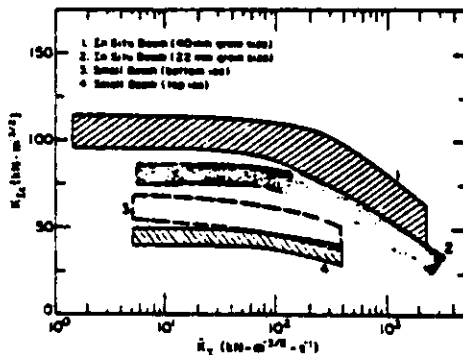


Figure 44. Effect of loading rate on K_{1c} for sea ice (data from [72]).

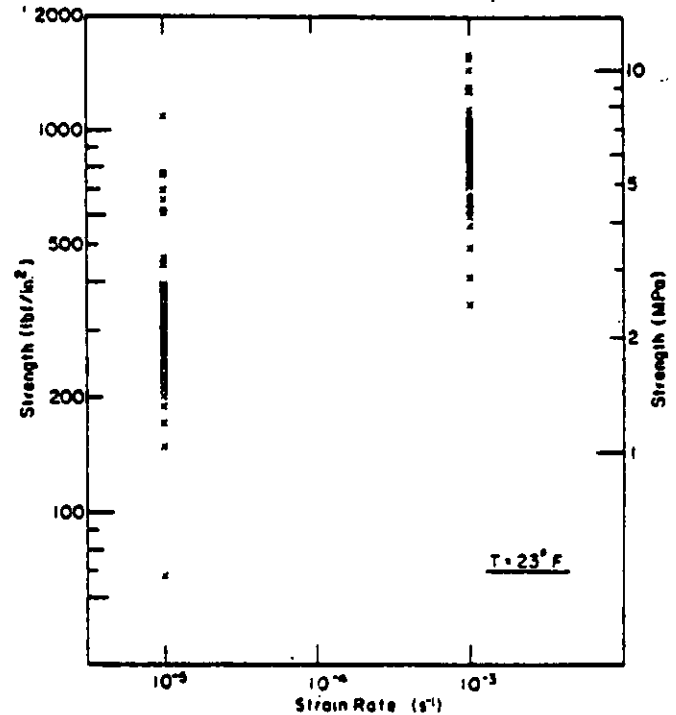


Figure 45. Uniaxial compressive strength of multiyear sea ice at -5°C and strain rates of 10^{-5} and 10^{-3} s^{-1} [43].

state. Isotropic fine-grained ice behaved differently from anisotropic ice, and strength varied with loading direction in anisotropic ice. Values of ϕ for the Mohr-Coulomb criterion were mostly in the range 30° to 50° , with extreme values of 14° and 55° . "True" triaxial tests ($\sigma_1 \neq \sigma_2 \neq \sigma_3$) have been made on anisotropic saline ice [104], but so far the results are too complicated to be summarized concisely.

One potential problem in triaxial testing is that failure could be influenced by differences of loading rates for the principal stresses, or by variations in the ratio σ_1/σ_2 . Because a complex stress field in natural ice is likely to fluctuate with the ratio of principal stresses staying fairly constant, a new triaxial test device has been developed to keep the ratio σ_1/σ_2 constant throughout a test [105].

Very little work has been done on the mechanical properties of multi-year sea ice, and it is still hard to generalize about differences between "new" and "old" ice. Some studies suggest that multiyear ice is weaker than first-year ice [106], but recent detailed studies [43] do not support this idea. Actually, it is not easy to make comparisons because of the great variability of strength in multiyear ice, which contains many different types of ice. Figure 45 gives some values of σ_c at strain rates of 10^{-5} and 10^{-3} s^{-1} , with a temperature of -5°C . If Figure 45 is compared with Figures 37 and 38, it can be seen that the strength range for multiyear ice is similar to that for granular first-year ice at -10°C . At 10^{-3} s^{-1} , the multiyear ice is about the same strength as columnar first-year ice, but at 10^{-5} s^{-1} the columnar ice is weaker than multiyear ice except when tested in the "hard fail" direction.

Uniaxial tension tests on multiyear ice are being made as part of a current program at CRREL, and the indications so far are that σ_T is always less than 1 MPa.

3.4 Ice Island Ice

The earlier notes on ice islands indicate a rather complicated structure, with four different types of ice distinguishable. Since mechanical tests have not been made on ice islands to any significant extent, it is useful to simplify the earlier picture so as to draw some conclusions about probable mechanical behaviour.

Of the listed constituents for ice islands, two are non-saline ice: lake ice, and snow ice (which is just glacier ice). The properties of lake ice as such have not been reviewed here, but they can be inferred from the general properties of granular and columnar non-saline ice. A more specific review of lake ice properties can be found elsewhere [7]. Snow ice is the material that makes up glaciers, ice caps and ice shelves. Unless it has been metamorphosed by strong shearing, it is typically isotropic, with grain size and porosity varying. For polar glacier ice, grain size varies from around 1 mm in "snow," where the bulk density is less than 0.6 Mg/m^3 , to around 5 mm in very dense ice (porosity ≈ 0) from the deep layers. The properties of porous glacier ice have already been summarized, and the properties of "snow" and "snow ice" for lower ranges of bulk density are dealt with elsewhere [6], [107].

The remaining two constituents of ice islands are saline ice types (sea ice, brackish ice), but salinity is likely to be very low. The sea ice component is very old sea ice, and therefore perhaps comparable to some of the multiyear ice that has just been discussed. Not much is known about ice formed from brackish water, but a first guess might be that it would be similar to lake ice.

Actually, the small ice island fragments that drift into shallow coastal waters have suffered ablation from both top and bottom surfaces, and they may not include all the ice types that have been listed. From impressions gained during visits to a

number of small ice islands, and from drilling and blasting work on ice islands, one of us is inclined to regard them simply as small icebergs.

3.5 Fragmented Ice

There is a tendency to assume that the problems created by floating ice are solved once the ice is broken. In fact, accumulations of fragmented ice can, in some circumstances, resist ship movement and load structures much more severely than an unbroken ice sheet.

Fragmented ice covers a broad spectrum, from fine-grained mush ice, through blocky brash ice, up to floe ice, rafted ice, and ridged ice. As far as ships and structures are concerned, the accumulations of fragmented ice that are of most concern are mush, brash, and first-year pressure ridges.

Mush ice is something like waterlogged snow, with fluid properties while it is floating freely, and high cohesion when it is compacted or drained. Although it can cause real problems for ships and marine structures, systematic study of mush ice is only just starting and, apart from a small amount of information in the snow mechanics literature, data are not yet available.

Brash ice has more or less equant particles in the size range 0.02 to 2.0 m. The tendency has been to treat it analytically as a granular "c- ϕ " material that conforms to a Mohr-Coulomb failure criterion, but for horizontal penetration of a uniform layer the stress-free upper and lower boundaries appear to permit yielding in conformance to a criterion of the von Mises type [108]. However, measurements of ϕ have been made in a number of studies.

Large ice blocks pushed together into pressure ridges also form a "granular" material which initially has cohesion c and internal friction (shear resistance) ϕ . The scale of this material is too big for conventional measurements of its bulk properties, but some deductions can be made from analysis of natural processes.

The properties of fragmented ice are summarized and discussed elsewhere [2].

4. CONCLUSION

From this brief survey of the different varieties of ice encountered in arctic waters, it is evident that there are large gaps in the available data. There are virtually no data derived from direct studies on icebergs and ice islands. Although major studies on these ice masses are perhaps unnecessary, some exploratory studies would be useful in order to confirm that icebergs and ice islands are, in fact, similar to their parent ice bodies. Studies on first-year sea ice have been made almost entirely on ice which has formed near the coast. This kind of sea ice is believed to have strong c-axis alignments in the horizontal plane, but only in a few cases has the orientation of the stress field relative to c-axis orientation been taken into consideration. The most significant shortcoming at the present time is lack of information on multiyear ice, which is the most common material in the central arctic pack, and probably the most threatening material for offshore structures. Finally, little is known about the properties of marine frazil ice. It may be more common than was previously thought to be the case, and the fine-grained coherent ice formed from frazil may be stronger than first year congelation ice.

As far as the acquisition and interpretation of test data is concerned, the field of sea ice research is moving into a new phase. Some of the older test

methods, and the data generated by them, have had to be discarded, a process that has forced both of the present authors to junk some of their older work. Current activity is based on test techniques that are more refined and more carefully selected, and there are moves towards standardization of test techniques worldwide. Tests can be designed, conducted and interpreted with better appreciation for the relevant constitutive relations and failure criteria, and with less slavish conformance to methodologies borrowed from other technical fields. Some experimental areas are still deficient, and more emphasis needs to be given to multiaxial stress states and to loadings of long duration.

The things we call basic mechanical properties are, of course, only meaningful within the framework of underlying theory, and they have to be applied to engineering design through the appropriate theory. At present there is only loose coordination of ice engineering research in the areas of theoretical mechanics, experimental determination of properties, and solution of practical boundary value problems. Consequently, there is a danger that efforts in these various areas might be mismatched. For example, theoreticians might be calling for highly complex data from polyaxial tests on rate-dependent anisotropic material at a time when design engineers are struggling to progress beyond simple elastic analysis and maximum principal stress failure criteria. Some measure of coordination is needed in order to satisfy the legitimate demands of both basic research and practical engineering.

In spite of all these difficulties, the general situation is encouraging. Ice mechanics has made considerable progress in recent years and may, in fact, be making some new contributions to applied mechanics and materials science. There is a good collection of basic data, and many practical problems can be tackled with confidence. Perhaps the greatest problem at the present time is that the accelerated leasing schedule for the Beaufort, Chukchi and Bering Seas will create a heavy demand for high quality data, while the number of experienced research people, the physical facilities for ice research, and the levels of funding support are all severely limited. To overcome this problem, the very least that is needed is an expansion and intensification of collaboration between academia, industry and government.

REFERENCES

1. Weeks, W.F. and Ackley, S.F., The growth structure and properties of sea ice. USACRREL Monograph 82-1, 130 pp., 1982.
2. Mellor, M., Mechanical behavior of sea ice. USACRREL Monograph 83-1, 92 pp., 1983.
3. Coon, H.D., Brown, C.B., Cox, G.F.N., Ralston, T.D., Shapiro, L. and Weeks, W.F., Research in Sea Ice Mechanics, Marine Board, Assembly of Engineering, National Res. Council, National Acad. Press, 80 pp., 1981.
4. Weeks, W.F. and Mellor, M., Some elements of iceberg technology, in Iceberg Technology, ed. A.A. Hussein, pp. 45-98, Pergamon Press, 1976.
5. Schwarz, J. and Weeks, W.F., Engineering properties of sea ice. J. Glaciology, vol. 19, no. 81, pp. 499-530, 1977.
6. Weeks, W.F. and Assur, A., The mechanical properties of sea ice. USACRREL Monograph II - C3, 80 pp., 1967.
7. Weeks, W.F. and Assur, A., Fracture of lake and sea ice. USACRREL Research Report 269, 77 pp., 1969.
8. Hobbs, P., Ice Physics, Oxford Univ. Press, 837 pp., 1974.

9. Bragg, W.H., The crystal structure of ice. Proc. Phys. Soc., vol. 34, pp. 98-103, 1922.
10. Lepparanta, M., Observations of icebergs in the Barents Sea in July 1980. Iceberg Research, No. 2, pp. 3-4, 1982.
11. Robe, R.Q., Iceberg drift and deterioration, in Dynamics of Snow and Ice Masses, ed. S.C. Colbeck, pp. 211-59, Academic Press, New York, 1980.
12. Rigsby, G.P., Study of ice fabrics, Thule area, Greenland, Snow, Ice and Permafrost Research Establishment Report 26, 6 pp., 1955.
13. Gow, A.J. and Williamson, T., Rheological implications of the internal structure and crystal fabrics of the West Antarctic ice sheet as revealed by deep core drilling at Byrd Station. Geol. Soc. Amer. Bull., vol. 87, pp. 1665-77, 1976.
14. Rigsby, G.P., The complexities of the three-dimensional shape of individual crystals of glacier ice. J. Glaciology, vol. 7, no. 50, pp. 233-52, 1968.
15. Scholander, P.F. and Nutt, D.C., Bubble pressure in Greenland icebergs, J. Glaciology, vol. 3, no. 28, pp. 671-678, 1960.
16. Smith, E.H., Arctic ice, with special reference to its distribution in the North Atlantic Ocean, U.S. Coast Guard Bull. No. 19: I-X, 221 pp., 1931.
17. Weeks, W.F., The structure of sea ice: a progress report, in Arctic Sea Ice, U.S. Nat. Acad. Sciences - Nat. Res. Council Pub. 598, pp. 96-98, 1958.
18. Cherepanov, N.V., Spatial arrangement of sea ice crystal structure. Prob. Arkt. i Antarkt., vol. 38, pp. 176-181, 1971.
19. Weeks, W.F. and Gow, A.J., Preferred crystal orientations along the margins of the Arctic Ocean. J. Geophys. Res., vol. 84, no. C10, pp. 3105-3121, 1978.
20. Weeks, W.F. and Gow, A.J., Crystal alignments in the fast ice of arctic Alaska, J. Geophys. Res., vol. 85, no. C2, pp. 1137-1146.
21. Kovacs, A. and Morey, R., Radar anisotropy of sea ice due to preferred azimuthal orientation of the horizontal c-axes of ice crystals, J. Geophys. Res., vol. 83, no. C12, pp. 6037-6046, 1978.
22. Langhorne, P., Laboratory experiments on crystal orientation in NaCl ice. Annals of Glaciology, vol. 4, 1983.
23. Kovacs, A. and Morey, R.M., Investigations of sea ice anisotropy, electromagnetic properties, strength, and under-ice current orientation, CRREL Report 80-20, 18 pp., 1980.
24. Tabata, T. and Ono, N., On the crystallographic study of several kinds of ice, Low Temp. Sci., vol. A20, pp. 199-214, 1962.
25. Gow, A.J. and Weeks, W.F., The internal structure of fast ice near Narwhal Island, Beaufort Sea, Alaska, CRREL Report 77-29, 8 pp., 1977.
26. Lofgren, G. and Weeks, W.F., Effect of growth parameters on the substructure spacing in NaCl ice crystals, J. Glaciology, vol. 8, no. 52, pp. 153-164, 1969.
27. Nakawo, M. and Sinha, N.K., Brine layer spacing of first-year sea ice. Draft manuscript, 1982.
28. Zorikov, I.A., Zagorodnov, V.S. and Raikovski, J.V., Core drilling through the Ross Ice Shelf (Antarctica) confirmed basal freezing. Science, vol. 207, no. 4438, pp. 1463-1465, 1980.
29. Weeks, W.F. and Assur, A., Structural control of the vertical variation of the strength of sea and salt ice, in Ice and Snow - Processes, Properties and Applications, ed. W.D. Kingery, pp. 258-276, MIT Press, 1963.
30. Weeks, W.F. and Lofgren, G., The effective solute distribution coefficient during the freezing of NaCl solutions, in Physics of Snow and Ice, ed. H. Oura, Inst. Low Temp. Sci., Hokkaido, vol. 1, no. 1, pp. 379-597, 1967.
31. Nakawo, M. and Sinha, N.K., Growth rate and salinity profile of first-year sea ice in the high Arctic, J. Glaciology, vol. 27, no. 96, pp. 315-330, 1981.
32. Lake, R.A. and Lewis, E.L., Salt rejection by sea ice during growth, J. Geophys. Res., vol. 75, no. 3, pp. 583-597, 1970.
33. Niedrauer, T.M. and Martin, S., An experimental study of brine drainage and convection in young sea ice, J. Geophys. Res., vol. 84, no. C3, pp. 1176-1186, 1979.
34. Assur, A., Composition of sea ice and its tensile strength, in Arctic Sea Ice, U.S. Nat. Acad. Sciences - Nat. Res. Council Pub. 598, pp. 106-138, 1958.
35. Sinha, N.K., Technique for studying structure of sea ice, J. Glaciology, vol. 18, no. 79, pp. 315-323, 1977.
36. Gow, A.J., Ackley, S.F., Weeks, W.F. and Govoni, J.W., Physical and structural characteristics of Antarctic sea ice. Annals of Glaciology, vol. 3, pp. 113-117, 1982.
37. Cherepanov, N.V., Using the methods of crystal optics for determining the age of drift ice. Problemy Arktiki, vol. 2, pp. 179-184, 1957.
38. Schwarzscher, W., Pack-ice studies in the Arctic Ocean, J. Geophys. Res., vol. 64, pp. 2357-2367, 1959.
39. Yaykut, G. and Untersteiner, N., Some results from a time-dependent thermodynamic model of sea ice, J. Geophys. Res., vol. 67, pp. 1550-1567, 1971.
40. Walker, E.R. and Wadhams, P., Thick sea ice floes, Arctic, vol. 32, no. 2, pp. 140-147, 1979.
41. Wadhams, P., Sea ice topography of the Arctic Ocean in the region 70° W to 25° E. Phil. Trans. Roy. Soc. London, vol. A302, no. 1464, pp. 45-85.
42. Tucker, W.B., Sodhi, D. and Govoni, J., Structure of first-year pressure ridge sails in the Prudhoe Bay region, in The Beaufort Sea - Physical and Biological Environment, eds. P. Barnes, D. Schell and E. Reimnitz, Academic Press, 1983.
43. Cox, G.F.N., Richter, J., Weeks, W.F., Mellor, M. and Bosworth, M., The mechanical properties of multi-year sea ice, Phase I: Test results. USACRREL Report 81-, 1983.
44. Cray, A.P., Arctic ice island and ice shelf studies, in Scientific Studies at Fletcher's Ice Island, T-3, 1952-1955, Vol. III, ed. V. Bushnell, pp. 1-37, Air Force Cambridge Research Center Geophysical Research Paper No. 63 (AFCRC-TR-232(3)), 1960.
45. Marshall, W.F., Structure and stratigraphy of T-3 and the Ellesmere Ice Shelf, in Scientific Studies at Fletcher's Ice Island, T-3, 1952-1955, Vol. III, ed. V. Bushnell, pp. 45-57, Air Force Cambridge Research Center Geophysical Research Paper No. 63 (AFCRC-TR-232(3)), 1960.
46. Pagle, R.H., Blair, R.G. and Persson, L.E., Ice core studies of Ward Hunt Ice Shelf, 1960. J. Glaciology, vol. 5, no. 37, pp. 39-59, 1964.
47. Smith, D.D., Ice lithologies and structure of ice island Arlis II. J. Glaciology, vol. 5, no. 37, pp. 17-38, 1964.
48. Nakawa, M., Moriguma, J. and Higuchi, K., Glaciological studies on Fletcher's Ice Island (T-3). Arctic Institute of North America Research Paper No. 21, 1962.
49. Cherepanov, N.V., Structure of sea ice of great

- thickness. Trudy Arkt. i Antarkt. N.I. Institut, vol. 367, pp. 13-13, 1964.
50. Lyons, J.R., Savin, S.M. and Tamburi, A.J., Basement ice, Ward Hunt Ice Shelf, Ellesmere Island, Canada. J. Glaciology, vol. 10, no. 58, pp. 93-100, 1971.
 51. Mellor, M., Glacier mechanics, IAHR Internat. Sympos. on Ice, Quebec, Canada, Vol. II, pp. 455-473, 1981.
 52. Mellor, M. and Cole, D., Deformation and failure of ice under constant stress or constant strain-rate, Cold Regions Sci. Tech., vol. 5, pp. 201-219, 1982.
 53. Mellor, M. and Cole, D.M., Stress/strain/time relations for ice under uniaxial compression, Cold Regions Sci. Tech., 1983.
 54. Gold, L.W., Some observations of the dependence of strain on stress for ice, Canad. J. Phys., vol. 36, no. 10, pp. 1265-1275, 1958.
 55. Hawkes, I. and Mellor, M., Deformation and fracture of ice under uniaxial stress. J. Glaciology, vol. 11, no. 61, pp. 103-131, 1972.
 56. Sinha, N.K., Short-term rheology of polycrystalline ice, J. Glaciology, vol. 21, no. 85, pp. 457-473, 1978.
 57. Sinha, N.K., Rheology of columnar-grained ice, Experimental Mechanics, vol. 18, no. 12, pp. 464-470, 1979.
 58. Carter, D., Brittle fracture of snow ice, Proceed. IAHR Sympos. Reykjavik, Iceland, Paper 5.2, 1970.
 59. Haynes, F.D., Effect of temperature on the strength of snow-ice, USACRREL Report 78-27, 18 pp., 1978.
 60. Mellor, M. and Testa, R., Effect of temperature on the creep of ice, J. Glaciology, vol. 8, no. 32, pp. 131-145, 1969.
 61. Paterson, W.S.R. and Budd, W.F., Flow parameters for ice sheet modeling, Cold Regions Sci. Tech., vol. 6, no. 2, pp. 175-177, 1982.
 62. Budd, W.F., The dynamics of ice masses. Australian Nat. Antarctic Research Expedition, Scientific Report 108, 1969.
 63. Mellor, M., A review of basic snow mechanics. Snow Mechanics Sympos., Grindelwald, LAHS Pub. No. 114, pp. 251-291, 1974.
 64. Currier, J.H. and Schulson, E.M., The tensile strength of ice as a function of grain size. Acta Metallurgica, vol. 30, pp. 1511-1514, 1982.
 65. Mellor, M. and Cole, D., Cyclic loading and fatigue in ice. Cold Regions Sci. Tech., vol. 4, pp. 41-53, 1981.
 66. Mellor, M., Mechanical properties of polycrystalline ice. Physics and Mechanics of Ice, IUTAM Symposium, Copenhagen, Springer-Verlag, pp. 217-245, 1979.
 67. Jones, S.J., Triaxial testing of polycrystalline ice. Third Internat. Conf. on Permafrost, Edmonton, pp. 670-674, 1973.
 68. Haynes, F.D., Tensile strength of ice under triaxial stresses. USACRREL Research Report 312, 1973.
 69. Frederking, R.M.W., Plane-strain compressive strength of columnar-grained and granular snow ice. J. Glaciology, vol. 18, no. 90, pp. 505-516, 1977.
 70. Deleted.
 71. Butkovich, T.R., Ultimate strength of ice, USA SIFRE Research Report 11, 1954.
 72. Urabe, N. and Yoshitake, A., Strain rate dependent fracture toughness (K_{IC}) of pure ice and sea ice. Internat. Sympos. on Ice, IAHR, Quebec, pp. 417-420, 1981.
 73. Miller, K.J., The application of fracture mechanics to ice problems, in Physics and Mechanics of Ice, ed. P. Tryde, Springer-Verlag, Berlin, pp. 265-277, 1979.
 74. Cox, G.F.N. and Weeks, W.F., Equations for determining the gas and brine volume in sea ice samples. CRREL Report 82-30, 7 pp., 1982.
 75. Langbein, M.P. and Pounder, E.R., Elastic parameters of sea ice, in Ice and Snow - Properties Processes and Applications, ed. W.D. Kingery, MIT Press, pp. 69-78, 1963.
 76. Tabata, T., Studies of the visco-elastic properties of sea ice, in Arctic Sea Ice, U.S. Nat. Acad. Sci. - Nat. Res. Council Pub. 598, pp. 139-147, 1958.
 77. Kohnen, W., Seismic and ultrasonic measurements on the sea ice of Eclipse Sound near Pond Inlet, N.W.T. in northern Baffin Island. Polarforschung, Jahrg 4, no. 2, pp. 66-74, 1972.
 78. Abele, G. and Frankenstein, G., Snow and ice properties as related to runways in Antarctica. USACRREL Technical Report 174, 37 pp., 1967.
 79. Brown, J.H., Elasticity and strength of sea ice, in Ice and Snow: Properties, Processes and Applications, ed. W.D. Kingery, pp. 79-106, MIT Press, 1963.
 80. Anderson, D.L., Preliminary results and review of sea ice elasticity and related studies, Trans. Engineering Inst. Canada, vol. 2, no. 3, pp. 116-122, 1958.
 81. Traetteberg, A., Gold, L.W. and P. Frederking, The strain rate and temperature dependence on Young's modulus of ice, International Symposium on Ice Problems, IAHR, Hanover, NH, USA, pp. 479-486, 1975.
 82. Kovacs, A., Weeks, W.F. and F. Michetti, Variation of some mechanical properties of polar snow, Camp Century, Greenland, CRREL Research Report 276, 33 pp., 1969.
 83. Vaudrey, K.D., Ice engineering - study of related properties of floating sea-ice sheets and summary of elastic and viscoelastic analyses, U.S. Naval Civil Engineering Lab., Tech. Rept. RB60, 1977.
 84. Murat, J-R. and R. Tinawi, Sea ice testing in flexure, Proceedings of POAC 77, St. John's, Newfoundland, vol. 2, pp. 638-653, 1977.
 85. Lainey, L. and Tinawi, R., Parametric studies of sea ice beams under short and long term loading, IAHR Internat. Sympos. on Ice, Quebec, Canada, pp. 440-452, 1981.
 86. Murat, J.R. and Lainey, L.M., Some experimental observations on the Poisson's ratio of sea ice, Cold Regions Science and Technology, vol. 6, no. 2, pp. 105-113, 1982.
 87. Deleted.
 88. Wang, Y.S., Uniaxial compression testing of arctic sea ice, POAC, Quebec, Canada, vol. 1, pp. 346-355, 1981.
 89. Mellor, M. and I. Hawkes, Measurement of tensile strength by diametral compression of discs and annuli, Engineering Geology, vol. 5, pp. 171-225, 1971.
 90. Wang, Y.S., Crystallographic studies and strength tests of field ice in the Alaskan Beaufort Sea, Proceedings of POAC 79, Trondheim, vol. 1, pp. 651-665, 1979.
 91. Schwarz, J., The pressure of floating ice-fields on piles. (In International Association of Hydraulic Research. IAHR Symposium: ice and its actions on hydraulic structures, Reykjavik, Iceland, 8-10 September 1970, Delft, International Association of Hydraulic Research, paper 6.3., 1971.
 92. Frederking, R.M.W. and Timco, G.W., NRC ice property measurements during the CANARIK VIGORIK trials in the Beaufort Sea, winter 1969-80, Nat. Res. Council Canada, Div. Building Res., DRB Paper No. 947, 1981.
 93. Wang, Y.S., Sea ice properties, in Technical Seminar on Alaskan Beaufort Gravel Island Design, Exxon, U.S.A., 1979.

94. Dykins, J.E., Ice engineering - tensile properties of sea ice grown in a confined system, U.S. Naval Civil Engineering Lab. Tech. Rept. R689, 1970.
95. Deleted.
96. Butkovich, T.R., On the mechanical properties of sea ice, Thule, Greenland, 1957. U.S. Snow, Ice and Permafrost Research Establishment. Research Report 54, 11 pp. and appendices, 1959.
97. Deleted.
98. Saeki, H. and Ozaki, A., Experimental study on flexural strength and elastic modulus of sea ice. POAC, Quebec, vol. 1, pp. 536-547, 1981.
99. Urabe, N., Iwasaki, T. and Yoshitake, A., Fracture toughness of sea ice. Cold Regions Sci. Tech., vol. 3, no. 1, pp. 29-37, 1980.
100. Urabe, N. and Yoshitake, A., Fracture toughness of sea ice - in situ measurement and its application. POAC, Quebec, Canada, vol. 1, pp. 356-365, 1981.
101. Deleted.
102. Shaniro, L.H., Metzner, R.C. and Johnson, J.B., Fracture toughness of sea ice. Report to Shell Development Company.
103. Panov, V.V. and N.V. Fokeev, Compression strength of sea ice specimens under complex loading. Problemy Arktiki i Antarktiki, vol. 49, pp. 81-86. (English translation pp. 97-104), 1977.
104. Hüusler, F.V., Multiaxial compressive strength tests of saline ice with brush-type loading plates. International Symposium on Ice, Quebec. IAHR, pp. 526-539, 1981.
105. Mellor, M., Cox, G.F.N. and H.W. Bosworth, The mechanical properties of multi-year sea ice, Phase I: Techniques for measuring the mechanical properties of ice. USACRREL Report for Shell Development Co., (to be published by CRREL), 1983.
106. Timco, G.W. and Frederking, R.M.W., Compressive strength of multi-year ridge ice, in Workshop on Sea Ice Ridges, Calgary, Alberta, Nat. Res. Council of Canada, 1980.
107. Mellor, M., Engineering properties of snow, Journal of Glaciology, vol. 19, no. 81, pp. 15-66, 1977.
108. Mellor, M., Ship resistance in thick brash ice, Cold Regions Science and Technology, vol. 3, no. 4, pp. 305-321, 1980.
109. Hamza, H. and D.B. Muggerridge, "Plain Strain Fracture Toughness (K_{Ic}) of Fresh Water Ice," POAC 79, vol. 1, pp. 697-707, 1979.





CRREL Monograph 82-1

November 1982

The growth, structure, and properties of sea ice

W.F. Weeks and S.F. Ackley

Unclassified

SECURITY CLASSIFICATION OF THIS PAGE (When Data Entered)

REPORT DOCUMENTATION PAGE		READ INSTRUCTIONS BEFORE COMPLETING FORM
1. REPORT NUMBER CRREL Monograph 82-1	2. GOVT ACCESSION NO.	3. RECIPIENT'S CATALOG NUMBER
4. TITLE (and Subtitle) THE GROWTH, STRUCTURE, AND PROPERTIES OF SEA ICE		5. TYPE OF REPORT & PERIOD COVERED
		6. PERFORMING ORG. REPORT NUMBER
7. AUTHOR(s) W.F. Weeks and S.F. Ackley		8. CONTRACT OR GRANT NUMBER(s)
9. PERFORMING ORGANIZATION NAME AND ADDRESS U.S. Army Cold Regions Research and Engineering Laboratory Hanover, New Hampshire 03755		10. PROGRAM ELEMENT, PROJECT, TASK AREA & WORK UNIT NUMBERS
11. CONTROLLING OFFICE NAME AND ADDRESS U.S. Army Cold Regions Research and Engineering Laboratory Hanover, New Hampshire 03755		12. REPORT DATE November 1982
		13. NUMBER OF PAGES 136
14. MONITORING AGENCY NAME & ADDRESS (if different from Controlling Office)		15. SECURITY CLASS. (of this report) Unclassified
		15a. DECLASSIFICATION/DOWNGRADING SCHEDULE
16. DISTRIBUTION STATEMENT (of this Report) Approved for public release; distribution unlimited.		
17. DISTRIBUTION STATEMENT (of the abstract entered in Block 20, if different from Report)		
18. SUPPLEMENTARY NOTES		
19. KEY WORDS (Continue on reverse side if necessary and identify by block number) Electrical properties Sea ice Ice Structural properties Mechanical properties Thermal properties Salinity		
20. ABSTRACT (Continue on reverse side if necessary and identify by block number) This monograph describes in some detail the current state of knowledge of the observed variations in the structural characteristics (grain size, crystal orientation, brine layer spacing) and composition (brine, gas and solid salts) of sea ice as well as the presumed causes of these variations. The importance of these variations in controlling the large observed changes in the mechanical, thermal and electrical properties of sea ice is also discussed.		

Unclassified

PREFACE

This Monograph was prepared by Dr. W.F. Weeks, Glaciologist, Snow and Ice Branch, Research Division, U.S. Army Cold Regions Research and Engineering Laboratory, and S.F. Ackley, Chief of the Snow and Ice Branch.

The work on which a portion of this paper is based has taken place over a number of years. The authors particularly thank the Oceanic Processes Branch of NASA, the Arctic Program of the Office of Naval Research, the Division of Polar Programs of the National Science Foundation, and the Arctic Program of the Outer Continental Shelf Environmental Assessment Program of NOAA for their support and patience. The OCSEAP program was supported by the Bureau of Land Management and is a multiyear program responding to needs of petroleum development of the Alaskan Continental Shelf.

Technical review of the manuscript was performed by Dr. Anthony J. Gow and Jacqueline A. Richter of CRREL.

CONTENTS

	Page
Abstract-----	1
Preface-----	11
Introduction-----	1
The atomic structure of ice-----	1
The sea ice phase diagram-----	4
Formation of the initial ice cover-----	12
The transition zone-----	23
The columnar zone-----	29
Substructure-----	35
Constitutional supercooling-----	41
Variations-----	47
Directional c-axis alignments-----	47
Frazil ice-----	52
Multiyear ice-----	63
The salinity profile-----	69
Observations-----	69
Initial salt entrapment-----	74
Brine drainage mechanisms-----	78
Solid salt crystals-----	88
Relationships between sea ice structure and properties-----	90
Models for the variation in the mechanical properties of sea ice-----	90
Models for the variation in the thermal properties of sea ice-----	98
Electrical properties of sea ice in the 0.1- to 40-GHz range-----	103
Concluding statement-----	117
Literature cited-----	117

ILLUSTRATIONS

Figure	
1. Structure of ice I -----	2
2. A portion of the phase diagram NaCl-H ₂ O-----	5
3. Freezing point of brine as a function of the ratio of the weight of dissolved salts to pure water-----	7
4. Phase relations for "standard" sea ice-----	8
5. Relative water content in percent versus temperature for sea ice-----	10
6. Probabilities of values for D _c for various ions-----	11
7. Temperature of the density maximum and of the freezing point for seawater of different salinities-----	12
8. Growth sequence for ice crystals in bulk water-----	13
9. Initial discs during the freezing of seawater-----	14
10. Stellar ice crystals growing in seawater-----	15
11. Stellar ice crystals grown from seawater-----	15
12. Initial ice crystal formation in calm seawater-----	16
13. A needle surrounded by crystals with their c-axes vertical-----	17

Figure	Page
14. Inked copy of a surface rubbing of an ice skim-----	17
15. The relation between the ice surface topography produced by etching and the lines on a rubbing-----	18
16. Grease ice forming on the surface of a lead-----	19
17. Pancake ice forming from frazil crystals-----	20
18. Composite ice sheet of pancakes and sheet ice-----	21
19. Aerial photograph of grease ice-----	22
20. Schematic drawing of the general effect of Langmuir circulation on grease and pancake ice-----	23
21. Rubbing of the bottom of an ice skim-----	24
22. Photomicrograph of the lower surface of sea ice-----	24
23. Orientation of the c-axes of sea ice crystals from different depths-----	26
24. Histograms showing the relative percentage of different c-axis orientations-----	27
25. Schematic diagram showing the process of geometric selection according to Perey and Pounder-----	28
26. c-axis orientation in a healed crack-----	29
27. Rubbing from just below the transition layer on an ice sheet-----	30
28. Histogram giving the angles between the c-axes of neighboring ice crystals-----	30
29. Vertical rubbing of columnar zone ice-----	31
30. The distribution of c- and a-axis orientations in the upper and lower portions of thin ice sheets-----	32
31. Lengths and widths of ice crystals at different levels in a sea ice sheet-----	32
32. Increase in crystal size with distance below the surface of an ice sheet-----	32
33. Plot of change in grain size with distance below the upper ice surface-----	34
34. Histograms of crystal diameters at different levels in an ice sheet-----	34
35. Horizontal thin section of sea ice from below the upper ice surface-----	36
36. Photographs of two thin sections showing cellular substructure in sea ice-----	37
37. Plot of $-\log(a_0v)$ versus $(\log 1/v)^2$ -----	38
38. Profiles of growth rate, salinity and brine layer spacing-----	39
39. Plot of average brine layer spacing versus corresponding rate of growth-----	40
40. Vertical thin section of sea ice from the lower portion of the core from site J-9, Ross Ice Shelf -----	41
41. Steady-state distribution of solute in the liquid ahead of an advancing solid/liquid interface-----	43
42. Constitutionally supercooled zone of liquid ahead of an advancing interface-----	43
43. A plot of the boundaries that separate growth conditions where a planar interface is stable and where it is unstable-----	44
44. Schematic of knife-edged cells-----	45
45. The c-axis orientations as determined by Cherepanov in the Kara Sea-----	47

Figure	Page
46. Sample site locations, mean c-axis alignments, and instantaneous current directions determined along the coast of the Beaufort Sea-----	48
47. Schmidt net plots of individual c-axis orientations for six different sampling sites-----	49
48. Mean crystal orientation in the horizontal plane, and the standard deviation as a function of vertical location in the ice sheet-----	50
49. Histogram showing the relative frequency of different deviations between the observed instantaneous current direction and the mean c-axis direction-----	50
50. Sketch showing the interface geometry of two crystals---	51
51. Site locations for sea ice core sampling from the USCGC <u>Polar Sea</u> -----	53
52. Salinity, structure and thin section photos from selected depths for Floe 42-A-1-----	54
53. Salinity, structure and thin section photos from Floe 43-A-2-----	55
54. Salinity, structure and thin section photos from Floe 44-G-3-----	56
55. Salinity, structure and thin section photos from Floe 49-G-2-----	57
56. Salinity, structure and thin section photos from Floe 61-G-2-----	58
57. Congelation ice vs ice thickness for all cores obtained in the Weddell Sea-----	59
58. Profiles of seasonal changes of temperature with depth in the water column typical of the Antarctic and the Arctic-----	60
59. Cross section of a multi-year floe-----	64
60. Winter's increment of ice growth plotted against the number of annual layers measured from the top of the floe-----	66
61. The distribution of salinity, temperature and the resultant density caused by the diffusion of a fresh-water layer over a saltwater layer-----	67
62. Salinity profiles of ice of Eclipse Sound at intervals of two weeks during the winter of 1977-78-----	69
63. Average salinity of ice sheet at Hopedale, Labrador-----	70
64. Average salinity of sea ice as a function of ice thickness-----	71
65. Average multiyear salinity profiles for hummocked and depressed areas-----	72
66. A cross section of an area of multiyear ice showing the variation of salinity with topography-----	72
67. Average salinity of sea ice as a function of ice thickness for warm sea ice-----	73
68. Plot of $\ln(1/k-1)$ versus v using the salinity entrapment data of Cox and Weeks-----	76
69. Plot of k vs $\delta v/D$ for the salinity entrapment data of Cox and Weeks-----	76
70. Plot of $\ln(1/k-1)$ versus v for columnar-grained sea ice-	77
71. Stable salinity or k versus growth rate-----	77
72. Relation between brine pocket migration velocity and ice temperature -----	80

Figure	Page
73. Relation between the temperature gradient in the ice and the brine pocket migration rate-----	80
74. Comparison between experimental salinity curves and theoretical salinity curves determined from a brine expulsion model-----	82
75. Plot of rate of change of salinity due to gravity drainage versus brine volume for different temperature gradients-----	83
76. Plot of rate of change of salinity due to gravity drainage versus low brine volumes for different temperature gradients-----	83
77. Schematic drawing of a cut through a brine drainage channel-----	84
78. Number of brine drainage channels developed in thin ice sheets versus the average growth rate-----	84
79. Relationship of maximum brine volume and salt advection required to maintain the steady-state salinity profile-----	88
80. Scanning electron micrographs of a vertical section of a brine pocket at -30°C, second replica-----	89
81. Rubbing of a broken segment of sea ice-----	91
82. Idealized diagram of the shape of the brine inclusions in sea and NaCl ice-----	92
83. An idealization of the structure of sea ice used in calculating its elastic modulus-----	95
84. Thermal conductivity of pure ice as a function of temperature-----	99
85. Thermal conductivity of sea ice-----	100
86. Density and thermal conductivity of bubbly ice as a function of the fractional air content-----	101
87. Effective thermal conductivity of sea ice as a function of temperature for various salinities and densities-----	101
88. Thermal conductivity of sea ice calculated using Ono's model-----	102
89. Thermal diffusivity of sea ice-----	102
90. Real and imaginary parts of the dielectric constant for brine and pure water-----	106
91. Brine layers at the bottom of the ice sheet showing necking off as the temperature is lowered-----	107
92. Ice salinity, temperature and brine volume profile from the Alaskan Arctic-----	110
93. Computed depth-dielectric constant profiles-----	111
94. Simulated returned power/incident power vs depth-----	112
95. Scattering albedo vs scatterer size to wavelength ratio for ice overlying fresh water-----	116
96. Changes in brightness temperature plotted against scattering albedo with the layer thickness to wavelength ratio as a parameter-----	116

TABLES

Table

1. Some properties of the solid salts presumed to occur in sea ice-----	9
---	---

THE GROWTH, STRUCTURE, AND PROPERTIES OF SEA ICE

W.F. Weeks and S.F. Ackley

INTRODUCTION

On the geophysical scale sea ice is a thin, fragile, dynamic, solid layer that forms under the thermodynamic conditions that occur near the Poles. There it serves as a boundary between two much larger fluid bodies — the ocean and the atmosphere. Typical scales of interest would be 10^3 to 10^6 m. In the present paper we take a more detailed view, focusing on the ice itself at scales ranging between 10^0 and 10^{-3} m, with an occasional glimpse at a scale of 10^{-10} m. It is our purpose to help the reader understand the internal structure of sea ice, how this structure develops, and how it affects the bulk properties of the ice. Although this is a subject that has received little attention in comparison to similar studies of metals and ceramics, it is, in our view, very important, as many details in the behavior of sea ice are structurally controlled. The variations in structure are, in turn, determined by the environmental conditions under which the ice has formed.

In the following, we will take many observations and theories based on studies of other materials and apply them to sea ice. This is a natural progression, in that it moves from the well studied to the little studied. The reader should, however, be warned that such transfers of ideas are, many times, far from straightforward. In fact, it is to be hoped that in the long run the study of sea ice as a material will be able to contribute as much to the study of other materials as it receives. The reasons for this optimism are several. First, the natural range of temperatures at which sea ice exists is just a few degrees off its melting point. In fact, sea ice normally is only partially solidified in that it contains melt inclusions. Second, this temperature range is one in which man can operate without special precautions or equipment. Therefore, experiments on sea ice are much easier than experiments on most metals and ceramics studied at similar near-melting temperatures. Finally, pure ice, the primary phase composing sea ice, is transparent. This makes it relatively easy to look inside the ice and to observe what is actually occurring. This is a luxury rarely available to workers in metallurgy and ceramics.

THE ATOMIC STRUCTURE OF ICE

One of the unusual characteristics of ordinary ice is that it is less dense than its melt. Geophysically this low density is quite important in that it causes ice to float on the surface of lakes and seas. If ice sank into its melt, as do most solids, there would be a tendency for natural water bodies to freeze completely to their beds, a situation hardly conducive to the development of aquatic life in either temperate or polar regions.

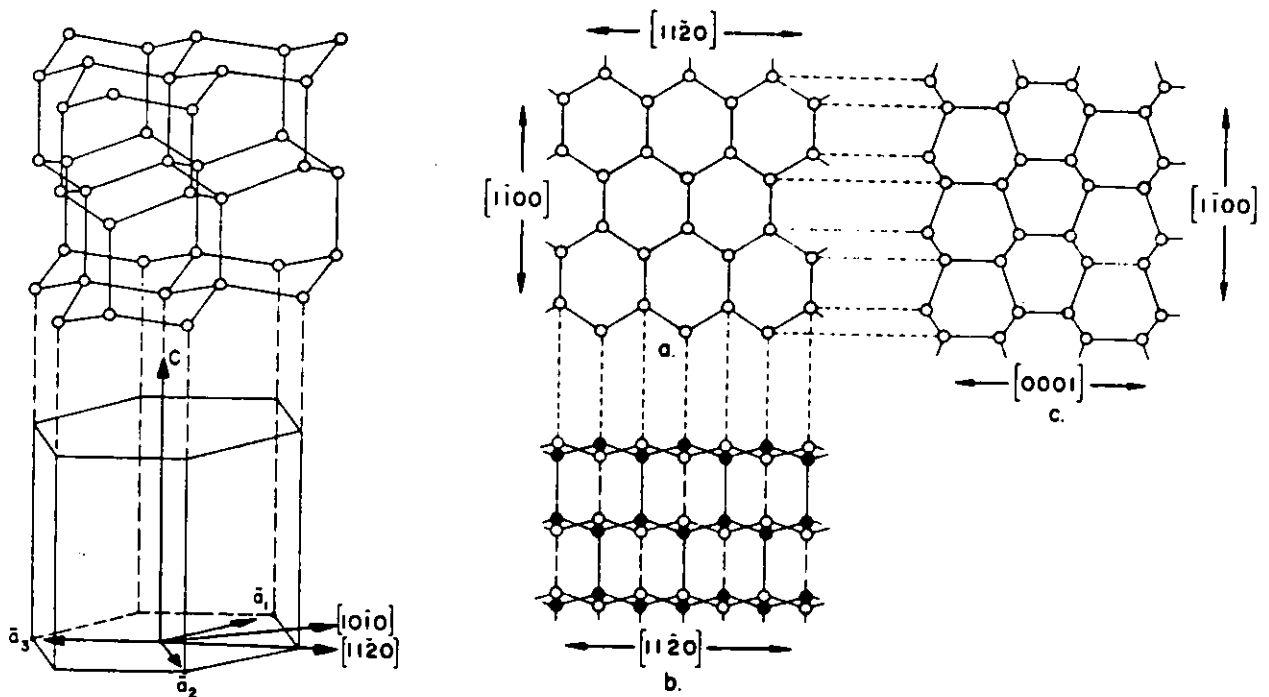


Figure 1. Structure of ice I.

The fact that ordinary ice is such an open, low density solid also suggests that there may be other, more compact atomic arrangements of H and O that would result in H_2O polymorphs with a higher density. There are, in fact, at least nine other polymorphs of H_2O (Hobbs 1974) that can be produced. However, ordinary ice (ice I) is the only one of these that exists in significant quantities under the physical conditions encountered at the earth's surface. In the remainder of this paper, when ice is referred to, the ice polymorph will always be ice I.

The geometric arrangement of the oxygen atoms, which in the ice structure are the principal diffracting centers for X-rays, is well understood, as ice was one of the first substances to have its structure determined (Bragg 1922, Lonsdale 1958, Owston 1958, Hobbs 1974). The results of these studies are shown in Figure 1. Each oxygen atom is located at the center of a tetrahedron with four other oxygen atoms located at each of the apices. The O-O distance is 0.276 nm at $0^\circ C$, resulting in an open, low-density structure. The tetrahedral coordination of the oxygen atoms results in a crystal structure possessing hexagonal symmetry, a fact that will affect many of the large scale characteristics of ice. An important feature of the structure of ice I is that the oxygen atoms are concentrated close to a series of parallel planes that are referred to as the basal planes. The direction perpendicular to these planes is referred to as the principal hexagonal or c-axis. The arrangement is such that, in any unit cell which contains four oxygen atoms, fracture along the basal or (0001)* plane involves

* The parentheses around the Miller indices signify a single plane or a set of planes; indices of a direction are given in brackets, i.e. $[11\bar{2}0]$, and the full set of equivalent directions of a form are indicated by carets, i.e. $\langle 11\bar{2}0 \rangle$ (Barrett 1952, p. 8-12).

the rupture of only two bonds. On the other hand, fracture along any plane normal to this plane requires the breaking of at least four bonds. Therefore, the fact that ice glides and cleaves readily on the basal plane can be easily rationalized in terms of its atomistic structure. When the positions of the oxygen atoms are projected parallel to the [0001] direction, the resulting hexagonal array (Figure 1a) can be seen to be composed of three close-packed rows of atoms. These rows lie in the $\langle 11\bar{2}0 \rangle$ direction parallel to the three secondary or a-axes. As will be seen, the a-axis directions, which are, of course, all equivalent, correspond to the directions of the arms of a) dendritic sea ice crystals growing from the melt, b) snowflakes growing from the vapor, and c) internal melt features that form inside ice crystals as the result of absorbed solar radiation; again all are external manifestations of the atomic structure.

This highly regular net of oxygen atoms is bonded together by a series of hydrogen bonds. The positions of the hydrogen atoms in these bonds are disordered and obey the so-called Bernal-Fowler rules: 1) two hydrogens are near each oxygen atom and 2) only one hydrogen atom can be on or near the line connecting two neighboring oxygen atoms. Within the constraints of these rules all configurations are considered to be equally probable. The average structure that results can be specified by assigning hypothetical "half-hydrogen" atoms to each of the $4N$ sites contained in any array of N oxygen atoms. Therefore each oxygen atom is tetrahedrally surrounded by four "half-hydrogens." This arrangement of "half-hydrogens" is in good agreement with both the observed zero-point entropy of ice (Pauling 1935, Nagle 1966, Suzuki 1967) and the results of single-crystal neutron diffraction studies (Peterson and Levy 1957). Any violation of the Bernal-Fowler rules can be considered as producing a defect in the ice structure, with a violation of rule 1 resulting in an ionic defect: an oxygen atom surrounded by three protons produces a positive ion $(H_3O)^+$ while one with only one proton produces the negative ion $(OH)^-$. When rule 2 is violated, a Bjerrum defect results: when two protons occur on the bond a so-called D-defect results, while a bond with no protons gives an L-defect.

Although beyond the scope of the present paper, an understanding of the nature of the hydrogen bonding in ice is certainly necessary to the study of its electrical, diffusive, thermodynamic and mechanical behavior. For instance, it is the nature of the highly directional hydrogen bond that is responsible for the anomalous physicochemical properties of ice and water. As was mentioned, the density of ice at $0^\circ C$ is less than that of water at the same temperature, with the density of water increasing to a maximum at $+4^\circ C$. The low density of ice is the result of the tetrahedral coordination of each water molecule by hydrogen bonding causing a very open structure. On melting, some of the hydrogen bonds are broken, allowing the molecules to assume a more closely packed structure with an associated increase in density. This process of further bond breakage and compaction of molecules continues with rising temperature until a point is reached ($+4^\circ C$) when density increases are more than compensated for by thermal expansion.

THE SEA ICE PHASE DIAGRAM

Now that we have a general knowledge of the structure of pure ice, we next need information on the phase relations of the ice-salt and ice-seawater systems that are of concern in the study of sea ice. By phase relations we refer to information that specifies the different phases that coexist at equilibrium at different temperatures and pressures in a system with a known bulk composition. One of the first questions that must be considered here is "Does the ice that forms from freezing salt solutions incorporate salt in solid solution?" Here by solid solution we refer to the process when the impurity atoms actually occupy lattice sites in the atomic structure of the ice crystal. Solid solutions form most readily when the foreign atoms have the right size to fit into the host structure, tend to form a similar type of chemical bond, and have an appropriate charge to maintain electrostatic neutrality. Impurities fulfilling these requirements for substitution into ice are rare. Because the ionic and atomic radii of fluorine and nitrogen are similar to those of oxygen, F^- , HF , NH_4^+ , and NH_3 are likely candidates to replace some of the water molecules in the ice structure. Other possibilities are NH_4OH , NH_4F , and the hydrohalogen acids (HCl , HBr , and HI). In all of the above cases some limited substitution in the ice structure is observed. Maximum substitution occurs at a concentration of 10^{-2} mol/L, which corresponds to a molar ratio of about 1 in 5000. However, none of the above materials are present in significant quantities in seawater.

How much of the common components of seawater enter substitutionally into ice crystals grown from it? There is, to our knowledge, no precise information on the subject, although the amounts would appear to be extremely small. Harrison and Tiller (1963) estimate that for most solutes in ice the equilibrium solute partition coefficient k_o ($k_o = X_A^s / X_A^l$ where X_A^s and X_A^l are the mole fraction of solute A in the solid and liquid respectively) is less than $k_o < 10^{-4}$. In short, although thermodynamic arguments can be made that suggest that at equilibrium a finite amount of impurity should exist in the ice structure, this amount is apparently so small that for most purposes the ice can be considered as a pure phase. Therefore, as ice forms from a salt or seawater solution essentially all the solute is rejected back into the liquid or melt. So, as more and more ice forms with gradually decreasing temperature the melt that coexists in equilibrium with the ice becomes saltier and saltier. The phase relations simply specify the number and composition of the different phases (brine, ice, solid salts) that coexist at the different temperatures and pressures. Although, in principle, it is possible to calculate the phase relations from thermodynamic information, in fact phase diagrams, and particularly those for complex systems such as seawater, are invariably determined experimentally. The results of such experimentation are then displayed in the form of a phase diagram.

For example, Figure 2 shows the water-rich portion of the $H_2O - NaCl$ phase diagram, which is the simple two-component system that most closely approximates seawater. What happens when we start with an $NaCl$ solution and gradually cool it down past its freezing point until it becomes completely solidified can be seen on this diagram. Consider an

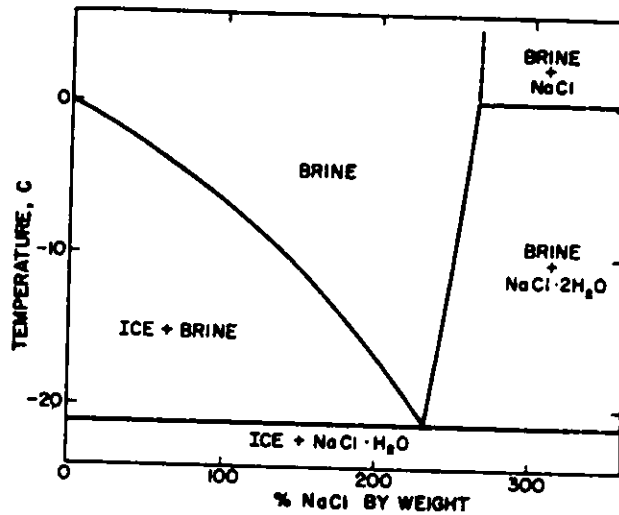


Figure 2. A portion of the phase diagram NaCl-H₂O.

NaCl solution with a composition of 35⁰/₀₀ NaCl at a temperature of +5°C. The phase rule is $P + F = C + 2$, where P is the number of phases that coexist, C is the number of components, and F is the number of degrees of freedom (for details refer to any standard physical chemistry text). However, in our case we have fixed one degree of freedom by the fact that our experiment was carried out at a constant pressure of 1 atmosphere and, therefore, the appropriate formulation of the phase rule becomes $P + F = C + 1$. We have a two-component system, H₂O and NaCl (so $C = 2$), with only one phase (the brine solution) present ($P = 1$). Therefore, $F = 2$ and two variables (temperature and bulk composition) must be specified to fix the state of the system. Figure 2 shows that experimentally ice is observed to start forming from a 35⁰/₀₀ NaCl solution at -2.0°C. Once ice forms P becomes 2, C remains 2, and $F = 1$, indicating that the system is now univariate. Therefore, as long as ice and brine coexist it is only necessary to specify the temperature or the bulk composition to fix the state of the system. In our case we initially specified the composition of the system, so if we additionally specify the temperature we have also fixed the composition of the brine that can coexist in equilibrium with the ice. The liquidus curve, in fact, gives the composition of the NaCl brine that is in equilibrium with ice at different temperatures. As the system continues to cool, more and more pure ice forms from the brine, causing the remaining brine to decrease in volume and become more saline. For example, at -5°C ice coexists with a brine containing 80⁰/₀₀ NaCl, while at -10° and -20°C the brine compositions are respectively 140 and 225⁰/₀₀. If cooling is continued to -21.2°C a third phase (the solid salt NaCl·2H₂O) is observed to form. Now P has become 3, C remains 2, and F must equal 0. The system is now referred to as being invariate, and this point (where the curve giving the composition of the brines that are in equilibrium with ice meets the curve giving the composition of the brines that are in equilibrium with NaCl·2H₂O) is called the eutectic point. As the system is invariate further cooling cannot continue until one of the phases disappears. Solidification continues at the eutectic temperature, with the two solids ice + NaCl·2H₂O crystallizing until all of the remaining brine has disappeared. The system is now composed of a

mixture of the two solids ice + NaCl·2H₂O, and a further decrease in temperature can proceed.

The above can be summarized as follows. When an NaCl solution with a composition similar to seawater (35‰ salt) is frozen, the first ice crystals start to form at -2.0°C. As freezing proceeds, more and more pure ice forms, with the remaining brine gradually becoming saltier and saltier. As long as ice and brine coexist the composition of the brine at each temperature is fixed. The formation of ice continues with further cooling, and the amount of brine becomes less and less until at a temperature of -21.2°C the eutectic point is reached and an additional phase, the sodium chloride dihydrate, is formed. At temperatures below the eutectic temperature all brine has solidified and only the two phases ice and NaCl·2H₂O exist.

When seawater is frozen a similar but more complex series of events occur. In this case we are dealing with an eight-component system for artificial seawater and a greater-than-eight-component system for natural seawater. Therefore, these systems never become invariable exhibiting eutectic points. With cooling, ice forms and the remaining brine becomes more saline. As cooling continues, different solid salts also precipitate from the brine. However they precipitate over a temperature range as opposed to a fixed eutectic temperature. At a temperature of -70°C there is still a measurable amount of brine believed to be present in the ice (Richardson and Keller 1966), and at least five solid salts are presumed to be present (CaCO₃·6 H₂O, Na₂SO₄·10H₂O, NaCl·2H₂O, KCl, MgCl₂·12H₂O).

Present phase information on sea ice is largely based on three different experimental studies (Ringer 1906, Gitterman 1937, Nelson and Thompson 1954). All these contributions are very creditable, but the first two works are old and the investigators were not aware of many potential problems that must be overcome in any proper determination of the phase relations (Tsurikov and Tsurikova 1972). Also, the Nelson and Thompson study was not focused on sea ice (they were interested in the possibility of the formation of sulfate deposits by freezing) and, therefore, certain desirable parameters of importance in the study of sea ice were not determined.

Without going into details concerning who did what and why, we feel that current deficiencies in the experimental studies of the sea ice phase diagram are as follows:

1. There has never been a direct determination of the composition of the solid salts that form in sea ice (their composition has always been inferred from changes in the composition of the brine).
2. Although equilibrium is always assumed in such studies, there does not appear to have been any attempt to verify this assumption by approaching the same state via different cooling (and heating) paths.
3. It is very important in phase studies to assure that the liquid phase is always compositionally homogeneous and can react with all the solid phases in the system. It is almost certain that this was not true in the three studies we mentioned. The general experimental technique

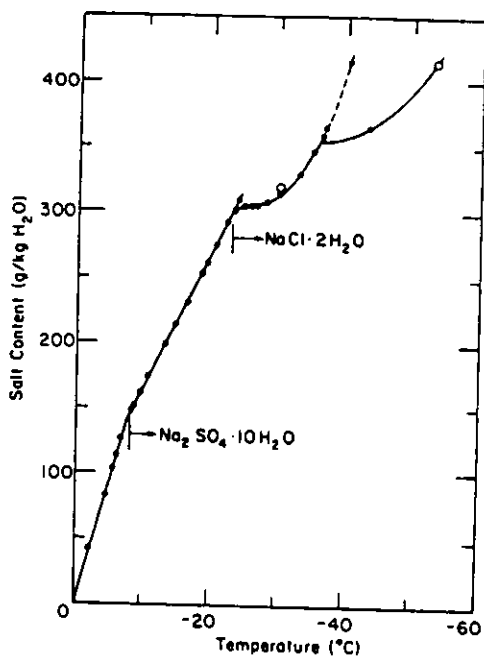


Figure 3. Freezing point of brine as a function of the ratio of the weight of dissolved salts to pure water (linear relations used to -24°C). Solid dots computed from data of Nelson and Thompson (1954). Open circles computed from Ringer (1906). The dashed line indicates a possible path if salts precipitate in a different order (after Assur 1958).

has been to freeze a solution to a desired temperature, remove the ice from the brine, and if necessary prepare a new solution for further freezing based on the composition of the remaining brine. This is an excellent procedure as long as the brine remains homogeneous and is in continuous contact with all the phases present. However, if isolated brine pockets form in the ice phase then the liquid and solids in these pockets can no longer react with the bulk liquid. This problem becomes particularly pronounced if there are reactions between the brine and previously formed solid phases. Several such reactions have been suggested by Gitterman and also by Savel'ev (1963), although the evidence for their occurrence cannot at present be considered conclusive.

4. All experimental work to date has ignored the carbonate content of the brine, although $\text{CaCO}_3 \cdot 6\text{H}_2\text{O}$ would appear to be the first solid salt to form during the formation of sea ice.

Considering the above problems, is our present knowledge of the phase diagram useful or just misleading? We feel that in most cases it is useful. The phase diagram as commonly utilized was worked out by Assur (1958), based on the work of Nelson and Thompson and of Ringer. Figure 3 shows the freezing point of the brine derived from standard seawater as a function of its composition (expressed as grams of salt per kilogram of H_2O). The different experimental determinations are in good agreement. Note that there are pronounced breaks in slope at temperatures where major solid salts start to crystallize. Figure 4 presents the phase diagram for standard sea ice, which is defined as sea ice of such a composition that its meltwater will have the same relative concentration of ions (to each other) as normal seawater (Assur 1958). The idea of standard sea ice is a useful one and is an extension of the observation that although the absolute amounts of salt in seawater may vary widely, the ratios of the ions relative to each other remain surprisingly constant. How applicable this observation is to sea ice will be examined later. It should be noted here that if the ratios of the

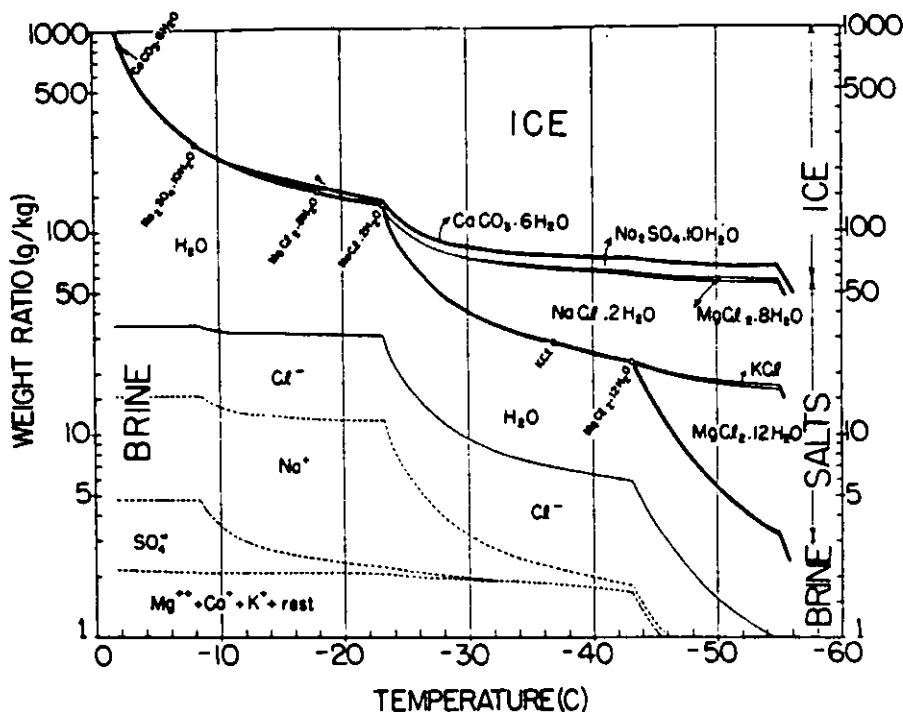


Figure 4. Phase relations for "standard" sea ice. Circles on the brine-salt line indicate temperatures at which solid salts precipitate (Assur 1958).

ions were to change, the crystallization temperatures of the solid salts would also be changed.

Figure 4 shows that at -10°C 1000 g of standard sea ice with a salinity of 34.325‰ is composed of 768 g of ice, 4.2 g of solid salt (4.0 g of $\text{Na}_2\text{SO}_4 \cdot 10\text{H}_2\text{O}$ + 0.2 g $\text{CaCO}_3 \cdot 6\text{H}_2\text{O}$) and 228 g of brine composed of 195 g H_2O and 32 g of various ions. At -30°C , on the other hand, the amount of ice and of solid salt present has risen to 917.0 and 43.4, respectively (76% of the solid salt is $\text{NaCl} \cdot 2\text{H}_2\text{O}$), while the amount of brine has decreased to 39.5 g (the exact figures can be found in Assur (1958)). The initial temperatures of crystallization of the various solid salts believed to be present in sea ice are given in Table 1. Also listed are some other characteristics of these salts, including their eutectic temperatures in pure salt- H_2O solutions. The differences in these temperatures are the results of the presence of the other ions in seawater brine that are not present in the aqueous solutions of the individual salts.

To change precisely from measurements of the weight of brine per kilogram of sample to the volume of brine per kilogram of sample, accurate measurements must be available of the density of the seawater brine coexisting with ice at different temperatures. As Nelson and Thompson only reported brine densities at $+4^{\circ}\text{C}$, this calculation cannot be made with the confidence desired. A table of the estimated values of the relative volume of brine (usually indicated by the symbol v_b) for standard sea ice is given in Assur (1958) for the temperature range of -0.1 to -54°C . In sea ice with a salinity of 1‰ only 0.075‰ of brine remains at -54°C as compared with 24‰ existing at -2.0°C (a

Table 1. Some properties of the solid salts presumed to occur in sea ice.

Salt Composition	Mineral Name	Crystal System	Density (Mg/m ³)	Eutectic Temperature of the Salt in an Aqueous Solution (°C)	Temperature of Initial Salt Formation in Seawater Brine (°C)
CaCO ₃ ·6H ₂ O	Mirabilite	Monoclinic	1,771	?	- 2.2
Na ₂ SO ₄ ·10H ₂ O		Monoclinic	1,464	- 3.6	- 8.2
MgCl ₂ ·8H ₂ O	Hydrohalite	Monoclinic	1,630 (0°C)	-33.6	-18.0
NaCl·2H ₂ O		Monoclinic	1,984	-21.1	-22.9
KCl	Silvite	Cubic	1,984	-11.1	-36.8
MgCl ₂ ·12H ₂ O	Antarcticite	Monoclinic	(1.24)	-33.6	-43.2 (erratic)
CaCl ₂ ·6H ₂ O		Hexagonal	1,718 (4°C)	-55.0	<-55.0

320-fold increase). In most applications where extreme accuracy is not deemed essential, the fact that v_b can be linearized as a function of $1/\theta$ and S_1 , where θ is the temperature and S_1 is the salinity of the ice, is utilized, and the empirical equations developed by Frankenstein and Garner (1967)

$$v_b = S_1 \left(\frac{45.917}{\theta} + 0.930 \right) \quad -8.2 \leq \theta \leq 2.0^\circ\text{C} \quad (1)$$

and

$$v_b = S_1 \left(\frac{43.795}{\theta} + 1.189 \right) \quad -22.9 \leq \theta \leq -8.2^\circ\text{C} \quad (2)$$

are used (note that different relations are used on the opposite sides of the Na₂SO₄·10H₂O crystallization temperature). At temperatures above and below the stated ranges it is necessary to refer directly to Assur's original table. It should be noted that both Assur's table and the above equations assume that sea ice has a constant density of 0.926 Mg/m³. Therefore, to determine the applicable brine volume for sea ice having a known bulk density of ρ , the calculated brine volume should be multiplied by $(\rho/0.926)$. Equations incorporating this density change and allowing the calculation of both the brine and the gas volumes in sea ice of known densities can be found in Cox and Weeks (1982).

The best check on the adequacy of Assur's brine volume diagram is a study by Richardson and Keller (1966) in which the amount of liquid water present in artificially frozen seawater was determined as a function of temperature by the use of nuclear magnetic resonance (NMR) techniques. These values were then compared with a curve of the same parameter based on Nelson and Thompson's chemical measurements. The results are shown in Figure 5. The agreement is very good at temperatures above -43°C (the MgCl₂·12H₂O crystallization temperature). At lower temperatures systematic differences were noted, with NMR giving the higher water contents. Fortunately, natural sea ice rarely exists at temperatures below -40°C.

Based on the NMR study can one assume that the phase relations published by Assur are adequate at temperatures above -40°C? This is a hard question to answer at present. The problems arise in two different but similar ways. First, as was mentioned, brine pockets may form,

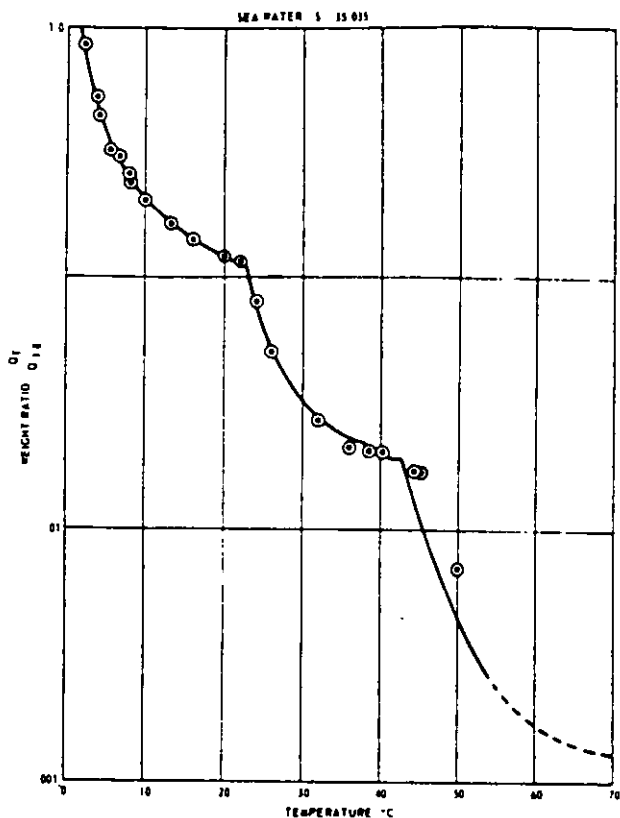


Figure 5. Relative water content in percent versus temperature for sea ice (sea-water sample 35.035‰ salinity). The curve is based on Nelson and Thompson's analytical data. The points are measured by NMR techniques (after Richardson and Keller 1966).

isolating portions of the brine and solid salts, and changing the sequence of possible reactions between these phases and the ice. Second, and probably more important, it is possible that as sea ice ages and brine drainage proceeds, the solid salts will remain fixed in the ice. This process would result in the enrichment of ions that are present in the early-formed solid phases. For instance, if the upper surface of sea ice were to be maintained at a temperature of -20°C for a long period of time, $\text{CaCO}_3 \cdot 6\text{H}_2\text{O}$ and $\text{Na}_2\text{SO}_4 \cdot 10\text{H}_2\text{O}$ would form while all the Cl^- ion would remain in the brine. If brine drainage were to proceed, this could produce changes in the $\text{SO}_4^{2-}/\text{Cl}^-$ and $\text{CO}_3^{2-}/\text{Cl}^-$ ratios. If these changes were large enough the standard sea ice phase diagram of Assur would no longer be applicable, with appreciably different phase relations being exhibited by ices that have had different thermal histories. As the thermal history of most pack ice is relatively unknown, we would be reduced to either performing a complete chemical analysis on each sea ice specimen or developing a technique that could easily be used to determine brine volume directly. Both of these methods would presumably be much more time consuming than the present technique of determining the salinity, density and temperature of a sample and determining the amount of brine, gas and solid salt in the ice from Assur's tables or Cox and Weeks' equations.

Do significant changes occur in the ratios of the ions in sea ice? The evidence is mixed. In newly formed ice, and in first-year ice that has not been subject to low temperatures for long periods of time, most measurements (Bennington 1963b, Blinov 1965, Addison 1977) suggest that major changes in the ion ratios are small. For thicker ice, and particularly for multiyear ice where the changes in ion ratios would be expected to be largest, experimental results are quite variable. The most

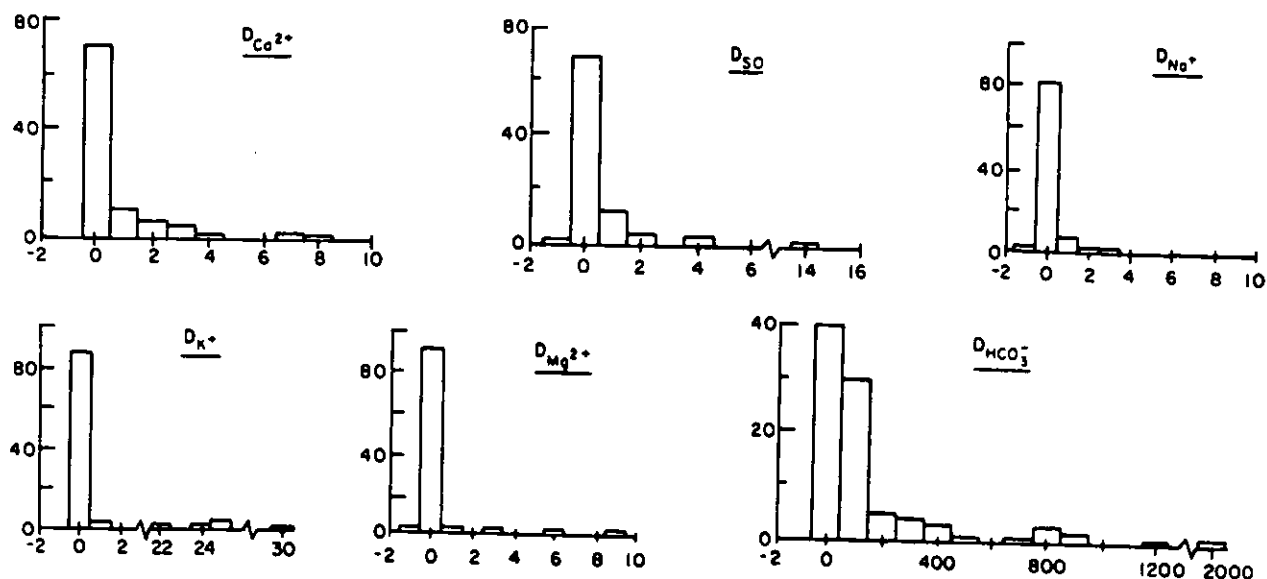


Figure 6. Probabilities (expressed as percentage) of values for D_c for various ions (Tsurikov 1974).

thorough study of the problem is by Tsurikov (1974, 1976), who calculated the ratio

$$D_c = \frac{(c/Cl)_i - (c/Cl)_w}{(c/Cl)_w} \quad (3)$$

where c is the concentration of the ion of interest and i and w indicate ice and water respectively. Positive values of D_c indicate that the content of ion c in the ice is higher than in the water. The chloride ion was chosen as the "standard" as it is retained completely within the brine at temperatures above -22.9°C and, therefore, should show extensive depletion via drainage. Figure 6 shows the relative frequencies of the D_c values calculated for several different ions. Although negative D_c values do occur, all the histograms show pronounced positive skews. The most interesting case is that of $D_{HCO_3^-}$; only 60% of the samples showed non-zero $D_{HCO_3^-}$ values indicating measurable changes in the relative ratios of (HCO_3^-/Cl) in the ice as compared to the seawater from which the ice formed. One sample showed a 2000-fold enrichment in HCO_3^- and several values near 800 were observed. That higher values might be observed for $D_{HCO_3^-}$ is not too surprising as $CaCO_3 \cdot 6H_2O$ is the first solid salt to form in sea ice (-2.2°C) which would presumably tend to immobilize the CO_3^{2-} ion, resulting in enrichment. However, such large values would appear difficult to explain. The other histograms show similar but much less striking trends, with near-zero values occurring in excess of 70% of the time. A 14-fold enrichment was noted for D_{SO_4} , which is not surprising. However, a 30-fold enrichment was observed for D_K , which is surprising in that the first K salt (KCl) does not form until -36.8°C and therefore K^+ should be more mobile than Cl^- . The effects of these ratio changes on the sea ice phase relations, and in particular on current techniques for estimating brine volume, are not presently clear. Certainly this is an area worthy of further study. To add to the confusion, the most recent paper on the subject (Reeburgh and Young, in press) obtained data that suggest an initial change in the

$\text{SO}_4^{2-}/\text{Cl}^-$ ratio during the formation of first-year ice but no change in the ratio for multiyear ice. As in most of the previous studies, the sampling was sparse (1 first-year and 1 multiyear site).

FORMATION OF THE INITIAL ICE COVER

In comparison to the rather voluminous literature devoted to the freezing of bodies of "fresh" water, little attention has been paid to the initial formation of sea ice. It is possible, however, by piecing together the available information on sea ice and comparing it with the "fresh" water observations, to arrive at a fairly complete qualitative picture of the gross features of the process. This initial crystal formation is unique in that, although the cold source is the overlying air, the velocity of crystal growth is probably largely limited by the rate of heat and solute dissipation through the liquid. It is, therefore, the only portion of the growth of a sea ice sheet that can be considered as true dendritic growth, i.e. that type of branched external crystal morphology that is characteristic of growth into "thermally" supercooled melts.

Because normal seawater has a salinity greater than 24.7‰ , therefore possessing a freezing point higher than its temperature of maximum density (Fig. 7), surface cooling creates an unstable vertical density distribution, causing convective mixing. This process transports the sensible heat stored in the lower layers of the water to the surface where it is dissipated. At the time of initial ice formation a several-meter-thick upper layer of the sea will have been lowered to or slightly below the freezing point.

The amount of supercooling necessary to initiate ice formation in seawater has apparently not been investigated. Considering the large number of solid impurities in any small volume of natural seawater, it is almost certain that homogeneous nucleation never occurs. Also, in polar regions snow crystals are fairly continuously being deposited on the upper water surface, providing nuclei for further growth. The amount of supercooling is probably a few hundredths to tenths of a degree Celsius.

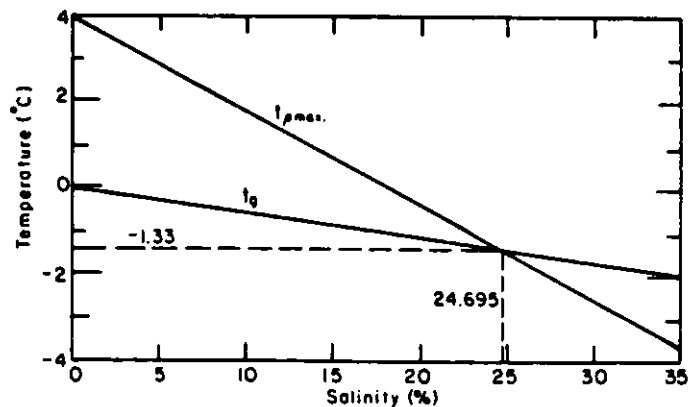


Figure 7. Temperature of the density maximum t_{pmax} and of the freezing point t_g for seawater of different salinities.

In general, the freezing of seawater appears to be similar to that of fresh water, and it is reasonable to assume that the first crystals to form will be minute spheres of pure ice (Hobbs 1974). Growth rapidly changes these spheres into thin circular discs in the general growth sequence spheres to discs to hexagonal dendritic stars, as shown schematically in Figure 8 (Arakawa 1954). The disc-like shape is the result of a highly anisotropic surface energy of ice which, although specifying a planar form, does not specify any particular growth direction in this plane. At small undercoolings, when heat and solute dissipation problems are not important, the growing disc can minimize its surface-to-volume ratio by maintaining a circular outline. That the growth rate of ice is strongly dependent on the growth direction is well known (Hillig 1958, 1959, Macklin and Ryan 1966). In ice discoids this plane of maximum growth is the (0001) or basal plane, which is the plane of maximum reticular atomic density in an ice crystal (Owston 1958). Therefore, ice growth can be said to be well described by Bravais' law: the smaller the reticular density of a crystal surface, the faster it grows normal to itself. The final crystal consists only of those surfaces showing the slowest normal growth, the close-packed surfaces (Rosenberg and Tiller 1957). Crystal growth parallel to the c-axis is orders of magnitude slower than growth in the (0001) plane, and the resulting kinetics are consistent with the classical Volmer-Stranski models, which are based on the assumption that two-dimensional nucleation and growth is the rate-controlling mechanism (Hillig 1958).

The maximum diameter to which discs grow is, at least in fresh water, on the order of 2 to 3 mm, and is a function of the supercooling. A discussion of the morphological stability of such disc crystals, including a specific discussion of ice discs growing in pure water, is given by Fujioka and Sekerka (1974). Related work concerning the morphological stability of ice cylinders freezing from aqueous solutions has been published by Hardy and Coriell (1973).

Figure 9 shows a large number of such discs developing in the upper centimeter of seawater (observations were made at Thule, Greenland). Note the characteristic notched edges on several of the tilted plates. Limited experimental observations (Kumai and Itagaki 1953) indicate that under comparable growth conditions the maximum disc size is depressed by the presence of an appreciable amount of solute in the water. Discs did, however, form in all cases when inorganic solutes were used (Arakawa and Higuchi 1954). This decrease in maximum disc size is quite

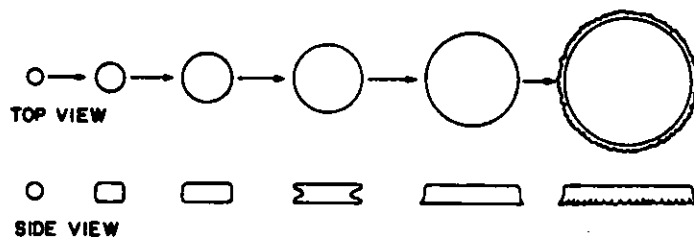


Figure 8. Growth sequence for ice crystals in bulk water (Arakawa 1954).



Figure 9. Initial discs during the freezing of seawater. Disc size is approximately 1 mm (Thule, Greenland).

reasonable since it is necessary for an ice crystal growing in seawater to dissipate both heat and solute into the surrounding liquid. As the radius of curvature of the disc increases, the ease of heat and solute dissipation decreases, until at some critical radius — determined by the thermal conductivity of the melt, the diffusion coefficient of the solute in the melt, and the growth velocity (Glen 1955) — the discoidal growth form becomes unstable, breaking up into a hexagonal dendritic star which again offers a much smaller tip radius of curvature. Although the change to a stellar form causes an increase in the relative amount of surface, this is apparently compensated for by the fact that the crystal is now more readily able to dispose of heat and solute at the advancing interface (the so-called "point effect of diffusion"). The disc-to-star transition is therefore marked by an appreciable increase in the growth velocity (Kumai and Itagaki 1953). That most, if not all, of the stellar crystals initially went through a discoidal stage can be seen by examining the centers of the stars under a high magnification (Fig. 10 and 11). The arms of the stars form parallel to the a -axis direction $\langle 11\bar{2}0 \rangle$ in the ice crystal, which, as was mentioned, is the shortest lattice vector in the (0001) plane.

Optically, these initial crystals, both discoidal and stellar, show a small but definite biaxiality. Optic angles of 3 to 5 degrees were observed in crystals from ice skins formed at Hopedale, Laborador, and Thule, Greenland. Golovkov (1936) reported 2V values as great as 20 degrees from crystals of Kara Sea ice. This biaxiality is undoubtedly



Figure 10. Stellar ice crystals growing in seawater.

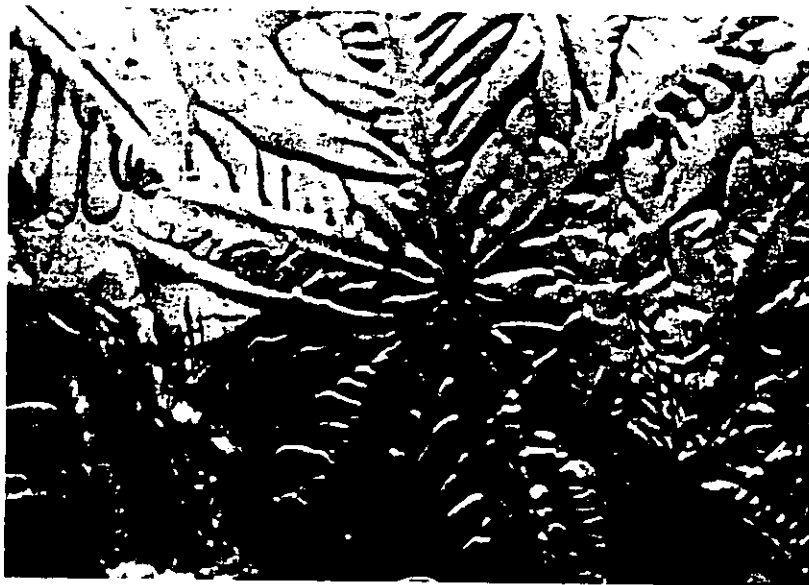


Figure 11. Stellar ice crystals grown from seawater.

produced by strains introduced in the crystals during their growth. Due to its low birefringence, ice is optically extremely stress-sensitive.

The star-like crystals grow rapidly across the surface of calm seawater until they overlap and freeze together, forming a continuous thin ice skim. Because of the tabular nature of both the initial ice discoids and stars, they float with their basal planes (0001) in the plane of the water surface. Ideally this would produce an ice skim with a completely c-axis-vertical orientation. However, since water conditions are rarely completely calm a number of discoids or stars are usually



Figure 12. Initial ice crystal formation in calm seawater.

caught in an intermediate position, i.e. with their c-axes inclined at some angle to the vertical. This is well shown in Figures 9 and 12 which are photomicrographs of initial ice crystal formation in seawater of 32‰ salinity. A petrofabric diagram of such a skim will appear similar to the first fabric diagram in Figure 23, a strong c-axis-vertical maximum and a few crystals in other orientations.

During the initial freezing of fresh water at low supercoolings, surface needles are extremely common (Fujino and Suzuki 1959, Hallett 1960). The needles form when a disc becomes inclined at an angle to the water surface. Subsequent growth then proceeds rapidly, in the form of long, thin, needle-like crystals, from the points where the disc intersects the surface. The needles appear to be confined strictly to the thin surface layer of water that is appreciably supercooled. If crystal growth were to continue downward along the basal plane, the crystal would immediately encounter water that is not supercooled and the growth would stop. If larger supercoolings are encountered more complex morphologies develop—simple double pyramids between -2.7 and -5.5°C and, at yet lower temperatures, complex double pyramids showing secondary and higher order non-rational growth directions (photographs of such crystals can be found in Macklin and Ryan (1966) or in Hobbs (1974)).

The limited observations available on the freezing of sea- and salt-water indicate that although surface needles are occasionally encountered, they appear to be rarer than in fresh water (Fukutomi et al. 1949, Arakawa and Higuchi 1954, Suzuki 1955, Fujino and Suzuki 1959). This observation is readily explained by the fact that prior to the nucleation of the initial sea ice crystals, convective mixing has lowered an appreciable thickness of the water layer to the freezing point. This makes it possible for inclined discs to grow both downward as well as along the water surface. A significant downward growth component causes the disc to develop as a dendritic star instead of a needle, and also produces a moment due to buoyancy forces which tends to rotate the



Figure 13. A needle surrounded by crystals with their c-axes vertical (normal to the plane of the photograph) (right 2/3 of photograph).



Figure 14. Inked copy of a surface rubbing of an ice skim.

stellar crystal until its (0001) plane is parallel to the water surface. Possibly needle-like growth in seawater occurs only when part of the needle has frozen to or is spatially restricted by other ice crystals, so that the needle is prevented from rotating when a downward growth component develops. Figure 13 is a photomicrograph of the upper surface of a thin ice skim showing the tip of such a needle (the surrounding ice is of an essentially c-axis-vertical orientation). Figure 14 is an inked copy of a rubbing of the upper surface of a similar ice

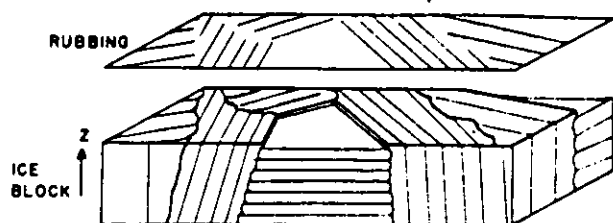


Figure 15. The relation between the ice surface topography produced by etching and the lines on a rubbing.

skim. This technique, which has been successfully applied to both glacier and lake ice for grain size measurements and texture analysis (Seligman 1949, Ragle 1962), utilizes the fact that projections on the ice surface appear as lines or "ticks" on the rubbing, while "smooth" (0001) surfaces appear as white or uniformly shaded areas. Each group of parallel lines represents a single crystal of sea ice. Figure 15 shows schematically the relation between the ice surface topography and the lines that appear on the rubbings. The majority of the surface of the ice skim in Figure 14 is composed of crystals with their c-axes roughly perpendicular to the freezing surface, although several needles and crystals with their c-axes inclined are present. A study of a number of such rubbings from ice skims formed during calm conditions shows that commonly >50% of the upper ice surface is composed of crystals with their c-axes approximately vertical. The curved dendritic growth patterns often noted on freshwater ponds do not appear to occur in sea ice. This is in keeping with the experimental results of Knight (1962a), which indicate that an increase in solute content tends to eliminate the curvature.

Available experiments suggest that the ice crystal morphologies developed during the freezing of pure water and of aqueous solutions are similar. Also, the presence of solutes appears to reduce the supercooling necessary for crystal growth to occur in non-rational crystallographic directions (Ryan and Macklin 1968, Ryan 1969). Therefore, one might expect to find reports of single and double pyramidal crystals forming during the freezing of seawater. We are not aware of such reported occurrences. We can, therefore, conclude that either natural supercoolings are not sufficient for pyramidal growth to develop or that no one has bothered to look. Both are probably true.

Crystal growth processes like those described above occur during calm, cold periods when there is no turbulence in the upper layer of the sea. The resulting ice cover "presents a smooth unbroken surface on which there are no highly evident horizontal changes in the structure of the ice layer" and has been termed "sheet ice" by Wilson et al. (1954). Commonly, however, in the open ocean there is some wave-induced turbulence during initial ice formation. This mixing introduces more nuclei into the area of active freezing and provides the energy to overcome the buoyancy forces so that the initial crystals may be "stirred" throughout a depth of up to several meters (Savel'ev 1958, Martin and Kauffman 1981). The effective supercooling is reduced, more crystals form per unit volume, and abrasive action between crystals is increased. As a result, extensive discoidal growth is favored. Even if stars were to form, their arms would commonly be broken off. It should be mentioned that in this freezing mode it has been found that it is not necessary for each individual crystal to nucleate separately.



Figure 16. Grease ice forming on the surface of a lead and being driven by the wind into its downwind end (Martin and Kauffman 1981).

Wind action herds the resultant ice crystals, which are generally termed frazil, into agglomerations that take on various forms. For instance, grease ice is an agglomeration of frazil crystals into a soupy layer that can be distinguished as a result of the low reflectivity, matte-like appearance of its upper surface (Fig. 16). Its major distinction from thicker and/or more compact agglomerations of frazil is in its mechanical behavior where it exhibits viscous fluid-like properties as opposed to the rafting and bending behavior of thicker or more compact floes. Martin and Kauffman (1981) describe a wave-damping experiment indicating that a general concentration of about 40% by volume of frazil ice crystals is necessary for the mechanical properties to transition to more solid characteristics. These wind-driven frazil accumulations can reach thicknesses of 1 m as opposed to the 0.01- to 0.1-m-thick frazil accumulations that occur before transitioning to columnar ice when quiescent conditions (no wind or waves) are present.

Pancake ice, roughly circular pieces of new ice with upturned edges, also results from frazil accumulations (Fig. 17). During the initial stages of the development of pancakes from frazil ice the pancakes are only semi-consolidated slush. When touched by a probe this will break up into horizontally floating discoids that will not sustain their own weight when removed from the water. The areas between the pancakes are usually relatively free of crystals and act as source areas for the growth of new crystals. Wave action then causes oscillatory

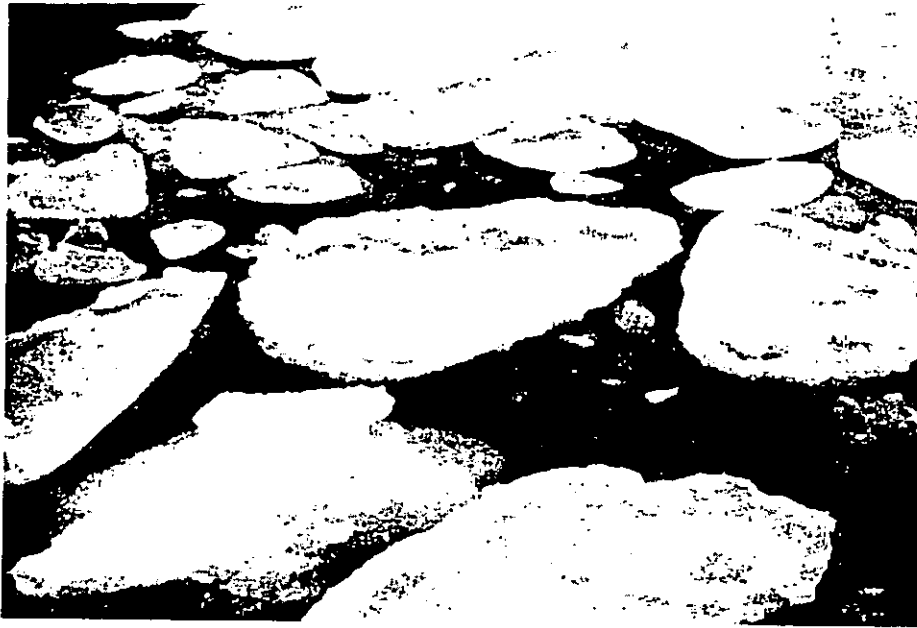


Figure 17. Pancake ice forming from frazil crystals (Dunbar and Weeks 1975).

motions that result in repeated contacts and separations between the floes, pushing the newly formed frazil crystals up to build the characteristic raised pancake rims. Bonding between frazil particles takes place when they are brought into contact, and is also a necessary process in forming these features. These intercrystal bonds develop by deformation and by surface energy forces (described in Hobbs (1974) and Colbeck (1979)). Two effects weld the particles. The first is regelation, where the force pressing the particles tends to locally depress the melting point, leading to heat flow away from and freezing at other contacts. As well, when the stress is removed, the unfrozen contact will change its freezing point and refreeze. The second mechanism is dependent on the radius of curvature and generally takes place in the unsaturated or above-sea-level portions of the pancake ice. Small particles in contact with the water and vapor that is present are thermodynamically unstable with respect to the equilibrium pressures between solid-liquid, solid-vapor and liquid-vapor at the surfaces of larger particles. The imbalance in pressures tends to deform the ice particles, leading to a flattened solid interface between them and causing them to be welded together at a solid boundary. A distinction between grease ice and pancake ice in the formation process may be related to the ability of the pancake floes to drain somewhat and increase the likelihood of freezing contacts developing by the non-equilibrium pressures due to radius of curvature effects between particles. Generally, in the completely saturated case when the ice crystals are immersed in seawater, bond development is not as dramatic as in the unsaturated compacts. These processes are, however, invoked cautiously as speculative models since they have been developed primarily to explain wet snow properties. The specific application to seawater-ice crystal systems has not been made, and since the thermodynamics is affected by dissolved impurities a complete formulation of the problem is necessary with the seawater parameters specified. It seems clear, however, that the physical processes are qualitatively similar and that bonding between particles is necessary to build these ice forms. When such crystals are



Figure 18. Composite ice sheet of pancakes and sheet ice, Gulf of St. Lawrence (Dunbar and Weeks 1975).

packed together into pancakes by wave motion and the movement of slush pancakes against one another, visual observations show that there is some tendency for the discoids to be stacked in a vertical position (c -axis horizontal) so that a closer lateral packing of discoids is permitted. The degree of orientation produced by this packing process is, of course, far from perfect, and in many cases the overall orientation may be close to random. Unfortunately, fabric diagrams of this type of ice are apparently lacking. The initial ice cover that results when a slush layer congeals is usually fine-grained equigranular in texture. A series of excellent vertical and horizontal photomicrographs of such ice are shown in Tabata and Ono (1957, Fig. 10 and 11-1 to -6).

The general shape of the initial pancakes depends upon their position in relation to the wave motion and shore. In the open ocean, away from the edge effects of shore, the pancakes tend to be circular in outline due to constant abrasion by other pancakes, which removes sharp corners. Close to shore the pancakes are commonly unequidimensional, with their long axes parallel to the shoreline.

During periods of wave action, as the growing ice sheet moves out from shore there is commonly a definite sequence in its development. There is a change from open water containing frazil crystals to grease ice to agglomerating pancakes and grease ice to loosely joined pancakes and finally to a complete sheet of joined pancakes. If at any given time during this process turbulence subsides, grease ice will form between the pancakes, producing a composite ice sheet (Fig. 18). Also, after the initial ice sheet has formed, sheet ice will develop beneath the pancakes and grease ice. Photographs illustrating the different aspects of the formation of both sheet and composite ice sheets can be found in Weeks and Lee (1958, 1962) and the illustrated ice glossaries (Armstrong et al. 1966, U.S. Navy Hydrographic Office 1952, Rodhe 1959).

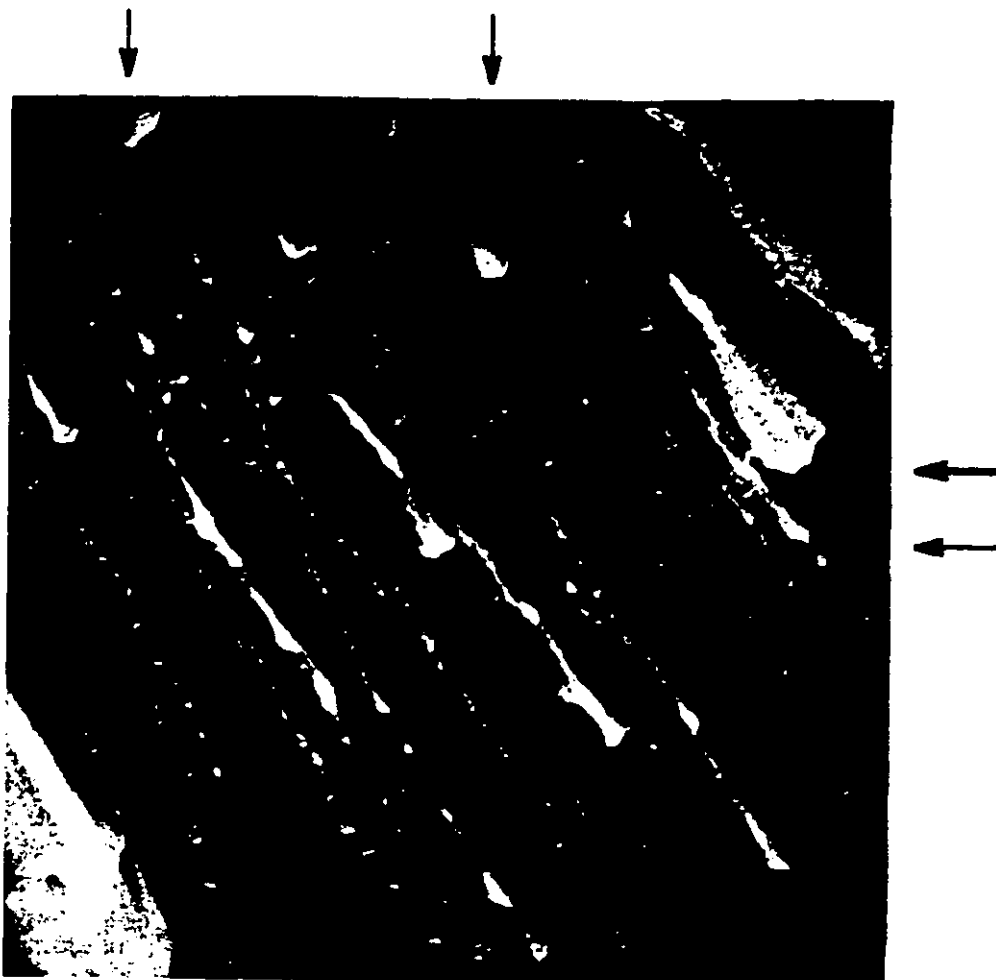


Figure 19. Aerial photograph from elevation of 147 m of grease ice showing tadpole shapes in a large polynya in the Bering Sea (Martin and Kauffman 1981).

In larger open-water regions, such as polynyas and open ocean-ice edge regions, cold, windy conditions cause grease ice and frazil crystals to stream out approximately parallel to the wind in long plumes. Figure 19 shows these plumes developing at surface temperatures of about -20°C and wind speed of 15 m/s in a polynya near Nome, Alaska. Dunbar [private communication; quoted in Martin and Kauffman (1981)] first suggested that a Langmuir circulation causes this organization of grease and pancake ice. Figure 20 schematically shows such a circulation. At the downwind head of such plumes a broadening occurs, usually consisting primarily of pancake ice. Such features have been dubbed "tadpoles" by Dunbar and Weeks (1975) because of their broad head - narrow tail shape. When formed by the offshore winds along shorelines or ice shelves these ice plumes eventually either disappear across regions of open ocean with warm conditions or form the relatively intact ice covers of larger fields of sea ice. Estimates of the ice production in such polynyas are large, with the possibility that an equivalent thickness of 2 m of ice can develop in as little as 20 hours, as opposed to an entire season's growth of 2 m of ice that would form under undisturbed conditions (Martin 1981).

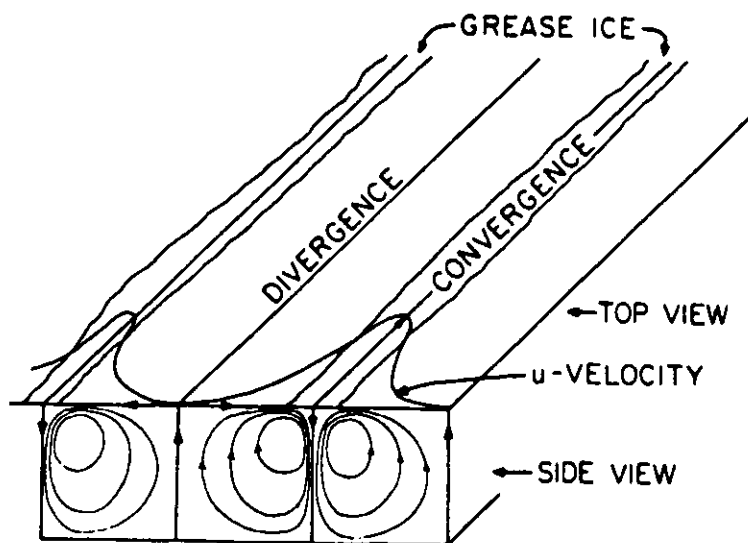


Figure 20. Schematic drawing of the general effect of Langmuir circulation on grease and pancake ice (Martin and Kauffman 1981).

As will be seen later, frazil ice formation can influence deep ocean circulation. It does this through salt fluxes caused by high ice production rates and through mechanical effects like the Langmuir circulations. Based on our most recent observations of Antarctic ice covers, frazil ice appears to be much more widespread than was previously thought. The mechanisms of ice-ocean interaction that contribute to frazil ice other than the initial forms we have just discussed are just being developed. We discuss the evidence for these other features and for possible mechanisms that could lead to increased occurrences of this ice type in a later section.

THE TRANSITION ZONE

Once a continuous skim of ice has formed across the sea surface, the possibilities for crystal growth due to purely "thermal" supercooling are greatly reduced. An ice skim now separates the melt (seawater) from the cold source (air). The latent heat is, therefore, extracted entirely through the ice sheet, and the growth rate is determined by the temperature gradient in the sheet and its effective conductivity. In addition, when a continuous ice layer has formed, the ice crystals lose a degree of growth freedom: only if the grain boundaries are exactly perpendicular to the freezing interface can crystal growth proceed without one grain interfering with the growth of another. Any tendency for anisotropic growth will produce geometric selection, with the crystals in the favored orientation eliminating the crystals in the unfavored orientation by cutting them off from the melt. Since "free-floating" ice crystals, forming both from fresh- and seawater, show pronounced anisotropic growth (ratios as high as 100:1; Hallett 1960), with the plane of maximum growth parallel to the (0001) crystallographic plane (Hobbs 1974), it is reasonable to suppose that geometric selection will occur. In fact, this phenomenon always does occur in natural ice sheets, and the ice layer in which the preferred orientation "wins out,"

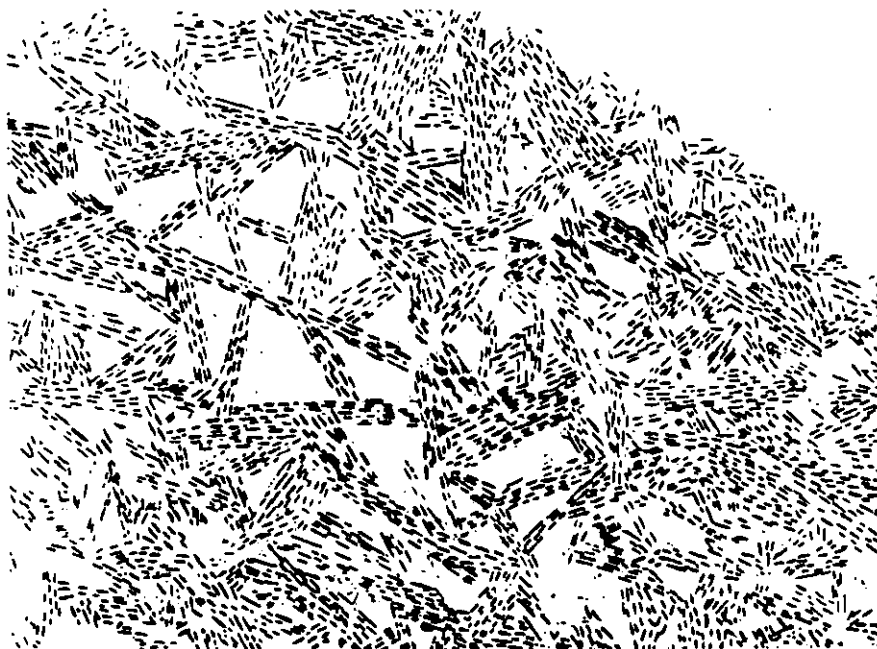


Figure 21. Rubbing of the bottom of a 2.5-cm-thick ice skim that is undergoing geometric selection (Hopedale, Labrador, 1955).



Figure 22. Photomicrograph of the lower surface of sea ice showing a triangular crystal being eliminated by geometric selection.

producing a characteristic growth fabric, has been termed the transition layer by Perey and Pounder (1958). In sea ice, the orientation change is usually essentially completed within a vertical distance of 5 to 10 cm, although the base of the transition layer may be located at distances in excess of 1 meter below the upper ice surface if the initial ice sheet is composed of a thick layer of frazil (Pounder and Little 1959, Weeks and Gow 1980).

A typical rubbing of the bottom surface of a 2.5-cm ice skim in which the process of geometric selection is obviously occurring is shown in Figure 21. The blank plane-sided polygonal areas are where c-axes vertical or near-vertical crystals occur. These crystals grow appreciably slower than the surrounding c-axes horizontal crystals. They therefore form depressed (\approx 2- to 5-mm) areas on the bottom surface of the ice skim and do not show in the rubbings. A photomicrograph of the bottom surface of an ice skim showing such a depressed area due to the presence of a c-axis vertical crystal is shown in Figure 22. If this ice were allowed to continue growing, the crystal in the center of the photomicrograph would be rapidly eliminated by the surrounding crystals as a result of selected growth parallel to the (0001) plane. Once the c-axes vertical crystals are eliminated, rubbings from the lower levels in the ice sheet are similar to Figure 27.

A more quantitative picture of this process can be obtained by making a series of c-axis orientation measurements at different levels in the ice sheet using a 4-axis universal stage. Figure 23 shows these results plotted on a Schmidt net from a layer of sheet ice that formed during a calm night. It is quite clear that the majority of c-axes vertical crystals are eliminated in the upper 1 cm of the ice sheet. By the 5-cm level, all the remaining crystals have their c-axes within a few degrees of the horizontal. Since the azimuthal distributions of c-axes in Figure 23 and in other studied examples (Tabata and Ono 1957) did not show any pronounced pattern, it was assumed that they are random and only the angle between the c-axis and the vertical need be considered. Figure 24 is a diagram prepared on the basis of this assumption. It clearly shows that in the initial skim, as well as in the top 1.5 cm of the ice sheet, ice crystals exist with all different orientations. Therefore, to form the characteristic c-axis orientation of the columnar zone (below the transition layer), it is not necessary to nucleate new grains with a c-axis horizontal orientation. The new orientation presumably forms by the survival of those grains with the favored orientation that are present in the initial ice skim. Similar conclusions have been reached from the study of the solidification of metal ingots (Walton and Chalmers 1959).

The process of geometric selection in ice can easily be rationalized in terms of crystal growth theory. The theory predicts that atoms from the melt arriving at a crystal surface will have a much higher probability of remaining if they arrive at a step in the surface than if they arrive at an atomistically smooth face. Therefore, growth normal to the closest packed plane [the (0001) plane in ice] requires either the existence of step-producing defects or the nucleation of an embryo that will then grow laterally to form a new plane of atoms. The activation energy for this latter process is quite high, necessitating a larger supercooling, δT . These conclusions have been verified for ice by Hillig (1958, 1959), who found that the kinetics of ice growth parallel to the c-axis was consistent with the classical two-dimensional nucleation and growth model, while the growth kinetics parallel to the (0001) plane could be explained by a screw dislocation model (Hillig and Turnbull 1956).

When the initial downward growth starts in the ice sheet, the crystals in the most favorable orientations rapidly grow ahead of crystals

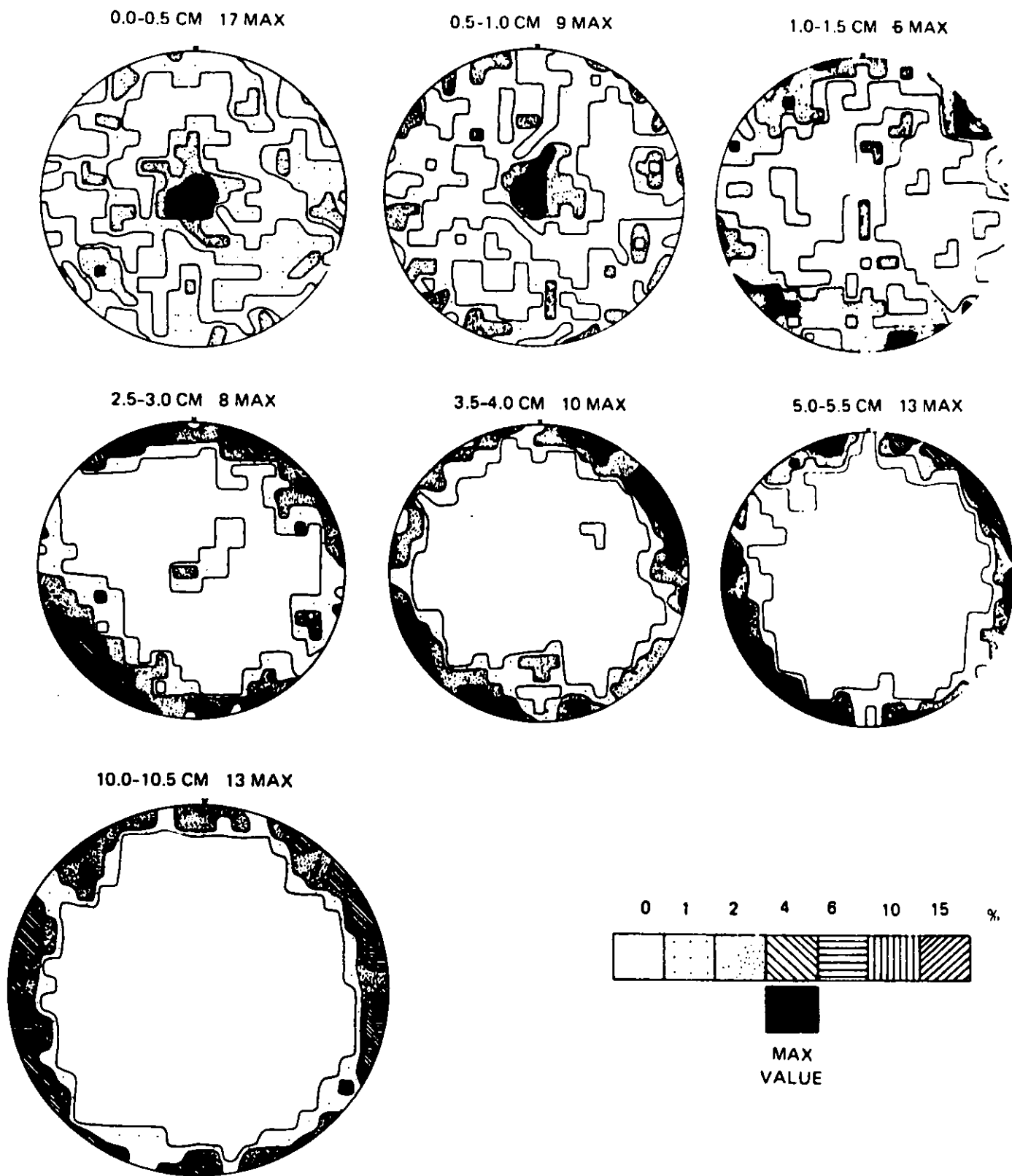


Figure 23. Orientation of the c-axes of sea ice crystals from different depths below the upper surface of an ice sheet (Thule, Greenland, 1957) plotted and contoured on the upper hemisphere of a Schmidt net. The diagrams are in the horizontal plane. Contour intervals (per 1% circle) as indicated.

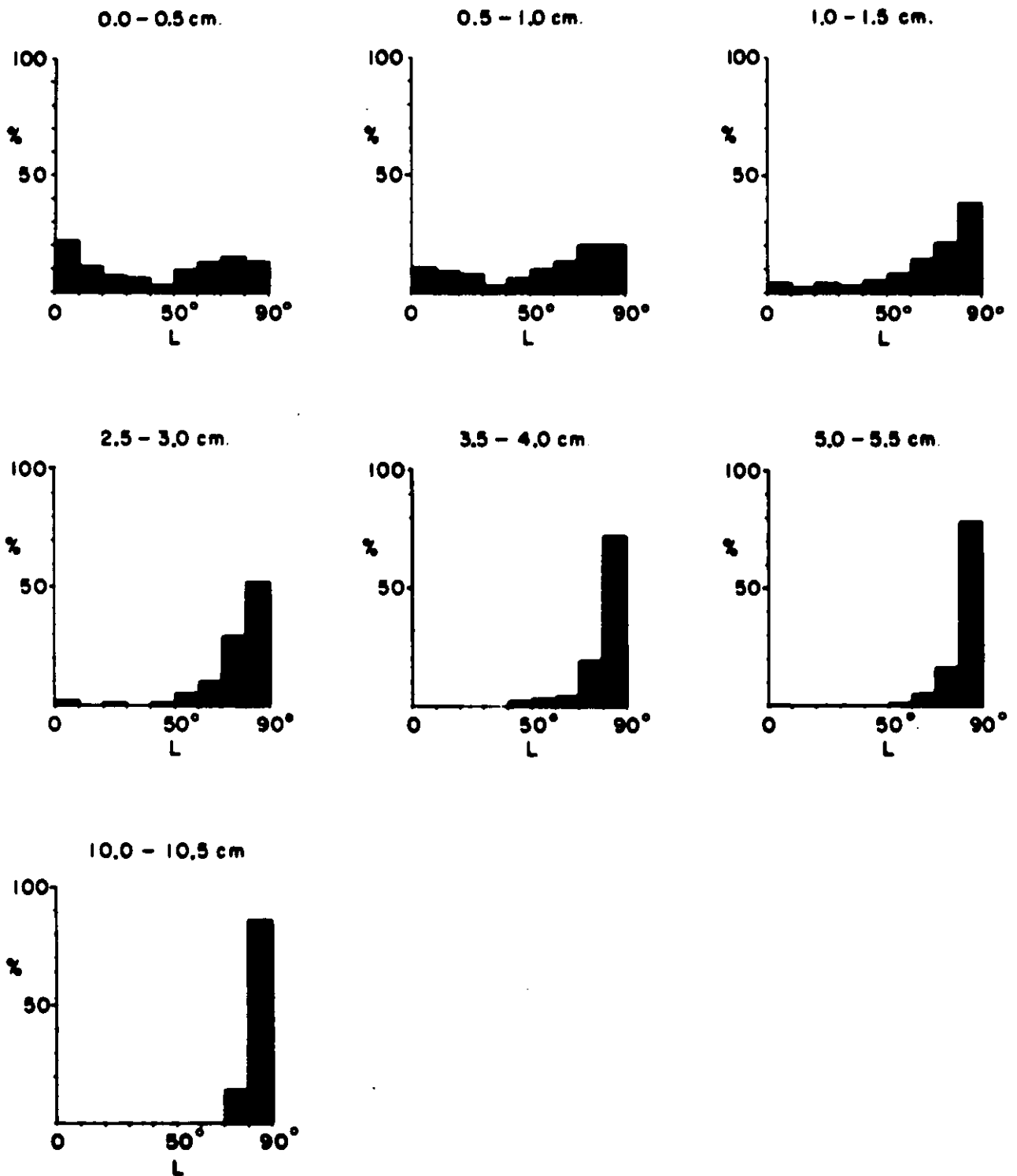


Figure 24. Histograms showing the relative percentage of different c-axis orientations (0° = vertical, 90° = horizontal) in the ice studied in Figure 23.

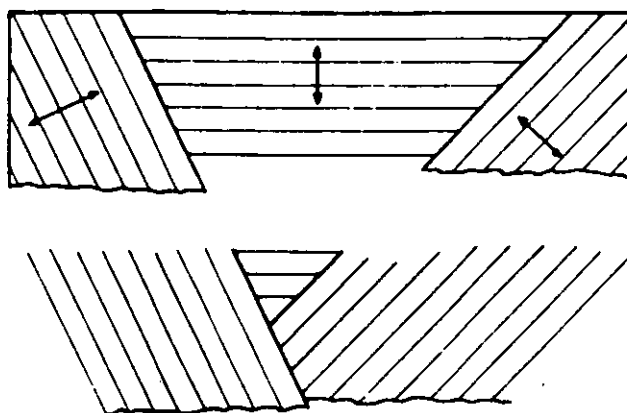


Figure 25. Schematic diagram showing the process of geometric selection according to Perey and Pounder (1958). The arrows indicate the direction of the c-axes.

with less favored orientations since they 1) can grow more rapidly at any given supercooling — at the same growth velocity, growth in a high index direction generally occurs at a much smaller δT than growth in a low index direction — and they 2) have to grow a smaller linear distance to advance the same distance parallel to the axis of heat flow. In addition, the latent heat evolved and the solute rejected by the more rapidly growing crystals reduces the effective interface supercooling of their slower neighbors. This selective growth process is shown diagrammatically in Figure 25 (Perey and Pounder 1958).

In the final growth orientation, all the (0001) planes are aligned approximately parallel to the thermal gradient (Fig. 23, diagrams from depths of greater than 5 cm). This orientation has been found repeatedly in studies of both sea and NaCl ice (Shumskii 1955, Tabata and Ono 1957, Perey and Pounder 1958, Weeks and Lee 1958, Weeks and Assur 1963, Langhorne 1980, Weeks and Gow 1980). In sea ice, because the heat loss into the atmosphere is unidirectional there is no obvious reason why the (0001) planes should have any particular orientation in the horizontal plane of the ice sheet. Early field observations appeared to verify this, at least for relatively thin ice (Tabata and Ono 1957, Weeks 1958).

However, if the heat loss were two-directional, as it is during the refreezing of small vertical cracks in sea ice, then heat would be lost both to the air and to the cold ice that composes the sides of the crack. The ice crystals that form would therefore be expected to have their c-axes horizontal and parallel to the axis of the crack. Figure 26 is a diagram showing the c-axis orientations observed in healed sea ice cracks at Hopedale, Labrador. The orientations are exactly as expected. Similar observations from lake ice have been reported by Taylor and Lyons (1959, p. 13). In fact this pronounced orientation in the refrozen crack explains why once a crack heals it commonly does not re-fracture in tension but new cracks develop parallel to it (the crack has a crystal orientation that gives the highest possible tensile strength in the direction normal to the crack).

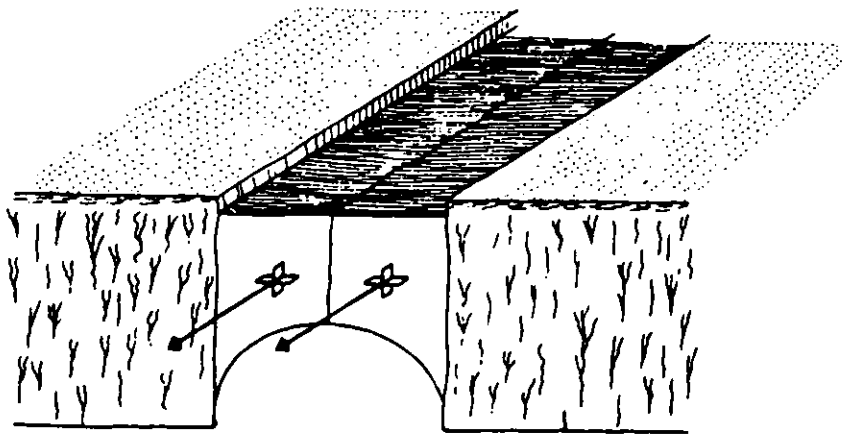


Figure 26. c-axis orientation in a healed crack at Hopedale, Labrador.

The percentage of a winter's ice sheet composed of transition zone ice is small. But the importance of this zone exceeds its size. By studying the transition one can examine the processes that control the structure of the underlying columnar zone, the zone which contains the majority of the sea ice.

THE COLUMNAR ZONE

Below the transition layer in sea ice, the ice has all the characteristics associated with the so-called "columnar" zone in metal ingots [i.e. a strong crystal elongation parallel to the direction of heat flow, a pronounced crystal orientation, and an increase in crystal size over crystals closer to the cold source (Walton and Chalmers 1959)]. Therefore, it is useful to apply this term to sea ice. Because the transition layer is thin and occurs at or near the ice/air interface, it commonly sublimates away or recrystallizes into the snow cover as the ice sheet grows. Therefore, the complete thickness of a one-winter sheet of ice can, to a good approximation, be considered as being in the columnar zone. Compared with the pronounced changes occurring in the transition layer, the changes in the columnar zone are considerably more subtle.

Fabric diagrams from the columnar zone are extremely monotonous, as shown by Figure 23 (diagrams below 5 cm). All c-axes are oriented within a few degrees of the horizontal plane. An inked rubbing of columnar zone ice showing the grain boundaries and the trace of the (0001) plane for each crystal is presented in Figure 27. This rubbing was made just below the transition layer on the lower surface of a 5-cm ice skim formed at Thule, Greenland. The grain boundaries are highly sutured, the details of the boundaries corresponding to the locations of individual platelets. Even with this suturing, it is usually quite easy to distinguish the boundaries of individual crystals. Suturing is usually clearly evident both in horizontal rubbings (Fig. 27) and thin sections (Fig. 35) and appears to be a common characteristic of ice grown with a dendritic solid/liquid interface (see Knight, 1962d, p. 323). A histogram showing the angles between the c-axes of neighboring crystals from the rubbing in Figure 27 is presented in Figure 28. If the diagram were

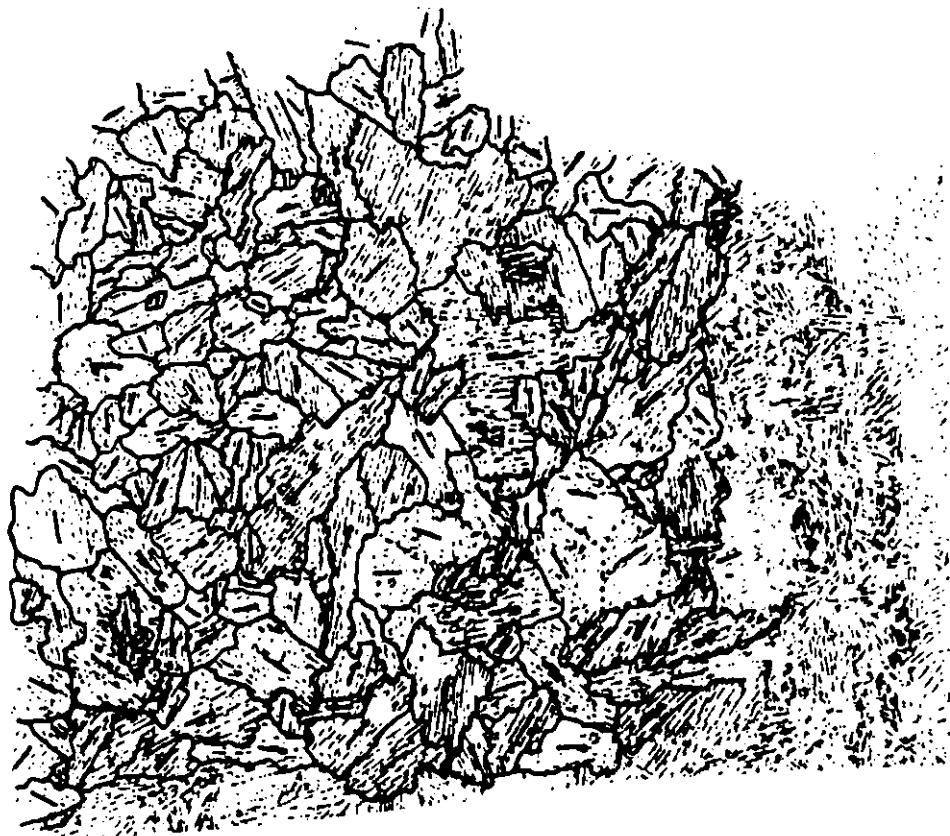


Figure 27. Rubbing from just below the transition layer on a 5-cm-thick ice sheet at Thule, Greenland. The inked "tick" marks indicate the trace of the (0001) plane.

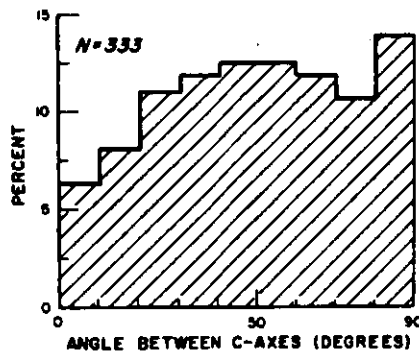


Figure 28. Histogram giving the angles between the c-axes of neighboring ice crystals shown in Figure 27.

isotropic, the theoretical frequency in each class would be 37 (11.1%). A chi-squared test shows that there is no reason to doubt that this fabric is isotropic at the 0.05 significance level. Similar results have been obtained by Tabata and Ono on thin sheets (<33 cm) from Hokkaido, Japan.

As compared with horizontal rubbings, vertical rubbings in the columnar zone are relatively uninformative. A typical example is shown in Figure 29. The lines reflect the vertical orientation of the plate-like sea ice structure. The change in horizontal spacing of the lines is produced by changes in both the plate spacing at different positions in the ice sheet and the angle at which the plates intersect the plane of the rubbing.

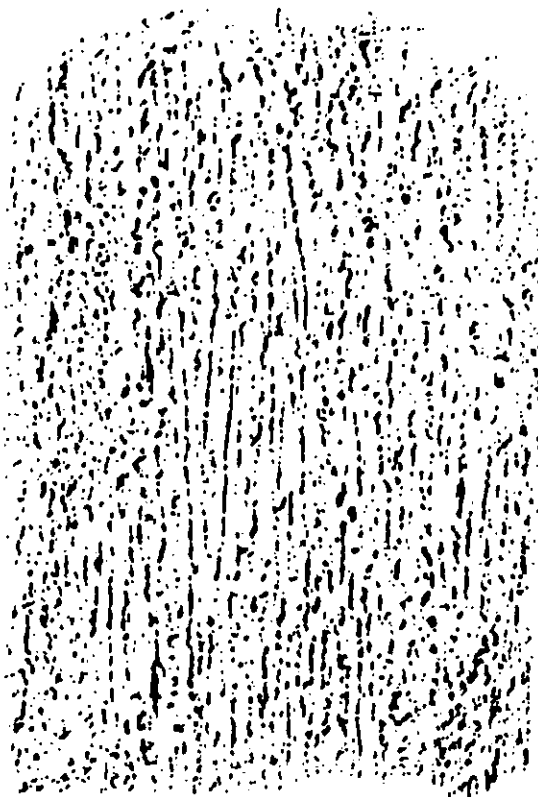


Figure 29. Vertical rubbing of columnar zone ice.

Although the *c*-axis orientations of sea ice have received considerable attention, the orientations of the *a*-axes have not been examined, as they are harder to measure. The one exception to this is a recent study by Kawamura and Ono (1980), who studied both *c*- and *a*-axis orientations in sheets of thin (4.0 to 8.5 cm), newly formed sea ice at Barrow, Alaska. Measurements were made at two different levels in the ice. Although formally both these samples would probably be considered to be from the transition zone, the samples from near the bottom of the ice sheets showed strong *c*-axis-horizontal orientations (88%). The relative frequency of the *a*-axis orientations of the different grains from the bottom centimeter of the sheets is shown in Figure 30. The vertical angle between the horizontal and the *a*-axis nearest the ice surface is indicated by the symbol θ . As can be seen, the most frequent *a*-axis orientations are either horizontal to near-horizontal (38%) or at 30 degrees (17%). This suggests that the favored *a*-axis growth direction is close or equal to either $\langle 11\bar{2}0 \rangle$ or $\langle 10\bar{1}0 \rangle$.

We would like to suggest that once the columnar zone has developed and all the remaining crystals are oriented with their *c*-axes essentially horizontal, it is the crystal with the most favorable *a*-axis orientation that has the growth advantage and will ultimately dominate at the interface. We would guess that the favored growth direction would be $\langle 11\bar{2}0 \rangle$, that is parallel to the *a*-axis as opposed to normal to the first-order hexagonal prism $\langle 10\bar{1}0 \rangle$. We would also guess that the growth advantage of $\langle 11\bar{2}0 \rangle$ would be small, and that a strong $\langle 11\bar{2}0 \rangle$ orientation

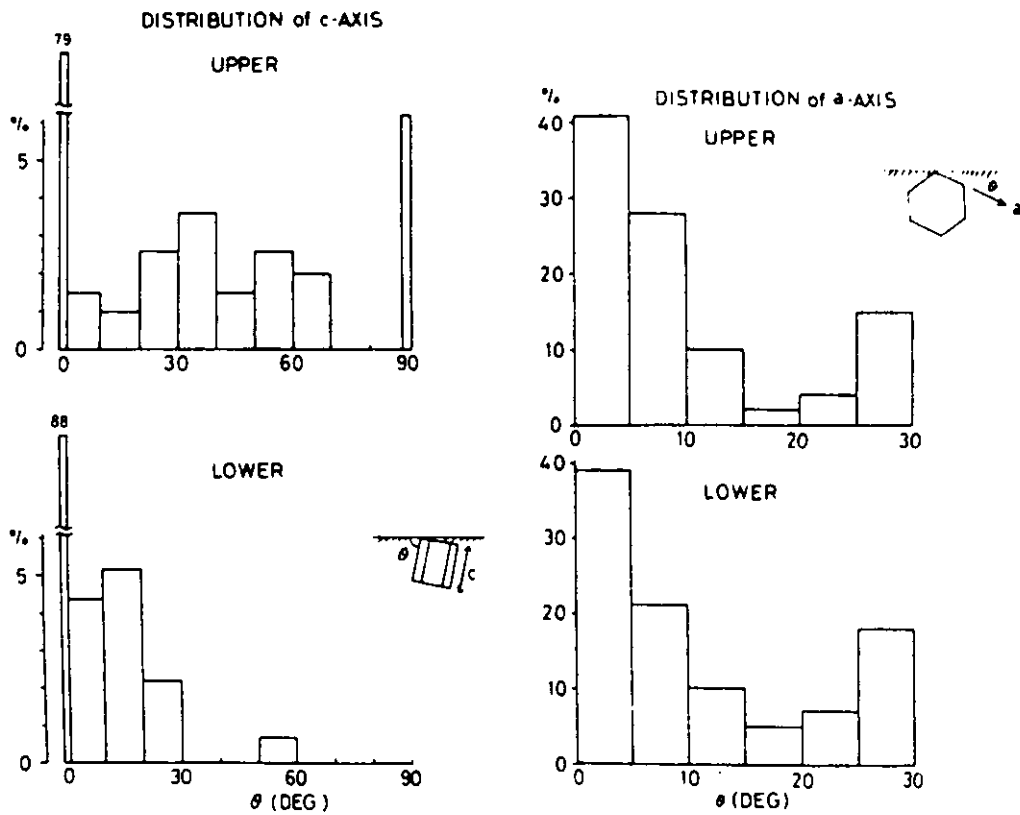


Figure 30. The distribution of c- and a-axis orientations in the upper (4.0-7.7 cm) and lower (17-22 cm) portions of thin ice sheets examined at Barrow, Alaska (Kawamura and Ono 1980).

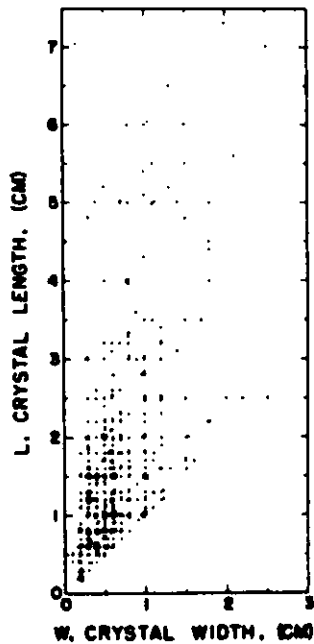


Figure 31. Lengths and widths (in the horizontal plane) of ice crystals at different levels in a sea ice sheet at Thule, Greenland.

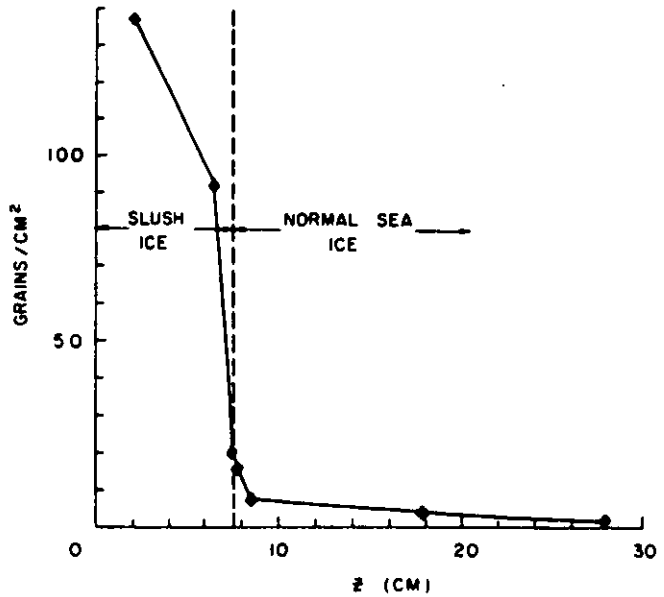


Figure 32. Increase in crystal size with distance below the surface of an ice sheet at Barrow, Alaska (Weeks and Hamilton 1962).

in the vertical direction would take a prolonged period of ice growth before it would dominate. It should not be difficult to check these contentions by using etch techniques on samples collected from thick undeformed first-year and multiyear sea ice.

Another interesting aspect of the columnar zone is the variation in crystal size. The general relation between the maximum length L and the maximum width W of a number of crystals measured in horizontal thin sections has been studied by Weeks and Hamilton (1962) using relatively thin (31.4 cm) ice from Point Barrow, Alaska. Length measurements were always taken parallel to the (0001) plane and width measurements parallel to the c -axis. The data are reasonably well fitted by a linear regression line giving approximately a 2:1 length-to-width ratio. This indicates that the ratios of sidewise to edgewise growth of the individual crystals do not differ nearly as much as might be expected from the studies of growth anisotropy in free-floating ice crystals. Figure 31 shows a plot of the length-width values of a number of crystals measured from horizontal thin sections made at 5-cm intervals through the upper 60 cm of the fast ice at Thule, Greenland. Here L refers to the maximum dimensions of the crystal and W the value measured at right angles to L (i.e. the crystallographic orientation was not considered). Therefore, by definition, the $L:W$ ratio can never be less than 1. Keeping this difference in mind, the Thule results are quite comparable to those from Point Barrow.

The most noticeable change in the upper part of the columnar zone is the marked increase in grain size with increase in depth in the ice sheet. This change is clearly shown in Figure 32 (Weeks and Hamilton 1962), which plots the number of crystals per square centimeter at different depths in the ice sheet. Once the rapid grain size change at the base of the slush layer is completed, there is a slow but regular increase with depth. The grain size curve in this ice sheet is quite comparable to grain-coarsening effects observed in the columnar zones of both pure and impure metals (Walton and Chalmers 1959, Fig. 11-12, p. 451). The change in the grain size characteristics has been studied in some detail from the upper 60 cm of a 125-cm-thick ice sheet at Thule, Greenland. The measurements were stopped at the 60-cm level because a large number of crystals were not completely contained in a given thin section. Fortunately, as a result of the fact that all grains in sea ice are columnar, the investigator is not faced with the problem of the thin section not cutting the "centers" of the crystals. The crystal "diameter" d ($d \equiv \sqrt{LW}$) was measured and the average value d computed for several levels in the ice sheet. There is a pronounced linear increase in d with increasing depth in the ice. Also plotted in this figure are d values from Point Barrow (Weeks and Hamilton 1962) and Hokkaido (Tabata and Ono 1962). The slopes of all three curves are similar. This suggests that if a transformation is made correcting for the initial grain size at ($Z = 0$), all these curves can be considered as identical. Figure 33 shows a plot of $[d - d(Z = 0)]$ versus Z . The least-squares line through the origin has a slope of 0.033. The $[d(Z = 0)]$ value for Hokkaido (0.87) was obtained by least squares extrapolation and the value for Point Barrow (0.22) by setting ($Z = 0$) at the slush-normal sea ice boundary. This preliminary examination suggests that grain size may prove to be an interesting and useful parameter. If further measurements support the hypothesis of "equal slopes," once the

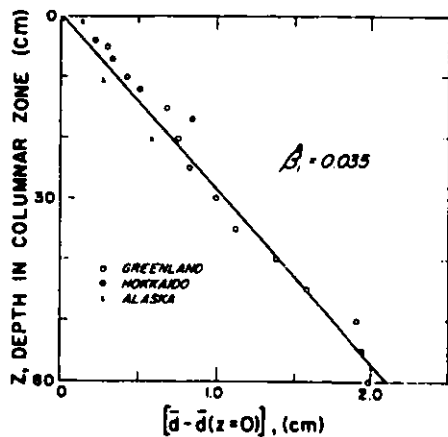


Figure 33. Plot of change in grain size with distance below the upper ice surface. The grain size curves are shifted to zero at the ice surface.

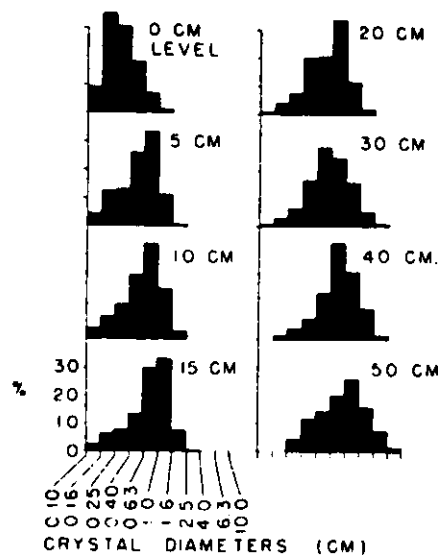


Figure 34. Histograms of crystal diameters at different levels in an ice sheet at Thule, Greenland.

average grain size is determined at one level in an ice sheet it would specify the grain size for the complete sheet. This presumably could only be the case for continuously grown one-winter ice sheets since nucleation of new crystals would cause a discontinuity in the grain diameter curves. We would anticipate that the simple "equal slopes" hypothesis will not be verified and that the rate of increase in the mean grain diameter will be a function of the growth rate of the ice, with the largest values of the slope occurring at the lowest ice growth rates. More will be said later in this paper about grain size variations in sea ice with strong c-axis alignments.

There are, in fact, data already available in the literature that tend to cast doubt on a simple relation between d and the vertical position in the ice sheet. For instance, Koerner (1963) observed that sea ice cores from Jones Sound off Devon Island in the Canadian Arctic showed a smaller initial grain size and a more rapid increase in crystal size with depth than ice collected closer to shore. He also suggested that this difference might be the result of changes in growth rates. Also, in old sea ice incorporated into the ice island Arlis II, Smith (1964) observed areas as large as 10 m on a side with almost perfect c-axis alignment. Using a slope of 0.033 it would require an ice thickness of approximately 300 m to give such an average grain size. Ice thicknesses of this magnitude appear quite unreasonable at the present.

Figure 34 shows a series of histograms of the distribution of crystal diameters for different levels in the ice sheet from Thule, Greenland. The abscissa is scaled to permit ready comparison with similar data on lake ice presented by Marshall (Wilson et al. 1954). The sea ice crystal diameter distributions in sea ice, with the exception of the

upper surface which would be in the transition layer, are negatively skewed, while the lake ice distributions have a tendency to appear normal or even rectangular. Whether these differences are generally true between lake and sea ice is impossible to ascertain with the presently available data.

The preceding intracrystalline petrographic parameters are best measured in horizontal thin sections. There are also several petrographic features that are only clearly seen in vertical thin sections. In contrast to the preceding parameters, which are either constant or change gradually with position in the ice sheet, these commonly appear as sharp bands that extend for large lateral distances. Small scale horizontal banding in sea ice has been noted at widely separated regions (Shumskii 1955, Tabata and Ono 1957, plate XVI, Langleben 1959, Fig. 3, Bennington 1963a, Fig. 1, Paige 1966). For example, Shumskii observed a total of 58 secondary layers in a 291-cm section of old pack ice, giving an average layer thickness of 5 cm. The layers are produced by changes in the amount of impurities (brine and air) trapped in the ice. Similar effects are well known in studies of metals. As far as is known, this type of layering is not accompanied by the nucleation of new crystals. Air bubble layering in lake ice is also well known (Taylor and Lyons 1959, p. 16-19, Swinzow 1966, Gow and Langston 1977). These differences in impurity content are produced by changes in the growth rate of the ice and can make convenient horizontal markers in the ice sheet throughout any region where the weather is laterally homogeneous. Langleben (1959) has, quite effectively, used this layering as a reference mark in studying the location of the transition layer throughout the growth season. A similar technique should also be useful in studying the relative amounts of ablation from the lower and upper surfaces of pack ice during the melt season. This has been done for lake ice by Gow and Langston (1977). A theoretical analysis of the effect of changing the freezing velocity on the amount of impurity incorporated into the solid phase, assuming that solute transfer in the melt takes place by diffusion only, has been published by Tillier et al. (1953) and Smith et al. (1955). Up to the present time, there have been two attempts to apply this theory to bubbles in freshwater ice grown in the laboratory (Carte 1961, Bari and Hallett 1974) and one example using field observations (Gow and Langston 1977). Apparently, no work has been done on sea ice, although we would expect similar relations to hold.

There are several other important aspects of the structure of the columnar zone (e.g. variations in the width of the substructure in the ice crystals, brine drainage channels, annual layering in multiyear ice, directional c-axis alignments in the horizontal plane). These subjects will be treated in detail later in the paper.

SUBSTRUCTURE

One invariably identifies sea ice by the presence of a characteristic cellular substructure consisting of reasonably evenly spaced ice platelets or cells separated by small angle grain boundaries. It is along these boundaries that the salt in sea ice is present in the form of liquid and solid inclusions. This cellular substructure is clearly shown in Figures 35 and 36. It has been known for some time that the spacings of this substructure change with vertical location in the ice

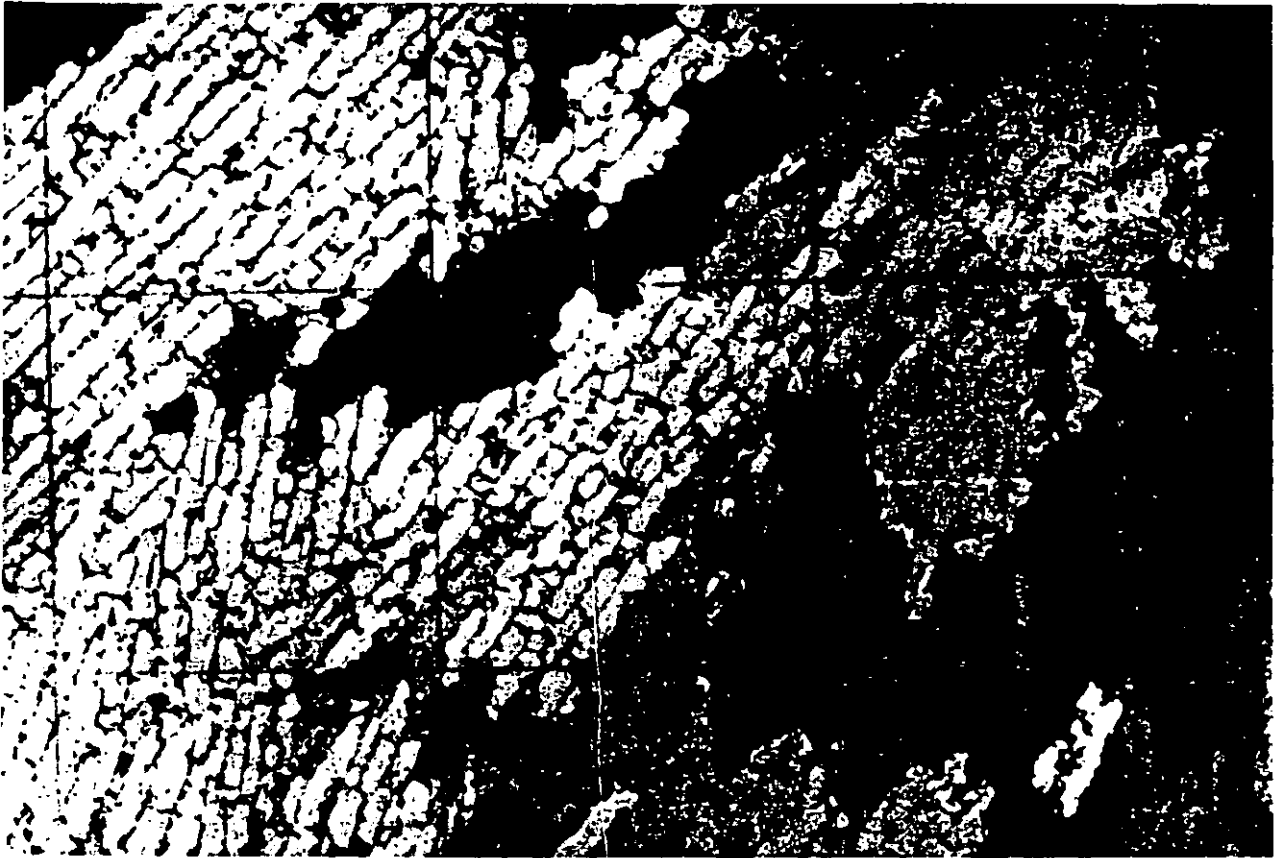


Figure 35. Horizontal thin section of sea ice from 27.9 cm below the upper ice surface, Point Barrow, Alaska (Weeks and Hamilton 1962). Grid is 1 cm on a side.

sheet (Fukutomi et al. 1953). In an attempt to understand these variations, observations have been carried out on natural sea ice (Tabata and Ono 1962, Weeks and Hamilton 1962, Paige 1966, Gow and Weeks 1977, Nakawo and Sinha, in press) and experiments have been undertaken on a variety of salt ices (Weeks and Assur 1963, Rohatgi and Adams 1967 a,b, Lofgren and Weeks 1969). The most important parameter in characterizing the substructure is the brine layer spacing a_0 (also referred to as the plate width), which is the distance between adjacent layers of brine pockets measured parallel to the c-axis (see Fig. 36; double-headed arrow indicates the c-axis direction).

Laboratory experiments have shown that in NaCl ice formed under conditions of unidirectional freezing, there is a gradual increase in the value of a_0 with increasing distance from the upper ice surface or from the constant temperature cold plate. An analysis of the factors controlling the variation in a_0 has been published by Bolling and Tiller (1960) for the case where the solute transfer in the liquid ahead of the advancing interface is by diffusion only. Although the final form of the analysis is approximate, the physical reasoning behind the analysis is clear. The exact solution to the steady-state solute distribution in the liquid ahead of an advancing plate tip consists of both plane and non-plane wave terms. These latter terms cause lateral diffusion and can be considered to extend some effective distance y into

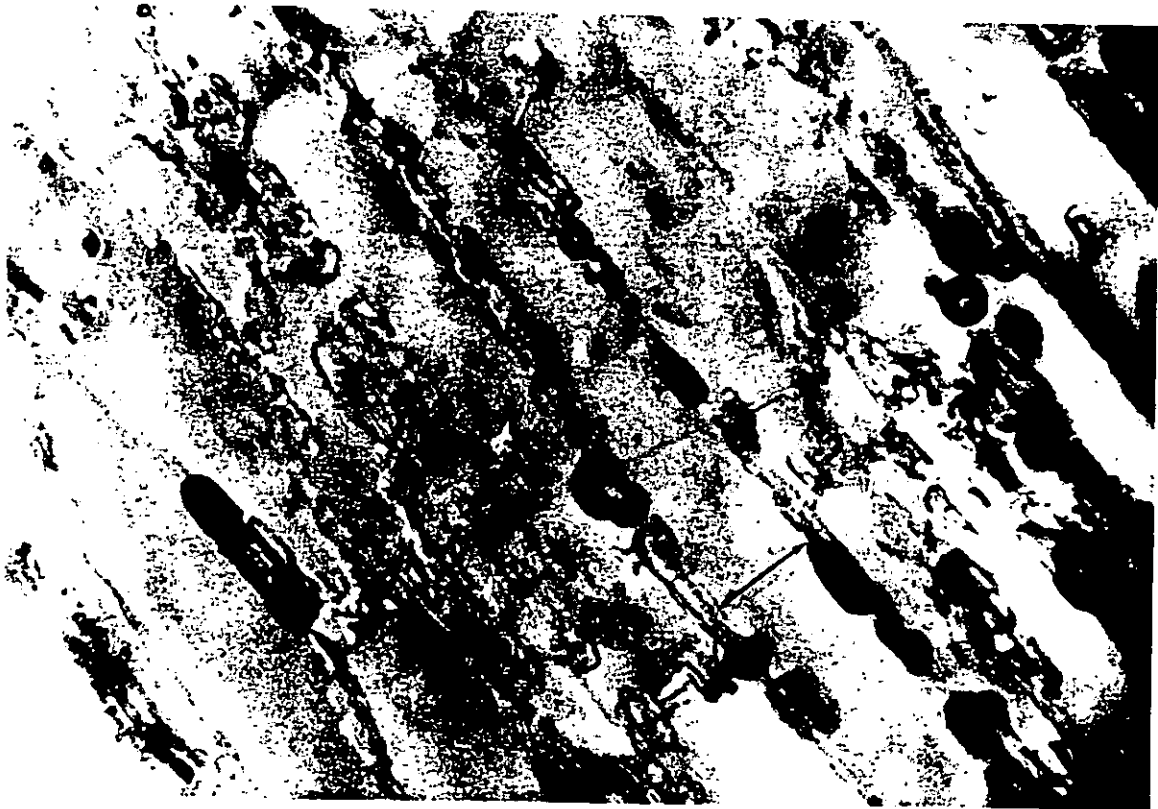
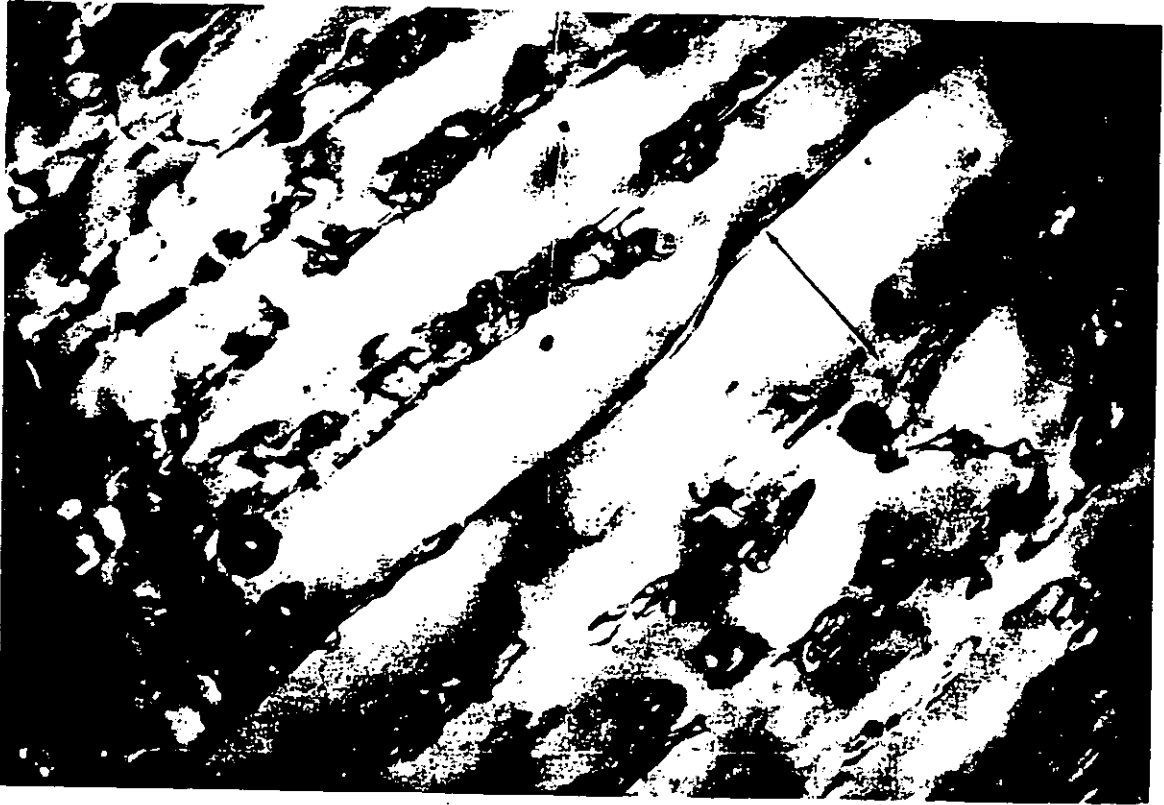


Figure 36. Photographs of two thin sections showing cellular substructure in sea ice. The c-axis direction is in the plane of the section and normal to the platy structure. The spacing between brine layers is approximately 0.6 mm.

the liquid. Once lateral diffusion starts it continues until it is terminated by the advancing interface. The time allowed for diffusion is $t = (y+y^+)/v$ where y^+ is a function of interface shape and v is the interface velocity. The distance that the solute can diffuse in this time is $x = \sqrt{Dt}$. Assuming that $x = a_0/2$ results in

$$a_0 = \frac{D}{2\pi v} \left\{ 1 + \left[1 + \frac{16\pi^2 v}{D} \left(\frac{0.6 \gamma}{\Delta S G'_0} \right)^{1/2} \right]^{1/2} \right\} \quad (4)$$

Here γ is the solid/liquid interfacial energy, ΔS is the entropy of fusion per unit volume, and G'_0 is the effective temperature gradient at the tip of the cell. This equation indicates that a_0 increases with an increase in C_0 , the bulk composition of the freezing solution (G'_0 decreases as C_0 increases), and that the functional form of the relation between a_0 and v is $a_0 v = A$ for small values of v and $a_0 \sqrt{v} = A$ for large values of v (here A is a constant).

The experimental studies (Rohatgi and Adams 1967 a,b) corresponding to this theory are in reasonable agreement (Lofgren and Weeks 1969), indicating that a_0 increases as a linear function of C_0 and that $a_0 v = A$. Lofgren and Weeks also found Bolling and Tiller's predictions to be compatible with their data for experiments where convection was not occurring at the freezing interface. When convection was predominant $a_0 \sqrt{v} = A$ at high values of v while at low values of v , a_0 became roughly constant. Figure 37 shows the test data; the fitted relation is of the form

$$\log(\bar{a}_0 v) = \log A + n_1 \left(\log \frac{1}{v} \right)^2 \quad (5)$$

where A and n_1 are constants.

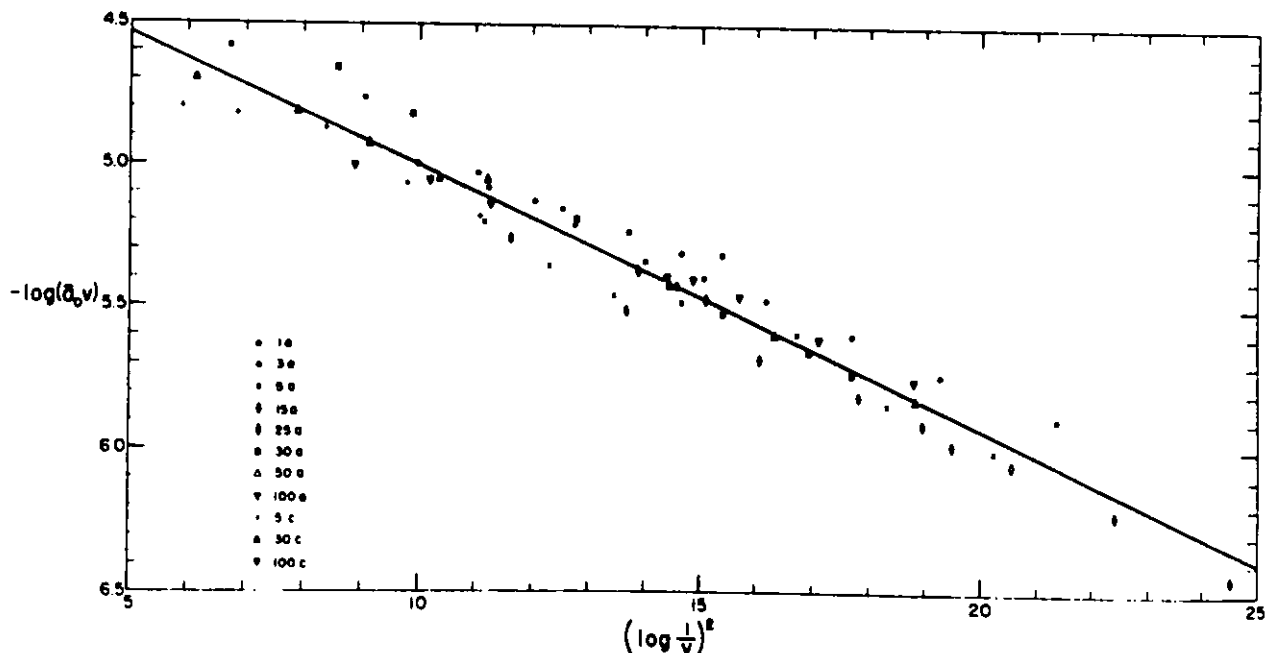


Figure 37. Plot of $-\log(a_0 v)$ versus $(\log 1/v)^2$ (Lofgren and Weeks 1969).

The field observations have in general shown an increase in a_0 with increasing depth Z in the ice sheet (Tabata and Ono 1962, Weeks and Hamilton 1962, Paige 1966). However, at Narwhal Island, Alaska, a decrease in a_0 with increasing Z was noted by Gow and Weeks (1977), and at Eclipse Sound, Baffin Land, a rather complex variation was observed by Nakawo and Sinha (in press). Typical a_0 variations would range from 0.4 mm near the upper ice surface to 1.0 mm at $Z = 2.0$ m in first-year sea ice. At a given level in the ice sheet the distribution of a_0 values is approximately normal about the mean (Weeks and Hamilton 1962), as might be expected from the Central Limit Theorem.

The best available study of the relation between a_0 and growth velocity in a natural ice cover was undertaken at Eclipse Sound, N.W.T., by Nakawo and Sinha (in press). Curve (a) in Figure 38 shows the calculated growth rate plotted as a function of Z , the vertical position (depth) in the ice sheet. Curve (b) is the mean of the growth rate for an interval of ± 50 mm centered on the 25-mm segment for which it is plotted. There is a pronounced variation in growth rate with Z , with the maxima at about 0.2, 0.5, and 1.0 m corresponding to the observed cold periods in November, December, and January. Curve (c) presents the salinity profile obtained from an adjacent core. There is clearly a positive correlation between growth rate and salinity. More will be said about this later. The curve on the right shows the corresponding values of a_0 and indicates an inverse proportionality with growth rate in agreement with the work of other investigators. Figure 39 shows the same data presented as an a_0 versus v plot. The dashed line is a least-squares fit of the Bolling and Tiller equation. The agreement is quite reasonable if the two a_0 values from near the bottom of the ice sheet are disregarded. The ice studied here showed a pronounced c-axis alignment, not only in the horizontal plane but specifically in the

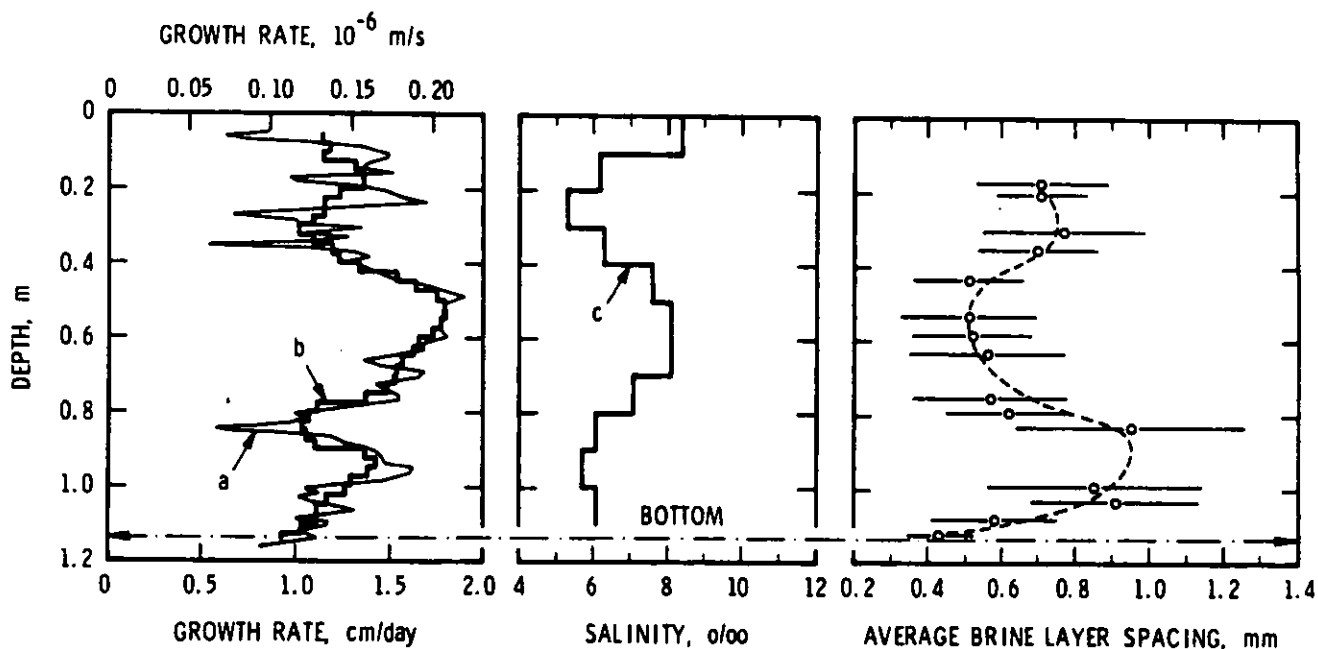


Figure 38. Profiles of growth rate, salinity and brine layer spacing. Curve b represents the mean of calculated growth rate, curve a, for an interval of ± 50 mm for every 25 mm (Nakawo and Sinha, in press).

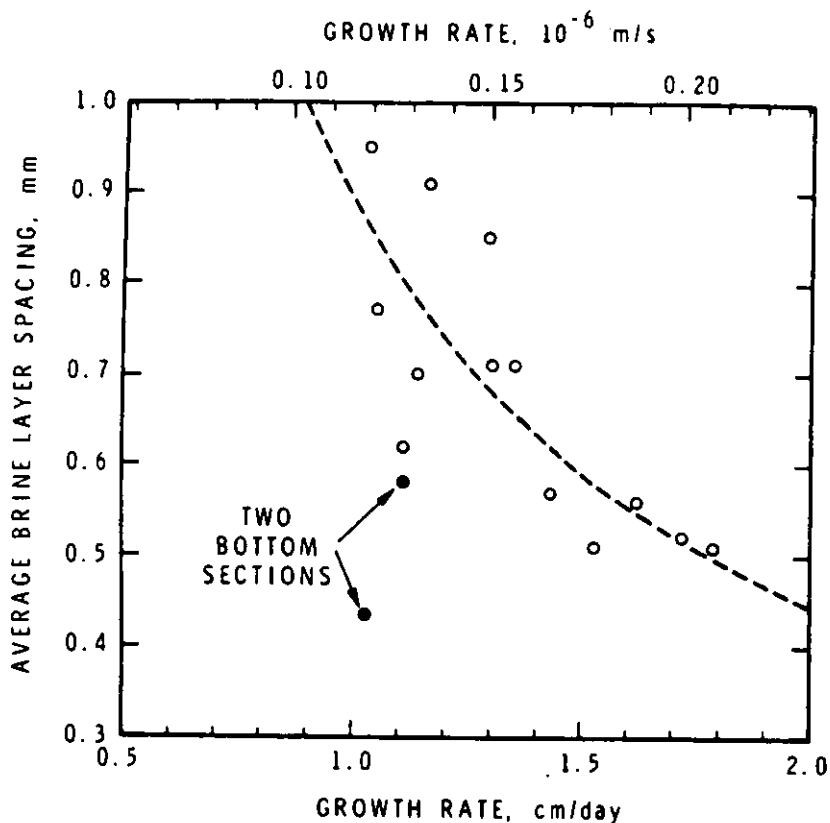


Figure 39. Plot of average brine layer spacing versus corresponding rate of growth from curve b (Fig. 38). Broken line shows a least squares fit, assuming that the spacing is inversely proportional to the growth rate (Nakawo and Sinha, in press).

NE-SW direction in that plane. At a given level in the ice sheet (i.e. at a constant growth velocity) limited data suggest that a_0 is a maximum value when the c -axis is parallel to the favored direction, and that it systematically decreases when the angle to this direction increases. If this can be verified it both complicates the picture and makes studies of a_0 variations very interesting indeed.

The hypothesis that slower growth corresponds to larger a_0 values is quite strongly supported by field observations on very thick sea ice — ice that in all probability grew extremely slowly. Cherepanov (1964) obtained a_0 values of 1.5 mm on old sea ice 10 to 12 m thick observed on drifting station NP-6; Gow (personal communication) obtained a_0 values of 1 to 1.5 mm on thick sea ice that formed as part of the Koettlitz Ice Tongue, McMurdo Sound, Antarctica; and finally Zotikov et al. (1980) obtained a_0 values of 5 mm from sea ice formed on the base of the 416-m-thick Ross Ice Shelf. Figure 40 shows a vertical thin section from the bottom of this core. The core was oriented so that the plane of the thin section was in general normal to the (0001) planes containing the brine pockets. The growth velocity at the sample site (Camp J9) was estimated to be 2 cm/year, far slower than could readily be obtained in the laboratory.



Figure 40. Vertical thin section of sea ice from the lower portion of the core from site J-9, Ross Ice Shelf, Antarctica. The scale is marked in units of 5 mm (thin section prepared by A.J. Gow). The ice shelf at site J-9 is 416 m thick.

CONSTITUTIONAL SUPERCOOLING

Up to the present time we have demonstrated that the ice phase that forms from seawater should be pure ice. If this were strictly true it would be simple to desalinate seawater simply by freezing it. The reason this is not done is that salt becomes entrapped in the ice phase, largely in the form of liquid inclusions located along the boundaries between the ice plates. To understand why this salt entrapment occurs one must first understand why sea ice grows with a platelet-like structure in the first place. In short, why does sea ice form with a non-planar, dendritic interface, resulting in brine entrapment, while lake ice forms with a planar interface, resulting in almost complete impurity rejection back into the melt. Both result from the freezing of impure melts; it is only a matter of degree ($35^{\circ}/_{\infty}$ as compared with $<0.1^{\circ}/_{\infty}$). The answer is that sea ice is a classic example of a material that invariably shows pronounced constitutional supercooling.

What is constitutional supercooling (C.S.) and how does it work? Briefly stated, the answer is as follows (Rutter and Chalmers 1953, Tiller et al. 1953, Elbaum 1959). Consider a salt solution freezing as

the result of one-dimensional cooling. For such a system the distribution coefficient k_0 (defined as the ratio of the solute content of the solid to the solute content of the liquid when the two phases are at equilibrium) has a value of 10^{-4} or less (Harrison and Tiller 1963). Next assume that:

- (a) Diffusion in the solid is negligible.
- (b) Convection and mixing in the liquid, due to causes other than diffusion, are negligible (for salt solutions this is a good assumption only if we freeze from the bottom up).
- (c) k_0 is constant.

If the origin of the coordinate system is taken to be at the freezing interface, then freezing can be viewed as moving this liquid toward the interface at a velocity v producing a net flow out of a unit volume of $v(dC/dx)$ where C is the concentration and x is the distance normal to the interface. At the same time there is a diffusive flow of impurity into the volume element of $D(d^2C/dx^2)$, where D is the diffusion coefficient. If a steady state is achieved these two terms must be equal, leading to the differential equation

$$D \frac{d^2C}{dx^2} + v \frac{dC}{dx} = 0 \quad (6)$$

The boundary conditions are

$$\begin{aligned} C_L &= C_0 \text{ at } x = \infty \\ C_L &= C_0/k \text{ at } x = 0. \end{aligned}$$

Here C_L is the concentration in the liquid and C_0 is the initial concentration in the liquid (the composition far removed from the interface). The steady-state solution is then

$$C_L = C_a \exp(-(vx)/D) + C_0 \quad (7)$$

where $C_a \equiv C_1 - C_0$ and C_1 is the composition of the liquid at the interface. This ultimately leads to

$$C_L = C_0 \left[1 + \left(\frac{1-k}{k} \right) \exp\left(-\frac{v}{D} x\right) \right] \quad (8)$$

indicating that there should be a thin layer of liquid at the interface that shows an exponential decrease in C_L as one moves away from the interface. This is shown schematically in Figure 41. Because of these compositional variations there are associated changes in the equilibrium freezing temperature of the liquid (Fig. 41) inasmuch as

$$T_E = T_0 - m C_L \quad (9)$$

where T_E is the equilibrium freezing temperature, T_0 is the melting point of the pure solvent (ice), and m is the slope of the liquidus line from the phase diagram. This results in

$$T_E = T_0 - m C_0 \left[1 + \frac{1-k}{k} \exp\left(-\frac{v}{D} x\right) \right]. \quad (10)$$

Next, take the actual temperature distribution in the liquid to be given by

$$T = T_0 - m \left(\frac{C}{k} \right) + G_L X \quad (11)$$

where G_L is the temperature gradient in the liquid. The first two terms on the right side of this equation give the temperature at the interface. For some compositional profiles and temperature profiles the composition is such that the liquid ahead of the interface become super-cooled (see Fig. 42). Hence the term "compositional supercooling."

When the slope of the actual temperature profile is less than the slope of the T_E curve at the interface, constitutional supercooling occurs. The criterion for this condition is

$$\frac{G_L}{v} < \frac{mC_0}{D} \left(\frac{1-k}{k} \right) \quad (12)$$

a relation obtained by differentiating eq 10 and 11 with respect to x and evaluating them at $x = 0$. This relation has been found to be in good agreement with experimental observations in metal systems (Walton et al. 1955). When eq 12 is applied to the freezing of both salt solutions and seawater, it is found that even when optimum conditions for the maintenance of a planar interface occur ($v = 10^{-6}$ cm/s, $G = 1.0$ C/cm, and $k_0 = 10^{-4}$), the ratio $G/v = 10^6$. For this ratio C.S. should exist (Fig. 43) even for salinities representative of typical lake water (≈ 100 ppm or $0.1^\circ/_{\infty}$), not to mention the salt contents studied in this paper ($24.7^\circ/_{\infty}$ and greater).

Although the existence of a C.S. layer ahead of the advancing solid/liquid interface is necessary for cell formation, it is not necessarily sufficient. In addition, there is considerable uncertainty in the preceding calculation as the result of possible variations in G . This difficulty can be avoided by calculating if the growth conditions are such that the steep-walled cell boundary grooves associated with the

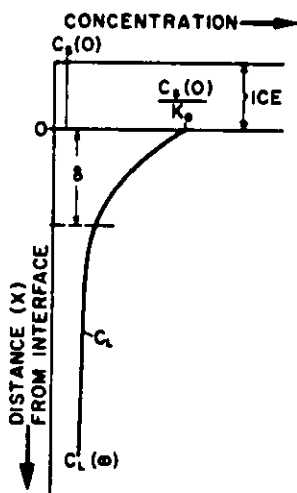


Figure 41. Steady-state distribution of solute in the liquid ahead of an advancing solid/liquid interface.

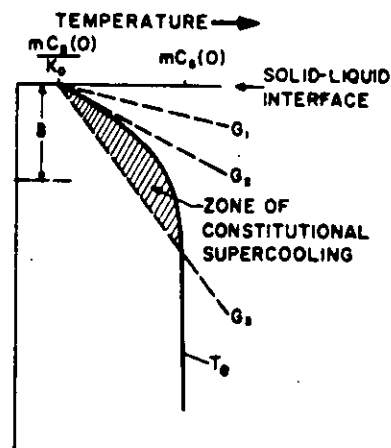


Figure 42. Constitutionally supercooled zone of liquid ahead of an advancing interface.

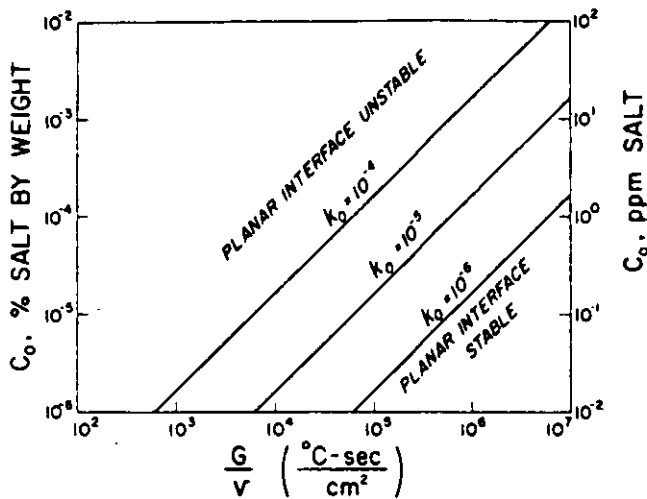


Figure 43. A plot of the boundaries that for different k_0 values separate growth conditions where a planar interface is stable and where it is unstable. Solute transfer in the liquid is assumed to be by diffusion only.

entrapment of brine along plate boundaries are stable. The stability criterion for the formation of these grooves (Tiller 1962) is

$$\frac{G_B}{v} < \frac{-m C_1 (1 - k)}{D} \quad (13)$$

where G_B is the temperature gradient in the solid and C_1 is the composition of the liquid at the interface. If transfer in the liquid is by diffusion only, $C_1 = C_0/k$ and eq 13 becomes similar to eq 12 with G_B substituted for G_L . Equation 13 is a more stringent criterion than eq 12 because for ice-solute systems $G_B > G_L$. Now, if

$$t = \frac{\rho L h^2}{2 \kappa \Delta T_0} \quad (14)$$

(Carslaw and Jaeger 1959), where t = time, ρ = density of the solid, L = latent heat of fusion, ΔT = difference between the upper surface (i.e. cold plate/ice) temperature of the ice and the freezing temperature of the seawater, h = thickness of the ice, and κ = thermal conductivity of the ice, then

$$v = \frac{dh}{dt} = \frac{\kappa \Delta T_0}{\rho L h} \quad (15)$$

and

$$G_B = \frac{\Delta T_0}{h} \quad (16)$$

Therefore, eq 13 becomes

$$\frac{\rho L}{\kappa} < \frac{-m C_0 (1 - k)}{D k} \quad (17)$$

in which C_0 is the only parameter under the control of the experimenter. Substitution of numerical values in eq 17 shows that for all seawater and brackish water salinities cell boundary grooves are stable if solute transfer in the liquid is by diffusion only. In actuality, because natural sea ice freezes from the top down, the primary mechanism of solute transfer is free convection (Farhadieh and Tankin 1972, Wakatsuchi 1977), which causes C_1 to approach C_0 . This explains the

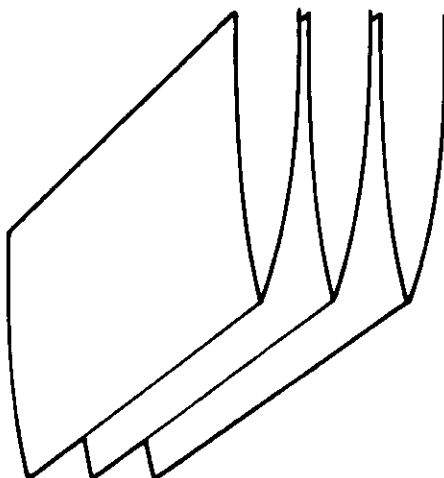


Figure 44. Schematic of knife-edged cells (Harrison and Tiller 1963).

observations of Weeks and Lofgren (1967), who recorded transitions from a non-planar to a planar interface during the freezing of 1‰ (unstirred) and 3‰ (stirred) NaCl solutions.

Once C.S. is established and a cell-boundary groove is stable, the planar ice/water interface breaks down into parallel rows of cellular projections within each grain (Harrison and Tiller 1963). Concentrated brine is accumulated in the grooves that develop between the rows of cells (Fig. 44) and is eventually trapped when adjacent cells develop lateral connections. The entrapped brine leaves a permanent record of the positions of the intercellular grooves. It is the distance between the midpoints of these intercellular grooves that was termed the brine layer spacing a_0 earlier in this paper.

The relations we have just presented are useful in understanding the general phenomenon of C.S. However, a treatment of C.S. that is truly adequate for sea ice does not as yet exist. It will have to deal explicitly with the fact that the liquid is mixed by free convection and that the appropriate boundary layer is not a diffusive one, but a convective one.

It should also be mentioned that considerable work is currently underway to further develop and apply a more sophisticated interface stability theory, one that is based on the dynamics of the whole system rather than just the thermodynamics of the liquid and is capable of describing the time evolution of a perturbed interface and the accompanying temperature and concentration fields. A review of these developments has been published by Sekerka (1968). The diffusion equations are solved for a planar interface with a sinusoidal perturbation of a small amplitude δ superimposed upon it. The growth velocity of the perturbation δ is then calculated, a velocity which is a function of the wavelength of the perturbation λ and several thermal parameters. If δ is greater than zero, the instability grows and develops into cells. The stability criterion involves the function $S(\omega)$, which for $k \ll 1$ is

$$S(\omega) = -T\Gamma \omega^2 - G_l + mG_c + \left(\frac{k_s - k_l}{k_s + k_l} \right) G_l - \frac{Lv}{k_s + k_l} \quad (18)$$

Here T is the melting temperature of a flat interface; $\Gamma = \gamma/L$ where γ is the specific liquid/solid interfacial free energy, and L is the latent heat of the solvent per unit volume; $\omega = 2\pi\lambda$; k_s and k_l are the thermal conductivities of the solid and liquid; and G_s , G_l , and G_c are respectively the temperature gradient in the solid at the interface, the temperature gradient in the liquid at the interface, and the concentration gradient in the liquid at the interface. When $S(\omega) < 0$ the interface is stable. The principal stabilizing terms are G_l as the temperature gradient is positive and the first and last terms, which are usually small. Because for ice $k_s > k_l$, the conductivity weighted term in G_l offsets the stabilizing effect of G_l alone. The principal term leading to instability is mG_c .

This relation is only strictly applicable to the study of perturbations about the steady-state solution. When expressed as a stability criterion it is usually stated as

$$|m| \frac{vC_1}{D} < \frac{2 k_l G_l}{k_s + k_l} + \frac{Lv}{k_s + k_l} \quad (19)$$

where C_1 is the concentration in the liquid at the interface. Sekerka et al. (1967) have also expressed this relation as

$$\left[\frac{1}{k} - \left(\frac{1}{k} - 1 \right) e^{-t/t_{\text{rise}}} \right] |m| \frac{vC_0}{D} < \frac{2 k_l G_l}{k_s + k_l} + \frac{LV}{k_s + k_l} \quad (20)$$

where C_0 is the bulk composition of the freezing solution, t is time and $t_{\text{rise}} = D/(kv^2)$ is a characteristic time of solute buildup at the growing interface. In eq 20 the term in brackets increases monotonically from a value of 1 at $t = 0$ to a value of nearly $1/k = 10^4$ for $t = t_{\text{rise}}$. In inserting the appropriate values for seawater, Sekerka et al. (1967) found that a seawater/ice interface is effectively instantaneously unstable with respect to the time t_{rise} associated with the buildup of salt at an advancing ice interface.

Modifications of this theory incorporating coupled convective and constitutional interface instabilities are under development. The equations are quite complicated (Coriell et al. 1980) and have not, as yet, been applied to the freezing of seawater.

It should also be mentioned that this theory can be used to estimate λ_{max} , which is presumably equivalent to the brine layer spacing a_0 . The resulting equations suggest that

$$\lambda_{\text{max}} \propto v^{-1/2} \quad (21)$$

and that for seawater freezing with a velocity of 10^{-5} cm/s, a_0 should have a value of ≈ 0.2 mm. In fact, a_0 values from 0.5 mm to 0.95 mm are encountered, in reasonable agreement.

VARIATIONS

Directional C-Axis Alignments

In the earlier portions of this paper we have pointed out that the crystals in the columnar zone have their c-axes oriented in the horizontal plane. We have also shown some early fabric diagrams (Fig. 23) in which the c-axis alignments within the horizontal plane were either random or near-random. It was reasonable to expect that this might be the case as the heat flow was apparently one-dimensional. Also, such random radial c-axis alignments were common in the solidification of metals.

However, in the early 1960's Peyton (1963, 1966, 1968), while examining a 3x3-m block of 1.6-m-thick sea ice from Barrow, found that the bottom meter exhibited a near-constant c-axis orientation over the entire 9-m² cross section. In his studies of mechanical properties, Peyton utilized this ice to investigate the effect of changes in the orientation of the uniaxial stress to the c-axis direction on the failure strength. At roughly the same time Cherepanov (1964) and Smith (1964) observed that old sea ice incorporated in the ice islands SP-6 and Arlis II showed near-perfect c-axis alignment over large areas (on SP-6 the entire 80-km² area of the "island" showed a similar c-axis alignment). Clearly such alignments were not statistical fluctuations, and specific efforts to study this phenomenon (or these phenomena) were in order.

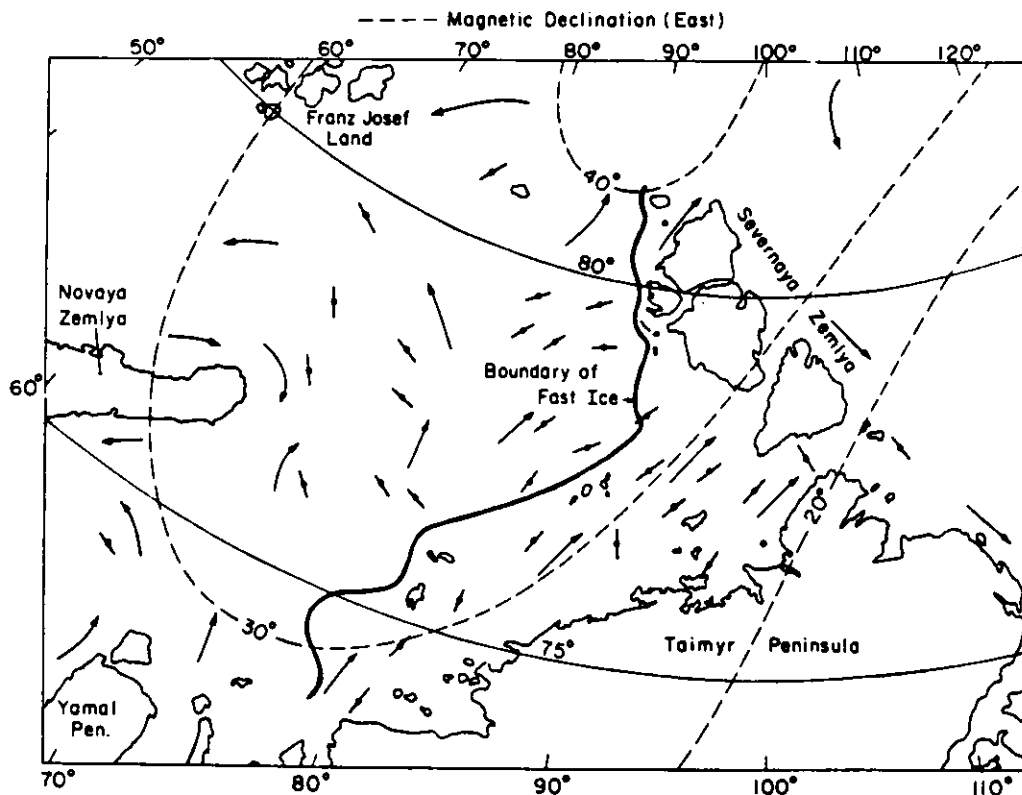


Figure 45. The c-axis orientations as determined by Cherepanov (1971) in the Kara Sea. The arrows indicate the estimated directions of the surface currents obtained from U.S. Navy sources (Weeks and Gow 1978).

In 1971 a quite remarkable set of c-axis observations (Fig. 45) were published by Cherepanov, who observed nearly constant c-axis alignments over thousands of square kilometers in the Kara Sea. This was followed by studies of the directional dependence of the electrical properties of sea ice from widely separated sites in the Canadian Arctic that also supported the contention that c-axis alignments might well extend over lateral distances of the order of tens of kilometers (Campbell and Orange 1974, Kohnen 1976). This work was followed by a series of three papers that provided a detailed look (Fig. 46) at crystal alignments along the coast of arctic Alaska (Gow and Weeks 1977, Weeks and Gow 1978, 1980). Similar studies are now available for the Mackenzie Delta portion of the Beaufort Sea (Langhorne 1980), for the ice surrounding artificial gravel islands that are used for drilling platforms (Vittoratos 1979), for channels in the Canadian Arctic Islands (Nakawo and Sinha, in press), and for the Antarctic (Serikov 1963, Gow et al. 1981).

The results of these observations indicate the following:

1. In all sea ice formed by unidirectional freezing, c-axis-horizontal orientations develop rapidly after an initial ice skim forms, and they dominate the rest of the ice growth.

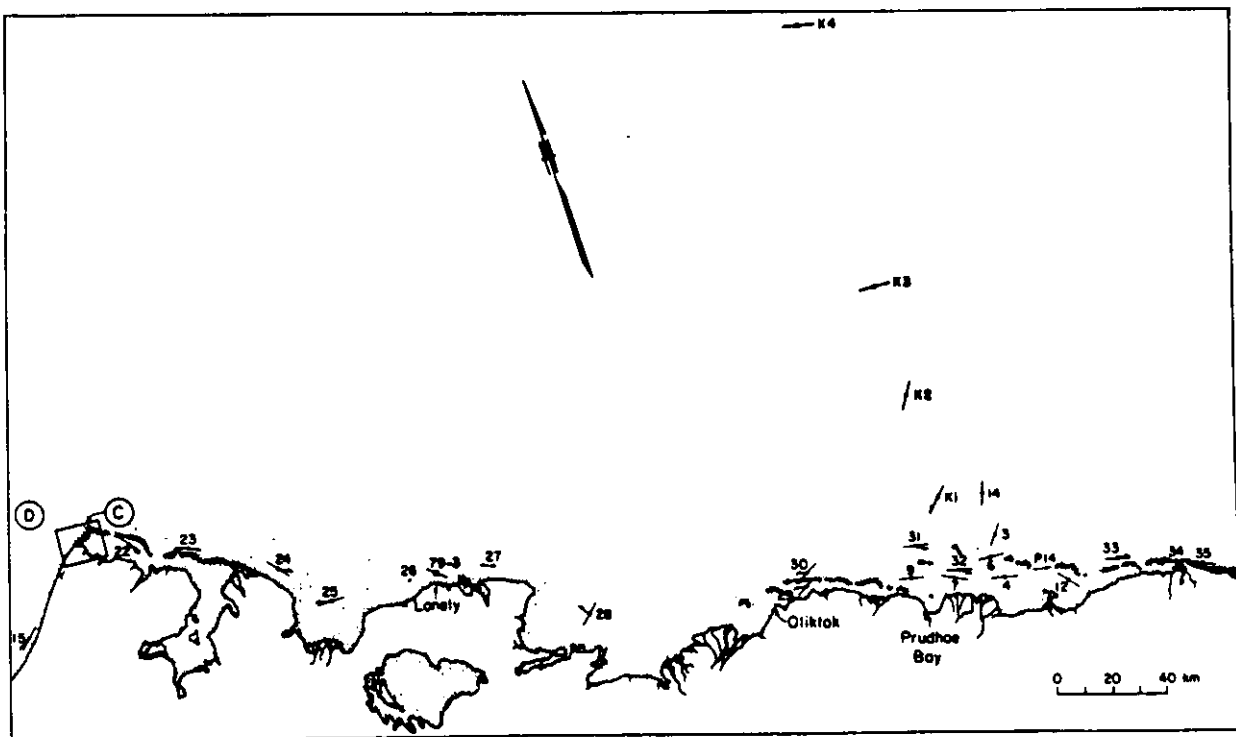


Figure 46. Sample site locations (dots), mean c-axis alignments (bars), and instantaneous current directions (arrows) determined along the coast of the Beaufort Sea. All the samples were collected during 1978 except site 79-3 north of Lonely and the low "out-of-sequence" sites (3, 4, 6, 7, 9, 12, 14 and P14) north of Prudhoe Bay, which were collected during 1977 (Weeks and Gow 1978) and are included for comparative purposes. Also shown are four orientations determined by radar (sites K1-K4) by Kovacs and Morey (1980).

2. In much of the ice examined (95% of the sample sites along the Alaskan coast; Weeks and Gow 1980) strong c-axis alignments also develop within the horizontal plane. Figure 47 shows a sampling of published fabric diagrams. Standard deviations around the mean are usually $<10^\circ$ for ice collected from near the bottom of ice sheets in excess of 1.5 m thick.

3. Alignments may occasionally be present in ice 20 cm thick and they invariably become stronger (show less scatter around the mean) with increasing depth in the ice (Fig. 48).

4. Although the mean c-axis direction is not constant at different levels in the ice sheet, the variations are commonly $<20^\circ$.

5. Mean c-axis directions at the same site commonly appear to be similar from year to year; however, the "strength" of the alignment may vary.

6. In the nearshore regime the c-axes generally parallel the coast, swing around both natural and artificial islands in a streamlike pattern, and are aligned parallel to the axes (throats) of passes and inlets.

7. Limited information (Fig. 45 and 46) indicates that strong crystal alignments can also develop in areas of pack ice.

There have been several different suggestions concerning the cause of these alignments. Cherepanov (1971) initially suggested that some

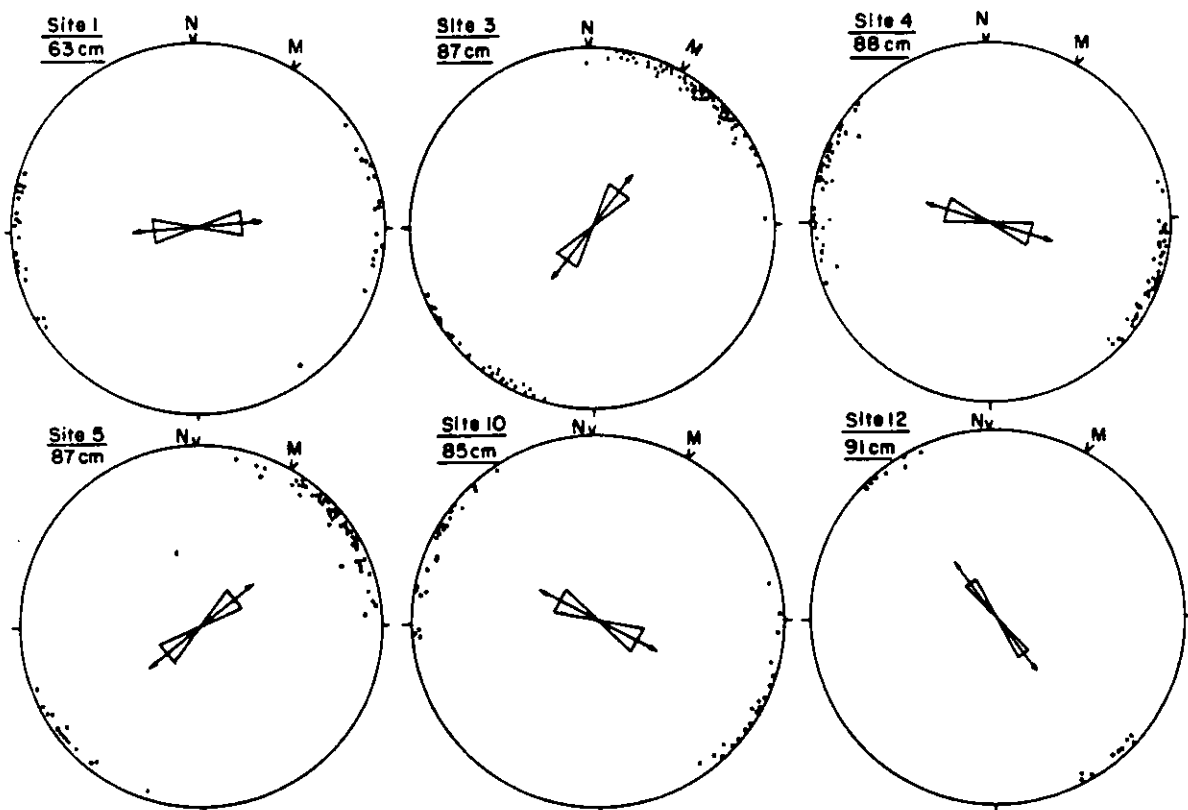


Figure 47. Schmidt net plots of individual c-axis orientations for six different sampling sites along the coast of the Beaufort Sea (Weeks and Gow 1978).

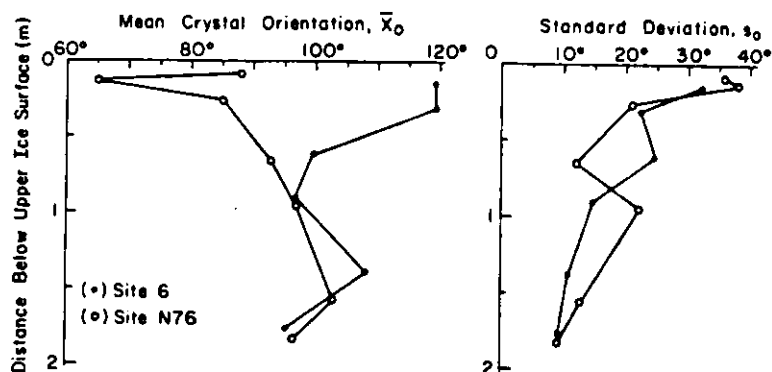


Figure 48. Mean crystal orientation in the horizontal plane, $\bar{\alpha}_0$, and the standard deviation, s_0 , as a function of vertical location in the ice sheet. Sites along the coast of the Beaufort Sea (Weeks and Gow 1978).

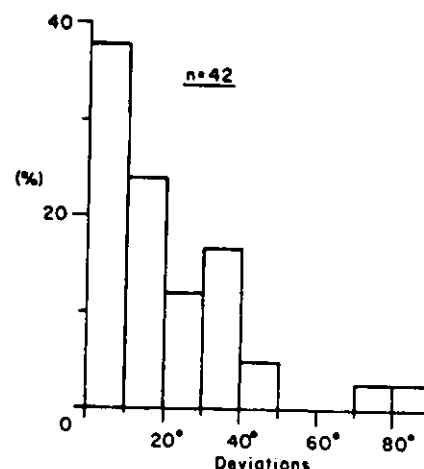


Figure 49. Histogram showing the relative frequency of different deviations between the observed instantaneous current direction and the mean c-axis direction (Weeks and Gow 1980).

interaction between the earth's magnetic field and the electric potential produced at the freezing interface caused them. No information was given concerning how such couplings might work. Weeks and Gow (1978) rejected this suggestion, pointing out that a) there does not appear to be a theoretical reason why the sea ice crystal orientation should be affected by the earth's magnetic field, b) similar alignments have not been observed in experiments on the unidirectional freezing of NaCl solutions in magnetic fields 80,000 times stronger than the earth's, and c) Cherepanov's own measurements show many examples of crystal alignment that are not in agreement with the direction of the geomagnetic field at the time the samples were collected.

Weeks and Gow then suggest, after examining a variety of alternatives, that the mechanism most likely to produce the aligned crystals works through the control that the current has on the composition of the liquid at the dendrite tips, and thus on the interface temperature. If the current is parallel to the basal ice plates, then a stable boundary layer can build up along a dendrite tip. If, however, the flow is perpendicular to the plates (i.e. parallel to the c-axis), then mixing will be enhanced at each plate tip, and the thickness of the diffusion-limited solute boundary layer reduced. A reduced boundary layer thickness should give the crystals in this orientation a very slight growth advantage, permitting them to grow sideways at the expense of neighboring crystals. Although approximate calculations suggest that the Weeks and Gow hypothesis is plausible, its mechanisms are far from proved. It is, however, possible to test the suggested correlation between mean current direction and the direction of the c-axis alignment. These observations have been collected by Weeks and Gow (1978, 1980) and by Kovacs and Morey (1978). Figure 49 shows the relative frequency of different angular deviations between the observed "instantaneous" current direction determined just under the ice and the mean c-axis direction. The

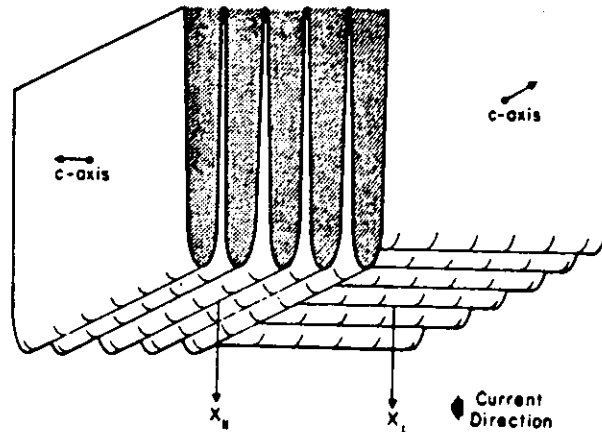


Figure 50. Sketch showing the interface geometry of two crystals of sea ice oriented so that the c-axis in one crystal (the left) is parallel to the current direction, while in the other crystal (the right) the c-axis is oriented normal to it (Weeks and Gow 1978).

agreement is quite good, considering that short-term current measurements are known to commonly show significant deviations from the long-term average current direction because of eddies. It should also be noted that Weeks and Gow measured a 7-hour average of the current vector at a site near Barrow and obtained an average value that differed from the mean c-axis alignment by only 4° .

Recently, Stander and Gidney (1980) have proposed a very different model to explain c-axis alignments: that the alignments are the result of stress-activated mechanisms such as grain boundary sliding and dislocation generation. Although details are not given, the authors state that their model is similar to that of Kamb (1959) [see review by Patterson (1973)], which discusses preferred fabrics in metamorphic rocks that are produced by recrystallization in an anisotropic stress field. We feel that it is quite clear that this theory is not applicable to c-axis alignments in sea ice. The fabrics in sea ice are the result of preferred directions of crystal growth from the melt. The orientation seen at each level in the ice is the orientation that was present when the ice layer initially formed. During this initial phase of crystal growth, each crystal is composed of a series of separated platelets that extend downward into the melt (Fig. 50). These platelets do not touch each other until approximately 2.5 cm above the gross solid/liquid interface. It is a bit difficult to talk about stress transfer between crystals at a level in the ice where the crystals are not in direct contact. Finally, if the Stander and Gidney hypothesis were correct, there should be evidence that the sea ice has recrystallized. There is no indication that this has occurred, with the possible exception of the upper levels of multiyear ice where a completely different process is believed to be at work. Although we would agree that the sea ice substructure is not stable in a thermodynamic sense, it persists because the grain and sub-grain boundaries are locked in by the presence of innumerable brine and air pockets located along them. For

recrystallization to occur, the grain and sub-grain boundaries would have to break away from these inclusions, a process that creates additional surfaces within each crystal, thereby raising the surface free energy and creating a barrier to recrystallization. For larger stresses this barrier would be overcome and recrystallization would occur. However, a simple petrographic examination clearly shows that in both aligned or unaligned sea ice this has not occurred, as the grain size and substructure remain unchanged.

It should be possible to resolve by experiments many of the questions about the mechanisms that lead to the c-axis alignments. Such work is now underway (Langhorne 1980). If the c-axis direction is a measure of the mean current direction it might at first glance be concluded that alignments would only be found in ice that was fast when the alignment developed. Two pieces of information suggest that this is not always true. Cherepanov (1971) found alignments in first-year ice in areas of the Kara Sea that were identified as pack (Fig. 45), and Kovacs and Morey (1980) obtained similar results for offshore areas of the Beaufort Sea (Fig. 46). This can be explained if the current velocity at the ice/water interface remains reasonably constant relative to the ice long enough for an alignment to develop. As both these sets of observations were made in the later winter when the ice pack in the Beaufort and Kara Seas was extremely tight, this would appear to be a plausible explanation.

Present observations suggest that very significant portions of the world's fast ice show strong c-axis alignments. The percentage of the pack that shows such alignments is unknown. We would guess that pack ice that forms at locations such as the Bering Sea, Baffin Bay, and much of the Antarctic, where the ice is highly mobile and the floes are free to rotate, would show random alignments in the horizontal plane. Where the pack ice becomes very tight during the ice growth season, restricting the possible rotation of floes, then aligned ice may be the dominant form. Systematic field observations should be made to resolve these questions.

Frazil Ice

Given an initial ice skim formed from individual discs or particles of ice, the ice cover was believed to usually take on the characteristic congelation or columnar ice structures so frequently observed. Frazil ice was thought to account for only the top 5% or so of the ice cover (e.g. Martin 1979), with congelation or columnar ice providing the vast majority (95% by volume) of most sea ice. This condition has been found in fast ice regimes in the Arctic Basin (Weeks and Gow 1978, 1980), in the Labrador Sea (Weeks and Lee 1958), and more recently in the fast ice region of Antarctica near McMurdo sound (Gow et al. 1981).

In ice edge regions and in large polynyas where substantial open water can be maintained, Martin and others have described rapid frazil ice generation that could conceivably result in frazil ice thicknesses of up to a meter prior to the development of a columnar congelation structure.

Work in the Weddell Sea has, however, indicated even greater potential for frazil growth. A serious revision of ideas concerning the

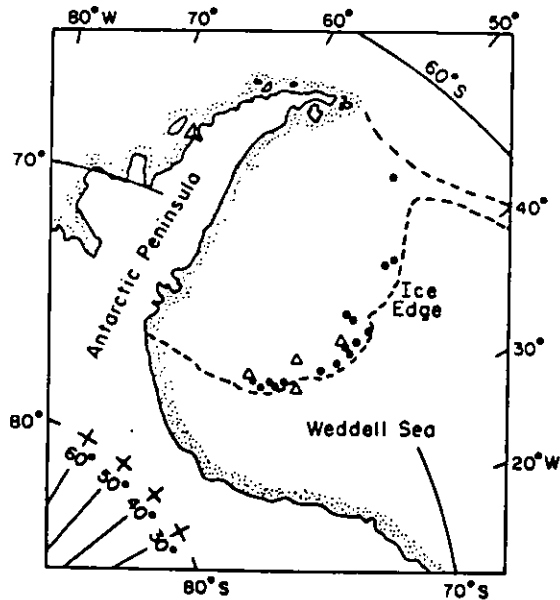


Figure 51. Site locations for sea ice core sampling from the USCGS Polar Sea in Feb-March 1980.

importance and distribution of frazil ice, at least for the Antarctic pack ice regions, appears to be in order. If frazil ice is more widespread than once believed, mechanisms for ice-ocean interaction must also be modified. We first give the evidence for these new frazil structures and then discuss some preliminary ideas for the ice-ocean mechanisms leading to the formation of the observed structures.

Figure 51 shows the location of sites in the Weddell Sea sampled during February-March 1980. Complete cores were obtained from 66 individual floes (13 multiyear floes), with a total of 138 m of core being retrieved. Salinity and fluorescence measurements were also taken at 10-cm intervals over the entire length of core. The crystal structure was defined in two ways. The first was by preparing two to six horizontal thin sections per core (depending on its length). This method gave only point samples of the structure, albeit at several locations along the core length. To verify the frazil percentages initially estimated from these point samples, vertical thick (2 to 3 mm) sections were then prepared of the ice. When these sections were viewed between crossed polaroids, the differences between relatively fine-grained equiaxed crystals (frazil) or coarse-grained columnar crystals (congelation ice) could easily be distinguished. These changes were then sketched schematically (cartooned) as a function of the distance along the core.

We will now briefly describe the structure of several representative floes (after Gow et al. 1981).

Floe 42-A-1 (see Fig. 52). This is an example of thick (4.8 m) multiyear ice with a maximum salinity of 9‰ and an average salinity of 3.5‰. The floe was composed of 4% snow ice (designated S in the vertical structure profile), 61% frazil ice (designated F) and 35% congelation ice (designated C). The congelation ice component is characterized by a very strong alignment of the crystallographic c-axes as indicated by the arrows in the photographs of thin

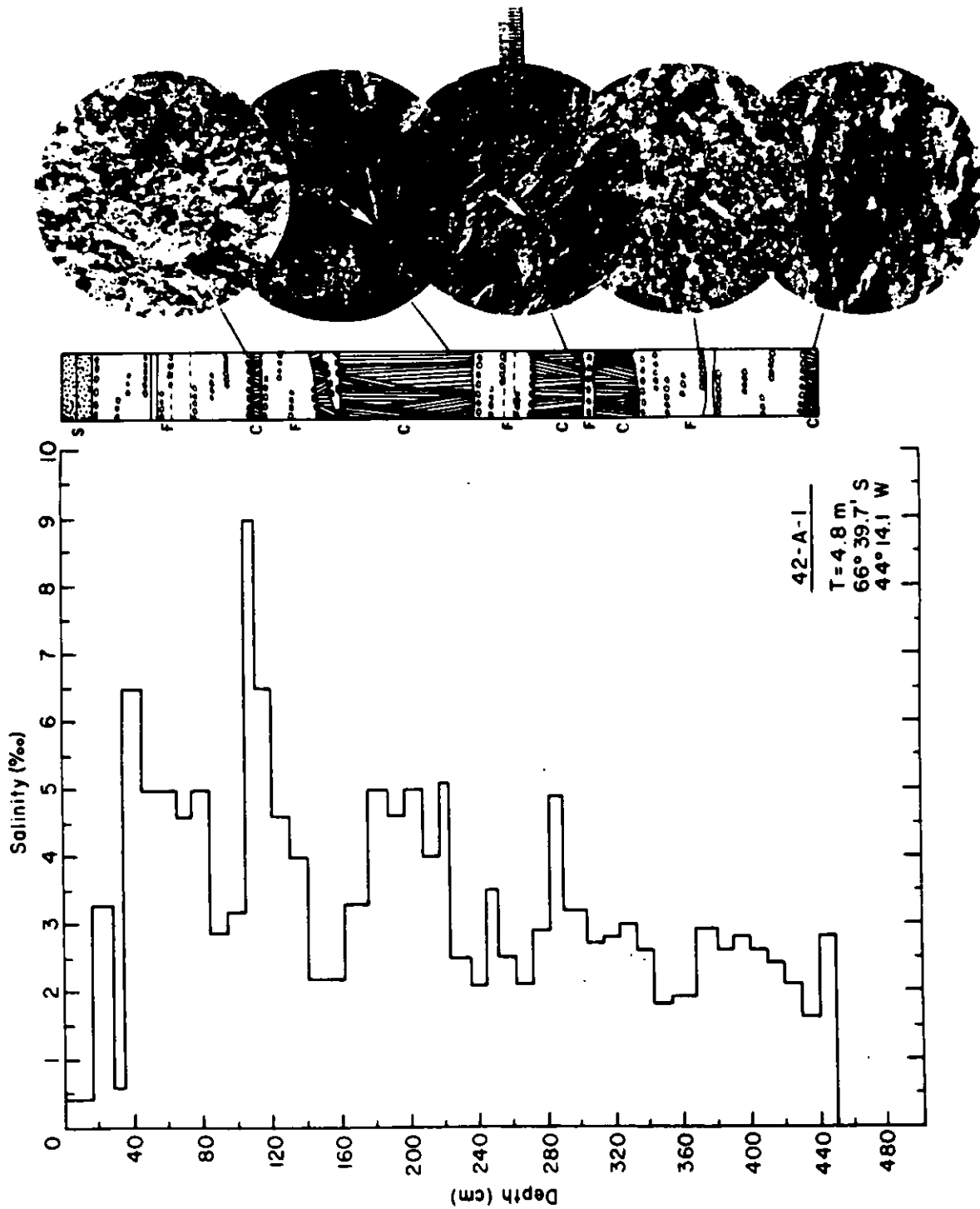


Figure 52. Salinity, structure and thin section photos from Floe 42-A-1. The key to the ice structure diagram is as follows: S = snow ice, F = frazil, C = congelation ice.

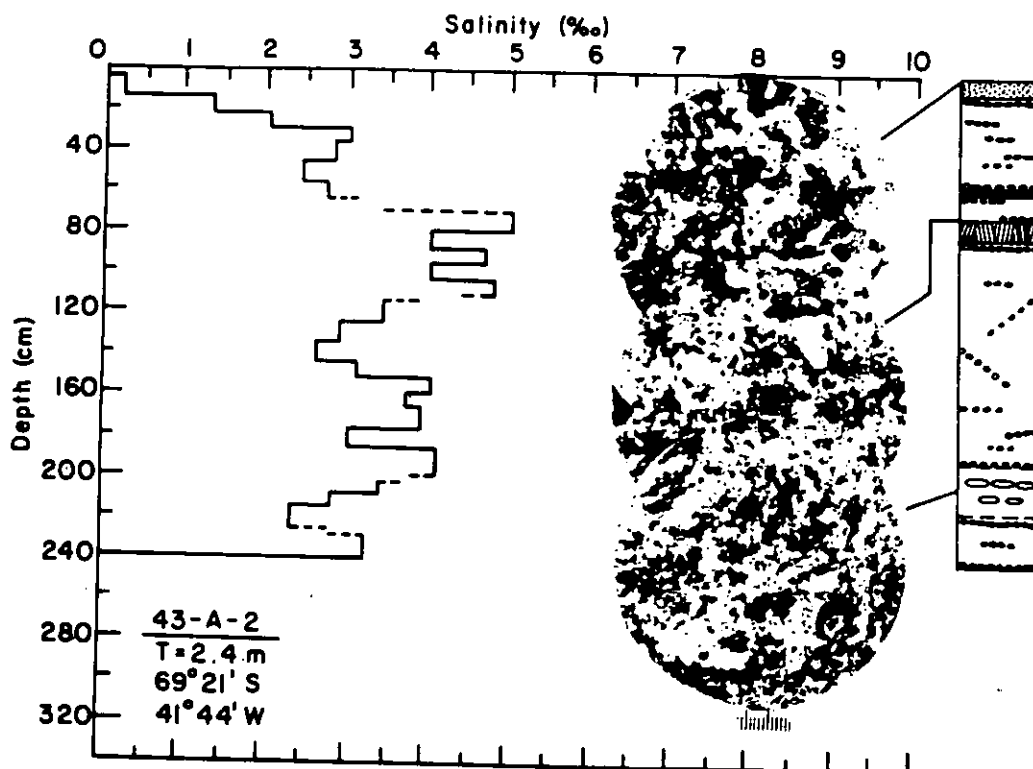


Figure 53. Salinity, structure and thin section photos from Floe 43-A-2. A key to the ice structure diagram is given in Figure 52.

sections from 2.24 m and 2.93 m. In this and other profiles presented here the much smaller crystals and the absence of brine lamellae-ice plate structure serve to distinguish frazil ice from the generally fibrous-textured congelation ice.

Floe 43-A-2 (see Fig. 53). The exact age and origin of this 2.4-m-thick floe are difficult to assess. However, a maximum salinity of 5‰ and an average value of about 3‰ would indicate that this particular floe is multiyear. It is composed of 90% frazil ice of variable grain size with congelation ice composing less than 6% of the floe thickness.

Floe 44-G-3 (see Fig. 54). This floe was located in a region of recently disintegrated sheet ice that produced floes measuring approximately 30 m in length. Identified as first-year ice with an average salinity of 5‰ it is composed almost entirely of congelation ice (95%) with crystals showing well developed brine lamellae-ice plate structure and a very strong alignment of the crystallographic c-axes. The constancy of this alignment (indicated by arrows) would suggest either a fast ice origin or growth of ice in place in a relatively immobilized part of the winter pack.

Floe 49-G-2 (see Fig. 55). This first-year floe was composed mainly of congelation ice (72%) but had some frazil ice (22%) incorporated in a zone at 0.26-0.70 m depth. The thin section from 0.70 m exhibits a texture that is transitional between fine-grained frazil and coarser-grained congelation ice. The bottom section is composed of ran-

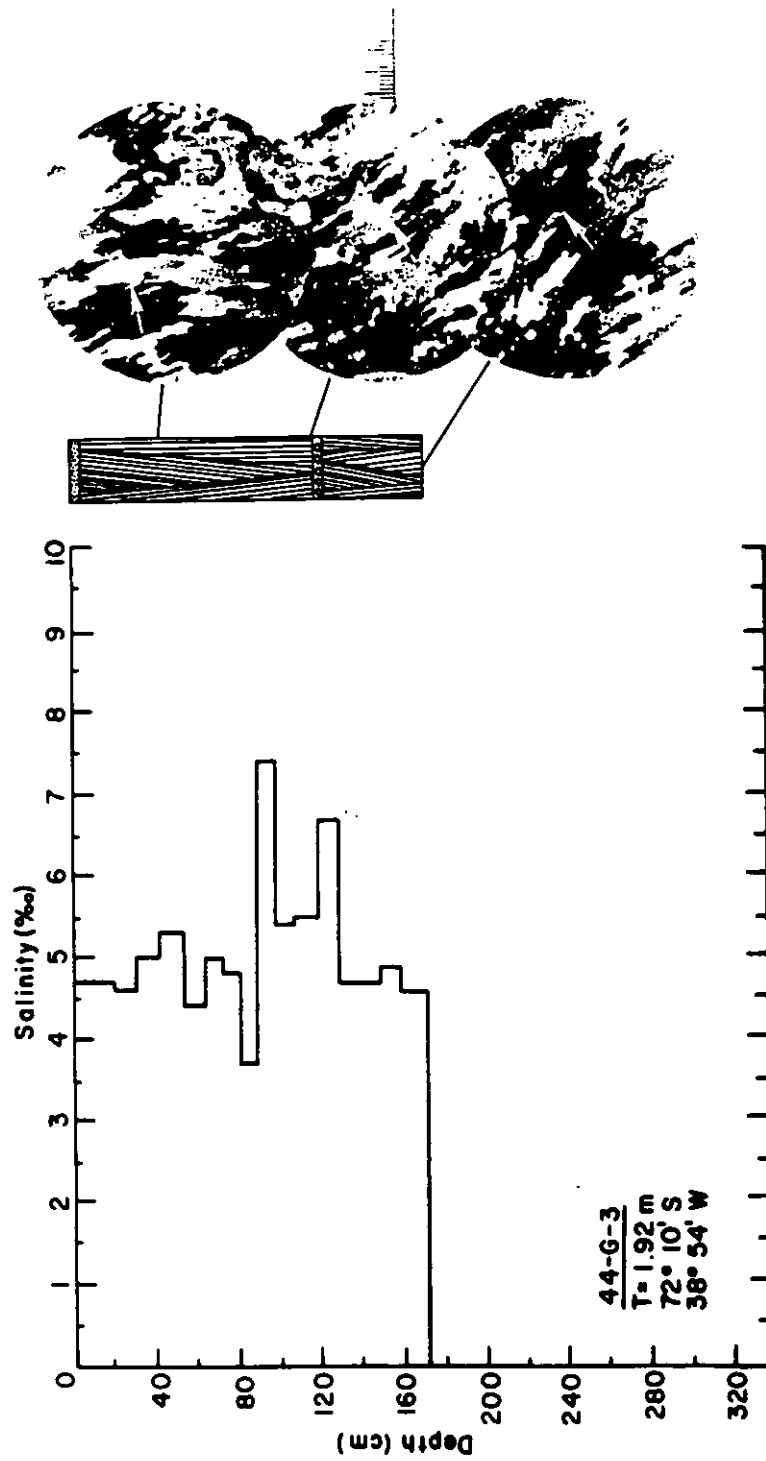


Figure 54. Salinity, structure and thin section photos from Floe 44-G-3. A key to the ice structure diagram is given in Figure 52.

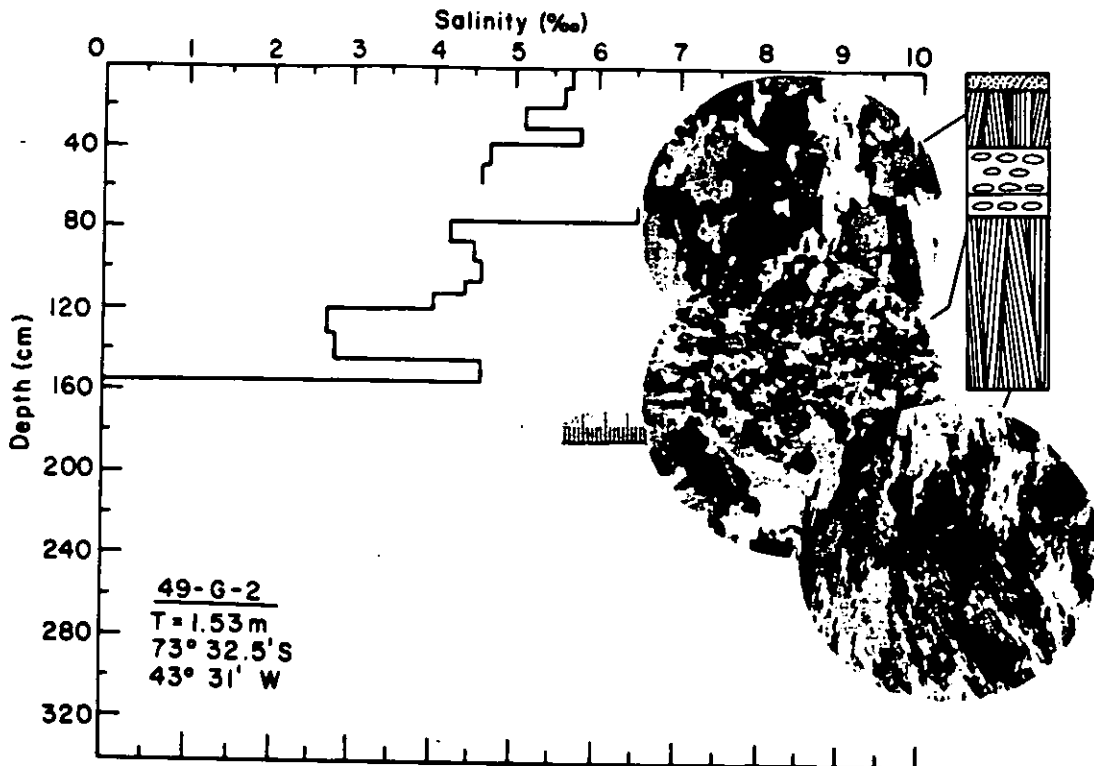


Figure 55. Salinity, structure and thin section photos from Floe 49-G-2. The key to the structure diagram is given in Figure 52.

domly aligned fibrous-textured crystals. The average salinity of the floe is 4.7‰ .

Floe 61-G-2 (see Fig. 56). This is a multiyear floe with an average salinity of 3.5‰ . The upper meter of ice is mostly composed of congelation ice with moderately aligned crystals, underlain by 2.9 m of frazil ice of highly variable grain size. Crystals of frazil range in size from 0.4 to 4 mm and are usually arranged in layers that would suggest several separate episodes of frazil generation.

It was found that of the total length of multiyear core (35.85 m samples), about 75% was frazil and only 19% was congelation, with the remainder (6%) being fine-grained but of indeterminate origin. For the first-year ice (85.7 m) the frazil congelation percentages were 46% and 47% respectively, with 7% of indeterminate structure. These characteristics are shown in Figure 57, where congelation ice percentage is plotted as a function of ice thickness. The data indicate a slightly higher percentage of congelation ice for ice less than 1 m thick and roughly equal (but highly varied) percentages for ice between 1 and 2 m thick. However, no floe exceeding 2 m in thickness is composed of more than 50% congelation ice. Therefore the thickest ice in the Weddell Sea (>2 m) is composed primarily of ice with frazil structure.

One's first reaction in looking at these statistics is that it is the almost complete reversal of what would be presumed based on the commonly held assumptions about the growth of sea ice. Instead of the

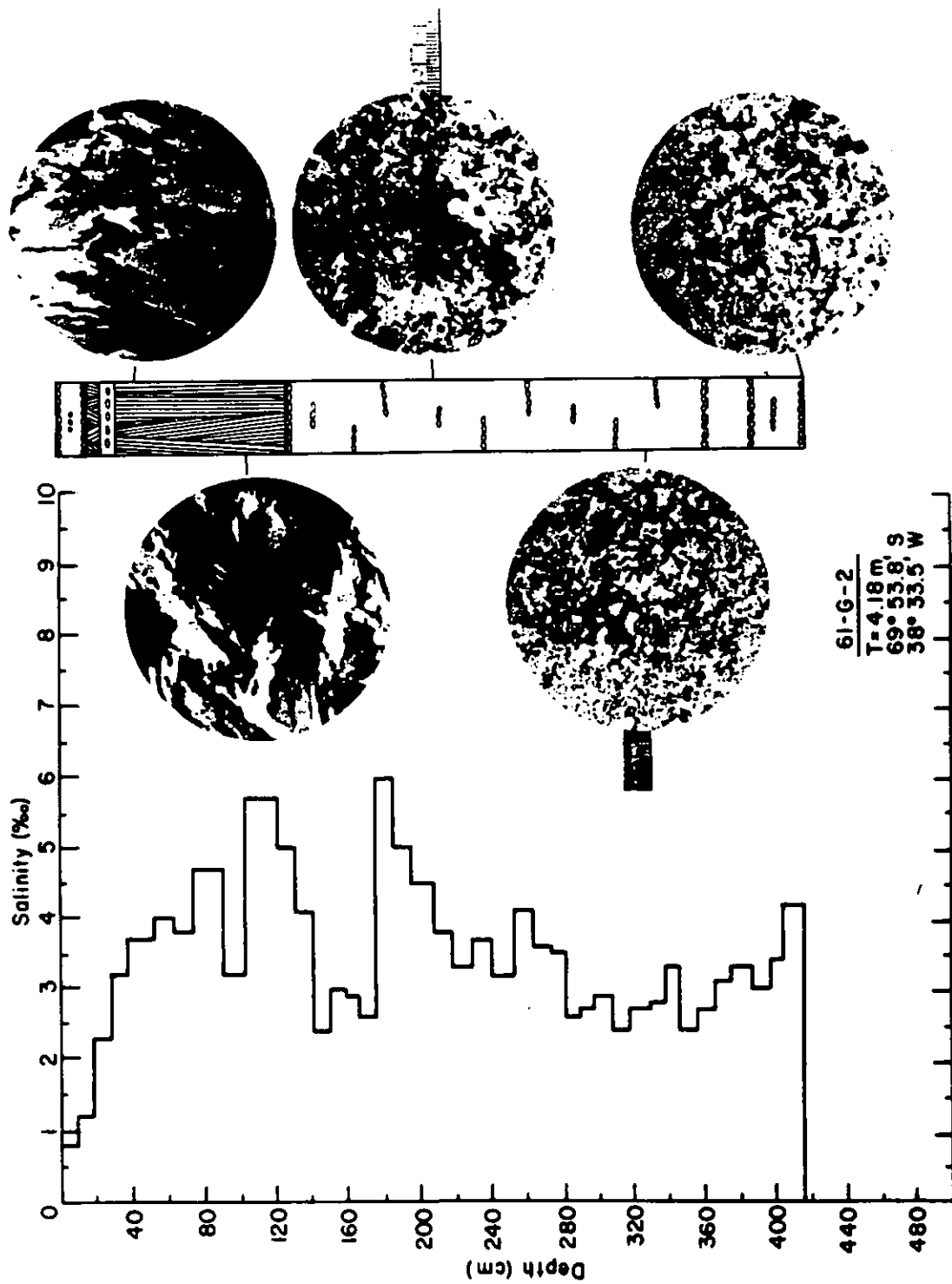


Figure 56. Salinity, structure and thin section photos from selected depths for Floe 61-G-2. A key to the ice structure diagram is given in Figure 52.

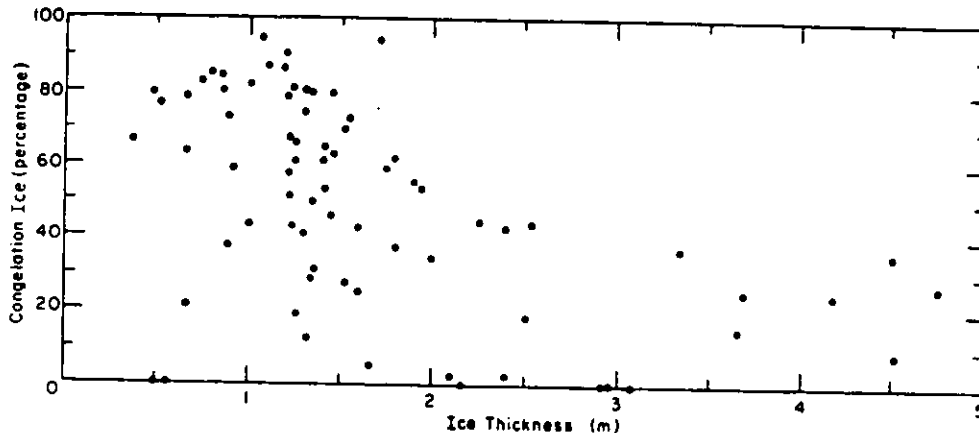


Figure 57. Congelation ice (percentage) vs ice thickness for all cores obtained in the Weddell Sea.

thinnest ice (<1 m) being primarily composed of frazil, it is the thickest ice that commonly contains the largest percentage of frazil.

Such frazil ice as occurs in the Weddell Sea pack ice is particularly interesting in that its origin and properties are very different in most all respects from the congelation ice upon which most work has been concentrated. This will be seen quite clearly later in this paper when the effect of ice structure on ice properties is discussed. We will now discuss some possible mechanisms for the generation of oceanic frazil ice.

Mechanisms of Frazil Generation in Oceans

To generate fine-grained frazil ice during freezing from the melt, the observations from rivers, lakes and oceans suggest one necessary condition, namely turbulence. Frazil generation originates as a result of the large-scale (> cm scale) mixing of waters and during its development has been likened to a blizzard (an upside-down one) in the water column. However, some basic differences exist in the momentum and heat flow characteristics of rivers and oceans. In rivers the turbulence is nearly always purely mechanically derived from accelerations in the flow by increasing discharge, varying bed geometry (falls and rapids) or the like. Although the literature is not clear on this point, it appears that a threshold velocity of 0.6 m/s is necessary under freezing conditions to allow the onset of frazil formation (Ashton, pers. comm.). The constraint is primarily a mechanical one; while frazil generation requires efficient heat transfer between the cold atmosphere and the water, sufficient mechanical shear is necessary to mix the flow and carry the newly formed ice crystals rapidly away before a complete skim of ice can form. In the ocean, however, these mechanical influences are much less pronounced. Four possible sources of turbulence that can affect freezing conditions leading to frazil formation in the ocean are as follows.

(1) Wind- and wave-induced turbulence. As we previously described, this effect can only account for limited frazil production in wide leads and polynyas and near ice edges due to the extreme damping of these effects when a significant percentage of the sea surface is covered by ice.

(2) Water which is at a depressed freezing point due to pressure at depth and is suddenly adiabatically brought to the surface (Foldvik and Kvinge 1974). Water of this type typically exists under large ice shelves, and the ascent occurs near the front. If this were the only mechanism producing frazil one might expect the percentage of frazil in floes to increase as ice shelves are approached. Correlations of this type have not as yet been observed. As well, the amount of ice production available by this mechanism (since possible freezing point depressions are only a few tenths of a degree) does not seem compatible with the large amount of frazil ice observed ($\approx 50\%$ of the observed ice).

(3) Contact between two water masses of significantly different salinity but both at their freezing point. We will discuss this mechanism further in relation to multiyear ice structure since this type of ice formation occurs in under-ice melt ponds (of primarily fresh water) which drain into the ocean from melting surface ice and are stratified due to density differences. Freezing then occurs due to double diffusion (transfer of heat at a faster rate than salt) from the cold ($< -1^{\circ}\text{C}$) seawater to the fresh water on top of it (Martin 1974). This process could also occur associated with the drainage of river or glacier water into seawater that is colder than the fresh water freezing point. Again these effects are undoubtedly local in the regions they affect and it is difficult to see how they could account for the observed ice conditions in the Weddell Sea.

A process of sufficient generality that occurs over a broad enough region to account for much of the observed frazil production is:

(4) thermohaline convection initiated by surface cooling and freezing. Figure 58 indicates some differences between Arctic and Antarctic water column structure that indicate more potential for frazil ice generation in the Antarctic. In general, the mixed layer in the Antarctic is both considerably deeper than in the Arctic and is, also, totally at its local freezing point. Martin (1974), in a study of ice stalactites, indicated that the heat loss of a descending brine plume could be, when the water was at its freezing point, as much as 50% accounted for by frazil production. As the temperature of the brine plume is closer to the freezing point of the surrounding water, there is less tendency for stalactite forms to occur, implying all the heat loss could be taken out by frazil ice formation. We note, however, that in

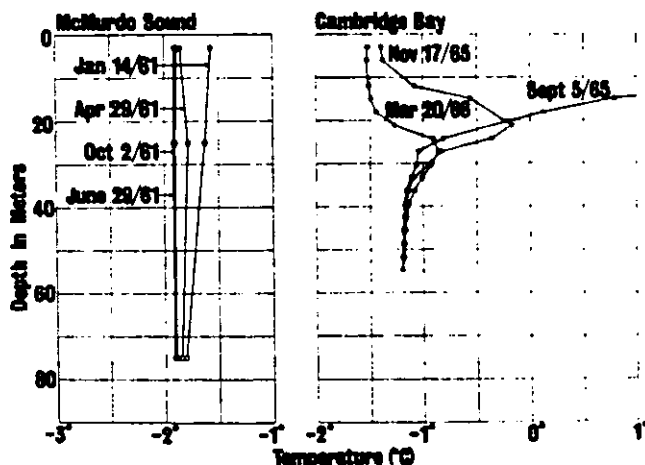


Figure 58. Profiles of seasonal changes of temperature with depth in the water column typical of the Antarctic (McMurdo Sound) and the Arctic (Cambridge Bay). The Antarctic near-surface waters remain closer to the freezing point at greater depths than do the Arctic waters (Lewis and Lake 1971).

Martin's study the frazil crystals appeared to be entrained downward with the descending plume. More likely is that frazil crystals are generated in waters adjacent to the descending plume for two reasons. One effect is buoyancy. That is, the energy necessary to force an ice crystal downward with a density defect approaching 10% compared to surrounding waters is considerable and much larger than the relative density differences that can lead to water column overturning. Secondly, if the waters of a descending cold brine plume are entraining surrounding waters then the mixture will also be in equilibrium at its freezing point. That is, there should not be any ice production, merely a more saline mixture at a temperature intermediate between the cold brine plume and the surrounding water. A simpler mechanism that preserves the buoyant characteristic of the ice crystals and still allows ice production at depth is to maintain the integrity of the descending brine plume and allow it to gain heat at a different rate than salt. This is known as double diffusion and has been observed in several other contexts in the ocean (e.g. Turner 1973). In this mechanism, the descending brine plume gains heat but diffuses salt at a much lower rate, thereby cooling adjacent waters to temperatures below their freezing point (at their given salinity). An ice crystal is then nucleated and rises due to buoyancy, and the remaining water also descends at a new equilibrium freezing temperature and salinity. While the process appears to be diffusion-limited by the ability to extract heat from the brine plume, the convection is continuously strengthened by the ice formation so the effect is a convection cascade which should quite effectively use the heat sink of the brine plume and establish a circulation boosting the convective process. Based on the observed structures (Fig. 52-56), we also see that frazil forms under thicker ice. Advecting surface-generated frazil downward underneath this thicker ice is again a problem of overcoming strong upward buoyancy forces. A generation mechanism whereby ice crystals are formed at depth due to thermohaline convection is not constrained in this way. Descending brine plumes in leads and polynyas will set up a local circulation that could bring the ascending arm (containing some of the frazil) underneath adjoining ice. As well, substantial shear usually exists between the ice and the water column due to wind action on the ice, so motion of the ice cover would tend to bring a different piece (possibly thicker) into position over the ascending frazil crystals, if they are formed at depths greater than a few meters.

None of the above-mentioned mechanisms have, as yet, been detailed to any substantial degree. Whether they do indeed account for the observed frazil ice structures and whether frazil structures are more widespread than previously thought or are only an anomaly of the Weddell region remain subjects for future study.

Suspended Material in Frazil Ice

One very interesting aspect of frazil ice is that it may contain large amounts of fine-grained sediment and algae. Our observations in the Weddell Sea (Ackley 1982, Buck and Garrison 1982, Garrison and Buck 1982) indicate that enough algae was incorporated into thin (<20 cm), young (=1 day old) ice to give the ice significant coloration. Of primary importance is that our measurements indicated that the concentration of algae in this thin ice was several times the concentration in

the water column in which the ice was growing. This observation is strongly in opposition to our past experience with growing ice sheets from the melt, where water impurities, dissolved or suspended, are for the most part rejected and lesser concentrations are generally observed in the ice than in the water. Similar evidence from the Arctic has been gathered (T. Osterkamp and J. Gosink, personal communication) where, in coastal waters, bottom sediments that are stirred up and incorporated into the growing ice are at higher concentrations than observed in the water column itself.

The short time scales (a few hours) observed in the growth of the algae-loaded ice in the Antarctic mitigates against biological growth affecting the increase in the concentration in the ice relative to the water column. Two possible mechanisms, both relying on frazil ice formation processes, can be proposed to explain these increases in concentration of suspended material in the ice relative to the water column. The first is ice nucleation by foreign particles. Concentration by ice nucleation can occur if frazil ice crystals preferentially nucleate on suspended particles. Since the small observed supercoolings limit the volume of ice formed to a small fraction of the volume of water, the effect is to have the same number of foreign particles in a much smaller volume, that is, to increase the concentration of particles in the ice phase. We note, however, that this process still requires the ice to form in the water column (frazil ice) rather than on top of the water column (congelation ice).

The second mechanism, which we call concentration by ice scavenging, occurs by collision of the frazil ice crystal with particles as it travels through the water column to the upper water surface. Each crystal could collect several particles, depending upon how much the length of the path that the ice crystal travels exceeds the mean distance between particles in the water column.

We have microscopically examined thin sections of some of the Antarctic ice samples and have found evidence suggesting that for algae particles both nucleation and scavenging operate. This examination indicates that cells are found within individual ice crystals, suggesting that the cell nucleated the crystal, and also are found at grain boundaries between individual crystals, suggesting that the crystal scavenged the cell.

It appears, however, that scavenging is the dominant mechanism for incorporation of material. If nucleation were the only mechanism, a limit on the amount of material incorporated would be the number of crystals (one cell per crystal) per unit volume. Frazil ice crystal sizes observed are of the order of ≈ 1 mm diameter, implying an upper bound of $\approx 10^6$ cells/liter if nucleation is the only mechanism. Measured concentrations of algae exceed this by one to two orders of magnitude ($\approx 10^8$ cells/liter), indicating scavenging may be the more effective mechanism for incorporating algae. Another observation is that most foreign materials allow water supercoolings of the order of a few degrees Celsius to exist before they become effective as ice nuclei (Hobbs 1974). Although supercoolings of a few tenths of a degree have been observed at the surfaces of Arctic leads (Katsaros 1973) these values are characteristically less than required for most suspended mineral matter

to serve as a nucleating agent. Biological materials, especially living cells from cold waters, have not been well studied as to their effectiveness as nucleating agents, and this behavior should be investigated. In conclusion, in the few cases studied the total particle concentration relative to the ice crystal size as well as the wide range of organic and inorganic materials incorporated in the ice support the contention that scavenging is a more important incorporation mechanism than nucleation.

Multiyear Ice

Considering that vast areas of the polar seas are covered with multiyear ice, there is an amazing lack of information on its structure and properties. In the following discussion we will use the term "multiyear ice" to refer to ice that has survived at least one summer's melt season. This rather casual usage corresponds to the way that the word "multiyear" is commonly utilized by sea ice specialists. This differs from the recommended WMO usage in which second-year ice has survived one melt season, multiyear ice has survived two or more melt seasons, and the phrase old ice is used to characterize both of these ice types.

In the Arctic, multiyear ice is distinguished by two main characteristics: 1) its rolling, hummocky surface, which is the result of differential melt, and 2) its salinity profile, which indicates values near zero for the ice above sea level and shows a gradual increase to values of 3.0 to 3.5‰ for the ice in the lower portion of the floe. As will be discussed later, this profile appears to be primarily produced by the flushing of nearly pure surface meltwater downward through the ice sheet.

What is the structure of this ice? The limited work that has been performed on multiyear ice has largely focused on the horizontal layers that are produced by the summer melt cycle. The reason for this interest is obvious: the annual layering allows one to establish a minimum age for thick floes of pack ice. Previous to these studies age estimates were based upon subjective criteria such as the amount of pressuring and the detailed morphology of the ice surface. Age estimates have also been made from the ice thickness and from the locations of the maxima and minima in the salinity profiles (Savel'ev 1958). As will be discussed later, although there is a general tendency to form a low salinity layer on the underside of the ice during the summer melt period, this salinity distribution is rapidly modified by brine migration and is difficult to use in estimating ice age except in extremely simple cases.

The first study of a horizontal "translucent-longitudinal" section of a thick (291 cm) pack ice floe was by Shumskii (1955) when in July of 1954 he made a brief visit to the drifting station SP-3. As a result of the above-freezing temperatures during the period of field work, very few detailed observations were made. The ice was divided into two main types, infiltrated (0-38 cm) and normal sea ice (38-291 cm). The infiltrated ice layer was described as resembling the firn of arctic glaciers and contained four distinguishable layers which were interpreted as annual. The normal sea ice was also classified into two

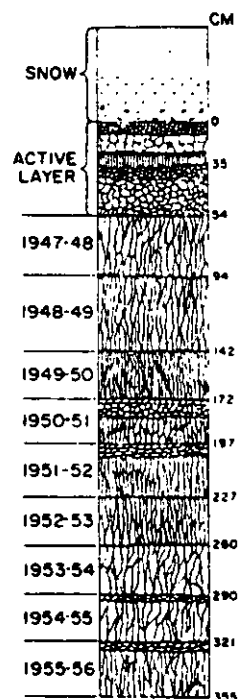


Figure 59. Cross section of a multi-year floe (Cherepanov 1957).

types. The upper part (38 to 150 cm) contained lens-like irregular strata that were believed to be the result of thaw cycles. These strata were absent in the lower portion (150 to 291 cm) of the ice. Therefore, Shumskii reasoned that the lower portion of the sea ice (141 cm thick) was formed after the end of the thaw period while the 4-year accumulation of infiltrated ice was forming at the surface of the ice sheet. The upper 112 cm of the sea ice was believed to be older. The total age of the floe was estimated at not less than 6 to 7 years. Shumskii also suggested that the presence of infiltrated ice indicated that the snow line in the central Arctic is presently at sea level.

Following this preliminary study, detailed investigations of the horizontal layering in pack ice were made on SP-4 (Cherepanov 1957) and Station Alpha (Schwarzacher 1959). It was found that the annual layering is readily observable in the lower part of the ice sheet and less clearly defined nearer the upper surface where the effects of the summer melt are more pronounced. Cherepanov found ten recognizable annual layers in a 335-cm-thick floe (Fig. 59), while Schwarzacher found either seven or eight layers in a 345-cm-thick floe. The boundaries between the annual layers were of two different types. The most common was a thin (2-5 mm) layer of milky white ice with a sharp upper boundary and an irregular lower boundary. The details of the formation of this layer are not known but it apparently develops during the period when the ice growth has stopped. The milky color of the layer may, in some way, be connected with the biological activity beneath the ice during the summer months. The formation of the milky layer is apparently not associated with either recrystallization or the nucleation of new grains, since when ice growth starts in the fall the crystals of the previous winter commonly resume growth with the same crystallographic orientation (Schwarzacher 1959).

The other type of summer layer is considerably thicker (1 to 10 cm) and shows a sharp decrease in grain size relative to the overlying winter ice. The grain shapes in this layer have been described as slightly elongated in the vertical direction. The c-axis orientations are in general horizontal but they show deviations up to 30 degrees (Schwarzacher 1959). In the ice studied by Cherepanov the crystals were equi-axed and the orientation was random. This ice does not show the platy substructure so characteristic of sea ice and has a much lower salinity (1 to 1.5‰) than the surrounding ice. The formation of annual layer is clearly the result of the formation during the summer of a stable layer of fresh meltwater between the lower surface of the ice and the underlying dense seawater. This process has been known for some time (Malmgren 1927) and has been described in considerable detail on Station Alpha by Untersteiner and Badgley (1958). They found that many of the freshwater melt ponds that develop during the summer drain through core holes, forming an irregular layer of fresh water between the ice and the seawater. At the interface between the fresh (0°C) and saltwater (-1.6°C), ice crystals formed and floated upward until the fresh water was filled with a mesh of fragile crystals. When the crystals forming at the fresh/saltwater boundary could no longer rise, the formation of a solid layer of freshwater ice began. The formation of such a layer is to be expected under any floe occupied by a scientific station because the large number of core holes drilled in the floe for technical studies readily facilitate the rapid transfer of meltwater to the underside of the ice. On an unoccupied floe early in the melt period, meltwater will either be channeled into open leads where wave action will favor mixing with the seawater or it will form large melt pools toward the interior of the floe. Only later in the melt period when deterioration is far advanced do drainage holes form in all areas of the floe (Bennington 1959). Even during this period, the lower density of the fresh meltwater inhibits it from percolating completely through the floe. When a freshwater layer does form, it is usually localized under the thinner portions of the ice floe and is particularly prevalent near open leads. This layer, if preserved by freezing, is very useful as a marker; Cherepanov found that four out of the nine annual boundaries in the NP-4 floe were marked by "fresh" ice layers (Fig. 59). On the other hand, Schwarzacher (1959) has noted from examination of a large number of cores in the vicinity of Station Alpha that the "fresh" ice layers do not contribute significantly to the total ice growth.

Schwarzacher (1959) observed that the top 50 cm of the floes he examined contained ice which formed at or near the surface of the floe. This ice was predominantly the result of the freezing of meltwater pools that form during the summer and was characterized by c-axes-vertical orientations. A fine-grained granular ice may also be formed by snow falling in the meltwater pools, producing a slush which subsequently freezes. This melt and refreezing associated with the upper ice surface tends to obliterate the annual layering in the upper part of the ice sheet and makes the accurate estimation of the age of the ice in a floe difficult if only one cross section is examined. For example, of the 150 cores collected by Schwarzacher in the summer of 1958 from areas that did not show signs of old pressure ridges, only 25% consisted of undisturbed ice and only 2% were sufficiently unaltered to show an annual layering throughout the complete thickness of the floe (eight

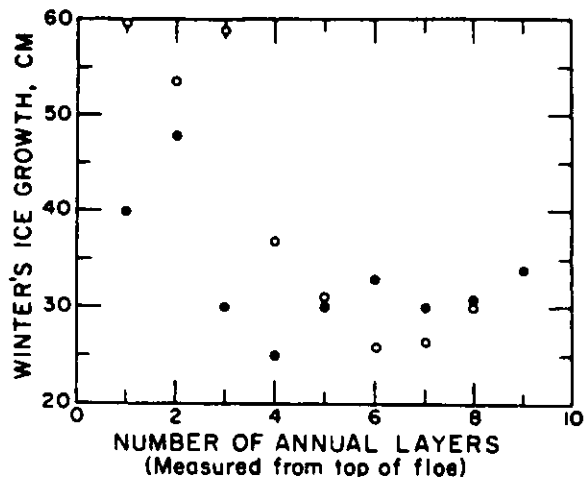


Figure 60. Winter's increment of ice growth plotted against the number of annual layers measured from the top of the floe. Data from Cherepanov (1957) and Schwarzacher (1959). The circles and dots represent observations on Stations Alpha and SP-4 respectively.

layers to 1950). Inasmuch as neither Schwarzacher, Cherepanov, or Bennington observed any annual stratification or superimposed firn, this casts considerable doubt on Shumskii's suggestion that the snow line in the central Arctic is currently at sea level. Both Cherepanov and Schwarzacher have noted that the formation of infiltrated ice is strictly local and is highly dependent upon the details of the surface relief. If infiltrated ice forms at all it will form in small depressed areas where old heavy snowdrifts are present. In most areas on both NP-4 and Alpha, both the snow cover and 20 to 30 cm of ice thawed during the summer (Untersteiner 1961). It therefore seems quite likely that the ice identified by Shumskii as superimposed firn was actually ice formed by melting and refreezing in the upper part of the ice sheet. If this is the case the SP-3 floe would be a minimum of 9 years old instead of 6 or 7 as suggested by Shumskii.

It is also of interest to point out that the thicknesses of the annual layers can be used to determine if the top annual layer is the layer representing the year when the ice sheet initially formed. Figure 60 shows the winter increments of ice growth plotted against the number of the annual layer measured from the top of the floe. The data are from Cherepanov (1957) and Schwarzacher (1959). For the last 7 years (SP-4) and 5 years (Alpha) it is clear that the ice thickness has approximately reached a steady state, the ice growth in the winter being the same as the expected ablation during the summer. Even the thickest annual layer measured on Alpha indicates an existing ice thickness of 260 to 280 cm at the end of the summer prior to the accumulation of the layer if the empirical relations of Schwarzacher (1959, p. 2365) and Untersteiner (1961, p. 165) are used. Inasmuch as 280 cm is the maximum one winter's fast sea ice accumulation known in the Canadian Arctic (Eureka, 1946-47; see Bilello 1961), this indicates that although the floe studied by Schwarzacher contained 8 years' accumulation of ice, the initial floe formed a minimum of 9 years prior to the time of measurement. Because the accumulation of winter ice in the Arctic Basin is usually considerably less than 260-280 cm [160 cm at NP-2 (Petrov 1954-55), 173 cm at NP-4 (Cherepanov 1957, Fig. 4, p. 183) and 180 cm at Alpha (Frankenstein, personal communication)] the estimate of 9 years for the age of the floe at Alpha is probably quite conservative, and the floe at NP-4 must be more than 11 years old.

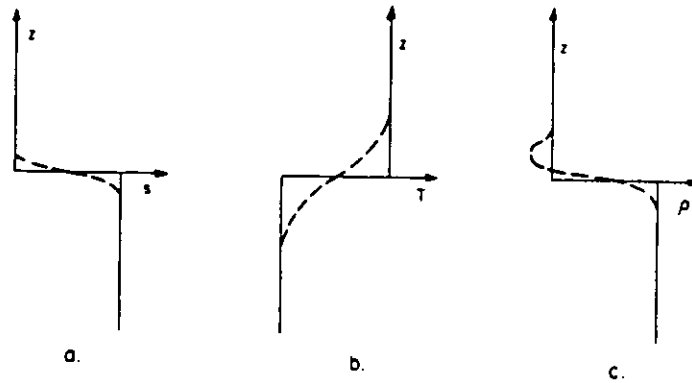


Figure 61. The distribution of a) salinity, b) temperature and c) the resultant density caused by the diffusion of a freshwater layer over a saltwater layer, with both layers at their respective freezing points. The size of the density inversion is exaggerated. (Martin and Kauffman 1974.)

One interesting aspect of the freezing of the freshwater layers that can form beneath multiyear ice floes is that the heat transfer rates are 5 to 10 times those calculated assuming that all heat transfer is by thermal diffusion (Martin and Kauffman 1974). What appears to happen is as follows. When the surface meltwater flows off the pack into the ocean, and ultimately beneath the ice, we have an ice layer at its melting point ($\approx 0^{\circ}\text{C}$) underlain by a nearly freshwater layer at its freezing point ($\approx 0^{\circ}\text{C}$), in turn underlain by seawater at its freezing point (-1.8°C). At the boundary between the fresh- and seawater a zone of water forms which, because of the rapid diffusion of heat relative to salt and the fact that the density of water with a salinity of <24.7 decreases on cooling, is both supercooled and less dense than the overlying water (Fig. 61). The resulting density distribution is unstable, with a Rayleigh number of 10^3 to 10^4 , and free convection results. When this supercooled water rises, it is nucleated by the overlying ice layer and forms a mesh of thin vertical interlocking ice crystals that ultimately grow down to the fresh water/seawater interface. At this time the presence of ice crystals throughout the complete thickness of the freshwater layer eliminates supercooling, constrains both temperature and salinity to lie on the freezing curve, and permits them to diffuse in the vertical direction until both quantities become horizontally uniform. The combination of these processes results in the lateral growth of the ice crystals, which continues until a horizontal ice sheet forms. Excellent photographs showing the growth of ice crystals during a laboratory simulation of this process can be found in Martin and Kauffman (1974).

Just what is the structure of multiyear ice? The only thing that can be said at present is that we don't know. As was discussed, we used to think that we did, that multiyear ice was a layer-cake of annual growth layers with a layer thickness roughly equaling the amount of summer ablation. As has been shown, this type of ice clearly exists. However, based on the limited samples (150 cores) collected by Schwarzscher in the Arctic Ocean from multiyear ice that appeared to be unde-

formed, only 25% of the ice actually was undeformed and only 2% showed annual layering throughout the complete thickness of the floe. These results should be coupled with the results obtained in the Weddell Sea by Gow et al. (1982) where 75% of the multiyear ice was frazil. It should also be noted (Meeks et al. 1974) that recrystallized ice has tentatively been identified in the low salinity, above-water-level portions of thick multiyear floes studied in the Beaufort Sea during the 1972 AIDJEX pilot experiment. Perhaps the multimaximum fabric reported by Savel'ev (1958, Fig. 5) from a hummock on a multiyear flow is from this type of ice (similar fabrics are produced by recrystallization in glacier ice). If this interpretation is correct, we will not be surprised, as we have believed for a long time that sea ice would probably recrystallize if the brine inclusions, which presumably lock in the substructure, were drained from the ice. This drainage, in fact, does occur in the upper part of thick multiyear floes.

When all the above information is combined, we frankly must admit that we do not know what to think. However, we do know what is needed: a program that systematically obtains cores from different regions of the Arctic and Antarctic pack ice and studies their structure. Such a program is not hard to accomplish, but it requires good logistic support.

In concluding this section it should be pointed out that understanding why the structurally different types of sea ice form and being able to estimate how much of each ice type will exist at different locations at different times of the year is not only of academic interest. It is also a problem of considerable applied importance as each of these different ice types has different physical properties. At the present time we at least know what the problem is. This alone should stimulate further work in this area.

This is a convenient place to also mention that although undeformed multiyear ice commonly has a steady-state thickness of between 2.5 and 5 m (Maykut and Untersteiner 1971) it appears to be possible to obtain undeformed multiyear sea ice with thicknesses of at least 12 m under present climatic conditions (Walker and Wadhams 1979). Examples of such thick ice would appear to be the floe upon which NP-6 was situated (10-12 m, Cherepanov 1964), a floe from Nansen Sound, Ellesmere Island, described by Serson (1972, 10 m thick), and the sea ice portions of the Koettlitz Glacier, McMurdo Sound, Antarctica (15 m, Gow and Epstein 1972) and the Ward Hunt Ice Shelf off Northern Ellesmere Island (20 m, Lyons et al. 1971). The formation of such thick ice requires rather special conditions in that the oceanic heat flux must be near zero and the annual snowfall must be sufficient to maintain a high surface albedo without allowing the accumulation of snow on the ice surface. Walker and Wadhams (1979) have calculated that under such conditions a thickness of 12 m would be reached in about 65 years, with a final equilibrium thickness of roughly 20 m requiring about 200 to 300 years.

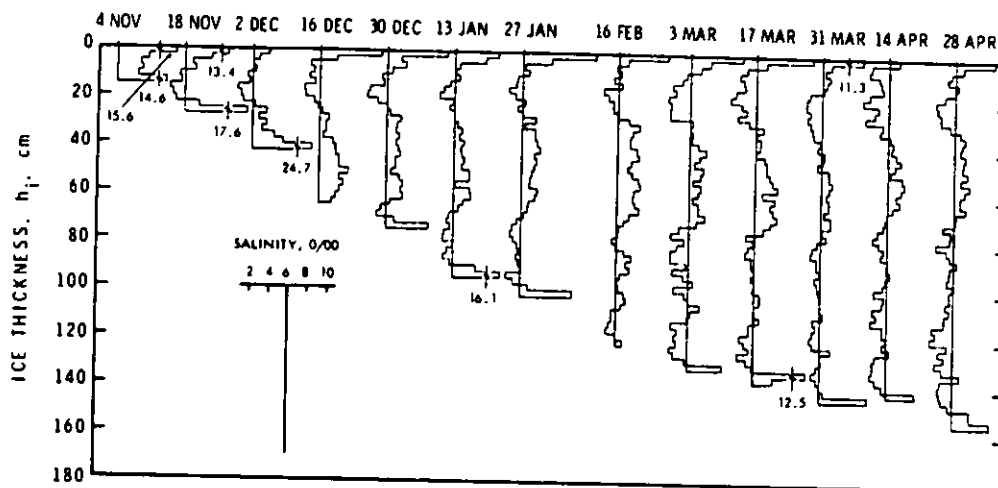


Figure 62. Salinity profiles of ice of Eclipse Sound at intervals of two weeks during the winter of 1977-78. Scale for salinity is shown in insert. Vertical solid lines represent a value of 6‰ and are given as reference (Nakawo and Sinha 1981).

THE SALINITY PROFILE

Observations

There are ice salinity data scattered through the sea ice literature. However, most of this information is very spotty - a profile here, a profile there. There are only a few exceptions where reasonably systematic salinity observations were made at a given site throughout the complete growth season. The best example of this type of study is by Nakawo and Sinha (1981), who obtained salinity profiles from a site in Eclipse Sound near Pond Inlet, Baffin Island, on a weekly basis from November 1977 to April 1978. The profiles are shown in Figure 62 (a two-week interval is used here for clarity). A plot of the variations in mean daily air temperature which can be consulted in the original reference shows values that were below -10°C for all but a very few days just after freeze-up and commonly were below -20°C . These profiles show characteristics that are similar to those of innumerable other profiles obtained from ice in the high Arctic. Note that there is initially a rapid decrease in the salinity at a given level in newly formed ice [see also Malmgren (1927) and Weeks and Lee (1958, 1962)]. After this initial rapid decrease, which appears to occur within a week after the ice forms, the salinity values attain quasi-stable values which then decrease very slowly throughout the growth season. In many ice sheets the uppermost layer of ice shows a higher salinity, as does the lowermost layer. This results in the profiles having a C-shaped appearance.

The other set of reasonably complete salinity measurements was obtained at Hopedale, Labrador, by Weeks and Lee (1958). The climate at Hopedale was very different than at Pond Inlet, with several thaw periods occurring when air temperatures went above -10°C and at times above freezing. The continuous, relatively rapid desalination that was observed (Fig. 63) even in December and January is presumably caused by

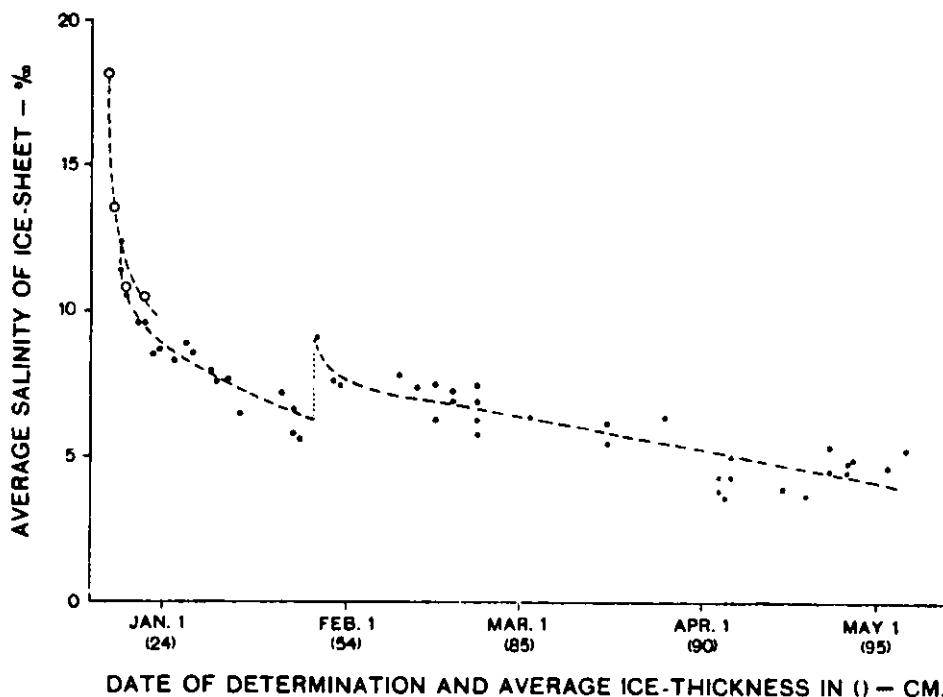


Figure 63. Average salinity of ice sheet at Hopedale, Labrador, plotted against ice thickness and date of measurement (Weeks and Lee 1958).

the higher air temperatures, which in turn produced higher ice temperatures, resulting in increased brine volumes and enhanced brine drainage. Nakawo and Sinha note that at Pond Inlet similar rapid desalination also occurred but not until May and June (data not shown in Fig. 62).

It should be remembered in examining salinity profiles that even in the most homogeneous-appearing ice there is a small-scale, apparently random variation in the salinity. In the only available study performed to date of such variations (Thule, Greenland), a standard deviation of $0.62^{\circ}/_{\infty}$ was obtained at a given depth level in ice that would seem to be completely uniform (Weeks and Lee, 1962).

Plots of the average ice salinity for the complete ice sheet versus ice sheet thickness have been prepared by Cox and Weeks (1974) for first-year sea ice using data from a wide variety of sources and locations. The results are rather surprising in that they are not only consistent but also show only a small amount of scatter (Fig. 64). Initially there is a rather rapid linear drop in the average salinity until an ice thickness of approximately 0.4 m is reached. At this and larger thicknesses the curve of average salinity versus ice thickness is also linear but with an appreciably decreased slope. Recent work by Gow et al. (1982) shows that the bulk salinity of Antarctic sea ice tends to be greater than that of sea ice of comparable age and thermal history in the Arctic.

When in the spring the upper surface of the ice starts to melt, there initially is a rapid decrease in the salinity of the above-sea-

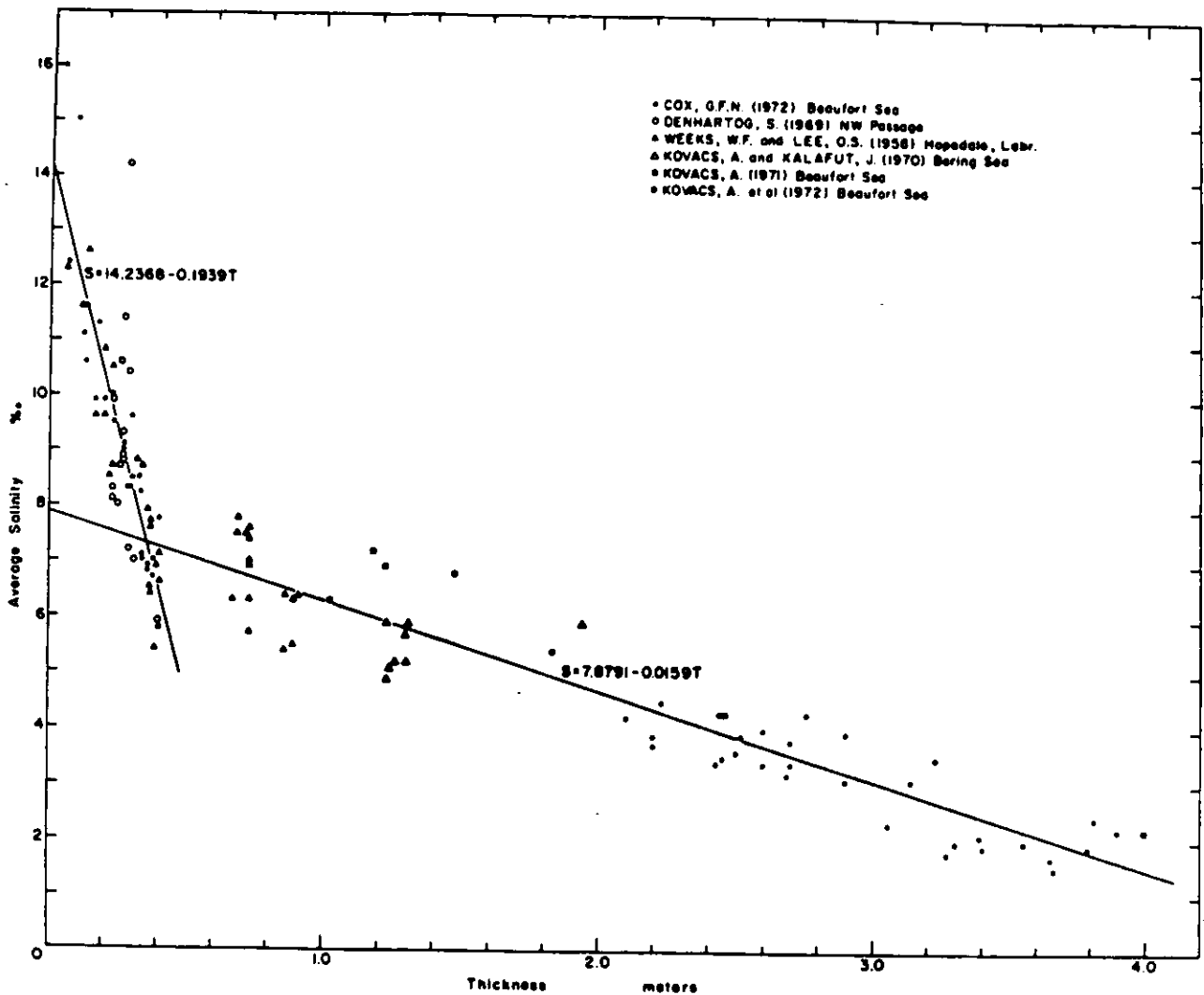


Figure 64. Average salinity of sea ice as a function of ice thickness for cold sea ice sampled during the growth season (Cox and Weeks 1974).

level portions of the ice. The best example of the final salinity profile for multiyear ice is by Schwarzacher (1959) based on 40 cores and 2060 salinity determinations (Fig. 65, curve C). In the more recent study by Cox and Weeks (1974) multiyear salinity data were separated into two classes depending upon whether the core was selected from a hummock (Fig. 65, curve A) or from a depression (curve B). Based on these data Schwarzacher's curve appears representative of hummocky ice or at least ice with a high freeboard. Note the significant amount of scatter in the measurements. The same is presumably true of Schwarzacher's data, although he only presented average values. Note the extremely low salinity of the near-surface ice from the hummocky areas. In many of the thicker floes that have been studied this ice is sufficiently pure that it can be melted and utilized for drinking water. The near-surface ice from the depressed areas (curve B) is more saline by 3 to 4‰. Some general feel for the lateral and vertical variations in ice salinity with changes in ice topography can be gained from Figure 66. Note the high salinities of the newly formed ice in the lower portion of the ice sheet and the great variability in the upper

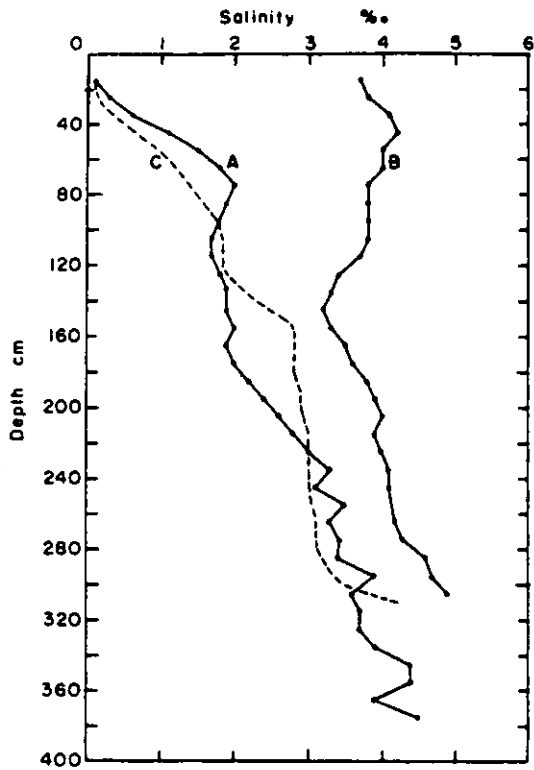


Figure 65. Average multiyear salinity profiles for hummocked (curve A) and depressed (curve B) areas. Curve C is the average multiyear salinity profile determined on Station Alpha by Schwarzacher (1959) (from Cox and Weeks 1975).

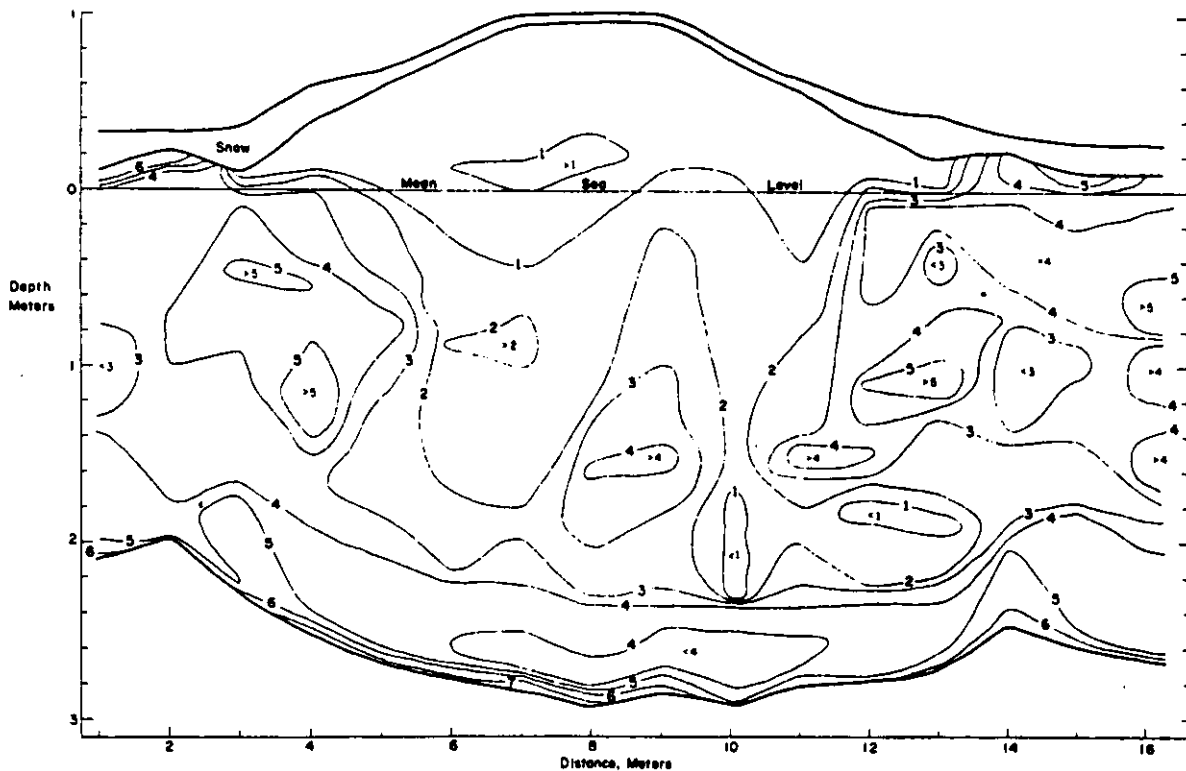


Figure 66. A cross section of an area of multiyear ice showing the variation of salinity with topography (Cox and Weeks 1975).

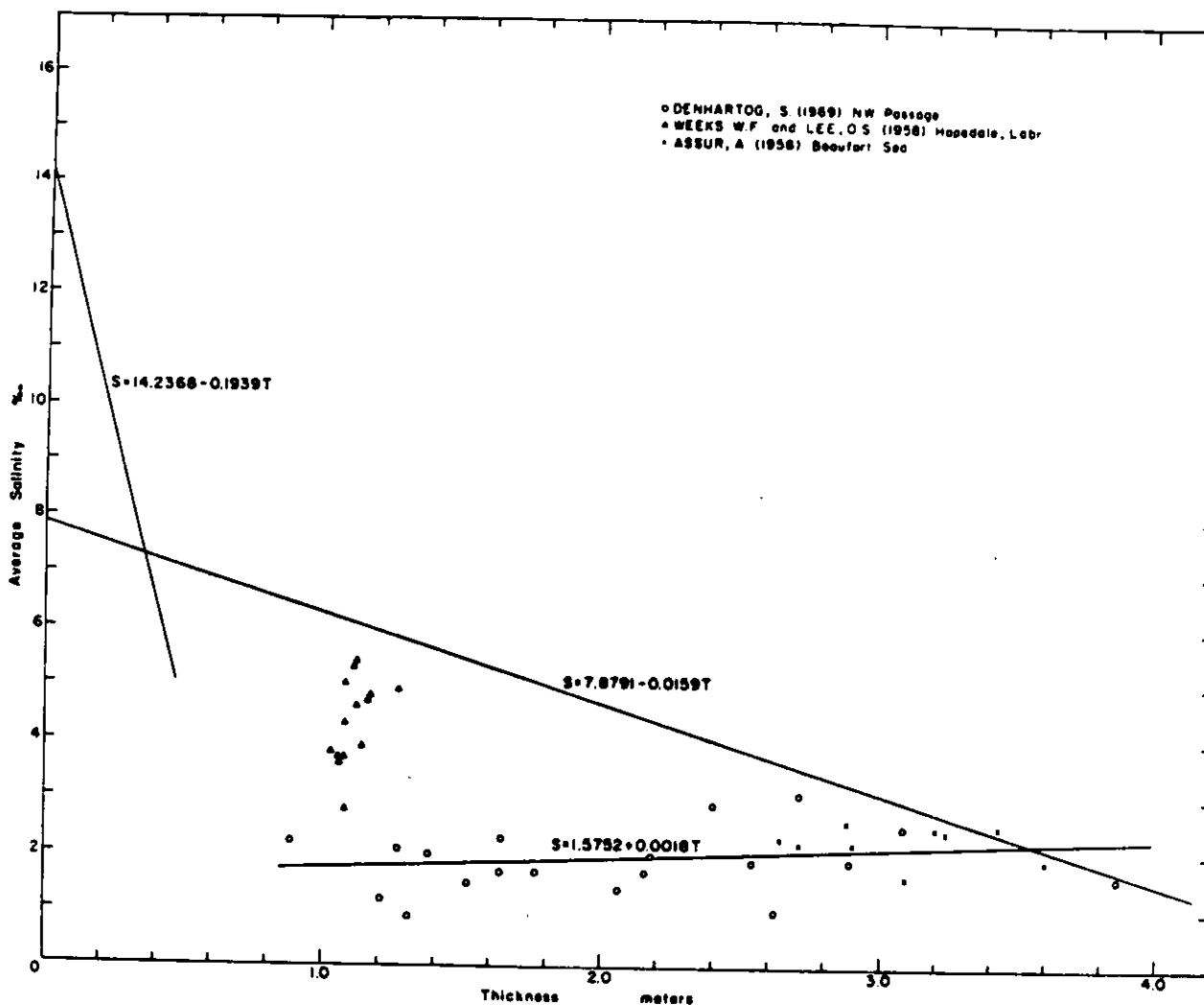


Figure 67. Average salinity of sea ice as a function of ice thickness for warm sea ice sampled during the end of the melt season (Cox and Weeks 1975).

portion of the profile. Figure 67 shows a plot of average salinity versus average ice thickness for multiyear ice. There is an appreciable amount of scatter and a very slight increase in mean salinity with increasing ice thickness.

There appear to be several factors that contribute in different degrees to determining the salinity profile that exists at any given time:

1. The initial amount of salt entrapped in the ice.
2. The migration of liquid inclusions through the ice crystals.
3. Brine expulsion or the squeezing of brine out of the ice as the result of differential volume changes in the different phases composing the sea ice.
4. Brine drainage.
5. Flushing.

We will now discuss each of these factors in turn.

Initial Salt Entrapment

The first step in unraveling the variations in the salinity profile of ice is to understand how much salt is initially entrapped in the ice as a function of growth conditions and structure. Surprisingly little work has been carried out on this subject. Fortunately, there has been considerable work on this general subject for other similar materials to serve as a guide to understanding the situation for sea ice.

Early studies focusing on the salt entrapment problem are those of Johnson (1943) and Adams et al. (1963). In some aspects these results were contradictory in that Johnson's results indicated that although there was a linear relation between the salinity of the ice S_i and the salinity of water S_w , changes in the growth velocity of the ice v did not appear to cause appreciable changes in the effective solute distribution coefficient $k \equiv S_i/S_w$. On the other hand, Adams and co-workers obtained experimental data indicating quite clearly that S_i was an approximately linear function of v . In an attempt to resolve these differences, Weeks and Lofgren (1967) and Cox and Weeks (1975) performed a number of experiments using NaCl ice as a model for related behavior in sea ice. These two sets of experiments were similar in purpose but quite different in technique. In the Weeks and Lofgren study, ice sheets up to 25 cm thick were formed during freezing runs that lasted between 48 and 110 hours. At the end of the run the ice was removed and cut into 1-cm-thick slices, and the salinity of each slice measured. Because the freezing runs were very short, brine drainage was neglected, which is, of course, a rather questionable assumption because of the rapid drop in salinity that usually occurs during initial ice growth. Water salinities were also calculated for each stage of ice growth by considering the amount of salt rejected from the ice. The values of k were then determined by combining the ice salinities with the water salinities that were appropriate for that ice level.

In the Cox and Weeks study the radioactive isotope ^{22}Na was used as a tracer and the salinity of both the ice and water was determined by sequentially measuring the gamma ray emission from different levels of the sample which, as in the previous experiment, was produced by unidirectional freezing. After considerable processing of the resulting data it was possible to obtain, via non-destructive observations, replicate salinity profiles that were in good agreement with more directly determined values. As these freezing runs took over 900 hours, it was no longer possible to neglect brine drainage. Therefore, only the salinities from the newly formed ice located just above the skeleton layer (that essentially no-strength layer at the bottom of a growing ice sheet where there are no lateral bonds between the ice platelets that compose each crystal) were used. It was assumed that the skeleton layer had a constant thickness of 3 cm.

In analyzing these results Weeks, Cox and Lofgren used the theory of Burton et al. (1953) which has been quite effective in treating experimental results in the field of metallurgy. They assumed that because of mixing the concentration C will approach a constant value of C_δ at some distance δ from the growing interface. For distances less than δ the velocity component normal to the interface approaches that due to crystal growth v . For a steady state at $x < \delta$, the continuity equation is

$$D \frac{d^2C}{dx^2} + v \frac{dC}{dx} = 0 \quad (22)$$

with the boundary conditions

$$(C_1 - C_s) v + D \frac{dC}{dx} = 0 \quad \text{at } x = 0 \quad (23)$$

where C_1 and C_s are the concentrations in the liquid at the interface ($x = 0$) and in the solid respectively and

$$C = C_2 \text{ at } x \geq \delta.$$

The solutions to eq 22 with these boundary conditions are given by

$$\frac{C - C_s}{C_2 - C_s} = \exp \left[\frac{v}{D} (\delta - x) \right] \quad (24)$$

and the concentration C_1 of the liquid at the interface is

$$\frac{C_1 - C_s}{C_2 - C_s} = \exp \left[\frac{\delta v}{D} \right]. \quad (25)$$

If δ is chosen properly this last equation can be forced to give the correct value of C_1 . Because $C_s/C_1 = k_0$, eq 25 can be rewritten as

$$k = \frac{k_0}{k_0 + (1 - k_0) \exp \left[-\frac{\delta v}{D} \right]}. \quad (26)$$

Here k_0 can be considered to be the value of k at $v = 0$ (provided that a cellular interface were to remain stable). Inasmuch as $k_0 < 1$ for salt-water systems eq 26 can be rearranged as

$$\ln \left(\frac{1}{k} - 1 \right) = \ln \left(\frac{1}{k_0} - 1 \right) - \frac{\delta v}{D} \quad (27)$$

which is a straight line on a plot of $\ln (1/k - 1)$ vs v with a slope of $-\delta/D$ and a zero intercept of $\ln (1/k_0 - 1)$. Figure 68 shows the resulting plot of Cox and Weeks' (1975) data. The data are quite linear with the exception of the values obtained at very low v values. Based on Lofgren and Weeks' observations, the drift toward higher $(1/k - 1)$ values in the low v range is undoubtedly related to changes in the morphology of the solid/liquid interface as conditions are approached where a planar interface becomes stable. Ignoring the values at low v , least-squares gives $k_0 = 0.26$ and $\delta/D = 7243$ s/cm. The results obtained by Lofgren and Weeks were similar but the value obtained for δ/D was lower (5090 s/cm). Figure 69 shows the later data set presented as a plot of k versus $[\delta v/D]$. Note that at higher growth velocities essentially all the salt in the solution is trapped in the ice.

How do these results compare with field observations? Figure 38 showed a plot of v as a function of depth in the ice against salinity S_1 . There is clearly a positive correlation between v and S_1 as predicted by the BPS theory. Replotting these results (Nakawo and Sinha 1981) as shown in Figure 70 clearly shows the linear relation suggested by the BPS theory. Presenting these results in a more direct manner by

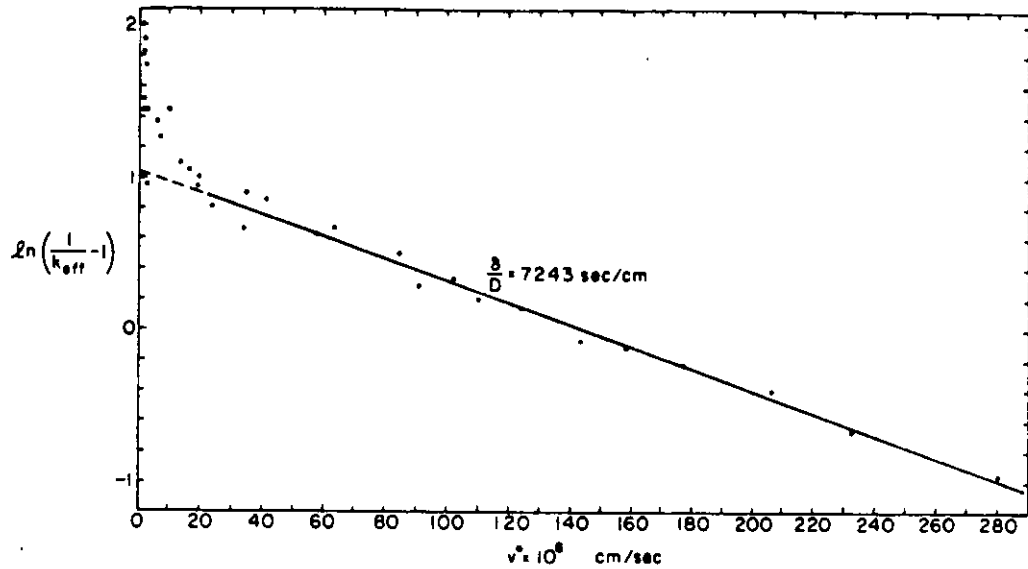


Figure 68. Plot of $\ln(1/k-1)$ versus v using the salinity entrapment data of Cox and Weeks (1975).

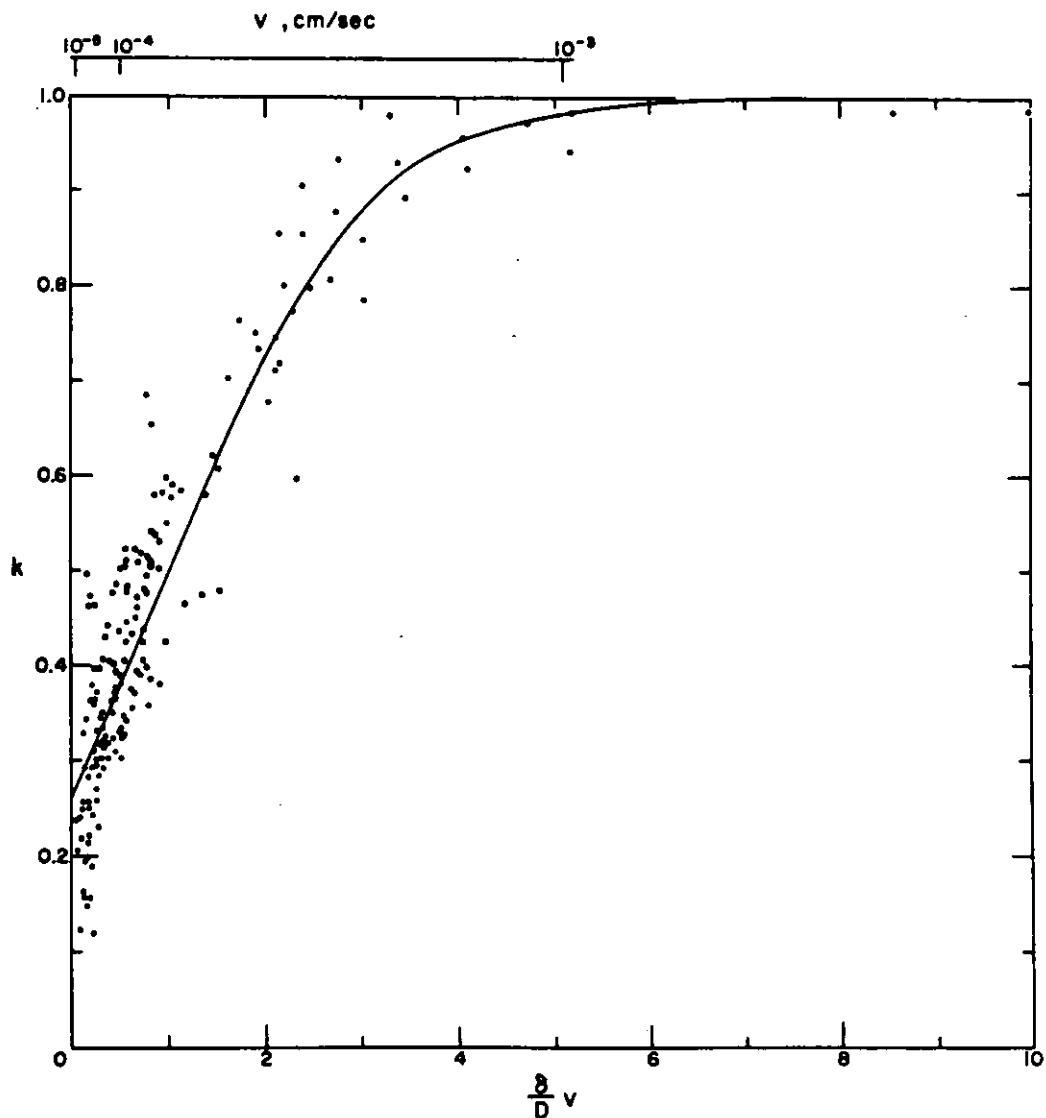


Figure 69. Plot of k versus $\delta v/D$ for the salinity entrapment data of Weeks and Lofgren (1967). The curve is a least-squares fit of eq 26.

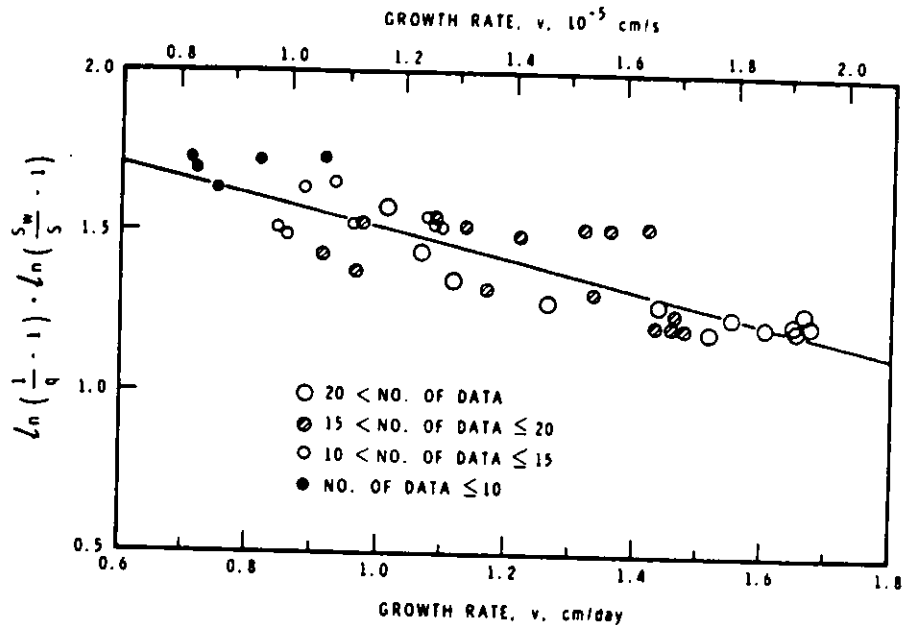


Figure 70. Plot of $\ln(1/k-1)$ versus v for columnar-grained sea ice from depths between 25 and 125 cm, Eclipse Sound, NWT. The solid line is a least-squares fit of eq 26. After Nakawo and Sinha (1981).

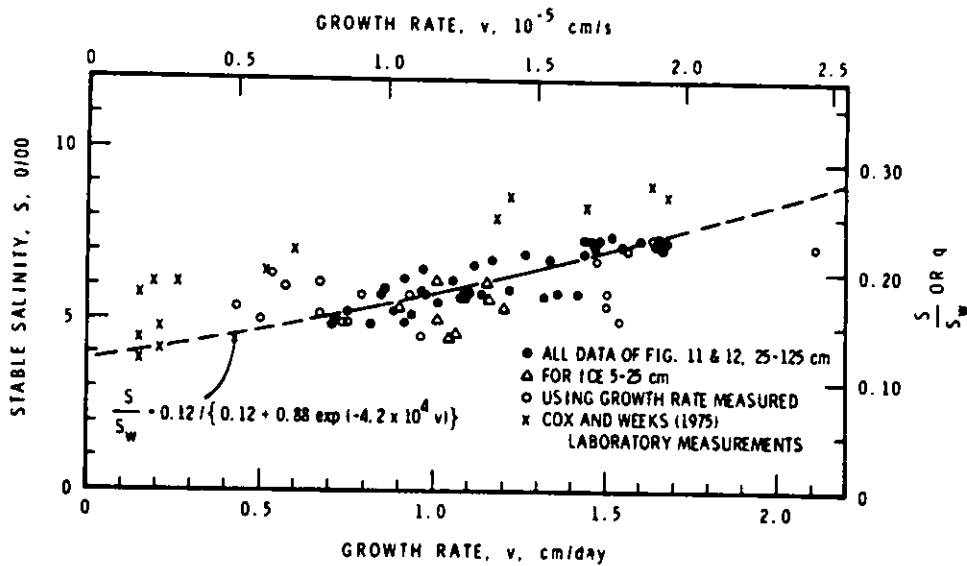


Figure 71. Stable salinity or k versus growth rate (Nakawo and Sinha 1981). The figure numbers refer to figures in the original paper.

plotting k versus v gives Figure 71. Here the ice between 5 and 25 cm consists of discontinuous columnar grains, with the length of the columns less than 1 cm. Below 25 cm the ice consists of long columnar grains. Note that there does not appear to be any appreciable difference between discontinuous columnar grains and continuous columnar grains. The BPS theory appears to work quite satisfactorily. Also shown in Fig. 71 are data points obtained by Cox and Weeks. These

latter observations consistently show more salt present in the ice, a not unexpected result inasmuch as they were determined by nondestructive testing and did not experience the brine drainage that commonly occurs during normal sampling procedures. Therefore, at the present time the best way to estimate the amount of salt initially entrapped in sea ice is to use the relation

$$S_i = S_w \left[\frac{k^*}{k^* + (1 - k^*) \exp \left(- \frac{\delta v}{D} \right)} \right] \quad (27)$$

with $k^* = 0.12$ and $\delta/D = 4.2 \times 10^4$ s/cm (Nakawo and Sinha 1981). Here we have replaced k_0 with k^* to distinguish it from the true equilibrium k_0 value.

Although it would appear that our knowledge of initial salt entrapment is in reasonable shape, there are some disturbing aspects. Although the BPS theory appears to work it is based on a series of assumptions that strictly apply only to impurities that are incorporated in solid-solution in the solid phase. In the sea ice case we are clearly dealing with bulk entrapment of the melt at a dendritic interface. There have been some attempts to analyze this situation (Edie and Kirwan 1973, Myerson and Kirwan 1977a,b, Ozüm and Kirwan 1976). In the last reference this approach was applied to the freezing of stirred NaCl-H₂O solutions with considerable success. It would be interesting to modify these relations in order to treat free convection as the mixing process and then apply this analysis to the case of sea ice.

Brine Drainage Mechanisms

Brine Pocket Migration

In the first published discussion of a possible mechanism of removing salt from sea ice, Whitman (1926) pointed out that a temperature gradient in the ice establishes a concentration gradient in a brine pocket if phase equilibrium is to be maintained. This, in turn, during the winter causes the diffusion of solute from the cold, saline upper end of the brine pocket to the warmer, less saline lower end of the pocket. Associated with this diffusion, the ice at the warm end of the pocket dissolves while freezing occurs at the cold end, resulting in the migration of the brine pocket toward the warm side of the ice.

Since this early paper the phenomenon of liquid inclusions or liquid zones migrating through solid crystals has received considerable attention in the crystal growth and crystal purification literature (Wernick 1956, Pfann 1958, Tiller 1963) where it is referred to as temperature gradient zone melting (TGZM).

The theory is as follows. Because for salt-water systems the equilibrium value of k is very small, for the migration of a small inclusion such as a brine pocket effectively all the salts can be considered to be excluded from the ice phase. Therefore J , the flux of solute at the freezing interface of a brine pocket, is

$$J = C_v (1-k) = C_v. \quad (28)$$

For the steady state, eq 28 can be written in terms of the concentration gradient dC/dx as

$$Cv = -D \frac{dC}{dx} \quad (29)$$

where D is the diffusion coefficient of the salt (or salts) in water. Then substituting

$$\frac{dC}{dx} = \frac{dC}{d\theta} \cdot \frac{d\theta}{dx} \quad (30)$$

where θ = temperature and $(dC/d\theta)$ is specified by the phase diagram, it follows that

$$v = -\frac{D}{C} \left[\frac{dC}{d\theta} \cdot \frac{d\theta}{dx} \right]. \quad (31)$$

Here D , C , $dC/d\theta$ and v are all dependent on the temperature θ . In eq 31 the appropriate temperature gradient is the gradient in the liquid G_ℓ .

For a spherical droplet a solution of Laplace's equation provides a relation between G_ℓ and the temperature gradient in the solid G_s which is specified

$$\frac{G_\ell}{G_s} = \frac{3\kappa_s}{(2\kappa_s + \kappa_\ell)}. \quad (32)$$

Here κ indicates the thermal conductivity. As κ_{ice} is approximately 4 times κ_{brine} , the gradient ratio is fairly insensitive to small changes in κ_{brine} caused by variations in the brine composition. Also, as the values of κ change slowly with temperature, the G_ℓ/G_s ratio is roughly constant. Substituting appropriate thermal conductivity values Seidensticker (1965) obtained $G_\ell = 1.34 G_s$. Making an additional correction caused by the density (ρ) differences between the ice and the brine Seidensticker finally obtained

$$v = \left(\frac{d}{mC} \right) \left(\frac{2\kappa_s}{(2\kappa_s + \kappa_\ell)} \right) \left(\frac{\rho_\ell}{\rho_s} \right) = 1.46 \frac{D}{mC} \quad (33)$$

as the equation giving the velocity of migration in a unit thermal gradient. In eq 33 $m = d\theta/dC$ and is the slope of the liquidus curve from the phase diagram (note that the units of C do not matter as long as m and C are in compatible units).

How do the predictions of eq 33 agree with observed brine pocket migration rates? There have been a number of studies of the migration of brine inclusions through ice crystals (Kingery and Goodnow 1963, Hoekstra et al. 1965, Harrison 1965, Jones 1973, 1974). That the theory and observations are in reasonable agreement is shown by Figures 72 and 73. Figure 72 shows the relation between migration velocity and ice temperature at a constant temperature gradient of $1^\circ\text{C}/\text{cm}$ in the ice. The general shapes of the curves are in good agreement although the theory predicts velocities that are $\approx 20\%$ higher than observed. That v is a linear function of G_s , the temperature gradient in the ice, is clearly shown in Figure 73. Analysis of the experimental data shows that the rate of droplet migration is, indeed, almost completely con-

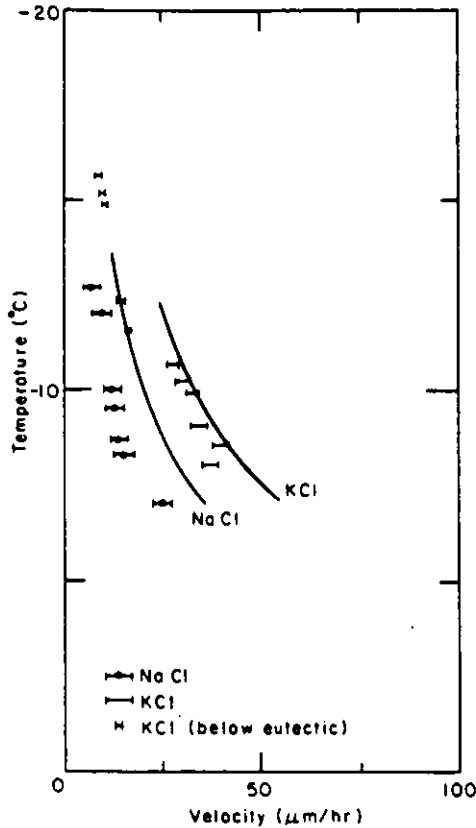


Figure 72. Relation between brine pocket migration velocity and ice temperature at a constant temperature gradient of $1^{\circ}\text{C}/\text{cm}$. The curves are calculated using eq 33. (Hoekstra et al. 1965, Seidensticker 1965.)

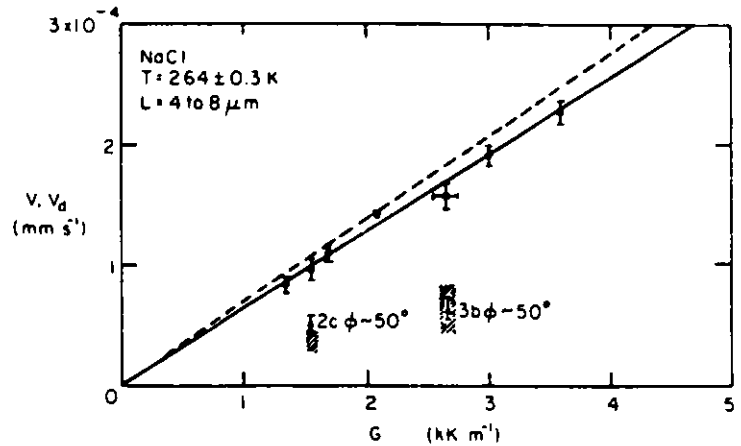


Figure 73. Relation between the temperature gradient in the ice and the brine pocket migration rate (Jones 1973). Each brace marked with a solid circle gives the mean and mean deviation of the velocities of about 10 separate droplets; the braces marked by solid triangles comprise rather smaller samples. The dashed line indicates, to an accuracy of $\pm 10\%$, the maximum (diffusion-limited) values of V determined from calculated values of D . The cross-hatched areas give values of $V \cos^2 \phi$ for those droplets migrating diagonally.

trolled by the rate of transport of solute through the liquid. At the present time the results suggest that in some, if not all, of the cases studied droplet migration depends on the presence of crystal defects (presumably screw dislocations) in the solid ahead of the high temperature interface (Jones 1973).

The obvious problem with brine pocket migration as an effective contributor to desalination is the fact that brine pockets appear to migrate extremely slowly. In fact Untersteiner (1968) has calculated that, if representative values for the temperature distribution in multiyear ice are used, a brine pocket between 10 and 20 cm below the ice surface would migrate 2 cm downward between August and April and then between May and July experience an essentially equal migration upward for a net year's travel of near zero. As an example of an extreme case of brine pocket migration consider a 30°C temperature difference across a 1-m-thick piece of first-year ice giving a temperature gradient of $0.3^{\circ}\text{C}/\text{m}$. If the temperature at the brine pocket location is -6°C , eq 33 gives a migration velocity of $14.0 \mu\text{m}/\text{hr}$, which corresponds to almost exactly 1 cm migration per month.

In closing this discussion, we note that the brine pockets that have been studied have all been very small (4 to 80 μm). In inclusions this small there is little chance for convective motions to occur in the brine. In much larger inclusions, with diameters on the order of 1 mm, convection becomes possible, and the transfer of solute in the inclusion is much more efficient, with effective "diffusion" coefficients of 10^{-3} as opposed to 10^{-6} for pure diffusion. Migration rates should be accordingly enhanced. It should also be noted that the convection will only occur when the temperature increases downward (during the winter). During the summer, when the temperature gradient is reversed, the salt is produced at the bottom of the brine pocket, resulting in a stable density distribution in the liquid. It would be interesting to see this problem explored further.

Brine Expulsion

In his studies of sea ice Bennington (1963a) noted that when the ice was cooled, a pressure buildup occurred in the brine pockets where the liquid portion of the inclusion had separated from the vapor bubble. At times this pressure becomes sufficient to cause the surrounding ice to fail along the basal plane, allowing brine to escape and migrate toward the warm side of the ice sheet. This process is called brine expulsion, and its contribution to the overall removal of brine from sea ice has been explored by Untersteiner (1968) and by Cox and Weeks (1975). Untersteiner has used a simple model which gives S , the decrease in the bulk ice salinity, from its initial value of S_0 when the temperature drops from θ_0 to θ , as

$$S = S_0 (\theta_0 / \theta)^{\Delta\rho / 1 - \Delta\rho} \quad (34)$$

where $\Delta\rho = 0.1$ is the difference in density between water and ice. This relation only holds while the temperature is continuously dropping from θ_0 to θ . Therefore the salinity of the ice at any time $t > 0$ depends on the initial salinity of the sample and on all subsequent periods of cooling that the ice has undergone in its history. Equation 33 is then applied to estimating the salinity profile of a multiyear floe. The resulting salinity values indicate that the near-surface ice should have a salinity of a few tenths of a part per thousand (as observed), and that below the near-surface ice the salinity profile in all but the lowest part of the ice is very slightly concave upwards (which is not observed).

Cox and Weeks develop a more complex model and utilize it via the application of a finite difference scheme to calculate the change in salinity that should occur in first-year ice. A portion of the results are shown in Figure 74, where the solid curves give the initial and final experimental salinity profiles and the broken curves were calculated from the model. From this, combined with a number of other comparisons, it was concluded that brine expulsion plays only a small role in the desalination of first-year ice. However, the change in salinity is significant and cannot be neglected. This is especially true during periods of rapid ice growth when the rate of change of temperature at each level in the ice sheet is high. In a way it is unfortunate that brine expulsion is not the dominant desalination mechanism as it is independent of the ice permeability in that the volume changes rupture the

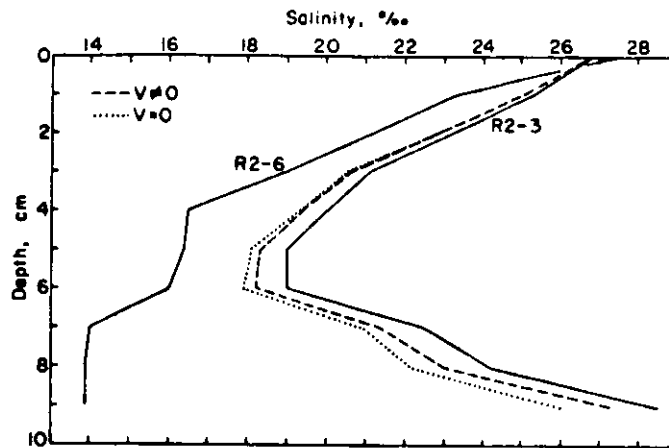


Figure 74. Comparison between experimental salinity curves and theoretical salinity curves determined from a brine expulsion model. R2-3 and R2-6 are the initial and final observed curves. The other curves were calculated. The dashed curve considers the effect of brine velocity; the dotted curve does not (Cox and Weeks 1975).

ice, allowing the brine to migrate (no permeability is required as the process makes its own). Therefore a detailed knowledge of the brine pocket and brine channel structure is not required. Photomicrographs showing the effects of brine expulsion in multiyear ice can be examined in Knight (1962c).

Gravity Drainage

If brine pocket migration and brine expulsion are not sufficiently vigorous processes to explain the observed changes in the salinity profiles of growing sea ice then gravity drainage must be the culprit (unless there is something "undiscovered" taking place). Here by gravity drainage we refer to all processes where brine, under the influence of gravity, drains out of the ice sheet into the underlying seawater. As an ice sheet grows, its surface gradually rises higher above sea level to maintain isostatic equilibrium. This in turn produces a pressure head in the interconnected brine system, driving the underlying brine out of the ice (Eide and Martin 1975). In addition, because the density of the brine in equilibrium with ice is determined by the temperature distribution, during the period of time when the temperature within the ice increases downward an unstable vertical density distribution exists within the brine channels in an ice sheet. This should produce a convective overturn of the brine within the ice as well as an exchange between the denser brine within the ice and the underlying seawater. In such a process the rate of brine drainage should be a function of the temperature gradient in the ice, which determines the brine density gradient and the brine volume, which is presumably related to the permeability. Whether or not this is true in an ice sheet was examined by Cox and Weeks (1975). Figures 75 and 76 indicate that as either the brine volume or the temperature gradient in the ice sheet increases, the rate of change of salinity also increases. In fact gravity drainage

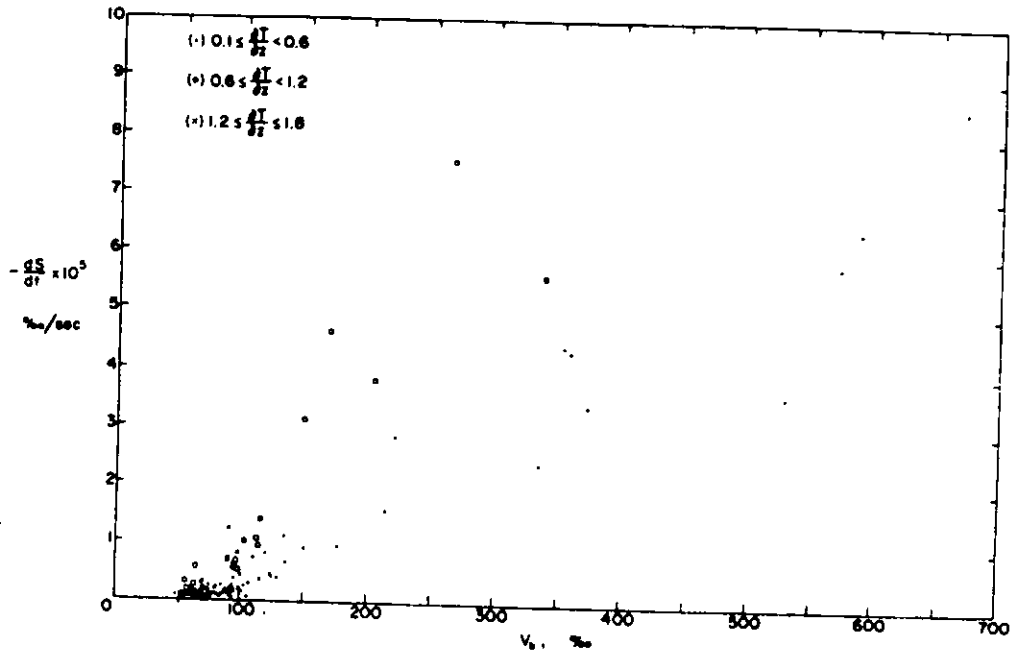


Figure 75. Plot of rate of change of salinity due to gravity drainage ds/dt versus brine volume for different temperature gradients $\partial t/\partial z$ ($^{\circ}\text{C}/\text{m}$) (after Cox and Weeks 1975).

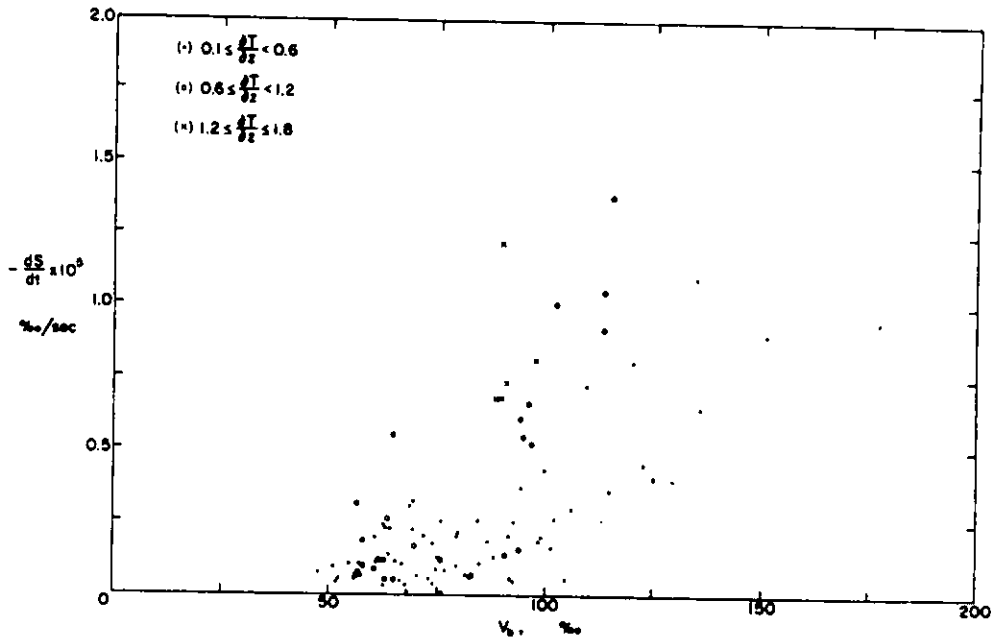


Figure 76. Plot of rate of change of salinity ds/dt due to gravity drainage against brine volume (at low brine volumes) for different temperature gradients $\partial t/\partial z$ ($^{\circ}\text{C}/\text{m}$) (after Cox and Weeks 1975).

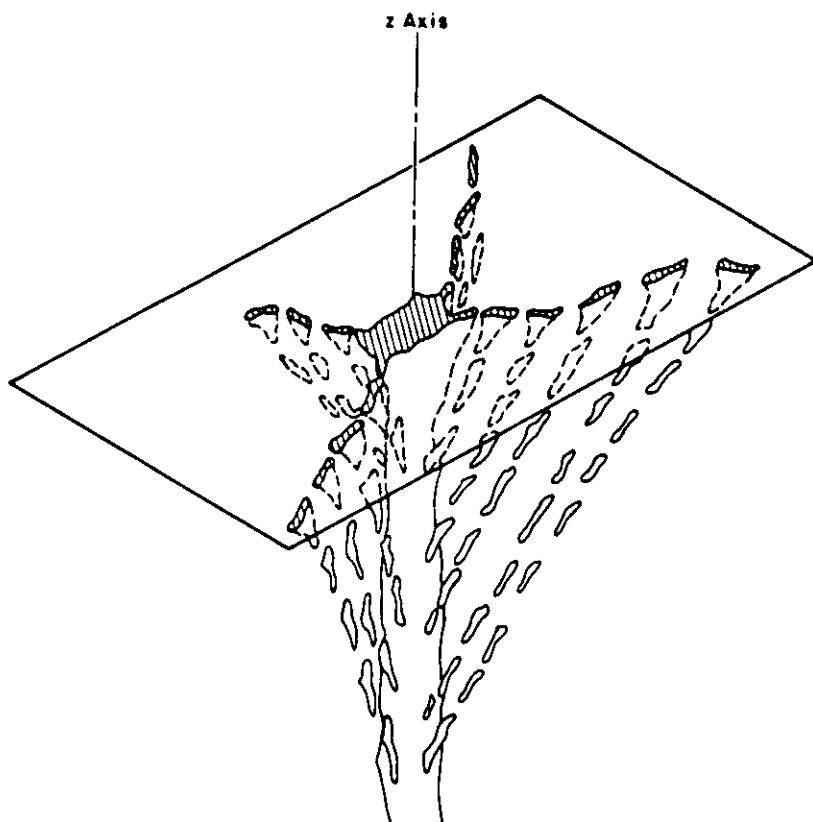


Figure 77. Schematic drawing of a cut through a brine drainage channel (Lake and Lewis 1970).

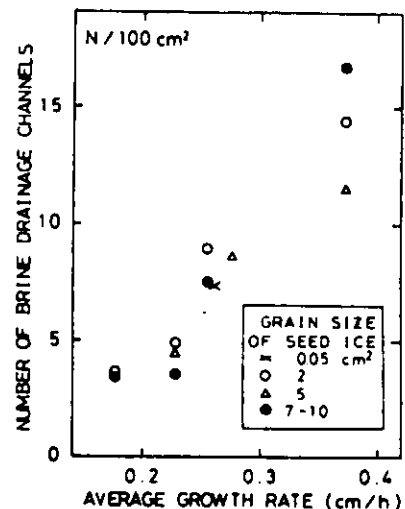


Figure 78. Number of brine drainage channels developed in thin ice sheets versus the average growth rate (Saito and Ono 1980).

does appear to be the dominant mechanism for removing salt from growing sea ice.

The fact that gravity drainage is the dominant mechanism is not surprising. That this is the case was suggested by Kingery and Goodnow in 1963, although in 1968 Untersteiner still remained skeptical that gravity drainage was important in ice thicker than a few tens of centimeters. What is surprising is how gravity drainage works. Although it might be reasonable to expect that gravity drainage would be a process that occurs in a uniform manner at any given level in the ice sheet, this clearly does not appear to be the case. Knight (1962b) and Lake and Lewis (1970) first noted that in natural sea ice large vertical tubular brine drainage structures are attended by smaller tributary tubes, much as in a vertically oriented, radially symmetric river system. Figure 77 shows a schematic drawing of such a brine drainage tube (Lake and Lewis 1970). Representative diameters of the tubes at the bottom of a 1.55-m-thick ice sheet were 0.4 cm, and there was one large channel every 180 cm². In a given horizontal plane the large channels show a starburst pattern, with the arms of the star generally following the crystal boundaries. In thick ice (<10 cm) it has been found (Saito and Ono 1980) that the number of brine drainage channels is related to the average growth rate (Fig. 78) but not to the average grain size. Even at the lowest growth velocities studied there were three channels per 100 cm² or 33 cm² per channel as compared to the 180 cm² per channel

noted in thicker ice by Lake and Lewis. Presumably, some of the channels in the thin ice merge in the same manner as river systems join as the ice thickens.

The nature of brine drainage channels has been investigated in a series of papers by Martin and his coworkers (Dayton and Martin 1971, Martin 1974, Eide and Martin 1975, Niedrauer and Martin 1979). The flow from the channels is oscillatory, with the duration of the downward flow being typically shorter than the duration of the upward flow. Oscillatory periods of approximately 1 hour have been described, with an 8- to 15-minute inflow followed by a 45-minute outflow (Eide and Martin 1975). Dayton and Martin (1971) have described the drainage of brine from such channels at a rate of approximately 1 liter/minute. They have also noted channel diameters of the order of 10 cm although most channels appear to have diameters ranging between 0.1 and 1.0 cm.

When the cold, saline brine streamers leave the base of the ice sheet, hollow tubes of ice form around them. These ice stalactites (Paige 1970) can be very large. Dayton and Martin (1971) present excellent photographs of such features and note stalactite lengths of 1.5 to 6.0 m (lengths of 20 to 50 cm are probably more representative). Once the ice tube is formed around the brine streamer, the horizontal transfer of heat between the brine and the surrounding seawater occurs through the ice wall. However, lateral transfer of salt cannot occur. Immediately after a tube forms, the "relatively" warm brine is in contact with the inner ice wall. For phase equilibrium to be maintained, this brine must be both cooled and diluted back to the composition specified by the eutectic curve. This is accomplished by melting the inner tube wall, with the heat of melting coming from ice accretion on the outer wall. Therefore, the stalactite both accretes on the outside and ablates on the inside while at the same time lengthening.

A similar enlargement appears to take place in brine channels within the ice sheet. Let a flow of cold, dense brine occur through a brine channel from the upper (cold) part of the ice to the lower (warm) part. To warm the cold brine there is a lateral flow of heat (through the ice) to the brine channel. As in the stalactite the brine warms above its equilibrium temperature. To reestablish equilibrium the channel wall melts, cooling the ice and diluting the brine. Therefore, the results of pumping brine down through the ice are both the cooling of the adjacent ice and an increase in the diameter of the brine channel (Martin 1974).

Because the seawater beneath growing sea ice is at its freezing point, there is an important difference between brine drainage channels and river systems. A river system usually continuously widens as its mouth is approached. Brine channels, on the other hand, neck just above the ice/water interface (a similar neck also occurs at the tips of growing stalactites; Eide and Martin 1975). Two factors appear to determine this necking. Not only is the seawater below the ice sheet at its freezing point, but it is also less dense than the brine flowing from the ice. This density difference $\Delta\rho$ creates a buoyancy force $\Delta\rho g$ which acts upward and opposes the pressure gradient force F_p , which drives the brine out of the ice. The value of F_p can be calculated (Martin 1974) by assuming that the volume flux q in the neck is imposed on the

neck by the nature of the upper portion of the drainage channel and that the flow through the neck is Poisseuille flow. Then

$$F_p = \frac{8\rho_b v_b q}{\pi a^4} \quad (35)$$

where a is the radius of the neck. For a sufficiently small value of a , $F_p > \Delta\rho g$, causing brine to flow out of the neck. For a larger neck radius $F_p < \Delta\rho g$, and buoyant seawater intrudes into the neck. When this occurs, because the seawater is at the freezing point and the ice is colder than the water, ice forms on the side of the neck, reducing the value of a . The ratio of these two forces E , which is referred to as the "entrainment number," is given by

$$E = \frac{\pi \Delta\rho g a^4}{8 \rho_b v_b q} = \frac{\text{buoyancy force}}{\text{pressure gradient force}} \quad (36)$$

For stalactite tips the tip radius is nearly predicted by $E = 1$ (Martin 1974). The sequence of adjustments in the tip radius is as follows. First, the brine flows uniformly out of the tip, causing the tip radius a to increase so that $E > 1$. The flow then decreases and seawater intrudes into the neck, freezing to the walls and reducing the radius back to the subcritical value ($E < 1$), at which time the whole process starts anew.

For very slow ($q \rightarrow 0$) flows salt diffusion is important and the above criterion is not valid. In this situation Lake and Lewis (1970) have argued that a Rayleigh number criterion

$$\frac{g \frac{1}{\rho} \frac{\partial \rho}{\partial x} a^4}{D\mu} = 68 \quad (37)$$

(where $\partial\rho/\partial z$ is the density gradient inside the tube caused by the temperature field in the ice, μ is the viscosity, and D is the salt diffusivity) determines the minimum tube radius. Substituting appropriate values into eq 37 we obtain $a = 0.3$ mm, which is of the observed order, indicating that in the limit of $q = 0$ the channels will remain open.

The reason that oscillations occur is that the brine level inside the ice oscillates between two positions of hydrostatic equilibrium. When cold, dense, saline brine from the upper levels of the ice fills the drainage channel the equilibrium brine level is lower than when warmer, less saline seawater fills the channel. When the tip radius has increased until $E > 1$ then any small mass perturbation in the stalactite results in a large pressure imbalance in the brine drainage tube, which accelerates seawater up the tube until the second higher equilibrium level is reached. At the same time, ice growth associated with the influx of seawater is decreasing a , causing $E < 1$. In addition, the seawater is being cooled to a brine and the process starts over again. The important factor in governing the oscillations would appear to be the geometry of the brine channels (Martin 1974).

In conclusion, although this has not been investigated, it would appear that the brine drainage channel - stalactite combinations, in addition to providing an efficient mechanism for removing brine that is within the channel, also facilitate desalination by three other mechanisms:

1. The increase in the diameter of the brine channel both entrains brine pockets and reduces the viscous drag on the downward-flowing brine.
2. The pressure drop associated with the formation of the stalactites facilitates the drainage of brine into the channel.
3. The cooling of the ice surrounding the channel causes the expulsion of brine into the channel (Martin 1972).

There are many aspects of brine drainage that have not been explored at all. In particular, we refer to the effects of the formation of ice in the brine drainage system and the effective permeability of such systems. We would expect that features similar to brine drainage tubes develop during the solidification of other materials.

Flushing

Although flushing is actually a particular type of gravity drainage, it is considered separately in that the pressure head necessary to overcome capillary retention is provided by the hydrostatic head resulting from surface meltwater. Therefore, flushing can only occur in the spring and summer when surface melt is possible. The other requirement for flushing is that the ice be permeable. The presence of significant amounts of surface meltwater also suggests that the ice is either at or near the pressure melting point. Such near-melting ice temperatures result in very high brine volumes for a given salinity, and high brine volumes generally correlate with large permeabilities.

It is generally believed that flushing is the most effective mechanism for desalination. The reason for this belief is the fact that the time when flushing starts corresponds to the time during the spring and early summer when major changes occur in the salinity of sea ice. It is also reasonable to believe that the continual percolation of fresh water down and through sea ice should result in significant decreases in the salinity. Considering its probable importance as well as the fact that flushing is undoubtedly similar to (and probably simpler than) processes that have been extensively studied in soils and other permeable materials it is surprising that the only discussion of flushing is by Untersteiner (1968).

In this study, it is assumed that a steady-state salinity profile will be achieved when the downward flux of salt F_g is balanced by the upward flux $\omega \cdot s$. Here ω is the velocity of upward ice displacement (in the Arctic Ocean $\omega = 30$ cm/yr) and s is the ice salinity in g/cm^3 . To specify F_g it is assumed that $\partial F_g / \partial z$ is a function f of the largest brine volume v_m attained during the period when melt is occurring at the upper surface of the ice floe. Letting $+z$ be the vertical axis (positive downward) the steady-state case is given by

$$\frac{\partial s}{\partial t} = -\omega \left(\frac{\partial s}{\partial z} \right) + f(v_m) \equiv 0. \quad (38)$$

Then, following Assur (1958), by letting $v_m = c(s/\theta_m)$ where $c = \text{constant} \approx -55$ and θ_m and v_m are the highest temperature and highest brine volume attained during the year, Untersteiner obtains

$$\omega \frac{\partial s}{\partial z} = f\left(c \frac{s}{\theta_m}\right). \quad (39)$$

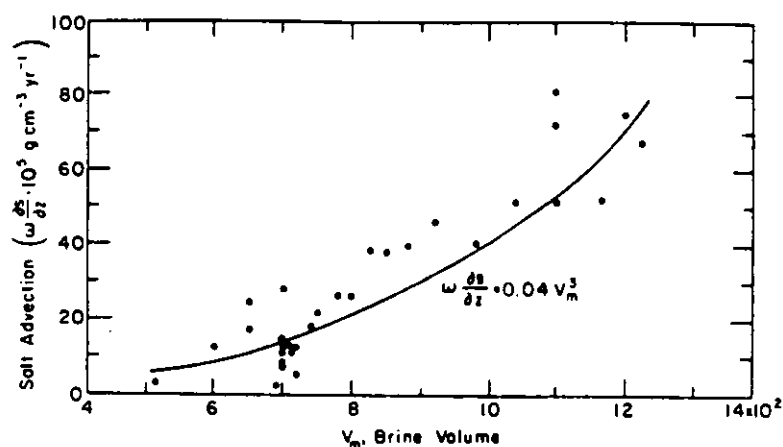


Figure 79. Relationship of maximum brine volume and salt advection required to maintain the steady-state salinity profile shown as curve C in Figure 65 (Untersteiner 1968).

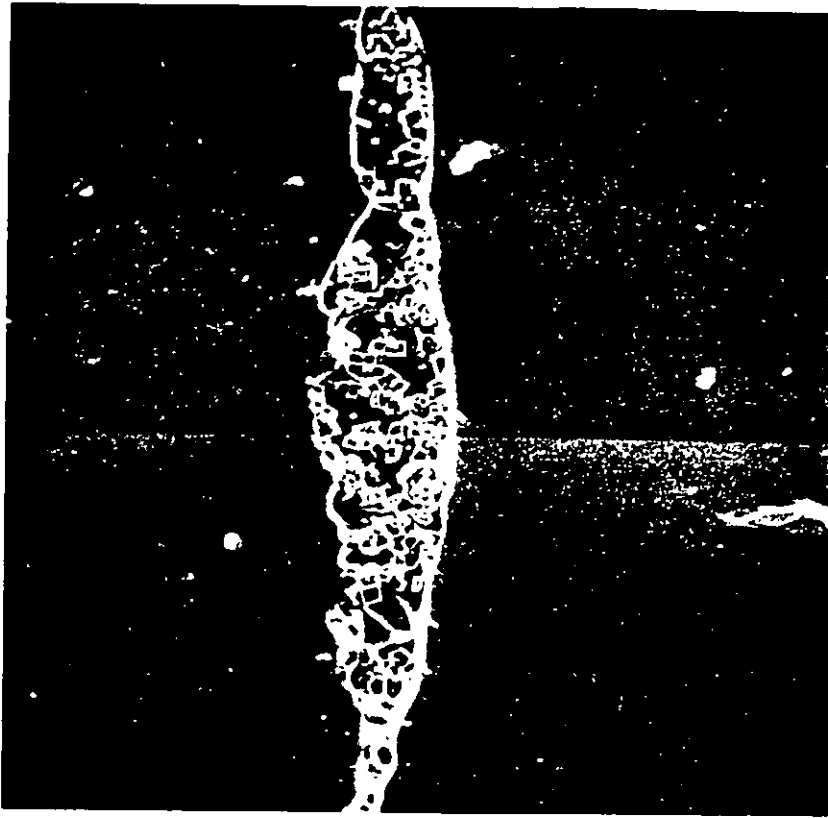
Untersteiner then presents field data obtained on drifting station Alpha showing vertical profiles of v_m and (ds/dz) . Both relations are similar, supporting the suggestion that the greatest salt loss occurs at the level where v_m reaches its highest value. Based on the observed salinity profile, the values of salt advection necessary to maintain the profile are then calculated and plotted against v_m (Fig. 79). Based on this plot, it is assumed that $F_s = 0$ at $v_m = 0.05$ (5%). The steady-state case then becomes

$$\omega \left(\frac{ds}{dz} \right) \equiv \omega \left(\frac{ds}{dz} \right) \equiv \frac{ds}{dt} = 0.04 v_m^3 \quad (40)$$

a relation that can be used to recalculate the salinity profile. The resulting salinity profile shows a very reasonable agreement with the observed salinity profile for multiyear ice (see Untersteiner, 1968, Fig. 1). However, as was also pointed out by Untersteiner, this apparent agreement between "theory" and observation is probably misleading in that the reasoning is somewhat circular: first a salinity profile characteristic of multiyear sea ice was selected, then a relation was selected between $(\partial s/\partial t)$ and v_m that would maintain the steady-state salinity profile. This relation (eq 40) then allowed the recalculation of the original salinity profile. Although encouraging, the agreement can hardly be considered proof that the multiyear salinity profile is the result of flushing. However, flushing certainly does appear to be the most likely (and almost the only) candidate.

Solid Salt Crystals

There is only one paper that examines the nature of the solid salt crystals in sea ice (Sinha 1977). In this work a microtoming and replicating technique was used to examine the nature of the brine pockets and the precipitation pattern of the salt crystals at low temperatures (-30°C , which is below the crystallization temperature of $\text{CaCO}_3 \cdot 6\text{H}_2\text{O}$, $\text{Na}_2\text{SO}_4 \cdot 10\text{H}_2\text{O}$, $\text{MgCl}_2 \cdot 8\text{H}_2\text{O}$ and $\text{NaCl} \cdot 2\text{H}_2\text{O}$). Figure 80 shows vertical scanning electron micrographs of a brine pocket. Although the individual crystals were not positively identified the majority of the crystals are undoubtedly $\text{NaCl} \cdot 2\text{H}_2\text{O}$. Note the random distribution of the



a. 140X magnification.



b. 800X magnification.

Figure 80. Scanning electron micrographs of a vertical section of brine pocket at -30°C , second replica (Sinha 1977).

salt crystals. Most crystals appear to be loosely packed in the cavities and can be removed either by preparing successive replicates or by washing the microtomed surface with kerosene before the replicates are prepared.

Some brine pocket replicates were also made at -10°C , a temperature at which only $\text{Na}_2\text{SO}_4 \cdot 10\text{H}_2\text{O}$ should be present in the ice in appreciable quantities. In this case the walls of the pockets were quite smooth and it appears that many of the salt crystals remained in the liquid brine. If this is the case it is difficult to see how the presence of $\text{Na}_2\text{SO}_4 \cdot 10\text{H}_2\text{O}$ could have a significant effect on the strength of sea ice as suggested by Peyton (1966).

Clearly more work using these or related techniques to examine the solid salt crystals is needed. It certainly would also be useful to positively identify the different crystals that are observed.

RELATIONSHIPS BETWEEN SEA ICE STRUCTURE AND PROPERTIES

In the above we have discussed a number of aspects of our current understanding of the internal structure of sea ice. We will now review selected examples of how the physical properties of sea ice are affected by changes in its internal structure. Here we will start with the mechanical properties, then discuss the thermal properties, and finally treat our limited understanding of the electromagnetic properties of sea ice. In this last section we will stress electromagnetic properties in the microwave range in that these properties are important in developing and interpreting several different types of remote sensing observations that are currently used in sea ice research.

Models for the Variation in the Mechanical Properties of Sea Ice

Failure Strength

Early studies of the mechanical properties of sea ice revealed that the fracture surface was commonly controlled by the pronounced sea ice substructure. For example Figure 81 (Anderson and Weeks 1958) clearly shows the fracture surface in a sample subjected to tension to tend to run parallel to the (0001) planes of the ice crystals. Additional rubbings showing similar trends have been published by Tabata (1960) and by Paige and Kennedy (1967). Clearly the breaks are following the planes in which the brine pockets and air bubbles are concentrated. That these planes, if correctly oriented, should be planes of weakness is reasonable in that the gas and brine inclusions reduce the percentage of the failure plane that is solid (ice), allowing failure to occur at lower bulk stress levels. Therefore it would be expected that sea ice samples with low porosities would, being essentially pure ice, have strengths similar to that of freshwater ice. Also that sea ice with higher porosities would have very low strengths. Experimental observations (Schwarz and Weeks 1977, Weeks and Assur 1967, 1969) support this reasoning.

What was needed was a model that could be used to extrapolate and interpolate strength values at intermediate values of porosity and that was based on a reasonable model of the pore geometry of real sea ice.

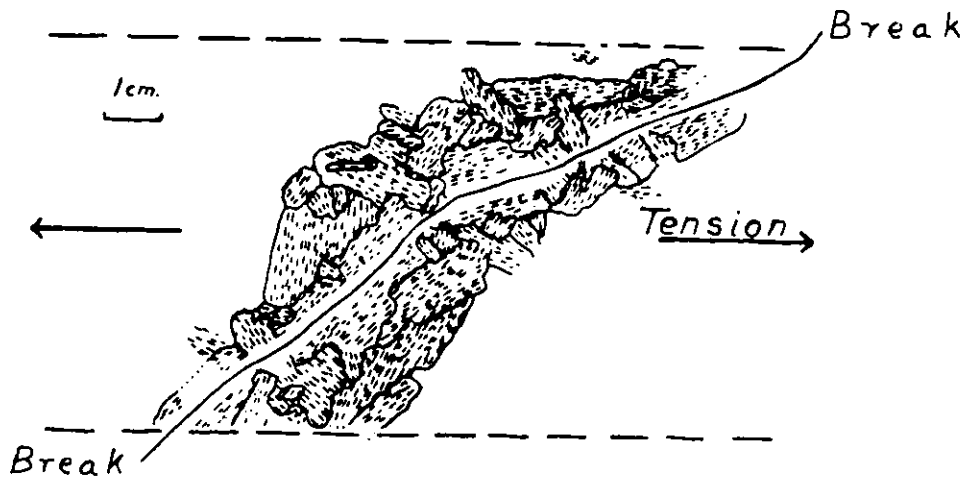


Figure 81. Rubbing of a broken segment of sea ice (Anderson and Weeks 1958).

Such a model was developed by Assur (1958), Anderson and Weeks (1958) and Anderson (1958, 1960). They assumed that it should be possible to express the variation in the failure strength σ_f for sea ice produced by variations in its porosity in the general form

$$\frac{\sigma_f}{\sigma_0} = 1 - \psi \quad (41)$$

where σ_0 is the basic strength of sea ice (i.e. the strength of an imaginary material that contains no brine, but still possesses the sea ice substructure and fails as the result of the same mechanism(s) that cause failure in natural sea ice) and ψ is the "plane porosity" or relative reduction in the area of the failure plane as the result of the presence of brine and air inclusions. The critical value of ψ in the failure plane is

$$\psi = f(v) = f(v_a + v_b) \quad (42)$$

where v is the void volume or porosity and v_a and v_b are the volume of air and brine respectively in the sea ice. Usually it is considered that $v_b \gg v_a$ (that the volume of brine is sufficiently larger than the volume of air so that v_a can be neglected).

It is now necessary to express ψ in terms of v_b through a simplified model of the brine geometry in real sea ice. Figure 82 shows such a model given by Assur (1958). Here the relative brine volume is

$$v_b = \frac{F_g}{a_o b_o g_o} \quad (43)$$

where F_g is the average area of a brine inclusion in the BG plane and defining

$$\beta_o \equiv \frac{b_o}{a_o} \quad (44)$$

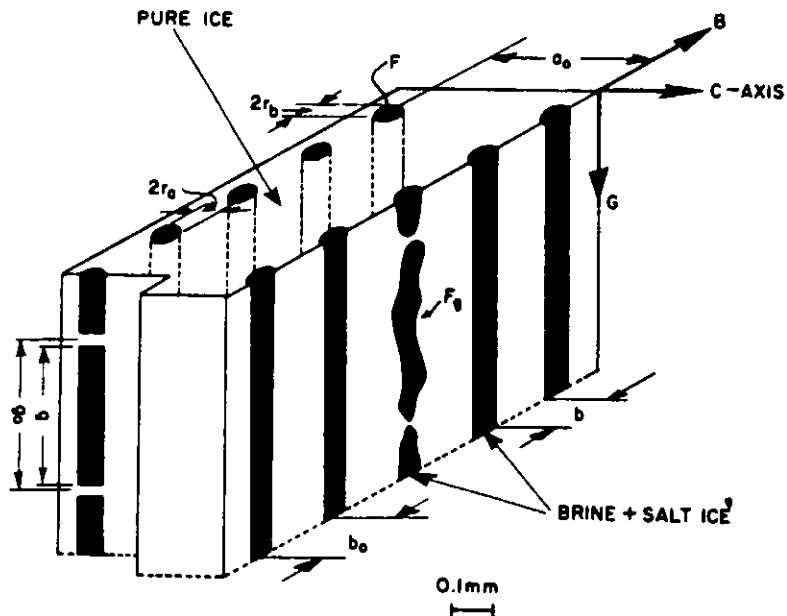


Figure 82. Idealized diagram of the shape of the brine inclusions in sea and NaCl ice (Assur 1958).

$$\gamma = \frac{g}{g_o} \quad (45)$$

the reduction in the cross-sectional area caused by the presence of the brine pockets is

$$\psi = \frac{2r_b g}{b_o g_o} = \frac{2r_b \gamma}{\beta_o a_o} \quad (46)$$

The question now is: How do the geometric parameters r_b and ψ vary with v_b ? A number of assumptions are possible; however, two are commonly used. The simplest is to assume that geometric similarity is maintained along the B-axis (see Fig. 82) and that the width as well as the relative length (γ) of the brine pockets remain constant. In this instance r_b changes proportionally to v_b and an equation of the form

$$\frac{\sigma_f}{\sigma_o} = 1 - c v_b \quad (47)$$

is obtained. The other assumption commonly made is that the average length and spacing of the brine pockets remain constant and that changes in v_b are reflected only in the BC cross section. In this case the resulting equation is

$$\frac{\sigma_f}{\sigma_o} = 1 - c v_b^{1/2} \quad (48)$$

These two models can be represented as straight lines in σ_f, v_b^k coordinates where k is 1 and 1/2 respectively. The σ axis intercept is σ_o and

$$c = v_o^{-k} \quad (49)$$

where v_0 is the volume of brine required to cause the ice to have zero strength.

Two specific models that have been utilized in discussing strength results are the constant width and elliptical cylinder models. In the constant width model

$$F = 4 r_a r_b \quad (50)$$

and

$$v_0 = \frac{2r_a}{a_0} = \frac{d_0}{a_0} \quad (51)$$

Here d_0 is the minimum width of a parallel brine layer before it splits as the result of interfacial tension to produce individual brine pockets. It is commonly assumed that $d_0 = \text{constant}$ (values of $\approx 7 \times 10^{-3}$ cm have been measured in natural sea ice).

In the elliptical cylinder model

$$\epsilon = \frac{r_b}{r_a} \quad (52)$$

and

$$F = \pi r_b r_a = \frac{\pi r_b^2}{\epsilon} \quad (53)$$

and eq 48 becomes

$$\frac{\sigma_f}{\sigma_0} = 1 - 2 \sqrt{\frac{\epsilon \gamma}{\pi \beta_0}} \sqrt{v_b} \quad (54)$$

Additional details can be obtained from Weeks and Assur (1967, 1969).

Plots of σ_f versus v_b , $v_b^{1/2}$, and $v_b^{2/3}$ (this last case is where all brine pockets remain of a similar shape during changes in v_b) have been made for a number of different sets of test data, and it has commonly been found that eq 48 gives the best fit. Therefore, some authors have routinely plotted strength measurements of every type against $\sqrt{v_b}$. As is pointed out by Mellor (1982), such indiscriminate application of eq 48 is to be avoided, particularly in cases where the structure of the ice is unknown, when the orientation of the pore structure to the principal stresses and to the failure stresses is uncertain, and when the fracture mechanisms are not fully understood.

For instance, it would clearly be inappropriate to apply the details of such models to marine frazil ice (a material whose mechanical properties have not, as yet, been investigated), as its structure is very different from that of congelation sea ice (see Fig. 52-56). Structurally, marine frazil ice appears to be similar to compact snow, with the included brine and air distributed between the grains (as contrasted to within the grains as is the case for congelation ice). If, as a first approximation, the brine and air inclusions can be assumed to be

randomly distributed throughout the ice in a fashion similar to that observed for dense snow then we would expect strength to decrease as a linear function of v_b , since in such a case the relative plane porosity in any cross section is equal to v_b . Also the properties of the ice would not depend upon the orientation of the sample relative to the applied stresses.

In this section we have discussed the effect of brine and gas inclusions in the ice on the bulk properties of the ice. Nothing has been said concerning the effect of the presence of solid salts. There have as of now been two attempts to develop a theory for the effect of solid salts. Assur (1958) postulated two different situations based on a model of the reinforcement of the brine pocket walls by a continuous layer of intermixed ice and solid salt. In the first case the elastic modulus (E) of the salt-ice reinforcement is similar to that of pure ice, and rupture occurs within the reinforcement. As a result a relatively thin layer of salt-ice should abruptly increase the ice strength, but little further increase would be observed with the thickening of the reinforcement. In the second case a substantial difference in E between the salt-ice mixture and the pure ice is assumed, with the strength of the mixture being sufficiently high so that the initial failure occurs in the ice as opposed to in the mixture. It was suggested that the first situation might apply to the precipitation of $\text{Na}_2\text{SO}_4 \cdot 10\text{H}_2\text{O}$, where only a small amount of salt forms, with the second case applying to the precipitation of $\text{NaCl} \cdot 2\text{H}_2\text{O}$, when much larger quantities of salt form. Further work on this problem was later undertaken by Peyton (1966), who utilized a similar salt reinforcement model.

There are two obvious problems here. First, the very limited direct observations on the nature of the distribution of solid salt crystals in brine pockets reported by Sinha (1977) show a random distribution of loosely packed crystals. This clearly does not support the geometric assumptions of Assur's model. However, more important there is still no adequate set of strength tests on real sea ice against which the predictions of any model can be tested. The closest to an adequate study of this problem was by Weeks (1962), who performed ring-tensile tests on $\text{NaCl} \cdot 2\text{H}_2\text{O}$ ice. He found that the strength of $\text{NaCl} \cdot 2\text{H}_2\text{O}$ ice was a) essentially independent of temperature and the volume of $\text{NaCl} \cdot 2\text{H}_2\text{O}$, and b) comparable to the strength of freshwater ice. This plus Sinha's observations suggest that solid salts may well have little effect on the failure strength of sea ice. What is clearly needed now is a set of high quality tests that are specifically focused on resolving this problem.

Elastic Modulus

It is only recently that a similar model has been suggested to explain the variation in the elastic modulus (E) of sea ice with changes in the volume of brine included in the ice (Bergdahl 1977). First, stress in the vertical direction (G -direction, see Figure 83) is considered. Also, the value of v_a is assumed to be negligible and the vertical interruptions in the brine cylinders are neglected. Then the deformation for the brine inclusions and for the ice matrix are set equal ($\nu = 0$) and the loading is considered to be dynamic. Then

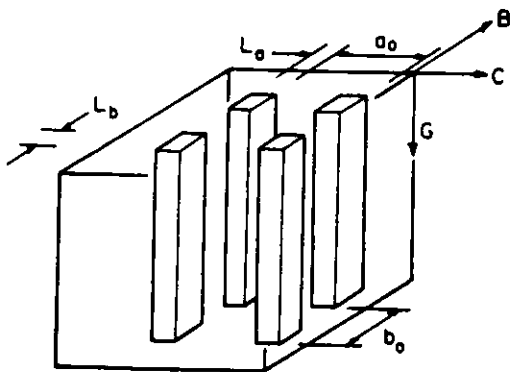


Figure 83. An idealization of the structure of sea ice used in calculating its elastic modulus (Bergdahl 1977). The rectangular areas represent brine inclusions.

$$\epsilon = pK = \sigma_1/E_1 = \sigma/E \quad (55)$$

where ϵ = strain
 p = pressure in the brine pockets
 σ_1 = stress in the ice
 σ = stress averaged over the cross section A, $\sigma = P/A$
 E = bulk elasticity of sea ice.

From eq 55

$$\sigma = E \epsilon \quad p = \epsilon/K \quad \sigma_1 = \epsilon E_1 \quad (56)$$

and the average stress is

$$\sigma = \sigma_1 (1 - A_b) + p A_b \quad (57)$$

where A_b is the relative cross-sectional area of brine. These equations give

$$E = E_1 + (1/K - E_1) A_b \quad (58)$$

or, if $v_b = A_b$,

$$E = E_1 + (1/K - E_1) v_b \quad (59)$$

suggesting that E should prove to be a linear function of the brine volume. This, of course, has been shown to be the case experimentally (see Mellor 1982, Weeks and Assur 1967, or Schwarz and Weeks 1977).

When horizontal deformations in the sea ice cover are considered, a more complex model must be utilized. In doing this Bergdahl approximates the brine pockets as rectangular tubes with a horizontal cross-section area $L_a \cdot L_b$ (see Fig. 83). Deformation along the c-axis is then given by

$$a_0 \epsilon = a_0 \sigma/E_h = L_a \sigma/E_b + (a_0 - L_a) \sigma/E_1 \quad (60)$$

with

ϵ = average strain along the c-axis
 a_0 = brine layer spacing
 σ = average stress
 E_h = bulk modulus of elasticity
 E_b = bulk modulus of the brine layer
 E_1 = elasticity of pure ice.

The bulk elasticity can ultimately be simplified to

$$E_h = E_1 / (1 - (1/K - E_1) v_b / E_b) \quad (61)$$

indicating that the elastic modulus in the horizontal direction would be expected to be a function of both the brine volume and the shape of the brine pockets. As in the equations for failure strength, to evaluate eq 61 a relation must be assumed between the ratio L_b/L_a and v_b .

There are many problems with the utilization of such models. Obviously they represent gross simplifications of the structure of real sea ice, which in actuality is very complex. One difficulty is that there is very little information on how brine pocket shapes actually change with changes in v_b . Also, usually the total void volume is assumed to equal v_b , the brine volume (i.e. v_a is assumed to equal zero). Now this is not strictly true, even for young sea ice, while for low salinity multiyear ice v_a may be much larger than v_b . There are, at present, no good observations to support the common assumption that air bubbles are localized along the same substructure as the brine pockets. This, of course, seems reasonable, and many times the total void volume v is taken to be the sum $v_a + v_b$. Finally, there are very few sets of measurements of the mechanical properties of sea ice available in which both v_a and v_b were determined. Even considering these weaknesses, the geometric models for the variations in the mechanical properties of sea ice have proven to be very useful and they undoubtedly will continue to be utilized in treating a variety of different problems.

Applications

We conclude this section with a discussion of one such application. As was discussed earlier it is known that some elements of the substructure of sea ice vary systematically with changes in the growth velocity. The growth velocity is in turn controlled by the meteorological conditions. If changes in the substructure affect the mechanical properties of the ice, it is then possible to formulate relations between the meteorology and the ensuing ice properties. For example, let us first assume that the relation between brine layer spacing a_0 and growth velocity v can be expressed as

$$a_0 \sqrt{v} = c \quad (62)$$

where c is a constant. Then if the ice growth equation can be approximated by

$$c = \frac{\rho L h}{\Delta \theta} \left[\frac{1}{e} + \frac{h}{2\kappa} \right] \quad (63)$$

where t is time, h is ice thickness, ρ is the density of the ice, L is the latent heat of fusion of the ice, $\Delta \theta$ is the difference between the ambient air temperature and the freezing temperature of seawater, k is the thermal conductivity of sea ice, and e is the overall coefficient of surface heat transfer, by rearranging and differentiating we can obtain

$$v = \frac{dh}{dt} = \frac{\Delta \theta}{\rho L \left[\frac{1}{e} + \frac{h}{\kappa} \right]} \quad (64)$$

This relation, when combined with eq 62, gives

$$a_o = \sqrt{\frac{c^2 \rho L}{\Delta \theta} \left[\frac{1}{e} + \frac{h}{\kappa} \right]} . \quad (65)$$

For thin ice a_o is independent of ice thickness h , as $1/e \gg h/\kappa$. For thick ice, on the other hand, $h/\kappa \gg 1/e$, giving a_o varying proportional to \sqrt{h} .

The structural parameter a_o , however, appears in the ice strength equations. For instance, in the constant width model as

$$\frac{\sigma_f}{\sigma_o} = 1 - \frac{v_b}{v_o} = 1 - \frac{a_o v_b}{d_o} \quad (66)$$

and the elliptical cylinder model as

$$\frac{\sigma_f}{\sigma_o} = 1 - 2 \sqrt{\frac{\gamma \epsilon a_o}{\pi b_o}} \sqrt{v_b} . \quad (67)$$

Therefore, combining these relations with eq 65 we obtain, respectively,

$$\sigma_f = \sigma_o \left[1 - \frac{cv}{d_o} \sqrt{\frac{\rho L}{\Delta \theta} \left[\frac{1}{e} + \frac{z}{\kappa} \right]} \right] \quad (68)$$

and

$$\sigma_f = \sigma_o \left[1 - 2 \sqrt{\frac{v_b \gamma \epsilon c}{\pi b_o}} \sqrt{\frac{\rho L}{\Delta \theta} \left[\frac{1}{e} + \frac{z}{\kappa} \right]} \right] \quad (69)$$

where z is the position of a given ice layer below the surface and $\Delta \theta$ is the temperature difference when that layer formed. Combining all the constants and considering only thin ice, the two different models give, respectively,

$$\sigma_f = \sigma_o \left[1 - \text{const} \frac{v_b}{\sqrt{\Delta \theta}} \right] \quad (70)$$

and

$$\sigma_f = \sigma_o \left[1 - \text{const} \sqrt{\frac{v_b}{\Delta \theta}} \right] . \quad (71)$$

These equations support the intuitive conclusions of early Soviet investigators (see Sharp 1947), who claimed that the strength of young sea ice was in some way affected by its growth conditions. For thick ice we obtain

$$\sigma_f = \sigma_o \left[1 - \text{const} v_b \sqrt{\frac{z}{\Delta \theta}} \right] \quad (72)$$

and

$$\sigma_f = \sigma_o \left[1 - \text{const} \sqrt{v_b \sqrt{\frac{z}{\Delta\theta}}} \right]. \quad (73)$$

More details and a consideration of the effect of a snow cover on the sea ice can be found in Assur and Weeks (1964). The important point here is that similar studies can easily be made of the effect of vertical variations in a variety of structural characteristics of sea ice upon the profile properties of the sheet, provided that the relations between the characteristics and the ice growth conditions have been established. A related study that examines the effect of growth conditions on the salinity and brine profiles of first-year sea ice has been published by Weeks and Lofgren (1967).

Models for the Variation in the Thermal Properties of Sea Ice

By the thermal properties of sea ice we specifically refer to the parameters that compose the thermal diffusivity term in the thermal diffusion equation, i.e. the specific heat, the density and the thermal conductivity. Of these three terms the first two depend only on the temperature and the composition of the ice. The geometric distribution of the components is not a factor. Therefore they will not be discussed here. Good recent reviews and studies of these two properties can be found in Bergdahl (1977), Yen (1981) and Cox and Weeks (1982).

Thermal Conductivity

The thermal conductivity of sea ice and the thermal diffusivity which contains the thermal conductivity are dependent on the spatial arrangement of the different phases composing the sea ice: the pure ice, the brine, the entrapped gas and, if the ice is sufficiently cold, the solid salt hydrates. Figure 84 gives thermal conductivity (λ_1) of pure polycrystalline ice determined by several investigators (see Yen 1981 for references). For practical purposes Yen suggests that the complete set be used, resulting in the relation

$$\lambda_1 = 9.828 \exp(-0.0057 T) \quad (74)$$

where λ_1 is in W/m K and T is in kelvins. The effect of crystal orientation on λ_1 has been little studied (Landauer and Plumb (1956) suggest that λ_1 parallel to the c-axis is approximately 5% higher than values measured normal to the c-axis). Note that at 273K, λ_1 is roughly 2.2 W/m K, which is about 4 times the thermal conductivity of water at that temperature. There are, as yet, no measurements on the conductivity of seawater brine in equilibrium with ice. However, data on other salts suggest that λ_b is strongly dependent on concentration and less dependent on temperature. Based on λ_b measurements for NaCl and Na₂SO₄ solutions, Schwerdtfeger (1963) has suggested that the value for seawater brine can be approximated by

$$\lambda_b = 0.4184 (1.25 + 0.030 \theta + 0.00014 \theta^2) \quad (75)$$

where λ_b is in units of W/(m K) and θ is in K. As Schwerdtfeger

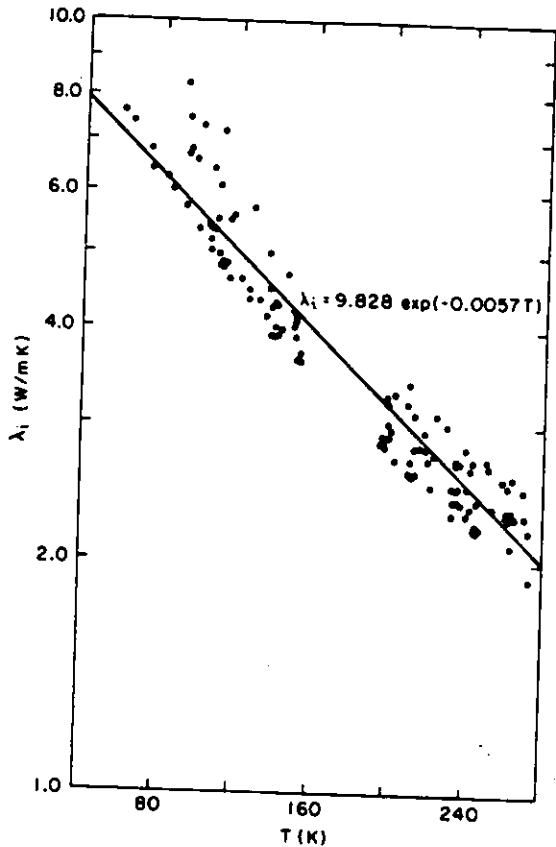


Figure 84. Thermal conductivity of pure ice as a function of temperature. See Yen (1981) for the data sources.

points out; although eq 75 becomes less accurate at lower temperatures, the value of λ_b is less important under such conditions because the relative volume of brine becomes negligible. The thermal conductivity of air (λ_a) is approximately 0.03 W/(m K) at temperatures between -30°C and 0°C , or roughly 1% of the conductivity of the ice. Therefore, for most purposes λ_a is taken as nil. The conductivities of the solid hydrates at temperatures below -8.7°C are not well known and they are usually neglected inasmuch as they would be expected to have only a very small effect on the bulk conductivity of sea ice.

Next it is necessary to consider the effect of the geometry of the brine and gas inclusions on the bulk conductivity of the sea ice. This was first done by Anderson (1958, 1960), who considered the presence of brine in several different spatial configurations. Among these were the cases with the brine distributed

- a) in isolated spherical bubbles
- b) in parallel cylinders or layers between ice platelets with the conductivity measured in the direction of the brine layers (analogous to electrical conduction in parallel), and
- c) in parallel layers with the conductivity measured perpendicular to the layers (analogous to electrical conduction in series).

These results are shown in Figure 85. Note that the conductivity measured parallel to the c-axis (perpendicular to the brine layers) is appreciably lower than the equivalent value measured perpendicular to the c-axis. This difference in thermal conductivity with crystal orienta-

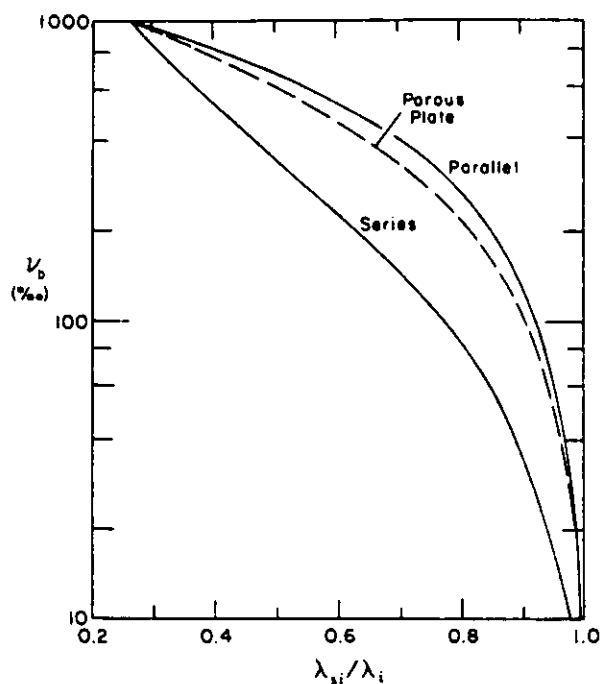


Figure 85. Thermal conductivity of sea ice (Anderson 1958). The different curves represent different arrangements of the brine inclusions.

tion is undoubtedly an important contributing cause of the fact that in the transition layer in the upper part of newly formed sea ice the crystals with their c-axes horizontal are observed to grow ahead of crystals in other orientations (the c-axis-horizontal crystals have their direction of maximum thermal conductivity aligned in the vertical, parallel to the direction of heat flow (Weeks 1958)).

Inasmuch as the heat flow in sheets of undeformed sea ice is essentially one-dimensional (in the vertical) and the great majority of congelation ice is oriented with its c-axes horizontal, this is clearly the case that should be considered in most practical problems. Schwerdtfeger (1963) expanded upon Anderson's treatment by considering the presence of air in the sea ice. This was done by assuming that the air in sea ice consists of a series of uniform, randomly distributed spherical air bubbles. Then, using a relation developed by Maxwell (1891), which incidentally is the same relation Anderson used in calculating the "porous plate" conductivity given in Figure 85,

$$\lambda_{bi} = \frac{2\lambda_i + \lambda_a - 2V_a(\lambda_i - \lambda_a)}{2\lambda_i + \lambda_a + V_a(\lambda_i - \lambda_a)} \lambda_i \quad (76)$$

where λ_{bi} is the thermal conductivity of pure ice containing randomly distributed bubbles as stated and V_a is the volume of air per unit volume of sea ice. Figure 86 gives the resulting values of λ_{bi} (and of the density of bubbly ice ρ_{bi}) for temperatures in the 0 to -20°C range. Here λ_i and λ_a were respectively taken to be 2.09 and 2.51×10^{-2} W/m K. Schwerdtfeger then considered sea ice as the composite material composed of layers of brine and layers of pure ice containing air bubbles, with a resulting thermal conductivity λ_{si} given by

$$\lambda_{si} = \lambda_{bi} - (\lambda_{bi} - \lambda_b) \left(\frac{\sigma \rho_{si}}{\alpha \rho_w \theta} \right) \quad (77)$$

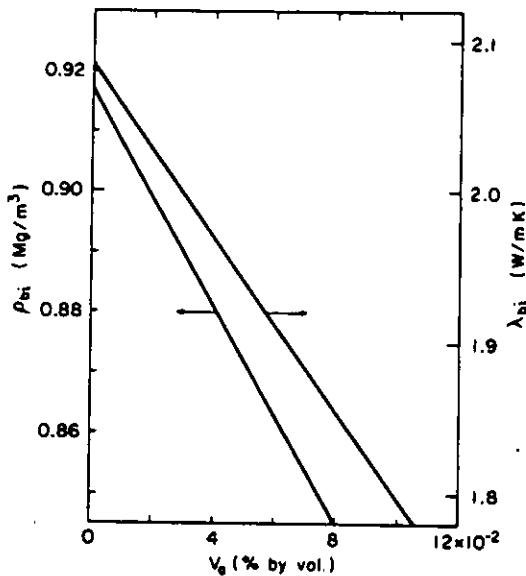


Figure 86. Density and thermal conductivity of bubbly ice as a function of the fractional air content (Schwerdtfeger 1963).

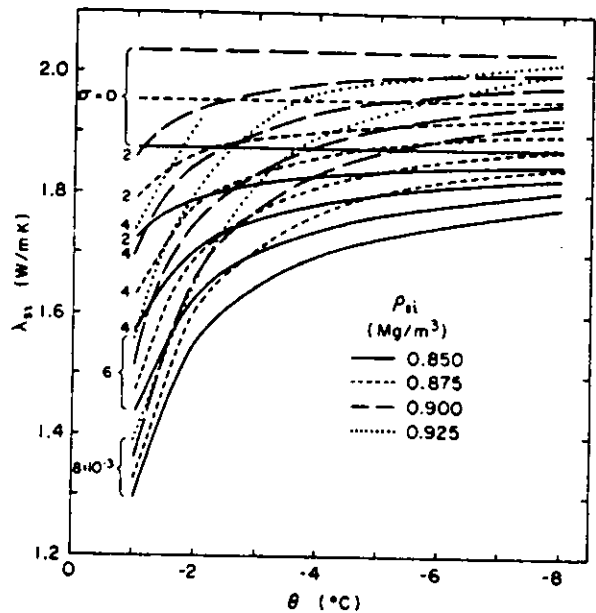


Figure 87. Effective thermal conductivity of sea ice as a function of temperature for various salinities and densities (Schwerdtfeger 1963).

Here λ_b is the thermal conductivity of the brine, σ is the salinity of the ice, α is the constant in the relation $s = \alpha\theta$ where s is the fractional salt content and θ is temperature, and ρ_w and ρ_{gi} are the densities of pure water and of bulk sea ice respectively. The results of Schwerdtfeger's calculations are shown in Figure 87, redrawn by Yen (1981). As is apparent in this figure and has been noted by Schwerdtfeger, even at temperatures of -8°C the curves in Figure 87 exhibit asymptotic behavior, with the conductivity of sea ice approaching the value for pure ice at low temperatures. Therefore at low temperatures it is the air content of the sea ice that controls its thermal conductivity, while at temperatures near the melting point it is the brine volume in the ice that is important and which in turn at a given temperature is controlled by the salinity.

The most recent work on the conductivity of sea ice is by Ono (1968) who realized through his studies of its internal structure that it was probably not realistic to assume that air bubbles are only trapped in the ice matrix. He therefore developed a model in which the air bubbles are spherical and are uniformly dispersed through both the ice and the brine, with identical concentrations in both phases. However, as in the previous models the layers of bubbly ice and bubbly brine are assumed to be arranged in parallel. The results of Ono's calculations are shown in Figure 88. The conductivity curves are for air-free sea ice. The effect of the presence of air is included by first using the figure to determine the point specified by the ice temperature and salinity and moving vertically downward parallel to the conductivity (y) axis an amount specified by the v_a inset scale.

The requisite petrographic data necessary to quantitatively determine which model, Schwerdtfeger's or Ono's, is the most appropriate to

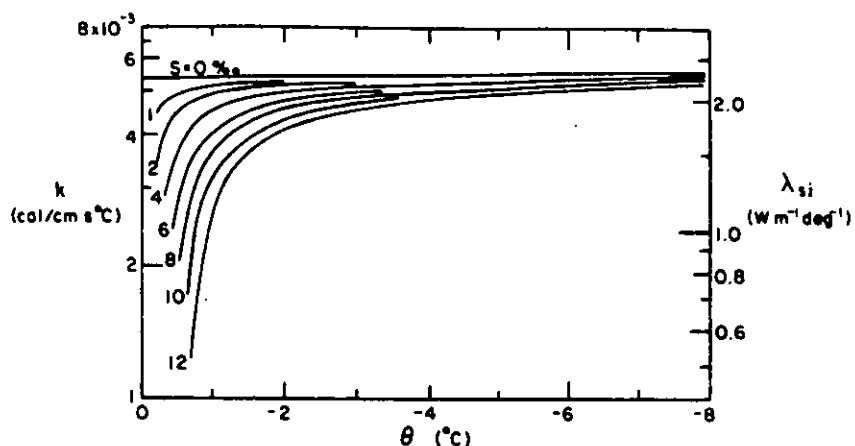


Figure 88. Thermal conductivity of sea ice calculated using Ono's model (Ono 1968).

different types of congelation ice are not available. It is our impression, however, that Ono's model is the most realistic. A further improvement would probably be to consider the case where the amounts of air bubbles in the brine and in the ice are different. However, we doubt that there is much profit in the fine-tuning of these models unless it is required by some specific problem. It should also be noted that present models do not suitably describe marine frazil ice. An adequate model of this material could undoubtedly be obtained by combining models that independently consider randomly distributed brine and air inclusions.

Thermal Diffusivity

The thermal diffusivity $\sigma_{si} = \lambda_{si} / (\rho_{si} c_{si})$ of sea ice as calculated by Ono (1968) is given in Figure 89. As can be seen σ_{si} is

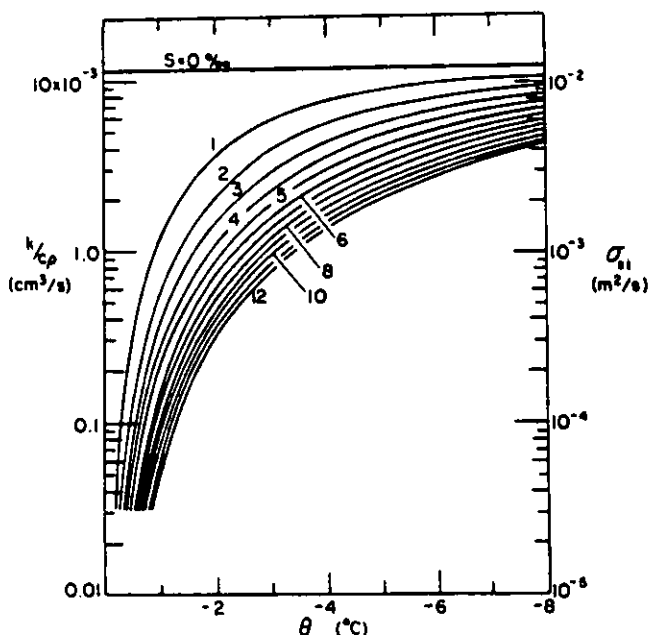


Figure 89. Thermal diffusivity of sea ice (Ono 1968).

strongly dependent on the temperature of the ice. This is not surprising in that, as noted by Schwerdtfeger, all three terms composing σ_{gi} are monotonic functions of temperature. As temperature rises λ_{gi} decreases while the two terms in the denominator (ρ_{gi} and c_{gi}) both increase. Therefore the thermal diffusivity σ_{gi} shows a decrease that is more temperature-dependent than any of its constituent parameters. However, it should be noted that the values of σ_{gi} are not appreciably affected by changes in the air content of the ice. This insensitivity can clearly be seen by examining Table VI in Schwerdtfeger (1963). The same insensitivity to changes in air content occurs in the thermal diffusivity of freshwater ice (Bergdahl 1977, p. 70-71).

The particular importance of σ_{gi} is that it is the most directly observable thermal property, as it can be directly calculated from the rate of change of the temperature profile in an ice sheet. For a convenient method of determining σ_{gi} the reader is referred to Ono (1965, 1968) and to Yen (1981). Determinations of σ_{gi} from observed temperature profiles of natural sea ice have been made by Lewis (1967), Weller (1968) and Ono (1965, 1968). In all cases the observed and calculated σ_{gi} and λ_{gi} values proved to be in reasonable agreement. In fact we are rather surprised with the agreement in that, at least in warm first-year sea ice with large brine volumes, we would expect convective processes, that are not considered at all in current thermal conductivity models, to be very important. For instance, it is hard for us to believe that the processes occurring in brine drainage tubes that alternatively expell cold brine and take in "warm" seawater would not have an effect on the observed σ_{gi} values. These matters should clearly be explored further.

Electrical Properties of Sea Ice in the 0.1 to 40 GHz Range

Active radar and passive microwave emission measurements over sea ice (generally in the frequency range between 0.1 and 40 GHz) have been used extensively over the past decade to obtain information on ice thickness, ice age, and ice concentration on vertical scales (for thickness) of the order of one to a few meters and on horizontal scales (for ice age and concentration) of the size of the Arctic Basin and the area covered by the maximum extent of Antarctic sea ice (≈ 20 million km^2). Universal to an interpretation of this information, whether emission characteristics (passive methods) or reflection characteristics (active methods), is some model for the dielectric characteristics of the various ice types that we have discussed previously. These characteristics are manifested in the physical-structural nature of the ice cover, for example its salinity, temperature, and density (air content) profiles, and to some extent crystal structure in that it controls the configuration of the other phases (air, brine and solid salt) within the ice structure. Since these properties control the dielectric properties, variations in measured dielectric properties as observed by satellite, aircraft, or ground-based systems hold the promise of providing useful information for geophysical and engineering purposes on the variability of these physical parameters.

For sea ice, different formulations of the dielectric properties are necessary, depending on 1) the frequency range of the remote sensing device and, in combination with this, 2) the description of the ice as

"high loss" (generally correlated with first-year and younger ice types) or "low-loss" (which is almost exclusively associated with multiyear ice). The distinction arises relative to the level of electromagnetic theory needed to model the various phenomena observed. Since sea ice consists of a mixture of constituents with variable dielectric properties, in some cases (primarily at low frequencies or longer wavelengths) the sizes of the individual dielectric inhomogeneities (brine pockets, air bubbles, and solid salt particles) only influence the reflection/emission characteristics as they contribute to the average properties of the medium. This constraint, that the individual particle sizes can be neglected, and only the total volume be considered, applies as long as the particle sizes are less than ≈ 0.1 wavelength of the incident (or outgoing) radiation.

If, on the other hand, the particle sizes are commensurate with the wavelength, then scattering by individual particles becomes a factor. More complex theories that account for the geometry and interaction of the particles, as well as the average dielectric properties of the medium, are then necessary. The description of these materials is by Rayleigh scattering methods, and a body of theory pertaining to aerosols and atmospheric scattering problems is available. The necessity to apply scattering theory only applies to "low loss" materials (in our case multiyear ice) since "high loss" materials (first-year and younger ice) either attenuate active signals or confine thermal microwave emissions to such a thin layer that the scattering is relatively low. As well, in the younger ice types, the dielectric inhomogeneities are primarily brine pockets with size scales of a millimeter or less, while in old ice the air bubbles (with sizes approaching several millimeters) are the inhomogeneities. The air bubbles therefore affect properties at more frequencies of interest between 0.1 and 40 GHz than do brine pockets. The cutoff where scattering from air bubbles is relatively important is for frequencies above 2-3 GHz, while for brine pockets scattering may be important only above about 20-30 GHz.

We first discuss the basic translation of physical properties into electrical parameters, i.e. the dielectric constants of sea ice as functions of its constituents (and their configurations), then the effects of structural and physical properties on active radar sounding, and finally on the passive microwave emission characteristics of sea ice.

Dielectric Properties of Sea Ice

Since sea ice consists, to a greater or lesser degree, of four phases, ice, brine, air and solid salts, each with different dielectric properties, we therefore need a formulation of the dielectric properties as functions of the relative proportions of these constituents. In reality, however, the dielectric properties are dominated either by the relative amounts of ice and brine or, when the amount of brine is small, the amounts of ice and air. Solid salts do not have a strong effect since their dielectric properties (between 0.1 and 40 GHz) are generally close to those of ice so the presence of a small amount of solid salts is generally indistinguishable at these frequencies. In formulating the dielectric properties, therefore, two-phase formulations accounting for ice and brine or ice and air have generally been adopted. The dielectric properties of both brine and air present sufficient contrast with

those of ice to give a distinct contribution to the dielectric properties relative to that of pure ice.

Dielectric properties of ice and air. The complex dielectric constant of most materials is defined (in the pure phase) as

$$\epsilon = \epsilon' - j\epsilon'' \quad (78)$$

where ϵ' is the real part (sometimes also called the dielectric constant), ϵ'' is the dielectric loss or imaginary part (and can also be related to the conductivity of the media) and $j = \sqrt{-1}$.

As noted earlier, the ability of ice to reject salts is large, that is the solubility of salts in the pure ice phase is invariably down by several orders of magnitude relative to the liquid phase. The ice phase in sea ice is, therefore, relatively pure, and its dielectric properties correspond closely to those observed for pure ice as reviewed, for example, in Evans (1965). The dielectric loss is of the order 10^{-2} to 10^{-4} which, in the sea ice context, is relatively insignificant as we will show later. The real part of the dielectric constant ($\epsilon_1 = 3.2$) is constant over the frequency range from 0.1 to 40 GHz. Similarly, the air component is relatively loss-less and has the value $\epsilon_a = 1$ in its real part.

Dielectric properties of brine. Of the four components in sea ice, brine shows the greatest variability in dielectric properties over the frequency range of our interest (0.1 to 40 GHz). An equation of the Debye form is necessary to describe its behavior due to the relaxation brine undergoes in this frequency range. After Stogryn (1971), this is

$$\epsilon_2 = \epsilon_\infty + \frac{\epsilon_0 - \epsilon_\infty}{1 - j2\pi f\tau} + j \frac{\sigma}{2\pi f\epsilon_0} \quad (79)$$

where ϵ_0 , ϵ_∞ , ϵ_0 , f , τ , σ are the static and high frequency dielectric constants of the brine, the free space permittivity, the frequency, the relaxation time and the ionic conductivity of the dissolved salts. As frequency increases, the contribution to dielectric loss from ionic conductivity (third term in eq 79) drops off but the second term on the right-hand side contains the water dipole relaxation at $\omega = 1-25$ GHz so the dielectric loss which is related to attenuation also increases for frequencies between 1 and 25 GHz. If we reformulate eq 79 so that $\epsilon_b = \epsilon'_b - j\epsilon''_b$ as in eq 78, then Figure 90 compares the real and imaginary parts of the dielectric constant (here labeled K' and K'') for pure water and brine at the same temperature (-10°C). Unlike air and pure ice, the dielectric properties of brine undergo substantial changes between 0.1 and 40 GHz. As also implied in this figure, the values of the dielectric constants at any given frequency are dependent on the concentration of salts in the brine. To compute dielectric properties of the brine in sea ice, it is therefore necessary to know the temperature and salinity of the mixture and then compute the brine concentration based on the phase diagram for sea ice.

From Figure 90, we note that compared to ice, the dielectric loss of either brine or pure water is several orders of magnitude higher than that of pure ice (e.g. 10 to 100 at 1 GHz compared to 10^{-4} for ice).

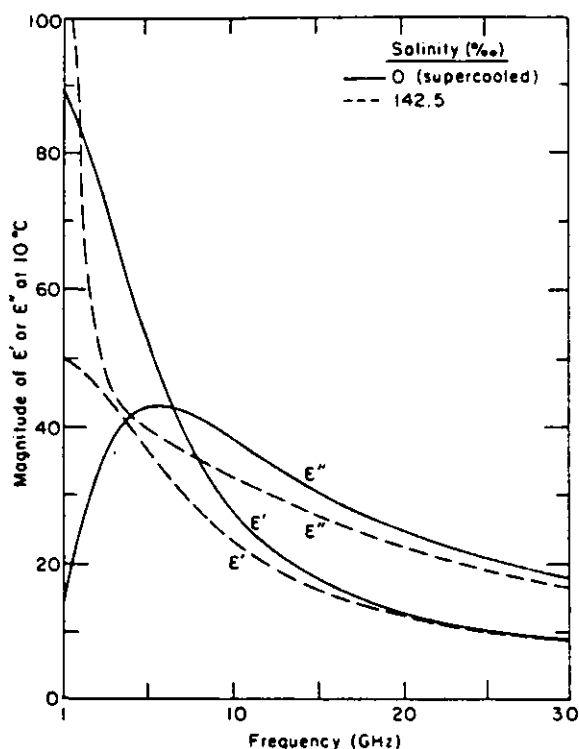


Figure 90. Real (ϵ') and imaginary (ϵ'') parts of the dielectric constant for brine and pure water (Poe et al. 1972).

The change in the dielectric constant is also substantial but, relative to ice, only increases by about a factor of 10 to 30 (one order of magnitude). Therefore, since the amounts of brine in sea ice are small, the contribution of brine to the real part of the dielectric constant is small, but the electromagnetic loss (imaginary part of the dielectric constant) is almost completely accounted for by the brine. Ice, therefore, controls the behavior of the real part while brine dominates the loss behavior.

Averaged or composite dielectric properties of sea ice. As mentioned earlier, both the low frequency and the high frequency dielectric behavior require at least a formulation of the composite dielectric behavior of ice. Poe et al. (1972) reviewed several formulations of the available evidence to establish a bulk dielectric constant using several empirical formulations. More recently, however, Vant et al. (1975) showed that a more analytical formulation of the mixture constant after Tinga et al. (1973) gave a theoretically justifiable dielectric constant based on analytic solutions from electrostatics. Golden and Ackley (1981) have also used Tinga et al.'s formulation in explaining some active radar properties of sea ice so we will pursue that formulation here as well. Some differences in formulation are noted between Vant et al. and Golden and Ackley, however, since the possibility of dielectric horizontal anisotropy of sea ice was not allowed for in Vant et al.'s formulation. The overall sea ice structure taken is that discussed by Anderson and Weeks (1958) and here earlier. Essentially, brine layers (Fig. 91a) formed at the dendritic growth interface neck with decreasing temperature (Fig. 91b) further up in the ice sheet and freeze out into cylinders (Fig. 91c) and eventually into elliptical cylinders (Fig. 91d). An idealized model of a brine inclusion is a non-degenerate ellipsoid ($a > c > b$, where a , b are in the x , y plane and c in the z plane or in the depth direction) with surface defined by:

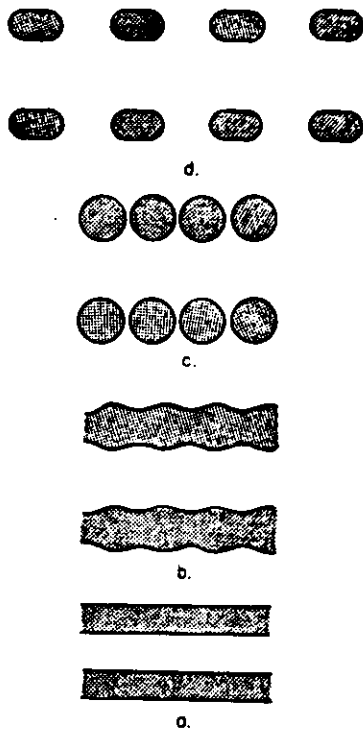


Figure 91. Brine layers at the bottom (a) of the ice sheet showing necking off as the temperature is lowered (Anderson and Weeks in Golden and Ackley 1981).

$$\frac{x^2}{a^2} + \frac{y^2}{b^2} + \frac{z^2}{c^2} = 1. \quad (80)$$

Tinga et al. (1973) derived an expression for the complex dielectric constant ϵ_k of a mixture consisting of ellipsoids (brine) of complex dielectric constant ϵ_2 , relative volume V_b and uniform axial alignment, dispersed in a homogeneous medium (ice) of complex dielectric constant ϵ_1 , when the mixture is subjected to an initially uniform electric field directed along one of the principal axes of the ellipsoid:

$$\epsilon_k = \epsilon_1 + \left[\frac{V_b \epsilon_1 (\epsilon_2 - \epsilon_1)}{n_k (1 - V_b) (\epsilon_2 - \epsilon_1) + \epsilon_1} \right] \quad (81)$$

where n_k is the depolarization factor of the ellipsoid:

$$n_k = \frac{abc}{2} \int_0^\infty \frac{ds}{(k^2 + s) \sqrt{(a^2 + s)(b^2 + s)(c^2 + s)}}. \quad (82)$$

This solution allows an accounting for cases when the field is aligned with one of the ellipsoid axes as sometimes occurs in active sounding. If the field is not aligned with one of the axes or if the axes are randomly aligned with respect to any direction of the field, then in the case of random alignments, Ackley and Keliher (1979) show the dielectric constant is

$$\epsilon \equiv \frac{1}{3} \epsilon_a + \frac{2}{3} \epsilon_b \quad (83)$$

(when the E-field is in the a-b plane).

The brine volume can be obtained either directly from the phase diagram or by using one of the equations of Frankenstein and Garner

(1967) or Cox and Weeks (1982) for the appropriate temperature range. Salinity and temperature also control the concentration in the brine and, therefore, the real and imaginary values of ϵ_2 , the dielectric constant of the brine. Since the dielectric constant of the brine is a complex number, the composite dielectric constant ϵ_k is also complex.

For ice covers where air is the primary second component, the effects of geometry on the mixture dielectric constants are not usually included. Normally the primary electromagnetic effects are confined to the top portion of the ice cover down to the freeboard level where salinity usually increases, leading to a dominance of ice-brine dielectric mixtures below these depths. In the top portions of the ice cover, especially in multiyear ice where the air content is most significant, several factors appear to discount other geometries of the air bubbles besides spherical as being very important for dielectric modeling purposes. The ice above freeboard typically arises from several sources: a) Brine-drained ice of usually frazil structure from the previous year or years of growth. The inclusions are probably at least random if not spherical, leading to little difference than treating them as spherical. b) Recrystallized ice. Here again the tendency is for the air bubbles to trend toward more spherical shapes because of the annealing at the melting point that has taken place. c) Snow-ice or snow infiltrated by meltwater and refrozen. Again, spherical air inclusions would dominate. Even if the inclusions are non-spherical, the dielectric contrast between ice and air is small (3.2 to 1) so the ice component dominates the real part of the dielectric constant at the low percentages of air (<20%) typically found in sea ice covers. This behavior is in contrast to the imaginary part of ice-brine mixtures where the brine dominates. Since the pure ice dielectric properties are homogeneous and isotropic (at these frequencies) the air-ice dielectric properties are also mostly isotropic, even if some anisotropy exists in the inclusions. The changes in dielectric constant can be related to the density of the ice and, after Gudmandsen (1971), this is:

$$\epsilon = (1 + 0.85 \rho_1)^2. \quad (84)$$

As the radar sounding of sea ice via the use of active methods depends directly on the dielectric properties as shown in the mixture constants we will discuss these next.

Active Radar Sounding of Sea Ice

To emphasize this point again, the mixture dielectric constants given in eq 81 have an apparent dependence on the inclusion geometry. However, this geometric dependence appears only in the depolarization factor n_k which can be solved for in terms of axial ratios of the major and minor dimensions of the inclusions. Therefore the same dielectric effect would be attributed to large inclusions as to small inclusions if 1) the total volume occupied was similar and 2) the axial ratios were the same. The geometry is, therefore, decoupled from the wavelength as long as $a, b, c, \ll \lambda$. The apparent effect arises from the boundary conditions on Maxwell's equation at the surface of the inclusions, in that much more surface area of the included medium is present to particular views of the electric field if the inclusions are anisotropic.

In active sounding, an electromagnetic wave polarized in one direction travels into the sea ice and is reflected by any dielectric discontinuities it encounters. The major discontinuities are the top (air/ice) and bottom (ice/water) interfaces of the ice sheet. Recently radar measurements in the frequency range from 0.1 to 0.5 GHz (100 to 500 MHz) have been used to obtain thickness information on sea ice (when dielectric properties are either known or assumed), primarily from ground-based transceivers but also by instruments mounted in helicopters. We have formulated the dielectric constant of sea ice in a form that includes anisotropy because one of the effects seen recently (Campbell and Orange 1974, Kovacs and Morey 1978) is anisotropy in the strength of the return from impulse radar soundings in these thickness soundings of sea ice.

The effect seen is marked dependence of returned radar signal strength, depending on the orientation of the linearly polarizing antenna of the radar system on the surface. The strongest return also coincided with the azimuthal orientation of the c-axes in the ice cover, while the weakest return was found to be at 90° from the direction of the c-axis. This implied a structural control on the radar signal return primarily through the major elements affecting radar attenuation in sea ice, the brine inclusions. We have previously shown how brine platelet spacing aligns well with c-axis direction within any given crystal and also that large areas of sea ice have pronounced azimuthal alignments of the c-axes in response to currents under the ice cover. These alignments also control the brine inclusion geometry and affect the strength of the radar returns. To examine the observed radar anisotropy, Golden and Ackley (1981) used the mixture dielectric constants with some assumptions regarding brine pocket geometry to model the radar behavior of sea ice. Figure 92 shows a typical salinity temperature profile from the Alaskan Arctic and the computed brine volume profile. To depict the radar behavior, the profile was divided into 10-cm lengths with the dielectric constant at each level computed by eq 81 from the computed brine volume at that level. Direct information on the brine inclusion geometry was not available for this data set (nor are such observations generally available), so an assumed profile was taken to compute the depolarization factor as a function of depth. Since the depolarization factor is dependent only on the axial ratio, these were varied from the top to the bottom of the ice. At the bottom, previous measurements (Anderson and Weeks 1958, Kovacs and Morey 1978, Weeks and Assur 1967) indicated reasonable ratios of the ellipsoidal axes were of the order of $a:b:c = 30:1:5$ (here the a-axis direction is in the vertical plane and normal to the direction of the crystallographic c-axis). Near the top of the ice sheet a frazil-like initial layer probably formed, with more isotropic characteristics of the brine inclusions. These were assumed to be in the ratio $a:b:c = 1:1:0.5$. The brine inclusion geometries (a and c dimensions) were then taken to vary linearly between these values. Later data (Langhorne et al. 1980) on brine inclusion geometry in oriented ice showed the variation in axial ratios to follow similar patterns to the brine volumes so the most extreme excursions were concentrated in the bottom few centimeters.

As we show later, this can only enhance the behavior derivable from the assumed linear changes. The dielectric constant profiles for the two directions are shown as a function of depth in Figure 93. The

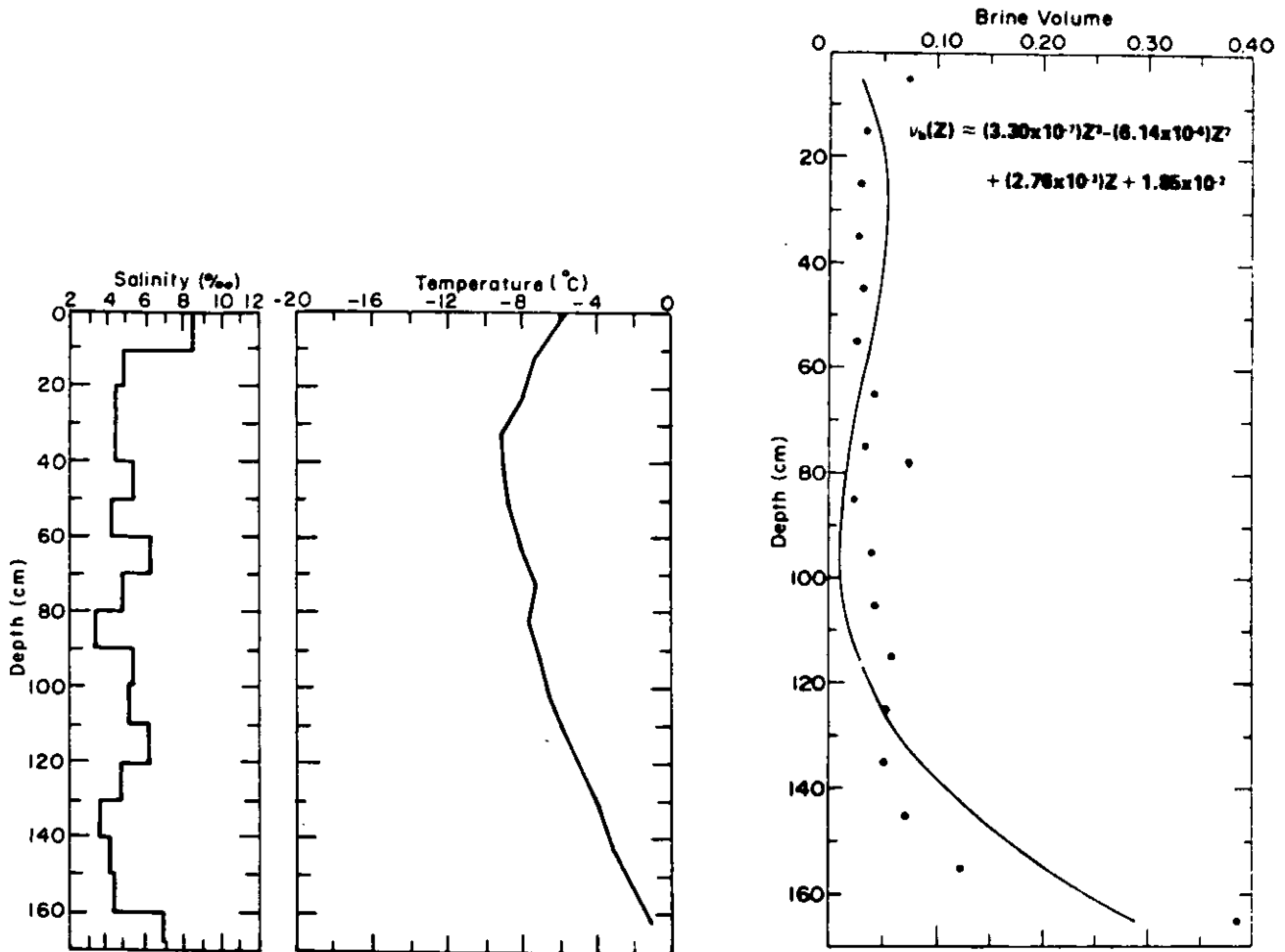


Figure 92. Ice salinity-temperature and brine volume profile from the Alaskan Arctic (Harrison Bay) (Golden and Ackley 1981).

normal polarization indicates the E-field parallel to the preferred c-axis (normal to the long axes of the ellipsoids) while the tangential polarization refers to the direction perpendicular to the c-axis. We see the strong anisotropy in the dielectric constants (particularly in $\epsilon''_{n,t}$), especially near the bottom of the ice where the brine volume and axial ratios dramatically increase. It is easy to imagine that if the inclusion geometry were allowed to vary directly with the brine volume then this behavior would be even more pronounced.

Figure 94 shows the power returned as a function of depth when a multilevel reflection, attenuation, and beam spreading model is used to calculate the returned power. The returned power for the two polarizations is down by more than one order of magnitude (6% compared to 0.3%), compatible with the radar attenuation observations. Large electric field penetration into the brine layers for the highly attenuated direction allows conduction effects to attenuate the wave. This in turn reduces the power returned from the ice/water interface relative to the other direction.

The radar properties of sea ice, therefore, exhibit a response to the structural controls given by the ice sheet and are dependent

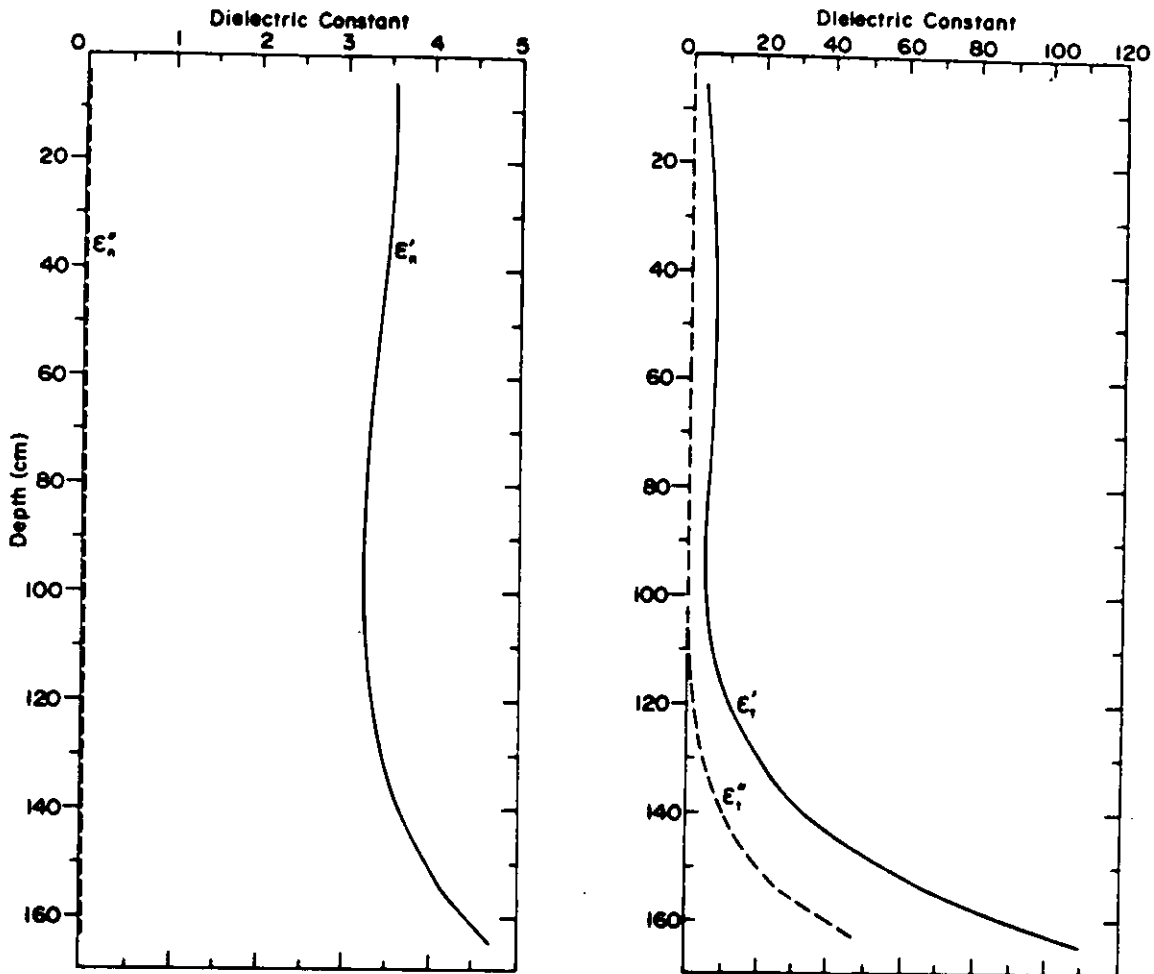


Figure 93. Computed depth-dielectric constant profiles using the brine volume profile from Figure 92 and assumed axial ratios of the inclusions at the top $a:b:c = 1:1:0.5$ and at the bottom $a:b:c = 30:1:5$ (Golden and Ackley 1981).

specifically on the salinity-temperature profile (determining the brine volume) and, where strong anisotropy is observed, on the macroscopic manifestations of the brine inclusion geometries as given by the depth variation of the axial ratios of the inclusions.

In the future by suitable radar modeling and sounding of sea ice, active radar measurements could provide a nondestructive means of determining sea ice structure by inverting the return radar signals and calculating the brine volume and brine inclusion geometry profiles that lead to the observed power levels.

Passive Microwave Emission Characteristics of Sea Ice

As we noted in the last section, active radar returns reflect the physical properties of the medium. Similarly, passive emissions are another technique used to acquire information on the intrinsic dielectric properties and also upon factors such as surface roughness, layering, and internal or volume scattering of the ice. Passive microwave emission is the thermal emission at microwave frequencies due to black

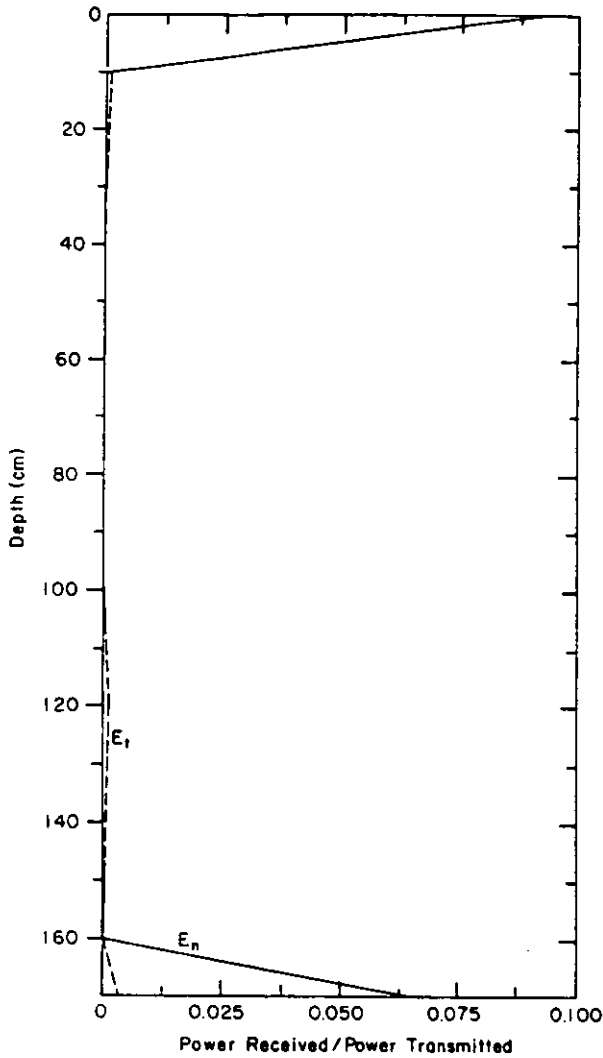


Figure 94. Simulated returned power/ incident power vs depth for profiles shown in Figures 92 and 93 (Golden and Ackley 1981).

body radiation by the material. It therefore has the additional characteristics of dependence on the thermal temperature as well as the dielectric properties of the material.

Stogryn (1970) developed the theory for a vertically structured medium that is smooth, flat, and semi-infinitely extended and shows continuous variations in dielectric properties and temperature with depth. If the dielectric properties and thermal temperature are known with depth, and if the brightness temperature of the radiation incident upon the surface is known, then the brightness temperature (horizontally polarized) at polar angle θ and frequency ν is

$$T(\theta, \nu) = |R_h(\theta, \nu)|^2 T_{\text{sky}}(\theta, \nu) + 4 \left(\frac{2\pi\nu}{c}\right)^3 \cos\theta \int_{-\infty}^0 T(z') |A(z')|^2 \text{Im}[\epsilon(z', \nu)] dz' \quad (85)$$

where T_{sky} , the incident radiation, is due to atmospheric attenuation and reradiation of cosmic noise, and R_h , c , $T(z')$, $\epsilon(z', f)$ are the horizontal reflection coefficient, the speed of light, the temperature at depth z' , and the complex dielectric constant respectively ($\text{Im}[\epsilon(z', \nu)]$ is the imaginary part of the dielectric constant).

For application to sea ice we note the clear dependence of the parameters mentioned, first the temperature with depth and second the dielectric constant. The dependence of the brightness temperature on the imaginary part of the dielectric constant is also of note, since for first-year sea ice this is controlled almost exclusively by the brine volume profile. As with the radar model previously mentioned, the only dependence here is on the aggregate or mixture properties of the material and not on the individual geometries of the other components of the other materials in the ice matrix (air, brine, and solid salts). However, a comparison of such a theory with observations of brightness temperature of sea ice did not give good agreement (Poe et al. 1972). Similarly, theoretical results from a surface roughness theory using Kirchoff approximations also did not provide good agreement, although parameterization of the surface backscatter coefficients appears to be a necessary component in any of these models.

A discussion of surface backscatter is both beyond our scope and somewhat independent of our theme, which is to understand some of the relationships between internal sea ice properties and observed emission characteristics. We therefore only mention it as one of the necessities in the complete description of the emission characteristics. England (1975) notes that surface roughness, while not easily treated theoretically, is visually apparent, so cautious interpretations of its effect can be made.

For the case of sea ice at microwave frequencies, a more important effect which must be included to improve the agreement between theory and observation is a consideration of volume scatterers within the ice. The field intensity calculations from scattering phenomena are somewhat burdened with notation, so the more interested reader is advised to consult the references for details. Scattering can be conveniently divided into three tasks (England 1975). These are 1) the derivation of the direct field intensity resulting from self emission of the medium and from sky radiance, as we discussed earlier based on the work of Stogryn (1970), 2) the derivation of the diffuse field resulting from radiation singly or multiply scattered from the direct field (this calculation involves the third task), and 3) the derivation of the relative scattering strength or scattering albedo in terms of wavelength, scatterer size and concentration, and dielectric properties. The derivation of the diffuse field is the notation-ridden exercise, while task 3, the scattering albedo, gives conditions more directly comparable to our purpose since it related most directly to the physical properties under discussion. A brief derivation of the scattering albedo, therefore, follows after England (1975). Simplifying assumptions are that the embedded particles are spherical and effectively separated so that interaction effects between scatterers are not considered. The Rayleigh scattering cross section σ is related to the size parameter (the ratio of scatterer diameter to free space wavelength) and to the dielectric constant (the ratio of the dielectric constant of the scatterer (brine or air) to that of the layer (ice)). Spheres of diameter d and dielectric constants ϵ_2 embedded in a medium whose dielectric constant is ϵ_1 have an average dipole moment (Stratton 1941)

$$\bar{P} = 4\pi\epsilon_1 \epsilon_0 \left[\frac{\epsilon_2/\epsilon_1 - 1}{\epsilon_2/\epsilon_1 + 2} \right] \frac{\bar{d}^3}{8} E_0 \quad (86)$$

where ϵ_0 is the free space permittivity, E_0 is the incident electric field strength (or emitted radiation strength from below), and \bar{d} is the mean diameter of the scatterers. The average outward energy flow \bar{P} from the scatterer is

$$\bar{P} = \left(\frac{\mu}{\epsilon_1 \epsilon_0}\right)^{1/2} \frac{\omega^4 \bar{P}^2}{12\pi} \left(\frac{\epsilon_1}{c^2}\right) \quad (87)$$

where μ is the permeability ($\mu = \mu_0$ for the dielectrics of interest), $\omega (= 2\pi f)$ is the angular frequency of the incident wave, and c is the free space velocity of light. Poynting's relation yields the energy flow per unit area of the source wave (the energy flow prior to scattering encounter),

$$\bar{S} = \frac{1}{2} (E_0)^2 (\epsilon_1 \epsilon_0 / \mu_0)^{1/2} \quad (88)$$

so that the average scattering cross section $\sigma = \bar{P}/\bar{S}$ is

$$\bar{\sigma} = \frac{2}{3} \pi^5 \left(\frac{\bar{d}}{\lambda_0}\right)^3 \frac{\epsilon_1^2}{\lambda_0} \bar{d}^3 \left[\frac{\epsilon_2/\epsilon_1 - 1}{\epsilon_2/\epsilon_1 + 2}\right]^2 \quad (89)$$

where $\lambda_0 = \frac{2\pi c}{\omega}$ and $\mu_0 = \frac{1}{c^2 \epsilon_0}$ are used.

If f^* is the volume fraction of scatterers in the layer (related to the ice density for air inclusions) then

$$f^* = \bar{N} \frac{4}{3} \pi \left(\frac{\bar{d}}{2}\right)^3 = \bar{N} \pi \frac{\bar{d}^3}{6} . \quad (90)$$

The scattering loss is the number of scatterers times the scattering cross section per scatterer or

$$\bar{N} \bar{\sigma} = \frac{2\pi (\epsilon_1)^{1/2} \tan \delta_1}{\lambda_0} S_c f^* \quad (91)$$

where $\tan \delta_1 = \epsilon''_1 / \epsilon'_1$ is the loss tangent and

$$S_c = (2\pi)^3 \left(\frac{\bar{d}}{\lambda_0}\right) \left[\frac{\epsilon_1}{\tan \delta_1}\right]^{3/2} \left[\frac{\epsilon_2/\epsilon_1 - 1}{\epsilon_2/\epsilon_1 + 2}\right]^2 . \quad (92)$$

The total loss α_1 in the layer is the sum of the scattering loss $N \sigma$ and the dielectric loss $2\beta_1$ where

$$\alpha_1 = \bar{N} \bar{\sigma} + 2\beta_1 \quad (93)$$

and

$$2\beta_1 = [2\pi(\epsilon_1)^{1/2}/\lambda_0] \tan \delta_1 . \quad (94)$$

(Here the appropriate values for ϵ_1 , $\tan\delta_1$ could be the mixture dielectric constant and loss tangent instead of the ice constants if scattering is small, in analogy to the active radar parameterization shown earlier.)

A useful parameter to estimate the influence of scattering is the scattering albedo ω_0 which is defined as the ratio of scattering loss to total loss in the layer or

$$\omega_0 = \frac{\overline{N} \overline{\sigma}}{\overline{N} \overline{\sigma} + 2\beta_1} \quad (95)$$

Naturally, if ω_0 is small then the contribution to total loss from scattering is small so we can define combinations of frequency ranges, concentrations of scatterers and dielectric properties where scattering has to be taken into account. We will now show a few simulations of these parameters of interest.

Figure 95 shows the scattering albedo versus d/λ_0 (ratio of scatterer size to wave length) with the volume fraction as a parameter for ice overlying fresh water. We note the middle three curves $f = (.05, .1, .2)$ are typical air content values seen in multiyear sea ice (Meeks et al. 1974). These curves indicate that "significant" contributions to the total loss from scattering occur at a minimum fractional diameter to wavelength ratio of about 0.1. From the limited data on multiyear sea ice, air bubble sizes varying from 0.5 mm to several millimeters (Poe et al. 1974) are observed, indicating a wavelength cutoff of about 0.5 to 1 cm where scattering losses become important and indeed dominate the emission character of multiyear ice. This corresponds to frequencies greater than 1-3 GHz.

The effects of brightness temperature as would be sensed by an above-surface radiometer are shown in Figure 96 where the scatter-induced brightness temperature change is plotted versus scattering albedo as a function of the layer thickness to wavelength ratio. Generally for thin layers (low D/λ_0) the brightness temperature induced by scattering increases, while for thick layers (high D/λ_0) the brightness temperature drops for almost all values of scattering albedo. The conclusion is that where we have "significant" values of scattering albedo (>0.5) the major effect seen will be for thicker layers of scattering material and that change will be a drop in brightness temperature. This behavior is what is typically observed for multiyear ice in the Arctic, with lower brightness temperatures implying significantly more scattering and layer thickness at the higher frequencies than for first-year ice. As the dielectric loss (non-scattering part, $2\beta_1$) increases, the effect of layer thickness drops off. This behavior also is indicated in the equation for scattering albedo ω_0 , where increasing numbers of scatterers would be required for the scattering to dominate the ordinary dielectric loss, $2\beta_1$. For first-year ice, which is both lossy and of lower air content, the influence of scatter-induced changes on brightness temperature are commensurately less than for multiyear ice. In first-year ice, the scatterers are primarily the brine pockets, which have a dimension of about 0.1 mm and are effective as scatterers only at high frequencies (20-40 GHz). However, this point is still inconclusive

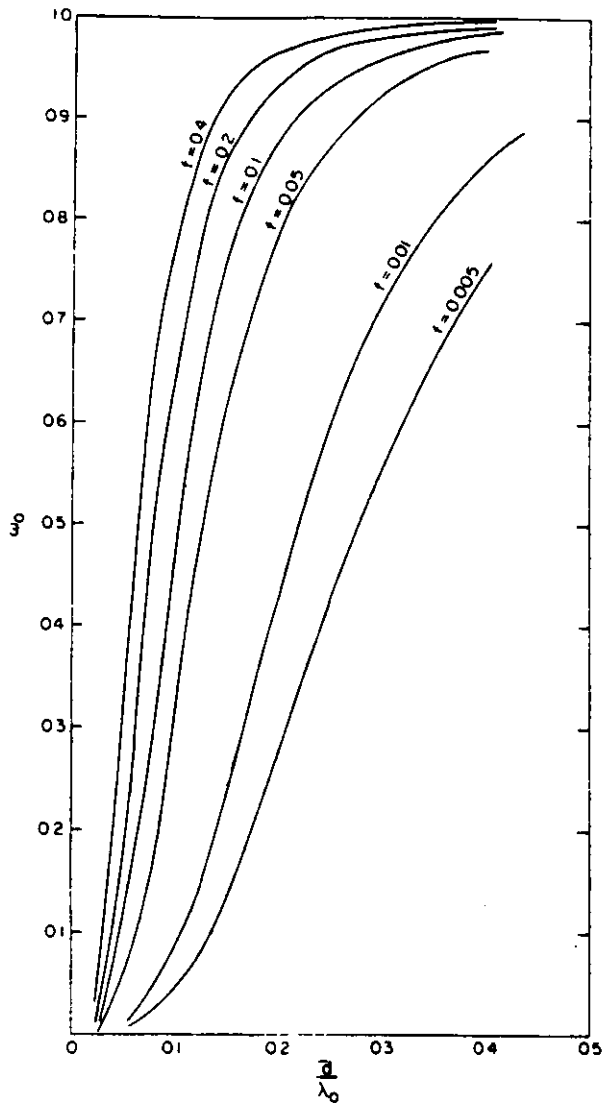


Figure 95. Scattering albedo (ω_0) vs scatterer size to wavelength ratio (d/λ_0) for ice overlying fresh water. The volume fraction of scatterers (f) is the parameter on the curves (England 1975).

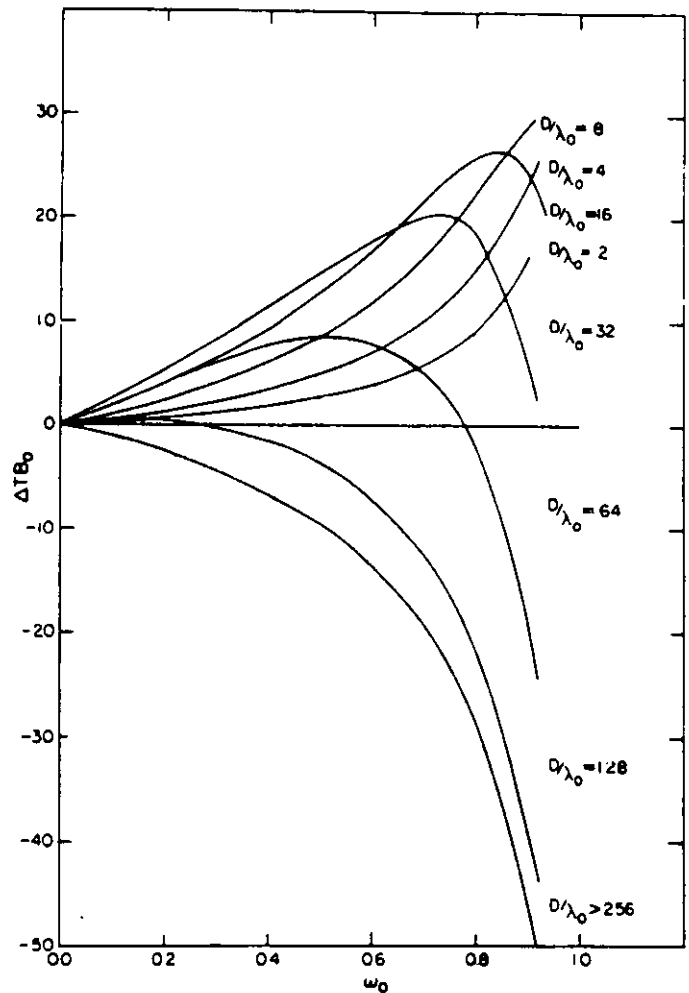


Figure 96. Changes in brightness temperature (ΔTB_0) plotted against scattering albedo (ω_0) with the layer thickness to wavelength ratio (D/λ_0) as a parameter (England 1975).

without detailed information on the brine pocket geometries or a solid theoretical base which would permit calculations of scattering from strong fluctuations (Poe et al. 1974). While the general behavior can be seen from this type of calculation, other authors (Poe et al. 1972, Fung 1981) note that correlation function techniques (small perturbation method), the distorted Born approximation, and generally more sophisticated solutions to the wave equation are probably necessary in order for a complete specification of the sea ice scattering problem. These calculations are, however, significantly limited by the current lack of data on the physical properties of sea ice, specifically a detailed knowledge of the brine pocket and air bubble geometries, and the variation in the mean values of the dielectric constants as function of depth.

CONCLUDING STATEMENT

In this paper we have attempted to give the reader a general knowledge of the current state of understanding of the structure of sea ice, how and why it develops and varies, and a few examples of how these variations can affect the bulk properties of the ice. Progress in this field has been slow, largely as the result of a lack of support for such work. This is unfortunate in that, as we hope was shown in the paper, an understanding of the ice structure is essential as the foundation upon which the science of the property variations of sea ice must be built.

LITERATURE CITED

- Ackley, S.F. (1982) Ice scavenging and nucleation: Two mechanisms for incorporation of algae into newly forming sea ice. AGU-ASLO Ocean Sciences Meeting, San Antonio (abstract to be published in EOS).
- Ackley, S.F. and T.E. Keliher (1979) Ice sheet internal radio-echo reflections and associated physical property changes with depth. J. Geophys. Res., vol. 84, no. 80.
- Adams, C.M., D.M. French and W.D. Kingery (1963) Field solidification and desalination of sea ice. In Ice and Snow: Properties, Processes and Applications (W.D. Kingery, Ed.), Cambridge, Mass.: MIT Press, p. 277-288.
- Addison, J.R. (1977) Impurity concentrations in sea ice. J. Glaciol., vol. 18, no. 78, p. 117-127.
- Anderson, D.L. (1958) A model for determining sea ice properties. In Arctic Sea Ice. U.S. National Academy of Sciences - National Research Council, Pub. 598, p. 148-152.
- Anderson, D.L. (1960) The physical constants of sea ice. Research, vol. 13, no. 8, p. 310-318.
- Anderson, D.M. and W.F. Weeks (1958) A theoretical analysis of sea ice strength. Trans. Am. Geophys. U., vol. 39, no. 4, p. 632-640.
- Arakawa, K. (1954) Studies on the freezing of water, II. J. Faculty Sci. Hokkaido Univ., Ser II, vol. 4, p. 311-339.
- Arakawa, K. and K. Higuchi (1954) On the freezing process of aqueous solutions. Low Temp. Sci., A 12, p. 73-86 (in Japanese).
- Armstrong, T., B. Roberts and C. Swithinbank (1966) Illustrated glossary of snow and ice. Scott Polar Research Institute, Special Pub. No. 4, 60 p.
- Assur, A. (1958) Composition of sea ice and its tensile strength. In Arctic Sea Ice. U.S. National Academy of Sciences - National Research Council, Pub. 598, p. 106-138.

- Assur, A. and W.F. Weeks (1964) Growth, structure, and strength of sea ice. USA Cold Regions Research and Engineering Laboratory, Research Report 135, 19 p.
- Bari, S.A. and J. Hallett (1974) Nucleation and growth of bubbles at an ice-water interface. J. Glaciol., vol. 13, no. 69, p. 489-520.
- Barrett, C.S. (1952) Structure of Metals. New York: McGraw-Hill.
- Bennington, K.O. (1959) Preliminary report on sea ice crystal fabrics on Station Charlie. In Semi-Annual Report, 1 December 1959, Drifting Station Charlie, Project Husky Nonr. 477(24) T.O. 307-252.
- Bennington, K.O. (1963a) Some crystal growth features of sea ice. J. Glaciol., vol. 4, no. 36, p. 669-688.
- Bennington, K.O. (1963b) Some chemical composition studies on arctic sea ice. In Ice and Snow - Processes, Properties, and Applications (W.D. Kingery, Ed.), Cambridge, Mass.: MIT Press, p. 248-257.
- Bergdahl, L. (1977) Physics of Ice and Snow as Affects Thermal Pressure. Göteborg, Sweden: Chalmers University of Technology, Department of Hydraulics, Rept. Series A:1, 158 p.
- Bilello, M.A. (1961) Ice thickness observations in the North American Arctic and Subarctic for 1958-59, 1959-60. USA Cold Regions Research and Engineering Laboratory, Special Report 43, 43 p.
- Blinov, L.K. (1965) The salt content of sea water and sea ice. Trudy Gos. Okeanograf. Inst., no. 81, p. 5-55.
- Bolling, G.F. and W.A. Tiller (1960) Growth from the melt. I: Influence of surface intersections in pure metals. J. Appl. Phys., vol. 31, p. 1345-1350.
- Bragg, W.H. (1922) The crystal structure of ice. Proc. Phys. Soc., vol. 34, p. 98-103.
- Buck, K.R. and D. Garrison (1982) Sea ice algal communities in the Weddell Sea. II: Population comparisons between the water column and sea ice. AGU-ASLO Ocean Sciences Meeting, San Antonio (abstract to be published in EOS).
- Burton, J.A., R.C. Prim and W.P. Slichter (1953) The distribution of solute in crystals grown from the melt. Part I: Theoretical. J. Chem. Phys., vol. 21, p. 1987-1991.
- Campbell, K.J. and A.S. Orange (1974) The electrical anisotropy of sea ice in the horizontal plane. J. Geophys. Res., vol. 79, no. 33, p. 5059-5063.
- Carlsaw, H.S. and J.C. Jaeger (1959) Conduction of Heat in Solids. Oxford University Press, 510 p.
- Carte, A.E. (1961) Air bubbles in ice. Proc. Phys. Soc. (London), vol. 77, no. 495, p. 757-768.

- Cherepanov, N.V. (1957) Using the methods of crystal optics for determining the age of drift ice. Problemy Arktiki, vol. 2, p. 179-184 (in Russian).
- Cherepanov, N.V. (1964) Structure of sea ice of great thickness. Trudy Arkt. i Antarkt. N.I. Institut, vol. 367, p. 13-18.
- Cherepanov, N.V. (1971) Spatial arrangement of sea ice crystal structure. Prog. Arkt. i Antarkt., vol. 38, p. 176-181.
- Colbeck, S. (1979) Grain clusters in wet snow. J. Coll. Inter. Sci., vol. 72, no. 3.
- Coriell, S.R., M.R. Cordes, W.J. Boettinger and R.F. Sekerka (1980) Convective and interfacial instabilities during unidirectional solidification of a binary alloy. J. Cryst. Growth, vol. 49, no. 1, p. 13-28.
- Cox, G.F.N. and W.F. Weeks (1975) Brine drainage and initial salt entrapment in sodium chloride ice. USA Cold Regions Research and Engineering Laboratory, Research Report 354, 85 p.
- Cox, G.F.N. and W.F. Weeks (1974) Salinity variations in sea ice. J. Glaciol., vol. 13, no. 67, p. 109-120.
- Cox, G.F.N. and W.F. Weeks (1982) Equations for determining the gas and brine volumes in sea ice samples. USA Cold Regions Research and Engineering Laboratory, CRREL Report (in press).
- Dayton, P.K. and S. Martin (1971) Observations of ice stalactites in McMurdo Sound, Antarctica. J. Geophys. Res., vol. 76, p. 1595-1599.
- Dunbar, M. and W.F. Weeks (1975) Interpretation of young ice forms in the Gulf of St. Lawrence using side-looking airborne radar and infrared imagery. USA Cold Regions Research and Engineering Laboratory, Research Report 337, 41 p.
- Eddie, D.D. and D.J. Kirwan (1973) Impurity trapping during crystallization from melts. Ind. Eng. Chem. Fundam., vol. 12, p. 100-106.
- Eide, L. and S. Martin (1975) The formation of brine drainage features in young sea ice. J. Glaciol., vol. 14, no. 70, p. 137-154.
- Elbaum, C. (1959) Substructures in crystals grown from the melt. Prog. Met. Phys., vol. 8, p. 203-253.
- England, A.W. (1975) Thermal microwave emission from a scattering layer. J. Geophys. Res., vol. 80, no. 32, p. 4484-4496.
- Evans, S. (1965) Dielectric properties of snow and ice: A review. J. Glaciol., vol. 5, p. 773.
- Farhadieh, R. and R.S. Tankin (1972) Interferometric study of freezing of sea water. J. Geophys. Res., vol. 77, p. 1647-1657.

- Foldvik, A. and T. Kvinge (1974) Conditional instability of sea water at the freezing point. Deep Sea Res., vol. 21, p. 169-174.
- Frankenstein, G. and R. Garner (1967) Equations for determining the brine volume of sea ice from -0.5° to -22.9°C . J. Glaciol., vol. 6, no. 48, p. 943-944.
- Fujino, K. and Y. Suzuki (1959) Observations on the process of ice rind formation on the surface of still water. Low Temp. Sci., A 18, p. 149-155 (in Japanese).
- Fujioka, T. and R.F. Sekerka (1974) Morphological stability of disc crystals. J. Cryst. Growth, vol. 24/25, p. 84-93.
- Fukutomi, T., K. Kusunoki and T. Nagashima (1949) On the formation of crystal ice and the structure of ice crust. Low Temp. Sci., vol. 2, p. 73-76 (in Japanese).
- Fukutomi, T., M. Saito and Y. Kudo (1953) Study of sea ice (the 16th report): On the structure of ice rind, especially on the structure of thin ice sheet and ice-sheet block. Low Temp. Sci., vol. 9, p. 113-123 (in Japanese).
- Fung, A. (1981) Microwave scattering and emission from sea ice. Proceedings of Second Workshop on Microwave Remote Sensing of Sea Ice and Icebergs, NASA Langley Research Center.
- Garrison, D. and K.R. Buck (1982) Sea ice algal communities in the Weddell Sea. I: Biomass distribution and the physical environment. AGU-ASLO Ocean Sciences Meeting, San Antonio (abstract to be published in EOS).
- Gitterman, K.E. (1937) Thermal analysis of sea water. Trudy Solyanoy Lab. Akad. Nauk SSR, No. 15(1) (in Russian).
- Glen, J.W. (1955) Comments on the paper of Professor Arakawa on the growth of ice crystals in water. J. Glaciol., vol. 2, p. 483.
- Golden, K.M. and S.F. Ackley (1981) Modeling of anisotropic electromagnetic reflection from sea ice. J. Geophys. Res (in press).
- Golovkov, M.P. (1936) K petrografii l'da Karskogo moria (The petrography of Kara sea ice). Leningrad: Vsesoiuznyi Arkticheskii Institut, Trudy 60, p. 7-40.
- Gow, A.J. and S. Epstein (1972) On the use of stable isotopes to trace the origins of ice in a floating ice tongue. J. Geophys. Res., vol. 77, no. 33, p. 6552-6557.
- Gow, A.J. and D. Langston (1977) Growth history of lake ice in relation to its stratigraphic, crystalline and mechanical structure. USA Cold Regions Research and Engineering Laboratory, CRREL Report 77-1, 24 p.
- Gow, A.J. and W.F. Weeks (1977) The internal structure of fast ice near

- Narwhal Island, Beaufort Sea, Alaska. USA Cold Regions Research and Engineering Laboratory, CRREL Report 77-29, 8 p.
- Gow, A.J., S.F. Ackley, W.F. Weeks and J.W. Govoni (1982) Physical and structural characteristics of Antarctic sea ice. Third International Symposium on Antarctic Glaciology, Ohio State University, Annals Glaciol.
- Gow, A.J., W.F. Weeks, J.W. Govoni and S.F. Ackley (1981) Physical and structural characteristics of sea ice in McMurdo Sound. Ant. J. U.S. (in press).
- Gudmandsen, P. (1971) Electromagnetic probing of ice. In Electromagnetic Probing in Geophysics (J.R. Wait, Ed.), Boulder, Colorado: Golem Press, p. 321-338.
- Hallett, J. (1960) Crystal growth and the formation of spikes in the surface of supercooled water. J. Glaciol., vol. 3, p. 698-702.
- Hardy, S.C. and S.R. Coriell (1973) Surface tension and interface kinetics of ice crystals freezing and melting in sodium chloride solutions. J. Cryst. Growth, vol. 20, p. 292-300.
- Harrison, J.D. and W.A. Tiller (1963) Controlled freezing of water. In Ice and Snow - Processes, Properties, and Applications (W.D. Kingery, Ed.), Cambridge, Mass.: M.I.T. Press, p. 215-225.
- Harrison, J.D. (1965) Measurement of brine droplet migration in ice. J. Appl. Phys., vol. 36, no. 12, p. 3811-3815.
- Hillig, W.B. (1958) The kinetics of freezing of ice in the direction perpendicular to the basal plane. In Growth and Perfection of Crystals (R.H. Doremus, Ed.), New York: Wiley, p. 350-359.
- Hillig, W.B. (1959) Kinetics of solidification from nonmetallic liquids. In Kinetics of High Temperature Processes (W.D. Kingery, Ed.), New York: Wiley, p. 127-135.
- Hillig, W.B. and D. Turnbull (1956) Theory of crystal growth in undercooled pure liquids. J. Chem. Phys., vol. 24, p. 914.
- Hobbs, P. (1974) Ice Physics. Oxford University Press, 837 p.
- Hoekstra, P., T.E. Osterkamp and W.F. Weeks (1965) The migration of liquid inclusions in single ice crystals. J. Geophys. Res., vol. 70, no. 20, p. 5035-5041.
- Johnson, N.G. (1943) Studies av isen i Gullmarfjorden. Svenska Hydrog. - Biol. Komm. Skr., Ny Serie: Hydrografi, 18, p. 1-21.
- Jones, D.R.H. (1973) The temperature-gradient migration of liquid droplets through ice. J. Cryst. Growth, vol. 20, p. 145-151.
- Jones, D.R.H. (1974) Determination of the kinetics of ice-brine interfaces from the shapes of migrating droplets. J. Cryst. Growth, vol. 26, p. 177-179.

- Kamb, W.B. (1959) Theory of preferred crystal orientation developed by crystallization under stress. J. Geol., vol. 67, p. 153-170.
- Katsaros, K.B. (1973) Supercooling at the surface of an arctic lead. J. Phys. Ocean., vol. 3, no. 4, p. 482-486.
- Kawamura, T. and N. Ono (1980) Freezing phenomena at seawater surface opening in polar winter. III. Measurement of crystallographic orientation of newly grown sea ice. Low Temp. Sci., A(39), p. 175-180.
- Kingery, W.D. and W.H. Goodnow (1963) Brine migration in salt ice. In Ice and Snow: Properties, Processes and Applications (W.D. Kingery, Ed.), Cambridge, Mass.: MIT Press, p. 35-47.
- Knight, C.A. (1962a) Curved growth of ice on surfaces. J. Appl. Phys., vol. 33, p. 1808-1815.
- Knight, C.A. (1962b) Migration of liquid inclusions parallel to the c-axis in single ice crystals: An origin for some striations. Can. J. Phys., vol. 40, p. 1681-1682.
- Knight, C.A. (1962c) Polygonization of aged sea ice. J. Geol., vol. 70, p. 240-246.
- Knight, C.A. (1962d) Studies of arctic lake ice. J. Glaciol., vol. 4, p. 319-335.
- Koerner, R.M. (1963) The Devon Island expedition, 1960-64. Arctic, vol. 16, p. 57-62.
- Kohnen, H. (1976) On the dc resistivity of sea ice. Z. Gletsch. und Glaz., vol. 11, no. 2, p. 143-154.
- Kovacs, A. and R. Morey (1978) Radar anisotropy of sea ice due to preferred azimuthal orientation of the horizontal c-axes of ice crystals. J. Geophys. Res., vol. 83, no. C12, p. 6037-6046.
- Kovacs, A. and R.M. Morey (1980) Investigations of sea ice anisotropy, electromagnetic properties, strength, and under-ice current orientation. USA Cold Regions Research and Engineering Laboratory, CRREL Report 80-20, 18 p.
- Kumai, M. and K. Itagaki (1953) Cinematographic study of ice crystal formation in water. J. Faculty Sci., Hokkaido Univ., Ser. II, 4, p. 235-246.
- Lake, R.A. and E.L. Lewis (1970) Salt rejection by sea ice during growth. J. Geophys. Res., vol. 75, no. 3, p. 583-597.
- Landauer, J.K. and H. Plumb (1956) Measurements of anisotropy of thermal conductivity of ice. USA Snow, Ice and Permafrost Research Establishment, Research Report 16.
- Langhorne, P. (1980) Crystal anisotropy in sea ice in the Beaufort Sea.

Proceedings, Workshop on Remote Estimation of Sea Ice Thickness,
Memorial University, St. Johns, Newfoundland, C-CORE Pub. 80-5, p.
189-224.

- Langhorne, P.J., J.R. Rossiter and T.E. Keliher (1980) Remote estimation of the properties of sea ice, ice core analysis, Beaufort Sea, March 1979. Memorial University, St. Johns, Newfoundland, C-CORE Pub. 80-7, 172 p.
- Langleben, M.P. (1959) Some physical properties of sea ice. II. Can. J. Phys., vol. 37, p. 1438-1454.
- Lewis, E.L. (1967) Heat flow through winter ice. In Physics of Snow and Ice (H. Oura, Ed.), Institute of Low Temperature Science, Hokkaido, vol. 1, no. 1, p. 611-631.
- Lewis, E.L. and R.A. Lake (1971) Sea ice and supercooled water. J. Geophys. Res., vol. 76, no. 24, p. 5836-5841.
- Lofgren, G. and W.F. Weeks (1969) Effect of growth parameters on the substructure spacing in NaCl ice crystals. J. Glaciol., vol. 8, no. 52, p. 153-164.
- Lonsdale, K. (1958) The structure of ice. Proc. Roy. Soc. (London), vol. 247, p. 424-434.
- Lyons, J.B., S.M. Savin, and A.J. Tamburi (1971) Basement ice, Ward Hunt Ice Shelf, Ellesmere Island, Canada. J. Glaciol., vol. 10, no. 58, p. 93-100.
- Macklin, W.C. and B.F. Ryan (1966) Habits of ice grown in supercooled water and aqueous solutions. Phil. Mag., vol. 14, p. 847-860.
- Malmgren, F. (1927) On the properties of sea ice. Sci. Results Norwegian North Pole Exped. "Maud", 1918-1925, vol. 1, no. 5, 67 p.
- Martin, S. (1972) Ice stalactites and the desalination of sea ice. Naval Research Reviews, vol. XXV, no. 9, p. 17-26.
- Martin, S. (1974) Ice stalactites: Comparison of a laminar flow theory with experiment. J. Fluid Mech., vol. 63, no. 1, p. 51-79.
- Martin, S. (1979) A field study of brine drainage and oil entrapment in sea ice. J. Glaciol., vol. 22, no. 88, p. 473-502.
- Martin, S. (1981) Frazil ice in rivers and oceans. Ann. Rev. Fluid Mech., vol. 13, p. 379-397.
- Martin, S. and P. Kauffman (1974) The evolution of under-ice melt ponds, or double diffusion at the freezing point. J. Fluid Mech., vol. 64, no. 3, p. 507-527.
- Martin, S. and P. Kauffman (1981) A field and laboratory study of wave damping by grease ice. J. Glaciol., vol. 27, no. 96.

- Maxwell, J.C. (1891) Electricity and Magnetism, 3rd ed., Vol. I. New York: Dover.
- Maykut, G. and N. Untersteiner (1971) Some results from a time-dependent thermodynamic model of sea ice. J. Geophys. Res., vol. 76, p. 1550-1576.
- Meeks, D.C., G.A. Poe and R.O. Ramseier (1974) A study of microwave emission properties of sea ice - AIDJEX 1972. Aerojet Electro-systems Company, Azusa, California, Final Report No. 1786FR-1.
- Mellor, M. (1982) Mechanical behavior of sea ice. U.S. Army Cold Regions Research and Engineering Laboratory, CRREL Report (in press).
- Myerson, A.S. and D.J. Kirwan (1977a) Impurity trapping during dendritic crystal growth. 1. Computer simulation. Ind. Eng. Chem., Fund., vol. 16, no. 4, p. 414-420.
- Myerson, A.S. and D.J. Kirwan (1977b), Impurity trapping during dendritic crystal growth. 2. Experimental results and correlation. Ind. Eng. Chem., Fund., vol. 16, no. 4, p. 420-425.
- Nagle, J.F. (1966) Lattice statistics of hydrogen bonded crystals. I. The residual entropy of ice. J. Math. Phys., vol. 7, p. 1484-1491.
- Nakawo, M. and N.K. Sinha (1981) Growth rate and salinity profile of first-year sea ice in the high Arctic. J. Glaciol., vol. 27, no. 96, p. 315-330.
- Nakawo, M. and N.K. Sinha (in press) Brine layer spacing of first-year sea ice. J. Geophys. Res.
- Nelson, K.H. and T.G. Thompson (1954) Deposition of salts from sea water by frigid concentration. J. Marine Res., vol. 13, no. 2, p. 166-182.
- Niedrauer, T.M. and S. Martin (1979) An experimental study of brine drainage and convection in young sea ice. J. Geophys. Res., vol. 84, no. C3, p. 1176-1186.
- Ono, N. (1965) Thermal properties of sea ice II. A method for determining the K/c_p value of a non-homogeneous ice sheet. Low Temp. Sci., vol. A23, p. 177-183 (in Japanese).
- Ono, N. (1968) Thermal properties of sea ice. IV. Thermal constants of sea ice. Low Temp. Sci., vol. A26, p. 329-349 (in Japanese).
- Owston, P.G. (1958) The structures of ice I, as determined by X-ray and neutron diffraction analysis. Adv. Phys., vol. 7, p. 171-188.
- Ozum, B. and D.J. Kirwan (1976) Impurities in ice crystals grown from stirred solutions. A.I.Ch.E. Sympos. Series, vol. 72, no. 153, p. 1.
- Paige, R.A. (1966) Crystallographic studies of sea ice in McMurdo Sound,

- Antarctica. Naval Civil Engineering Laboratory, Technical Report R494, 31 p.
- Paige, R.A. (1970) Stalactite growth beneath sea ice. Science, vol. 167, p. 171-172.
- Paige, R.A. and R.A. Kennedy (1967) Strength studies of sea ice — effect of load rate on ring tensile strength. Naval Civil Engineering Laboratory, Technical Report R545, 25 p.
- Patterson, M.S. (1973) Nonhydrostatic thermodynamics and its geologic applications. Rev. Geophys. Space Phys., vol. 11, p. 355-389.
- Pauling, L. (1935) Structure and entropy of ice and of other crystals with randomness of atomic arrangements. J. Am. Chem. Soc., vol. 57, p. 2608-2684.
- Perey, F.G.J. and E.R. Pounder (1958) Crystal orientation in ice sheets. Can. J. Phys., vol. 36, p. 494-502.
- Peterson, S.W. and H.A. Levy (1957) A single-crystal neutron diffraction study of heavy ice. Acta Crystallographica, vol. 10, p. 70-76.
- Petrov, I.G. (1954-55) Fiziko-mekhanicheskiye svoystva i tol'shchina ledyanogo pokrova (Physical and mechanical properties and thickness of ice cover). In Materialy Nablyudeniy Nauchno-Issledovatel'skoy Dreyfuyushchey Stantsii 1950-51 Goda (Observations of the Drifting Research Station of 1950-51) (M.M. Somov, Ed.), Arkticheskiy Nauchno-Issledovatel'skiy Institut 2, Leningrad, p. 103-165.
- Peyton, H.R. (1963) Some mechanical properties of sea ice. In Ice and Snow--Processes, Properties, and Applications (W.D. Kingery, Ed.), Cambridge, Mass.: MIT Press, p. 107-113.
- Peyton, H.R. (1966) Sea ice strength. Geophysical Institute, University of Alaska Rept. UAG-182, 187 p.
- Peyton, H.R. (1968) Sea ice strength — effects of load rates and salt reinforcement. In Arctic Drifting Stations (J.E. Sater, Ed.), Arctic Institute of North America, p. 197-217.
- Pfann, W.G. (1958) Zone Melting. New York: Wiley, 230 p.
- Poe, G., A. Stogryn and A.T. Edgerton (1972) Microwave emission characteristics of sea ice. Aerojet General Corp., Rept. 1749R-2.
- Poe, G.A., A. Stogryn, A.T. Edgerton and R.O. Ramseier (1974) Study of microwave emission properties of sea ice. Aerojet General Corp., Rept. 1804FR-1.
- Pounder, E.R. and E.M. Little (1959) Some physical properties of sea ice. I. Can. J. Phys., vol. 37, p. 443-473.
- Ragle, R.H. (1962) The formation of lake ice in a temperate climate. U.S. Army Cold Regions Research and Engineering Laboratory, Research Report 107.

- Reeburgh, W.S. and M.S. Young (1982) New measurements of sulfate and chlorinity in natural sea ice. J. Geophys. Res. (in press).
- Richardson, C. and E.F. Keller (1966) The brine content of sea ice measured with a nuclear magnetic resonance spectrometer. J. Glaciol., vol. 6, no. 43, p. 89-100.
- Ringer, W.E. (1906) De Veranderingen in Samenstelling van Zeewater by Het Bevriezen. Chemisch Weeleblad, vol. 3, p. 223-249.
- Rodhe, B. (1959) The Baltic ice code. Sveriges Meteorologiska och Hydrologiska Institut, Stockholm, Ser. E, No. 10, 59 p.
- Rohatgi, P.K. and C.M. Adams (1967a) Freezing rate distributions during unidirectional solidification of solutions. Trans. Metall. Soc. A.I.M.E., vol. 239, no. 6, p. 850-857.
- Rohatgi, P.K. and C.M. Adams (1967b) Ice-brine dendritic aggregate formed on freezing of aqueous solutions. J. Glaciol., vol. 6, no. 47, p. 663-679.
- Rosenberg, A. and W.A. Tiller (1957) The relationship between growth forms and the preferred direction of growth. Acta Met., vol. 5, p. 565-573.
- Rutter, J.W. and B. Chalmers (1953) A prismatic substructure formed during solidification of metals. Can. J. Phys., vol. 1, p. 15-39.
- Ryan, B.F. (1969) The growth of ice parallel to the basal plane in supercooled water and supercooled metal fluoride solutions. J. Cryst. Growth, vol. 5, p. 284-288.
- Ryan, B.F. and W.C. Macklin (1968) The growth of ice in supercooled aqueous solutions. J. Cryst. Growth, vol. 2, p. 337-340.
- Saito, T. and N. Ono (1980) Percolation of sea ice. II. Brine drainage channels in young sea ice. Low Temp. Sci., vol. A39, p. 127-132.
- Savel'ev, B.A. (1958) Izucheniye l'dov v rayone dreyfa stantsii SP-4 v period tayaniya i razrusheniya ikh v 1955 g (Study of ice in the region of the drift of station SP-4 during melting and break-up in 1955). Problemy Severa, vol. 2, p. 47-79.
- Savel'ev, B.A. (1963) Structure, composition, and properties of the ice cover of sea and fresh waters. Izd. Moskovskogo Univ., 541 p. (in Russian).
- Schwarz, J. and W.F. Weeks (1977) Engineering properties of sea ice. J. Glaciol., vol. 19, no. 81, p. 499-530.
- Schwarzacher, W. (1959) Pack-ice studies in the Arctic Ocean. J. Geophys. Res., vol. 64, p. 2357-2367.
- Schwerdtfeger, P. (1963) The thermal properties of sea ice. J. Glaciol., vol. 4, no. 36, p. 789-807.

- Seidensticker, R.G. (1965) Comment on paper by P. Hoekstra, T.E. Osterkamp and W.F. Weeks, "The migration of liquid inclusions in single ice crystals." J. Geophys. Res., vol. 71, no. 8, p. 2180-2181.
- Sekerka, R.F. (1968) Morphological stability. J. Cryst. Growth, vol. 3/4, p. 71-81.
- Sekerka, R.F., R.G. Seidensticker, D.R. Hamilton and J.D. Harrison (1967) Investigation of desalination by freezing. Office of Saline Water, Westinghouse Research Laboratories, Pittsburgh, Contract No. 14-01-0001-605, Final Report.
- Seligman, G. (1949) Growth of glacier crystal. J. Glaciol., vol. 1, p. 254-268.
- Serikov, M.I. (1963) Structure of Antarctic sea ice. Infor. Bull. Soviet Antarctic Exped., vol. 4, no. 5, p. 265-266.
- Serson, H.V. (1972) Investigation of a plug of multi-year old sea ice in the mouth of Nansen Sound. Defence Research Establishment, Ottawa, Technical Note 72-6, 4 p.
- Sharp, R.P. (1947) Suitability of ice for aircraft landings. Trans. Am. Geophys. Union, vol. 28, p. 111-119.
- Shumskii, P.A. (1955) K izucheniiu l'dov severnogo ledovitogo okeana (A study of ice in the Arctic Ocean). Vestnik Akademii Nauk SSSR, 25, No. 2, p. 33-38.
- Sinha, N.K. (1977) Technique for studying structure of sea ice. J. Glaciol., vol. 18, no. 79, p. 315-323.
- Smith, D.D. (1964) Ice lithologies and structure of ice island Arlis II. J. Glaciol., vol. 5, no. 37, p. 17-38.
- Smith, V.G., W.A. Tiller and J.W. Rutter (1955) A mathematical analysis of solute redistribution during solidification. Can. J. Phys., vol. 33, p. 723-745.
- Stander, E. and G.A. Gidney (1980) The measurement of finite strain in sea ice by impulse radar techniques. Proceedings Workshop on Sea Ice Field Measurement, Memorial University, St. Johns, Newfoundland, C-CORE Pub. No. 80-21, p. 127-164.
- Stogryn, A. (1970) The brightness temperature of a vertically structured medium. Radio Science, vol. 5, no. 12, p. 1397.
- Stogryn, A. (1971) Equations for calculating the dielectric constant of saline water at GHz frequencies. IEEE Trans. Microwave Theory and Techniques, vol. 19, no. 8, p. 273.
- Stratton, J. (1941) Electromagnetic Theory. New York: McGraw-Hill, p. 563-573.
- Suzuki, Y. (1955) Observations of ice crystals formed on sea surface. J. Ocean. Soc. Japan, vol. 11, p. 123-126.

- Suzuki, Y. (1967) On disorder entropy of ice. In Physics of Snow and Ice, Institute of Low Temperature Science, Hokkaido University, Vol. 1, No. 1, p. 21-41.
- Swinzow, G.K. (1966) Ice cover of an arctic proglacial lake. USA Cold Regions Research and Engineering Laboratory, Research Report 155, 43 p.
- Tabata, T. (1960) Studies on the mechanical properties of sea ice V. Measurement of flexural strength. Low Temp. Sci., vol. A19, p. 187-201.
- Tabata, T. and N. Ono (1957) On the structure of sea ice. Low Temp. Sci., vol. A16, p. 197-210 (in Japanese).
- Tabata, T. and N. Ono (1962) On the crystallographic study of several kinds of ice. Low Temp. Sci., vol. A20, p. 199-214 (in Japanese).
- Taylor, L.D. and J.B. Lyons (1959) Ice structures, Anglussa Lake, northwest Greenland. Geophysics Research Directorate, Air Force Cambridge Research Center, TN-59-461, 33 p.
- Tiller, W.A. (1962) Effect of grain boundaries on solute partitioning during progressive solidification. Acta Met., vol. 1, no. 4, p. 428-437.
- Tiller, W.A. (1963) Migration of a liquid zone through a solid. J. Appl. Phys., vol. 34, no. 9, p. 2757-2762.
- Tiller, W.A., K.A. Jackson, J.W. Rutter and B. Chalmers (1953) The redistribution of solute atoms during the solidification of metals. Acta Met., vol. 1, p. 428-437.
- Tinga, W.R., W.A. Voss and D.F. Blossey (1973) Generalized approach to multiphase dielectric mixture theory. J. Appl. Phys., vol. 44, no. 9, p. 3897-3903.
- Tsurikov, V.L. (1974) Statistics of salt composition in sea ice. Oceanology, vol. 14, no. 3, p. 360-367.
- Tsurikov, V.L. (1976) Liquid Phase in Sea Ice. Moscow: Nauka, 210 p. (in Russian).
- Tsurikov, V.L. and Tsurikova, A.P. (1972) The brine content of sea ice (statement of the problem). Oceanology, vol. 12, no. 5, p. 663-672.
- Turner, J.S. (1973) Buoyancy Effects in Fluids. Cambridge University Press, 367 p.
- U.S. Navy Hydrographic Office (1952) A functional glossary of ice terminology. Washington, D.C., 88 p.
- Untersteiner, N. (1961) On the mass and heat budget of arctic sea ice. Arch. Meteorol. Geophys. Biok., vol. 12, p. 151-182.

- Untersteiner, N. (1968) Natural desalination and equilibrium salinity profile of perennial sea ice. J. Geophys. Res., vol. 73, no. 4, p. 1251-1257.
- Untersteiner, N. and F. Badgley (1958) Preliminary results of thermal budget studies on arctic pack ice during summer and autumn. In Arctic Sea Ice, U.S. National Academy of Sciences-National Research Council Pub. 598, p. 85-98.
- Vant, M.R., R.O. Ramseier and V. Makros (1975) The complex dielectric constant of sea ice at frequencies in the range 0.1-40 GHz. J. Appl. Phys., vol. 49, no. 3, p. 1264-1280.
- Vittoratos, E.S. (1979) Existence of oriented sea ice by the McKenzie Delta. In POAC 79, Trondheim, Norway, p. 643-650.
- Wakatsuchi, M. (1977) Experiments on haline convection induced by freezing of sea water. Low Temp. Sci., vol. A35, p. 249-258 (in Japanese).
- Walker, E.R. and P. Wadhams (1979) Thick sea-ice floes. Arctic, vol. 32, no. 2, p. 140-147.
- Walton, D. and B. Chalmers (1959) The origin of the preferred orientation in the columnar zone of ingots. Trans. Metal. Soc. Am. Inst. Min. Met., Eng., vol. 215, p. 447-457.
- Walton, D., W.A. Tiller, J.W. Rutter and W.C. Winegard (1955) Instability of a smooth solid-liquid interface during solidification. J. Metals 7, Eng., vol. 215, p. 447-457.
- Weeks, W.F. (1958) The structure of sea ice: A progress report. In Arctic Sea Ice, U.S. National Academy of Sciences-National Research Council, Pub. 598, p. 96-98.
- Weeks, W.F. (1962) Tensile strength of NaCl ice. J. Glaciol., vol. 4, no. 31, p. 25-52.
- Weeks, W.F. and A. Assur (1963) Structural control of the vertical variation of the strength of sea and salt ice. In Ice and Snow - Processes, Properties, and Applications (W.D. Kingery, Ed.), Cambridge, Mass.: MIT Press, p. 258-276.
- Weeks, W.F. and A. Assur (1967) The mechanical properties of sea ice. USA Cold Regions Research and Engineering Laboratory, CRREL Monograph II-B3.
- Weeks, W.F. and A. Assur (1969) Fracture of lake and sea ice. USA Cold Regions Research and Engineering Laboratory, Research Report 269, 77 p.
- Weeks, W.F. and A.J. Gow (1978) Preferred crystal orientations along the margins of the Arctic Ocean. J. Geophys. Res., vol. 84, no. C10, p. 5105-5121.

- Weeks, W.F. and A.J. Gow (1980) Crystal alignments in the fast ice of arctic Alaska. J. Geophys. Res., vol. 84, no. C10, p. 1137-1146.
- Weeks, W.F. and G. Lofgren (1967) The effective solute distribution coefficient during the freezing of NaCl solutions. In Physics of Snow and Ice (H. Oura, Ed.), Institute of Low Temperature Science, Hokkaido, vol. 1, no. 1, p. 579-597.
- Weeks, W.F. and O.S. Lee (1958) Observations on the physical properties of sea ice at Hopedale, Labrador. Arctic, vol. 11, p. 134-155.
- Weeks, W.F. and O.S. Lee (1962) The salinity distribution in young sea ice. Arctic, vol. 15, p. 92-108.
- Weeks, W.F. and W.L. Hamilton (1962) Petrographic characteristics of young sea ice, Point Barrow, Alaska. Am. Mineral., vol. 47, p. 945-961.
- Weller, G.E. (1968) The heat budget and heat transfer processes in Antarctic plateau ice and sea ice. ANARE Scientific Reports, Series A (IV), Glaciology, Pub. No. 102, 155 p.
- Wernick, J.H. (1956) Determination of diffusivities in liquid metals by means of temperature-gradient zone melting. J. Chem. Phys., vol. 25, no. 1, p. 47-49.
- Whitman, W.G. (1926) Elimination of salt from sea water ice. Am. J. Sci., Ser. 5, vol. 11, no. 62, 126 p.
- Wilson, J.T., J.H. Zumberge and E.W. Marshall (1954) A study of ice on an inland lake. USA Snow, Ice and Permafrost Research Establishment, Research Report 5, 78 p.
- Yen, Y.C. (1981) Review of thermal properties of snow, ice and sea ice. USA Cold Regions Research and Engineering Laboratory, CRREL Report 81-10, 27 p.
- Zotikov, I.A., V.S. Zagorodnov and J.V. Raikovski (1980) Core drilling through the Ross Ice Shelf (Antarctica) confirmed basal freezing. Science, vol. 207, no. 4438, p. 1463-1465.

A facsimile catalog card in Library of Congress MARC format is reproduced below.

Weeks, W.F.

The growth, structure and properties of sea ice / by W.F. Weeks and S.F. Ackley. Hanover, N.H.: U.S. Cold Regions Research and Engineering Laboratory; Springfield, Va.: available from National Technical Information Service, 1982.

vi, 136 p., illus.; 28 cm. (CRREL Monograph 82-1.)

Bibliography: p. 117.

1. Electrical properties. 2. Ice. 3. Mechanical properties. 4. Salinity. 5. Sea ice. 6. Structural properties. 7. Thermal properties. I. Ackley, S.F. II. United States Army. Corps of Engineers. III. Army Cold Regions Research and Engineering Laboratory, Hanover, N.H. IV. Series: CRREL Monograph 82-1.



Mr Franz U. Häusler

MECHANICAL PROPERTIES OF SEA ICE

Introduction

For all marine engineering activities in ice covered oceans and seas the knowledge of the mechanical properties of sea ice is necessary:

- In the project stage this knowledge is needed for design and dimensioning purposes, e.g. for estimating the overall ice force and local ice pressures on an offshore structure or for evaluating the required power for an icebreaking ship.
- During the model test stage of such a project the mechanical properties of sea ice are needed as full-scale reference, which is to be scaled down to model values.
- In the final stage of full-scale trials and operation in ice the actual mechanical properties of the ice encountered must be known as reference values for measured performance properties of the ship structure. These reference values are used both for checking whether the design assumptions were right or not and for improving the data basis for further projects.

The objective of the present lecture is:

- to give a review of the today's knowledge on the most important mechanical properties of sea ice
- to describe, how some of them can be determined in the field.

The mechanical sea ice properties considered here are: uniaxial compressive strength and tensile strength, shear strength, flexural strength, elastic modulus and friction coefficient. Most of these properties depend more or less on temperature, salinity, crystal orientation and on the rate of load application or deformation.

Some words will be spent on the stress-strain characteristics of saline ice under multiaxial load conditions. A summary of possible multiaxial testing methods and a description of some failure criteria applicable to sea ice will be presented. Finally a rough idea will be given of how to apply such a failure criterion to the determination of ice forces on a structure.

Uniaxial compressive strength

The testing procedure for a uniaxial compression test is in general as follows: an ice sample of cylindrical, cubic or prismatic shape is loaded onto two opposite end forces until fracture occurs or until a desired strain is reached. The time histories of the applied load and of the resulting displacement(s) are recorded.

The conventional way of load application is to use stiff polished steel platens. Here commonly a triaxial stress state exists near the end planes of the specimen because of the radial constraint which is produced by friction between the platens and the specimen. The usual procedure to overcome these end-effect difficulties is to use specimens, which are long enough to provide for a mid-section with a fairly uniaxial stress state.

Another method has been suggested by the International Association for Hydraulic Research (IAHR) Working Group on Standardizing Testing Methods in Ice (IAHR, 1975): load is applied through a platen of low-modulus urethane, which is laterally confined by an aluminium cylinder (Fig. 1). The advantages of these "compliant platens" are:

- a reasonably uniaxial stress state over the whole specimen length
- allowance for shorter specimen
- wide tolerances in specimen preparation acceptable; the soft platen material can conform to minor irregularities of the end planes.

For more information see Haynes and Mellor (1977) and Law (1977).

In most of the tests published in the past conventional testing machines were used, which allowed at best a constant cross-head speed. The problem with these conventional testing machines is that at nominally equal strain rates (cross-head speed over specimen length) the actual strain rate in the sample tested, and so the strength measured, depends on the system stiffness of the testing machine. (Sinha and Frederking, 1979 and Sinha, 1981 b).

This problem has been solved by application of the closed-loop control technique, where e.g., the actual strain value, obtained from a strain transducer attached to the specimen tested, is controlled by comparing it with and keeping it automatically equal to a setting value taken from a dynamic setting means. This technique provides theoretically for an infinitely stiff testing system. Some few results on the compressive strength of saline and sea ice obtained with closed loop controlled testing machines can already be found in the literature (e.g. Wang, 1979 and 1981 and Häusler, 1981).

The dependencies of the uniaxial compressive strength of sea ice on the most important parameters are qualitatively as follows:

- the ice gets stronger with decreasing temperature (brine volume decreases)
- the ice gets weaker with increasing salinity (brine volume increases)
- the ice strength increases with increasing strain rate in the ductile failure range and remains roughly constant in the brittle failure range (limit $\dot{\epsilon} \approx 10^{-4}$ to 10^{-3} s^{-1})
- the ice strength parallel to the growth direction (vertical) usually is much greater than in plane with the ice cover (horizontal).

For sea ice investigation usually the strength dependencies on temperature and salinity are combined by using the brine volume as parameter. The brine volume v_b can be evaluated by means of the empirical formula

$$v_b = S_I \left(0.532 - \frac{49.185 \text{ } ^\circ\text{C}}{T_I} \right)$$

(Frankenstein and Garner, 1967), with S_I the absolute ice salinity and T , the ice temperature in $^\circ\text{C}$. This formula is valid only between -0.5 and -22.9 $^\circ\text{C}$. The reduction in sea ice strength with increasing brine volume can be explained by the reduction of effective cross-sectional area of ice-to-ice bonding in the failure surface, since increasing brine volume leads to increasing void inclusions (porosity) of the ice.

From geometrical considerations Assur (1958), Anderson and Weeks (1958), and Anderson (1958 a) concluded an equation of the general form

$$\sigma = \sigma_0 (1 - C v_b^k)$$

with $k = \{1, \frac{1}{2} \text{ or } \frac{2}{3}\}$ depending on the model of geometric similarity. For details see also Weeks and Assur (1967 or 1969). Up to now in most cases satisfactory results have been obtained using the square root of brine volume as parameter ($k = \frac{1}{2}$). The imaginary strength σ_0 is the theoretical strength of ice containing no brine inclusions but still showing the typical sea ice substructure.

In his most comprehensive study Peyton (1966) analyzed among others the dependency of the compressive strength of sea ice on brine volume variations (Fig. 2). In order to cut off stress rate effects he used a corrected strength σ_R defined as $\sigma_R = \sigma_C \left(\frac{\sigma_0}{\sigma} \right)^{0.22}$ with δ the rate of stress application and δ_0 unity stress rate. The comparably high strength values in the low brine volume range are explained by solid salt reinforcement due to precipitation of $\text{NaSO}_4 \cdot 10 \text{ H}_2\text{O}$ at temperature below -8.7 $^\circ\text{C}$.

Peyton's equation is

$$\sigma_R = 1.08 \text{ MPa} \left(1 - \sqrt{\frac{v_b}{0.672}} \right).$$

Weeks and Assur (1967) suggested an equation

$$\sigma_R = 1.65 \text{ MPa} \left(1 - \sqrt{\frac{v_b}{0.725}} \right)$$

which describes also the low brine volume data points of Peyton's study but is limited to values of $v_b \leq 0.25$. At higher v_b - values σ_R is assumed to remain constant.

Peyton (1966) also studied the dependency of uniaxial compressive strength on sample orientation (Fig. 3). The maximum strength direction he found was parallel to the growth direction; while the plane with the ice cover and under an angle of 45° to the crystal's c-axis.

The strength parallel to the c-axis reaches 75% of the vertical samples strength.

Peyton's results on horizontal specimen are rather consistent with the findings of Wang (1979), which are shown in Fig. 4.

The vertical to horizontal ratio corresponds rather well to the tendency found by Butkovich (1956, 1959), who reported a ratio of about 4, while the results of Häusler (1981) on laboratory grown NaCl-ice yield a ratio of 4.9.

The results of Schwarz (1971) on sea ice from the Baltic Sea (Lübecker Bucht) are in contrast to these findings (Fig. 5). Schwarz and Weeks (1977) explain the effect of the vertical samples being weaker than the horizontal ones by easy separation along the grain's longitudinal axes due to tensional strain occurring normal to the load axis.

The strain rate dependency in the ductile range found by Wang (1979) (Fig. 4) resembles the dependency known from fresh ice (e.g. Michel, 1978). The general equation is

$$\sigma_c = \sigma_0 \left(\frac{\dot{\epsilon}}{\dot{\epsilon}_0} \right)^a$$

with σ_0 being the imaginary compressive strength at unity strain rate $\dot{\epsilon}_0$, ranging from 0.34 to 1.03 GPa for horizontal samples of Arctic sea ice at -10°C , and $a = 0.538$ being an empirical exponent. The corresponding values for S2-fresh ice at -10°C are $\sigma_0 = 0.134$ GPa and $a = 0.343$ (Michel, 1978).

The transition from ductile to brittle failure, which is characterized by the maximum strength in the strength versus strain rate plot was found by Schwarz (1971) at a strain rate of about $\dot{\epsilon} = 3 \times 10^{-3} \text{s}^{-1}$ (Fig. 5) while Wang's (1979) data (Fig. 4) yield a transition strain rate of about $\dot{\epsilon} = 2 \times 10^{-4} \text{s}^{-1}$. This can be explained by the different stiffnesses of the testing systems: Wang (1979) used a 100 kN capacity closed-loop testing machine with rigid steel platens, while

Schwarz (1971) reports the use of plywood sheets between the sample and the machine platen.

For field tests on the compressive strength of sea ice the IAHR Working Group on Standardizing Testing Methods in Ice (Schwarz, et al., 1981) recommends the use of "compliant platens" together with a portable testing machine.

Uniaxial tensile strength

The maximal tensile strength can only be determined through direct tension test. In the past often indirect testing methods, such as ring tensile, frazil or beam tests have been used, but they all induce more or less complicated stress states which make the analysis of the results difficult.

The standard procedure is to prepare dumbbell shaped specimens, the end of which are frozen into metal end caps (Hawkes and Mellor, 1972). The load is applied through two standard steel cables. LVDT's are attached between the two end caps.

A new method proposed by Mellor (Schwarz, et al., 1981), which allows the use of right circular cylinders, seems most promising: Synthane (bonded Bekelite) end caps are scarified on a lathe to form a rough "hairy" bonding surface. The end caps have the same diameter as the specimen and are frozen directly to its end faces.

Up to now the most comprehensive studies on the tensile strength of sea ice have been carried out by Dykins (1970) and again by Peyton (1966), both using dumbbell shaped specimen.

Peyton's (1966) results on the tensile strength of natural sea ice show a similar dependency of the strength on sample orientation as already discussed in the chapter on the compressive strength. (Fig. 3). The absolute tensile strength values are round about one quarter of the compressive strengths of the same sample orientations.

Dykin's (1970) results base on extensive investigations on ice frozen in the laboratory from sea waters. The brine volume was varied widely by investigating two different salinities at various temperatures. Both horizontal as well as vertical specimen were tested. The results shown in Fig. 6 exhibit a linear dependency of the tensile strength on the square root of brine volume

$$\sigma_T \text{ (vertical)} = 1.542 \text{ MPa} \left(1 - \sqrt{\frac{v_b}{0.312}}\right)$$

$$\sigma_T \text{ (horizontal)} = 0.816 \text{ MPa} \left(1 - \sqrt{\frac{v_b}{0.140}}\right).$$

Varying the stress rate from 13 to 755 kPa s⁻¹ the tensile strength was found to be rate insensitive for stress rates up to 180 kPa s⁻¹. For stress rates higher than 180 kPa s⁻¹ Dykins (1970) observed that the tensile strength decreased by up to 52% of the initial value. Schwarz and Weeks (1977) explained this effect by the high number of stress concentrators in sea ice such as e.g., brine pockets.

For field testing the IAHR Working Group recommends duplicating as far as possible laboratory standards and procedures.

Shear strength

A pure shear strength test is difficult to perform, and has not yet been standardized.

Schwarz and Weeks (1977) refer to Paige and Lee (1967) and to Dykins (1971) as the best sets of shear strength data. Dykins (1971) reports "confined" shear strength values in the range of 200 to 400 kPa, which were reasonably unaffected by the variations of the load direction and of the temperature. Paige and Lee (1967) present a dependency of shear strength on the square root of brine volume similar to that of the flexural strength.

In order to establish the shear coefficients of a multiaxial failure criterion for saline ice Häusler (1982) used the data of uniaxial compressive strength tests under an angle of 45° to the growth direction. These data allow the determination of the xz-shear coefficient "e" of the failure criterion applied (see chapter on multiaxial testing), which was found to be $e = 3.12 \text{ MPa}^{-2}$ for the Smith-yield criterion for saline ice of 10.6 ‰ NaCl at the moment of sampling, -10°C and $\dot{\epsilon} = 2 \times 10^{-4} \text{ s}^{-1}$. The corresponding pure shear stress parallel to the growth direction is 0.57 MPa. The uniaxial strengths of this ice for comparison are 2.1 MPa in plane with the ice cover and 10.1 MPa normal to it (vertical).

Flexural strength

In many cases of ice structure interaction the ice fails in bending, e.g., ice ride-up or conventional icebreaking by ships. Even if not a basic material property, the flexural strength of an ice cover yields a useful index value both for analyzing measured ship or structure performances (full scale and model scale) or predicting them theoretically.

The flexural strength is normally obtained by simply supported beam tests or by cantilever beam tests, both carried out in-situ.

In the past extensive testing has been carried out on small scale beams cut out of larger ice covers (e.g. Lawrov, 1971 or Dykins, 1971). These tests are most valuable for a fundamental clarification of the flexural behaviour of ice.

But for estimating the flexural properties of an ice cover large scale in-situ testing is the state of the art, because in this way an average of the nonhomogeneous strength properties of the ice cover is obtained, drainage of the brine entrapped within the ice is avoided, and the temperature conditions are only changed minimally.

The cantilever beam test is usually preferred because it is rather simple to be carried out in the field. For this reason, the flexural strength obtained from in-situ cantilever beam tests is also one of the most important reference values used at ice model basins.

Doubtless the interpretation of strength data from in-situ cantilever beam test is somewhat problematic. The standard procedure, which is recommended by the IAHR Working Group on Standardizing Testing Methods in Ice (Schwarz, et al., 1981), is the application of the simple cantilever beam formula

$$\sigma_f = \frac{6 F l}{b h^2},$$

but it is emphasized, that this strength value should only be used as an index because of the list of simplifications and because it neglects necessary (compare Svec and Frederking, 1981):

- the ice cover is assumed to behave linearly elastic, and to be homogeneous and isotropic
- the buoyant support is neglected
- shear stresses are neglected:
- the cantilever behaves as a slender beam
- stress concentrations at the root of the beam are ignored
- the root is assumed to be an infinitely stiff, clamped support
- inertia effects are neglected.

The assumption of linear elastic behaviour is not too bad as long as the loading times are short enough. Loading times of 1 - 3 seconds minimize creep effects sufficiently but keep inertia effects still small (Svec and Frederking, 1981; Määttänen, 1976 and Schwarz et al., 1981). The reduction of the bending moment at the root of the cantilever beam is small for relatively short beams. From this point of view beam length to thickness ratios of less than 10 are recommended (Frederking and Häusler, 1978).

On the other hand the neglect of shear stresses and the assumption of slender beam behaviour requires larger beam lengths:

The latter assumption requires in addition a limited beam width, while on the opposite side, the number of crystals covered by the beam width must be large enough to eliminate grain size effects. Combining all these requirements the IAHR Working Group recommends a beam length of 7 - 10 times ice thickness and a beam width of 1 - 2 times ice thickness (Schwarz, et al., 1981).

Stress concentrations at the root of the cantilever beam, which have been found to reduce the apparent flexural strength of freshwater ice by up to 50% when compared with results from simply supported beams (Gow, 1977), seem not to be so much significant in sea ice due to its more plastic behaviour (Schwarz and Weeks, 1977).

The same conclusion can be drawn from Dykins' (1971) results which are shown in Fig. 8. For brackish water ice from the Baltic Määttänen (1976) found a reduction in apparent flexural strength of 32% when reducing the root radius of the cantilever beam from 1.5 m to 0.05 m, but for further root radius decrease the tests showed no decrease of the strength results. The latter was concluded to be a grain size effect. Accordingly, the IAHR Working Group does recommend the cantilever beam test only for sea ice covers and demands a root radius of less than 1/15 of the beam width (Schwarz et al., 1981).

The effect of compliant clamping at the root combined with plate effects was demonstrated by Svec and Frederking (1981) in a finite element study, the results of which were confirmed by a small series of in-situ cantilever beam tests on freshwater ice. Their calculations using thin plate bending elements showed for shorter beams ($l = 4$ m, $h = 0.4$ m) a maximum bending moment somewhat in front of the beam root, an effect, which coincided well with their observations, that beams tested, often broke 10 to 20 cm away from the root. In addition the computed maximum centerline moment was found to be about 1.5 times the moment at the root obtained from the simple cantilever beam theory (the buoyant effect was negligible). They finally concluded that in the analysis of short beams (l/h less than 12 to 15) the plate theory should be used and the ice cover to which the beam is attached be included.

A lot of results from in-situ cantilever beam tests can be found in the literature, some of which are plotted versus the square root of brine volume in Fig. 9 (Weeks & Anderson, 1958; Brown, 1963; Butkovich, 1956; Frederking & Häusler, 1978; Dykins, 1971).

The considerations on a sea ice model of Assur (1958) led to the conclusion that sea ice strength should depend on the square root of the brine volume $\sqrt{v_b}$.

First a linear dependency was tried. The results of Weeks and Anderson (1958), Butkovich (1956) and Brown (1963) have been condensed by Weeks and Assur (1969) to the formula

$$\sigma_g = \begin{cases} 0.69 \text{ MN/m}^2 \left(1 - \sqrt{\frac{v_b}{0.202}}\right) & \text{for } \sqrt{v_b} \leq 0.35 \\ 0.20 \text{ MN/m}^2 & \text{for } \sqrt{v_b} > 0.35 \end{cases}$$

while Dykins (1971), see also Fig. 8, developed from large scale in-situ cantilever beam and simple beam tests together with small scale simple beam tests a dependency which can be expressed as

$$\sigma_f = 1.08 \text{ MN/m}^2 \left(1 - \sqrt{\frac{v_b}{0.209}}\right).$$

Frankenstein (1970) analyzed his cantilever beam test results according to a proposal by Assur (1967), which considers the strength and elasticity inhomogenities over the ice thickness.

The basic assumptions of this analysis are as follows:

- the strain distribution over the beam's thickness is linear
- Young's modulus and ice strength can be expressed as functions of the brine volume (Weeks, Assur, 1967)

$$\sigma_f = \sigma_0 (1 - \sqrt{v_b})^2$$

$$E = E_0 (1 - v_b)^4$$

(Frankenstein (1970) used a simple quadratic formula for E)

- the brine volume distribution can be established by measuring the salinity and temperature profile and by application of the formula

$$v_b = \frac{S}{1000 \text{ ‰}} \left(0.532 - \frac{49.185 \text{ °C}}{T_i}\right)$$

found empirically by Frankenstein & Garner (1967), with S salinity in ‰ and T_i ice temperature in °C.

Together with a measured bending moment at the root of a cantilever beam an actual stress distribution and the variation of strength over the ice thickness can be established. This allows to evaluate the fictive strength value σ_0 which Frankenstein (1970) has found to be a constant $\sigma_0 = 0.76 \text{ MN/m}^2$. This is in reasonable agreement with the value of $\sigma_0 = 0.85 \text{ MN/m}^2$ reported by Frederking and Häusler (1978).

Accordingly the IAHR Working Group also demands to establish the flexural strength via Frankenstein method for each tested beam.

Even if not finally proved by a sufficient amount of experimental data, the Frankenstein method already allows to evaluate a reference value for the flexural strength of sea ice with a minimum of effort. This is important for instance in connection with full scale ice-breaker trials, where a reference ice strength is urgently needed but time usually does not allow to test very much beams, if any.

Elastic modulus

The elastic modulus E can be described as the slope of a stress over strain curve at the origin.

In the past, attempts have been made to determine E from static or quasistatic as well as from dynamic tests.

In static tests normal strength test procedures are used. From the slope of the measured stress-strain curve the elastic modulus can be determined. Here only the in-situ cantilever beam test shall be considered since this test is rather easy to perform in the field. Correspondingly a lot of publications on elastic modulus determinations by in-situ cantilever beams can be found in the literature. Up to now the standard procedure usually was to measure the tip deflection w under load relatively to the surrounding ice cover and to apply the simple cantilever beam formula

$$E = \frac{4 F}{w b} \left(\frac{l}{h}\right)^3$$

with F , the load, l , beam length, b , beam width and h , ice thickness. But usually this simple formula is not applicable because

- the beam is elastically supported by buoyancy
- the beam rotates and deflects at the root; the ice cover does not give a rigid clamping
- shear deformation becomes important if the beam is relatively short.

The well known inhomogeneity and anisotropy of the ice cover can be ignored as long as overall index values of the elastic modulus are the points of interest.

Most recently, several authors discussed the problem of improving the analysis on cantilever beam test with respect to the elastic modulus: Tatinclaux and Hirayama (1982) propose to make use of the theory of

beams on an elastic foundation and to analyze the tip deflection of beams of different lengths, but they ignore rotation and deflection at the root.

Frederking and Häusler (1978) measured these deflections over the beam length and applied a curve fitting method together with the model of a rigidly clamped cantilever beam on an elastic foundation. Häusler (1982) proposed the model of an elastically clamped cantilever beam. The problem of determining the spring constants of the elastic clamping at the root is detoured by measuring at least four deflections over the beams length and by applying a curve fitting method. In the presented form this method can only be applied to shorter beams, when the effect of buoyancy is negligible. This method systematically yields higher E values than those obtained by means of the simple cantilever beam formula with or without elastic foundation. A most sophisticated method for flexural strength analyses was presented by Svec and Frederking (1981): the cantilever beam was studied together with the surrounding ice cover by means of a finite element computer program using triangular plate bending elements and including buoyancy (see above). Together with an iterative procedure this method promises high quality results even on the quasistatic elastic modulus of floating ice covers.

In the dynamic tests usually the velocity of wave propagation is measured. Depending on the type of wave, different equations must be applied:

- the compressional wave in a long rod has a wave velocity of

$$c_L = \sqrt{\frac{E}{\rho}}$$

- the wave velocity of a compressional seismic wave (P - wave)

B is

$$c_B = \sqrt{\frac{E(1-\mu)}{\rho(1+\mu)(1-2\mu)}}$$

- the shear wave (S - wave) velocity c_s is

$$c_s = \sqrt{\frac{E}{2\rho(1+\mu)}}$$

with ρ ice density and μ Poisson ratio (Pounder, 1965).

Consistently the elastic modulus of sea ice with zero brine volume as determined by dynamic methods is reported by different authors (e.g. Langleben and Pounder, 1963 or Anderson, 1958 b) to be in the range of $E = 9$ to 10 GPa, a value which corresponds rather well with the elastic modulus known from fresh water ice (see e.g. Michel, 1978).

With increasing brine volume the elastic modulus decreases. The results of Langleben and Pounder (1963) from small scale acoustic tests on young sea ice can be described by the linear equation

$$E = 10.0 \text{ GPa} (1 - 0.00351 v_b).$$

Anderson's (1958b) results show a steeper decrease with an elastic modulus of about 4.5 GPa at $v_b = 40$ ‰ and about 1.0 GPa at $v_b = 100$ ‰ brine volume.

Laboratory tests on the flexural strength and elasticity of saline ice as determined in flexure (Schwarz, 1975), support a relationship between elastic modulus E , flexural strength σ_f and brine volume v_b , which was proposed by Weeks and Assur (1967) in connection with studies on a physical sea ice model (see above, chapter flexural strength).

The combination of the two equations gives the plot shown in Fig. 11. For σ_0 and E_0 , Schwarz (1975) reports values of 7.8 MPa and 1.7 GPa respectively. For the E/σ_f ratio of natural sea ice as determined in flexure and tension, values are varying between 2000 and 5000 (Schwarz and Weeks, 1977). This ratio is important for model scale investigations, in which it should be the same as in nature in order to fulfil the similarity rules.

Frederking and Häusler (1978) evaluated an elastic modulus of 2.0 GPa from a series of in-situ cantilever beam tests carried out on young sea ice at Spitzbergen in April 1977. In their analysis they used (see above) the static model of a rigidly clamped cantilever beam on an elastic foundation.

Häusler (1982) analyzed the Spitzbergen 1977 data again using the model of an elastically clamped cantilever beam and got an average value of $E = 2.2$ GPa.

Friction

Friction is one of the most important aspects of investigations on ship resistance in ice and on ice forces on structures.

Pounder (1965) gives a concise description of different theories, which have been proposed to describe ice friction phenomena:

- pressure melting theory
- frictional heating theory
- vapour film theory
- molecular rotation theory.

He finally concludes that only the pressure-melting theory seems to be ruled out from the present state of knowledge, but all the three other theories tend to overlap, merging smoothly one into another.

This uncertainty on the physical nature of friction may be the reason for the paucity of information on this subject. Schwarz and Weeks (1977) have collected friction data published in literature.

They found static friction coefficients between ice and steel of different surface conditions to be varying between $C_f = 0.03 - 0.04$ for sea ice and wet smooth steel and up to $C_f = 0.40 - 0.70$ also for sea ice and steel, all being rather independent of surface pressure. A range of $C_f = 0.1$ to 0.5 seems to be a reasonable first estimate of the static friction coefficient. The dynamic friction coefficient was found to be significantly lower ranging from $C_f = 0.025 - 0.045$

for brackish ice (0.9 ‰ salinity) and smooth steel up to $C_f = 0.07 - 0.250$ for sea ice and steel and furthermore up to $C_f = 0.31$ for snow and rough steel. Typical values seems to be for sea ice and steel $C_f = 0.06$ to 0.20 and for snow and steel $C_f = 0.05$ to 0.24 . Dry snow is said to raise the friction coefficient relative to dry ice by a factor of four, while wet snow seems to yield the same friction coefficient as ice.

The IAHR Standardizing Working Group has made some recommendations on the performance of friction tests, (Schwarz, et al, 1981) which shall briefly be reported here:

- a block of ice should be towed over the material surface, not vice versa; no rotating disc should be used (clogging cavities, frictional heating)
- ice block and surface should be plane
- the surface tested must be perfectly horizontal; to eliminate mistakes due to inclinations of the surface, each test is to be repeated immediately in the reverse towing direction
- one data point should be established by five to ten of such double measurements
- ice block dimensions, temperature and normal force are to be measured; horizontal towing force and velocity should be recorded. In addition a general description of ice and material surface is requested.

Multiaxial strength

Multiaxial testing of ice is a rather new field. Only very few publications on this topic can be found in the literature. In rock and soil mechanics testing of materials under multiaxial stresses is well established. Already in 1910 Th. v. Kármán designed and used a load cell for triaxial tests on marble (v. Kármán, 1911).

This ingenious design, usually called "Standard Triaxial Cell", was subject to only slight improvements and is used worldwide until today. A biaxial apparatus with rigid loading platens had already been developed by Föppl one decade earlier (Föppl, 1900). Föppl clearly recognized the disturbing influence of lateral strain constraint, and used a lubricant to minimize friction between platens and specimen.

In 1975 an international cooperative study on multiaxial testing methods for concrete was undertaken (Gustle, 1976). In principle, the results of this study can be transferred to ice. Six different testing methods have been studied (Fig. 12). Table 1 shows the advantages and disadvantages of each method in a concise form.

Four of these methods have up to now been applied to ice in general: the standard triaxial cell (Fokeyev, 1976 and Jones, 1978), the rigid steel platen (Frederking, 1977 and Timco and Frederking, 1983), the lubricated rigid platens (Duval, 1981) and the brush type loading platens (Häusler, 1981). But only three of these papers deal with sea ice or saline ice (Fokeyev, 1976, Häusler, 1981 and Timco and Frederking, 1983). Fokeyev (1976) performed an extensive test series on saline ice frozen in the laboratory.

The experimental data are presented in terms of Mohr-circles plotted for different temperatures and salinities. Unfortunately the testing apparatus used apparently did not allow a strain rate control. Knowing from uniaxial testing the strong dependency of ice strength on the strain rate, the lack of corresponding information limits the utilisation of Fokeyev's data.

The multiaxial sea ice data of Timco and Frederking (1983) will be presented during the POAC '83 - Conference subsequent to the WEGEMT '83 - Course. So they cannot be discussed here. What can be discussed is the testing apparatus, which is the same as used by Frederking (1977) during his studies on S-2 columnar grained fresh-water ice: A brick shaped specimen is loaded along its longitudinal axis by means of two rigid platens. The transverse expansion under load is hindered in one direction by two rigid confining platens, which are attached to two opposite long sides of the specimen, and which are rigidly clamped to each other. Under load, this transverse confinement creates a normal stress onto the confined forces, however, the magnitude of this stress depends on the Poisson ratio, which can only be estimated. So the exact biaxial stress state is not known. Together with test results from uniaxial compressive and tensile strength tests, the data obtained from this biaxial stress allow the determination of the coefficients of the 5-parameter Pariseau yield function for a material, which exhibits planar isotropy, as columnar grained ice does.

The triaxial testing machine used by Häusler (1981) has three individually closed loop controllable axes, each with brush-type loading platens especially designed for ice tests. In principle this arrangement allows all possible stress states in the cubic specimen from triaxial compression until triaxial tension. However, up to now, no tensional tests have been performed with this device because of bounding problems. The average values of 16 different uniaxial, biaxial and triaxial compressive strength tests are plotted in Fig. 13 together with the 5-parameter Pariseau yield surface and the 7-parameter Smith yield surface for planar isotropic materials. The procedure of coefficient determination and further details are presented by Häusler (1982).

The yield functions determined there on basis of a reduced strength data set are as follows:

Pariseau 5-parameter yield function

$$\begin{aligned}
 f(\sigma_{ij}) = & 0.688 \text{ MPa}^{-2} (\sigma_x - \sigma_y)^2 \\
 & + 0.0188 \text{ MPa}^{-2} [(\sigma_y - \sigma_z)^2 + (\sigma_z - \sigma_x)^2] \\
 & + 1.45 \text{ MPa}^{-2} \tau_{xy}^2 \\
 & + 3.08 \text{ MPa}^{-2} (\tau_{yz}^2 + \tau_{zx}^2) \\
 & - 0.971 \text{ MPa}^{-1} (\sigma_x + \sigma_y) \\
 & - 0.279 \text{ MPa}^{-1} \sigma_z \\
 & - 1 \leq 0
 \end{aligned}$$

Smith 7-parameter yield function

$$\begin{aligned}
 f(\sigma_{ij}) = & 0.647 \text{ MPa}^{-2} (\sigma_x - \sigma_y)^2 \\
 & + 0.0106 \text{ MPa}^{-2} [(\sigma_y - \sigma_z)^2 + (\sigma_z - \sigma_x)^2] \\
 & + 1.34 \text{ MPa}^{-2} \tau_{xy}^2 \\
 & + 3.12 \text{ MPa}^{-2} (\tau_{yz}^2 + \tau_{zx}^2) \\
 & - 0.971 \text{ MPa}^{-1} (\sigma_x + \sigma_y) \\
 & - 0.279 \text{ MPa}^{-1} \sigma_z \\
 & + [0.222 \text{ MPa}^{-1} (\sigma_x + \sigma_y) - 0.128 \text{ MPa}^{-1} \sigma_z]^2 \\
 & - 1 \leq 0,
 \end{aligned}$$

with σ_{ij} the stress tensor.

The most significant difference between these criteria occurs in the stress state of hydrostatic compression which the 5-parameter Pariseau yield function yields infinitely high, while the 7-parameter Smith yield function gives an ultimate hydrostatic compression of

$\sigma_x = \sigma_y = \sigma_z = 22.7$ MPa. The measured value was 14.2 MPa. The uniaxial and biaxial compressive strengths in plane with the original ice cover have been measured as $\sigma_x = 2.1$ MPa and $\sigma_x = \sigma_y = 9.4$ MPa respectively, while the uniaxial strength parallel to the growth

direction was measured to be as high as $\sigma_z = 10.1$ MPa. Last, but not least the biaxial strength, one load applied parallel, the other perpendicular to the growth direction, exhibited a biaxial strength of only $\sigma_x = \sigma_y = 2.5$ MPa.

This pronounced anisotropy of strengths with respect to the vertical and horizontal direction is reflected by the strain curves recorded during each strength test. An example is given in Fig. 14 which shows the stress strain behaviour of a cubic specimen under a compressive stress state of $\sigma_x = \sigma_y = \sigma_z = 3:2:1$ with σ_y being parallel to the growth direction.

The application of such multiaxial strength data onto ice engineering problems such as forces on a flat structure have been repeatedly reported in the past (e.g. Ralston, 1978) or Reinicke and Remer, 1978). So the present lecture can be restricted to a rough sketch (adapted from Reinicke and Remer, 1978):

- A yield function $f(\sigma_{ij}) \leq 0$ is an algebraic combination of the elements of the stress tensor σ_{ij} , which for $f < 0$ characterizes elastic or stable stress states and for $f = 0$ describes in elastic or yield stress states.
- The plastic limit analysis (PLA) can be used to solve engineering problems of ultimate strength by means of a known yield function.
- The lower bound theorem of the PLA states that plastic collapse of a material will not occur if a stress field can be found which satisfies equilibrium requirements and yields $f(\sigma_{ij}) \leq 0$ in the whole regime studied.
- The upper bound theorem of the PLA states that plastic collapse must occur, if for any compatible velocity field considered as plastic only, the rate at which the external forces do work exceeds the rate of internal dissipation of energy.
- The velocity field used in the upper bound analysis is to be constructed by means of the normality rule, which yields the strain rates to be normal to the yield surface $f(\sigma_{ij}) = 0$.

Acknowledgements

The author gratefully acknowledges the Hamburgische Schiffbau-Versuchsanstalt (HSVA) for the permission to present this lecture. Thanks are expressed to Dr. Schwarz for his kind cooperation.

References

Anderson, D.L. (1958 a):

A model for determining sea ice properties.
In: Arctic sea ice, Washington, D.C., pp. 148-152
U.S. National Academy of Sciences - National Research
Council Publication 598.

Anderson, D.L. (1958 b)

Preliminary results and review of sea ice elasticity and
related studies.
Transactions of the Engineering Institute of Canada, Vol. 2,
No. 3, pp. 116-122.

Anderson, D.L. and W.F. Weeks (1958):

A theoretical analysis of sea-ice strength.
Transactions, American Geophysical Union, Vol. 39, No. 4, pp. 632-640.

Assur, A. (1958)

Composition of sea ice and its tensile strength.
In: Arctic sea ice. Washington, D.C., pp. 106-138.
U.S. National Academy of Sciences - National Research
Council Publication 598.

Assur, A. (1967)

Flexural and other properties of sea ice sheets.
In: Oura, H., ed. Physics of snow and ice: international conference
on low temperature science....1966...., Proceedings, Vol. 1, Pt. 1,
Sapporo, Institute of Low Temperature Science, Hokkaido University,
pp. 557-567.

Brown, J.H. (1963):

Elasticity and strength of sea ice.
In: Kingery, W.D., ed., Ice and snow; properties, process and
applications: proceedings of a conference held at the Massachusetts
Institute of Technology, Febr. 12-16, 1962, Cambridge, Mass.,
M.I.T. Press, P.79-106.

Butkovich, T.R. (1956):

Strength studies of sea ice.
U.S. Snow, Ice and Permafrost Research Establishment,
Research Report 20

Butkovich, T.R. (1959):

On the mechanical properties of sea ice, Thule, Greenland, 1957.
U.S. Snow, Ice and Permafrost Research Establishment,
Research Report 54.

Duval, P. et al. (1981)

Primary creep and experimental method for testing ice in various conditions of strain rates and stresses.

By: P. Duval, M. Maitre, A. Manouvrier, G. Marec and J.C. Jay.
Proceedings, International Association for Hydraulic Research,
IAHR International Symposium on Ice, July 27-31, 1981,
Quebec, Canada, Vol. II, pp. 596-602.

Dykins, J.E. (1970):

Ice engineering - tensile properties of sea ice grown in a confined system.

Naval Civil Engineering Laboratory, Port Hueneme, California,
Technical Report R 689.

Dykins, J.E. (1971)

Ice engineering - Material properties of saline ice for a limited range of conditions.

Naval Civil Engineering Laboratory, Port Hueneme, California,
Technical Report R 720.

Föpl, A. (1900):

Die Abhängigkeit der Bruchgefahr von der Art des Spannungszustandes.
Mitteilungen aus dem Mechanisch-Technischen Laboratorium der
TU München, Heft 27.

Fokeyev, N.V. (1976)

Determination of the compressive strength of artificial ice specimens of different salinities under conditions of combined stress.

Proceedings of the Arctic and Antarctic Research Institute,
Vol. 331, 1976, pp. 189-202

(Orig. in russ., engl. transl. Ottawa 1980).

Frankenstein, G.E. (1970)

The flexural strength of sea ice as determined from salinity and temperature profiles.

National Research Council of Canada, Associate Committee on
Geotechnical Research, Technical Memorandum No. 98, pp. 66-73.

Frankenstein, G.E. and R. Garner (1967):

Equation for determining the brine volume of sea ice from
-0.5 to -22.9 °C.

Journal of Glaciology, Vol. 6, No. 48, pp. 943-944.

Frederking, R.M.W. (1977):

Plane strain compressive strength of columnar-grained and granular-snow ice.

Journal of Glaciology, Vol. 18, No. 80, 1977 p.505-516.

Frederking, R. and F. U. Häusler (1978):

The flexural behaviour of ice from in situ cantilever beam tests. Proceedings, Part 1, IAHR International Association for Hydraulic Research, Symposium on Ice Problems, Lulea, Sweden, Aug. 7-9, 1978, pp. 197-215.

Gerstle, Kurt H. et al. (1976):

Strength of Concrete under Multiaxial Stress States. McHenry Symposium, Mexico City, October 1976, pp. 103-131.

Gow, A.J. (1977):

Flexural Strength of ice on temperate lakes. Journ. of Glaciology, Vol. 19, No. 81 (1977), pp.247-256 (Proc. of the "Symposium on Applied Glaciology", Cambridge, 13-17 Sept, 1976).

Gow, A.J., H.T. Ueda and J.A. Ricard (1978):

Flexural strength of ice on temperate lakes. Comparative tests of large cantilever and simply supported beams. Cold Region Research and Engineering Laboratory, Hanover, N.H., Report No.78-9.

Häusler, F.U. (1981):

Multiaxial Compressive Strength Tests on Saline Ice with Brush-Type Loading Platens. Proc. International Association for Hydraulic Research, International Symposium on Ice, July 27-31, 1981, Quebec, Canada, Vol. II, pp. 526-539.

Häusler, F.U. (1982):

Comparison between different yield functions for saline ice. International Glaciological Society, 2nd Symposium on Applied Glaciology, August 23-27, 1982, Hanover, N.H. Annals of Glaciology, Vol. 4 (in press).

Häusler, F.U. and P. Jochmann (1982)

Eine verfeinerte Methode zur Bestimmung der Elastizitätseigenschaften von Eisdecken. Proceedings, INTERMARITEC '82, International Conference on Marine Research, Ship Technology and Ocean Engineering, Sept. 29/30, 1982, Hamburg, paper IMT 82-202.

Hawkes, I. and M. Mellor (1972):

Deformation and fracture of ice under uniaxial stress. Journal of Glaciology, Vol. 11, No. 61 (1972), pp. 103-131.

Haynes, F.D. and M. Mellor (1977):

Measuring the uniaxial compressive strength of ice. Journal of Glaciology, Vol. 19, No. 81 (1977), pp. 213-223.

Hilsdorf, Hubert (1965):

Bestimmung der zweiachsigen Festigkeit des Betons.
Deutscher Ausschuß für Stahlbeton, Heft 173, Berlin 1965.

IAHR (1975):

Report of the task-committee on standardizing testing methods for ice.
In: Frankenstein, G.E., ed. Proceedings, Third International
Symposium on Ice Problems, 18-21 Aug. 1975, Hanover, N.H.
International Association for Hydraulic Research,
Committee on Ice Problems; p. 607-618.

Jones, Stephen J. (1978):

Triaxial testing of polycrystalline ice.
Third International Conference on Permafrost, Edmonton, Alberta,
10-13 July, 1978, Vol. I, p. 670-674.

Káramán, Th.v. (1911):

Festigkeitsversuche unter allseitigem Druck.
VDI-Heft 42 (1911), pp. 37-68.

Langleben, M.P. and E.R. Pounder (1963):

Elastic parameters of sea ice.
In: Knigery, W.D., ed. Ice and Snow; properties, processes, and
applications. Proc. of a conference held at the Massachusetts Institute
of Technology, Febr. 12-16, 1962, Cambridge, Mass. MIT Press,
pp. 69-78.

Lavrov, V.V. (1969):

Deformatsiya i prochnost l'da
Leningrad, Gidrometeorologicheskoye Izdatel'stvo.
English translation: Deformation and strength of ice.
Translated by T. Pelt. Edited by G.N. Yakolev. Jerusalem,
Israel, Program for Scientific Translations Ltd.
Available from National Technical Information Services,
U.S. Dept. of Commerce, Springfield, Virginia 22151.

Law, K.T. (1977):

Design of a loading platen for testing ice and frozen soil.
Canadian Geotechnical Journ. Vol. 14, No. 2 (May 1977) pp. 266-271.

Määttänen, M. (1976):

On the flexural strength of brackish water ice by in-situ tests.
In: Proc. Vol. I, 3rd International Conference on Port and Ocean
Engineering under Arctic Conditions, Fairbanks, Alaska,
University of Alaska, 11-15 August 1975, pp. 349-359.

Michel, B. (1978):

Ice Mechanics.
Les Presses de l'Université Laval, Quebec, Canada, 1978.
I.S.B.N. 0-7746-6876-8.

Paige R.A. and C.W.Lee (1967):

Preliminary studies on sea ice in McMurdo Sound,
Antarctica, during "Deep Freeze 65".
Journal of Glaciology, Vol. 6, No. 46, pp. 515-528.

Peyton, H.R. (1966):

Sea ice strength.
University of Alaska, Geophysical Institute.
Report No. UAG-R 182 p. 285.

Pounder, E.R. (1965)

The physics of ice.
Pergamon Press, Oxford - London, 1965.

Ralston, T.D. (1978):

An analysis of ice sheet indentation.
Proc., International Association for Hydraulic Research,
IAHR Symposium on ice problems, Lulea, Sweden,
August 7-9, 1978, Part 1, pp. 13-31.

Reinecke, Kurt and R. Remer (1978):

A Produce for the Determination of Ice Force -
Illustrated for Polycrystalline Ice.
Proc. IAHR Symposium on Ice Problems, August 7-9, 1978,
Lulea, Sweden, p. 217-238.

Schwarz, J. (1971):

The pressure of floating ice-fields on piles.
In: International Association for Hydraulic Research,
IAHR Symposium: ice and its action on hydraulic structures,
Reykjavic, Iceland, 7-10 Sept. 1970, paper 6.3;
Delft, Intern. Association for Hydraulic Research.

Schwarz, J. (1975):

On the flexural strength and elasticity of saline ice.
Proceedings Third International Symposium on Ice Problems,
18-21 Aug. 1975, Hanover, N.H. Guenther E. Frankenstein, ed.,
Intern. Association for Hydraulic Research.

Schwarz J. and W.F. Weeks (1977):

Engineering properties of sea ice.
Journ. of Glaciology, Vol. 19, No. 81 (1977), pp. 499-531.

Schwarz, J. et al. (1981):

Standardized testing methods for measuring mechanical
properties of ice.
Prepared by the Working Group on Standardizing Testing Methods in Ice,
IAHR Section on Ice Problems,
Cold Regions Science and Technology, Vol. 4 (1981), pp.245-253.

Sinha, N.K. (1981 b):

Comparative Study of Ice Strength Data.
Proceedings, International Association for Hydraulic Research,
International Symposium on Ice, July 27-31, 1981, Quebec, Canada,
Vol. II, pp. 581-595.

Sinha, N.K. and R. Frederking (1979):

Effect of Test System Stiffness on Strength of Ice.
Proceedings, 5th International Conference on Port and Ocean
Engineering under Arctic Condition (POAC '79), August 13-18, 1979,
Trondheim, Norway, Vol. 1, pp. 708-718.

Svec, O.J. and R.M.W. Frederking (1981):

Cantilever beam tests in an ice cover: influence of plate
effects at the root.
Cold Regions Science and Technology, Vol. 4, No. 2 (1981),
pp. 93-101.

Tatinclaux, J.C. (1982):

In situ measurements of the mechanical properties of ice.
Proceedings INTERMARITEC '82, Hamburg, September 29-30, 1982,
pp. 326-334.

Tatinclaux, J.C. and K.-I. Hirayama (1982):

Determination of the flexural strength and elastic modulus
from in-situ cantilever beam tests.
Cold Regions Science and Technology, Vol. 6, No. 1 (1982),
pp. 37-47.

Wang, Y.S. (1979):

Cristallographic Studies and Strength Tests of Field Ice in
the Alaskan Beaufort Sea.
Proc., 5th Intern. Conference on Port and Ocean Engineering
under Arctic Conditions (POAC '79), August 13-18, 1979,
Trondheim, Norway, Vol. 1, pp. 651-666.

Wang, Y.S. (1981):

Uniaxial Compression Testing of Arctic Sea Ice.
Proc. 6th Intern. Conference on Port and Ocean Engineering under
Arctic Conditions (POAC '81), July 27-31, 1981, Quebec, Canada,
Vol. 1, pp. 346-355.

Weeks, W.F. and D.L. Anderson (1958):

An experimental study of strength of young sea ice.
Transactions, American Geophysical Union, Vol. 39, No. 4,
pp. 641-647.

Weeks, F.W. and A. Assur (1967):

The mechanical properties of sea ice.
U.S.Cold Regions Research and Engineering Laboratory, Hanover, N.H.,
Cold regions science and engineering,
Pt. II, Sect. C3 - CRREL-Monograph II-C3.

Weeks, W.F. and A. Assur (1968):

The mechanical properties of sea ice.
National Research Council of Canada, Associate Committee on
Geotechnical Research, Techn. Memorandum No. 92, Ottawa, March 1968
(Proc. of the Conference on "Ice Pressures against Structures",
Laval University, Quebec, 10-11 November 1966), pp. 25-78.

Weeks, W.F. and A. Assur (1969):

Fracture of lake and sea ice.
U.S.Cold Regions Research and Engineering Laboratory, Hanover, N.H.,
Research Report RR 269.

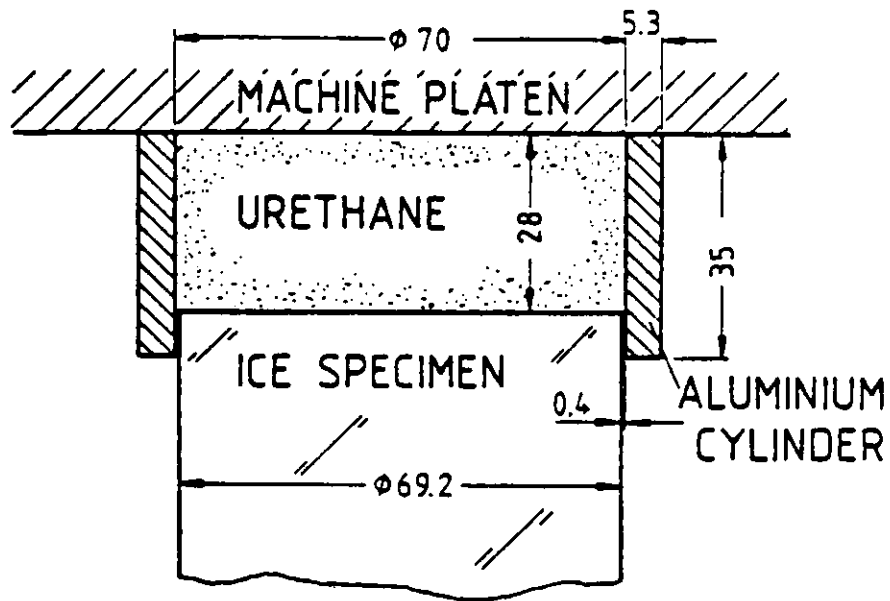


Fig. 1. Compliant Platens (Haynes and Mellor, 1977).

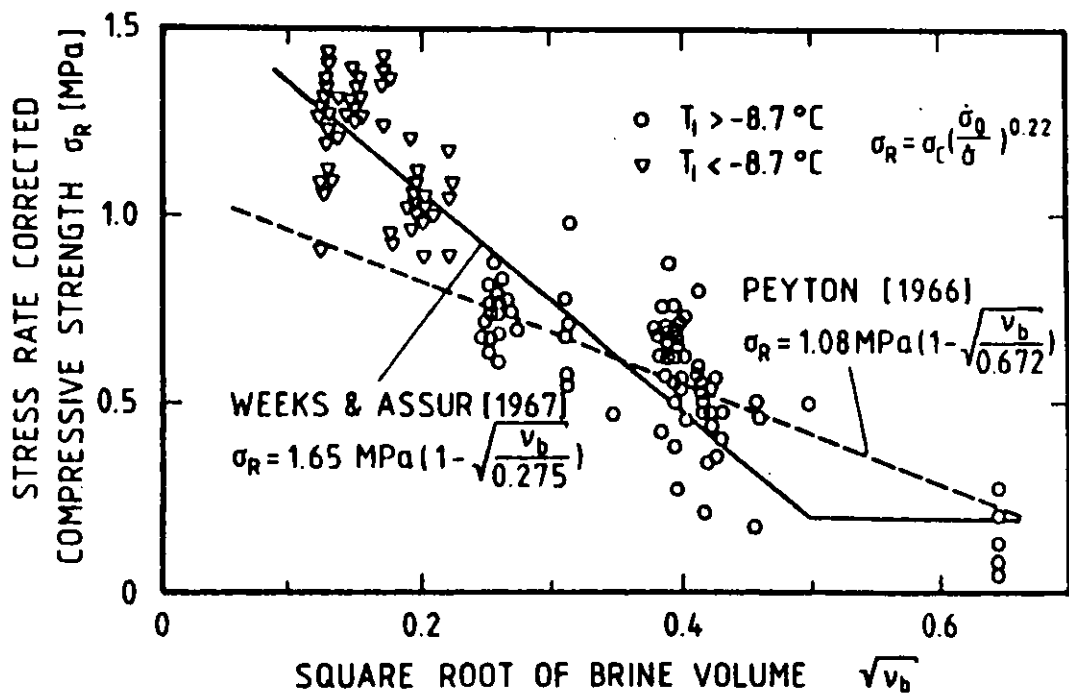


Fig. 2. Stress rate corrected compressive strength versus square root of brine volume (Payton, 1966).

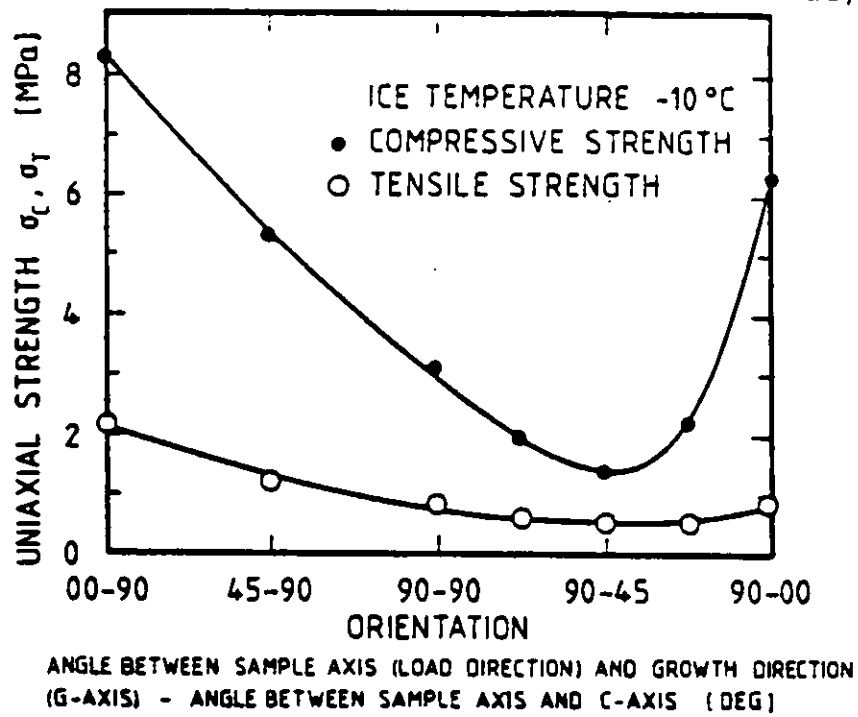


Fig. 3. Average failure strength in compression and direct tension versus orientation (Peyton, 1966).

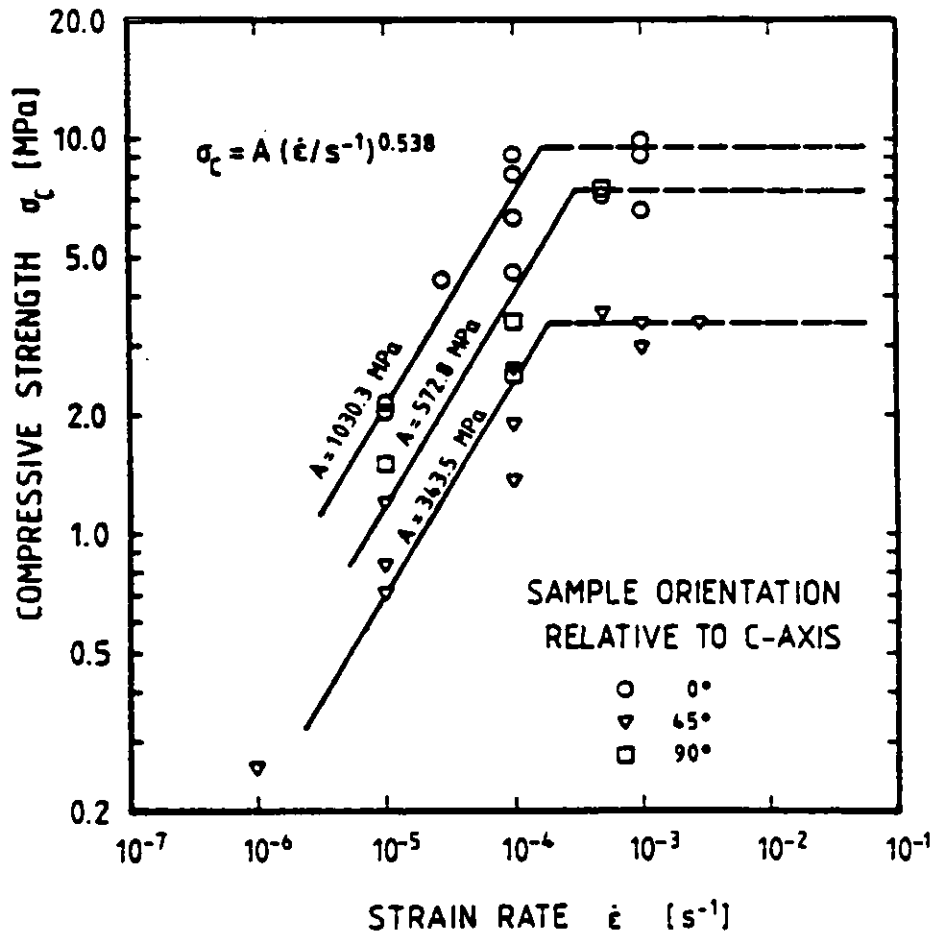


Fig. 4. Compressive strength of horizontal sea ice samples from Reindeer Island at -10 °C versus strain rate (Wang, 1979).

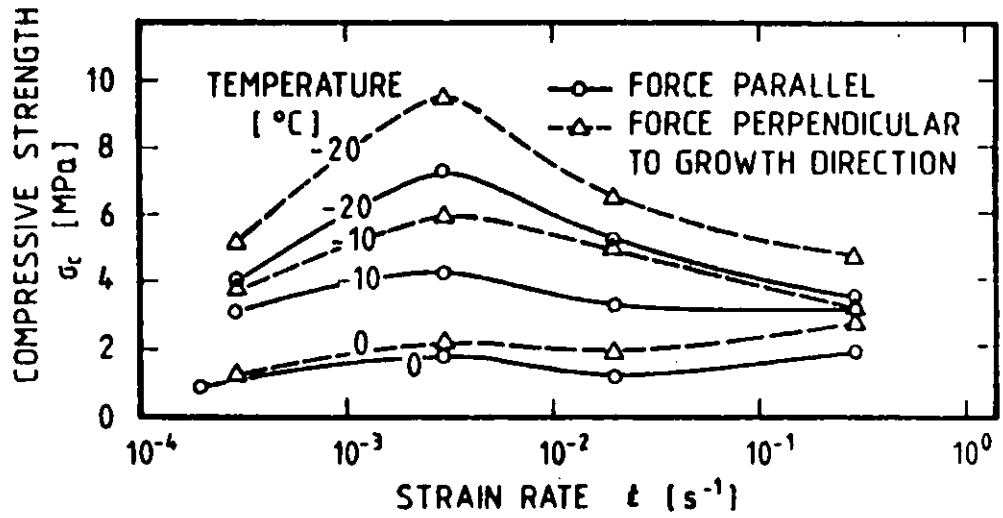


Fig. 5. Compressive strength of Baltic Sea ice versus strain rate for various temperatures and sample orientations (Schwartz, 1971).

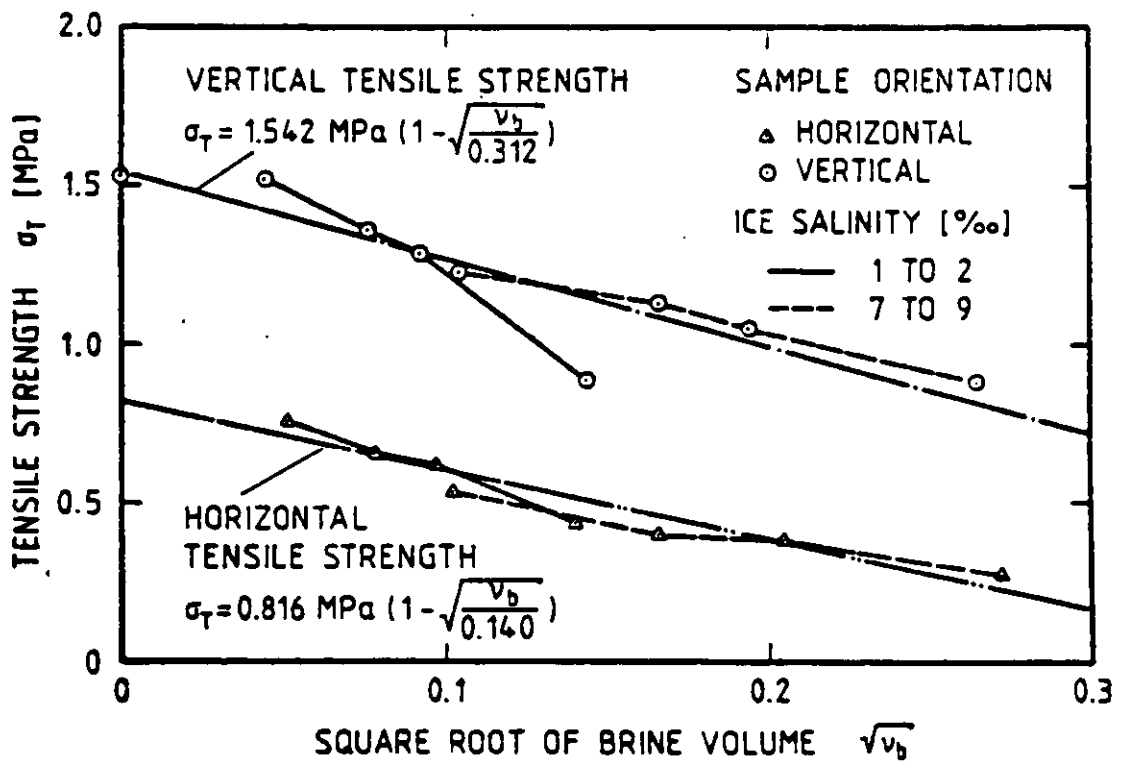


Fig. 6. Tensile strength of sea ice versus square root of brine volume (Dykens, 1970).

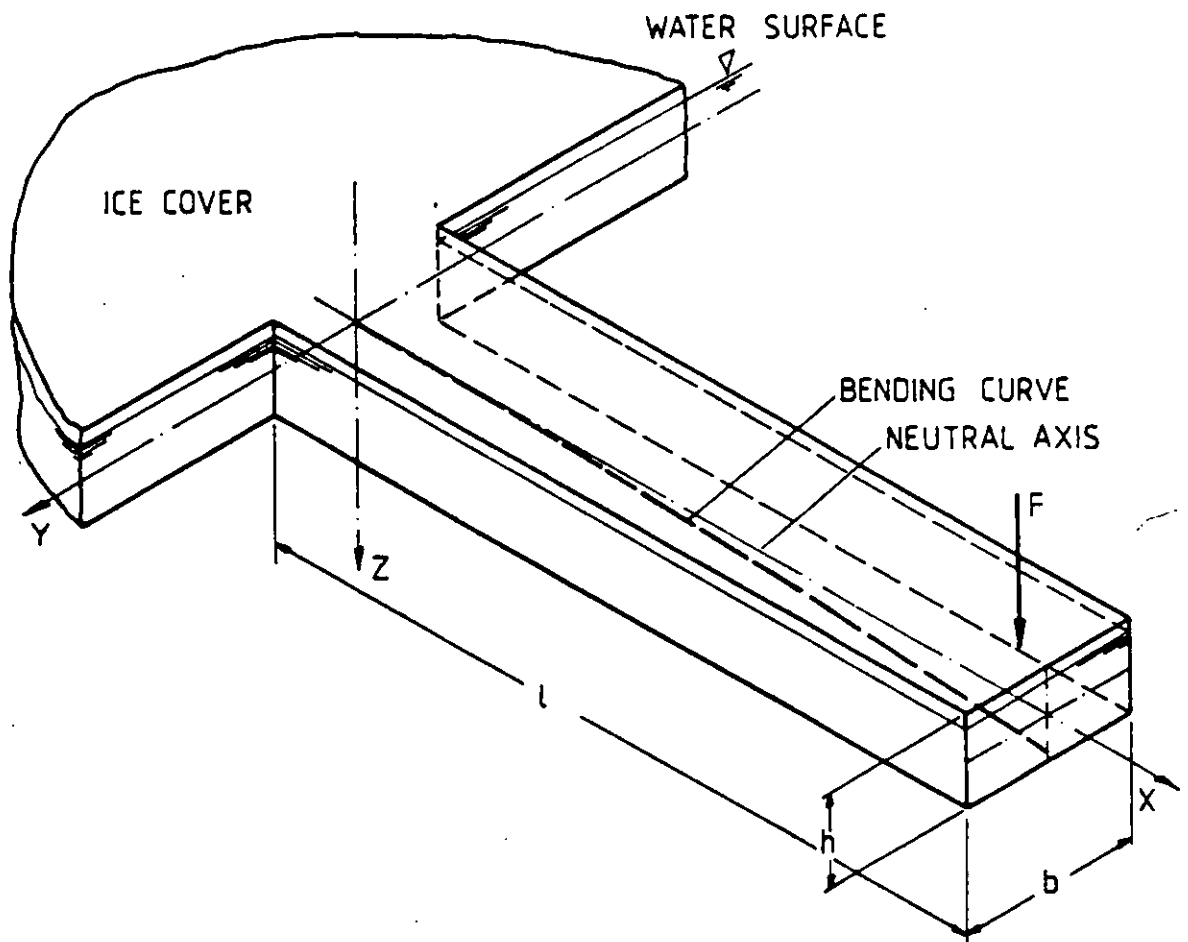


Fig. 7. Schematic of a buoyantly supported in situ cantilever beam.

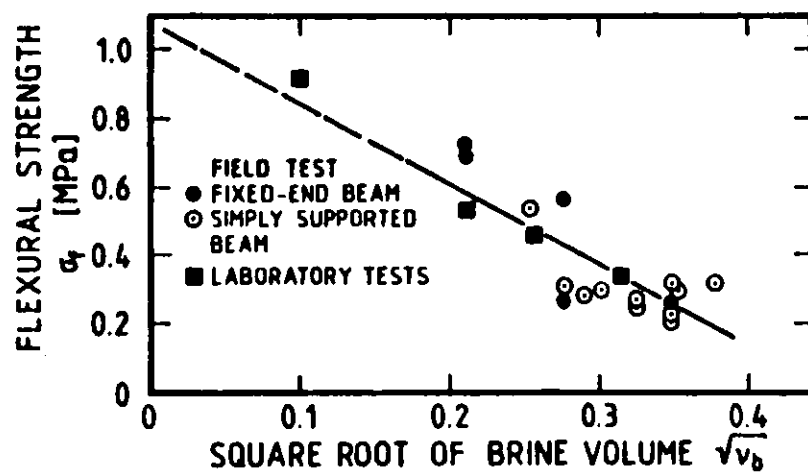


Fig. 8. Flexural strength from simple supported and in situ cantilever beam tests versus square root of brine volume (Dykins, 1971).

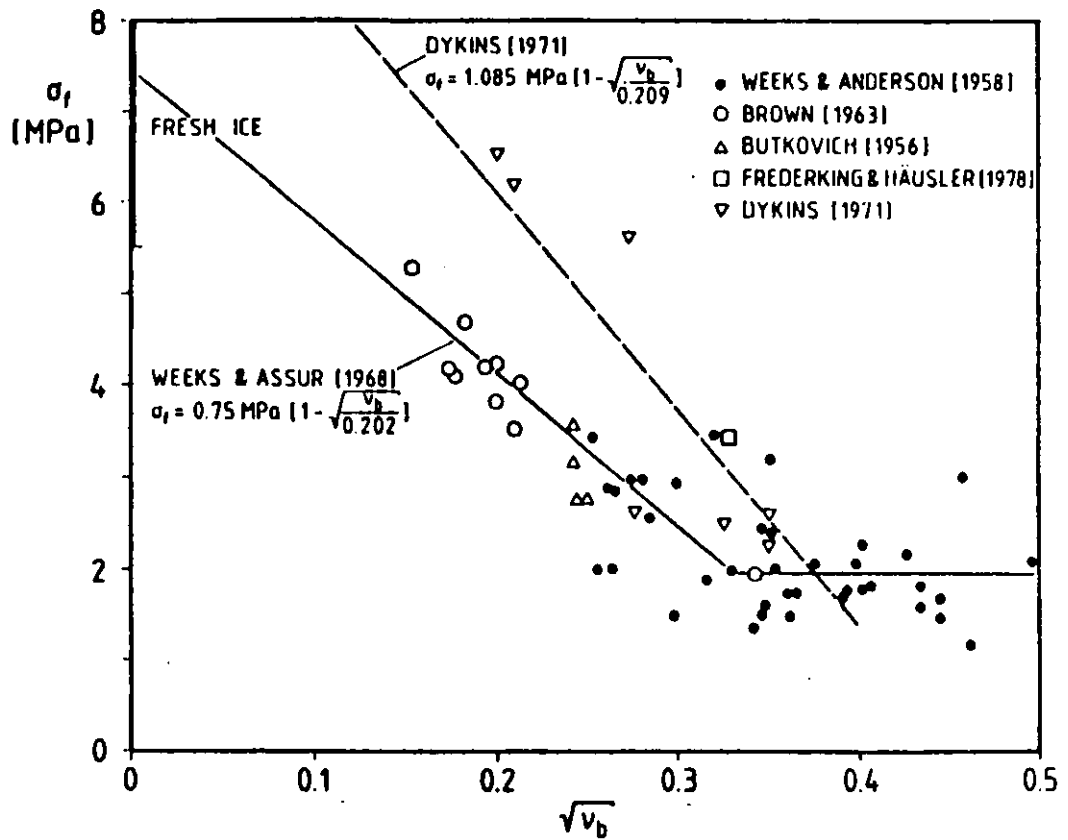


Fig. 9. Flexural strengths as measured from in situ cantilever beam tests versus square root of brine volume.

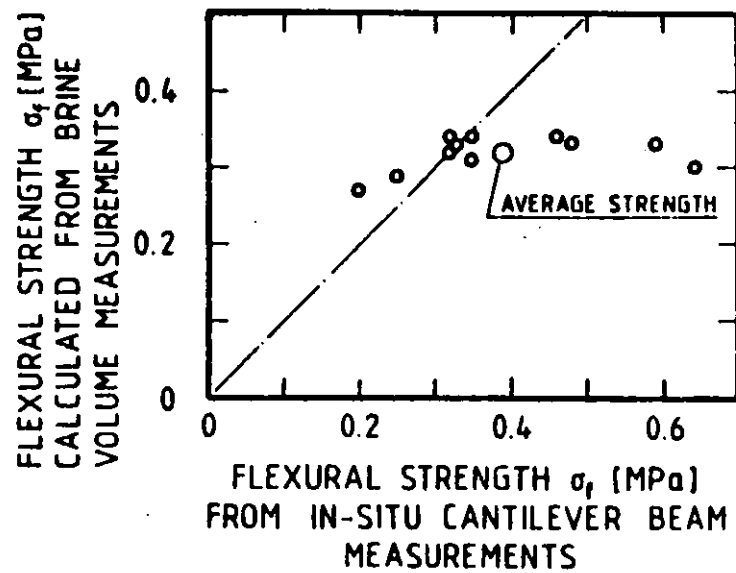


Fig. 10. Flexural strength as calculated from brine volume measurements versus flexural strength as measured in cantilever beam tests (Frederking and Häusler, 1978).

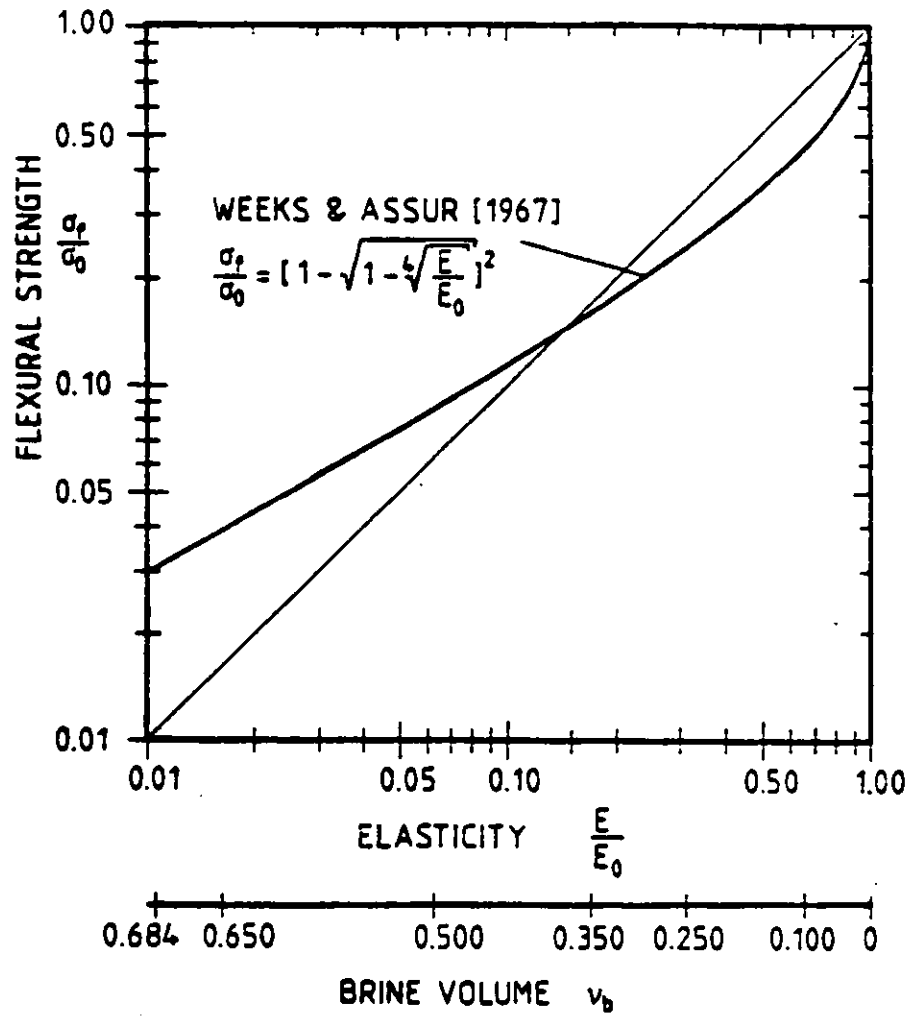


Fig. 11. Normalized flexural strength versus elastic modulus for saline ice (Schwarz, 1975).

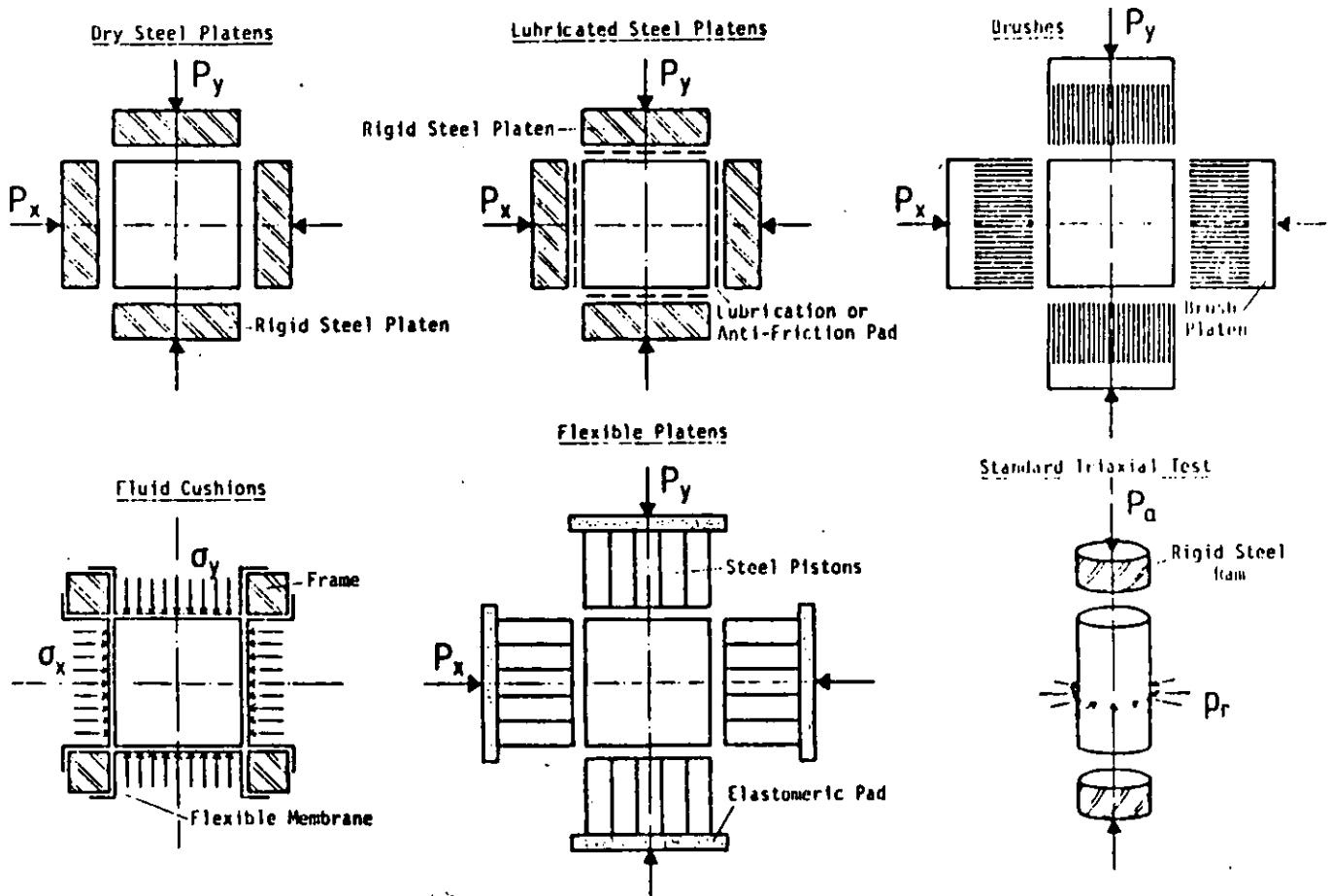


Fig. 12. Multi-axial test methods, (Gerstle, et al., 1976).

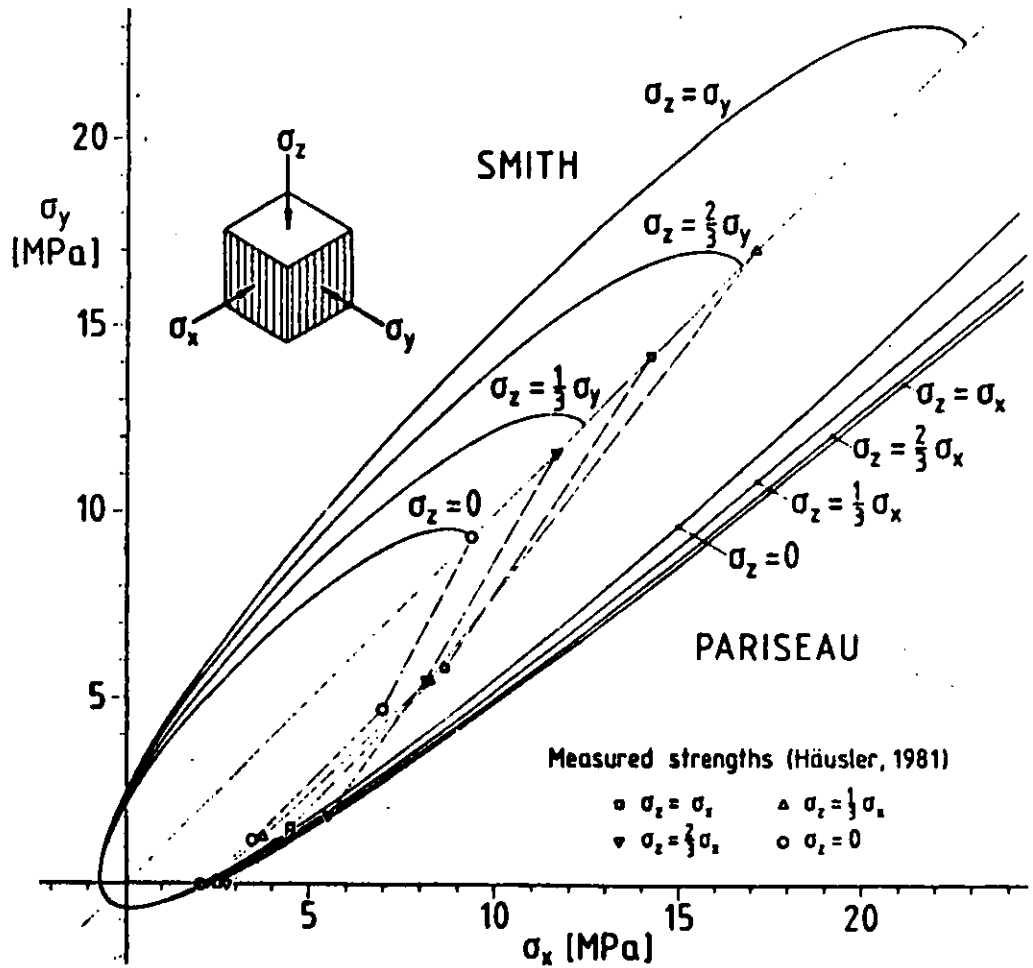


Fig. 13. Yield surfaces for columnar grained saline ice of 10.6 ‰ NaCl (when sampled), -10 °C at $2 \times 10^{-4} \text{s}^{-1}$ strain rate (Häusler, 1982).

	Dry Steel Platens	Lubricated Steel Platens	Brushes	Fluid cushions	Flexible Platens	Standard Triaxial Test	
						axial	radial
Normal boundary constraint	very high	high	high	no	low	very high	no
lateral boundary constraint	high	low	low	no	low	high	no
strain measurement at the specimens in triaxial tests	no	no	at the edges	with pressure- tight gauges	at the edges	with pressure- tight gauges	
multiaxial tension possible	yes*)	no	yes*)	no	no	yes	no
necessary accuracy in specimen prepara- tion	high	medium	very high	low	medium	high	low

*) not yet solved

Table 1 Characteristics of Multiaxial Testing Methods



Mr Thomas Thompson

ICE SURVEILLANCE TECHNIQUES

Ice and ice regimes.

Ice floating on the ocean surface is generally divided into 3 major types: sea ice, glacier ice and river ice. The first type is formed from freezing of sea water, the second originates from glaciers discharging icebergs and growlers into the ocean and the third is freshwater ice discharged into the sea by rivers. The two first types are the most common and of greatest importance for operations in northern waters. Sea ice forms when the temperature falls below the freezing point for salt water (around -1.8°C) and melts when the temperature rises above. Over large areas ice therefore forms during autumn/winter and melts during spring and summer. This ice is called first-year ice. In the Arctic basin the ice only melts partly during summer and most of the ice remains from year to year and this ice is called multi-year ice or old ice. The ice present in the Arctic basin at the time of minimum extension, which normally occur during August/September, is practically all multi-year ice. The ice present at the time of maximum ice extension which normally occurs during February/March, is in some areas purely first-year, in others a mixture of first-year and multi-year ice. In e.g. the Baltic, Gulf of St. Lawrence, Sea of Okhotsk the ice is first-year. In areas where ice is drifting out of the Arctic basin, such as the Norwegian Sea, Baffin Bay, Bering Sea, the ice is a mixture of first- and multi-year ice. Figure 1 shows the extreme minimum and maximum ice extension in the northern hemisphere. The ice extension at the same time of the year may however vary considerably from year to year. One example is the Baltic where the ice a severe winter covers an area of about 366000 km^2 and a mild winter only 37000 km^2 . This is illustrated in Figure 2.

Important features of the ice.

Except for the fast ice along the coasts the pack ice is in constant movement caused by winds and currents. This movement creates many of the typical features of sea ice such as floes of different sizes, openings as cracks and leads, variable concentration, rafting and ridges etc. Had the ice been homogenous and level it would have been an easy task to construct and build ships which could maintain regular traffic even in very thick ice. The fact that the ice field is utterly unhomogenous with ridges with a depth of 10-30 metres in first-year ice and 30-40 metres in multi-year ice makes it necessary to use specially constructed icebreakers to assist the traffic in ice. Even for icebreakers it may be difficult to force the ice and it is therefore necessary to constantly observe and

surveille the ice in order to find the easiest and most economic way through it.

When mapping the ice one has to identify a number of ice parameters in order to obtain a full picture of the situation. The most important parameters are:

- a. The distribution of the ice.
- b. The concentration (the proportion the water surface covered with ice.)
- c. The thickness of the level ice.
- d. The form of the ice.
- e. The deformation of the ice.
- f. Surface features (snow, melt water etc).
- g. The movement of the ice.

Observational methods.

A variety of methods can be used to observe the different ice parameters. The simplest is the visual observation by human eye. This method has however severe limitations, and is restricted by darkness, limited visibility and the fact that what is observed has to be recorded. The human observer has therefore gradually been replaced or supplemented by other techniques such as remote sensing.

Remote sensing.

Remote sensing means that one from distance record electromagnetic waves emitted or reflected from an object and by processing obtain information about the physical properties of the object. The electromagnetic waves covers a wide spectrum of wavelengths from only millionths of a millimeter to centimeters, meters and kms. Only a few ranges of the spectrum can however be used due to the absorption in the atmosphere and to technical limitations. Figure 3 shows the absorption of the atmosphere in the various wavelengths and the parts of the spectrum for which techniques have been developed for remote sensing. These parts are called

- visual (VIS)
- infrared (IR)
- microwave (MW).

The instruments which have been developed to measure in the three wavelengths mentioned above are called sensors. They use various techniques to cover a given surface.

The most common sensors are:

- a) Scanning radiometers that scan the surface from side to side while the carrier (platform) moves forward and thus covers a swath of the surface. These types of sensors normally measure the emission in a number of narrow spectral intervals in the VIS, the IR or the MW region of the spectrum (multispectral technique). The scanning technique is illustrated in Figure 4.

- b) Radars which emit energy and measure the reflected energy from the surface. For ice mapping the Side-Looking Airborne Radar (SLAR) is the most useful. This type of radar is usually mounted on an aircraft and looks out to the side of the aircraft covering a 20-100 km wide strip on one or both sides as it moves ahead. When operating a sidelooking radar from high altitudes a special technique is used to increase the resolution. This technique is called synthetic aperture. The radar is then called SAR (Synthetic Aperture Radar). A SAR can give high resolution images even from satellites. The SLAR or SAR technique is illustrated in Figure 5.
- c) Profilometers using light (LASER) or short pulse microwaves (radar). These instruments measure the profile of the ice surface and give a picture of the ice roughness.
- d) Under-water profilers using sound waves (sonar). This method is mainly used from submarines and gives the underwater roughness of the ice.

The latter two sensors give only line information along the path of the carrier in the form of profiles of the upper and the lower surface of the ice while the others provide an image of a surface area.

The sensors have to be carried by some form of platform that moves through, over or under the ice. It could be a ship, a submarine, an aircraft (or helicopter) or a satellite. It could also be a stationary platform using an omnidirectional technique eg. conventional radar.

The efficiency of the system will however depend on the field of view and the speed with which the platform is moving. Table 1 gives an example of the time it takes to observe a given area with different methods. We can see from the table that the time required to cover the same area (20000 km²) is for a ship 14 days, an aircraft 10 min. and a satellite 1 second.

platform	field of view	speed	time
ship	3 km	20 km/h	14 days
aircraft	200 km	400 km/h	10 min.
satellite	3000 km	400 km/min.	1 sec.

Table 1.

Observations from the surface, e.g. a ship, allow many direct measurements of a number of parameters such as concentration, form of ice, thickness, deformation, surfaces features etc. provided daylight and

good visibility. It is however not possible to obtain a synoptic picture of the ice situation over a large area unless one uses a large number of ships and collect all the observations at one processing centre. This is quite unpractical. By use of aircraft and helicopter larger areas can be covered but the result will depend on the weather and daylight and the individual capability in observing and recording. For an efficient operational ice surveillance system remote sensing techniques therefore become necessary. The remote sensing information may be supplemented by conventional observations which in many cases can give more details about the ice.

Operational Remote Sensing System.

The sensors described above have to be carried by some sort of platform and preferably one that can cover a large surface area in short time. The most efficient platforms for remote sensing are therefore aircraft and satellites.

Aircraft.

The sensors that can successfully be carried by aircraft are

- a) VIS and IR scanners
- b) SLAR or SAR
- c) Profilometers
- d) Photographic cameras

Of these the SLAR/SAR has proved most useful as it is daylight- and weatherindependent. It can cover swaths up to 50 km on each side of the aircraft although a lot of details are lost outside the 25 km range. Figure 6 gives an example of a SLAR registration from the Hall Basin in the strait between Ellesmere Island and Greenland. The SLAR information is normally registred onboard the aircraft as an image on photographic paper or on magnetic tape for later processing. It is also possible to transmit the information to a ground station, but it is a limited amount of information that can be transmitted this way. Normally the information is processed after landing and combined with other available information at an ice central in preparation of the final products to be distributed to the users.

Infrared scanners and laser profilometers are also useful airborne instruments. Their use is however limited by clouds, fog and other weather phenomena.

Satellite.

A large number of satellites are in operation today, providing vast amounts of information about the atmosphere and the earths surface. The satellites are of two major types:

- a) Geostationary which at 36000 km altitude above equator moves with the same angular speed as the earth and therefore maintains a stationary position relative to a point at the equator.
- b) Polar orbiting which at 800-900 km passes over or near the poles with a speed of about 100 min. per orbit. These satellites cover the whole globe as the earth turns around its axis in 24 hours.

The geostationary satellites give near continuous information for the same area as they keep constant position all the time. Due to the earth's curvature the resolution of the information decreases to the north and south with the distance from the equator and for ice surveillance the geostationary satellites are therefore of little interest for areas north and south of about 55°.

The polar orbiting satellites give information for a given area about 10 times per day in the polar region. The following information can be obtained:

- Visual and infrared data in 5 wavebands with a resolution of 1 km (NOAA weather satellites).
- Visual and infrared data in 7 wavebands with a resolution of 30-80 m (LANDSAT). The LANDSAT sensors cover only a 185 km wide strip on each orbit and can therefore not give full daily global coverage. North and south of 82° the LANDSAT satellites give no information.
- Microwave data in 5 wavebands with a resolution of 20-30 km (NIMBUS-7). Weather and daylight independent and give full global coverage every 3 days.
- SAR data has been successfully received from a USA satellite (SEASAT-1) which operated during a few months in 1978. This satellite provided data with a resolution of 25 m. A new European microwave satellite with SAR instrumentation is planned for 1987. An example of a SAR image in the Beaufort sea is given in Figure 7.

With the satellites NOAA, NIMBUS and LANDSAT it is possible to obtain ice information with the resolution of 20-30 km, 1 km and less than 100 m respectively. The microwave data from NIMBUS provide large scale information in all weather conditions. The NOAA satellites provide visual and IR data on a medium scale but cannot see through clouds and heavy fog. The LANDSAT satellites provide visual and infrared data with high resolution, but are also hampered by clouds and fog.

Data collection and processing.

The satellite data is transmitted from the satellites to receiving ground stations in digital form. In order to obtain useful information the data has to be processed by computer whereby it is checked and corrected for radiometric and geometric errors. The information from the various spectral intervals are combined to derive the optimal information about

a particular object such as sea ice. This is done through an interactive process between the operator/interpreter and the computer and the results, optimized for its particular purpose, are normally presented as colour images. Examples of such images, but in black and white, are given in Figures 8-10. Figure 8 shows a NOAA-6 image (one channel) covering the area from northern Scandinavia to the North Pole. The image give general information on the distribution of the ice and its concentration. Figure 9 shows a section of Figure 8 with the White Island in the lower central part of the image. From this image more information about the concentration, form and age of the ice can be derived. Figure 10 shows a LANDSAT image of the ice around the White Island. From this image many details about the ice can be derived.

Ice surveillance systems.

None of the sensors mentioned above will give a satisfactory mapping of all ice parameters required. The VIS and IR scanners give information about the distribution and concentration of the ice (ice contra water), the form of ice and to some extent the age and thickness. The microwave scanners will give the large scale distribution and concentration and some information about the age. The SLAR or SAR will e.g. give information about the extension, concentration and the roughness of the ice with high resolution. In order to obtain an optimum information about the ice a combination of sensors and platforms will have to be used. The information from the various sensors will have to be collected, compiled, interpreted and transferred to ice maps which can be transmitted to the users. A typical ice surveillance system will include:

- a. Satellite data processed on daily routine basis.
- b. Aircraft reconnaissance including SLAR, IR-scanners, profilometers etc. To be used when required to supplement the satellite information.
- c. Surface observations from ships and fixed installations.

The total system will further include, besides the above observational system, reception of data at a central processing centre, processing and interpretation, presentation and transmission of ready products to the users.

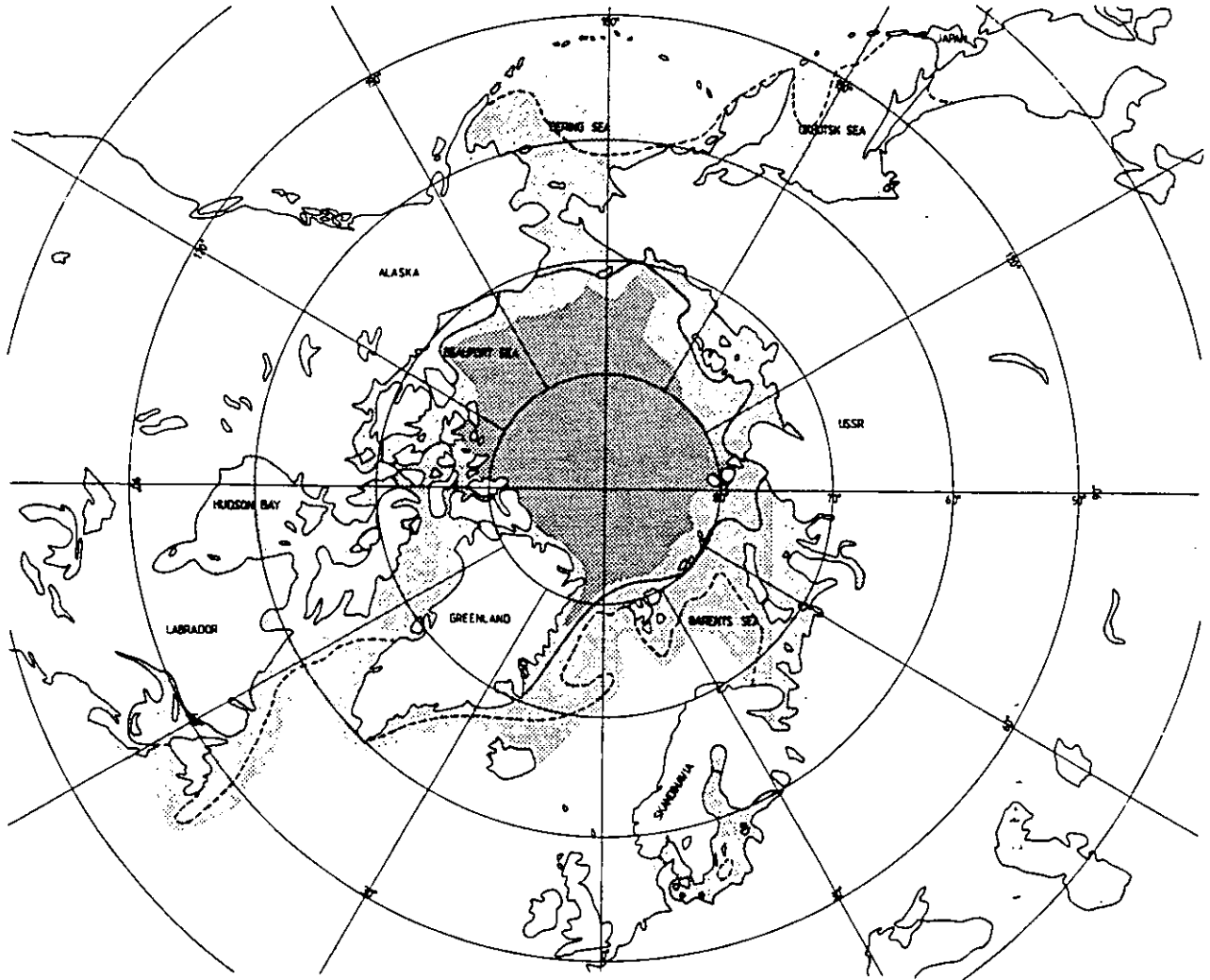


Fig. 1. Extention of the ice in the Northern Hemisphere.

▬ Extreme maximum
extention.

▨ Extreme minimum
extention.

--- Mean maximum
extention.

— Mean minimum
extention.

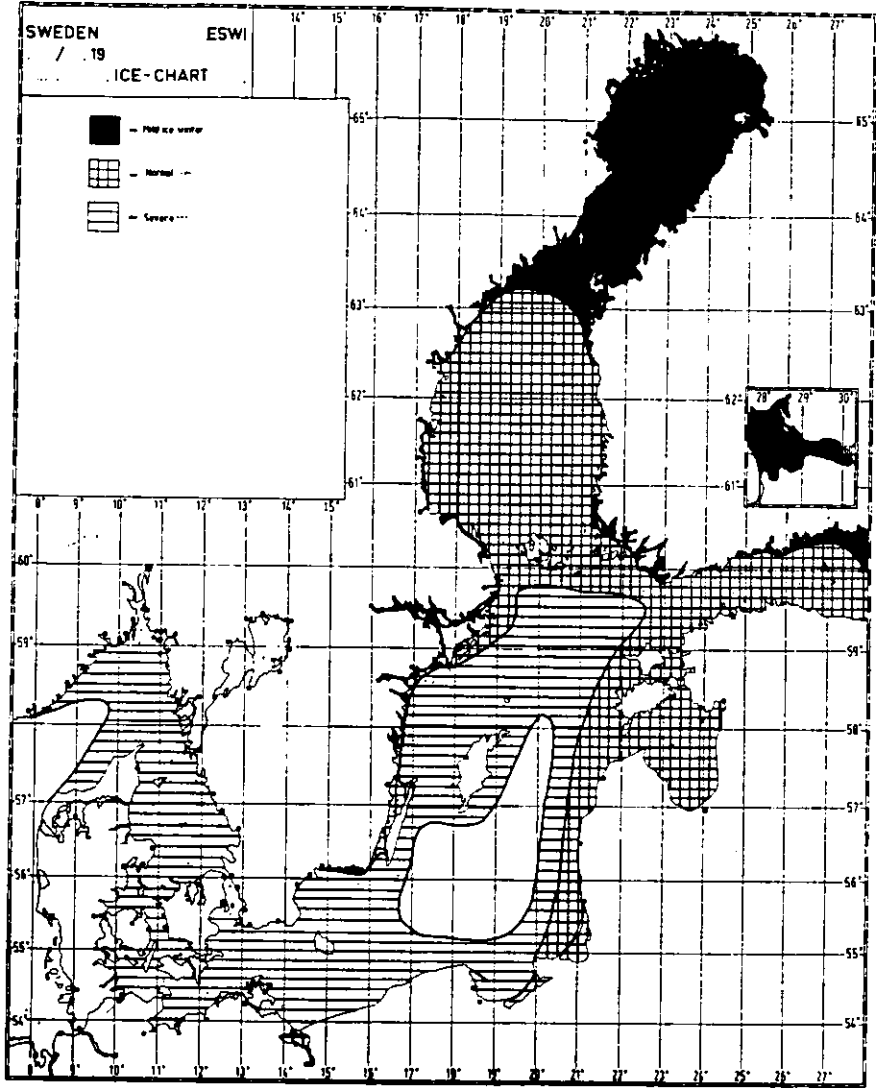


Fig. 2. The ice extention in the Baltic during a mild, normal and severe winter.

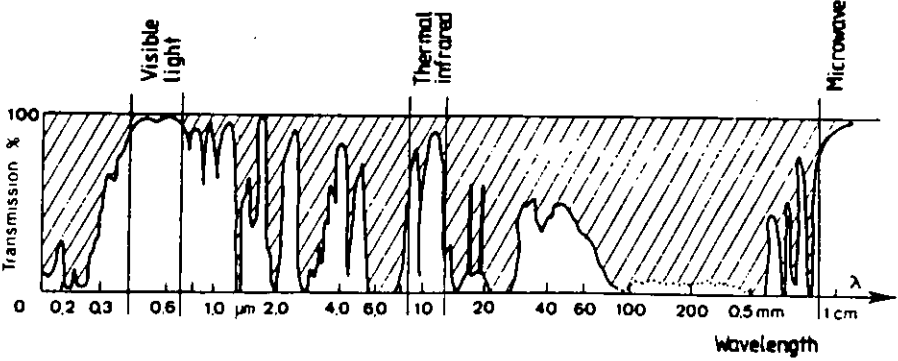


Fig. 3. Atmospheric absorbrion at various wavelenghts.

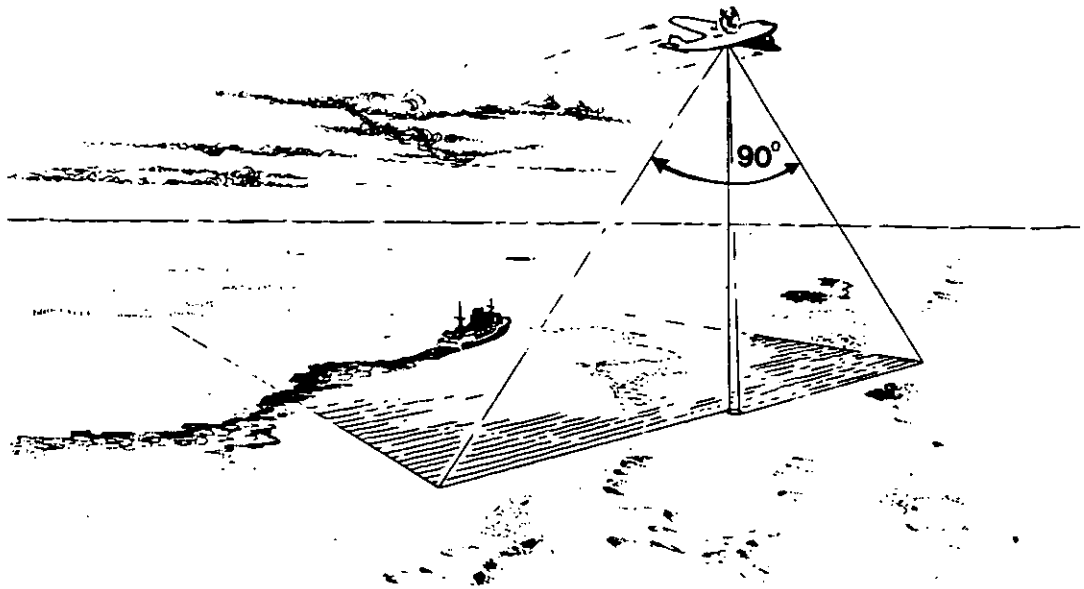


Fig. 4. Principle for airborne line scanning.
Same principle used from satellite.

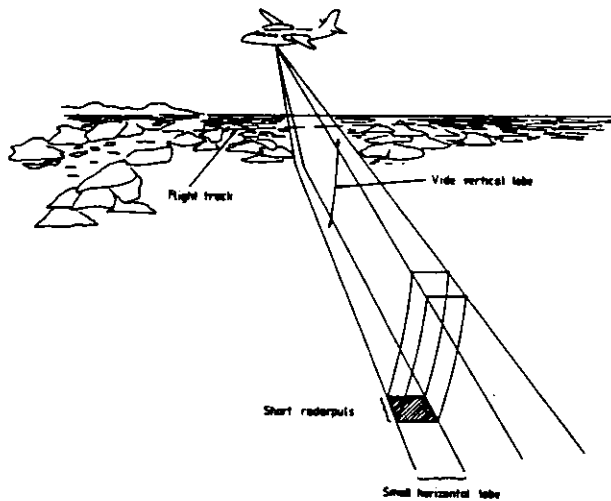


Fig. 5. Principle for Sidelooking Airborne Radar (Slar).
Same principle is used from satellite (SAR).

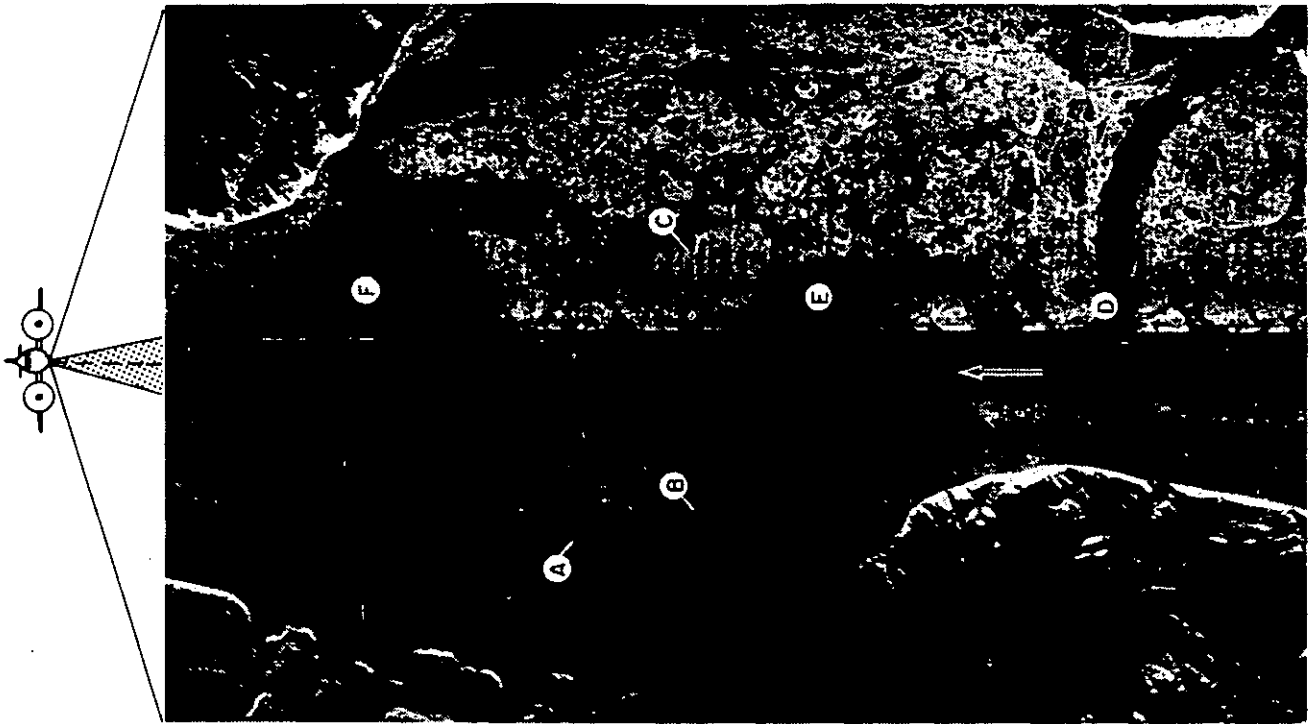


Figure 6. Example of a registration from a Sidelooking Airborne Radar over the Hall Basin between Greenland and Ellesmere Island (From M. Dunbar)

A, B, C = Multi-year ice (old ice).

D, E, F = First-year ice (young ice).

SEASAT SAR

SCALE 1:250000

FRAME CENTRE 74 5 18 N 124 53 33 W

BANKS ISLAND, N.W.T.
ORBIT 205 JULY 11, 1978
25M RESOLUTION 4 LOOKS
SATELLITE HEADING 282.72 DEG

GROUND RANGE

8:45:
38.878



Fig. 7. Example of a synthetic Aperture Radar image from the satellite SEASAT-1.

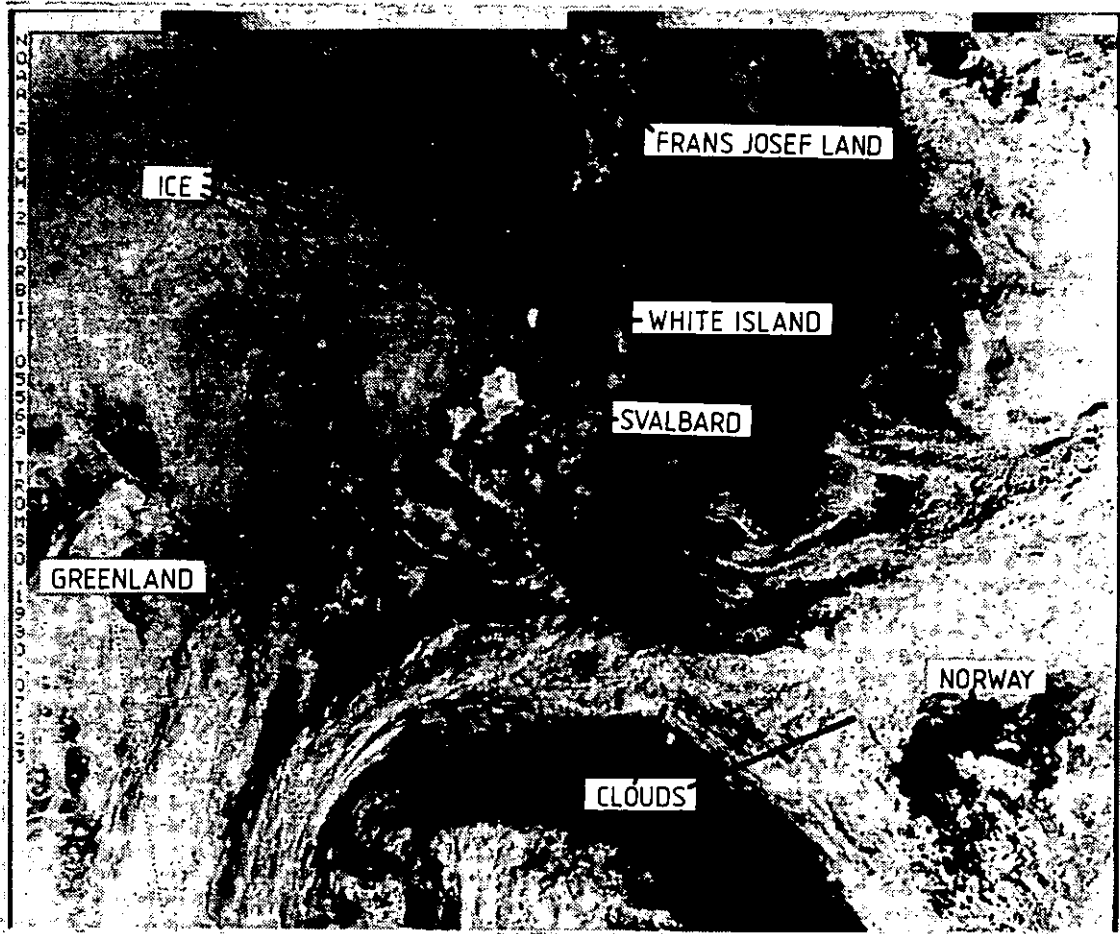


Fig. 8. NOAA-6 satellite image from 23 July 1980, covering part of eastern arctic.

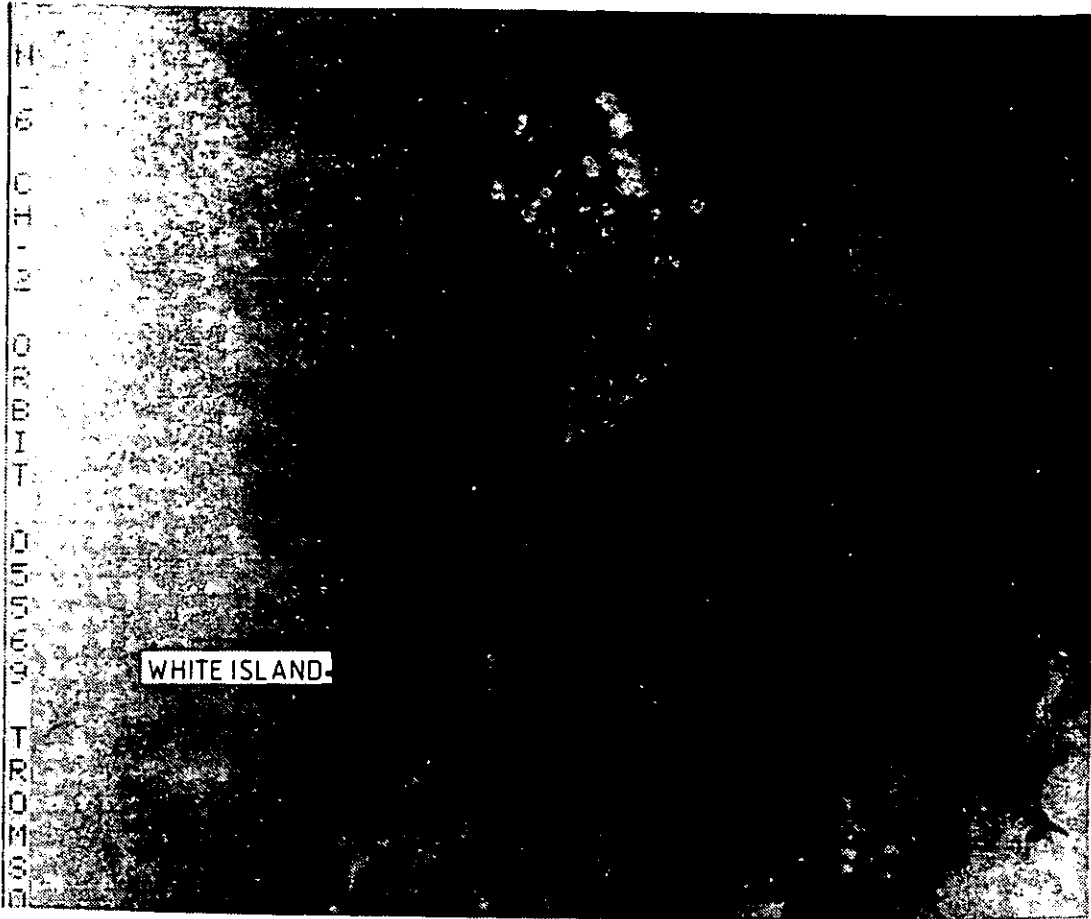


Fig. 9. NOAA-6 satellite image from 23 July 1983, from the area between Svalbard and Franz Josefs Land. (Detail of Figure 8.)



Fig. 10. LANDSAT image from July 1980, showing the ice around White Island.

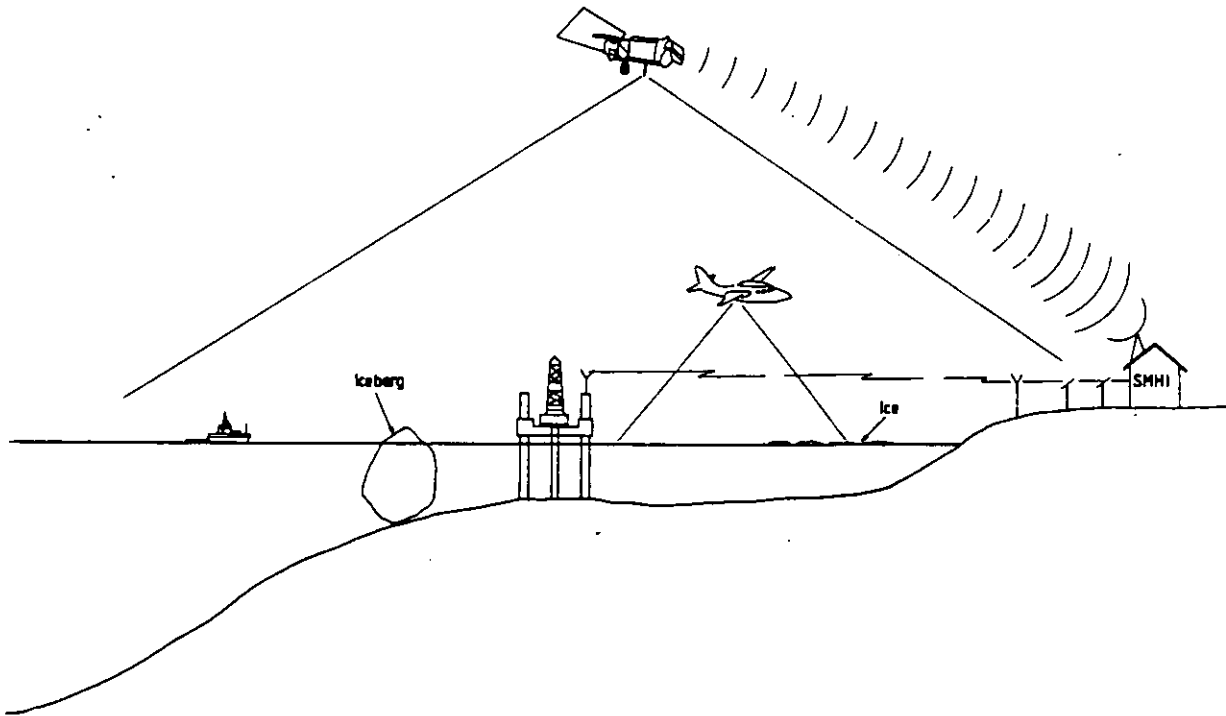


Fig. 11. Ice surveillance system.



Mr Kaj Riska

Mr Petri Varsta

STRUCTURAL ICE LOADS IN THE BALTIC

1 INTRODUCTION

This lecture included in the course "Ships and structures in Ice" describes the ice loads encountered by ships in first year relatively thin ice appearing e.g. in the Baltic. From the designers point of view these ice loads can at present be adequately taken into account. This is reflected for instance in the decision which the committee updating the Finnish-Swedish ice class rules made i.e. the strength level in the present rules from year 1971 is adequate with an exception of some minor problems in longitudinally framed ships / 1/.

This level of knowledge was not, however, reached by a deep understanding of the nature and thus the calculation of ice loads in the Baltic. On the contrary, it is based on extensive strength analysis of about 200 ice damaged vessels in the Baltic /3/. The analysis provided the adequate strength levels for each structural member without a recourse to a deep analysis of ice loads.

The present lecture tries to describe how to evaluate the design ice loads from the knowledge gathered about the mechanics of ice loads. The lecture is divided into

two parts, first the ship-ice interaction and its modelling is described. In the second part the structural ice loads are evaluated based on the research done in this area.

First, however, a brief description of ice and ice conditions in the Baltic is given.

2 ICE CONDITIONS IN THE BALTIC

2.1 Occurrence of ice

The climate in the Baltic can be characterized as sub-arctic in sense that the annual 0°C -isotherm passes close to the northern Baltic. The freezing of sea follows closely the passage of 0°C -isotherm which happens on average in the end of October in the northern regions and in the beginning of December in the Gulf of Finland. The freezing starts about a month after the passage of 0°C -isotherm.

After the freeze-up ice thickens on average linearly reaching its maximum thickness in April, see Fig. 1. The maximum thickenss is about 1 m in the northern regions and about 80 cm in the Gulf of Finland /5/, Fig. 2. The maximum extent of ice cover is reached in the beginning of March when on average the Gulf of Bothnia and the Gulf of Finland are ice covered /6/. During the most severe winters the ice edge can be well south of the island Gotland. All ice disappears during May and thus ice in the Baltic is first year ice.

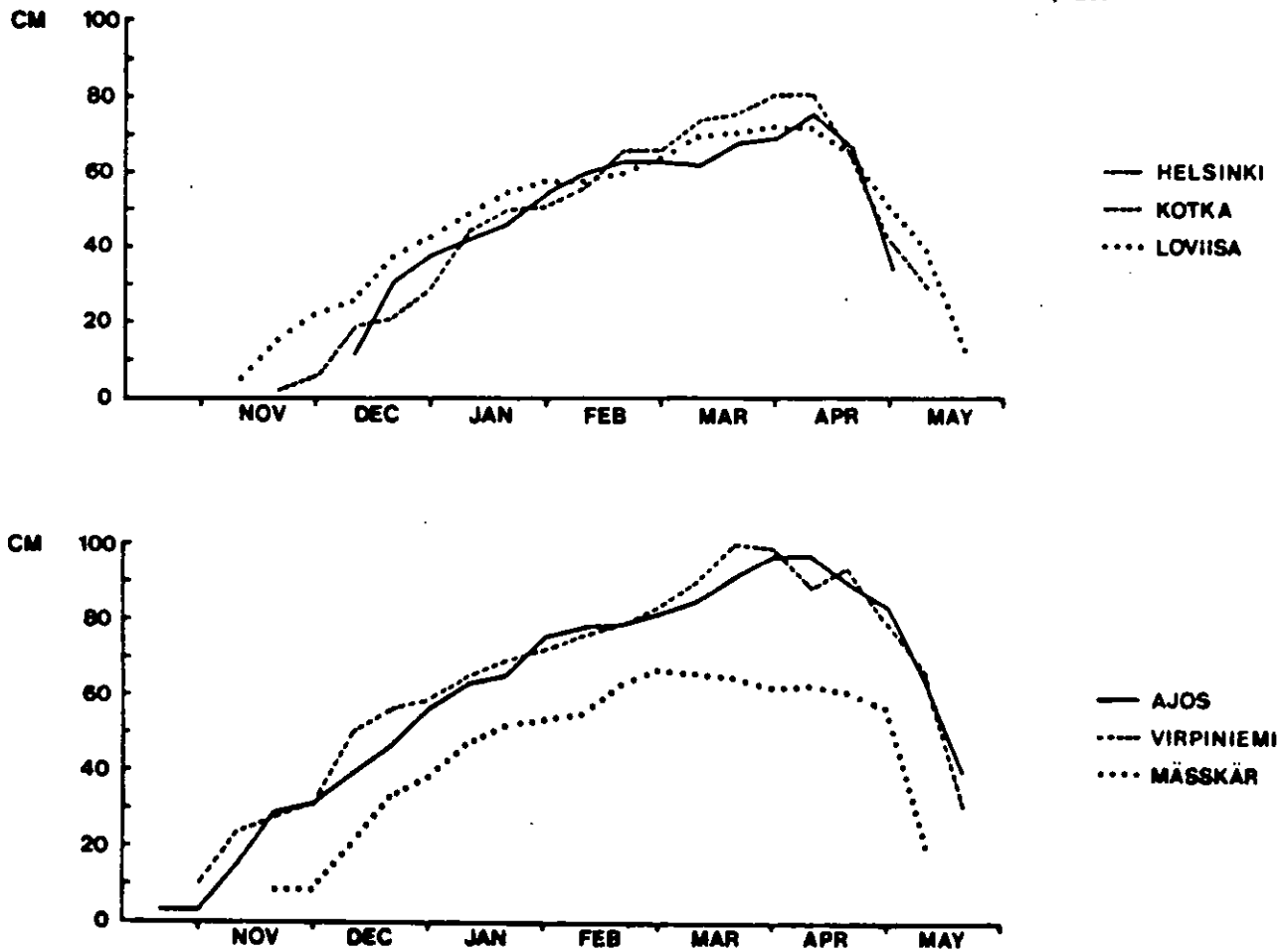


Fig. 1. Time evolution of the maximum level ice thickness in the Gulf of Finland and in the northern Baltic /6/.

Ice cover in the Baltic can be divided into two areas; shore fast zone and the area outside the coast where ice is moving. The movement causes ice cover to ridge and also quite wide leads occur, Fig. 3. The ridges in the Baltic can be about 20 m thick. The ridge fields can be quite extensive along the edge of the shorefast ice zone. In this area there can be some tens of ridges along a track 1 km long. These common ridge fields present a great obstacle for winter navigation in the Baltic.

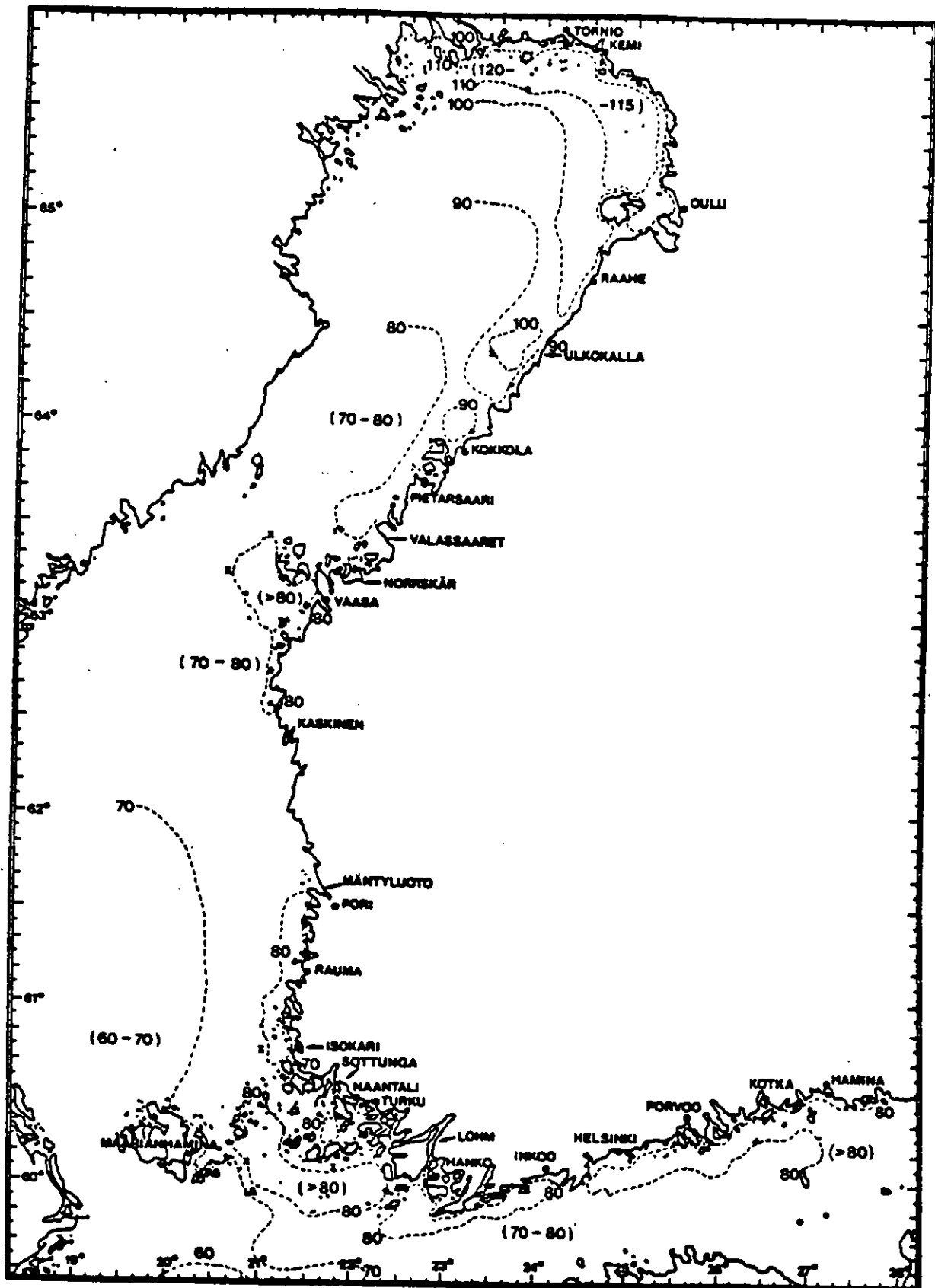


Fig. 2. Maximum level ice thickness [cm] along the Finnish coast in 1920 - 1980 /6/.

MERENTUTKIMUSLAITOS
HAVSFORSKNINGSINSTITUTET
INSTITUTE OF MARINE RESEARCH

No: **37** **25. 2. 1982**

Thick ice, continuous in level and depth
Continued, narrow or very thin ice up to 10-15%
Subsistence, narrow or very thin ice

Area of ice
Area of ice up to 10-15%
Area of ice up to 10-15%

Area of ice up to 10-15%
Area of ice up to 10-15%
Area of ice up to 10-15%

Area of ice up to 10-15%
Area of ice up to 10-15%
Area of ice up to 10-15%

Area of ice up to 10-15%
Area of ice up to 10-15%
Area of ice up to 10-15%

Area of ice up to 10-15%
Area of ice up to 10-15%
Area of ice up to 10-15%

Area of ice up to 10-15%
Area of ice up to 10-15%
Area of ice up to 10-15%

Area of ice up to 10-15%
Area of ice up to 10-15%
Area of ice up to 10-15%

Area of ice up to 10-15%
Area of ice up to 10-15%
Area of ice up to 10-15%

Area of ice up to 10-15%
Area of ice up to 10-15%
Area of ice up to 10-15%

Area of ice up to 10-15%
Area of ice up to 10-15%
Area of ice up to 10-15%

Area of ice up to 10-15%
Area of ice up to 10-15%
Area of ice up to 10-15%

Area of ice up to 10-15%
Area of ice up to 10-15%
Area of ice up to 10-15%

Area of ice up to 10-15%
Area of ice up to 10-15%
Area of ice up to 10-15%

Area of ice up to 10-15%
Area of ice up to 10-15%
Area of ice up to 10-15%

Area of ice up to 10-15%
Area of ice up to 10-15%
Area of ice up to 10-15%

Area of ice up to 10-15%
Area of ice up to 10-15%
Area of ice up to 10-15%

Area of ice up to 10-15%
Area of ice up to 10-15%
Area of ice up to 10-15%

Area of ice up to 10-15%
Area of ice up to 10-15%
Area of ice up to 10-15%

Area of ice up to 10-15%
Area of ice up to 10-15%
Area of ice up to 10-15%

Area of ice up to 10-15%
Area of ice up to 10-15%
Area of ice up to 10-15%

Area of ice up to 10-15%
Area of ice up to 10-15%
Area of ice up to 10-15%

Area of ice up to 10-15%
Area of ice up to 10-15%
Area of ice up to 10-15%

Area of ice up to 10-15%
Area of ice up to 10-15%
Area of ice up to 10-15%

Area of ice up to 10-15%
Area of ice up to 10-15%
Area of ice up to 10-15%

Area of ice up to 10-15%
Area of ice up to 10-15%
Area of ice up to 10-15%

Area of ice up to 10-15%
Area of ice up to 10-15%
Area of ice up to 10-15%

Area of ice up to 10-15%
Area of ice up to 10-15%
Area of ice up to 10-15%

Area of ice up to 10-15%
Area of ice up to 10-15%
Area of ice up to 10-15%

Area of ice up to 10-15%
Area of ice up to 10-15%
Area of ice up to 10-15%

Area of ice up to 10-15%
Area of ice up to 10-15%
Area of ice up to 10-15%

Area of ice up to 10-15%
Area of ice up to 10-15%
Area of ice up to 10-15%

Area of ice up to 10-15%
Area of ice up to 10-15%
Area of ice up to 10-15%

Area of ice up to 10-15%
Area of ice up to 10-15%
Area of ice up to 10-15%

Area of ice up to 10-15%
Area of ice up to 10-15%
Area of ice up to 10-15%

Area of ice up to 10-15%
Area of ice up to 10-15%
Area of ice up to 10-15%

Area of ice up to 10-15%
Area of ice up to 10-15%
Area of ice up to 10-15%

Area of ice up to 10-15%
Area of ice up to 10-15%
Area of ice up to 10-15%

Area of ice up to 10-15%
Area of ice up to 10-15%
Area of ice up to 10-15%

Area of ice up to 10-15%
Area of ice up to 10-15%
Area of ice up to 10-15%

Area of ice up to 10-15%
Area of ice up to 10-15%
Area of ice up to 10-15%

Area of ice up to 10-15%
Area of ice up to 10-15%
Area of ice up to 10-15%

Symbol	Description	Scale	Notes
C	Ice concentration (1/10)	10-100	10-100
C	Top of concentration in level	10-100	10-100
C	Year concentration	10-100	10-100
C	Continuation	10-100	10-100
C	Stop of concentration	10-100	10-100
C	Form of surface	10-100	10-100
C	Form of surface	10-100	10-100

Derivoiden pinta- ja pinnan keskiarvo
yhteensä matalampi
sea surface temperature

Year	Value	Notes
21.02.	(1966-80)	
21.02.	(1966-80)	
21.02.	(1966-80)	

LIKENNEMÄÄRÄJÄRJYTYKSET
TRAFIKBÄNSÄMNINGARNA
RESTRICTIONS TO NAVIGATION

Location	Restrictions	Start Date	End Date
Porvoo, Oulu, Rauma	I A	2000	1.2.1982
Rovaniemi, Pori, Rauma	I A	2000	8.2.1982
Vaasa, Rauma, Pori, Rauma	I A, I B	2000	8.2.1982
Uusikaupunki	I, II	1200	15.1.1982
Helsinki, Turku, Vaasa, Rauma, Oulu, Rauma	I, II	1200	15.2.1982
Rauma, Rovaniemi	I, II	900	15.2.1982
Porvoo, Loviisa, Rauma, Helsinki	I A, I B I C, II	1200 2000	15.2.1982

Rajajärjestelmä on voimassa alkaen...
Päätyä...
Välillä...

Location	Restrictions	Start Date	End Date
Porvoo, Oulu, Rauma	I A	2000	1.2.1982
Rovaniemi, Pori, Rauma	I A	2000	8.2.1982
Vaasa, Rauma, Pori, Rauma	I A, I B	2000	8.2.1982
Uusikaupunki	I, II	1200	15.1.1982
Helsinki, Turku, Vaasa, Rauma, Oulu, Rauma	I, II	1200	15.2.1982
Rauma, Rovaniemi	I, II	900	15.2.1982
Porvoo, Loviisa, Rauma, Helsinki	I A, I B I C, II	1200 2000	15.2.1982

MERENTUTKIMUSLAITOS - HAVSFORSKNINGSINSTITUTET
PL 100
00701 Helsinki 14
PB 100
Fors 14

Vuoksu
Tammikuu 25. 2. 1982

Fig. 3. Ice conditions in the Baltic.

2.2 Baltic sea ice

Seawater in the Baltic is brackish. The salinity in the mid-Baltic is about 6 o/oo and it decreases towards northern Baltic being in the northernmost areas about 3 o/oo. The salinity of ice is usually under 1 o/oo. The brine drainage phenomenon is apparent in salinity and ice is usually devoid of salt in the end on winter.

The ice cover in the Baltic consists of three layers. Bottom layer is columnar-grained ice, sometimes called black ice. In this layer the ice crystals are candlelike the long axis being vertical. The middle layer is snow ice formed from frozen slush and on top of that there is snow cover, Fig. 4.

When modelling the ice loads the data about mechanical properties serve as input data. Especially the behaviour of ice when loaded should be determined. Ice under load behaves principally in two different ways. Depending on the strain rate and temperature the response of ice is purely elastic with brittle failure or viscoelastic with ductile failure. In the ship-ice interaction the strain rate is so high that ice can be considered as elastic

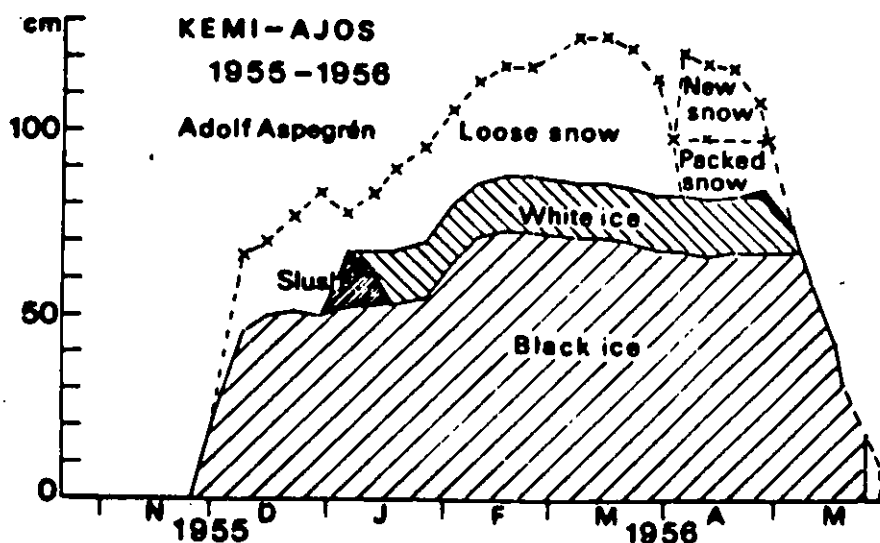


Fig. 4. Ice layer in the northern Baltic /5/.

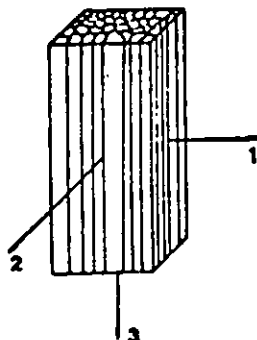
and brittle material /2/. The structure of columnar-grained ice is anisotropic. Thus also the mechanical properties reflect the anisotropy the type of which is called transverse anisotropy i.e. the horizontal plane is a plane of isotropy.

The main part of the thickness of first year ice in the Baltic is S2 type columnar-grained ice. The mechanical behaviour of S2 ice in ship-ice interaction can be characterized by a constitutive equation and a failure criterion.

The constitutive equation for columnar-grained ice includes five independent elastic parameters. Further improvement from the values given in reference /7/ has been done on the basis of the field measurements carried out by VTT/Ship Laboratory in the Bothnian Bay close to Kemi. These elastic constants were evaluated by compressive tests and are given in Table 1.

Table 1. Elastic parameters of S2 columnar-grained ice in elastic brittle range. Ice temperature $T_i = -6$ °C.

E_1 [GN/m ²]	E_3 [GN/m ²]	G_{13} [GN/m ²]	ν_{12}	ν_{13}
7.28	10.16	2.48	0.59	0.34



- E_i Young modulus in the i -direction
- G_{ij} shear modulus in the ij -plane
- ν_{ij} Poisson's ratio, when stress is in the i -direction.

The failure criterion used for S2 ice should be flexible enough to take into account the anisotropy of ice and also the different tensile and compressive strengths. The Tsai-Wu macroscopic failure criterion is well suited for S2 ice. It includes seven strength parameters which have been evaluated based on measurements and literature. These are presented in Table 2.

Table 2. Strength values for columnar-grained ice at temperature -6°C .

S_{1C}	= 3.70 MN/m ²	S_{iT}	tensile strength in the i-direction
S_{3C}	= 5.16 MN/m ²	S_{iC}	compressive strength in the i-direction
$U_C(45^{\circ})$	= 2.80 MN/m ²	$U_C(\theta)$	off axis compressive strength, where the 3-axis has been inclined by angle θ
S_{1C}^{P2} / S_{1C}	= 3.5	S_{iC}^{Pj}	confined compressive strength in the i-direction, where restraint is in the j-direction.
S_{1C}^{P3} / S_{1C}	= 1.0		
S_{1T}	= 0.55 MN/m ²		
S_{3T}	= 1.0 MN/m ²		

The macroscopic failure criterion can predict the stress state under which the specimen fails. The applications of Tsai-Wu criterion are presented in reference /7, 9/.

The properties of snow ice in the top layer are important when considering the bending failure of ice cover. The tensile strength is most important parameter for bending failure. However, there is a discrepancy between values measured with bending tests and direct tensile tests and therefore the bending test results can be considered most reliable for Baltic sea ice. The values for flexural

strength are /9/

top layer $S_{1B} = 0.92 \text{ MN/m}^2$
bottom layer $S_{1B} = 0.55 \text{ MN/m}^2$

3 THE SHIP-ICE INTERACTION

3.1 Background

The modelling of ship-ice interaction can be separated into two items; describing the response of ship and ice under the contact force and determination of the contact force. The contact force arises when ship hits ice edge and crushes it, Fig. 5. The contact force can be presented using the average contact pressure p_{av} and contact length l_c in form /9/

$$F_n = p_{av} l_c \frac{2}{\sin 2\beta_n} \cdot \xi_c \quad (1)$$

$$= C_p \xi_c$$

The relationship between displacements of ice cover and ship and crushing depth /10/ is

$$\frac{F_n}{C_p} = w_{ns} - w_{ni} \quad (2)$$

In ship displacement w_{ns} is included the rigid body motions and also the possible vibratory response. The displacement of ice cover includes rigid body motions and bending deformation. The motions can be determined from

equations of motion and the bending of ice cover can be solved with e.g. finite element method which accounts also for the added mass of water under the ice.

In the first year ice like in the Baltic, the rigid body motions are negligible and thus Eq. (2) reduces to

$$\frac{F_n}{C_p} = v_n t - w_{ni}, \quad (3)$$

where v_n is the normal speed of the ship.

The average pressure forms the basis of structural loads in the Baltic. The load length and load height i.e. crushing depth could also be determined analytically by modelling the dynamic bending of ice cover. This approach is, however, only touched in this lecture.

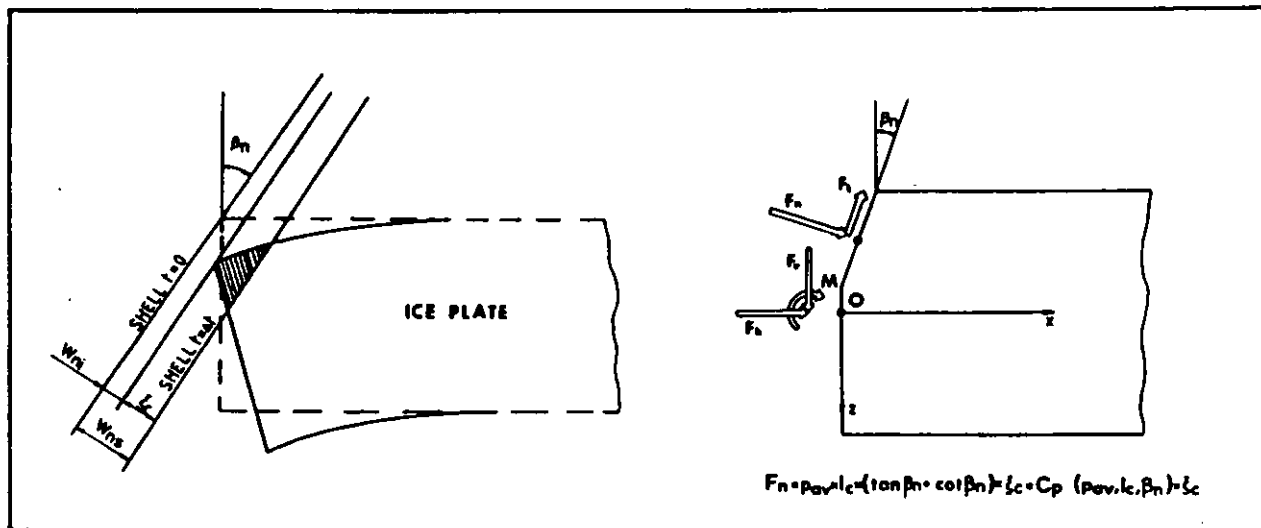


Fig. 5. The ship-ice interaction.

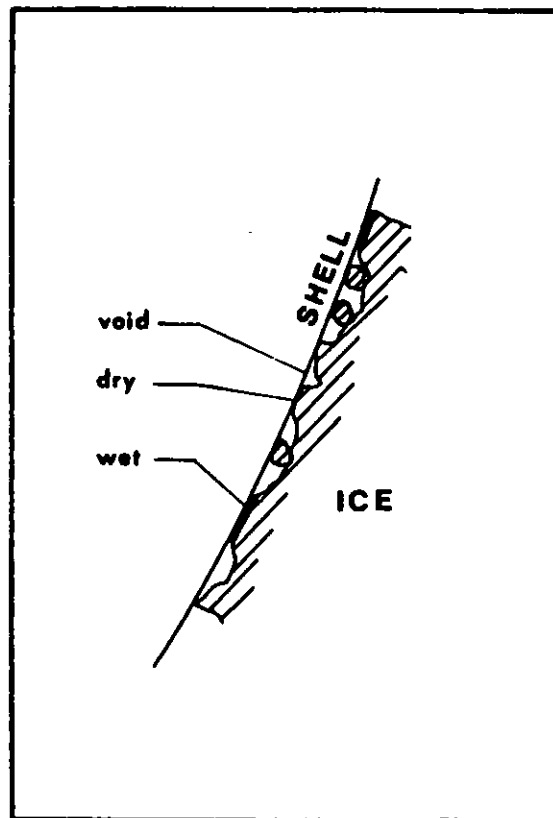


Fig. 6. Schematical presentation of the contact between the ice edge and shell and the contact types.

3.2 Ice pressure

The contact between ship and ice is not an ideal one between two solids, steel and ice. On the contrary it is quite irregular but it can be broken down to three different types of contact within the apparent contact area, Fig. 6. The contact can either be direct or transferred through a viscous layer or there can exist areas of no contact at all. It can be shown /9/ that if contact is transmitted through a viscous layer the pressure is greatest. This nominal pressure depends on ice parameters (which depend on temperature), frame angle and geometry of ice edge i.e. the so called constraint effect /9/.

The nominal 'wet' ice pressure p_{max} can be calculated knowing the ice parameters and the geometry of ice edge. It has also been measured with a special ice pressure

gauge /4, 10/, Fig. 7. The highest measured value in Fig. 7 is about 8 MPa but values up to 10 MPa has been measured in long-term measurements but the corresponding temperature is not known.

For dimensioning purposes it is suitable to establish the average ice pressure, p_{av} , which can be used to analyze larger structural areas. The strength of test specimens depends exponentially on their volume /9/. Similarly the average ice pressure depends on the load length because the load height was fixed. Also the stiffness of the structure influences the average pressure by changing the shape of ice pressure. The average pressure can be presented as

$$p_{av} = k_I \left(\frac{l}{s}\right) k_f(s, t) p_{max}. \quad (4)$$

The different flexibilities of frames and plating produce a pressure shape of triangular form /4, 8, 9/, Fig. 8. The exact shape can be calculated by assuming the ice to behave as a Winkler foundation. The load shape reduced the average pressure. The pressure reduction is a function of frame spacing s and plate thickness t . Also load height influences it out only slightly if load height is more than $s/2$. The pressure reduction can be taken into account by constant k_f which is equal to one for stiff structures. This constant is presented in Fig. 9.

k_f : contact length constant

The length contact can be evaluated based on measurements in which loads on different sized areas are measured. The results of measurements on board I.B. Sisu are presented in Fig. 10. Based on these measurements the form of the length constant is

$$k_I = \left(\frac{l}{s}\right)^{-0.27} \quad (5)$$

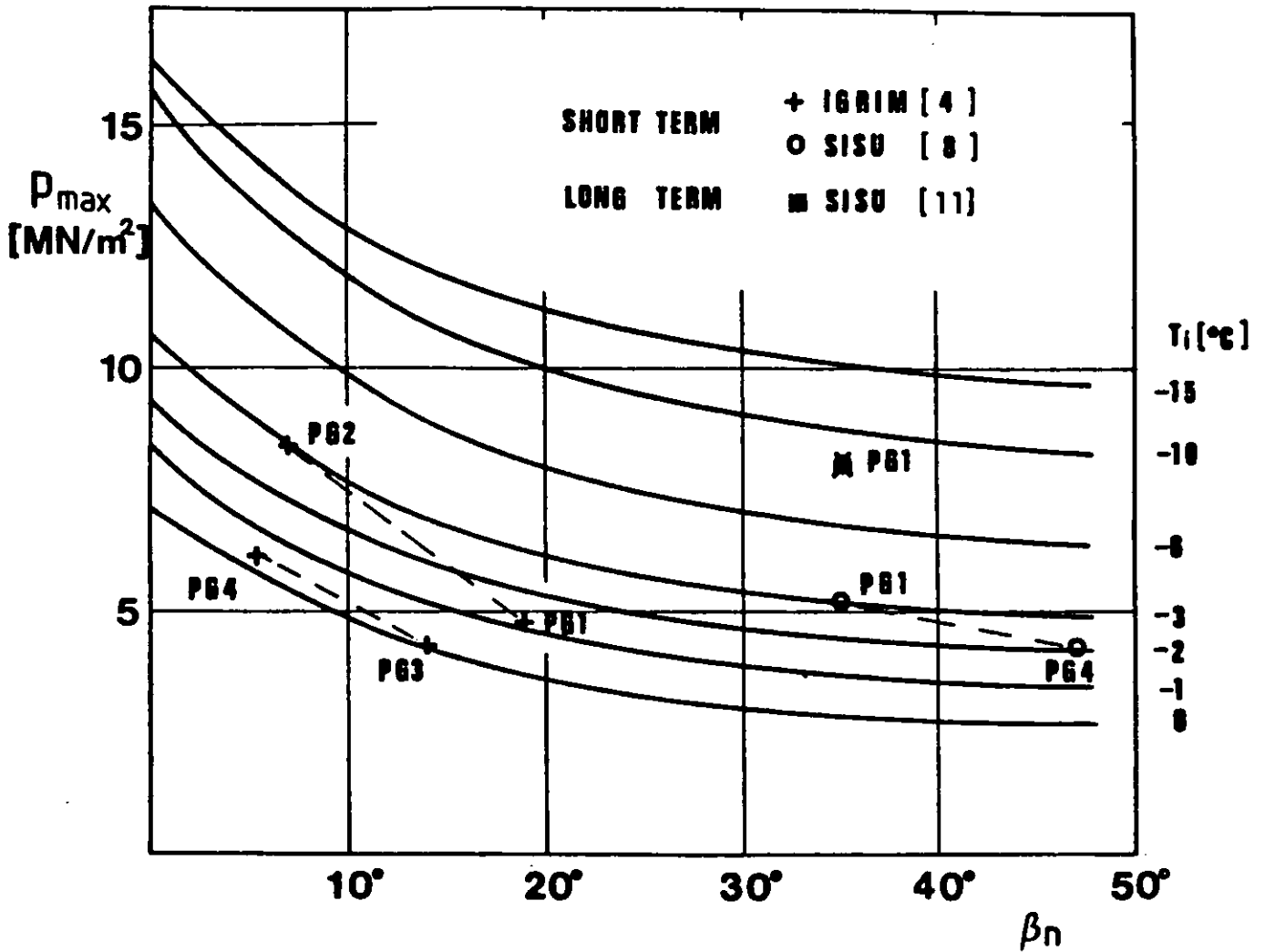


Fig. 7. The maximum ice pressures versus ice temperature and frame angle /9/. Also some results of measurements are shown.

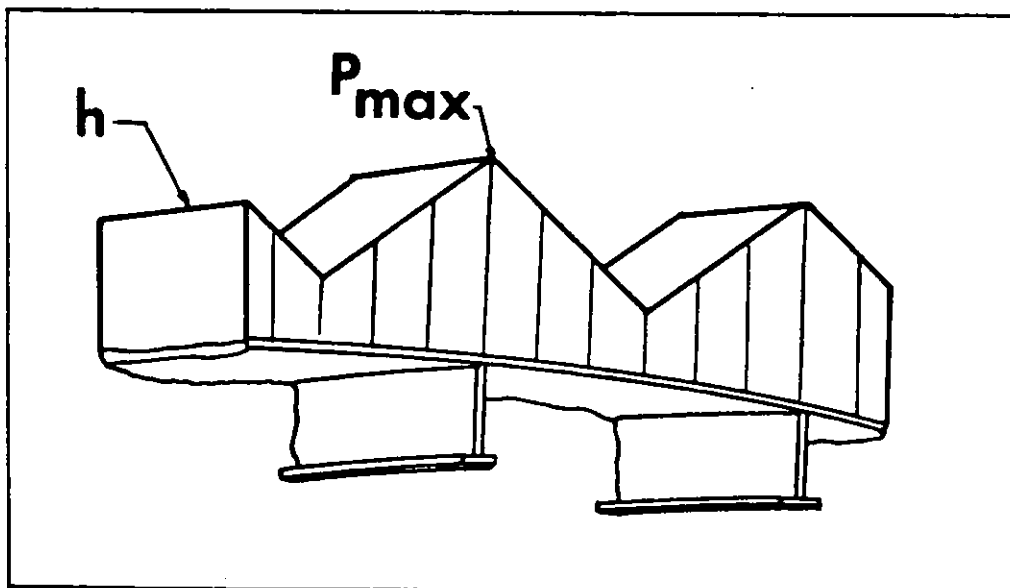


Fig. 8. The actual load shape.

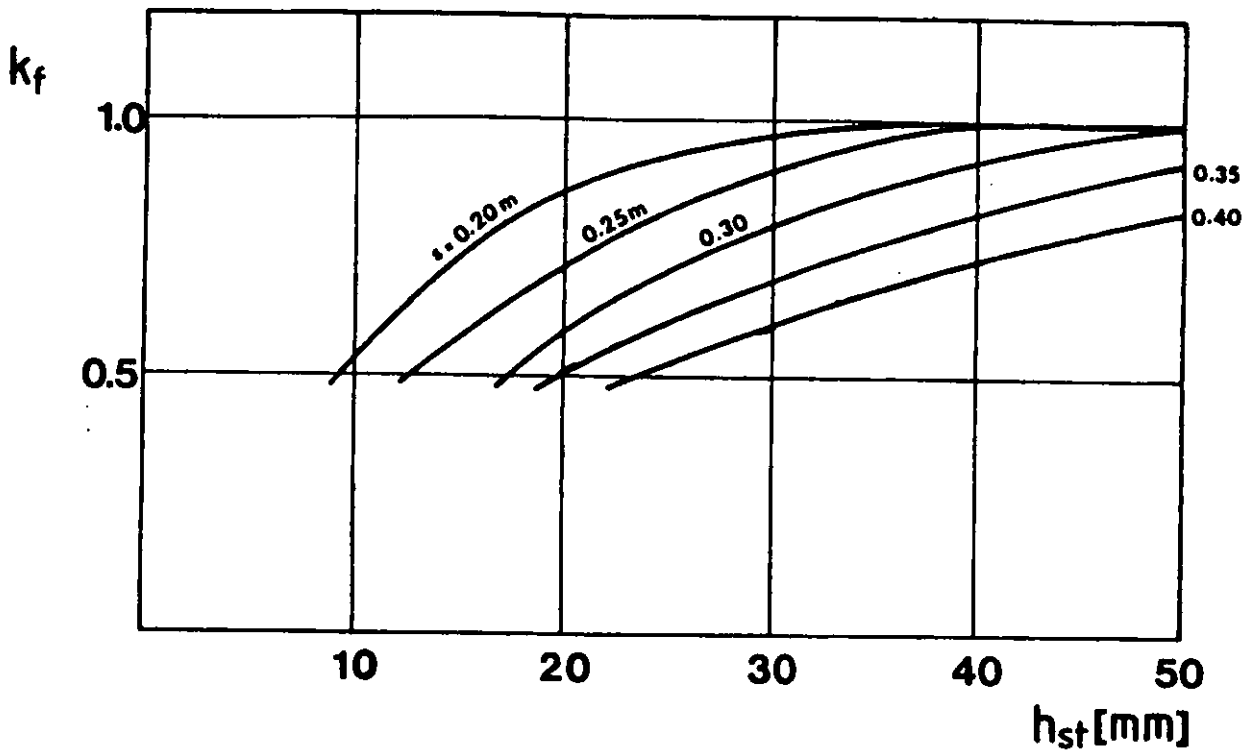


Fig. 9. The flexibility coefficient k_f as a function of plate thickness h_{st} and frame spacing /9/.

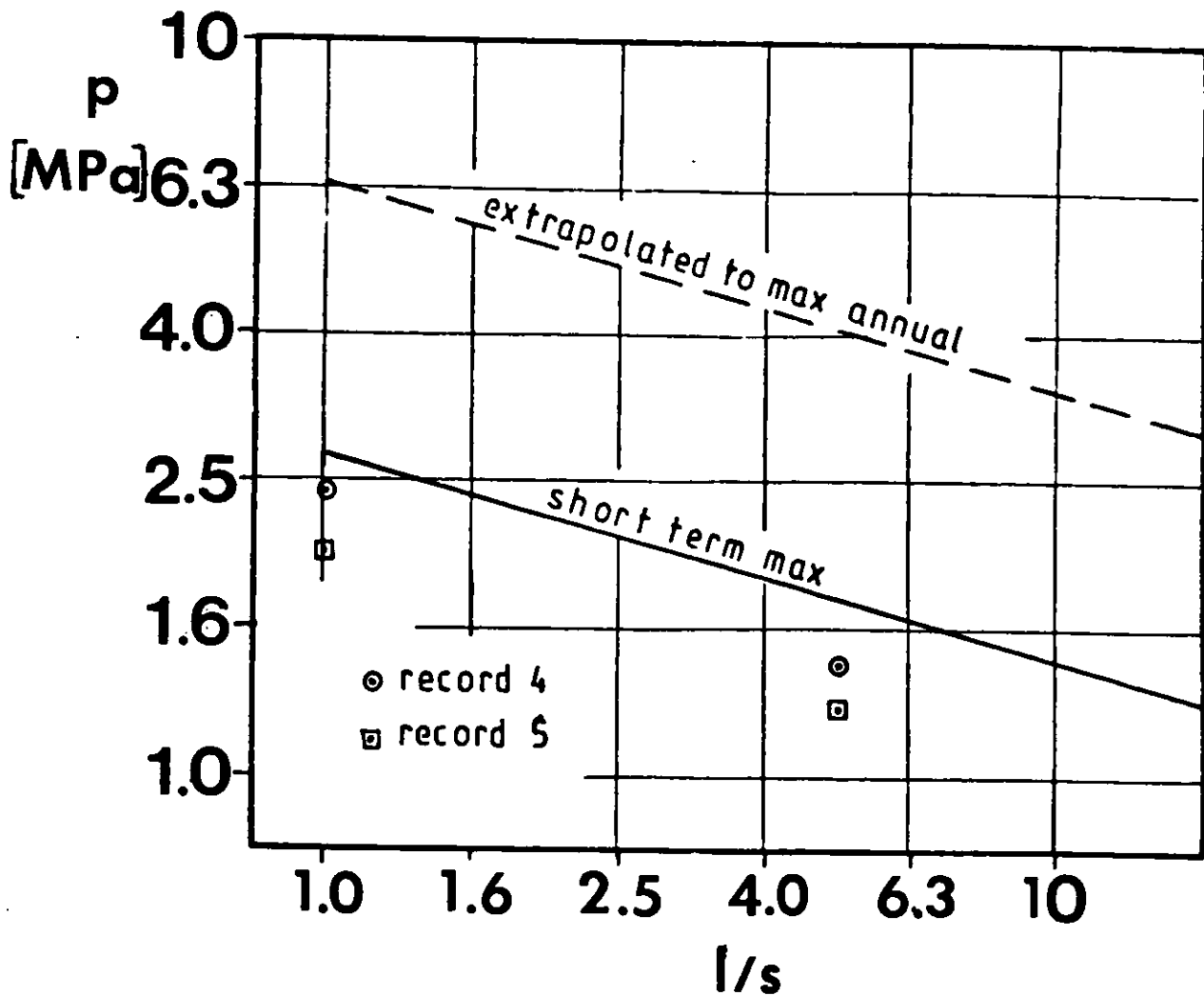


Fig. 10. Ice load versus load length based on short-term measurements /8/.

3.3 Ice load

The ice load, F_n is Eq. (1), depends mainly on the ice edge geometry, frame angle and ship's speed normal to the hull. Once the relationship between p_{av} versus crushing depth ξ_c is known, the dynamic bending could be modelled numerically. The highest load occurs when ice cover breaks and thus also a failure criterion for ice is needed. These kind of calculations provide a load height but the load length cannot be determined.

The effect of frame angle and normal ship's speed on ice load is presented in Fig. 11. In this figure also values from full scale test are plotted. The calculation and tests were performed with a selected ice edge geometry, in which the load length was 3.5 m. The ice thickness influences ice load much, see Fig. 12. The consequence of the uncertainty of tensile or flexural strength of ice cover is also clearly seen in the figure.

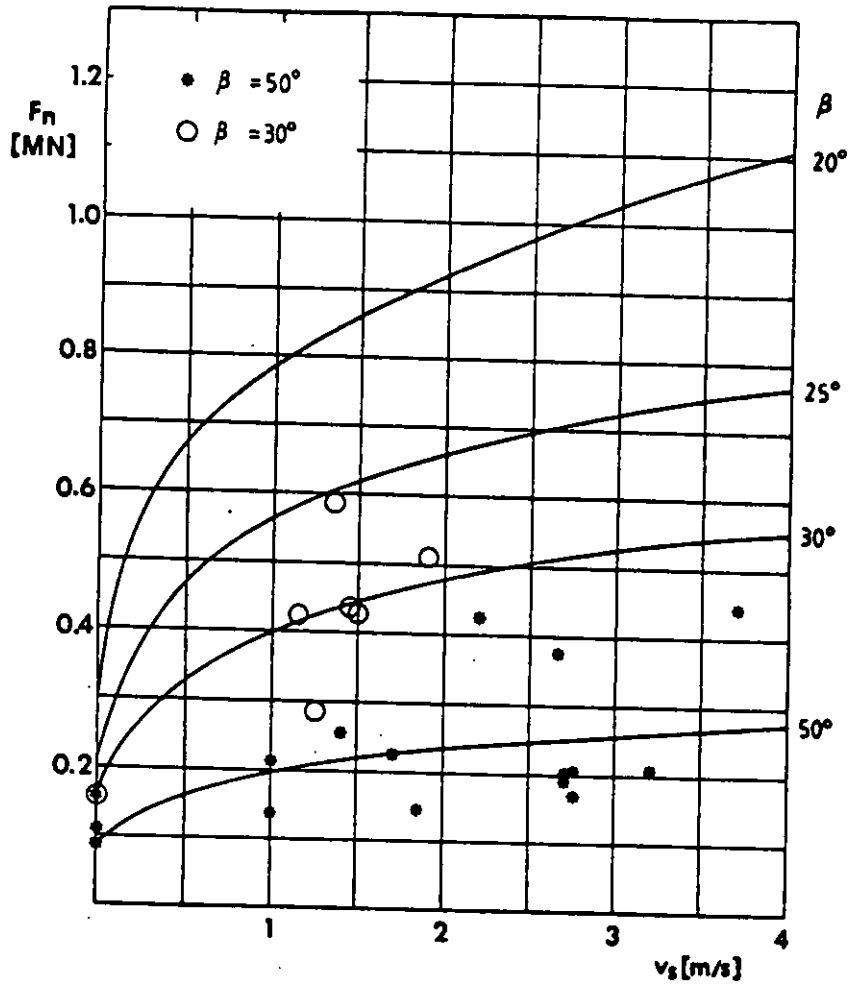


Fig. 11. Ice load versus ship's speed and frame angle /9/. Test results from full scale trials are also shown. Load length 3.5 m.

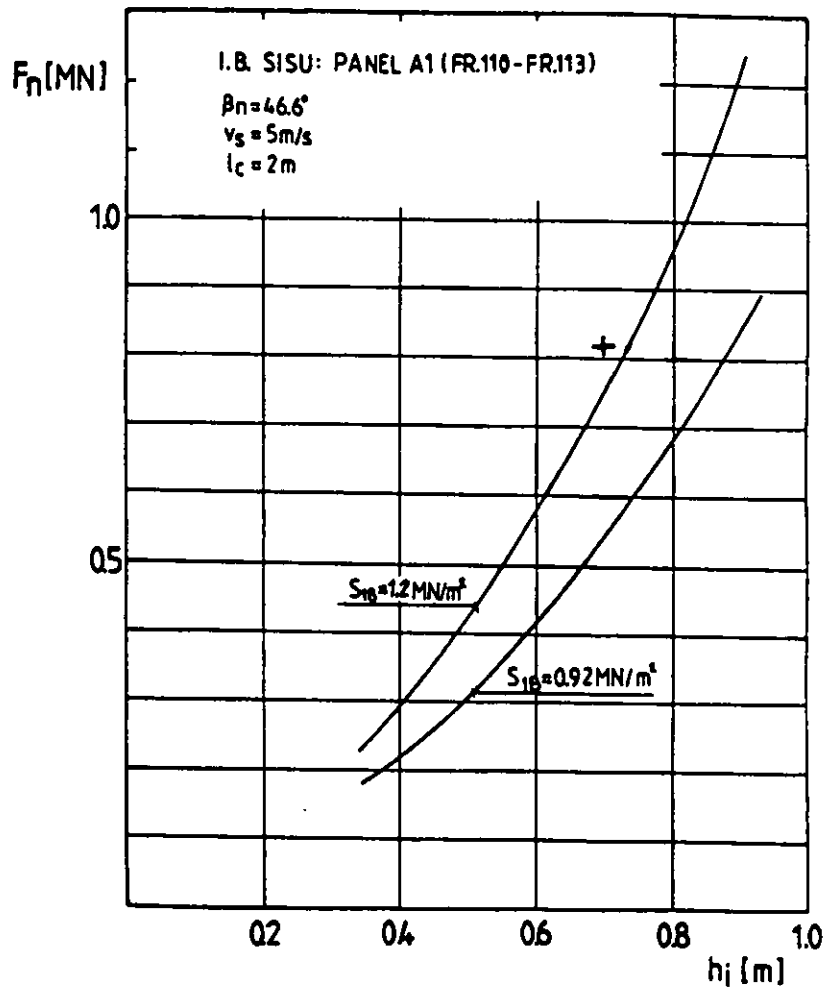


Fig. 12. Ice load versus ice thickness and flexural strength of ice cover [9]. A full scale test result is also shown. In the full-scale tests ice thickness varied between 60 cm and 80 cm and the value shown is the maximum measured value.

4 STRUCTURAL ICE LOADS IN THE BALTIC

4.1 Design approach

The representation of ice load as a distributed pressure load is very suitable design approach. When representing ice loads in this way many factors stemming from as well from structural as navigational and operational points of view should be taken into account. These factors are usually incorporated into the design ice pressure in form of coefficients i.e. the design ice pressure p is

$$p = C_1 C_2 p_0 \quad (6)$$

where C_1 and C_2 are coefficients the meaning of which is explained subsequently and p_0 is the structural ice pressure.

More powerfull ships attain higher speed when proceeding in ice. Also ships with bigger displacement can due to their inertia have high instantaneous speeds. Higher speeds again cause higher loads, cf. Fig. 11. The speed coefficient C_1 is commonly presented $/1, 3/$ with the aid of square root of power and displacement, see Fig. 13. It should be noted that the fore part and midship and aft parts differ because normal speeds encountered are different.

The other coefficient included should describe the operational use of ships. This is done in the Baltic by separating the ships into different ice classes. The ships in lower ice classes are navigated more cautiously than ships in higher classes. As a reference the coefficient C_2 proposed for Finnish-Swedish ice class rules is given in Table 3.

Table 3. Factor C_2 .

Ice class	Fore part of ship	Midship	After part of ship
1A super	1.00	1.00	0.75
1A	1.00	0.85	0.65
1B	1.00	0.70	0.45
1C	1.00	0.50	0.25

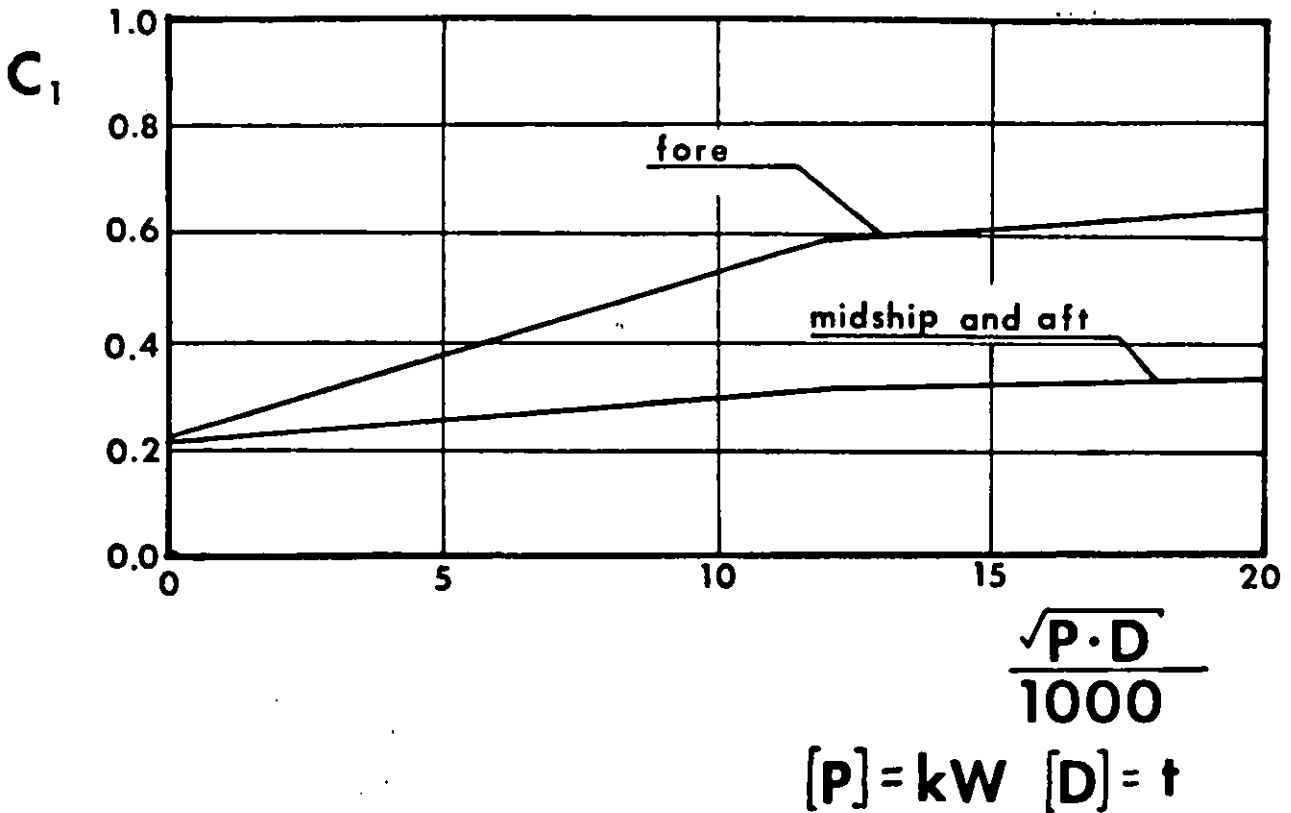


Fig. 13. Values of coefficient C_1 versus square root of power and displacement /1/.

The division into different ice classes is reflected also in another aspect. Ships in higher ice classes usually proceed in thicker ice. Thus for design purposes the height of the ice pressure i.e. loaded area should be determined. As a guidance Table 4 can be presented /1/.

Table 4. Height of the load area in different ice classes.

Ice class	Height of the load area [m]
1A super	0.35
1A	0.30
1B	0.25
1C	0.22

4.2 Structural ice pressure

The determination of structural ice pressure p_o described in this chapter is based on the research presented in chapter 3. For stiffeners the structural ice pressure is equal to the average ice pressure in Eq. (1). To apply the concept average pressure, p_{av} , it should first be noted that in structural hierarchy of ships different structural members have different load length associated with them, see Table 5. This load length is taken into account by the coefficient k_1 , Eq. 3. For plating and frames in transversely framed ships the load length is frame spacing and thus $k_1 = 1$.

Table 5. Length of the load area.

Structural element	Length of the load area l_a
Transversely stiffened plates	Frame spacing [m]
Longitudinally stiffened plates	Span of the frame [m]
Transverse frames	Frame spacing [m]
Longitudinal frames	Span of the frame [m]
Ice stringers	Spacing of the web frames [m]
Web frames	Spacing of the web frames [m]

The stiffeners are not sensitive to the load shape and the average pressure is only important. It enables us to use in design calculations uniform pressure distribution. The shell plating is, however, sensitive to the load shape. The response of plating to triangularly shaped pressure is less than to uniform pressure eventhough the average pressure is the same. To obtain an uniform pressure for desing purposes for plating the average pressure p_{av} should be reduced. This is done by introducing an additional coefficient k_{pl} ^{*} the values of which are presented in Fig. 14. Thus the structural ice pressure for plating is

* FOR OTHER ELEMENTS $k_{pl} = 1$

$$p_o = k_l k_f k_{pl} p_{max} \quad (7)$$

The final question which remains in determining the structural ice pressure in the Baltic is which value should p_{max} attain. The most reliable answer at the moment is given by full scale long term ice pressure measurements. Based on the measurements by VTT/Ship Laboratory the maximum value measured is 10 MPa. This seems to be quite suitable value for design purposes.

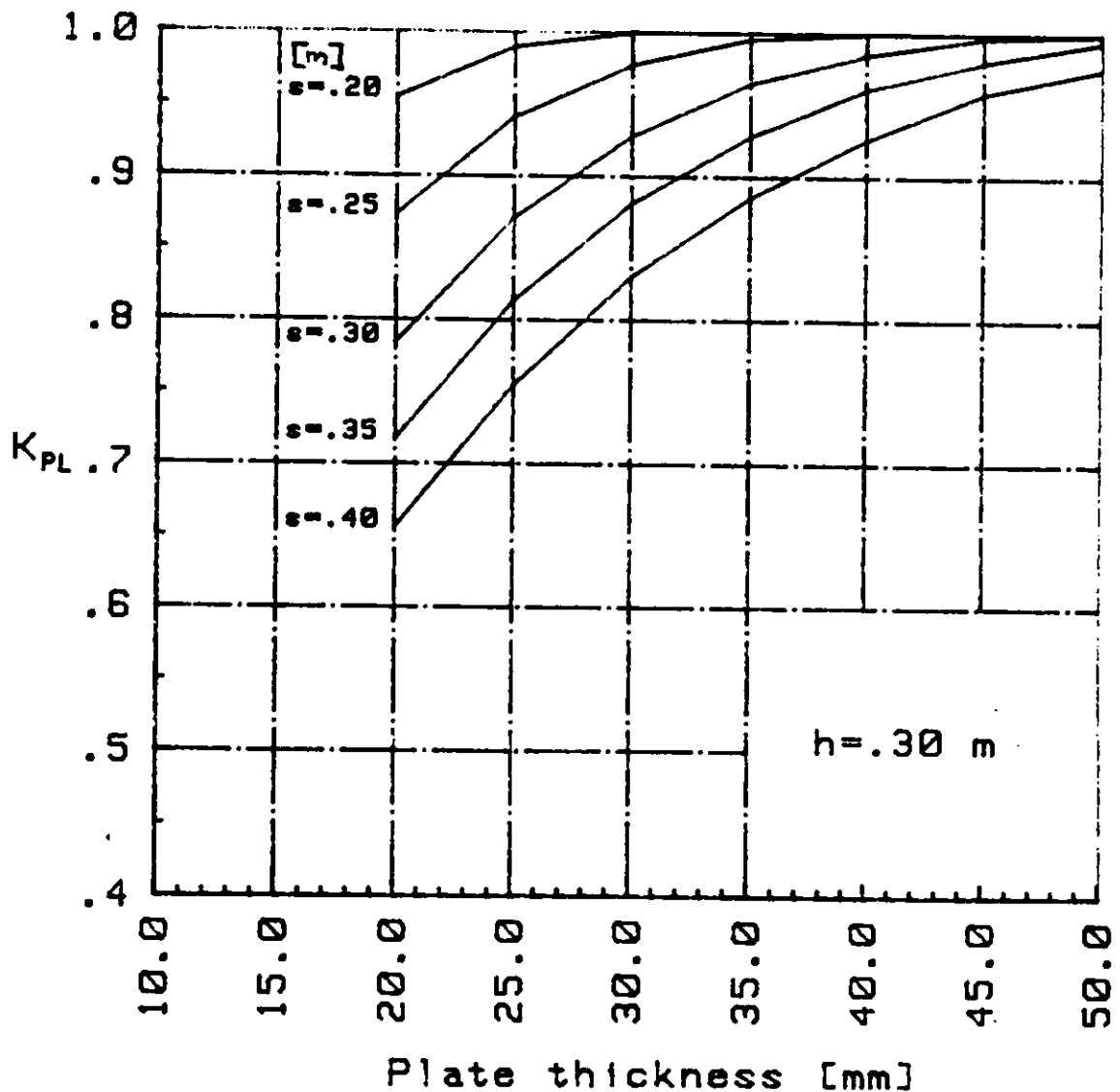


Fig. 14. Coefficient k_{pl} versus frame spacing and plate thickness.

REFERENCES

1. Up-dating Baltic ice class regulations: design formulae for hull structure elements in ice-strengthened ships. Espoo 1982, VTT/Ship Laboratory Report. 28 p. Unpublished.
2. ENKVIST, E. et al., The ship-ice interaction. POAC 79, proceedings vol. 2 Trondheim, August 13 - 18, 1979. The University of Trondheim and the Norwegian Institute of Technology. Trondheim 1979. pp. 977 - 1002.
3. JOHANSSON, B., On the ice-strengthening of ships hulls. International shipbuilding progress 14(1967). pp. 231 - 245.
4. KORRI, P. & VARSTA, P., On the ice trial of a 14500 dwt tanker on the Gulf of Bothnia. NSTM -79, Helsinki, 1979. Publ. LARADI, Helsinki 1979. 31 p.
5. PALOSUO, E., Absolute greatest thickness of level ice on the Baltic Sea. Geophysica 17(1982)1-2. pp. 133 - 142.
6. PALOSUO, E., et al., Formation, thickness and stability of fact ice along the Finnish coast. Helsinki 1982 Winter Navigation Research Board, Report No. 36. 19 p.
7. RISKKA, K., On the role of failure criterion of ice determining ice loads. Espoo 1980. VTT/Ship Laboratory, Report No 7. 31 p.
8. RISKKA, K. & al., Ice load and pressure measurements on board I.B. Sisu. To be published in POAC 83.

9. VARSTA, P., On the mechanics of ice load on ships in level ice in the Baltic sea. Helsinki 1982. VTT/Ship Laboratory Research Report (unpublished).
10. VARSTA, P., Modelling of impact between ship hull and ice. To be published in POAC 83.
11. VUORIO, J. et al., Long-term measurements of ice pressure and ice-induced stresses on the icebreaker SISU in winter 1978. Helsinki 1979. Winter Navigation Research Board, report no. 28. 50 p.



Dr. Arno Keinonen

ICE LOADS ON SHIPS IN THE CANADIAN ARCTIC

Abstract

In Canada during the last few years, the state of the art of ice impact pressure and force determination has progressed rapidly.

This paper presents some of the main developments based on tests with Dome Petroleum's icebreaker Carmar Kigoriak.

The new data suggests three changes (1, 2, 3) in the Canadian Arctic Shipping Pollution Prevention Regulations (CASPPR) and those changes should address the implications of two other (4, 5) findings:

1. A proposed increase of limiting local ice pressure in the ships bow from 10.34 to 20 MPa;
2. A proposed addition of ice force carrying capacity requirements over large areas of the bow;
3. The introduction of global strength requirements for ship hull girders due to impacts with extreme ice features;
4. In impacts with extreme ice features, there is an important amount of dampening taking place which reduces the stress levels in the hull girder; and,
5. There is some evidence that scaling up the existing data from Kigoriak to bigger ships will give relaxation to the global load requirements.

ACKNOWLEDGEMENTS

The work to determine ice loads and ship response has been made possible by Dome Petroleum's economic support as well as that of the Canadian Coast Guard.

The technical work has been performed largely by employees of Dome Petroleum. The Technical Research Centre of Finland has been the main contractor measuring ice pressures, loads, and stresses on the Kigoriak.

The personal cooperation and strong support of Mr. John McCallum of the Canadian Coast Guard is also acknowledged.

1. INTRODUCTION

Ice navigation history in the Canadian Arctic is much shorter than in the Soviet Union or in those sub-Arctic areas of the northern hemisphere which experience significant although less severe ice conditions. In fact, all present ship operations in the Canadian Arctic are extended summer operations which focus on avoiding ice rather than on attempting to efficiently and regularly break ice.

The ice conditions in the Canadian Arctic are more severe than for any other areas where ships have thus far operated on a year-round basis. The continuous existence of significant amounts of glacial ice as well as the large areas experiencing thick multi-year ice introduce different as well as more stringent requirements than for areas experiencing seasonal ice only.

Currently, all shipping operations in the Canadian Arctic are governed by the CASPPR. The CASPPR were written about 10 years ago based mainly on the Baltic regulations. There was no significant experience at that time in Canadian Arctic ice conditions where the existence of glacial and multi-year ice introduces new problems. The limitations of the regulations has resulted in the Canadian Arctic Coast Guard initiating the development of research to lead to the development of new CASPPR regulations via numerous analytical, model scale and full scale studies.

In this presentation, the past development related to Arctic ship operations are first introduced to give some background to the present situation. Then, the related anticipated future development of technology is outlined and the roles of glacial and multi-year ice as related to future developments are discussed.

The text consists principally of an approach for developing ice load criteria for future Arctic ships as used by Canadian Marine Drilling Ltd. (Canmar). This includes full scale impact tests with the Canmar Kigoriak, introduction of their results, discussion of their meaning, and use of the results for determination of ice loads for future Arctic tankers.

2. ICE HAZARDS AND SHIP NAVIGATION IN THE CANADIAN ARCTIC

From a ship navigation point-of-view, there are several ice features of significance found in the Canadian Arctic. The first of these is slowly moving glacial ice and ice islands or their fragments (Fig. 1). There isn't yet a final solution to coping with the danger they pose to shipping in the region. The second important feature is multi-year ice (Fig. 1).

Glacial ice poses a problem due to its size - tens of times the size of a ship. Multi-year ice, while often of lesser size, is extremely dangerous because of its strength and thickness.

3. DEVELOPMENTS IN NAVIGATION

High latitude shipping in Canada in the post-war years has been limited to service on a summer basis to small communities, government establishments and resource exploration and production operations. The factor which has begun to change this situation rapidly is the discovery of marketable quantities of gas and oil in Alaska, the Beaufort Sea and the High Arctic Islands.

Due to these discoveries, a major component of a number of Canadian Arctic projects over the last decade has been the development of new technology with the capability of extending the operational season for icebreaking ships. The most far-reaching in these projects is the planned

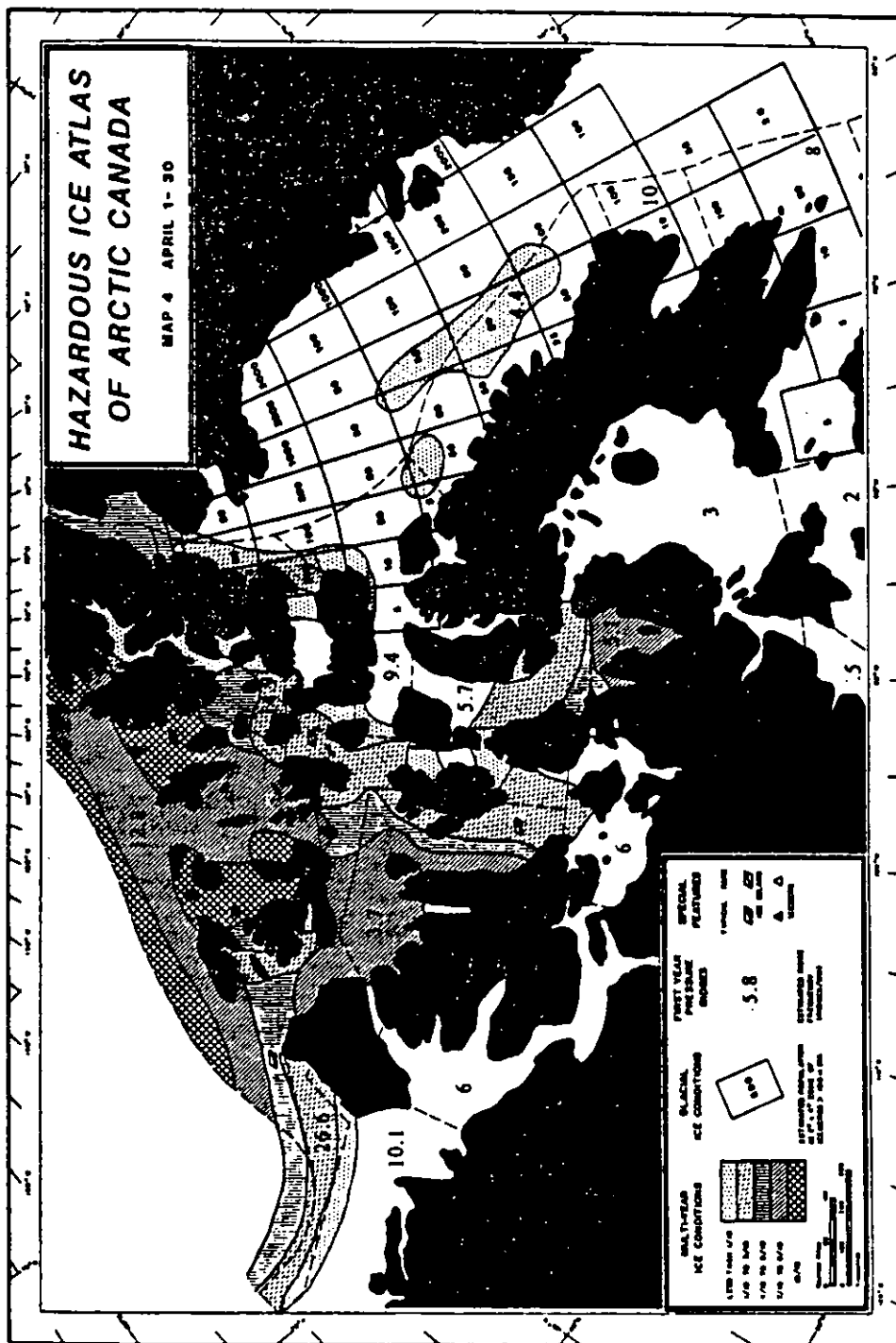


FIG. 1 ICE HAZARDS IN THE CANADIAN ARCTIC FOR A TYPICAL APRIL 1-30 PERIOD. (REF. 2)

development of an Arctic LNG carrier and oil tanker capable of year-round transportation of gas or oil to world markets either via the North West Passage to the East or via the Beaufort Sea and Bering Strait to the west. The first important development project was the summer transit of the Manhattan through the North West Passage in 1979. The purpose of that voyage was to determine whether a refitted ship could successfully complete the voyage. The results indicated that while such a ship could complete the voyage on an experimental basis; much remained to be learned concerning ice loads before sufficient knowledge would exist to write adequate safety regulations for Arctic shipping.

To give some idea of the density of commercial traffic in 1978 in the Canadian Arctic north of latitude 60°, there were approximately 300,000 shipkilometers (Ref. 6) recorded that year. One-third of those shipkilometers were recorded north of latitude 70°. Further, local Canadian Beaufort exploration shipkilometers by Canmar that year were approximately equal to all the traffic above latitude 70°.

From a limited accident data base, the safety record for navigation in the Canadian Arctic does not compare favourably with shipping in southern Canadian waters. In a comparison between the St. Lawrence Seaway (Ref. 6) and the Arctic, the density of accidents turns out to be six times higher per distance travelled in the Arctic. Statistics indicate that the prime causes of these accidents have been unsuccessful attempts to avoid collision with large ice features or not detecting the hazardous ice feature or detecting it but not understanding its potential hazard to the ship.

3.2 DEVELOPMENT TRENDS

Assurance of ship safety will be a key feature to both government approval for any major year-round Canadian Arctic shipping project as well as to the day-to-day success, economic and political, of that operation. While nobody can predict at what date such operations could begin, present indications are that year-round navigation will occur within the next decade. Further, based on new developments in ice loads research in the Canadian Arctic, it seems that a re-evaluation of the CASPPR is required to make such operations successful.

To answer many of the questions which will result in both an economic and safe year-round large tanker operation, some basic questions effecting the ice load criteria for ships operating year-round needs be addressed. Many of these issues indeed will have no final answer until these large ships actually gather operational experience in the Canadian Arctic ice regime. Such issues include: Is a collision with an iceberg a structural design requirement for these ships? If it is, what kind of collision, and what critical consequences are there? If all icebergs can be avoided, what is the actual limiting occurrence for the structural integrity of the ship? What are the ice forces and responses of a ship in collision with an iceberg? What is the acceptable risk for different kinds of consequences of accidents? How can the risk be determined? Since accurate answers are not currently known to these questions, conservative designs are required which will prevent serious accidents in which ships and lives are lost and Arctic waters are polluted.

At the present time, there is considerable work going on in Canada to try to find answers to all these questions.

The ice load criteria put forward for an Arctic ship by Johansson et al (Ref. 7) and background to those given in this paper by Canmar is mainly based on the 1979-1981 full scale tests and the associated analytical work with the icebreaker Canmar Kigoriak.

4. ICE LOAD DETERMINATION

4.1 GENERAL

Currently in Canada, there are several projects underway attempting to solve parts of the problem of extreme ice loads determination and ship reaction to these loads.

The M.V. Arctic, a partially experimental Arctic bulk carrier, has been instrumented for determination of global as well as local ice loads and response of structure. The Louis St. Laurent and the Pierre Raddison, Canadian Coast Guard icebreakers, have been tested to measure local ice loads while obliquely hitting multi-year ice. Dome's Canmar Kigoriak was specifically instrumented and twice tested in head-on collisions with extremely heavy ice to measure local and global loads.

A large part of the results of these tests is confidential; however, a part of the Kigoriak data has been released by Dome in this paper and in Ref. 4 to encourage communication and discussion in the international scientific community.

4.2 ALTERNATIVE SCENARIOS

In these projects, the key ship/ice interaction scenarios have emerged and include:

1. head on collision with an iceberg;
2. oblique impact with an ice edge; and,
3. beaching on grounded or infinite size ice.

Common to all of these is that two force peaks and associated ship responses are experienced. That is, when the impact takes place a dynamic force peak is caused and when the ship is lifted high up a second static force peak is caused.

In this presentation, emphasis has been placed on analyzing a head on collision with an iceberg which is considered the ultimate challenge for a ship and showing both impact and static components for it. The other cases which can be actual extreme impacts are then modifications to this analysis and generally interpolations to less severe load levels. Thus, knowing what happens in a collision with an iceberg gives a good sound basis for calculating a limiting load analysis.

4.3 DESCRIPTION OF A 'HEAD ON' IMPACT

1. The Impact Phase (Fig. 2)

The impact phase extends from the point of time when the bow first touches the ice to the moment when the bow is actually sliding up on the edge of the ice. This is the fastest dynamic phase introducing the following phenomena:

- (a) The ship's surge velocity changes from V_0 to V_1 .

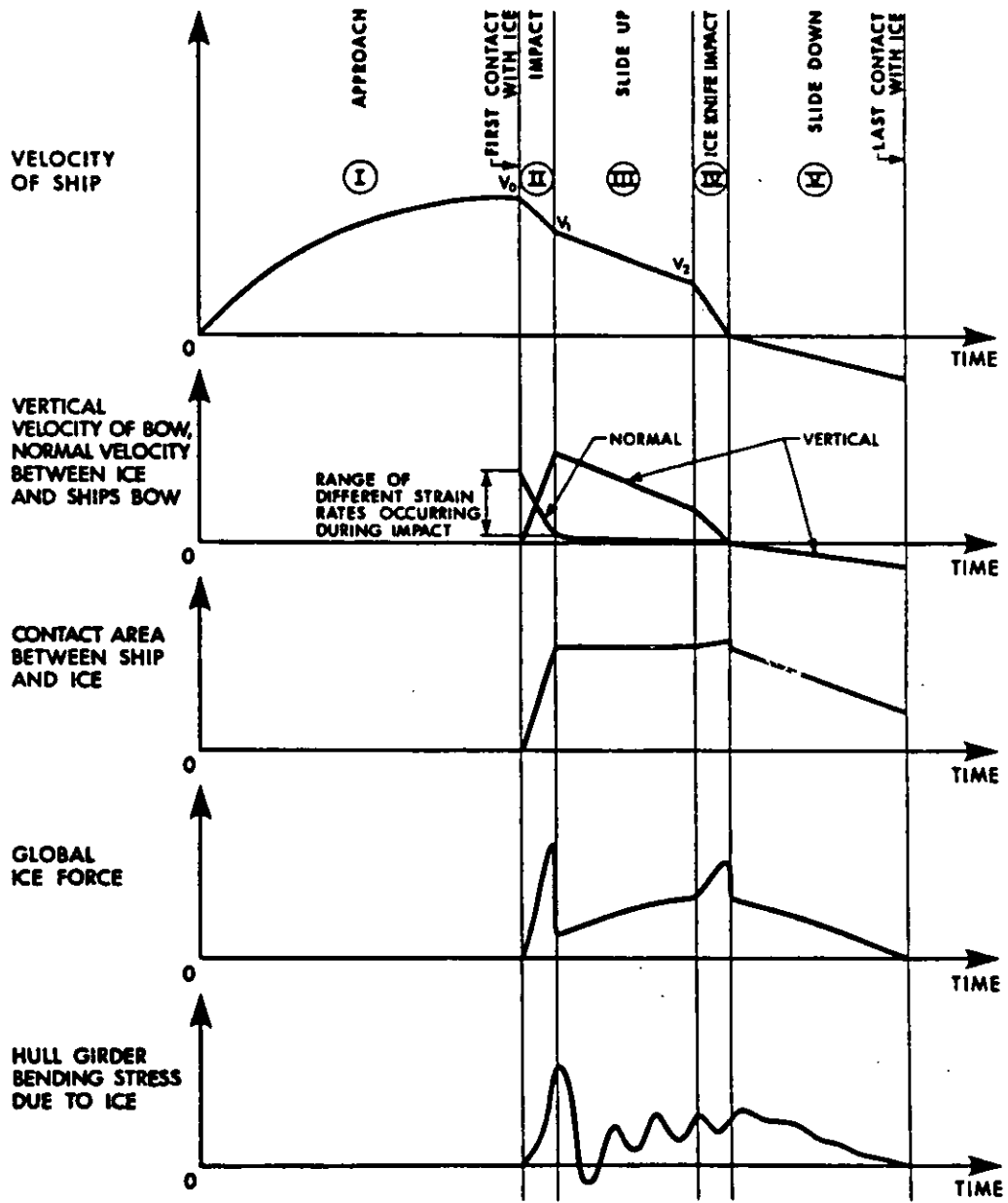


FIGURE 2 DESCRIPTION OF TYPICAL RAM SCENARIO

- (b) There is an increase in the vertical velocity of the bow from zero to its maximum value. Decrease of the normal velocity between the ship's bow and the ice occurs with the initial value of $V_0 \sin \varphi$, where φ is the stem angle, dropping to virtually zero. This guarantees that all strain rates for ice crushing are present during the impact.
- (c) The contact area increases from zero to its maximum value during the ram.
- (d) The global ice force increases to its maximum value at or close to the end of the impact.
- (e) The peak of the dynamic response of the hull girder is observed towards the end of this phase.

2. Slide-Up Phase

After the impact is over and the ship slides up on its stem area, there is a gradual transfer of kinetic energy to potential energy which shows as a decrease of all velocity components and an increase of the ship's trim and rising vertical position. Frictional losses also dissipate part of the energy. There are some minor amounts of ice destroyed in the interface during this phase.

This phase ends when all the kinetic energy is expended (at low velocities) or when there is a second impact between the vertical ice forefoot, if the ship possesses one, and the ice.

3. Ice Forefoot Impact

when there has been enough initial kinetic energy (ie. high enough impact velocity), the ice forefoot will hit the ice and stop the ship by expending the remaining kinetic energy.

The magnitude of the global ice force will reach a second peak during this phase which can be of the same order of magnitude as the first impact peak.

At the end of this phase, the static beaching force maximum is seen.

4.4 LOCAL ICE PRESSURES IN THE BOW

The smallest area of interest for the ship designer is the single shell plating unit. The ice pressure or load on this area is an important input to the problem of ice loads on the bow.

The theory is that for these plates, the limiting pressure factor for big ships is the crushing strength of the ice itself. For small ships, the limiting pressure will be less, due to lesser confinement. Two recently proposed formulae for determining this local pressure are:

1. Johansson et al (Ref. 7)

$$p_0 = 3 + 0.85 \sqrt{\Delta P} \quad (1)$$

where

p_0 = ice pressure on bow

Δ = ships maximum displacement in millions of kilograms

P = ship shaft power in MW

2. Tunik (Ref. 9) interpreted by Glen (Ref. 5)

$$p_0 = 2 + 6p^{0.18} - \Delta^{0.05} \quad (2)$$

Figure 3 compares these two equations and also shows the line corresponding to the present regulations (CASPPR). The limiting value which appears both in Johansson's and Tunik's proposals seems to be 20 MPa for local ice pressure when the present rules would be asking for 10.34 MPa as a maximum independent of ship size.

An important item to note concerning local loading is that the measured small scale compressive strength of ice, uniaxial or borehole jack, does not have a constant relationship with the ice pressures on the bow of the Kigoriak as reported by Ghoneim and Keinonen (Ref. 4). The factor between measured local ice pressure on the ship's bow and the uniaxial compressive strength of ice is between 2 and 5 depending on the type of ice, the factor being small for stronger ice. In a similar way, the borehole jack strength does not relate to the maximum pressure.

During the full scale tests of Canmar Kigoriak, the highest local pressures were measured during the impact phase of a collision. Another lesson learned from the Kigoriak tests (Ref. 4) was that no impact velocity dependency was detected for local maximum pressures measured on a 0.18 m diameter area. This can be understood from Fig. 2. The actual crushing rate for the ice may have varied stochastically in different peak pressure measurements, which would effectively hide any velocity dependence.

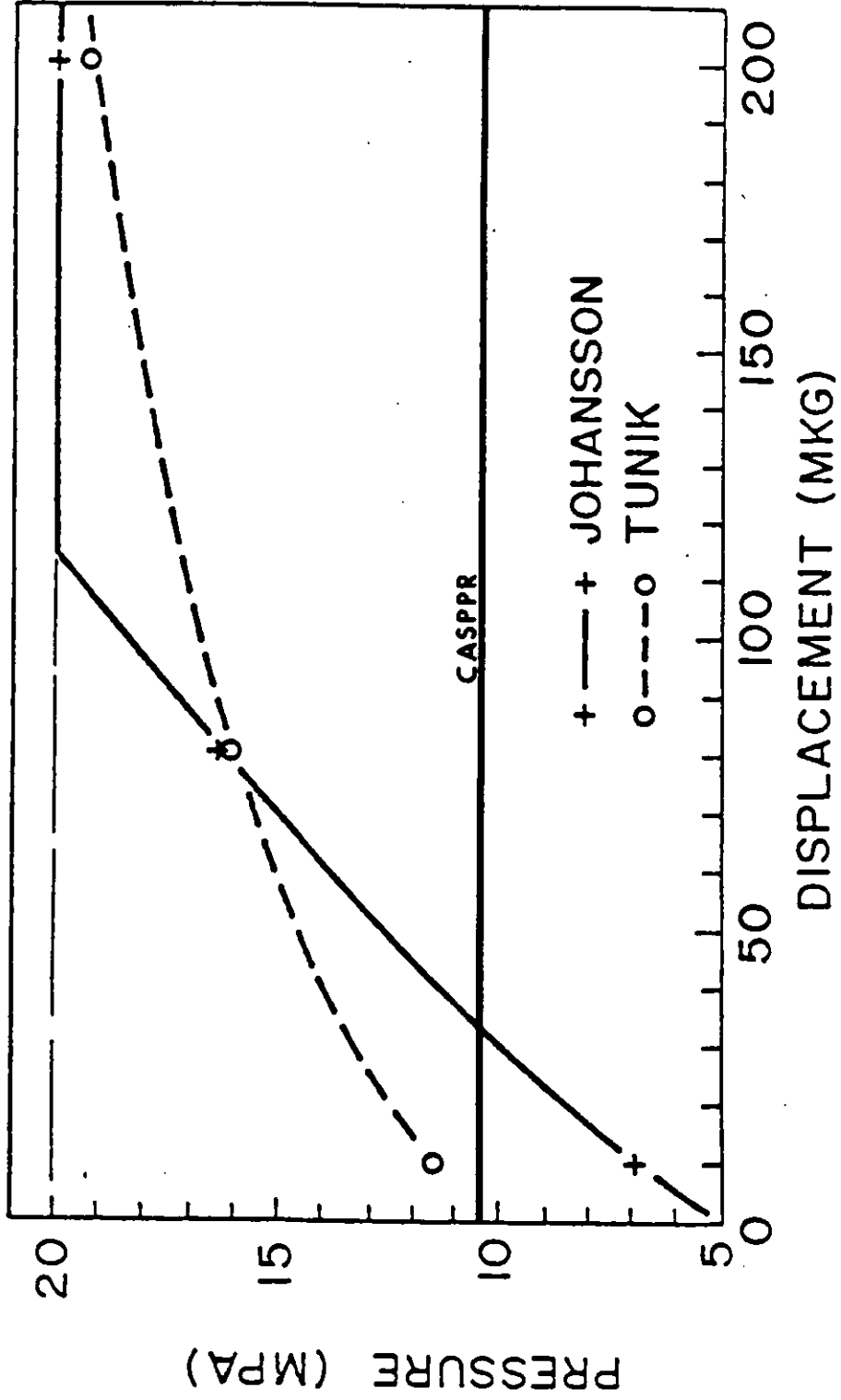


FIG. 3 PRESSURE VS. DISPLACEMENT. (REF. 5)

4.5 ICE LOADS ON THE BOW

Loads acting on larger areas of a ship's bow are of importance to a ship's designer in order to correctly determine the required strength of the larger load carrying members. These loads are mainly dictated by the ship characteristics; however, the crushing behaviour of ice also plays an important role. From Fig. 2, it can be seen that the dynamic peak force occurs at or close to the end of the impact phase. The static peak force occurs at the moment when the ship is highest up and is a result of beaching. Also, dependent on the configuration of the ice forefoot, the second impact between it and the ice may be associated with the highest force.

Johansson et al (Ref. 7) propose a formula to determine the maximum bow force for a ship, not specifying but

implying that the force occurs during the first impact:

$$F_m = v \cdot \Delta^{0.9} \quad (3)$$

where

F_m = maximum force in MN
 v = ship's impact in m/s

Tunik (Ref. 9) also proposes a formula for maximum bow force:

$$F_m = kv^{1.5} \cdot \Delta^{2/3} \quad (4)$$

where

K = coefficient depending on ship parameters

Again, Glen (Ref. 6) has made a comparison between these two proposals as seen in Fig. 4. It can be seen there that Johansson's formula gives lower loads for small ships in the same size range where all the existing full scale data lies. When extrapolating to larger ships, Johansson employs more conservatism than Tunik and thus, his formula yields higher ice loads. The comparison applies only to ships with Kigoriak geometry, that is, a flat stem and a spoon-shaped bow. To develop a formula for the force for a general ship shape, a geometric modification has been made to the Johansson formula:

$$F_m = 2.5 \cdot \sin \varphi \Delta^{0.9} \quad (5)$$

Another essential piece of information for the calculation of ice loads is the size and shape of the contact area over which the force is applied plus, if possible, the pressure distribution within that contact.

Johansson et al (Ref. 7) propose that this be represented by:

$$A_m = \sqrt{81 + 12F_m} - 9 \quad (6)$$

where

A_m = maximum area in m^2

The shape of the contact area is observed to be a narrow horizontal band with an aspect ratio of up to 1:5.

Tunik proposes a lengthy contact shape giving a maximum contact height [b(meters)]:

$$b = 0.4 + 0.1 (P \cdot \Delta)^{0.2} \quad \text{where} \quad (7)$$

b = maximum contact height

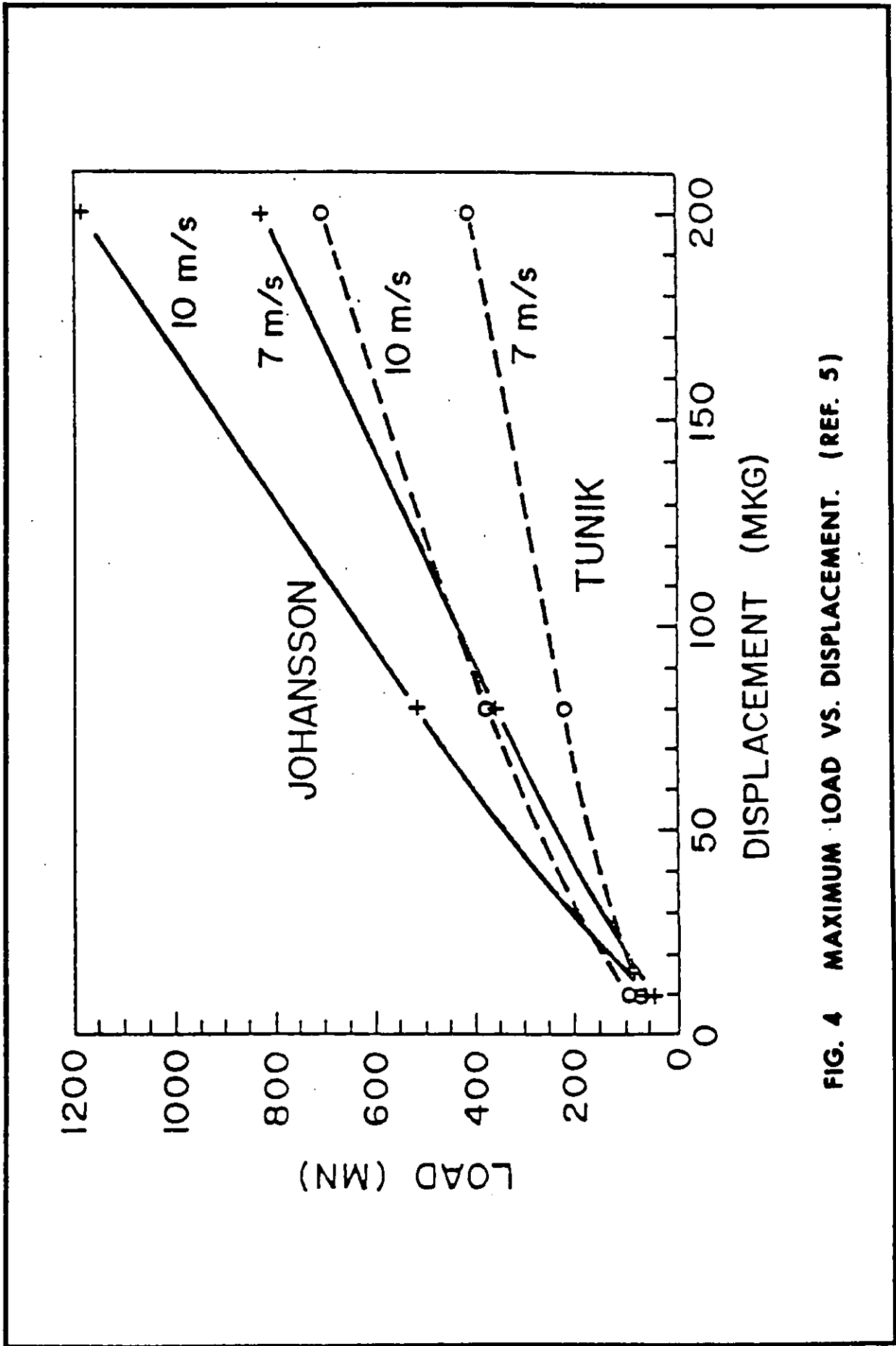


FIG. 4 MAXIMUM LOAD VS. DISPLACEMENT. (REF. 5)

These two formulae are not fundamentally dissimilar and both recognize the fact that contact areas tend not to be square in shape for example.

The experimental data from the Kigoriak full scale tests (Ref. 4) are plotted against Johansson's (Ref. 7) formulae in Fig. 5. The line has been plotted representing Johansson's formulae as well as the test results in the form of limiting curves for all test data lying at or below those lines shown for the August and October Kigoriak impact tests. Table 1 summarizes the environmental data represented by these curves. Also, in Fig. 5 the present yield limit of the structure of the bow is shown. During the tests, several yield exceedences were seen. The Kigoriak, a Class 3 (CASPRR) ship, was operating in the heaviest ice during these tests which means Class 10 requirements as shown in Fig. 5.

The other result from these tests with Kigoriak was the verification of the effect of velocity on the force. Figure 6 shows the increase of the mean of the peak forces during the impact phase of ramming with increasing impact velocity at the bow of the Kigoriak. It also shows a decrease or at least no increase beyond about 5 m/s impact velocity. This reversal from the expected trend is felt to be attributable to the crushing and cracking behaviour of that specific ice type which is described in Table 1.

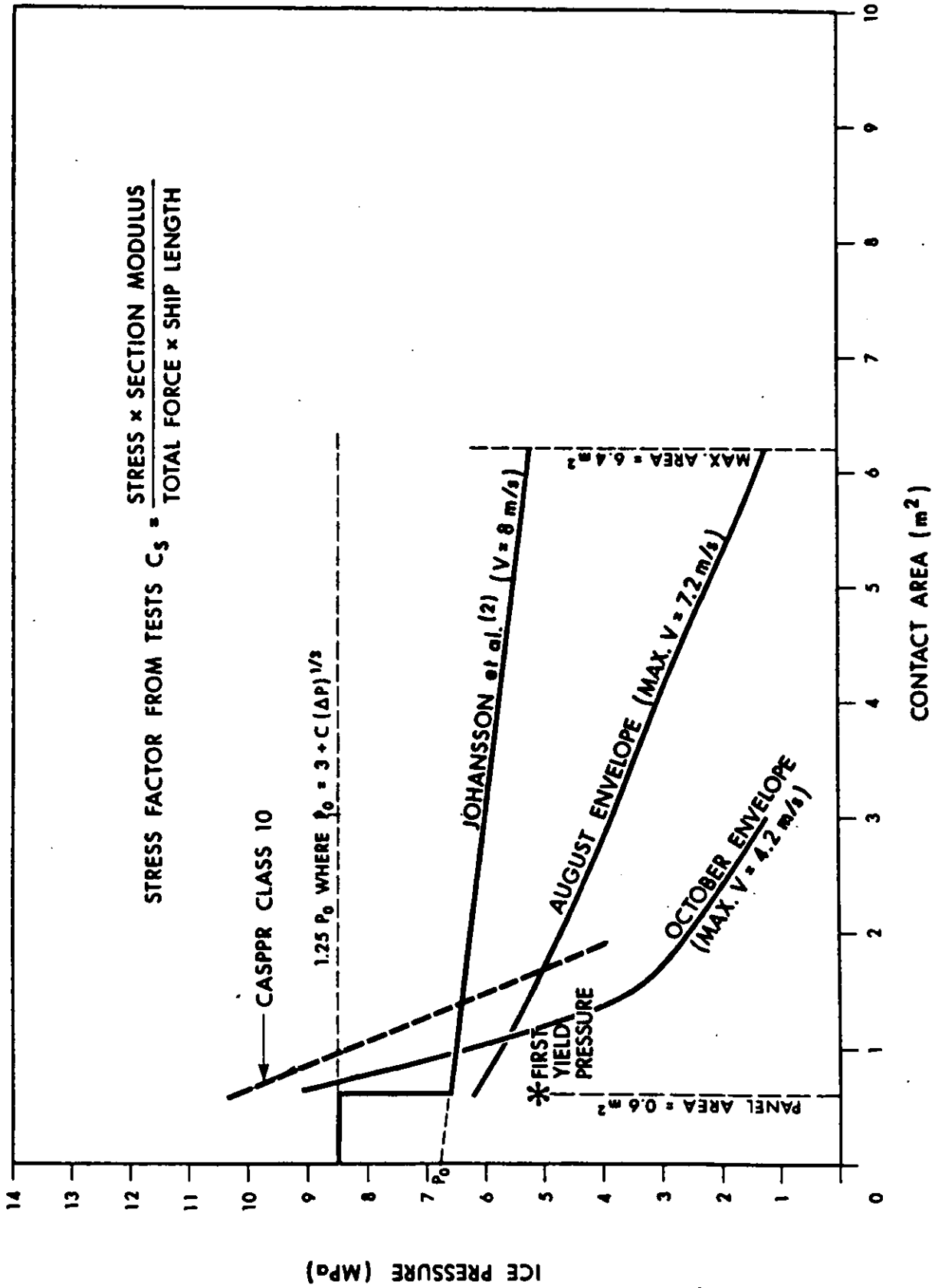


FIG. 5 COMPARISON OF PREDICTED AND MEASURED PRESSURES AS A FUNCTION OF CONTACT AREA. (REF. 4)

TABLE 1
COMPARISON BETWEEN AUGUST AND OCTOBER
TEST CONDITIONS

PARAMETER		AUGUST	OCTOBER
VELOCITY (m/s)	RANGE	1.3 - 7.2	0.5 - 4.2
	MEAN	4.9	2.0
ICE THICKNESS (m)	RANGE	12.0 - 30.0	5.0 - 12.0
	MEAN	15.0	6.0
ICE SURFACE TEMPERATURE (°C)	RANGE	0 - (-1)	(-1) - (-3)
	MEAN	(-0.5)	(-2.5)
UNIAXIAL STRENGTH* (MPa)	RANGE	1.8 - 3.7	3.0 - 7.4
	MEAN	2.9	4.3
BOREHOLE JACK STRENGTH (MPa)	RANGE	3.5 - 12.5	13.5 - 21.7
	MEAN	7.4	18.2
CRYSTALLOGRAPHY		COLUMNAR-GRAINED ICE	GRANULAR ICE

NOTE: The uniaxial compressive strength was measured in the vertical direction. The C-axis had a moderately preferred horizontal orientation. Strain rates used were on the average $5 \times 10^{-5} s^{-1}$.

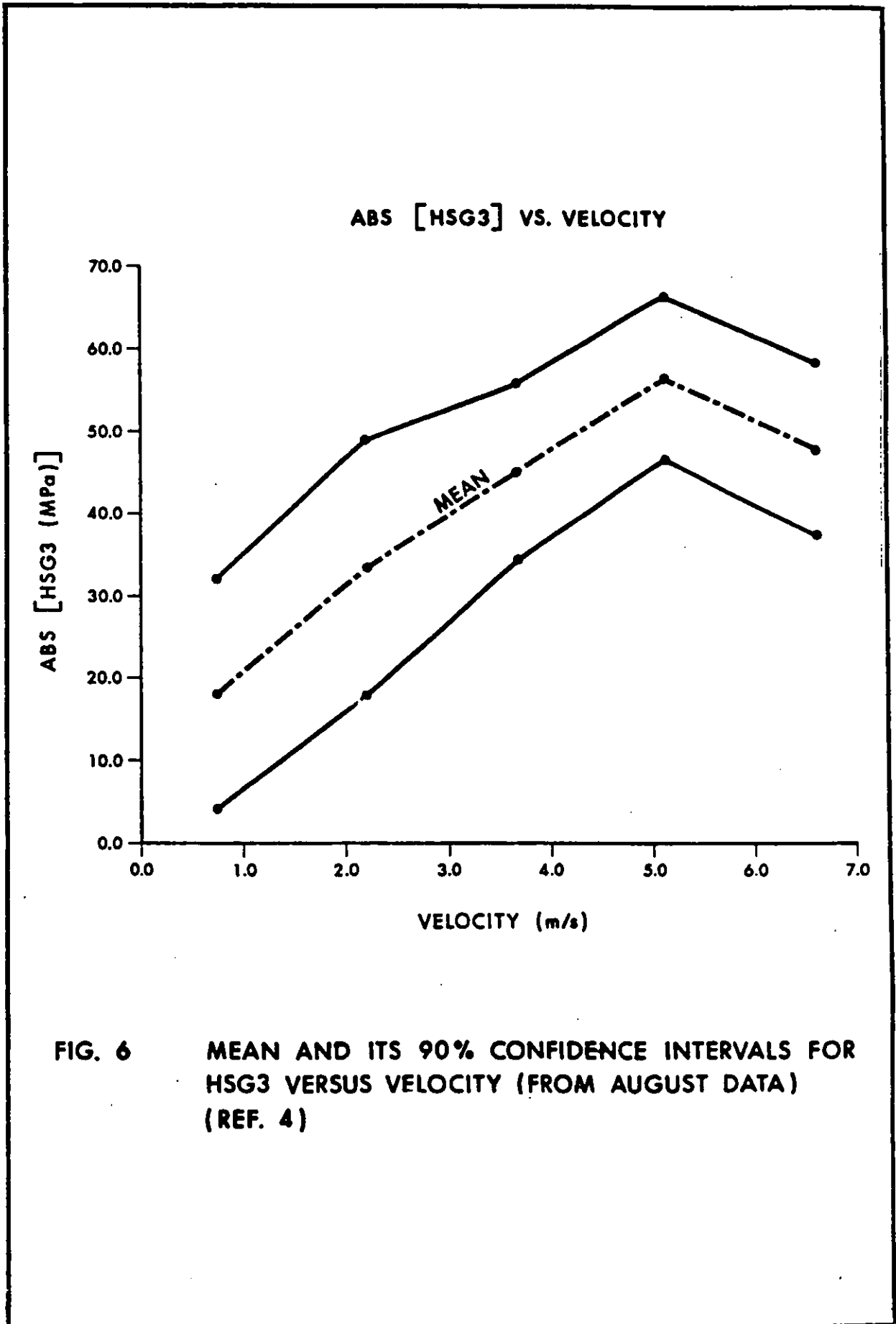


FIG. 6 MEAN AND ITS 90% CONFIDENCE INTERVALS FOR HSG3 VERSUS VELOCITY (FROM AUGUST DATA) (REF. 4)

4.6 HULL RESPONSE

Ice loads locally and globally when hitting ice are not separable from the response of the ship to ice contact. The actual ice load will change depending on the dynamic characteristics of the structure of the ship.

In local areas, the most important consideration in this respect is the varying stiffness of the hull causing redistribution of pressures with the stiffer members having to carry more load. This principle has been introduced in Ref. 3.

Globally, the new parameter introduced to the equation is the dynamic transmission of the energy of impact through the hull. This can result in dynamic magnification or dynamic dampening to the actual response of the hull.

The practical evidence from Kigoriak tests show what the dynamic behaviour is. A simple beam formula for Kigoriak to arrive at a static relationship between force in the bow and corresponding stress on the deck has been developed.

$$\sigma = c \cdot \frac{F \cdot L}{S} \quad (8)$$

where

- σ = stress on the deck at midship in MPa
- C = beam coefficient, 0.15 to 0.2 for Kigoriak
- F = force at bow in MN
- L = length of waterline in m
- S = section modulus, midship, m³

When applying this formula for the purpose of interpreting the measured deck stress in terms of force

at the bow, results yielding only approximately one-third of those forces determined directly from measurements at the bow and from rigid body motions are produced. This suggests that there is a radical dynamic dampening by a factor in the order of 3. Nonetheless, it must be recognized that deck stresses increased to 60 per cent of yield during Kigoriak tests which points out the need to take into account the global strength of the hull in impacts, no matter what the force has been causing this magnitude of stress.

A comment on the importance of the impact relative to the beaching force is needed since, at present, the CASPPR do not recognize impact requirements for hull girder strength determination. Practical evidence from Kigoriak has been that the stresses on the deck were regularly higher during the impact phase than during the beaching phase.

5. SCALING

After having reached a satisfactory level of accuracy for ice pressures and forces on Kigoriak's hull, the question of scaling must be addressed. The approach adopted to date has been one using a time domain simulation of an impact between a ship and an ice obstacle.

The model that has been used assumes a three dimensional ice obstacle with such variable parameters as dimensions and geometry as well as average crushing pressures. The ship is a rigid body with six degrees of freedom, thus allowing unsymmetric as well as symmetric analysis. Added water mass is handled by analytical equations. The program analyses the momentary contact area for each time step between the ship and the ice obstacle. Based on the contact area, using given equations or constants for average pressure over that contact area, the program calculates the total force and its location on the ship.

This force is used to calculate the change of the motion of the ship during one time step.

The logic of the calibration and the actual scaling after the calibration are as follows:

1. Parametric impact simulations are run with the computer program for the Kigoriak, varying ice crushing pressure, impact velocity, and other impact conditions to match those during full scale tests.
2. Resulting accelerations and force traces are compared with the full scale test data from Kigoriak. The key parameter chosen for calibration of the output of the simulations program is a crushing pressure of the ice. An independent check for the validity of the simulations program is a comparison of the duration of the impact yielding from the simulation with that for the same impact parameters from the full scale tests.
3. With the calibrated simulation model a parametric series of simulations are run for a rigid body ship of the kind that is required.

Figure 7 depicts the plotted output from several Kigoriak simulations showing the peak force during impact versus velocity. Average ice pressure was 3 MPa. This output in Fig. 7 is calibrated based on the Kigoriak full scale test results. The equations presented by Johansson et al (Ref. 7) are based on the impact simulation model before the Kigoriak collision tests were performed.

The ice load requirements for a large tanker are shown in Fig. 8 from Johansson et al (Ref. 7), deduced by using the output of the impact simulation model.

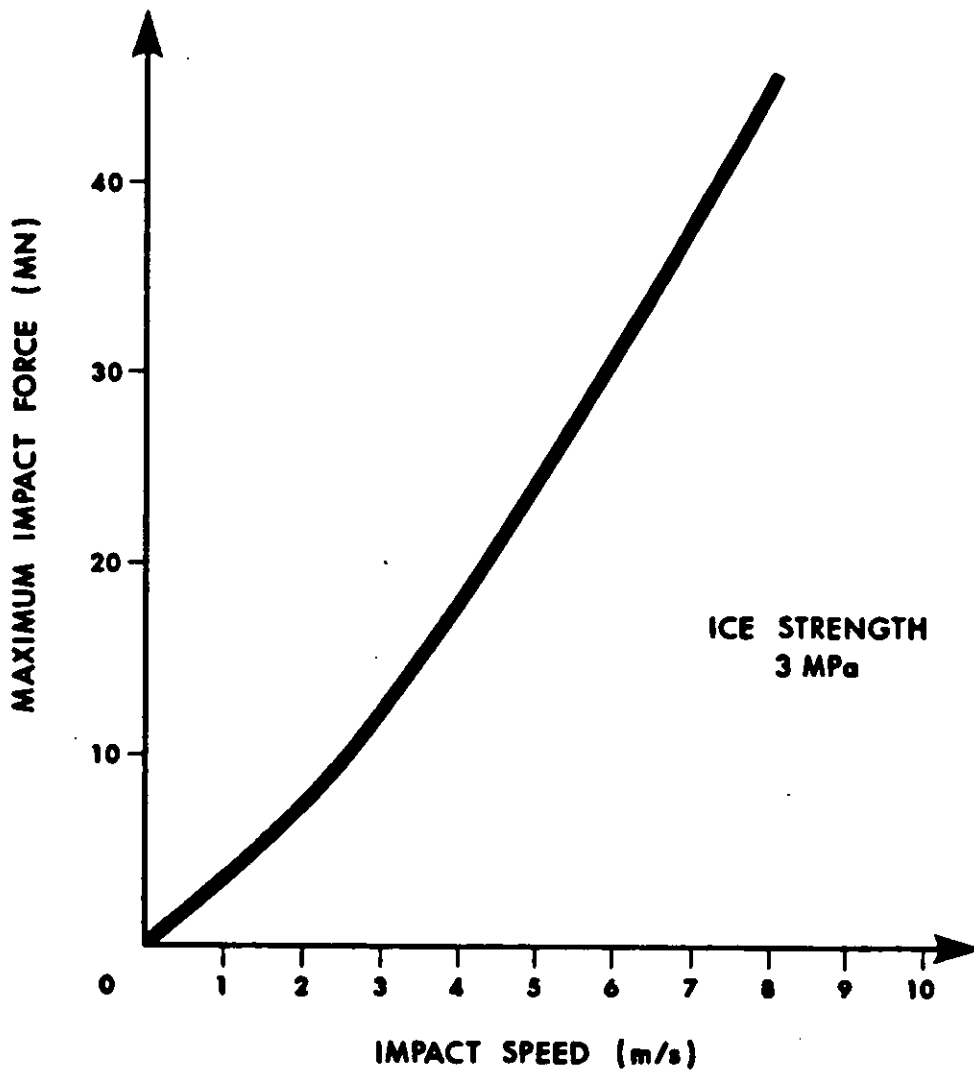


FIG. 7 PEAK IMPACT FORCE FOR KIGORIAK FROM
IMPACT SIMULATION PROGRAM.

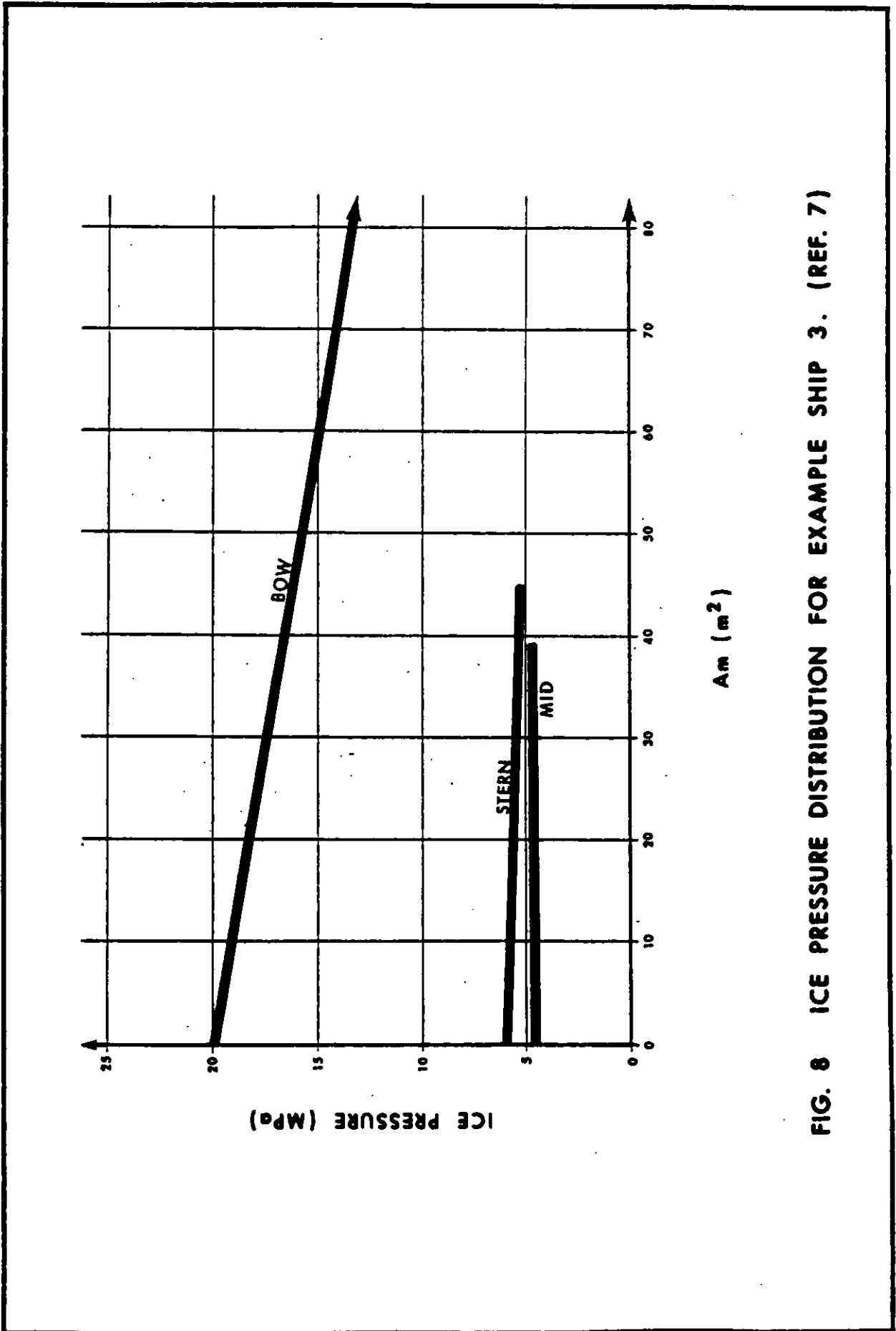


FIG. 8 ICE PRESSURE DISTRIBUTION FOR EXAMPLE SHIP 3. (REF. 7)

6. EVALUATION OF PRESENT KNOWLEDGE

6.1 CASPPR REGULATIONS VS. NEW KNOWLEDGE

As has been shown, there is quite a difference between the ice load requirements based on the present CASPPR and two recently proposed revisions to those regulations which introduce more stringent requirements. The major difference between the existing rules and recent practical experience occurs when extrapolating to larger ship sizes. Yet with a small ship like Kigoriak, there are indications that the forces on its bow are higher than those interpreted from the rules for a ship of its class. Further, the rules have so far omitted the possibility that an impact with ice can create critical stresses in the hull girder. The Kigoriak tests indicate that these are clearly the most critical hull girder stresses for this ship at least. A relaxation to this is introduced in the form of dynamic dampening which reduces midbody stresses experienced during impacts.

Concerning local pressure requirements, the technology has only recently advanced to the stage where reasonably accurate measurements can be made. From these measurements, another discrepancy between the rules and full scale measurements emerges. Practical experience shows that considerably higher pressures exist than those accounted for in the CASPPR.

There is virtually no disagreement between the ice pressures and loads proposed by Johansson et al (Ref. 7) for midship and stern ice pressures and those used in the present CASPPR. In both, these requirements are radically lower and the Kigoriak experience doesn't suggest any departures from them.

6.2 NEW KNOWLEDGE - GAPS

The single biggest unknown in a collision between a ship and an iceberg is the large scale fracturing behaviour of the ice and its effects on ice loads. The fact that forces on the Kigoriak during impact tests did not increase beyond impact velocities of 5 m/s points out the possibility that, due to global failure mechanisms of the ice, there may be some relaxation introduced to the maximum force at high velocities. Thus, the present assumptions of linear force velocity dependence may be conservative. There is, as yet, no data to indicate how much relaxation and under what circumstances.

Using Kigoriak data, and extrapolating forces from fall multi-year ice to mid-winter hard multi-year ice and even further to glacial ice, introduces an unknown. This may mean that the Johansson proposal is less conservative than is currently indicated.

The third unknown is the global behaviour of a ship and how that will effect the ice load in impacts based on the Kigoriak experience. Presently, considerable dampening rather than dynamic amplification is implied. One big unknown, perhaps the most challenging one for research, is that of the scaling laws for local ice pressures. The present view is that the limiting local ice pressure will be determined by the crushing strength of the ice as well as the confinement; however, it is not yet possible to choose the right strength parameters of ice which can be translated into this limiting local pressure.

In this presentation, only the extreme impacts on the bow have been discussed even though it is obvious that the midbody, the stern, and the bottom of the ship will require ice strengthening. It is true that even less is known about the ice forces on these other parts of the

ship. The approach taken has been to study the extreme case which is the bow impact. Then, after understanding determination of the bow force, the same principles can be applied to these other parts after determining which interaction scenarios are acceptable for design. The problem requires interpolation, which should be easy assuming the right choice of ship/ice interactions.

7. DESIGNER'S APPROACH

Even though the development of ice load definition for Canadian Arctic conditions has been rapid, it must be admitted that there is a need for even overly-careful approaches to designing safe Arctic ships. This is true at least until practical operating experience has provided sufficient confidence in the quantities of ice loads that can be expected during navigation of Canadian Arctic waters.

The experience with the Kigoriak, as well as other operational experience in the Beaufort Sea with occasional multi-year ice invasions resulted in the production of a design philosophy which addressed the problems of ice loading as follows:

1. Design has been developed for a ship to withstand, according to best ice load estimates, an unlimited collision with an infinite size iceberg, with, at the most, minor structural damage.
2. Design is underway for an efficient ice obstacle detection system to efficiently avoid iceberg, and other, collisions.
3. Largest safety factors have been introduced into the global strength.

4. A non-polluting tank arrangement has been introduced in the case of hull penetration.
5. This first Arctic tanker will be extensively instrumented and tested in collisions with icebergs, as well as other ice loading situations. The potential ice load related operational limits will be found, if any.
6. A permanent stress monitoring system will be installed.

This is considered to be the most satisfactory approach for the actual first ship, as well as for development of a real ice load data base for any further ships that will be designed for and operated in the Canadian Arctic.

8. CONCLUSIONS

The state of knowledge of ice loads in ships in Canada has progressed during the last few years so much that today it is felt that without any further developments the design of a first structurally safe generations of ships for year-round operation in the Canadian Arctic is possible. Any uncertainties in ice loads will be overcome by applying the design philosophy presented herein. This development is possible, based on the lessons learned during the last few years in operations in areas experiencing incidences of multi-year ice .

The lack of basic understanding of how the ice behaves under high impact velocities and at very high load levels is the limiting factor today in being able to predict more accurately ice loads in collisions.



COLLAPSE ANALYSIS OF SHIP
SHELL PANELS

by

Tore H. Søreide

To be presented at WEGEMT Seventh Graduate School on Ships
and Structures in Ice

Helsinki University of Technology, March 1983

ABSTRACT

The paper deals with capacity of stiffened ship shell panels subjected to lateral loads from ice. An introduction is given into the basis for plastic analysis of plated structures and collapse models for stiffeners and plate elements are presented. The stiffening effect from membrane forces is discussed and analytical models are described in which membrane forces are included. A brief description is given of nonlinear computer programs based upon the finite element method of analysis. These programs account for elasto-plastic material behaviour as well as the geometric effects of large deflections. The applicability of such programs is discussed and recommendations are given for design formulas.

1. INTRODUCTION

The use of plastic methods in design of structures has increased remarkably during the last decade. Most of the codes for steel structures in Europe /1/ base their ultimate load design on simplified plastic techniques which account for redistribution of stresses after plastification. In the design of offshore platforms plastic methods of analysis are of special interest for estimating damage due to explosion or ship/platform collision /2/ and for studying the progressive collapse of a platform in damaged condition.

In the conventional elastic method of design "first yield" was used as a criterion for the load-carrying capacity of flexural members. However, it is well known that even in the service-ability state most steel plated structures undergo local yielding due to the presence of residual stresses. The ductility of steel makes a redistribution of stresses possible. The idea behind the ultimate limit state design is to make the criteria for maximum load more realistic in the sense that a plastic model of analysis better simulates the real behaviour of structures under extreme loading.

The recent development of large capacity computers has made the use of numerical techniques such as the finite element method more attractive for design purposes. The implementation of nonlinear material and geometric effects combined with step-by-step loading makes it possible to follow the development of plastic zones in the structure throughout the load history. Thus, the nonlinear finite element technique gives much more information about the pre-collapse behaviour of the structure and also accounts for elastic deformations. So far, the method has not been used to any extent for design purposes, but has proven to be very valuable in the study of special phenomena related to plastic collapse and buckling of structures.

The design of ships and offshore structures in ice represents a new and challenging area in which the latest development of design methods should be brought further. The big uncertainty lies on the estimation of load on the structure concerning intensity, extent and time variation. The description of load is beyond the scope of this paper, the aim being to present applicable strength formulas. An overview of load criteria applicable in structural design against ice loads is presented in Ref. /3/.

2. LOAD-CARRYING BEHAVIOUR OF STIFFENED PANELS

Stiffened plates are usually considered as subregions of the total structure and may be treated individually, see Fig. 1. The factors that governs the behaviour of such a panel are

- a. Loading, type and extent
- b. Geometry of plate elements and stiffeners
- c. Boundary conditions

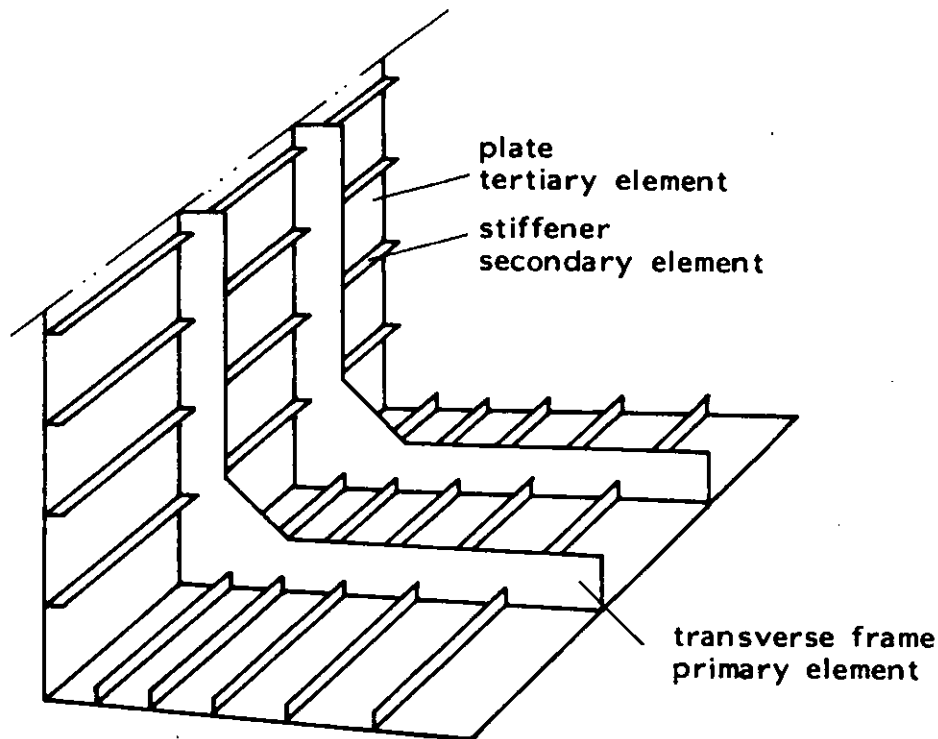


Fig. 1 Ship plate structure

Considering the panel between two transverse frames in Fig.1 the boundary conditions for deflections may easily be set, e.g. zero deflection along all edges. However, rotational and in-plane restrictions are much more complicated to define. In case of partial loading, the edges should be considered as rotationally free. For uniform loading of the panel, e.g. water pressure, it is more realistic to assume the boundaries to be fixed against rotation.

The assumption of free inplane movement in most cases overestimates stresses and deflections, leading to an overconservative design. As is demonstrated in Chapter 5, plated structures under lateral loading experience a high degree of membrane action even at deflections in the range of the plate thickness. The main contribution to this inplane stiffness comes from adjacent plating. In order to predict this restraint a separate analysis of the plating should be carried out so that the mutual dependency between out-of-plane behaviour and inplane restraints could be taken care of by some sort of elastic springs at the panel boundaries.

The stiffened panel shown in Fig. 1 may be divided into three basic structural components. These are

- a. Frame elements, acting as primary structural elements
- b. Stiffeners acting as secondary structural elements between frames
- c. Plate element acting as tertiary structural elements between stiffeners

A complete analysis of the structural behaviour of the panel in Fig. 1 requires a full representation of the interacting effects between the three structural components. Chapter 6 demonstrates how such an analysis can be performed by advanced numerical techniques. However, by conventional design methods some simplifications on the structural behaviour must be introduced.

Given the ice loads on the ship plating the load transfer in the structure follows the opposite of the rank above:

- a. The external ice load is carried by the plate element and transferred to the stiffeners
- b. The stiffeners are supported on the frame elements and transfer the loads to these
- c. The frame elements give concentrated loads along the hull girder

The design procedure now follows the above line implying the subsequent design criteria for plate and stiffeners:

- a. The plate is designed for carrying the load between stiffeners
- b. The stiffeners are designed with their effective width of plate to carry the load between transverse frames

The subsequent chapters give theoretical models for ultimate load design according to the above structural integrity.

The aspect ratio of plate elements is usually in the range of four or more. Thus, the analysis of the rectangular plate element can be approximated by a simple platestrip model with span equal to the stiffener spacing. Chapter 3 gives analytical models for this simplified analysis while Chapter 4 concerns aspect ratios below four for which a two-dimensional plate analysis is necessary.

3. COLLAPSE MODELS FOR PLATESTRIIP AND STIFFENER.
NO MEMBRANE EFFECTS

3.1 Elasto-Plastic Deformation

Consider the simply supported beam (or alternatively platestrip) in Fig. 2. The beam is subjected to a uniform load with intensity q .

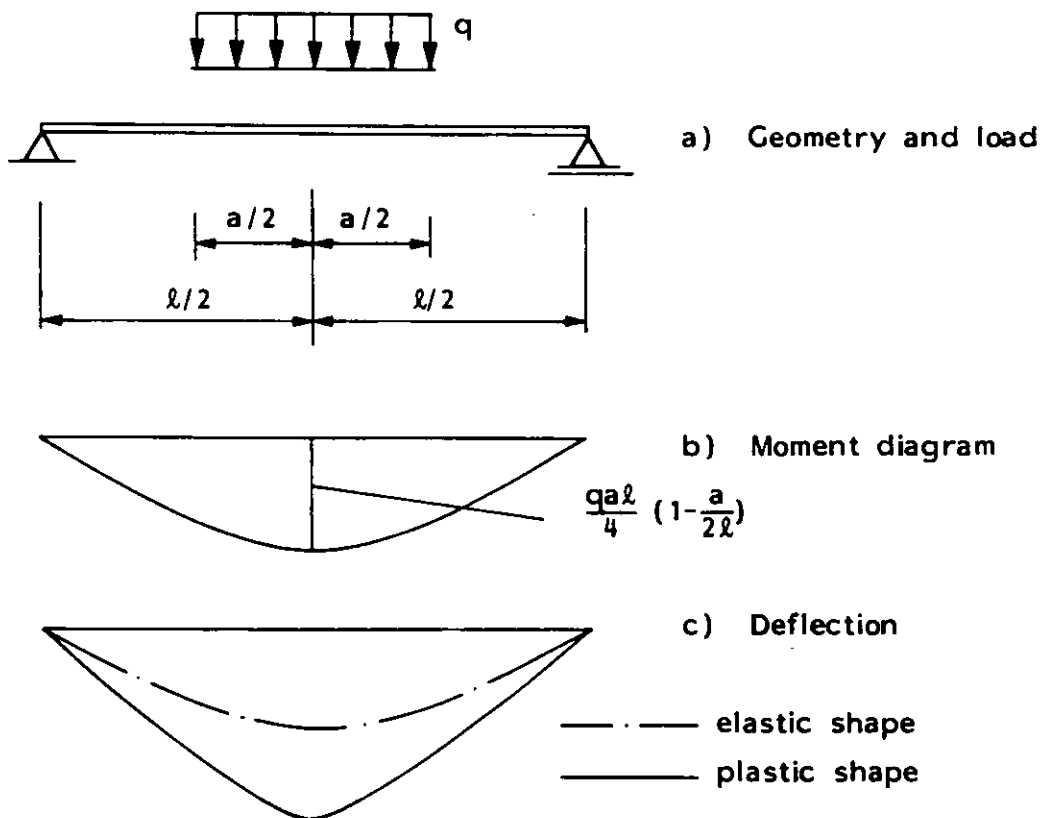


Fig. 2 Elasto-plastic bending of beam

The system in Fig. 2 is statically determinate and the moment curve is of the same shape also after plastification has occurred. While the beam is purely elastic the curvature at any point along the beam is given by

$$\frac{d^2w}{dx^2} = -\frac{M}{EI} \quad (1)$$

where EI denotes the elastic cross section stiffness. However, after plastification in the central region of the beam, the moment/curvature relationship is no longer linear in this part. As full plastification is obtained at the centre of the beam, the curvature at this point tends towards infinity. This concentration of curvature in the central plastic region is also indicated by the deflection curve in Fig. 2c. It is seen that as full plastification develops the beam turns into a mechanism with plastic hinge at the centre.

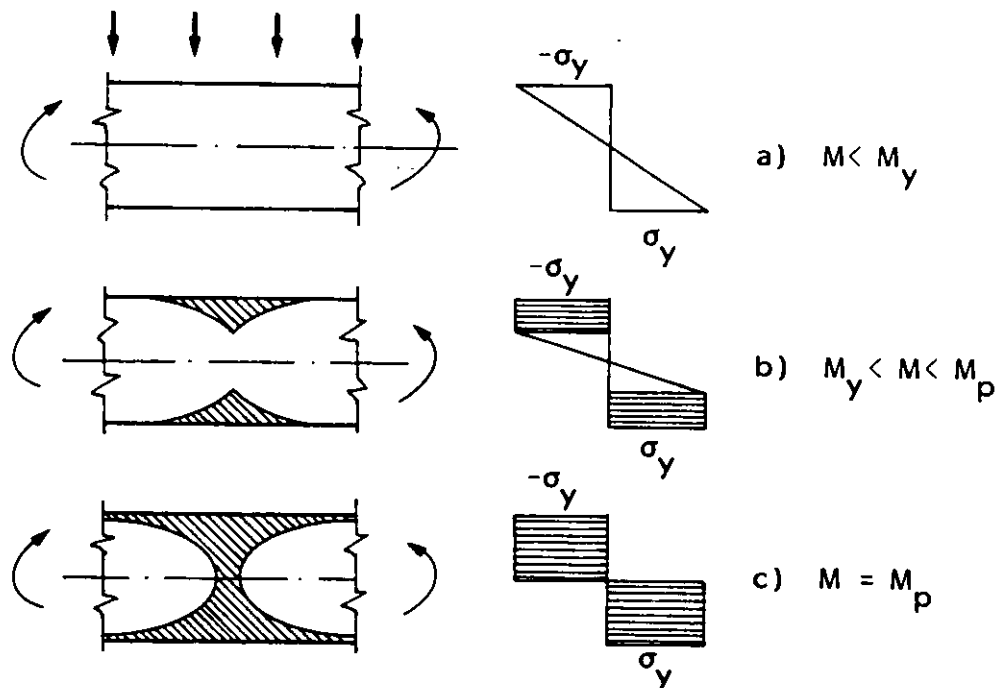


Fig. 3 Development of plastic hinge

The development of plastic hinge at the centre of the beam is illustrated in Fig. 3. Case a) is the level of loading at which first yield occurs at the outer fibres. In case b) the cross section is partly yielded and the stress distribution is constant over the plastic fibres and linear over the remaining

lastic part of cross section. Case c) indicates full plasti-
fication in the central cross section. At this stage a plastic
hinge is formed and the beam turns into a mechanism. No extra
load reserve can be gained so that this situation represents
the real physical collapse of the structure.

3.2 Simply Supported Beam. Virtual Work Equations

In this section a kinematic procedure for calculating the
collapse load q_c is presented based upon energy considerations.
Consider the deformed configuration in Fig. 2c for which the
external load q has just reached its maximum value q_c . Since
the deformed shape represents an equilibrium configuration, the
Principle of Virtual Displacements can be applied. The virtual
displacement field δu_i should satisfy the following requirements

- a. $\delta u_i = 0$ on part of boundary where displacements
are prescribed
- b. δu_i fulfills the compatibility requirements throughout
the structure

The virtual displacement field may be any pattern satisfying
the two restrictions.

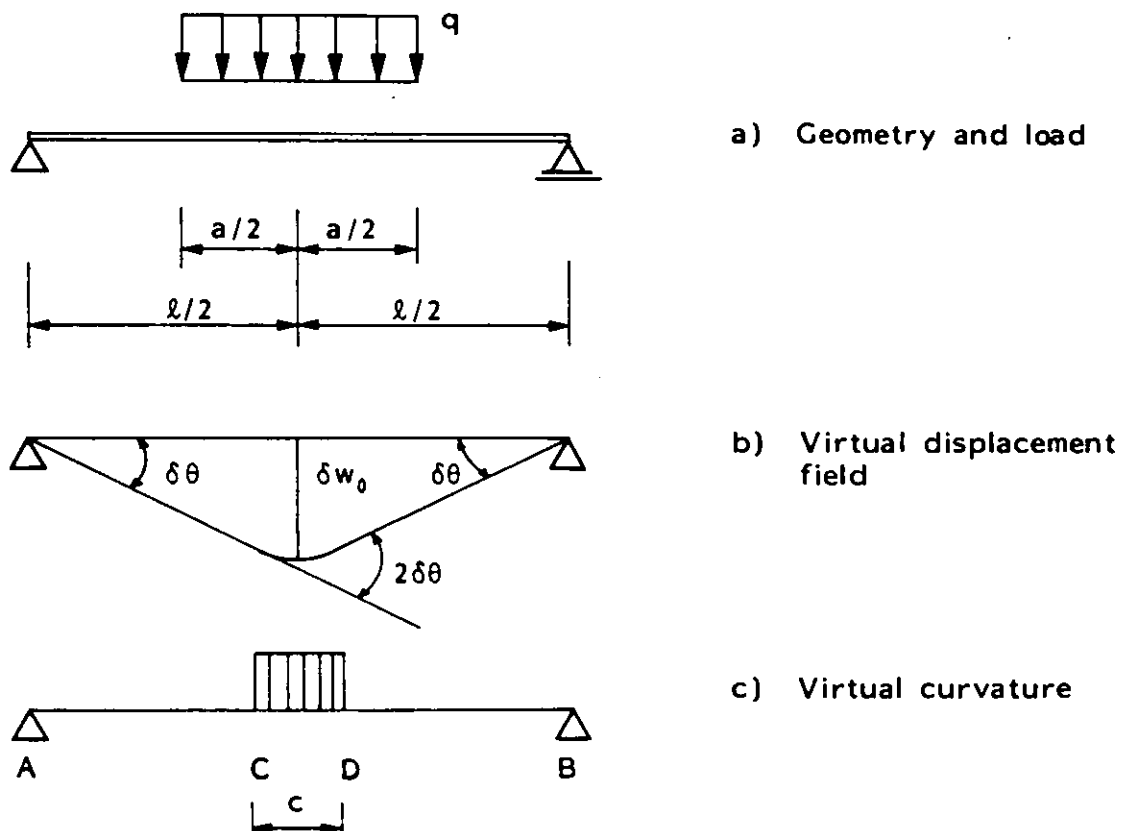


Fig. 4 Virtual displacement field for simply supported beam

Fig.4 shows a virtual displacement field that satisfies restrictions a) and b). The virtual displacement pattern is chosen so that parts AC and DB of the beam have zero virtual curvature while $\delta\kappa$ is different from zero over CD with length c. The following virtual work equations emerge

$$\text{External virtual work: } \delta W_e = \int_a^l q \delta w \, dx \quad (2)$$

$$\text{Internal virtual work: } \delta W_i = \int_c^l M \delta \kappa \, dx \quad (3)$$

Considering now the load level at which a plastic hinge is formed at midpoint and introducing at limiting case $c \rightarrow 0$ Eq.(3) turns into

$$\delta W_i = M_p \cdot 2\delta\theta \quad (4)$$

where M_p is the plastic moment capacity.

Kinematically, the following relations are valid for $c \rightarrow 0$

$$\delta w_0 = \frac{\ell}{2} \delta\theta \quad (5)$$

$$\delta W_e = q \int_a^l \delta w \, dx = qa \left(1 - \frac{a}{2\ell}\right) \cdot \delta w_0 \quad (6)$$

where δw_0 is the virtual deflection at midpoint.

Equating external and internal virtual work leads to collapse load

$$q_c \cdot a = \frac{8M_p}{\ell(2-a/\ell)} \quad (7)$$

Thus, in case of uniformly distributed load over the total beam ($a=\ell$) the collapse load is estimated to

$$q_c = \frac{8M_p}{\ell^2} \quad (8)$$

A concentrated load P at midspan gets its critical value
($a=0, qa=P$)

$$P_c = \frac{4M_p}{l} \quad (9)$$

3.3 Clamped Beam

Fig.5 gives the virtual displacement field for a partially loaded beam with rotational restraints at the ends. The external virtual work equation (6) is still valid while the expression for internal virtual work turns into

$$\delta W_i = M_p \cdot 4\delta\theta \quad (10)$$

Thus, the collapse load for clamped ends comes out to be twice the capacity for rotationally free ends

$$\bar{p}_c \cdot a = \frac{16M_p}{l(2-a/l)} \quad (11)$$

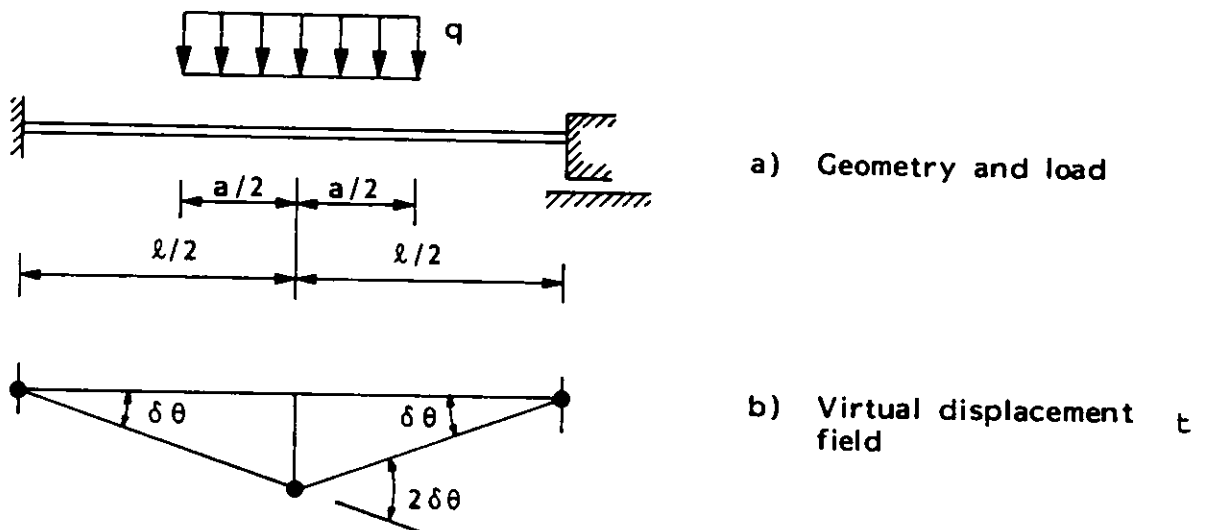


Fig.5 Virtual displacement field for clamped beam

In case of uniformly distributed load over the total beam
($a=l$) the load intensity at collapse reads

$$\bar{p}_c = \frac{16M_p}{l^2} \quad (12)$$

and for a concentrated load at midspan there comes out
($a=0, qa=P$)

$$\bar{P}_c = \frac{8M_p}{l} \quad (13)$$

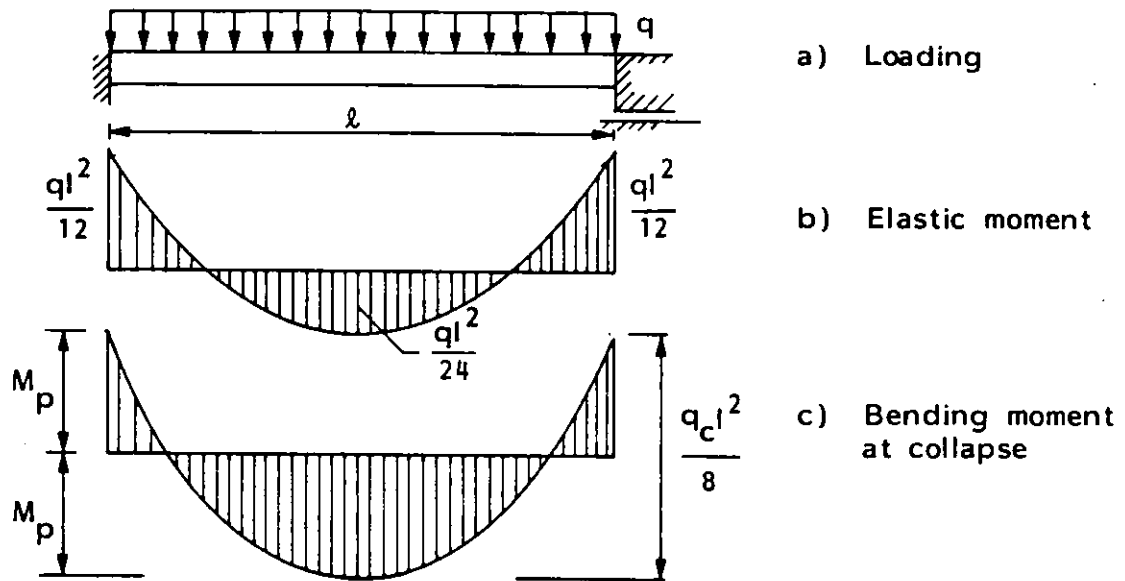


Fig.6 Elastic and plastic moment distributions for clamped beam

For a statically indeterminate structure like the clamped beam in Fig.6 with uniformly distributed load q over the total length the form of moment distribution changes during the development of plastic zones. Increasing the load q from zero the behaviour is at first elastic with the bending moment distribution in Fig.6b. The elastic response continues until the maximum bending moments at the ends reach the level of first yield. By further increasing the load the final collapse configuration in Fig.6c is reached for which the load intensity is defined by Eq. (12).

3.4 Plastic Moment Capacity of Platestrip

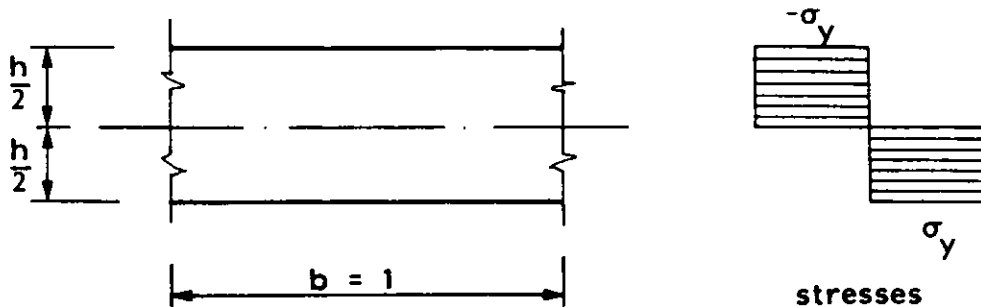


Fig.7 Full plastification of platestrip

In Fig.7 a platestrip with unit width is considered in fully plastified condition. Denoting the plastic section modulus by Z the plastic bending moment per unit width is given by

$$m_p = \sigma_y Z \quad (14)$$

where σ_y is the yield stress. For the rectangular cross section in Fig.7 the plastic section modulus reads

$$Z = \frac{h^2}{4} \quad (15)$$

3.5 Plastic Moment Capacity of Stiffener

When checking the capacity of stiffeners between transverse frames the cross section in Fig.8 can be used. The effective width of plating denoted by b_e interacts with the stiffener profile to give an effective stiffener cross section.

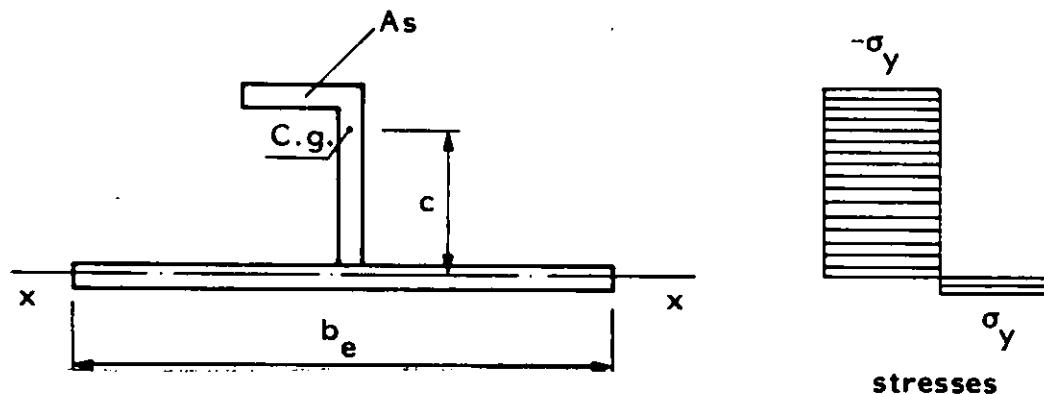


Fig.8 Full plastification of stiffener

The position of the plastic neutral axis $x-x$ is so that the areas on both sides of this axis are equal. For most practical cases the plastic neutral axis falls within the plate, and the plastic section modulus simplifies to

$$Z = A_s \cdot c \quad (16)$$

where A_s is the stiffener area (without effective plate) and c is the distance from centre of stiffener area A_s to plastic neutral axis $x-x$.

It should be emphasized that the location of the plastic neutral axis x-x must be verified before applying the above simplified consideration.

The calculation of effective width of plate represents a special problem in the sense that the effective width and therefore also the plastic moment capacity may vary along the stiffener.

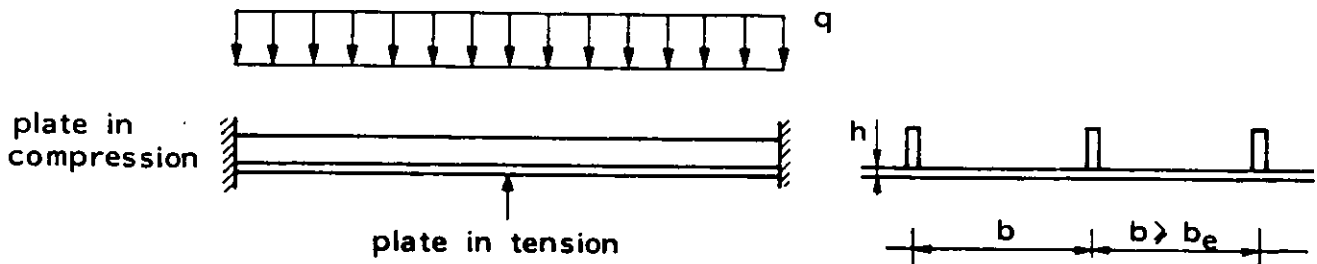


Fig.9 Flat bar stiffeners in bending

For the model in Fig.9 the plate is on the compression side at the ends of the panel and on the tension side at midspan. With the plate on the compression side the effective width should be reduced due to buckling phenomena. The effective width of plate used to calculate the plastic section modulus can be taken as /4/

$$\frac{b_e}{b} = \frac{1.8}{\beta} - \frac{0.8}{\beta^2}, \text{ max } 1.0 \quad (17)$$

where β is the so-called slenderness factor

$$\beta = \frac{b}{h} \sqrt{\frac{\sigma_y}{E}} \quad (18)$$

Eq.(17) is based on initial deflections equal to $0.01 b$ and residual stresses of $0.2 \sigma_y$.

When calculating the plastic moment capacity at midspan the total stiffener spacing is used as effective plate width.

The load intensity at collapse can now be written

$$\bar{q}_c = \frac{8(z_1 + z_2)\sigma_y}{l^2} \quad (19)$$

where Z_1 and Z_2 are the plastic section modulus for partial and full effective plate width, respectively. Eq. (12) is a special version of Eq. (19) with $Z_1 = Z_2$.

4. COLLAPSE MODELS FOR RECTANGULAR PLATE ELEMENTS

For plate elements with small aspect ratios in the range one to three the platestrip model above may be too conservative and a twodimensional analysis is necessary. The displacement field for such a plate is shown in Fig. 10 for the case of simply supported edges with no horizontal restraints.

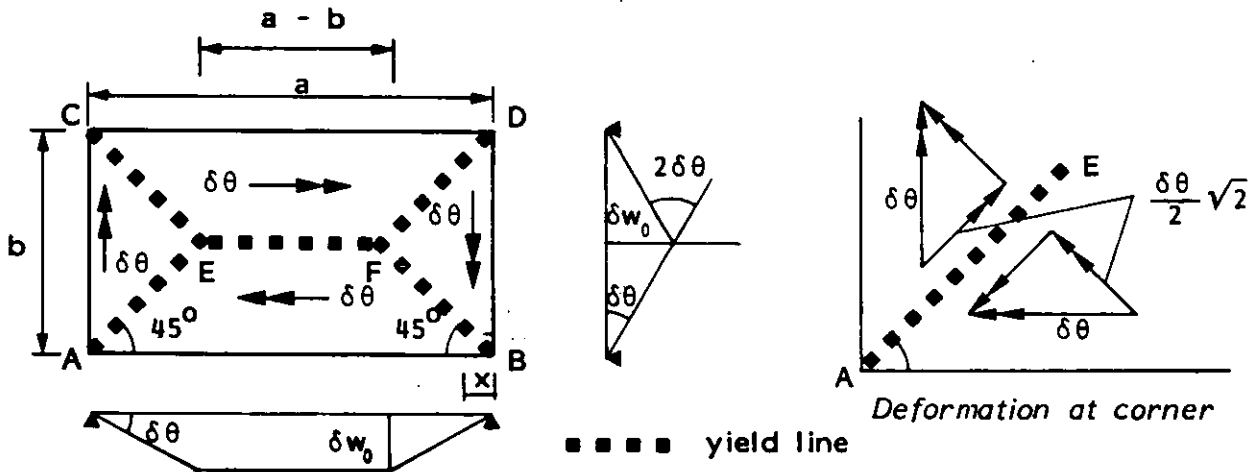


Fig.10 Displacement field for simply supported rectangular plate

The virtual deformations of the plate are concentrated along the dotted lines which correspond to the plastic hinges for beams. The virtual energy dissipation is now calculated by integrating along the plastic zones.

The mechanism in Fig.10 is based on an angle of $\phi=45^\circ$ at corners between plate edge and yield lines. The approximation introduced by this assumption is of minor importance /2/.

The energy dissipation per unit length along a yield line is found as the product of plastic moment capacity m_p (Eq.14) and virtual relative rotation between the two adjacent elements. Thus, for the line EF in Fig.10 the energy dissipation reads

$$\delta W_i^{EF} = 2m_p (a-b) \cdot \delta \theta \quad (20)$$

Considering Fig.10 it is seen that the relative rotation along inclined yield lines is

$$\delta\beta = 2 \frac{\delta\theta}{2} \sqrt{2} = \delta\theta\sqrt{2} \quad (21)$$

and the plastic virtual work along these lines is

$$4\delta W_i^{AE} = 4m_p b \delta\theta \quad (22)$$

The sum of Eqs. (20,22) gives the total internal energy dissipation

$$\delta W_i = 2M_p b \left(\frac{a}{b} + 1 \right) \delta\theta \quad (23)$$

where a/b now is the aspect ratio of the plate.

The external virtual work due to distributed load p is

$$\delta W_e = \int_{A_p} p \delta w \, dA \quad (24)$$

where integration is taken over the loaded area A_p . In case of uniform load Eq. (24) turns into

$$\delta W_e = p \int_{A_p} \delta w \, dA = p \delta V \quad (25)$$

and δV is the volume covered by the virtual displacement field over the loaded area A_p . For uniform load p over the total plate element δW_e gets the form

$$\delta W_e = \frac{pb^3}{12} \left\{ 3 \left(\frac{a}{b} - 1 \right) + 2 \right\} \delta\theta \quad (26)$$

Combining Eqs. (23,26) the load intensity at collapse comes out to be

$$\bar{p}_c = \frac{24m_p \left(\frac{a}{b} + 1\right)}{b^2 \left(3\left(\frac{a}{b} - 1\right) + 2\right)}, \quad \frac{a}{b} > 1 \quad (27)$$

Eq. (27) is based upon the approximation $\phi = 45^\circ$ at corners. Wood /5/ gives the following expression for an upper bound on the collapse load

$$\bar{p}_c^* = \frac{24m_p}{b^2 \left(\sqrt{3 + \frac{b^2}{a^2}} - \frac{b}{a}\right)^2}, \quad \frac{a}{b} > 1 \quad (28)$$

The corresponding lower bound solution obtained by static considerations reads

$$\bar{p}_L = \frac{24m_p}{b^2} \left(\frac{1}{3} + \frac{b}{3a} + \frac{b^2}{3a^2}\right) \quad (29)$$

Table 1 gives a comparison of the different collapse load formulas for simply supported plates. It is seen that the alternative two-dimensional expressions in Eqs. (27,28,29) differ very little. Further, even for aspect ratio $\frac{a}{b} = 6,0$ use of the platestrip approximation in Eq. (8) implies an error of about 20 percent on the conservative side in the design.

$\frac{a}{b}$	1.0	1.5	2.0	2.5	3.0	3.5	4.0	5.0	6.0	∞
$\frac{\text{Eq. (27)}}{\text{Eq. (8)}}$	3.0	2.14	1.80	1.61	1.50	1.42	1.37	1.29	1.24	1.0
$\frac{\text{Eq. (28)}}{\text{Eq. (8)}}$	3.0	2.12	1.77	1.58	1.47	1.39	1.33	1.26	1.21	1.0
$\frac{\text{Eq. (29)}}{\text{Eq. (8)}}$	3.0	2.11	1.75	1.56	1.44	1.37	1.31	1.24	1.19	1.0

Table 1 Alternative solutions for the collapse load of simply supported rectangular plate related to the platestrip formula in Eq. (8).

For a rectangular plate with the edges clamped against rotation plastic zones along the edges has to be included in the displacement field of Fig.10. Thus, the internal energy dissipation in Eq.(23) is doubled while the external virtual work is still given by Eq.(26). The collapse pressure comes out as twice that for a simply supported plate

$$\bar{p}_c = \frac{48m_p \left(\frac{a}{b} + 1\right)}{b^2 \left\{3\left(\frac{a}{b} - 1\right) + 2\right\}} \quad (30)$$

5. INFLUENCE FROM MEMBRANE FORCES ON THE PLASTIC CAPACITY OF PLATES

The previous derivations concern beams and plates with no horizontal restraints. The lateral load is carried on bending action, and there is no redundancy in the structure after formation of a plastic mechanism. However, it is well known that for plated structures the activation of membrane forces can have a significant strengthening effect.

5.1 General Introduction

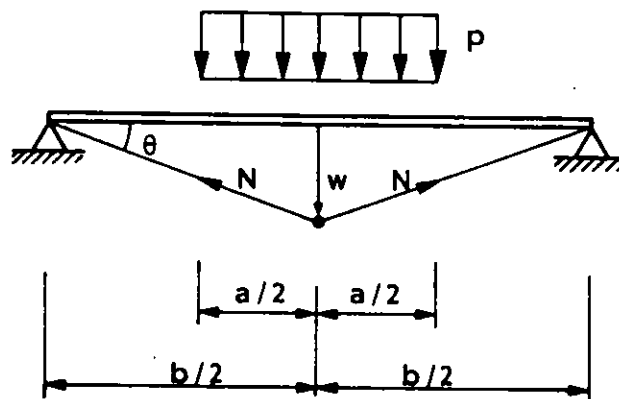


Fig.11 Simply supported platestrip with horizontally fixed ends.

The platestrip in Fig.11 has free end rotations but is fixed against horizontal displacement. The model is partially loaded by a distributed load p and in the subsequent derivations a unit width of the plate is considered.

One special problem arises when deriving the load-displacement relations with membrane forces included. In the previous models of horizontally free platestrips the ultimate load was found explicitly from a virtual work consideration. The magnitude of deformation at collapse did not enter into the equations. The physical explanation for this is that as a plastic mechanism is formed the load-displacement relation is undetermined. However, in case of membrane forces the load carrying effect of these depends on the magnitude of deflection. Thus, the deflection W enters into the expression for lateral load and the following new phenomena arise

- a. The one-to-one relationship between lateral load and deflection makes it possible to estimate the amount of deformation for given load.
- b. The load-displacement relationship gives no collapse criterium in the form of a maximum load level as far as lateral loading is concerned.

Due to the coupling between lateral load and deformation even in the plastic range a choice of material behaviour has to be taken. The simplest alternative is chosen in the form of ideal rigid-plastic stress-strain curve of the type indicated in Fig.12, neglecting elastic deformations.

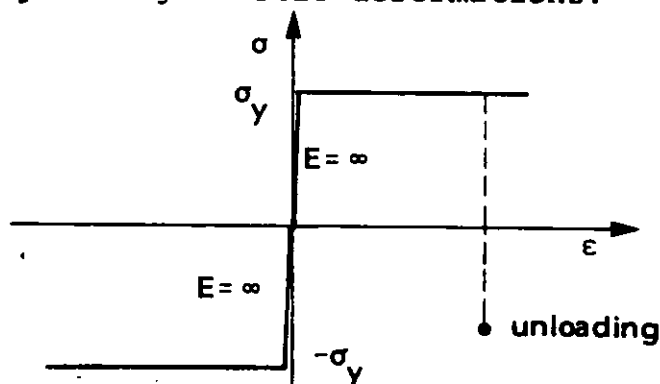


Fig.12 Stress-strain curve for ideal rigid-plastic material

5.2 Moment - Axial Force Interaction

The stress distribution over the height of the platestrip is indicated in Fig.13 for the case of simultaneously acting bending moment and axial load.

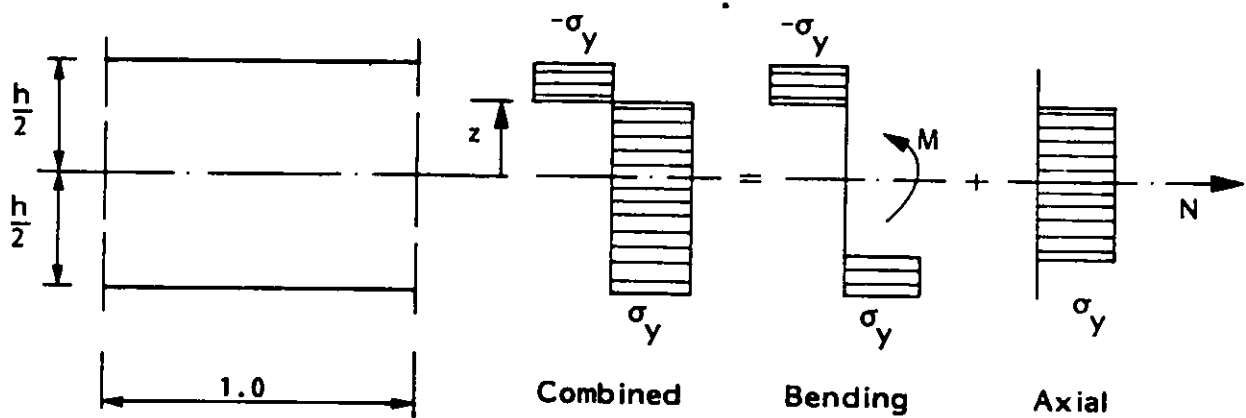


Fig.13 Stress distribution over cross section for combined bending moment and axial force.

The resulting forces on the cross section are given by

$$N = 2z\sigma_y \quad (30)$$

$$M = \frac{h^2}{4}\sigma_y - \frac{(2z)^2}{4}\sigma_y = \frac{h^2}{4}\sigma_y \left(1 - 4\frac{z^2}{h^2}\right) \quad (32)$$

For the limiting situation $z = \frac{h}{2}$ the full plastic axial load is given by

$$N_p = h\sigma_y \quad (33)$$

and correspondingly the full plastic moment for $z = 0$

$$M_p = \frac{h^2}{4}\sigma_y \quad (34)$$

It should be emphasized that M and N now denote forces per unit width of the platestrip.

For combinations of bending moment and axial force the interaction formula is obtained by eliminating z from Eqs. (31,32)

$$\frac{M}{M_p} + \left(\frac{N}{N_p}\right)^2 = 1 \quad (35)$$

The collapse criterium is illustrated in Fig.14.

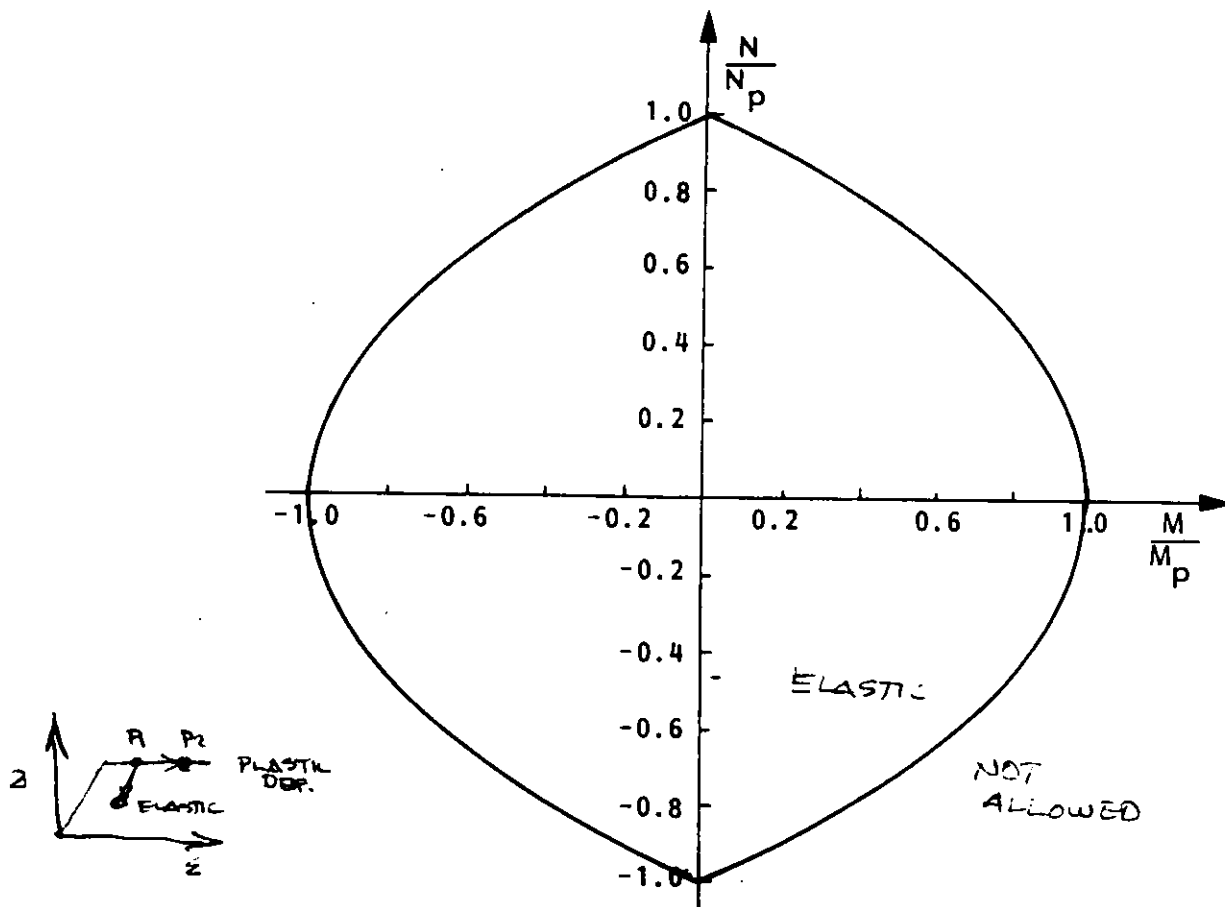


Fig.14 Interaction diagram according to Eq.(35)

The above interaction curve can be seen as a yield surface in light of the flow theory of plasticity /5/. Combinations of M and N which lie inside the curve are allowable and represent no plastic deformations. Points outside the yield surface are not allowed and combinations on the curve correspond to fully plastic cross sections for which plastic flow occurs.

The rate of deformation is now defined by the associated flow rule which requires the strain rate vector to be perpendicular to the yield surface

$$\frac{N_p \dot{\epsilon}}{M_p \dot{\kappa}} = \frac{\partial F / \partial (N/N_p)}{\partial F / \partial (M/M_p)} \quad (36)$$

where $F(\frac{M}{M_p}, \frac{N}{N_p})$ is given by Eq.(35).

5.3 Load - Deflection Curve for Simply Supported Platestrip

Considering one half of the platestrip in Fig.11 and using the deflection amplitude w as "time parameter" the following strain expressions emerge

$$\dot{\epsilon} = \frac{b}{2} \cdot \frac{\partial}{\partial w} \left(\frac{1}{2} \theta^2 \right) = \frac{2w}{b} \quad (37)$$

$$\dot{\kappa} = \frac{\partial \theta}{\partial w} = \frac{\partial}{\partial w} \left(\frac{2w}{b} \right) = \frac{2}{b} \quad (38)$$

Incorporating the work rate of external forces the complete energy equation reads

$$\left(N \frac{2w}{b} + M \frac{2}{b} \right) \cdot 2 = \int_a^b p w(x) dx \quad (39)$$

Combining Eqs. (36,37,38) gives

$$\frac{N}{N_p} = \frac{2w}{h} \quad (40)$$

$$\frac{M}{M_p} = 1 - \frac{4w^2}{h^2} \quad (41)$$

The work from distributed loading gets an expression similar to Eq.(6). The final version of Eq.(39) gets the form

$$\frac{p}{p_c} = 1 + \frac{4w^2}{h^2}, \quad w < \frac{h}{2} \quad (42)$$

where p_c is the collapse load neglecting membrane forces (see Eq.(7))

$$p_c \cdot a = \frac{8M_p}{b(2-a/b)} = \frac{2h^2 \sigma_y}{b(2-a/b)} \quad (43)$$

Eq.(42) is valid as long as $N < N_p$, or from Eq.(40) $w < \frac{h}{2}$. For $w > \frac{h}{2}$ the bending moment vanishes and the load-deflection relationship turns into

$$\frac{p}{p_c} = 4 \frac{w}{h}, \quad w \geq \frac{h}{2} \quad (44)$$

The total load-deflection curve is now defined by Eqs. (42,44) and is illustrated in Fig.15 below.

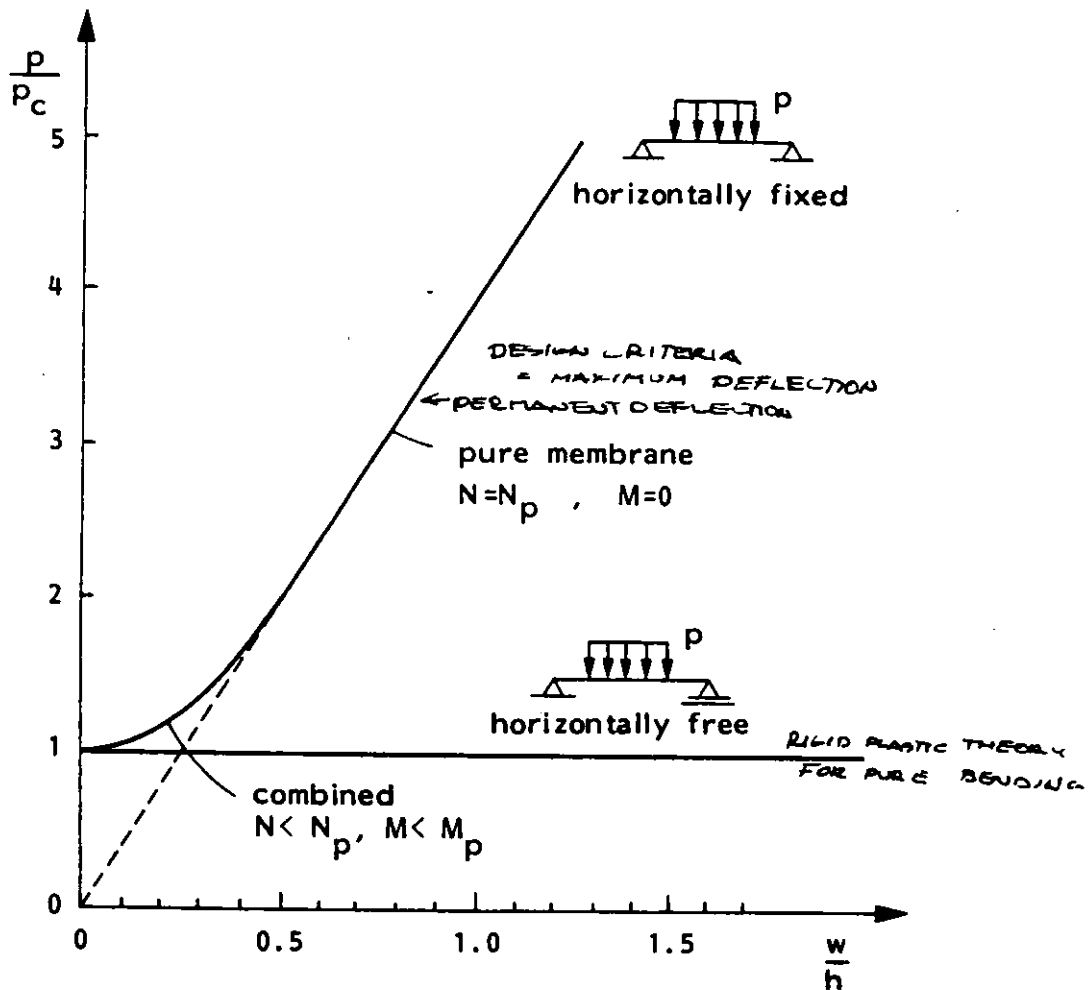


Fig.15 Load-deflection curve for simply supported platestrip under partial loading.

According to the above considerations full membrane action in the plate takes place at maximum deflection equal to half the plate thickness. However, special care must be taken when applying this simplified estimate since elastic deformations are neglected. This is illustrated in Fig.16 where comparison is made with more exact finite element solution for rather slender platestrip under uniformly distributed loading.

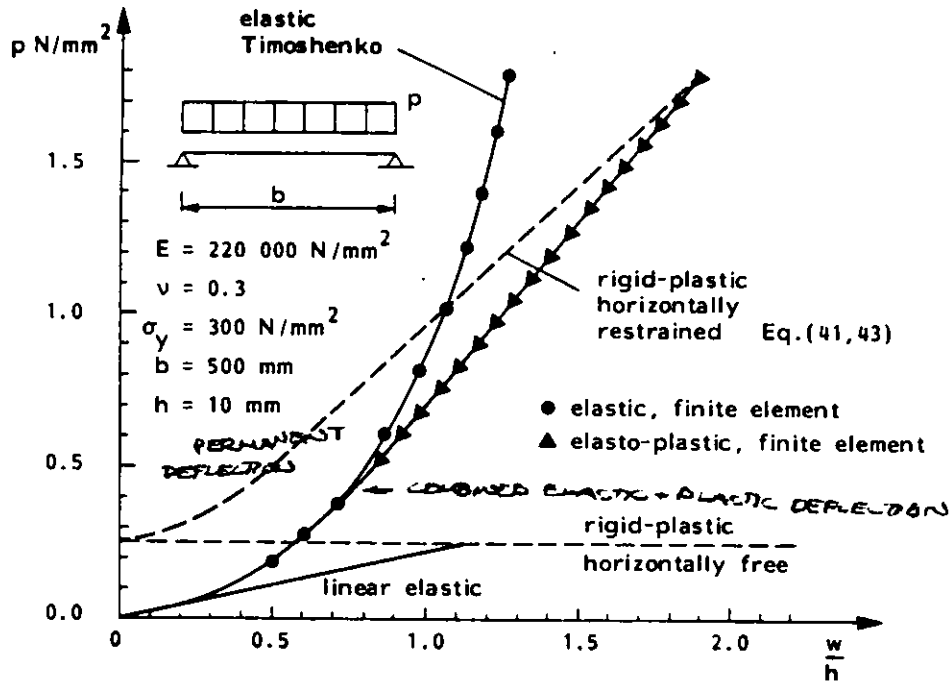


Fig.16 Simply supported platestrip under uniformly distributed load

The computer program is described in Chapter 6, and includes elastic as well as plastic material behaviour. The rigid-plastic technique is seen to be nonconservative in the sense that it overestimates the plate capacity for a given magnitude of deflection. The two methods become closer at larger deflections for which the relative contribution from elastic deformation is smaller.

6. NONLINEAR COMPUTER PROGRAMS BASED ON THE FINITE ELEMENT TECHNIQUE

6.1 Description of the Finite Element Method

The finite element method is essentially a product of the use of high speed electronic digital computers and the development in the field of numerical analysis of engineering problems. The basis of the finite element method is the representation of a body or a structure by an assemblage of subdomains called finite elements. These elements are connected at joints which are called nodes or nodal points, see Fig. 17.

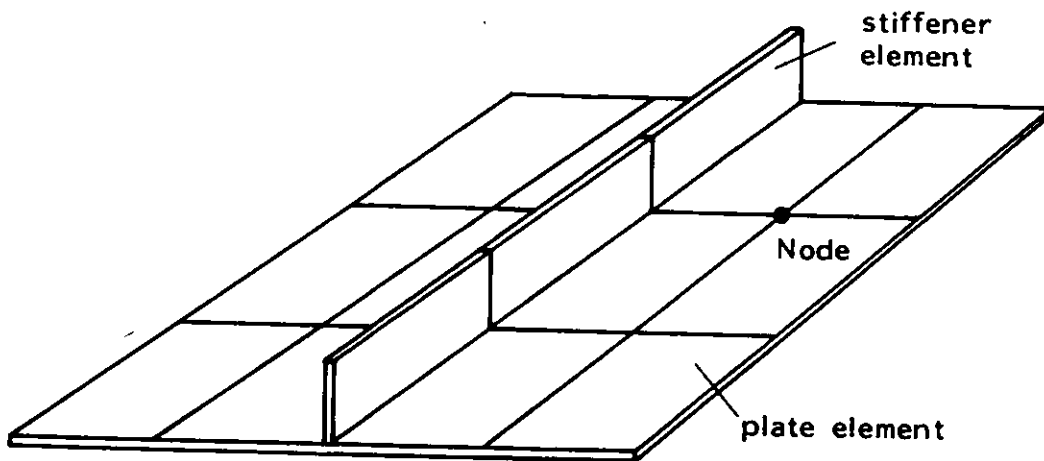


Fig.17 Stiffened plate represented as an assemblage of elements

The process of selecting a certain number of discrete points in the body is termed discretization. Any given function is approximated locally over each finite element by continuous functions which are uniquely defined in terms of the values of the function itself (and possibly of the values of its derivatives up to a certain order) at the nodal points belonging to each element. Such functions may for example be chosen to represent the variation of displacements over each element. These functions are chosen to satisfy some minimum continuity requirements, the so-called compatibility conditions.

The unknowns are the displacements (and derivatives of displacements) at the nodes. By this procedure displacement and strain fields can be derived for each single element with the nodal displacement values as parameters.

The virtual work equation is employed to obtain a set of equilibrium equations for each element. This variational way of establishing the equilibrium equations gives only a mean and not a pointwise equilibrium.

It is an important aspect of the finite element method that the structure is discretized into elements, which first are analysed independently. By combining the equations for the individual elements in such a way that continuity of node parameters is preserved, the equilibrium equations for the entire body are established. Boundary conditions in the form of prescribed displacements and stresses are imposed and the system of equations is solved to obtain node displacement values. The displacement and strain variations may now be calculated within each element and the stresses are found through the material law in the form of a stress-strain relation.

As a consequence of the above description the finite element method is divided into two main parts. These are

a. The element analysis

Involves study of each individual element.

b. The system analysis

Considering the whole body as an assemblage of elements.

In the case of geometric and/or material nonlinearity the description given is recapitulated in a step-by-step procedure. The problem is then to find incremental stiffness relations for the elements. After each load step, displacement and stress increments are added to their previous values. For such problems a combination of a step-by-step procedure and an iteration method may be effective.

The subsequent sections of this chapter are devoted to the evaluation of stiffener and plate elements, accounting for material as well as geometric nonlinear effects. Further, a short description is given on the most common solution procedures.

6.2 Nonlinear Stiffener Element

6.2.1 Incremental stiffness equations

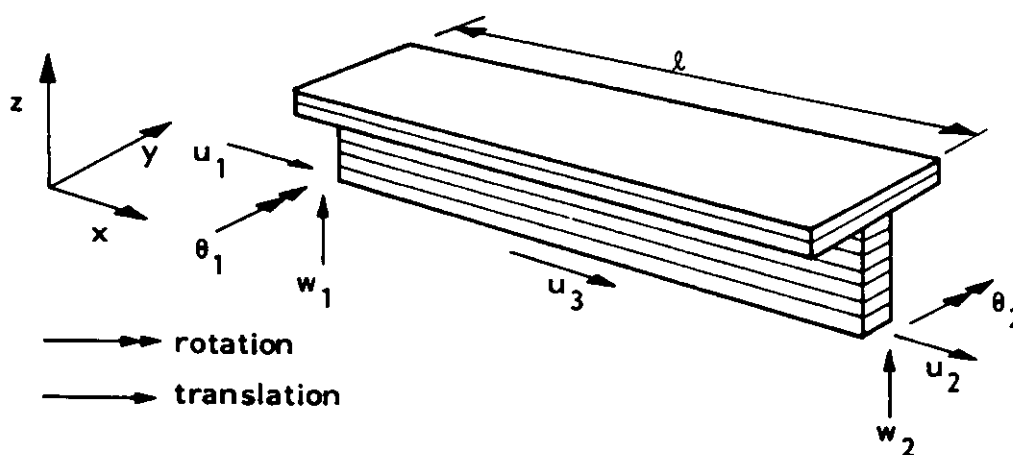


Fig.18 Nonlinear stiffener element

The elasto-plastic large deflection stiffener element is shown in Fig.18. The node parameters are axial displacement at the ends and at midpoint and deflection and rotation at the two ends. It is assumed that the deformation satisfies the Navier hypothesis also in the nonlinear range so that plane cross sections remain plane in deformed configuration.

The so-called Total Lagrangian Description is used in which deformation is referred to initial, undeformed configuration and large deflection effects are taken care of by nonlinear terms in the strain-displacement expressions.

The axial displacements of points on the nodal point line are represented by the vector

$$u = [u_1 u_2 u_3]^T \quad (45)$$

and the deflection have parameters

$$w = [w_1 \theta_1 w_2 \theta_2]^T \quad (46)$$

Initial deflection of the element is taken care of by a corresponding set of parameters

$$\bar{w} = \left[\bar{w}_1, \bar{\theta}_1, \bar{w}_2, \bar{\theta}_2 \right]^T \quad (47)$$

In matrix notation the nodal point line displacements may be written

$$u_0(x) = a^T(x)u \quad (48)$$

$$w(x) = b^T(x)w \quad (49)$$

$$\bar{w}(x) = b^T(x)\bar{w} \quad (50)$$

The axial displacement $u(x,z)$ of a point with coordinates x, z becomes

$$u(x,z) = u_0(x) - z w_{,x}(x) \quad (51)$$

where comma denotes differentiation. The lateral deflections w and \bar{w} are supposed to be constant across the height of the stiffener. Shear deformation of the stiffener is not included.

The axial strain is now found by the von Karmen strain expression /6/

$$E_{xx} = u_{,x} + \bar{w}_{,x} w_{,x} + \frac{1}{2}(w_{,x})^2 \quad (52)$$

and on incremental form

$$\Delta E_{xx} = \Delta u_{,x} + \bar{w}_{,x} \Delta w_{,x} + w_{,x} \Delta w_{,x} + \frac{1}{2}(\Delta w_{,x})^2 \quad (53)$$

The constitutive equation is described in Section 6.2.2, and can be written.

$$\Delta S_{xx} = D \Delta E_{xx} \quad (54)$$

on incremental form where D now is the incremental material stiffness coefficient, elastic or elasto-plastic.

Incorporating an incremental form of the virtual work principle the incremental load-displacement relationship for the stiffener element reads

$$\Delta P = k \Delta v \quad (55)$$

where P is the vector of nodal forces and v the corresponding displacement vector in the following order

$$v = \left[u_1 \ w_1 \ \theta_1 \ u_2 \ w_2 \ \theta_2 \ u_3 \right]^T \quad (56)$$

k is the so-called incremental element stiffness matrix, and may conveniently be separated into three contributions

$$k = k_L + k_{NL} + k_G \quad (57)$$

where

k_L = Linear geometry matrix.
Does not take care of large deflection effects.

k_{NL} = Nonlinear geometry matrix.
Large deflection incorporated.

k_G = Geometric matrix
Effect from membrane forces on lateral stiffness.

6.2.2 Constitutive equations

The so-called flow theory of plasticity is adopted giving an incremental stress-strain relationship on the form of Eq. (54). As postulated by Ziegler /7/ the plastic behaviour of a material is characterized by the following ingredients

- a. An initial yield condition defining the elastic limit of the material
- b. A flow rule relating the plastic strain increments to the stresses and stress increments
- c. A hardening rule specifying the conditions for subsequent yielding from a plastic state.

Since most experimental work on steel support the von Mises yield criterion this is used for initial yielding on the form

$$f = \bar{\sigma} - \sigma_y = 0 \quad (58)$$

where σ_y is the uniaxial yield stress and $\bar{\sigma}$ is the so-called equivalent stress.

The expression (58) gives a simple continuous functional representation of the yield condition and makes the von Mises criterion especially attractive from a programming point of view.

The first assumption made in the derivation of the flow rule is that the total strain ϵ may be decomposed into a recoverable elastic part ϵ_e and an irrecoverable plastic part ϵ_p

$$\epsilon = \epsilon_e + \epsilon_p \quad (59)$$

The plastic deformation is postulated to be incompressible

$$\epsilon_{px} + \epsilon_{py} + \epsilon_{pz} = 0 \quad (60)$$

It is also assumed that a loading function f exists at every stage of plastic deformation. The special value $f = 0$ constitutes the yield condition. For hardening materials f depends on the stress state σ , the plastic strain ϵ_p and a hardening parameter κ

$$f = f(\sigma, \epsilon_p, \kappa) \quad (61)$$

The material state may be

$$f < 0 \text{ elastic} \quad (62)$$

$$f = 0 \text{ plastic} \quad (63)$$

$$f > 0 \text{ inadmissible} \quad (64)$$

Taking the differential of f from a plastic state gives

$$df = \frac{\partial f}{\partial \sigma} d\sigma + \frac{\partial f}{\partial \epsilon_p} d\epsilon_p + \frac{\partial f}{\partial \kappa} d\kappa \quad (65)$$

Now, three different loading conditions can be defined

$$\frac{\partial f}{\partial \sigma} d\sigma < 0, f = 0 \text{ unloading} \quad (66)$$

$$\frac{\partial f}{\partial \sigma} d\sigma = 0, f = 0 \text{ neutral loading} \quad (67)$$

$$\frac{\partial f}{\partial \sigma} d\sigma > 0, f = 0 \text{ loading} \quad (68)$$

The third assumption is that the material is stable as defined by Drucker /8/. This postulate has two implications, namely convexity of yield surface and outward normality of the plastic strain increment vector $d\epsilon_p$ to the yield surface. The normality implication may be expressed as

$$d\epsilon_p = d\lambda \frac{\partial f}{\partial \sigma} ; d\lambda > 0 \quad (69)$$

Eq. (69) indicates that the loading function f plays the role of plastic potential. For materials obeying the von Mises yield criterion and the isotropic hardening rule in Eq. (61), Eq. (69) turns into the Prandtl - Reuss equation

$$d\epsilon_p = \frac{3}{2} \frac{s}{H' \bar{\sigma}} d\bar{\sigma} \quad (70)$$

where s now is deviatoric stress and H' is given by

$$H' = \frac{E \cdot E_T}{E - E_T} \quad (71)$$

E and E_T are defined in Fig.19 as elasticity modulus and elasto-plastic tangent slope on stress-strain curve, respectively.

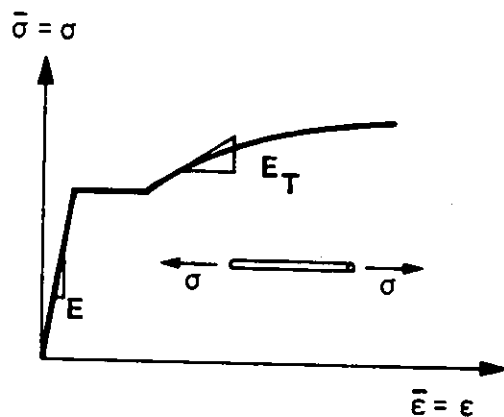


Fig.19 Uniaxial stress-strain relation

Eq. (70) indicates that an incremental stress-strain relationship is obtained. For a more detailed description of the flow theory of plasticity the fundamental works by Hill /9/ and Naghdi /10/ are recommended.

The integration of stiffness is carried out by specifying integrating points in longitudinal x -direction and using several layers over the stiffener height, see Fig.18. The usual number of such integrating stations is 3 longitudinally and 6-10 over the cross section. Accumulated strains and stresses are stored at each integration station.

6.3 Nonlinear Plate Element

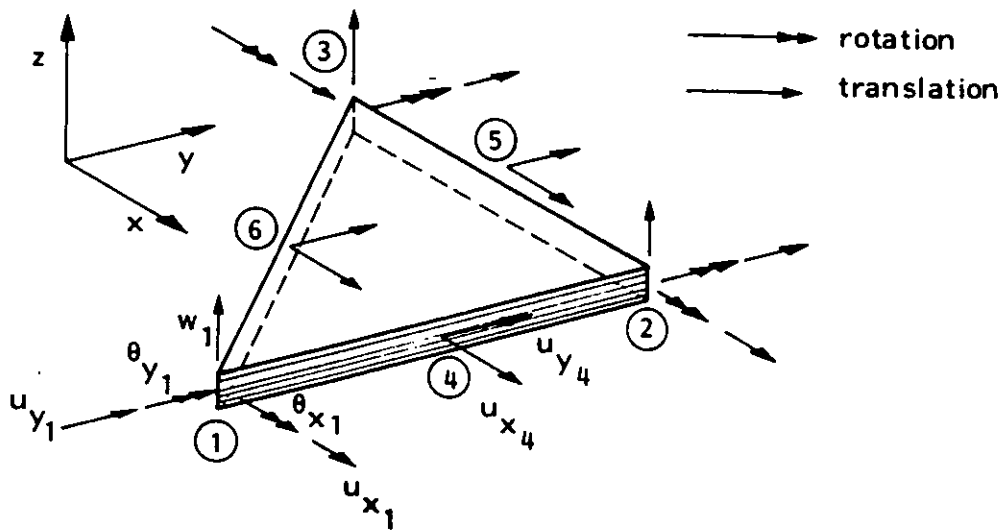


Fig. 20 Nonlinear plate element

The plate element chosen is a triangular element with six nodes as shown in Fig. 20. The corner nodes have inplane parameters u_x, u_y and out-of-plane parameters w, θ_x, θ_y while the midside nodes only have coupling to u_x, u_y . The xy -plane coincides with the middle surface of the plate in its initial undeformed configuration, and the z -axis is normal to the middle surface.

The development of incremental stiffness is similar to the procedure described for the stiffener element, the main difference being the new set of nonlinear strain-displacement relations

$$E_{xx} = u_{x,x} + \bar{w}_{,x} w_{,x} + \frac{1}{2} (w_{,x})^2 \quad (72)$$

$$E_{yy} = u_{y,y} + \bar{w}_{,y} w_{,y} + \frac{1}{2} (w_{,y})^2 \quad (73)$$

$$2E_{xy} = u_{x,y} + u_{y,x} + \bar{w}_{,x} w_{,y} + \bar{w}_{,y} w_{,x} + w_{,x} w_{,y} \quad (74)$$

where \bar{w} denotes initial deflection prior to load application.

The corresponding stress-strain expression on incremental form gets the form

$$\Delta\sigma = D\Delta\epsilon \quad (75)$$

where

$$\sigma = \begin{bmatrix} S_{xx} & S_{yy} & S_{xy} \end{bmatrix}^T \quad (76)$$

$$\epsilon = \begin{bmatrix} E_{xx} & E_{yy} & 2E_{xy} \end{bmatrix}^T \quad (77)$$

and D is the 3 by 3 constitutive matrix.

Incorporating the incremental virtual work principle, the load-displacement relation comes out on the form (55) where P and W now are vectors of 21 elements each.

6.4 Solution Techniques

As has been described nonlinearity occurs in two different forms. These are material nonlinearity that results from nonlinear constitutive laws and geometric nonlinearity caused by finite displacements. Most nonlinear structural problems involve both effects.

The "best" technique to solve the nonlinear equations largely depends on what form the mathematical equations have. The choice of method is generally much more difficult than in the case of linear problems. While in linear analysis the solution always is unique this may no longer be the fact in nonlinear situations. Thus the solution achieved may not necessarily be the solution sought. Physical insight into the nature of the structural problem may therefore be essential in addition to pure mathematical knowledge to derive a successful method of solution. Often a combination of several methods is utilized in an attempt to obtain a technique which combines precision, reliability and low cost.

The solution is carried out by applying the external loading in steps, ΔR . For each load step the incremental stiffness is assumed to be constant and the corresponding incremental equilibrium equations must be solved. For step number i this may be written in matrix notation

$$K_I^{i-1} \Delta r^i = \Delta R^i \quad (78)$$

where K now is the total system matrix on incremental form, and r and R are displacement and load vectors, respectively. The total load is now

$$R^i = R^{i-1} + \Delta R^i \quad (79)$$

and the first approximation for the displacement vector at this load level is

$$r^i = r^{i-1} + \Delta r^i \quad (80)$$

The incremental stiffness matrix K_I is a function of the current configuration of the structure, and for elasto-plastic problems, the entire deformation history.

The simple Euler-Cauchy incrementation method outlined above has a tendency of drift-off from the exact solution path. A more efficient technique is achieved by use of a so-called step-iterative solution technique where the discrepancy between external loads and internal stress resultants is eliminated by equilibrium iterations at each load level.

Since the tangent stiffness matrix is readily available, the so-called Newton-Raphson iteration is most suitable, see Fig. 2†

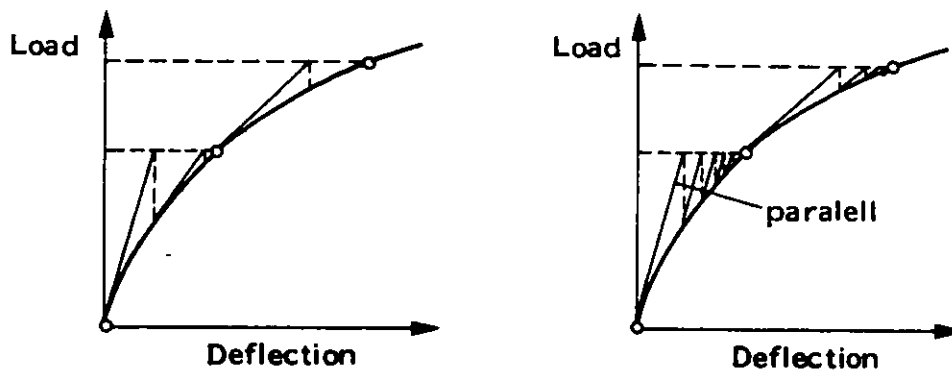


Fig.21 Step-iterative solution techniques

General discussions on solution techniques have been given by Oden /11/ and Bergan and Sørense /12/.

A flowchart of a computer program based on the above theory is shown in Fig.22.

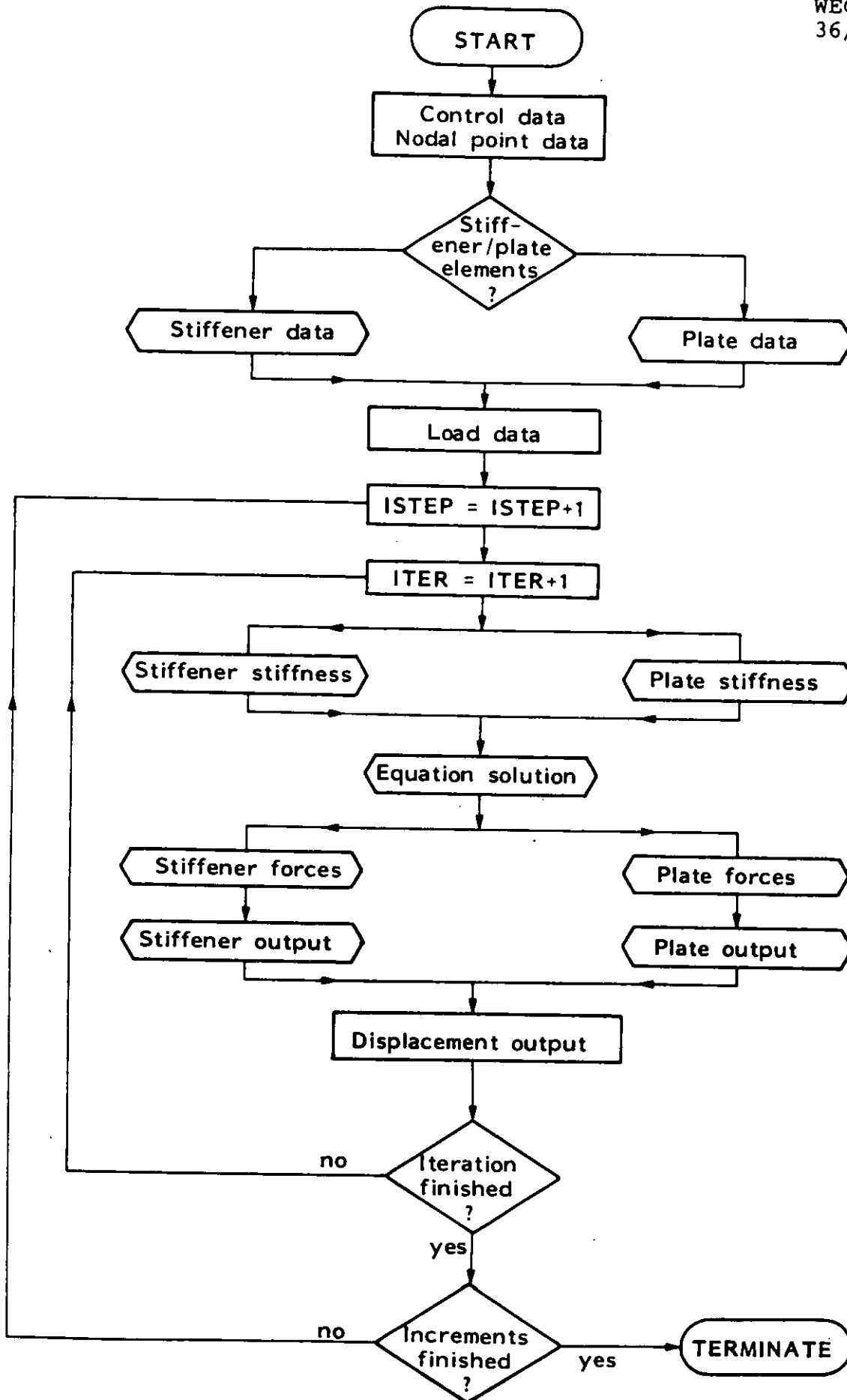


Fig. 21. Flowchart for nonlinear structural program TOTLAG.

7. RECOMMENDED DESIGN PROCEDURES

The finite element method represents an interesting alternative to the conventional design procedures. However, the nonlinear computer programs are rather costly and complicated to use, and are more practical for a final design than early preliminary designs. These programs should also be used for verification of the simpler rigid-plastic methods.

The requirements for the analytical methods are:

- a. The method must be reasonable accurate, and the level of approximation should be documented.
- b. The analytical model should simulate the real mode of collapse.
- c. The method should be close to normal design practice

The rigid-plastic techniques presented satisfy all these three criteria and represent a good basis for forming design recommendations. However, in order to choose the appropriate collapse model, boundary conditions and type of loading on the structural element must be identified. Further, these methods require full plastic hinges to develop and care must be taken to ensure high material ductility at low operating temperatures.

7.1 Design Loads

An overview of existing design load criteria is given in Ref./3/. What is of special importance for the choice of collapse model is the extent of the distributed load. The vertical extent of the load is approximately equal to the ice thickness. In Ref./3/ a so-called effective level ice thickness is defined and used as the vertical extent of the load, taking into account irregular ice features. With reference to the stiffening system in Fig.1. the vertical extent of the load is of special importance for the design of plate and transverse frames.

The horizontal distribution of the load along the ship side have interest for the design of longitudinal stiffeners. Ref /3/ considers the loaded area to be longer than one frame space. Thus, considering a stiffener element over one frame space, the load should be imposed as a distributed load along the total span of the stiffener.

Based on these load distributions analytical models can be set for the three structural elements as in the subsequent sections.

7.2 Plate Element

From the derivations in Section 5.3 it is seen that for simply supported platestrip full membrane action takes place even at a deflection amplitude equal to half the plate thickness. However, once more it should be emphasized that elastic deformations are neglected so that the maximum total deflection is somewhat larger.

In case of ice strengthening plating the slenderness of plate is low, usually in the range $b/h = 10 - 25$, and the elastic deformations prior to plasticity is of minor importance. Assuming uniformly distributed pressure from ice over the total width of plate and using the load/displacement relation (44) for a platestrip, the following formula emerges

$$p = 8 \frac{hw}{b^2} \sigma_y \quad (81)$$

Eq. (81) is in accordance with the formula proposed by Jones /13/.

The notation used is

p = load intensity

h = plate thickness

b = plate width equal to stiffener spacing

w = deflection amplitude

σ_y = yield stress of plate material

Since elastic deformations are of minor importance for the actual range of slenderness w is also an approximate measure on the maximum permanent deflection. Setting this tolerance limit equal to the plate thickness the following design formula comes out

$$P_{\max} = 8 \frac{h^2}{b^2} \sigma_y \quad (82)$$

or expressed as minimum plate thickness requirement

$$h_{\min} = b \sqrt{\frac{P}{8\sigma_y}} \quad (83)$$

Safety factors are not incorporated in the above equations.

Most classification societies base their ultimate load design of plates on the simple mechanism model with only bending action. Using the three hinge model in Fig.5 for a plate strip the expression for ultimate load intensity read

$$P_{\max} = 4 \frac{h^2}{b^2} \sigma_y \quad (84)$$

which is half the capacity in Eq.(82).

7.2 Stiffener Design

For stiffeners between transverse frames membrane action is of less importance and the design should be based on a three hinge bending mechanism giving the following ultimate load

$$P_{\max} = \frac{16Z}{l^2} \sigma_y \quad (85)$$

where

Z = plastic section modulus

l = frame space

σ_y = yield stress

By formula (85) full credit is given to the rotational restraints at supports.

REFERENCES

1. European Convention for Constructural Steelwork (ECCS): "European Recommendations for Steel Construction", 1978.
2. Søreide, T.H.: "Ultimate load Analysis of Marine Structures", Tapir Publishing Company, Trondheim, Norway, 1981.
3. Ship Structure Committee: "A Rational Basis for the Selection of Ice Strengthening Criteria for Ships", U.S. Coast Guard Headquarters, 1981.
4. Det norske Veritas: "Rules for the Design, Construction and Inspection of Offshore Structures-Appendix C Steel Structures", Oslo 1977.
5. Hodge, P.G.: "Plastic Analysis of Structures", McGraw-Hill, New York, 1959
6. Fung, Y.C.: "Foundations of Solid Mechanics," Prentice Hall, 1965.
7. Ziegler, H.: "A Modification of Pragers Hardening Rule", Quarterly of Applied Mathematics, Vol.17, No.1, 1959. pp. 55-65
8. Drucker, D.C.: "A More Fundamental Approach to Plastic Stress-Strain Relations", Proceedings of the First U.S. National Congress on Applied Mechanics, (Chicago 1951), New York, 1952.
9. Hill, R.: "The Mathematical Theory of Plasticity", Oxford University Press, 1950.

10. Naghdi, P.M.: "Stress-Strain Relations in Plasticity and Thermoplasticity", in Proceedings of the Second Symposium of Naval Structural Mechanics, (editors: E.H.Lee and P.S. Symonds), Pergamon Press, 1960.
11. Oden, J.T.: "Finite Elements in Nonlinear Continua", McGraw-Hill, New York, 1971.
12. Bergan, P.G. and Sørense, T.H.: "A Comparative Study of Different Numerical Solution Techniques as Applied to a Nonlinear Structural Problem", presented in Computer Methods in Applied Mechanics and Engineering, Vol.2, 1973, pp.185-201.
13. Jones, N.: "Plastic Behaviour of Ship Structures", Transactions, Society of Naval Architects and Marine Engineers, New York, NY, Vol.84, 1976.



STRENGTHENING OF HULL
STRUCTURES IN ICE

By

Christian Mürer

Principal Surveyor

A. GENERAL PHILOSOPHY OF ICE STRENGTHENING

1. ICE LOAD CRITERIA

1.1 General

In general, ice loads will have to be related to:

- Ice properties.
- Ice conditions/features/trade route.
- Interaction ice - ship structure.
- Structure response calculation criteria and acceptable level of risk.

In the following, these factors will be shortly discussed, based upon a selection of literature sources.

In addition, these topics are covered in more detail in other lectures.

1.2 Ice Properties

Natural sea ice is generally an anisotropic material with mechanical properties varying in different directions. Riska (1) has shown that the ice structure consists of vertical column-like crystals, and according to this, may be termed as an isotropic material in the transverse direction.

Ice may fail in tension, flexure, shear compression or buckling. For estimating ice loads, the compression, shear and bending failure modes, together with the E-modulus are the most important properties. Important factors affecting these properties are:

Porosity (containment of brine and air).

Hysing (2) refers to a dominating influence, especially on E-modulus and flexural strength.

Salinity. Fresh water ice is generally stronger than salt water ice, which, on the other hand, increases its strength with age, due to loss of salinity.

Temperature has great influence, strength increasing with reduced temperature.

Load/strain rate is very important, especially with respect to crushing (compression) strength, which has a special bearing on the ice load problem.

Coburn (3) has illustrated the general effect of strain rate, see fig. 1.

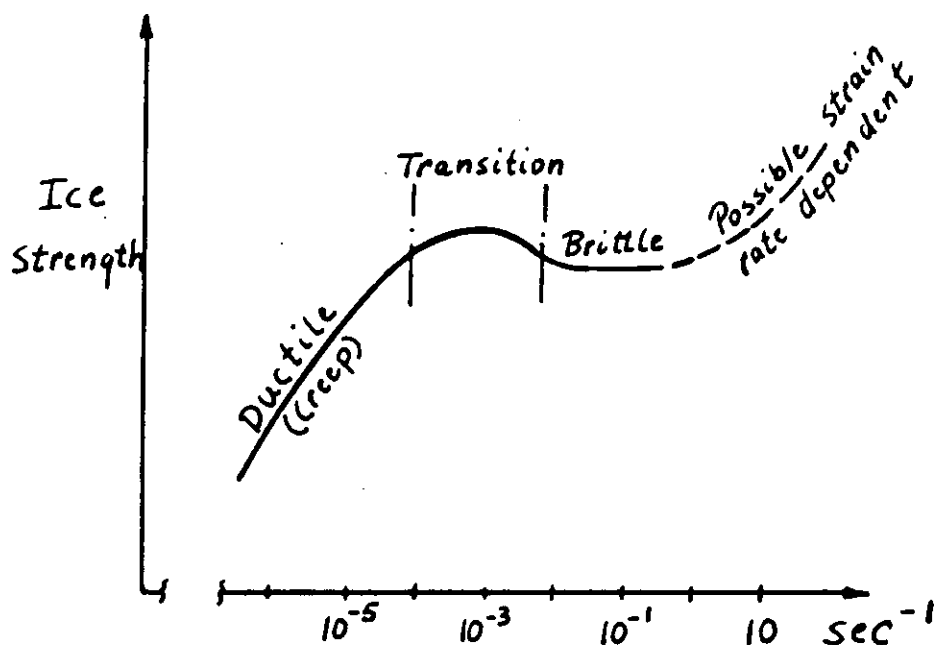


Fig. 1 General effect of strain rate.

At low strain rates (creep), the ice shows a plastic (ductile) behaviour, then there is a transition to brittle behaviour from about 10^{-4} to 10^{-2} sec^{-1} strain rates. This is discussed by Ralston (4), who refers to a series of indentation strength tests as compiled in Fig. 2.

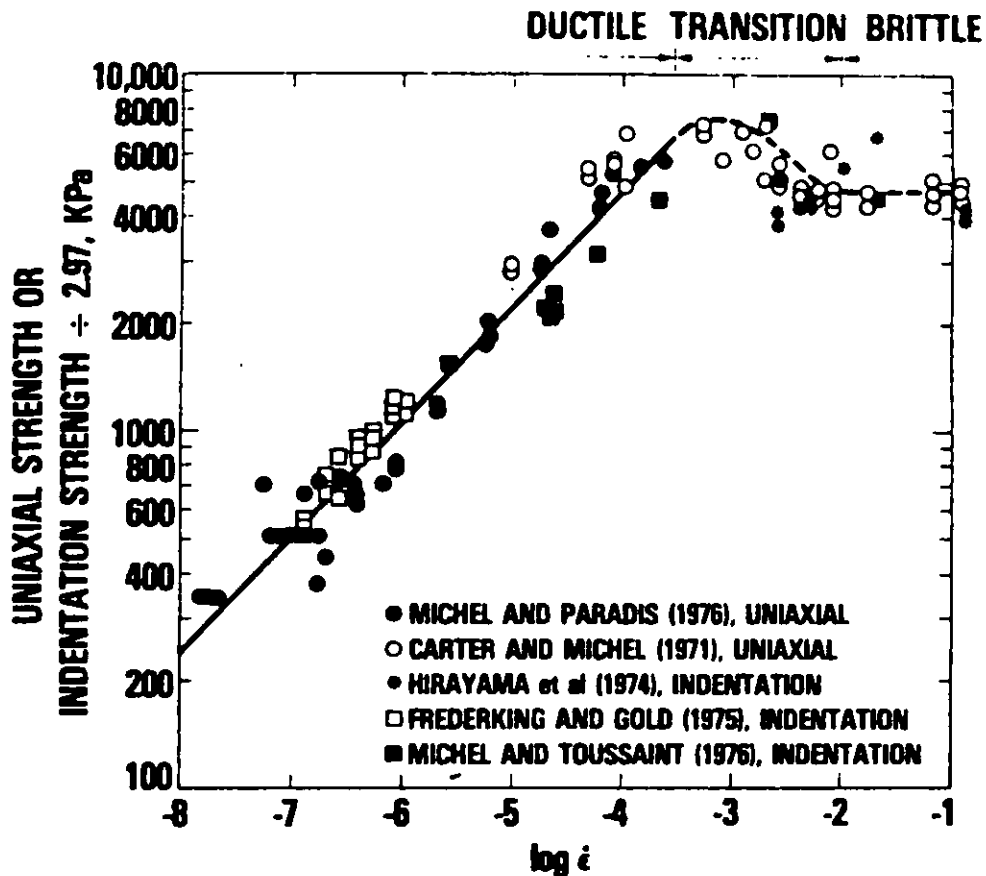


Fig. 2 Uniaxial crushing strength and indentation strength of ice at -10°C .

Applied load condition also has a significant influence on compression strength. Tests in multi-axial compression give much higher values than on uniaxial test specimens. In ref. (4), reference is made to laboratory tests where the influence of the applied load aspect ratio (width of load/ice thickness) on uniaxial strength has also been investigated. In fig.3, these results are shown, compared also with computed values from a plastic limit analysis developed in the paper.

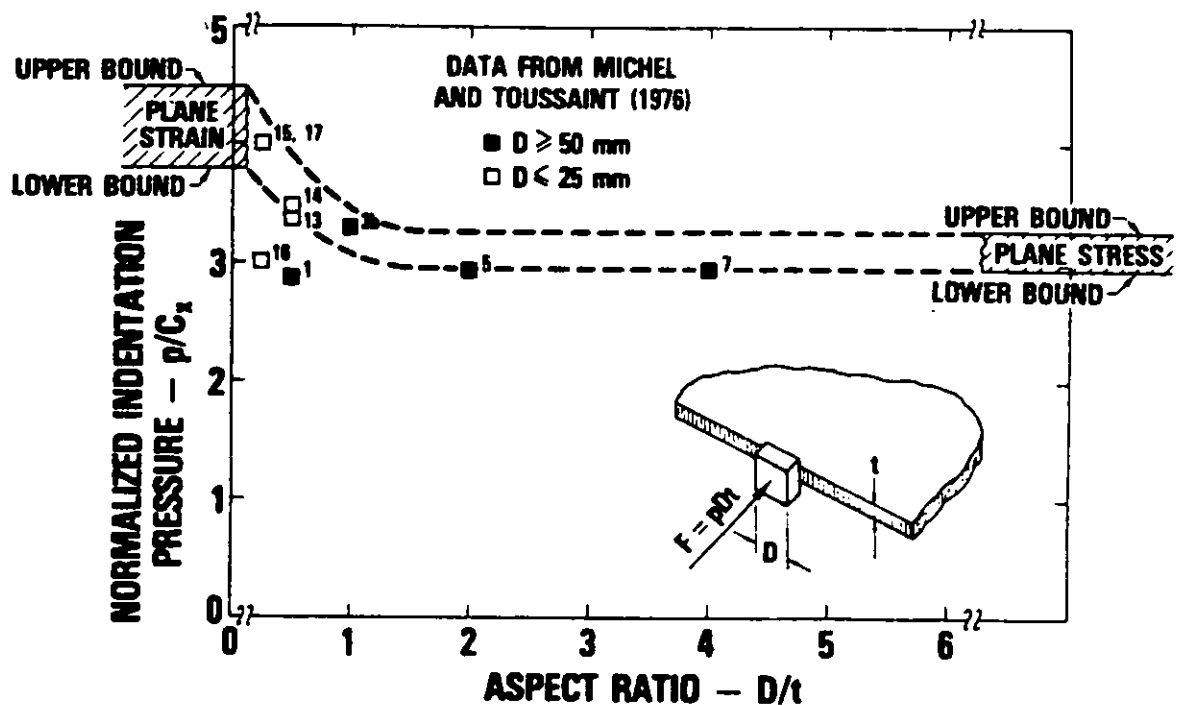


Fig. 3 Comparison of computed indentation pressure with test data. $C_x = 2.244$ MPa.

The large number of parameters referred to, makes the assessment of ice loads rather uncertain. Most data are from laboratory tests, and ice properties may be different in full scale. For sea ice exposed to short load durations relevant to the ship structures, the following typical values are given in ref (2):

- Tension: 0.8 - 1.0 MPa
- Bending: 1.0 - 1.2 MPa
- Shear : 0.3 - 1.0 MPa
- Uniaxial compr.: 5 - 10 MPa
- E-modulus : $2 - 5 \cdot 10^3$ MPa

In ref.(3) and also in more detail in ref.(5), a rational basis for selecting ice strengthening criteria has been proposed. Uniaxial crushing strength values have there been indicated in the range of 1.5 - 3.0 MPa from first-year "warm" ice to multi-year mid-winter ice. This must refer to unconfined strength at rather low strain rates.

According to ref.(4), these values should be multiplied by a factor of at least 2, to take care of the ice being confined in the transverse direction.

1.3 Ice Conditions

The influence of ice age on the strength properties has been mentioned in 1.2. For the Baltic Sea, only first year ice exists. The salinity, however, is very low, and this should be taken into account when estimating ice strength.

Other types than normal level ice (uniform thickness) to be met with are:

- Pressure Ridges
- Icebergs and icelands
- Growlers and bergy bits
- Broken ice.

The first three types represent great problems to shipping in terms of greater ice strength and large masses. Especially icebergs, icelands, bits and growlers may lead to very heavy impacts on ship structures. Strengthening to take care of such forces is not very practical, and they are to be avoided by proper navigation. Ridges should also be avoided by ice-strengthened merchant ships, except for the higher Arctic classes.

1.4 Interaction Ice - Ship Structure

The different cases of ship - ice interaction should be considered in relation to the ice condition mentioned above:

- Continuous ship motion in level ice.
- Impacts from broken ice floes.
- Hull striking on unbroken ice edge (ramming).
- Compression of hull in moving ice.

The first two cases involve rather small forces, and will mainly be considered in case of moderate ice conditions or when ships are assisted by icebreakers, as normally in the Baltic Sea.

As mentioned in 1.2, full-scale data on ice loads are rather limited. Mathematical models have been developed, see refs. (6) and (7), treating the collision of a ship with ice as a rigid body phenomena. A resulting force is calculated in a time step sequence, considering factors as: Ice crushing and bending, rigid body motions of ship, hydrodynamic added mass and damping, hull shape, speed and size of ship and properties and thickness of ice.

Results of such calculations are given also in ref.(5). Some observations are:

- In level ice, failure occurs in bending after initial crushing. Total load increases with increasing ice thickness. Size of ship has little influence. For large ice masses compared to ship mass, higher impact loads are expected.
- The total load increases with increasing crushing strength and with impact speed.

In ref. (2), analytical models for prediction of global ice loads are given, estimating the crushing, buckling and bending failure for level ice conditions and multiyear ridges. Normally, buckling loads seem to be higher than the crushing loads, whilst bending failure reduces the load significantly. A ship side sloping angle of 8° (see ref.(7)) has been mentioned as a transition from compression to bending of the ice.

During crushing of the ice, the pressure on the ship structure will be redistributed according to the local stiffness of the steel structure. Such a redistribution from plating to stiffeners and from stiffeners to girders and bulkheads is mentioned in refs. (7), (8) and (9). This phenomenon has been further discussed during the development of the new Baltic ice rules, see part C.

At the contact points where crushing takes place, a state of multiaxial compression occurs. The magnitude of the ice pressure in that case has been estimated by Hysing (2) to be:

$$P_1 = 6 \left(\frac{A}{A_0} \right)^{-0.165} \cdot \sigma_c$$

A = local load area

A₀ = standard area taken as 0.35 cm²

σ_c = maximum uniaxial crushing strength of ice.

Also Popov et al (7) have developed theoretical/empirical models for ice loads and ice/hull interaction, being the basis for the Russian ice rules.

2. HULL STRUCTURE RESPONSE CRITERIA

2.1 Hull Girder Strength

For merchant ships operating in ice conditions relevant to their design, longitudinal hull girder bending moments of any great magnitude will not be imposed. Ships with heavier strengthening and special ice bow configuration may be subject to bow rise, thus given a certain bending moment. This is, however, normally considered small compared to the standard open water wave bending moment to which the ships are designed. Only in case of high Arctic classes and for icebreakers should the longitudinal strength be specially considered.

2.2 Local Strength

Local structural response may in general have to be considered for a variety of modes, such as elastic deformation, yielding, ultimate plastic collapse, buckling and fatigue fracture. These various modes should be reflected in a set of simple and easy to use regulations.

When considering shell plating subject to external ice loads, buckling and fatigue are normally not considered to be of significant importance. Thus, the plating between stiffeners may be analysed on the basis of elastic bending with yielding as a limit criteria, or on a plastic deformation evaluation applying a one-dimensional model (plate - strip beam) with three plastic hinges, or finally, on a more sophisticated large deformation theory applying, for instance, a finite element analysis. When applying the simple elastic theory, one should keep in mind that yielding as a limit is very conservative. The load carrying capacity of plating is up to four times higher.

Service experience has indicated that framing, rather than plating has been subject to a certain degree of failure, such as plastic collapse, buckling and fractures in details.

A pure elastic bending analysis or a simple plastic analysis with three hinges are normally used as response criteria for framing. In addition, it is very important to take care of local design problems, such as proper end connections and use of tripping brackets to avoid collapse by instability.

3. MATERIALS

As long as ice-strengthened ships are intended to work for longer periods in cold climate waters, the importance of considering the steel material behaviour at lower than normal temperatures would seem quite obvious, especially for Arctic waters. Material toughness has to be sufficient to avoid brittle fracture at low temperature exposure.

Until now, however, special quality material requirements have not been included in, for instance the Baltic ice regulations, applied by many of the classification societies. Failure statistics do not seem to indicate any special brittle fracture problem under Baltic service.

What is more surprising, is that no special requirements as to brittle fracture toughness are given in the Canadian Ice Regulations, which are supposed to cover the highest classes of Arctic icebreakers. Recent experience seems to show that ships designed for Arctic (or Antarctic) service should be built with special steels in exposed areas.

In the USSR Register of Shipping rules, grade A steel is not permitted in important plate strakes in deck and in ice belt for the higher ice classes. For icebreakers, grade E steel is required in the ice belt plating.

Recently, the classification societies have introduced a recommendation (IACS Rec. No.7), as to the selection of proper materials for structures subjected to low temperatures. These regulations are based on the estimation of an ambient service temperature, considering that for normal world-wide service, a temperature of 0°C has been chosen. It seems quite obvious that these recommendations are well-suited for material selection in relation to both Baltic and Arctic ice strength regulations. A relevant definition of the ambient service temperature would have to be given, for instance the lowest monthly isotherm in the area of operation.

The selection of appropriate steel qualities is, in addition to temperature, to be based on stress level in structure, existence of details giving notch effect and considerations on consequence of failure. The IACS recommendation referred to contains a table (see Table 1) giving limiting thicknesses for the various ship steel qualities in relation to temperature and application category. Where applied thicknesses are above the limits for E (or EH) grade steel, special steels with high impact energy values at low temperatures are to be selected. Impact test temperatures are to be chosen in relation to plate thickness as follows:

$$t_{\text{test}} = t_{\text{serv}} + \frac{1}{2}(30 - t_{\text{pl}})$$

- t_{test} = test temperature ($^{\circ}\text{C}$)
 t_{serv} = service temperature ($^{\circ}\text{C}$)
 t_{pl} = plate thickness (mm)

Table 1 Thickness limitations (mm) for various design temperatures and application categories

Category	Grade	Minimum design temperature ($^{\circ}\text{C}$)					
		0	-10	-20	-30	-40	-50
Secondary	A	30	20	10	x	x	x
	B	40	30	20	10	x	x
	D	50	40	30	20	10	x
	E	50	50	50	50	45	35
	AH	40	30	20	10	x	x
	DH	50	50	45	35	25	15
	EH	50	50	50	50	45	35
Primary	A	20	10	x	x	x	x
	B	25	20	10	x	x	x
	D	35	25	20	10	x	x
	E	50	50	50	40	30	20
	AH	25	20	10	x	x	x
	DH	45	40	30	20	10	x
	EH	50	50	50	40	30	20
Special	A	x	x	x	x	x	x
	B	15	x	x	x	x	x
	D	20	10	x	x	x	x
	E	50	45	35	25	10	x
	AH	15	x	x	x	x	x
	DH	30	20	10	x	x	x
	EH	50	45	35	25	10	x
NOTE		Interpolation of thicknesses for intermediate temperatures may be considered.					

B. ICE RULE DEVELOPMENT AND PRESENT STATUS

1. INTRODUCTION

A special strengthening of the hull structure for ships intended for traffic in ice-infested waters may be traced back to the early twenties in the rules of some classification societies.

In addition, the authorities in some countries, especially those in the northern hemisphere with a coastline facing ice-troubled waters, developed their own regulations:

- Canada (Arctic Shipping Pollution Prevention Regulations, see ref.(10)) ASPR 1972
- Soviet-Union (Regulations of the USSR Register of Shipping) ^{GENERAL 1980} _{GEN. RULES 1982}
- Finland / Sweden (Finnish/Swedish Ice Class Regulations 1971) ^{ICE BREAKERS 1982}
PROPOSAL FOR NEW BALTIC RULES

In the following, a short review of this development will be given. A general trend has been a close cooperation between the authorities and the classification societies.

2. FINNISH/SWEDISH ICE REGULATIONS

2.1 In ref.(11), Siivonen has given a historic review of the Baltic Sea ice regulations. As mentioned, the first start was made in the twenties when the Finnish Board of Navigation assigned ships into categories, of which the highest was related to the existing rules of some classification societies. The next step was taken in 1932, when a new set of rules were established on the basis of the rules of six classification societies (Lloyd's Register of Shipping, British Corp., Germanischer Lloyd, Bureau Veritas, American Bureau of Shipping and Det norske Veritas). The main requirements were:

- Ice belt from somewhat above load waterline to somewhat below ballast waterline.
- Intermediate frames introduced.
- Scantlings of plating, frames, stringers, etc. given a percentage increase (15 to 25) above normal class rules.

Further classification societies (USSR Register of Shipping, Polish Register of Shipping and DDR Register of Shipping) were accepted later on, and in 1965 a new, higher Ice class (IA Super) was introduced.

2.2 Present Rules

The percentage system of arriving at hull scantlings were strongly criticized during these years, and in 1971 the existing Finnish/Swedish Ice Regulations were introduced. The Finnish authorities established a cooperation with the Swedish Authorities, and in addition, with some classification societies. The aim was to establish rules based upon direct ice-load/structure response criteria in which service experience should be incorporated. The theoretical background for these rules is to be found in the work by Johansson(12), and discussions and interpretations are given in the papers of Böckenhauer(13) and Jantzén(8).

With the background of part A, and also as a basis for the new rule development explained in part C, a review of the main highlights of the 1971 rules will be given.

2.2.1 Ice Loads

The evaluation of the design pressures was based on an empirical relation between pressure and displacement/engine power. More absolute, physical laws were not considered due to the statistical nature of

the ice loads. Thus, based on the assumption that the pressure

$$P = f(\sqrt{\Delta P_S})$$

where Δ = max. displacement of ship
 P_S = maximum shaft horse power,

about 200 ships trading in the Baltic were analysed with respect to strength and structural damage due to ice loads.

The strength analysis consisted of estimating the ultimate ice response that frames and plating could withstand without permanent deformations occurring. This ultimate pressure was plotted against the P_S - factor, as shown in Fig. 4, which covers the bow region of the ice class 1A ships. Similar diagrams were made for the middle and the aft regions, and for the other ice classes.

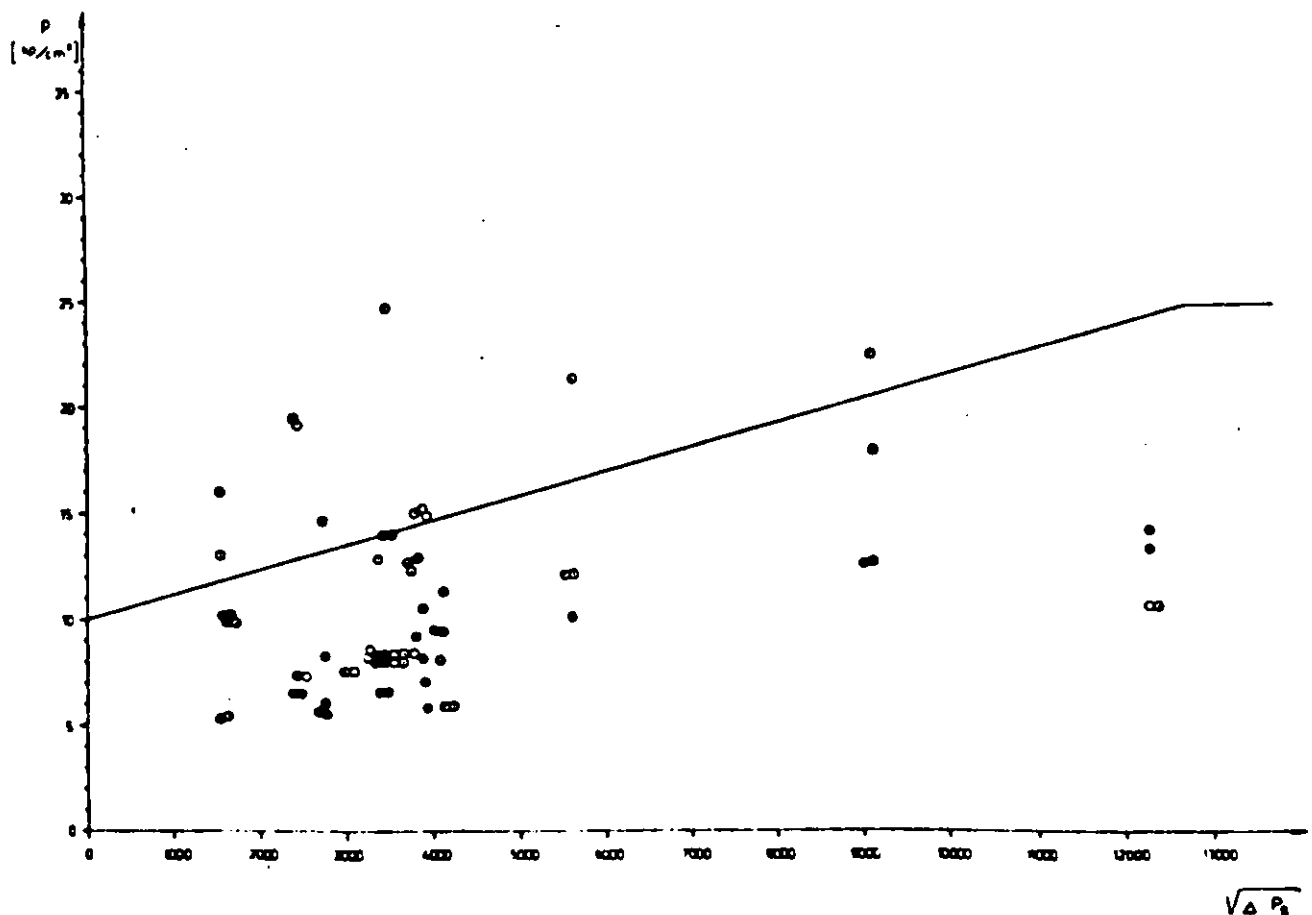


Fig. 4 Strength capability of analysed ships.

In the figure, the black spots indicate that a ship has sustained damage, whilst the white spots indicate that no damage has occurred. Certain lines were drawn on the diagrams, representing the proposed ice pressures, in such a way that most of the black spots fell below the line. By dimensioning the hull structures according to these design loads, a much more uniform design strength standard could be obtained.

2.2.2 Strength Analysis

General. Having chosen the ice load standard, Johansson based his strength analysis of plating and frames on the plastic theory. Considering the plating and also the frames as more or less fixed at their supports, the limiting load carrying capacity (permanent set) is reached when three plastic hinges have developed.

For a simple beam with uniform load, the plastic yield moment is given from Fig. 5:

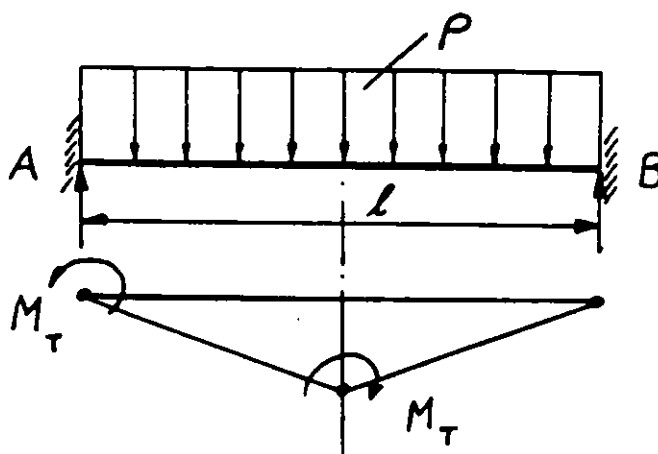


Fig.5 Plastic beam model.

$$M_y = -M_y + A l/2 - pbl^2/8$$

$$A = pbl/2$$

This gives:

$$M_y = \frac{pbl^2}{16}$$

where

p = uniform pressure

l = span of beam

b = breadth of load area

This yield moment should be equal to or less than the fully plastic section modulus times the yield stress:

$$M_y = W_p \sigma_y = pbl^2/16$$

Thus, the general requirement to the plastic section modulus based upon the ultimate strength criteria is:

$$W_{pt} = \frac{pbl^2}{16 \sigma_y} \quad (1)$$

Plating. Considering now the plate field between two transverse frames, the normal approximation is to take a plate strip fixed at the frames and loaded by a uniform ice pressure. The plastic section modulus of the plate is $W_p = \frac{bt^2}{4}$ and the general requirement to plate thickness with spacing s becomes from eq.(1):

$$t = 0.5s \sqrt{\frac{p}{\sigma_y}} \quad \text{or} \quad 500s \sqrt{\frac{p}{\sigma_y}} \quad (2)$$

with s in metres.

Now Johansson decided to use a constant ice pressure thickness of 0.8 m. In a plate field supported by transverse framing, a small part of the load will be transferred to the plating above and below the pressure area, and a small reduction in actual ice pressure was introduced:

$$P_1 = p(1.1 - \frac{s}{3})$$

with s in metres.

In addition, an increase of the plating ice pressure compared to the pressure on the framing was introduced, based upon the theory that the initial crushing of the ice edge between frames will lead to a redistribution to the plating from the framing. The increase was initially made variable from 40% at zero pressure to zero at max. ice pressure $P_0 = 3$ MPa. In the final rules, this factor was taken constant and equal to 1.2 for transverse framing and 1.4 for longitudinal framing forward. This factor has later been criticized, and as will be shown in part C, for transverse framing, a redistribution from plating to framing will actually take place.

Framing. For transverse framing, a load from the 0.8m thick ice was again assumed. This load acting at the middle of the span will give the following expression for the ultimate bending moment:

$$M_y = \frac{pbh}{8} (1 - \frac{h}{2}) \quad (3)$$

With b equal to the frame spacing s, the required plastic section modulus becomes:

$$W_p = \frac{M_y}{\sigma_y} = \frac{psh}{8\sigma_y} (1 - \frac{h}{2}) \quad (4)$$

For longitudinal framing, which was introduced in the rules for the first time, Johansson assumed that with standard ice thickness 0.8 m, the pressure area would cover three longitudinals. Further, he assumed that a part of the load on the middle frame was transferred to the adjacent frames. With plate thickness t , frame spacing s , and pressure on transverse frames P_t , the pressure on longitudinals was taken as:

$$P_l = P_t - \frac{t^2 \sigma_y}{s^2} \quad (5)$$

The plastic section modulus requirement based upon equation (1) becomes:

$$W_{pl} = \frac{P_l s l^2}{16 \sigma_y} \quad (6)$$

with l = span of longitudinal.

2.2.3 Final Modifications

The ice pressure level actually introduced in the final 1971 rule edition was reduced by a factor 1.75, and the allowable stress level simultaneously reduced by a factor 1.75. This in fact means that section modulus requirements to the initial beam were transferred to the elastic range, and now with a factor of safety against yield of 1.75. Thus, the final formulae in the present Finnish/Swedish ice rules are:

Plating. From eq.(2) with constant multiplied by $\sqrt{1.75}$:

$$t = 667s \sqrt{\frac{kp}{\sigma_y}} + 2 \quad (\text{mm})$$

For transverse framing:

$$k = 1.2 \left(1.1 - \frac{s}{3} \right)$$

For longitudinal framing:

$$k = 1.4 \text{ in forward region} \\ = 1.2 \text{ elsewhere}$$

kp is limited to 16.5 kp/cm^2 (1.62 MPa).

Transverse framing:

To obtain the requirement to the elastic section modulus, eq. (3) has been multiplied by 1.75/1.4 and with ice thickness $h=0.8\text{m}$:

$$W = \frac{ps (1 - 0.4)}{8 \sigma_y} \cdot 10^6 \quad (\text{cm}^3)$$

Longitudinal framing:

From eq. (6), multiplied by 1.75/1.4:

$$W = \frac{p_1 s l^2}{13 \sigma_y} \cdot 10^6 \quad (\text{cm}^3)$$

The pressure P_1 has been given, based on eq. (5):

$$\begin{aligned} P_1 &= 0.64 p \text{ in forward region} \\ &= 0.70 p \text{ elsewhere} \end{aligned}$$

For all framing, the requirements to ordinary frames and possible intermediate frames are the same.

Ice stringers supporting transverse frames have been treated on the basis of eq. (1) with $b = h = 0.8\text{m}$, multiplied by 1.75, divided by 1.5 (plastic/elastic section modulus ratio) and finally the pressure has been reduced by 25%, assumed carried by the frames to adjacent supports:

$$W_s = \frac{K p S^2}{22 \sigma_y} \cdot 10^6 \quad (\text{cm}^3)$$

S = span of stringer in m.

$$k = 1.1 - \frac{S}{10}, \quad 0.7 < k < 1.0$$

The factor K gives a certain reduction in load with increased length of load area.

Web frames supporting stringers have been assumed to carry at the middle of the span a point load equal to 80% of the total stringer load:

$$\begin{aligned} p_s &= 0.8 \cdot 0.75 \cdot K p S h \\ &= 0.48 \cdot K p S \end{aligned}$$

giving a plastic limit bending moment based upon fixed support at bottom and 50% fixed at deck:

$$M = \frac{p_s Z}{7}$$

and required section modulus

$$W_w = \frac{1.75 M}{1.5 \sigma_y} = \frac{kpSZ}{12.5 \sigma_y} \cdot 10^6 \quad (\text{cm}^3)$$

In addition to the general formulae for plating, frames, stringers and web frames, detailed requirements are given to end connections of frames, tripping brackets, shear areas and local buckling stiffening of decks and stringers.

Finally, for the various ice strength classes, vertical extension of plating and framing has been given in relation to the maximum load waterline and the minimum ballast waterline.

3. THE CANADIAN ASPPR ICE RULES

The Canadian ice rules were introduced in 1972, see ref.(10). Quite naturally, they are intended for ships sailing under Arctic winter conditions, and as many as 9 different ice classes were given (1, 1A, 2, 3, 4, 6, 7, 8 and 10). In addition, 5 lower classes were added (A, B, C, D and E), corresponding to the Baltic ice classes and also to the ice classes of the classification societies.

3.1 Ice Loads

The ice pressures given for the higher ice classes are higher than in other ice rules, varying from 0.7 MPa amidships in class 1 to 10.5 MPa in the forward region of class 10. A comparison of the various rules is discussed in more detail in item 5.

The ice pressure within each region of the side and bottom shell varies nearly linearly with the ice class. As for the Baltic ice rules, the height of the ice pressure area is assumed to be 0.8 metres irrespective of class.

3.2 Strength Requirements

The basis for calculating the strength of plating and framing is the same as in the Baltic rules. A standard beam analysis has been made based on the three-plastic-hinges criterium for plating with uniform load, for transverse frames with a 0.8 m load acting at midspan.

Plating. Equation (1) has been used, and from the plastic section modulus of a plate strip, a safety factor of 1.75 introduced, and the plate thickness is given by:

$$t = 667s \sqrt{\frac{p}{\sigma_y}} \quad (\text{mm})$$

with frame spacing s in metres.

This is very nearly the same formula as in the Baltic rules. In view of the much higher ice pressures, the Canadian rules require higher plate thicknesses.

Framing. For the transverse framing eq.(4) is used, and with 0.8m ice thickness and $W_p/W_e = 1.4$, the requirement to elastic modulus:

$$W_e = \frac{ps(1 - 0.4)}{8 \sigma_y} \cdot 10^6 \quad (\text{cm}^3)$$

with l and s in metres, means that a factor of safety of 1.75 has been used. Since no similar reduction in ice pressures seems to have been made (as with the Baltic rules), this high factor of safety may be questioned.

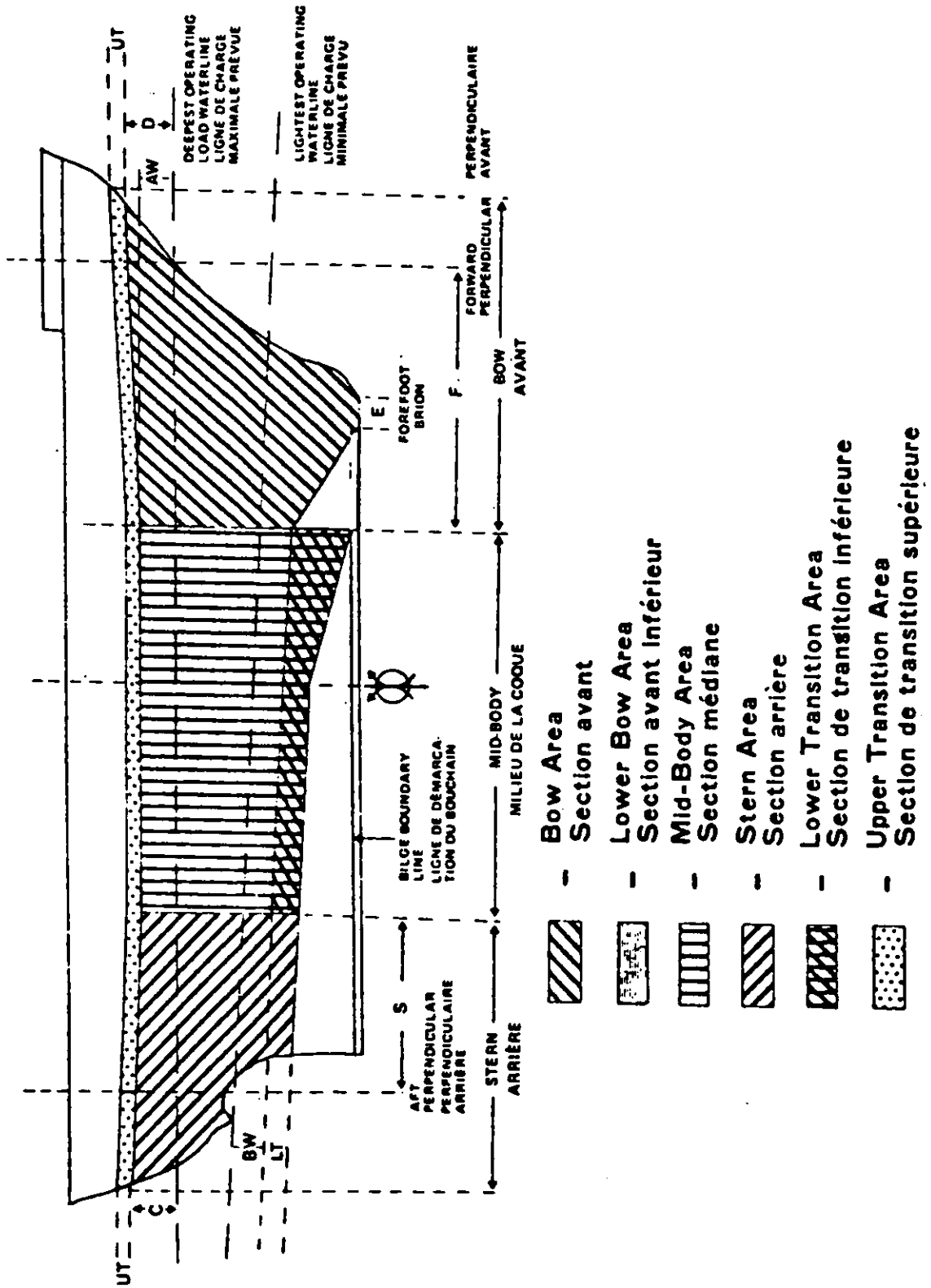


Fig. 6 Canadian ASPPR ice strengthening regions.

As shown in Fig.6, the strengthened areas extend higher above the load waterline and lower than the ballast waterline than in the Baltic rules. This seems quite logical as long as these rules are based on Arctic conditions and intended also for ships and icebreakers traversing continuous level ice and ridges.

4. THE ICE RULES OF USSR REGISTER OF SHIPPING

4.1 Rule Development

The rules of the Russian classification society have since 1968 been based on the work of Popov et al (7), mentioned earlier in connection with general theory on ice loads. Before 1982, the USSR-rules for ships in general contained 6 different ice classes ($Y\lambda$, $Y\lambda$, $\lambda_1, \lambda_2, \lambda_3$ and λ_4) of which the first one applies to icebreakers and the second to semi-icebreakers.

Ice loads were given for classes Y and 1, and were based on the theory that in the bow region (fore part), the ship sustains impact loads from collisions with ice floes. This leads to expressions for loads being functions of hull shape and ship size, thus for the fore part:

$$p = kL \left(1 + \frac{2L}{1000} \right) \alpha^{4/5} u$$

k = constant varying with class and type of structure

L = length of ship

α = angle between centerline and waterline, at $0.1L$ aft of F.P. for plating and $0.2L$ for framing.

u = a function of the vertical slope angle of the frames.

For the rest of the length, the ice pressure was given by:

$$P = L - C_1 \quad \text{for plating}$$

$$P = C_2 L \quad \text{for frames}$$

with the following minimum values (in MPa):

	$Y\lambda$	λ_1
Plating	0.75	0.5
Frames	0.45	0.27

Plate thickness is given by:

$$t = 356 s \sqrt{\frac{p}{\sigma_y}} \quad (\text{mm})$$

Transverse frames by:

$$W = 5ksl \frac{p}{\sigma_y} \cdot 10^3 \quad (\text{cm}^3)$$

$k = 16$ for single-deck ships

$= 13.5$ for multi-deck ships

For the highest ice class ($Y\lambda A$), no specific requirements were given, however, subject to special approval.

For the lower ice classes, the requirements are given directly as percentage increases of the normal ship scantlings.

4.2 The 1982-rules.

New general ice rules were issued in 1982, based upon a revision of number of classes and ice loads.

The number of classes have been reduced to 5 ($\lambda 4$ deleted). A general statement is that the highest class ($Y\lambda A$) is supposed to have icebreaking qualities almost equivalent to icebreakers of the lowest categories. The other four classes are said to correspond to ice classes of other classification societies.

The new ice classes are coupled to certain geographical regions and navigational periods. The strengthening required is said to be related to the operation in Arctic seas north of the USSR, however, also the Baltic Sea.

The ships of ice category YλA are to have the hull configuration of an icebreaker, with specific requirements to stem slope ($\varphi = 20^\circ - 30^\circ$), slope of side forward ($\beta_1 = 40^\circ$) and amidships ($\beta_2 = 8^\circ$) and waterline slope in forebody ($\alpha = 20^\circ - 30^\circ$). The side slope angle amidships of 8° is considered to be a lower limit for ships expected to be subject to side compression in ice. As mentioned earlier, bending collapse of the ice should then occur, and the loads are substantial, however not inadmissible. In this connection, it should be mentioned that a side slope angle larger than 17° is considered necessary to obtain a positive lifting out of the hull.

4.2.1 Ice Loads

As stated earlier, the ice loads are based on the ship impact forces in the ice field and on the hull compression by ice. In the fore part, the impact forces are decisive, and the pressure formulae arrived at are functions of the mass (displacement) of the ship and a form factor depending on waterline slope and vertical frame slope. In the midship and aft regions, both criteria have been introduced.

For plating, the pressure in the forward region is given by:

$$p_f = a_1 \left(a_2 + a_3 \frac{\Delta}{1000} \right) \Delta^{1/6} v \cdot 10^{-2} \quad (\text{MPa})$$

a_1 = factor varying with ice class

a_2 and a_3 = factors depending on the displacement (Δ)

v = form factor given by:

$$v = \left(0.278 + 0.18 \frac{x}{L} \right) \cdot \sqrt[4]{\frac{\alpha^2}{\beta}} \quad \text{for } x/L \leq 0.25$$

$$= \left(0.343 - 0.08 \frac{x}{L} \right) \cdot \sqrt[4]{\frac{\alpha^2}{\beta}} \quad \text{for } x/L > 0.25$$

not to be taken greater than 0.72.

x = distance of hull section from F.P.

α and β = angles defined earlier.

For the 3 highest classes a correction factor for high shaft horse power is also given

$$k = \left(\frac{N_S}{N_R} \right)^{1/6}$$

N_S = actual power

N_R = rule power given.

In the **midship** and **aft** regions the pressures are given by:

$$p_m = p_f \left(a_4 - a_5 \frac{\Delta}{1000} \right)$$

$$p_a = a_6 p_m, \quad \text{max. } 0.75 p_f$$

a_4 to a_6 are again factors depending on ice class and displacement.

For framing, the same formulae as above are to be used for the forward and midship regions, whilst there is also introduced constant pressure values for the midship and aft regions varying from 1.6 to 0.35 MPa for the various ice classes. The latter values are the estimated crushing strength of the ice at low strain rates (plastic body creep) varying with expected ice thickness.

In Table 2, pressure heights have been calculated for the three different displacements.

TABLE 2. Ice Pressures. USSR-Rules.

$\Delta(t)$	Region	Item	p (MPa)				
			$\gamma \lambda A$	$\gamma \lambda$	λ_1	λ_2	λ_3
5000	Forward	Plating	2.92	1.65	1.23	1.00	0.84
		Frames	2.92	1.65	1.23	1.00	0.84
	Midship	Plating	1.82	1.03	0.65	0.43	0.27
		Frames	1.20	0.65	0.60	0.43	0.27
	Aft	Plating	2.19	1.03	0.52	0.27	0.14
		Frames	1.68	0.65	0.48	0.29	0.18
15000	Forward	Plating	4.72	2.67	1.99	1.62	1.36
		Frames	4.72	2.67	1.99	1.62	1.36
	Midship	Plating	2.36	1.33	0.89	0.57	0.34
		Frames	1.20	0.65	0.60	0.45	0.34
	Aft	Plating	3.30	1.33	0.72	0.36	0.17
		Frames	1.68	0.65	0.48	0.29	0.18
45000	Forward	Plating	6.01	3.40	2.53	2.06	1.73
		Frames	6.01	3.40	2.53	2.06	1.73
	Midship	Plating	3.00	1.70	1.14	0.72	0.43
		Frames	1.20	0.65	0.60	0.45	0.35
	Aft	Plating	4.21	1.70	0.91	0.46	0.22
		Frames	1.68	0.65	0.48	0.29	0.18

The vertical distribution of the ice loads is not given for the plating, however formulated for the framing in the forward region:

$$b_f = c_1 u \quad (\text{m})$$

c_1 = constant varying with ice class

$$u = (0.635 + 0.61 \frac{x}{L}) \sqrt{\frac{\alpha}{\beta}} \quad \text{when } \frac{x}{L} \leq 0.25$$

$$= (0.862 - 0.30 \frac{x}{L}) \sqrt{\frac{\alpha}{\beta}} \quad \text{when } \frac{x}{L} > 0.25$$

$$u_{\max} = 0.8$$

We notice that the pressure height here is independent of ship size.

In the **midship** and **aft regions**, the height is given by:

$$b_m = b_a = \frac{3.04}{\beta} (c_2 + c_3 \frac{\Delta}{1000})^{4/3} \text{ for sloped side}$$

$$= c_2 + c_3 \frac{\Delta}{1000} \text{ for straight side}$$

C_2 and C_3 are factors depending on ice class and displacement.

The load height varies between 0.5 and 0.7 metres in the forward region, and between 0.4 and 1.2 metres midships and aft.

4.2.2 Strength Requirements

Plating. Plate thickness is given by the formula (with both transverse frames and longitudinals):

$$t = 18.4s \sqrt{\frac{p}{\sigma_y}} + c$$

Here, p is given in KPa and σ_y in MPa. With both having same units:

$$t = 582s \sqrt{\frac{p}{\sigma_y}} + c \text{ (mm)}$$

$C = 3\text{mm}$ for the three highest classes
 $= 2\text{mm}$ for the rest.

Framing. The section modulus for **transverse framing** is given by:

$$W = k\phi s l b \frac{p}{\sigma_y} \cdot 10^4 \text{ (cm}^3\text{)}$$

$$\phi = (1 - 0.7 \frac{b}{l}) \phi_1$$

ϕ_1 = factor depending on extension of frames.

k = factor depending on end connections.

The section modulus for **longitudinals** is given by:

$$W = 6.5 s l^2 \frac{p}{\sigma_y} \cdot 10^4 \quad (\text{cm}^3)$$

4.2.3 Extension of Ice Belt

In view of a tendency for the broken ice floes to be pushed down by the ship, and thus cause impact forces on the hull rather deep below the lowest waterline, the extension downwards of the ice belt has been increased compared to earlier rules. Values from 0.7 to 1.2 metres below the waterline have been required for the ice classes.

In the fore part, a certain length of the bottom has been included in the ice belt.

5. COMPARISON BETWEEN ICE REGULATIONS

A comprehensive comparison between the various ice regulations in force in 1979 has been made in ref. (5). In the following a short review of the latest rule revisions compared to the older rules will be given, including:

- a) Canadian ASPPR Regulations
- b) USSR Register of Shipping 82-rules
- c) Baltic 71-rules
- d) Proposed revision of Baltic Rules (see Part C2).

In Fig. 7, the ice pressures given for the forward part framing have been plotted on the basis of the K-factor used in the Baltic rules. In addition to the four regulations mentioned, also some points from the USSR Register of Shipping Icebreaker rules have been given, and the pressure applied for the design of the USCG Polar-class icebreakers.

As pointed out, the Baltic rules give ice pressures at the low end of the scale, comparable with the lowest USSR ice classes. In addition, the variation of pressure with

ice class is very small, and for the new Baltic there is no variation at all. As will be shown, variation in scantlings is obtained by differences in ice load heights.

The USSR icebreakers are seen to be designed for the same pressure levels as the Canadian vessels, and the highest USSR ship class (Y Λ A) corresponds to the lowest icebreaker class($\lambda\lambda$ 4).

In Figs. 8 and 9, the plate thicknesses and the transverse frames forward (section modulus) have been plotted, based on a frame spacing $s = 0.4\text{m}$ and a span of $l = 2.5\text{m}$.

As not only the pressures, but also the load heights are decisive for the scantlings, a comparison has been given in the following table:

Regulation	ASPPR	USSR	USSR Icebr.	Baltic 71	New Baltic
Load heights (m)	0.8	0.5-0.8	0.5-1.2	0.8	0.22-0.35

When considering the Baltic rules in relation to the USSR rules, the question arises whether the scantlings variations of the former in fact are too small, and why maintain 4 classes. This will be further discussed in Part C. As will be seen, a small increase in frame scantlings have been proposed in the new rules.

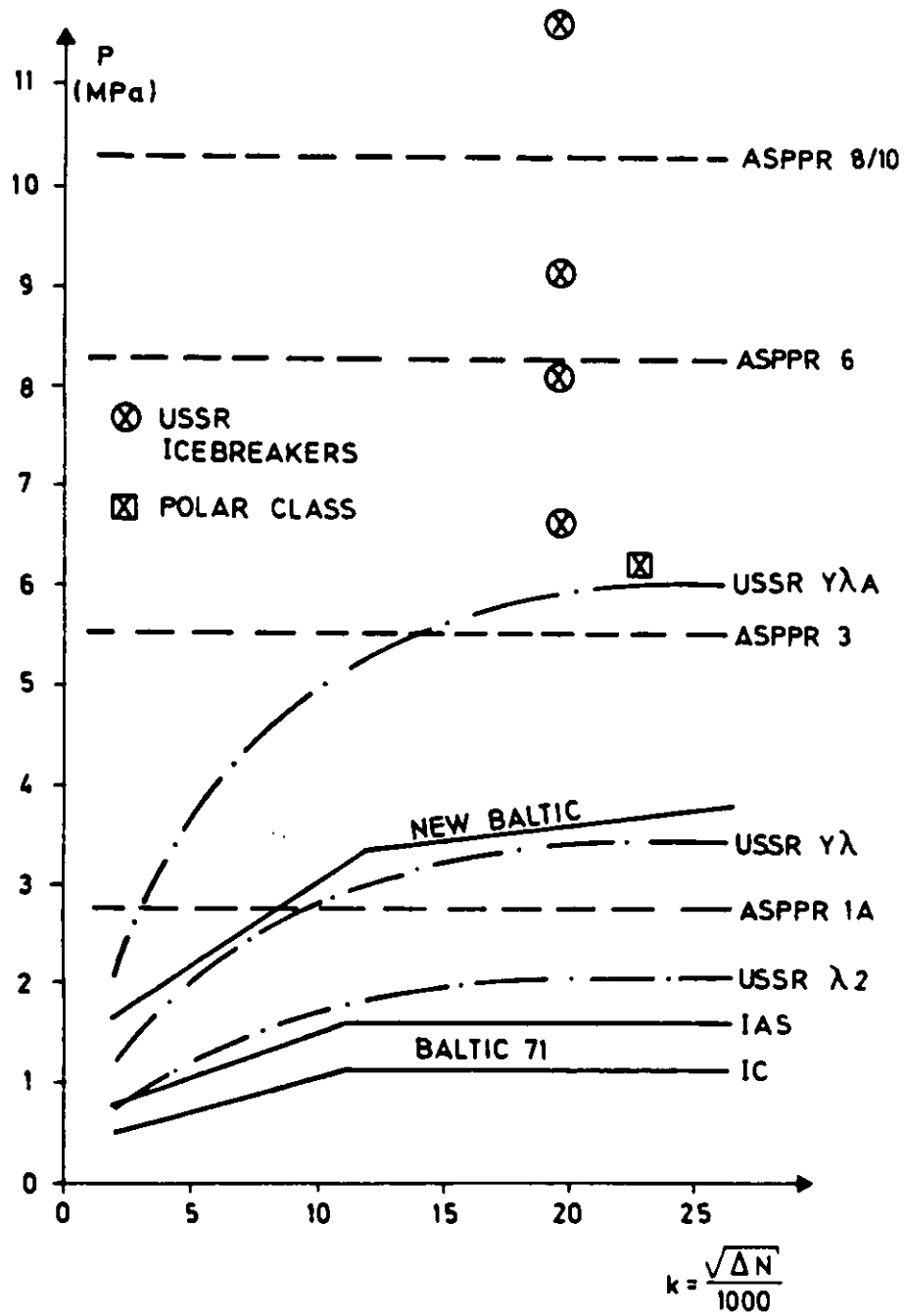


Fig. 7 Comparison of ice pressure forward.

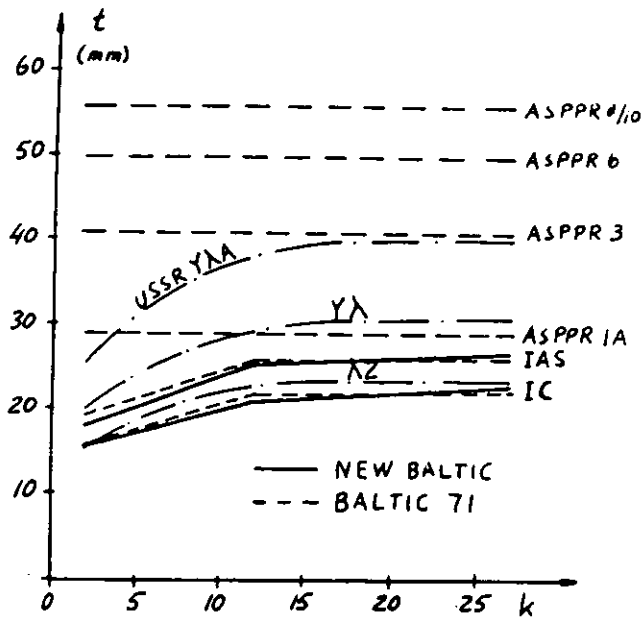


Fig. 8. Comparison of plate thickness forward.

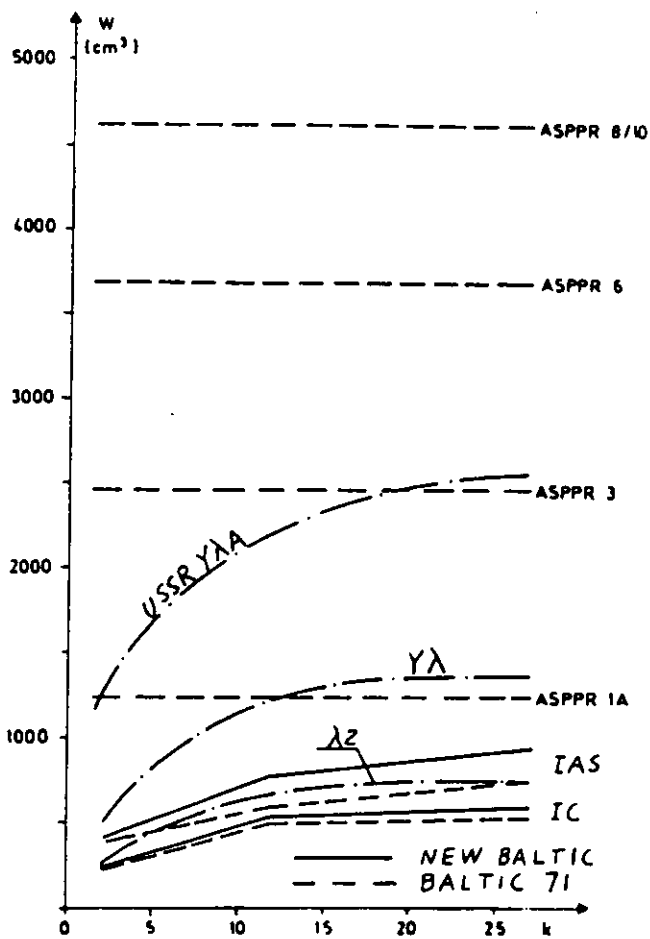


Fig. 9. Comparison of frame section modulus forward.

C. **FUTURE TRENDS IN STRENGTH REQUIREMENTS**

1. **GENERAL**

From the review of ice strength rule development given in Part B, and the comparison between some of the most important requirements, it is quite clear that there is a great difference between the strength levels for:

- a) Ships for one-year ice versus multi-year ice
(Baltic - Arctic/Antarctic)
- b) Merchant ships being assisted by icebreakers versus ships built for breaking of ice.

Further rule development will take these differences into account. Considering that the Baltic Sea and the St. Lawrence river area will also be important waters for general shipping traffic in the future, special rules for these areas will be of great interest for the classification societies. A revision of existing rules has thus been supported as described in the succeeding section.

The increasing importance of Arctic and also Antarctic ship traffic in connection with oil and gas exploitation should encourage the classification societies to reconsider their rules for Arctic vessels and icebreakers. Experience with present regulations and the outcome of research going on in the fields of ice conditions, ice properties and loads, interaction between ship and ice and the structural response criteria will create the background for improved requirements.

2. **FINNISH/SWEDISH RULES**

2.1 Introduction

Based upon nearly 10 years experience with the 1971 Baltic Rules, the Finnish/Swedish authorities in 1979

decided to initiate work in amending and modernizing the rules. Some of the classification societies were invited to participate in the revision work, principally those with a certain number of ships with Baltic Ice Class Notations. Also, an initial contact was made with the USSR Register of Shipping and the Canadian Authorities. Two working groups were established, one for hull and one for machinery and propellers. In addition to representatives from the Finnish and Swedish authorities, experts from Germanischer Lloyd, Lloyds Register of Shipping, Bureau Veritas and Det norske Veritas have participated in the work.

The number of ice classes were discussed initially, and the need for both the lower classes was questioned. A distribution of ice class certificates issued in Finland during the winter of 78-79 (see Table 3), shows that, while class IA is by far the most popular class, there are also many ships in the two lower classes. Thus, it was concluded that all four classes should be maintained.

TABLE 3.

Ice Class	IAS	IA	IB	IC	Total
No.of Cert.	48	369	121	157	695
Per cent	6.9	53.1	17.4	22.6	

For the hull structure, the ultimate goal was to establish a new set of rules based upon the experience and noted shortcomings, basing the general requirements on parts of the design philosophy discussed in Part A. As the overall strength of the Baltic service fleet was considered satisfactory, it was the intention of the work not to make significant alterations in the scantlings, other than what would be the result of applying a system of rational design concepts to all structures on the same basis.

2.2 Ice Loads

The basis for the ice load presentation will be a distributed pressure over a certain length, however, taking into account the redistribution of load discussed in A 1.4. Due to the deflection of the plating relative to stiffeners and girders, the ice load will concentrate on the frames and the other stiff structures. As outlined in Part A, the local pressure may be well in excess of the normal uniaxial crushing strength, and values according to the multiaxial or confined stress field concept discussed in A 1.2 may be reached. Full-scale measurements referred to in ref. (9) and (14) performed by the Technical Research Centre of Finland (VTT), confirm this theory. Thus, the principle load distribution for the plate/frame combination can be presented by the pressure curve shown in fig.10.

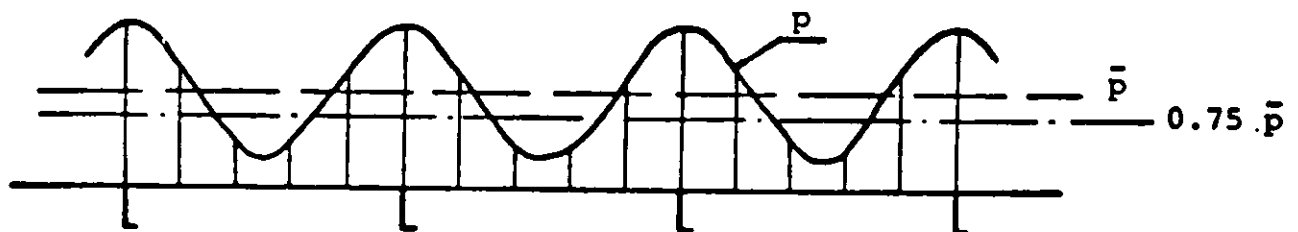


Fig. 10 Ice load distribution.

For the framing, the design pressure will be taken as the mean value \bar{p} of the load curve, and for the plating, a value estimated to be $0.75 \bar{p}$.

Furthermore, the full-scale measurements referred to have shown that the real ice loading acting on the ship's side is concentrated in a narrower band than the nominal ice thickness. For the four ice classes, nominal ice thicknesses (h_0) are chosen, and the ships are assumed to operate in level ice conditions corresponding to this. The actual load height (h) is assumed to be a fraction of the ice thickness, as given in Table 4.

TABLE 4.

Ice Class	Nominal ice thickness h_0 (m)	Height of load area h (m)
IAS	1.0	0.35
IA	0.8	0.30
IB	0.6	0.25
IC	0.4	0.22

It should be noted, however, that ships according to the ice regulations are assumed to be assisted by and operate under instructions from icebreakers in difficult conditions. Thus, the ships are not expected to withstand the load produced by heavy ice jamming when ice thickness is approaching h_0 .

The design pressure which will be defined in the new rules is based on some of the same parameters that govern the present requirements. Thus the displacement of the ship and the engine power have been kept in a factor $k = f(\Delta N)$. As before, 3 regions along the length of the ship will be defined, with varying ice pressures. Finally, there will be a certain variation of ice loads between the ice classes, not only due to the variation in load height given in Table 4, but also in the pressure itself.

The design ice pressure is given by the formula:

$$p = c_d c_1 c_a p_0 \quad (\text{MPa}) \quad (7)$$

where

$$c_d = \frac{ak + b}{1000} \quad , \quad k = \frac{\sqrt{\Delta N}}{1000}$$

Δ = displacement of ship (t)

N = engine power (KW)

a and b are factors given in Table 5.

TABLE 5.

Factor	Location of the load area			
	Fore part		Midship and after part	
	$k \leq 12$	$k > 12$	$k \leq 12$	$k > 12$
a	30	6	8	2
b	230	518	214	286

c_1 = a factor accounting for the probability that a certain ice pressure occurs in the different regions of the different ice classes, given in Table 6.

TABLE 6.

Ice Class	Fore part	Midship	After part
IAS	1.00	1.00	0.75
IA	1.00	0.85	0.65
IB	1.00	0.70	0.45
IC	1.00	0.50	0.25

c_a = a factor expressing the probability that the length of a certain load area will have full pressure, given by

$$c_a = \frac{47 - 5 l_a}{44}, \text{ max. } 1.0, \text{ min. } 0.5$$

l_a = length of load area in metres, to be taken as follows:

Structure	Type of framing	l_a (m)
Shell and frames	Transverse	Frame spacing
	Longitudinal	Span of long.
Stringers		Span of stringers
Web frames		Spacing of web frames

P_0 = nominal ice pressure = 5.6 MPa.
This is regarded to be a moderate value for the uniaxial crushing strength of first year ice (see Part A 1.2) at transition zone strain rates.

TABLE 7. Ice Pressures. New Baltic Rules.

$\Delta(t)$	Region	Item	p (MPa)			
			IAS	IA	IB	IC
5000	Forward	Plating	1.41	1.41	1.41	1.41
		Framing	1.88	1.88	1.88	1.88
	Midship	Plating	1.02	0.87	0.71	0.51
		Framing	1.36	1.16	0.95	0.68
	Aft	Plating	0.76	0.66	0.46	0.26
		Framing	1.02	0.88	0.61	0.34
15000	Forward	Plating	2.06	2.06	2.06	2.06
		Framing	2.75	2.75	2.75	2.75
	Midship	Plating	1.18	1.00	0.83	0.59
		Framing	1.58	1.34	1.11	0.79
	Aft	Plating	0.89	0.77	0.53	0.30
		Framing	1.19	1.03	0.71	0.40
45000	Forward	Plating	2.80	2.80	2.80	2.80
		Framing	3.73	3.73	3.73	3.73
	Midship	Plating	1.41	1.20	0.99	0.70
		Framing	1.88	1.60	1.32	0.94
	Aft	Plating	1.06	0.91	0.64	0.35
		Framing	1.41	1.22	0.85	0.47

In Table 7, the ice pressures are given for the various ice classes in the three regions, for plating (with transverse frames) and frames. The displacements are the same as used in Table 2, and with the engine powers 2500, 5000 and 13500 KW respectively.

2.3 Structural Response

2.3.1 General.

In contrast to the plastic design model chosen as a basis for the earlier ice regulations (see Part B 2.2.2), the new rules will be based on elastic response, both for plating and stiffeners. This might be regarded as a step back by some, however, found more convenient in cases where girder systems subject to ice loads would have to be checked by computer program calculations, normally based on elastic theory.

2.3.2 Plating.

For a plate strip between transverse frames, uniformly loaded, the maximum bending moment is given by:

$$M_e = \frac{pbs^2}{m}$$

With section modulus: $W_e = \frac{bt^2}{6}$ we normally get,
with yielding as limit:

$$t = 2448s \sqrt{\frac{p}{\sigma_y m}} \quad (8)$$

m = coefficient of end fixation

= 12 with fixed ends

s = frame spacing in m.

With the limited height of the load area, we know that there will be a certain redistribution of loads to the neighbouring plating. In the requirements for wheel loaded decks in the rules of Det norske Veritas, a general formula has been given applicable to ice loading. The distribution factor is given by:

$$f_1 = 1.3 - \frac{4.2}{\left(\frac{h}{s} + 1.8\right)^2}, \quad \text{max. } 1.0$$

In addition, an aspect ratio factor may be introduced:

$$f_a = 1.1 - 0.25 s/l$$

This factor is max. 1.0 when $s/l \leq 0.4$. Normally this will be the case for transverse frames.

When the length of ice pressure area is equal to s , the factor m becomes 13.6, and the final formula for plate thickness, with transverse frames, is:

$$t = 667s \sqrt{\frac{f_1 P_p}{\sigma_y}} + t_c \quad (\text{mm})$$

$P_p = 0.75 p$, when p = pressure on frames given in eq. (7).

t_c = corrosion and abrasion addition
 = 2 mm for ice class IA Super and IA
 = 1 mm for ice class IB and IC.

With longitudinal frames the factor f_1 becomes 1.0, and the plate thickness is given from eq. (8):

$$t = 667s \sqrt{\frac{P_1}{f_2 \sigma_y}} + t_c \quad (\text{mm})$$

f_2 = factor expressing the variation of coefficient m with the ratio $\frac{h}{s}$.

$$f_2 = 0.6 + 0.4 \frac{s}{h} \quad \text{for } \frac{h}{s} \leq 1$$

$$= 1.4 - 0.4 \frac{h}{s} \quad \text{for } 1 < \frac{h}{s} < 1.8$$

The magnitude of pressure p_1 to be inserted in this formula is still subject to discussion. As mentioned in B 2.2.2, Johansson (12) increased the pressure for longitudinally stiffened plating, and a finite element calculation performed by Lloyd's Register indicates an increase in stress for long plate panels. It would seem correct to introduce a factor in front of p giving:

$$P_1 = (1.1 - 0.35 \frac{s}{l}) p, \text{ max. } p$$

2.3.3 Framing.

The structural model for transverse frames is as given in Fig. 11.

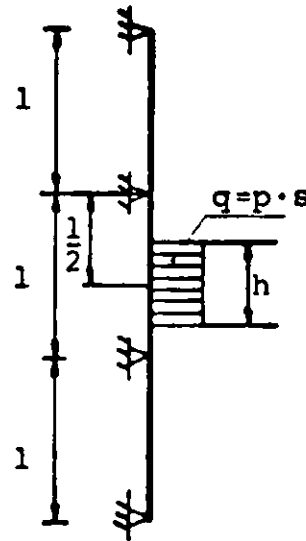


Fig. 11 Structural model of transverse frames.

The maximum elastic bending moment for this ideal case at midpoint of span is:

$$M = \frac{p h s l}{m_t} \quad (9)$$

where

$$m_t = \frac{40}{7 - 5 \left(\frac{h}{l}\right) + \left(\frac{h}{l}\right)^2}$$

The ratio h/l is normally small (< 0.3) and the square term may be deleted. Thus, m_t may be written more generally:

$$m_t = \frac{7 \cdot m_o}{7 - 5 \left(\frac{h}{l}\right)}$$

m_o is then a factor depending on the end fixations of the frame, for the case with a point load at mid span. For the case given in Fig. 11, $m_o = 5.7$.

The usual design method for merchant ships with ice strengthening is to apply ordinary main frames and fit intermediate frames in between. The end fixations of main frames and intermediate frames may be different, and the working group has made a special study of this problem. A finite element analysis was carried out,

see ref. (15), on a 3-dimensional model of a typical cargo vessel covering 3 main frames and 4 intermediate frames between web frames. A typical load case 1, with continuous load strip on upper span ($h = 0.2$ m), is shown in Fig. 12. Other load conditions were shorter loads (equal to 1 and 2 times frame spacing) in both upper and lower span, illustrated by load case 8 in Fig. 12. In Table 8, some of the results are given, showing fixation factor m_o .

In order to arrive at a simplified expression for the bending moment, the following reasoning has been made, based on the results of the investigation. For a point load on a simple beam, the m_o -factor will vary between 4 (free-free) and 8 (fixed ends). Normally, main frames will have boundary conditions between these values. Some examples are:

Side frame in bulk carrier, fixed at hopper tank, free at deck: $m \approx 5.2$

Same frame considered partly fixed in top wing tank:
 $m \approx 6.5$

Side frame in cargo vessel with several decks, lower hold: $m \approx 5.5$

Side frame in cargo vessel with tween deck:
 $m \approx 5.8$

Double side with stringers:
 $m \approx 7.0$

All these m -values are valid for one separate frame, i.e. no load distribution from or to other frames.

Now from the GL-report, we learn that a redistribution of loads takes place, from the frames with smaller constraint to the frames with bigger. This generally leads to a leveling out of the bending moments. In case of short ice loads (load cases 3 to 5 in the report), we also get a reduction in bending moment due to load transfer to unloaded frames.

With long ice loads (load case 1), the normally stiffer main frames will take a bigger share of the load and endure higher bending moments as shown in Table 8. The bending moment in the main frame becomes higher, the smaller degree of fixation the intermediate frame has.

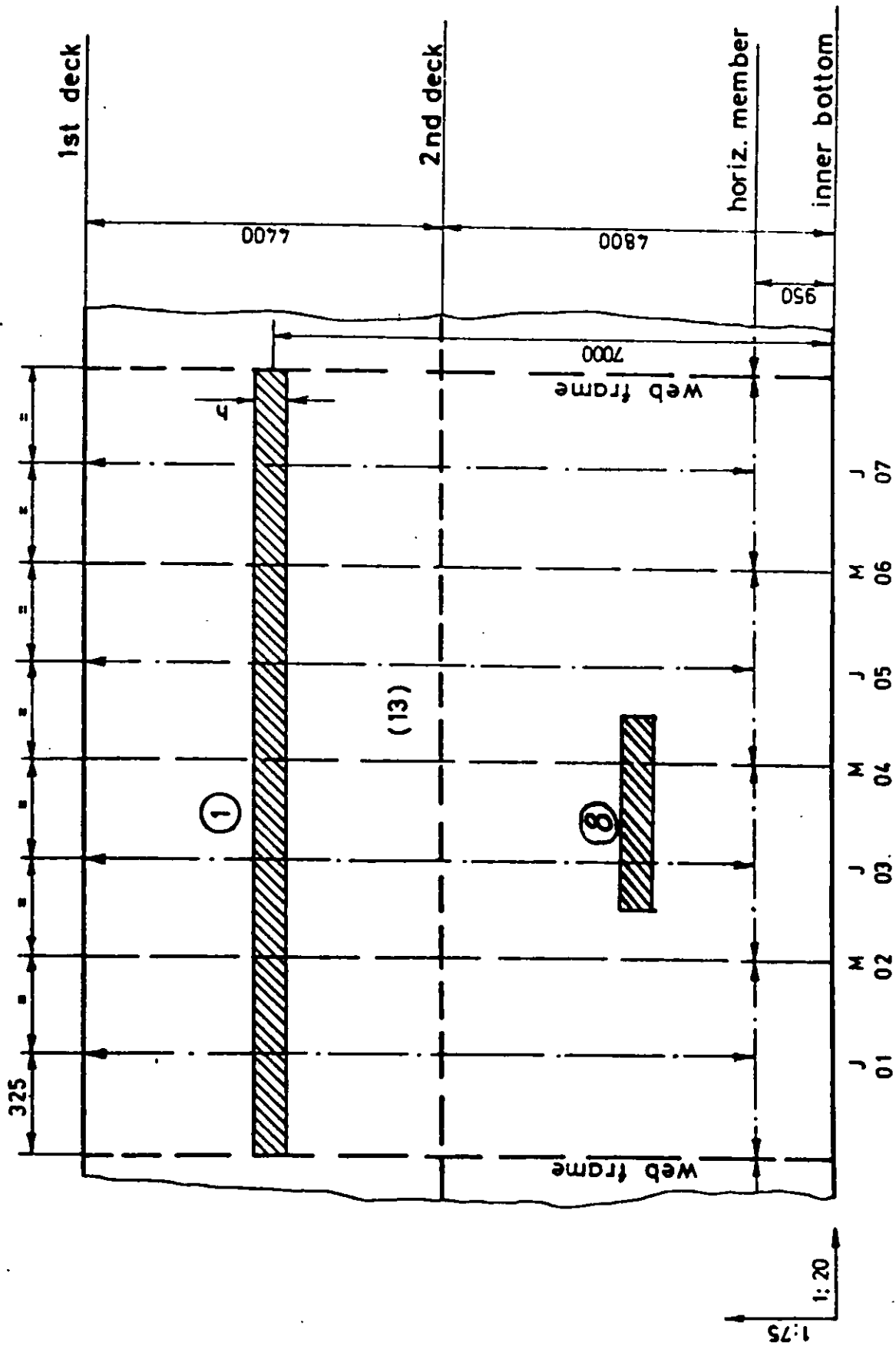


Fig. 12 Typical load cases.

From this it is logical to assume that a main frame will take a bigger share of the load from the intermediate frame, the higher degree of fixation the main frame has. Thus, a main frame with a high degree of fixation, and initially having a smaller bending moment, will experience a bigger increase in bending moment than a main frame with small degree of fixation and initially having a higher bending moment. Thus, a leveling out of the resulting bending moment in the main frames of different fixations will take place.

TABLE 8.

Boundary condition	Load case	Frame no.	Frame type	m
As built	LC1. Continuous along model	02	main	5.72
		03	intermediate	6.60
		04	main	5.44
		05	intermediate	6.60
		06	main	5.72
	LC3.One frame	04	main	10.59
	LC4.One frame	03	intermediate	11.44
	LC5. Two frames	04	main	7.22
Interm. frames released at 2.deck	LC1. Continuous along model	02	main	5.17
		03	intermediate	6.60
		04	main	4.74
		05	intermediate	6.60
		06	main	5.17

For normal types of main frames, which may be considered to be at least partially constrained at each end, m_o -values have been given in Table 9. Corresponding values for intermediate frames are also given, both as a function of the boundary condition of the intermediate frame.

TABLE 9.

Boundary condition of intermediate frame	m_o	
	Main frame	Interm. frame
Free-free	4.7	6.5
Continuous	5.2	6.5
Free-fix	5.4	6.5
Fix-fix	7.0	7.0

The m_o -values given are based on a long pressure strip covering several frames. For short load areas we have seen that there is a reduction in moments due to load distribution to adjacent frames. In section 2.2 it was stated that the load length l_a for transverse frames is to be taken equal to one frame spacing, giving a c_d -factor of approximately 1.0.

In this case the moments should be reduced, and bigger m_o -values used. On the other hand, we have seen in Part A 1.2, that the ice pressure at very small aspect ratios (see fig. 3) increases above the linear tendency of factor c_d . To take care of this increase at short load lengths, it has been decided that the short load should be combined with m_o -values corresponding to the longer load areas. It is felt that this solution should be reconsidered. Maybe a c_d -variation in line with fig.3 should be given, and corresponding m_o -values worked out. Maximum values of the c_d/m_o -ratio would then give the requirement to transverse frames.

The existing proposal is, however, that the section modulus for both main frames and intermediate frames will be given by the expression:

$$W = \frac{pshl}{m_t \sigma_y} 10^6 \quad (\text{cm}^3)$$

$$m_t = \frac{7 m_o}{7 - 5 \frac{h}{l}}$$

and with the following mean m_o -values:

Boundary condition of intermediate frame	Fix-Fix	Fix-Free	Continuous	Free-free
m_o	7	6	5.7	5

For single-deck ships as bulk carriers, $m_o=7$ should be used. For ships with tween-decks and/or ice stringers, $m_o=5.7$ would be normally applicable.

For longitudinal frames, the load distribution has previously been considered as a uniform ice load along the frame, with a certain redistribution through the plating to adjacent frames. Considering, however, that the longitudinal frame subject to ice pressure will be a more flexible structure than the web frames supporting the longitudinal, the same redistribution of load as shown for plating in Fig.10 may be expected to take place.

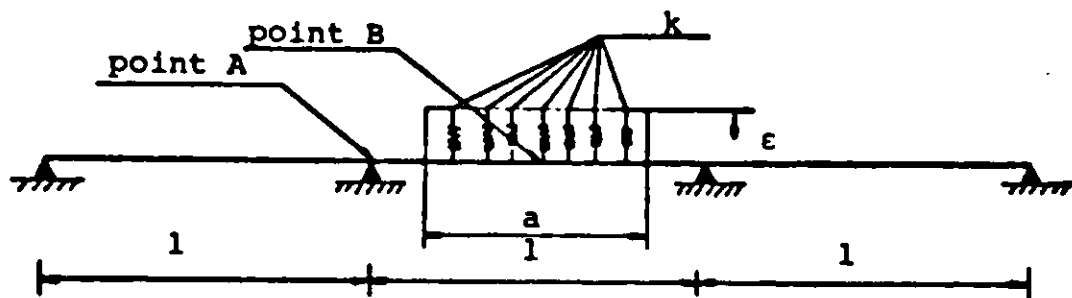


Fig. 13 Structural model of longitudinal.

This problem has been investigated by the Technical Research Centre of Finland (VTT). On a model as shown in Fig.13, the ice load was simulated by a number of springs (20), where the spring constant was given by:

$$k = 1.7 \cdot 10^{10} A_L \quad (\text{N/m})$$

based on the assumption that the ice load from an ice wedge is given by:

$$F = kx = 1.7 \cdot 10^{10} A_L x \text{ (N/m}^2\text{)}$$

$$A_L = \text{contact area} = h \cdot \Delta l$$

$$\Delta l = \text{distance between springs}$$

$$x = \text{displacement of load area}$$

Calculations were made for typical frame cross sections and for various lengths of load contact (a) from 0.08 l to 1.0 l. The maximum bending moment was found to be at point B (see Fig.13) for a load length $a=0.5 l$. The bending moment was then about 55% of the bending moment corresponding to a uniformly distributed ice load on the whole span. Thus it was decided to introduce a reduction factor of 0.6 in the formula for longitudinal frames.

The section modulus for longitudinals is given by:

$$W = \frac{f_3 f_y p s l^2}{m_1 \sigma_y} 10^6 \text{ (cm}^3\text{)}$$

$$f_3 = (1 - 0.2 \frac{h}{s}) \frac{h}{s} \text{ (redistribution to adjacent longitudinals)}$$

$$f_y = 0.6 \text{ (longitudinal redistribution)}$$

$$m_1 = \text{boundary factor}$$

$$= 13.3 \text{ for continuous longitudinal}$$

For both types of frames, it is very important that the connection area to stringers and web frames is able to carry the total ice load on the frame.

Minimum area is given by:

For transverse frames:

$$a_{ct} = \frac{\sqrt{3} p s h}{\sigma_y} 10^4 \text{ (cm}^2\text{)}$$

For longitudinal frames:

$$a_{cl} = \frac{\sqrt{3} f_3 p s l}{\sigma_y} 10^4 \text{ (cm}^2\text{)}$$

The necessary sectional area of the frames would be half of the areas given above.

Also for ice stringers supporting transverse frames, a special investigation has been made by the Technical Research Centre of Finland (VTT). In the continuous beam model shown in Fig. 14, the frames are represented by springs, and the spring constants are obtained by the model shown in Fig. 15.

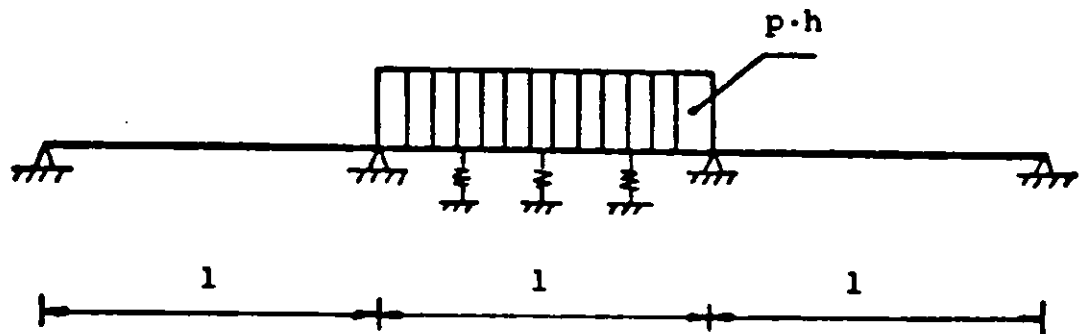


Fig. 14 Model of stringer.

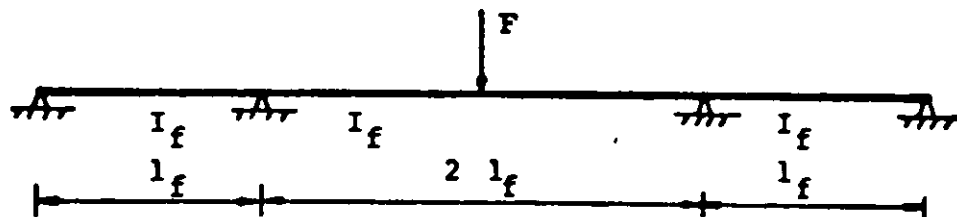


Fig. 15 Model of transverse frame.

The maximum bending moment and shear force in the stringer were calculated with the springs fitted, and for comparison also without springs. The results show that both bending moment and shear force are reduced by about 12 per cent, due to the load carried by the frames.

Requirements to section modulus and cross-sectioned area are thus given by:

$$W_s = \frac{f_5 p h l^2}{m_s \sigma_y} 10^6 \quad (\text{cm}^3)$$

$$A_s = \frac{\sqrt{3} f_6 p h l}{2 \sigma_y} 10^4 \quad (\text{cm}^2)$$

m_s = boundary factor
 $= 13.3$ for continuous stringer
 $f_5 = f_6 = 0.88$ for normal designs.

More exact formulae will be given as an alternative.

In addition, approximate formulae for web frames supporting stringers or longitudinals will also be given.

2.4 Ice Belt and Ice Draughts.

As to the vertical extension of the ice belt, it has been proposed to increase the downward distance below ballast waterline for the higher classes. In addition, the bottom forward in class IAS will have increased thickness.

For ships with high speed, ice damages have been experienced in some cases in the forward part above the normal ice belt. High speed ($v > 18$ kn) in combination with bulbous bow seem to be of special importance. Based on this, it has been decided to require a local extension of the plating and ice framing in the fore part, somewhere between 1 and 2 metres above the normal ice belt for such ships.

In the present Baltic rules, the maximum ice draught has been related to the summer load waterline (ships with length above 100 metres), considering the Baltic Sea as a salt water ocean. In view of the rather low salinity of the water, there has been much discussion about actual waterline, overloading and greater possibility for ice damages above the ice belt. On this background, it has been decided to propose basing the new rules on the fresh water summer load line, giving the normal maximum draught. For ships with timber load line, this should be applied.

Finally, a special ice draught marking on the ship's side will be proposed, enabling the ice class certificate surveyors to easily check that the ship is not overloaded. This would also give the designer and shipowner more flexibility in choosing a special ice load line, for instance limited by a deficiency in installed engine power.

3. ARCTIC RULES DEVELOPMENT

As mentioned in section 1, the classification societies are expected to be interested in a further development of their Arctic and icebreaker rules. Some short remarks on possible design principles will be given.

3.1 Ice Loads

For ships intended to operate in ice-infested waters without assistance from icebreakers, the loads will have to be significantly increased above the load level of the Baltic rules, as shown from the Canadian and USSR rules.

Special hull form parameters are to be given:

- The stern line angle with the vertical
- Angle between longitudinal axis and waterline forward and at the forward shoulder
- The slope of the side to the vertical forward and in the midship region.

3.1.1 Impact Loads.

As mentioned in Part A, the smaller impact loads between ship and ice floes being the basis for the Baltic ice strengthening will be exceeded by the much higher pressures due to ramming and turning in continuous level ice, for icebreakers also in ridges.

In the bow area, consideration should be given to consecutive rams, and the impact loads will be functions of:

- displacement of vessel
- operational speed in ice
- the hull form parameters in the bow area
- crushing strength of ice.

For the rest of the ship, impact forces from sideways contact should be evaluated, considering the various failure modes of level ice and ridges mentioned in Part A and discussed in, for instance ref.(2). The load parameters will be the same as mentioned above, the shear and flexural strength of the ice will have to be added.

3.1.2 Sideways compression.

As discussed earlier, these loads are especially important in the midship region, where the side slope angle is the main parameter. With $\beta < 8-10^\circ$, direct crushing of the ice will take place, and the forces will be very high. Thus, angles above these values are recommended, giving pressures below the confined crushing strength in the creep zone (0.5 - 1.5 MPa).

3.1.3 Local loads.

The local loads used to calculate scantlings of plating and stiffeners are to be estimated on the basis of the global loads given in items 1 and 2, defining relevant load lengths in each case.

3.2 Longitudinal Strength

The vertical and horizontal bending moments and shear forces on the hull girder due to the calculated impact forces, of which the bow impacts are the most important, are to be estimated.

Hull girder vibrations due to the impact forces should be taken into consideration by estimating relevant dynamic load factors.

3.3 Scantlings

Calculation of scantlings based on the above loads may be performed according to some of the methods discussed in Part A.

In view of the high pressures and large loads, more refined methods will have to be considered in the future. Both stiffeners and more complicated framing structures should be subject to complete structural analysis, evaluating all design factors involved and applying the criteria of partial load factors and limit response factors.

Finally, the fatigue problem should not be forgotten. The dynamic nature of the ice loads, especially in connection with ice breaking, will impose cyclic stress patterns. Thus, the fatigue properties of the steels and the local design details should be considered.

REFERENCES

- (1) Riska, K.: "On the Role of Failure Criterion of Ice in Determining Ice Loads." Technical Research Centre of Finland (VTT), Ship Laboratory Report 7, March 1980.
- (2) Hysing, Th.: "Marine Structures and Ships in Ice." Norwegian Maritime Research, No.2, 1981, p.13.
- (3) Coburn, J.L.: "A Rational Basis for Hull Ice-Strengthening Criteria." SNAME, STAR Symposium, Paper No.10, Ottawa, June 1981.
- (4) Ralston, T.D.: "An Analysis of Ice Sheet Indentation." IAHR-78, University of Luleå, Sweden.
- (5) Coburn, J.L. et al: "A Rational Basis for the Selection of Ice-Strengthening Criteria for Ships." SSC-309, Washington 1981.
- (6) Major, R.A. et al: "A Model to Predict Hull-Ice Impact Loads in the St. Lawrence." SNAME Ice Tech. Symposium, Montreal, April 1975.
- (7) Popov, Y.N. et al: "Strength of Ships Navigating in Ice" and "Durability of Ships Designed for Ice Passage." (Translation) Sudostroenie, Leningrad 1967/68.
- (8) Janzén, St.: "Critical Review of Ice Rules, also related to Arctic Traffic." (In Swedish) NSTM 79, Helsinki.
- (9) Vuorio, J. et al: "Long Term Measurements of Ice Pressure and Ice-Induced Stresses on the Icebreaker Sisu in Winter 1978." Winter Navigation Research Board Rep.No.28. Helsinki and Stockholm, April 1979.
- (10) "Arctic Waters Pollution Prevention Act." Canada Gazette, Part II, Vol.106, No.20, October 1972.
- (11) Siivonen, O.: "The Development of Finnish Ice Class Rules." Ice, Ships and Winter Navigation, Symposium Oulu University 1977, p.154.

References (cont.)

- (12) Johansson, B.M.: "On the Strengthening of Ship Hulls."
International Shipbuilding Progress,
Vol.14, June 1967, p.231.
- (13) Böckenhauer, M.: "Comments to the Revised Rules for
Ice Strengthening of Germanischer Lloyd."
(In German) Hansa, Vol.106, No.3,
1971, p.259.
- (14) Varsta, P.: "Measurements and Analysis of Ice-Induced
Stresses on the Shell of an Icebreaker."
Winter Navigation Board, Research Rep.21.
Helsinki and Stockholm 1977.
- (15) Böckenhauer, M. et al: "Updating of Ice Class Rules.
Transverse Frames under Ice Pressure."
Germanischer Lloyd, STB Report No.978/81.



WEGEMT - COURSE "STRUCTURES AND SHIPS IN ICE"

P. Varsta
Acting Professor
HUT, Finland

K. Riska
Research Scientist
Technical Research Centre of Finland
Ship Laboratory

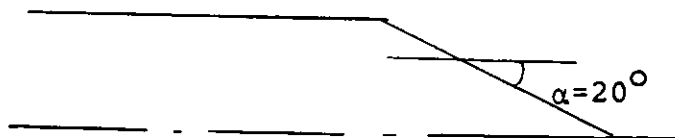
CASE STUDY - ICE LOADS

An ice-going merchant vessel for arctic is studied in this case study. The dimensions of the ship are assumed to be the following

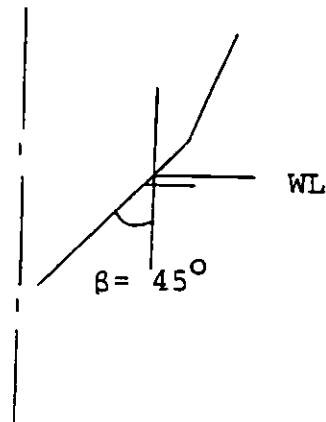
L = 170 m
B = 25 m
T = 10 m
 $C_B = 0,60$
 $v_s = 10$ knots

The bow lines are simplified and consist of plane surfaces:

Water lines



Bow frames



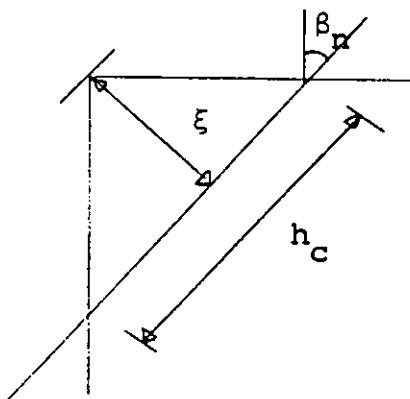
1. Determine the ice pressure and the contact area in impact at bow with an ice floe of infinite mass and horizontal diameter 50 m. Ice temperature is -10°C .

The following formulas can be used in the work (refs.: /1/ Popov & al.: Strength of ships sailing in ice, /2/ Varsta, P. & Riska, K., Structural ice loads in the Baltic).

Ice pressure $p_{av} = p_{max} \cdot k_f \cdot k_l$ assume $k_f = 0.75$
 $k_l = 0.80$

See Fig. 7 in /2/.

Contact geometry /1/:



$$A_c = l_c h_c$$

A_c contact area
 h_c contact height
 l_c contact length
 R radius of ice floe

$$A_c = C_A \xi^a, \quad C_A = \frac{4}{3} \frac{\sqrt{2R}}{\cos^{3/2} \beta_n \sin \beta_n}$$

$$a = \frac{3}{2}$$

$$\xi_{max} = \left(\frac{5}{4} \frac{M_N v_n^2}{p_{av} C_A} \right)^{\frac{2}{3}}$$

$$M_N = \frac{M_S}{C'}, \text{ reduced mass of ship,}$$

$$C' = 2.0$$

$$l_c = \frac{5}{3} \sqrt{\frac{2R\xi_{\max}}{\cos\beta_n}}$$

v_n normal speed
 β frame angle
 α water line angle

$$v_n = v_s \frac{\sin\alpha \cos\beta}{\sqrt{1 - \sin^2\alpha \sin^2\beta}}$$

$$\beta_n = \frac{\pi}{2} - \arccos \left(\frac{\cos\alpha \sin\beta}{\sqrt{1 - \sin^2\alpha \sin^2\beta}} \right)$$

2. Determine the scantlings of shell plating and transverse frames in the impact assuming frame spacing $s = 0.4$ m and frame span $L = 4$ m.

Use the following assumptions and formulae

Plating

Ice pressure $p_{PL} = k_f \cdot k_l \cdot k_{PL} p_{\max}$, assume $k_{PL} = 0.8$

$$t = \frac{77.4 k_a \sqrt{k_w C \cdot s p_{PL}}}{\sqrt{m \cdot \sigma_y}}$$

[t] = mm

[p_{PL}] = kN/m²

[σ_y] = MPa

[s] = m

$$k_a = 1.1 - 0.25 \frac{s}{L} \quad \text{max 1.0 for } \frac{s}{L} = 0.4$$

$$k_w = 1.3 - \frac{4.2}{\left(\frac{C}{s} + 1.8\right)^2} \quad \text{max 1.0 for } a \geq 1.94 s$$

$$C = \begin{cases} l_c & \text{for } l_c < s \\ s & \text{for } l_c > s \end{cases}$$

$$m = \frac{38}{\left(\frac{k}{s}\right)^2 - 4.7 \frac{1}{s} + 6.4} \quad \text{for } \frac{1}{s} \leq 1.0$$

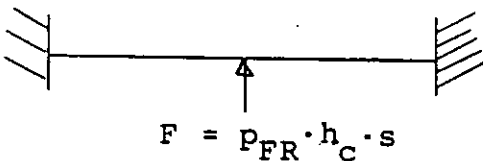
$$= \frac{87}{\left(\frac{1}{s}\right)^2 \left(\left(\frac{1}{s}\right)^2 - 6.3 \frac{1}{s} + 10.9\right)} \quad \text{for } 1.2 \leq \frac{1}{s} \leq 2.5$$

$$= 12 \quad \text{for } \frac{1}{s} \geq 3.5$$

$$\sigma_Y = 240 \text{ N/mm}^2$$

Frames

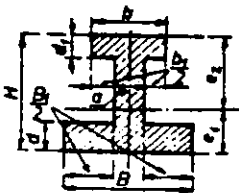
Assume the following situation



$$W = \frac{M_{\max}}{\sigma_Y} = \frac{F \cdot L}{8 \sigma_Y}$$

Ice pressure $p_{FR} = k_f \cdot k_1 \cdot p_{\max}$

The frame is a T-profile for which the following formulas are valid



$$I_x = \frac{1}{12} (B e_1^3 - B_1 h^3 + b e_2^3 - b_1 h_1^3)$$

$$e_1 = \frac{a H^2 + B_1 d^2 + b_1 d_1 (2H - d_1)}{2(aH + B_1 d + b_1 d_1)}$$

$$e_2 = H - e_1$$



Modeling Techniques in Various Ice Model Basins

by Joachim Schwarz

History

Ever since the 1950's engineers and scientists have been attempting to use model tests in ice to predict the corresponding full scale phenomena. The first ice model basin was built in 1955 at the Arctic and Antarctic Research Institute in Leningrad. This 13,4 m x 1,85 m x 1,3 m size basin is still in operation and many good results, as for example, the icebreaking concept of the 75.000 HP icebreaker ARKTIKA have been produced there.

A major motive for simulating icebreaking phenomena in model tests was the discovery of oil, gas and other resources in the Arctic in the 1960's which led to the MANHATTAN ice voyages in 1968 and 1969. In connection with the design of the icebreaking forebody of the MANHATTAN an ice model basin was built by WARTSILÅ in 1969, followed by ARCTEC Inc., USA, and HSVA in Hamburg, West-Germany, in 1971.

Currently twelve ice model basins are in operation and four more are under construction. The main data of all these facilities are summarized in Table 1. In this table the ice model basins are divided into three categories. The small ice tanks built in the 1950's are those of the first generation. To the second generation belong those of medium dimensions and to the third generation the new WARTSILÅ tank and those under construction at HSVA and at NRC, which have 60 m testing length necessary for self propulsion tests.

TABLE 1

Year built	Operating Organisation	Country	Length for testing m	Width m	Depth m	Model ice in use	Remark
<u>Ice Model Basins in Operation</u>							
1955	Arctic + Antarctic Research Institute	USSR	13,4	1,8	1,3	saline ice	1. Generation
1969	WARTILA Shipyard	Finland	29,0	4,8	1,05	saline ice	
1971	HSVA	W.-Germany	30	6,0	1,2	carbamide ice	
1971	Offshore Technology Corporation	USA	89,9	14,6	4,6	synthetic ice	
1974	Arctec Inc.	USA	30	3,6	1,5	saline + synthetic ice	
1977	Arctec Canada	Canada	30,5	4,9	1,8	saline/carbamide synthetic ice	2. Generation
1979	CRREL	USA	36	9,2	2,5	carbamide ice	
1981	Ship Research Institute, Tokyo	Japan	30	6,0	1,2	saline ice	
1981	Iowa Institute for Hydraulic Research	USA	20	4,5	2,0	carbamide ice	
1981	NRC, Ottawa	Canada	21	7,0	1,25	carbamide ice	
1982	Nippon Kokan	Japan	20	6,0	1,8	saline ice	
1983	WARC	Finland	60		2,3	saline ice	3. Generation
<u>Ice Model Basins under Construction</u>							
?	Arctic and Antarctic Research Institute Leningrad	USSR					
?	Krylov Institute Leningrad	USSR					
1984	HSVA, Hamburg	W.-Germany	60	10,0	2,5/5,0	carbamide ice	3. Generation
1985	NRC, St. John's	Canada	60	12,0	3,5	carbamide ice	3. Generation

Areas of Testing in Ice

Three different areas of model or small scale testing in ice can be identified

- Hydraulic modeling of ice phenomena
- Model testing of icebreaking ships
- Model testing of offshore structures (ice forces)

Hydraulic modeling is concerned with the ice management in rivers. In this field the roughness coefficient of the ice underside (ice ripples) in relation to temperature and flow conditions is determined. Ice breakup processes in rivers are simulated in order to study the mechanics of ice jam formation and to establish means for its prevention.

Frazil ice formation is another problem area which is studied in model and full scale tests. So-called "ice booms" have been developed to prevent the formation of frazil ice which occasionally blocks the whole flow cross section of rivers. Such ice booms have been investigated in model tests before they were built in prototype, e.g. in the St. Marie's River.

Model testing of icebreaking ships is used to determine the most efficient hull form for icegoing ships in respect to resistance and power consumption (Fig. 1 and 2). For a long time (up to 1977) the icebreaker models were only investigated in resistance tests.

This procedure led to the dissatisfying performance of some icebreakers, i.e. low resistance but also of low propeller efficiency in ice. The lowest icebreaking resistance occurs when the shape of the forebody is such that the ice, after being broken, is only submerged without being pushed sideways. Hereby most of the broken ice slides along the bottom of the ship toward the propeller area, where it causes potential propeller damage and a reduction in the propulsion efficiency. This means that in addition to resistance tests, self propulsion tests are necessary in order to fully investigate the icebreaking capability of ships. Today, most ice research facilities follow this philosophy.

The performance of self propulsion tests has an additional advantage

in that the results of model and full scale tests can be compared directly via power or thrust without converting resistance (measured in model tests) into thrust (sometimes measured in full scale tests) by making assumptions on the thrust deduction fraction.

Besides the prediction of the icebreaking capability of vessels in level ice, model tests are being carried out to investigate the ships performance in pressure ridges, in rubble ice fields and in broken ice, going ahead and astern. In the latter case, investigations are focused on the problem of ice ingestion into the propellers and whether or not possible propeller ducts are getting clogged.

Another aspect of icebreaker performance is the ramming ability of the ship. This is necessary if the ice cover is thicker than the ship is able to break in the continuous mode. The result of these ramming tests may be the relationship between the impact speed of the ship with the ice and the length of indentation of the hull into the ice.

In some cases - e.g. for icebreaking offshore supply ships or for long tankers - it is important to have good manoeuvrability. This can be investigated by model tests in which the Y_0 = transverse deviation per ship length is established.

Some ice basins provide the opportunity to investigate the icebreaking performance under lateral pressure; hereby the ice cover is pushed by a side-pressure-unit against the side of the passing ship model while the icebreaking performance data are being recorded.

Model testing for offshore structures is becoming more and more important. While ten years ago small scale tests were carried out in order to investigate ice forces on simple structures like piles, bridge piers or conical structures, today, more sophisticated concepts for exploration or production platforms are being tested.

We distinguish between fixed and floating offshore structures.

Fixed structures (bottom founded, Fig. 3)

Type of structures

- piles
- bridge piers
- light houses
- caissons
- monocones
- multilegged structures
- vertical piles with conical ice deflectors

Objective: Determination of ice forces as a function of

- speed (strain rate)
- ice strength
- ice condition
(level ice, rubble ice ridges)

Floating structures (Fig. 4)

Type of structures

- single point mooring bouy
- conical drilling barge (moored)
- semisubmersible

Objective: Determination of

- mooring cable forces
 - system forces
 - motions in 3 axes and
 - rotations around 3 axes
 - accelerations
- for parameters like
- ice thickness
 - speed
 - ice strength
 - ice conditions

While in the case of the model tests for fixed structures the determination of ice loads is relatively simple, the investigation for floating structures requires the simulation of the dynamic response to the ice attack of the entire structure system as well as of each single member.

Similarity Requirements

The rules of similitude for modeling in ice can be obtained by dimensional analysis or by establishing correlation functions between model and full scale tests.

Laws of similitude for modeling ice phenomena have been presented by Nogid (1959); Michel (1970, 1975); Edwards and Lewis (1970); Atkins (1975) and Vance (1975). Common to all publications is the statement that Froude scaling laws are applicable for ice.

$$Fr = \frac{V}{\sqrt{gI}} \quad (1)$$

Complete similitude of ice tests is achieved if geometric, kinematic and dynamic similarity is reached.

The corresponding scaling functions are as follows (p = prototype; m = model)

Geometric similarity

$$L_p = \lambda L_m \quad (2)$$

(L = geometric length)

Kinematic similarity

$$V_p = \sqrt{\lambda} V_m \quad (3)$$

$$t_p = \sqrt{\lambda} t_m \quad (4)$$

(V = velocity; t = time)

Dynamic similarity

$$F_p = \lambda^3 F_m \quad (5)$$

(F = force)

In addition to these similarity requirements the failure of an ice sheet must be similar in model and full scale tests in respect to failure force and failure mode.

Assuming elastic theory (Hooke's law)

Shear failure forces:

$$F_t = \tau h L C_1 \left(\frac{a}{L}, \frac{b}{L}, \frac{c}{L}, \nu \right) \quad (6)$$

Crushing failure forces:

$$F_c = \sigma_c h L C_s \left(\frac{a}{L}, \frac{b}{L}, \frac{c}{L}, \nu \right) \quad (7)$$

Flexural failure forces:

$$F_b = \sigma_f h^2 C_3 \left(\frac{a}{\ell}, \frac{b}{\ell}, \frac{c}{\ell}, \nu \right) \quad (8)$$

where F_t , F_c and F_b are the forces producing failure; τ , σ_c and σ_f are the shear, compressive and flexural strength of ice; L , a , b and c are representative lengths (the last three for conditions of loading), ν is Poissons's ratio, and ℓ is a characteristic length of the ice sheet that is related to the position of the line of flexural fracture.

The ratio of these shear, crushing and flexural forces in model and prototype should correspond to the scale ratio of forces as given in Equ. (5).

Hereby

$$\lambda^3 = \frac{\sigma_p}{\sigma_m} \lambda \lambda \quad (9)$$

or

$$\lambda = \frac{\sigma_p}{\sigma_m} \quad (10)$$

The elasticity of a material is simulated correctly if the Cauchy number

$$Ch = \frac{V^2 \rho}{E} \quad (11)$$

is equal in model and full scale tests. When assuming elastic deformation, also the ratio of the Elastic Moduli should be equal to λ .

Hence, it follows that the ratio of E/σ should be equal in model and prototype.

MAIN PROBLEM IN MODEL TESTS

The friction coefficient, μ , should be the same in model and full scale test conditions. This follows from Coulomb's friction law

$$F_t = \mu F_n \quad (12)$$

where

F_t = tangential force

F_n = normal force and

μ = static or dynamic friction coefficient.

As in open water tests, the Reynolds' number (effect of viscosity) can not be fulfilled simultaneously with Froude's and Cauchy's model laws. In order to minimize the error due to Reynolds' effects, the models should be as large as possible.

The following table summarizes the scaling functions for model - full scale correlations.

Table II. Similarity Relations for Modeling Vessels in Ice

Length	=	$L_p = \lambda L_m$	
Beam	=	$B_p = \lambda B_m$	
Draft	=	$T_p = \lambda T_m$	
Force	=	$F_p = \lambda^3 F_m$	
Displacement	=	$\nabla_p = \lambda^3 \nabla_m$	
Velocity	=	$v_p = \sqrt{\lambda} v_m$	
Time	=	$t_p = \sqrt{\lambda} t_m$	
Torque	=	$Q_p = \lambda^4 Q_m$	
Thrust	=	$TH_p = \lambda^3 TH_m$	
Power	=	$P_{dp} = \lambda^{3.5} P_{dm}$	
Gravity	=	$g_p = g_m$	
Thickness	=	$h_p = \lambda h_m$	
Flexural Strength	=	$\sigma_p = \lambda \sigma_m$	COMPRESSIVE } SHEAR } STRENGTH
Elastic Modulus	=	$E_p = \lambda E_m$	
Coefficient of Friction	=	$\mu_p = \mu_m$	
Viscosity	=	$\nu_p = \nu_m$	
Density of Water	=	$\rho_{wp} = \rho_{wm}$	
Density of Ice	=	$\rho_{ip} = \rho_{im}$	
Poisson's Ratio	=	$\mu_{pp} = \mu_{pm}$	

p = prototype; m = model; and λ = geometric scale factor

Tank and Model Sizes

The tank utilized should be large enough to allow at least three characteristic lengths between the point of application of the ice load, i.e. the bow of the vessel, and the extreme boundary. The characteristic length (ℓ) is defined by the following relationship:

$$\ell^4 = \frac{E h^3}{12 (1-\mu_p^2) \gamma_w} \quad (13)$$

where

- ℓ = characteristic length in meters
- h = ice thickness in meters
- E = ice modulus of elasticity in pascals
- μ_p = Poisson's ratio
- γ_w = specific weight of water in newtons per cubic meter

As a rule of thumb, to simulate unrestricted ice boundaries and deep water conditions at low speeds, tank width should be at least 6 times the characteristic length for continuous ice sheets and the tank depth should be greater than $D = \sqrt{BT}$, where D is depth in meters, B is the model beam in meters and T is the model draft in meters. The tank should be long enough to allow at least one full ship length of penetration at steady state for each resistance data point obtained. The speed of the carriage for resistance tests should be maintained to within ± 0.02 mps and the resistance readings should be measured to within 0.5 %. Due to the uncertainties of scale effects, large scale ratios should be avoided and geometric scale ratio should not exceed 50 if possible; however, scale ratios in the area of less than 30 are preferred (ITTC-1978).

Measured Values in Model Tests

In model tests for icebreaking ships or offshore structures the following parameters should be measured:

Ice conditions

Ice thickness and its variation along track of icebreaker
Flexural strength
Compressive strength
E-Modulus
Ice density
Ice crystal size and structure
Size of broken ice pieces and degree of ice coverage
Density of broken ice in case of broken channel tests
Lateral pressure in ice covers
Ridge geometry
Ridge consolidation (percentage)
Ridge piece size
Ridge shear strength

Offshore structure data

Particulars of structure model and test set up
Gyradii
Friction coefficient between structure and ice
Draft
Area or height of ice attack
Natural frequency of model
Elastic properties of mooring cables
Ice forces in x, y and z directions
Movements in x, y and z directions (surge, sway, heave)
Pitch, roll and yaw angles
Speed
Accelerations

In all tests the ice-hull-structure interactions should be documented by video, movie and still pictures.

Ship model data

Vessel particulars incl. appendices
Gyradius
Model speed
Icebreaking resistance
Friction coefficient between hull and ice
Vessel draft (fore and aft)
Pitch angle
Roll angle
Shaft thrust
Shaft torque
Shaft rpm
Propeller pitch
Accelerations
Penetration distance in case of ramming tests
Rudder angle
Turning radius or deviation in case of manoeuvring tests

Various Techniques of Testing in Ice

1. Model ice -----

Presently there are three different kinds of model ice in use at the various ice laboratories (see Table 1): Saline ice; synthetic ice and carbamide ice. In the case of saline ice and carbamide model ice, brine is used to reduce the strength and the E-modulus. Since the brine content depends on the salinity of the water, freezing rate and temperature, all three parameters are used to temper the ice properties. A high freezing rate which is obtained by the liquid nitrogen system applied by ARCTEC Inc. and ARCTEC Canada increases the brine content and lowers the strength. Almost all other ice model basins use the Freon refrigeration system which provides lower freezing rates of 1 to 3 mm/h at air temperatures ranging between -10° C and -35° C. Some of the ice tanks use the natural convection freezing method (HSVA 1971 tank, WARTSILA 1983 tank, Leningrad 1955 tank, Tokyo tank, NKK tank) while others try to speed up the freezing rate by means of a forced air circulation system (CRREL tank, Iowa tank, NRC tank, St. John's 1985 tank and the new HSVA 1984 tank).

In order to increase the strength reduction, a warm-up method applied to the ice cover was introduced by Schwarz 1975. This method is presently in use at most ice tanks. This process causes the brine content to increase and has the effect of reducing the strength, especially of the top layer of the model ice cover. This top layer consists of random oriented crystals and has therefore, before tempering, an unproportionally high strength.

The size of the ice crystals is reduced by a water spray method. By this method water is sprayed at a certain air pressure into the approximately -10° C cold air in the ice tank room. The droplets freeze and form ice crystals which settle on the water surface, whereby the formation of a fine grained ice cover is initiated. The crystals of the top layer (2 - 3 mm) are randomly oriented. Below this layer, the ice crystals line up vertically to form columnar grained ice (Fig. 5). This crystal structure combination is similar to saline level ice in nature, where the top layer, for example, is approximately 5 cm thick. At low freezing rates (as for

example presently 1 mm/h at CRREL, USA) the top layer is unproportionally thick (5 - 10 mm).

The problem with saline model ice is that the strength and E-modulus can not be reduced by the same scale rate as is required by Cauchy's model law. This follows from the relationship between flexural strength and brine volume on one side and E-modulus and brine volume on the other side as proposed by WEEKS and ASSUR (1958) and verified by Schwarz (1975) (Fig. 6). Fig. 6 shows for model scales > 15 the strength to deviate drastically from $E/\sigma = \text{const.}$ This means that at large model scales the strength is too large compared to the elasticity or that at the correctly scaled strength, the model ice has almost no elasticity, but deforms mostly plastically. This plastic deformation requires, however, too much energy to break the ice, which is demonstrated in Fig. 7.

Up until 1981, HSVA tried to compensate for this error of too high resistance results at low strengths by not testing models below a flexural strength of the saline model ice of 50 kPa and by extrapolating the resistance-strength curve to the required, correctly scaled strength. Hereby the E/σ -ratio was kept close to full scale values. This method incorporates the inaccuracy of every extrapolation method. Therefore for this reason among others (self-propulsion tests), HSVA has adopted the carbamide model ice technique, developed by TIMCO (1979).

WARTSILA currently uses saline model ice, also only scaled down to a certain minimum strength, which generally is above the properly scaled strength. By running the models through unbroken ice and through presawn ice, WARTSILA establishes the various portions of icebreaker resistance:

- the breaking portion
- the submerging portion (low speed)
- the inertia portion (speed effect).

By using the carbamide model ice, the E/σ -ratio stays within the range of full scale values (2-3000) even at very low flexural strengths (10 - 20 kPa). The lowest strength at which the model ice can be considered solid is about 10 kPa. If we assume a flexural strength in nature of 500 kPa a maximum scale of 50 can be used for model tests in ice.

It should be mentioned that not all ice laboratories have been successful in adopting the carbamide model ice. The reason for this may be that the carbamide ice properties are very sensitive to the freezing rate, the water temperature in the ice tank, the warm-up temperature and its gradient.

Synthetic model ice is presently used for certain tests by ARCTEC Inc. and ARCTEC Canada. The exact formula of this ice is kept proprietary. It is, however, known that the basic ingredient is parafine or wax. Certain additives provide the correct strength and elasticity reduction. Shortcomings of this material are the non-crystalline isotropic structure (sea ice in nature is generally plan-isotropic) and especially the sticky-frictional behavior of this synthetic ice. The argument, that the correct friction coefficient between the model ice and the model ship can be obtained by providing the hull with an extremely smooth surface is insufficient since the effect of friction between the broken ice pieces, which causes a too high resistance, is ignored.

The simulation of rubble ice or pressure ridges in the various ice model basins is hampered by the insufficient knowledge of the mechanical properties of these ice formations. What is reasonably well established are the geometric dimensions of pressure ridges in the Arctic and their degrees of consolidation. Therefore most model ice basins restrict the simulation to these parameters. Nevertheless, some means of quality control of the mechanical properties is desirable. The methods of modeling pressure ridges may be different at the various establishments. HSVA builds pressure ridges as follows:

A parental ice sheet is created by growing a level ice cover of about 20 mm thickness. This parental ice cover is broken into small ice blocks by cutting the ice cover into longitudinal strips of about 100 mm width using a cutting rake, which is fixed to the main towing carriage. Then the strips are further cut into pieces manually to achieve the required maximum ice piece dimensions of no more than 5 times the parental ice sheet thickness. The fragmented ice is pushed by means of the carriage's pushing board into the ridge casts, one side of which is held somewhat below and the other above the water surface. The casts are constructed of a pipe frame connected by strengthened plastic foil. This cast is adjusted in depth such as to produce the desired ridge keel depth. The sail height is modeled manually.

During the freezing period of the final ice cover, the degree of consolidation of the ridges is influenced by covering the ridges with insulating blankets. Hereby the freezing together of ridge ice pieces is slowed down.

Before the test starts, the ridge casts are lowered down to the bottom and pulled to the side wall of the ice tank.

The dimensions of the ridges including the depth of consolidation are measured at the remaining sections after each test.

Some quality control is established through an in situ shear box test in which the shear strength of the ridge ice in the horizontal direction is measured.

The mechanical properties of the model ice are established by cantilever beam tests (flexural strength), uniaxial compression tests and deflection measurements (E-modulus). The testing methods should follow the recommendations of the IAHR-Working Group on Standardizing Testing Methods in Ice (Schwarz et al. 1981). In cantilever beam tests, the breaking load applied at the free end of the beam is measured. The beam dimensions are related to the ice thickness h , such that the beam length is $6 \times h$ and the beam

width $2 \times h$. The load should be applied at about 1 second times $\lambda^{-1/2}$. The flexural strength is then calculated from the failure force measurements by using the equation

$$\sigma_f = \frac{6F l}{b h^2} \quad (14)$$

where

F = failure load [N]
l = length of the beam [m]
b = width of the beam [m]
h = thickness of the ice [m]

It should be kept in mind that the flexural strength established as recommended above is an "index" value because several assumptions are not correct, as for example

- elastic theory (Hooke's law)
- linear deformation across the thickness
- isotropy
- homogeneity.

The compressive strength tests should be obtained under controlled conditions in respect to temperature, strain rate, and load direction vs. crystal direction. The use of compliant platens for applying the load to the sample is recommended (see IAHR-recommendations Schwarz et al. 1981).

The modulus of elasticity can be obtained by measuring the deflection of the cantilever beam or of the ice plate. In the case of the cantilever beam method, care must be taken to avoid errors due to deflection of the ice cover at the root of the beam and due to plastic deformation along the length of the beam. This error can be avoided if the deflection is measured at several locations along the beam length (see Häusler, 1982).

A better method of establishing the E-modulus is possible through the

"plate test", whereby certain loads are applied on to the ice cover while simultaneously, the deflection of the ice cover is measured at the center of the applied load.

The modulus of elasticity is then calculated from the following equation:

$$E = 1.94 \cdot 10^5 \cdot \left(\frac{F}{W}\right)^2 \frac{1 - \nu^2}{\rho_w \cdot g \cdot h^3} \quad (15)$$

where

- E = modulus of elasticity [MPa]
- F = load [N]
- W = deflection [mm]
- ν = Poissons ratio (0.3)
- g = acceleration due to gravity (9.814 m/sec²)
- h = ice thickness [mm]
- ρ = density of water in t/m³ (1.0025 t/m³ at T = 0° C).

2. Resistance Testing

When the correct thickness, strength and modulus of the ice sheet are obtained, the model is set to the correct displacement and trim and every effort should be made to set the longitudinal radius of gyration to the values established by the ITTC Seakeeping Standards. In towed model tests, the carriage is run at a steady speed through the ice sheet for at least one - better two or three - model length, the speed can then be increased and another data point obtained. Fig. 8 gives an example of a test record showing the time functions of speed, resistance, roll, and pitch.

Upon completion of the level ice tests, the broken ice can then be utilized for the broken channel ice test. In these tests, the procedure is similar to that for the level ice except that the model should be run through at least two model lengths of broken channel. The critical measurement in these tests is the degree that the channel is filled with ice. One should ensure that for a channel 100 % filled with broken ice, no open water patches are visible. Lesser degrees of ice in the channel should be documented with overhead photographs and movie film or video tapes.

Resistance tests in level ice with pressure ridges incorporated are carried out in the same manner as resistance tests in level ice without the ridges. Of course, the icebreaker model should penetrate the ridge completely before the test condition is changed (speed).

Resistance tests in ice fields under lateral pressure have been carried out (for example at HSVA), the technique should be improved and the results be compared with full scale data.

It should be noted that resistance tests alone without information on the ice-propeller interaction is insufficient to predict the icebreaker performance and the resistance values alone are of not much worth.

It should further be mentioned that due to the lateral guidance of the

model in resistance tests (normal procedure at some ice tanks), the results may be effected by unrealistic friction effects when the model is pressed by the guide against the level ice cover.

Techniques (as those currently in use at HSVA) which provide a certain degree of freedom to sway are one way of minimizing this error.

3. Self Propelled Testing

Today, self propelled testing for icebreaking ships is standard at most of the ice model basins. The tests are carried out by fitting the model with propellers and dynamometers that measure torque, thrust, and rpm. (The propellers may be stock model propellers that have the approximate full scale propeller characteristics.) The model must be free to heave, pitch and roll as it transits the length of the tank. This can be accomplished with an umbilical cord trailing from the towing carriage, through the use of telemetry systems, or directly from the carriage using differential dynamometers. A rudder and rudder control mechanism should be installed to control the direction of the model if the model is not guided by the carriage. Upon proper ballasting and trimming the model is running the length of the tow basin in open water at various speeds. These tests should be carried out at the model self propulsion point, the ship self propulsion point, and overload conditions. Analysis of the data will yield an estimate of the quasi-propulsive coefficient in open water (ITTC-78).

The self propelled tests described above are then repeated in ice, either level ice or broken channel ice and the same data collected. These data will yield an estimate of the quasi-propulsive coefficient in an ice environment. Thus such self propelled tests will yield the effectiveness of the total ship propulsion system, i.e. hull form and propeller-hull-ice interaction. Many researchers feel that the self propelled tests are the more significant tests in evaluating a ship's performance in ice.

Due to the more critical nature of the Reynolds effects in propeller interactions, it is recommended that the models used be as large as possible.

In order to reach steady state test conditions in speed and propeller ice interactions the required testing length is longer than in resistance tests. This is one reason why the 3rd generation ice model basins (WARTSILAX, HSVA and NRC) all have a testing length of 60 m.

Fig. 9 shows a record of a self propulsion test with time functions

of speed, torque, thrust, rpm, pitch and roll. This record clearly indicates the effect of the ice-propeller interaction on the torque, rpm and also on thrust.

The prediction of the overall icebreaking ability of a ship can be expressed in terms of speed as a function of ice thickness (see Fig.10).

- 1) CONSTANT SPEED
FIXED MODEL $\rightarrow R(V)$ SELF PROPULSION POINT INTERPOLATED
- 2) CONSTANT RPM
FREE MODEL \rightarrow SPEED (RPM, T)
= MEASURED $R(V) = 0$

4. Ramming Tests

If an ice cover is too thick for an icebreaker to navigate continuously, then the ice is broken by ramming. Model tests for investigating the ramming ability of an icebreaker are performed such that the model approaches the ice cover at a certain speed and penetrates the ice over a certain length. The result may be given by the length of the ship's penetration as a function of impact speed. The test is carried out with the self propelled model.

5. Manoeuvring Tests

Due to the limited width of the existing ice tanks, manoeuvring tests can only be considered qualitative in nature. However, by determining the transverse deviation per ship length (γ_0) the manoeuvrability of icegoing ships can be described. The rudder angle would be another parameter.

6. Offshore Structure Tests

The scope of model tests on offshore structures is the determination of the forces which various ice features may exert against structures. The models may be fixed or floating. The fixed structures may be mounted on to the platform of an underwater carriage (HSVA). While the model structure is pulled via the underwater carriage through the ice, the forces of the ice-structure interaction are measured. Another testing technique is to keep the structure in place and to move the ice cover or broken ice by means of the main carriage against the model structure. In the case of level ice, this testing technique may be hampered by the unrealistic unconfined stress condition of the ice cover which is caused by cutting off the ice from the sidewalls of the ice tank in order to allow ice movement. Also difficult or perhaps impossible to simulate is structure-ridge interaction, if the structure is to stay in place and the ice moved against it.

In the case of model tests for floating offshore structures the dynamic effect of the floating structure model must be considered in addition to all other similarity requirements for fixed offshore structure tests.

While in icebreaker model tests generally mean values are important, in the case of offshore structure tests, the maximum ice forces are relevant and are considered in design work.

Due to the stochastic processes of ice/ship or ice/structure interactions, probability approaches are necessary and are being used by most ice model basins to evaluate the model test results.

Comparison of Model Test Results of Various Ice Model Basins

In 1980, Melville Shipping Ltd., Canada, provided model test results to the ITTC-Ice Committee which were conducted by three different ice model basins (Arctec Inc., HSVA, and WARTSILÅ) for the same icebreaking LNG tanker project. These results and also those of the Arctic and Antarctic Research Institute in Leningrad have been used by the ITTC-Ice Committee for comparative purposes. Unfortunately, each ice model basin used a different surface roughness of the tanker model. Also the scale was different. The Committee published the following statement (ITTC 1981 Proceedings):

"Predicted ice total resistance results for the four tanks which have here presented data compare reasonably well when the differences in prediction friction coefficients for the results are considered, and where the other prediction parameters of E , σ and h are the same with each tank using its present methods.

There are two fundamentally different prediction methods used, both based on experience with model/ship correlations.

a) From Ice Resistance Tests:

This method is based on a large amount of correlation experience. The open water thrusts, for given powers and speeds are compared with predicted ice resistance data.

b) From Propulsion Tests:

Recently prediction methods based on detailed model propulsion tests in ice have been used in order to more accurately take account of the effects of broken ice on the propulsion factors. Only a few correlations have been made so far using this method. The method involves using true prediction hull/ice friction values, appropriate to the conditions, and equating thrust data corrected for the in ice thrust deduction from propulsion tests to the ice total resistance.

Both of the above prediction methods may be used at present with some confidence, the second test method is more detailed and yields more data related to the performance of the propulsion system."

By correcting for the different friction coefficients used in the various ice model basins, the speed - ice thick relationships established by the four ice model basins fall almost on the same curve (Fig.11).

Model Test Results - Theoretical Prediction

The most advanced theoretical approach to predict the icebreaking resistance of ships is that of Milano (1972, 1982). From 1972, when his first prediction theory was published till 1982, Milano has improved his theory considerably. A comparison of model test results with his theoretical prediction is shown in Fig. 12. Since the model test results also compare well with full scale data (Fig. 13) it can be concluded that the performance of icebreaking ships can be predicted by model tests and by theoretical means to a high degree of confidence.

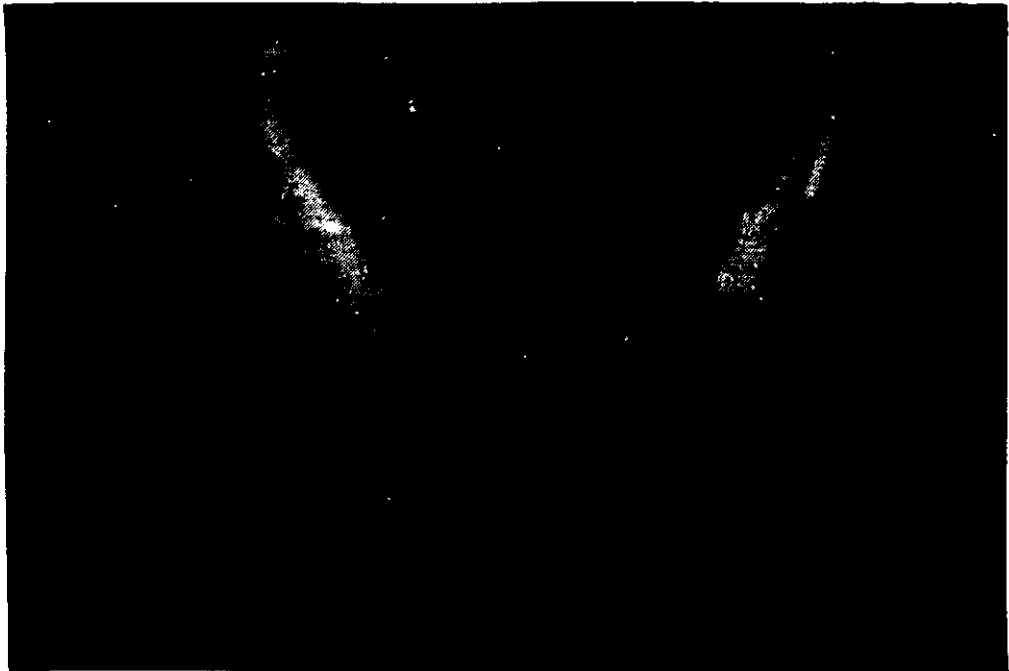
References

- Nogid, L.M.(1959): "Model representation of a ship going through a continuous ice field or pack ice" Trans. of the Leningrad Ship Building Institute, No. 45.
- Michel, B. (1970): "Ice Modeling in Hydraulic Engineering" Proc. I.A.H.R. Ice Symposium, Reykiavik, Paper 4.13.
- Michel, B. (1975): "Techniques of ice modeling including distortion". Report GCT-75-01-01, Civil Eng. Dept., Laval University.
- Edwards, R.Y., Lewis, J.W. (1970): "Modeling the motion of ships through polar ice fields using unconstrained, self-propelled models" Proc. I.A.H.R. Symposium "Ice and its action on hydraulic structures" Reykjavik, Iceland, paper 4.14.
- Atkins, A.G. (1975): "Icebreaking Modeling", Journal of Ship Research Vol. 19, No. 1
- Vance, G.P. (1975): "A scaling system for vessels modeled in ice" Paper presented to "The Society of Naval Architects and Marine Engineers" Ann. Meet., Ap.9-11
- ITTC 1978 - Report of Ice Committee

- Weeks, F.W. and A. Assur (1967): The mechanical properties of sea ice. U.S.Cold Regions Research and Engineering Laboratory, Hanover, N.H., Cold regions science and engineering, Pt. II, Sec. C3 - CRREL-Monograph II-C3.
- Schwarz, J. (1975): "On the Flexural Strength and Elasticity of Saline ice" Proc. of 3rd. Intern. IAHR-Symposium on Ice Problems, Hanover, N.H. 1975 (Frankenstein editor)
- Timco, G.W. (1979): The Mechanical and Morphological Properties of Doped Ice: A Search for a better Structurally Simulated Ice for Model Test Basins. POAC 79/ Port and Ocean Engineering under Arctic Conditions, Norway.
- Schwarz et al (1981): Standardized Testing Methods for Measuring Mechanical Properties of Ice. Cold Regions Science and Technology, Vol. 4.
- Häusler, F.U. (1982): Comparison between different yield functions for saline ice. International Glaciological Society, 2nd. Symposium on Applied Glaciology, Aug. 23-27, 1982, Hanover, N.H. Annals of Glaciology, Vol. 4 (in press)-
- Milano, V.R. (1973): Ship Resistance to Continuous Motion in Ice, Transaction SNAME Technical Bote 39-2
- Milano, V.R. (1982) "Correlation of Analytical Predictions of Ship Resistance in Ice", (Visiting Scientist at HSVA), Intermaritec 82, Hamburg, W-Germany, September 1982.



Fig. 1. Model of Icebreaking ship in ice tank.



a)



b)

Fig. 2. View through bottom window of ice tank on bow and stern of icebreaker model.

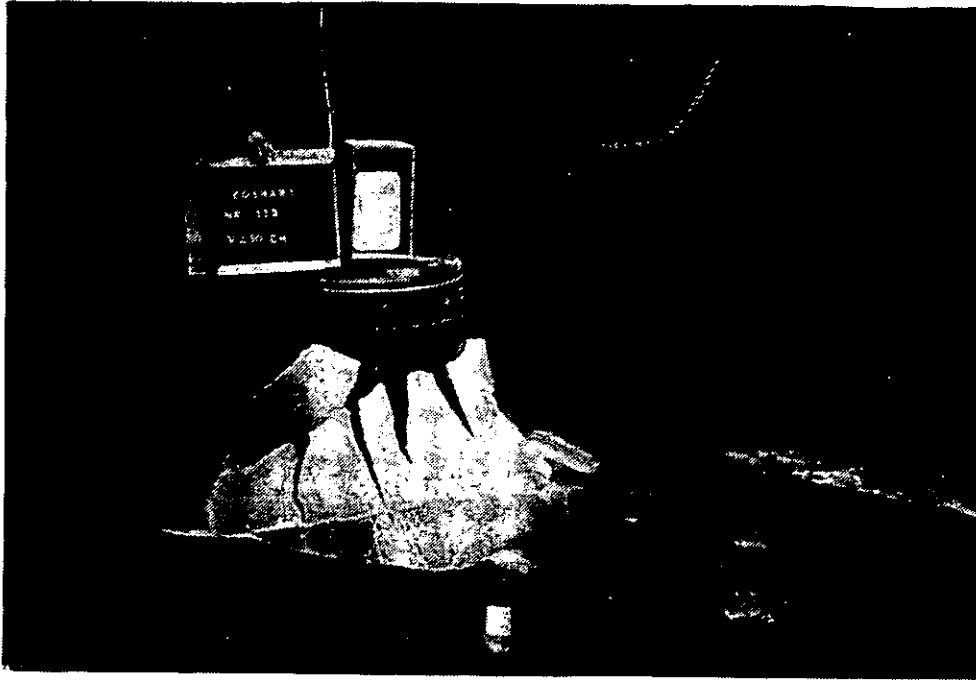


Fig. 3. Model of fixed conical offshore structure in ice.

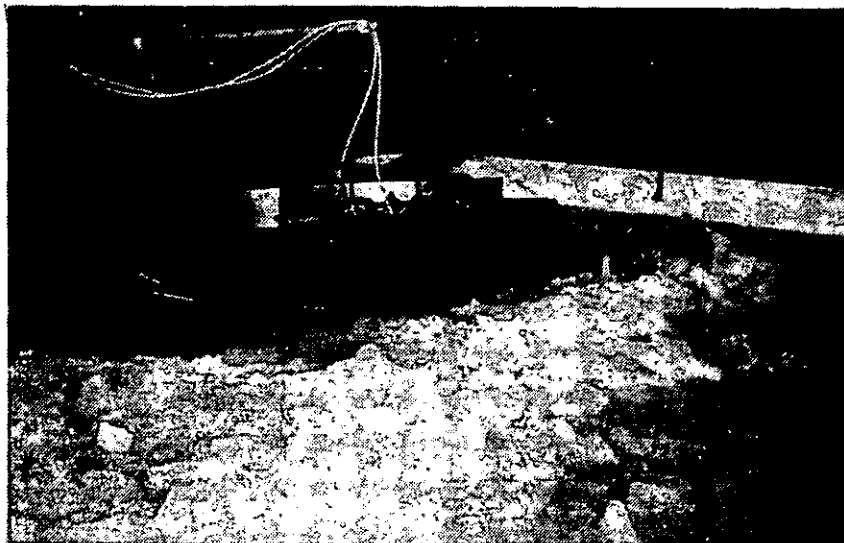


Fig. 4. Model of floating conical offshore structure.



Fig. 5. Vertical cross section of crystal structure carbamide model ice.

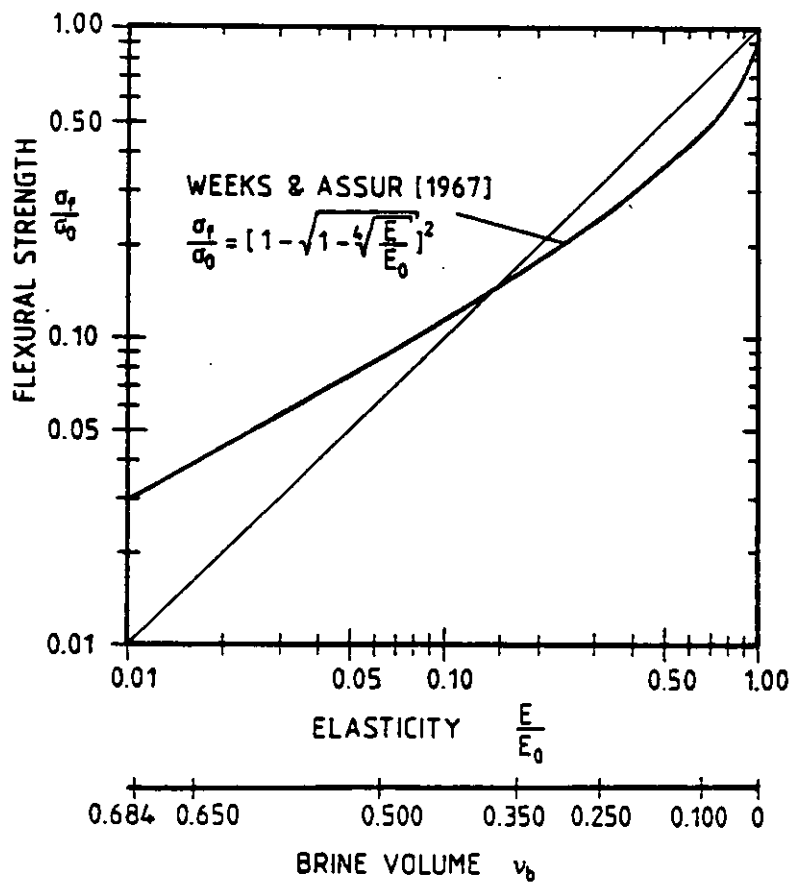


Fig. 6. Normalized flexural strength versus elastic modulus for saline ice.

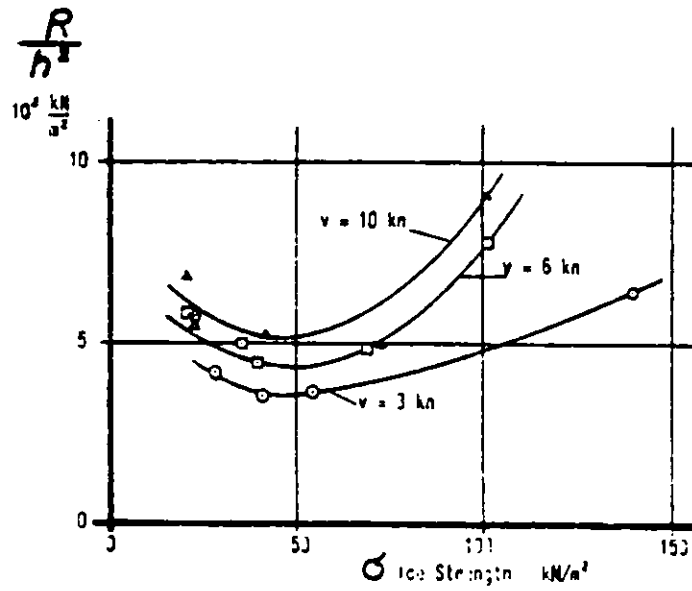


Fig. 7. Icebreaking resistance versus flexural strength of model ice.

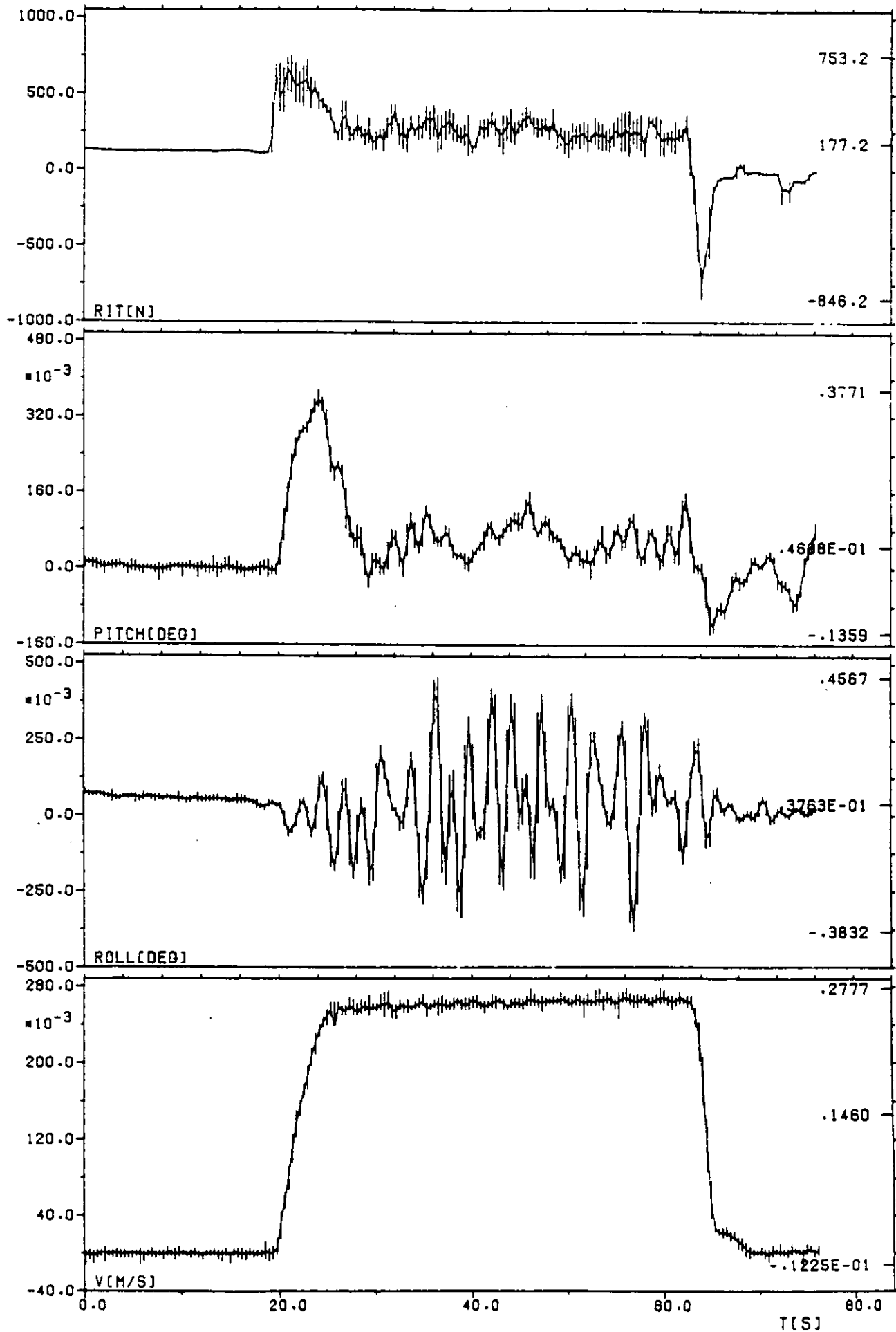


Fig. 8. Resistance test results obtained in ice model basin.

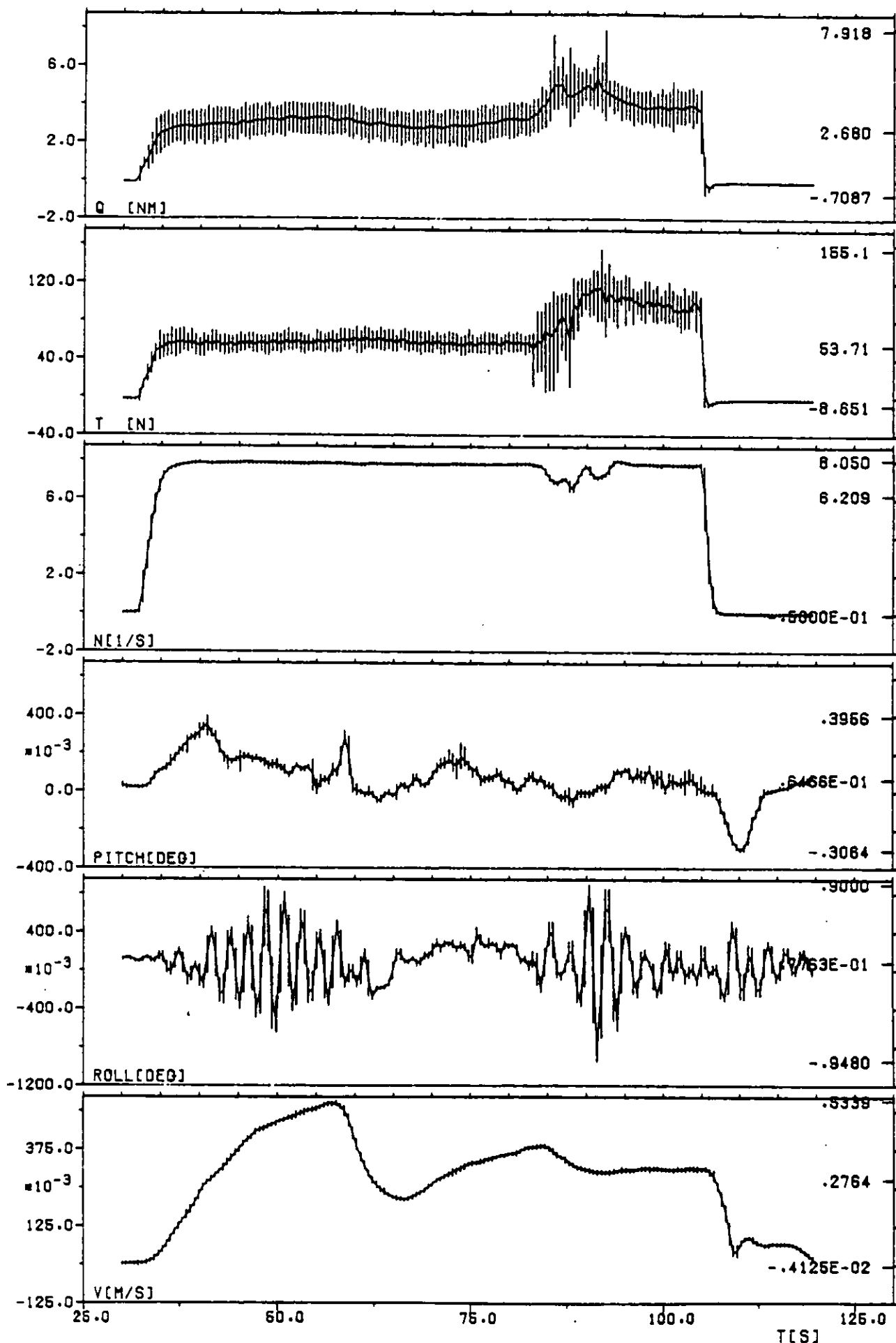


Fig. 9. Self-propulsion test results obtained in ice model basin.

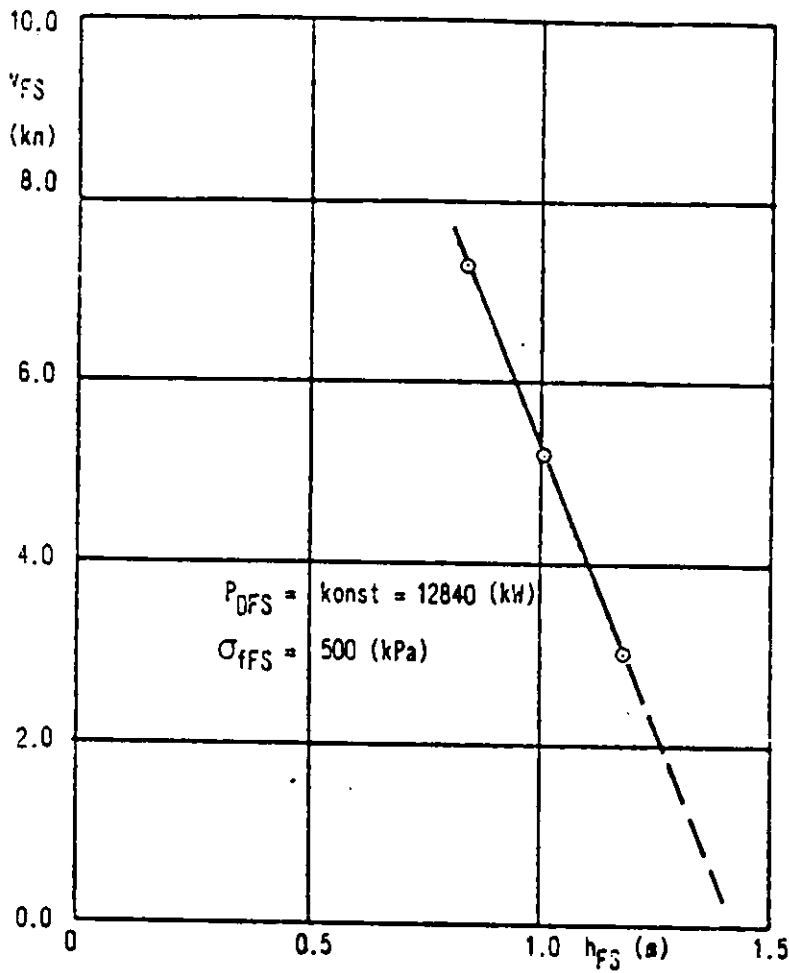


Fig. 10. Prediction for icebreaker speed as a function of ice thickness based on model test results.

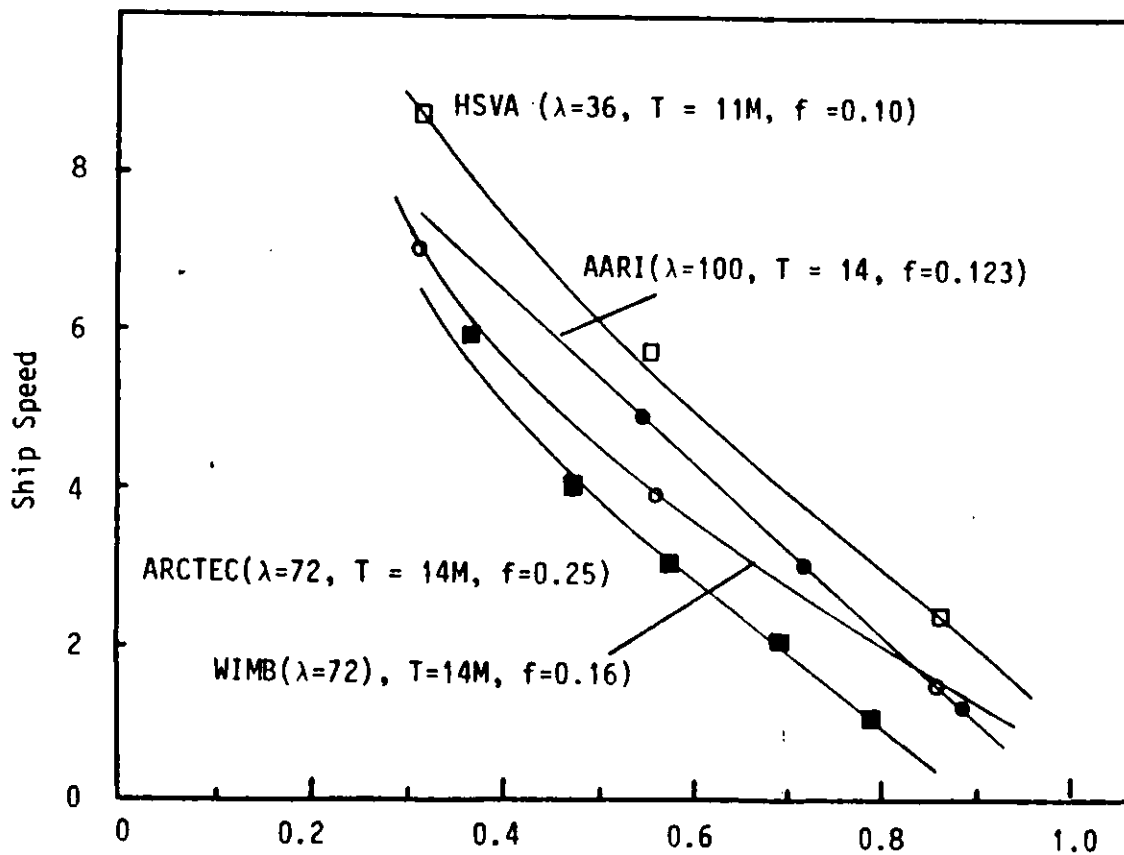


Fig. 11. Comparison of resistance test results established by four different ice model basins.

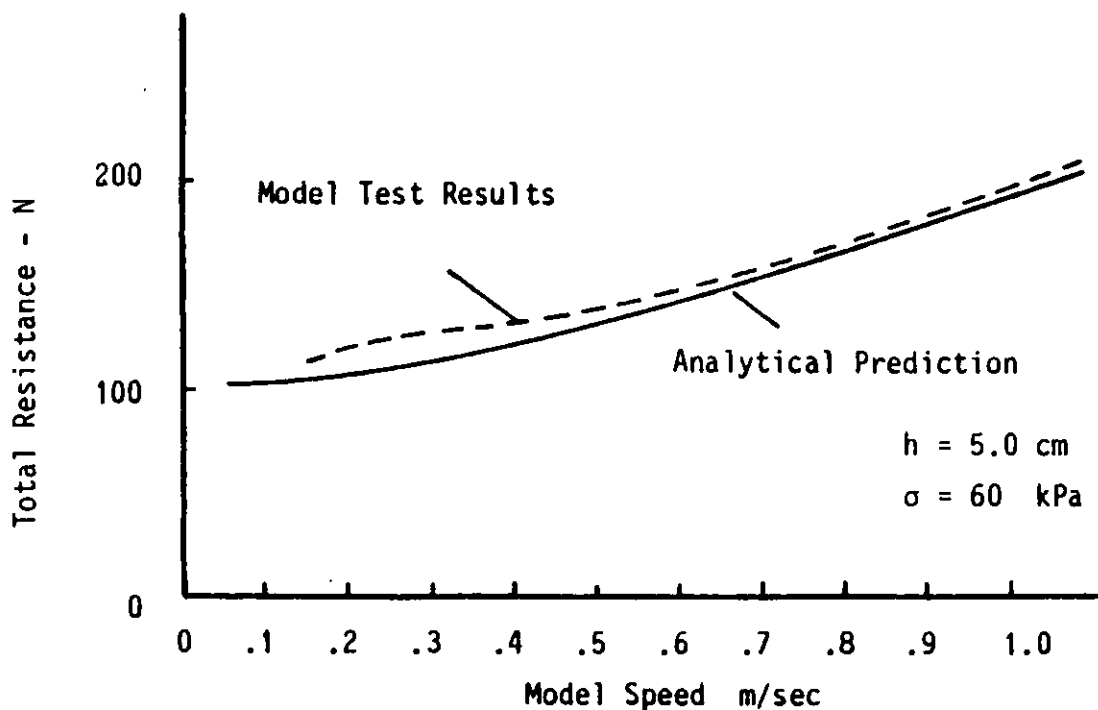


Fig. 12. Comparison between theoretically predicted and experimentally established icebreaker resistance vs. speed.

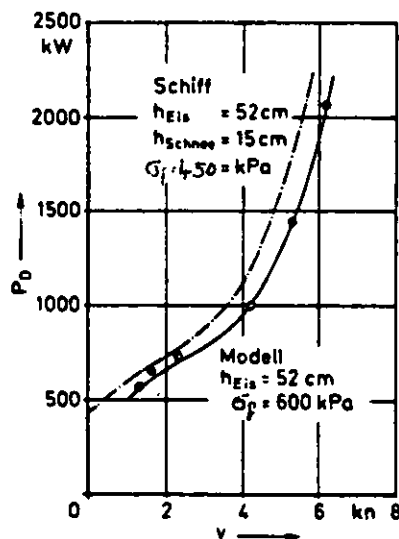


Fig. 13. Comparison between model and full scale test results of power vs. speed for an icebreaker.



Prof. Ernst Enkvist

LEVEL ICE RESISTANCE

1

INTRODUCTION

The term Level Ice is used for virgin ice of constant thickness and 100 % coverage. This ice condition is a theoretical one and it is often hard to find such ice even for testing purposes. For many icebreakers and icebreaking ships level ice is not a proper design condition. Still, it is important enough to be investigated, and it is easier to define than any of those realistic conditions including ice of less than 100 % coverage, refrozen channels, various kinds of ridges etc. Snow is a problem. You may define level ice as snowless, but there usually is snow on top of it. If the snow is hard and weathered it may contribute to ice resistance just as much as if the ice thickness were increased by the snow thickness. Usually the contribution is smaller, say 1/3 to 1/2 of an equal increase in ice thickness.

In ship contracts, it is general practice to guarantee a certain speed at full power in deep, calm water. This can be tested by acceptance trials. For icebreakers and tugs a bollard pull at full power is usually guaranteed. This can also be checked by means of a dynamometer - with some difficulty as the pull may be meganewtons. Now, any responsible naval architect negotiating an icebreaker contract to the shipowner employing him may try to have the builders guarantee an icebreaking performance in level ice. In this situation the responsible naval architect on the shipyard's side must consider whether such performance can be properly demonstrated in acceptance trials. In addition the environmental conditions can vary so much, that such a guarantee must still be considered hazardous. An experienced icebreaker operator will judge the performance quite generally from the power and size and will not require any guarantee for the thickness of level ice broken.

The term Ice Resistance means that the water resistance is deduced from the total resistance. The water resistance is considered not to be influenced by the presence of the ice cover.

2
BREAKDOWN OF RESISTANCE

You are riding a ship in a beautiful field of level ice and wish to find out its resistance. Stop the ship. Descend the pilot's ladders and sample your field for thickness and strength. Increase power slowly until the ship just starts. You read RPM and pitch (if controllable) and compute towing force, i.e. ice resistance to find point A in the plot below. Now, the ship will pick up some speed. Do not touch controls. Read your speed by police radar or sighting poles. When it is constant, take readings and compute point B. Then increase power. When velocity has stabilized, take readings, find C. If there is still level ice around, repeat to get D.

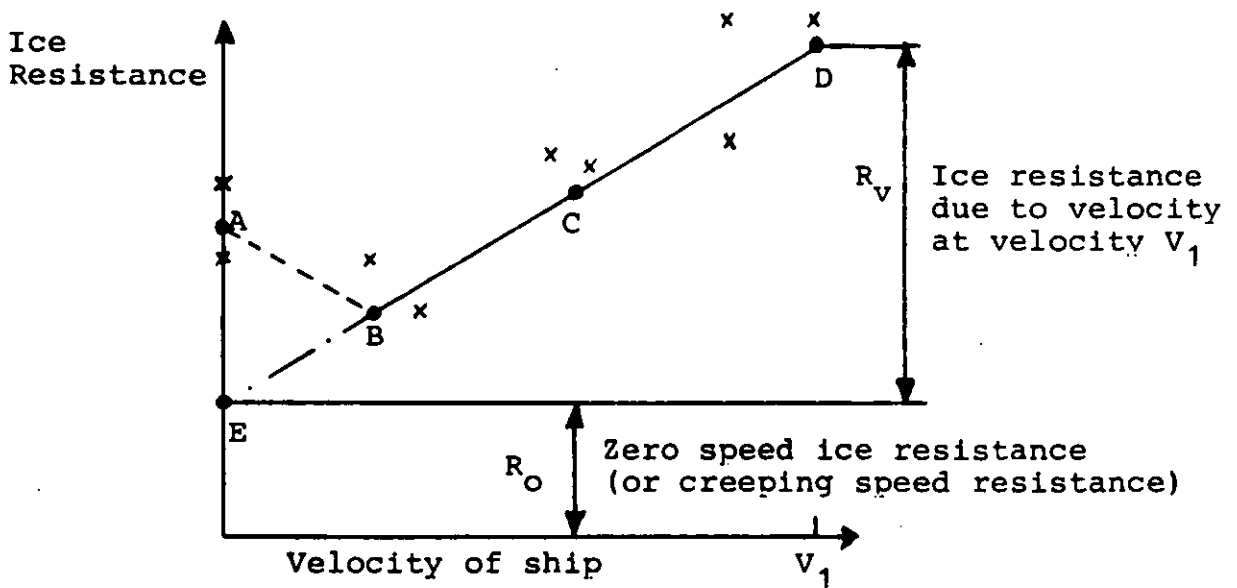


Fig. 1. A full-scale test result.

A thorough look at fig 1 will teach us many basic things, and prevent misonceptions which were common up to abt. 1970.

The x-points added indicate what happens if you repeat your testing - you get scatter even in the same field at constant thickness. Accept it, you have to live with it.

The relatively high starting resistance at A is due to static friction between the ship hull and ice. When it is overcome i.e. changed to sliding friction you get B. The broken line between A and B indicates a part of the thrust-velocity curve for the propulsion system at partial power. If you could decrease power from B you would end up in point E. This is not easy to do in practice. The curve between B and D is more or less a stright line. Considering the complicated phenomena behind it, it can impossibly be a stright line, but considering the scatter you may look at 20 full scale test plots without finding proof of anything else than a stright line.

The plot in fig 1 shows that there is a finite resistance at zero speed, and that it will increase further with velocity. This fact has been self evident to icebreaker operators for about 100 years. Still, litterature before abt 1970 often treated the ice resistance as caused by the mechanical breaking only, ref [1], [2]. Without involving sophistications, such as strain rate dependence etc. the breaking would not cause any velocity dependence.

In ref. [3], followed by [4] and [5] the basic breakdown into components was established as follows:

$$R_{ice} = R_b + R_s + R_v \quad (0)$$

R_b = resistance due to breaking ice

R_s = resistance due to submerging ice

R_v = resistance due to velocity

$$R_o = R_b + R_s$$

In addition, mechanical friction was considered to influence all three components. They all cause their own normal forces against the hull and this will result in tangential friction forces, the longitudinal component of which contributes to resistance.

The student may be interested in the fact that there are other definitions of breakdown, such as in [6]. But these are generally more complicated.

The breakdown of expr. (0) is somewhat illogical, but generally accepted. Breaking and submersion are physical causes of resistance, velocity is a ship operating condition, which will cause a number of physical phenomena.

In ref. [7] friction is defined as a separate component. This is practical, if you vary the coefficient of friction in a model test and plot the ice resistance versus coefficient of friction. The same could be true of any other single parameter, influencing resistance. In fact, expr. 1 relies on an assumption of superposition. This assumption is at least as doubtful as in case of open water resistance.

There are presentations, such as [4] and [5] in which the components are nondimensionalized, just as in open water practice. 10 years of testing, predicting and analysis at Wärtsilä has not left anybody convinced that this is of any assistance, and thus it will not be explained here.

3

ENERGY CONSIDERATIONS

Before starting any analysis of the physical phenomena causing resistance components it might be worthwhile to consider a few basic principles.

The ship's motion through the ice field will cause breaking, crushing and many secondary actions of the ice cover. These phenomena invariably cause a loss of mechanical energy. If the loss can be computed for a particular distance travelled, then the ice resistance is obtained by dividing this energy by the distance:

$$\text{Resistance} = \frac{\text{Energy loss}}{\text{Distance travelled}}$$

This fact seems stupidly simple, but appears to be overlooked when separate forces are used in analysis. Nearly all forces involved in the icebreaking process are intermittent and variable as to direction and size. Energy does not depend on direction, which will simplify analysis.

Take the force to break off a cusp from the edge of a semi-infinite ice cover. According to /1/ it is approximately

$$F = 0,52 \sigma h^2$$

where h is ice thickness and σ is ice bending strength. From this expression most people seem to draw the conclusion that the resistance due to breaking the ice cover is proportional to the ice thickness squared. Consider deflection at breaking:

$$\delta = F / \sqrt{kD}$$

where k is the foundation modulus and D is the flexural rigidity of the plate

$$D = Eh^3 / 12 (1-\nu^2)$$

where E is the apparent modulus of elasticity and ν is Poisson's ratio. The work you have to do to break off a cusp is:

$$F \cdot \delta \cdot 0,5$$

and then you may advance until you must break off the next cusp. The travel between these short energy-loss processes is proportional to cusp width, which is dependent upon the characteristic length (not equal to it):

$$L_C = \sqrt[4]{D/k}$$

To cut it short, if you use these basic formulations you end up with a resistance due to breaking the ice cover, which is proportional to

$$R_b \propto Bh\sigma \cdot \frac{\sigma}{E}$$

where B = ship beam

The truth is much more complicated, and experimental results show an exponent for h which is between 1 and 2.

Finally, consider the following saw-teeth-diagrams:

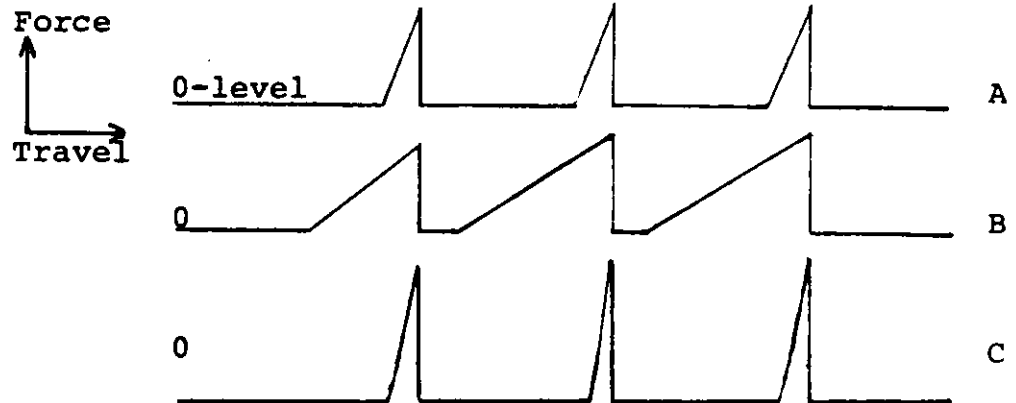


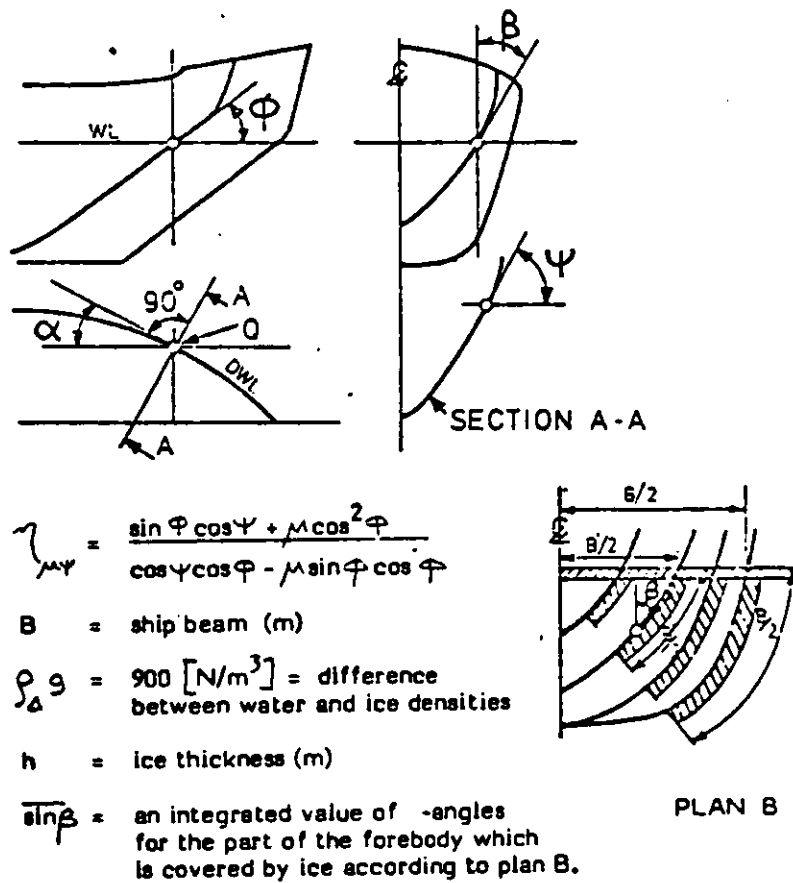
Fig. 2.

These could illustrate the process of breaking off cusps or any other local intermittent process with an arbitrary direction of the original force. The force in the diagram, however, is transformed to longitudinal resistance force by means of direction cosines. The area of the teeth represent energy, and as the distance between teeth is constant it also represents relative resistance. Case C has the highest force, but the smallest resistance. Case B shows a high resistance at the same peak force level as A.

If A represent the work to break ice in pure bending B could show what happens if this process is slowed up by edge crushing or stem shearing, or too low modulus of elasticity in case of model ice. In the latter case the deflection before breaking would be too large.

4
FORM AND DIRECTION COSINES

For icebreaking ships, the form parameters used in general ship design are insufficient. The coefficients of fullness (block-, prismatic etc.) are of no particular significance for the ice resistance. The half angle of entrance of the design waterline, α , is significant. The stem angle with horizontal, ϕ is important but insufficient alone. There is no international standard of angles for icebreaking ship forebodies, but the following notation is used by Wärtsilä:



The angles for μ_{ψ} for the purpose of expression (1) are selected approximately at $B/4$ to simulate a point of contact for a rectangular presawn ice floe.

Fig. 3. Symbols and definitions for expression (1).

Fig. 3 also shows the cumulative friction formfactor $\eta_{\mu\psi}$. This is a kind of direction cosine and is defined by

$$\eta_{\mu\psi} = \frac{\text{momentary total longitudinal force}}{\text{momentary vertical net force}} = \frac{F_x}{F_z}$$

This factor could be applied locally, using the local angles, or for the whole forebody, using average angles. For its derivation, see ref [2].

Any similar direction cosines may be derived. Friction will be an important factor. For a presentation of direction cosines, see ref. [3].

For $\eta_{\mu\psi}$ the influence of friction will be most critical in case of steep bow angles. The ice edge will not be pushed down if μ is too high and angles too steep. Then, the ice would fail in buckling instead of bending, which would increase resistance enormously.

In practice, there are no single factors, like $\eta_{\mu\psi}$, which are sufficient to explain the influence of form on level ice resistance. Still, form is important, friction is very significant, and analysis based on $\eta_{\mu\psi}$ above is worthwhile, as long as conclusions are not stretched, producing radical innovations in form, which will cause "off-design"-trouble in open water, bad turning ability or other modes of navigation in ice, such as slush or ridges.

In the icebreaking process, the broken ice slides down and covers a large part of the underwater hull surface. Still, the form parameters near the stem and along the bows near the waterline have a dominating influence on ice resistance.

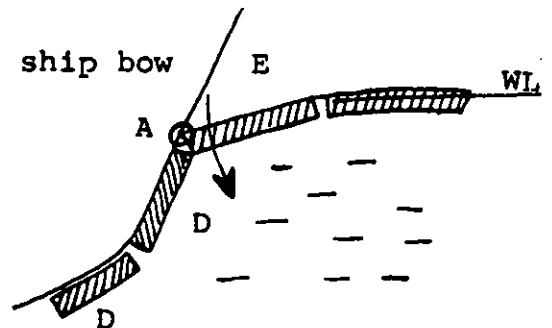
5
CAUSE OF RESISTANCE COMPONENTS

The following presentation is a personal, qualitative, undocumented, brief presentation of the real physical phenomena behind the components. It is based on experience in analysis and observations of full-scale and model tests. The causal explanations are put roughly in order of quantitative importance.

Mechanical friction is not separately mentioned, it is associated with all phenomena causing normal forces against the shell, and it is of large quantitative importance.

R_b , breaking resistance

- crushing of ice edge at A (fig. 4)
- crushing and shear of ice edge at stem, along B
- Bending failure, circumferential crack C



R_s , submersion resistance

- turning floes after breaking. Point A slides down along hull pushing previously broken floes D further down
- the sliding of floes D until maximum submersion, i.e. the hull will slide along a cover of submerging floes, see fig. 3, plan B
- the sliding of the hull along fully submerged floes covering a part of the parallel midbody
- sliding along floes pressed against hull by wedging or ice pressure.
(This may be a very large resistance in a really pressurised ice field)

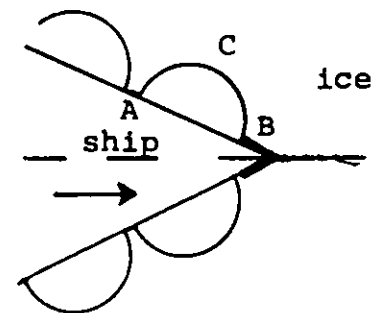


Fig. 4.

R_v , velocity resistance

- turning floes against hydrostatic pressure due to ventilation, i.e. air at E, fig. 4
- accelerating floes including a dominant entrained mass of water in the turning down process and including the train of previously broken floes, D
- turning floes against the bow-wave pressure

At high velocity dynamic phenomena must interfere heavily with the static phenomena included in R_b and R_s . Thus, the size of broken floes becomes much smaller at high speed. Model tests have indicated that the breaking resistance is not speed dependent at moderate velocities, but the test material is not large.

6
RELATIVE IMPORTANCE OF COMPONENTS

The static components, R_b and R_s , are measured together, and therefore it has not been quite clear what their proportion is. If R_b is derived theoretically from bending failure only it comes out as insignificantly small. This is not true. In a recent publication, ref. [8] an experimental survey was presented, which produced the following result:

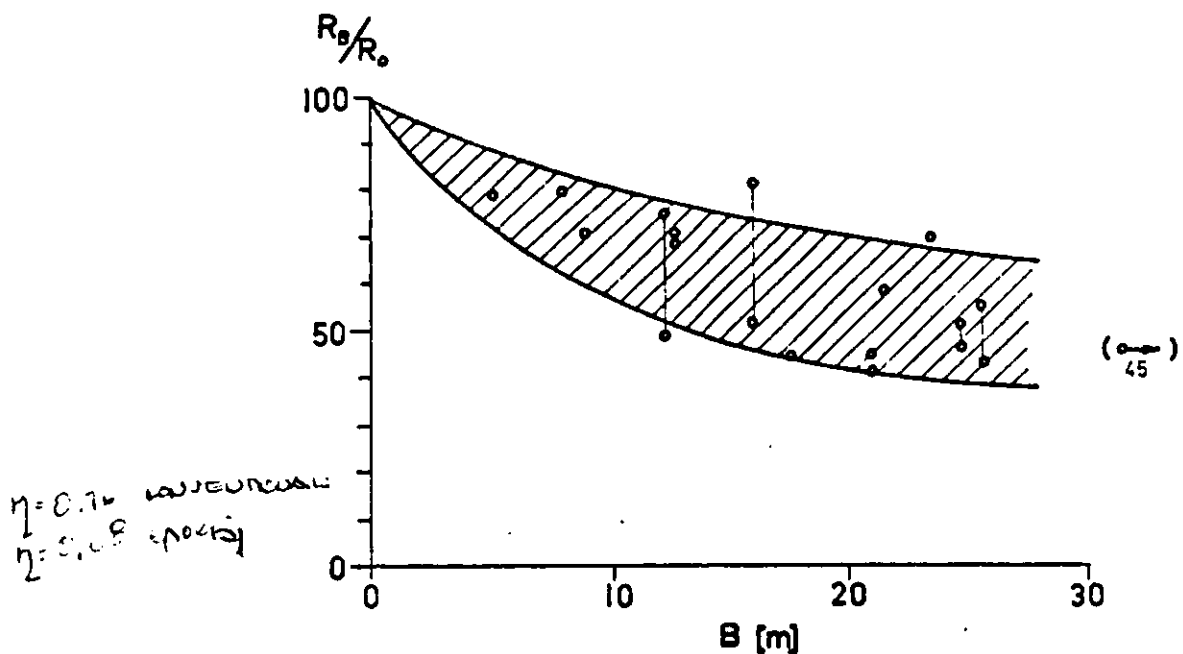


Fig. 5. Percentage of R_b to total zero speed resistance R_0 versus ship beam.

This plot was obtained from a large experimental material combining model- and full scale results. In model tests R_b may be eliminated by presawing, i.e. simulating breaking cracks by sawing them before testing. From such tests a semi-analytical expression was derived:

$$R_s = \rho_{\Delta} g (3,9 B^2 h \mu \sin \beta + 12,2 \cdot B h^2 \eta_{\mu \psi}) \quad [N] \quad (1)$$

Then the total $R_0 = R_b + R_s$ at zero speed was obtained from 16 full-scale tests. When their R_s was computed from (1) and deduced from R_0 fig. 5 was obtained, and R_b came out as 40...80 % of R_0 , the highest percentages for the smallest ships.

If you have no better methods of prediction you may use expression (1) combined with fig. 5 to find out point E in fig. 1.

Having applied such an approach it only remains to predict the velocity resistance. Instead of presenting any original expression I prefer referring to [3], [5] and [9].

If you are in a terrible hurry and your supervisors ask for a tentative estimate immediately, then use:

$$R_v \approx 45 B h^{1,3} \quad [kN] \quad \text{at } 3 \text{ [m/s] velocity}$$

Even if you use a sophisticated prediction method, your result may be grossly optimistic if you have to test the ship in $-40^{\circ}C$ and 40 cm of hard arctic snow.

7
RESISTANCE PREDICTIONS AND DESIGN

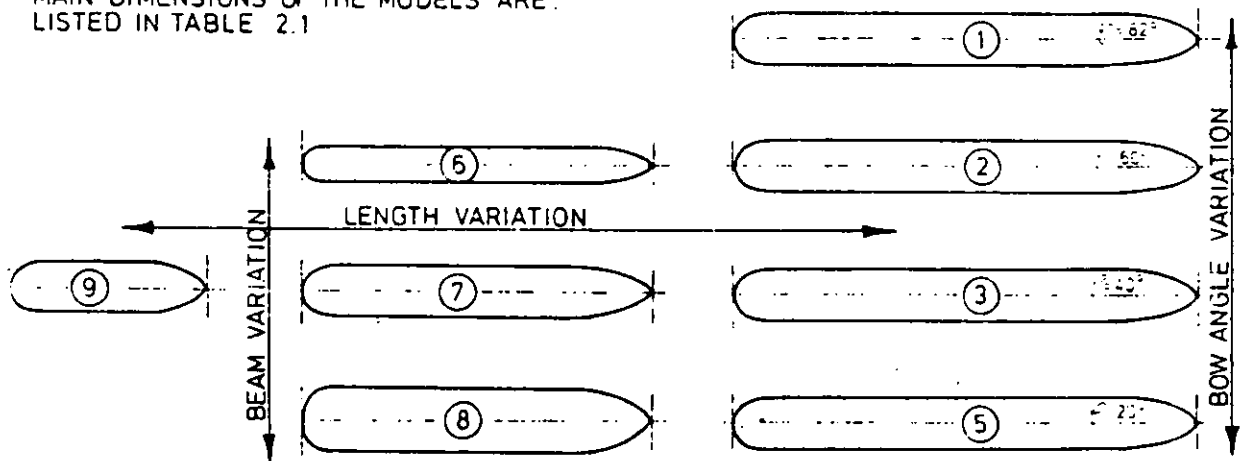
In paragraph 6 an approach to prediction was presented. Generally, it might be stated that the highest levels of confidence are obtained if you possess a large number of full scale results, feed them all into a regression analysis, test a number of form parameters for correlation and establish a prediction formula, which has nothing to do with the real physical phenomena in icebreaking. This may work admirably, as long as your new cases resemble those, which formed the data basis for your analysis.

If you make innovations, and have to find out their effect on resistance, then a model test is probably the most cost effective method.

In laying down the proportions and lines for a new design it might be of interest to consider the influence of certain parameters one by one. Ref. [10] reports on a nearly systematic model test series, fig. 6.

8 MODELS WITH SYSTEMATICALLY VARYING PARAMETERS

MAIN DIMENSIONS OF THE MODELS ARE LISTED IN TABLE 2.1



MODEL No. 4 WITH BULBOUS BOW

⑨ = MODEL No. 2

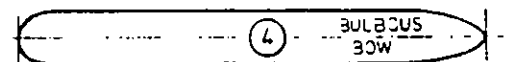


Fig. 6. Marad series.

The influence of bow angle ϕ came out as fig. 7 shows.

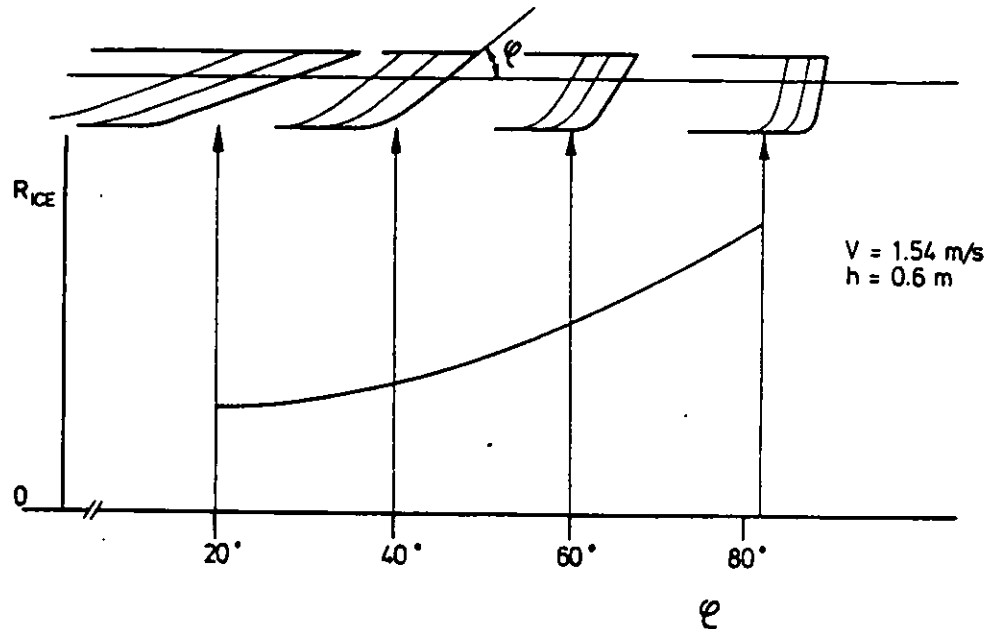


Fig. 7. Bow angle influence from marad-series.

An increase in the bow angle of entrance, α , will generally cause a decrease in resistance. The ultimate case is a landing craft bow, which is not considered ship-shape for openwater passages and may cause pushing of broken floes or bad steering.

Beam is an important parameter. For moderate variations resistance may be taken as proportional to beam. For influence of narrow channels, see ref. [11].

Lentht will increase resistance, but much less than beam. In pressurised ice length is critical.

Draft has an insignificant influence on resistance but low draft results in propulsion difficulties.

REFERENCES

REFERENCES

1. Runeberg R.: Steamers for Winter Navigation and Icebreaking. Minutes of Proceedings of the Institution of Civil Engineers, Vol. XCVII, session 1888-1889, part III.
2. Шиманский, Е.А.: Условные измерители ледовых качеств судов. (Conditional Standards of Ice Qualities of a Ship). Труды ДАНИИ Т 130, 1939.
3. Каштелян, В.И., Позняк, И.И., Рывлин, А.Я.: Сопротивление льда движению судна. (Ice Resistance to Motion of a Ship). "Судостроение", Ленинград 1968.
4. Lewis, J.W., Edwards, R.Y.: Methods for Predicting Ice-breaking and Ice Resistance Characteristics of Icebreakers. SNAME, 1970.
5. Ernst Enkvist: On the Ice Resistance encountered by Ships operating in the Continuous Mode of Icebreaking. Report No 24, 1972.
6. Milano, V.R.: Ship Resistance to Continuous Motion in Ice. Dissertation. Stevens Institute of Technology, 1972.
7. Poznyak, I.I. & Ionov, B.P., The Division of Icebreaker Resistance into Components. Spring Meeting/STAR Symposium, Ottawa 1981, SNAME.
8. Ernst Enkvist: A Survey of Experimental Indications of the Relation between the Submersion and Breaking Components of Level Ice Resistance to Ships. POAC-83.
9. Jack W.Lewis, Frank W. DeBord, Vanya A.Bulat: Resistance and Propulsion of Ice-Worthy Ships. SNAME-82.
10. Great Lakes Ore Carrier Series Ice Resistance Model Test Program for MARAD, WIMB Test Report No.18, December 29, 1972, Helsinki.
11. V.I.Kashtelyan and L.G.Tsoy: Study of Ship Ice Performance in Narrow Channels. SNAME, STAR Symposium-81.
12. Naegle, J.N.: "Ice-Resistance Prediction and Motion Simulation for Ships in the Continuous Mode of Icebreaking". Ph.D.Dissertation, University of Michigan, Ann Arbor, 1980.

MARKED RELEVANT
MAY 1975





Dicks Wright

WEGEMT 1983
XVI

W ESTERN
E UROPEAN
G RADUATE
E DUCATION
M ARINE
T ECHNOLOGY

SEVENTH GRADUATE SCHOOL
SHIPS AND STRUCTURES
IN ICE

LECTURE NOTES
ON
PROPULSION COEFFICIENTS
AND PROPELLER DESIGN FOR
ICEBREAKING SHIPS

BY
JACK W. LEWIS, PRESIDENT

NOMENCLATURE

- C_B = block coefficient
- C_p = prismatic coefficient
- C_x = midship's area coefficient
- f = hull-ice friction factor
- g = acceleration of gravity
- h = ice thickness
- n = propeller shaft speed
- t_i = constant of proportionality or thrust deduction factor in ice
(the subscript "i" is used to denote icebreaking)
- t_p = constant of proportionality or the so called "thrust deduction
factor" while towing. (The subscript "p" is used to denote
pulling)
- w_i = $(V-V_a)/V$ = wake fraction, icebreaking
- w_p = wake fraction, towing
- B = maximum beam at operating waterline
- D = propeller diameter
- E = ice elastic modulus
- EHP = useful output power
- DHP = developed horsepower
- DHP_i = developed horsepower, icebreaking
- EHP_i = useful output power, icebreaking
- F = a function
- G = a function
- H = ship draft
- J_a = V_a/nD , propeller advance coefficient
- J_m = V/nD , measured advance coefficient

- $K_Q = Q_0/\rho n^2 \eta^5$ = torque coefficient, open water
- $K_{QBP} = Q_{BP}/\rho n^2 D^5$ = measured torque coefficient, towing
- $K_T = T_0/\rho n^2 D^4$ = thrust coefficient, open water
- $K_{TBP} = T_{BP}/\rho n^2 D^4$ = measured thrust coefficient, towing
- L = ship length at operating waterline
- P = tow rope pull
- P/D = propeller pitch-diameter ratio
- Q_{Ri} = shaft torque, icebreaking
- Q_{BP} = shaft torque measured just before the stern tube bearing towing
- Q_0 = propeller torque measured without the ship present
- R_i = pure hull ice resistance
- R_{iw} = ice and water hull resistance (towed)
- R_{ow} = open water hull resistance (towed)
- T_{Bi} = shaft thrust (behind in ice)
- T_{BP} = shaft thrust (behind pulling)
- T_0 = propeller thrust measured without the ship present
- V = ship speed
- V_a = advance speed of propeller
- ∇ = ship displacement
- ΔR_{iw} = hull resistance augmentation due to propeller hull-ice interactions (in ice covered water)
- ΔR_{owp} = hull resistance augmentation due to propeller hull interactions (in ice free water)
- α = attack angle on propeller
- β = advance angle of propeller

- ϕ = pitch angle of propeller
- ρ_i = mass density of ice
- ρ_w = mass density of water
- σ_c = ice crushing strength
- σ_f = ice flexural strength
- $\eta_{\eta p}$ = EHP/DHP = quasi-propulsive efficiency, towing
- η_o = open water propeller efficiency
- η_{HP} = hull efficiency, towing
- η_{RP} = relative rotative efficiency, towing
- η_{D_i} = EMP_i/DHP_i = quasi-propulsive efficiency, icebreaking
- η_{H_i} = hull efficiency, icebreaking
- η_{R_i} = relative rotative efficiency, icebreaking

At the heart of the ship design process is the problem of selecting power required and the propeller to deliver it. The problem is faced not only by ice-worthy ship designers; open water surface ship designers and submarine designers have dealt with the problem for decades. The data required to solve this design problem falls into three groups.

- First, we need data on the resistance of the hull. For ice-worthy ships this includes not only water resistance, but also resistance in various ice conditions which are to be encountered along the trade route.
- Next, we need design data on suitable propellers. Normally, these are in the form of thrust and torque characteristics as a function of shaft speed, advance speed, pitch/diameter ratio, expanded area ratio, etc.
- Finally, we require data on the interaction coefficients of these propellers with the ship's hull. In the case of ice-worthy ships this must include the effects of ice.

In the design of ice-worthy ships, large gaps exist in the available data necessary to solve this problem. In the following lecture, and others during this course, attention will focus on the estimation of the hull ice resistance. This lecture will focus on the almost total lack of data concerning propeller/hull/ice interaction coefficients, namely thrust deduction, wake fraction, and relative rotative efficiency. We will then proceed to describe design procedures for selecting propellers utilizing the available data.

I. PROPULSION: THE INTERACTION BETWEEN HULL, PROPELLER AND ICE

The operating regime of a propeller on an ice-worthy ship is similar to that for a tugboat. For example numerous route analysis studies of proposed icebreaking tankers have shown that the majority of shaft horsepower hours accumulated during a round trip voyage occur at low ship speeds under nearly full power operation. Minimum fuel consumption considerations dictate that the propeller be designed for maximum efficiency under "over-load" conditions. This means that information regarding propulsive coefficients under overload conditions must be available. Thrust deduction, wake fraction, and relative rotative efficiency coefficients are considerably different under overload conditions when compared to free running conditions. Consequently, the discussion will start with an investigation of the propulsive coefficients under open water overload conditions and then continue with a discussion of ice effects on these parameters.

A. Thrust Deduction

The force balance equation for a single screwed ship under towing conditions is shown in Figure 1 and can be expressed as

$$T_{BP} = P + R_{ow} + \Delta R_{owp} \quad (1)$$

where T_{BP} = shaft thrust (Behind Pulling)

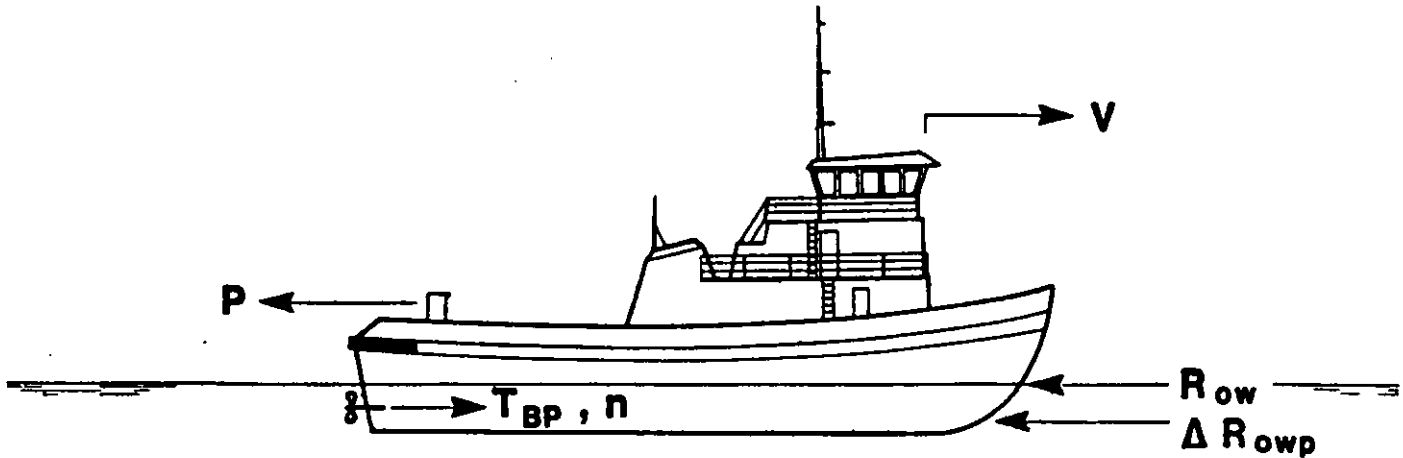
P = tow rope pull

R_{ow} = open water hull resistance (towed)

ΔR_{owp} = hull resistance augmentation due to propeller-hull interactions.

It is general practice to express ΔR_{owp} as a fraction of T_{BP} . That is

$$\Delta R_{owp} = t_p * T_{BP} \quad (2)$$



$$T_{BP} = P + R_{ow} + \Delta R_{owp}$$

Figure 1. Overload condition force balance.

where t_p = constant of proportionality or the so-called "thrust deduction factor" while towing. (The subscript "p" is used to denote pulling)

Substituting (2) into (1) and rearranging gives

$$t_p = \frac{T_{BP} - (P + R_{ow})}{T_{RP}} \quad (3)$$

Usually, thrust deduction factors are plotted as a function of ship speed, V . But this is inappropriate for the towing conditions. Since R_{ow} is a function of ship speed and T_{BP} is a function of ship speed and shaft speed, n , then t_p must be a function of V and n . Harvald [1963] shows that the thrust deduction factor can be expressed as a function of the measurable advance coefficient

$$J_m = V/nD \quad (4)$$

where V = ship speed
 n = shaft speed
 D = propeller diameter

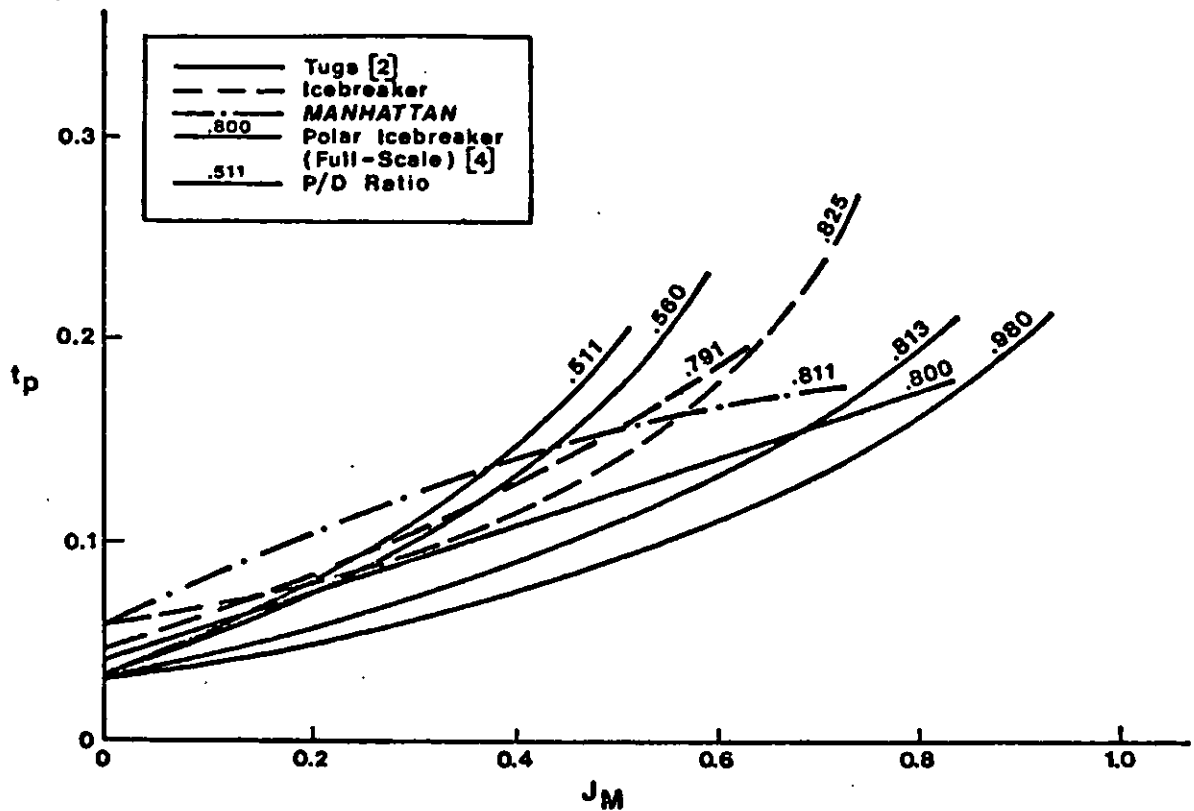


Figure 2. Thrust deduction while towing.

Harvald analyzed the Parker and Dawson [1962] tugboat data and showed that the thrust deduction factor varies from a low of about 0.04 at $J_m = 0$ to a high of about 0.20 at values of J_m depending upon the pitch-diameter (P/D) ratio of the propellers. Similar results can be obtained from overload model tests of ice-worthy ships. Figure 2 shows thrust deduction factors as a function of J_m for several ice-worthy ships along with the tug data analyzed by Harvald. This data clearly indicates that there is little thrust deduction at near bollard condition and that thrust deduction varies almost linearly

with J_m over the range of normal towing speeds. These results were further confirmed during full-scale over-propulsion tests of a triple screw icebreaker conducted by DeBord, et al. [1981].

Open water model tests are usually used to determine thrust deduction factors. Captive, towed model tests are used to measure R_{ow} and self-propelled, overload model tests with varying values of tow rope pull and model speed are used to measure shaft thrust. Equation (3) is then used to compute the thrust deduction factors from the measured data. These calculations are very prone to error because t_p is computed based on the difference between two very large numbers (T_{RP} and $P + R_{ow}$).

Full-scale trials can also be conducted to determine thrust deduction factors. While these tests are expensive they are important for determining model-prototype correlation. Recently, such full-scale tests were conducted by DeBord, et al. [1981] on a large polar icebreaker. These tests indicated that towing thrust deduction factors measured in a model agreed reasonably well with those measured during ship trials. Consequently, it can be safely assumed that model-scale effects on open water thrust deduction are negligible.

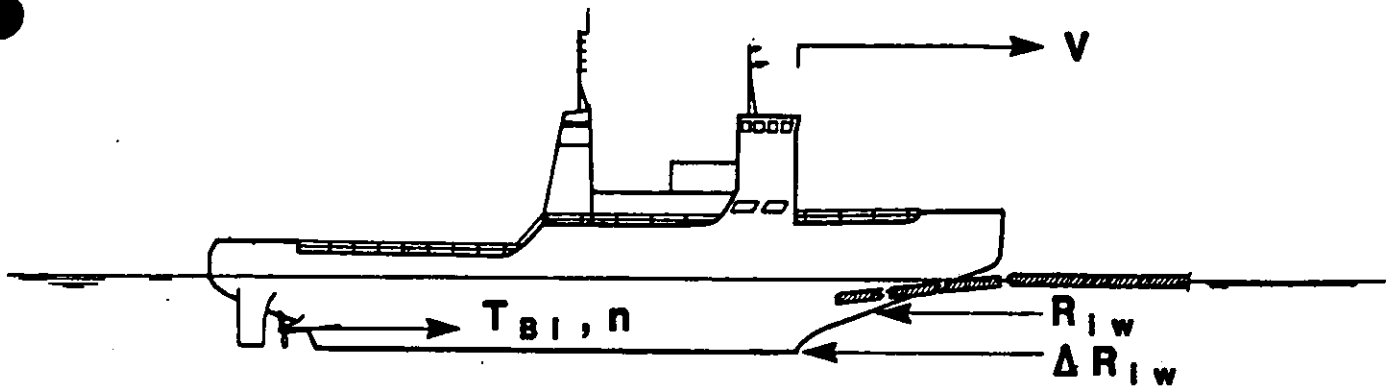
Consider now the following force balance equation for an ice-worthy ship breaking level ice, as shown in Figure 3.

$$T_{Bi} = R_{iw} + \Delta R_{iw} \quad (5)$$

where T_{Bi} = shaft thrust (Behind in ice)

R_{iw} = hull resistance in ice and water (towed)

ΔR_{iw} = hull resistance augmentation due to propeller
hull-ice interactions.



$$T_{Bi} = R_{iw} + \Delta R_{iw}$$

Figure 3. Icebreaking condition force balance.

As before, ΔR_{iw} is expressed as a fraction of T_{Bi}

$$\Delta R_{iw} = t_i \times T_{Bi} \quad (6)$$

where t_i = constant of proportionality or thrust deduction factor in ice (The subscript "i" is used to denote icebreaking)

Substituting (6) into (5) and rearranging gives

$$t_i = \frac{T_{Bi} - R_{iw}}{T_{Bi}} \quad (7)$$

Equation (7) is quite similar to Equation (3) and this similarity suggests an important means (hereafter referred to as the "shaft thrust method") to infer full-scale hull ice resistance from full-scale trials data. As is the case with the determination of open water thrust deduction, the accuracy of t_i is compromised by the calculation of the difference of two large values, (T_{Bi} and R_{iw}). In addition these values are subject to large fluctuations due to nonhomogenous ice conditions and the periodic nature of icebreaking action.

If we assume that the thrust deduction factor in ice (t_i) is equal to the thrust deduction factor during open water towing (t_p) then

$$R_{iw} = P + R_{ow} \quad (8)$$

Thus, given the function t_p versus J_m from model tests, and given a set of values v , n and T_{Bi} from full-scale trials, one could obtain R_{iw} by computing J_m , looking up t_p , and multiplying by T_{Bi} to get R_{iw} .

$$R_{iw} = (1-t_p) \times T_{Bi} \quad (8a)$$

To investigate the validity of the assumption that $t_i = t_p$, self-propelled model data collected during icebreaking and open water towing must be analyzed. It should be understood, before discussing the results, that a self-propelled model test in ice has only recently been attempted and hence little data is available. In order to compute t_i , a means of estimating R_{iw} must be available. For model tests, this estimate is obtained by first conducting captive, towed resistance tests in ice and then fairing the results. Unlike open water testing, a great deal of scatter exists in ice model test data and this considerably complicates the problem of estimating t_i . The results of one such analysis, shown in Figure 4, clearly reveal the problem. In this figure, values for t_i computed using Equation (7) and the ice model data are plotted along with the open water test results. The scatter in the t_i data is so great that all one can say is that the data provides no evidence which would indicate that t_i is or is not equal to t_p . Much more work is needed in this area. In particular, more self propelled ice model test data are needed in order to isolate data trends.

B) Propulsive Efficiency, Wake Fraction and Relative Rotative Efficiency

The input power required to sustain a given towing speed in open water depends on the propulsive efficiency. This efficiency can be expressed as the ratio of the useful output power (or EHP) to the required input power (developed horsepower or DHP). In the case of towing, EHP must include the towrope pull. Thus

$$EHP = \frac{(P + R_{ow}) V}{550} \quad (9)$$

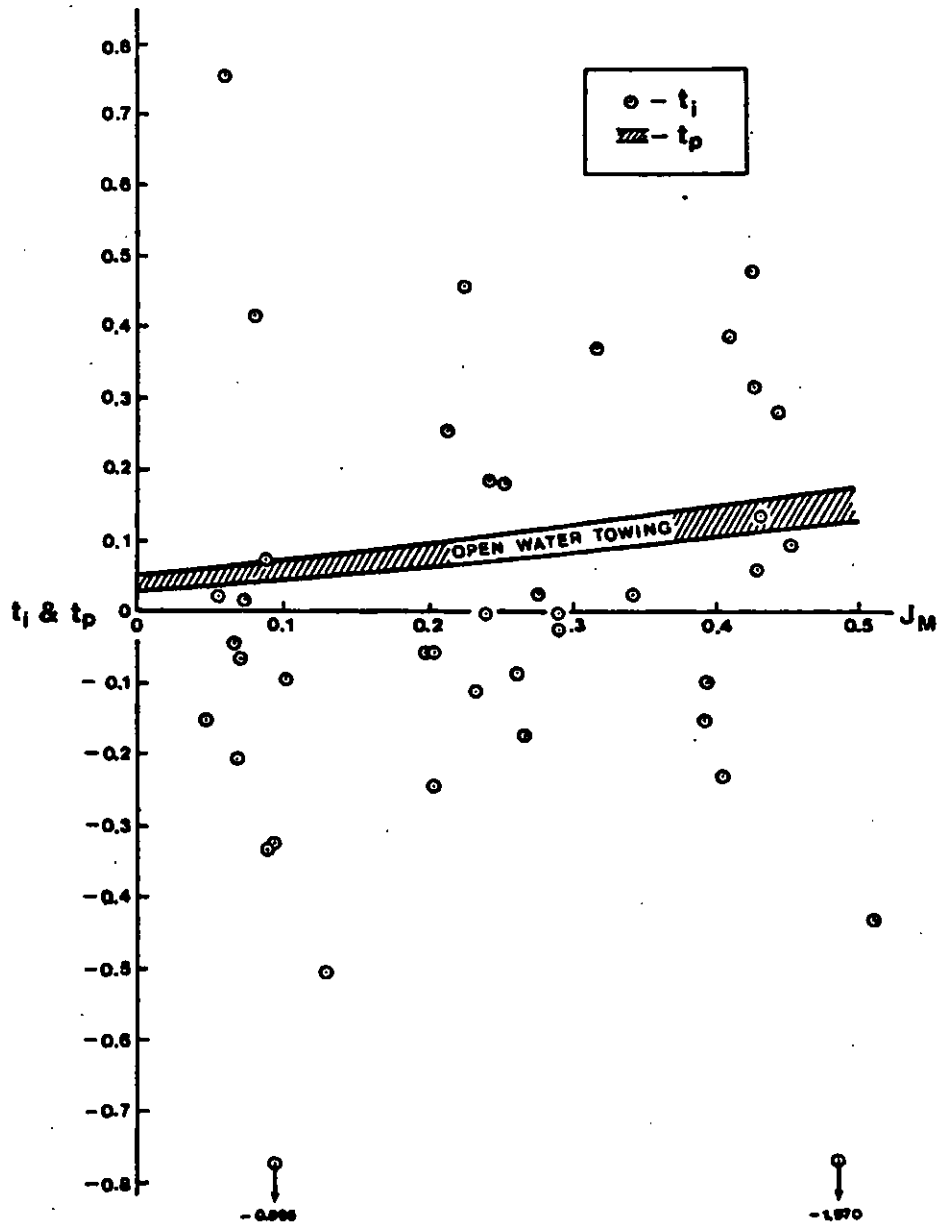


Figure 4. Thrust deduction factors during icebreaking and towing from model scale tests.

It should be noted that in the towing case the EHP is not exclusively a function of hull form as it is in the free running case.

The input or developed horsepower is given by:

$$DHP = 2\pi n Q_{BP} / 550 \quad (10)$$

where Q_{BP} = shaft torque measured just before the stern tube bearing

The ratio of EHP/DHP is generally referred to as the quasi-propulsive efficiency, η_{DP} , and for towing is equal to

$$\eta_{DP} = \frac{EHP}{DHP} = \frac{(P + R_{ow})V}{2\pi n Q_{BP}} \quad (11)$$

The subscript P is used as a reminder that this is for the towing condition.

The quasi-propulsive efficiency is generally subdivided into three components: open water propeller efficiency, hull efficiency and relative rotative efficiency. The open water propeller efficiency, η_0 , is given by

$$\eta_0 = \frac{T_0 V_a}{2\pi n Q_0} \quad (12)$$

where T_0 = propeller thrust measured without the ship present

Q_0 = propeller torque under same conditions

n = propeller shaft speed

V_a = advance speed of propeller

The advance velocity of the propeller and the ship speed are related by the "wake function" which is by definition

$$w_p = \frac{V - V_a}{V} \quad (13)$$

Then:

$$\frac{V}{V_a} = \frac{1}{1 - w_p} \quad (13a)$$

Equations (3), (12) and (13a) may be substituted into (11) to give

$$\eta_{DP} = \frac{1 - t_p}{1 - w_p} \times \frac{T_{BP}}{T_o} \frac{Q_o}{Q_{RP}} \times \eta_o \quad (14)$$

The first term on the right hand side of Equation (14) is called the hull efficiency while towing, η_{HP} . The second term is called the relative rotative efficiency while towing, η_{RP} . Obviously, in order to compute the power required to overcome the total resistance ($P + R_{OW}$) while towing, it is necessary to have information on the relative efficiency and the wake fraction, as well as the thrust deduction.

The relative rotative efficiency is an artifice of data analysis procedures. That is, it exists in Equation (14) because of our desire to separate out of the quasi-propulsive efficiency that part due to the open water propeller efficiency. As such, the value of the relative rotative efficiency depends on the method (torque or thrust identity) used to obtain the open water propeller efficiency. In the thrust identity method (used throughout this lecture), the value of K_{TBP} is calculated from measured data and used as the entering argument for the open water propeller curves. Thus, T_{BP} is assumed equal to T_o (hence the name thrust identity) and as a result

the relative rotative efficiency is equal to Q_0/Q_{BP} . The value of J_a found from the K_T curves is then used to find K_{Q0} and hence Q_0 . The relative rotative efficiency is then easily computed. Frequently, relative rotative efficiency is reported in model test reports without reference to the method used to compute it. This misleading practice probably contributes to the mystery which seems to surround this coefficient.

The method (torque or thrust identity) used to obtain open water propeller efficiency also affects the value obtained for wake fraction. Hence, it too is an artifice of data analysis procedures. In addition to this complication a careful analysis of propulsion data under towing conditions reveals that values for wake fraction can be considerably different from those at the self-propulsion point. This is of great importance in tugboat design and is frequently overlooked by designers who usually work only at the self-propulsion point.

Harvald gives much insight into the behavior of wake fractions at extreme propeller loadings. A very useful concept was taken from his work and used in the analysis of ice-worthy ship propulsion. The wake fraction can be determined by use of propeller diagrams in which curves of the propeller coefficients behind the ship (K_{TBP} and K_{QBP}) are plotted against the advance coefficient in addition to the corresponding open water propeller curves. The following equations for V and V_a ,

$$V = J_m nD \quad (15)$$

$$V_a = J_a nD \quad (16)$$

are substituted in Equation (13) to give

$$w_p = \frac{J_m - J_a}{J_m} \quad (17)$$

Consequently, wake fraction can be obtained directly from the propeller diagrams using either the thrust or torque identity method.

Figure 5 shows the application of this graphical method to determine w_{pQ} (torque identity) from K_Q curves. Values for w_{pT} can be obtained in a similar manner using k_T curves (thrust identity).

Figure 6 shows the propeller characteristics and resulting relative rotative efficiency and wake fraction for a typical icebreaking hull form under open water towing conditions obtained from model data. The data clearly shows the large differences in wake fraction under towing and free running conditions. The choice of J_m as the abscissa for plotting η_{Rp} and w_p is arbitrary. However, it will be seen later that this eliminates ambiguity when attempting to use relative rotative efficiency and wake fraction data during propeller design.

The input power required to sustain a given ship speed while icebreaking can be expressed in a manner similar to that used for towing. The quasi-propulsive efficiency for icebreaking becomes

$$\eta_{Pi} = \frac{EHP_i}{DHP_i} = \frac{R_{iw} V}{2 \pi n Q_{Pi}} \quad (18)$$

where the subscript i is used as a reminder that this is for icebreaking.

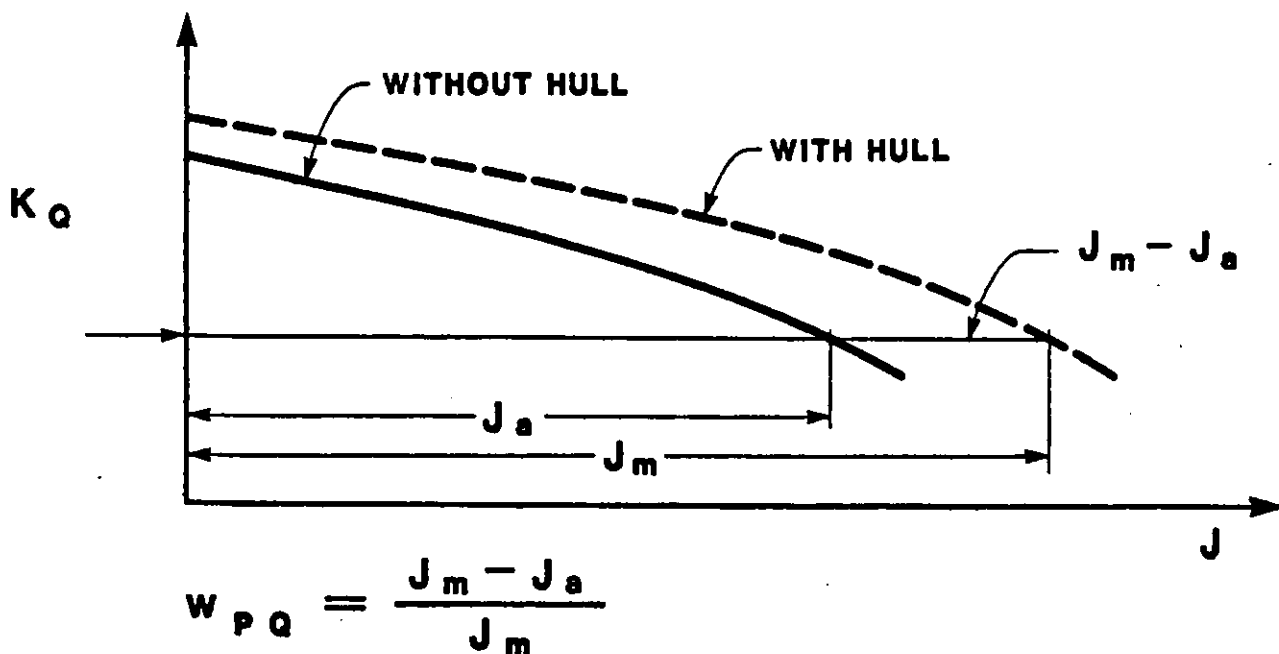


Figure 5. Graphical determination of wake fraction.

The quasi-propulsive efficiency for icebreaking can also be subdivided into the open water propeller efficiency, hull efficiency and relative rotative efficiency. The latter two efficiency definitions are given by:*

$$\eta_{H_i} = \frac{1 - t_i}{1 - w_i} \quad (19)$$

and

$$\eta_{R_i} = \frac{T_{B_i}}{T_0} \frac{Q_0}{Q_{B_i}} \quad (20)$$

where

$$w_i = \frac{V - V_a}{V} \quad (21)$$

* Juurmaa and Segercrantz [6] take a different approach. They give $\eta_{p_i} = \eta_{H_i} \eta_{R_i} \eta_{0_i}$ where η_{0_i} is obtained from model propeller dynamometer tests in ice without the hull. This approach has not been followed in the present paper because model propeller dynamometer tests in ice are not yet known to produce meaningful results. It should also be carefully noted that Juurmaa and Segercrantz's η_{H_i} and η_{R_i} differ from those used by the present authors because the definitions of w_i differ.

There is great similarity between Equations (10) and (11) and this similarity suggests yet another means (hereinafter referred to as the "shaft torque method") to infer full-scale hull ice resistance from full-scale trials data. If the quasi-propulsive efficiency in ice equals the towing quasi-propulsive efficiency, then hull resistance can be obtained as follows.

A plot of quasi-propulsive efficiency for towing is prepared from open water model or full-scale data as a function of developed horsepower and ship speed. Values for developed horsepower and ship speed during icebreaking are then used as entering arguments for this plot and the quasi-propulsive efficiency obtained. Equation (18), with $\eta_{ij} = \eta_{jp}$, is then used to compute R_{iw} .

To investigate the validity of the assumption that η_{ij} equals η_{jp} , it is necessary to determine if both the hull efficiency and relative rotative efficiency while ice-breaking are the same as when towing. The hull efficiency involves both thrust deduction and wake fraction. Thrust deduction in ice has already been discussed so attention will now be given to wake fraction and relative rotative efficiency in ice.

Fortunately, both of these latter parameters can be determined from full-scale data using the previously discussed method suggested by Harvald. Plots of K_{TBi} and K_{QB_i} vs J_m are prepared from the full-scale trials data and plotted along with the corresponding open water propeller curves. Figure 6 shows full-scale thrust identity wake fraction and relative rotative efficiency data in ice for the icebreaker previously discussed in Figure 3. The open water towing wake fraction and relative rotative efficiency is also shown in this figure for purposes of comparison. It can be seen that the icebreaking wake fraction is considerably different from the towing wake fraction, but the relative rotative efficiencies are roughly the same.

Plots similar to those shown in Figure 7 have been prepared for several icebreakers in which full-scale data is available. In each case, the influence of icebreaking on relative rotative efficiency and wake fraction was found to be similar to that shown in Figure 7. Apparently the submerged ice pieces, which surround the hull and strike the propeller while icebreaking,

significantly change the water flow pattern into, and the speed of, the propeller causing the propeller to observe a great decrease in advance velocity.

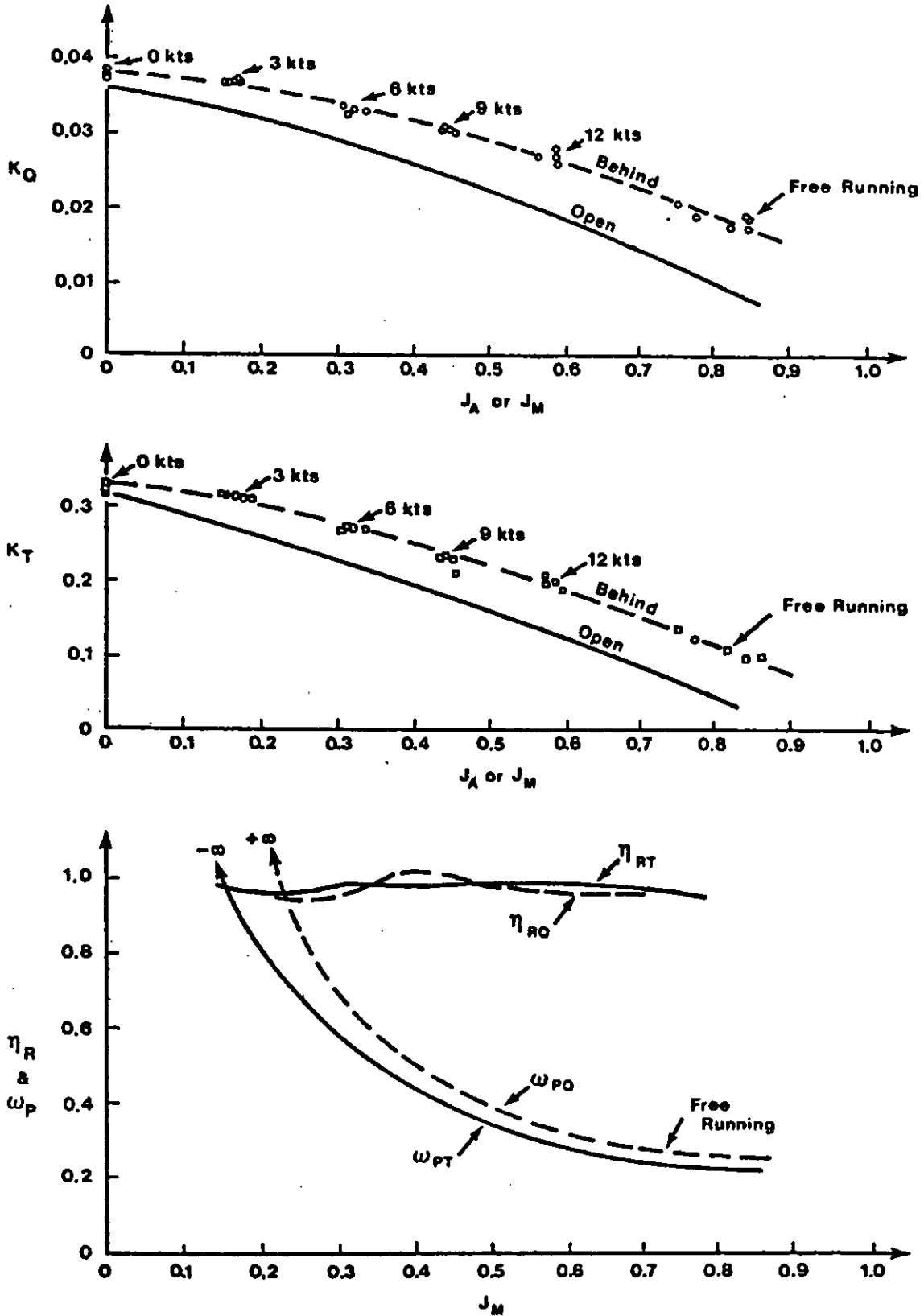


Figure 6. Relative relative efficiency and wake fraction in ice free water (free running to bollard condition)

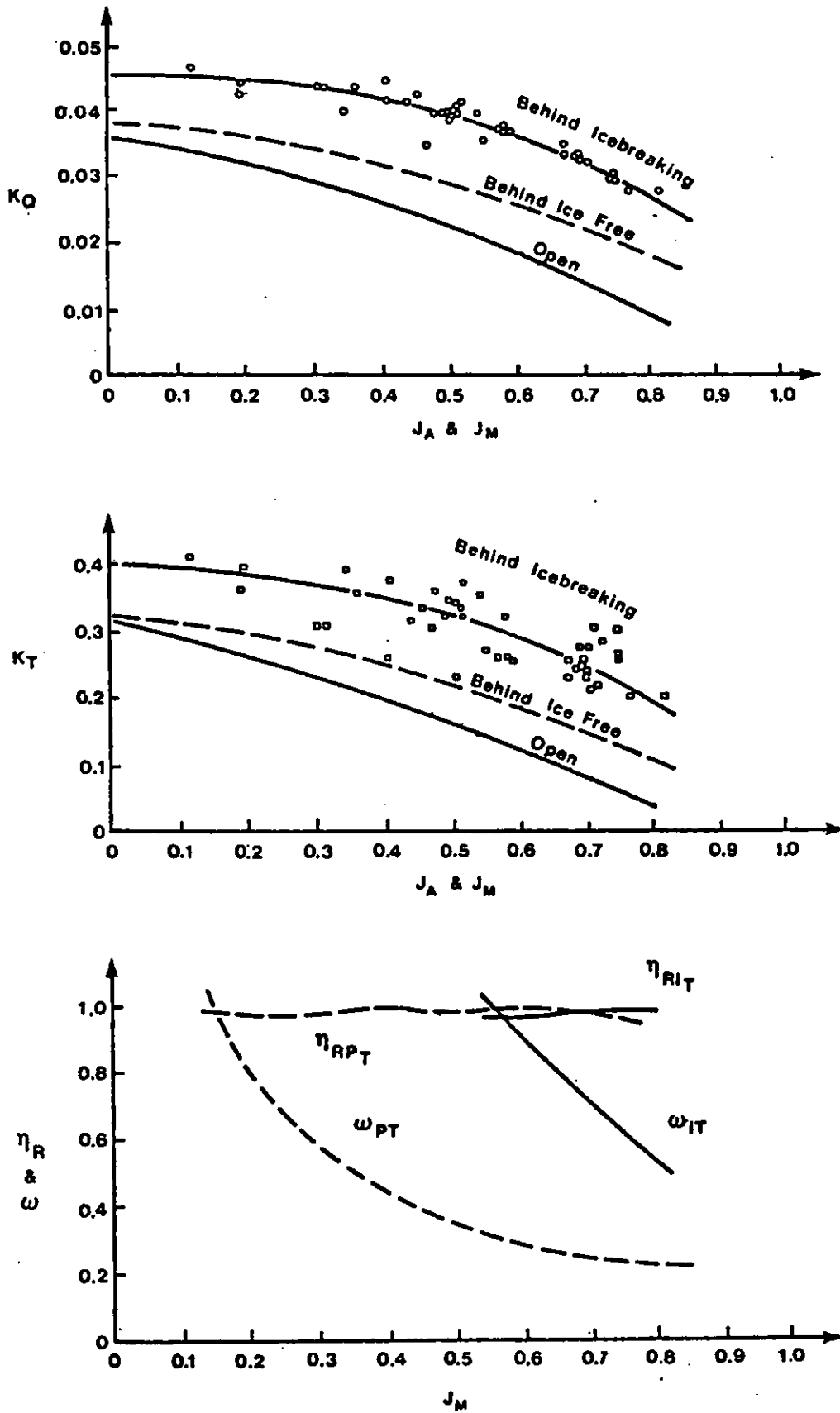


Figure 7. Relative rotative efficiency and wake fraction during icebreaking (light to heavy ice conditions)

Referring back now to the discussion of the validity of the assumption that $\eta_i = \eta_p$, it is obvious that the wake fraction difference will render this assumption invalid unless there are compensating changes in the ice thrust deduction. Previous discussion of ice thrust deduction however shows that no such compensating changes are present. It is therefore concluded that η_i is not equal to η_p and consequently the "shaft torque method" of inferring full-scale hull ice resistance from icebreaking trials data should not, in general, be used.

Before leaving the subject of ice-worthy ship powering, it is of interest to investigate the input powering requirements obtained from self-propelled icebreaking model tests. Figure 8 shows plots of the K_{TBi} and K_{QB_i} versus J_m for both the model and prototype. These data indicate that thrust measurements obtained during self-propelled model tests in ice are similar to those obtained during full-scale trials. The torque data from the self-propelled model tests in ice, on the other hand, are considerably higher than the full-scale trials data and the scatter is significantly greater.* Consequently, the powering requirements obtained from the self-propelled model test data are in excess of actual ship powering requirements. It is not clear at this time why this happens. It is believed that the problem may be due to the improper scaling of crushing strength of the model ice. The self-propelled model ice tests were conducted in saline model ice which is known to have too high a crushing strength (by a factor of 2 to 4) when flexural strength is properly scaled as it was in these tests. Since the

* Similar results from self-propelled icebreaking model tests have been reported by Narita and Yamaguchi [1981].

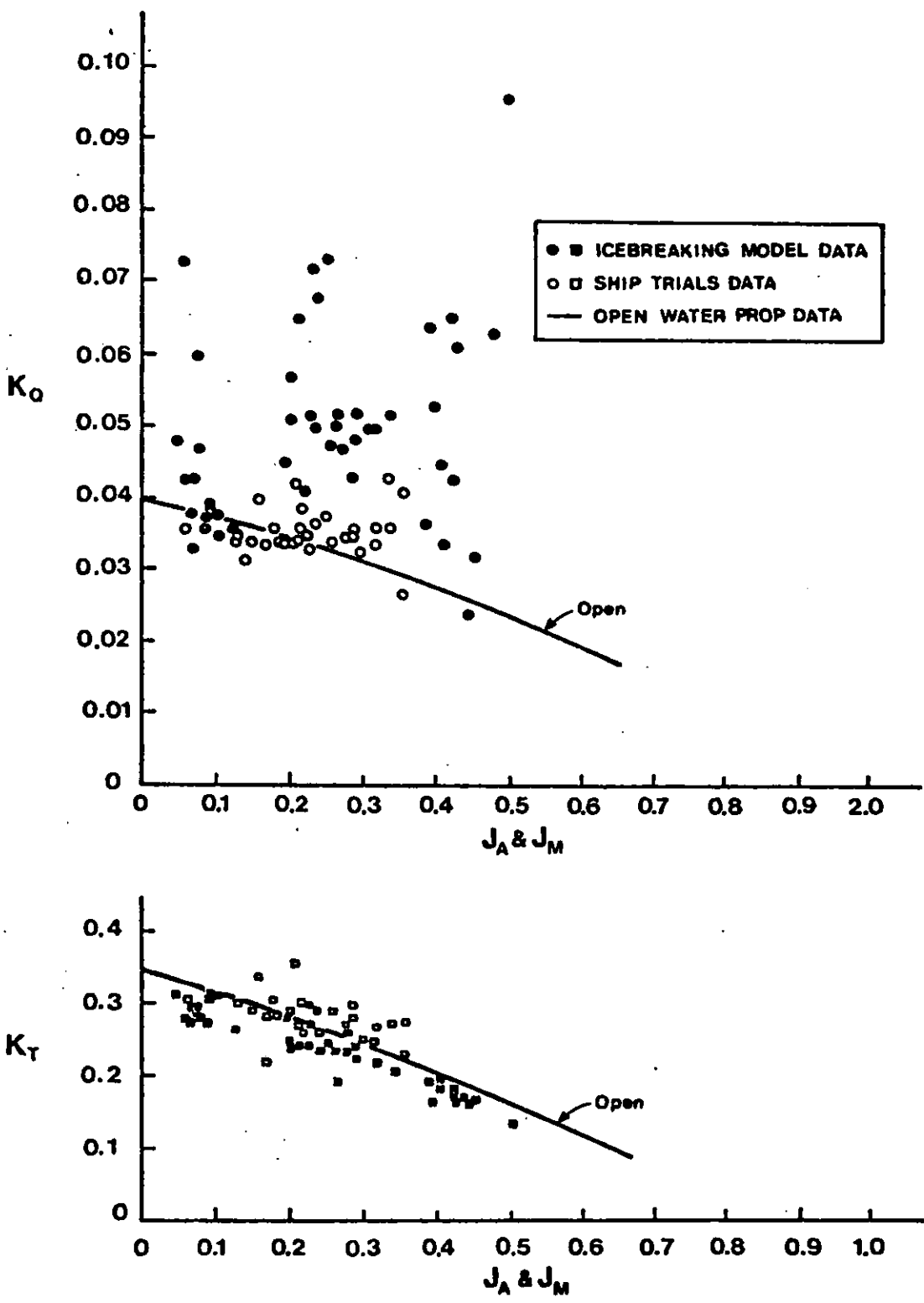


Figure 8. Comparison of self propelled icebreaking model and icebreaking ship trials data.

propellers frequently mill ice when icebreaking, it is reasonable to assume that too high a crushing strength would result in the long term average model shaft torque being too high while possibly having little influence on long-term average shaft thrust. This phenomena might also explain the increased scatter in torque data as compared to thrust data since torque would be greatly influenced by the quantity of ice impacting the propellers.

II. PROPELLER DESIGN

The design of propellers for ice-worthy ships is not straightforward. As indicated thus far, there is not a great deal of information available concerning needed hull-propeller-ice interaction coefficients. Furthermore, there is much confusion concerning methods for applying what data is available. The design procedures discussed today will, hopefully, eliminate at least some of the confusion and provide a sounder basis for propeller selection.

Classic works in this field are found in the papers by Ignatjev [1966], and Enkvist and Johansson [1968]. These authors give particularly practical information regarding the selection of propellers for optimum efficiency while icebreaking. The work of Enkvist and Johansson is of particular interest because they recommend departures from traditional tugboat and icebreaker design practice. The traditional approach generally involves designing propellers for maximum thrust in bollard conditions or some intermediate speed using the standard series propeller data without giving consideration to the ice. Usually this practice results in the largest practical diameter propeller consistent with cavitation criteria associated with submergence, and a rather small pitch-diameter ratio. Enkvist and Johansson claim, however, that when ice interaction with the propeller is considered, smaller diameters and larger pitch-diameter ratios result in a more efficient propeller. Their conclusions appear to be based on laboratory studies of model propellers in water-ice mixtures. Unfortunately, easy to use design data is not provided in their paper. Their paper also does not mention thrust deduction, wake fraction or relative rotative efficiency.

Kader [1975] describes the procedures he used to design the propeller for a recent U.S. Coast Guard icebreaking tugboat (KATMAI BAY). He employed the traditional approach. Kader mentions the work of Enkvist and Johansson but apparently could not accept the approximate 10 percent decrease in open water thrust associated with reducing propeller diameter. While Kader's approach is referred to as traditional, it also points out some of the confusion surrounding icebreaker propeller design.

Kader sought values for propeller pitch-diameter and expanded area ratios which maximized thrust at five knots given the propeller diameter and delivered horsepower (2500 hp). In order to perform such calculations, it is necessary to know relative rotative efficiency, wake fraction and thrust deduction. Kader makes no mention of relative rotative efficiency. A check of his calculations show that he assumed it to be unity.

For wake fraction, Kader used wake fraction data at the self-propulsion point for 5 knots. This is completely inappropriate, for at 5 knots the self-propulsion power requirement was only around 50 horsepower, not 2500 horsepower. Consequently, the wake field at the self-propulsion point would be entirely different from that at a 5 knot towing condition using 2500 horsepower. Kader made no attempt to use wake fraction data under towing conditions which were collected by West [1975], and made only passing reference to thrust deduction in his design even though such data must have been available (although not reported) from West's work. It is interesting to note that Kader goes on in his report to present results of detailed lifting line propeller calculations for the propeller selected with the incorrect wake fraction.

A. Basic Concepts

These discussions point out some of the interesting problems facing the ice-worthy ship propeller designer. In order to explain the design procedure recommended in this paper, it is necessary to describe in more detail the behavior of wake fraction under towing and icebreaking conditions previously discussed. Consider the blade velocity diagram shown in Figure 9. The advance coefficient, J_a , is directly proportional to the tangent of the angle β . The thrust and torque is directly related to the attack angle α which is in turn a function of the difference between the pitch angle ϕ and the advance angle β . During icebreaking, ice interacting with the propeller can slow its speed as discussed in the paper by Enkvist and Johansson. If the advance speed of the propeller, V_a , were to remain constant, then the attack angle on the blade could rapidly decrease and even go negative. Thrust and torque would quickly diminish and the thrust could go negative. Such shaft speed variations, however, are non-steady phenomena and are of concern to the propeller designer only insofar as they affect the long term average propeller thrust and torque.*

In the analysis of the full-scale ice trials data previously described, such long term averages of thrust and torque were obtained and used in the computations of relative rotative efficiency and wake fraction. Consequently, these coefficients represent average or long term values suitable for the design of propellers.

* Adequate blade strength assumed.

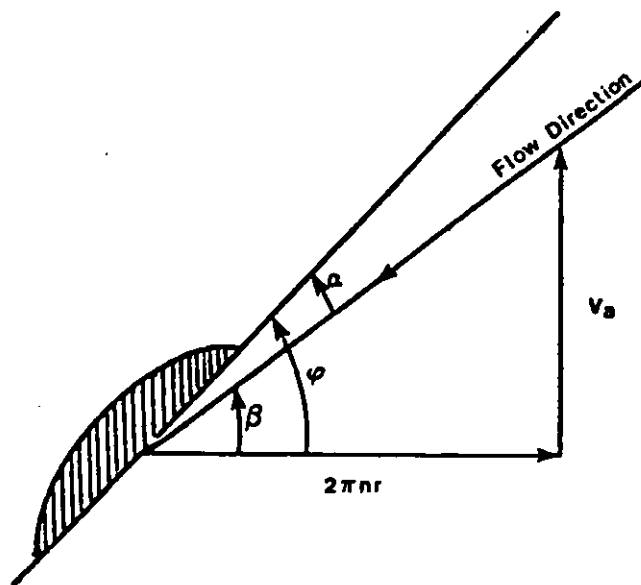


Figure 9. Propeller blade - velocity diagram.

Consider now the plot of $(1 - w_p)$ shown in Figure 10, and the associated blade velocity diagrams and K_T - J curves. Imagine an icebreaker towing a load in open water which gradually increases from nothing (self-propulsion point) to such a magnitude that it stalls (bollard point) the ship. Throughout this maneuver, the following equation applies:

$$V_a = V(1 - w_p) \quad (22)$$

At the free-running condition, V_a will equal approximately $0.8V$. As the load increases, V_a slowly decreases until at some finite ship speed, V_a becomes zero. At this point the angle of attack on the propeller equals roughly the pitch angle. Note that this occurs when $J_a = 0$ on the K_T - J curve yet this is not bollard condition. Further, increase in load causes V_a to go negative. This does not mean thrust goes negative. It does mean, however, that the propeller is now operating in a regime not normally tested in open water propeller tests. To get data for a propeller in this quadrant, the

propeller must be turning ahead but towed backwards. When the load is finally increased to the point where it stalls the ship, Equation (22) can no longer be used to calculate V_{ap} because the equation is indeterminate. That is, as V approaches zero, $(1-w_p)$ approaches negative infinity. While this behavior may at first seem hard to believe, it becomes more palatable when one understands that the $(1-w_p)$ curve was derived from self-propelled overload model tests for the KATMAI BAY.

The situation depicted in Figure 10 does not necessarily occur with all icebreaker hulls. It is also possible for $1-w_p$ to exhibit behavior as shown in Figure 11. In this case the K_{TBP} curve crosses over the K_T curve at a certain value of J_a (equal to J_m) and then continues below K_T for values for

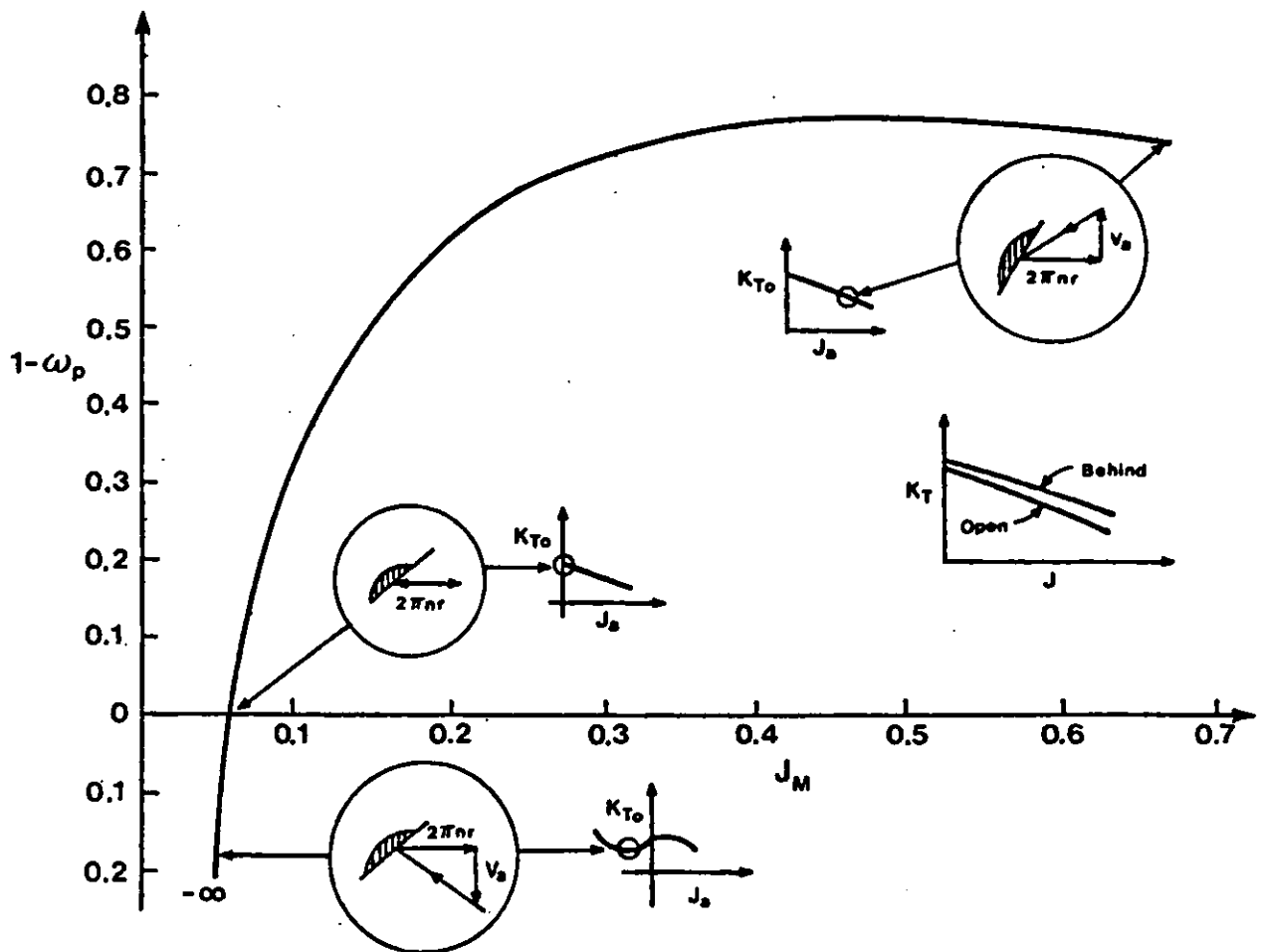


Figure 10. Typical wake fraction under towing conditions.

m

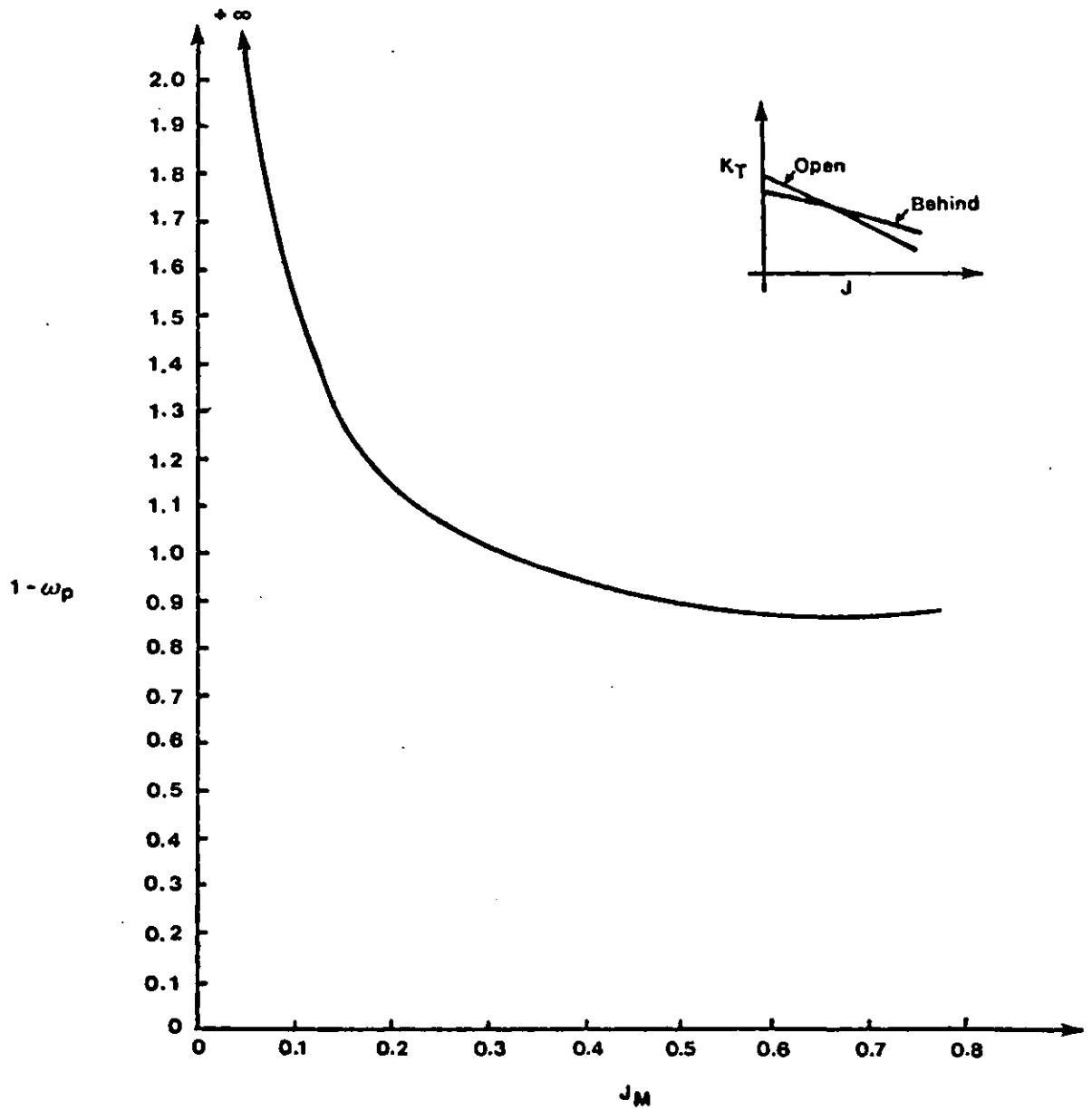


Figure 11. Another typical wake fraction under towing conditions.

J_a less than this cross-over J_a . This completely different behavior of $(1-w_p)$ clearly shows how dependent w_p is on the definition equation for w_p as well as the stern for the icebreaker. Figure 11 is derived from actual model overload test data presented in the aforementioned report by Murdey. The same behavior was found during full-scale tests of a large polar icebreaker as reported by DeBord [1981].

In considering wake fraction during icebreaking, there are at least two approaches that can be taken. One approach is to use an entirely new "open water" K_T - J curve for referencing wake fraction computations. Juurmaa and Segercrantz [1981] suggest this approach in their paper. The new "open water" K_T - J curves are obtained by conducting propeller dynamometer tests in an ice water mixture, i.e., without the ship being present. They show that this new "open ice-water" K_T - J is similar to, but slightly below, the normal "open water" K_T - J curves. If sufficient data were available and could be trusted to have no model-scale effects, then thrust identity wake fractions could be obtained by referencing the wake fractions to these new curves. The present disadvantages associated with this method are: (1) such data is not readily available to a designer; (2) the "open ice-water" K_T - J curves depend on the amount of ice entering the propeller; and (3) model-full-scale correlation has not been established.

Another approach is the one suggested in this paper. That is, full-scale ship trials K_{TB1} - J_m data is plotted along with normal open water K_T - J data and thrust identity wake fractions for icebreaking are obtained by referencing the wake fraction calculations to the open water K_T - J curves. The present disadvantage of this method is the scarcity of data. Both of the

suggested methods suffer from the fact that open water propeller data is not normally collected in the "positive n negative V_a " quadrants and this is sometimes necessary.

Consider now an icebreaker starting at its full power free-running speed, encountering a level ice field whose thickness gradually increases with distance of penetration. The speed of the icebreaker will decrease slowly until it reaches the ice thickness which stalls ($V=0$) the ship. The ice related wake coefficient ($1-w_i$) for this situation is shown (actual computations using KATMAI BAY ice trials data) in Figure 12. It can be seen that the situation described for the icebreaker while towing in open water applied to the icebreaking situation also. Only in the icebreaking case, the speed (ship) at which J_a equals zero will be higher and the propeller will therefore operate in the positive n negative V_a quadrant over a larger range of ship speeds.

B. Design Procedure

The procedure recommended here for designing the optimum efficiency propeller for an icebreaker will now be described. First it is presumed that thrust deduction, wake fraction and relative rotative efficiency data have been obtained from full-scale icebreaking trials and model tests for a similar ship as required. Thrust identity coefficients should be used and plotted as a function of J_m . The ship speed for optimization is then selected based on preliminary routing studies. The maximum diameter propeller should be selected consistent with adequate hull clearances for vibration and ice clearing. It is also presumed that open water K_T - J and K_Q - J propeller curves are available as a function of pitch-diameter and expanded area ratio. For those not familiar, Figure 13 shows a typical representation of open water propeller test data.

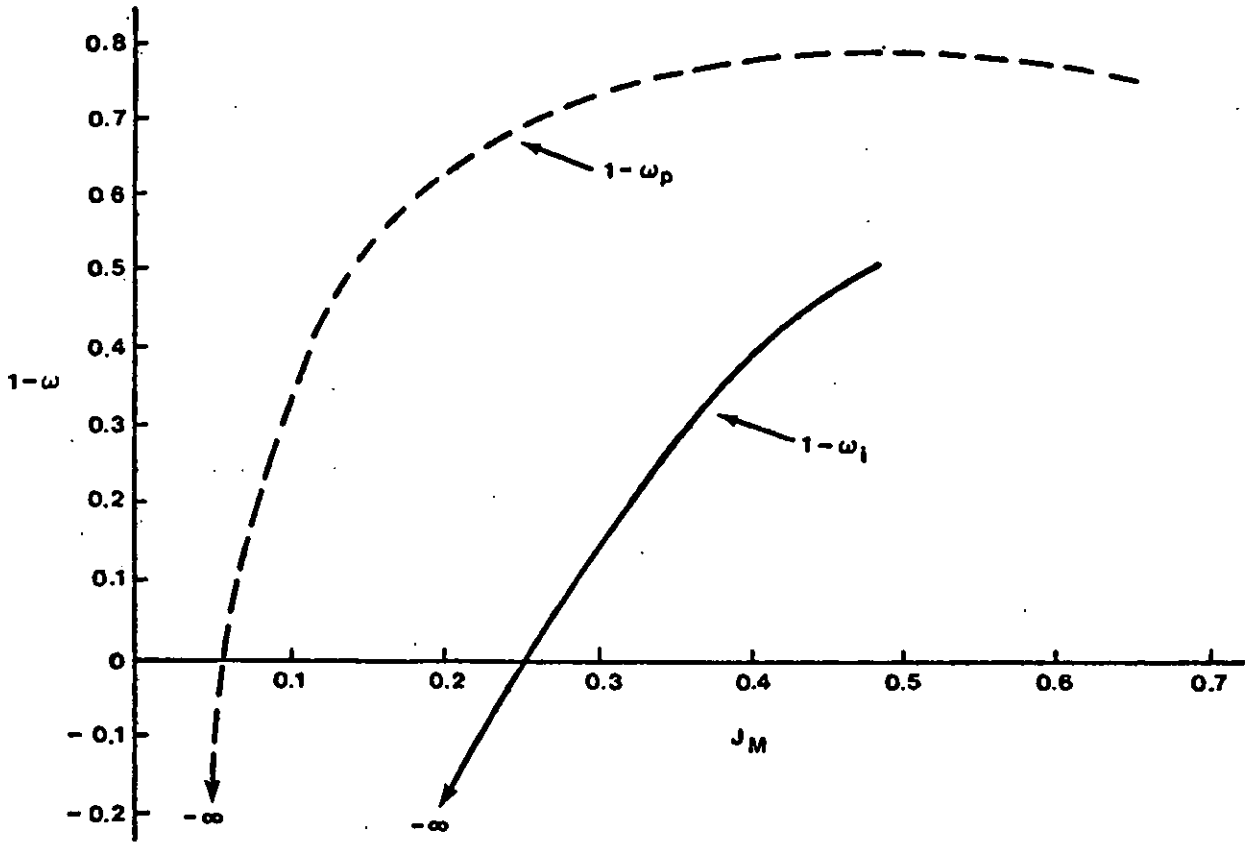


Figure 12. Typical wake fraction under icebreaking conditions.

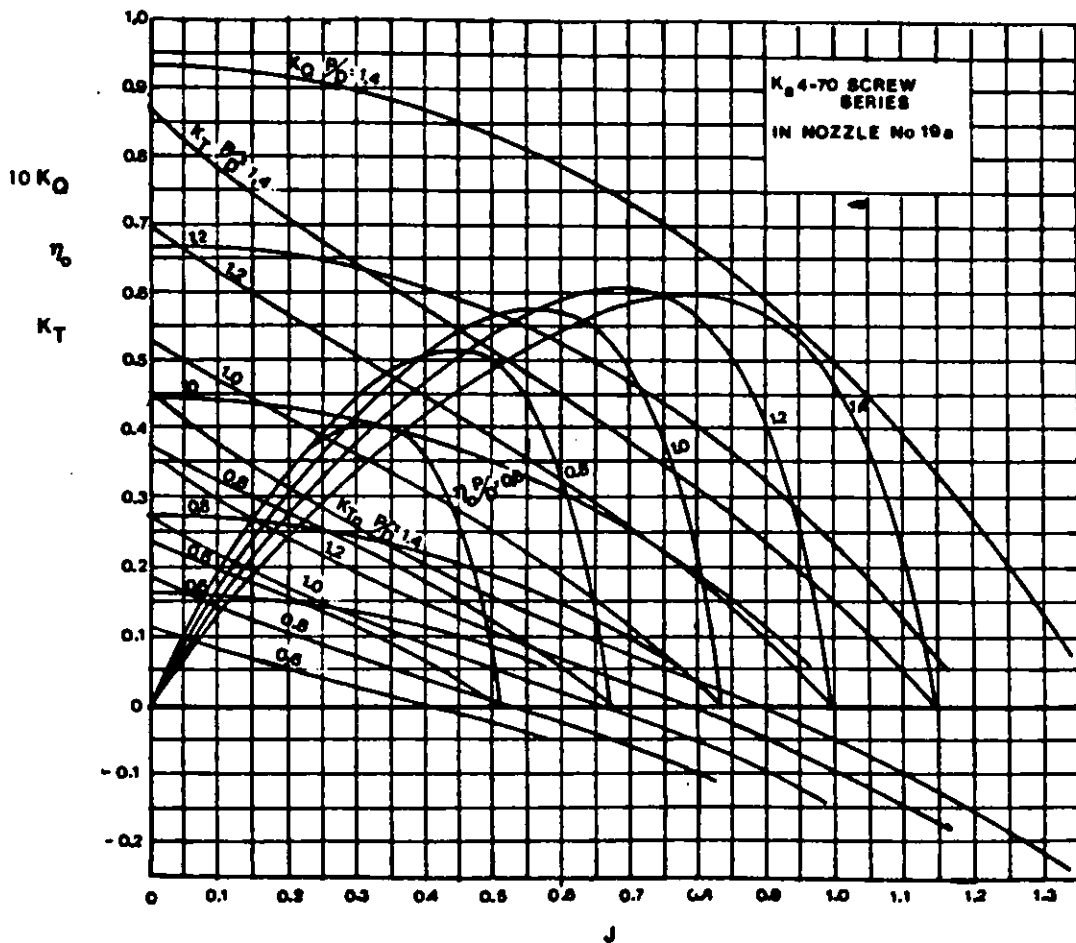


Figure 13. Open water propeller curves (from Oosterveld 1970)

Two general cases may then be investigated. In one case the shaft horsepower to be installed is unknown and in the other case the shaft horsepower is given. The first case is the more general design problem and will be discussed first.

In this case, the total hull resistance is first computed given the ice thickness, ice strength, ship characteristics, etc. using the given ship speed. Next values for pitch-diameter and expanded area ratio are arbitrarily selected. A trial value of shaft speed is next selected and used to compute J_m . Values for $(1-t_i)^*$, $(1-w_i)$ and R_i are then found from plots. The value of J_a is calculated using $(1-w_i)$ and J_m . K_{T_0} for this value of J_a is found and used to determine T_0 . From this, the total resistance which can be overcome is found by multiplying T_0 by $(1-t_i)$. If the value of total resistance so found does not agree with total resistance required, shaft speed is changed and the above process is repeated until acceptable agreement is found. Once convergence is achieved, the value of J_a at convergence is used to find K_{Q_0} . This can then be used in conjunction with the values of R_i and n at convergence to obtain the required shaft horsepower for the values of pitch-diameter and expanded area ratio used. The procedure is repeated for several values of pitch-diameter and expanded area ratios. The pitch-diameter ratio which gives minimum horsepower for each expanded area ratio is then selected. Table 1 shows a sample of this type of calculation for an icebreaking tanker with the given parameters. Using the curves of Figure 13 for a 4 bladed shrouded propeller.

* Obtained by assuming $(1-t_i) = (1-t_p)$ where t_p is from overload model tests.

PARAMETERS

Ship Velocity	6.5 knots
Resistance	2.34 MN
Propeller Diameter	8.53 M
Expanded Area Ratio	0.70
Propeller Configuration:	KA blade series
	4 blades
	Nozzle 19A

It can be seen that the optimum P/D for this set of parameters lies between 0.8-0.9. Cavitation charts such as suggested by Enkvist and Johansson are used to select the expanded area ratio which minimizes shaft horsepower while providing sufficient safeguard against cavitation.

For the case in which shaft horsepower is given, the procedure involves seeking the pitch-diameter and expanded area ratio which maximizes thrust available for icebreaking while providing sufficient safeguard against cavitation. First, values for pitch-diameter and expanded area ratio are arbitrarily selected. Next a trial value for shaft speed is chosen and used to compute J_m . Values for $(1-t_1)$, $(1-w_1)$ and R_1 are found. Two values for K_Q are then computed.

The first value of K_Q , referred to in Table 2 as $K_{Q_{available}}$, is calculated using the relation:

$$K_{Q_{avail}} = \frac{C \cdot DHP \cdot \eta_{r1}}{2\pi \cdot p \cdot n^3 D^5} \quad (23)$$

where: C = constant depending on units

DHP = given Horsepower

η_{r1} = Relative Rotative efficiency

n = assumed shaft speed (ups)

D = Propeller Diameter

TABLE 1 SAMPLE DESIGN

CASE I

a) Sample iteration varying N for P/D to obtain TR = Ri
Select P/D = .7

N (rpm)	90	89	88	87.7
J _m	0.261	0.264	0.2672	0.2681
(1-w _i)	0.560	0.564	0.568	0.570
J _a	0.146	0.149	0.1519	0.1528
K _{T0}	0.231	0.2297	0.228	0.228
T ₀	2.828	2.75	2.671	2.648
(1-t _i)	0.885	0.884	0.884	0.8835
T _{Bi} (MN)	2.503	2.430	2.362	2.340
K _Q				0.0200
DHP (HP)				24,325

b) Results for various P/D ratios

P/D	0.6	0.7	0.8	0.9	1.0
N (rpm)	98	87.7	79.7	73.3	68
J _a	0.125	0.1528	0.179	0.205	0.229
K _{T0}	0.1817	0.228	0.278	0.3303	0.384
T ₀ (MN)	2.632	2.648	2.67	2.682	2.682
(1-t _i)	0.889	0.8835	0.879	0.874	0.870
T _{Bi} (MN)	2.340	2.340	2.343	2.344	2.334
K _Q	0.0153	0.0200	0.0261	0.0335	0.0423
DHP	25,960	24,325	23,780	23,780	23,980

The second value is obtained by calculating J_a using $(1-w_i)$ and J_m , and finding K_Q from the open water K_Q - J curves. If the two values found do not match, another value for shaft speed is chosen and the process repeated until convergence of the K_Q values is achieved. Once convergence has been achieved, the value of J_a at convergence is used to obtain K_T from the open water K_T - J curves. The values of shaft speed and $(1-t_i)$ at convergence are then used to compute available thrust for the values of pitch-diameter and expanded area ratios chosen. The procedure is repeated for several values of pitch-diameter and expanded area ratios. The pitch-diameter ratios which provide maximum thrust are then selected for each expanded area ratio considered.

Table 2 shows sample calculations for the same propeller as Figure 1 at various ship speeds with an assumed rpm and given horsepower. This represents the all too frequent case where the designer is presented with a ship's machinery specifications and required to generate values of thrust available to overcome resistance. Each entry in Table 2 is at the P/D ratio providing maximum thrust for each ship velocity. This calculation may be repeated for different expanded area ratios. Finally, the expanded area ratio which provides the required margin against cavitation and maximum available thrust is selected. Figure 14 shows the thrust curve resulting from these calculations.

The design procedure recommended here is not considered by the authors to be the final word on this subject. Considerably more work in this area is required. More work following the approach taken by Juurmaa and Segercrantz [1981] could prove very valuable. It would be extremely interesting, for example, to have the Troost propeller series tested using their dynamometer in a model ice which had crushing and shearing strength properly scaled. More

self-propelled model icebreaking tests are also needed and these data should be compared with full-scale ice trials data to more adequately describe ice related thrust deduction, wake, and relative rotative coefficients using methods suggested in these notes.

TABLE 2 THRUST CALCULATION - DESIGN CASE 2

DHP = 41,550

RPM = 77

$K_{Qavail} = 0.0495$

SHIP SPEED (knots) P/D	0 1.05	2 1.05	4 1.05	6 1.06	8 1.07
K_Q	0.0494	0.0494	0.0492	0.0494	0.0490
K_T	0.5669	0.5571	0.5202	0.4745	0.4300
T_0 (MN)	5.080	4.992	4.661	4.252	3.853
t_i	0.061	0.082	0.102	0.120	0.136
TB: (MN)	4.770	4.582	4.186	3.742	3.329

SHIP SPEED (knots) P/D	10 1.09	12 1.12	14 1.15	16 1.19
K_Q	0.0490	0.0494	0.0492	0.0494
K_T	0.3923	0.3593	0.3229	0.2888
T_0 (MN)	3.515	3.220	2.893	2.587
t	0.151	0.163	0.174	0.184
TB: (MN)	2.984	2.695	2.390	2.111

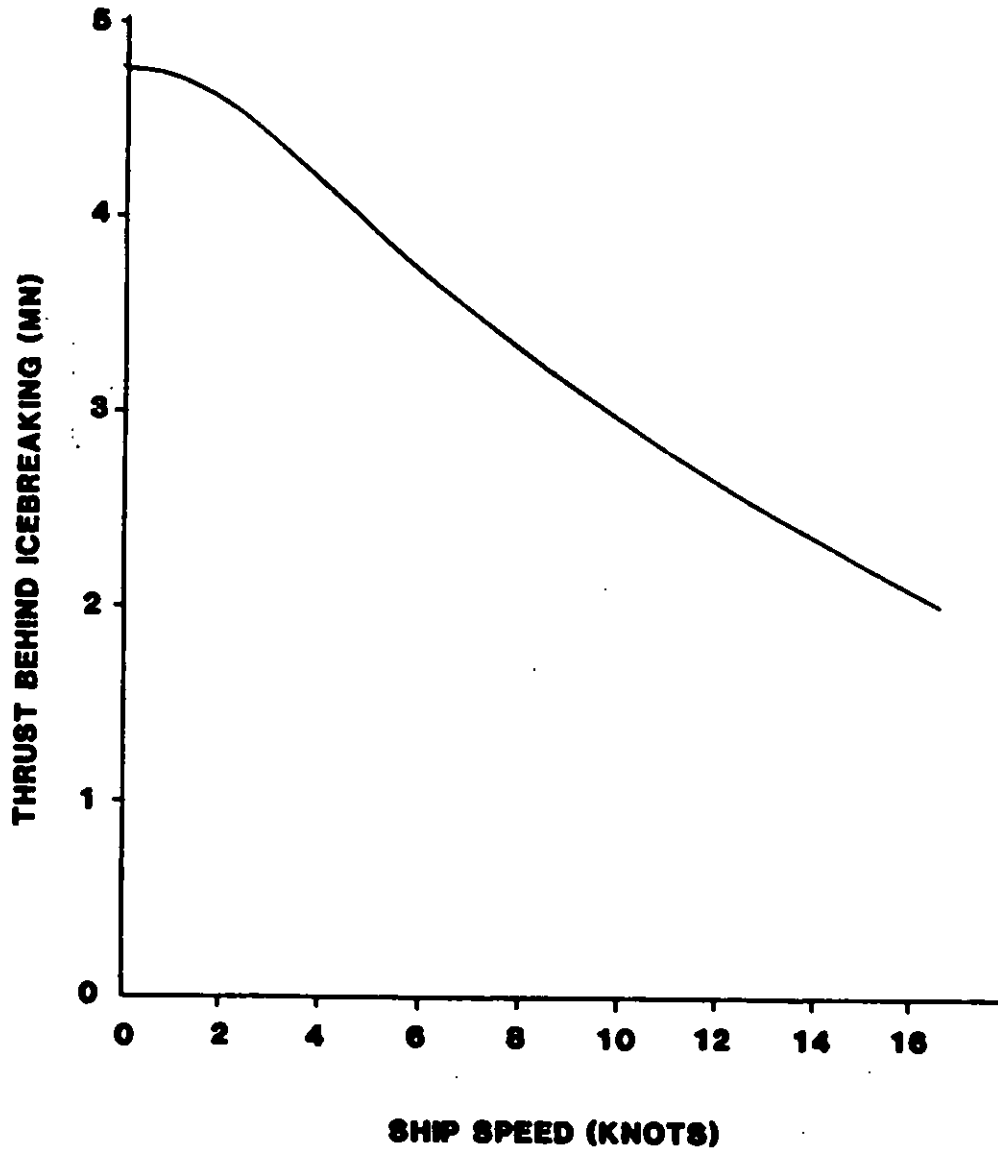


Figure 14. Calculated thrust for a CP propeller in ice

REFERENCES

- DeBord, F. W., R. P. Voelker, F. A. Geisel, J. L. Coburn and K. E. Dane, "Winter 1981 Trafficability Tests of the USCGC POLAR SEA; Volume V - Bollard and Tow Rope Pull Tests," ARCTEC, Incorporated Report No. 583C-3, Columbia, MD, 1981.
- Enkvist, E. and Johansson, B. M., "On Icebreaker Screw Design," *European Shipbuilding Journal of the Ship Technical Society*, Vol. 17, No. 1, 1968.
- Harvald, S. A., "Tug Propulsion: Wake, Thrust Deduction, and R.P.M." *European Shipbuilding*, Vol. 12, No. 3, 1963.
- Harvald, S. A., "Wake and Thrust Deduction at Extreme Propeller Loadings," Publication of the Swedish State Shipbuilding Experimental Tank, No. 61, Goteborg, 1967.
- Ignatjev, M. A., "Screw-Propellers for Ships Navigating in Ice," Published by Sudostrojenie, Lennigrad, 1966.
- Juurmaa, K. and H. Segercrantz, "On Propulsion and Its Efficiency in Ice," *Proceedings, Sixth Ship Technology and Research (STAR) Symposium*, Paper No. 17, SNAME, New York, NY, 1981.
- Kader, R. D., "The Design of a Propeller for a U.S. Coast Guard Icebreaker Tugboat," Naval Ship Research and Development Center Report No. SPD-223-19, Bethesda, MD, October 1975.
- Lewis, J. W. and R. Y. Edwards, Jr., "Methods for Predicting Icebreaking and Ice Resistance Characteristics of Icebreakers," Presented at the Annual Meeting, SNAME, New York, NY, 1970.
- Lewis, J. W., F. W. DeBord and V. A. Bulat, "Resistance and Propulsion of Ice Worthy Ships," *Transactions*, 1982 SNAME Meeting, New York, NY, 1982.
- Murdey, D. C., "Resistance and Propulsion Experiments with Model 327-1 and Propellers 66C and 66R," NRC MDSL Report LTR-SH-269, 1980.
- Narita, S. and M. Yamaguchi, "Some Experimental Study on Hull Forms for the New Japanese Antarctic Research Ship," *Proceedings, Sixth Ship Technology and Research (STAR) Symposium*, Paper 20, SNAME, New York, NY, 1981.
- Oosterveld, M. W. C., "Wake Adapted Ducted Propellers," NMR Publication No. 345, Wageningen, Netherlands.
- Park, M. N. and J. Dawson, "Tug Propulsion Investigation," TRINA, 1962.
- West, E. E., "Powering Predictions for the United States Coast Guard 140-Foot WYTM Represented by Model 5336," Naval Ship Research and Development Center, Report No. SPD-223-16, Bethesda, MD, April 1965.



W ESTERN
E UROPEAN
G RADUATE
E DUCATION
M ARINE
T ECHNOLOGY

SEVENTH GRADUATE SCHOOL
SHIPS AND STRUCTURES
IN ICE

LECTURE NOTES
ON
RECENT DEVELOPMENTS IN
THE PREDICTION OF LEVEL
ICE RESISTANCE

BY
JACK W. LEWIS, PRESIDENT

NOMENCLATURE

A_c	= area or crushed ice
A_0	= dimensional coefficient for ice resistance
A_1	= dimensional coefficient for ice resistance
A_x	= midship area
B	= maximum beam at operating waterline
C_0, C_1, C_2	= dimensionless icebreaking coefficients
C_B	= block coefficient
C_p	= prismatic coefficient
C_x	= midship area coefficient
D_c	= cusp depth
D_w	= wedge depth
E	= Elastic modulus
F_N	= Froude number
H	= ship draft
H_{bw}	= height of the bow wave
H_c	= horizontal extent of crushing
J_a	= V_a/nD , propeller advance coefficient
J_m	= V/nD , measured advance coefficient
L	= ship length at operating waterline
P_n	= force normal to the hull
P_v	= force vertical to the ice sheet
R_i	= pure hull ice resistance
R_{iw}	= ice and water hull resistance (towed)
R_m	= resistance due to mass forces
R_N	= Reynolds number

R_{ow}	= open-water hull resistance (towed)
T_{Ri}	= shaft thrust (behind in ice)
U	= V = forward velocity of ship
W_c	= cusp width
W_w	= wedge width
Z_b	= vertical extent of deflection
b	= width of crushed ice
f	= hull-ice friction factor
g	= acceleration of gravity
h	= ice thickness
l_c	= characteristic length of ice
n	= propeller shaft speed
t_i	= constant of proportionality or thrust deduction factor in ice (subscript i is used to denote icebreaking)
t_p	= constant of proportionality or the so-called "thrust deduction factor" while towing (subscript p is used to denote pulling)
x, y, z	= distance in the surge, sway, and heave directions
α	= waterline angle
β	= hull flare angle
β'	= normal flare angle
∇	= ship displacement
δ	= angle between hull and ice sheet
η_3	= average direction cosine between hull normal and vertical axis
θ	= angle of inclination between cusp and water surface
ρ_i	= mass density of ice
ρ_w	= mass density of water
ρ_Δ	= density difference between water and ice
σ_c	= ice crushing strength
σ_f	= ice flexural strength
τ	= shear strength of ice
ϕ_0	= stem angle

ICEBREAKING HULL RESISTANCE

Means for determining hull ice resistance must be available to the designer of an ice-worthy ship in order to estimate powering requirements. Full-scale data can be used for this purpose and in the first part of this lecture, available full-scale data will be analyzed and formulas for determining hull-ice resistance developed.

Use of full-scale data for determining hull ice resistance, however, has its limitations. It is very expensive and data is available for only a relatively few number of hull forms. Icebreaking model tests represent a much more cost effective approach to obtaining such data, provided the results are reliable. We will investigate today the correlation between full-scale and model test data and show how model data can be used to derive effects of hull form on ice resistance.

The use of analytical theories for determining hull ice resistance is the least expensive means available. Use of analytic methods will be discussed today, with particular emphasis placed on a recently developed theory.

I. HULL ICE RESISTANCE BASED ON FULL-SCALE TRIALS DATA

There are so many hull, ice, water, and motion variables which could influence hull resistance that it is currently impossible to explain the effect of every one on resistance. For the time being then, one must be satisfied with methods which predict hull ice resistance only to a first order approximation.

Two basic steps are involved in the use of full-scale trials data to predict the hull ice resistance. First is the analysis of the measured data to estimate ice resistance.

During the preceding discussion of propulsive coefficients, two methods for inferring hull resistance in ice were described. These methods were referred to as the "shaft thrust method" and the "shaft torque method". Uncertainties exist in each method; however, it appears that fewer uncertainties exist with the shaft thrust method and therefore this method is to be preferred.

The concept of "pure hull ice resistance" comes from the assumption that the total hull resistance can be subdivided into two additive components. One component is the open water resistance of the hull as obtained from towed model tests in calm water, and the other is obtained from subtracting the open water resistance from the total resistance. Thus pure ice resistance is defined as

$$R_i = R_{iw} - R_{ow} \quad (1)$$

where R_{iw} = total hull resistance in ice and water

R_{ow} = hull resistance in open water

This division of the total resistance into two components is arbitrary and without an analytical basis. However, it will be useful later when the full-scale trials data of several ships are analyzed and compared to model scale test predictions.

It is assumed that a set of full-scale data consisting of measurements of shaft thrust, shaft speed and ship speed is available. For each "run" in this set of data, the measurements should be time averaged over several ship lengths of travel at a relatively steady speed.

To infer pure ice resistance from this set of data, it is also necessary to have available two sets of open water model test results or equivalent full-scale data. The first set consists of the open water towed resistance test data and the second set consists of the open water, self-propelled overload or towing test data. The latter set of data is

absolutely essential and great care should be given to its collection to ensure that a sufficient number of towing speeds are used to span the full-scale data and that shaft thrust is measured.

The model data is then reduced and plots of t_p versus J_m and R_{ow} vs V are prepared. The full-scale data is reduced as follows. The value of J_m is calculated for each run using the measured shaft speed and ship speed, and the diameter of the propeller. The value of t_p is obtained from the plot of the model data. The total ice and water resistance is computed using the measured shaft thrust for the run and the equation

$$R_{iw} = (1-t_p) T_{Ri} \quad (2)$$

The open water resistance is found by entering the plot of model open water resistance versus speed with the value of ship speed for the run. Equation (1) is used to obtain the pure ice resistance for the run.

The procedure is repeated for each run in the set of full-scale data. The data is then tabulated and the ship speed, ice thickness, ice flexural strength and any other pertinent data tabulated along with the pure ice resistance.

One set of full-scale data, reduced as described above, is of somewhat limited value. However, as I will show in the next section, when many sets of such data are analyzed together, meaningful design data can be obtained. In order to utilize the data obtained from full-scale trials, data must be analyzed to determine the functional relationship between resistance and the independent variables involved. This is the second step in the analysis of full-scale data to make useful predictions possible.

Past analysis of full-scale trials and model test data in level ice has shown that pure ice resistance is composed of two additive components: one speed independent and the other speed dependent. Analysis of near zero speed data shows that the speed independent terms varies roughly with the

square of the ice thickness. The speed dependent term varies approximately linearly with the product of the ice thickness and the ship velocity. In equation form, these past analyses show

$$R_i = A_0 h^2 + A_1 hV \quad (3)$$

where A_0 and A_1 are constants for the particular ship in the particular ice field study.

Through the use of dimensional analysis, it is possible to develop dimensionless variables which can greatly facilitate the analysis of data by allowing diverse sets of data to be combined, and by reducing the total number of independent variables involved. For example, consider the following functional expression for pure ice resistance:

$$R_i = F(L, B, H, \nabla, A_x, h, \sigma_f, \sigma_c, E, \rho_i, \rho_w, g, f, V) \quad (4)$$

where

F = the function being sought

L = ship length at operating waterline

B = maximum beam at operating waterline

H = ship draft

∇ = ship displacement

A_x = midship area

h = ice thickness

σ_f = ice flexural strength

σ_c = ice crushing strength

E = ice elastic modulus

ρ_i = mass density of ice

ρ_w = mass density of water

g = acceleration of gravity

f = hull-ice friction factor

V = ship speed

The number of variables in Equation (4) may be reduced through application of classical dimensional analysis. By selecting the force group $\rho_w g B h^2$ for nondimensionalizing R_i , one can obtain the following dimensionless version:

$$\frac{R_i}{\rho_w g B h^2} = G \left(C_B, C_P, C_X, \frac{R}{h}, \frac{L}{h}, \frac{H}{h}, \frac{\rho_i}{\rho_w}, \frac{E}{\sigma_f}, \frac{\sigma_c}{\sigma_f}, \frac{\sigma_f}{\rho_w g h}, \frac{V}{g h}, f \right) \quad (5)$$

where G is a different function from F .

Although Equation (5) is only slightly less complicated than Equation (4), it does provide a basis for combining data from several different size hulls in various types of ice into one data base. Furthermore, experience has shown that many of the independent variables shown have negligible influence on the dependent variable.

Past analysis of ice resistance data indicates that much of the variation associated with the ice resistance data is removed when the ice resistance is divided by the force group $\rho_w g B h^2$. This is consistent with the findings indicated in Equation (3), since dividing this equation by h^2 leaves it in the form

$$\frac{R_i}{h^2} = A_0 + A_1 \frac{V}{h} \quad (6)$$

That is, R_i/h^2 is a linear function of V/h .

It is possible to form several groups of the independent dimensionless variables given in Equation (5) which will give a V/h term for a particular ship. One such group is

$$VLB = \left(\frac{V}{\sqrt{gh}} \right) \frac{(L/h)}{(B/h)^{1/2}} \quad (7)$$

Using this group, the dimensionless equivalent of Equation (6) becomes

$$\frac{R_i}{\rho_w g B h} = C_0 + C_2 \left(\frac{V}{\sqrt{gh}} \right) \frac{(L/h)}{(B/h)^{1/2}} \quad (8)$$

Multiplying both sides of Equation (8) gives the dimensional equation

$$R_i = C_0 \rho_w g B h^2 + C_2 \rho_w g^{1/2} B^{1/2} L h V \quad (9)$$

It can be seen that Equation (9) is equal to Equation (3) if

$$A_0 = C_0 \rho_w g B$$

and

$$A_1 = C_2 \rho_w g^{1/2} B^{1/2} L$$

The validity of Equation (8) must be checked against actual data. Note that this equation indicates that the speed independent term is proportional to the beam of the ship and that the speed dependent term is proportional to the product of the square root of the beam and the length of the ship. In order to check this, it is therefore necessary to have data for several ships with varying beams and lengths.

Four sets of full-scale ice trials data were analyzed to determine if Equation (8) reasonably fits these data. The ships varied in length from 39.6m to 295.7m and their beams varied from 7.3m to 45.7m. Each set of trials data was linearly regressed with Equation (8) to obtain values for coefficients, C_0 and C_2 , and the corresponding correlation coefficient. The results are given in Table 1.

Before discussing these results, it is important to point out that so far no consideration has been given to possible effects of ice strength, hull form or hull-ice friction factor on pure ice resistance. This was done for two reasons. First, these variables were purposely omitted at this stage of the analysis in order to determine how much of the data variation could be explained by considering only length, beam, speed of the ship, and the ice

thickness as independent variables. Second, except for ice strength, it is difficult to quantify these variables. Table 2 shows a matrix of test conditions associated with each ship trial that are relevant to ice strength (Ice Type), hull form (Row Type) and hull-ice friction (Hull Surface Condition)

TABLE 1
RESULTS OF REGRESSING INDIVIDUAL ICEBREAKING
SHIP TRIAL DATA AGAINST EQUATION (9)

SHIP	C_0	C_2	CORRELATION COEFFICIENT
SS MANHATTAN	4.354	0.194	0.956
USCGC MACKINAW	7.161	0.222	0.736
USCGC KATMAI BAY	6.065	0.230	0.705
CCGC PIERRE RADISSON	1.556	0.203	0.945

TABLE 2
FULL-SCALE ICE TRIALS INFORMATION REGARDING
HARD TO QUANTIFY INDEPENDENT VARIABLES

SHIP	ICE TYPE	ROW TYPE	HULL SURFACE CONDITION
SS MANHATTAN	SEA (284)*	MODERN	PAINTED STEEL
USCGC MACKINAW	FRESH (920)*	OLD	PAINTED STEEL
USCGC KATMAI BAY	FRESH (661)*	MODERN	LOW FRICTION COATING PARTIALLY WORN
CCGC PIERRE RADISSON	SEA (376)*	MODERN	LOW FRICTION COATING

* MEAN FLEXURAL ICE STRENGTH IN kPa

The mean flexural ice strength is indicated in parentheses in this table.

The results given in Table 1 clearly indicate that the speed dependent coefficient, C_2 , for each ship is essentially identical. This shows that the speed dependent pure ice resistance component most likely varies as the product of the square root of the beam, the length, the ice thickness and the velocity ($B^{1/2} LhV$). In view of the possible variations in ice strength, hull form and friction factor indicated in Table 2, the similarity of C_2 could also indicate that this coefficient is not greatly affected by these variables.

The speed independent coefficient, C_0 , is not the same for each ship data set. It is most likely that this coefficient is influenced by the variables indicated in Table 2. It is difficult however to isolate this influence. An attempt was made to include the effect of ice strength by combining all of the trials data into one set and performing a multiple linear regression with the following equation:

$$\frac{R_i}{\rho_w g B h^2} = C_0 + C_1 \left(\frac{\sigma_f}{\rho_w g h} \right) + C_2 \left(\frac{V}{\sqrt{gh}} \right) \frac{(L/h)}{(B/h)^{1/2}} \quad (10)$$

The results gave $C_0 = 3.8989$, $C_1 = 0.0123$ and $C_2 = 0.223$ and a correlation coefficient of 0.85.

Although Equation (10) does not show any variation in resistance with hull form or hull-ice friction factor, it is of immense value to a designer in the initial stages of ice-worthy ship design. The equation first of all is derived entirely from full-scale trials data collected on ships ranging from very small to quite large. It also includes two ship variables (length and beam), two ice variables (ice thickness and ice strength) and the ship speed.

II. HULL ICE RESISTANCE BASED ON MODEL-SCALE TESTS

Model-Full Scale Correlation

Due to the difficulties associated with attempts to isolate effects of hull form and hull-ice friction on pure ice resistance using full-scale trials data, it is natural to turn to another, less expensive, approach. The works of Edwards, et al. [1976] and Lecourt, et al. [1978] address these problems and present very useful design data. Still the validity of model test data is frequently questioned and therefore it is important to take every opportunity to address the question of model-prototype correlation when such data becomes available.

Within the last several years, two new sets of full-scale data have been collected for ships which were extensively tested in the model ice basin. In addition, field trials data from one old test (Edwards, et al. [1972]) were reanalyzed using the "shaft thrust method" referred to in the previous lecture. The corresponding model test data is old, but still valuable.

The approach taken in this model-prototype correlation study was as follows. For each ship model test the experimenter involved presented a data smoothing equation which best fit the model data. This equation was used to predict full-scale ice resistance by substituting values of the full-scale independent variables (i.e., values for ice thickness, ice strength, ship speed, hull friction, etc.). The ice resistance predicted by the model data smoothing equation was then plotted against the full-scale ice resistance as inferred using the shaft thrust method.

The results of this model-full-scale correlation analysis are shown in Figures 1, 2 and 4. On each of these plots there are three lines. The solid line represents the line for perfect match of model and full-scale data. The

other two lines represent $\pm 20\%$ variation between model and full-scale data.

Figure 1 shows correlation for the USCGC MACKINAW ice trials and model tests. These data were previously presented and analyzed by Edwards, et al. [1972]. The trials data used in Figure 1, however, differs from that presented by those authors in three respects. First, the trials data was reanalyzed for this paper using the "shaft thrust method" instead of the "shaft torque method" used by them. Second, the thrust deduction factor was taken into account in this reanalysis. Third, trials data in very thin ice was excluded from the analysis, because these could not be tested in the ice model basin. Of the resulting twenty-nine (29) data points, sixteen (16) fall within the $\pm 20\%$ limits, nine (9) are above the upper 20% limit and four (4) are below the lower 20% limit. The ship speed is indicated beside each data point to show that there are no trends in the scatter associated with speed as had been previously observed by Edwards, et al. [1972].

Figure 2 shows correlation for the USCGC KATMAI BAY ice trials and model data. The ice trials data for this ship were presented by Vance, et al. [1981] and the model data by Lecourt, et al. [1978]. Vance's raw data were reanalyzed using the shaft thrust method referred to previously. Vance suggested using a hull-ice friction factor of 0.15 and this was used in Lecourt's model data smoothing equation. The KATMAI BAY had a low friction coating but was reported by Vance as deteriorated. Thrust deduction factors required had to be estimated using the data presented in Figure 3 because West [1975] did not report thrust measurements taken during the open water towing model test program. Of the sixteen (16) data points shown, nine (9) are within the $\pm 20\%$ limit, one (1) is above the upper 20% limit and six (6) are below the lower 20% limit. Notice that the range of absolute resistance

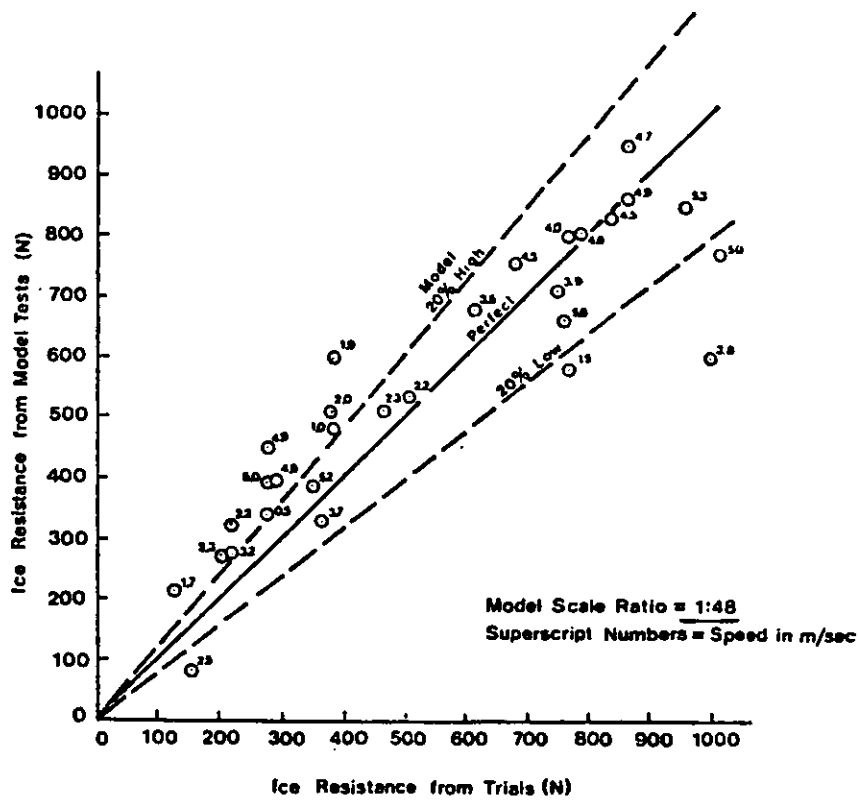


Figure 1 Model-full scale correlation-USCGC MACKINAW

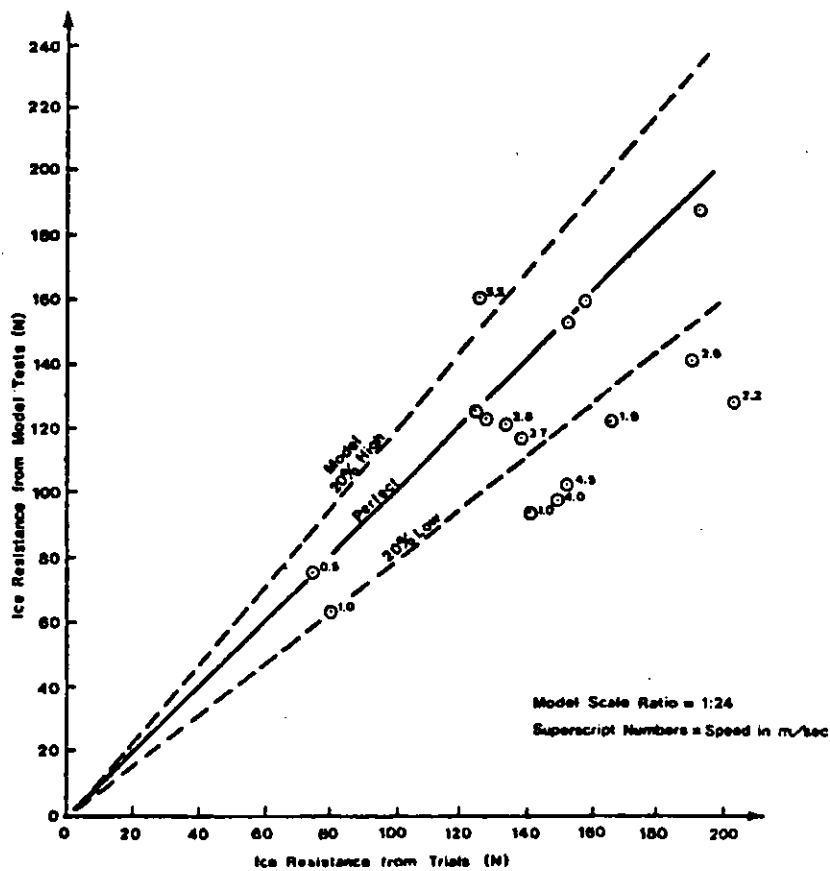


Figure 2 Model-full scale correlation - USCGC KATMAI BAY

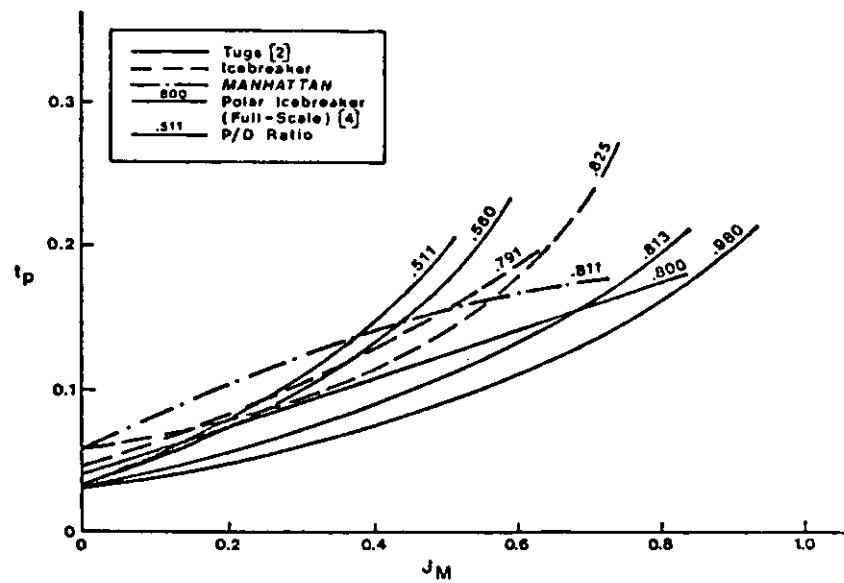


Figure 3 Thrust deduction while towing

values associated with these trials is only one-fifth that associated with the MACKINAW trials. Also note that the scale factor for the KATMAI RAY model (1/24) is twice that of the MACKINAW (1/48).

Figure 4 shows correlation for the CCGS PIERRE RADISSON ice trials and model data. The ice trials data for this ship were presented by Edwards, et al. [1981] and the model data by Bulat [1981]. Edwards' raw data were reanalyzed using the shaft thrust method. Thrust deduction factors and open water resistance required for application of this method were taken from the

excellent work of Murdey [1980].* The full-scale trials data for this ship is the most extensive ever collected and is a tribute to the skills and foresight of those involved with these trials. Of the one hundred two (102) data points shown, sixty-seven (67) are within the ± 20 percent limits, twenty (20) are above the upper 20% limit, and fifteen (15) are below the lower 20% limit. Ship speed is not shown with the data for purposes of clarity; however, no speed effects were noted. Several of the data points above the upper 20% limit were associated with the highest ice thickness conditions, which may show a tendency for the model to over-predict resistance at high ice thicknesses. It is also of interest to point out that the model tests were conducted with a hull-ice friction factor of around 0.05.

Out of the 147 data points presented in Figures 1, 2, and 3, 63% are within the $\pm 20\%$ limits, 20% are above the upper 20% limit and 17% are below the lower 20% limit. It would appear that the $\pm 20\%$ limits correspond to roughly one standard deviation between model and full-scale data.

Effect of Hull Form on Pure Ice Resistance

The most extensive investigation of the effects of hull form on pure ice resistance to date is contained in the paper by Edwards, et al. [1976]. I can add little to this work. However, for the sake of continuity, this section of the present paper will present a brief review of that part of the Edwards, et al. paper which pertains to hull form effect on pure ice resistance.

*This report of open water towing and other trials can be used as an outstanding example of how such tests should be conducted, and how the data should be analyzed and reported

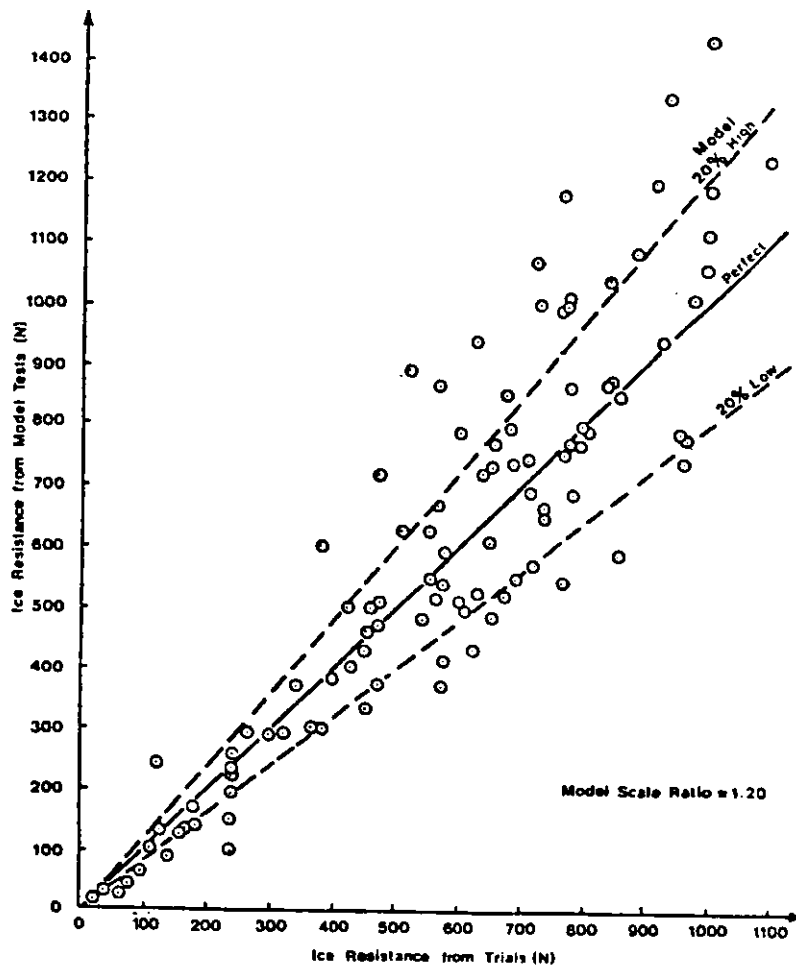


Figure 4 Model - full scale correlation CGS PIERRE RADISSON

A series of seven different icebreaker models and two parallel mid-bodies were tested in order to determine the effect of varying length, beam, draft and block coefficient on icebreaking resistance of a typical modern icebreaker. Each of these variables was varied independently, insofar as was possible, over three discrete steps. For each model, ice flexural strength, ice thickness and ice friction factor were also varied. One hundred and ninety-six (196) data points were acquired in the test program and later subjected to a stepwise multiple regression analysis which accepted independent variables at the 95% confidence level.

The resulting equation which is given below had a multiple correlation coefficient of 0.99:

$$\begin{aligned} \frac{R_i}{\rho_w g B h^2} &= 5.7 + 0.147 \frac{H}{h} - 7.83 C_B^2 \\ &+ \frac{\sigma_f}{\rho_w g h} (-0.318 + 0.265 f + 0.394 C_B) \\ &+ \frac{V}{gh} (-68.16 + 0.048 \frac{\sigma}{\rho_w g h} \\ &+ 223.73 C_B - 181.3 C_B^2 + 0.249 \frac{H}{h}) \end{aligned}$$

The equation was stated as valid over the following ranges of the independent variables:

$$\begin{aligned} 104 &> \frac{\sigma_f}{\rho_w g h} > 8 \\ 2.5 &> \frac{V}{gh} > 0.2 \\ 0.625 &> C_B > 0.500 \\ 73 &> \frac{H}{h} > 10 \end{aligned}$$

No range for the friction factor f was given.

Equation (11) is rather complex and it is difficult to see how the various independent variables influence the resistance. In order to see the effect of varying C_B and (H/h) more clearly, Figure 5 shows plots of dimensionless resistance as a function of dimensionless speed with C_B and (H/h) as parameters with f and $(\sigma_f/\rho_w g h)$ held constant at 0.15 and 50, respectively. These plots show that dimensionless ice resistance increases as C_B and H/h increase.

It is interesting to note that Equation (11) does not contain ship length. This variable was not found to be significant in the regression analysis in spite of the fact that it was varied up to 40% more than the parent hull form. This is in disagreement with the full-scale data analysis we have just examined. However, the variation in length among the full-scale data is far greater than 40%. Equation (11) also appears to me to give too much variation in resistance with ship draft.

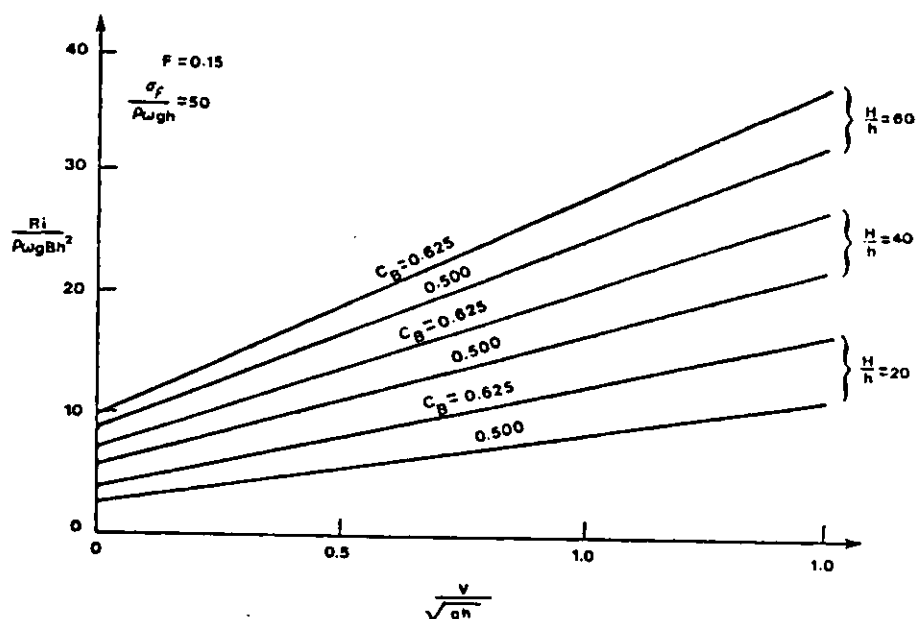


Figure 6 Variation of ice resistance with speed, hull size and hull form

If the designer is considering icebreaker type ships, consideration should be given to the hull forms discussed by Noble and Bulat [1979]. These forms use the CGCS PIERRE RADISSON as a parent. Since that ship obviously has outstanding icebreaking characteristics parametric form variations about this parent should be of great interest and value.

III. HULL ICE RESISTANCE BASED ON ANALYTICAL STUDIES

Predicting ice resistance analytically is an extremely complex problem. Ice may be treated, for example, as an elastic plate on an elastic foundation for purposes of analysis. But even simple equations for this model involve 4th order, nonlinear, partial differential equations. Further, full-scale and model-scale test data clearly show that the strength of ice has only a minor influence on the total icebreaking resistance. Even if the aforementioned differential equations could be solved, one may find that only a fraction of the problem had been solved.

This complex problem has been tackled by several investigators over the years starting perhaps with Runeburg [1888]. The most significant contributions in recent times were published by Kashteljan, Poznak and Rylvlin [1968]. While their work cannot be strictly referred to as analytical, their contribution gives great insight into the problem. Another significant contribution to the field is the work of Enkvist [1972]. His order of magnitude analysis of ice resistance components gives even greater insight into the factors contributing to icebreaking resistance.

Perhaps the first person to investigate the problem completely analytically was Milano [1972, 1973]. Milano's algorithm, however, shows ice resistance to be greatly influenced by ice flexural strength and only slightly influenced by hull-ice friction. This is in disagreement with full-scale trials and ice model test data we have examined.

Vance (1982) recently provided a comparison of a number of different analytical techniques with full-scale and model test results, shown in Figure 6. The comparison shows the results of Milano's technique, Kashteljan's technique, the ICEREM technique and model test results as reported by E. J. Lecourt in an ARCTEC report "Icebreaking Model Tests of the 140 Foot WYTM" prepared for the U.S. Coast Guard. ICEREM is a proprietary analytical model licensed by ARCTEC. The figure is for 12 inch level ice with no hubble system in effect. As can be seen in the figure, the Milano technique predicts high, and the Kashteljan technique is high at low speeds and of the wrong slope. The model tests are the best prediction with ICEREM predicting high, but with the correct slope. It should be noted that ICEREM is very sensitive to the friction coefficient and a slight error in this factor could cause the differences noted. A $t_f = .4$ was assumed for the full-scale data, as this was the value deduced by Vance from the full-scale tests.

IV. THE NAEGLE MODEL AND SPLICE

Recently, a major contribution to the field has been made by Naegle [1980]. Naegle's algorithm produces results and trends which agree reasonably well with full-scale trials and ice model test data. For this reason, Naegle's model is considered to be the best one available in the open literature today.

ARCTEC, Inc. has used the Naegle formulation as the basis for a new analytical model for the prediction of ship performance in level ice (SPLICE).

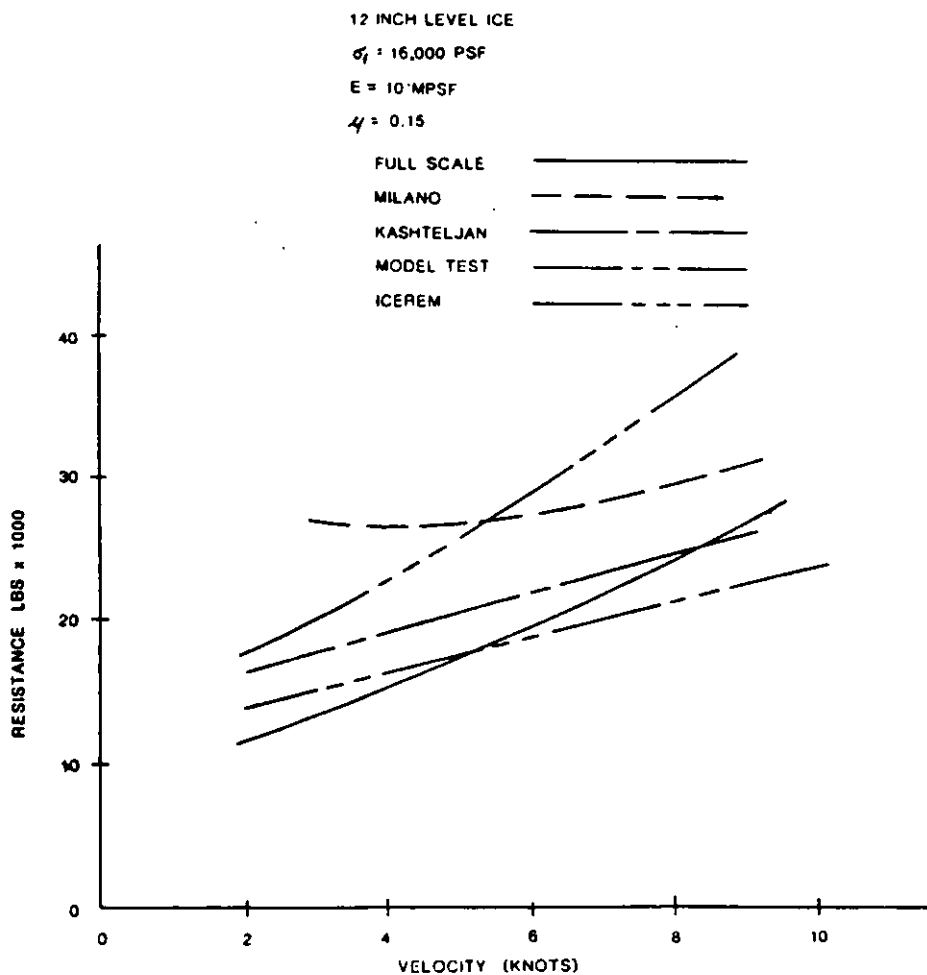


Figure 6 Ice resistance for USCGC KATMAI BAY

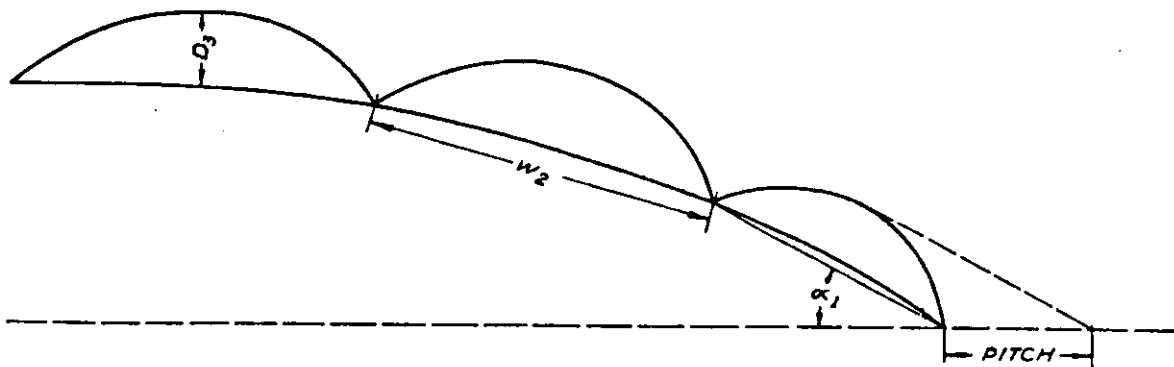
In the process of formulating SPLICE, some modifications were made to Naegle's algorithm. I will now discuss both the basic algorithm and these changes in some detail.

Naegle approaches the hull ice resistance problem as a mechanics problem. All forces acting on the hull are explicitly written and Newton's Law is applied. The resulting coupled differential equations are solved numerically to determine rigid-body motions. Ice resistance is determined by setting the surge-direction velocity to a constant value and calculating average values for the surge direction forces.

Naegle considers both ice and non-ice (fluid and propulsion) forces, but only the ice related forces will be discussed here. His treatment covers those ice forces related to breaking of the ice, turning of broken ice pieces, submersion of the broken ice pieces and mechanical friction between the hull and the ice.

A. Breaking Pattern

In order that a steady-state resistance might be achieved, Naegle assumed that the ice breaks in a consistent and predictable manner. He referred to this breakage profile as the ice breaking pattern. In its simplest form, this breaking pattern can be viewed as a series of cusps, modelled as semi-ellipses, running from the stem along the hull as shown in Figure 7. The total number of cusp rows is determined by adding rows, beginning at the stem, until the distance from the center of the outer cusp to the centerline of the ship is greater than the ship's half-beam. The maximum number of rows permitted by his program is three.



$$\begin{aligned}
 \text{ROW 1} & \quad D_1 = (0.0247 + 0.5439 \bar{n}_s) L_c \\
 & \quad W_1 = 4 D_1 \\
 & \quad \text{Pitch} = D_1 / \sin \alpha_1 \\
 \text{ROW 2} & \quad D_2 = 2 \text{ Pitch} \sin \alpha_2 \\
 & \quad W_2 = 4 D_2 \\
 \text{ROW 3} & \quad D_3 = 4 \text{ Pitch} \sin \alpha_3 \\
 & \quad W_3 = 6 D_3
 \end{aligned}$$

Figure 7. Definition of naegle ice-breaking pattern.

As an initial attempt to represent the breaking pattern, the algorithms in the Naegle model were quite good. The use of cusp-shaped ice pieces agreed well with model and full-scale data. Likewise, the inclusion of hull geometry terms which influenced piece size was commendable. However, on further examination and use it became clear that a few problems remained due to the simplicity of the pattern, but that with modest modifications the routine could be substantially improved. The first of these difficulties was due to the failure of the model to account for the effect of ship speed on piece dimensions, a phenomenon many investigators have observed. The second came from the stepwise nature of the resistance versus ice thickness curve. This discrete aspect resulted whenever a cusp was added to or deleted from the pattern due to a slight change in ice conditions. The third problem stemmed from the inability of the model to account for the wedge-shaped pieces of ice existing between the broken cusps.

The first step taken to overcome these difficulties was to reanalyze the cusp depth data for the STATEN ISLAND, JELPARRI and FINNCARRIER. The result of this work was the formulation of an equation expressing cusp depth as a function of ice conditions and deflection velocity:

$$\eta_c = l_c * \left[2.42205 + 6.02256 \left(\frac{\sin \alpha}{\tan \beta'} \right) \left(\frac{U}{\sqrt{g l_c}} \right) \right]^{-1} . \quad (12)$$

At a later point in this work a coefficient was introduced into the cusp depth equation in order to judge whether hull geometry effects were present. To do this computation, optimal values of the coefficient were found for a series of four icebreakers. The coefficients were then regressed against a variety of hull geometry terms. The equation which resulted was highly correlated with the data; it may be expressed as:

$$\eta_c = \bar{n}_3 l_c * \left[1.7153 + 4.2653 \left(\frac{\sin \alpha}{\tan \beta'} \right) \left(\frac{U}{\sqrt{g l_c}} \right) \right]^{-1} \quad (13)$$

where \bar{n}_3 is as defined by Naegle--the average direction cosine in the forward 20% of the ship's length.

In parallel with the redefinition of cusp depth, an effort was directed towards recasting the equation predicting cusp width, w_c . The equation which was finally chosen may be expressed as:

$$\frac{w_c}{\eta_c} = \sqrt{\frac{10.0 \text{ m}}{h}} . \quad (14)$$

In general, for thin ice where cusp depth is small the ratio is large (-5), thereby reducing the number of cusps required. Similarly when the ice is thick the ratio is small (-3) and the number of cusps increase. Also as shown by the range of values adopted, this expression produces ratios in agreement with the values commonly cited. In conjunction with the above equation, the maximum allowed number of cusp rows was increased from three to ten.

The next required step was to minimize the discrete or stepwise aspects of the breaking pattern with regard to ice resistance. This task was accomplished by fairing the outer cusp into a line parallel with the centerline, located at or beyond the half-beam of the ship as shown in Figure 8. As an example, if the line of maximum extension is defined as tangent to the hull at maximum beam, then cusps are added until the lip of the outer cusp exceeds the half-beam of the ship. At this point the outer cusp's dimensions are reduced until the lip just touches the boundary line. From full-scale observations, a channel wider than the ship's beam is usually seen; the

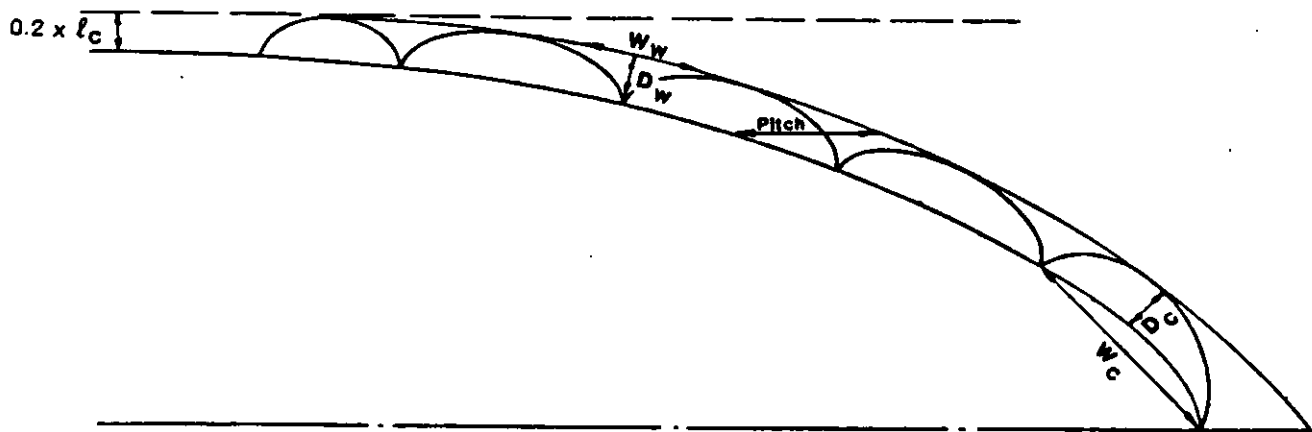


Figure 8. Breaking pattern in splice.

extension of this channel beyond the half-beam of the ship is typically stated as between 15% and 30% of the characteristic length of ice. Consequently, the boundary line chosen was that extending $0.2 \cdot l_c$ beyond the ship's half-beam.

The last major modification to the breaking pattern subroutine was the addition of wedge-shaped ice pieces between the cusps. These pieces were included in order that a complete envelope of broken ice surrounds the bow region. These wedges were defined as having a depth, D_w , equal to the average depth of their neighboring cusps. The one exception to this rule is the first wedge which has a depth equal to Naegle's original definition of "pitch". The wedge's width, W_w , was determined by requiring that the wedge area be equivalent to the area left between the cusps.

Finally, Naegle's original concept of pitch was redefined. In SPLICE, pitch is taken as the distance between a point on the hull and the surrounding envelope of unbroken ice on a line parallel to the centerline of the ship. Pitch is calculated for the apex of every wedge and the center of every cusp. Also, the criterion for a breaking cycle is based solely on pitch--only when the ship has advanced a distance equal to a row's pitch will a new breaking cycle for that row begin. This latter statement is not true for the Naegle program in which a new breaking cycle was permitted whenever a cusp turned parallel to the hull.

B. Level Ice Forces

The subprogram developed by Naegle to predict the acting level ice force divides this force into three components. The first component is due to the crushing of the ice-sheet prior to the breaking of the ice; the second is due to the turning and acceleration of the cusp parallel to the ship's side; the third is due to the forced submergence of the ice beneath the hull. Each

of these three components is further subdivided into two subcomponents--one associated with the normal force and the other associated with the frictional force. I will discuss only the normal forces here.

1) Breaking Forces

The ice sheet from which the individual cusps are broken is assumed to behave as an edge loaded, semi-infinite elastic plate resting on an elastic foundation. A representation of this assumption is provided in Figure 9. The free edge is assumed to crush when interacting with the advancing hull until stresses in the ice sheet exceed the ultimate strength of the ice in flexure, σ_f . The force normal to the hull, P_n , during crushing is taken as:

$$P_n = \sigma_c A_c \quad (15)$$

where: σ_c = ultimate strength of ice in crushing, and

A_c = area of crushed ice.

Figure 10 shows a definition sketch of an ice piece undergoing crushing and deflection. For a width of crushed area, b , (perpendicular to the page) the area of crushed ice is given by:

$$A_c = \frac{H_c b}{\sin \beta'} \quad (16)$$

where: H_c = horizontal extent of crushing, and

β' = normal flare angle.

The vertical force, P_v , is then given as:

$$P_v = \sigma_c H_c h. \quad (17)$$

Nevel's solution [1965] to the semi-infinite plate problem is used to arrive at the following approximate solution for deflection, expressed in non-dimensional form:

$$\frac{Z_b \rho g l_c^2}{P_v} = 0.4697 \exp(-0.4396 H_c / l_c) \quad (18)$$

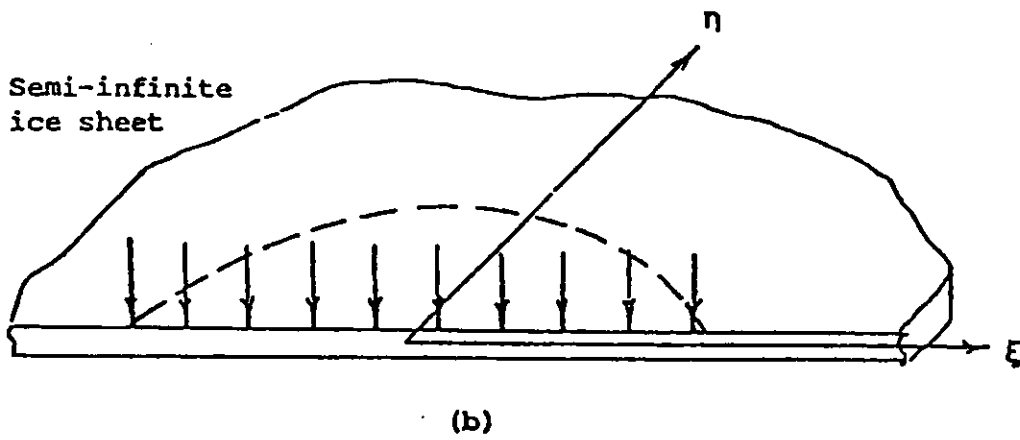
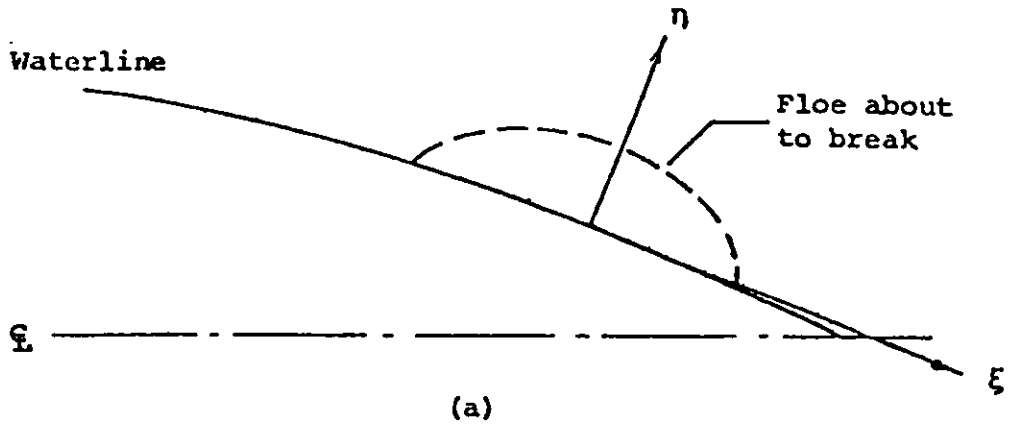
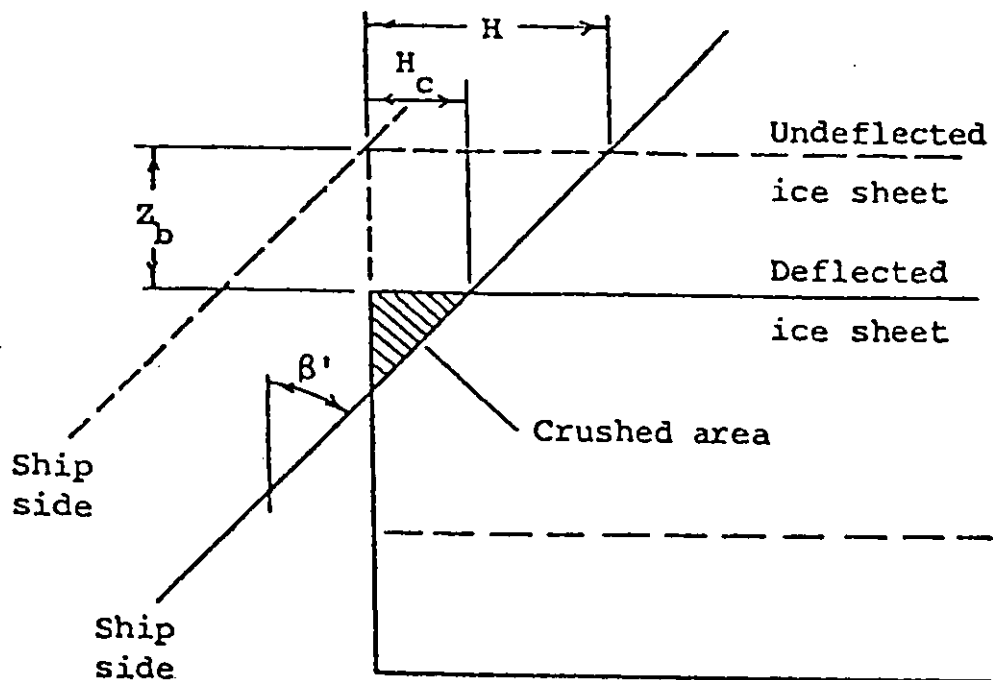


Figure 9. Assumption of an edge-loaded, semi-infinite ice sheet.



H = Horizontal penetration into the plane of the undelected ice sheet

H_c = Horizontal extent of crushing

z_b = Vertical ice sheet deflection due to bending

Figure 10. Geometry of the deflecting ice sheet.

where Z_b equals the vertical extent of deflection. Using the identity:

$$Z_b = \frac{H - H_c}{\tan \beta} \quad (19)$$

where H is the total extent of advance into the unbroken ice, H_c may be recast as:

$$H_c = \frac{H \rho g l_c^2}{\rho g l_c^2 + 0.4697 \sigma_c h \tan \beta \exp(-0.4396 H_c / l_c)} \quad (20)$$

By the definition:

$$H = \Delta x \sin \alpha \quad (21)$$

where Δx is the incremental advance in the surge-direction from the point of initial contact and α is the waterplane angle at the center of contact, H_c may then be estimated.

The acting bending stress, σ , also falls from Nevel's work in his solution for the maximum bending moment:

$$\sigma = \frac{1.5929 Z_b \rho g l_c^2 \exp(-0.5629 H_c / l_c)}{h^2} \quad (22)$$

As long as the stress calculated by the above expression is less than σ_f , the ice sheet does not break.

Naegle further assumed that the mechanism of ice breakage at the stem was distinct from those processes considered above. He assumed that this mechanism was one of shear with the force normal to the stem, P_n , given by:

$$P_n = \frac{\tau h^2}{2 \sin \phi_0} \quad (23)$$

where: τ = shear strength of ice, and

ϕ_0 = stem angle.

This component has been removed from the final formulation due to our introduction of the new breaking pattern and Naegle's original uncertainty about this term.

The other major components of the breaking force which have been modified in the final formulation of SPLICE are:

- The radius of deflection of the ice during breaking was redefined based on Enkvist's data. [1972]
- The effective length of crushing was redefined as somewhat less than the cusp width due to the curvature of the hull.
- Equations for wedge crushing and breaking have been included based on work by Nevel. [1961]
- Lastly, an effort was made to include dynamic effects of the breaking process with the resulting stress being a function of hull geometry.

2) Turning Focus

After the cusps have broken from the ice sheet, the advance of the ship forces them to turn on edge until parallel with the hull. During this phase of icebreaking Naegle considers two forces acting over the cusp as shown in Figure 11. The first is the head, H_h , due to the combined effects of the hull-induced pressure field represented by the bow wave and the ventilation occurring above the cusp. The percent of ventilation is taken as 3.33 times the ship Froude number. The second acting force is that due to the inherent buoyancy of the cusp, F_B . By integrating these forces times a moment arm throughout the semi-ellipse and then solving the moment equation, Naegle resolves the normal force, P_n , as:

$$P_n = 0.5 \pi \rho_{\Delta} g W_C D_C h \cos \beta' \tan \delta + 0.3151 \rho g W_C D_C (3.33 F_n D_C \sin \theta + H_{bw}) / \cos \delta \quad (24)$$

where: ρ_{Δ} = the difference in density between water and ice, and

θ = the angle of inclination between cusp and water surface.

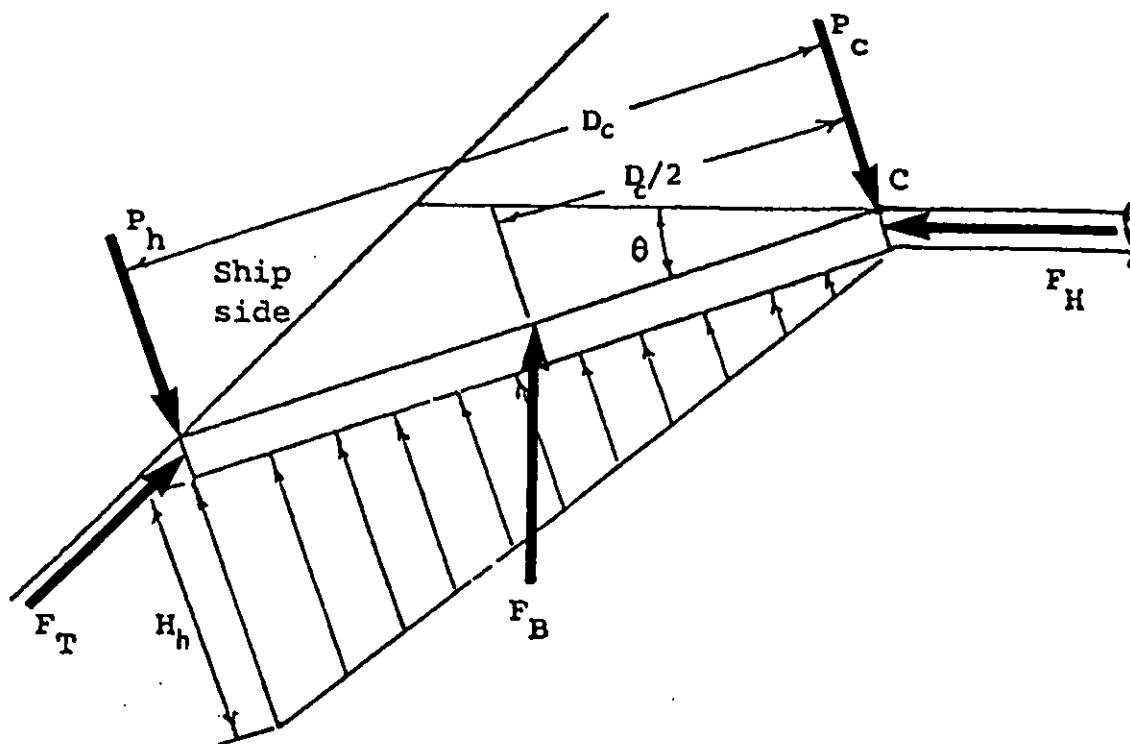


Figure 11. Force distribution on turning cusp.

Also included in the turning force subprogram is the average resistance, R_m , due to mass forces. These mass forces are defined as the forces required to accelerate the cusps from zero speed to that speed equal to the forward velocity of the ship times the tangent of the buttock angle. This resistance can then be written as:

$$R_m = \frac{U^2 \tan^2 \alpha \sin \alpha}{4 \tan^2 \beta} (\pi \rho l h W_c + \frac{\pi}{6} \rho D_c W_c) \quad (25)$$

where: ρ_i = density of ice, and
 β = hull flare angle.

The modifications in the calculation of turning forces in the SPLICE model are less extensive than those to the breaking routines.

- Pressure due to the bow wave and Froude dependency on ventilation were reconsidered and more sophisticated treatments used.
- Turning forces were calculated for the smaller, wedge-shaped ice pieces in a manner similar to that for the broken cusps.
- The final modification is the inclusion of viscous drag as a turning force, which was totally neglected by Naegle.

After the cusps are upended and in contact with the hull, it is assumed that they remain in contact with the hull and slide under its length up to amidships. Scale model tests show this phenomenon to be true at low to medium speeds. At higher speeds, however, the pieces are pushed sharply downward and do not necessarily maintain contact. The model, therefore, assumes that the speed of the icebreaker is in the low to medium range.

3) Submergence Forces

Submergence forces are calculated by multiplying the projected area of the ice upon the hull by $\rho \Delta gh$.

I have not discussed the hydrodynamic equations of motion utilized in the SPLICE model. These relations are well documented in the available literature and the Runge-Kutta routines used by Naegle are standard numerical analysis fare as well.

Results produced with the final version of the Naegle based SPLICE model are shown in Figures 12 through 16. Comparisons are made with full-scale data available for the KATMAI BAY, PIERRE RADISSON, STATEN ISLAND, MACKINAW, and POLAR STAR. The plots show predicted versus measured ice resistance. Obviously, perfect correlation would have the points lying on the diagonal with no scatter around this line. Also included on the graphs are the bands of 10% and 25% deviation. These regions are illustrated in order to get a quantitative sense of the reliability of the model in predicting resistance.

In order to evaluate the relative merit of SPLICE, it is necessary to compare its predictive powers against other analytic techniques. In general, these techniques can be divided into two classes: mathematical models and empirically-based predictor equations. With regards to the former, only one math model is known to have been built outside ARCTEC and this model is the Milano program [1973]. Inadequacies in its performance have already been well documented by White et al. [1973] so that any effort to use it as a basis of comparison would be inappropriate. On the other hand, the predictor equations enjoy fair popularity in the preliminary design of icebreaking vessels. A

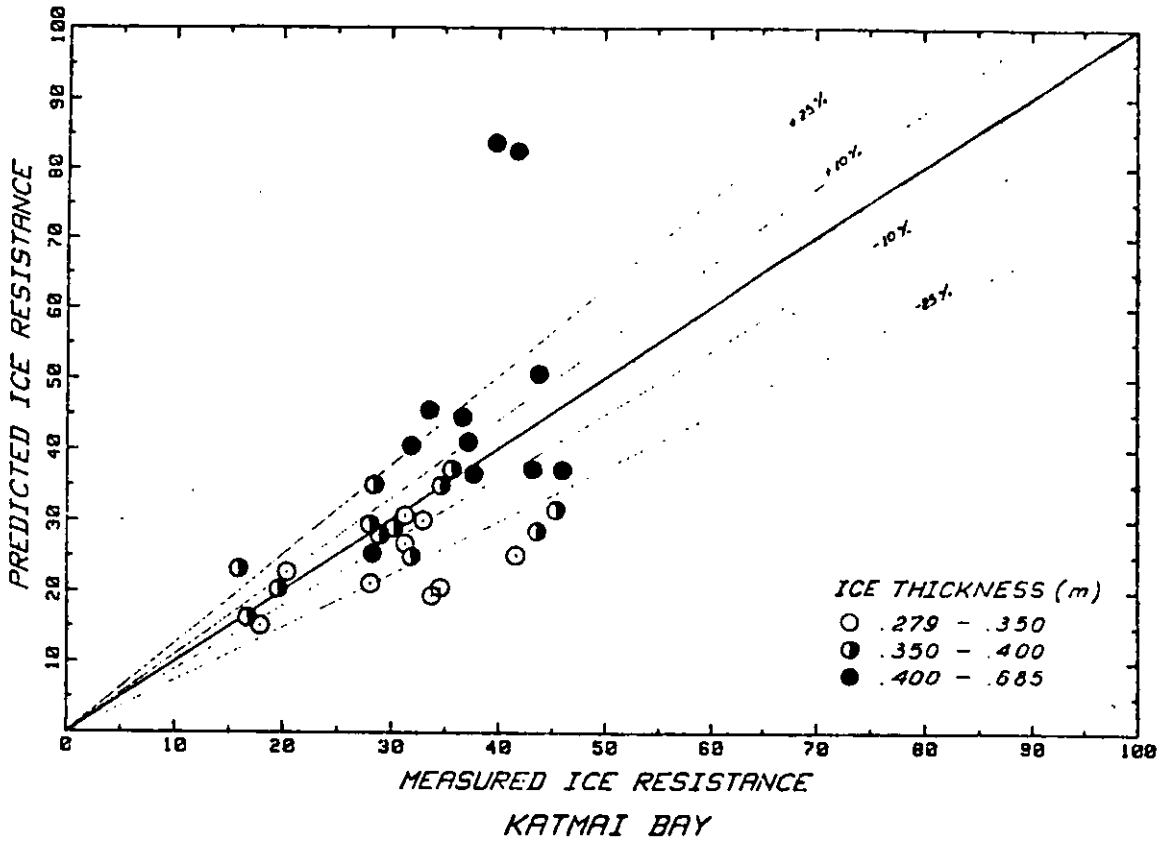


Figure 12. Splice final run: Katmai Bay.

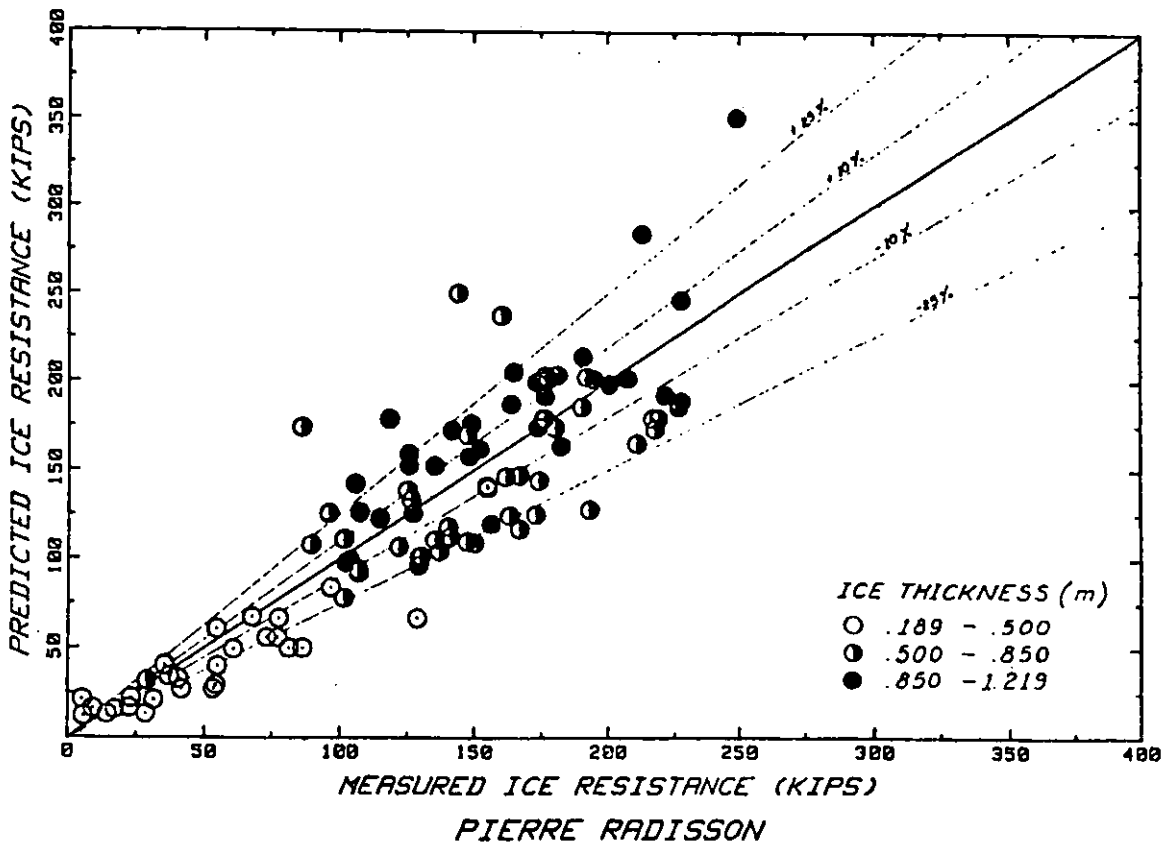


Figure 13. Splice final run: Pierre Radisson.

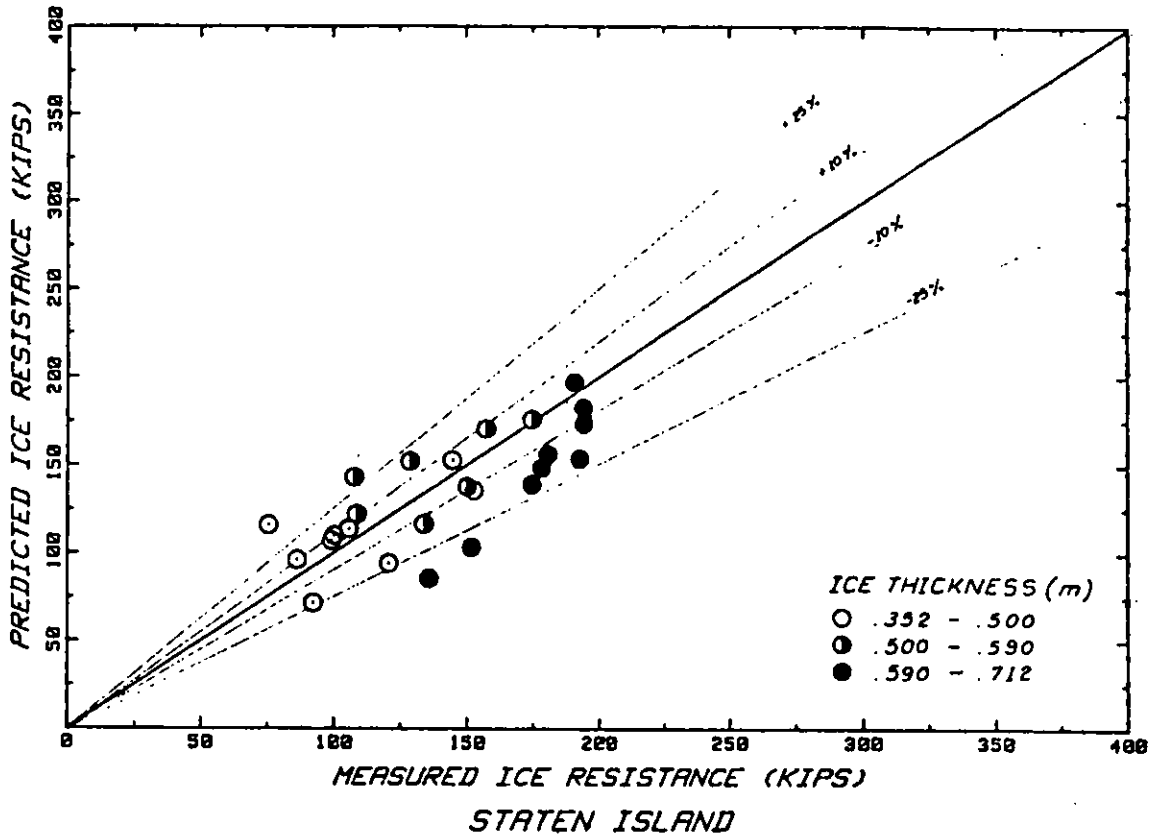


Figure 14. Splice final run: Staten Island.

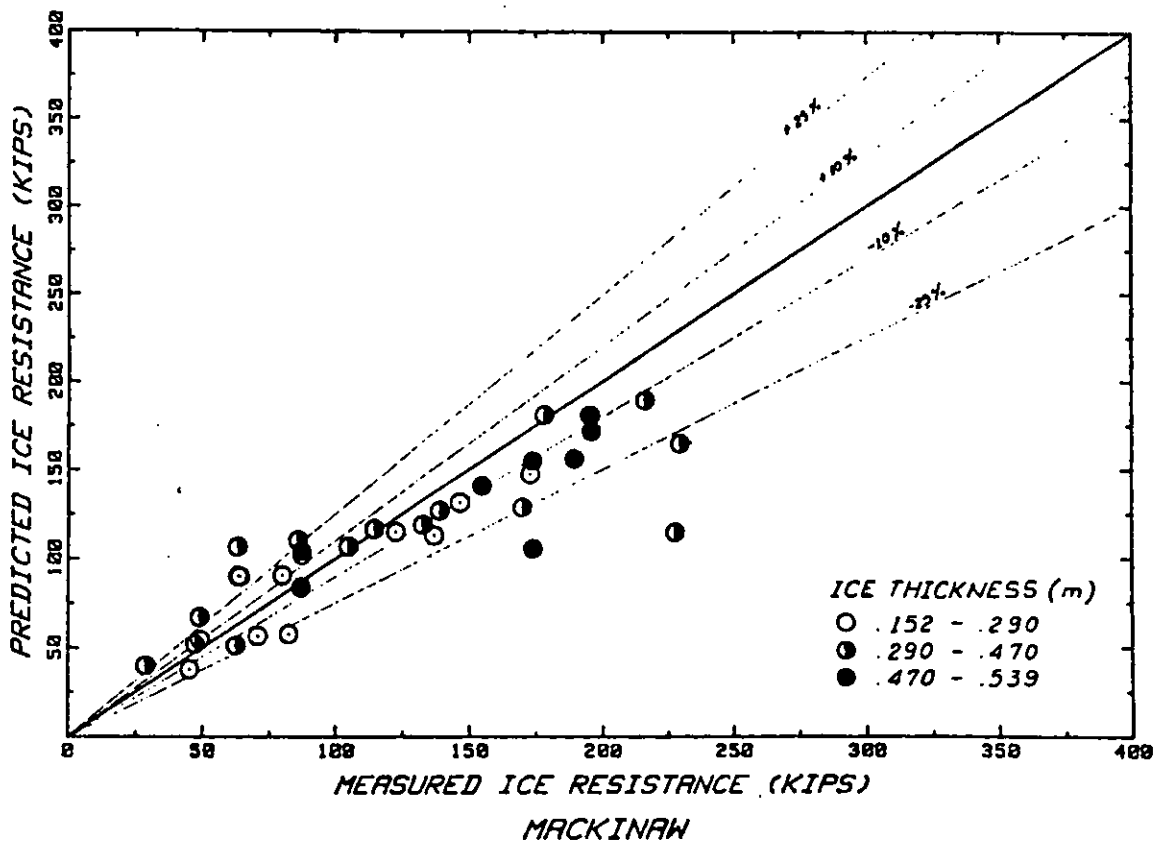


Figure 15. Splice final run: Mackinaw.

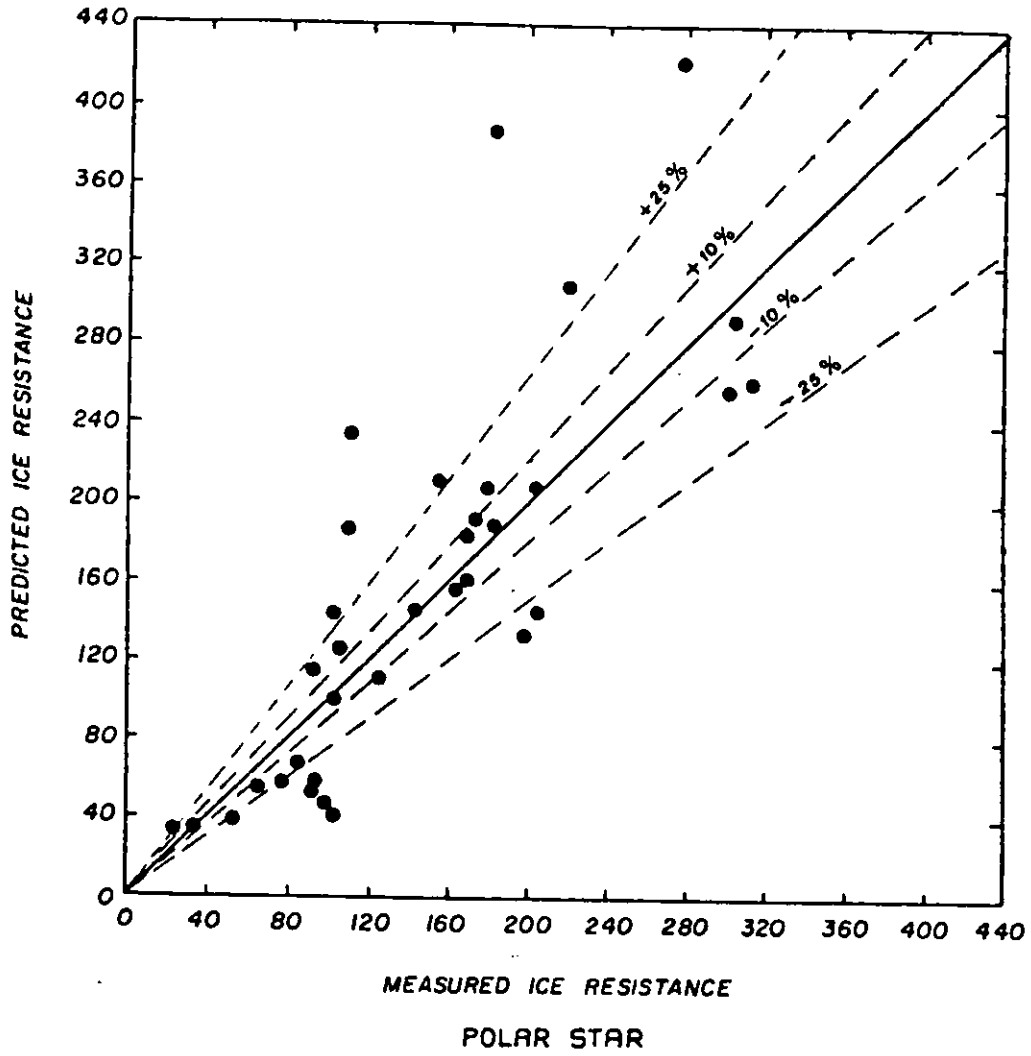


Figure 16. Splice run with snow cover effects: Polar Star.

Large number of such equations exist with the most recent being the Lewis equation given in my recent SNAME Paper [1982]. This equation was developed against the largest, most reliable database assembled to date. This predictor equation predicts ice resistance, R_i , in the form:

$$R_i = \rho g R h^2 \left[3.8989 + 0.0123 \left(\frac{\sigma_f}{\rho g h} \right) + 0.223 \left(\frac{U}{\sqrt{g h}} \right) \left(\frac{L/h}{\sqrt{R/h}} \right) \right]. \quad (26)$$

Table 3 compares the results of the above equation against the SPLICE Model's predictions for the four ships used previously. In the case of the MACKINAW, the accuracy of the SPLICE Model over the prediction equation is nominal and if such results were typical of all ships, one would wonder as to the value of this program. However, the advantages of a more complex approach become apparent when looking at the results for the other ships. For the STATEN ISLAND, nearly five times as many points lie within the 10% band when comparing the mathematical model against the predictor equation. For the KATMAI BAY, the SME for the SPLICE Model is nearly half that of the predictor equation. And finally for the PIERRE RADISSON, the predictor equation breaks down and the merits of the theoretical approach are clear.

The inherent problem with simple predictor equations is their inability to account for a host of factors which influence ice resistance. The two primary considerations are hull form and frictional characteristics, but even these parameters do not portray the entire picture. Without a breakdown of the theoretical components and a structuring of these components into a rational approach, the ability to predict resistance in absolute terms for a variety of hull forms and ice conditions is marginal at best. In consequence, it is our belief that the SPLICE Model is the most sophisticated and accurate prediction technique developed so far.

TABLE 3
COMPARISON OF SPLICE MODEL AND LEWIS EQUATION*

	<u>MACKINAW</u>			<u>STATEN ISLAND</u>	
	SPLICE	LEWIS		SPLICE	LEWIS
±10%	22.9%	22.9%	±10%	34.6%	7.7%
±25%	71.4%	62.8%	±25%	84.6%	76.9%
SME	139.3 KN	141.3 KN	SME	112.4 KN	149.3 KN

	<u>KATMAI BAY</u>			<u>PIERRE RADISSON</u>	
	SPLICE	LEWIS		SPLICE	LEWIS
±10%	31.3%	21.9%	±10%	26.5%	2.0%
±25%	68.8%	34.4%	±25%	71.7%	16.7%
SME	57.7 KN	91.9 KN	SME	142.7 KN	510.4 KN

*This table presents the percent of full-scale data points lying within both 10% and 25% of the values predicted by the two techniques along with the standard measure of error calculated over the complete database for each ship.

REFERENCES

- Bulat, V. and I. F. Glen, "The Testing of a Ship Model in Ice for the National Research Council," ARCTEC CANADA Limited Report No. 335C-3, Kanata, Ontario, 1981.
- Bulat, V. A., Discussion on: "Performance of CCGS FRANKLIN in Lake Melville, 1980" by M. Michailidis and D. C. Murdey, Sixth Ship Technology and Research Symposium, The Society of Naval Architects and Marine Engineers, 1981.
- Comstock, J. P., *Principles of Naval Architecture*, The Society of Naval Architects and Marine Engineers, 1967.
- Edwards, R. Y., J. W. Lewis, J. W. Wheaton and J. L. Coburn, "Full-Scale and Model Tests of Great Lakes Icebreaker," Presented at the Annual Meeting, SNAME, New York, NY, 1972.
- Edwards, R. Y., R. A. Major, J. K. Kim, J. G. German, J. W. Lewis and D. R. Miller, "Influence of Major Characteristics of Icebreaker Hulls on Their Powering Requirements and Maneuverability in Ice," Presented at the Annual Meeting, SNAME, New York, NY, 1976.
- Edwards, R. Y., B. Johnson, M. Dunne, G. Comfort and V. Bulat, "Results of Full-Scale Trials in Ice of CCGS PIERRE RADISSON," *Proceedings*, Sixth Ship Technology and Research (STAR) Symposium, Paper No. 23, SNAME, New York, NY, 1981.
- Enkvist, E., "On the Ice Resistance Encountered by Ships Operating in the Continuous Mode of Icebreaking, Report 24, The Swedish Academy of Engineering Sciences in Finland, 1972.
- Kashteljan, I. I., Poznjak and A. J. Ryvlin, "Ice Resistance to Motion of a Ship," (Translation), Sudostroenie, Leningrad, 1968.
- Lecourt, E. J., R. A. Major, H. L. Thomas and J. N. Naegle, "Recent United States Coast Guard Efforts to Improve Icebreaking Efficiency," Presented at the Spring Meeting (STAR) Symposium, SNAME, New London, CT, 1978.
- Lewis, J. W. and R. Y. Edwards, Jr., "Methods for Predicting Icebreaking and Ice Resistance Characteristics of Icebreakers," Presented at the Annual Meeting, SNAME, New York, NY, 1970.
- Lewis, J. W., F. W. DeBord and V. A. Bulat, "Resistance and Propulsion of Ice-worthy Ships," *Transactions*, SNAME, The Society of Naval Architects and Marine Engineers, 1982.
- Mathis, P. B., M. P. Lasky and L. B. Crook, "Powering Predictions and Flow Observations for the United States Coast Guard Proposed Icebreaker Design (M-14-3) Represented by Model 5245," Report P-223-H-09, Naval Ship Research and Development Center, 1971.

- Milano, V. R., "Ship Resistance to Continuous Motion in Ice," *Transactions*, SNAME, Vol. 81, New York, NY, 1973.
- Milano, V. R., "Ship Resistance to Continuous Motion in Ice, Ph.D. Dissertation, Stevens Institute of Technology, Hoboken, NJ, 1972.
- Motora, S. and R. B. Couch, "Maneuverability of Full-Bodied Ships in Restricted Waters, University of Michigan, 1961.
- Murdey, D. C., "Resistance and Propulsion Experiments with Model 327-1 and Propellers 66C and 66R," NRC MDSL Report LTR-SH-269, 1980.
- Naegle, J. N., "Ice-Resistance Prediction and Motion Simulation for Ships Operating in the Continuous Mode of Icebreaking, Ph.D. Thesis, University of Michigan, 1980.
- Nevel, D. E., "The Narrow Free Infinite Wedge on an Elastic Foundation, U.S. Army Cold Regions Research and Engineering Laboratory, 1961.
- Nevel, D. E., "A Semi-Infinite Plate on an Elastic Foundation, Report 136, U.S. Army Cold Regions Research and Engineering Laboratory, 1965.
- Newman, J. N., "Marine Hydrodynamics," The MIT Press, 1977.
- Noble, P. and V. Bulat, "Final Report on Optimization of Bow Forms for a Medium Icebreaker," ARCTEC CANADA Limited, Report No. 461C, Kanata, Ontario, 1979.
- Nogid, L. M. and D. V. Dubrovin, "On Viscous Resistance of Icebreakers, Sudostroenie, 1962.
- Pennington, R. H., "Introductory Computer Methods and Numerical Analysis, The Macmillan Company, 1965.
- Popov, Y. N., O. V. Faddeev, D. E. Kheisin, and A. A. Yakovlev, "Strength of Ships Navigating in Ice, Sudostroenie, 1968.
- Runeburg, R., "On Steamers for Winter Navigation and Icebreaking," *Proceedings*, The Institution of Civil Engineers, Vol. 97, Part 3, London, 1888.
- Saunders, H. E., "Hydrodynamics in Ship Design," The Society of Naval Architects and Marine Engineers, 1965.
- Vance, G. P., A. S. Gracewski and M. J. Goodwin, "Full-Scale Icebreaking Tests of the USCGC KATMAI RAY," *Proceedings*, Sixth Ship Technology and Research (STAR) Symposium, Paper No. 25, SNAME, New York, NY, 1981.
- Vance, G. P., Discussion on: "Resistance and Propulsion of Ice-Worthy Ships," by J. W. Lewis, F. W. DeBord and V. Bulat, 1982 Annual SNAME Meeting, New York, NY, 1982.

Wangdahl, G. E., "The External Penalty Function Optimization Technique and Its Application to Ship Design, Report 129, University of Michigan, 1972.

West, E. E., "Powering Predictions for the United States Coast Guard 140-Foot WYTM Represented by Model 5336," Naval Ship Research and Development Center, Report No. SPD-223-16, Bethesda, MD, April 1975.

White, R. M., "Prediction of Icebreaker Capability," The Institute of Naval Architects, 1969.

White, R. M., G. P. Vance and J. W. Lewis, Discussions on 1979 *SNAMF Transactions*, The Society of Naval Architects and Marine Engineers, 1973.



SHIP PERFORMANCE AND RESISTANCE IN ICE RIDGES

Prepared by:

Dr. Arno J. Keinonen,
Manager

ABSTRACT

Ice ridges offer the most serious obstacles to the practical operation of icebreaking ships in Arctic environments.

Using both data from the Baltic and the Canadian Arctic, this paper introduces a theory of ridge resistance accompanied by a review of model and full scale testing methodologies and results related to ship performance and resistance in first-year ridges. The main text is complimented by two extensive appendices detailing the mathematical methodology for deriving the components of pure ridge resistance as well as providing a computer program listing for ridge resistance analysis.

ACKNOWLEDGEMENTS

The Baltic information contained in this paper relating to both full scale model tests and theoretical methodology comes from Wärtsilä Helsinki Shipyard. The data related to the Canadian Arctic comes from Dome Petroleum Limited and Canadian Marine Drilling Ltd. both from Calgary. These companies have provided me with a unique opportunity to work at the leading edge of technology in the field of icebreaking science and further, to use that knowledge in this presentation.

NOMENCLATURE

TEXT SYMBOL	DEFINITION
g	acceleration of gravity
h (or H)	ridge thickness
h_s	height of ridge at parallel side plane
\bar{h}_s	average pressure height
h_x	added ridge thickness due to development
l', m', n'	direction cosines of a force for x, y, z-axes
$l, 2, 3, 4, Y, i$	penetrations for ridge growth
p	pressure
p_B	pressure against hull with B-inclination
$r(1, 2, j)$	moment levers
α	half angle of entrance of waterline
α'	half angle of entrance of waterline or normal plane to total hull force
β	angle of friction between ship's hull and ice
β	angle between vertical plane and parallel middle body side
β'	inner angle of friction of ridge mass
ϕ (or ψ')	angle between horizontal plane and ship's buttock
ϕ' (or ψ')	angle between horizontal plane and buttock of normal plane to total hull force
$\gamma(1, 2)$	angle between horizontal plane and breaking plane (for upper breaking plane, lower breaking plane)
δ	angle between horizontal plane and increasing thickness under ship's bottom
ϵ	index for end plane

NOMENCLATURE

TEXT SYMBOL	DEFINITION
μ	coefficient of friction between ship's hull and ice
μ_B	solidity of ridge mass
ν	Poisson's ratio for ridge mass
ρ_Δ	density of water less density of ice, buoyant density of ice
σ	normal stress
σ_H	normal stress against ship's hull
$\sigma_Y(1,2)$	normal stress against breaking plane (upper, lower)
σ_E	normal stress against end plane
τ	shear stress
τ_0	cohesion of ridge mass
$\tau_Y(1,2)$	shear stress in breaking plane (upper, lower)
τ_E	shear stress in end plane
A	area
A_{PB}	cross sectional area of ice under parallel hull
A_S	contact area between ice and parallel sides of hull
$A_Y(1,2)$	area of breaking plane (upper, lower)
A_E	area of end plane
B	breadth of ship
$F(x, y, z)$	force (its axial components)
F	shear friction resistance
$F_{G_1}(\sigma_Y, \tau_Y, \tau_0)$	buoyancy force, (components normal and parallel to breaking plane, total)

NOMENCLATURE

TEXT SYMBOL	DEFINITION
$F_{N(x,y,z,xy,xz)}$	normal force (its components)
F_{PB}	buoyant ice force against flat bottom of ship
$F_{TOT(0,1,2)}$	total hull force (due to upper, lower breaking plane)
F_{ϵ}	force to break end plane
$F_{\sigma\gamma,\tau\gamma}$	normal force, shear force to breaking plane
$F_{\mu(x,y,z)}$	frictional force (its axial components)
F_{τ_0}	cohesive force
$G_{(1,2,3)}$	volume of ice for buoyancy force (its components)
L_p	length of parallel waterline
L_{pp}	length of parallel part of hull
L_p'	effective parallel hull length
R	resistance
R_{ICE}	total ice resistance
R_{PB}	total ice resistance flat ship's bottom
R_{PS}	total ice resistance parallel ship's side
R_{TOT0}	pure ridge resistance, totally at 0-speed
$R_{\gamma_{1,2}}$	total ice resistance, γ -plane breaking (upper, lower)
$R_{\epsilon(1,2)}$	resistance due to end plane breaking (upper, lower)
T	ship's draught
V_1, V_2, V_3	subdivisions of buoyant ice mass
b	length of γ -breaking plane

NOMENCLATURE

TEXT SYMBOL	DEFINITION
ψ	angle between horizontal plane and a section perpendicular to waterline
ψ'	angle between horizontal plane and a section perpendicular to total hull force
∇	volume of displacement
A_{PB}	cross sectional area of ice at parallel sides of hull
CONSTANTS	
C1	area of γ -breaking planes (Eq.(2.17)a)
C2	$\frac{1}{\cos\gamma} + \frac{1}{\tan\psi}$, geometric coefficient
C3	buoyancy force (Eqs.(2.17)c,(2.23),(2.40))

1.0

INTRODUCTION

It has been shown in practical operations of icebreakers and other ice navigating ships that the most serious obstacle to their passage is offered by ice ridges. In the Canadian Arctic, in Beaufort Sea, a ship can spend more than 80 per cent of its navigation time in midwinter penetrating ridges (Ref. 1). Also, in the Baltic there is evidence that the practical navigation velocity drops to a fraction of the velocity in undeformed level ice when ships have to penetrate ridges (Ref. 2). Thus, it is quite obvious that in order to estimate or to improve navigation performance of ships in ice-covered waters, research related to the performance and resistance of ships in ice ridges as well as research related to ridges themselves should have a high priority.

In the past, the majority of icebreaking research has been directed towards research into the performance of ships in level ice. The research on ridges and on ship performance in ridges have not been very popular until quite recently. This has been a consequence, I believe, of the fact that it is very difficult to define characteristics of ridges and to measure them. Also, ships testing in ridges and modelling techniques for this research have been considerably more difficult than corresponding techniques for level ice research. Furthermore, most research related to ridges has been done in the past for reasons not related to ship performance, and consequently not all the appropriate parameters have been observed for such a specific use.

Actual full scale tests of ships in ridges have been performed in a scientifically meaningful manner only during about the past 10 years. Reference (3) gives the first documented example of these kinds of studies. Related model testing techniques have existed also for about the last 10 years. References (4, 5) show some of the milestones. There seems to be neither any international

agreement on modelling techniques for ridges nor any generally accepted standards for testing a ship model in them. The same holds true for full scale testing of ships in ridges and their associated parameters. Also theoretical approaches are virtually nonexistent, Reference (4) being the only major study published on this. The full range of problems in determining ships' performance in transitting through ridged ice covers is depicted in Fig. 1.

The intent of this paper is to provide a sufficient summary of ridges to give the reader a basic understanding of their characteristics. The specific aspects of ship performance and resistance are covered in greater detail but also in a summarizing way rather than in specific details. Where details are required, appropriate references are given.

In this paper I will introduce a theory of ridge resistance. Also, I will review model and full scale testing methodologies and results related to ship performance and resistance in first-year ridges. The parameters and methodologies given here are by no means the only possible combination of those for use in research and development work related to icebreaking performance in ridges. They are, however, all consistent within this presentation and give a range of tools which can be used for analytical, full scale and model testing work.

The practical ways of translating the specified resistance and performance of a ship into actual transiting velocity on a practical route is a different level of problem from those introduced here. Thus, it is deleted from this presentation. For the purposes of actual transit efficiency determination additional specific input data is required on the number of ridges, their sizes, distribution and morphology. Also, a time domain simulation based on specific resistance and performance knowledge is required (or an alternative tool based on energy balance analysis or simply an analysis of time consumption) in order to arrive at transit time for a ship.

It is obvious that multi-year ridges form even more severe obstacles than those in first-year ice. In this presentation, only first-year ridges are covered. Comparisons to other such research is difficult since research in this area has been mostly kept proprietary. It appears, based on operational experiences in the Canadian Arctic in multi-year ice, that quite different methodologies are required to arrive at meaningful results related to ship performance in multi-year ridges.

2.0 RIDGES

The formation of ridges can be a consequence of two ice fields being pushed together. The edges of those ice fields start to break into small ice blocks which will be pushed above and below the parent ice sheets. Also, major ridge formations can be initiated from within a solid stationary ice sheet. Subsequently, the pressure within the ice sheet increases beyond the carrying capacity of the thinnest ice in that ice field, and the consequence is initiated cracking and movement and formation of ridges. It has been seen in the Beaufort Sea that hundreds of square kilometers of 0.6m thick ice has formed ridged ice fields overnight.

From a ship's performance point of view, ridges are divided into single ridges, ridge fields where single ridges are formed right next to each other and ridged ice fields where there is some unbroken level ice between the ridges. For the sake of completeness, the ridged ice field should be defined as an ice field where ridges are so close to each other that a ship which penetrates the ice field does not have sufficient distance to accelerate to its undisturbed speed in level ice between those ridges. When ridges are further apart they behave as individual entities.

Figure 2 depicts a typical newly deformed single ridge. There are three parts to a ridge. The sail is that part of the ridge which can be seen from above. It consists of broken ice blocks and potentially, snow. Underlying the sail, is the level ice which continues on both sides of the ridge and normally reaches the vicinity of the centre line

underneath the sail from both sides. For a newly formed ridge there are still two separate level ice sheets within the ridge not frozen together. The third part of the ridge is the keel where the majority of the broken ice blocks and potentially snow have been submerged.

When a ridge gets older some of ridge parameters change. The sail may accumulate more snow content both inside it between ice blocks and around the sail. This results in a change in the frictional properties of the sail. The thickness of the level ice increases both inside the ridge and around it. The thickness growth within the ridge is called consolidation. It appears that the thickness growth is more rapid inside the ridge than in the surrounding level ice field. The keel also will get some refreezing action due to pressure between the ice blocks in it and due to the cold temperature of ice during ridge formation. Ridges in the Arctic exhibit more consolidation than in the Baltic which may be because they form in much colder temperatures.

When the summer comes, ridges disappear from the Baltic where there is no leftover ice after the summer. In the Arctic, ridges may survive the first summer, or melting period, so-called, and then become second-or multi-year ridges thereafter. At this point, their characteristics from a ship performance point of view, change radically. Most or all of the gaps between ice blocks in the sail and the keel will be filled with ice during the melting period and during the second winter the salt content virtually disappears. Thus, the ridges become essentially pieces of solid ice and it becomes gradually impossible to differentiate between the sail, the consolidated layer, and the keel.

A comparison between Baltic ridges, first-year Arctic ridges and multi-ridges is shown in Table 1. It should be noted that the ridges do not seem to form from the thickest ice in the area. Typically, most ridges are formed of ice less or about half of the thickness of the thickest level ice. The reason that ridges are formed in the Canadian Arctic from the thickest first-year ice as well is that the driving force to form those ridges comes from the even thicker multi-year ice. Also, the thickness of ridges does not increase in proportion to the thickness of level ice.

Figure 3 shows an actual ridge field cross-section for the Baltic as well as one for the Canadian Beaufort Sea.

TABLE 1
RIDGES IN BALTIC VS IN CANADIAN ARCTIC
BALTIC DATA FROM REF. (14)
ARCTIC DATA FROM REF. (15)

	BALTIC	CANADIAN ARCTIC	
	FIRST-YEAR ICE	FIRST-YEAR ICE	MULTI-YEAR ICE
No. of Ridges/km in Ridged Areas	4.9	7 approx.	
No. of Ridges/km Through All Ice	1.25	2 approx.	
Size of Ridges, Sail to Keel (m)	1.25		
Thickness of Ice for Ridge Formation (m)	4	~ 6	~8
Thickness of Thickest Consolidated Layer as a % Level Ice (m)	0.25 - 0.7	0.25 - 2.5	-
Thickness Before Melting Period (m)	~1.5	3.5	All of the Ridge
Ave. Maximum Thickness Level Ice Before Melting Period (m)	1	2.5	3.5

The amount of ridges is expressed in the terms of the number of sails crossed when travelling a unit distance, here, a kilometer, along a path. Table 1 shows the density of ridges in these terms in the Baltic and in the Canadian Arctic. This parameter yields average numbers. Both in the Baltic and in the Arctic there are areas with virtually no ridging as well as areas with virtually nothing else but ridges. One rule of thumb can be given. In archipelago's both in the Baltic and the Canadian Arctic, ridging density decreases with the increasing density of islands. In the Canadian Arctic, the heaviest ridges appear at the periphery of the Beaufort Sea in water depths of 15 to 40 meters.

There are some special cases related to ridging which will effect ship navigation. The most important is that in shallow coastal water ridges may actually ground to the sea floor and after grounding the ridge growth may continue. In such cases, sail will still increase in size. Then, new parameters are introduced to ridge characteristics of importance for ship navigation such as the overweight of the ridge due to pile up of ice after grounding. Also, the existence of the sea floor as the limiting boundary for ice to move is an important factor.

3.0 AN ANALYTICAL APPROACH FOR CALCULATING RIDGE RESISTANCE

If ridges as irregular ice features are difficult to define, the same certainly can be said about the analytical approaches in determining ships' behaviour in them. A number of simplifications and idealizations have to be made before one can even start to think of mathematical methods in determining the ridge resistance. Figure 4 shows our idealized ridge field which is the starting point for analysis. The ship which is shown in the middle of this idealized ridge field is on its way through it.

The first phase of resistance occurs between the bow of the ship and the ridge and the second phase between the parallel middle body of the ship and the ridge. To illustrate and to analyze these, a simplified ship geometry is assumed as shown in Fig. 5. The bow of the ship basically breaks the ridge and pushes the ice masses away from the path of the ship. The parallel middle body experiences a resistance component mainly of a static nature not pushing the ice aside anymore but introducing frictional losses due to ice leaning against the sides and the bottom of the ship.

There are three major components of resistance in the bow region:

1. resistance due to the consolidated ice layer;
2. resistance due to the pushing of ice masses in the sail and keel to the sides and underneath the bottom of the ship; and,
3. resistance due to the acceleration of the ice masses

Schematically, the first two components are shown in Fig. 6 for a low velocity level.

The first resistance component due to a consolidated ice layer is at this stage assumed to be the same as the level ice resistance of the ship in the same ice thickness. The validity of this assumption is debatable but I will return to this question when discussing the analysis of full scale tests in Chapter 5.5. For small ridges and for heavily consolidated ridges, the resistance due to consolidation may be the major resistance component.

The second component, also introduced and analyzed as pure ridge resistance, Reference (4), is studied in more detail in Appendix 1. For the purpose of analysis of the behaviour of ice rubble formed from ice blocks, a convenient assumption is that this ice mass in ridge sail and keel behaves like soil under a passive pressure (Passive means that external pressure is applied on the mass). The required mechanical ice parameters for determination of this behaviour are: the mass density, the cohesion, the inner friction and the Poisson coefficient of this mass. Figure 7 illustrates the passive behaviour analysis of this mass. Coulombs method (Ref. 4), can be used for this analysis. This method assumes a shear plane in direction as shown in Fig. 7. The force balance is governed by Coulomb's Equation 1 below:

$$F_G \sin(\gamma + \beta') + F_{T_0} \cos \beta' - F_{TOT} \cos(\gamma + \phi') = 0 \quad (1)$$

For ice resistance determination purposes, the ice and ship geometry and the friction between the ship and the mass needs to be known as well. The application of Equation 1 for ship purposes thus requires further

elaboration. Full development of the methodology for equations used in determining ships resistance are outlined in Reference (4). A short summary of this methodology is found in Appendix 1 and therefore, I will only touch upon the basic principles used in the analysis.

The interaction between the rubble mass and each cheek of the bow as defined in Fig. 8 can be treated separately. After analysis of the force geometry as shown in Appendix 1, the longitudinal component of the force applied by the cheeks of the bow to the rubble mass, taking account of the friction, is the second component of the ridge resistance, the pure ridge resistance. As shown in Appendix 1, this resistance is made up of components shown in Equation (2) below, and modifications of it, components using geometric transformations taking into account the ship geometry and ridge geometry.

$$R_{\text{toto}} = R_{\gamma 1} + R_{\gamma 2} + R_{\epsilon} \quad (2)$$

The first component $R_{\gamma 1}$ is the Coulomb shear plane breaking of the ice rubble mass governed by modifications of equation 1 as shown in Appendix 1. The second component $R_{\gamma 2}$ is due to a second lower breaking plane as seen in Fig. 9, and the third component R_{ϵ} due to the shear in the endplanes of the ice rubble shown in Fig. 8. This is governed by Equation 3.

$$R = \frac{F_{\epsilon} \cdot \cos \gamma \cdot \sin \alpha'}{\sin(\gamma + \psi')} + 2 \cdot A_{\epsilon} \cdot \frac{\cos \gamma \sin \alpha'}{\sin(\gamma + \psi')} \quad (3)$$

Different components of Equation 2 do change when the thickness of the ridge relative to the draft of the ship changes as well as with the penetration of the ship into the ridge field causing changes in the geometry of the ridge around the ship.

The resistance due to the ice surrounding the middle body during ridge penetration can be analysed using a method based on determination of the mass and geometry of the ice around the middle body. The friction coefficient between the ice and the hull as well as Poissons coefficient for the ice mass are needed as well. Appendix 1 provides complete equations for this resistance component, which are basically equations expressing contact areas multiplied by the average contact pressures and finally multiplying them by the ship-ice friction coefficient.

An example showing the relative importance of different resistance components is given in Fig. 10 . Ship A is an icebreaker with virtually no parallel middle body and Ship B is a ship with a fairly long parallel middle body. The main ship parameters are given in the figure as well.

It can be seen that by far the most important resistance component is due to the Coulomb plane of breaking of the ice mass. In order to simplify the analytical calculations of ridge resistance, the resistance component based on the behaviour of rubble mass can be handled only by calculating the breaking of the upper Coulomb plane and adding 15 per cent to take account of the end planes and adding another 10-25 per cent for the middle body resistance depending on the length of the ship.

Another comparison within the theory, is the study showing what the optimum bow geometry for low ridge resistance might be. Figure 11 shows this kind of comparison for the upper plane breaking component only. Basically, this suggests that a flat landing craft type of bow with a shallow stem angle would be optimal for the breaking of a ridge. Also, another point to note is the smaller friction coefficient, the smaller the optimum stem angle.

Resistance due to the acceleration of the ice masses has not been mathematically modelled to date. Multiplication of the velocity component of the level ice resistance by the mass of ice in the ridge relative to the mass of ice in the level ice should give a conservative estimate of this component.

4.0 RESISTANCE MODEL TESTS

In Wärtsilä icebreaking model basin, the first-year ice ridges have normally been modelled by means of a homogenous ice block structure with a constant thickness as shown in Fig. 12. This kind of model ridge has been chosen after many trials with different ridge types. This type of ridge field closely matches the theoretical idealized ridge field outlined in Section 3, used for the purposes of mathematically modelling ridge resistance. The consolidated portion of the first-year ridge has been totally left out. This ice block mass has been frozen only slightly on the top to prevent lateral movement of the mass. Then, in the subsequent analysis of these kinds of model tests, one has to add the resistance component related to the consolidated portion of the ridge, in the same way as in the theory presented in the previous section. A ship model is normally tested using a constant speed method in this type of ridge field.

The main parameters governing the model testing are: the thickness of this long rubble field, which is normally much longer than the ship model to be tested in it; the friction coefficient between the hull of the model and the ice. The resistance for a model also increases with continuing penetration of the model into the ridge field until the whole model is enveloped by the ridge.

Figure 13 depicts the basic stages of development of ice resistance for a simplified ship. When the model is fully in the ridge, we call the ridge resistance the fully developed ridge resistance, the same as in the mathematical model, found in Appendix 1. This fully developed resistance can be used to make comparisons with the theoretically calculated developed ridge resistance using the methods as introduced in the previous section. The development of the ridge profile during model penetration, as related to the development of resistance, follows the principle shown in Appendix 1, Figure 2.8.

Figure 14 shows the fully developed resistance from model tests in this kind of an homogenous ridge field with model parameters as shown in Table 2. This Table also lists a full range of values for model ridge parameters and components of ridge resistance as calculated based on the theory introduced in the previous section. An important thing to note is that both the model tests and the theory indicate a nearly linear relationship between the thickness of the rubble field and the developed ice resistance in it.

In all comparisons between the model test results and those based on the theory the agreement has been reasonably good within about 30 per cent. Differences appear in both directions, theory predicting at times high and at other times low values relative to model tests. The ice characteristics for purposes of full scale predictions and comparisons between model tests, theory and full scale tests are shown in Table 2 for a sample case. Actually, model ridges are the only ones where actual accurate measurements of the characteristics of the ice block mass can be made so that these basically identical parameters can be used as a first approximation of characteristics of natural unconsolidated first year ridges. The densities will vary though between different geographical areas.

An added requirement for the analysis of these kinds of model tests is the need to interpret the resistance, or energy, for penetration of shorter ridge fields or single ridges, and the exiting from them. Figure 15 illustrates a way of doing this type of interpretation.

A rectangular ridge is used representing a ridge field which could in nature look, for example, as shown by a dotted line. In Fig. 15a, first the resistance due to the bow develops to its maximum and remains at that level till the profile starts to decrease. If the ridge field is short enough, as in Fig. 15b, the resistance does not develop fully before it starts to decrease. The same applies to the resistance due to the middle body. If the length of the ridge field is shorter than the bow or parallel middle body, the highest value of the corresponding resistance component is in proportion of L_R/L_E or L_R/L_P respectively, to the full middle body resistance. This fully developed resistance value is derived out from the model tests, and from the theory.

5.0 FULL SCALE PERFORMANCE AND RESISTANCE TESTS

5.1 NAVIGATIONAL ASPECTS

When a ship penetrates a ridge field without having to ram into it, the key parameter in determining its performance is the energy required to penetrate the ridge field or alternatively the resistance. For big ships in small ridges this is the case. In the majority of ridge penetrations to date, ships are small and are not powerful enough to penetrate most ridge fields without being stopped. In that case, the ship has to execute a ram or several rams to penetrate the remaining part of the ridge or ridge field. Then, the navigation efficiency of the ship through ridges is determined by two key parameters. One is again the resistance or energy to penetrate the ridge field. The second parameter is the time factor. The rate of progress of the ship through a ridge field is determined by the length of penetration for each ram executed and the time that it took to execute the ram. Figure 16 schematically shows these parameters.

There is also another important factor involved. When the ship has been stopped by a ridge, it is essential that it can extract itself. If the resistance astern is higher than the thrust available for astern movement, a suitable auxiliary system or procedure will have to be applied for this purpose. In heaviest ridges in the Baltic, extraction contributes an important time component to ridge penetration. As shown in Ref. (3) it can use up to 54 per cent of the total ramming time. There is evidence that taking account of the extraction requirement is one of the key design requirements for icebreaking ships for the Arctic and that it has not automatically been assumed to be a key consideration in the design process.

Figure 16 shows schematically also the different phases of a ram. From this Figure, it can be seen that when using more time for a ram, one can use a longer acceleration distance and achieve a higher impact velocity, thus, helping to penetrate further. There is a limit, however, to the payoff of an added acceleration distance where the relative addition to the penetration length is less than the added time. This depends on the ridge, the ice conditions in the channel where acceleration takes place, and on the ice resistance, and the acceleration characteristics and mass of the ship.

5.2 RIDGE FIELD ASPECTS

Regrettably, one cannot choose idealizations for ship transit or for testing purposes but must experience the real ice conditions. Still, there is something one can do in order to achieve meaningful results for ships performance in ridges both for the purpose of determining operational capability of a ship as well as its resistance. One can choose the longest and generally thickest ridge fields. They are the closest match with the theory as well as with model tests. When the ships performance and resistance in this kind of extreme condition is known then determination of the performance (and resistance) of the ship in smaller size ridges and ridge fields is a matter of interpolation between performance in level ice (and resistance), and that determined in large ridge fields. A ridge field which is 100-200 m wide in cross-section in the direction of ship penetration and which has got a thickness 5-10 times that of the consolidated portion of the ridge is not too dissimilar to the idealized ridge field used for theoretical and model testing work.

Figure 3 depicts an example of one actual Beaufort Sea and one actual Baltic ridge field actually used for ship testing purposes.

The sails of full scale ridges vary drastically in shape and size in one ridge field producing on the average the same sail height as in the model ridge field. The same applies to the keel portion of the ridge fields and to the consolidated layer. The average thicknesses of our wide areas are the ones scaling to the idealized model of a ridge field. We have to recognize that at any point of time during penetration of a ridge field, a ship will not feel the ice resistance due to one point only in the ridge but over a large area determined by the width and the length of the bow of the ship, and that the middle body for long ships averages even larger areas. Then, the averaging of sail and keel profiles or the idealized ridge makes sense. Also, when one recognizes that both the theory and model tests show a linear dependency between the resistance and the thickness of the ridge, linear averaging does not cause any systematic errors. The validity of the averaging of the thickness of the consolidated portion of the ridge has not been accurately determined, but it appears that the variations of the thickness of this consolidation are considerably smaller than the variations in keel and sail profiles. Another important difference between full scale and model scale ridge fields is the existence of snow in natural ridges. In model ridges, no snow is used for modelling. The effect of this is an increase of friction in natural ridges due to the existence of snow.

The mechanical properties of natural ridge fields are not well known. Field measurements of ridge properties defining the global behaviour of a ridge do not exist. The block size distribution and the properties of ice blocks within the ridge as well as configuration properties have been measured on occasions. The best assumption for the Baltic to date is that inner friction and cohesion and Poissons coefficient for the ice mass in ridges are the same as those measured in ice model basins. Thus, a set of data for ridge properties representing Baltic ice ridges is as shown in Table 3. The least known, and at the same time the most critical, parameters are the adfreeze within the keel of a ridge and the effect of distribution of sizes of ice blocks within the ridge. The inner friction, cohesion and Poissons coefficient will vary with those.

The unknowns related to ice are not critical when thinking of the determination of performance or ice resistance of a ship during full scale tests or ship operations. Also, when scaling from full scale tests of one ship to another size of ship within the same ice regime, no problems should arise. The real need to know the right ridge parameters is when one attempts to use model tests or theories in predicting performance of a ship. The inaccuracies in such cases may be reduced by introducing semi-empirical and theoretical approaches calibrated against actual full scale ship tests.

5.3 CHARACTERIZATION OF RIDGES

The experiences during full scale ship trials have proven that a surprisingly simple approach can be taken when characterizing a ridge field for purposes of a ship test. The basic principle has been adopted that only the portion of the ridge profile above the water level has to be measured. The sail profile can then be translated into a relatively accurate estimate of the size of the keel profile as has been shown, both in the Baltic and in the Canadian Arctic (References 7 and 8). Using this procedure one can arrive at the estimate of a keel portion of a ridge field based on the fact that, on average, the balance of flotation of ice must exist. The other part of the ridge that has to be determined from the top side is the thickness of consolidation. Figure 3 shows the parameters measured for ship testing purposes.

The kind of ridge field cross-section as shown in Figure 3 is needed for the direction of a ship's approach to the ridge field which normally is perpendicular to the sail line. Critical visual evaluation of a ridge field is required in order to choose a profile for measurements and ship tests which represents the average sail heights in the ridge field.

5.4 TESTING PROCEDURE AND KEY PARAMETERS FOR TESTS

After having profiled a ridge field and having marked the line of penetration with reference marks on the ice, the appropriate testing procedures and associated parameters for these tests can be introduced as follows:

The parameters to be measured when calculating ship performance in ridges large enough to require ramming are:

1. ramming cycle;
2. entrance velocity; and,
3. penetration.

The power usage of the ship can also be documented for all these phases in order to fully determine the ramming characteristics of a ship. The rate of change of power effects the ramming behaviour and so does the ice propulsion interaction. During the extraction phase a gradual increase of power in order to determine the extraction capability can be implemented. Also, if any auxiliary devices or special procedures to extract the ship have been used such action can be documented.

In order to determine the ice resistance of a ship in ridges, the penetration phase has to be studied more carefully. The main parameters for that purpose are shown in Equation 3, which gives the resistance as a sum of lost kinetic energy from a ship and the energy available from its propellers.

The first parameter for resistance determination is the change of velocity over time during the penetration phase. Knowing that, and associated ship and added masses, the mass forces associated with the deceleration of the ship can be determined. The added mass in the case of a ship which is trimming considerably during the penetration phase may be closer to the added mass for trimming the ship rather than the longitudinal added mass to decelerate the ship. The added mass of ice effects the analysis of the resistance measurements. It has not been evaluated, but it is not felt to be critical at this early stage of development. When we compare ramming performance between any ships, the added mass of the ice can be considered to be the same.

The second parameter for resistance determination is the thrust of the propulsion during the penetration phase. Fairly rough methods of estimating this thrust during penetration are often times sufficient. This is for two reasons. Firstly, the thrust may only make a minor contribution to the resistance determination, due to high inertial forces which stop the ship. Secondly, the ways of determining thrust may not be that accurate when the propellers are operating in an environment full of large pieces of ice. The thrust deduction and wake fraction are difficult to estimate under such circumstances.

An important part of the testing procedure is to determine the relative position of a ship to the profiled ice ridge. Determining the moment of impact and the position of that impact point in the measured profile are essential. The position on the ridge profile where the ship has stopped needs to be determined. Also, in order to determine ship penetration, the vertical position of the ship at the end of a ram should be measured; thus, it is possible to calculate how much of the kinetic energy has been transferred into potential energy. This is so because the ship often tends to be in the lifted-up position at the end of a ram, and thus, part of the distance that the ship travelled from the moment of impact is used to lift the bow up along the stem rather than destroying and penetrating the ridge.

5.5 TEST RESULTS

From the testing procedure, it is fairly obvious how the determination of the speed of advance, or actual performance of a ship, in a ridge field can be analysed. It is governed by the equation in Fig. 16. Figure 17 displays the time phases for a set of rams. The penetrations can also be seen from this Figure. Figure 18 shows the actual speed of advance of the same Baltic icebreaker as a function of averaged ridge thickness over the total length of a ridge field. Several ridge fields are included in the plot. One has to note that the actual ridge thicknesses in the ice terminology, which are sail to keel maximum values, are normally 50-100 per cent higher than the thickness shown on the horizontal scale of Fig. 18 as an effective thickness of a ridge field.

In order to determine the ship's resistance in a certain type of ridge field at any point of time, a procedure must be adopted which can combine the ice profile in a meaningful way as compared to the progress of the ship through the ridge field. This kind of procedure is actually an averaging procedure which averages the ridge field in a similar manner as the ship averages it during penetration. The state of art of the knowledge of how the ship averages a ridge field is at an early stage. Accordingly, a simple procedure, shown below, is adopted, somewhat similar to that in Reference (3). First, the effective length of the bow of the ship has to be determined as distinguished from the parallel middle body of a ship. Fig. 5 gave a way to do this. Next the ridge thickness will be averaged for the ship penetrating it. The thickness of a ridge is defined for a position of the stem at the water line of the ship as the average of the thickness of this ridge counting back from the stem to the aft end of the bow. In a similar way the average thickness around the parallel middle body of the ship is determined starting from the point where the bow of the ship ends. Thus, each ship position in the ridge field corresponds to one specified ridge thickness for the bow and another one for the middle body of the ship. Plotting the momentary values of ship resistance against the corresponding ridge thickness, called effective ridge thickness, can be done as shown in Fig. 18.

From full scale experience with ships, the momentary values of resistance tend to vary quite significantly and a more appropriate approach is to consider the resistance during one ram as one resistance point. Then, the associated ridge thickness is the average of the curve showing the effective ridge thicknesses over the distance of penetration of that ram (Fig. 17). The ice resistance versus ridge thickness plot shows reasonable scatter, especially considering the complexity of the whole ridge penetration process which, has been used in plotting Fig. 18. There still is one more even simpler approach. It consists of averaging the whole cross-section of a ridge field and plotting it against an average ice resistance over all the rams in that ridge field. Then, the results may look as shown in Fig. 19. Another result from the Beaufort Sea shows basically similar scatter shown in Fig. 20. The interesting thing to note in the results from Beaufort Sea is that clearly the resistance vs. thickness relationship is linear but yet the straight line drawn through the results does not go to zero. This gives evidence that the consolidation resistance exists in clear measurable terms. Also, it was found that the point A which is shown in Fig. 20 corresponds to the consolidated thickness for the average consolidation in all the ridges where the tests were done approximately at a resistance value which the ship has in this thickness of level ice at the same velocity as the average velocities during penetration phases of the rams. The other interesting thing about Fig. 20 is that the two points which do not lie on the regression line represent departures from the average conditions during these tests. One of those points represents ramming velocities less than half of those used in other ridges. The other ridge field was built up out of ice blocks radically smaller than those on the average.

From the resistance one can then determine the energy of penetrating certain cross-sections of ridges. An example of this is shown in Fig. 21.

A shortcoming in the averaging procedures used is that the whole velocity component is averaged and we can only say the ice resistance represents the average velocity during the penetration phases over which the averaging occurred. It is also possible to tailor the results in their original form in order to extract a meaningful velocity component of the resistance as shown in Reference (4) for example. Yet, that turned out to be a major effort without yielding results one could confidently count on.

6.0 CONCLUSIONS

As seen in the presentation, there are ways to determine a ships performance in transitting ridged ice even though actual full scale measurements onboard ships are still rare. All aspects have not been covered in this connection but those ones related to ice resistance, energy of ridge penetration, and ramming were introduced in some detail.

In determining the transit performance of a ship the kinds of methodologies introduced here will lead to a good estimate. When using these methodologies, the biggest difficulty in evaluating the accuracy of such an estimate is not in the methodology itself but in the correctness of the input parameters. The biggest difficulty in estimating the transit performance of a ship in Arctic first-year ridges is the confidential nature of all the information that is available on actual ship performance in the actual Arctic ice conditions. Also, to date, the information in the public domain on characteristics of Arctic ridges is scarce.

The second biggest difficulty is in changing design concepts. For a reliable estimate, the performance of ships with radically new shapes has to be calibrated with full scale tests before making transit predictions for similar designs. It seems that introducing new concepts always introduce new aspects to performance in ice even though the basic methodologies are still valid.

REFERENCES

1. Keinonen, A.J., Duff, J., "Canmar Kigoriak-Demonstration of Arctic Capabilities", Proceedings, The 7th International Conference on Port and Ocean Engineering Under Arctic Conditions, Helsinki, Finland, April 5-9, 1983.
2. Gordin, S., Topp, A., "A Study on Ice Conditions Encountered by Ships and The Progress of Convoys in the Northern Part of the Gulf of Bothnia in the Winter of 1976", Basic Winter Navigation Centennial, Oulu, Finland, 1977.
3. Mäkinen, E., Keinonen, A.J., Laine, A., "Ice Resistance Measurements in Ridges with 1/B APV in the Baltic Sea", 3rd International Conference on Port and Ocean Engineering Under Arctic Conditions, Fairbanks, Alaska, 1975.
4. Keinonen, A.J., "An Analytical Method for Calculating the Pure Ridge Resistance Encountered by Ships in First-Year Ice Ridges, Ph.D. thesis, Helsinki University of Technology, Ship Hydrodynamics Laboratory, Otaniemi, Finland, 1977.
5. Keinonen, A.J., Nyman, T., "An Experimental Model - Scale Study on the Compressible Frictional and Cohesive Behaviour of Broken Ice Mass", IAHR Proceedings, Lulea, Sweden, 1978.
6. Enkvist, E., Varsta, P., Riska, K., "The Ship-Ice Interaction", The 5th International Conference on Port and Ocean Engineering Under Arctic Conditions", Norway, 1979.
7. Keinonen, A.J., "The Shape and Size of Ice Ridges in the Baltic According to Measurements and Calculations", Report 17, The Winter Research Navigation Board, Helsinki, Finland, 1979.
8. "Summary Compilation and Analysis of Ice Data Collected During Kigoriak Research Tests, 1979-80", Report #21, The Kigoriak Research Series, Dome Petroleum Ltd., (unpublished).

9. "1979-80 Full Scale Tests of the Canmar Kigoriak", Report #22, The Kigoriak Research Series, Dome Petroleum Ltd. (unpublished).
10. Gordin, S. (1977): LAIVIN C jäävastuskokeet (Ice Resistance Tests with SHIP C, in Finnish), Wärtsilä Test Report (unpublished).
11. Heideman, T. (1979): Utförande och analys av modellförsök i isvallar (Performance and Analysis of Model Tests in Ice Ridges, in Swedish). M.Sc.thesis, Helsinki University of Technology.
12. Laine, A. (1975): Full Scale Testing of SHIP A, Wärtsilä Test Report (unpublished).
13. Laine, A. (1977): SHIP B, Ice Resistance Tests, Wärtsilä Test Report (unpublished).
14. Keinonen, A.J., "Presentation of Sea Ice Ridges in General and Physical Characteristics of Baltic Ridges for Ship Resistance Calculations", Report #24, The Winter Navigation Research Board, Helsinki, 1978.
15. "Hazardous Ice Atlas of Arctic Canada", Prepared for Transport Canada, Ottawa, by Arctec Canada Ltd., January, 1983.

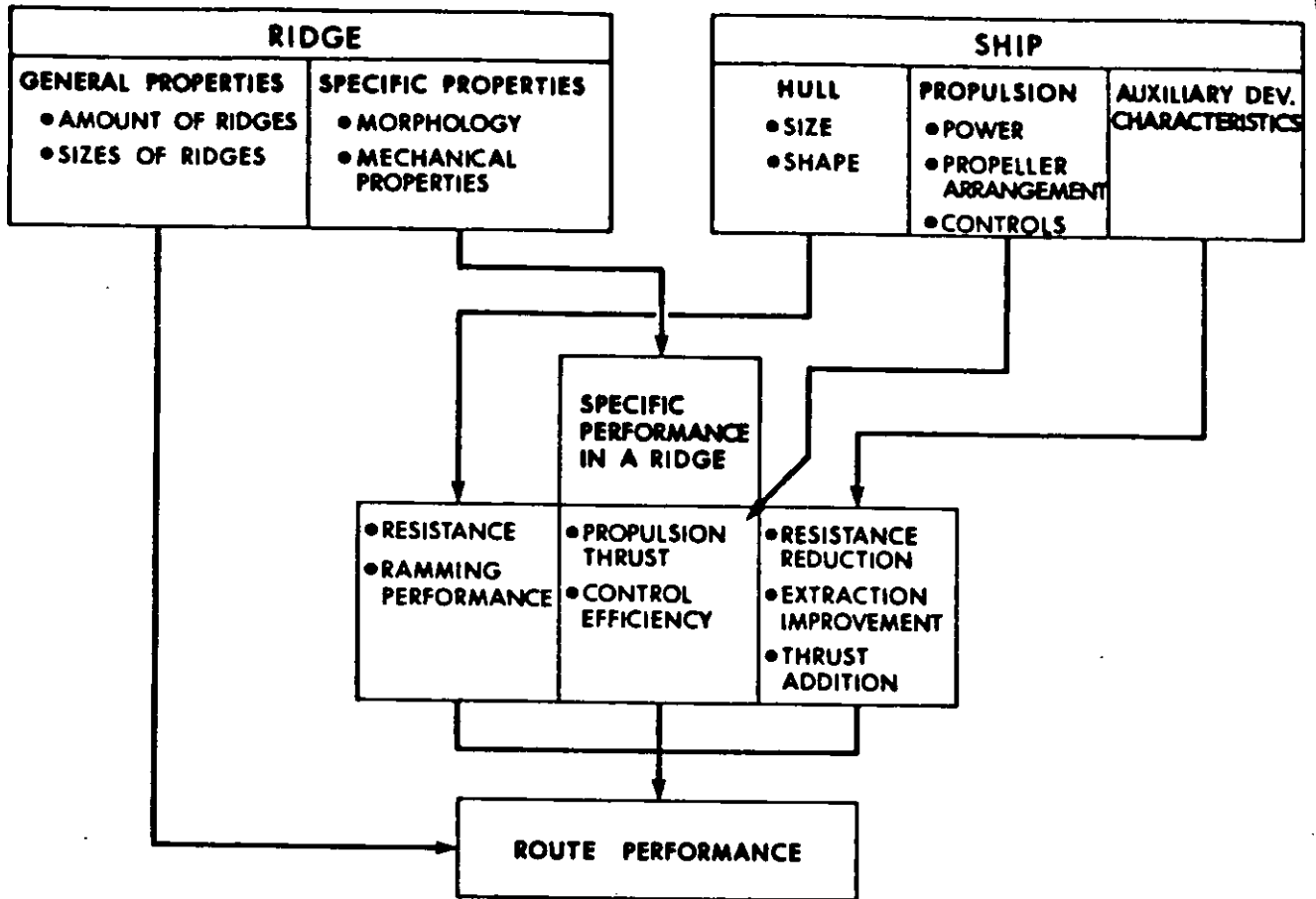


FIG. 1 RANGE OF RIDGE PERFORMANCE PROBLEMS

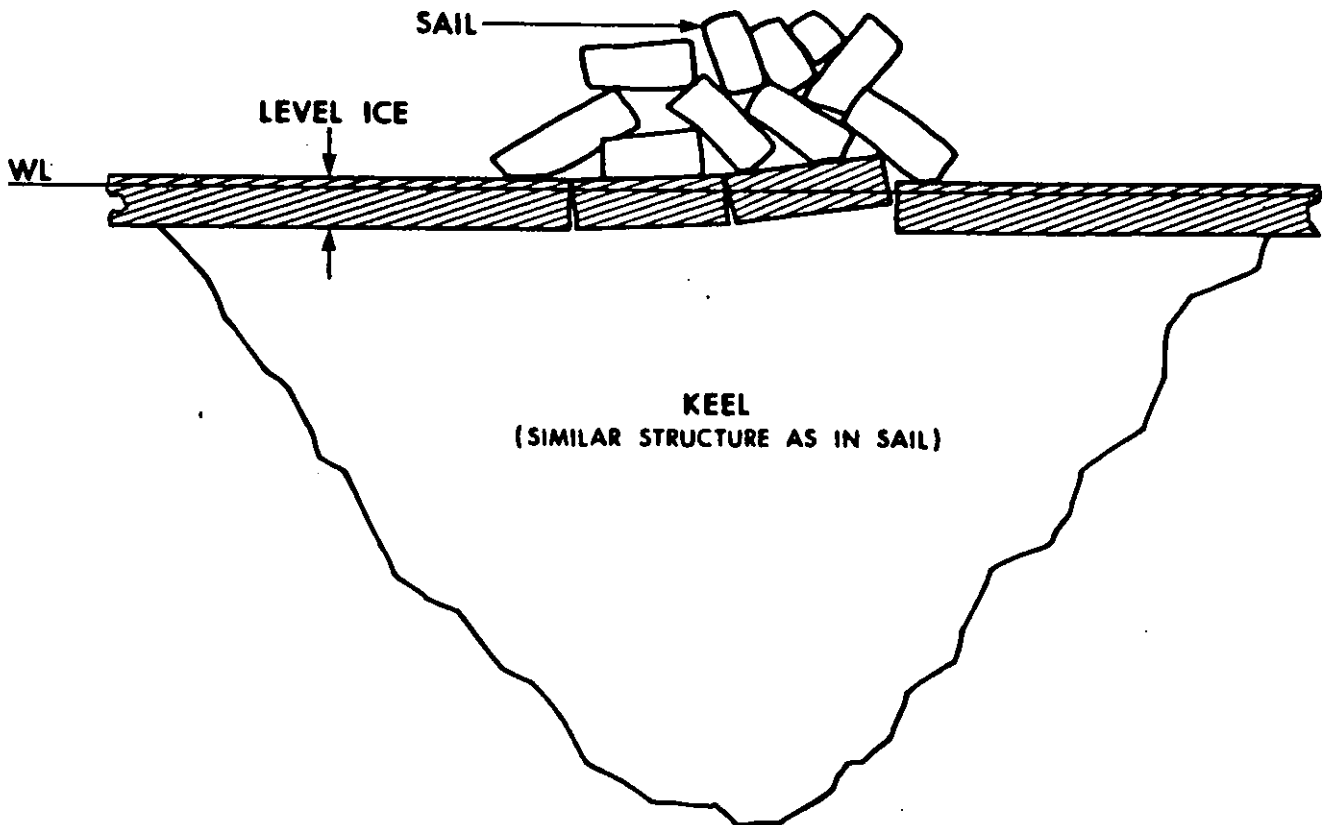


FIG. 2 A NEWLY FORMED RIDGE

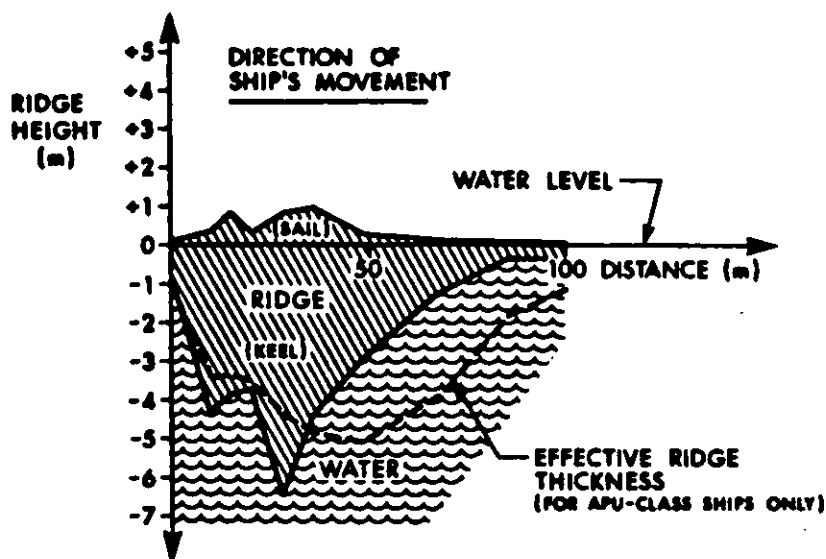


FIG. 3a AN EXAMPLE OF A RIDGE CROSS-SECTION IN THE BALTIC. REF. (3)

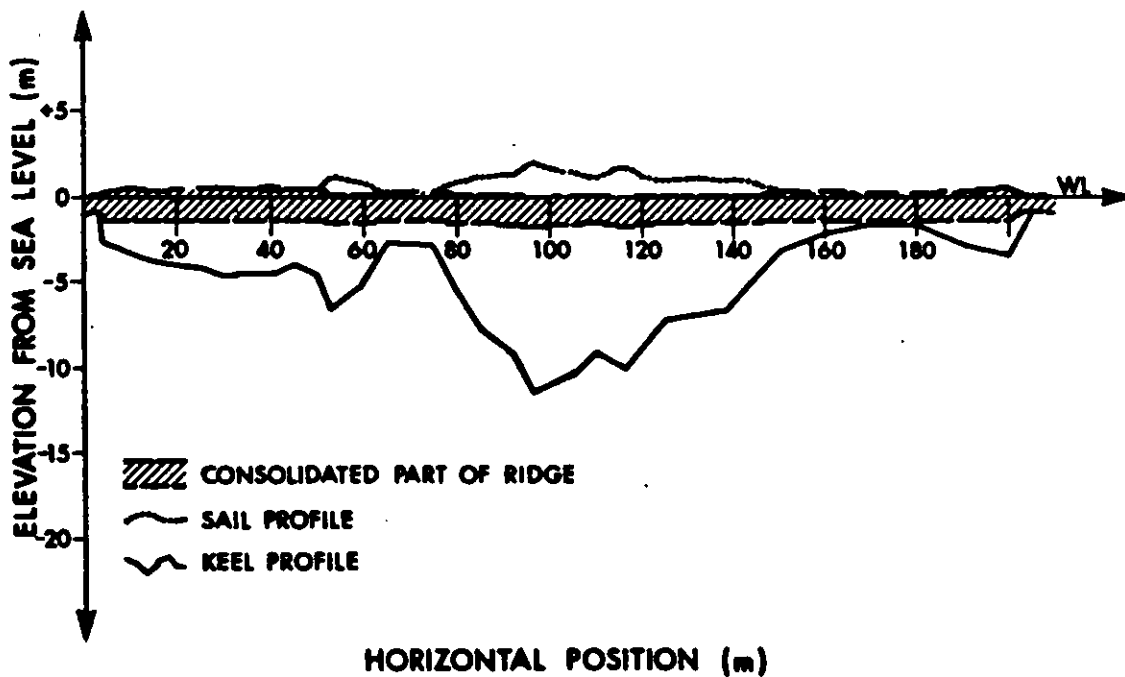


FIG. 3b AN EXAMPLE OF A RIDGE CROSS-SECTION IN THE BEAUFORT SEA. REF. (9)

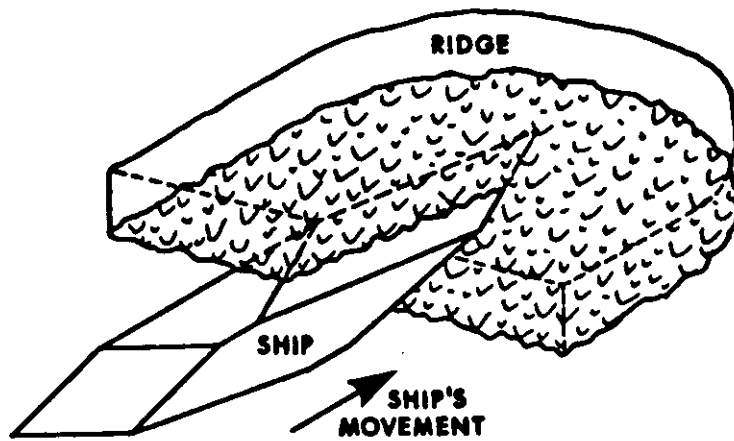
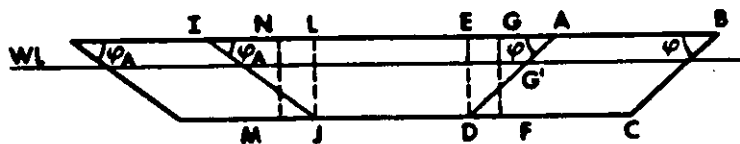


FIG. 4 INITIAL RESISTANCE CONDITION,
SUBMERGED PART OF SHIP HULL.
FOR SHIP GEOMETRY, SEE FIG. 5.
REF. (4)

XZ-PLANE



XY-PLANE

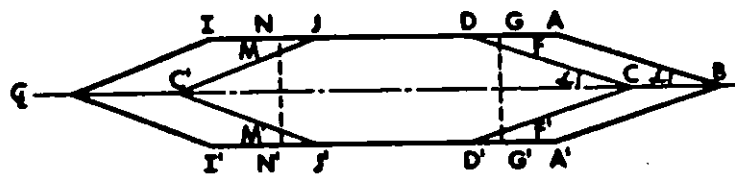


FIG. 5 SHIP'S GEOMETRY. REF. (4)

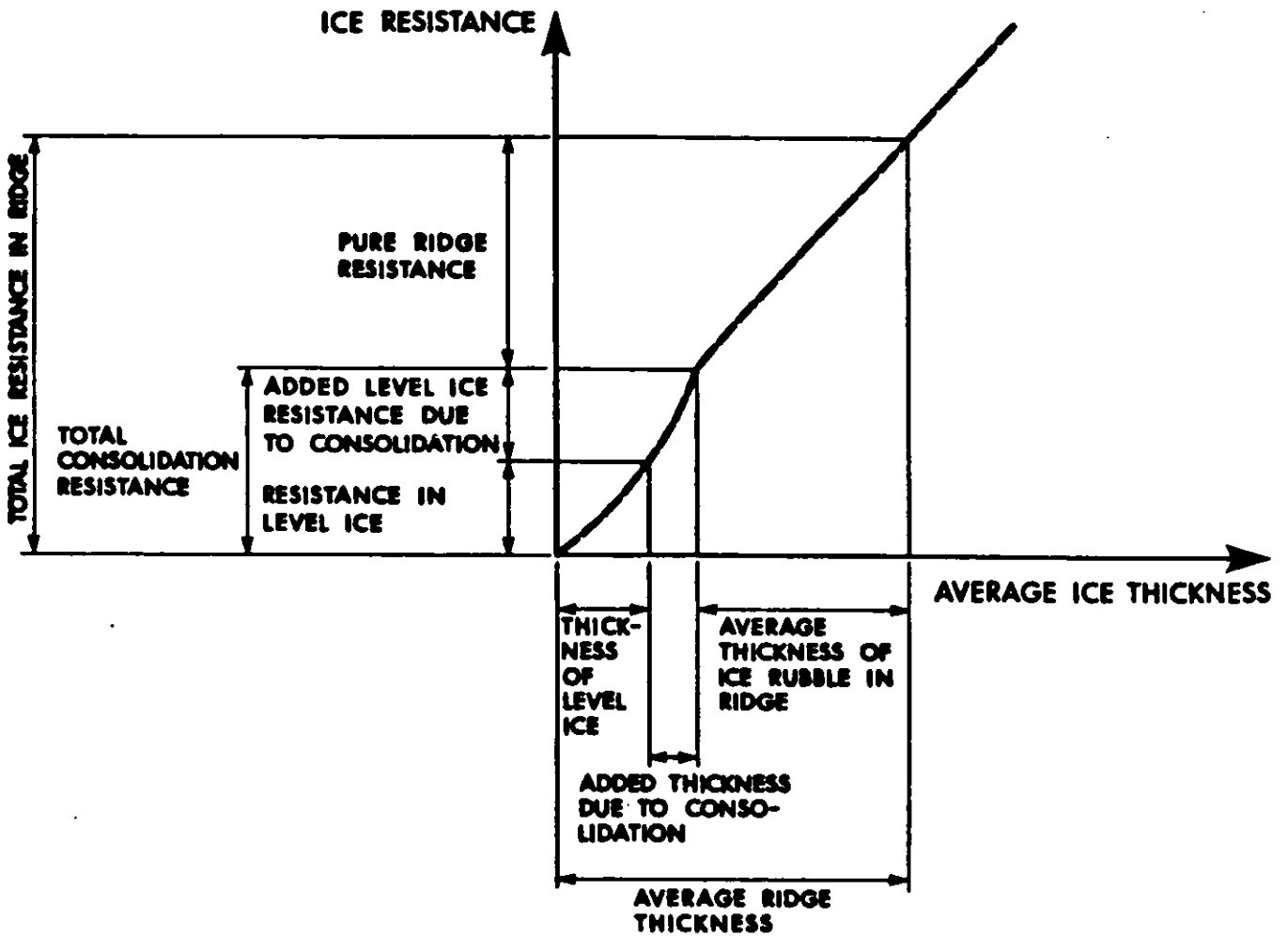


FIG. 6 RIDGE RESISTANCE COMPONENTS AT LOW VELOCITY

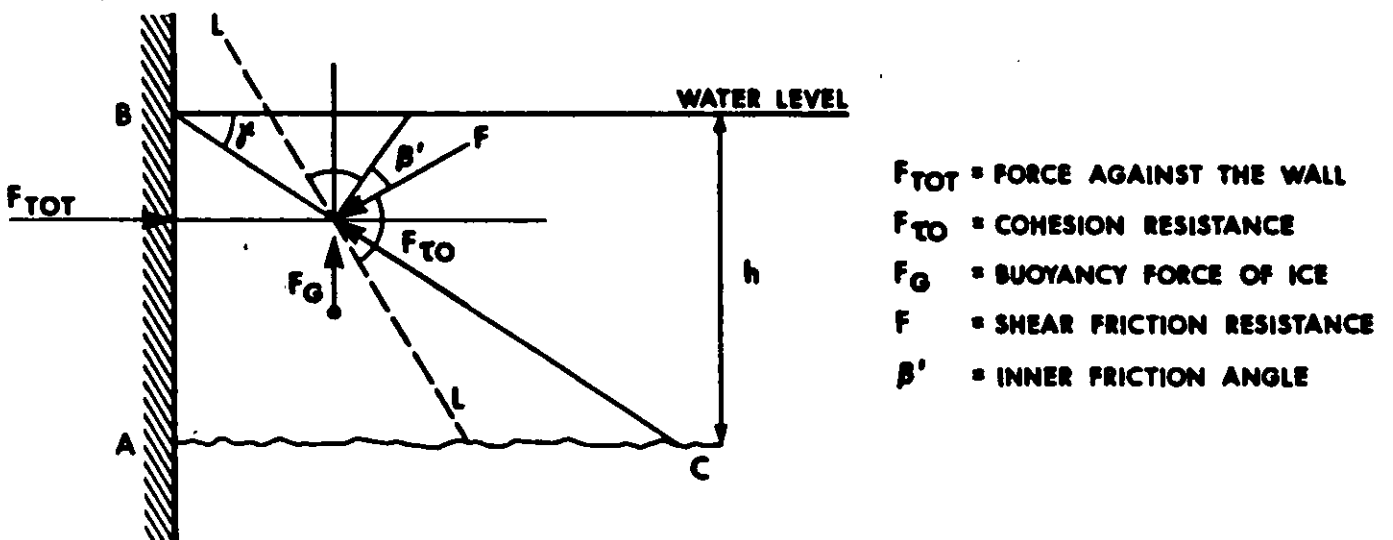


FIG. 7 COULOMB'S METHOD. REF. (4)

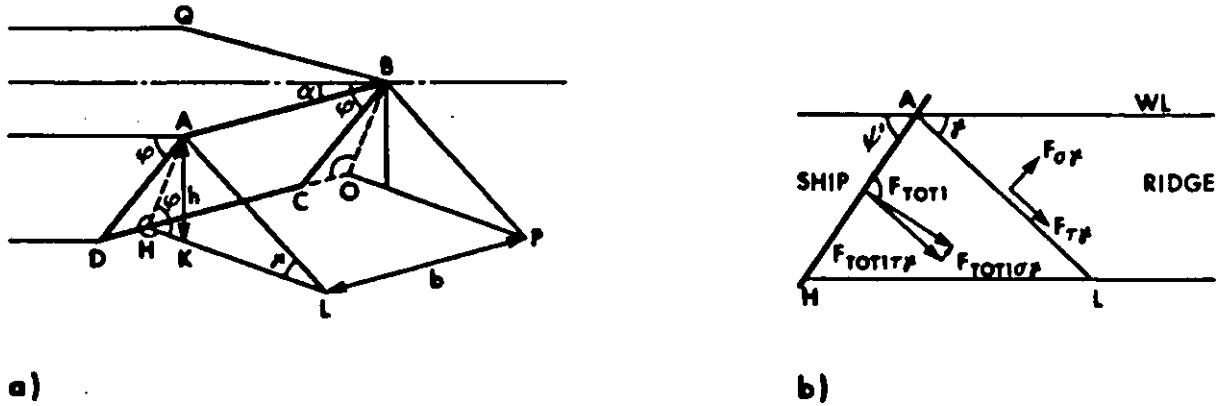


FIG. 8 a) STRESS ANALYSIS GEOMETRY FOR THE SIDE PLANE OF THE FORWARD BODY OF A SHIP (ABCD). b) COMPONENTS OF TOTAL SHIP'S FORCE IN β -PLANE. REF. (4)

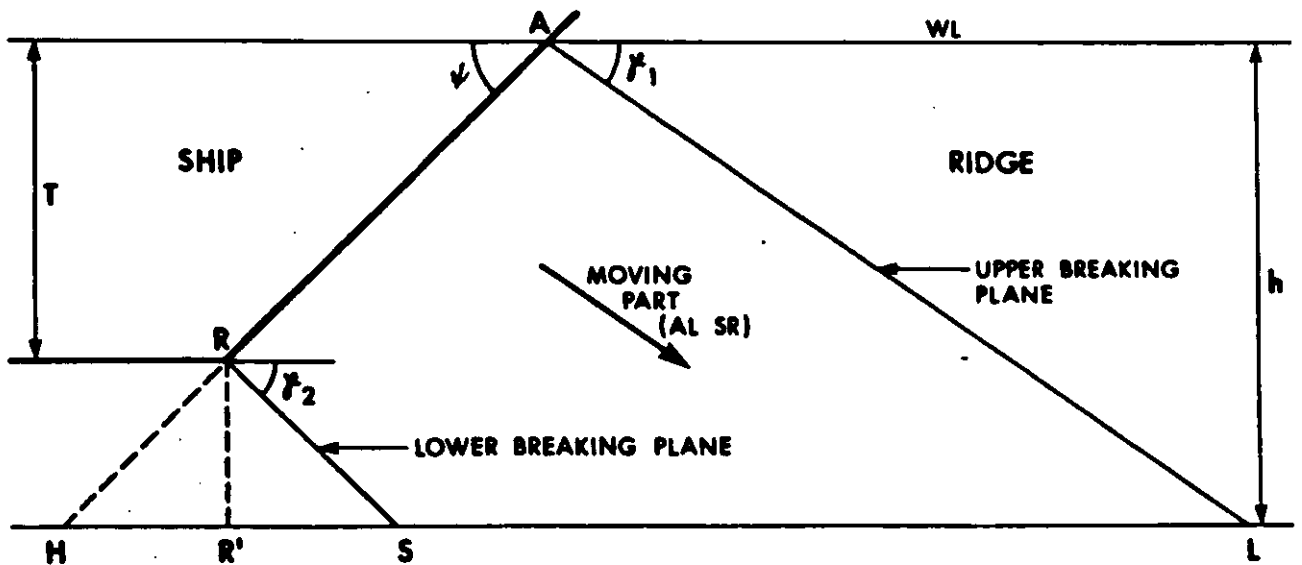


FIG. 9 INITIAL GEOMETRY FOR A RIDGE THICKER THAN SHIP'S DRAUGHT. REF. (4)

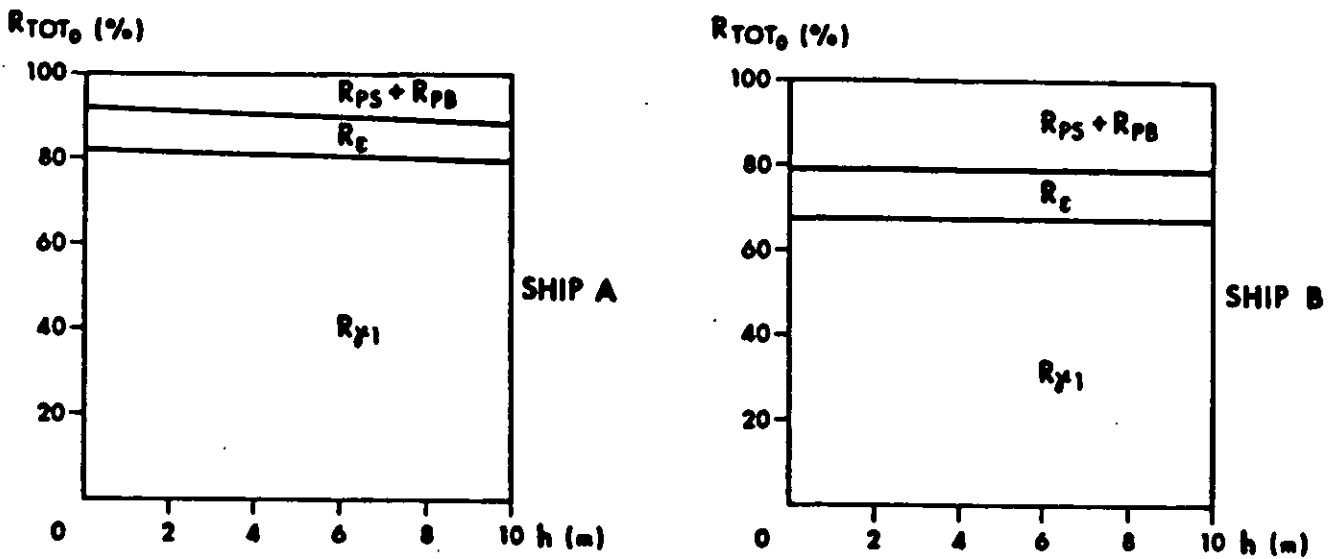


FIG. 10 DIVISION OF ANALYTICALLY COMPUTED COMPONENTS OF PURE RIDGE RESISTANCE. R_{y2} IS NEGLECTED, BECAUSE IT IS LESS THAN 0.2 PERCENT IN THESE EXAMPLES. REF. (4)

SHIP A

Ship Breadth (B)	12.600 M
Total Ship Draught (T1)	5.000 M
Parallel Middle Ship Length (L)	10.272 M
FII (N)	24.1 DEG, FII' = 33.9 DEG
Alfa (J)	22.8 DEG, ALFA' = 34.8 DEG
PSI (I)	49.1 DEG, PSI' = 49.7 DEG
Beta Middle Ship (B2)	12.0 DEG

Environment	(TANB) 0.160 In waterline direction (A1=0)
Hull Friction	(F1) 1.078
Ridge Friction	(N) 0.211
Ridge Cohesion (T0)	0.011 *10 ³ N/m ²
Ridge Poisson	(N) 0.211
Ice Density (D1)	875 KG/M ³
Water Density (D2)	1000 KG/M ³
Ridge Block Porosity (100*(1-K))	36 Percent

Developed Resistance 1000 *NEWTONS

Ridge Thicks M	Gamma Angle DEG	Side Res	Bottom Res	End Plane	Lower Plane	Upper Plane	Bow Total	Total
1.0	41	2.9	12.9	18.6	0.3	182.0	170.9	106.6
2.0	40	11.4	10.8	37.4	0.5	294.9	332.8	263.9
3.0	39	22.0	25.5	55.2	0.6	419.2	475.0	522.5
4.0	38	29.1	29.9	70.7	0.8	518.3	589.8	646.8
5.0	37	32.1	35.9	86.0	1.1	627.6	717.6	785.6
6.0	36	37.5	52.7	108.7	1.5	762.0	890.1	980.3
7.0	35	42.9	69.4	123.2	1.8	926.0	1061.1	1173.4
8.0	35	48.0	85.7	143.4	2.2	1099.8	1275.4	1369.1
9.0	35	53.1	101.9	163.7	2.5	1243.6	1409.8	1564.9
10.0	35	58.2	116.2	183.9	2.9	1397.3	1584.1	1760.5

SHIP B

Ship Breadth (B)	21.500 M
Total Ship Draught (T1)	9.500 M
Parallel Middle Ship Length (L)	67.500 M
FII (N)	29.7 DEG, FII' = 39.1 DEG
Alfa (J)	25.2 DEG, ALFA' = 36.5 DEG
PSI (I)	53.3 DEG, PSI' = 53.8 DEG
Beta Middle ship (B2)	8.0 DEG

Environment	(TANB) 0.160 In waterline direction (A1=0)
Hull Friction	(F1) 1.078
Ridge Friction	(N) 0.211
Ridge Cohesion (T0)	0.011 *10 ³ N/m ²
Ridge Poisson	(N) 0.211
Ice Density (D1)	875 KG/M ³
Water Density (D2)	1000 KG/M ³
Ridge Block Porosity (100*(1-K))	36 Percent

Developed Resistance 1000 *NEWTONS

Ridge Thicks M	Gamma Angle DEG	Side Res	Bottom Res	End Plane	Lower Plane	Upper Plane	Bow Total	Total
1.0	39	16.5	160.6	81.8	0.6	827.8	603.4	790.5
2.0	38	66.1	277.9	160.6	1.0	1034.8	1196.4	1540.6
3.0	38	148.6	352.0	237.5	1.3	1530.2	1789.0	2269.7
4.0	38	262.7	383.1	321.5	1.6	1998.4	2321.6	2967.3
5.0	37	378.5	457.6	405.3	1.8	2429.9	2837.1	3673.1
6.0	36	471.8	511.1	486.7	1.9	2813.3	3332.0	4284.9
7.0	36	533.5	565.6	546.9	2.3	3160.5	3709.6	4800.7
8.0	36	608.3	589.4	609.4	2.7	3463.2	4065.2	5252.8

TABLE 2 RIDGE RESISTANCE ANALYSES. REF. (4)

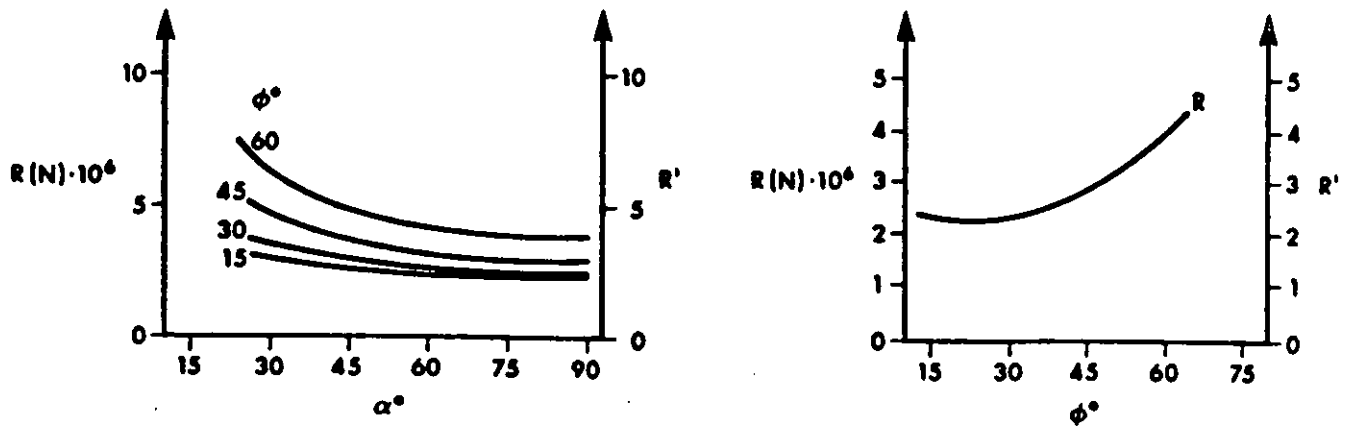
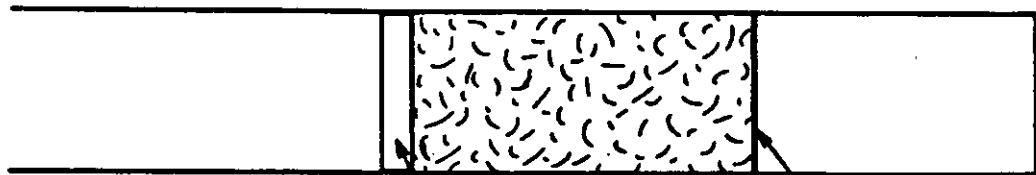


FIG. 11 COMPUTED MAIN BREAKING PLANE RIDGE RESISTANCE ACCORDING TO THE METHOD OF REF. (4) FOR $h = 5\text{ m}$, $B = 10\text{ m}$, $\mu = 0.2$ WITH STEM ANGLE ϕ AND WATERLINE ENTRANCE ANGLE α AS PARAMETERS. REF. (6)

a) OVERVIEW



b) SIDE VIEW

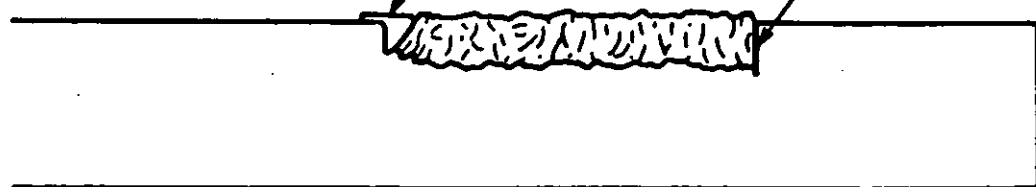


FIG. 12 MODELLED LARGE HOMOGENEOUS RIDGE FIELD a) FROM ABOVE AND b) FROM THE SIDE, FROM WÄRTSILÄ'S ICE MODEL BASIN. REF. (4)

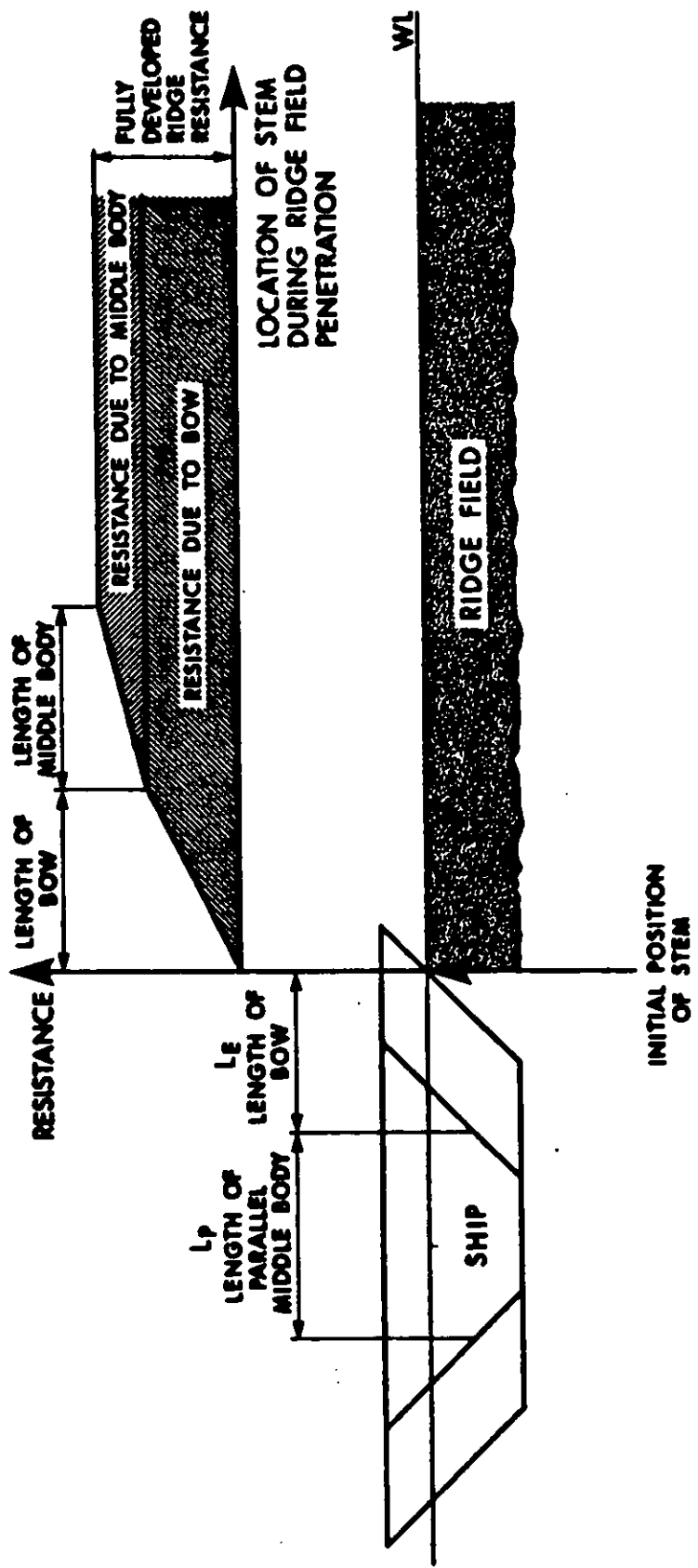


FIG. 13 DEVELOPMENT OF RIDGE RESISTANCE ACCORDING TO THEORY

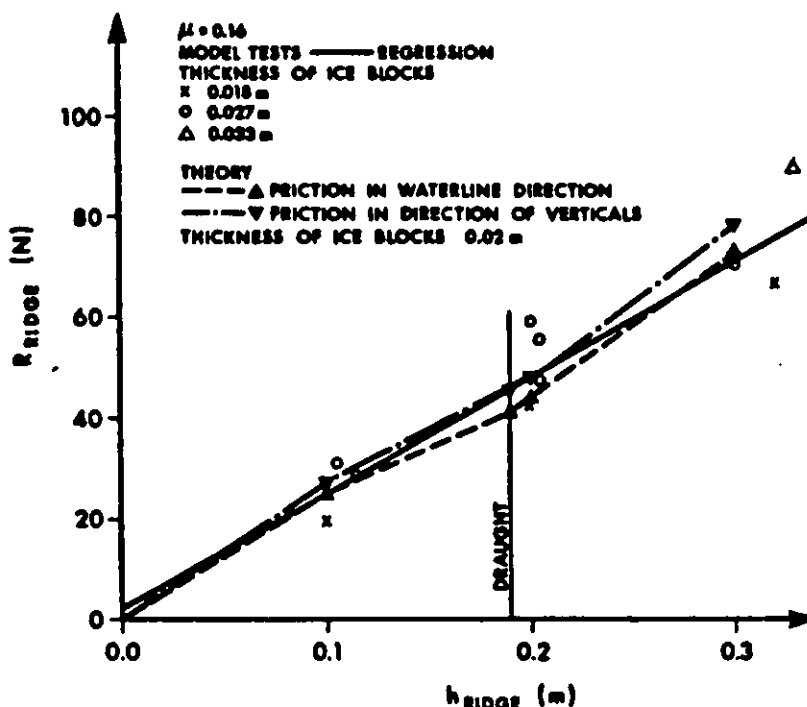


FIG. 14 RIDGE RESISTANCE MODEL SCALE CONSTANT SPEED. REF. (4)

Ship Breath (B)	0.470	M
Total Ship Draught (T1)	0.190	M
Parallel Middle Ship Length (L)	0.442	M
FII (N)	23.3	DEG, FII' = 34.5 DEG
Alfa (J)	18.3	DEG, Alfa' = 29.5 DEG
PSI (I)	53.8	DEG, PSI' = 54.4 DEG
Beta Middle Ship (B2)	18.0	DEG

Environment		
Hull Friction	(TANB1) 0.160	In waterline direction (A1=0)
Ridge Friction	(F1) 1.078	
Ridge Cohesion (T0)	0.011	*10 ⁺³ N/M ²
Ridge Poisson	(N1) 0.211	
Ice Density (D1)	910	KG/M ³
Water Density (D2)	1000	KG/M ³
Ridge Block Porosity (100*(1-M))	36	Percent

Developed Resistance 1 *NEWTONS

Ridge Thickn M	Gamma Angle DEG	Side Res	Bottom Res	End Plane	Lower Plane	Upper Plane	Bow Total	Total
0.10	37	1.6	0.9	3.0	1.2	19.7	23.9	25.8
0.15	36	1.5	1.2	4.4	1.6	27.9	33.1	35.8
0.20	35	1.9	1.4	5.8	2.3	33.5	41.6	44.9
0.25	36	2.3	2.4	7.2	3.3	44.1	54.6	59.2
0.30	36	2.7	3.3	8.9	4.3	54.7	67.8	73.8

Hull Friction		
(TANB1) 0.160		
In Direction of Verticals (A1=1)		
Ridge Friction	(F1)	1.078
Ridge Cohesion (T0)		0.011
Ridge Poisson	(N1)	0.211
Ice Density (D1)		910
Water Density (D2)		1000
Ridge Block Porosity (100*(1-M))		36

Developed Resistance 1 *NEWTONS

Ridge Thickn M	Gamma Angle DEG	Side Res	Bottom Res	End Plane	Lower Plane	Upper Plane	Bow Total	Total
0.10	34	1.0	0.9	3.4	1.3	21.2	25.9	27.7
0.15	33	1.4	1.1	4.9	1.8	29.0	35.7	38.2
0.20	32	1.8	1.3	6.4	2.7	35.8	44.8	47.9
0.25	33	2.2	2.3	8.0	3.7	47.2	59.0	63.4
0.30	33	2.6	3.2	9.9	4.9	58.6	73.4	79.2

TABLE 3 MODEL D RIDGE RESISTANCE ANALYSIS. REF. (4)

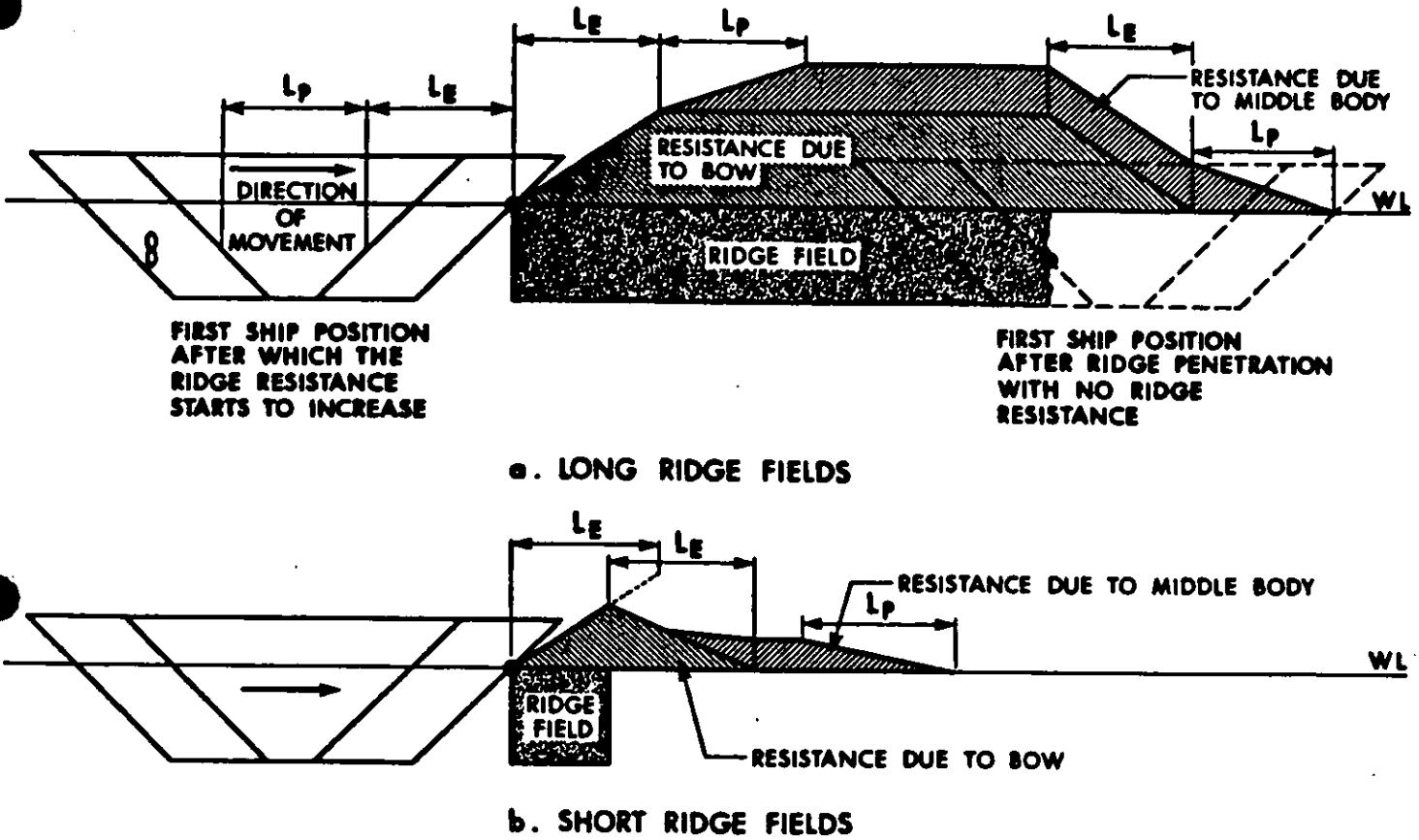


FIG. 15 DEVELOPMENT OF RIDGE RESISTANCE WHEN PENETRATING ACTUAL RIDGE FIELDS. RESISTANCE PLOTTED ACCORDING TO PENETRATION OF THE STEM THROUGH THE RIDGE FIELDS.

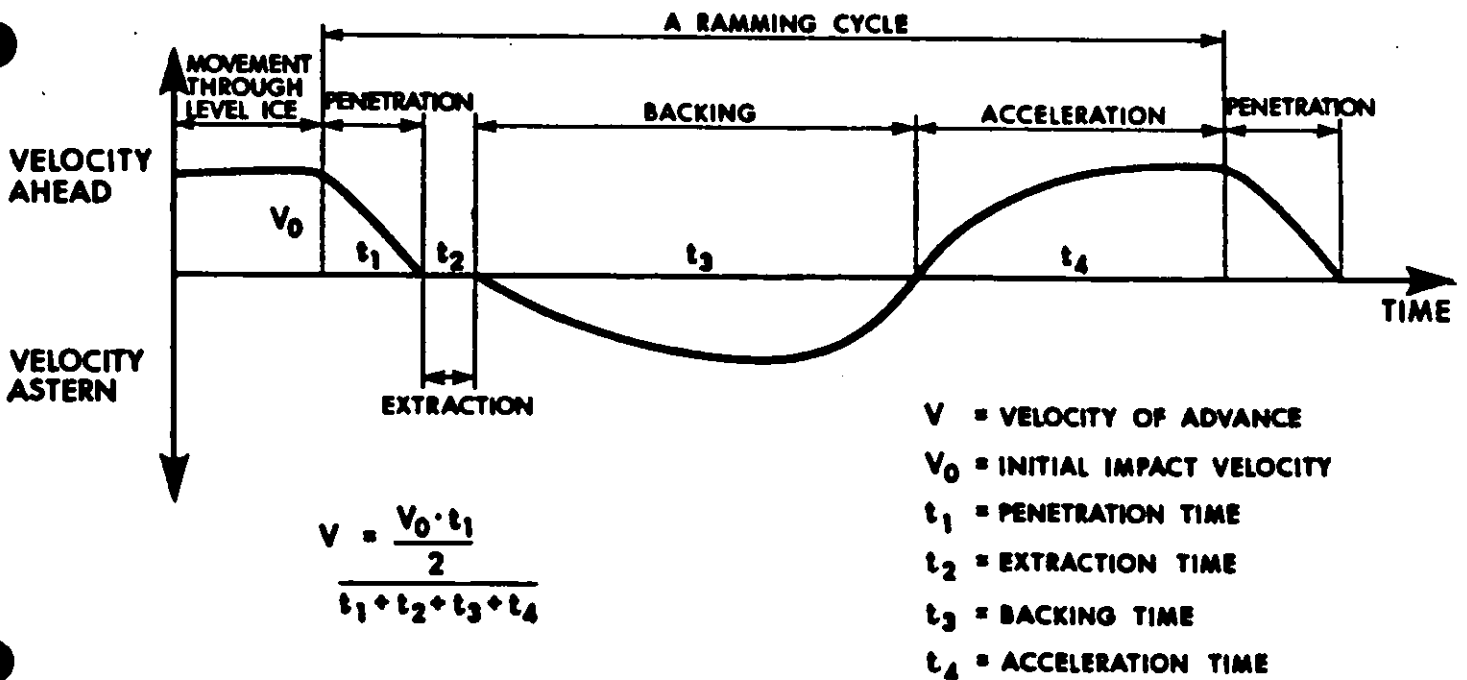


FIG. 16 RAMMING CYCLE PARAMETERS

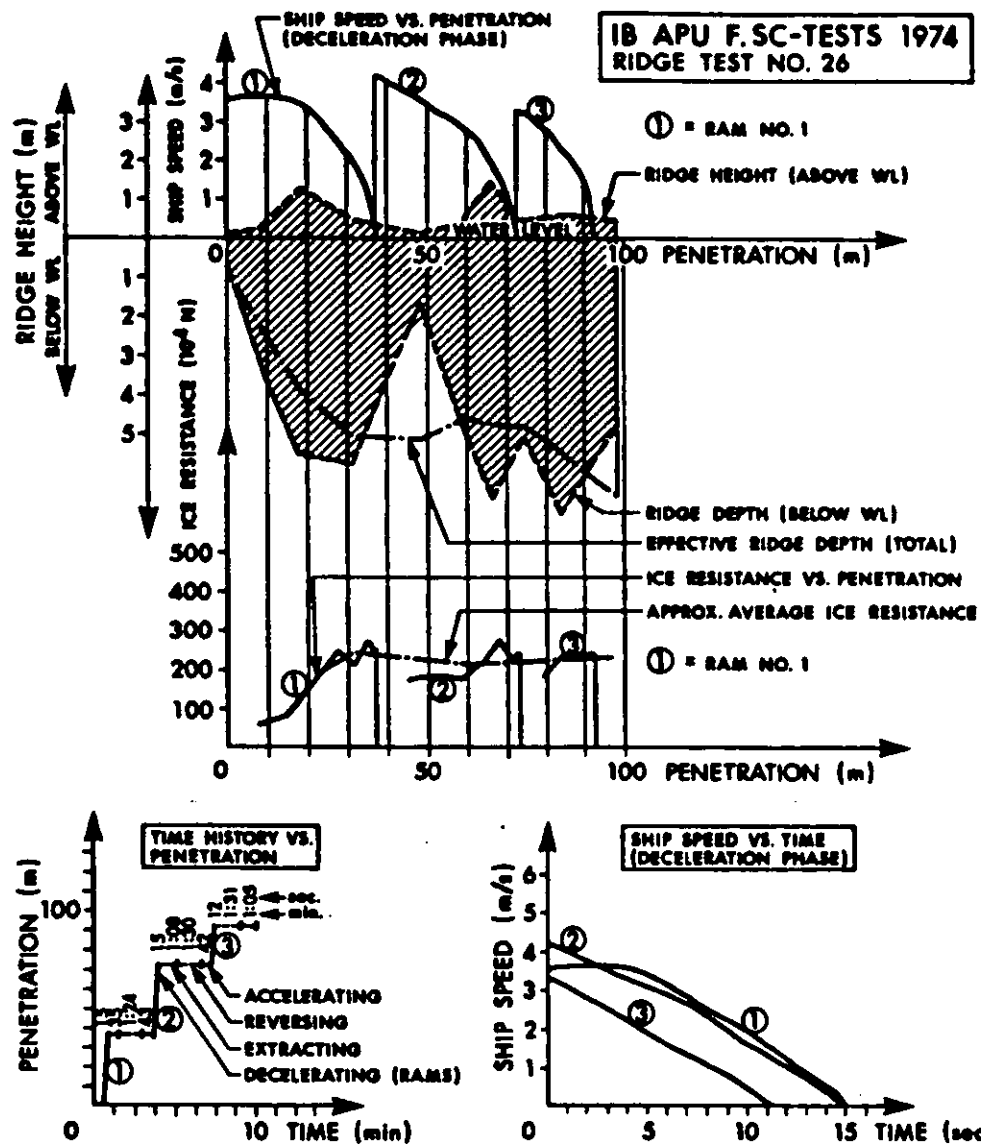


FIG. 17 AN EXAMPLE OF THE FORM INCLUDING INFORMATION OBTAINED FROM THE TEST IN ONE RIDGE. REF. (3)

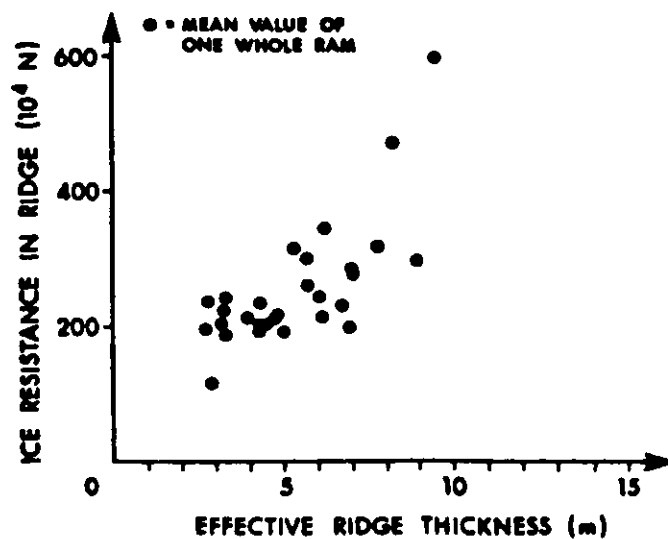


FIG. 18 ICE RESISTANCE IN RIDGE VS. EFFECTIVE RIDGE THICKNESS. AVERAGE VALUES OF INDIVIDUAL RAMS. REF. (3)

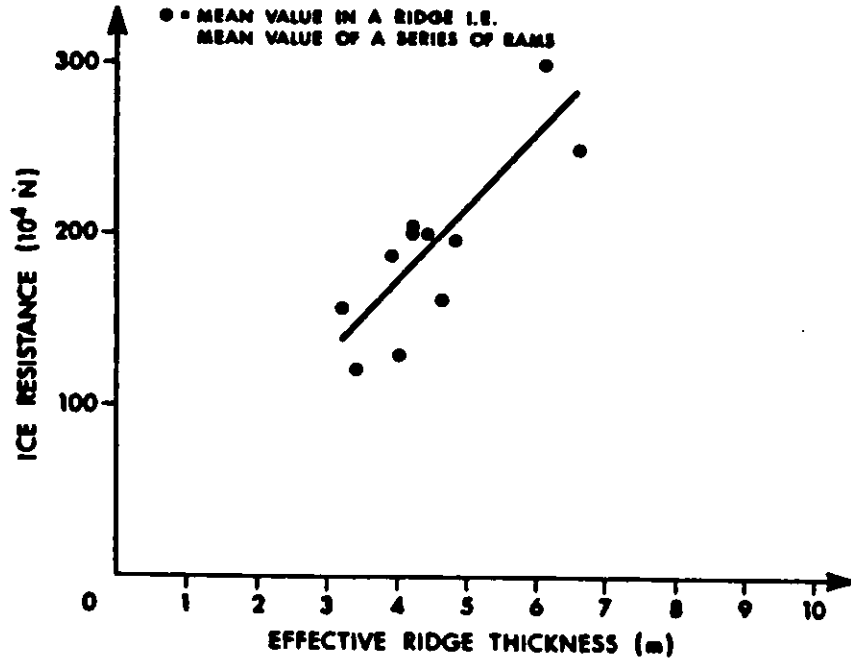


FIG. 19 ICE RESISTANCE IN RIDGE VS. RIDGE THICKNESS. AVERAGE VALUES OF EACH SERIES OF RAMS. REF. (3)

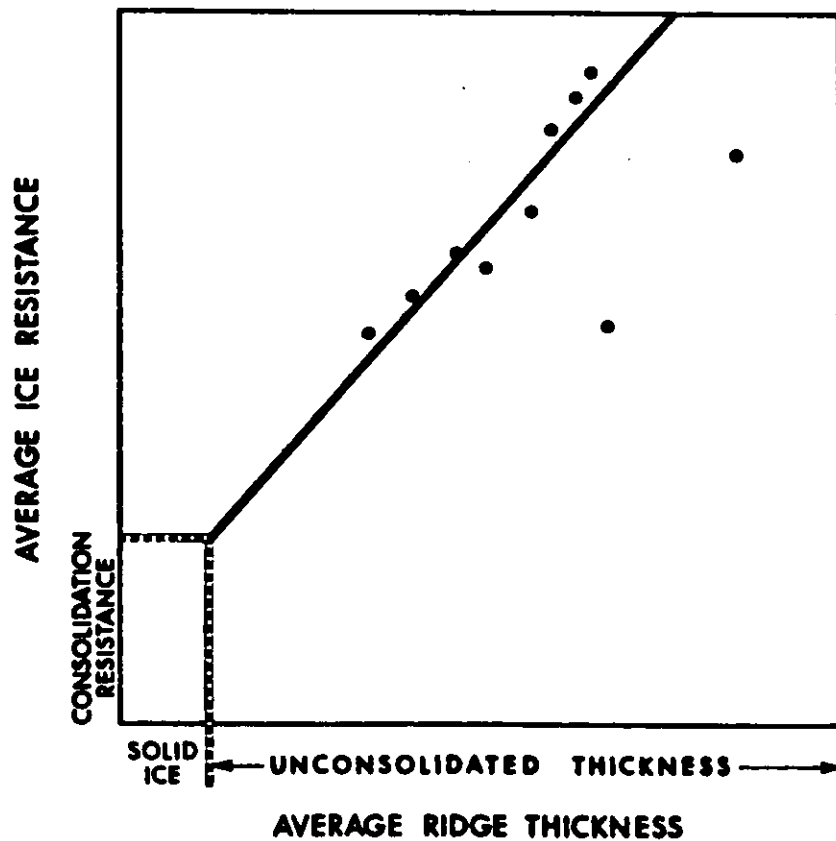


FIG. 20 AVERAGE PENETRATION RESISTANCE IN FIRST-YEAR RIDGES UNDER WINTER CONDITIONS. AVERAGE VALUES OF EACH SERIES OF RAMS IN THE BEAUFORT SEA. REF. (9)

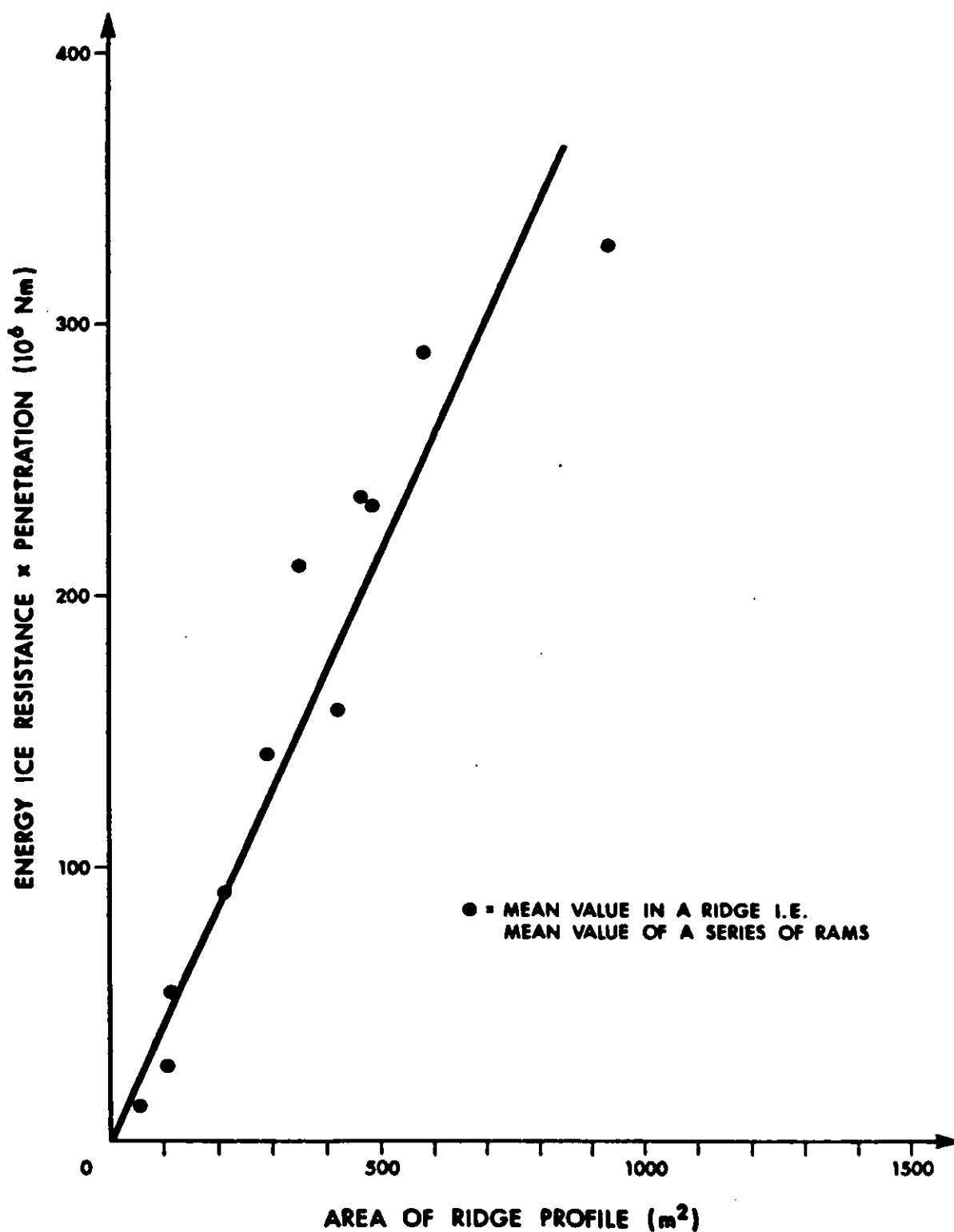


FIG. 21 ICE RESISTANCE INTEGRATED OVER PENETRATION VS. RIDGE THICKNESS INTEGRATED OVER PENETRATION. AVERAGE VALUES OF EACH SERIES OF RAMS. REF. (3)

DERIVATION OF COMPONENTS OF PURE RIDGE RESISTANCE

1.0 INTRODUCTION

This is a summary of the key components of ridge resistance based on a full description of an analytical model as presented in Ref. (4). This description does not give all the equations for all the resistance components presented in Ref. (4) as those of minor importance have been omitted and are treated as percentage additions to the major components.

1.2 GENERAL

Penetration of ridges by a ship is a complicated and extensive problem, if the whole process is considered. The most important factors affecting the penetration of ridges include:

1. resistance;
2. sticking in ice;
3. ice effects on propulsion; and,
4. inertial effects.

This study considers the resistance problem only. The inertial effects (added masses, accelerations in vertical and horizontal directions), which could be attached to the resistance problem, are not included in this paper. Due to the complicated interaction between ice and water in a ridge during ship's penetration, only the resistance problem for the case of slow passage is considered, where hydrodynamic or mass forces should not be of importance.

This work is limited to the consideration of free floating, first-year Baltic ridges. In contrast to the free floating ridges, there exist ridges on the shoals which stand on the seafloor. The contact between the keel of a ridge and the seafloor gives rise to

additional supporting effects on the ridge, which will not be analyzed here.

On the basis of their age, ridges are classified into first-year and multi-year ridges. In the Baltic, there are no multi-year ridges. The structure of multi-year ridges is considerably more rigid than that of first-year ridges, although the Arctic first-year ridges may be slightly more rigid than the majority of the ridges in the Baltic.

1.3 DETAILED CONSIDERATIONS

The analysis of full scale tests of ships in Baltic ice ridges References 10, 11, 12, 13 shows that the total ice resistance (total resistance = total ice resistance and resistance in ice free water) may be logically split into three components (see Figure 1.2):

1. level ice resistance;
2. aging resistance; and,
3. pure ridge resistance.

These components are at this stage assumed to be independent of each other. In Figure 1.1, the corresponding parts of the ridge are roughly sketched.

Level ice resistance is due to the fast, level ice field around and inside the ridge. In this work, no assumptions are made as to this part of the ice resistance. It may be determined through model tests, by full scale tests or by some theoretical or semi-empirical method, whichever is most practical.

Aging resistance means that part of the resistance which is related to the changes in the structure of a ridge due to its aging (or weathering). These changes involve an increase in the thickness of the frozen ice layer inside the ridge and the freezing together of ice-blocks in the sail and in the keel. Especially the freezing of rafted ice fields at the water surface causes a noticeable aging resistance component. This part of the resistance will be disregarded in the present approach to the resistance problem.

The remainder of the ice resistance, after subtraction of the level ice resistance and the aging resistance from the total ice resistance, will be called pure ridge resistance. This is by far the largest component of the ice resistance in large first-year ridges. Concentration will be placed on the analysis of this part of the resistance.

From the environmental point of view, consideration will be limited to a structurally homogeneous, large ridge field with a constant thickness. In natural conditions, the ridges may have a considerably varied cross-sectional profile. Nevertheless, the most difficult ridge conditions for a ship, is a long ridge field with continuously large keel depth profile. This approaches the case of constant thickness, because then the variations of the profile become unimportant compared with the continuously large amount of ice around the hull of the ship, especially when the ship can at any moment interact with a rather large part of the ridge field. The penetration of ridges, ice fields, or single ridges presents a less severe obstacle to ice navigation, but not one without some importance. Their penetration equations will be determinable by interpolation after analysis of the pure ridge resistance.

The pure ridge resistance will be handled according to the following scheme:

1. Initial resistance. The initial resistance is determined to be the resistance of a ridge field surrounding the forward body of a ship and having an initially constant thickness everywhere around the forward body of the ship. In Figure 1.3, a schematic illustration of the case of initial resistance is shown.

2. Developed resistance. The developed resistance is determined to correspond to a developed ridge profile around the hull of a ship. The developed ridge profile is a profile that stays constant under further penetration, once it has been established after a certain distance of penetration. The developed resistance may itself be divided further into two parts, that due to the forward body and that due to the parallel middle body of a ship. The decreasing aft body of the ship also comes into contact with ice, but as its effect on the resistance is minor and interacts with the propulsion, it will be ignored at this stage. In Figure 1.4, a schematic presentation of the developed resistance condition is shown.

The initial resistance will be used for a direct comparison with theory and with the corresponding basic experiments, due to the geometric simplicity of the condition. The developed resistance is directly comparable with scale model results in large homogeneous ridge fields, and for full scale test results it is an upper bound approach.

For the purposes of analysis, a simple geometry is chosen for the ship. This geometry is the combination of planes shown in Figure 1.5 as follows:

1. side planes of forward body (ABCD, BA'D'C');
2. bottom plane (DCD'J'C'J);
3. parallel side planes (ADJI, A'D'J'I');
4. side planes of aft body symmetrical to the forward body.

Assumptions are made such that the parallel middle body of a ship will be GFMN and such that the whole area of the parallel side planes and the bottom plane belong to the parallel middle body. Then, the resistance due to the forward body may be attributed to its side planes (ABCD and A'BCD'). Otherwise, a conventional ship's design is assumed with no forward screws nor any other departures from a smooth hull.

2.0 ANALYSIS OF THE PURE RIDGE RESISTANCE

2.1 GENERAL

In this analysis, the aim is to produce a quantitative, comparative presentation of the different resistance components of the pure ridge resistance as a function of ship and environmental parameters. The corresponding mathematical models representing each of the components will be kept at a simple level, because this is a first theoretical approach to the problem.

If one ignores the level ice and the weathering, a ridge field consists of loose, broken ice blocks both in the sail and the keel. Its response to ship movement may at any moment be determined as the force for breaking the mass, consisting of the loose ice blocks and removing it from the passage of the ship. In Section 2.2, a solution for this kind of breaking problem of masses is presented. The basis for the method is found in soil mechanics problems (Coulomb's method).

In Section 2.3, the initial resistance is analyzed for ridges shallower than a ship's draught. There, the basic method for the determination of pure ridge resistance is presented.

In Section 2.4, the initial resistance is touched upon for ridges deeper than ship's draught. The changes in the conditions for the basic method are presented.

In Section 2.5, the developed resistance condition is analyzed. A kinematic model for development of the ridge around the hull of a ship is presented, and the corresponding changes in the constants of the basic method are derived.

In Section 2.6, the resistance due to the parallel middle body of a ship is dealt with. This is a simplified approach based on Reference (1).

2.2 BASIS FOR THE BREAKING ANALYSIS

In the area of soil mechanics, problems of the carrying capacity of soil are solved in connection with loads caused by different types of structures. There exist a multitude of methods for these purposes.

A major part of an ice ridge is subjected, during ship penetration, to similar types of loads as soil. The difference between the earth and ice ridge problems is that the soil must not break, whereas an ice ridge must break. Thus, when using approximate methods, the desired direction of approach changes from the non-breaking condition to a breaking condition. At the same time, the purely static nature of the soil problem changes to a dynamic problem. Thus, in the ship problem, there is a need to analyze the problem beyond the stage of the breaking of the mass to gain knowledge of the development of the breaking condition. In addition, the complicated geometry of a ship, even when simplified, leads to a three-dimensional handling of the problem or at least to a need for boundary conditions to solve the end effects.

When choosing a method of analyzing the breaking forces in ship-ice interaction in ice ridges, it is considered most important that the analysis can be computerized so as to allow systematic calculations. It is also desirable to be able to vary the initial environmental conditions freely (friction, cohesion etc...). The analysis should be such that a practical kinematic model may be developed from the breaking model.

These conditions have led the author to Coulomb's method, a precis of which is given in the following text:

The method of Coulomb is based on an assumption of the breaking of the mass in a plane, when the mass is loaded with a wall. The breaking condition is solved by using a force balance calculation in possible breaking planes. The actual breaking plane where the breaking conditions are first reached is found by derivation. The method for a vertical frictionless wall is shown in Figure 2.1. BC is the breaking plane with an inclination γ from the horizon.

In the figure it can be seen that the action lines of the forces F_{TOT} , F_O , F_G and F pass through a single point, which lies in the breaking plane. In the condition of Figure 2.1, the method of Coulomb is accurate. The equation for projections of the forces onto the L-L-line normal to F is

$$F_G \sin(\gamma + \beta') + F_{T0} \cos \beta' - F_{TOT} \cos(\gamma + \beta') = 0$$

where β' is the inner friction angle of the mass. When substituting the condition for breaking,

$$\tau = \tau_0 + \sigma \tan \beta' \quad (2.1)$$

where τ_0 is the cohesion (the shear strength at zero normal load) of the mass and σ is the normal stress. τ is the actual shear strength.

And for a wall with a height h , determining

$$F_{\tau_0} = \tau_0 h / \sin \gamma$$

we get a formula for F_{TOT} per unit width

$$F_{TOT} = \frac{\mu_B \rho_A g h^2 \tan(\gamma + \beta')}{2 \tan \gamma} + \tau_0 h \frac{\cos \beta'}{\sin \gamma \cos(\beta' + \gamma)}$$

where μ_B is the solidity of the mass (0 = no ice; and 1 = only ice, now water between ice blocks).

When a minimum for this is searched for by varying γ , the breaking condition is determined. The minimum is found from the first derivative. For the vertical frictionless wall, the solution is

$$\gamma = (\pi/2 - \beta'/2).$$

This method overestimates the results somewhat when the coefficient of friction against the wall departs from zero. The method also becomes inaccurate when the wall is inclined and when the bottom of the ridge is not horizontal. All these changes cause one or several of the action lines of the forces to change, resulting in a rotating moment for which a correction should be made if theoretically fully analyzed. In any event, the actual changes of these are not known and the momentum equation is at this stage disregarded. The theory will be developed as Coulomb's method, and the results will be compared with appropriate test results. A departure from Coulomb's method will be made such that the friction between the ice and the wall is added to the analysis.

For convenience, the balance equation is split into two separate equations: the shear equation and the equation for the force normal to the breaking plane. Thus, the physically meaningful normal and shear stresses in the breaking plane are obtained directly from the analysis, if required.

2.3 INITIAL RESISTANCE, THIN RIDGES

2.3.1 General

In Figure 2.2, an initial resistance condition is shown with the notation that will be used in the analysis. The thickness of the ridge may not reach below the ship's draught in the case of a thin ridge.

In Sub-section 2.3.2, the relationship between the direction cosines of the forces and the hull angles are derived.

The force geometry in the basic condition is formulated in Sub-section 2.3.3, the method for the analysis of the breaking plane (plane ABPL in Figure 2.4), and the corresponding breaking force is derived in Sub-section 2.3.4.

2.3.2 Force geometry

In connection with initial resistance, the analysis of force direction cosines will be done. Several versions of such analysis exist, but to date all of these have been with assumptions appropriate to level ice resistance analysis. The earlier analyses were either done in order to determine the relationships between the net vertical force and the total resistive force, or do not include friction in a convenient manner.

For the purposes of this work, the direction of the frictional force will be given two possibilities, the direction of the waterline and the direction of the ship's verticals. The direction of the relative motion between ice and the hull of a ship actually lies between these two, and depends, in a complicated way, on the shape of the forward body of the ship, on the coefficient of friction, ridge thickness and ship's speed. The direction of friction for a landing craft bow shape is in the direction of the verticals in the flat part of the bow and that for a bow with a vertical stem and vertical sides is in the direction of the waterlines. The more the stem angle decreases, the more the direction of friction departs from this. The more the half-angle of the waterline decreases from 90 degrees, the more the direction of friction departs from the direction of the verticals.

In this work, both limiting cases are kept in the analysis throughout.

The notation of the hull angles is used as in Figure 2.2a. From Figure 2.2b-d the direction cosines for the normal force can be written

$$\frac{F_{Nx}}{F_N} = \sin\psi \sin\alpha, \quad \frac{F_{Ny}}{F_N} = \sin\psi \cos\alpha, \quad \frac{F_{Nz}}{F_N} = \cos\psi$$

$$\frac{F_{Nxy}}{F_N} = \sin\psi, \quad \frac{F_{Nxz}}{F_N} = \frac{\cos\psi}{\cos\phi} = \frac{\sin\psi \sin\alpha}{\sin\phi}$$

From the last of these the relationship between the hull angles α , ϕ and ψ can be determined and any one of these may be eliminated by expressing it in terms of the remaining two.

Using the expression $F_{\mu} = F_N \tan \beta$, where β is the friction angle between the hull of the ship and the ice, the direction cosines are developed for the total force as follows (see Figures 2.2 and 2.3):

a) for friction in the direction of the waterlines

$$F_x = F_{Nx} + F_{\mu x}$$

$$F_{Nx} = F_N \sin \psi \sin \alpha$$

$$F_{\mu x} = F_{\mu} \cos \alpha = F_N \tan \beta \cos \alpha$$

$$l' = \frac{F_x}{F_{TOT}} = \frac{F_N \sin \psi \sin \alpha + F_N \tan \beta \cos \alpha}{F_N / \cos \beta} \quad (2.2)$$

$$= \cos \beta (\sin \psi \sin \alpha + \tan \beta \cos \alpha)$$

$$F_y = F_{Ny} + F_{\mu y}$$

$$F_{Ny} = F_N \sin \psi \cos \alpha$$

$$m' = \frac{F_y}{F_{TOT}} = \frac{F_N \sin \psi \cos \alpha - F_N \tan \beta \sin \alpha}{F_N / \cos \beta} \quad (2.3)$$

$$= \cos \beta (\sin \psi \cos \alpha - \tan \beta \sin \alpha)$$

$$F_z = F_{Nz} + F_{\mu z}$$

$$F_{Nz} = F_N \cos \psi$$

$$F_{\mu z} = 0$$

$$n' = \frac{F_z}{F_{TOT}} = \frac{F_N \cos \psi}{F_N / \cos \beta} = \cos \psi \cos \beta \quad (2.4)$$

- b) for friction in the direction of the verticals, we correspondingly obtain

$$l' = \cos \beta (\sin \psi \sin \alpha + \cos \phi \tan \beta) \quad (2.5)$$

$$m' = \cos \beta \sin \psi \cos \alpha \quad (2.6)$$

$$n' = \cos \beta (\cos \psi - \sin \phi \tan \beta) \quad (2.7)$$

The apparent hull angles corresponding to the plane normal to the total force are next determined by means of these direction cosines. The apparent angles are labelled α' , ϕ' , ψ' .

$$\alpha' = \arctan(l'/m') \quad (2.8)$$

$$\phi' = \arctan(l'/n') \quad (2.9)$$

$$\psi' = \arctan(\tan \phi' / \sin \alpha') \quad (2.10)$$

It can be seen at once that, for example, in l' the difference between the two directions of friction is the substitution of $\cos \phi$ for $\cos \alpha$. Thus, if the α and ϕ angles are about the same, there is no difference between these two direction cosines (Equations (2.2), (2.5)).

2.3.3 Force Geometry in the Breaking Plane

In Figure 2.4, the waterline of the ship is ABQ, and h is the ridge thickness in this model, which means that the whole ridge will be considered, but as if it were completely submerged. The effects of this assumption on the results may be considered by a convenient choice of the coefficient of friction in those cases where it may not be assumed to be constant everywhere.

The plane ABCD is the side plane of the forward body of the ship. The part of the ridge that will be considered is ABPLHD, where the angle γ is a variable expressing the possible direction of breaking planes in the ridge.

A further assumption in the model is that ignoring the plane AHD of the ship's hull will be compensated for by the addition of BOC. The breaking, in addition to the γ -plane (ABPL), will be assumed to take place in ALH and BPO-planes, which will be called end planes. These planes are in the direction of the A-A-cut in Figure 2.4, (for A-A see Figure 2.2).

In addition, the sliding of the ice against the ship's hull in the ABCD-plane occurs, and this required us to consider a fully developed force of friction between the ship's hull and the ice. Also, the ridge mass is assumed to be incompressible.

The forces acting in the model are as shown in Figure 2.5:

1. As input, the total ship's force, F_{TOT} , transmitted from the hull of the ship to the ice. Due to friction, it is inclined away from the normal to the hull plane by the amount of the frictional angle.
2. The buoyancy force of ice, F_G , vertically upwards.
3. A force in an arbitrary, so-called γ - plane. This force is presented through its normal and tangential components, $F_{\sigma\gamma}$, $F_{\tau\gamma}$.
4. Forces in the end planes (ALH, BPO), presented through their normal and tangential components, the tangential component being F_{ξ} (not shown in Figure 2.5).

In Reference (1) it was seen that more than 80 per cent of the resistance is due to the shearing in γ plane. For the purposes of this presentation and for practical analyses, only this component will be considered.

In Figure 2.5, the components of the total ship's force are presented in the A-A plane. In this figure, the positive directions for the tangential (shear) and normal forces in the γ -plane are shown. It should be noted that ψ' , the apparent hull angle, is used instead ψ . Thus, friction is automatically included. The expressions for the components of the total force in the γ -plane are

$$F_{TOT1\sigma\gamma} = F_{TOT1} \sin(\gamma + \psi' - 90^\circ) \quad (2.11)$$

$$= -F_{TOT1} \cos(\gamma + \psi')$$

$$F_{TOT1\tau\gamma} = F_{TOT1} \cos(\gamma + \psi' - 90^\circ) \quad (2.12)$$

$$= -F_{TOT1} \sin(\gamma + \psi')$$

In Figure 2.6, the components of the buoyancy force in the γ -plane are shown. In this figure, the real ψ angle is used and the A-A plane is shown. The expressions for the components are thus

$$F_{G\sigma\gamma} = F_G \cos \gamma \quad (2.12a)$$

$$F_{G\tau\gamma} = -F_G \sin \gamma \quad (2.12b)$$

F_G is calculated according to

$$F_G = \mu_B \rho g G,$$

where ρ_Δ expresses the buoyant density of ice and G is the volume of ice corresponding to HAL. Furthermore,

$$G = b \cdot A_\xi,$$

where b is the length of the third dimension, (Figure 2.4), and A_ξ is the area of an end plane, given by

$$A_{\Sigma} = \frac{h^2}{2 \tan \gamma} + \frac{h^2}{2 \tan \psi} = \frac{h^2}{2} \left(\frac{1}{\tan \gamma} + \frac{1}{\tan \psi} \right) \quad (2.13)$$

$$b = \frac{B}{2 \sin \alpha}$$

Thus,

$$G = \frac{\rho h^2}{4 \sin \alpha} \left(\frac{1}{\tan \gamma} + \frac{1}{\tan \psi} \right),$$

and considering both sides of the ship,

$$F_G = \frac{\mu_B \rho g B h^2}{2 \sin \alpha} \left(\frac{1}{\tan \gamma} + \frac{1}{\tan \psi} \right) \quad (2.14)$$

2.3.4 Resistance to γ -plane Breaking

First, summing the forces in the γ -plane Equations (2.11), (2.12) and (2.14)

$$F_{\sigma\gamma} = F_{TOT1\sigma\gamma} + F_{G\sigma\gamma} \quad (2.15a)$$

$$= -F_{TOT1} \cos(\gamma + \psi') + \frac{\mu_B \rho g h^2 B}{2 \sin \alpha} \left(\frac{1}{\tan \gamma} + \frac{1}{\tan \psi} \right) \cos \gamma$$

$$F = F_{TOT1} + F_{G\tau\gamma} \quad (2.15b)$$

$$= F_{TOT1} \sin(\gamma + \psi') + \frac{\mu_B \rho g h^2 B}{2 \sin \alpha} \left(\frac{1}{\tan \gamma} + \frac{1}{\tan \psi} \right) \sin \gamma$$

The corresponding stresses are needed for determination of the breaking condition. The area of the γ -plane for two ship's sides is

$$A_{\gamma} = \frac{h}{\sin \gamma} \cdot \frac{B}{2 \sin \alpha} \cdot 2 \quad (2.16)$$

Then

$$\sigma_{\gamma} = \frac{F_{\sigma_{\gamma}}}{A} \quad (2.17a)$$

$$\tau_{\gamma} = \frac{F_{\tau_{\gamma}}}{A_{\gamma}} \quad (2.17b)$$

These formulae will be simplified by use of the following notation:

$$a. \quad C1 = A_{\gamma} = \frac{hB}{\sin \gamma \sin \alpha} \quad (2.18)$$

$$b. \quad C2 = \frac{1}{\tan \gamma} + \frac{1}{\tan \psi}$$

$$c. \quad C3 = \frac{\mu_B \rho_{\Delta} g h^2 B}{2 \sin \alpha}$$

Then, the stresses, Equations (2.17a, b), are expressed as

$$a. \quad \sigma_{\gamma} = \left[-F_{TOT1} \cos (\gamma + \psi') + C2 \cdot C3 \cdot \cos \gamma \right] / C1 \quad (2.19)$$

$$b. \quad \tau_{\gamma} = \left(-F_{TOT1} \sin (\gamma + \psi') - C2 \cdot C3 \cdot \sin \gamma \right) / C1$$

Next, the breaking condition, Eq. (2.1), $\tau_{\gamma} = \tau_0 + \sigma_{\gamma} \tan \beta'$ is used to arrive at the total force.

$$F_{TOT1} = \frac{\tau_0 C1 + C2 \cdot C3 \cdot (\sin \gamma + \cos \gamma \cdot \tan \beta')}{\sin (\gamma + \psi') + \tan \beta' \cdot \cos (\gamma + \psi')} \quad (2.20)$$

This expression will be used to determine the γ -plane for shear breaking of the ridge mass. The desired γ -plane is found by varying the value of γ . The actual breaking plane, denoted by γ_1 , is the one which gives a minimum value for F_{TOT1} . The resistive force is then obtained by using the direction cosine l' , Eqs. (2.2) and (2.5)

$$R_{\gamma_1} = l' F_{TOT1} (\gamma_1). \quad (2.21)$$

2.4 DEVELOPED RESISTANCE CONDITION

2.5.1 General

The principle for analyzing the resistance of the ice mass against breaking, presented in Section 2.3, is also applicable to the developed resistance condition. The main difference lies in the amount of ice that has to be taken into account in determining the buoyancy force. This means that the constant corresponding to the amount of ice (C3) must be analyzed for the developed condition separately. Before this can be done, a model must be devised for the development of the ridge profile around the hull of a ship during penetration. Such a model is presented in Sub-section 2.4.2 for a landing craft bow to show the basic principles for the growth. In Sub-section 2.4.2, a general model for ridge development is presented based on the principles contained in Sub-section 2.4.2. The results of this model are given in terms of the constant C3, applicable to the original calculation method, Eq. (2.20).

2.4.2 A Thickness Growth Model for a Landing Craft Bow

To illustrate the logic of the analysis, a kinematic ridge growth model for a landing craft bow will be developed. Only the case of a ridge with $h < T$ will be considered.

According to the breaking force analysis in Section 2.3, a straight rupture line is assumed for the kinematic model. When the γ -planes are used for sliding, the development of the ridge mass profile will take place as shown in Figure 2.8, for a landing craft bow.

In this example, a developed resistance condition in the forward body area is reached in Figure 2.8 (7).

The geometry of the ice in the developed condition is not important for the contents in the breaking analysis, but the amount of moving ice mass is. Nevertheless, the geometry is important as a basis for determination of the development of the profile in different ridge thicknesses and for different bow shapes.

The geometry of completed ridge growth around the forward body is shown in Figure 2.9. The initial analysis is changed such that the buoyancy force is increased by an amount corresponding to FEMN of Figure 2.9. Thus

$$F_{GTOT} (=FEMN) = \frac{Th\mu_B \rho \Delta gB \sin(\phi + \gamma)}{\sin\phi \sin\gamma}$$

The distance of penetration, starting from the initial resistance condition, that is needed for the completed ridge growth in the bow area is seen in Figure 2.10 as NN'. In Figure 2.10, the distance in front of the bow where the ridge starts to get thicker in the developed condition is AE. The expressions for these quantities are:

$$NN' = T \left(\frac{1}{\tan \gamma} + \frac{1}{\tan \phi} \right)$$

$$AE = \frac{h}{\tan \gamma}$$

For large values of ϕ -angle, which is at the same time the angle for ridge growth in front of the bow (see Figure 2.9), the ridge mass cannot stay piled up with a wall steeper than the natural slope of a ridge keel. In a dynamic condition, however, this is possible and also, as it is now set up, the geometry itself does not have any relevance in the analysis of the forces.

2.4.3 General Solution for Ridge Growth

Up to this point, we have considered the geometric mass shown in Figure 2.11 as DE'C'A. For a kinematic model, it is of importance to use the kinematic mass, which is given in Figure 2.11 as DECA. The difference arises from a consideration of the direction of the frictional force in the breaking geometry.

When the half angle of the waterline, α , is less than 90° , and so departs from the landing craft bow type, the ridge grows according to a different geometry. In a landing craft bow, the ice moves in the xz-plane only, with all ice passing under the hull. In the case of a normal bow shape, the ice moves also in the xy- and xz-planes, according to the same principles. In addition, the penetrations needed for the development of the ridge resistance have a different expression. Figure 2.11, shows the x-y image of one basic

geometry of the ridge growth. In this figure, it can be seen that a completed ridge growth around the forward body (= corresponding to the case of a landing craft bow type) will be achieved in the area AFEB, only. The corresponding bottom surface image in an xy-plane is shown in Figure 2.12. The bottom profile of the developed ridge is such that the ridge reaches its greatest depth in the line JK (Figure 2.12), and behind that when penetration is continued. At the points E, D and C no ridge growth will take place.

For determination of the buoyancy force the volume of the ice will be divided into three separate parts, which are shown for thin ($h \leq T$) and thick ridges ($h \geq T$) separately in Figures 2.13a and b.

Determination of F_{G1} is straight-forward and for the whole ship we obtain:

$$F_{G1} = \frac{h^2 \mu_B \rho g}{2 \sin \alpha} \left(\frac{1}{\tan \gamma} + \frac{1}{\tan \psi} \right) \text{ when } h \leq T \quad (2.22)$$

OR

$$F_{G1} = \frac{T^2 \mu_B \rho g}{2 \sin \alpha} \left(\frac{1}{\tan \gamma} + \frac{1}{\tan \psi} \right) \text{ when } h \geq T \quad (2.23)$$

Correspondingly, the expressions for F_{G2} in the two cases will be, for the whole ship,

$$F_{G2} = \frac{hB(T-h) \mu_B \rho g}{\sin \alpha} \left(\frac{1}{\tan \gamma} + \frac{1}{\tan \psi} \right) \text{ when } h \leq T \quad (2.24)$$

and

$$F_{G2} = \frac{TB(h-T) \mu_B \rho g}{\sin \alpha} \left(\frac{1}{\tan \gamma} + \frac{1}{\tan \psi} \right) \text{ when } h \geq T \quad (2.25)$$

The determination of F_{G3} is more complicated and, in addition to the division due to ridge thickness, another division will be made into two subcases which are shown in Figures 2.11a and b in xy-plane views.

The difference between the cases shown in Figures 2.11a and b is that in case (a) the ridge growth in the line JK will reach the maximum corresponding to complete growth for the case of a landing craft bow, whereas in the case (b), the thickness growth will not reach the same depth in the JK-line, Figure 2.12.

For determination of the total ice volume G_3 , the volume will be divided into three parts - V_1 , V_2 , and V_3 . As shown in Figures 2.12, V_1 and V_3 are equal, by symmetry. The general formulae for F_{G_3} is thus, for the whole ship,

$$F_{G_3} = (V_2 + V_1) \mu_B \rho_{\Delta} g \cdot 2 \quad (2.26)$$

and the general expressions for V_1 , and V_2 will be, for one ship's side,

$$V_1 = \frac{FE \cdot h_x \cdot DH}{6}$$

$$V_2 = \frac{FE \cdot h_x \cdot HG}{2}$$

where Figures 2.11 and 2.13 show FE, DH, HG and h_x for the different cases.

1. The Case of Figure 2.11a

This case is characterized by the fact that $DH = B/2$ and V_2 is thus limited by the breadth of the ship. First the case $h \leq T$ is considered (Figure 2.13a).

In the case $h_x = h$ and F_{G_3} can be expressed

$$F_{G_3} = \frac{C_2 h_x h (\sin \alpha' \tan \alpha + \cos \alpha') \mu_B \rho_{\Delta} g}{\tan \alpha \cos(\alpha' - \alpha)} \quad (2.27)$$

$$\cdot \left(\frac{B}{2} - \frac{h}{3} \frac{\cos \alpha'}{\cos(\alpha' - \alpha)} \right)$$

$$\text{where } C2 = \left(\frac{1}{\tan \psi} + \frac{1}{\tan \gamma} \right)$$

Next, for $h \geq T$ (Figure 2.13b), the equation will be changed. Then $h_x = T$.

$$F_{G3} = \frac{C2 h_x T (\sin \alpha' \tan \alpha + \cos \alpha') \mu_B \rho \Delta g}{\tan \alpha \cos (\alpha' - \alpha)} \left(\frac{B + h \cos \alpha' C2}{6 \cos (\alpha' - \alpha)} \right) \mu_B \rho \Delta g$$

2. The Case of Figure 2.11b

This case is characterized by the fact that $DG = B/2$. Then DH is constant ($=B/2$) and $h_x < h$. First, for $h \leq T$ (Figure 2.13a),

$$F_{G3} = \frac{Bh}{2} \left(\frac{1}{\tan \alpha} + \tan \alpha' \right) \left(\frac{1 - 2 \cos (\alpha' - \alpha)}{h C2} \right) \left(\frac{B + h \cos \alpha' C2}{6 \cos (\alpha' - \alpha)} \right) \mu_B \rho \Delta g \quad (2.29)$$

For $h > T$ (Figure 2.14b) we correspondingly obtain

$$F_{G3} = \frac{BT}{2} \left(\frac{1}{\tan \alpha} + \tan \alpha' \right) \left(\frac{\cos (\alpha' - \alpha) - 2}{T C2} \right) \left(\frac{B + T \cos \alpha' C2}{6 \cos (\alpha' - \alpha)} \right) \mu_B \rho \Delta g \quad (2.30)$$

The correct case out of these four is chosen by the division between $h < T$ and $h > T$. If h_x exceeds h when $h < T$, the correct F_{G3} value is found from Eq. (2.27) and if h_x exceeds T when $h > T$, the correct F_{G3} value is found from Eq. (2.31). When h_x does not exceed these limits, the correct value for F_{G3} is found for $h < T$ from Eq. (2.29) and for $h > T$ from Eq. (2.30), respectively.

The proper combination of F_{G3} Eqs. (2.22), (2.23), F_{G2} (2.24), (2.25) and F_{G3} Eqs. (2.27), (2.28), (2.29), (2.30) give $C3$ for the original method Eqs. (2.20), (2.14)

$$C3 = (F_{G1} + F_{G2} + F_{G3}) / C2$$

2.5 THE PARALLEL MIDDLE BODY

2.5.1 General

In ships which have a parallel middle body, this part of the hull will cause a resistance component, which is connected with the amount of ice mass around the parallel part of the ship, at the sides and below the ship's bottom. This resistance component is a linear function of the coefficient of friction between ship's hull and ice with the assumption that no change in the ice profile will occur due to a change in this coefficient.

Even a ship with no parallel middle body has approximately flat bottom and sides, as can be seen in the representation of a ship's hull considered in this work (Figure 1.5). The length of this apparently parallel body is shown in Figure 1.5 as $DF + MJ$ and is expressed as

$$L_p' = T/\tan\phi \quad (2.31)$$

In Subsection 2.5.2 the profile of the ice around the middle body will be analyzed.

In Subsection 2.5.3 the frictional resistance due to the ship's sides is analyzed using the profile from Sub-section 2.5.2 as input data.

In Sub-section 2.5.4 the frictional resistance due to the ice beneath the ship is analyzed.

It is important to get data on the length of a ridge field at which a developed resistance condition will be reached and when the ice starts to accumulate under the ship. The penetration lengths at which the different steps of the penetration are reached are analyzed in Sub-section 2.5.5.

2.5.2 Ice Profile Around the Parallel Middle Body

The development of an ice ridge in the forward body portion of a ship determines what kind of ice mass cross section enters the parallel part of the ship. This kind of cross section, when it once has reached its maximum dimensions, will be assumed to pass unchanged along the whole, parallel middle body during penetration. Underwater observation in the ice model basin support this kind of assumption in long homogeneous ridges.

The input data for determination of the ice profile is obtained from the analysis in Sub-section 2.4.3 and there are correspondingly four cases to be considered separately, two subcases for each of $h \leq T$ and $h > T$. Figures 2.14a-d present these cases. For clarity, the xy-planes are also drawn, as in Figure 2.12. A basic requirement for the cross-section DH' 'CG' 'H' is that its area has to be equal to that of the corresponding equivalent cross-section of the submerged part of the main beam of the ship. In addition, for symmetry reasons, DH' 'H' = CG' 'G' in each case.

The dimensions determined in Figures 2.14a-d are good for the idealized conditions of a vertical sided ship only. Also, the vertical slope of the ridge mass shown in Figures 2.14a and b is purely theoretical with no corresponding equivalent in nature.

The vertical wall of the ridge mass is eliminated by allowing the mass to break, as shown in Figure 2.15. The amount of ice that breaks and moves away from its original position under the hull to the sides is given in Figure 2.15 a by ABCE. This area is calculated by subtracting DEC from ABD

$$ABD = \frac{h^2}{2 \tan \beta'} \quad (2.32)$$

after geometric analysis

$$ABCE = \frac{h^2}{2 \tan \beta'} - \frac{1}{2} \cdot \left(\frac{h}{\tan \beta'} - \frac{B}{2} + \frac{h \cos \alpha'}{\cos(\alpha' - \alpha)} \right)^2 \quad (2.33)$$

$$\cdot \frac{\sin \alpha \operatorname{atan} \frac{\cos(\alpha' - \alpha)}{C^2 \cdot \cos \alpha'}}{\sin \left[\alpha - \operatorname{atan} \frac{\cos(\alpha' - \alpha)}{\cos \alpha' \cdot C^2} - \beta' \right]} \cdot \sin \beta'$$

If $DB < CB$, there does not exist any DEC triangle and instead of ABCE the breaking mass is ABD.

Eqs. (2.31) and (2.32) apply for a single ship's side.

The additional amount of ice now at the sides of the hull is the same as has broken away from below. When this ice is assumed to spread out evenly, the additional depth of the ridge at the sides is

$$\frac{ABCE}{B/2 - CB}$$

Thus, the limit where this kind of total breaking to the side takes place is at ridge thickness

$$2 \cdot h + \frac{ABCE}{B/2 - CB} = T$$

When $h = T$, the other limit is reached where no vertical wall exists and no breaking takes place. Between these two extremes, a linear interpolation of the amount of broken ice can be made.

In the case of Figure 2.15b (corresponding to 2.14b) the same type of determination is done for the breaking then,

$$ABD = \frac{h^2}{2 \tan \beta'} \quad (2.34)$$

thus

$$ABE = \frac{h^2}{2 \tan \beta'} - \frac{1}{2} \left[\frac{h}{\tan \beta'} \left(1 - \frac{h \cos \alpha'}{\cos(\alpha' - \alpha)} C_2 - \frac{B}{2} \right) / (2h) \right]^2 \quad (2.35)$$

$$\frac{\sin \operatorname{atn} \frac{h_x}{B/2}}{\sin \left(180^\circ - \operatorname{atn} \frac{h_x}{B/2} - \beta' \right)} \cdot \sin \beta'$$

which are for one ship's side, Eqs. (2.33), (2.35).

The additional depth of the ridge at the side is

$$\frac{ABE}{\frac{h \cos \alpha'}{\cos(\alpha' - \alpha)} C_2}$$

and the limits for total breaking and no breaking are

$$h + h_x + \frac{ABE}{\frac{h \cos \alpha'}{\cos(\alpha' - \alpha)} C_2} = T$$

and

$$h + h_x = T,$$

respectively. Again, interpolation between these limits is done linearly.

Finally, the total amount of ice below the hull is governed by the following equations. These equations are for the whole ship for A_{PB} (under the flat bottom) and for one ship's side for A_{PS} (at the parallel side).

Case a)(Figures (2.14)a, (2.15)a)

$$A_{PB} = \frac{h(B - h \cos\alpha')}{\cos(\alpha' - \alpha)} C_2 - ABCE \cdot 2 \quad (2.36)$$

$$A_{PS} = \frac{(B - h \tan\beta)h - A_{PB}}{2}$$

$$h_S = 2h + \frac{ABCE}{B/2 - CB} \quad (2.37)$$

Case b)(Figures (2.14)b, (2.15)b) (2.38)

$$A_{PB} = \frac{hB}{2} \left(1 - \frac{\frac{h \cos\alpha'}{\cos(\alpha' - \alpha)} C_2}{h - C_2} \right) - ABE \cdot 2$$

$$A_{PS} = \frac{(B - h \tan\beta)h - A_{PB}}{2}$$

$$h_S = h + h_x + \frac{ABE}{\frac{h \cos\alpha'}{\cos(\alpha' - \alpha)} C_2} \quad (2.39)$$

Case c)(Figure (2.14)c)

$$A_{PB} = (h - T)B + T \left(B - \frac{T \cos\alpha'}{\cos(\alpha' - \alpha)} C_2 \right) \quad (2.40)$$

$$A_{PS} = \frac{(B - T \tan\beta)T}{2}$$

$$h_S = h + T \quad (2.41)$$

Case d)(Figure (2.14)d)

$$A_{PB} = (h - T)B + \frac{BT}{2} \left(1 - \frac{T \cos \alpha' c_2 - \frac{B}{2}}{T c_2} \right) \quad (2.42)$$

$$A_{PS} = \frac{(B - T \tan \beta)T - A_{PB}}{2} \quad (2.43)$$

$$h^S = h + h_x.$$

In these equations h_S is the pressure height of the ridge and β the slope angle of the parallel side.

2.5.3 Side Resistance

The resistance of ice against the parallel part of the ship's sides is indisputably a purely frictional resistance due to friction between the ship's hull and the ice.

In Sub-sections 2.5.2, the geometry of the ice surrounding the parallel middle body was analyzed so that the pressure against the hull can be expressed as a function of the ice geometry.

The pressure in the vertical direction is $\mu_B \rho_A g h$ and in the horizontal direction $\mu_B \rho_A g h [\nu / (1 - \nu)]$. When the side of the ship is inclined at an angle β , an interpolation of the pressure for any desired β -direction will be made as

$$P_\beta = \mu_B \rho_A g h_S \left(\frac{\nu}{1 - \nu} (1 - \sin \beta) + \sin \beta \right), \quad (2.44)$$

h_S expresses the pressure height, P_β is the pressure.

When $h_S \leq T$, the average pressure height against the side of the ship is $\bar{h}_S = h_S/2$ (h_S Eqs.(2.37), (2.39) and when $h_S > T$ this is $\bar{h}_S = (2h_S - T)/2$ (h_S Eqs. (2.41) and (2.43). The resistance is then

$$R_{PS} = A_S \cdot p_{hS} \mu \quad , \quad (2.45)$$

where A_S is the contact area between the parallel ship's sides and the ice, p_{hS} is the average pressure against the ship's sides and μ is the coefficient of friction between hull and ice. Thus,

$$A_S = 2 \cdot L_p \cdot h_S / \cos \beta \quad \text{when } h_S \leq T$$

OR

$$A_S = 2 \cdot L_p \cdot T / \cos \beta \quad \text{when } h_S \geq T, \text{ for the whole ship.}$$

2.5.4 Bottom Resistance

The maximum resistance due to ice under the bottom is considered in the situation where the whole length of the bottom is covered by ice. In this case, resistance is a purely frictional force corresponding to the buoyancy force of the ice under the bottom. The buoyancy force is

$$F_{PB} = A_{PB} \cdot \mu_B \rho \Delta g \cdot L_p$$

with A_{PB} from Eqs. (2.36) (2.38) (2.40) or (2.42). The resistance is then

$$R_{PB} = \mu \cdot A_{PB} \cdot L_p \cdot \mu_B \rho \Delta g \quad (2.46)$$

The resistance is a linear function of the length of the parallel middle body covered by ice, starting from zero at the bow end.

2.6.5 Penetrations for Ridge Growth

Figure 2.16 shows an A-A-section of a ship with the notations used here for ridge growth. The different penetrations are marked, starting from the initial resistance condition. Their identification is

- l_1 = the distance of penetration required to reach the developed resistance thickness (= maximum thickness)
 l_2 = penetration required before (additional) ice starts to pass under the bottom
 l_3 = distance of increasing ice thickness under the bottom
 l_4 = (= $l_2 + l_3$) penetration required to reach the maximum ridge thickness below the bottom of the parallel middle body (= the minimum length of ridge to achieve developed resistance condition)
 l = the distance from the front of the stem at which the ridge growth starts
 l_i = penetration into the ridge before the initial condition is achieved

The expressions for these for $h \ll T$ are given in the direction of the ship's movement, by dividing the penetrations in the A-A-plane by $\sin \alpha$, as follows:

$$l_1 = \frac{T}{\sin \alpha} \left(\frac{1}{\tan \gamma} + \frac{1}{\tan \psi} \right) \quad (2.47)$$

For l_2 the volume (or areas) of ship penetration and that of ice growth are set equal, when ice starts to pass under the bottom.

$$h \left(\frac{1}{\tan \gamma} + \frac{1}{\tan \psi} \right) \cdot (T - h) = l_2 \sin \alpha \cdot h$$

thus

$$l_2 = \frac{(T - h)}{\sin \alpha} \left(\frac{1}{\tan \gamma} + \frac{1}{\tan \psi} \right) \quad (2.48)$$

$$l_3 = l_1 + l_4 - l_2$$

where

$$l_y = \frac{h}{\tan \gamma \sin \alpha}$$

$$l_3 = \frac{1}{\sin \alpha} \left[C_2 \cdot h + \frac{h}{\tan \gamma} \right] \quad (2.49)$$

$$l_4 = l_1 + l_y = \frac{T}{\sin \alpha} C_2 + \frac{h}{\tan \gamma \sin \alpha} \quad (2.50)$$

$$l_1 = \frac{h}{\tan \psi \sin \alpha} \quad (2.51)$$

When the thickness of the ridge is greater than the ship's draught, $h > T$, the expressions remain the same for l_1 , l_y and l_4 . The other expressions become

$$l_2 = l_y \quad (2.52)$$

$$l_3 = l_1 \quad (2.53)$$

$$l_1 = \frac{T}{\tan \psi \sin \alpha} \quad (2.54)$$

From Figure 2.19 the angle δ is determined as

$$a. \quad \delta = \arctan \frac{h_x}{l_3} \text{ for } h \leq T \text{ and } h_x \leq h \quad (2.55)$$

$$b. \quad \delta = \arctan \frac{h_x}{l_3} \text{ for } h \geq T \text{ and } h_x \leq T$$

2.7 SUMMARY OF RESISTANCE COMPONENTS

In the preceding sections (2.3 through 2.5) the pure ridge resistance (R_{TOT0}) has been analyzed into its components. Thus (R_{TOT0}) is expressed as the sum

$$R_{TOT0} = R_{Y1} + R_{Y2} + R_E + R_{PB} + R_{PS} \quad (2.56)$$

where the components are obtained as follows:

R_{Y1} (2.21)
 R_{Y2} see Ref.(4)
 R_E see Ref.(4)
 R_{PB} (2.46)
 R_{PS} (2.45)

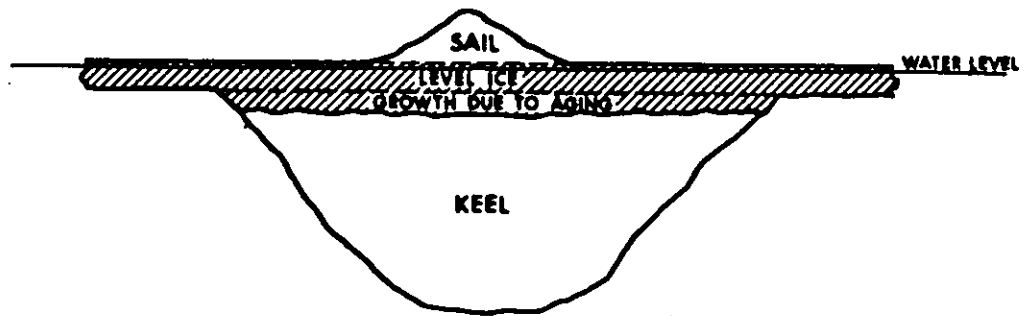


FIG. A-1 SCHEMATIC PROFILE OF A BALTIC RIDGE.
REF. (4)

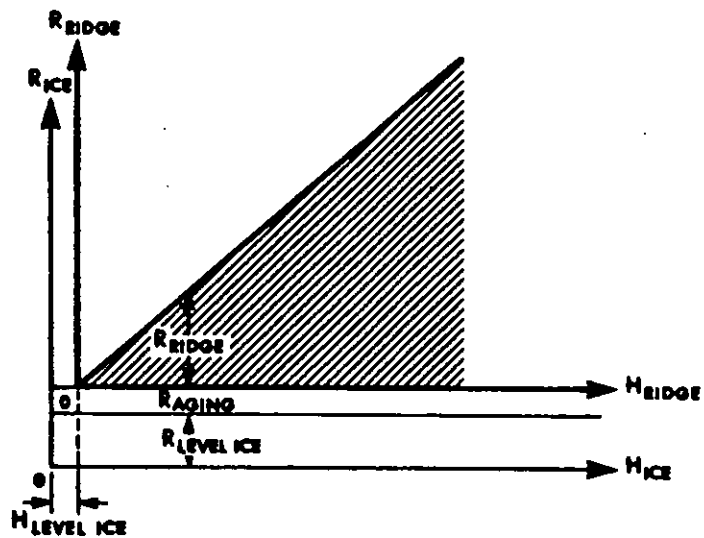


FIG. A-2 COMPONENTS OF TOTAL ICE RESISTANCE IN
RIDGES. REF. (4)

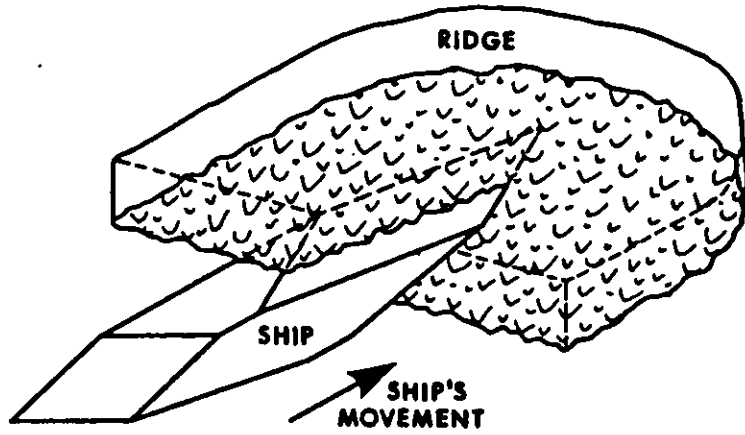


FIG. A-3 INITIAL RESISTANCE CONDITION,
SUBMERGED PART OF SHIP HULL.
FOR SHIP GEOMETRY, SEE FIG. A-5.
REF. (4)

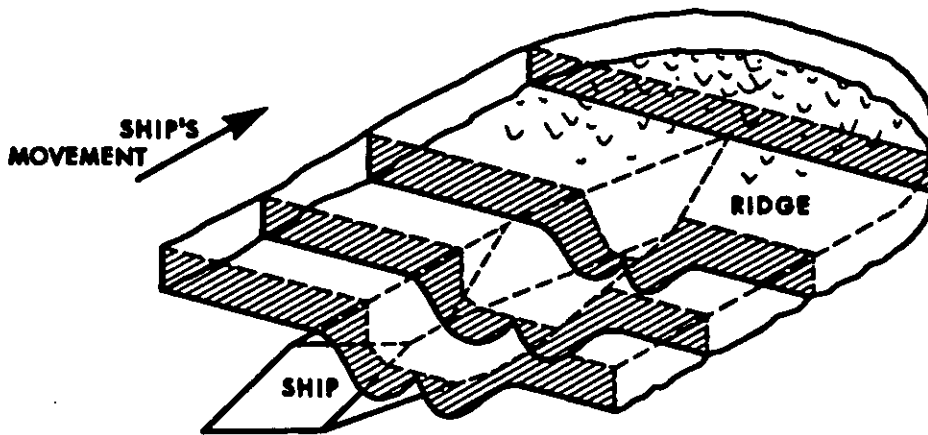
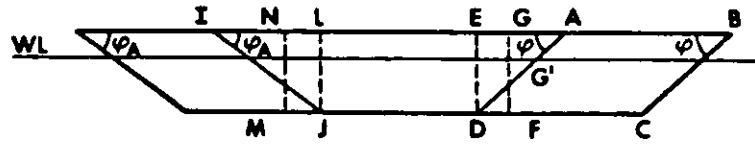


FIG. A-4 DEVELOPED RESISTANCE CONDITION.
REF. (4)

XZ-PLANE



XY-PLANE

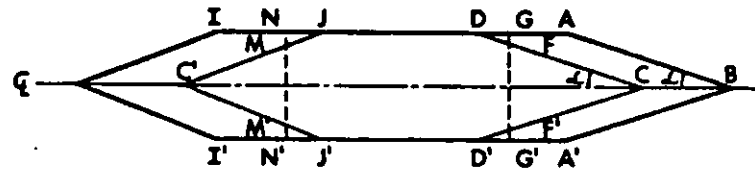
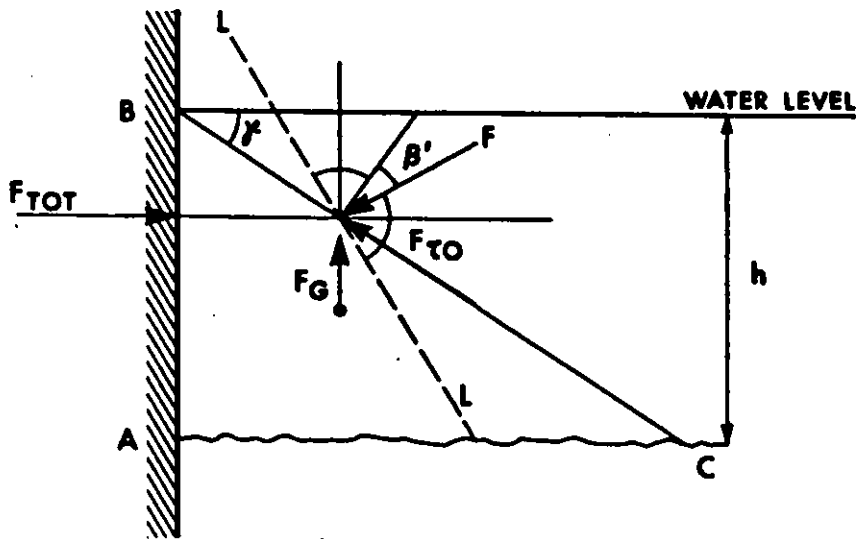


FIG. A-5 SHIP'S GEOMETRY. REF. (4)



- F_{TOT} = FORCE AGAINST THE WALL
- F_{T0} = COHESION RESISTANCE
- F_G = BUOYANCY FORCE OF ICE
- F = SHEAR FRICTION RESISTANCE
- β' = INNER FRICTION ANGLE

FIG. A-6 COULOMB'S METHOD. REF. (4)

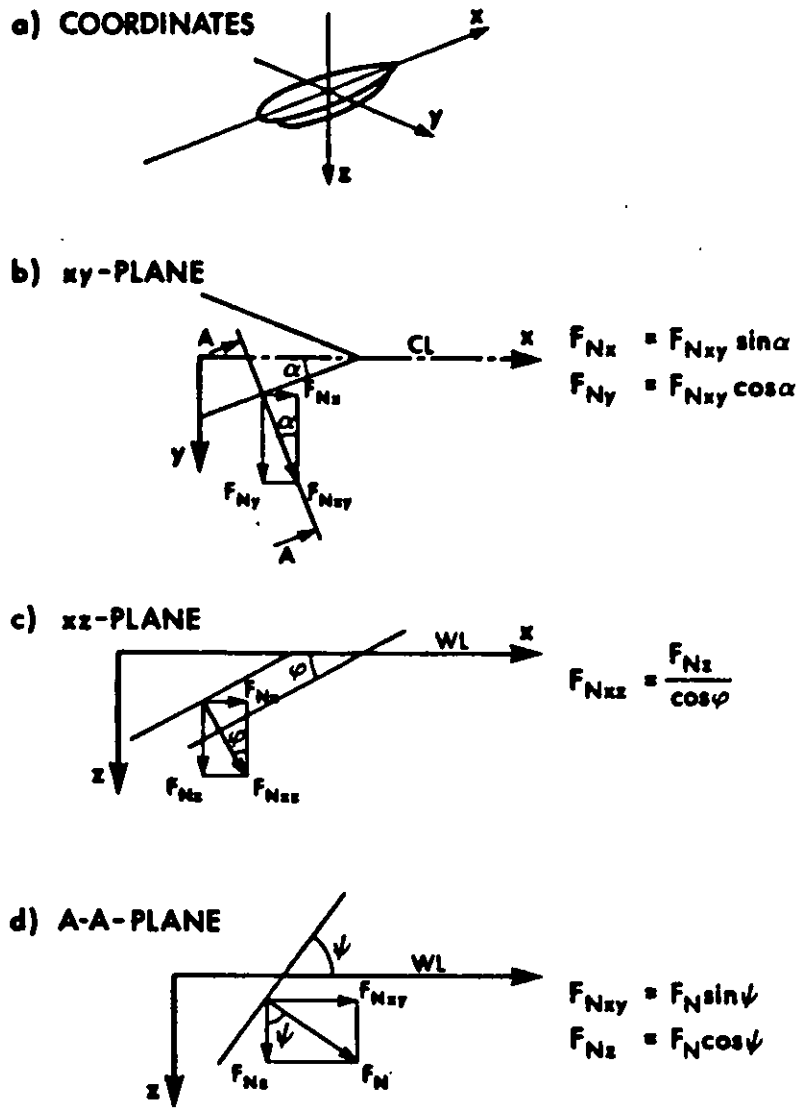


FIG. A-7 COMPONENTS OF NORMAL FORCE. REF. (4)

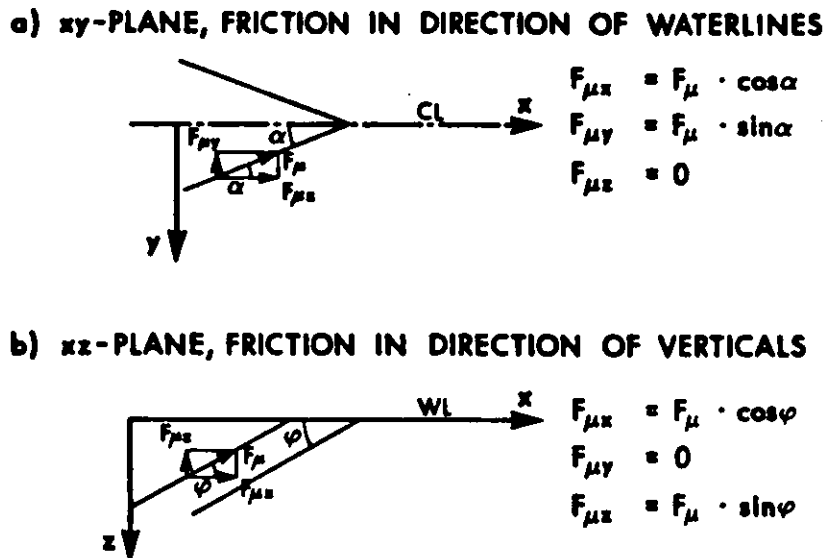


FIG. A-8 COMPONENTS OF FRICTIONAL FORCE. REF. (4)

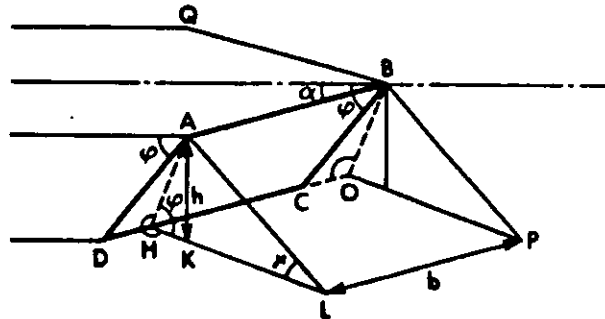


FIG. A-9 STRESS ANALYSIS GEOMETRY FOR THE SIDE PLANE OF THE FORWARD BODY OF A SHIP (ABCD). REF. (4)

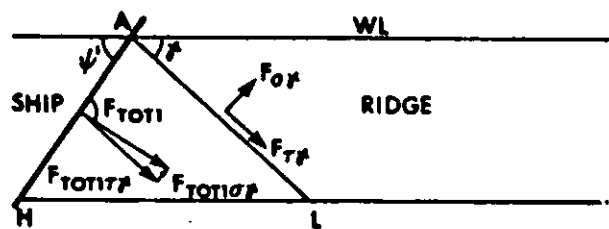


FIG. A-10 COMPONENTS OF TOTAL SHIP'S FORCE IN x - y -PLANE. REF. (4)

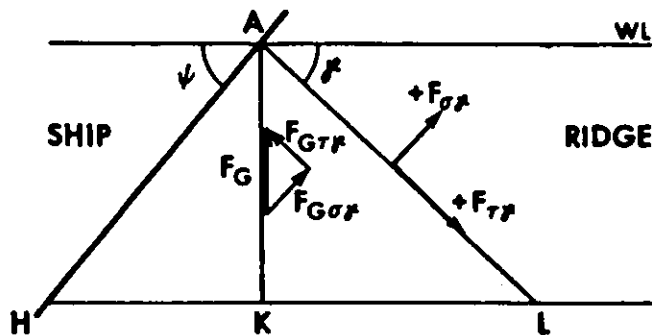


FIG. A-11 COMPONENTS OF BUOYANCY FORCE IN x - y -PLANE, AND THE END PLANE FORCE. REF. (4)

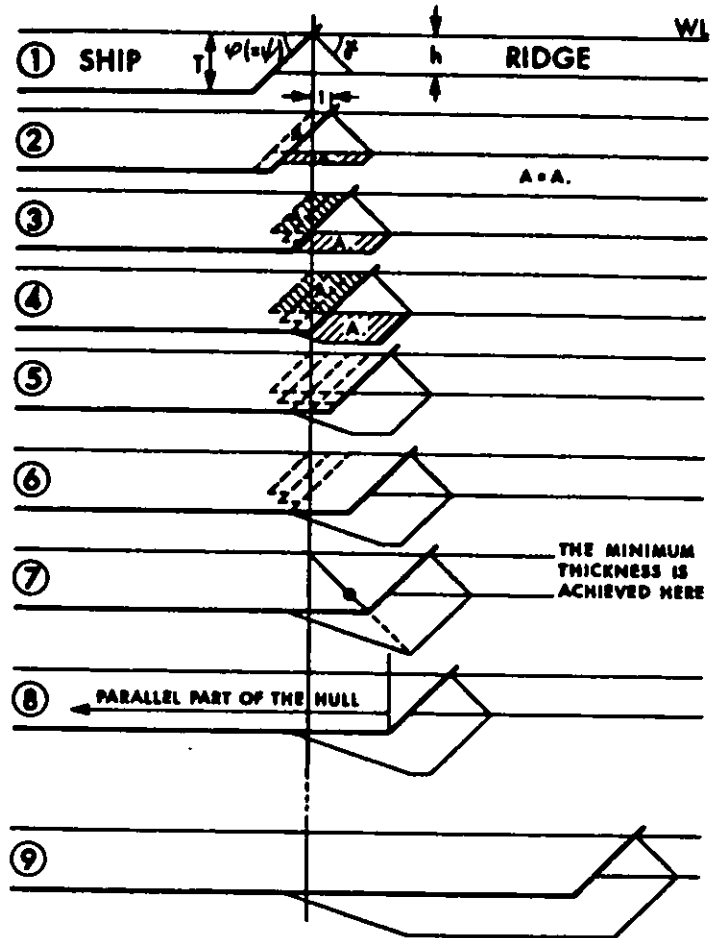


FIG. A-12 DEVELOPMENT OF RIDGE PROFILE AROUND A LANDING CRAFT BOW. REF. (4)

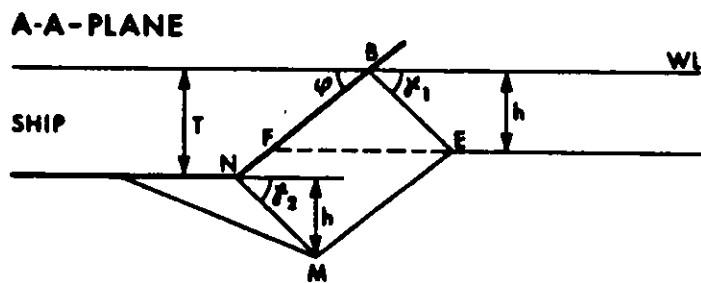


FIG. A-13 DEVELOPED GEOMETRY, LANDING CRAFT BOW. REF. (4)

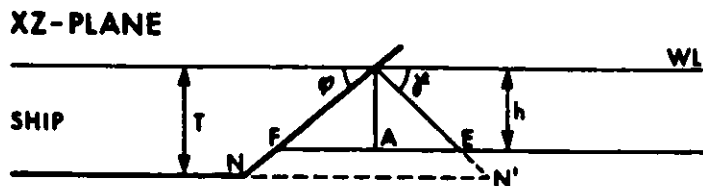


FIG. A-14 PENETRATION FOR RIDGE GROWTH, LANDING CRAFT BOW. REF. (4)

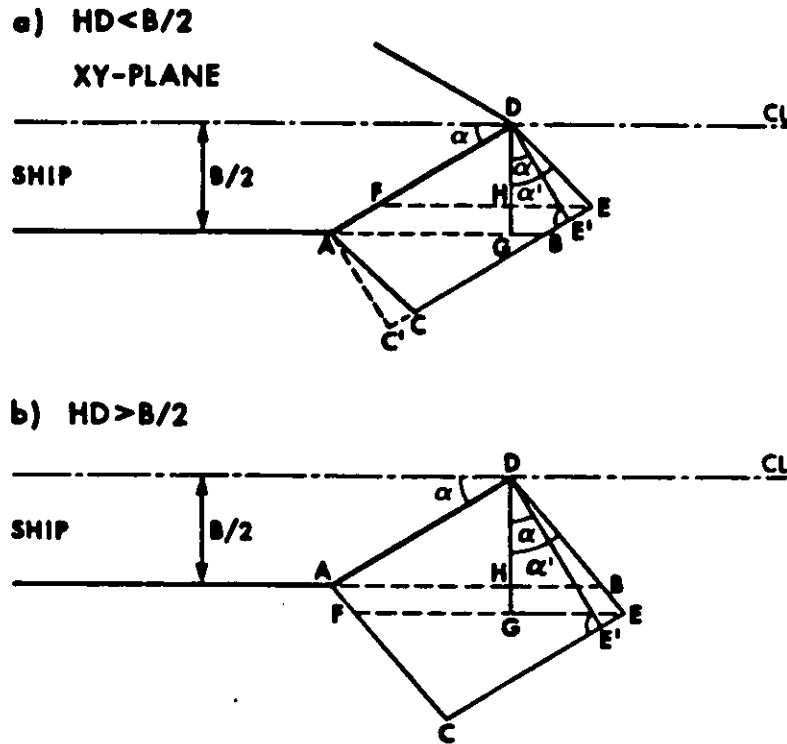


FIG. A-15 GEOMETRY FOR GROWTH MODEL. REF. (4)

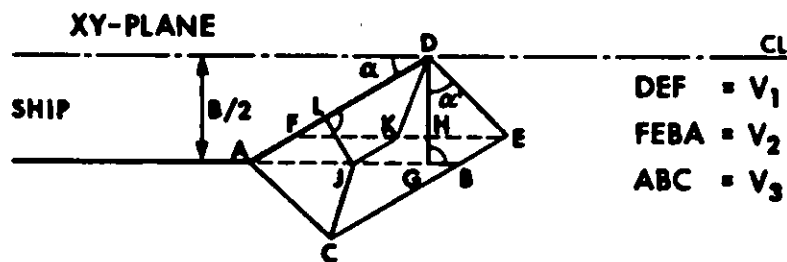


FIG. A-16 BOTTOM OF DEVELOPED RIDGE. REF. (4)

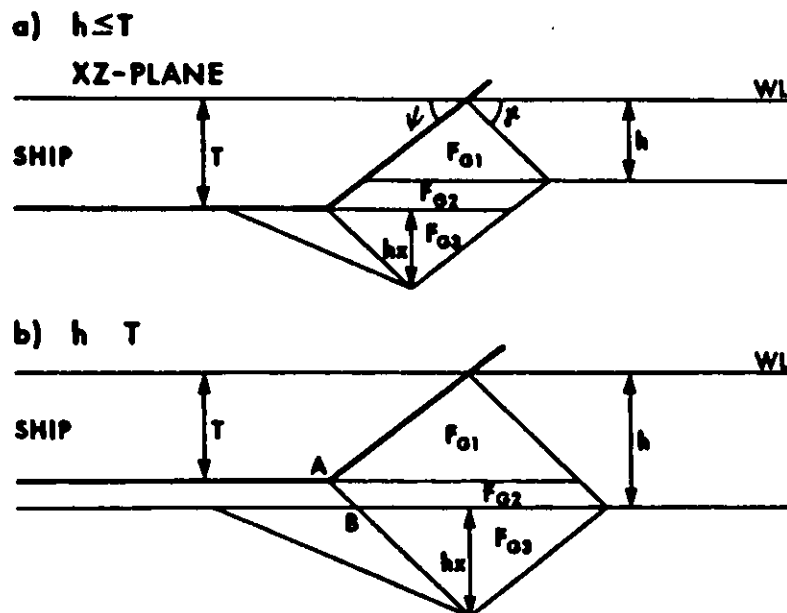
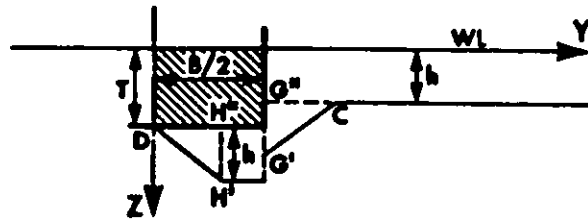


FIG. A-17 DIVISION OF ICE MASSES FOR THE DEVELOPED RESISTANCE CONDITION. REF. (4)



a)

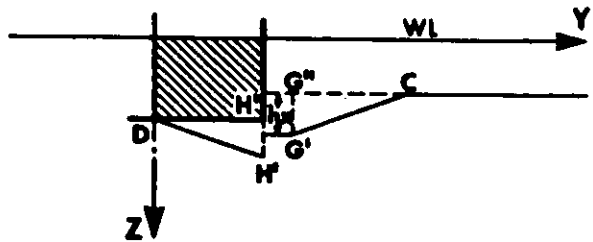
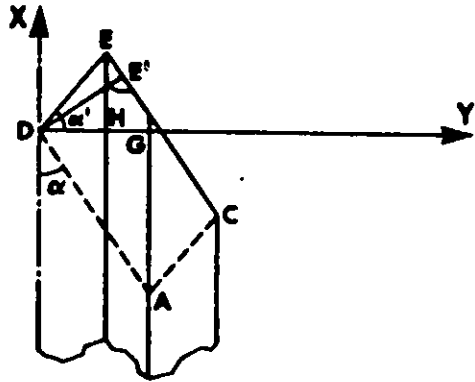
$$h \leq T$$

$$DG = \frac{B}{2}$$

$$HD = \frac{h \cdot \cos \alpha' \cdot C2}{\cos(\alpha' - \alpha)}$$

$$HG = \frac{B}{2} - HD$$

$$H'H'' = G'G'' = h_x = h$$



b)

$$h \leq T$$

$$DG > \frac{B}{2}$$

$$HD = \frac{B}{2}$$

$$HG = \frac{h \cdot \cos \alpha' \cdot C2}{\cos(\alpha' - \alpha)} - \frac{B}{2}$$

$$H'H'' = G'G'' = h_x = h \left(1 - \frac{HG}{DE'}\right)$$

$$DE' = h \cdot C2$$

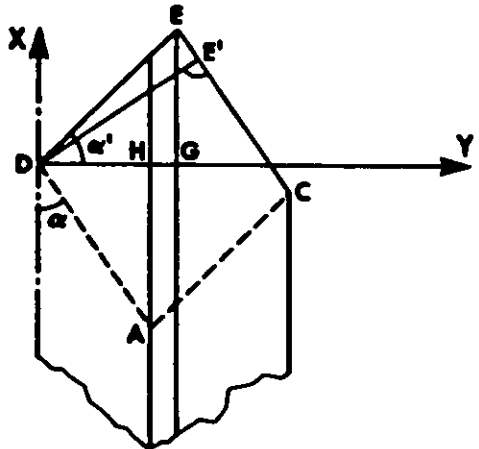
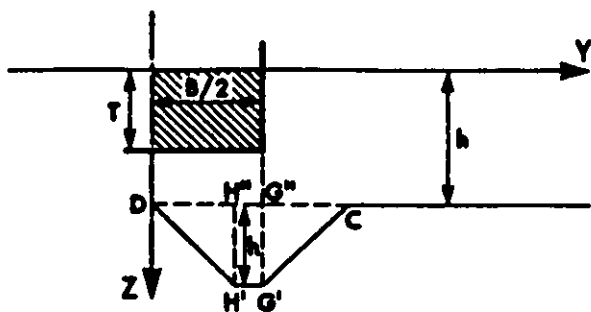


FIG. A-18 ICE PROFILE AROUND MIDDLE SHIP. REF. (4)



c)

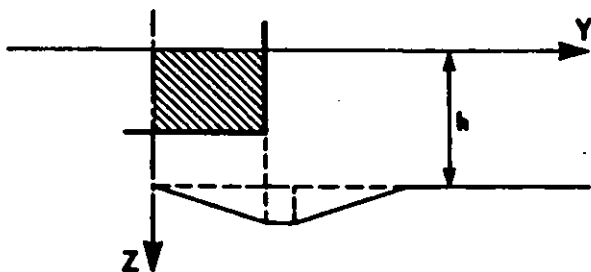
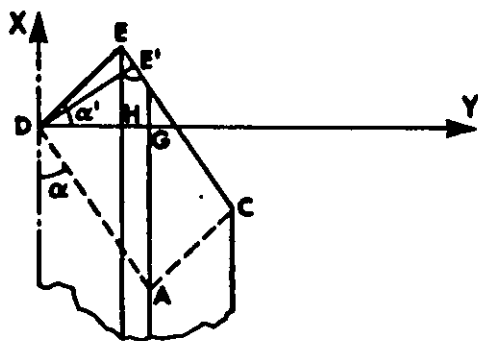
$$h \geq T$$

$$DG = \frac{B}{2}$$

$$DH = \frac{T \cos \alpha' \cdot C2}{\cos (\alpha' - \alpha)}$$

$$HG = DG - DH$$

$$H'H'' = G'G'' = h_x = T$$



d)

$$h \geq T$$

$$DG > \frac{B}{2}$$

$$HD = \frac{B}{2}$$

$$HG = \frac{T \cos \alpha' \cdot C2}{\cos (\alpha' - \alpha)} - \frac{B}{2}$$

$$H'H'' = G'G'' = h_x = T \left(1 - \frac{HG}{DE'}\right)$$

$$DE' = T \cdot C2$$

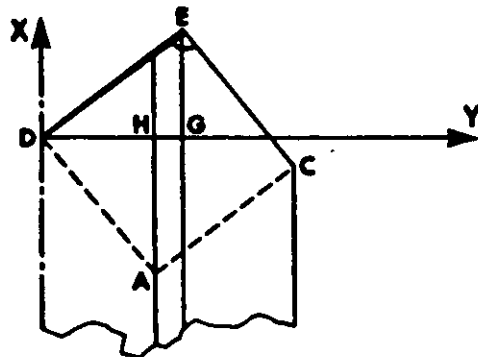


FIG. A-19 ICE PROFILE AROUND MIDDLE SHIP. (CONT'D)
REF. (4)

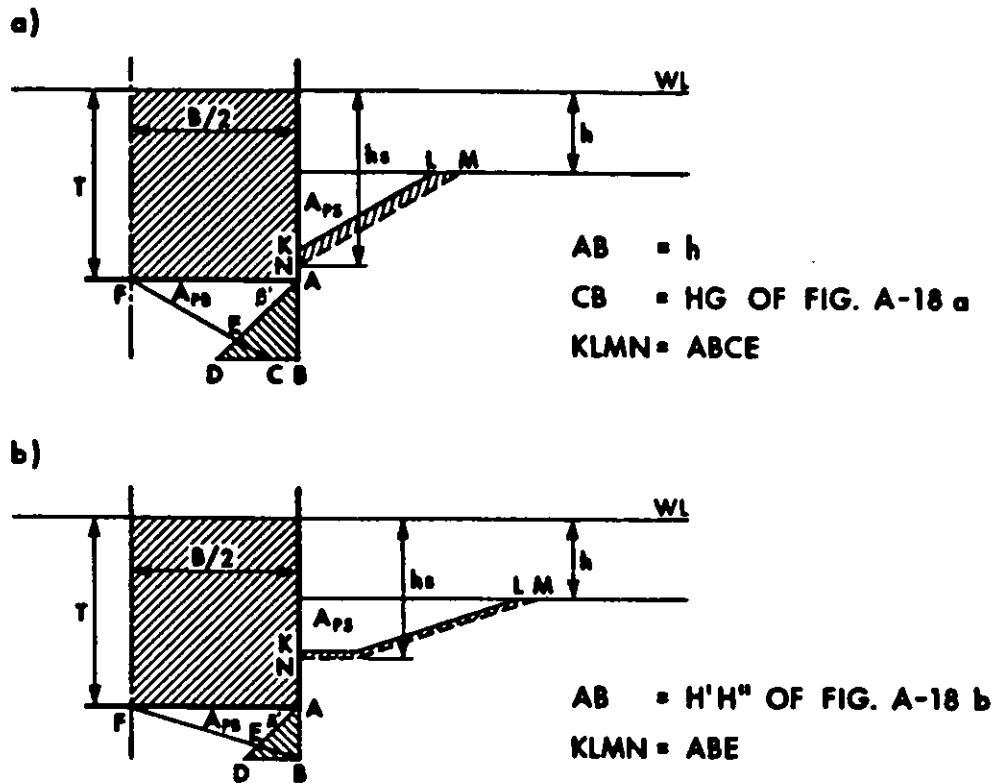


FIG. A-20 ELIMINATION OF THE VERTICAL RIDGE WALL.
REF. (4)

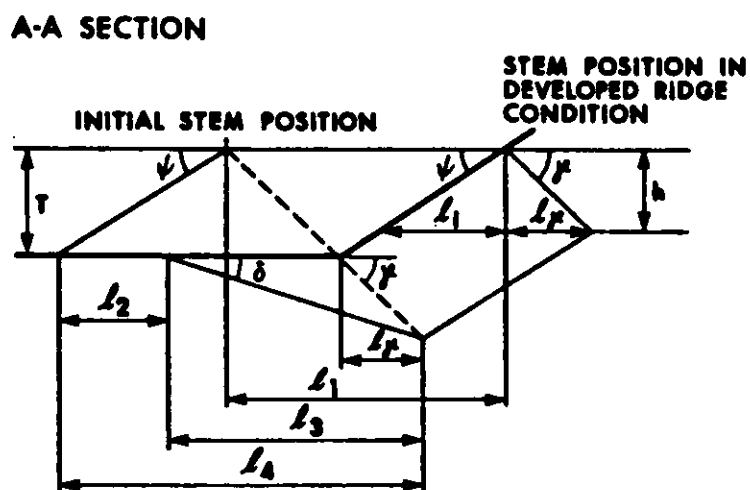


FIG. A-21 PENETRATIONS FOR RIDGE GROWTH. REF. (4)

REFERENCES

1. "The Canadian Arctic Shipping Pollution Prevention Regulations (CASPPR)," Chapter 33, The Arctic Waters Pollution Prevent Act, Queen's Printer, Ottawa, 1980.
2. Daley, C.G., Edworthy, J.T. (by Arctec Canada), Hazardous Ice Atlas of Canada, prepared for the Canadian Coast Guard, Ottawa 1983.
3. Enkvist, E., Riska, K., Varsta, P., "The Ship-Ice Interaction," POAC, 1979.
4. Ghoneim, G., Keinonen, A.J., "Full-Scale Tests of Canmar Kigoriak in Very Thick Ice," POAC, 1983.
5. Glen, I.F., Daley, C., "Ice Impact Loads on Ships", presented to the SNAME, Arctic Section, Calgary, May 1982.
6. Glen, I.F., Daley, C., Edworthy, J., Gareau, G., Studies Supporting Update of the CASPPR Regulations Group 1 and 2, Report 586A by Arctec Canada Ltd., for Canadian Coast Guard, 1982.
7. Johansson, B.M., Keinonen, A.J., Mercer, B., "Technical Development of an Environmentally Safe Arctic Tanker", SNAME, Spring Meeting/STAR Symposium, Ottawa, June 17-19, 1981.
8. Laskow, V., "Ship-Ice Interaction Models, Designer's Approach", presented to the SNAME, Arctic Section, Calgary, May 1982.
9. Tunik, A., "Ultimate Safe Conditions for Ship's Operation in Ice", presented to the SNAME, Arctic Section, Calgary, May 1982.



SHIPS AND STRUCTURES IN ICE

Propulsion in Ice

by

Kimmo Juurmaa

PROPULSION IN ICE

1 INTERACTION BETWEEN ICE AND PROPELLER

In principle there are three different ways of propeller - ice interaction. The first, and the most important as far as strength is concerned, is milling.

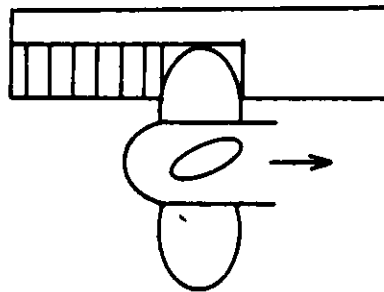


Fig. 1

Milling has been widely studied both theoretically and using model tests. The phenomenon, as well as its influence on propeller design, has been discussed in literature in such detail that there is no need to go any deeper here.

The second way of interaction is impulse contact, which implies that the propeller is hit by ice blocks that are subsequently thrown away from the propeller disc.

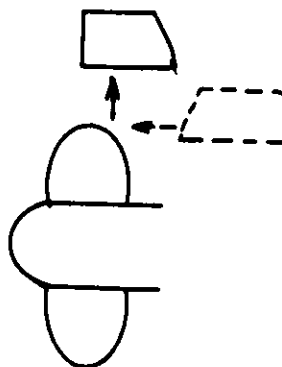


Fig. 2.

Impulse contact gives a lot of scope for optimizing the propeller blade form. Such optimizing leads to a similar blade form as is used for minimizing pressure impulses in uneven wakefield in open water, that is the so-called skew-back propellers.

The third possibility of interaction is that the ice block gets crushed when it hits the propeller blade.



Fig. 3.

In practice none of these contacts is dominating on its own, but they all appear to varying extents mixed with each other as will be seen in the following films. This means that it is most difficult to predict mathematically the behaviour of propellers in different conditions. Therefore, model tests and full scale tests are used for this purpose.

2

BASIC THEORY

In open water, propulsion efficiency is determined as the relation of effective power to delivered power, that is

$$\eta_d = \frac{P_e}{P_d}$$

and further

$$\eta_{bd} = \frac{R_t V}{2\pi nQ}$$

where

- R_t = towing resistance
- V = velocity of the ship
- n = required rpm to produce the propelling thrust
- Q = torque required to produce required rpm.

In ice we can use the same equation

$$\eta_{ice} = \frac{R_{ice} V}{2 \pi n_{ice} Q_{ice}}$$

When trying to compare the propulsion efficiency in open water to that in ice we will meet several problems:

- at the same speed, resistances are different
- with the same delivered power, rpm's are different
- with the same rpm, torques and speeds are different

To make the comparison, different analogies can be used:

- equal thrust
- equal torque
- equal ship speed
- equal speed of advance for the propeller
- equal propeller revolutions.

When selecting between the different analogies one should carefully consider the factors influencing the propulsion performance.

The performance of propulsion is mainly dependent on two factors:

- the amount of ice passing through the propeller
- the way in which the ice can get through the propeller.

The amount of ice that can get into contact with the propellers depends on the hull form, ice thickness, ship speed and flow velocity through the propellers.

For a model test where the propulsion behaviour is studied all these factors should be correctly scaled. Due to the existing model testing techniques, this is somewhat problematic. The use of any known model ice material results in incorrect strength properties and this leads to incorrect resistance values.

When trying to perform a self-propulsion test in these conditions either the ship speed, ice thickness or flow velocity through the propellers will be incorrect. To avoid this, the so-called towed self-propulsion test is used. In this test the propeller revolutions are selected so that the thrust will be as predicted. The prediction can be made either using theoretical calculations or by performing normal towing tests with pure hull. The thrust - rpm dependence is determined by overload tests in open water at different speeds. The propeller thrust is then compensated by counterweights. During the test the towing force is recorded. This force is a combination of resistance, counterweight and thrust:

$$F_{\text{tow}} = R_{\text{tp}} + F_{\text{cw}} - T_{\text{nice}}$$

In the actual self-propulsion point we naturally have

$$F_{\text{tow}} = F_{\text{cw}}$$

and

$$R_{\text{tp}} = T_{\text{nice}} = (1 - t_{\text{ice}}) T_{\text{ice}}$$

On the other hand, if the net thrust in ice is equal to the net thrust in overload condition in open water, the resistance in propulsion test should be equal to the resistance in towing test. This means also that the best way to compare the net thrusts in open water and in ice is to compare the resistance values of the towing test and the propulsion test when the latter is analyzed assuming

$$T_{\text{nice}} = T_{\text{noi}}$$

Now we can come back to the question of best analogy of comparing efficiencies in open water and in ice. The relation of these two efficiencies is called the ice efficiency of propulsion

$$\eta_i = \frac{\eta_{\text{dice}}}{\eta_d} = \frac{R_{\text{tice}} \times v_{\text{ice}}}{2\pi n_{\text{ice}} \times Q_{\text{ice}}} \times \frac{2\pi nQ}{R_t v}$$

By the use of overload tests we can create a situation where

$$v = v_{\text{ice}}$$

and

$$n = n_{\text{ice}}$$

at the same time. Thus we get

$$\eta_i = \frac{R_{\text{tice}} \times Q}{R_t \times Q_{\text{ice}}} = \frac{\frac{R_{\text{tice}}}{R_t}}{\frac{Q_{\text{ice}}}{Q}}$$

Since

$$R_{\text{tice}} = R_t - \Delta R$$

and

$$Q_{\text{ice}} = Q + \Delta Q$$

we get

$$\eta_i = \frac{1 - \frac{\Delta R}{R_t}}{1 + \frac{\Delta Q}{Q}}$$

where

ΔR = difference between the resistance values in towing test and self-propulsion test

R_t = net thrust from overload test

ΔQ = additional torque due to ice

Q = torque in open water.

3 PROPELLER EFFICIENCY

3.1 General

For a ship designer the efficiency of the whole propulsion is of great interest, but for a propeller designer the propeller efficiency is often of even greater interest. The propeller efficiency has also been studied by various methods. The most valuable studies have been performed with purpose built dynamometers in open water or ice model basins. As an example we can take some measurements that have been made in Wärtsilä's Ice Model Basin.

The propeller dynamometer is shown in Fig. 4. The dynamometer has been designed to be towed by the towing carriage in the basin. The ice formations are built in the basin as during normal model tests. The dynamometer is towed at a constant speed through the ice, and the torque, thrust and propeller revolutions are measured.

3.2 Examples of Propeller Efficiency in Channel

In order to show the influence of ice in the wakefield on propeller thrust and torque, and the variations in propeller thrust and torque that may be received by changing the propeller parameters, some model test results are presented below. Three different propellers were tested in medium ice conditions.

Propeller data:

propeller:	1	2	3	3B
D (m)	0.242	0.242	0.250	0.250
P/D	0.80	0.90	0.87	0.64
A_E/A_O	0.55	0.85	0.50	0.50
Z	4	4	4	4

Propellers 1, 2 and 3 were run through a built channel with a theoretical maximum contact depth of 17 % of the radius.

The results of these tests in "channel are presented in Figures 5, 6 and 7, expressed K_T , K_Q and η_o in open water, and in channel as a function of the number of advance J. In Figure 8 the ratio η_o in ice/ η_o in open water is presented for the propellers as a function of J.

In the channel tests almost no change in thrust is noted for propellers 1 and 2. With propeller 3 the thrust reduction is about 7 %. The torque is much more affected by ice. For propeller 2 the torque in ice is 6.5 - 15 per cent and for propeller 3 22 - 32 per cent. Thus the total reduction of the propeller efficiency is about 10 per cent for propeller 2, 15 per cent for propeller 1 and 25 per cent for propeller 3.

The following conclusions can be drawn from the results presented:

- The propeller torque is much more affected by the propeller - ice interaction than the propeller thrust.
- Although the ice conditions in the channel tests were quite difficult, almost no change in the thrust of propellers 1 and 2 was noted. Thus a thrust estimation could have been done from the propeller revolutions without any significant error.

With propeller 3 the error would be 7 per cent, i.e.

- with good propulsion - hull configurations the ice resistance can be evaluated from the propeller revolutions with a reasonable accuracy although the propeller works in a mixture of water and ice.

The tests above were all made with open propellers. Problems arise when doing tests with ducted propellers or with complicated propulsion - hull configurations as shown in the next chapter.

4 RESISTANCE AND PROPULSION EFFICIENCY

4.1 Full Scale Measurements

The overall performance of a ship in ice is relatively easy to determine in full scale. We only have to measure the power that is delivered to the propellers, the ship speed and the ice conditions. Problems arise when we try to separate the influence of hull resistance from the influence of propulsion efficiency.

If only full scale measurements are used, the possibilities of determining the hull resistance are rather limited and the result is always based on some assumptions. The assumptions between which we can select are:

- 1 the thrust deductions in ice and in open water are equal
- 2 the propulsion efficiency in open water is equal to that in ice
- 3 the thrust at given ship speed and propeller revolutions is equal in ice and in open water.

All these assumptions lead to an error of varying magnitude.

Assumption 1 means that the thrust must be measured. Possible error are related to the accuracy of the thrust measurement or to the contact between ice and the propeller, which leads to an increased thrust deduction.

The second assumption means that the delivered power must be measured. Possible errors in this case are related to the decrease of efficiency in ice.

Assumption 3 neglects the influence of ice on the thrust and the increased torque due to ice. This third assumption gives the smallest error.

4.2 Predictions Based on Model Scale

Resistance prediction based on model scale and applied in full scale is often based on resistance measurements in towing tests. This method also neglects the influence of propulsion. However, the prediction method is verified by full scale measurements and thus the propulsion efficiency is automatically included in the experimental correlation coefficients used by each model laboratory. For more precise predictions towed self-propulsion tests should be used together with the towing tests described in chapter 3.

4.3 Influence of Hull Form and Appendages

The accuracy of different methods to predict or in full scale to determine ice resistance depends on

- extent of propeller - ice interaction
- complicity of propulsion arrangements in the afterbody.

To give an example of this, some results of a model test series in Wärtsilä's Ice Model Basin are presented below. In this test series four different models were tested and resistance predictions were made separately for each model with two different methods.

Model 1 represents a conventional type of hull form. Models 2, 3 and 4 have basically the same hull form with half-tunnels to minimize the amount of ice that will get into the propellers. Model 3 has a nozzle of NSMB37 type, and 4 the same nozzle with increased protection. The philosophy here was on one hand to protect the cp propellers with the hull form and the nozzles and on the other hand to achieve more propulsive thrust.

All the models were tested in level ice and ridges with and without the propellers. Model speed, towing force, propeller torque and rpm were measured during the tests. The tests were performed as towed propulsion tests, where the thrust is compensated by counterweight and the model is towed through the ice. The net thrust to be expected at different rpm's and speeds was determined in overload tests in open water.

The resistance predictions were made by two different methods. First, from the pure towing tests, the resistance was predicted as described in reference 3. These results are presented in Fig. 9 as the 100 % line. These predictions gave no significant difference between the models. On the basis of these predictions the n_{ice} needed for the propulsion tests was determined.

The resistance predictions from propulsion tests were based on the assumption that the net thrust in ice is the same as in open water at the same speed and rpm. The results of these predictions are also presented in Fig. 9, which shows that the predictions differ quite much from each other. For the conventional hull form (model 1) the difference between the two predictions is 0 - 10 % in full scale speed range 0.5 - 1.5 m/s. For the half-tunnel stern (model 2) this difference is 0 - 5 %, which indicates that somewhat less ice is passing through the propellers. For the nozzle version the difference is 40 - 70 %, which indicates that the thrust is very seriously affected and the resistance increased due to the ice blocks passing through the nozzle or partially blocking it. With increased protection of the nozzle this difference can be decreased to 10 - 40 % (model 4).

Computing the ice efficiency, we get the results presented in Fig. 10. According to this figure the ice efficiency of propulsion varies from 0.78 to 0.66 for open propellers in the speed range of 0.5 - 1.5 m/s in full scale. The difference between the conventional hull and the half-tunnel hull is 3 - 5 %. For propellers with nozzles the ice efficiency of propulsion varies correspondingly from 0.46 to 0.19. By using better protection this efficiency can be increased up to 0.77 - 0.35 in the same speed range. It should be noted here that the models were not running at the actual self-propulsion point, because the differences between the various propulsion configurations were so obvious that there was no need to go to iteration to find out the actual self-propulsion point.

CONCLUSIONS

- 1 In full scale tests with a well designed propeller - hull configuration the ice resistance may with good accuracy be evaluated by considering the propeller net thrust the same as the net thrust in open water at the same propeller revolutions. With a complicated or badly designed hull configuration this assumption may lead to a significant error. In these cases model testing is necessary.
- 2 The propulsion efficiency in ice depends much on the propulsion - hull configuration. With complicated propulsion arrangements the efficiency is usually very low.
- 3 For a complicated propulsion - hull configuration the ice efficiency of propulsion

$$\eta_i = \frac{1 - \frac{\Delta T}{T}}{1 + \frac{\Delta Q}{Q}}$$

has to be determined when evaluating the icebreaking capability of the ship.

- 4 According to the results with open propellers, the change in propeller torque during propeller - ice interaction is more significant than the change in propeller thrust.
- 5 For optimizing purposes the propeller efficiency in ice can be separately examined by model scale tests, but the simulation of the actual wakefield is somewhat complicated.

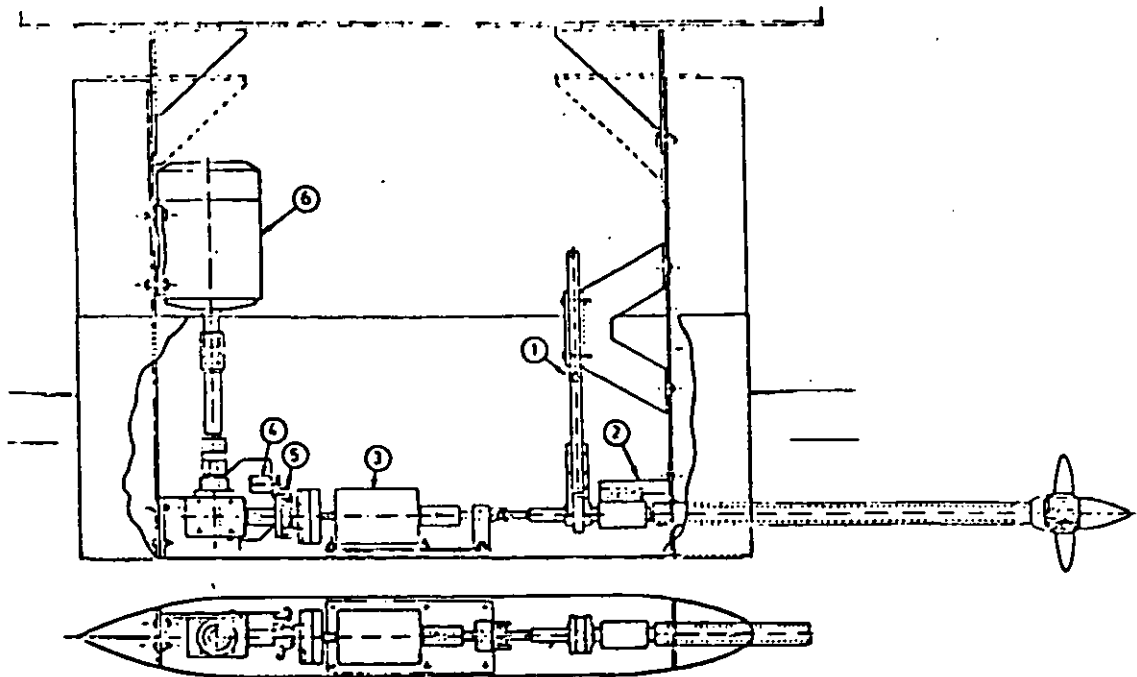


Fig. 4. The propeller dynamometer

- 1 thrust measuring device
- 2 slip ring assembly for transferring the blade forces
- 3 torque dynamometer
- 4 tachometer
- 5 pulse transmitter
- 6 AC motor connected to a frequency converter

P: η_0 OW, η_0 ICE
 □: K_1 IN ICE, K_0 IN ICE
 P: η_0 OW, η_0 IN ICE

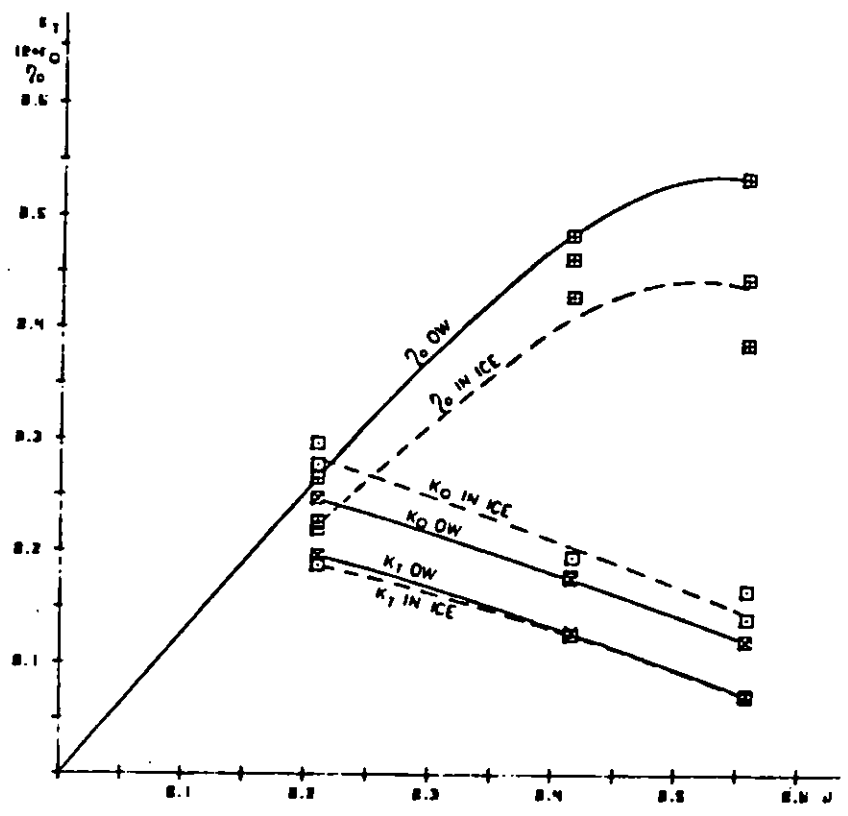


Fig. 5. Propeller 1 in open water and in channel

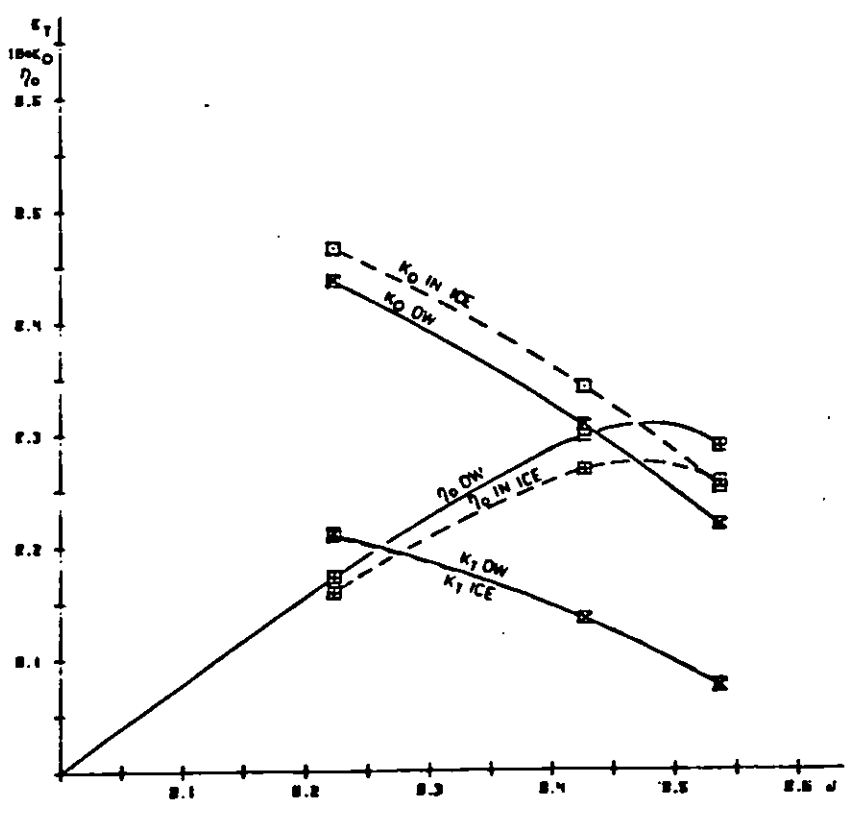


Fig. 6. Propeller 2 in open water and in channel

\square E_1 OW, E_0 OW
 \square E_1 IN ICE, E_0 IN ICE
 \square η_0 OW, η_0 IN ICE

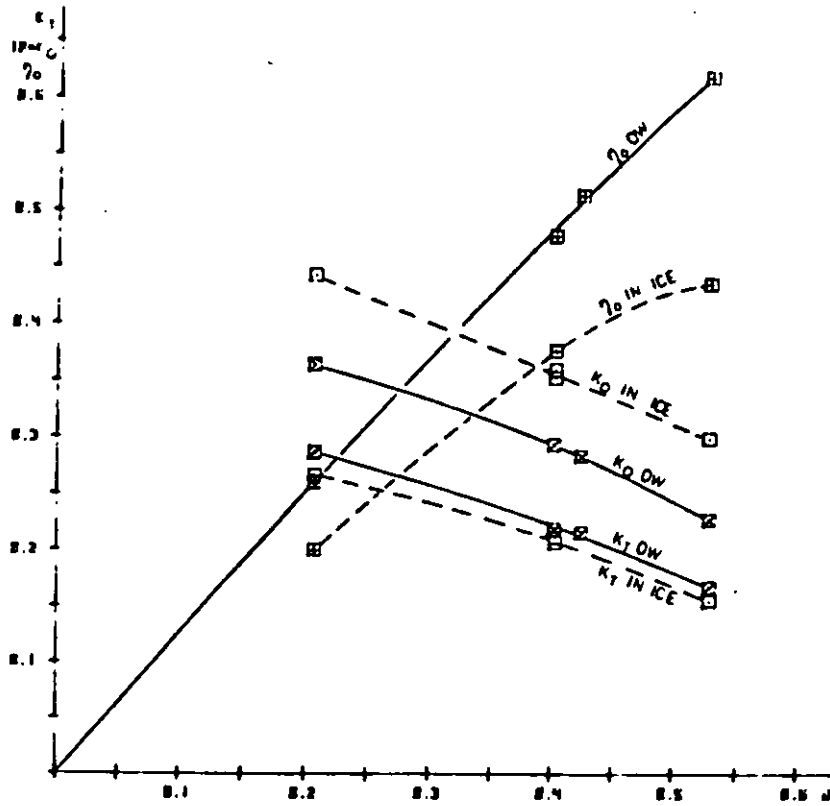


Fig. 7. Propeller 3 in open water and in channel

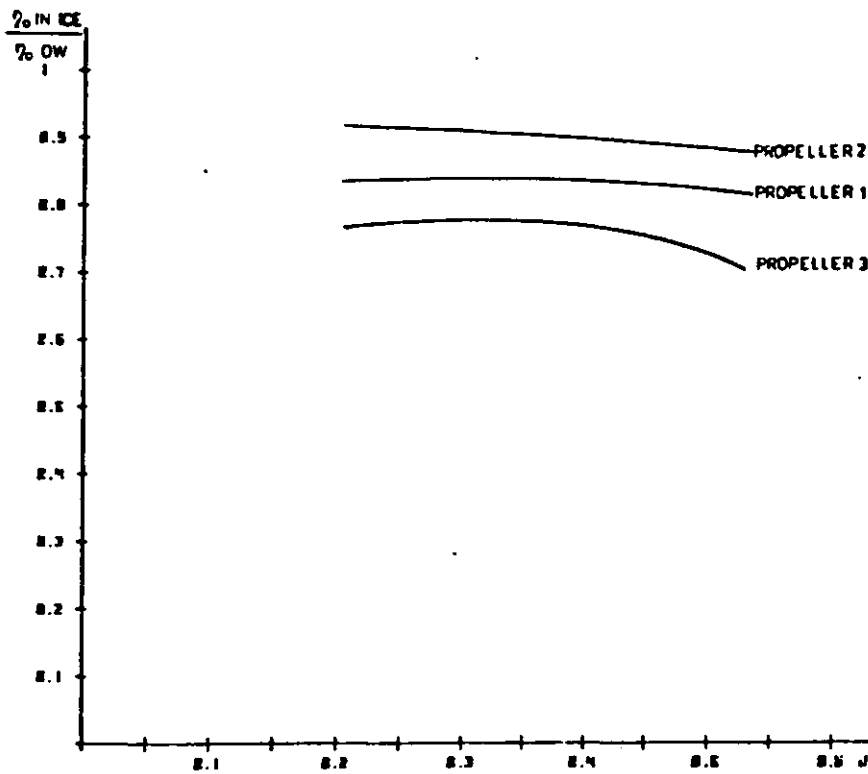


Fig. 8. The ice efficiency of the propellers in channel

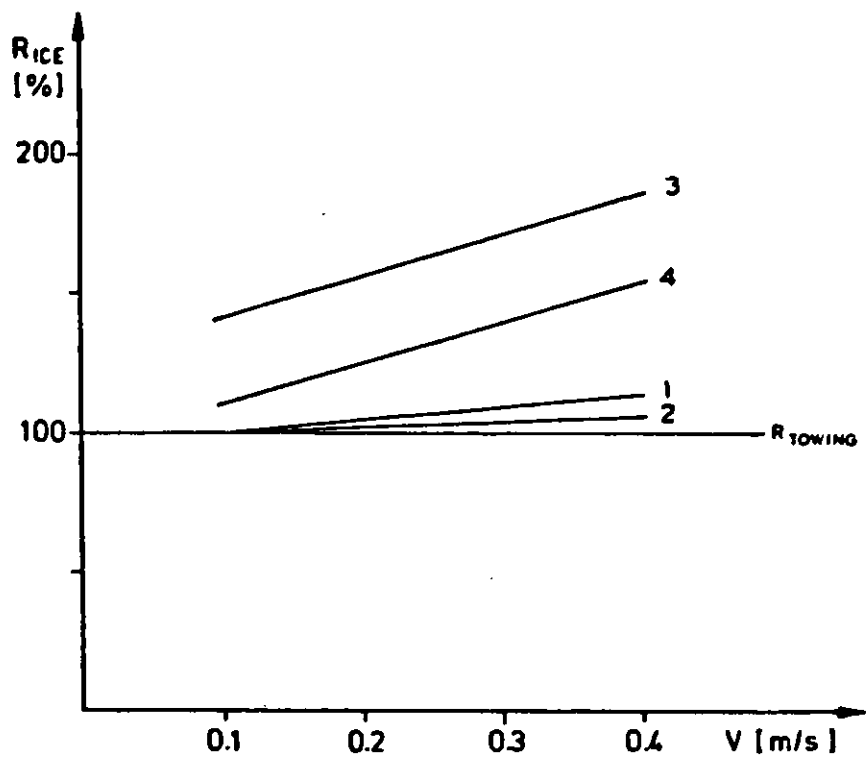


Fig. 9. Relative ice resistances with different hull forms determined by different test methods

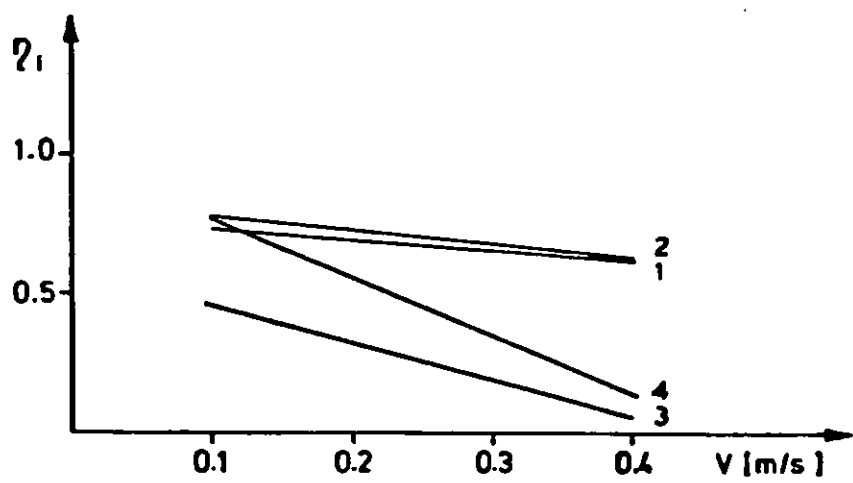


Fig. 10. The ice efficiency of propulsion for different hull forms



ICE LOAD RESPONSE IN SHAFTING

by Erik Sandberg
Det norske Veritas

ABSTRACT

This paper is a parameter study on the influences of flexibility and damping in a shafting system on the shock load level in the various components when the propeller is subjected to different types of ice shocks. Numeric time integration is used to solve the mathematics.

1. INTRODUCTION.

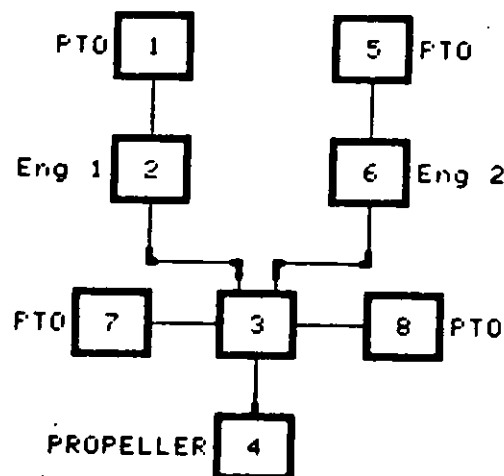
The finnish/swedish ice strengthening rules define the shock load level in the various components by means of the relative distribution of inertia . This is expressed by the term I/I_t in the formulae used throughout the rules for shafting (incl. gears, couplings etc.). The pure I/I_t relationship is only valid for infinitely rigid systems, which never is the case. On the other hand, the I/I_t is obviously a very important and also a rather practical parameter to include in the ice rules.

This paper contains examples on the influence of other parameters such as flexibility (long slender shaft and/or highly flexible couplings), damping (in flexible couplings), natural frequencies of the shafting system, duration and characteristics of the shock load on the propeller.

2. MATHEMATICAL MODEL.

2.1 Shafting System in general:

The shafting system is described as a lumped mass system (equivalent system, referred to propeller speed) with the following configuration.



2.2 Flexible Couplings

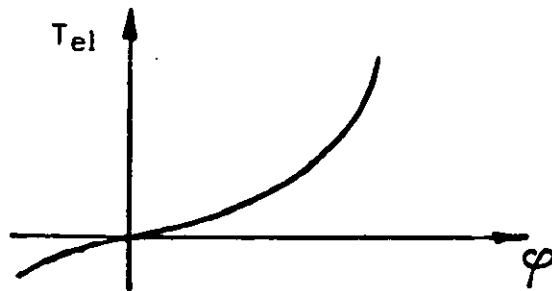
The numeric time integration method allows for nonlinear differential equations, jump function etc. This is an important advantage as most of the flexible couplings are progressive, few are linear, and some are degressive. Another important advantage is that the damping in the flexible couplings can be described in a more realistic way.

The usual way of presenting a flexible coupling is to express the elastic torque T_{el} by means of a (constant) stiffness K and the twist angle φ .

$$T_{el} = K \cdot \varphi$$

This is only true for a linear coupling. A more general approach is:

$$T_{el} = K_0 (\varphi + a \cdot \varphi^3 + b \cdot \varphi^5)$$



K_0 is the stiffness at zero twist, a and b are typical coupling particulars. Damping in the flexible coupling is usually described as a damping torque T_d expressed as structural damping by means of the (constant) stiffness K , the vibration frequency ω , the vibration velocity V and the dynamic magnifier M .

$$T_d = \frac{V}{\omega} \cdot \frac{K}{M}$$

This can also be used for nonlinear couplings when the constant stiffness K is replaced with

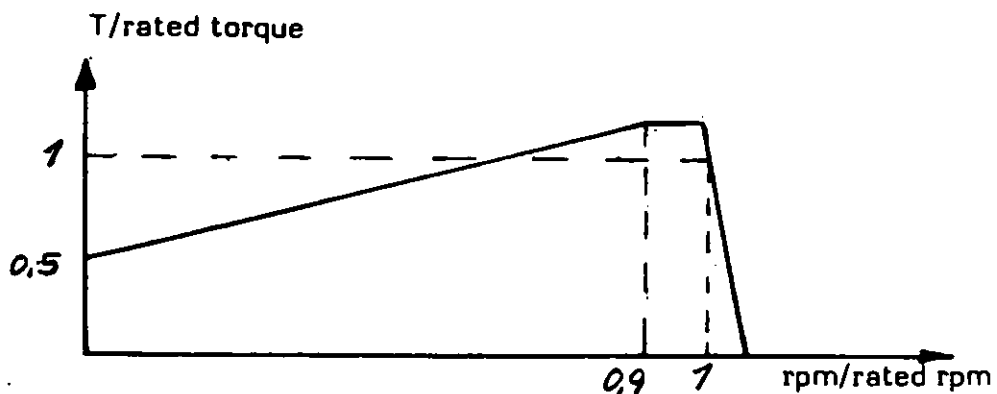
$$K = K_0(1 + 3a\phi^2 + 5b\phi^4)$$

However, even with this modification, further corrections should preferably be introduced for some types of progressive couplings.

2.3 Engine

The prime movers are assumed to be diesel engines with torque-speed characteristics as:

Speed droop = 5%, max overload torque 1,2 times rated torque



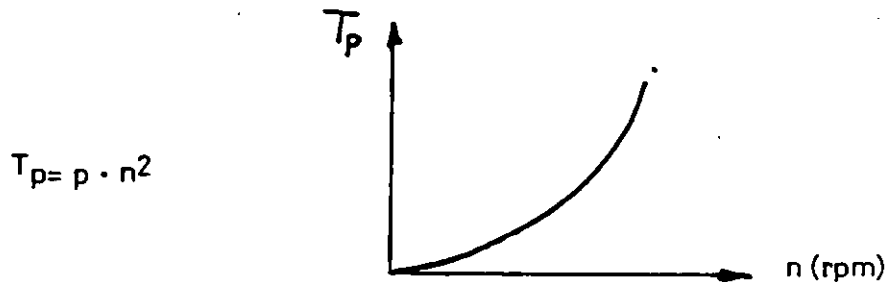
This figure indicates the max. available engine torque at various rpm. The speed governor and the injection system introduce time lag and phase shift in this dynamic system. When this is written, the true governor/injection model is not included in the program. However, in near future this will be included. For the time being the only simple way to include this influence, is by introducing relevant time lags. The absolute minimum time lag is appr. 1 engine revolution (infinitely quick governor, but time lag due to the firing sequence of the 4-stroke engine).

2.4 P.T.O.

The power take offs are assumed unloaded.

2.5 Propeller

The propeller demand torque T_p is according to the propeller law, i.e.



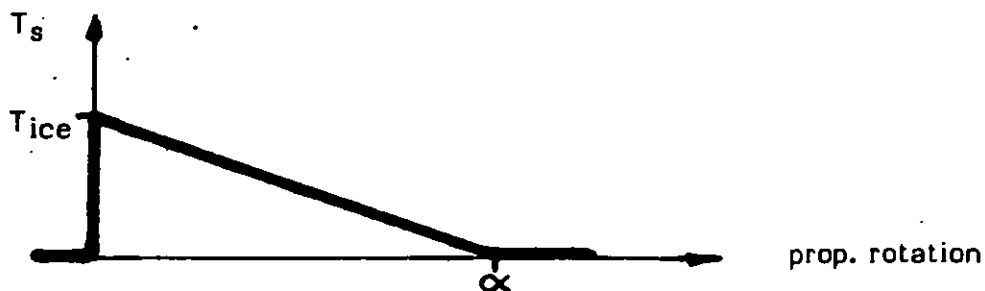
The p varies with the pitch setting, but for the sake of simplicity the p is taken constant during the influence of ice shocks.

2.6 Shock Torques

2. propeller shock torque (T_s) characteristics are applied. The peak shock torque is taken equal T_{ice} as determined by the finnish/swedish ice rules,

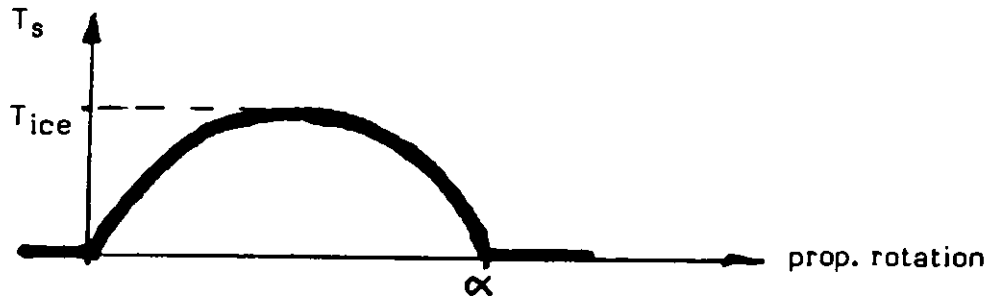
$T_{ice} = m \cdot D^2$
where m is ice class factor and D is propeller diameter.

The duration of the ice shock torque T_s is given as angle α of the propeller rotation. Most calculations have been carried out with a triangular shape of the shock torque.



The value of α is varied from 30 to 120 degrees.

Some calculations are carried out with a "half sinus" shape of the shock torque.



Here also $\alpha = 30$ to 120 degrees.

No examples have been made with consecutive shock torques.

3. THE PROPULSION PLANTS

3.1 Basic Data of 1st Plant

The basic plant has 2 engines on one reduction gear, with following data:

Equivalent mass moment of inertia (kgm^2)	
per engine	20 000
reduction gear	30 000
Propeller	30 000
Propeller shaft stiffness	48 000 kNm/rad
Rated engine (each) torque	470 kNm
Rated propeller torque	940 kNm
Rated speed	120 RPM
Propeller diameter	5,45 m
Ice class	1A super
Corresponding ice torque	625 kNm

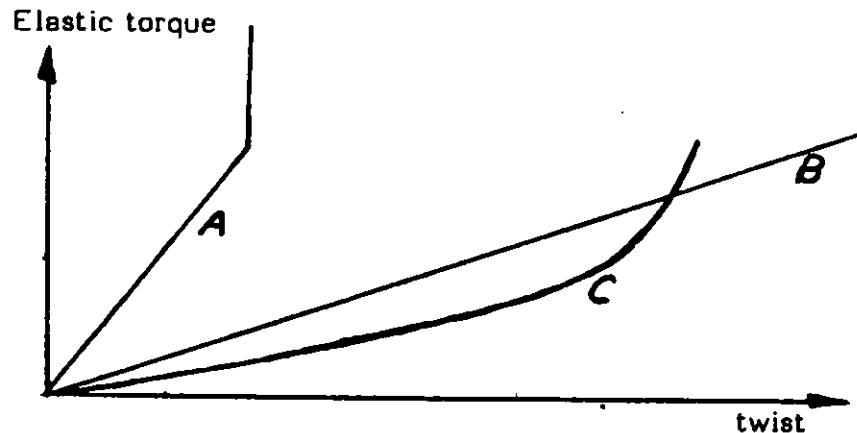
3.2 Variable Data of 1st Plant

3 different flexible couplings are used between the engine and reduction gear.

Coupling A has a linear stiffness of $32\,000 \text{ kNm/rad}$ (3° defl. at rated torque) and very high damping. The stiffness is linear until an elastic torque of 1,6 times 470 kNm is reached. From this deflection on the stiffness is 10 times higher. The damping torque has a crest value of 147 kNm .

Coupling B has a linear stiffness of 8 000 kNm/rad (12° defl. at rated torque) and average damping (magnifier of 10).

Coupling C has a highly progressive stiffness (15° defl. at rated torque) and a magnifier of 6 (which for the sake of simplicity is taken as constant).



Basically, the peak shock torque was put equal the ice impact torque T_{ice} according to Finnish-Swedish Ice Rules. Duration varied 30 - 120 degrees propeller rotation. In order to illustrate the effect of a jump function of coupling stiffness (A), a peak torque of $1,5 \cdot T_{ice}$ was used.

One serie of half sinus shock torques was made with coupling A in order to show this influence on the shapes of the response torques.

A large generator mass ($J = 30\ 000\ \text{kgm}^2$) was coupled to the front of engine no. 1 via a stiffness of 7500 kNm/rad. This variation was combined with couplings A, B and C.

For coupling A an extra alternative with a 4 times stiffer coupling was used.

The original gear mass is relatively high. An alternative gear mass of $5\ 000\ \text{kgm}^2$ was used in connection with coupling A and B.

When using highly flexible couplings it may sometimes be necessary to increase engine masses due to torsional vibrations and governor hunting problems. Therefore, another alternative was made with couplings A and B combined with 50 % larger engine masses and the "light" gear mass.

3.3 Basic Data of Plant No. 2

This plant has 1 engine with reduction gear.

Equivalent mass moment of inertia (kgm²)

engine	3 300
gear	650
propeller	2 000
Propeller shaft stiffness	12 000 kNm/rad
Rated propeller torque	100 kNm
Rated speed	240 rpm
Propeller diameter	2,7 m
Ice class	1A super
Corresponding ice torque	153 kNm

3.4 Variable Data of Plant No. 2

This plant was simulated with 2 different flexible couplings, H rather hard, S rather soft. Coupling H has a stiffness of 10 000 kNm/rad which corresponds to a coupling twist of 2° at rated torque (and engine speed), and a magnifier of 6.

Coupling S has a stiffness of 2 000 kNm/rad which corresponds to a twist of 10°, resp. a magnifier of 10.

4. RESULTS

4.1 General

The new version of the finnish-swedish ice strengthening rules, agreed upon in April 1982, defines an application factor K_A as:

$$K_A = 1 + \frac{T_{ice}}{u \cdot T} \cdot \frac{I}{I_t}$$

where

T_{ice} = ice torque (proportional to the square of the propeller diameter and an ice class factor).

$u \cdot T$ = rated torque at the considered component.
(on the propeller side of a reduction gear, $u = 1$. As all our examples are made with equivalent systems reduced to propeller speed, $u = 1$ throughout this paper).

I = mass moment of inertia (referred to propeller speed) of all rotating masses on the engine side of the considered component.

I_t = mass moment of inertia (ref. to propeller speed) of the entire rotating mass system.

This application factor K_A is assumed to indicate the expected peak response torque in the various components, due to the ice impact.

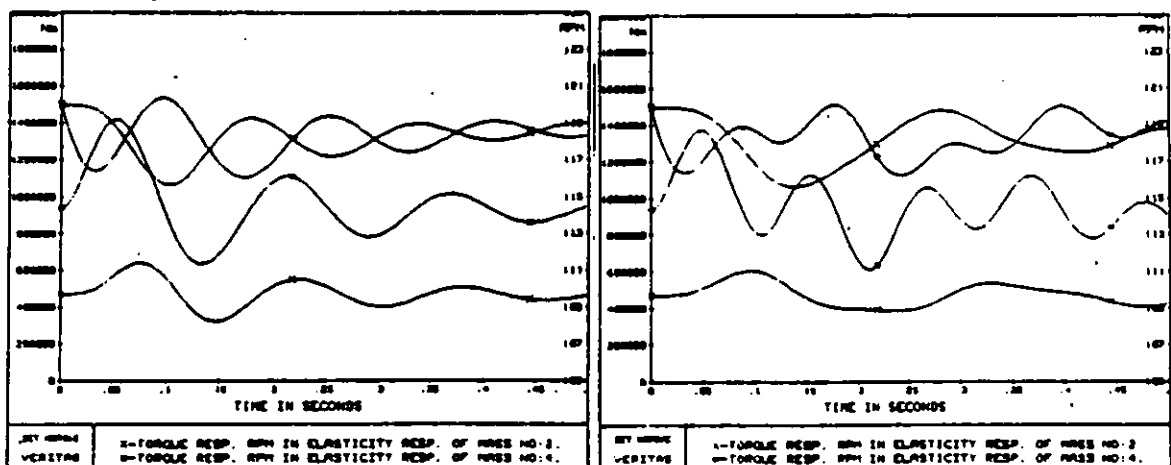
All results are plotted in diagrams with the factor K_A versus α (duration of shock). Additionally, the K_A factors according to the finnish-swedish rules are plotted as horizontal (constant K_A) lines in the various diagrams.

4.2 Governor Stability.

As mentioned previously, the governor influence was (preliminary) simplified as a given time lag, minimum corresponding to one rev. of the engine. This worked well together with rigid couplings. However, when introducing highly flexible couplings as e.g. the generator coupling, the system turned unstable. This was due to the too simple model of the governor function. It was necessary to increase the time lag to about 0,5 seconds in order to avoid "shake up" within the interesting time range. With this considerable time lag the engines do not pick up speed as fast as they theoretically could. On the other hand, when studying the response of only one shock load, the time lag has no practical influence. In case of consecutive shocks, it is necessary to find a better model for the governor influence.

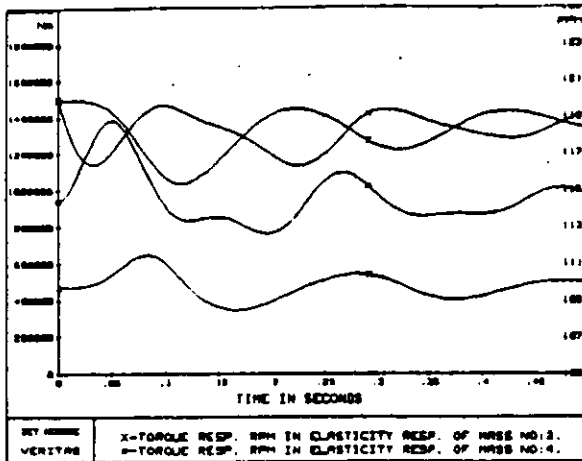
4.3 1st Propulsion Plant

The following 3 pictures show the computer plots of the basic system of 2 engines, gear and propeller, with main couplings A, B and C. The triangular ice shock torque appears at time zero and lasts over 60 degrees, i.e. appr. 0,08 sec. Two modes are visible. It should be noted that for highly flexible couplings the peak torque in the couplings is lagging the peak in the propeller shaft, thereby avoiding "adding up" as it is assumed in the finnish - swedish ice rules.



Picture No. 1

Picture No. 2



Picture No. 3

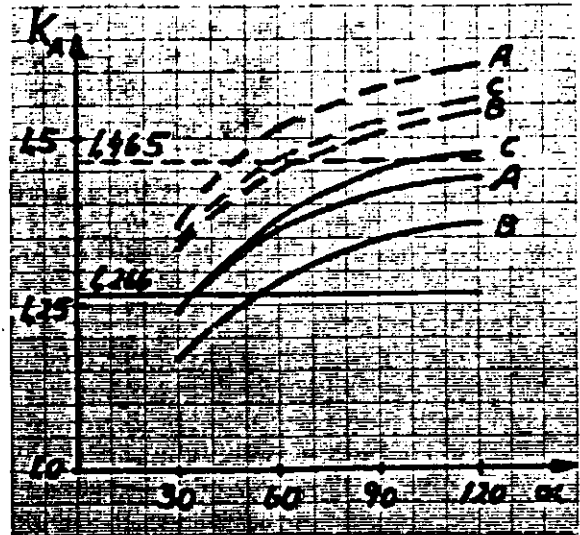


Fig. 1

In fig. 1, the complete results of $\alpha = 30 - 120$ with couplings A, B and C are plotted. The dotted curves are valid for the torque in the propeller shaft; the drawn curves for the torque in the couplings.

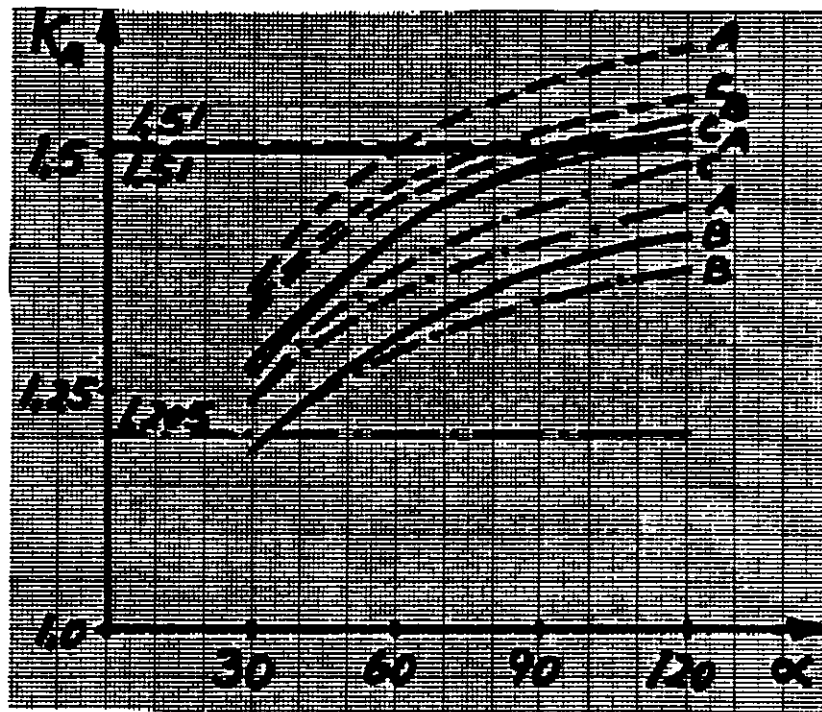


Fig. 2

Fig. 2 describes the results of the same variables as in fig. 1, but additionally a generator is flexibly coupled to the front of engine no. 1. The drawn curves refer to the torque in the main coupling at eng. no. 1, the broken curves to the main coupling at eng. no. 2. Coincidentally, the K_A factor according to Finnish-Swedish rules for both propeller shaft and main coupling at eng. no. 1 is equal 1,51.

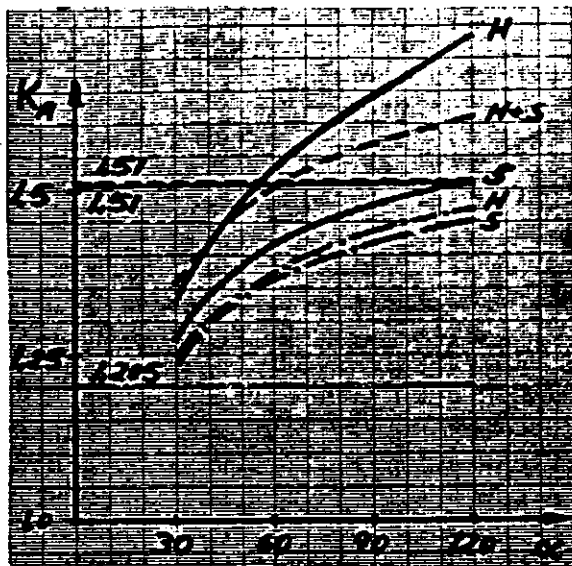


Fig. 3

Fig. 3 shows the influence of the stiffness of the flexible coupling between generator and engine no. 1. Using main coupling type A, the same curve description as in fig. 2, the variation of generator coupling is:

S = soft, as used in fig. 2; resp.
H = hard (4 times stiffer than S).

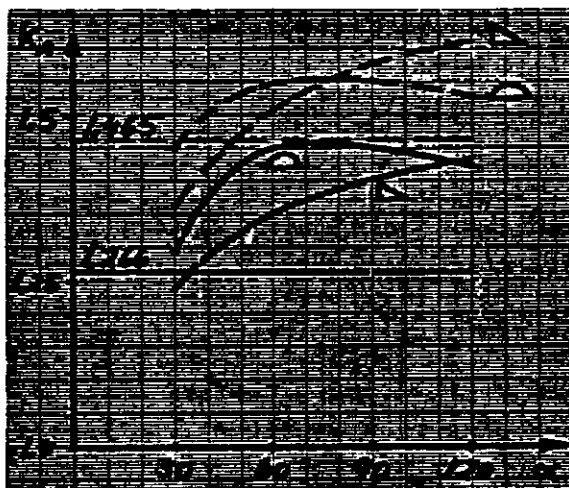
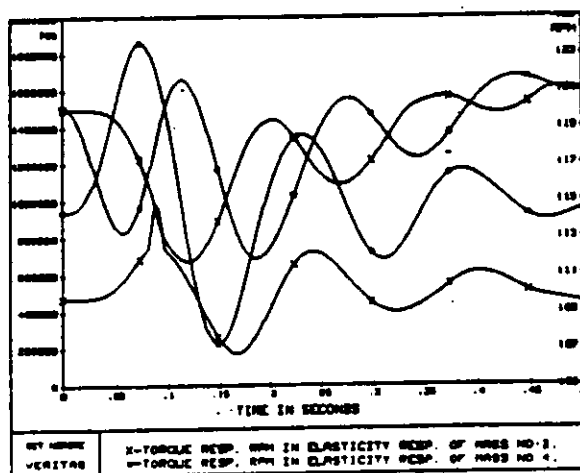


Fig. 4

Fig. 4 includes only the 2 engines, gear and propeller, coupling type A. The applied ice shock torque is of the "standard" triangular shape, resp. of the "half sinus" type.



Picture No. 4

Picture no. 4 shows the computer plot of a "half sinus" ice shock torque with a max. value of 1,5 times T_{ice} . Note the effect of a jump in coupling stiffness (coupling torque is the lower curve, propeller shaft torque starts at 970 000 Nm, both speeds start at 120 rpm and propeller speed drops faster than

the engine speed). This shape of the shock torque results in a smoother start of the propeller speed drop as well as the propeller shaft torque increase.

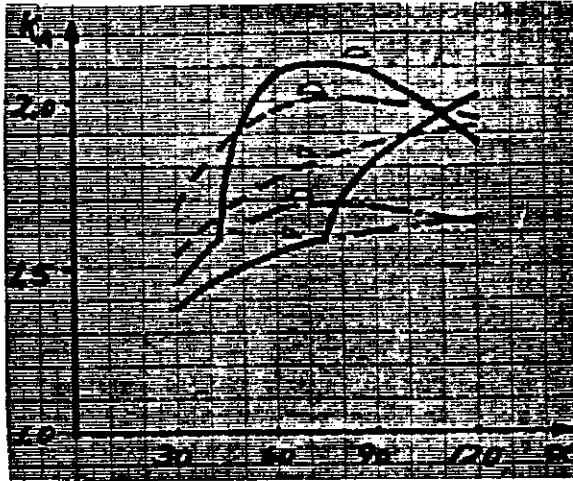


Fig. 5

Fig. 5 2 engines, gear, propeller and coupling type A (stiffness jump at $K_A = 1.58$). The ice shock torques (triangular resp. half sinus) are increased to 1,5 times T_{ice} . The dotted curve is for the torque in the propeller shaft, the drawn curves are for the torque in the couplings, and the broken curves indicate the torques in the couplings if no stiffness jump.

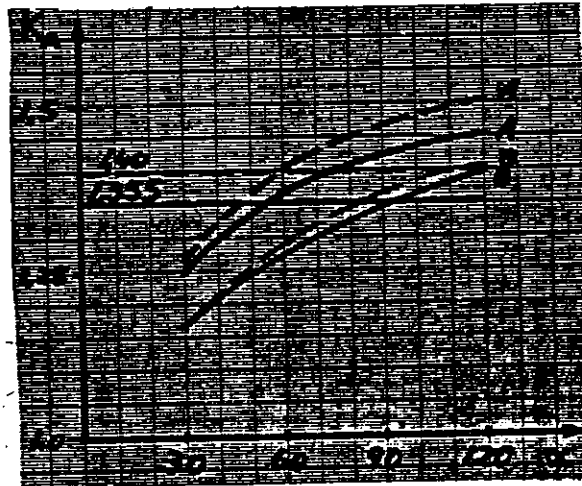


Fig. 6

Fig. 6 2 engines, reduced gear mass, propeller, and couplings A resp. B. "Standard" shock torques. Dotted curves for propeller shaft, drawn for couplings.

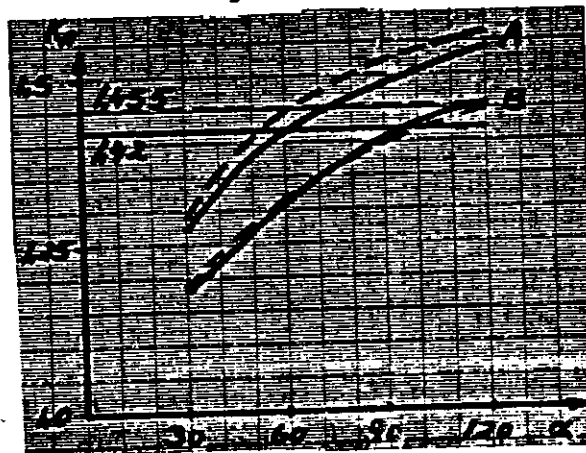


Fig. 7

Fig. 7 2 engines with 50 % increased inertia, reduced gear mass, propeller, and couplings A resp. B. Standard shock torques. Dotted curves for propeller shaft, drawn for couplings.

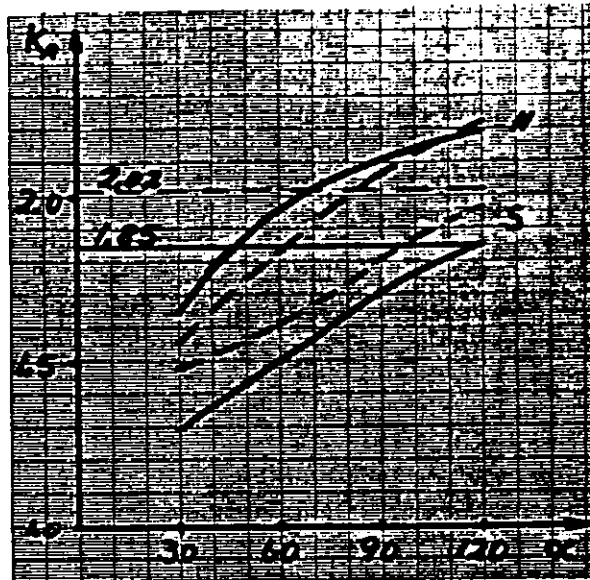


Fig. 8 shows the one engine plant with gear and propeller, with 2 different couplings S resp. H. S is the soft coupling, H the hard. Dotted curves for propeller shaft, drawn for coupling.

Fig. 8

5. CONCLUSIONS

We assume that the triangular ice shock torque with a duration of approx. 60 degrees is the most realistic one. With this assumption the figures indicate that the Finnish-Swedish ice strengthening rules present a good average for rigid couplings. For highly flexible couplings (referring to flexibility at full power!) the rules are too conservative. Compared with rather rigid couplings (2 - 3° twist at full power), a highly flexible coupling (10 - 15° twist at full power) can reduce the effect of ice shocks by 25 to 50 %.

In particular when large pto masses are put at the front of an engine, or branched from the engine branch, the selection of coupling flexibility is of great importance. A proper choice can almost "isolate" the pto mass.

However, the obvious advantage of highly flexible couplings should not be used without thorough system analysis such as governor stability and the influence of consecutive shocks.

The damping of the couplings have practically no importance on the peak effect of one single shock. In case of consecutive shocks (particularly if they match a natural frequency) the damping may be of greater importance. Governor behaviour is also very important and a realistic model for this purpose will be included.

Jumps in torsional stiffness within the expected torque range must be avoided, as this may cause considerable overloads of components as clutches, gear, etc. This important influence is now covered by the new Finnish-Swedish ice strengthening rules.

Last but not least, the simulation program can be used to analyse strain gauge measurements on shafting, when going in ice. The most significant torque fluctuations can be simulated mathematically and input data varied until the results match the measurements. This might give valuable information on the shape, duration and magnitude of the ice shock torques. So far the tangential loads on the propeller blades. Analogue simulations and measurements can be made for the axial ice impacts. I.e. with this simulation method and simple shaft strain and speed measurements it is possible to find valuable information on ice impact loads. Later on, this know how may be used to design optimum propulsion plants.

6. REFERENCES

Paul Martin, Erik Sandberg:

Computer program:

"Torsional Response in Power Plants with nonlinear Couplings Characteristics, due to Ice Impact Torques".



8

Professor Valter Kostilainen

MODELLING THE SHIP PERFORMANCE IN OLD ICE-CLOGGED
CHANNELS

1
BACKGROUND

The increase in commercial transportation in ice-covered waters has led to a situation in which, during a large part of the winter commercial ships, at least in the Baltic, are operating in old channels. A typical old channel is presented in fig. 1. There are no large ice blocks left and the dimensions of the ice-blocks in different directions are of the same order. The thickness of the layer of ice blocks increases continuously as long as the temperature remains below 0°C. The operation of commercial ships in these conditions is a significant change from typical icebreaker operations and in turn leads to different requirements of ship hull and propulsion.

The prediction of ship performance in ice-covered waters is at present more and more based on model tests in saline ice or in artificial material simulating the properties of scaled ice. Full-scale values are predicted using different methods and a certain degree of success in correlating the model data with full scale data is recognized. The difficulty in using saline ice techniques arises from the fact that ice is non-homogenous and non-isotropic. Thermal effects are difficult to handle.

Therefore the properties of ice even in laboratory conditions vary randomly. For example, if resistance is measured in ice model basins, the scatter of results is large and repeatability poor. Testing in ice is expensive. Sample sizes are small and statistical methods cannot be used. Particularly if broken channel conditions are simulated in an ice model basin, the maintenance of permanent conditions is difficult because the broken ice-block structure becomes slushy very rapidly. When using saline ice a full hydroelastic similarity is not possible in any case. If the strength of saline ice is scaled by the scale factor it will result in a highly plastic and slushy ice. Then the hydrodynamic modelling will suffer and viscous and friction effects are not necessarily the same as in full scale.

Considering the conditions in old broken channels where the ice blocks are solid and their dimensions in different directions are of the same order, the elasticity and strength of ice are supposed to be of minor importance in relation to hydrodynamic and friction effects. Therefore it was decided to adapt hydrodynamic similarity and ignore hydroelastic effects. Then systematic tests became practicable. The possible error due to ignoring hydroelastic effects can be checked with tests in saline ice and full-scale measurements.

Consequently an experimental set-up was developed for testing the performance of a ship in old ice-clogged channels. Ice fragments are simulated with plastic material, which has permanent physical properties at normal model testing temperatures. The new method has resulted in some interesting findings concerning the hydromechanical basis of the phenomena.

In the sections that follow an abridged description of the work done in the Ship Hydrodynamics Laboratory of the Helsinki University of Technology by H. Eskola, K. Hanhiova, P. Kannari, M. Lietepohja, I. Priha, P. Tuovinen and myself /1, 2, 3, 4, 5, 6, 7/ is given.



Fig. 1. A view over a typical old channel in the Northern Baltic Sea.

2
CHARACTERISTICS OF THE BROKEN CHANNELS

This section contains some results of the studies by P. Tuovinen /2/ and P. Kannari /6/.

2.1
Newly Broken Channels

In general navigation of merchant vessels in newly broken channel, which is protected by the islands, involves no problems. Ice fragments are larger and there are ample of clear water between. According to Tuovinen /2/ mean length of ice fragments in new channels in the Baltic is 3...5 meters.

2.2
Old Ice-Clogged Channels

When navigating in ice-covered waters, ships are usually gathered to form convoys led by an ice-breaker. Soon after a convoy has gone by, the broken track is pressed together by the moving ice fields. On lakes and in the shelter of archipelagos, where the fields are not moving, ice-clogged channels are formed. Newly broken channels are comparatively easy to navigate, but heavy traffic and temperatures below freezing point cause a fast growth of the brash ice mass in the channel. In an old ice-clogged channel there are no large ice blocks left and the dimensions of the ice blocks in different directions are of the same order.

In order to obtain reference data, the characteristics of old channels in the Gulf of Bothnia were measured and full scale performance tests were done during the winter of 1982 /6/.

Two of the observed channels lie in the northern part of the gulf near Kemi and Oulu, and one is outside Vaasa somewhat further south.

2.2.1 Channel Profiles

The transverse section of an old channel is not even. While passing through, ships tend to push the brash ice aside and thick ridgelike keels are formed on each side of the channel.

In order to find out the average transverse section, and to avoid local anomalies, several profiles were measured at 100 meter intervals.

The thickness measurements were taken from holes drilled into the brash ice layer. Each profile was measured at least 50 meters on each side of the centerline. Figure 2 shows a typical channel profile measured at Kemi. At the sides of the channel ice has piled up to form thick keels, which can reach almost three meters down. The thickness of the surrounding ice field was about 0,75 m.

Mean channel profiles at Vaasa, Kemi and Oulu are presented in fig. 3.

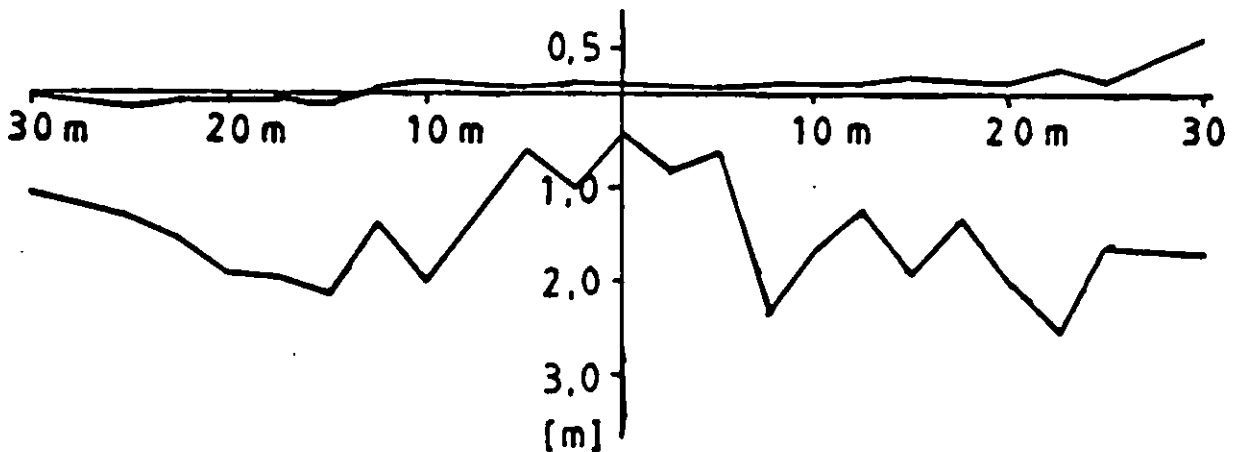


Fig. 2. Profile number 4 Kemi.

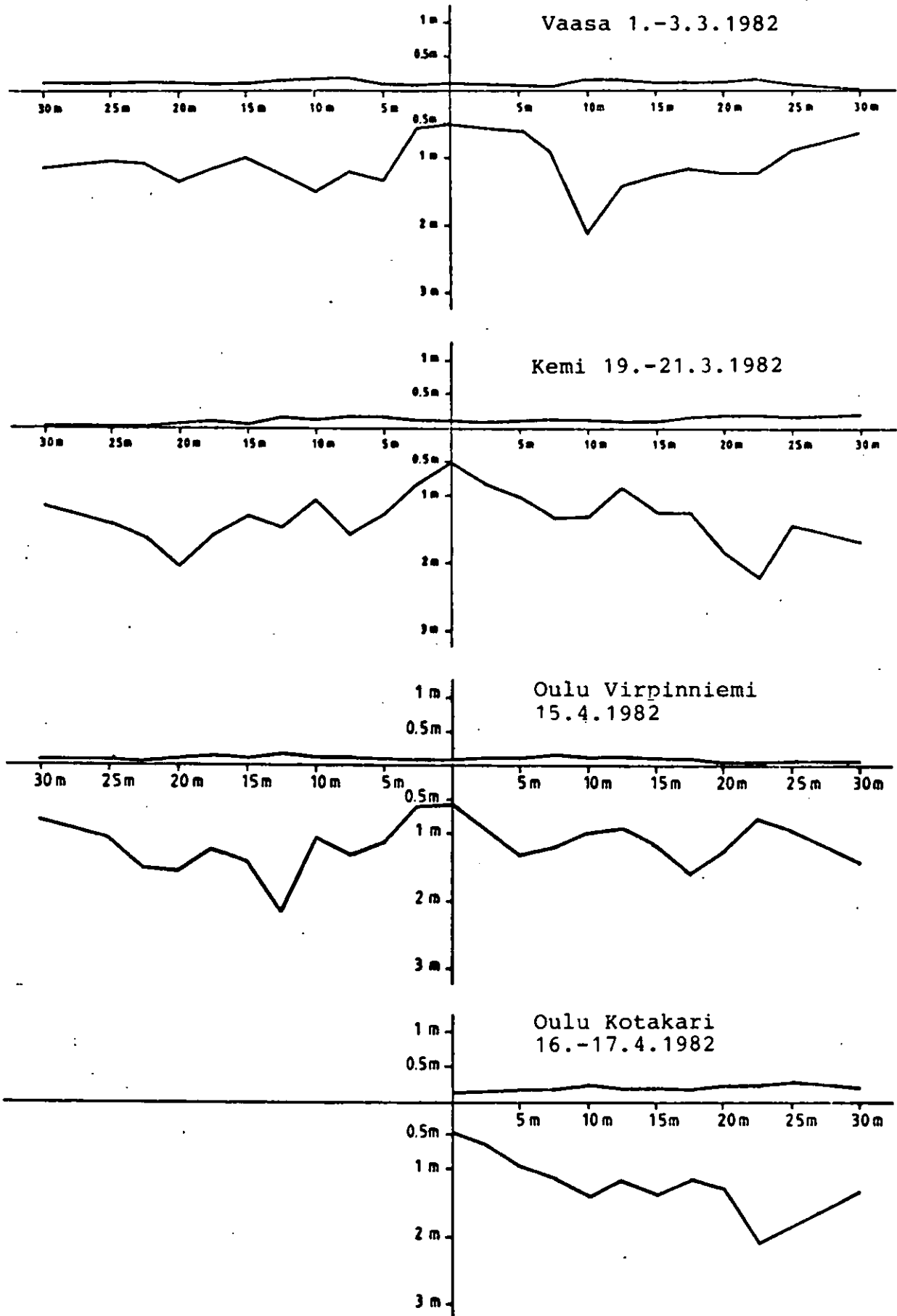


Fig. 3. Mean channel profiles in the Gulf of Bothnia 1982.

2.2.2 Channel Thickness

In order to present the characteristics of a channel some measures have to be defined /6/.

The accumulated mass thickness can be used to describe the growth of the brash ice mass in the channel. It is defined as the total cross sectional area (A) of the brash ice divided by the beam (B) of the widest ship that uses the channel regularly (fig. 4). Figure 5 shows the accumulated thicknesses of the measured channels as a function of the negative degree-days.

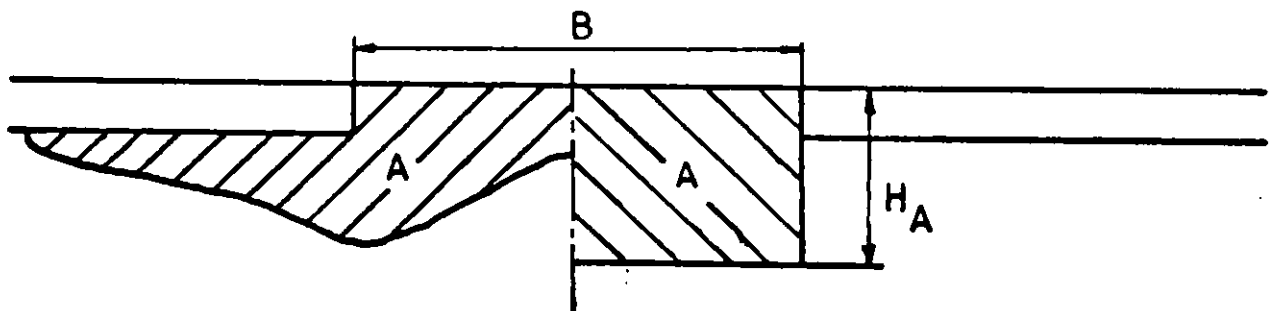


Fig. 4. Definition of the accumulated mass thickness (H_A).

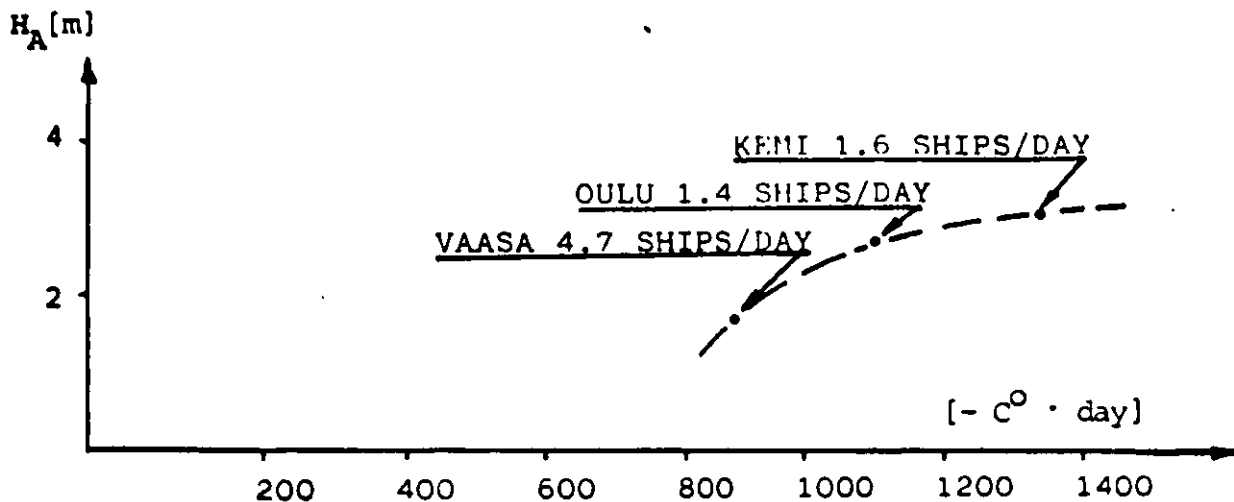


Fig. 5. The accumulated thickness of the measured channels.

A great part of the total brash ice mass lies at the sides of the channel far enough from the center line not to take part in forming the ice resistance. The effective breadth is defined as the part of the channel which forms the ice resistance. It is dependent on the beam of the ship in question and on the channel profile.

In the case of the Lunni-class product tanker and the channels measured in this study, the effective breadth is approximated at about $1.2 \times$ beam.

The effective mass thickness of a channel is defined as the mean thickness on the range of the effective breadth (fig. 6).

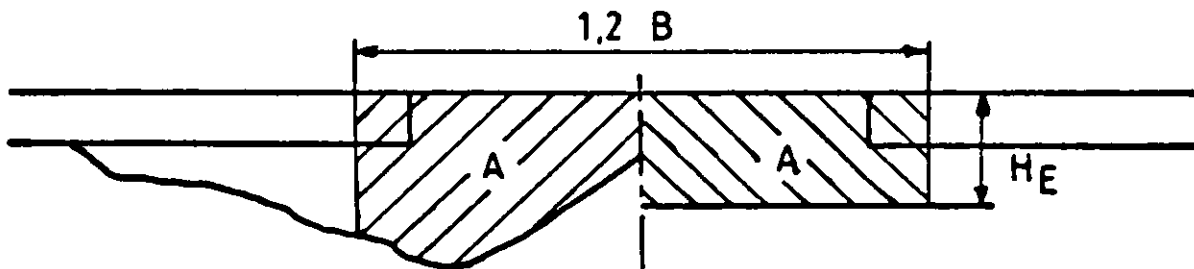


Fig. 6. Definition of the effective mass thickness (H_E).

Table 1 shows the accumulated and the effective thicknesses of the measured channels. The accumulated thickness of the Vaasa channel is more than 40 % smaller than that of the Kemi-channel but the difference in the effective thicknesses is only about 17 %. The reason for this is that in Kemi and Oulu the icebreakers have been used more efficiently to break side keels than in Vaasa.

Table 1. The average thickness of the channels.

	Effective mass thickness		Accumulated mass thickness	
	m	%	m	%
Kemi	1,22	-	3,06	-
Oulu V.	1,18	- 3,3	2,66	-13,1
Vaasa	1,01	-17,2	1,76	-42,5

2.2.3

The Longitudinal Section

In the Kemi channel a total of 5 cross sections were measured. Figure 7 shows the longitudinal profile of the channel in terms of the accumulated and the effective thicknesses. It is obvious that the channel is not uniform, especially with regard to the accumulated thickness.

The brash ice, which has been put into motion by the ship, keeps piling up unevenly. With regard to the effective thickness, the channel is much more uniform, but here also slight variations can be detected.

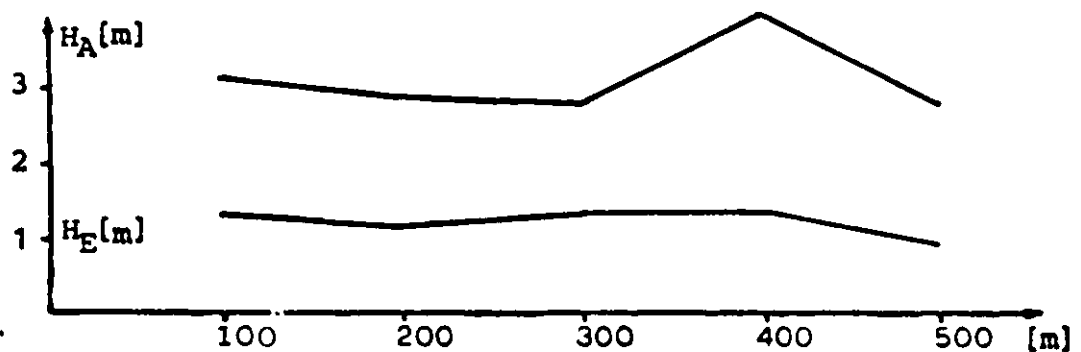


Fig. 7. Longitudinal section of the Kemi channel.

2.2.4
Block Size

The block sizes in the channel were measured from photographs taken from the forecandle of a ship. Scaling sticks, painted black and yellow had been placed in the channel before the ship's arrival.

From photographs it is possible to measure only the top layer of the brash ice, but the size distribution in the vertical direction can be assumed to be similar to that in the horizontal direction.

Figure 8 shows the measured volumetric size distribution in the Vaasa, Kemi and Oulu channels as a percentage of the total brash ice volume. The mean block diameter in Vaasa was 71 cm, in Kemi 79 cm and in Oulu 63 cm.

The size distribution is affected by the number of negative degree-days and the density of traffic. During the winter, weather in Kemi has been somewhat colder than in Oulu and Vaasa, and the traffic has been much lighter.

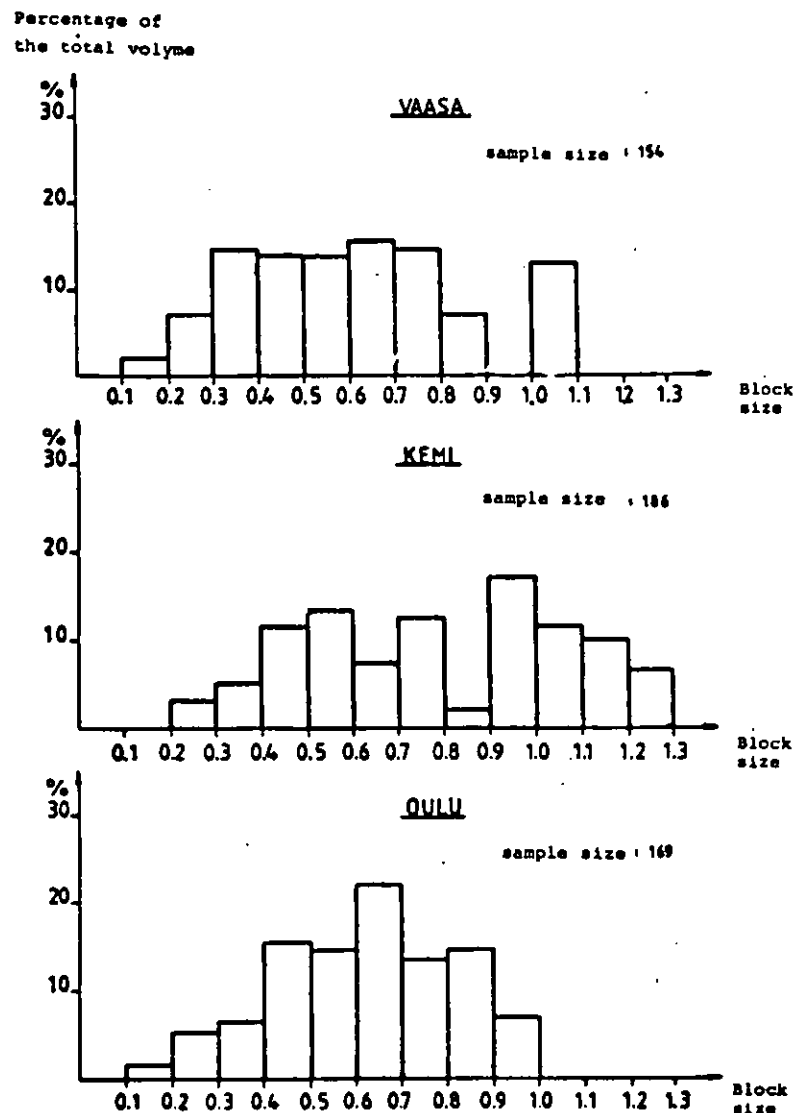


Fig. 8. Volumetric block size distributions.

2.2.5 Friction Coefficient

Frictional forces play an important role in the total channel resistance. The friction coefficient was measured using the cone method.

The cone, made of stainless steel, is pressed into the brash ice and rotated slowly around the vertical axis. The momentum needed to rotate is measured. Figure 9 shows the cone and the assumed pressure distribution of the brash ice, which keeps the cone afloat by its buoyancy. The pressure distribution is assumed to be linearly dependent on the thickness of the brash ice mass below the cone.

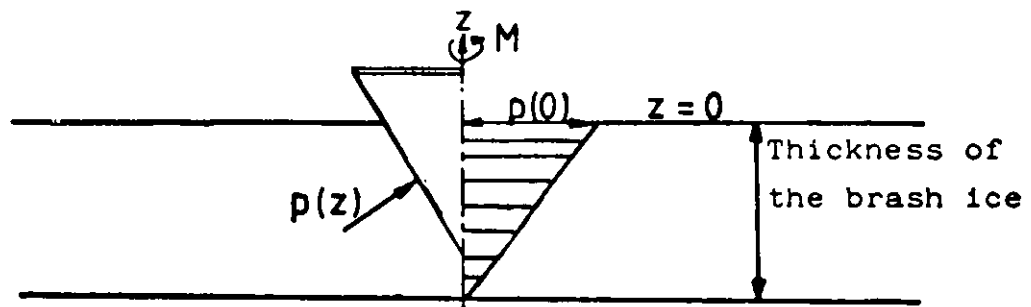


Fig. 9. The cone for friction measurements and the assumed pressure distribution.

The momentum caused by the viscous resistance and the bearing friction is determined by rotating the cone in icefree water.

Figure 10 shows the dynamic friction coefficient as a function of the medium pressure. The values are those between smooth stainless steel and wet brash ice. The relation between hull roughness and friction coefficient could be studied using the same method by roughening the cone.

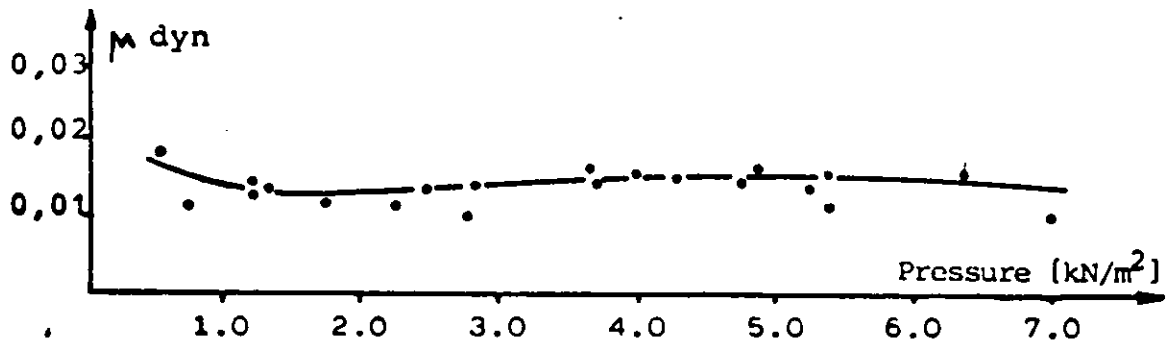


Fig. 10. Dynamic friction coefficient for smooth stainless steel on channel ice.

3

ELEMENTS OF SHIP RESISTANCE IN ICE-CLOGGED CHANNELS

Before any estimation of ship performance in ice-clogged channels based on model testing is made, it is important to examine the basic elements of the phenomenon itself. If all modes of movements are included, it is a most complex phenomenon. Therefore this examination is limited to a certain speed range, which has practical value and where some simplification can be made.

3.1

Selection of the Speed Range to be Considered

When the speed of the ship is very low, the ice fragments tend to accumulate at the bow region and the motion of the ship becomes unsteady. Tests in plastic pieces with a model of a ferry hull having a Baltic type ice-bow indicate the same phenomena at Froude number 0.06 and below. With bulbous and cylindrical bow models the upper limit of this unsteady speed range is higher. Motion of the ship in this unsteady speed range is dependent on the characteristics of the propulsion engines and on the dynamics of the total system. The determination of the model resistance in this speed range is difficult and it is left out of this resistance consideration.

The upper limit of the speed in this study is taken to be the service speed which is also the upper limit in practice if the layer of ice fragments in the channel is thin.

3.2 Components of Resistance

It will be notified in the sections following later, that the difference in resistance between a model in a simulated old channel and in clear water at the speed range specified in the preceeding Section, is practically independent of speed. This refers to the dominating effect of friction forces. Further it is supposed that the ship sides at the entrance are vertical and the thickness of the layer of ice fragments is considerably smaller than the draught at bow. On these basis the following simplified model of separating the net ice resistance in an old ice-clogged channel into components has been built up.

When a ship is in a steady ahead motion in an old channel and the interaction between the ship sides and only the layer of ice fragments is considered, frictional forces of the two kinds have an effect Tangential friction forces between the ship side and ice, and normal forces which push the ice fragments aside and which originate in internal frigtion between ice gragments. The former forces work in the entrance and in the parallel midship part of the ship and these forces are called side friction forces hereafter. The latter forces work in the entrance only and they are called internal friction forces hereafter. Work done by both kinds of forces are negligible in the run and will be ignored in this study.

When a ship proceeds a distance s , work which is done by internal friction forces is proportional to the area $2xA$, see fig. 11. This area is cleared of ice fragments. It can be seen that $2A = sB_{WL}$

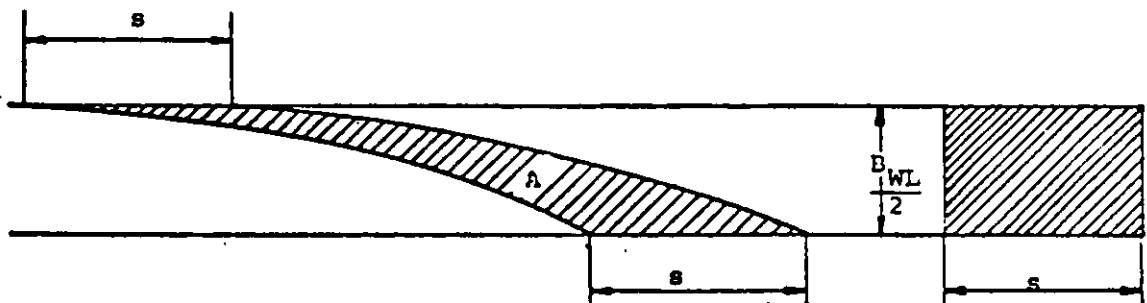


Fig. 11. Area cleared of ice fragments when ship is proceeding a distance s .

If the bow angle is small, this work can be approximated using an idealized two-dimensional model according to fig. 12.

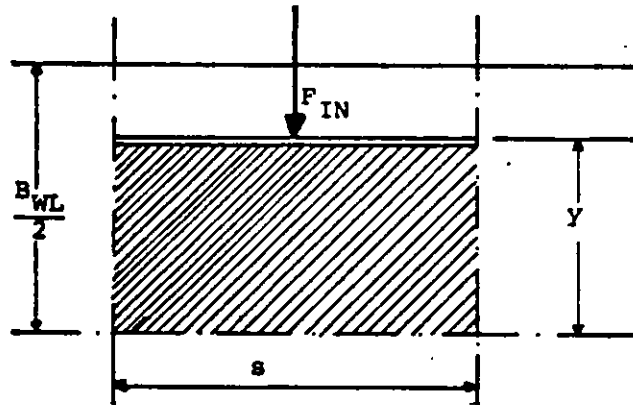


Fig. 12. Two-dimensional model for determination of normal force F_{IN} .

When the ship is proceeding ahead, y changes from 0 to $\frac{B_{WL}}{2}$

In steady motion the sides of the shaded square need not be considered.

Let F_{IN} be the normal force which pushes the ice fragments aside. Work done by the internal friction forces when the ship has proceeded distance s is denoted by W_{IF} . Then

$$W_{IF} = 2 \int_0^{\frac{B_{WL}}{2}} F_{IN} dy \quad (1)$$

The normal force F_{IN} of the two-dimensional model can be used to approximate the work done by the side friction forces. If the friction coefficient between the ice fragments and the ship sides is μ_s , then the work done by the side friction W_{SF} at distance s is the sum of work done by the friction forces in the parallel midship part and in the entrance:

$$W_{SF} = 2\mu_S s \left[L_P \frac{F_{IN} \left(\frac{B_{WL}}{2} \right)}{s} + L_E \frac{\int_0^{\frac{B_{WL}}{2}} F_{IN} dy}{s \frac{B_{WL}}{2}} \right] \quad (2)$$

Total work is then

$$W_{IT} = 2 \int_0^{\frac{B_{WL}}{2}} F_{IN} dy + 2\mu_S s \left[L_P \frac{F_{IN} \left(\frac{B_{WL}}{2} \right)}{s} + L_E \frac{\int_0^{\frac{B_{WL}}{2}} F_{IN} dy}{s \frac{B_{WL}}{2}} \right] \quad (3)$$

Thus the approximate formula for the net ice resistance of a ship in an old ice-clogged channel becomes:

$$R_I = 2 \frac{\int_0^{\frac{B_{WL}}{2}} F_{IN} dy}{s} + 2\mu_S \left[L_P \frac{F_{IN} \left(\frac{B_{WL}}{2} \right)}{s} + L_E \frac{\int_0^{\frac{B_{WL}}{2}} F_{IN} dy}{s \frac{B_{WL}}{2}} \right] \quad (4)$$

For the utilization of this formula it is necessary to know the force function $F_{IN}(y)$ for a certain distance s . This distance should exceed the size of the simulated ice fragments by one order. A method has been developed for the determination of this function using simple bottomless boxes, which have a piston moving into the layer of simulated ice fragments /4/. To eliminate the friction forces between the sides of the box and simulated ice, two widths of the boxes are used. In determining the integral

$$\int_0^{\frac{B_{WL}}{2}} F_{IN} dy,$$

this method seemed to be reliable and the repeatability of the tests is good. There seemed to be very clear linear dependence on the thickness of the layer of simulated ice. This result is in accordance with the earlier findings of the independence of the net ice resistance of speed, in old channel conditions. The determination of the terminal force $F_{IN} \left(\frac{B_{WL}}{2} \right)$ with this same method seems

to be more difficult, repeatability is poor and discrepancy large. In reality this force is not

constant for the whole length of prallel midship. It has its maximum value at forward shoulder and it then diminishes aft. One possibility is to approximate the terminal force on the basis of the work done by the internal friction forces. It can be taken to be proportional to the mean force in the entrance part;

$$F_{IN} \left(\frac{B_{WL}}{2} \right) \approx k_S \frac{\int_0^{B_{WL}} F_{IN} dy}{B_{WL}/2} \quad (5)$$

where k_S is a constant depending mainly on the form of the Waterline. Then

$$R_I \approx 2 \frac{\int_0^{B_{WL}} F_{IN} dy}{s} \left[1 + \frac{2\mu_S}{B_{WL}} (k_S L_P + L_E) \right] \quad (6)$$

This simple formula should be considered as a rough approximation for net ice resistance in an old ice-clogged channel. It can not be used in the case of full forward waterlines. It has been tested with a model of a Baltic-type product tanker. When the constant k_S is taken to be 1, then the difference in net ice resistance between model test results and results obtained from formula (6) was 10...30 %. The work done by the internal friction forces

$$\int_0^{\frac{B_{WL}}{2}} F_{IT} dy$$

can easily be determined by simple experiments, as was stated above.

In cases where larger amounts of ice fragments are moving below the bow and under the bottom, formulae (4) and (6) overestimate the net ice resistance. This was also observed in doing model tests in ballast conditions with the same product tanker.

4
MODEL SIMULATION OF SHIP AND PROPELLER OPERATION
IN ICE-CLOGGED CHANNELS

4.1
Simulation of Ice Blocks

A study of the size distribution of ice blocks was made by P. Tuovinen /1/. The measurement was done on the photographs of the channels. The results were presented as size distributions with histograms.

A size distribution function was found which fits all the three distributions surprisingly well.

The size distribution of the old channel is reproduced in fig. 13. This distribution was the basis of the size distribution of simulated ice-blocks. Finally the size distribution presented in fig 14. was arrived at. The lengths of this distribution correspond to the lengths of full size ice-blocks in the scale 1:25. Kannari made during the winter 1982 more profound studies on the size distributions /6/, which were presented in section 2.2.4. He also came to the conclusion, that volumetric size distributions should be used instead of linear size distributions. Unfortunately the volumetric size distributions of plastic pieces do not fit very well with the distributions presented in fig. 8. The final form of the plastic pieces is also presented in fig. 14. This form was selected to simplify the manufacture of the pieces. An inclined cut for two sides was chosen to prevent to compact formation of the layers of the pieces on the water surface.

The pieces were made of polypropene-plastic. This plastic has the same density as natural ice but is not strong that it survives propeller blades impact. The pieces had been made of two separate shipments of plastic bars and they proved to differ as to their friction coefficient by about 10 %. But since there were equal amounts of each brand in every size category, the mixture could be considered homogeneous. The friction coefficient was measured with a sleigh which had polypropene bars underneath. The sleigh was pulled on a sheet of plywood painted with the same paint as the model. On the edges of the plywood there were coamings so that water could be poured on. By placing weights on the sleigh and pulling it with a stepping motor at an even speed the wet friction coefficient could be deduced. It was found to be 0,183 and 0,213 respectively for each of the piece brands. Thus the mean friction coefficient was 0,198.

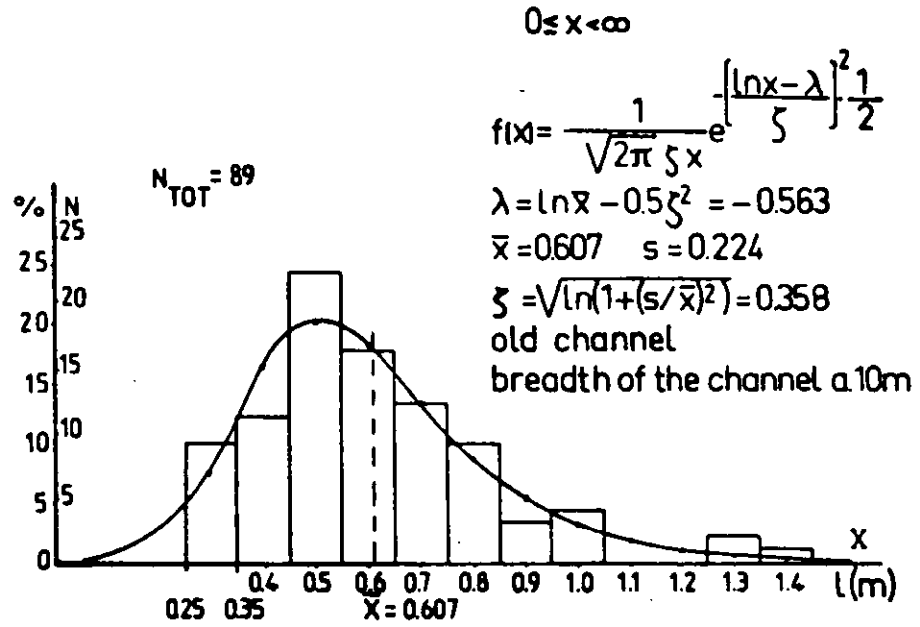


Fig. 13. The size distribution of ice blocks in an old channel according to /1/.

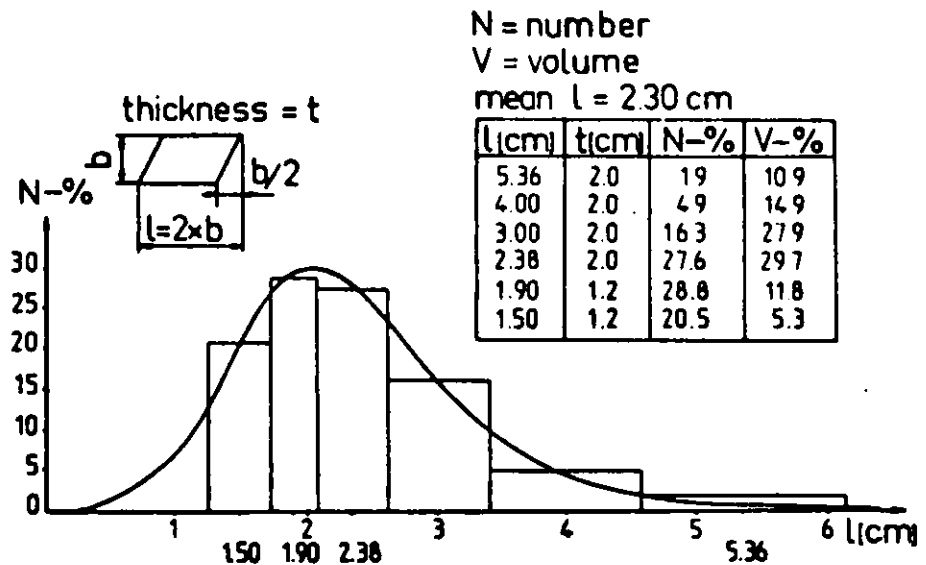


Fig. 14. The size distribution of plastic pieces used in the tests.

4.2 Manufacture of Propeller Models

Owing to the high impact loads of plastic pieces, materials generally used for propeller models, such as white metal or aluminium, can not be used. Therefore a new method of manufacturing model propellers for these tests was developed. By this method propeller blades are made of composite construction of metal plate and "Prestolith" plastic filler. At the beginning the core of the blade was made of bronze. These model propellers did however, have small local defects at the leading edge. Later the core and the edges of the propeller blades were made of stainless steel, which withstands the high impact loads of the plastic pieces.

The accuracy of these propeller models is not as good as propeller models manufactured by ordinary methods. Consequently measured efficiency was lower than corresponding Trost B-4 propeller. Propeller models used later on were made by modelmilling machine and the thickness of the blades of these new propellers are increased throughout.

4.3 Arrangement of the Propeller Experiments

The tests were made in the towing tank of the Helsinki University of Technology. The tank dimensions are 130 m x 11 m x 5,5 m. Only a narrow strip at the centerline of the tank was covered with plastic pieces. This strip was separated from the other parts of the tank by a removable channel consisting of net walls and bottom on light steel frames and tubular floatation elements. The cross-section of this channel is presented in fig. 15. To facilitate easy erection and removal of the channel it was made of ready-made sections of 6 m length. The ordinary measuring area is 24 m long thus consisting of 4 sections. These end sections were equipped with two double doors, which prevented the plastic pieces from getting out of the channel. These doors were opened during the run into and out of the channel by a frame installed in front and at the sides of the propeller and dynamometer arrangement. The whole arrangement was finally kept in position by nylon ropes fastened to the sides of the basin. The placing of the test channel in the towing basin is presented in fig. 16.

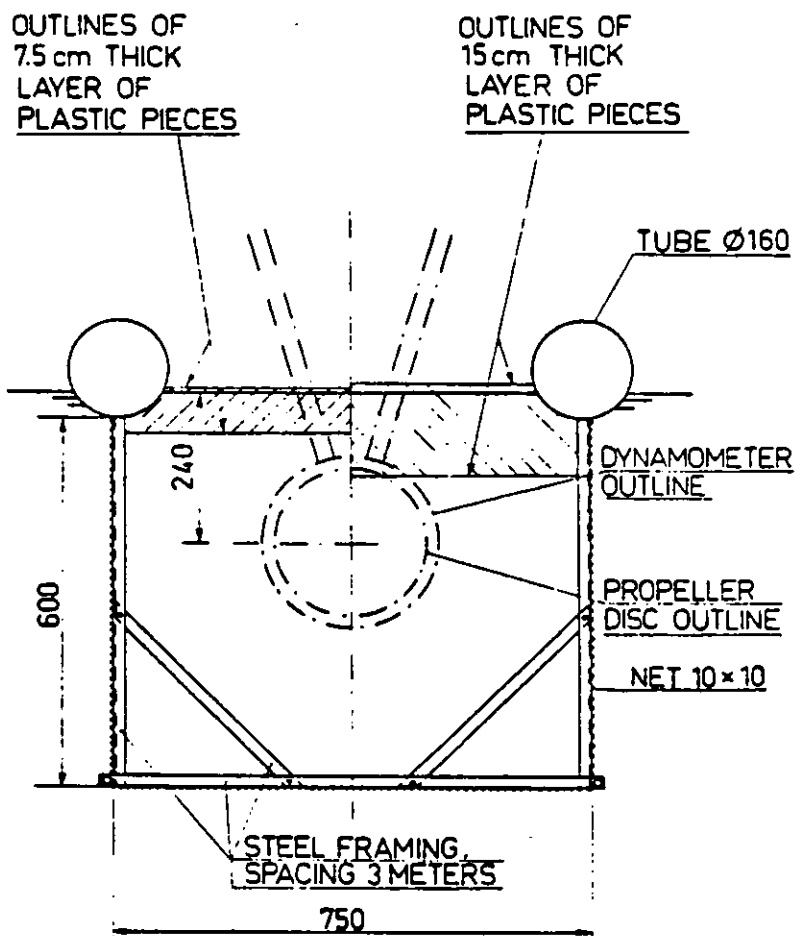


Fig. 15. Cross section of the testing channel.

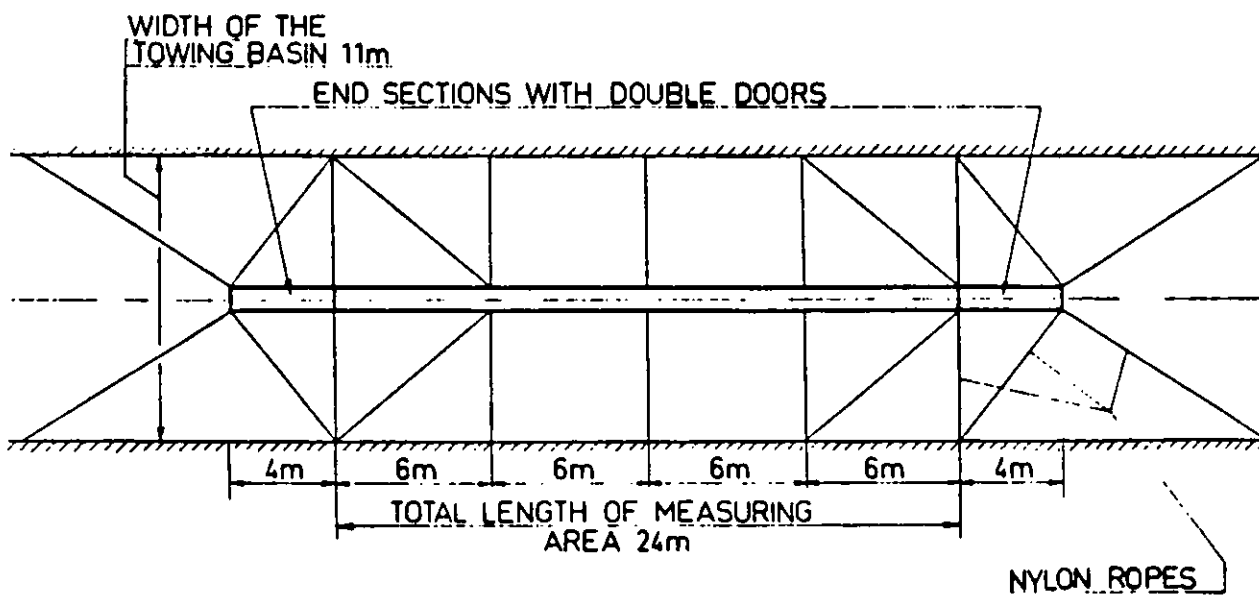


Fig. 16. General arrangement of the propeller testing channel.

So far only two thicknesses of the layer of plastic pieces on the surface of the test channel have been used, 7,5 m and 15 m.

The ordinary open water propeller dynamometer of the Laboratory could not be used in these tests. Therefore a new dynamometer which can withstand the high loads applied to propellers in these conditions, was designed /7/.

To eliminate the effect of friction and to facilitate the measurements of unsteady components of thrust and torque in possible subsequent studies, it was decided to measure the torque and thrust immediately after the propeller boss. The flecture consists of a stainless steel cylinder of 30 mm diameter and 1 mm thickness. On the outer surface of the cylinder a total of 8 miniature semiconductor strain gages are mounted. They form two full bridges, one for torque and another for thrust measurements. The installation of strain gages resembles the arrangement described by N. Brown /8/.

The propeller fits on one end of the flecture and the other end fits into a socket in the end of the shaft and is connected to an electrical cable in the hollow shaft. Slip rings are used to supply the exciting voltages to the gages and to take the output signals from the rotating shaft.

General layout of the dynamometer can be seen in fig. 17. The main body of the dynamometer is of stainless steel except fairing shape on the after end, which was made of epoxy-reinforced glass-fibre. The V-struts were made of hollow aerofoil-profiles of aluminium.

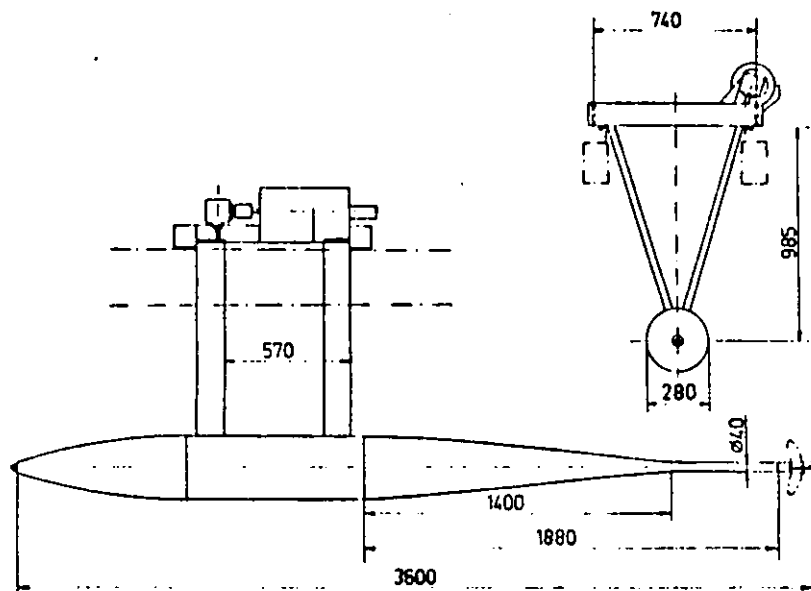


Fig. 17. Dynamometer arrangement.

4.4

Arrangement of the Resistance and Propulsion Experiments

Experiments were carried out in the same towing tank as propeller tests. A model simulating an old ice-clogged channel was erected there. It consisted of two separate plywood fields with a gap between. This gap was covered with plastic pieces which represented ice. The channel length was fixed at 40 m, while the width of the channel and the thickness of the plastic piece layer were varied as well as model. The channel was formed between two large plywood fields, which consisted of 8 modules of 5 m by 3,75 m. These could be easily lifted in and out of the basin. The modules were formed of 1,25 m by 2,5 m plywood sheets screwed together. The thickness of the finished plywood field was 32 mm. Each of the plywood fields was secured to the side of the towing tank with nylon ropes so that it could freely move up and down. At both sides of the channel there was a net fixed underneath the edge running the whole length of the channel. This restricted the plastic pieces from escaping and also limited the amount of plastic needed to within reasonable bounds. The net did not inhibit water from flowing sideways as the ship model proceeded in the channel. At each end of the channel there was a length of galvanized steel tubing with a net attached in order to keep the plastic pieces inside the channel. The arrangement is illustrated in pictures 18, 19 and 20. When taken underwater photographs, part of the net on one side of the channel was lifted up so that it lay flush with the bottom of the plywood and a plexiglass shield was installed in its place. Resistance tests and photographing were not performed simultaneously.

At the beginning of every test set, the layer of plastic pieces was first levelled by a device designed for this purpose. Then before testing, the model was run through the channel so that a natural profile would be created. It was only after this procedure that actual testing began. During the tests, layer thickness was carefully observed by plotter. As resistance is greatly affected by layer thickness any deviations could be noticed and promptly corrected manually during the test sequence. A typical channel profile is illustrated in figs. 21 and 22.

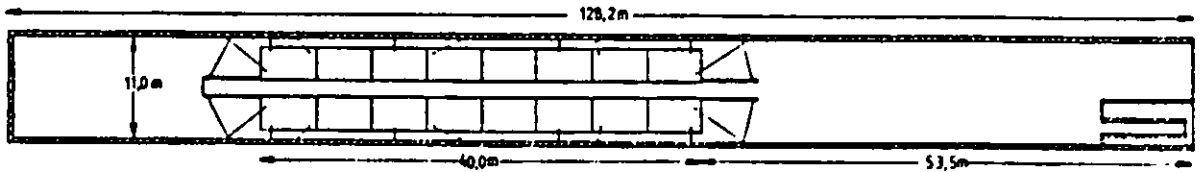


Fig. 18. Location of the plywood field in the basin
1:500.

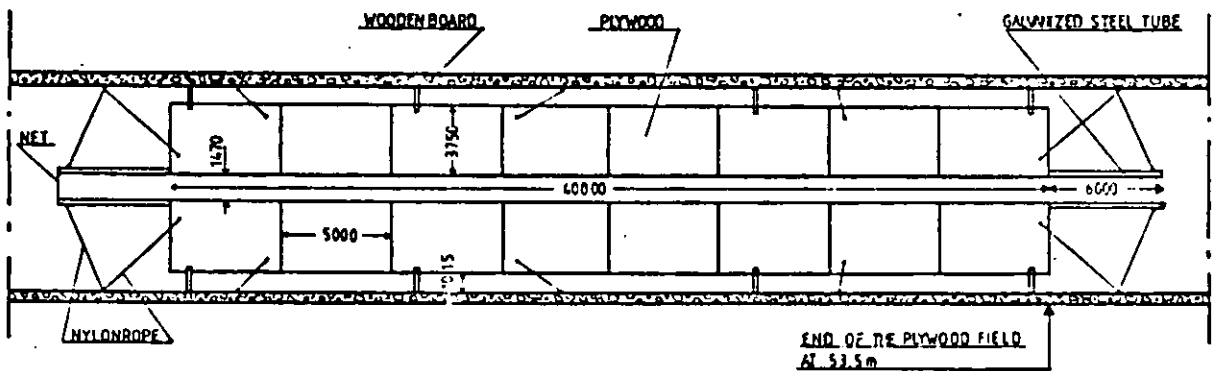


Fig. 19. Securing of the plywood field 1:250.

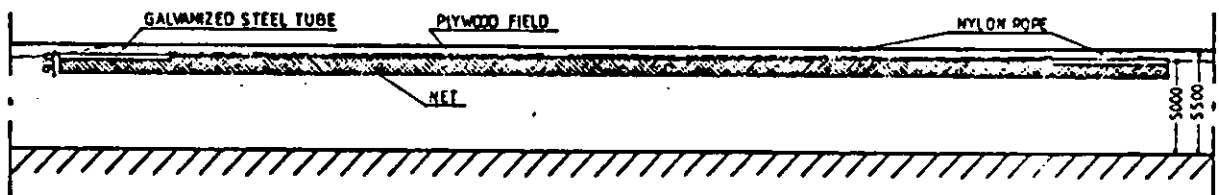


Fig 20. Longitudinal section of the plywood field
1:250.

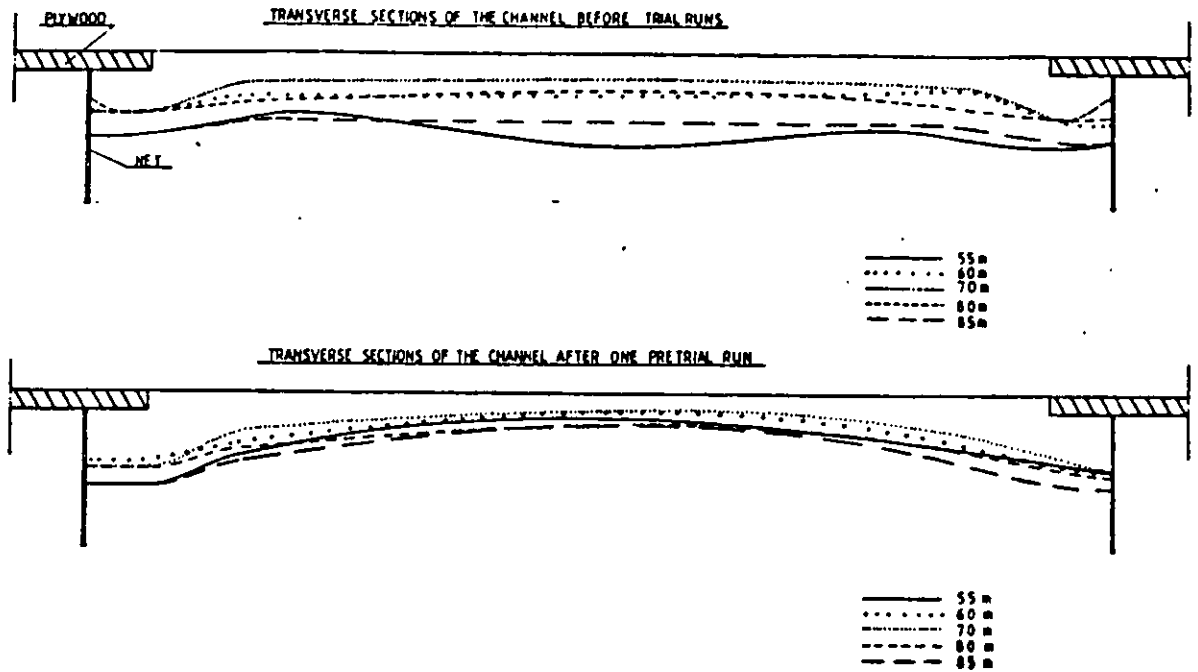


Fig. 21. Transverse sections of the channel 31.8.1981
Large model, $W/B_{WL} = 1,2$, $h_N/B_{WL} = 0,068$.

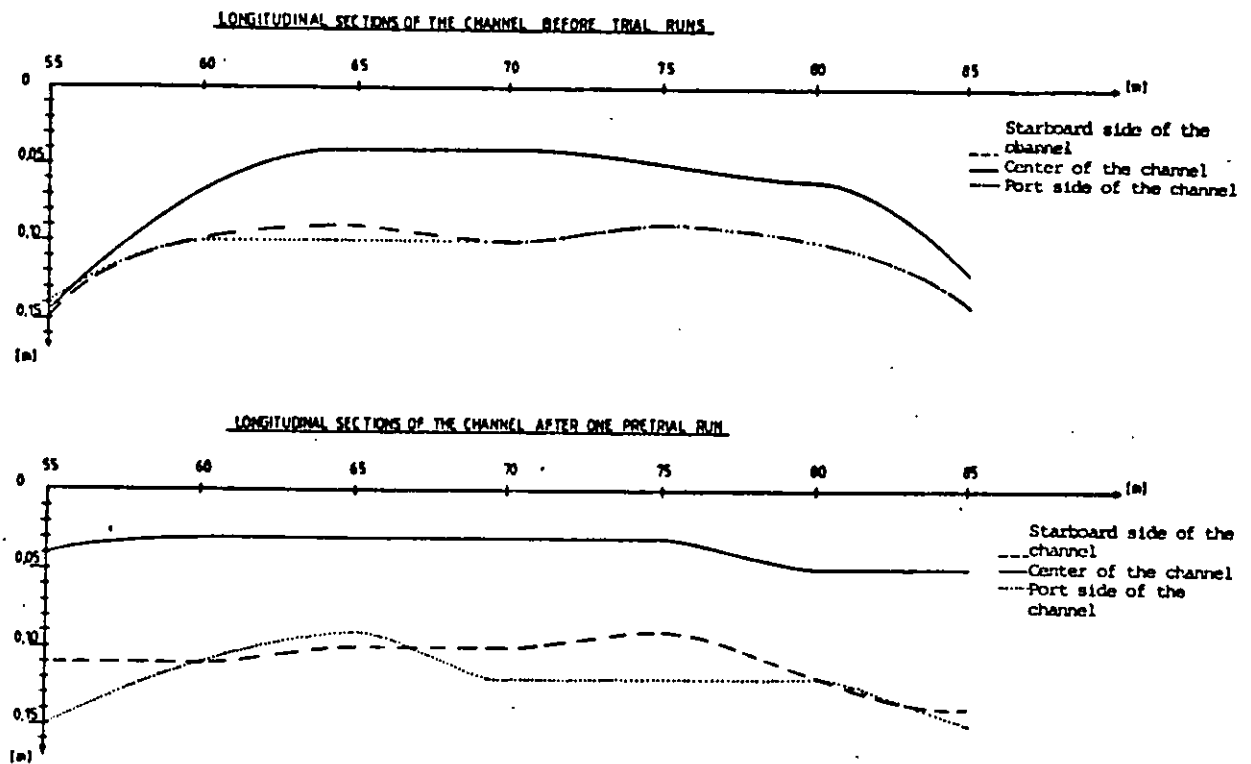


Fig. 22. Longitudinal sections of the channel 31.8.1981. Large model, $W/B_{WL} = 1,2$,
 $h_N/B_{WL} = 0,068$.

5
RESULTS

5.1
Propeller Tests

The main particulars of propeller models tested so far are presented in table 1. Blade profiles and outlines for all propellers were taken from the corresponding Wageningen B-propeller. The thickness of leading and trailing edges from .5 to 1.0 R was increased to .5 mm.

Table 2. Main Particulars of Propeller Models.

Propeller Nr	D m	A_{E0}	P_{MEAN}/D	d/D
p-34	.24	.55	.80	0.167
p-35	.24	.85	.90	0.167
p-38	.24	.55	1.17	0.167
p-40	.24	.85	1.26	0.167

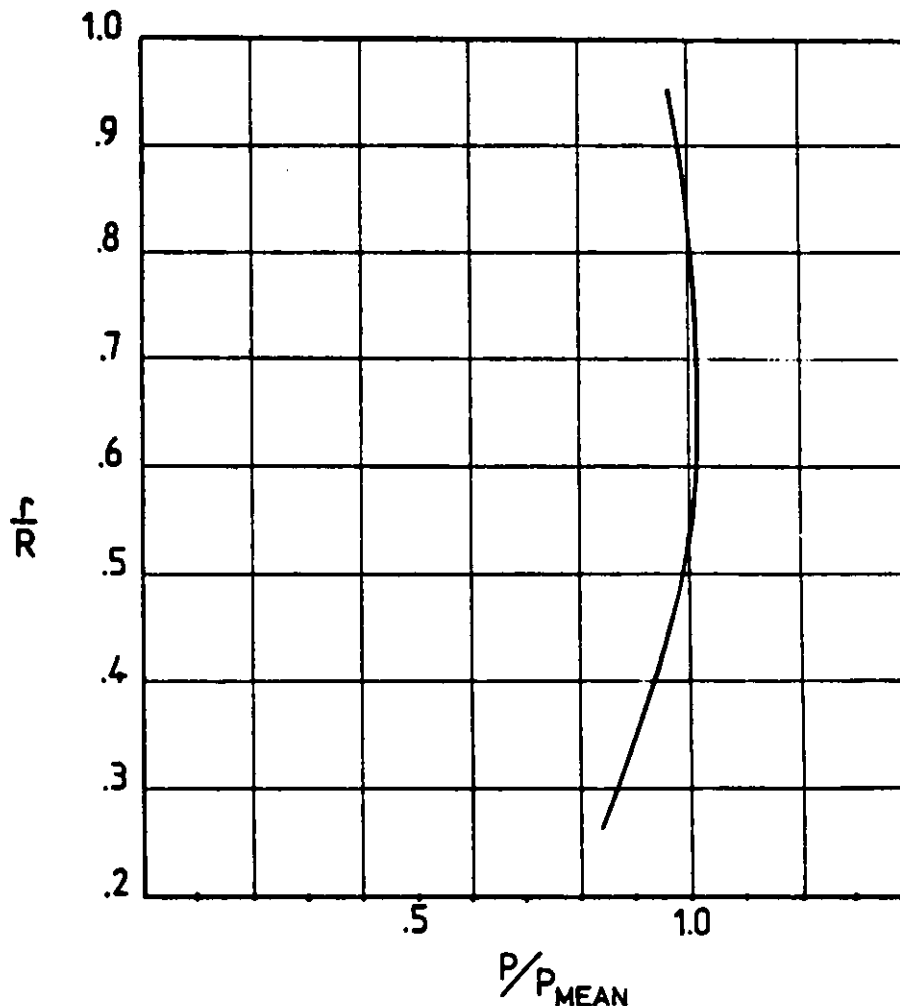


Fig. 23. Pitch distribution of the propeller models.

The results of the tests were faired and conventionally plotted with the coefficient:

$$K_T = \frac{T}{\rho n^2 D^4} \quad (7)$$

$$K_Q = \frac{Q}{\rho n^2 D^5}$$

$$\eta_0 = \frac{J}{2\pi} \cdot \frac{K_T}{K_Q}$$

as functions of the advance coefficient $J = V_A/nD$

No Reynolds-number correction was applied to the results. K_T -, K_Q -J diagrams of all tested propellers are given in fig. 24, 25, 26 and 27. The solid line represents the values of quantities in open water, without plastic pieces. The broken line represents the values in the testing channel with 7,5 cm thick layer of plastic pieces, the dotted line represents the values 15 cm thick layer of plastic pieces.

Measured torque signals specially in the 15 cm thick layer of plastic pieces varied, with large peak values compared with the mean. This together with the stochastic nature of the phenomenon resulted in considerable scatter in mean values as compared with the manually faired curves.

The most important finding of these tests is the experimental evidence of the importance of the clearance of the tips of the propeller blades. The situation can be explained with the help of fig. 15, where the propeller disc has been drawn in relation to the two layers of plastic pieces. When the thickness of the layer of plastic pieces is 7,5 cm, mean clearance between the tip of the propeller blade and the lower surface of the layer of plastic pieces is about 5 cm. In this case results of model tests indicate very small changes in thrust and torque coefficients even with higher loadings of the propeller. Visual observations confirm that very few of the plastic pieces were drawn by the suction of the propeller through the propeller disc. In the case of the 15 cm thick layer of plastic pieces, the tip of the propeller blades rotate through the layer of plastic pieces, the propeller tip is at rest about 1,5 cm above the lower surface of the layer of plastic pieces. As can be seen from figs.

9 to 12, the K_Q -values are increased and η_0 decreased throughout. Changes in K_T -coefficients are small. This means that thrust can be produced if the torque of the propeller motor can be increased. This is in general possible in icebreakers but not usually in commercial ships. Therefore the propeller of ice-transiting commercial ships should be placed as low as possible.

Owing to the large scatter of the measuring points no further conclusions can be drawn from the results of these tests. The number of test runs for each thickness of the layer of plastic pieces should be increased in subsequent tests.

Owing to the increased thickness of model propeller blades and the manufacturing method of propeller, the efficiency of tested propellers are poor. This should be taken into consideration if figures 23...27 are applied.

Tests were run in the usual way with as high Reynolds number as possible and results are presented in dimensionless form using the kinetic conditions. The buoyancy force of the plastic pieces is of great importance in these conditions. Before than application of the test results to the ship scale evaluation of propeller performance in ice clogged channel, scale effect studies should be made.

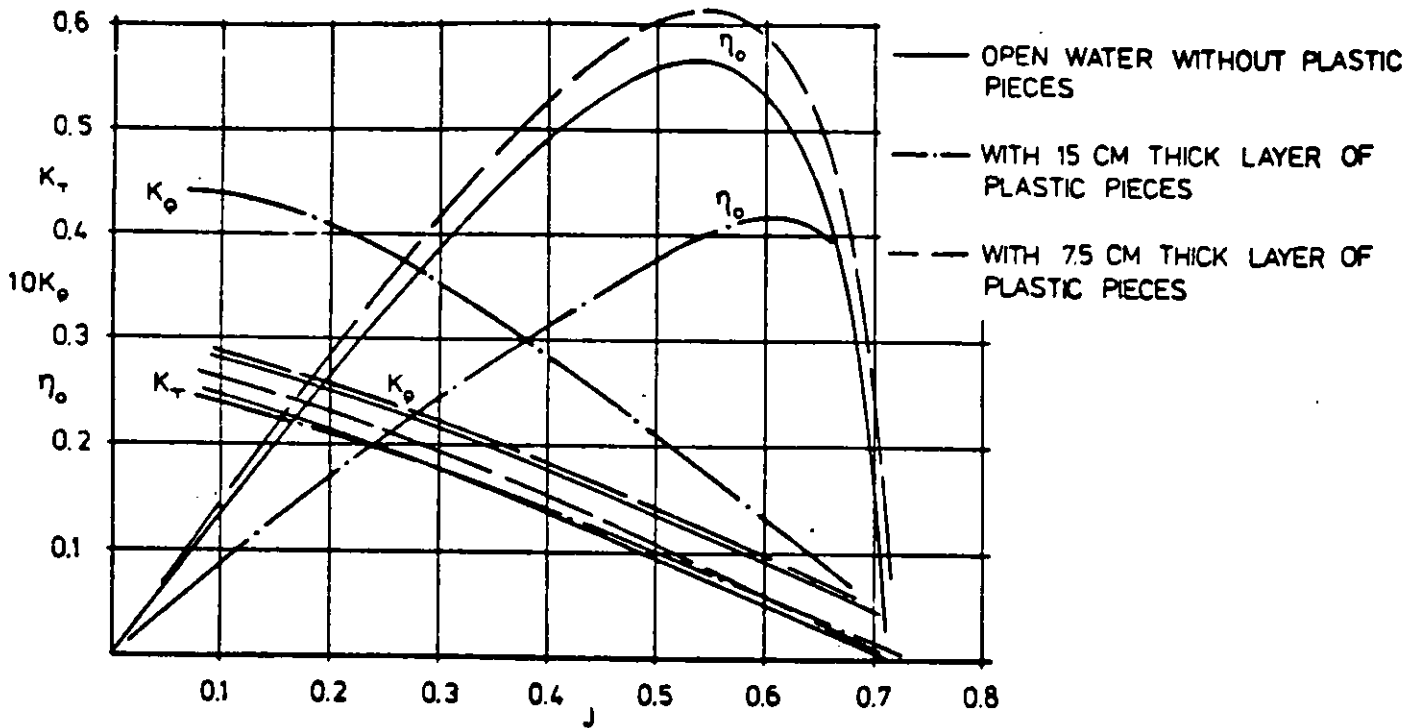


Fig. 24. K-J Diagrams of the propeller P-34,
 $P/D = .8, A_E/A_0 = .55$

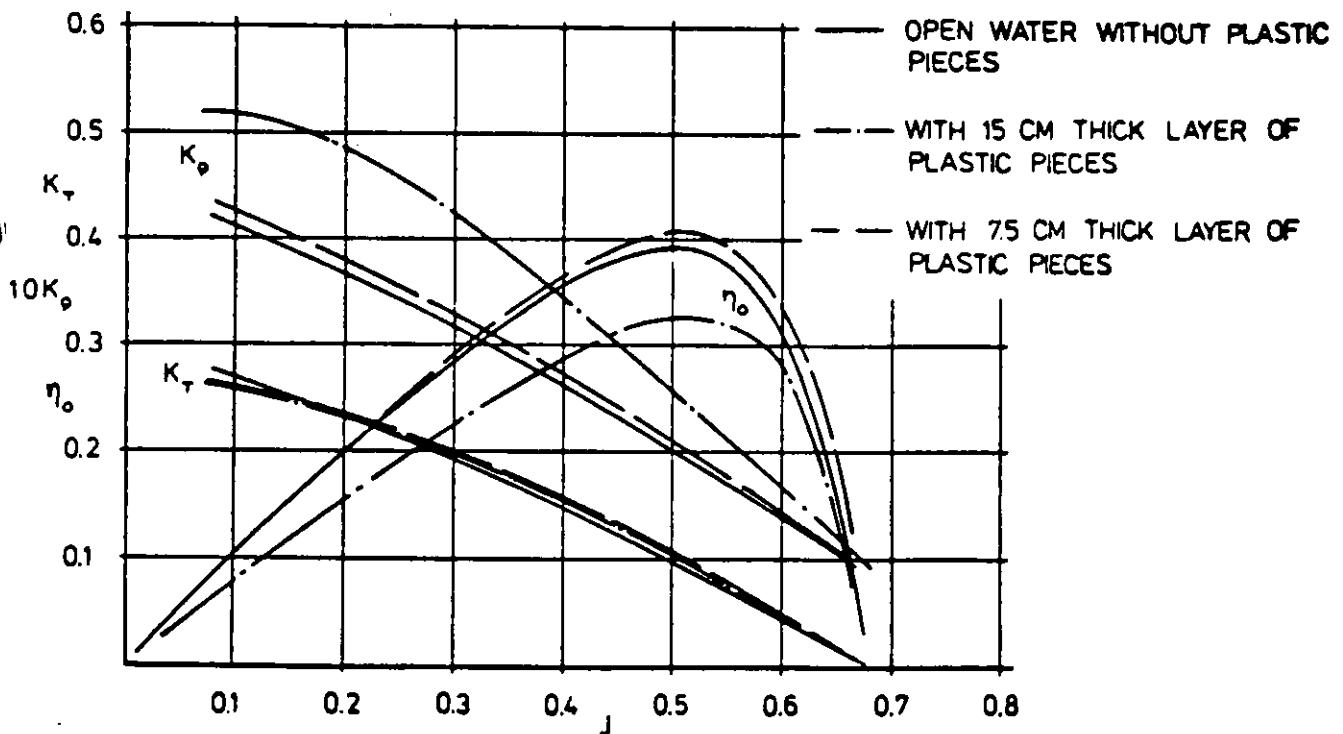


Fig. 25. K-J Diagrams of the Propeller P-35,
 $P/D = .9, A_E/A_0 = .85$

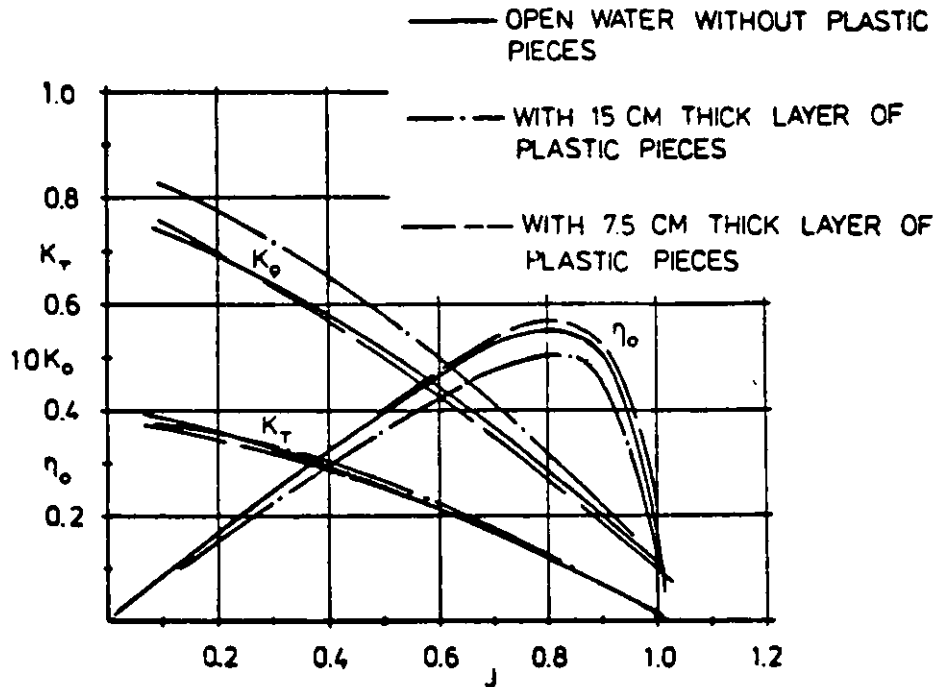


Fig. 26. K-J Diagrams of the propeller P-38,
 $D/D = 1.17$, $A_E/A_0 = .55$.

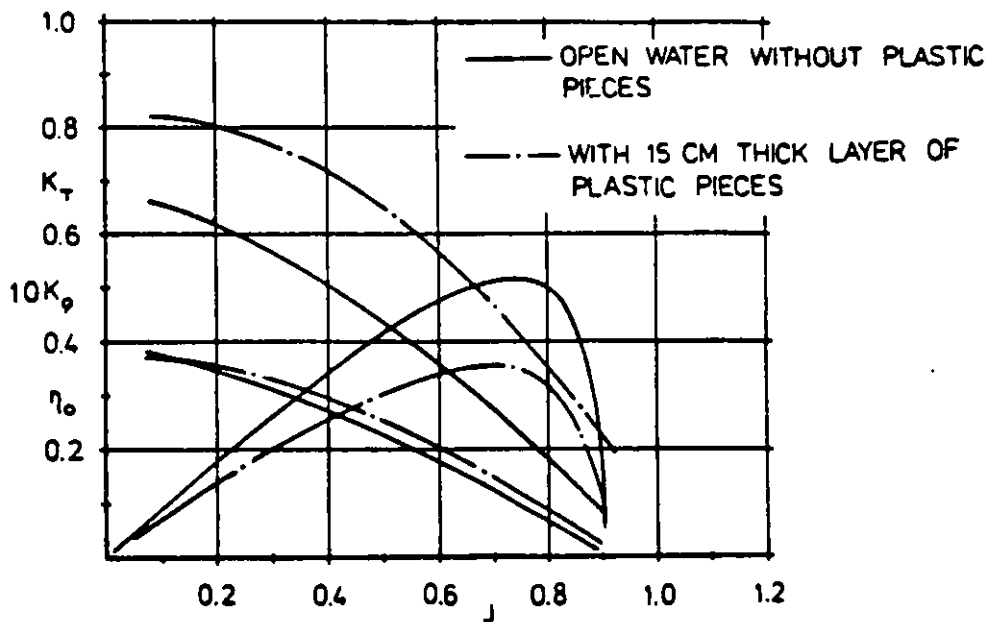


Fig. 27. K-J Diagrams of the propeller P-40,
 $P/D = 1.26$, $A_E/A_0 = .85$.

5.2
Resistance Tests

When ships are navigating in old channels, the environmental conditions vary randomly. Most of them are dependent on the meteorological time history and the density of traffic. On the other hand it was not possible to simulate more than one combination of conditions at this stage of the study. The effect of the one of the parameter, channel width, is considered here.

First, preliminary runs were made with channel width W , which was 10 % larger than waterline breadth B_{WL} . The measured resistance signal was very unsteady and repeatability of the mean values was poor. This was caused by the locking up of largen plastic pieces between the sides of the model and the edges of the channel. A series of tests was run with the two geosim models of the passenger ferry.

The combination of tested channel width ratios and thickness ratios of layer of plastic pieces for both model sizes is presented in table 3.

Table 3. Variation of Channel Width Ratio and Thickness Ratio of Layer of Plastic Pieces.

Model Scale Factor λ	h_N/B_{WL}	W/B_{WL}		
1 : 32	0,068		1.3	2.0
	0,036		1.3	2.0
1 : 18	0,068	1.2	1.3	2.0
	0,033			

The shape and size distribution of plastic pieces was the same in all combinations. The thicker layer of pieces with the largern model could not be included in the width series because the amount of plastic pieces was limited. The tests with the smaller model in small channel width ratio $W/B_{WL}=1.2$ resulted in unsteadiness of resistance recordings similar to results with the large model mentioned earlier when W/B_{WL} was 1.1. Therefore these results were omitted.

In reality the width of an old ice-clogged channel is a random parameter. In areas of busy traffic, width is large, thickness of the layer of ice fragments is thin in the center of the channel and increases towards the sides. The sides are often refrozen. Sparsely navigated channels and channels situated in narrow fairways are narrow.

The amount of plastic pieces is limited both from the point of view of the material and erection costs. Thus the very wide channel widths with large models are excluded. On the other hand the differences in resistance with the large model when channel width ratio was 1.2 and 1.3 proved to be small. The width ratio 1.1 was out of the question because of the locking up of plastic pieces. The size of the larger model corresponds to the normal size of models in normal clear water resistance and propulsion tests.

In the continuation of this type of model tests it was decided to use normal size models and channel width - model width ratio 1.2.

Test results of the two geosim models of a twin screw passage ferry (fig. 28) with scales 1:18 and 1:32 are presented in figures 29...36.

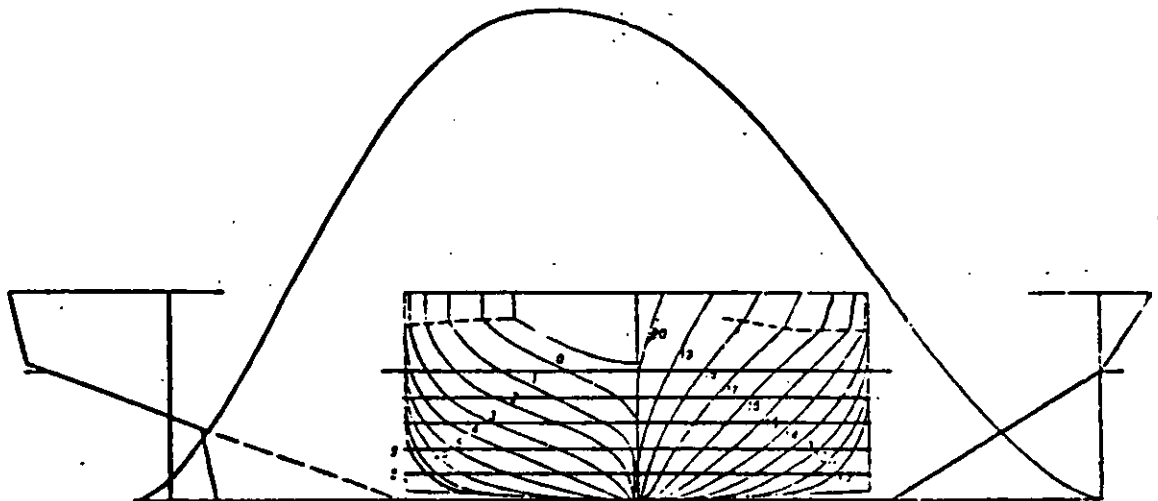


Fig. 28. The body plan of two geosim models. The original ship has the following main dimension:

$$\begin{array}{ll} L_{WL} = 142,4 \text{ m} & T = 5,78 \text{ m}_2 \\ B_{WL} = 22 \text{ m} & \Delta = 9702 \text{ m}^3 \end{array}$$

Resistance tests were carried out as usual. Underwater photographs were taken with equipment located near the halfway point of the channel. Visual observation of the behaviour of the plastic pieces close to the model was also conducted, by video tape recorder.

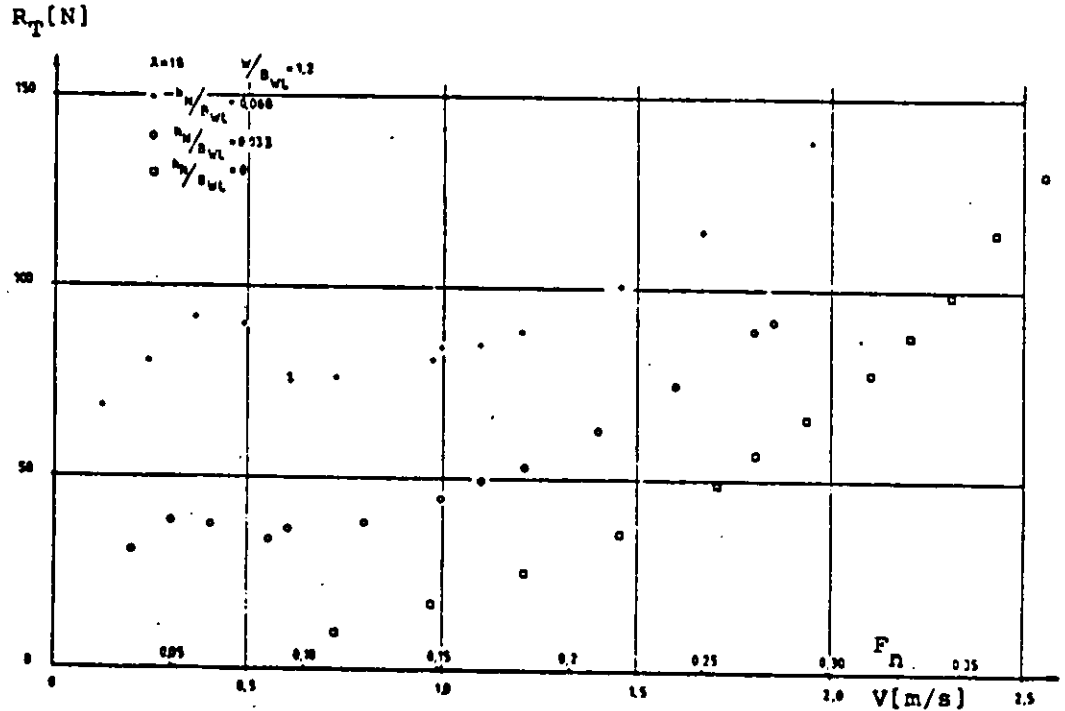


Fig. 29. Total resistance of large model in free-water and in the channel.

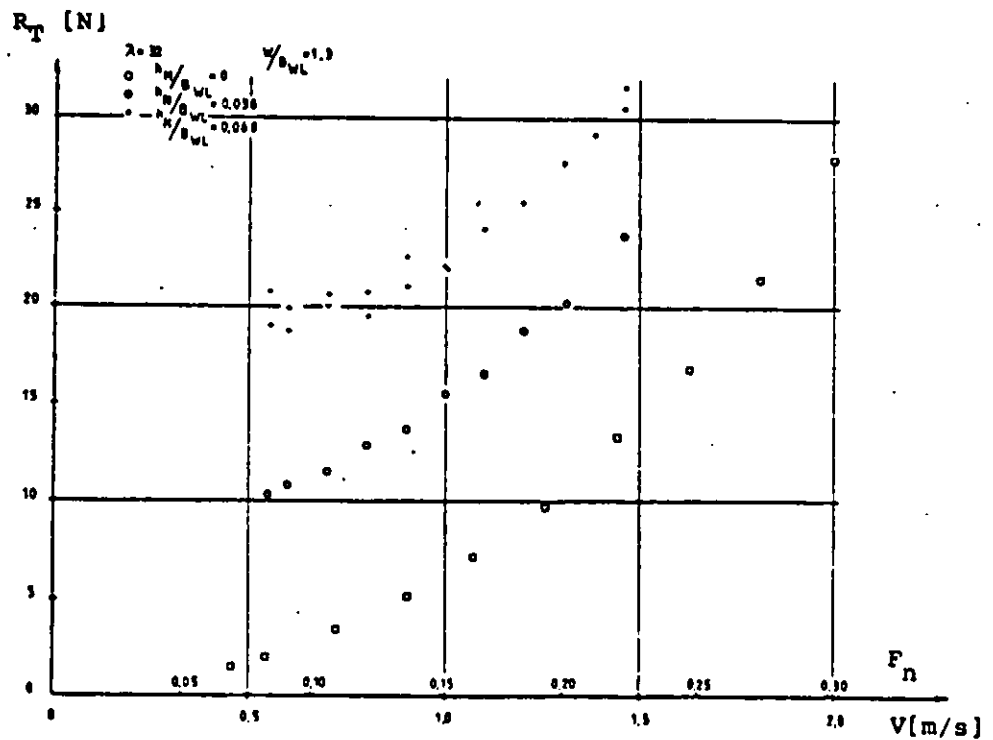


Fig. 30. Total resistance of small model in the channel.

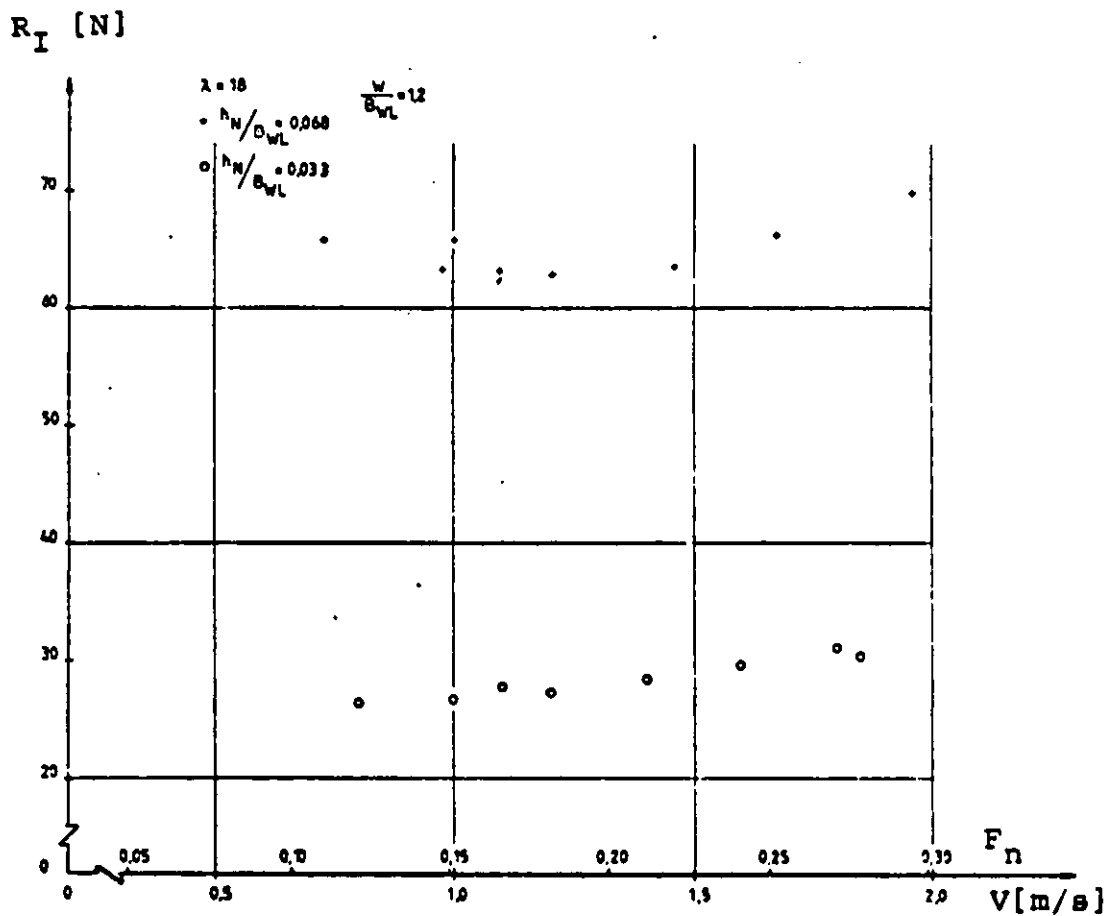


Fig. 31. The net ice resistance of large model at $W/B_{WL} = 1, 2$.

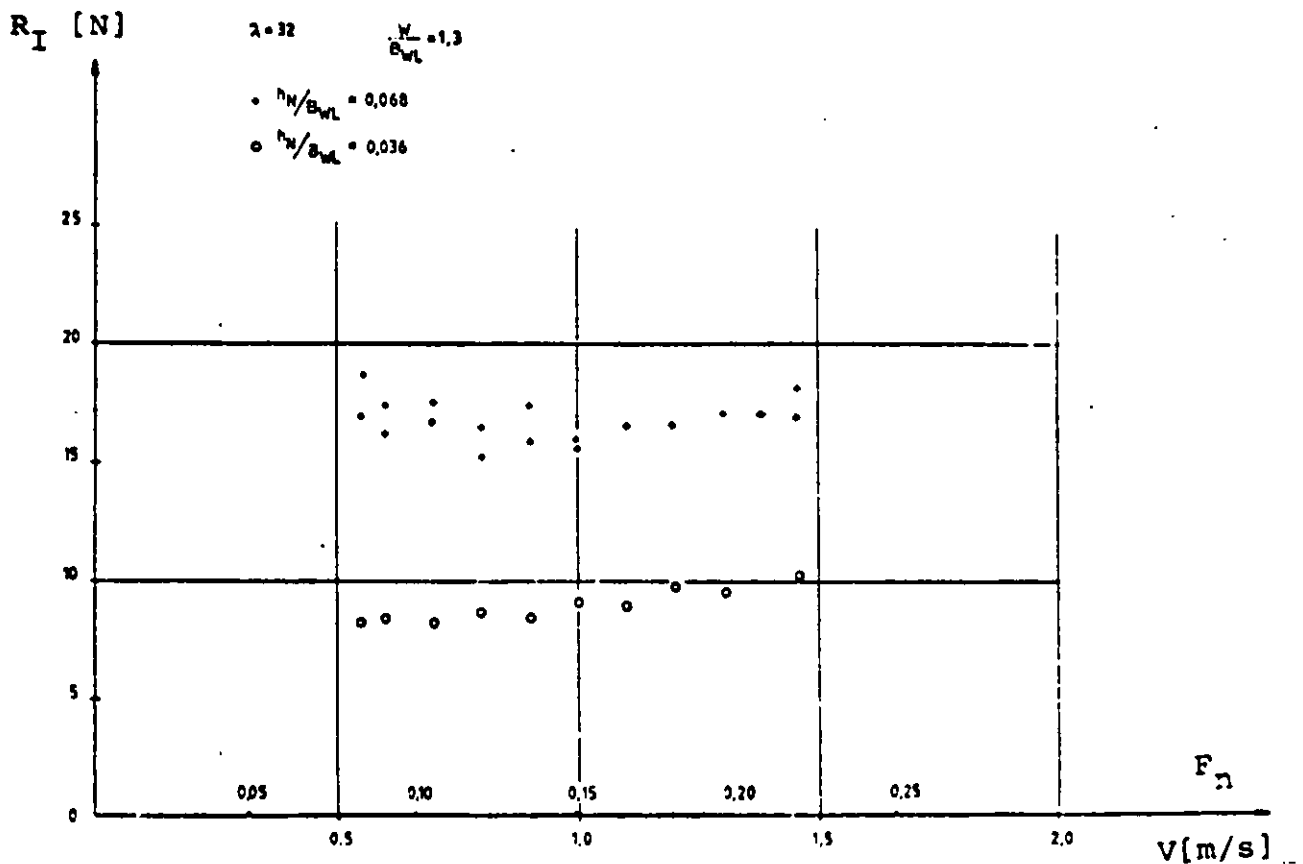


Fig. 32. The net ice resistance of small model at $W/B_{WL} = 1.3$

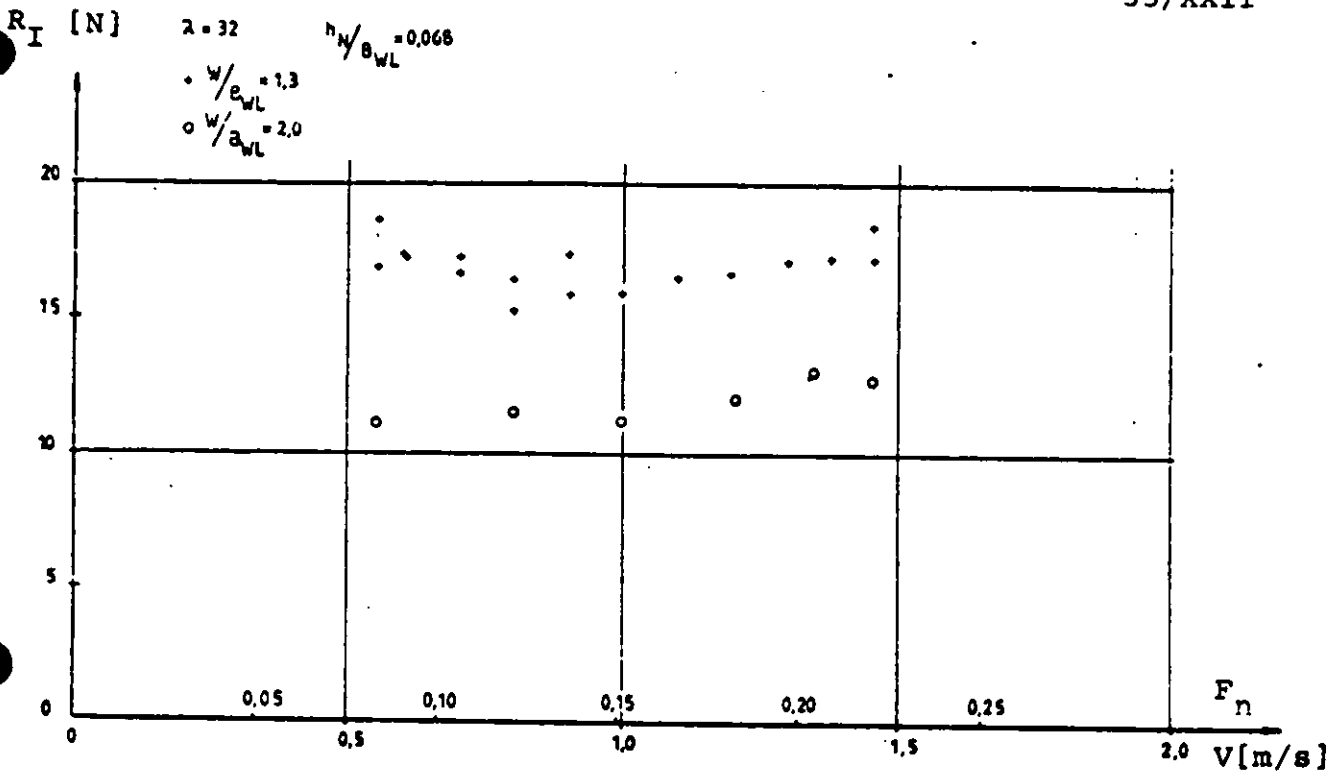


Fig. 33. The net resistance of small model at two W/B_{WL} ratios $h_N = 0,068$.

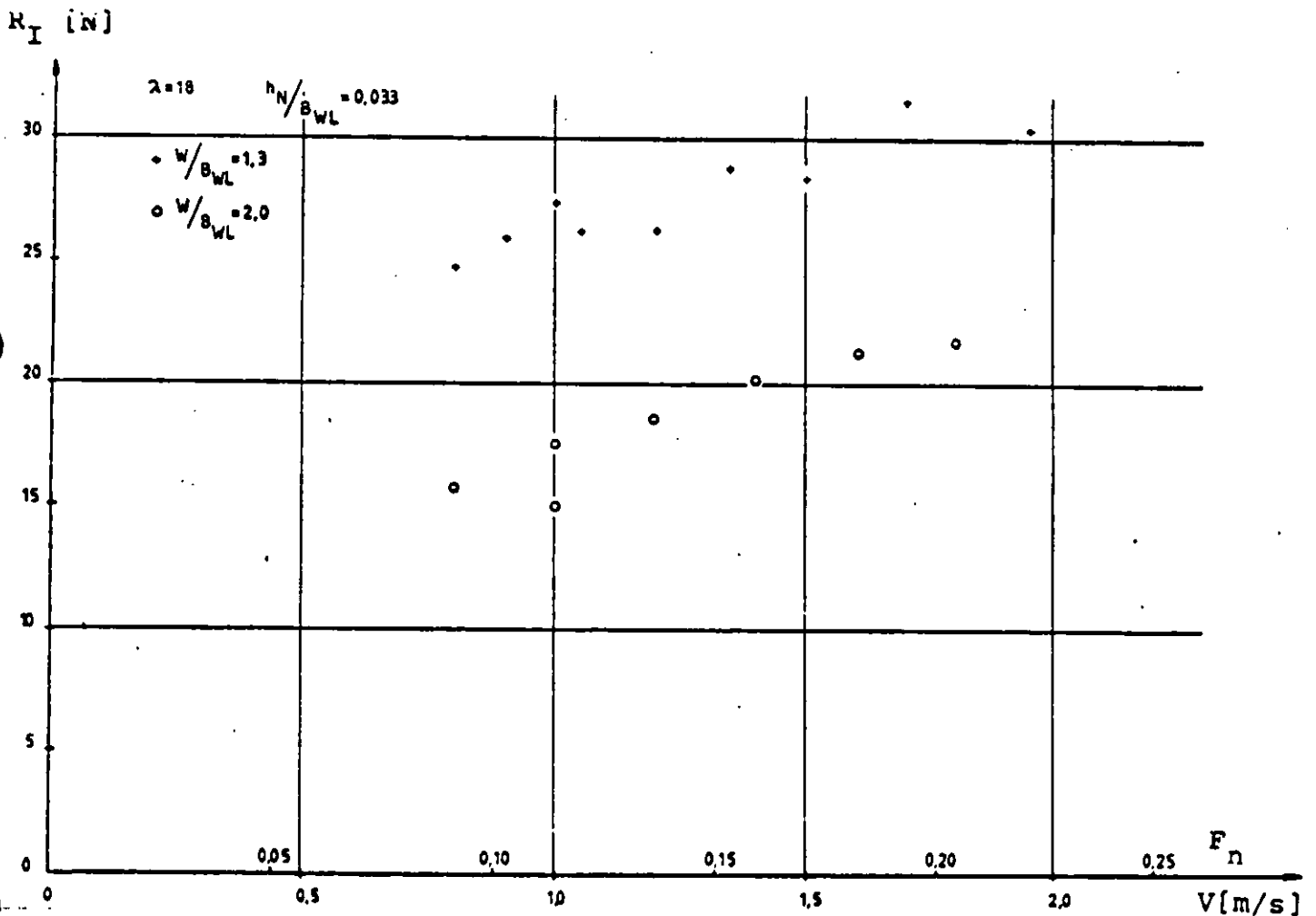


Fig. 34. The net ice resistance of large model at two W/B_{WL} ratios $h_N = 0,033$.

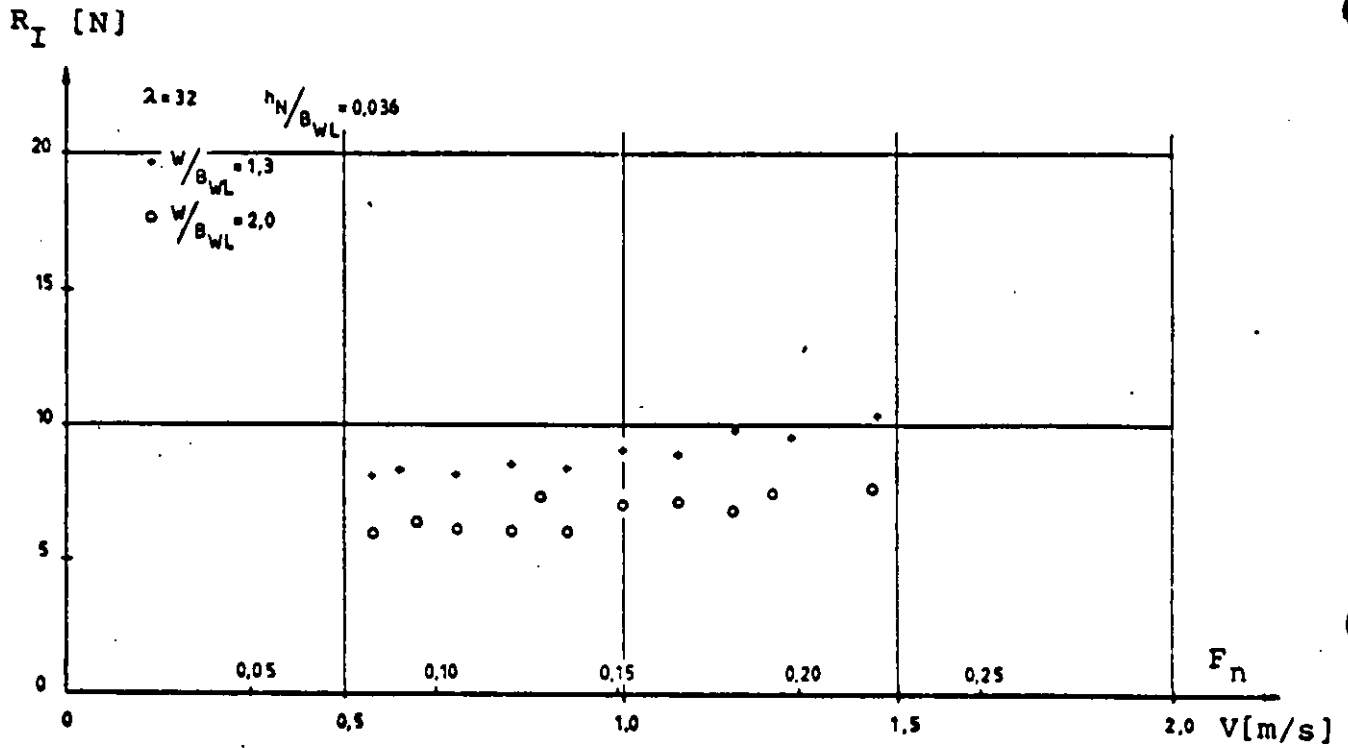


Fig. 35. The net ice resistance of small model at two W/B_{WL} ratios. $h_N/B_{WL} = 0,033$.

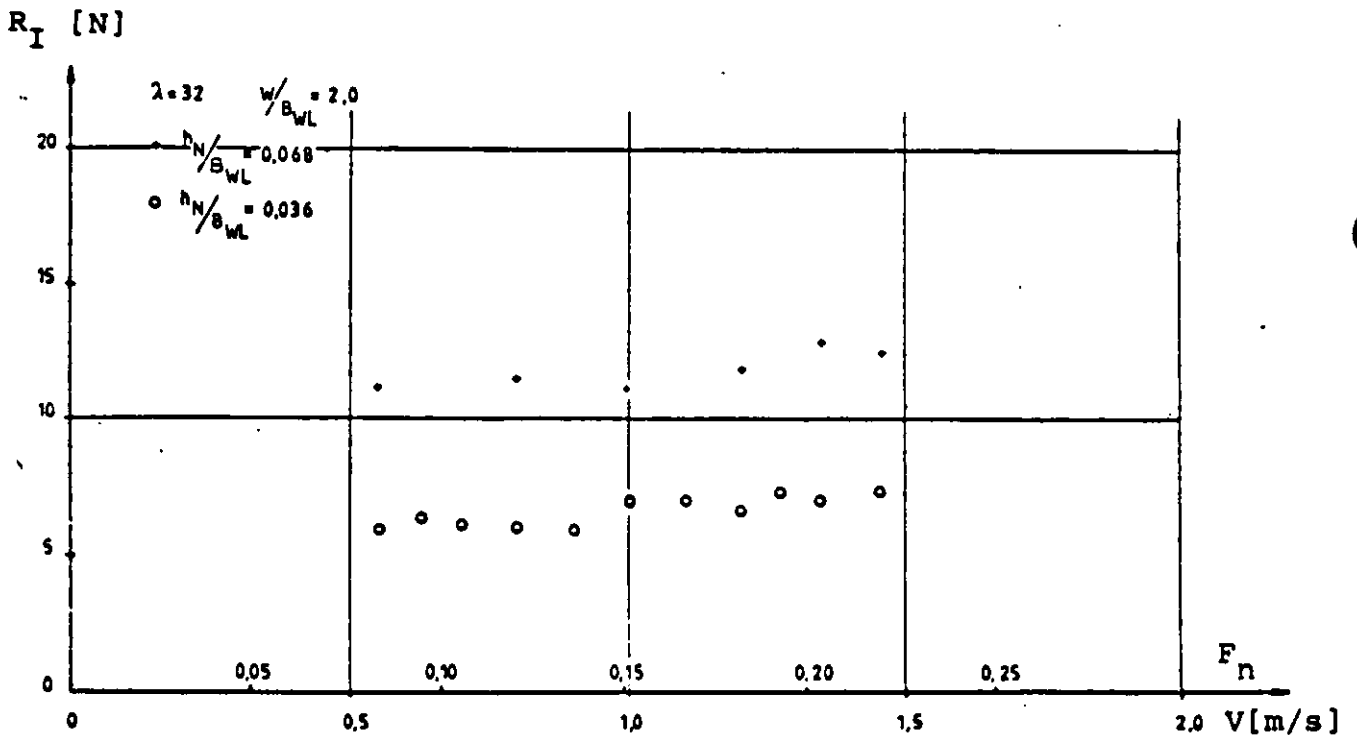


Fig. 36. The net ice resistance of small model at two h_N/B_{WL} ratios. $W/B_{WL} = 2,0$.

The most important discovery of the test series is that ice resistance shows only slight dependence on speed. This is indicated by figs. 29 and 30 which show total resistance corrected to 15 °C according to /2/ as all data presented. Fig 29 also shows that there seems to be a critical speed below which the plastic pieces attach to the bow of the model and cause a resistance increase with decreasing speed. This plug moving with the model can reach a length of about a quarter of L_{wl} and, depending on the layer thickness and the width of the channel, can cause scatter in measurement points at lower speeds. Figs. 31 and 32 which show ice resistance have been derived using a third degree regression polynomial for the free water resistance, like all subsequent figures, indicate very clearly how weakly R_I depends on speed.

In fig. 37 deduced from photographs, it can be seen how the pieces move past the model hull at different speeds and at the two layer thicknesses. When $h_N/B_{WL} = 0,036$ and at 4 knots the pieces slide along the side and stay well clear of the propeller bossings. At 8 knots the pieces reach the turn of the bilge and very few pieces go under the bottom. Still the pieces clear the bossings. At 12 knots, a few pieces go under the bottom and some reach the forward end of the bossings.

When $h_N/B_{WL} = 0,068$ and at 4 knots a few pieces go under the bottom and the turn of the bilge is covered with them, but only few pieces touch the bossings. At 8 knots there are some pieces under the bottom and the bossings are clear of them. At 12 knots lots of pieces go under bottom and quite a few pieces reach the forward end of the bossings.

As one considers the path of the pieces, there are two things which affect it when scaling it up to ships. The first is the friction coefficient between plastic and model which is larger than that of real ice and the second is different boundary layer. The boundary layer consists of two parts: one below and outside the plastic pieces and the other within the pieces. The differences in friction coefficients between plastic and model, plastic and plastic versus ice and ship, and ice and ice must surely have a strong influence on the way the pieces flow past the hull. Another fact that can affect the visual observation is the plexiglass shield which replaced the net while taking photographs.

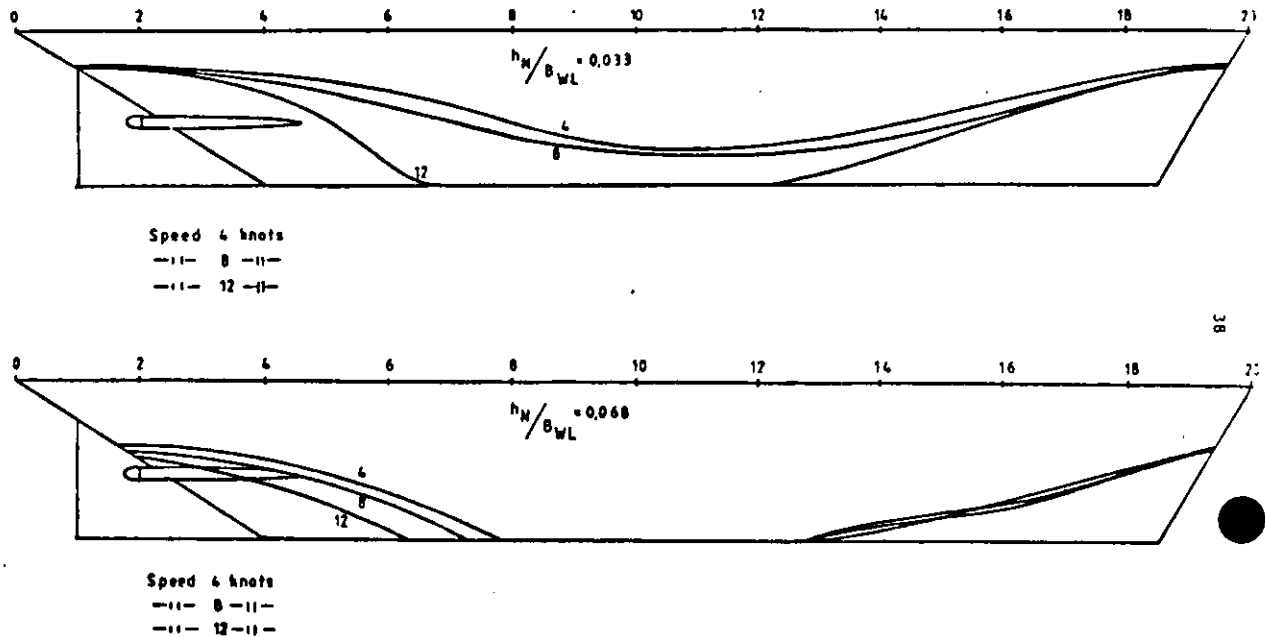


Fig. 37. The path of the pieces along the large model hull at different speeds.

As channel width increases R_I decreases as might be expected. Fig. 38 shows how channel width changes the effective layer thickness at midships, it can also be seen that large channel width requires less "compression" work.

Such marked behaviour of the pieces in attaching to the bow of the model with larger h_N/B_{WL} ratio as happened at $W/B_{WL} = 1,3$ could not be noticed at $W/B_{WL} = 2,0$, this can be seen in fig. 33. Figs 34 and 35 show how increase in channel width produces very uniform reduction in R_I independent of speed. Testing of the larger model at $W/B_{WL} = 2,0$ and with $h_N/B_{WL} = 0,068$ could not be executed because of the limited amount of pieces. Referring to figs. 35 and 33 one can see that increase of W/B_{WL} from 1,3 to 2,3 produces R_I reduction of about 25 % at $h_N/B_{WL} = 0,068$. Comparing figs. 32 and 36 reveals that change of h_N/B_{WL} from 0,036 to 0,068 produces an increase in R_I of about 70...80 % at $W/B_{WL} = 1,3$ disregarding the low speed hump, while at $W/B_{WL} = 2,0$ it is 70...85, so here the channel width does not have any effect on the percentage change.

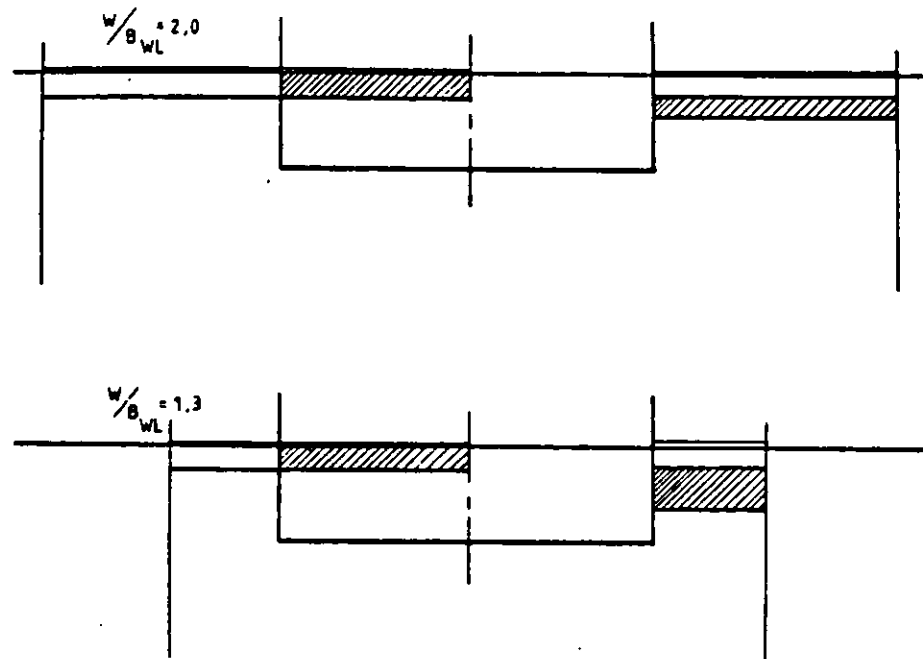


Fig. 38. The change of layer thickness as the area is pushed aside.

5.3

Propulsion Tests

This section contains the results of the study made by H. Eskola /5/. The test series described here included resistance and propulsion tests in four conditions: in clear water, in a channel with no plastic pieces and in two layer thicknesses of plastic pieces. The theoretical levelled layer thicknesses correspond to full scale values of 106 cm and 208 cm - in model scale 5.3 cm and 10.4 cm respectively.

The tested ship type was a 15955 tdw product carrier with icebreaking hull form. The main particulars of the model are listed in table 4. The model was tested both at full load and ballast draughts. Model was propelled with propeller P-34 described in section 5.1.

Table 4. Main particulars of model

Scale factor	λ	20
Length between perpendiculars	L_{PP}	7.223 m
Breadth on cwl	B	1.075 m
Draught at load waterline	$T_{AP} = T_{FP}$	0.475 m
Draught at ballast waterline	T_{FP}	0.280 m
	T_{AP}	0.320 m
Propeller diameter	D	0.24 m
Propeller pitch ratio	P/D	0.8
Disc area ratio	A_E/A_D	0.55

The propulsion tests were made by propelling the model near its self-propulsion point; overload tests were carried out only in clear water under ballast conditions. The fact that overload tests with several propeller loadings are essential if we wish to compare propulsion characteristics in different conditions, was not realised at first.

In this approach to analysing the propulsion characteristics, it has been attempted to calculate all possible efficiencies and not only the so-called "ice efficiency" described in /9/ and /10/. The main difficulties which arise with the analysis are connected with the propeller's "open water" characteristics and the similarity between resistance and propulsion tests.

5.3.1 Wake Fraction and Thrust Deduction

Taylor wake fraction was calculated by thrust identity method using fig. 24. This figure shows the results of the propeller tests in three different conditions but it is very possible that none of these are equal to the conditions behind a model in a thick layer of plastic pieces. And moreover these behind conditions - i.e. the flow of plastic pieces into the propeller - changes as a function of model speed and propeller loading.

Two means to solve this problem was used. Firstly, underwater photographs were taken of the propelled model in channel conditions. These photographs - combined with streamline tests - give information about the behaviour of plastic pieces under the model. The other method is to compare the thrust before the model arrives in the channel and the thrust measured in the channel. But it cannot be said for sure, whether the possible change in the thrust is due to the change in advance velocity of the propeller - affected by the plastic pieces - or if the propeller gives different thrust with the same advance ratios. Eskola made following assumptions: in all but one situation the propeller is working - as far as the thrust coefficient curve is concerned - in clear water. The only exception is the combination of ballast draught and thick (10.4 cm) layer of plastic pieces. In this case the propeller works in difficult conditions and it is assumed that the open water K_T -curve is slightly above that of the clear water.

Accurate measuring of resistance is essential if we want to calculate thrust deduction or - in general - propulsive efficiency from propulsion tests. A requirement of exactly similar conditions during the resistance and propulsion tests is not so easy to fulfil when using model ice. This is one reason why the scatter of e.g. the thrust deduction factor usually becomes too large.

Fig. 39 and 40 show the obtained values of w and t as a function of $J_V (= V_M/nD)$.

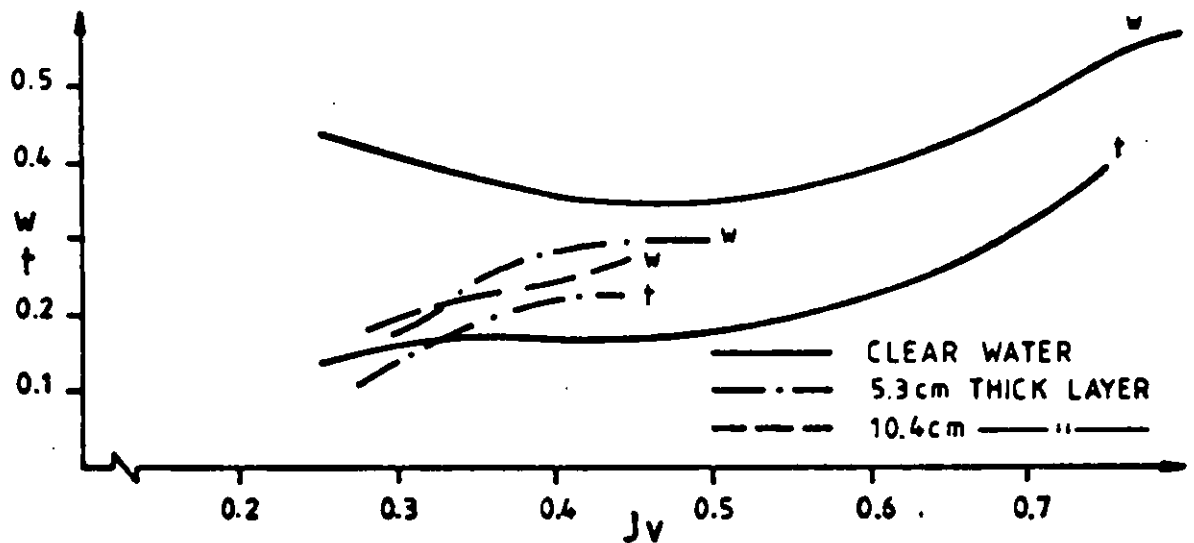


Fig. 39. t and w ; ballast draught.

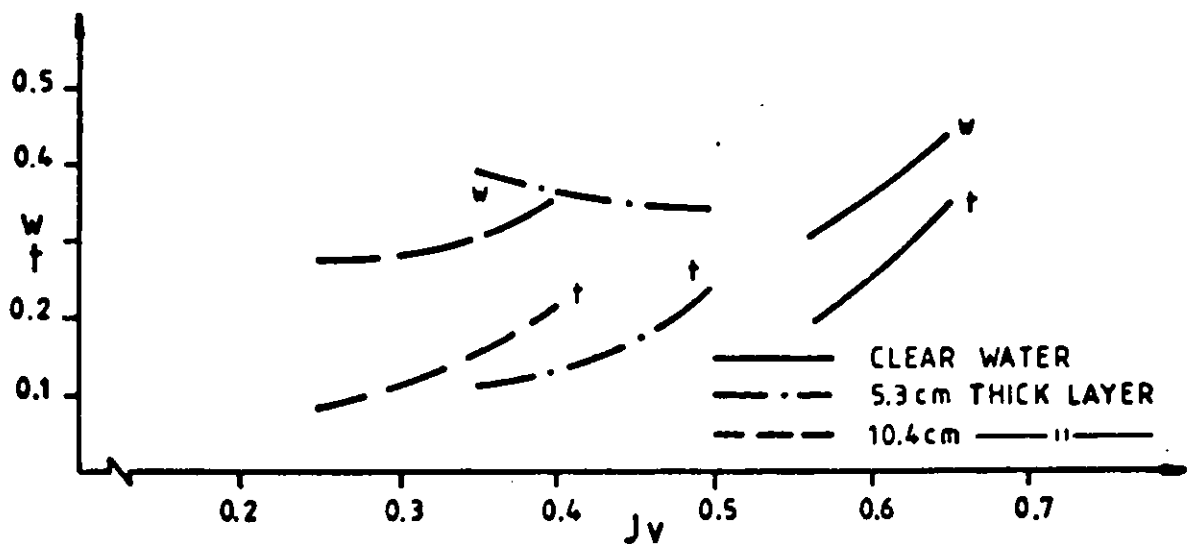


Fig. 40. t and w ; load draught.

5.3.2
Propulsion Efficiencies

In clear water, propulsive efficiency is defined as as

$$\eta_D = \eta_O \eta_R \eta_H \quad (8)$$

Eskola proposes to include the effect of plastic pieces in the relative rotative efficiency in ice, η_{IR} . In this way the open water efficiency $\eta_O (= J_0 K_{T0} / 2 K_{Q0})$ may become a little peculiar and does not necessarily correspond to any propeller working conditions but $\eta_O \eta_R (= \eta_B)$ still represent the propeller's efficiency behind the model as the η_B should, by definition, do. The obtained values of η_R , η_D and $\eta_H (1-t)$ are presented in fig. 41 and 42.

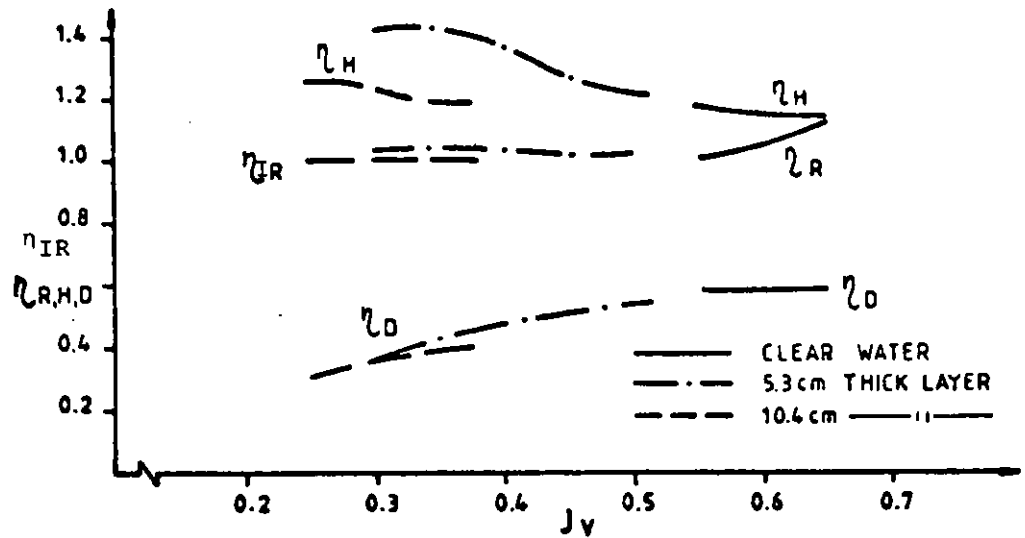


Fig. 41. Efficiencies; load draught.

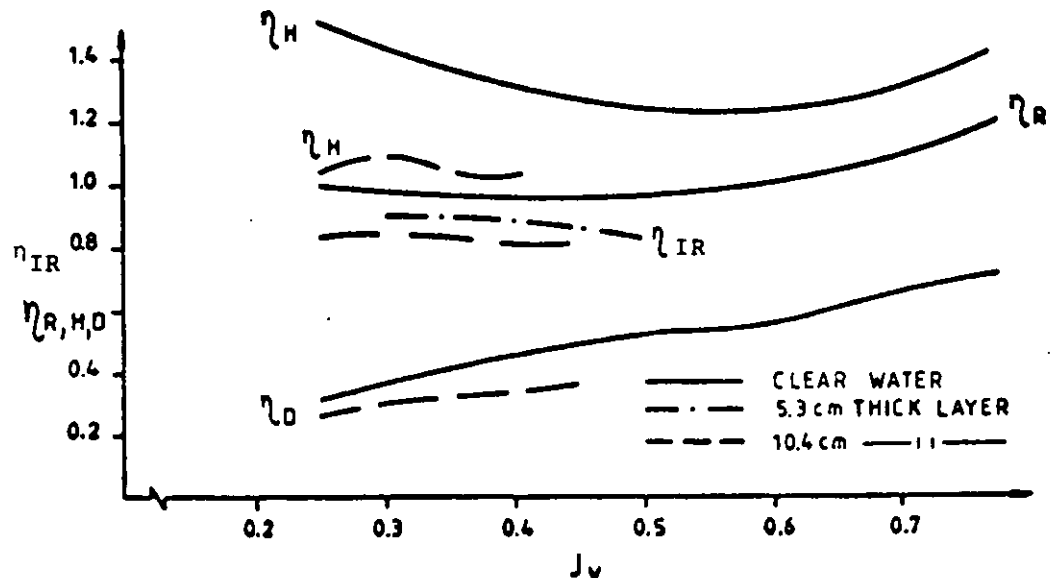


Fig. 42. Efficiencies; ballast draught.

Results seen in figs. 38...42 indicate that simulated ice can have a considerable effect on all propulsion factors and efficiencies. Therefore it may be dangerous to use only the results of clear water overload tests - not to mention tests at selfpropulsion point - when considering the performance of the hull - propeller system in ice. Whether or not an approach where hull efficiency is divided into wake and thrust deduction components, assuming e.g. thrust identity is accurate or reasonable in overload or ice conditions with heavy propeller loading, is another question.

Fig. 44 shows that at ballast draught the wake fraction in clear water can be twice as great as in channel conditions (the increase of w with larger J_V -values in the former situation is most likely due to very severe separation with relatively small loading).

At load draught the propulsion efficiencies have not changed much but the thrust deduction and wake fraction seem to behave differently in every condition.

NOMENCLATURE

A	area
B_{WL}	waterline beam
F_{IF}	force normal to ships axis acting in waterplane
F_{IN}	normal ice force on a body
F_{IT}	force tangential to ships axis
F_n	Froude number
h	layer thickness of fragments
h_N	nominal layer thickness of fragments
h_E	effective layer thickness of fragments at midships
J_O	V_A/nD , advance ratio
J_V	V_M/nD
K_Q	$Q/\rho n^2 D^5$, torque coefficient
K_{QO}	open water torque coefficient
K_T	$T/\rho n^2 D^4$, thrust coefficient
K_{TO}	open water thrust coefficient
k_I	fragment size coefficient
k_S	waterline form coefficient
L	length of a ship
L_E	length of entrance
L_P	length of parallel middle body
L_{WL}	length of waterline
l	length of fragments
n	propeller revolutions
Q	torque of propeller
R_I	net ice resistance
R_T	total resistance
s	distance
T	draught

T	thrust of propeller
t	thrust deduction factor
V_A	advance speed
V_M	model speed
v	velocity in general
W	channel width
W_{IF}	work done by internal friction forces
W_{IT}	total work
W_{SF}	work done by side friction forces
w	Taylor wake fraction
\bar{x}	mean length of fragments
y	coordinate
η_B	propeller efficiency behind the model
η_D	propulsive efficiency (= $RV/2\pi nQ$)
η_H	hull efficiency
η_O	propeller open water efficiency
η_R	relative rotative efficiency
η_{IR}	relative rotative efficiency in ice
λ	scale factor
μ_I	friction coefficient between simulated ice fragments
μ_s	friction coefficient between ice fragments and ship sides
ρ	water density
∇	displacement

REFERENCES

1. V. Kostilainen: Performance of Marine Propellers in Ice-Clogged Channels, Styrelsen för Vintersjöfartsforskning, Research Report No 33, 1981.
2. P. Tuovinen: The Size Distribution of Ice Blocks in a Broken Channel, Helsinki University of Technology, Ship Hydrodynamics Laboratory, Memorandum M-78, 1979.
3. V. Kostilainen, K. Hanhiova: Model Testing of Ships in Ice-Clogged Channels, Helsinki University of Technology, Ship Hydrodynamics Laboratory, Report No 22, Otaniemi 1982.
4. I. Priha: The Measurement of the Compression Force in Conditions Simulating a Ship Advancing in Ice-Clogged Channel (in Finnish). Helsinki University of Technology, Ship Hydrodynamics Laboratory, Memorandum M-97, 1982.
5. H. Eskola: Propulsion Tests of a Ship Model in Conditions Simulating Old Ice-Clogged Channel. (7th International Conference on Port and Ocean Engineering under Arctic Conditions. Helsinki 1983.)
6. P. Kannari: Measurements of Characteristics and Propulsion Performance of a Ship on Old Ice-Clogged Channels in the Baltic Sea in Winter 1982. (7th International Conference on Port and Ocean Engineering under Arctic Conditions. Helsinki 1983.)
7. M. Lietepohja: Construction and Trial Runs of Open Water Propeller Dynamometer. (In Finnish) M.Sc. Thesis, Helsinki University of Technology, Otaniemi 1980.
8. N. A. Brown: Periodic Propeller Forces in Non-Uniform Flow, MIT, Department of Naval Architecture and Marine Engineering, Report No 64-7, 1964.
9. K. Juurmaa, H. Segercrantz: On Propulsion and Its Efficiency in Ice, STAR Symposium, June 1981, Publ. SNAME, New York.
10. J. Schwartz, et. al.: Prediction of the Icebreaking Performance of the German Polar Research Vessel, STAR Symposium, June 1981, Pub. SNAME, New York.



MSc Kimmo Juurmaa

CASE STUDY

Propulsion in ice

Situation no. 1

- shallow draft icebreaking salvage/supply vessel
- $P_0 = 10.000 \text{ kW}$
- 2 propellers in nozzles
- estimated icebreaking capability $0.8 \text{ m} / 1.5 \text{ m/s}$
- hull form made from flat surfaces, not tested in ice
- during the ice trials the vessel could make only $0.5 \text{ m} / 1.5 \text{ m/s}$

Task no. 1

Prepare a research program to study the question what should be changed for the next vessel with similar features

Research program

- 1) Open water overload tests
- 2) Towing tests in ice
(one speed, one icethickness)
- 3) Propulsion tests in ice
(one speed, one icethickness)
- 4) Compute η_D , η_i , P_E ; P_D
- 5) Modification of the model
- 6) Repeat 1) to 4)

Calculation examples

Exercise 2

$$\eta_0 = 0.24$$

$$R_{tice} = 920 \text{ kN}$$

$$R_{sp} = 1470 \text{ kN}$$

$$Q_{ow} = 400 \text{ kNm}$$

$$Q_{tice} = 800 \text{ kNm}$$

$$\eta_i = \frac{1 - \frac{\Delta R}{R_t}}{1 + \frac{\Delta Q}{Q}}$$

$$\eta_i = \frac{1 - \frac{550}{1470}}{1 + \frac{400}{400}} = 0.31$$

$$\begin{aligned} \Delta R &= R_t - R_{tice} \\ &= 1470 - 920 = 550 \end{aligned}$$

$$\begin{aligned} \Delta Q &= Q_{tice} - Q_{ow} \\ &= 800 - 400 = 400 \end{aligned}$$

$$P_D = \frac{P_E}{\eta_i \times \eta_0} = \frac{920 \times 1.5}{0.31 \times 0.24} = 18548 \text{ kW}$$

Exercise 3

$$\eta_0 = 0.18$$

$$R_{tice} = 830 \text{ kN}$$

$$R_{sp} = 963 \text{ kN}$$

$$Q_{ow} = 385 \text{ kNm}$$

$$Q_{tice} = 460 \text{ kNm}$$

$$\eta_i = \frac{1 - \frac{963 - 830}{963}}{1 + \frac{460 - 385}{385}} = 0.72$$

$$P_D = \frac{P_E}{\eta_i \times \eta_0} = \frac{830 \times 1.5}{0.72 \times 0.18} = 9606 \text{ kW}$$



SHIPS AND STRUCTURES IN ICE

Propulsion Machinery Selection on Icebreakers

by

Jarmo Laakso

PROPULSION MACHINERY SELECTION ON ICEBREAKERS

1 INTRODUCTION

Due to the expansion of maritime trade into the arctic and antarctic waters even requiring year-round service, one has to pay more and more attention to the selection of propulsion machinery in the design of new vessels. The main machinery of the vessel is a vital element of the whole that ensures the successful maintenance of transportation in more and more tasking environmental circumstances.

During the last few years there has been a tremendous development in the propulsion machineries of icebreakers and icegoing cargo vessels, and besides pursuing technically more and more feasible solutions, a great attention is being paid to the overall operational economy of the vessel. Heavy fuel oil has become the standard fuel for all kinds of vessels, conventional solutions in auxiliary systems have had to give way, reserve systems have been added, the contents of harmful impurities in fuels have been increased, engine/propeller optimization has become the keyword of today, the power ratings of engines are reduced because of better fuel economy, scavenging air and cooling systems have been altered, etc.

The traditional special requirements laid down by navigation in ice for the propulsion machinery are to be added to what has been presented above, as for instance:

- full propeller power at every ship speed, i.e. adequate icebreaking capacity
- permanence of propeller speed when subject to ice loads
- strength of shaftline components in ice, dimensioning
- shallow water below the keel
- change of direction of short duration, many reversals
- stepless power control, ahead/astern
- protection of main machinery from overload
- cold suction air and sea-water
- supply of sea-water for cooling
- large shaft movements in sterntube seals.

Moreover, when conventional comparison criteria of the propulsion machinery, weight, space requirements and price as well as today's experience on winter navigation are considered, the establishment of a machinery solution for a demanding icebreaker project is not a simple task. The solution is always a compromise.

2 HISTORICAL BACKGROUND

Through the ages the typical icebreaker machinery has employed a diesel-electric system combined with a fixed-pitch propeller. As a direct-current application equipped with separate auxiliary machinery, it met with favour on all the seas in the 1950's and 1960's. To the joy of mechanics and electricians, the development of semi-conductor technology in the 1960's and 1970's made it possible to shift from direct-current generators to applications utilizing alternating current generators for propulsion. At the initial phase the regulation of the propulsion machinery was taken care of by diode rectifiers, in which case a separate auxiliary machinery was still needed for the electric network of the vessel.

The introduction of thyristor rectifier control for regulation of the direct-current motor enabled the use of the so-called power plant principle on ships whereby the main engines turned capable of satisfying both the propulsion power and the auxiliary power demand of the ship. Hence, the separate auxiliary diesel engines could be eliminated.

The electric engineers did not, however, stop here to wait for the product development in icebreaker design to gather experience of the solution in full scale, but soon introduced a new invention. Towards the end of the 1980's, the power plant principle will totally employ the alternating current machinery regulated through static frequency converters. The first installations on ships are being done at the moment, and after completion of the tests on the control system, the break-through of this system will only be a question of time.

Since the mid 70's there has, however, been a growing tendency to use a reduction gear - controllable pitch propeller application on icebreakers. This can be seen as a natural development as the experience of icegoing vessels is increasing, the methods of calculation and dimensioning have improved and the trends regarding propulsion machinery development presented earlier are being taken into account.

In addition, the vessels are frequently designed for both open water and icebreaking service which often causes the design criteria to conflict with each other, but the machinery with controllable pitch propeller offers an excellent compromise. Nowadays diesel engines almost exclusively are used as main engines in icebreaker applications for both electric and reduction geared machineries.

The compromising solution may seem very simple as far as the design and the operating of the ship are concerned, but it may in practice turn out to be rather troublesome as one machinery is principally supposed to meet the requirements set on two separate machineries. Various surprises will be everyday life on the yards during the design and starting-up stages of the new machineries.

3

DIESEL-ELECTRIC MACHINERY OF POWER PLANT PRINCIPLE

As advantages of the machinery employing the power plant principle can be mentioned, among others, the following:

- any one of the diesel engines can be engaged to the propeller together or separately
- onboard the ship there are diesel engines of one type only
- the damage or maintenance of any one of the diesel engines does not significantly affect the operation of the ship
- the power control of the propeller motor is fully stepless
- the number of diesel engines utilized can be freely selected and optimized
- full power to the propeller motor is attained over the whole speed range of the ship
- torque characteristics
- simple construction of the shaft line
- diesel engines rotate at a constant speed
- free location of the main engines
- fixed-pitch propeller.

At least the following disadvantages must also be mentioned:

- low efficiency of the machinery
- large space requirement and weight
- high price
- additional demand for crew.

A really interesting alternative for the ship's propulsion is offered by the frequency converter controlled alternating current motor. The regulation and behaviour of the motor as the source for icebreaker propulsion is fully corresponding to the characteristics of a direct-current motor. An equivalent torque curve can be accomplished with its good reversing characteristics.

A synchronous motor is by its construction considerably simpler than that of the direct-current motor; the lack of brushes reduces the need for maintenance decisively and the efficiency of the motor is improved by a few per cent.

There are already synchronous motor installations for low-power frequency converter applications and for even high-power controllable pitch propeller applications with constant speed. A frequency converter controlled synchronous motor will seriously be considered for propulsion in following icebreaker projects.

4 DIESEL - REDUCTION GEAR MACHINERY WITH CONTROLLABLE PITCH PROPELLER

When the propulsion machinery consists in general of a greater number of diesel engines coupled to the same gearbox, the most essential component for the faultless operation of the shaft line is the flexible clutch coupling combination, the selection of which for an icegoing vessel is to be made with greatest care. Besides the clutch having to be engageable and disengageable with the engine running, one has to take the following selecting criteria among others into consideration:

- torque and speed of the main engine
- minimum and maximum speeds of the main engine
- torsional vibrations
- movements of the engine and the gearbox in relation to each other, compensation values for thermal effects
- overdimensioning of the clutch coupling due to ice loads
- calculations for engagement and disengagement procedures
- weight of the clutch coupling.

When selecting a reduction gear for a propulsion unit on an icegoing vessel and on an icebreaker, one has to pay attention to the following items among others:

- construction of gear wheels
- tothing
- method of production
- rigidity of the gear body
- fastening to the foundation and deflections of the ship's hull
- factors for dimensioning
- location of the thrust bearing.

Due to the often relatively short and thick shaft line on icebreakers, a great attention is to be paid to the selection of sterntube bearing, particularly with regard to the reduction gear machinery. The possible wear-down of the water lubricated sterntube bearing leads to risks regarding the bearings of the gear bullwheel. Therefore, the oil lubricated bearing is in many cases the only alternative for sterntube bearing in reduction gear application.

There are, however, owners who insist on using water lubricated sterntube because of certain security risks. In order to eliminate leakage from sterntube, the seals must be selected so as to allow for all the shaft movements arising from navigation in ice and from vibrations without leaking. Moreover, the seal is to be protected with a reliable rope guard in the aft end.

The experience of the controllable pitch propeller on icegoing vessels and icebreakers as well as the numerous viewpoints of the advantages brought about by it have made the reduction gear-controllable pitch propeller solution more

and more popular. The measurements carried out in full scale and the development of calculation and dimensioning methods during the last 10 years have improved the strength of the controllable pitch propeller so that it can entirely safely be used in ice.

However, there are different propeller constructions, some of which are not applicable for icebreaker use. Furthermore, no propeller maker today has the means of reliably using the controllable pitch propeller as a fixed pitch propeller in case it is damaged. The automatic load control system for protecting the main engines from overload and the possibility of changing the propeller blade under the water surface make the controllable pitch propeller an equal competitor of the fixed pitch propeller in this respect, too.

5 ON SHAFT GENERATORS

On icegoing vessels and even on icebreakers it is becoming more and more common to equip the reduction gear machinery with a shaft generator which is used to supply the auxiliary power of the vessel.

Without going deep in the analysis of disadvantages and the development of technology, the shaft generator installation is often justified only by the lower fuel consumption of the main engine, cheaper fuel for the main engine and the minimization of the number and running hours of the engines utilized.

Today auxiliary diesel engines can burn the same heavy fuel oil as the main engines, and there is no great difference in fuel consumption either.

A shaft generator installation can be considered justifiable on a newbuilding if it serves to eliminate one or several auxiliary diesel alternator aggregates, if the shaft generator is cheaper than a separate auxiliary diesel alternator unit, if there are distinctly separate auxiliary power consumers onboard and, first of all, if the utilization of the shaft generator does not weaken the good efficiency of the propulsion machinery.

On an icebreaker the greatest demand for propulsion and auxiliary power is encountered during operation in ice. Due to the fluctuations in the propeller speed during ice operation, the use of a shaft generator as a supplier for the auxiliary network is very questionable. Therefore, the number of the vessel's auxiliary diesel engines cannot be reduced even if the shaft generator were installed.

The economy of the shaft generator in open water conditions is also greatly dependent on the operational profile of the vessel. If the shaft generator solution is not suitable for the operational profile, the annual fuel consumption of the main and auxiliary engines might end up 10 % higher than that using separate auxiliary engines. During operation at constant speed, both the propeller efficiency and the fuel consumption of the main engines are more unfavourable.

Adding to the above disadvantages the possible clutch and alignment problems that may be caused by the shaft generator, and the vibrations and additional loads caused by ice, there is good reason for considering the total elimination of the shaft generator on icegoing vessels.

6

ON STERN TUBE ARRANGEMENTS

Depending on alternative machineries, one often ends up in different stern tube arrangements: in a machinery fitted with a reduction gear, sometimes only an oil lubricated stern tube is possible, whereas in electrical machineries both water and oil lubricated bearings may be used, depending on the calculation of the shaft line reaction forces. With regard to an icebreaker application, the following factors related to the selection of the stern tube are worth emphasizing:

- both bearing alternatives have a certain lowest permissible continuous shaft speed
- both alternatives to be equipped with a reliable rope guard and a cutter arrangement
- for a water lubricated bearing it is possible to arrange direct sea-water flushing in case of the aft seal being damaged

- for water lubricated bearing a repair of the forward seal can be carried out at sea
- for water lubricated bearing a possible bearing damage does not immediately damage to the shaft
- a water lubricated bearing is sensitive to wear and tear, the wear down is to be taken into account in the shaft alignment, the maximum wear down is defined by rules and limited by technical aspects
- a water lubricated bearing is of considerable length, permitting lower surface pressures
- a water lubricated bearing is a more expensive solution, also regarding operation
- the flushing system of a water lubricated bearing is a complicated one, except when flushing through
- the lubrication capacity and the circulation is to be ensured also at low ambient temperatures
- a water lubricated bearing calls for more inspection and maintenance
- an oil lubricated bearing is always leaking some oil into the sea
- there is plenty of operational experience of both solutions on icebreakers.

7

ON CONSTRUCTION OF FIXED PITCH PROPELLER

In the propeller arrangement of a diesel-electric machinery there are two main constructional alternatives to choose from, fastening on a keyed cone or on a flange coupling. In both versions there is a possibility of changing a broken blade underwater, the possibility being necessary for an icebreaker in independent winter navigation service. Only small propellers are of monoblock construction. A keyless conical coupling in an icebreaker propeller does not guarantee adequate safety in operation.

The pros and cons of the conical fastening with key can be specified as follows:

- the shape of the hub is favourable in terms of casting techniques
- there are wide experiences of the construction
- special tools are needed for assembling and dismantling the propeller
- fretting corrosion occurs frequently on conical coupling faces

- a keyway weakens both the propeller hub and the shaft
- the machining of the cone and the keyway and the fitting work of the cone both during construction and possible repair work is an arduous task.

A corresponding list can be presented for a flanged coupling:

- the flange of the tailshaft requires a big forge and machine shop
- fastening bolts and dowels are to be manufactured and fitted
- symmetrical construction is favourable in terms of strength
- tailshafts and spare tailshafts are shorter and lighter in weight
- the propeller is lighter
- a similar solution has been realized with controllable pitch propellers

8

ON DIMENSIONING OF PROPULSION MACHINERY

When selecting the dimensioning criteria for the shaft line components of an icebreaker, all the factors affecting the magnitude of ice loads are to be analysed, those being among others:

- ice conditions
- draught of the ship
- hull form
- propeller immersion
- propeller diameter
- length of the ship
- number of propellers
- ship speed
- depth of free water under the keel

The effect of the aforementioned parameters on the dimensioning criteria can only be obtained by many year's experience in designing icebreakers, performing measurements in full scale and in model scale on as numerous and different icebreakers as possible and by developing new methods of calculation.

The dimensioning of the icebreaker propulsion shafting is accomplished normally in accordance with both shock loads and continuous fatiguing ice loads. Additionally, the requirements of the classification societies are to be taken into account.

It is of great importance to find the right dimensioning criteria for the propeller blade, components of the hub, shafting and its couplings, bearings (thrust + support), gearing, clutch couplings and seals.

The analysis of the shaft line vibration modes goes side by side with dimensioning, which, as far as icebreakers are concerned, requires a careful observation of the propeller induced ice excitations already at the project stage so as to avoid fateful surprises during ice trials.

With regard to the torsional vibrations, the selection of a wrong flexible coupling, omission of a certain operation condition or the implications of heavy fuel oil can lead to troublesome consequences for example through reduction gear hammering, clutch coupling damage, shaft line fatigue or propeller cone fretting corrosion. In the same way, the underestimation of the axial vibration can destroy the thrust bearing, sterntube seals or the tooth rim of the gearbox, and the strong ice excitations on the propeller can through a possible whirling vibration resonance cause problems as to tightening of sterntube seals, thrust bearing or fatigue strength of the shaft material.

9

PERMANENCE OF PROPELLER SPEED

It is important for an icegoing vessel to be capable of maintaining maximum propeller thrust when the propeller complex is subjected to ice loads, thus securing the smooth advance of the vessel in an ice field. Thus it is essential that the propulsion machinery has sufficient capacity to be able to run at maximum speed and develop full power all the time so as to minimize the risk of the propeller fully blocking. Regarding the propeller speed keeping capability of the propulsion machinery, its thrust and permanence of power output, the fundamental parameters having influence are as follows:

- magnitude of ice load
- duration of ice load
- intervals between ice loads
- total mass moment of inertia of the shaft line
- load control automation of the propulsion machinery
- torque capacity of the propulsion engine.

A comparison of the propulsion machinery alternatives in similar environmental conditions with regard to the permanence of the propeller speed is possible with the aid of a computer simulation programme developed by the yard. In addition to the parameters listed above, this programme uses as input data among others the following:

- characteristics of the diesel engine turbocharger
- characteristics of the diesel engine speed governor
- propeller geometry and hydro-dynamics.

The poorer torque capacity of the reduction gear machinery compared to the diesel-electric one can be compensated e.g. by the excessive main engine power rating, increased mass moment of inertia on the shaft line and the advanced load control system for the controllable pitch propeller. Thus under instantaneous dynamic loads the characteristics corresponding to the electric machinery can be effected. On the other hand, when the load is big and of long duration, there is a certain risk of bringing the geared propulsion machinery to its knees. Breaking the blocked propeller loose from the ice requires special action as far as the reduction gear machinery is concerned, whereas the propeller driven by electric motor can simply be broken loose by utilizing the greater torque capacity of the motor.

10 ON ANCILLARY SYSTEMS OF PROPULSION MACHINERY

10.1 Fuel Oil

Along with the development of the fuel price, the heavier fuels (1500-3500 SRI/100°F) have been adopted also for icebreaker engines. However, the fuel system of an icebreaker has in general also provisions for using diesel oil in regions where it is impossible to get heavy fuel.

Today operation on heavy fuel oil from pier to pier is aimed. At the same time new difficulties have emerged with the systems, for instance:

- inadequate burning of the fuel
- temperature optimization of the system liquids for the engine
- plenty of impurities in fuel
- varying fuel quality in different parts of the world
- high feeding temperature of the fuel
- problems of centrifuging, high specific gravity
- cavitation of feed pumps
- maintenance of the engine temperature, also in port
- driving the engine at low power
- need for heating the scavenging air
- high temperatures of tanks, etc.

Because of the special requirements related to an icebreaker machinery, such as numerous reversals, rapid load acceptance capacity etc., the introduction of heavy fuels for the icegoing fleet will not take place as rapidly as for normal merchant shipping.

10.2

Cooling System

An icebreaker using heavy fuel oil and intended for service in arctic conditions is to be equipped with a centralized cooling system. This is still more important if the vessel will operate in shallow waters, e.g. in estuaries, where sand and mud may penetrate into the cooling water system.

A central cooling system helps to create the adequate temperature of the cooling water and scavenging air and guarantees the proper burning of the heavy fuel oil even at low loads. In order to maintain the temperature in the scavenging air manifold, some engine manufacturers started to use a two-stage scavenging air cooler. To attain analogous function, a two-circuit cylinder cooling system has been employed in the Wärtsilä Vasa engines in a heavy fuel application. The risk of the scavenging air cooler getting frozen at low loads can also be prevented.

A special attention has to be paid on the risk of the cold suction air causing the surging of the turbocharger and the increasing cylinder pressures. These effects can be eliminated by passing part of the scavenging air back to the suction side of the compressor through overflow valves in the scavenging air manifolds.

11 OTHER COMPARISON POINTS OF VIEW

In addition to the criteria presented above, essential parameters having influence on the decision of the machinery solution are:

- annual fuel consumption
- total price of the machinery
- space requirement of the machinery
- influence of the machinery on the ship's principal dimensions
- weight of the machinery
- influence of the machinery on the general arrangement
- need for, and quality of, the crew required by the machinery
- installation and design costs
- availability of spare parts, service organisation
- life time of the machinery
- experiences of the subcontractors by the yard and the owner
- need for training of the crew
- operational principles of the owner
- domestic components

12 SUMMARY

When selecting the propulsion machinery for an icebreaker, the numerous positive and negative factors involved in every alternative must be carefully considered. Furthermore, there are certain compulsory requirements that must be fulfilled by the machinery in any case. Based on the experiences of the owner and the yard, the greatest emphasis is often laid on the simplicity of the propulsion machinery, proven technology, absolute reliability and suitability for fully independent navigation in ice.

In principle the same selection criteria are applied on all installations, but the relative value of different criteria varies with each installation. The owner is always compelled to make the final decision, and the yard together with the subcontractors must be able and ready to provide as objective information as possible. For an icebreaker the reliable operation of the propulsion machinery is the only guarantee for succeeding in the task it has been given. If an icebreaker is damaged, it may take several weeks to get help. By then the vessel may have been wrecked.



Senior Surveyor Lasse Norhamo

MACHINERY DAMAGES

0. BACKGROUND

Damage statistic presented in this paper is based on the analysis of damage history of 226 ships during a four years period starting from 1 November 1978. All together these ships have 450 winter seasons in the Northern Baltic ice conditions. Common features for these ships are Finnish ice certificate at least once during this period and Det norske VERITAS class, which have been the accept criteria into this study.

Information about actual ice conditions and duration in ice have not been available. It shall also be noticed that the ice certificate itself is not an evidene that the ship have been in ice, even if it is the most likely.

Finnish ice class certificate is issued only for the ships calling at Finnish ports. The certificate is valid for one winter navigation season (1st December - 30th April) and is issued not before the 1st November.

These 226 ships represent all kind of commercial tonnage with or without ice strengthening. About ten (10.6) percent of the ships are twin screwed. Ships in the ice class 1A are the largest group both in number (32%) and even more dominating when correlated to number of winter seasons (38%).

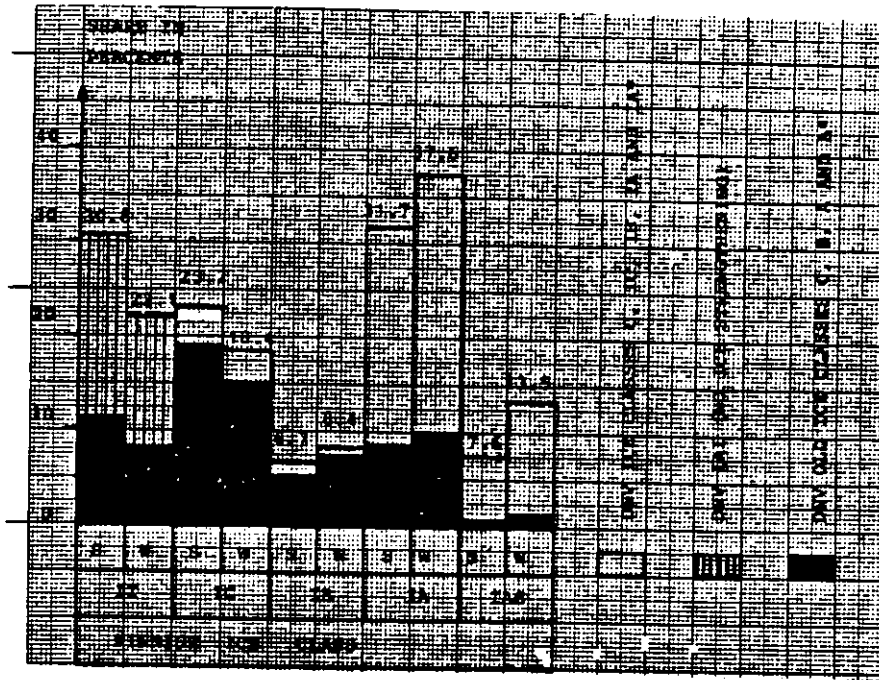


FIGURE 1
Number of Ships (S) and number of winter season (W)
versus Ice Class and Effect Group

In the figure 1 there are shown distribution of the ships and winter seasons versus DnV ice class and Finnish ice class respectively. Shaded part in each column represent "old" ice classes in DnV. It must be noticed that the ships built to the old ice classes are accepted into the respective Finnish ice class only when class drawings are approved not later than 1st May 1971 and that the ships are delivered not later than 1st January 1978.

Majority of the ships in Finnish ice classes IA and IAS are "new" and built to DnV's ice classes IA and IA* accordingly. In the ice classes IC and IB the majority of the ships are "old" and built to ice classes C or B accordingly.

Damage data used in this study have been obtained from VERITAS damage data bank for machinery damages.

All kind of damages reported during actual year(s) in ice starting on 1st November plus one following year are recorded. This means that the shortest searched period have been two years. However, for vessels having valid ice certificate in the season 1981/82 the reporting period was cut on 1st November 1982. For the group diesel engines the follow up period have been shortened with one year due to type of damages. Damage rate is represented then together with "world scale" damage rate in the same period. The world scale is based on the total VERITAS fleet in service. The damage rate is consequently not to be regarded as ice damages, but more as damage susceptibility of propulsion machinery on board the vessels operating in the Northern Baltic ice condition versus all vessels in world wide service.

1. PROPELLERS

The total number of propellers in "ice service" have been 250 representing totally 655 machinery years. In **figure 2** are the propellers are divided into two groups, fixed pitch (FP) and controllable pitch (CP) propellers and into three power groups according to propeller rating. In **figure 3** the same is shown for propellers in the world scale. CP-propellers are a clear majority (77%) on board the vessels with ice certificate. It might also be worth to notice that about 25% of all machinery years of large CP-propellers are found onboard these 226 vessels.

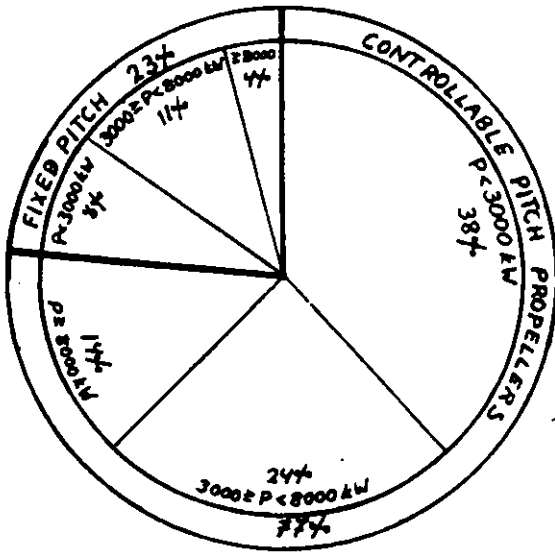


FIGURE 2
Propellers according to type
and effect group
(Totally 655 machinery years)

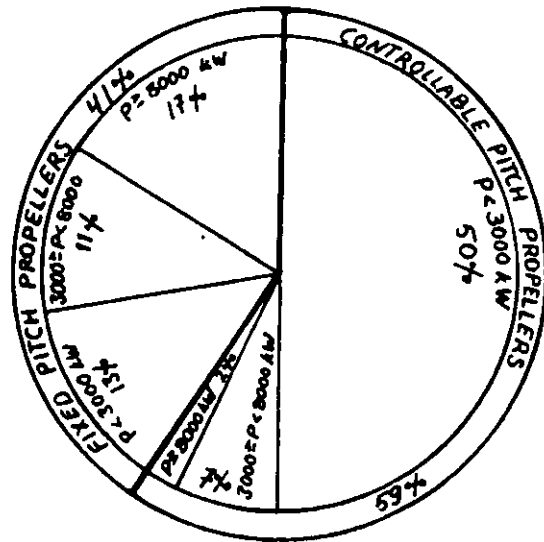


FIGURE 3
Propellers according to type
and effect group - world scale
(Totally 18200 machinery years)

In figures 4 and 5 there are distribution of FP- and CP-propellers shown versus Finnish ice classes and machinery years. There is no FP-propeller in the ice class IA Super. Nearly 70% of FP-propellers are found in the ice classes II-IC versus 35% of the CP-propellers.

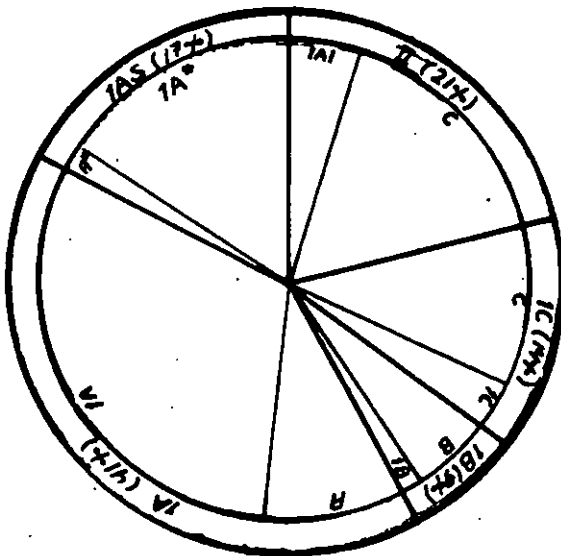


FIGURE 4
Controllable pitch propellers
according to ice class
(Totally 504 machinery years)

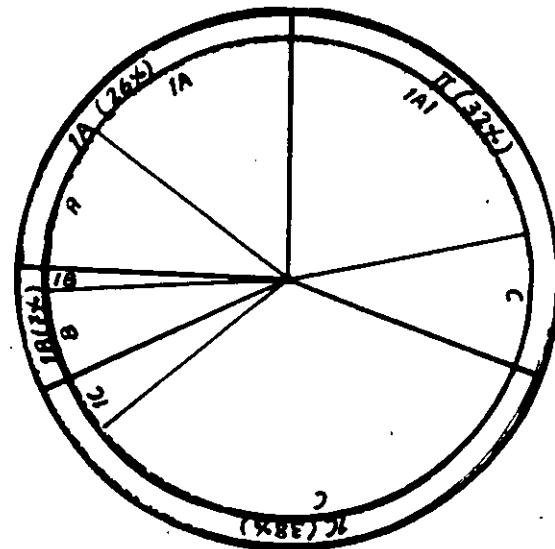


FIGURE 5
Fixed pitch propellers
according to ice class
(Totally 151 machinery years)

Stainless steel blades are found in 50% (56%) of searched CP-propellers and only 10% (4%) of FP-propellers. The figures in parantheses refer to machinery years.

Damage rate of FP- and CP-propellers versus ice class and effect group are shown in the figures 6 and 7 respectively. World scale damage rates are given for each group respectively. Shaded portion of the columns represent damage rate exceeding the world scale rate.

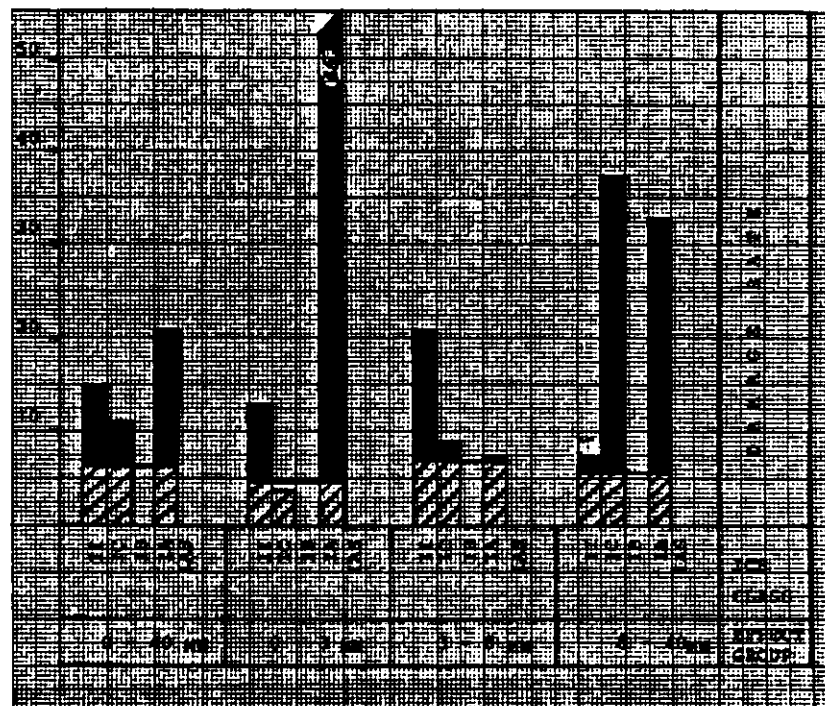


FIGURE 6
Fixed Pitch Propellers -
Damage Rate versus Ice Class and Effect Group

Average damage rate of FP-propellers is 14%. Damage rate of FP-propellers in the power group P < 3000 kW is very high in the ice class 1A. This is partly explained with only 8 machinery years and many damages on one propeller. This propeller, diameter 3.9 m, has old ice class A. The

power group $P \geq 8000$ kW shows also severe damage rate in 1C. This, however, should be representative and severe damage rate is also recorded in the ice class 1A. In this group only one damage has been recorded and consequently the figure is not representative for the ice class 1A. The damaged 1C propellers are all designed to old ice class C, where ice strengthening is based on per centage increase of blade thickness .

Damages on FP-propellers with ice classes C-A* have been recorded in 62% of the cases and for the propellers with ice classes 1C-1A* in 14% of the damage cases. Damage rate of old versus new ice classes 17% versus 3%.

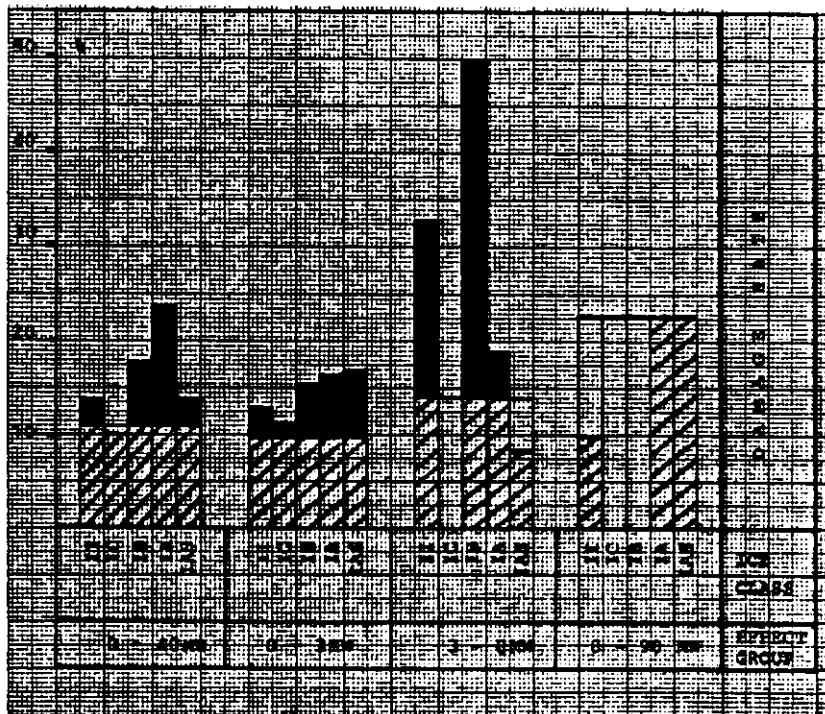


FIGURE 7
Controllable Pitch Propellers -
Damage Rate versus Ice Class and Effect Group

The average damage rate for CP-propellers is 16%. Of all damages recorded for CP-propellers 29% is in ice classes C-A* and 53% in ice classes 1C-1A*. Corresponding damage rates are 17 versus 16%.

Damage rate of FP- and CP-propellers is 17% versus 15% for ships in Finnish ice classes 1C or higher.

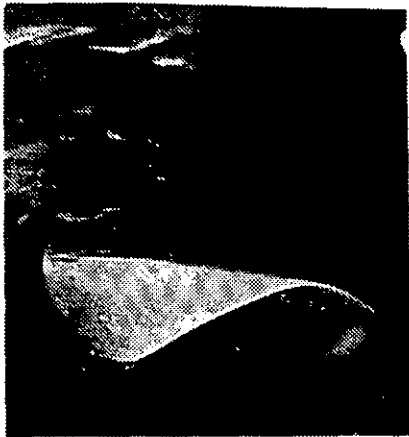
The damage rate is generally higher than for FP-propeller, increasing at increasing rate. Average world scale figures are 10% for CP-propeller versus 64% for FP-propeller. Damage rate for CP-propellers is more representative. However, in the power group $P \geq 8000$ kW ice class 1A damage rate is remarkably increased due to damages on highly scewed propellers, however, still not above the world scale.

In the figure 8 there are different types of damages presented in per cent of recorded damages.

Part	DAMAGE TYPE				
	Cracked	Fractured	Bent/ deformed	Cavitated/ eroded	Other
Blade tip	3	4	14	4	2
Blade	2	2	4	3	<1
Blade root & conn. to boss	5	3	<1	2	<1
Boss		<1	2	<1	3
Other	<1	5	4	2	22

FIGURE 8
Propeller damage types in per cents of total

Propeller blade is bent in 18% of all damage cases, however, in most cases at blade tip area. Propeller blade material, bronze versus stainless steel does not seem to have the expected influence. Bentpropeller blades are found as well in the bronze as stainless steel blades. It looks like stainless steel blades have even been more susceptible for being bent than NiAl-bronze blades. This is a somewhat surprising conclusion when taking into account that the yield strength (0.2%) relationship between bronze and stainless steel is in favour of stainless steel and that stainless steel blades are generally thicker than NiAl-bronze blades.



A picture of a damaged propeller blade which is heavily bent at the blade tip. Propeller diameter, 4.75 m, rating 5900 kW at 150 RPM material mangan bronze, no ice class.

2. SHAFTING

In the figure 9 there is shown the damage rate of shafting versus power group and ice class. As for the propellers world scale damage rate is given in each power group. Severe damage rate in the power group $P < 3000$ kW is not representative due to only few machinery years.

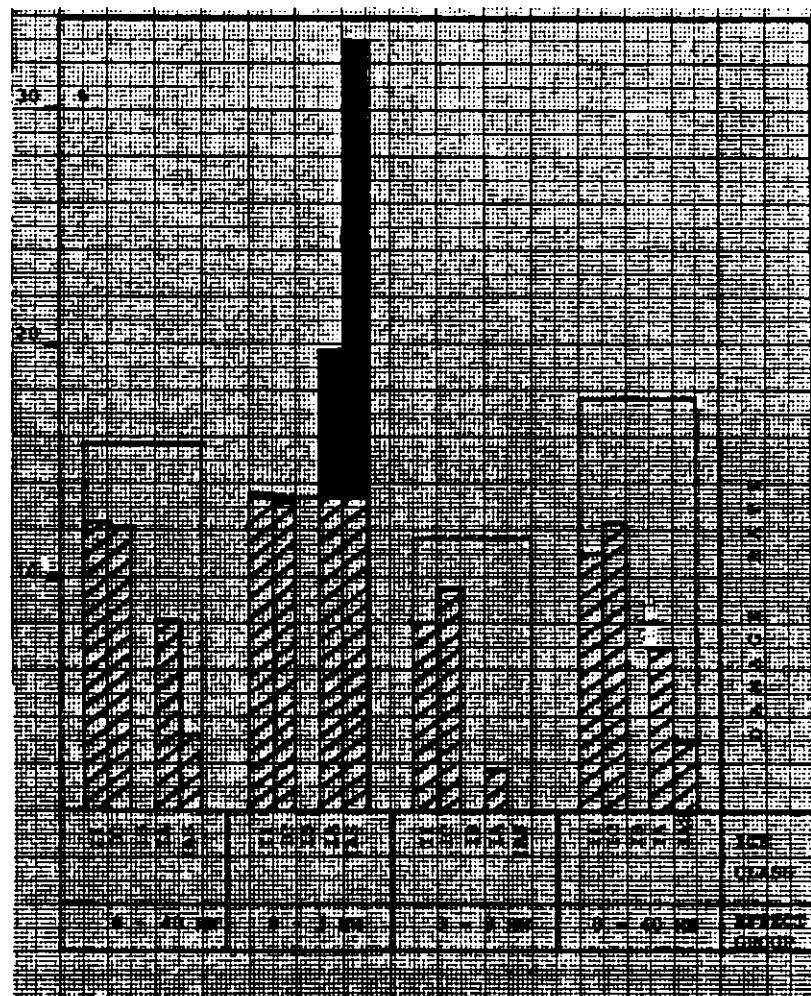


FIGURE 9
Shafting: Shafts, Bearings & Sealings
Damage Rate versus Ice Class and Effect Group

Average damage rate is 9.0%. The damage rate is generally below the world scale, except as mentioned above. About 50% of the recorded damages are found in outer- or inner stuffing boxes. In only two cases screw shaft have been bent. In both of the cases the propeller blade have also been bent. Blade materials have been NiAl-bronze and stainless steel respectively. One of the cases (NiAl-bronze blade) is caused by grounding. In such cases bending of screw shaft may be expected even if progressive strength is applied according to ice regulations. The actual ice classes were II (DnV's C) and IC (DnV's "old" C). Progressive strength principle have not been applicable for these ice classes.

Further there are found cracks in screw shafts in two cases and in one case screw shaft has fractured and the propeller lost. This vessel had a 3-bladed FP-propeller, diameter 1.75 m, and ice class "old" C.

3. MAIN REDUCTION GEAR

Total number of machinery years (366) represent about 55% of the respective figure for the propellers. As shown in the figure 10 the most of the years are found in the ice class 1A (33%) and in the class II (23%).

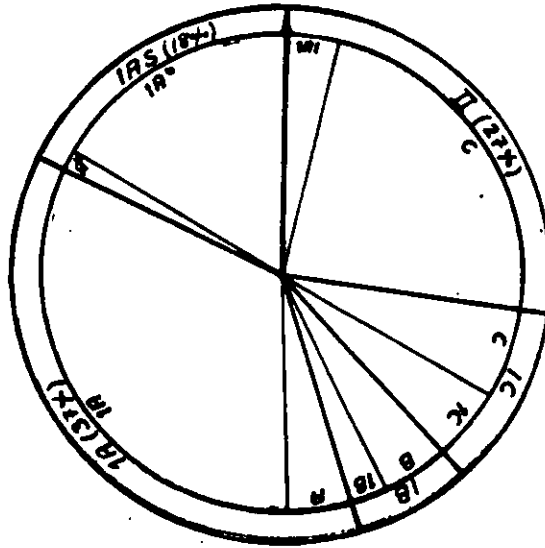


Figure 10
Main reduction gear according to ice class
(totalling 366 machinery years)

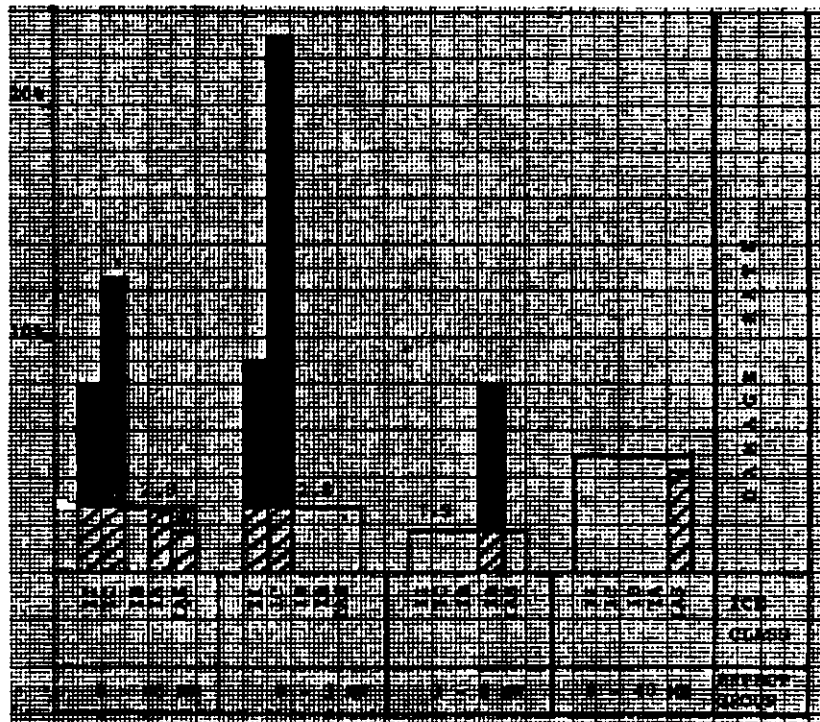


FIGURE 11
Main Reduction Gear -
Damage Rate versus Ice Class and Effect Group

Average damage rate is 5.5%. Damages in main reduction gears are concentrated in the two lowest ice classes and in to the lowest power group. Average damage rate is 5.5%, which is about 3% above the world scale. Damage rate decreases at increasing rating for the searched group of the reduction gears. Damage rates are 7.7 (2.8), 3.9 (1.9) and 1.8 (4.8) in the effect groups below 3 MW, 3-8 MW and above 8 MW. World scale damage rates are given in parantheses.

The gear damages in the two lowest ice classes are in the reduction gears, where ice strengthening is not required. Further the damages are concentrated to very few gears and are not generally representative.

4. MAIN DIESEL ENGINES

Main diesel engines are normally kept outside ice rules, except that concerning minimum output. Accordingly ice damages are not expected on this machinery part.

In the figure 12 there is number of diesel engines versus ice class shown.

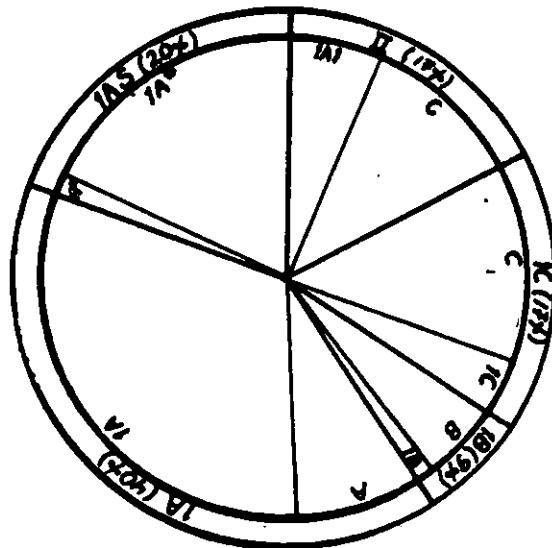


FIGURE 12
Diesel Engines according to Ice Class

Diesel engines damage rates versus ice class and power group are shown in the figure 13. World scale damage rate for each power group is given.

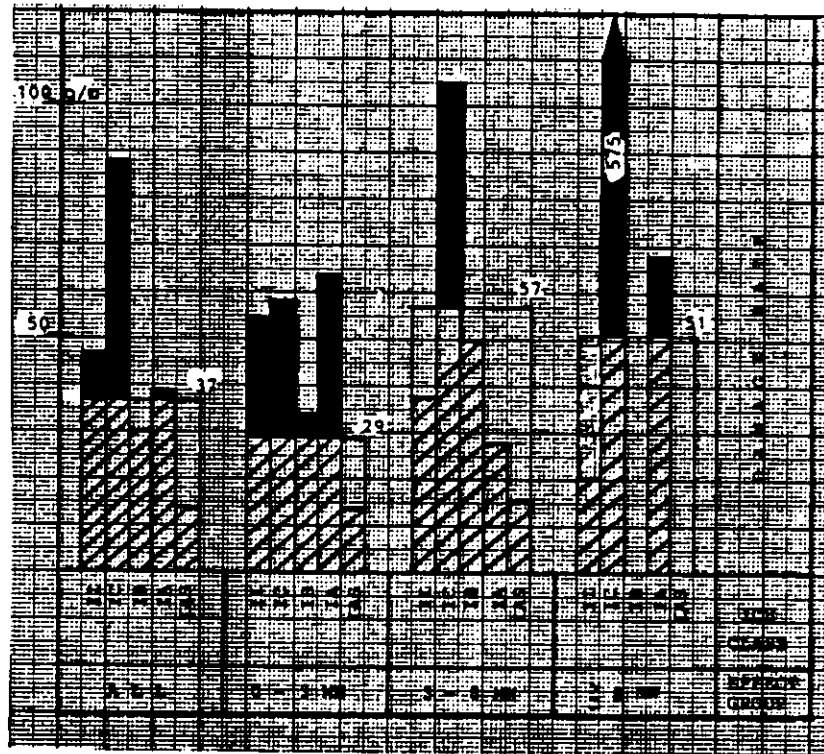


FIGURE 13

**Main Diesel Engines -
Damage Rate versus Ice Class and Effect Group**

Damage rate for diesel engines in the two lowest ice classes exceeds world scale rate remarkably. The same is valid also for 1A vessels in the lowest power group. This may be explained by usually low power and consequently a constant need to overload the engine in ice conditions.

Damage rate 57.5% of the power group ≥ 8 MW, ice class IC, is not representative due to only few (4) machinery years.

Most of the damages (39%) are found in the cylinder group (cylinder liner, piston, cylinder cover with valves). Almost 40% of these damages are cracks or similar. Bearing damages in crank shaft line show a damage rate of 12%. Exhaust turbo chargers are also represented with 12% damage rate.

Damage rate in the old ice classes C-A* is 70% versus 28% in the ice classes 1C-1A* related to the corresponding machinery years. Average damage rate for main diesel engines is 43%.

5. COMMENTS

Reliability of the damage statistic may be questionable in some cases. The statistical damage data for the propulsion machinery have also in many cases revealed a lack of generality. In order to obtain a more reliable statistical basis number of installations (years) must in these cases be larger.

The value of statistical data would also increase, if it could be supplied by and related to machinery time in different ice conditions.

Damages in ice conditions are also in many cases related to an operational "user" factor. Influence of this, probably an important factor, is not possible to take into account. The user factor influence could be studied in smaller groups of similar (sister) vessels operating in same ice conditions.

The ice damage statistic indicates that damage susceptibility of propulsion machinery is above the "world scale" in two groups, propellers and main diesel engines. On the other hand, vessels with ice class 1A Super are generally less susceptible to damage than other vessels operating in ice and these vessels also have damage rate well below the world scale, except for small CP-propellers.

Ice class 1B seems also to be a favourable ice class. It must, however, be noticed that there are only few "new" vessels in this ice class and that the statistic is most representative for the VERITAS old ice class B.

The statistic indicates that the CP-propeller damage susceptibility is equal to the propellers designed according to new or old ice classes. For the FP-propellers this trend is in favour of new ice classes. If the damages gained in the highly scewed CP-propellers are excluded, the damage susceptibility is turned in favour of the new ice classes.

Much higher damage rate of the main diesel engines in the old ice classes may be partly explained by higher average age of the engines in this group. Another negative factor is output of propulsion machinery versus ship size. Propulsion power per displacement of ship is in disfavour of the old ice classes. Diesel engine damages in ice conditions may in many cases be related to thermal overloading of the vulnerable components.

REFERENCES

1. Lists of the ice certificates of VERITAS classed ships, Finnish Board of Navigation
2. Machinery damage historical data, Det norske VERITAS, SPRINT-3 system.



Notes on Rudders and Steering for Ice Transitting Vessels

by P.G. Noble

Introduction

Maneuverability in ice represents a set of parameters of a ship on which depends its capacity to turn, stop, change direction, etc. The maneuverability of an icebreaker is very important since the performance of most of its basic missions depends on it. This is especially true for ramming in heavy ice, escorting of ships through ice fields and for the clearing of port facilities and other ice management duties. In the performance of these operations, an icebreaker must continually turn in the ice, back up, ram, etc.

Turns in ice are performed by turning as in normal open water with the rudder over, or by "herring bone". Normal turning is done by putting the rudder over, without ramming and without changing the mode of operation of the vessel. Turning by "herring bone" is accomplished with the aid of several maneuvers which lead to successive rams of the icebreaker into the ice with the bow and stern or with the bow only. Such maneuvers are accomplished by reversing the screws in combination with turning the rudder. The more serious ice conditions are, the larger the number of maneuvers is required to make one herring bone turn; therefore the more time is spent in turning. Maneuvers that are accomplished by an icebreaker during freeing of a non-icebreaking transport vessel stuck in the ice include both normal turning and herring bone turns.

The requirements imposed on the maneuverability of an icebreaker during ice navigation are extreme and diverse. Ice conditions substantially

complicate calculations of maneuverability characteristics as with the calculation of level ice resistance. However, analysis of maneuverability in ice is presently under development and some full scale data is available.

Directional stability is not as important for an icebreaker as maneuverability. Stability is of practical importance only for large icebreakers which are designed for leading convoys of ships over long distances and which also make long transits in open water from base to regions of ice operations. Most auxiliary and medium icebreakers rarely make such voyages since they are usually assigned to ports that are located in the immediate vicinity of their zone of operation.

The course keeping stability of an icebreaker during navigation in ice conditions is determined chiefly by the process of interaction between the hull and the ice. The basic feature of this process is its random character which is attributed to the non-uniformity of the ice cover and to the random character of forces contact between the hull and the ice. Since the properties of ice change from time to time, variations of these parameters on the motions of the icebreaker in ice are random and the deviations from the average values may be quite large. These variations cause the ice breaker to yaw, characterised by a yaw angle and period. As the non-uniformity of properties of the ice cover increases, the angle and period of yaw of the icebreaker under otherwise indentical conditions increase. In order to maintain the initial direction of motion of the icebreaker, the rudder must be turned from time to time and the angle to which the rudder is turned, of course, depends on the yaw angle. When an icebreaker sails in irregular ice cover, the rudder is used to counteract the varying forces and moments due to ice. The more effective the rudder is, the less the yaw angle will be. Thus, the yaw angle of an icebreaker depends not only on the non-unifromity of the ice but also on the rudder control and the quality of the helmsman's work.

During ice navigation, rudders, stocks and steering gears may be subjected to large dynamic loads, due to the ice striking the rudder blade during normal head-on operations or while turning, or due to backing into large ice floes during backing-down maneuvers, when carrying out herring bone turns or ramming in heavy ice. Special attention must be given to the design of

rudders and steering gear components to avoid sustaining serious damage under such conditions.

Design Consideration for Maneuvering in Ice

The primary influence of hull form on turning is the degree of side clamping due to wedging of broken ice pieces and the unbroken sheet ice against the ship's side. There are several methods for improving the performance of normal ship shapes when they must be used in ice. Traditionally, icebreakers have had no parallel mid body and have had a rounded hull form which allows for good maneuverability in ice. However, other methods such as widened bows, as were installed on the Manhattan, the Kigoriak and the Robert LeMeur, also give relief to side constraints in thin sheet ice. In addition, flare along the mid body of a ship can add to the improvement of maneuverability in ships with considerable mid body. Also, heeling large vessels "into the turn", so as to give an apparent increase in flare on the inside of the turns and so allow the inner bow to more effectively load the ice downward and break it, has been quite effective in trials in Eastern Canada.

In general, in order to turn in ice, it seems most effective to improve the ability of the forward part of the ship to break ice and to concentrate on supplying enough turning moment to hold the ship's stern against the outward side of the broken ice channel. Increasing the turning force so as to break ice with the ship's stern causes the problem of broken ice pieces flowing into the propeller and rudder area which is one of the more sensitive areas for damage on an icebreaking ship. Many icebreakers are multiple screw but since turning in thick ice requires considerable horse power, it is unusual to use differential power between screws to create a significant turning moment as reducing the thrust on the propeller on the inside of the turn reduces the total thrust available to overcome level ice resistance while producing only a small net turning moment through the asymmetrical thrust of the remaining one or two propellers. Similarly, if there is significant icebreaking around the bow, normal bow thrusters are not of much use, even at slow speed since the orifice of tunnel thrusters

is easily congested and blocked by ice pieces around the bow. Normal turning of an icebreaker must therefore be accomplished through use of the rudder alone.

Although turning tests for ice transitting ship have not been carried out extensively, Figure 1 shows the data for a number of icebreaking ships. These show both right and left hand turns and show the turning circle data as a function of ice thickness. The turning circle radius is non-dimensionalised on the ship length to produce a $\frac{r}{l}$ ratio. All of the ships shown on the plot are single rudder except the Werterdor which is twin-rudder and the Manhattan which is also twin-rudder. The 160m Polar Tanker and Katmai Bay are both single screw ships while the Labrador, Radisson and Wolfe are twin-screw vessels with centreline rudders. The data shows a wide scatter but some general trends are apparent at low ice thicknesses of the order of 12 inches or 30 centimetres. The turning circle radius is of the order of two and a half times the length of the ship in a ship with good turning capabilities but may be as high as eight or ten times the length in a ship with lesser turning abilities, while at 40 inches or one metre ice thickenss, the turning circle radius is of the order of eight to ten times the length of the vessel in a maneuverable icebreaker while it is of the order of twenty times in a ship that is less maneuverable. All of these data are based on continuous icebreaking and not using herring bone or ramming type turns.

Rudder System

The rudder system of an icebreaker must provide good control during navigation in ice and in open water. At the same time, the rudder, stock and steering gear all experience considerable ice loads. Because of this, great attention must be paid to their strength. The majority of icebreakers have a single rudder arranged on the centreline. This may either be a plate rudder with horizontal stiffening ribs which is common in the Soviet Arctic fleet or a built up, stream-lined rudder which is more common in the North American and Baltic fleets. A number of icebreakers used in non-Arctic conditions do use

multiple rudders but at the present time, it is unusual for Arctic vessels to have more than a single rudder.

Again, because of the high strength requirements, it is most common to use a rudder hung on a rudder post with multiple pintles in order to spread the load, although some light icebreakers do have semi-balanced spade rudders.

Figure 2 shows a typical icebreaker rudder installation on triple and twin screw icebreakers. It is important to note the large ice horn arranged above the upper part of the rudder blade which protects the rudder when backing down in heavy ice. A number of twin screw icebreakers are in service in both North America and the Soviet Union and these ships normally have single centreline rudders which, of course, leads to less effective turning ability due to the lack of propeller wash flow over the blade surface. Table 1 shows the rudder area and rudder stock size for two Soviet Arctic icebreakers and three Canadian heavy icebreakers.

When maneuvering in heavy ice, the rudder blade may see high loads which can be transmitted through the stock to the steering gear. A number of methods have been designed to minimize the potential damage to the system. One method, shown in Figure 3, is of pinning the rudder using a hydraulically retractable pin which can be driven from the ship shell into the upper edge of the rudder. This has the effect of locking the ship's rudder on the centreline and so removing any torque loading from the rudder stock. However, this load must be reacted out through the pin and in service this method has proved somewhat less than satisfactory as high side loadings can cause the rudder pin to jam, making it impossible to withdraw and therefore making the rudder inoperative for normal open water operations.

Another system is to incorporate a weak link in the upper rudder stock which can shear under high loading, allowing the rudder to be driven over and fetch up against hull stops, arranged to react out the ice loads. In this way, the steering gear and the main rudder stock are protected from overload

A third method incorporates the use of relief valves in the hydraulic system of the steering gear which reacts to over-pressure due to excessive torque and allows the steering gear to relax its torque on the rudder head and again allow the rudder blade to be driven over against hull stops which will then carry the load from the ice. All of these methods are still in use today.

Some measurements have been made on steering systems of heavy icebreakers while in thick ice. Figure 4 shows data of the measured torque over a period of several hours while operating in one metre of ice at 90 to 100% coverage. The ship's operating speed was between five and eight knots and the vessel was in a backing and ramming mode. It is interesting to note that the majority of torques were well below the maximum hydrodynamic torque but that there were individual occurrences of a few percent in which the ice torque was of the order of four times the maximum hydrodynamic torque.

Table 2 gives some indication of the frequency of rudder impacts during backing and ramming maneuvers for four North American icebreakers. Based on the maximum and mean torque recorded during backing and ramming trials of such icebreaking vessels, a set of design-oriented rudder torques have been developed at ARCTEC CANADA. The non-dimensional representation indicates that the higher the ratio of rudder stock length to diameter, the lower the impress torque.

The following example illustrates the step by step procedures which may be followed to design a rudder system for operation in ice

- °Choose diameter initially from hydrodynamic considerations, and length from design requirements.
- °Enter design curves (Fig. 5) for appropriate ice strength and calculated l_s/d_R .
- °Determine max and mean dimensionless torque.
- °Calculate corresponding torques for rudder geometry and ice thickness.
- °Calculate maximum and mean bending moment from

$$M_{\max, \text{mean}} = \left[\frac{Q'_R}{r} \right]_{\max, \text{mean}} \cdot K$$

where K is stiffness per unit load obtained from static flexure analysis.

- ° Calculate normal stresses, σ_n , due to bending $\left[\sigma_n = \frac{My}{I} \right]$
- ° Calculate in-plane stresses, σ_{ip} , due to bending by applying flexure/torsion strain ratios (maximum and mean).
- ° Calculate combined stress from

$$\sigma_e = \frac{1}{2} \sigma_t + \sqrt{\left(\frac{\sigma_t}{2}\right)^2 + \tau^2}$$

where σ_t is the vector resultant of flexural stress σ_n and σ_{ip} and τ is the shear stress due to torque Q_R .

Since the design curves do not at this time incorporate extreme ship/ice conditions allowable calculated stresses should not exceed 50% yield stress. The maximum and mean stresses should be calculated for all conditions of operations and the process repeated to reach a compromise design which satisfies the designer.

Auxiliary Steering Devices

As mentioned previously, the use of traditional tunnel thrusters in ice-breaking ships is not common due to the ease with which such thrusters become clogged and jammed with ice pieces. Two types of thruster have been fitted to icebreaking ships which have been reasonably effective. The first is a thruster which draws from a large sea chest type tank in the fore-peak and discharges either port or starboard. This type of bow thruster is fitted on the recent Canadian R Class icebreakers. The second type of thruster, the "Omni" thruster has been fitted to the most recent class of icebreaking anchor handling boats for Gulf Canada. This system draws water from below the keel of the vessel and again discharges either to port or starboard with a relatively high velocity jet. The "Omni" thruster has the added advantage that the same system can be used to drive a hull lubricating or hull washing system.

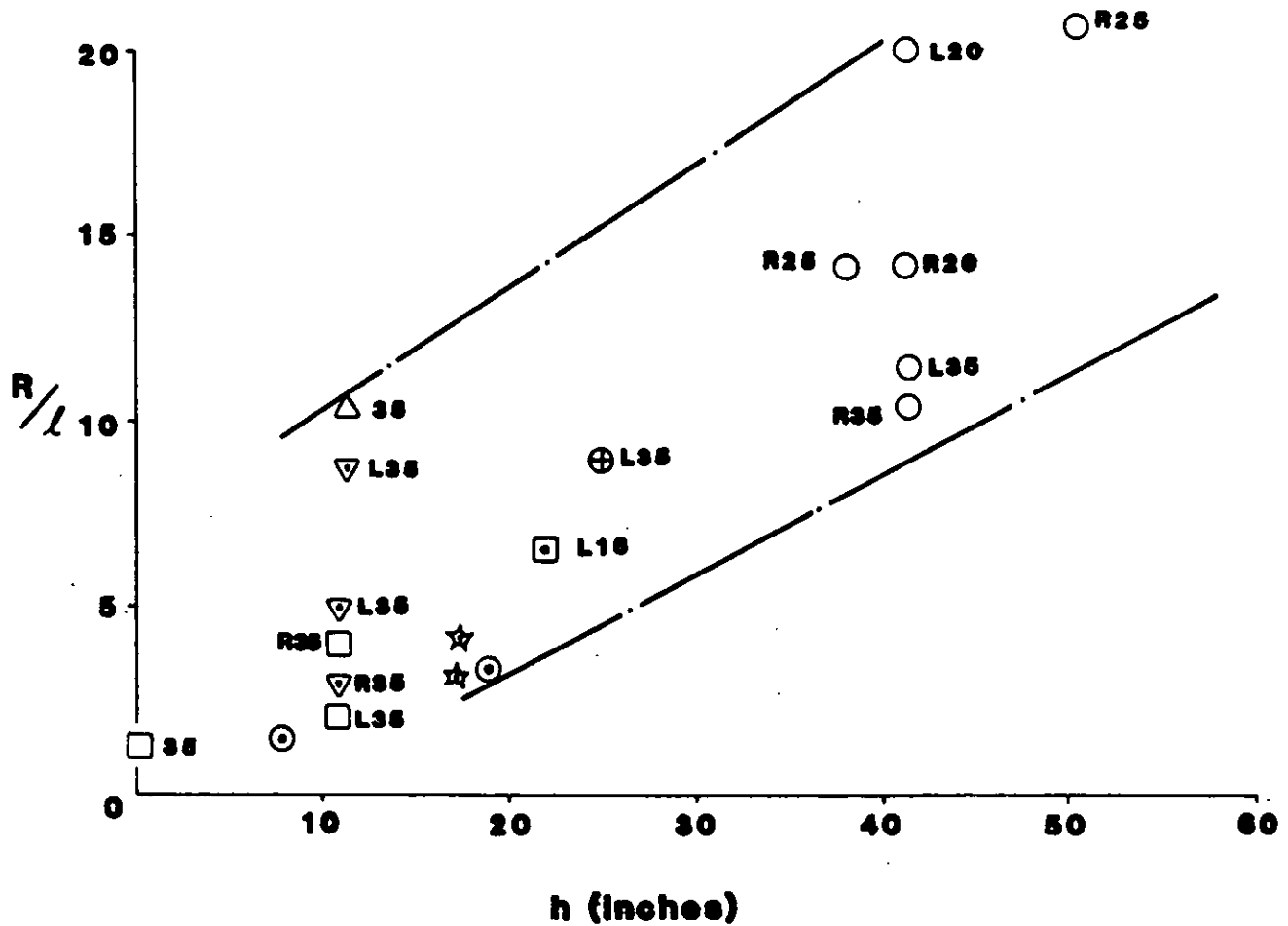
Other resistance-minimising devices such as air bubblers, which are sometimes fitted to ice transitting ships, can be used successfully as bow thrusters by discharging air or air and water combined through outlets on one or other side of the bow as appropriate. Other active steering enhancement devices, such as azimuthing thrusters, active rudders, steering nozzles, have not commonly been fitted on heavy icebreakers due to the risk of substantial damage to such equipment.

Summary

Steering systems for Arctic icebreakers can be successfully designed with today's technology. Special attention must be paid to relieving excess loads on the rudder system to avoid damage to the stock or steering gear and, in addition, it seems likely that in the near future it will be possible to design highly efficient, twin rudder systems for Arctic icebreakers which will give the added advantage of improved maneuverability, due to having the rudder blade in the prop-wash and also protection to the wing propellers during backing down maneuvers, by having a heavily strengthened rudder/ice horn combination immediately abaft each wing propeller. A further development now under consideration is a method whereby an "Omni" thruster type bow thruster system would have its control system connected to the main steering system in order that, when the helm was put over, both the rudders and the bow thruster would be simultaneously engaged to produce maximum turning moment.

Figure 1

TURNING CIRCLE DATA FOR ICEBREAKERS



LEGEND

- ◻ MANNATTAN
- ⊙ WERTERDOR
- ▽ 160m POLAR TANKER
- ☆ KATMAY BAY
- ◻ LABRADOR
- RADISSON (Summer)
- △ WOLFE
- ⊕ RADISSON (Winter)

L35 or R20 (Typical numbers) indicate amount of left or right rudder—in degrees.

BIBLIOGRAPHY FOR RUDDERS AND MANEUVERABILITY PAPERS

Kashteljan, "Icebreakers - Sections of Maneuvering and Rudders".

Bujakin, A.A. "Determination of the Diameter of a Rudder Shaft for Icebreakers and Icebreaking Ships". Sudostroenie, 23 December, 1962.

Laskey, N.V. "Design of Steering Gears, Rudders, Rudder Stocks and Propeller Protection for Canadian Arctic Class Vessels". Society of Naval Architects and Marine Engineers New England Section, April 1979.

Edah, et al. "Maneuvering Performance of Ships in Critical Channels". Society of Naval Architects and Marine Engineers Annual Meeting, 1982.

Kheysin, D.Y. "Use of Probability Methods in Estimating the Maneuvering Qualities of Ships in Ice". Sudostroenie.

Noble, P. and Menon, B. "Study of Steering System Components for Arctic Class Ships". Report 329, Canadian Coast Guard Ship Safety Division, November 1979.

FIGURE. 2

STERN CONFIGURATIONS (Not to common scale)

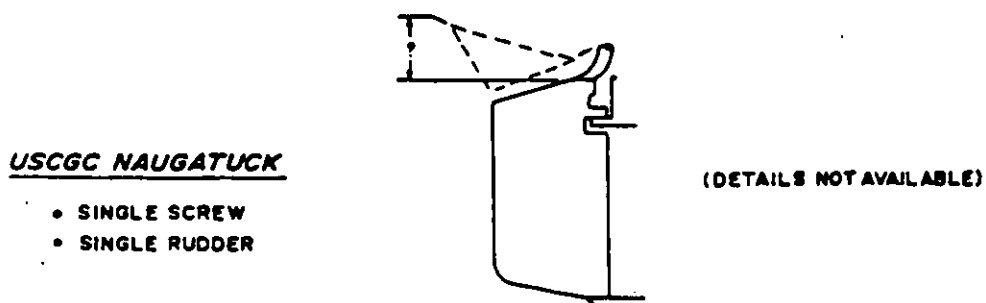
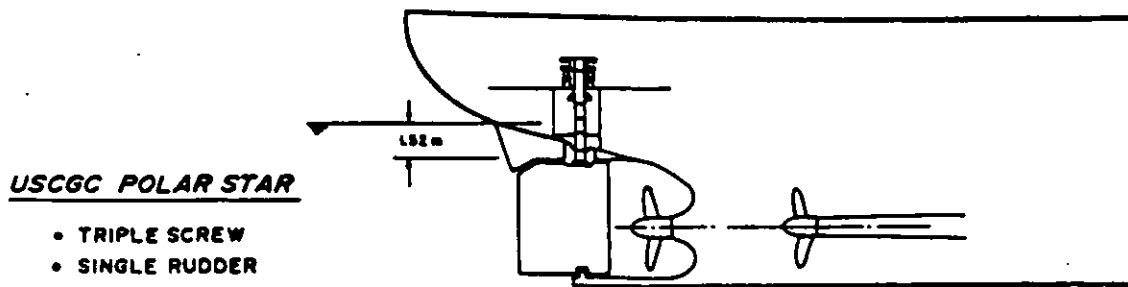
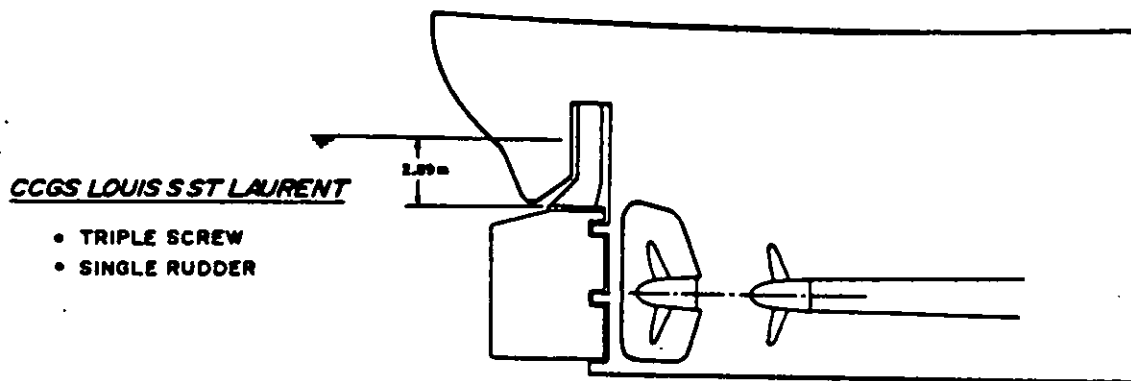
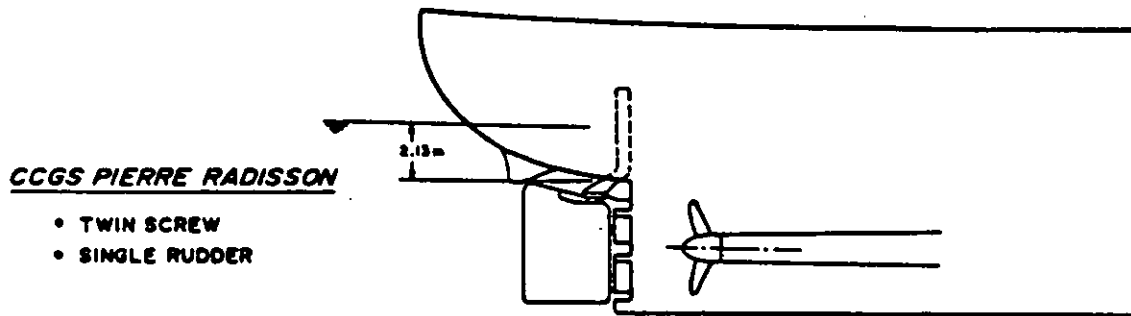
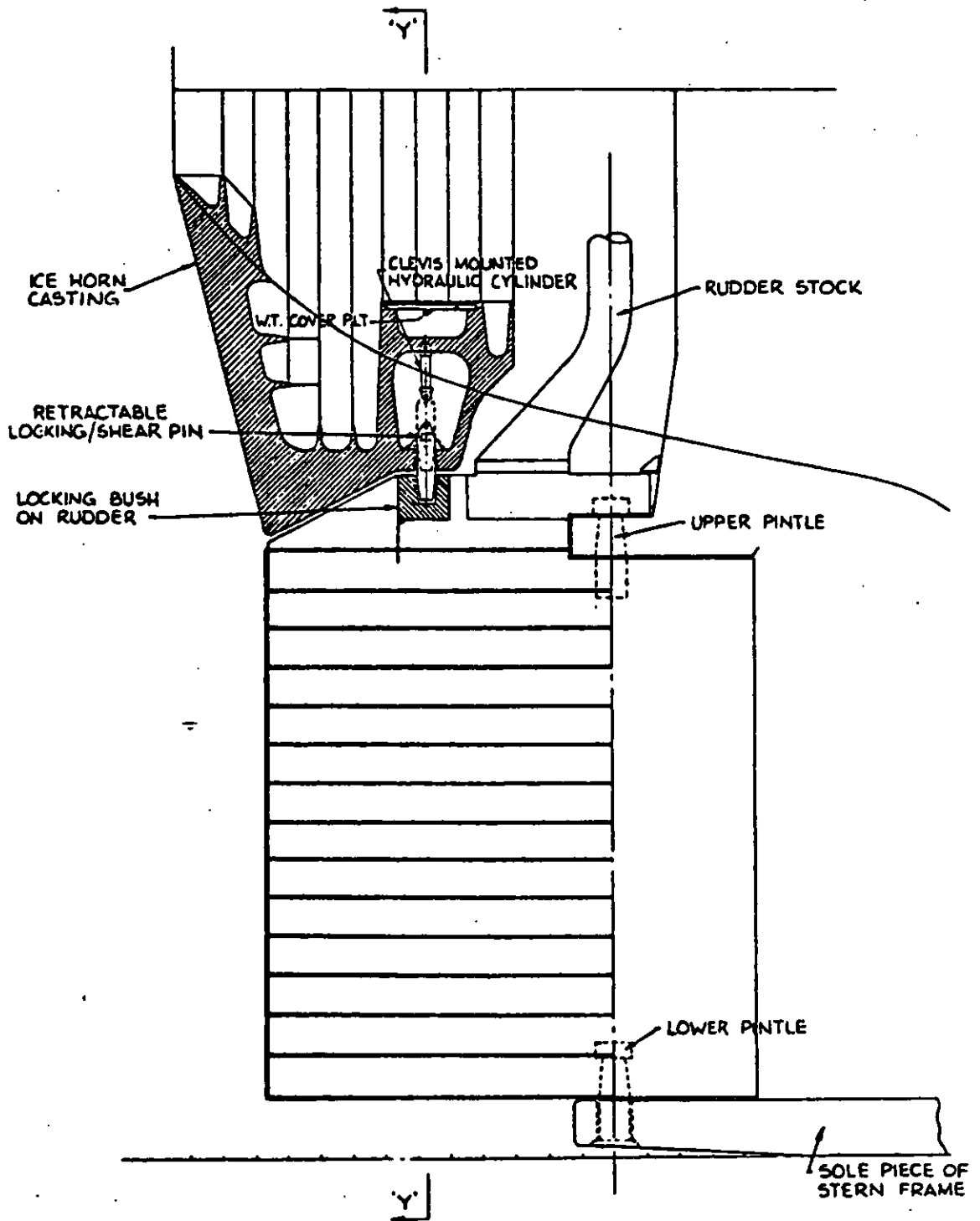


TABLE 1.

RUDDER AREA AND STOCK SIZE FOR VARIOUS ARCTIC VESSELS

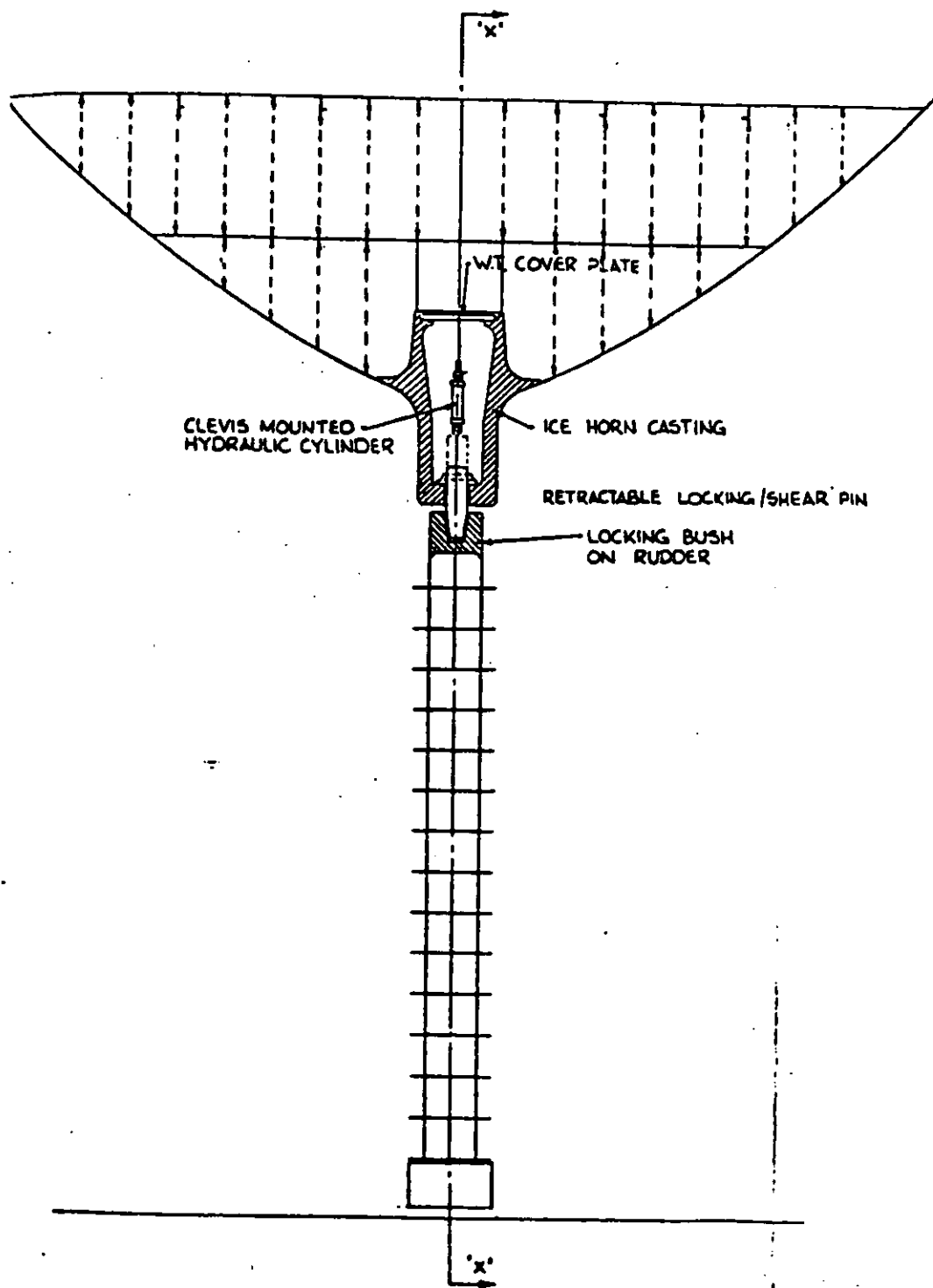
SHIP	COUNTRY	OPEN WATER SPEED	RUDDER AREA	AREA %L.P.	STOCK DIA.
Moskva	U.S.S.R.	18.6 kt.	13.7m	1.62%	540mm.
V.Pronchishchev	"	14.5	7.4	2.22	360
Labrador	Canada	16.0	12.74	2.17	406
d'Iberville	"	15.0	16.04	2.06	533
J.A.MacDonald	"	15.5	18.98	2.32	533

FIGURE 3a. RUDDER PINNING ARRANGEMENT.



SECTION THROUGH 'X-X'

FIGURE 3b. RUDDER PINNING ARRANGEMENT



SECTION THROUGH 'Y-Y'

FIGURE 4 RUDDER TORQUE MEASUREMENTS.

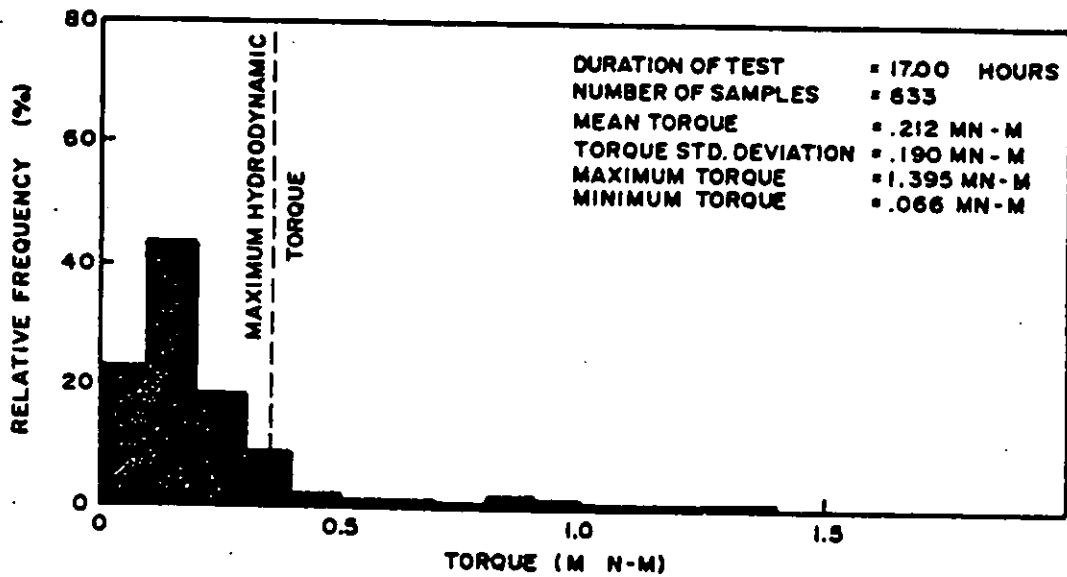


TABLE 2.

FREQUENCY OF IMPACTS FOR
BACKING AND RAMMING

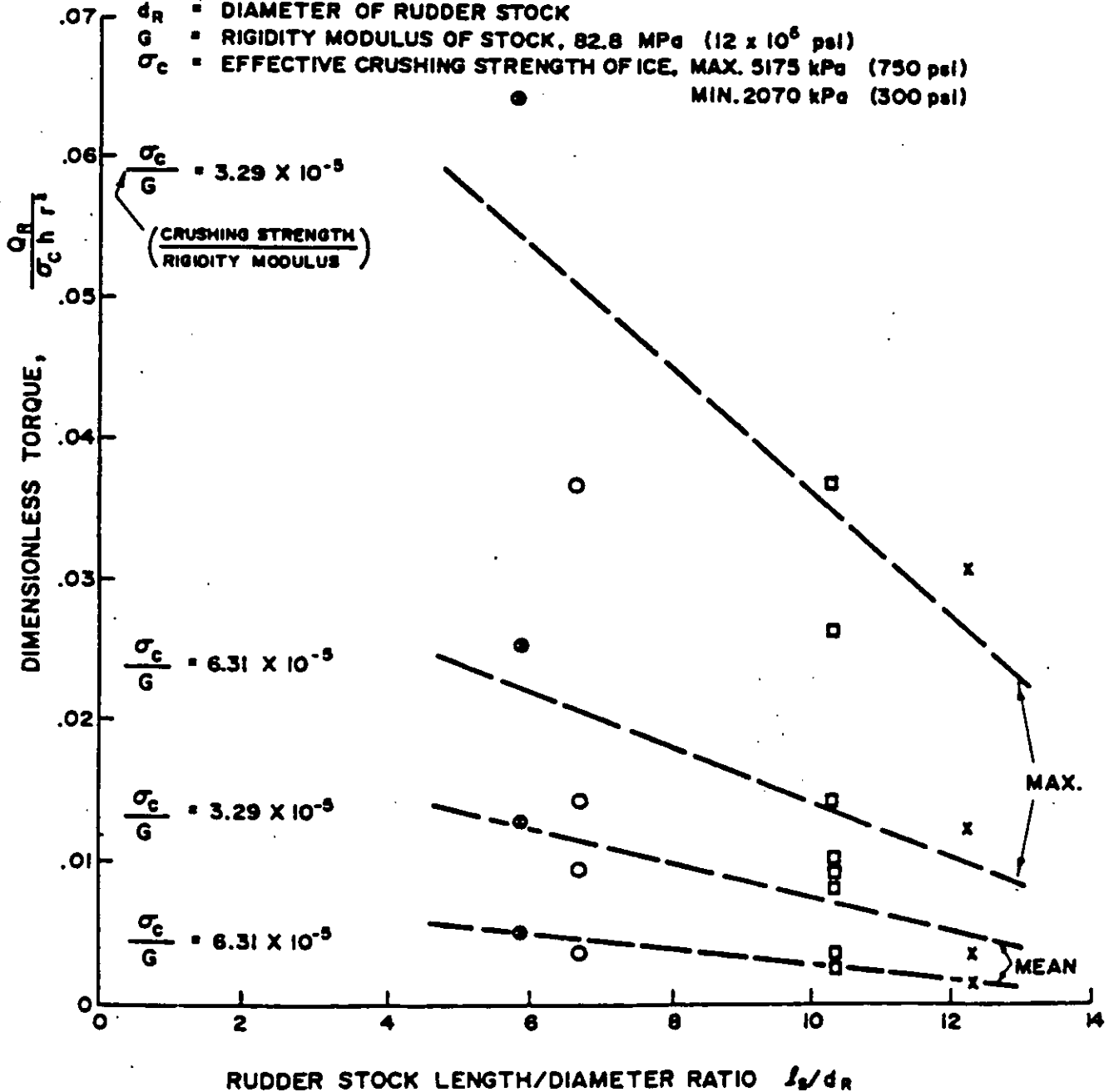
VESSEL	DRAFT AT RUDDER STOCK	ICE THICKNESS RANGE	NO. OF IMPACTS/HR.
POLAR STAR	1.52m	0.9m	54.1
RADISSON	2.13m	2.5-1.8m ridges	30.6
LOUIS	2.80m	1.7-1.5m	12.65
NAUGATUK	0.86m*	0.4-2.25 m with ridges up to 1.5m	16.2*

* Includes rudder/ice impact data for all cases and duration of each test is not accurate. Draft estimated based on best available information.

FIGURE 5.

NON-DIMENSIONAL REPRESENTATION OF RUDDER-ICE IMPACT TORQUES
OPERATION - BACKING & RAMMING

- Q_R ■ REACTION TORQUE IN RUDDER STOCK
- h ■ ICE THICKNESS
- r ■ DISTANCE FROM RUDDER STOCK AXIS TO TRAILING EDGE OF RUDDER
- l ■ LENGTH OF RUDDER STOCK FROM CROSS HEAD TO RUDDER PALM
- d_R ■ DIAMETER OF RUDDER STOCK
- G ■ RIGIDITY MODULUS OF STOCK, 82.8 MPa (12×10^5 psi)
- σ_c ■ EFFECTIVE CRUSHING STRENGTH OF ICE, MAX. 5175 kPa (750 psi)
MIN. 2070 kPa (300 psi)
- x POLAR STAR
- RADISSON
- LOUIS S ST LAURENT
- NAUGATUCK





MSc Sven-Ola Andersson

CPP IN ICE

Introduction

The controllable pitch propeller has traditionally been used for various kinds of ice-going vessels. Today's knowledge and technique in the field of ice-going propellers give guarantee for the reliable function of the CP propellers also in heavy ice.

Knowledge of magnitude and direction of the forces acting on a propeller blade when hitting ice is limited due to the complex nature of the problem and the difficulties in making accurate models or full scale measurements. Today, propeller-blades and -shafts for ice-going ships are dimensioned according to the ice class rules, while the selection of the hub is still a part of the fascinating art of propeller design. The main difficulties in this work are to gain an understanding of the ice loads for an actual propeller and to generalize this knowledge into methods of strength calculation.

There are different hub-types in service for a range of purposes. From the propellers for very fast patrol-boats, where the hub ratio must be small and the forces for pitch-setting are extremely big but the fastening of the blades can be relatively weak due to the uniform wake-field. To the very slow-running big propeller, where the forces for pitch setting are small but the fastenings of the blades must be strong due to the non-uniform wake-field. For the ice-strengthened propeller, both the pitch-setting mechanism as well as the blade-fastening must be extremely strong. These both requirements make the hub-ratio big.

The approach used by different classification societies can be divided into three main categories of rules for ice-strengthened propeller. In the first category the non-ice-dimensions are simply increased by a certain percentage, the rate depending on the prescribed ice class.

The second category uses special equations for calculations of ice-strengthened propellers and the common feature is the introduction of an ice torque factor. Multiplying this factor with the propeller diameter squared gives the shaft torque due to ice. The dimensions of blades (blade bolts) and shafts are then related to the sum of the hydrodynamic load at bollard pull and the ice torque. This concept is based on ice torque measurements in full scale, mostly on USSR and Finnish icebreakers.

The third category is still tentative but includes a force acting on a point normally at $0.9 R$ on the blade. The hub mechanism must be strong enough for this force.

For propellers in heavy ice it is necessary to get insight in the problem of calculating ice forces on blades and describe the geometry and the modes of ice destruction involved.

Two factors mainly influence the torque characteristics of the ice-going propeller, namely:

Variations in hull resistance due to variations in ice conditions which will indirectly influence the shaft torque.

Direct ice influence on the shaft torque as a result of mechanical contact between propeller blades and ice of various structure.

This paper deals with the latter.

The estimated ice loads provide basic guidelines to the selection of hub and blade dimensions for highly ice-strengthened propellers.

When the propeller blade hits the ice with the leading edge the forces acting on it are at its hardest. As long as there is torque available the blade is cutting ice. The torque required is low. The propeller blade is tremendously strong for forces acting on the leading edge. This is the best condition both for propeller and engine. It is the purpose of the control system to maintain this condition. It is also important that there is power available for cutting the ice.

Type of ice loads

For ships going steady in broken or very thin ice, the ice masses entering the propeller disc have comparatively small dimensions and are either accelerated through the propeller or just thrown out radially and pushed around the edge of the disc. The time for contact blade - ice is short and the loads moderate. Service experience from propellers operating in such ice conditions is good, indicating that a realistic stress level is obtained when dimensioned according to the class rules.

For ice-breakers and ships operating in unbroken or thick broken ice, large ice floes are constantly fed into the propeller disc and can occasionally be trapped between hull and propeller, commonly called wedging. When penetrating ice ridges or when breaking very thick ice, the available power is often less than the one needed for continuous breaking. In this case, the momentum of the ship is used to split the ice through ramming. The ice forces are enormous and gives the ship a yawing and swaging motion. If an ice channel is broken, the propellers can be pushed sideways into the ice at the edge of the channel. Ramming manoeuvres also necessitates frequent astern runs where the risk of getting ice into the propeller is high. All conditions above give severe shock loads on the propellers as the blade must cut or crush solid ice.

Ice properties

Although a well-known material, the physical properties of frozen seawater are uncertain to a high degree. Measurements show large variations in compression strength with density, salinity and temperature.

Sea ice is anisotropic, i.e. the strength is not equal in all directions and the mechanical behaviour is of a complex visco-elastic-plastic nature. A failure criterion is thus very difficult to formulate.

Uniaxial compression strengths in the range 0.2 to 8 N/mm² are reported in the literature but an average of about 2.5 N/mm² is common.

Shearing strengths between 0.6 and 1.3 N/mm² are measured. Jagodkin has calculated the crushing and shearing strengths of multiyear arctic pack ice based on a comparison between this mathematical model for ice torque and full scale tests. He assumed a ratio between the crushing strength σ_c and the shearing strength τ of $\sigma_c/\tau = 4$. This gave the average values:

$$\sigma_c = 2.55 \text{ N/mm}^2$$

$$\tau = 0.64 \text{ N/mm}^2$$

Since the proposed estimation method is based on Jagodkins model, strength values close to these can be expected to give good correlation between calculated and actual full scale ice loads.

Ice loads on propeller blades

Shaft torque, blade bending moment and thrust due to ice are calculated with a two-dimensional approach, assuming the forces on an equivalent blade section to be representative for the total blade forces.

To visualize the ice cutting mechanism, two different views of the blade in its maximum cut depth position are used. Figure 1. One is an expanded view of two consecutive equivalent blade sections and the other is a side view with two consecutive blade passages. The proceeding blade section is shown with dotted lines.

With a low ship speed and a high propeller rpm, the feeding of ice into the propeller disc is low and the blades cut ice by a combination of shearing and crushing. Figure 2. This is called the shearing mode and is analogous to the case of conventional milling in a lathe. The blades cut a channel in the ice block.

When the feeding is increased, the blades have to shear off more and more ice and at a certain point, the force needed to crush through ice with the projected blade area is less than the shearing force. The destruction mode is thus changed from a shearing - crushing combination to merely crushing. Figure 3 shows the blades when crushing ice. If constant ship speed and shaft rpm are maintained, regular notches are cut from the ice blocks.

In off-design conditions such as crash stop or crash forward the blade sections have very large angles of attack and the blades can partially shadow each other. Figure 4 shows ice crushing when the ship moves forward and the blades are set to astern pitch. The ice is crushed with the trailing part of the blade.

In the model ice milling tests (figure 5) there are indications of a "wedge" effect at small negative angles of attack, i.e. the normal force is equal to the integrated ice crushing pressure acting over the total blade area immersed in ice. No such effect appears at small positive angles of attack, at least for pitch settings in the normal range for a CP propeller.

Figure 6 shows the bending moment acting on the propeller blade at different pitches. The speed of the vessel is constant. About 10° pitch angle corresponds to zero slip and the bending moment is zero, because the propeller crushes the ice with only its leading edge.

For icebreakers with fixed pitch propellers it has been concluded that the propeller blades and shafts are damaged most severely when the rpm is reduced to zero due to counter-torques developed during the propeller interaction with ice or when the direction of shaft rotation does not correspond with the movement of the ship. That is to say, if the ship is moving ahead, the shaft should also be rotating in the ahead mode when the propeller impacts with ice.

The CP propeller should be kept turning, in which case the risk for blade failure is greatly minimized if the blade angle of attack at impact is correct. Of course, sufficient torque should be available to overcome the hydrodynamic and ice torques encountered.

In addition to appropriate ice-strengthening the ships must be operated properly. Crew training, navigational aids and communication practice should be improved.

CP-propellers_for_ice

It is a big task for the propeller manufacturer to prove that a CP propeller can compete with a diesel-electric machinery. First we must prove that the diesel-mechanic machinery can keep the propellers rotating while working in ice and then that the propeller is strong enough for the ice-loads. Of course the CP propeller has some obvious advantages in comparison with a diesel-electric machinery. The manoeuvrability of the ship is improved. The fuel consumption is less. The weight is considerably lower.

Figure 6 shows a common torque characteristic for a diesel-electric system and for a diesel-mechanic system. The diesel-mechanic system has a hydraulic coupling. With decreasing propeller rpm due to increasing ice-resistance the max engine torque is always available. It is a question of cooling capacity for how long it can slip down to zero rpm. A slip-coupling may be necessary for heavy ice condition.

Knowing that with the DE-system 3.5 times bigger torque is achieved at 0-30 % rpm than for the DM-system the question is, can the CP propeller mill ice at low pitch with 100 % torque better than the fixed pitch propeller at 350 % torque.

A thorough theoretical investigation is made by Mr Dan Johansson. It proves that with good margin the CP propeller is superior to the fixed pitch propeller.

At Wärtsilä in Finland some model tests (milling of rigid ice with a model propeller) have been performed. These tests indicate a reduction in torque of about 2/3 when reducing pitch from design to zero pitch.

For a Baltic ice-breaker I/B Varma built at Wärtsilä different machineries were investigated by Wärtsilä. For the very extreme ice-conditions it was calculated for, it was found that with the DE-machinery the screws stopped in three cases of four. With the DM-system they stopped only in one case of four, in which case also all the other alternatives stopped. The experience from the ice-breaker "Varma" in operation since 1969 is that its screws practically never were stopped.

It was thus considered possible to design an ice-breaker machinery with diesel engines, reduction gears and controllable pitch propellers which are capable to adequately maintain the revolutions. The lack of experience from the operation of controllable pitch propellers in heavy ice conditions however created a risk factor. Especially when there was no experience whatsoever considering the use of them as bow screws. In those days, the risk involved was considered too great to justify the mainly economical gain at the expense of proven reliability.

Since then some ice-breakers are built with cpp. The USCGC Polar Star was commissioned in Januari 1976. A diesel-electric plant provides 18 000 s h p through three propellers, for economical open-water and light-to-medium icebreaking. A gas turbine plant using the same shafting and propeller to deliver 70 000 s h p for heavy ice-breaking.

Propeller data

make	Escher Wyss
hub diameter	1690 mm
propeller diameter	4880 mm
hub ratio	36 %

The reputation for this propeller is not the best. But with reference to paper 14 presented at the Society of Naval Architects and Marine Engineers Symposium 1981 by Mrs Langrock, Wuehrer and Vassilopoulos, the owners and the propeller manufacturer have really worked on the task to get the most out of the tests. Stress measurements and calculations are made and improvements applied so that the propellers seem to function very well today. From the very beginning the experience with the system for ice-breaking and maneouvreability have been excellent.

Dome Petroleum in Canada have the ice-breaker, Kigoriak AMLX4, which is equipped with a nozzle.

Recently KaMeWa have delivered propellers for three artic ice-breakers built at Wärtsilä for V/O Sudoimport, Moskva.

Main characteristics of the ships are

Length o a	88.6 m
Breadth max	21.2 m
Draught	6 m
Displacement	5560 T
Speed in open water	16.5 knots

Propeller

Number	2
Diameter	4000 mm
Weight complete propeller	21000 kg
Weight propeller blade with flange	1860 kg
Material	30 % Cr Steel in the blades
Machinery	Wärtsiä Vaasa 8R32 4780 kW pro shaft

Requirements for CP-propeller

However the strength of the propeller must be proven. With given ice-strength and shaft torque the maximum ice-cutting depth is calculated. It may also be necessary to establish the magnitude of the torque variations related to time, ship speed and various ice conditions. It is obvious that the propeller system must be designed to cope with the worst situation one can expect for the ship type in question.

As an example main characteristics of the propeller are

Output (max)	3751 kW
Shaft speed (max)	170 RPM
Diameter of propeller	3800 mm
Number of blades	4
Hub diameter	1710 mm
Pitch diameter ratio (design)	0,932
Weight of propeller	21300 kg
Blade area ratio (expanded)	0,52

When the propeller is working in ice, mechanical forces from the ice are acting on the blades. The magnitude of these loads depends on the strength and thickness of the ice, the speed of the ship, the shaft speed and pitch of the propeller and so on. With the power specified 0.68 m ice can be milled continuously at full rpm. The pitch angle corresponds to zero slip in ice and the ice crushing strength is 2.55 N/mm^2 (26 kp/cm^2) see figure 7.

In this condition the blade loads are alternating between the max value when immersed in ice and the min value when in water. With the forces acting fatigue analysis of the hub components are made. The magnitudes for the non-ice-strengthened propeller at free-running are equal to the ice-strengthened in ice.

Maximum spindle torque occurs when the blades enter or leave the ice. At that moment half the blade is crushing ice, while the rest of the blade is in water. This gives a fluctuating force on the crank pin.

In figure 8 some parameters for this project are given. In order to give an idea of the tremendous strength of this hub, figures for a normally loaded non-ice-strengthened propeller is given as comparison in the table. In figure 9 the propellers are physically compared.

When comparing the figures for fatigue we must remember that during certain conditions the propeller blade is enormously strong. For example when ice-milling with the smallest projected area against the ice the safety factor may be, let's say 20 against fatigue cracks at 10^9 cycles and the crank-pin safety factor only 2 for the same ice condition. An opinion exists that if the leading edge of the blade hits the ice, the propeller and the shaft will be damaged because the blade is considerably stronger in its strongest direction than the blade fastening and the shaft. According to Ignatjev, the noted Russian, "Such an opinion is without reasons as the blade in this case only cuts into the ice".

For more severe ice condition, i.e. bow propellers crushing into deep pack ice ridges, all four (4) blades may cut ice simultaneously. This gives approximately four times the normal shaft torque. In that case the shaft speed drops to zero and the propeller is dragged through the ice by the momentum energy of the ship. This loads are very extreme and shall be considered as static loads only.

However, the shock loads may be so high during certain conditions that the blades are damaged. For instance when grounding or backing into an ice ridge with the propellers in ahead pitch. Therefore the pyramid strength philosophy is adopted.

When analysing the pyramid strength of the CP propeller

- the blade root section
- the blade bolts
- the crank pin ring and
- the bearing ring

are considered. (Other parts are not critical from the pyramid strength point of view).

When dimensioning these parts the propeller blade should be the weakest one. The strength of the other parts is therefore related to the blade strength.

The intention with this strength distribution is that if the propeller is overloaded, the blades should be bent or broken and no other damages should occur.

When calculating the breaking force of the blade, semiempirical formulas given by Ignatjev, are used. These formulas may be conservative. Observation on damaged blades as well as tests shows that the blades are practically never broken at the root section by bent. This gives less forces than when calculating for point of final fracture in the root section.

On the other hand it is probably not possible to reduce the pyramid strength requirement. Components designed for fatigue loads require materials and shape which automatically give necessary pyramid strength.

Above pyramid strength philosophy indicates that a propeller blade may be damaged but the hub is still intact. Therefore, today, it is normal to include a blade-exchange under water feature for ice-going CPP.

The very frequent maneuvering during a short period of time may cause unexpected problems. Even when there are propellers in service which make totally more maneuvering per year than an ice-going propeller the extreme maneuvering during short periods must be considered.

The use of a CP propeller in combination with a load control system makes it possible to minimize these torque variations and thus to maintain a more constant torque level. This will safeguard predetermined motor load and result in max possible thrust at each eventuality. Of course the first thing you have to calculate for an ice-going propeller is the strength. But you must also carefully design the complete propulsion system so that it really works as an attuned unit. The control system is important.

It has been well established that the CP propeller can cope with the variations in torque and rpm caused by ice, by adjustments of the propeller pitch. By doing so, it is possible to maintain the torque and rpm in such a way that the propelling machinery will be very little affected. In the case of direct or geared diesel drive it is of importance that overtorque and drop of shaft speed are avoided. When the highest permissible power level can be constantly maintained, it will not only increase the average speed of the ship in varying ice conditions but also increase the ice-breaking capability.

REFERENCES

1. Jagodkin, V. Ja.: Analytic Determination of the Resistance Moment of a Propeller During Its Interaction with Ice. Problemy Arktiki i Antarktiki 13, 1963, pp 79-88.
2. Khajkin, A. B., Jagodkin V. Ja.: Calculation of Statical Characteristics of Propeller-Electric Facilities of Ice-breaking Ships. Sudostroenie 32, January 1966, pp. 57-60.
3. Ignatjev, M. A.: Screw-Propellers for Ships Navigating in Ice. Sudostroenie, 1966.
4. Edwards Jr., R. Y.: Methods for Predicting Forces Encountered by Propellers During Interactions with Ice. ARCTEC Canada, Limited. Rep 75C-1, 1976. See also International Ship-building Progress Vol. 23, Dec 1976.
5. IAHR Symposium on Ice Problems. Luleå, Sweden. 1978.
6. Airaksinen, K., Martilla, M.: On Propulsion of Icebreakers. International Ship Building Progress Vol. 23, June 1976.
7. Airaksinen, K.: Translated Summary of Wärtsilä report "Modellförsök med en propeller i is". KMW Marine Laboratory R-169, 1970.
8. Sasaki, H., Yabuki, S., Sato, M.: Ice-Navigation and Shafting Strength of Ice-Breaker "Fuij". Bulletin of the M.E.S.J. Vol. 7, No. 1.
9. Jakonovskij, V.: Leningrad LCPKB
10. Nikitin, M.: Leningrad LCPKB.
11. Mäkinen, E., Roos, R.: Ice Navigation Capabilities of Lunni-Class icebreaking Tankers.
12. Lawrence, R. G. A.: Canadian Coast Guard Marine Operations in Artic Regions.
13. Johansson, D.: CPP in ice. Determination of forces acting on the propeller and blades when operated in ice condition.

Encl. 1.

Main characteristics for SA 15, ice-breaking, multi-purpose vessel for Südo import, Moskwa

The main characteristics for the ship are:

Length o a	174	m
Length waterline (at design)	164	m
Breadth max mld	24.5	m
Drought design	8.5	m
Displacement	23600	mt
Speed in open water	~ 17	knots

Propeller

Number	1	
Diameter	5.6	m
Hub diameter	2.35	m
Weight, complete propeller	67.5	ton
Weight, propeller blade with flange	5.1	ton
Material	13 %	Cr steel in the blades
Engine effect	15.4	MW (21000 HP) from Wärtsilä. Diesel-engines 14ZV40/400.

Time of adjustment (2 pumps) FF - FB	20 sec.
---	---------

Classification	USSR Register of Shipping for the notation KM ULA 2 A2 with the highest iceclass.
----------------	---

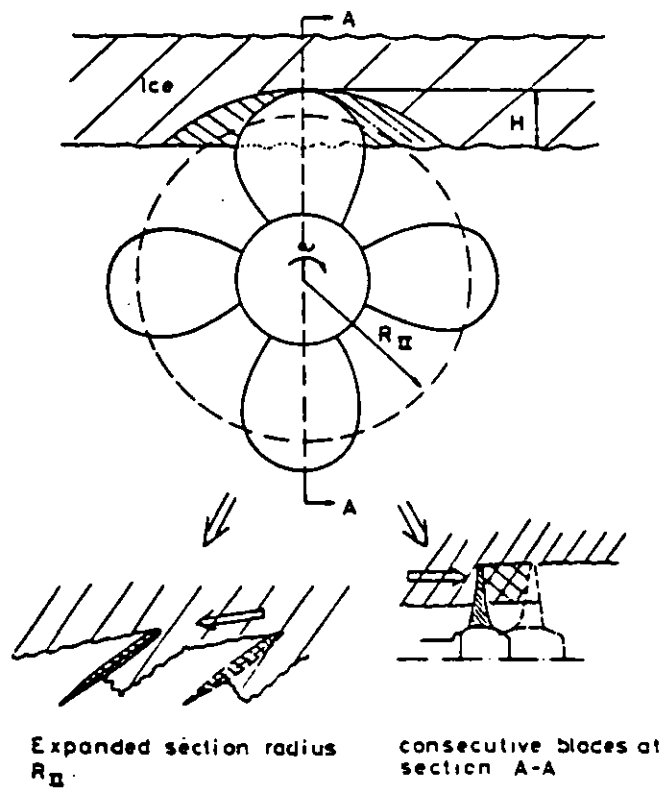


Fig. 1. Ice cutting views.

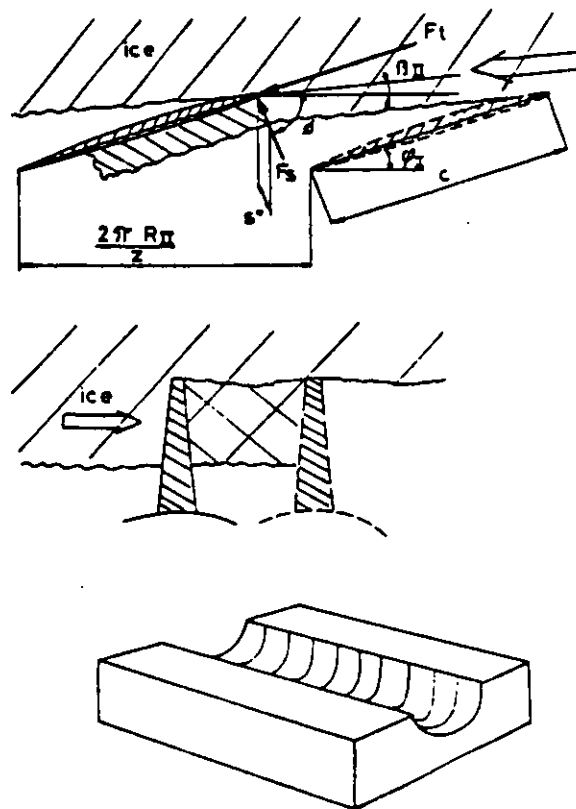


Fig. 2. Ice cutting, shearing mode.

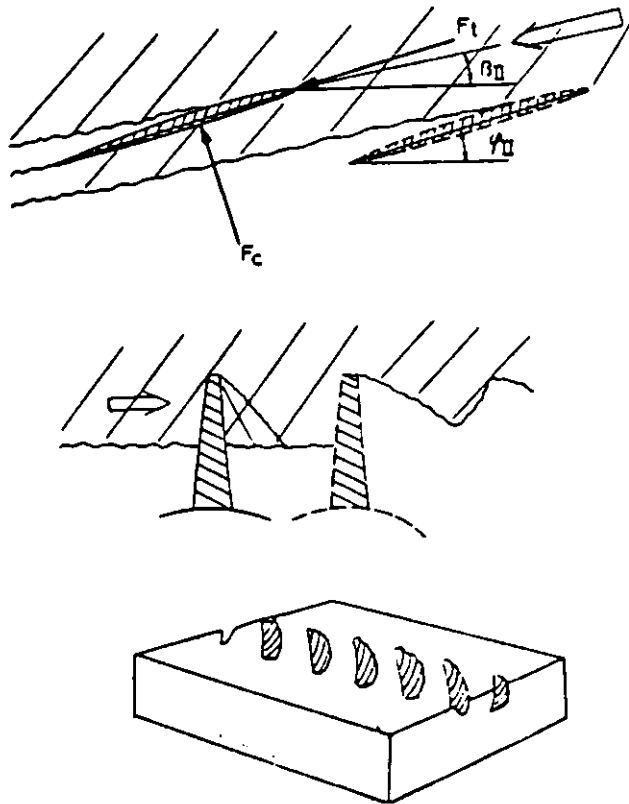


Fig. 3. Ice cutting, crushing mode.

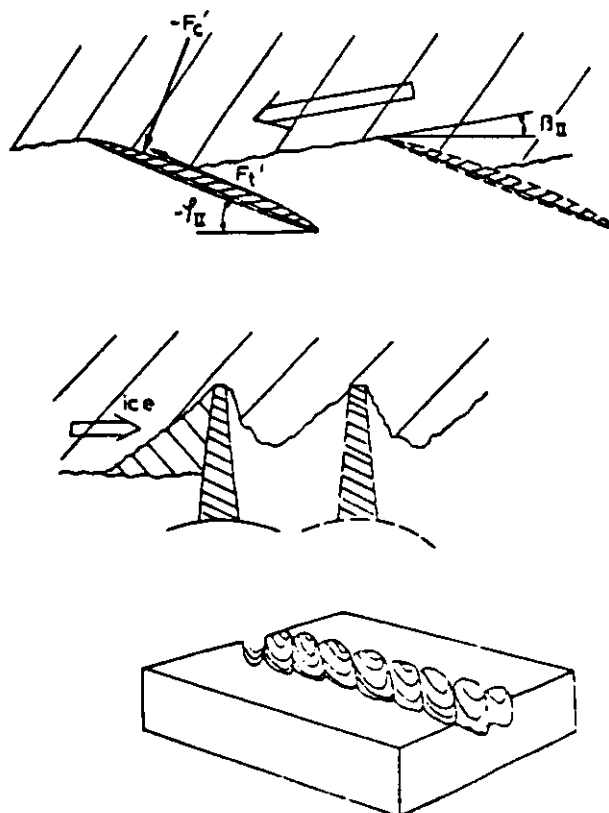
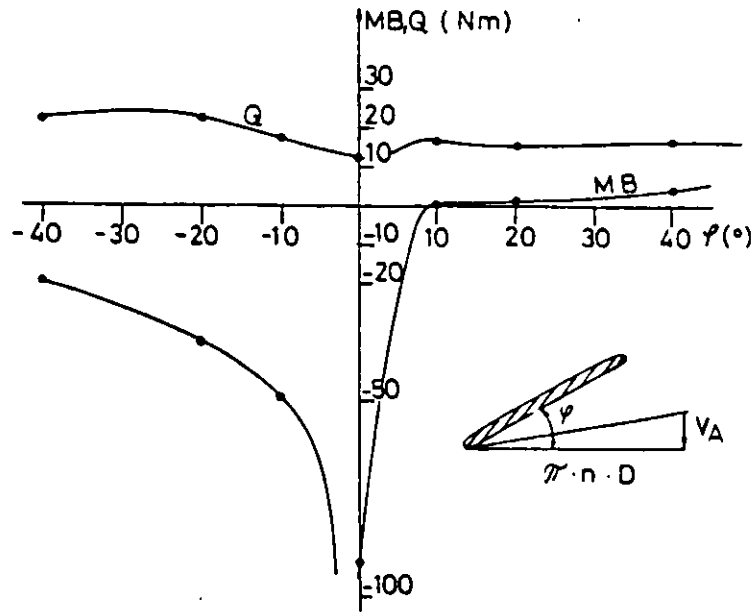


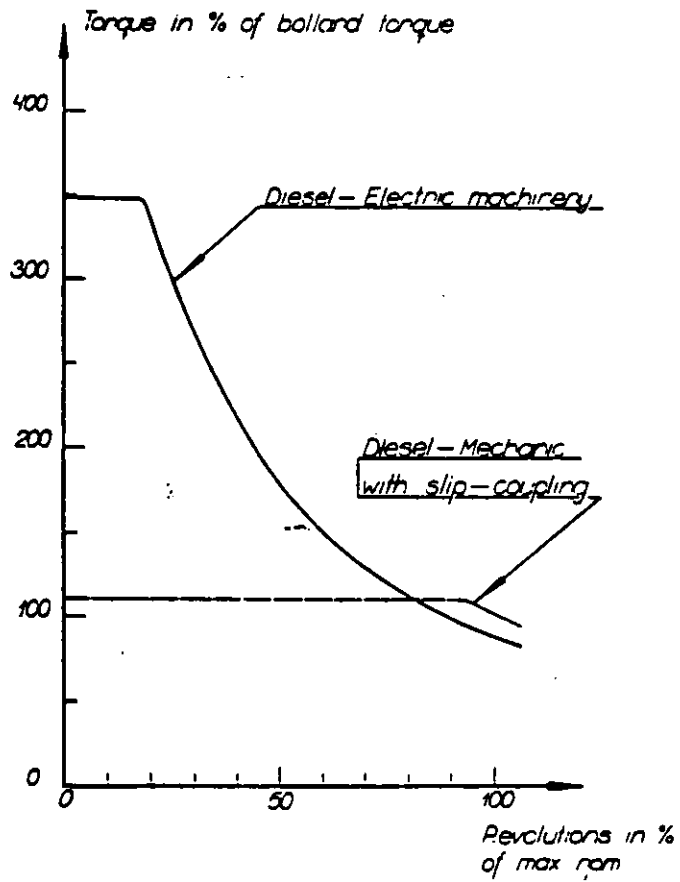
Fig. 4. Ice cutting with partially shadowed blades.



Acc. to Wärtsilä model tests.(7).

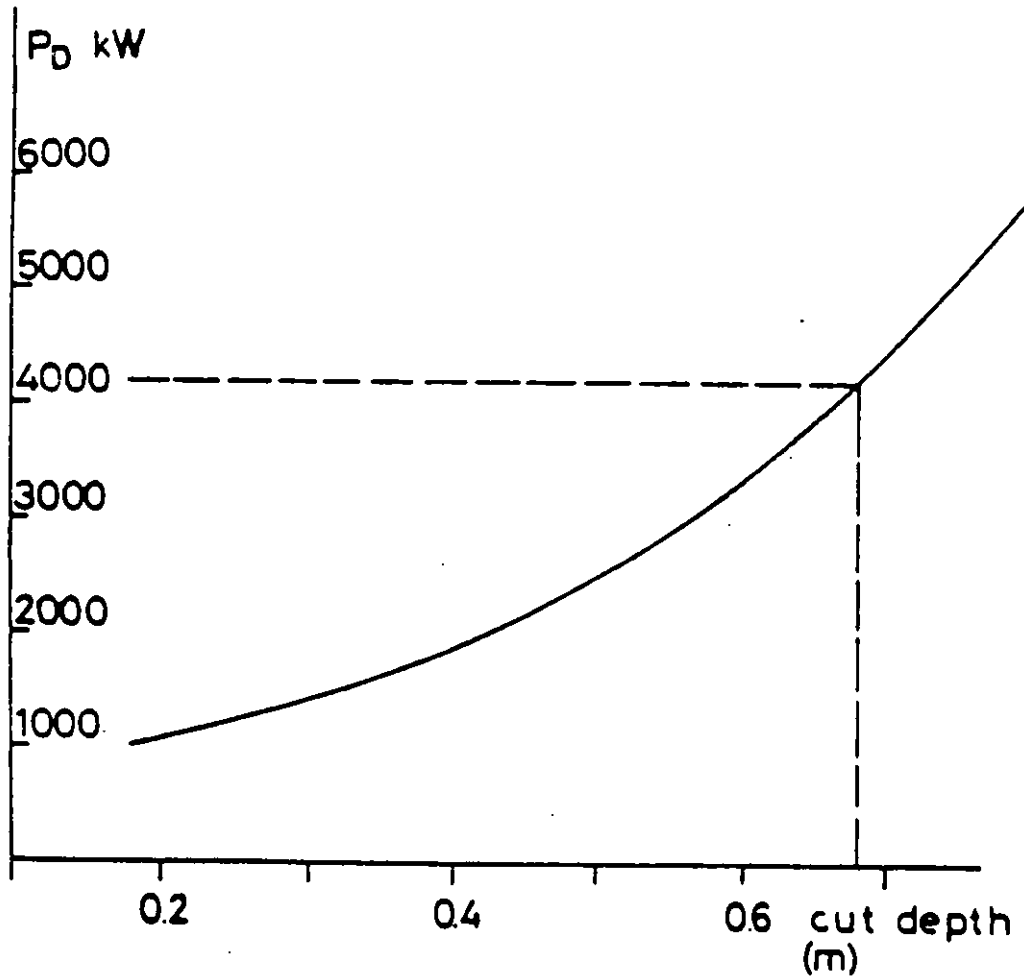
J = 0.152
 $D_{mod} = 0.3$ m
 RPM = 45.5
 Cut depth in ice = 0.03 m
 Blade form 2

Fig. 5. Shaft torque and blade bending moment vs. blade pitch angle.



Torque V.S rpm of typical DE- and DM-system

Fig. 6.



Required propeller power vs. cut depth
in ice.

$V_s = 6.5$ knots and RPM=180.

Pitch angle corresponding to zero
slip in ice, $\varphi \approx 6^\circ$.

Ice crushing strength = 2.55 N/mm^2
(26 kp/cm^2)

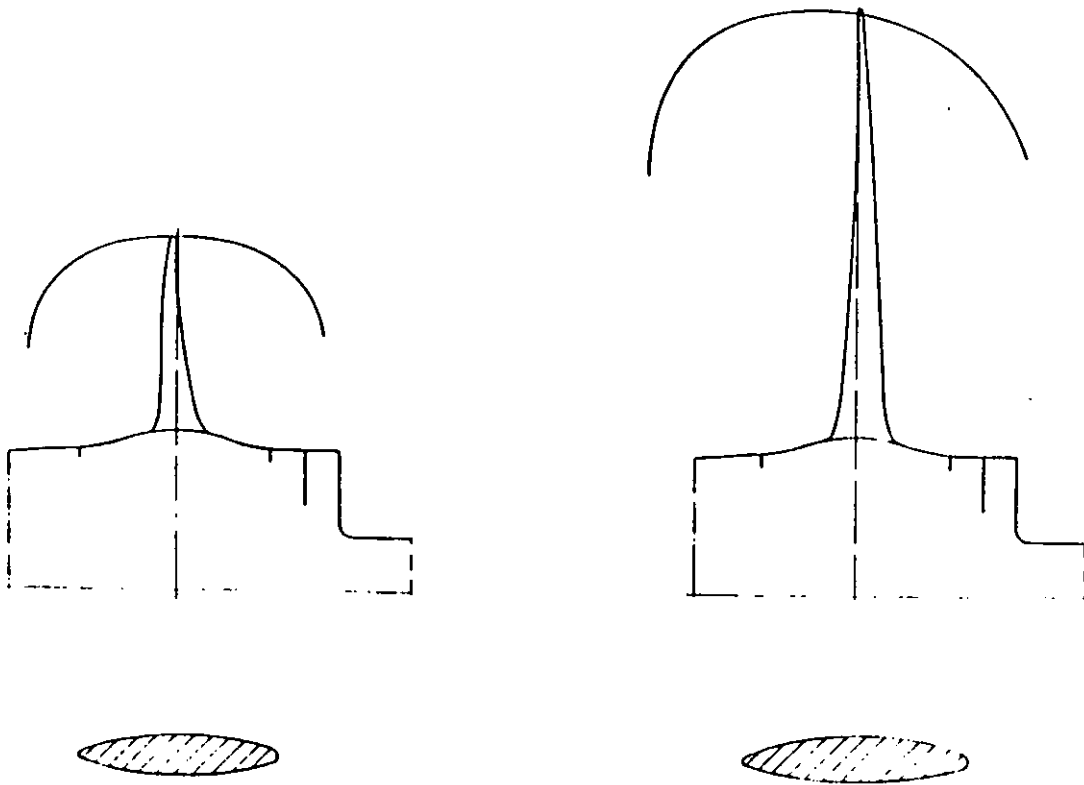
Fig. 7.

Comparison on highly ice strengthened bow propeller and a normal loaded non-ice-strengthened propeller

	Ice	Non-ice	
Power of propulsion pro propeller	3751	9326	kW
Speed max	12	16	knots
Hub diameter mm	1710	1710	
Number of blades	4	4	
Weight of one blade without flange	960	3160	kg
Hub - diameter ratio	0.45	0.267	
Diameter of propeller	3800	6400	mm
Shaft speed (max)	170	113	rpm
Stress factors at free running condition			
Blade bolts	424±1	431±3.5	
Blade flange fillets	16±6	52±24	
Crank pin ring	19±8	126±58.5	
Pyramid strength ratio blade bolt/blade	2.48	1.83	
bearing ring/blade	3.2	1.92	
Crank pin fillet (max)	61	134	
Stress factors when ice- milling with blade 0.68 m emerged in ice of strenght = 2.55 N/mm2			
Blade bolts	423±3.2		
Blade flange fillets	30±27		
Crank pin ring	20±19		
Crank pin fillet at pitch setting	268		
at constant pitch	89		

Fig. 8.

Fig. 8.



*Comparison between highly ice strengthened propeller and normally loaded propeller
Both propellers having same hub diameter.*

Fig. 9.



MSc Göran Wilkman

AUXILIARY SYSTEMS FOR ICEBREAKING

1 DEFINITION OF AUXILIARY SYSTEM

The main function of an auxiliary system is to help the ship in extreme ice conditions.

An auxiliary system is always something extra to the ship's construction.

Auxiliary systems can be classified in many ways. In this paper I have used the following classification, which is based on the functional characteristics of the systems.

2 DIFFERENT AUXILIARY SYSTEMS

2.1 Passive Systems

- Low friction coatings
- Extreme hull forms

2.2 Active Systems

- Heeling
- Trimming
- Bow propellers
- Air bubbling
- Air cushion
- Water washing
- Water & air washing

3 DESCRIPTION OF AUXILIARY SYSTEMS

3.1 Low Friction Hull Coatings

Standard marine coatings do not protect the ship hull when navigation in ice is concerned.

The hull plates will corrode and ageing progresses very rapidly. This increases resistance.

To prevent the increase of resistance, coatings that are able to withstand the wearing interaction between the ice and the hull plating have been developed. Also the use of stainless steel coating has been studied.

Results from the use of low-friction paints have been very encouraging and it has nowadays become practically a standard procedure to use these paints on icebreakers and icebreaking cargo vessels.

3.2 Heeling System

The main purpose of a heeling system is to free the vessel from a jammed position.

A heeling effect is created by transferring liquid from one side to the other. The heeling system consists of a series of side tanks and cross-over pipes with pumps. The angle of heel varies from 5 to 10 degrees and the time of one heeling movement is 30 to 60 seconds.

The heeling system requires a lot of space. The tank capacity depends on the ship's size. The existing systems have tank volumes from 100 to 1000 m³. The tank volume is function of the displacement of the vessel. In Fig. 1 there is a schematic drawing of a heeling system.

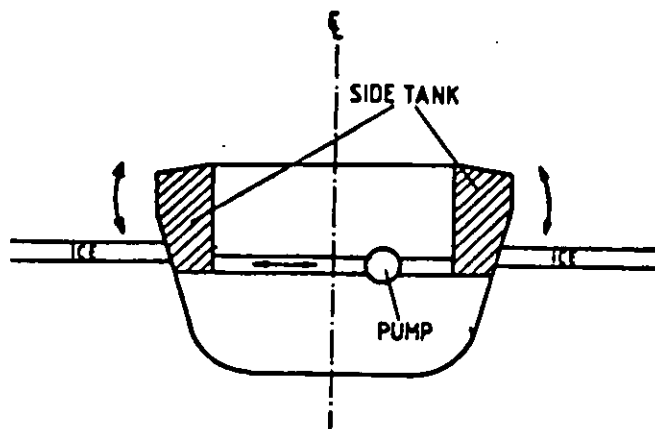


Fig. 1. The principle of a heeling system

Besides extracting the ship, the heeling system can also be used to help the ship to get started in extreme conditions.

3.3 Trimming System

The main purpose of a trimming system is very much the same as that of the heeling system.

In this system the water tanks are at both ends of the ship.

There are two different types of trimming systems:

- open system
- closed system.

In a closed trimming system liquid is pumped from the bow to the stern and back. In an open system water is pumped to and from the sea.

A schematic drawing of the trimming system is presented in Fig. 2.

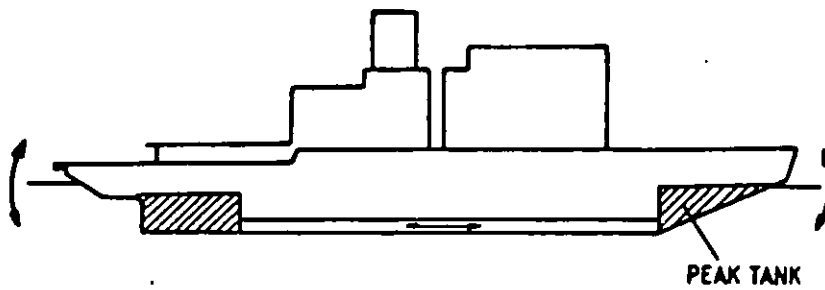


Fig. 2. Trimming system

3.4

Bow Propellers

Bow propellers were originally meant for flushing the bow area of the ship. The system was discovered after it was found out that in certain ice conditions ice-breakers moved better backwards than forwards. At first the number of bow propellers was one, but the system had a bad influence on the steering of the ship. To improve steerability, the number of the propellers was increased to two. In Fig. 3 various bow propeller arrangements are presented.

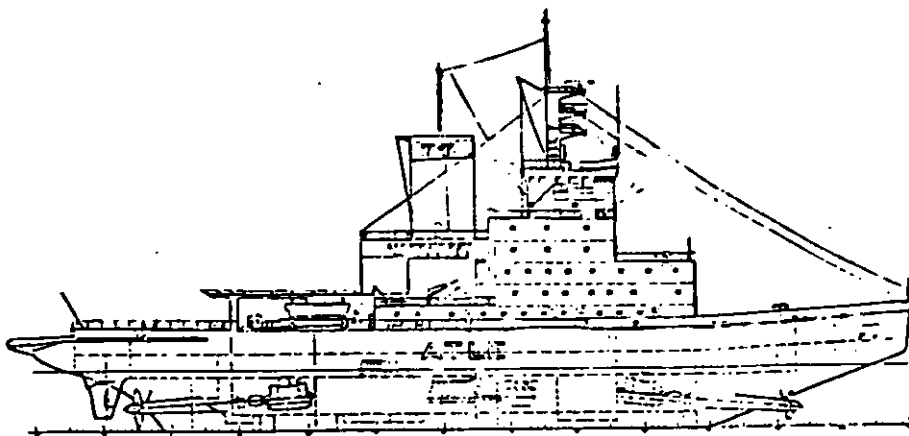


Fig. 3. Bow propeller arrangement, IB Atle

3.5 Air Bubbling

The Wärtsilä Air Bubbling System (WABS) was developed to replace the bow propellers. This system flushes the hull and can also be used as an additional steering system. In Fig. 4 there is the principal drawing of the WABS.

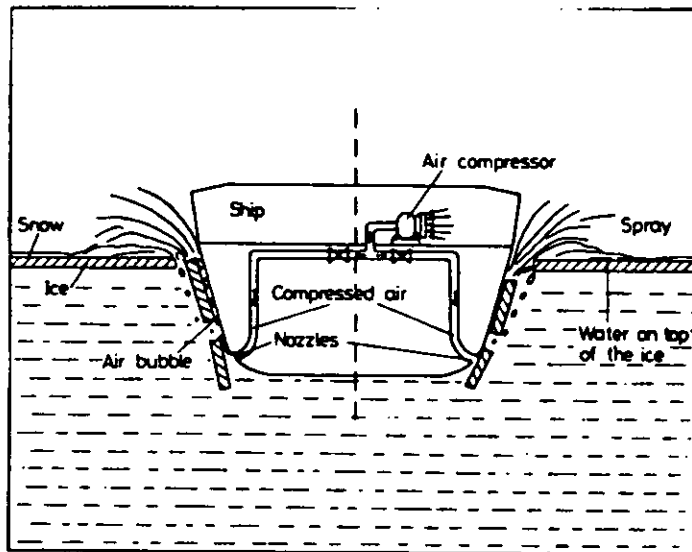


Fig. 4. Wärtsilä Air Bubbling System

3.6 Air Cushion

It is known that in certain conditions icebreaking is possible by using an air cushion technique. This can be done with a separate air cushion vehicle or with an air cushion platform in front of the ship. An air cushion arrangement is shown in Fig. 5.

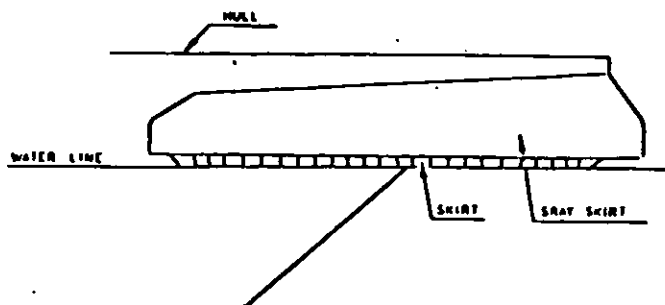


Fig. 5. Air cushion arrangement

3.7 Extreme Hull Form

On some occasions the shape of the ship's hull has a special purpose. In these cases the ship is usually effective only in one or two ice conditions. Examples of these kinds of configurations are for instance:

- Landing-craft bow
- Plough under the ship
- Reamers

3.8 Other Methods

Water Washing and Water and Air Washing

Principally there are two different types of water washing systems:

- Small nozzles (like air bubbling)
- One big nozzle like a thruster

4 PHYSICAL EFFECTS OF AUXILIARY SYSTEMS

What an auxiliary system can do to improve the ship's ice-going capability, varies according to the system employed. In the following and in chapters 5,6,7,8,9 and 10 I will compare the qualities of heeling, trimming, bow propellers, air bubbling and special paints.

Physical effects:

4.1 Heeling System

- In starting and stopping conditions the heeling system prevents
 $\mu_{dyn} \rightarrow \mu_{stat}$
- The heeling system creates peaks in the icebreaking forces which are directed separately to different parts of the hull.

4.2 Trimming System

- The trimming system creates a change in the equilibrium.
- The trimming system changes $\mu_{\text{static}} \rightarrow \mu_{\text{dynamic}}$ for a short moment.

4.3 Bow propeller(s)

- The bow propellers reduce the friction coefficient at the bow area.
- The bow propellers cut the ice into pieces.
- The bow propellers move the ice longitudinally.
- The shaft bossings of the bow propellers make it more difficult for the ice blocks to move.

4.4 Air Bubbling

- The Wärtsilä Air Bubbling System (WABS) reduces μ specially during operation in snow-covered ice.
- WABS prevents $\mu_{\text{dynamic}} \rightarrow \mu_{\text{static}}$ at zero speed.

4.5 Special Low Friction Paint

- Reduces friction

5 THE INFLUENCE OF AUXILIARY SYSTEMS ON THE SHIP'S ABILITY
TO PROCEED IN ICE-INFESTED WATERS

5.1 Heeling System

- Reduces the ice resistance in starting condition.

5.2 Trimming system

- Marginal

5.3 Bow Propellers

- Reduce the ice resistance in level ice when the power of the bow propellers is high enough.
- Help the ship to get through an ice ridge in constant movement at low speed.

5.4 WABS

- Reduces the ice resistance in all ice conditions

5.5 Special Low Friction Paint

- Reduces the ice resistance in all ice conditions.

6 INFLUENCE OF AUXILIARY SYSTEMS ON THE RISK TO GET STUCK /
ABILITY TO EXTRACT THE JAMMED VESSEL

6.1 Heeling

- Reduces the risk to get stuck.
- Helps the ship to be extracted.

6.2 Trimming

- Helps the ship to be extracted.

6.3 Bow Propellers

- The effect is not quite obvious. (The shaft bossings make the situation worse. The extraction of the vessel can be helped by using the propellers.)

6.4 WABS

- Reduces the risk to get stuck.
- Helps the vessel to be extracted.

6.5 Special Low-friction Coatings

- Reduces the risk to get stuck.

7 **ADVANTAGES DERIVED FROM THE USE OF AUXILIARY SYSTEMS IN
ICEBREAKING**

<u>System</u>	Proceeding in different ice conditions	Prevention of getting stuck. Getting extracted.
Heeling	2	5
Trimming	0	4
Bow propellers	2	1
Air bubbling (WABS)	5	4
Special low friction paint	4	3

Scale: 0-5

0 = no benefit at all

5 = much benefit

8 PRICE OF THE AUXILIARY SYSTEM, POWER CONSUMPTION AND
ADDITIONALWEIGHT / LOSS OF DISPLACEMENT

<u>System</u>	Price	Power consumption	Additional weight/ Loss of displacement
Heeling	2	1	5
Trimming	2	1	4
Bow propellers	5	2	3
WABS	3	5 (0)	1
Special low- friction paint	1	0	0

Scale: 0-5

0 = price, power consumption, additional weight
is negligible

5 = considerable

9 ADDITIONAL ADVANTAGES OF AUXILIARY SYSTEMS

Heeling 2 pcs

- Use for damping of the rolling motion is in principle possible
- Prevention of the ship from getting frozen

Trimming 0 pcs

Bow propellers 3 pcs

- Improves steerability especially when the vessel is moving backwards.
- Prevents ice accumulation on the underwater part of the hull.
- Removes ice between the ship and the quay when the ship is coming to the harbour.

WABS 6 pcs

- Steering
- Prevents ice accumulation on the underwater part of the hull.
- Reduces wave action around the ship.
- Can be used for emptying the ballast water tanks (heeling, trimming).
- Prevents the ship from getting frozed to the surrounding ice field during loading or unloading cargo in the Arctic.
- Removes ice between the ship and the quay when the ship is coming to the harbour.

Special low-friction paint 2 pcs

- Saves painting work.
- Decreases corrosion.

10 EXISTING COMBINATIONS OF AUXILIARY SYSTEMS

	Heeling	Trimming	Bow prop- ellers	Air bubbling	Special paint
Older sub-arctic icebreakers	x	-	x	-	x*
Newer sub-arctic icebreakers	x	-	x	-	x
Newest sub-arctic icebreakers	x	-	-	x	x
Older arctic icebreakers	x	-	-	-	-
Newer arctic icebreakers	x	x	-	-	-
Newest arctic icebreakers	x	x	-	x	x
Older icebreaking cargo vessels	-	-	-	-	-
Newer icebreaking cargo vessels	-	-	-	x	-(x)
Newest icebreaking cargo vessels	-	-	-	x	x

*The painting is done after several years of operation of the vessel.

11 TEST RESULTS FROM AUXILIARY SYSTEMS INSTALLED IN WÄRTSILÄ-TESTED VESSELS

11.1 Heeling System

Tests conducted with the heeling system are basically starting and extracting tests. In Figures 6 and 7 there are examples of the test results.

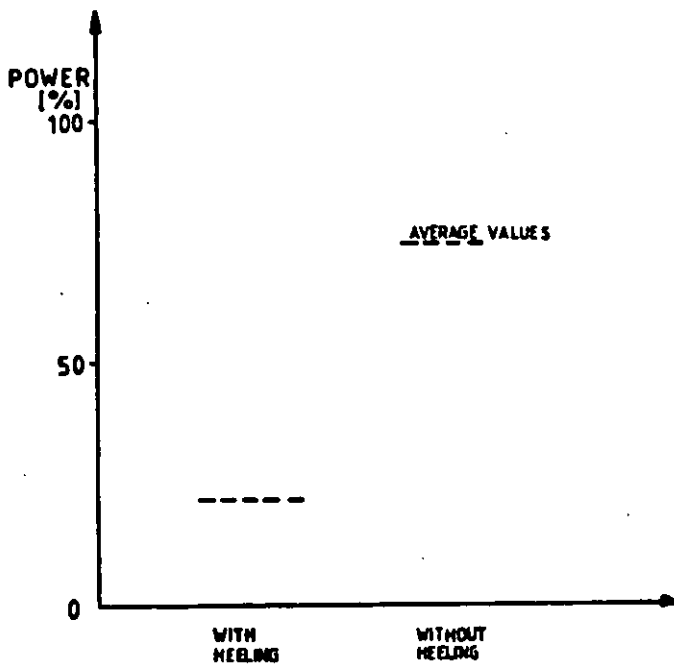


Fig. 6. Ymer extraction power in ridges

In Fig. 6 there is a very clear difference in the backing power when the heeling system is used.

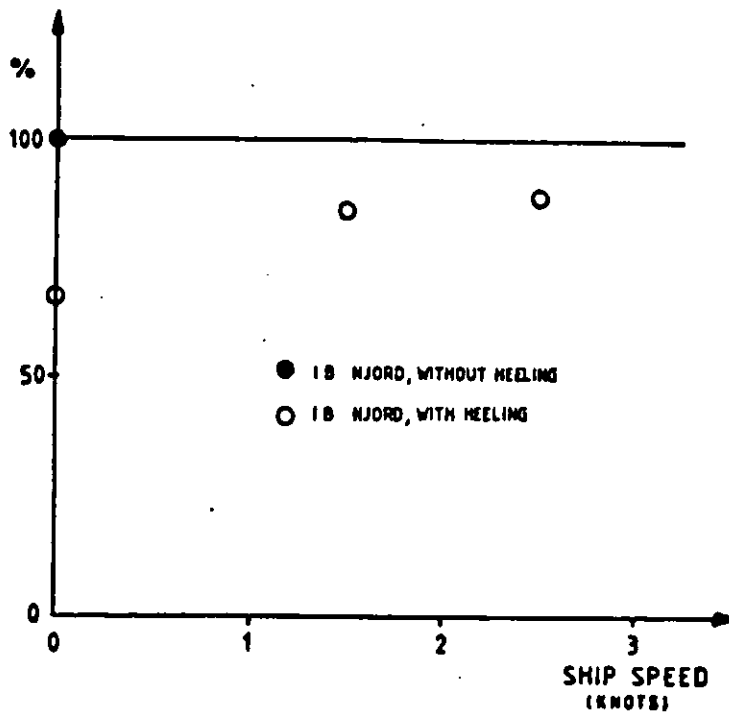


Fig. 7. IB Njord, the effect of the heeling system on the ice resistance in level ice.

In Fig. 7 the effect of the heeling system in starting condition abt. 35 % and in continuous motion 10-15 %.

11.2

Bow Propellers

Earlier sub-arctic icebreakers have bow propellers. Tests have been carried out very intensively in the Baltic area. Figure 8 shows the ice resistance with different bow propeller power compared to the resistance without the bow propellers.

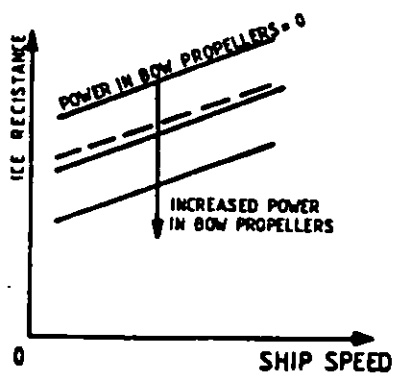


Fig. 8. The influence of the power of the bow propellers on the ice resistance in level ice.

- ship with bow propellers
- - - ship without bow propellers

In Fig. 8 we can see that if the bow propellers are used, they must have enough power to achieve the same level in ice resistance than the ship without the propellers at the bow.

11.3 Air Bubbling (WABS)

Modern icebreakers are equipped with an air bubbling system instead of bow propellers. Many tests have been carried out with WABS. When WABS is used we can increase the icebreaking capability of the ship. The power for WABS can be produced either separately from the propulsion power or within the propulsion power. In both cases we can increase the icebreaking capacity of the ship. The principle of the effect of WABS on the ice resistance is shown in Fig. 9.

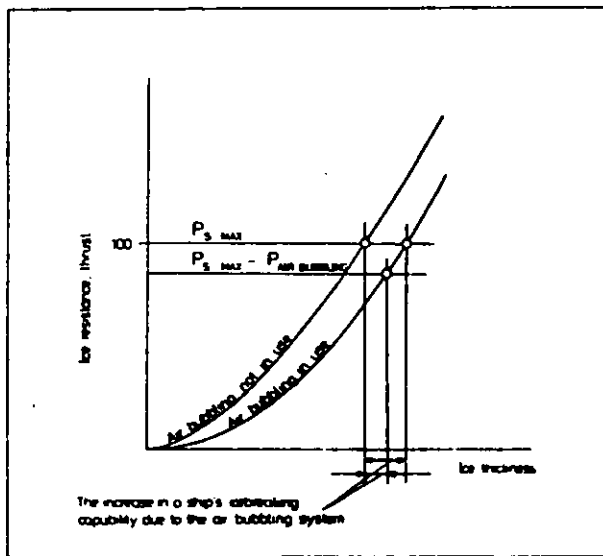


Fig. 9. The increase in a ship's icebreaking capability due to the air bubbling system, using both separate power and part of the propulsion power:

P_s = ship's power.

11.3.1 WABS, Level Ice

The influence of WABS on ice resistance in level ice is presented in Fig. 10. Tests have been carried out in the Baltic, in the Arctic and in the Antarctic areas with several ships. The reduction in ice resistance varies from 10 to 60 per cent.

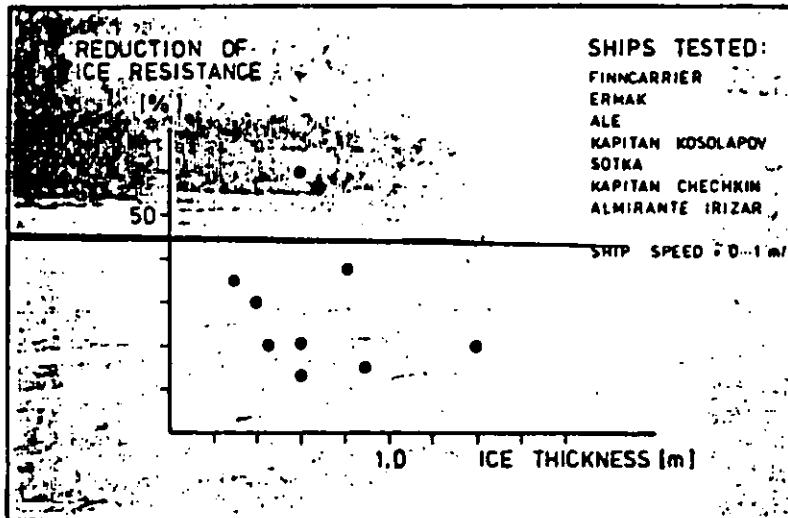


Fig. 10. Summarized results of full-scale measurements in level ice. Reduction of ice resistance due to WABS.

The variation in the results in level ice is very much dependent on the test conditions.

11.3.2 WABS, Broken Channel

Broken channel is a new channel made by the ship tested. The results in this condition are shown in Fig. 11.

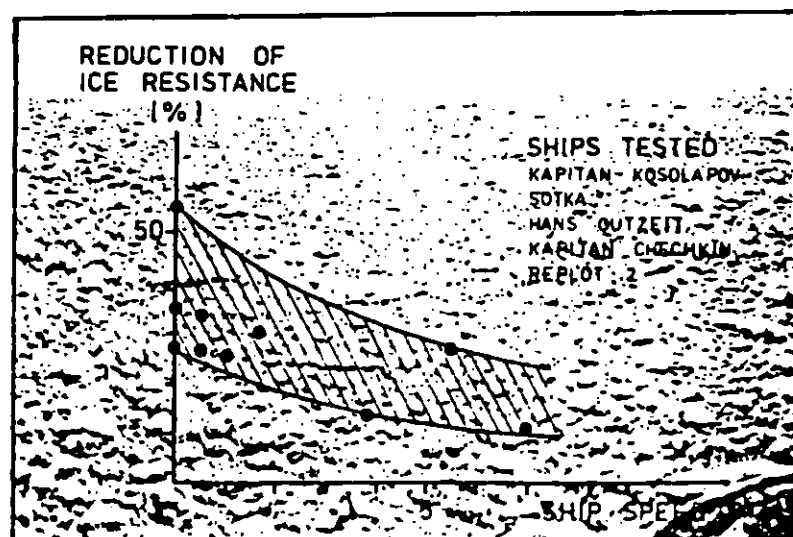


Fig. 11 Results of full-scale measurements in broken channels. Reduction of ice resistance due to WABS.

The effect of WABS in broken channels is obvious. Near zero speed the reduction in ice resistance is 25-55 %. At higher speeds it is somewhat lower.

11.3.3 WABS, Old Channel

An old channel means a channel which has very heavy traffic throughout the whole season. Test results in these ice conditions are shown in Fig. 12.

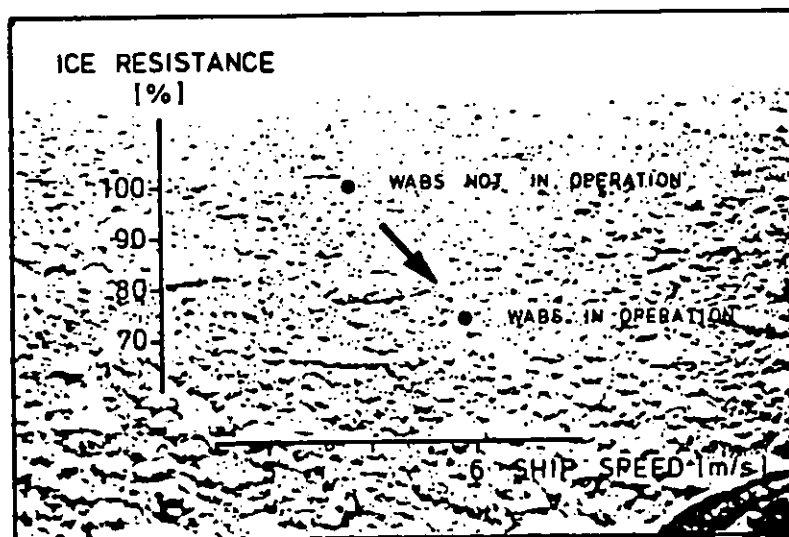


Fig. 12 Results of measurements in old channel.

In an old channel the vessel equipped with WABS reaches a higher speed at the same power level than the vessel without WABS.

11.3.4 WABS, Ridges

One very important ice condition is ice ridges. In this condition WABS reduces the risk of getting stuck in the ridge. It helps the ship to extract itself from a ridge. In Fig. 13 there are results of the extraction tests with IB Ale in ridges.

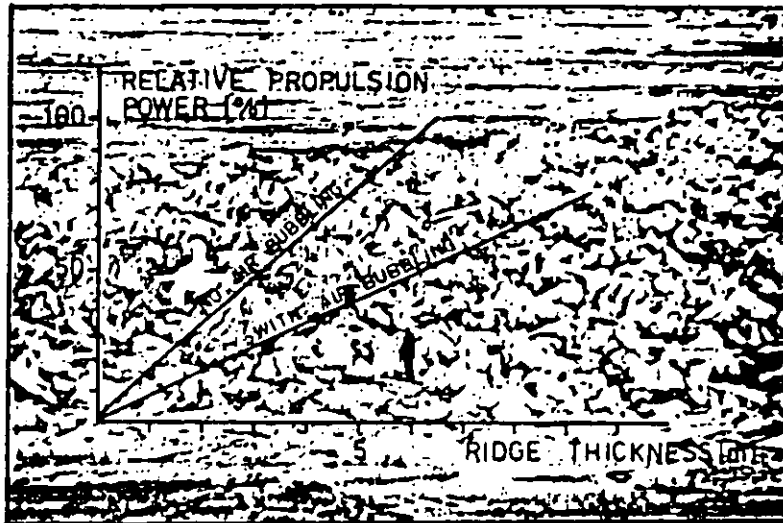


Fig 13. Power used to extract a ship from a ridge.

Full-scale tests with IB Ale.

11.4

Air Cushion

Air cushion vehicles represent a new branch in the highly specialized production of the Wärtsilä Helsinki Shipyard. The qualities of the ACV technique in icebreaking have also been studied. Fig. 14 shows the difference in ice resistance in level ice with and without an ACV platform in front of the ship. In level ice the power level is considerably lower with an air cushion platform which helps the icebreaking phenomena. When this combination, air cushion platform and a ship, is taken to old channel, the resistance with ACV is higher than without it which means that ACV is of disadvantage. This is presented in Fig. 15.

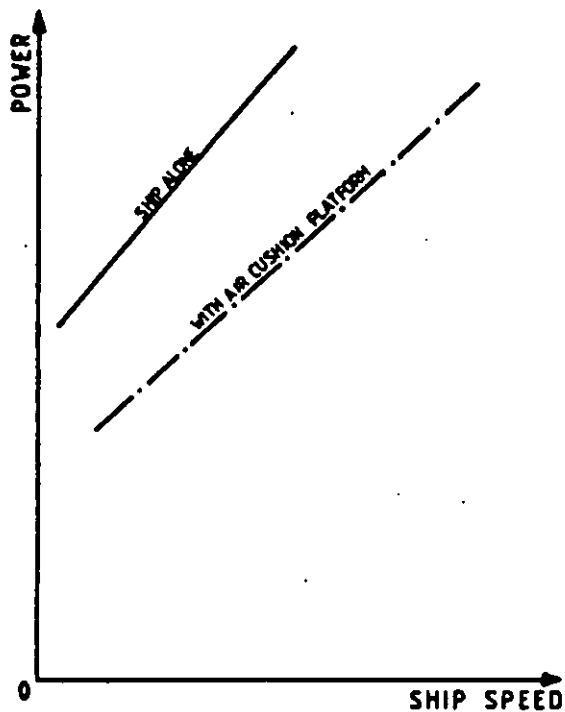


Fig. 14. Power consumption in level ice with and without air cushion platform in front of a ship.

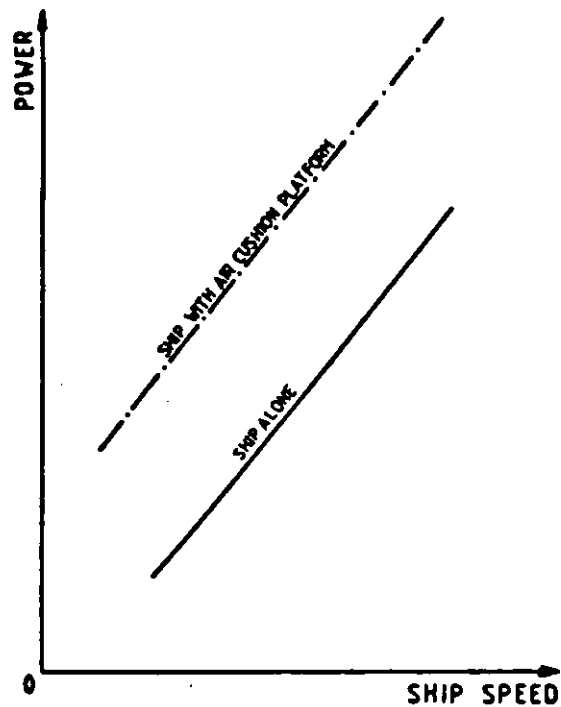


Fig. 15. Power consumption in old channel with and without air cushion platform in front of a ship.

11.5

Low Friction Coatings

Several ships painted partly or totally with a low friction coating have been tested. Fig. 16 shows the results from tests with two sister ships of different age. In 1972 the resistance of the older ship M/S "Silmä" was considerably higher than that of the younger "Valpas". Then the hull of the "Silmä" was painted with a low friction epoxy paint Inerta 160. When the ships were re-tested in 1974, their resistances were almost equal.

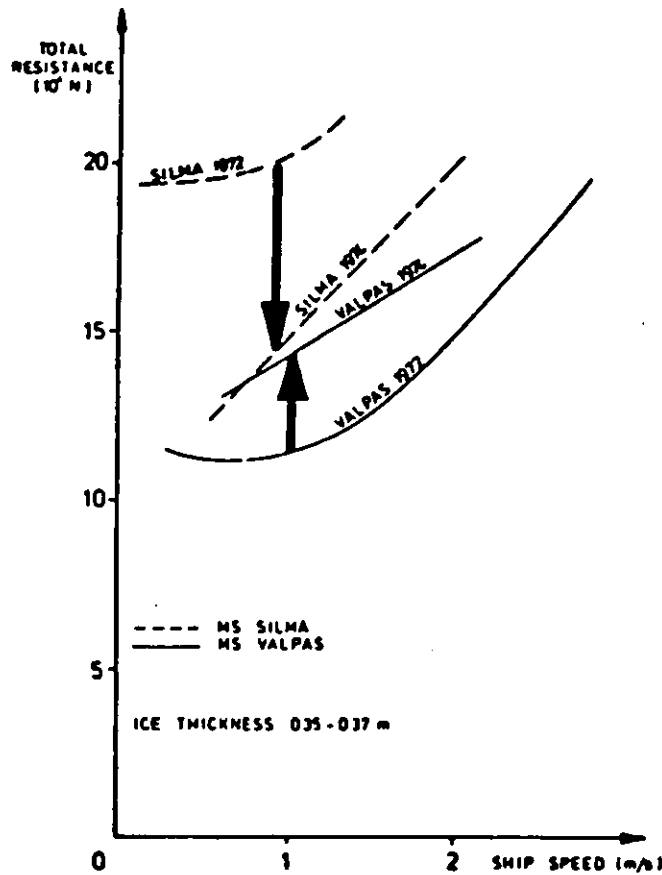


Fig. 16. The influence of a low friction coating on ice resistance

CONCLUSIONS

There are many systems to increase the ice performance of an icegoing vessel in extreme conditions. Some of them are good only in one ice condition, some have good qualities in all ice conditions that are faced by the vessel. It is highly dependent on the purpose of the vessel. To be able to choose the appropriate auxiliary systems for each project, we must know the circumstances in the area where the vessel will operate.



M.Sc. Jouko Virtanen

ICEBREAKERS

The following paper will present icebreakers, which are built in the last years and it is trying to show the development that has happend. The presentation is made primarily of icebreakers made at the Wärtsilä Helsinki Shipyard although the major icebreakers in the world are mentioned. The icebreakers are a demanding type of ship with excitement, rough conditions in remote areas of the world. There is always place for innovations and product development and in the future changes towards better icebreaker design will proceed with increasing speed.

1. BALTIC ICEBREAKERS

VOIMA

For good reasons icebreaker VOIMA can be called the pioneer of Wärtsilä's icebreaker production. This baltic icebreaker was delivered in 1954 to the Finnish Government. With her 10500 shp she was considered extremely powerful at that time. She has two bow propellers for the first time in an icebreaker and this four propeller lay-out has reminded unchanged in all later Baltic icebreakers. The heeling system was also installed already then . The displacement was 4350 t.

Three sisterships were ordered of Soviet Union, and they were the beginning of a long series of different kinds of icebreakers which Wärtsilä has built for the USSR. The names of those ships were Kapitan Belousov, Voronin and Melehov. Sweden ordered one similar icebreaker, Oden.

KARHU

The icebreaker KARHU was delivered in 1958 to the Finnish Government. It was decided to build a smaller icebreaker for use in sheltered waters. The power of the ship is 7500 shp and the displacement 3370 t. Two sisterships, MURTAJA and SAMPO, were delivered to the Finnish Government and one to Federal Republic of Germany, HANSE.

TARMO

The third class of Baltic icebreakers was TARMO, delivered in 1963. The power was increased to 12000 shp and displacement to 4890 t. Sweden ordered two, TOR and NJORD and Finnish Government a further two more, VARMA and APU.

URHO

The five icebreakers in the URHO class are URHO and SISU to Finland while the ATLE, FREJ and YMER were delivered to Sweden. The first was delivered in 1975. With her 22000 shp and 7900 t displacement she was almost double the size of the old icebreakers which were operating in the Baltic.

The aim of design was to secure year-round navigation to all major ports in the northern parts of Gulf of Bothnia, which means an ice thickness of 1,0-1,2 m with pressure ridges. The experience has shown that this also was achieved.

Machinery.

The propeller arrangement is still the same ;two at the bow and two at the stern. The five diesel engines are Wärtsilä-Pielstick 12 PC 2-5 type, 5000 bhp each. The main generators are 2x1735 kW DC. The propelling motors are 2x2455 kW at the stern and 2x1605 kW at the bow. The supplier of electric transmission system was Strömberg ,like for most of the Wärtsilä's icebreakers. The control system was made for unmanned engine room. The latest requirements for pollution control were fulfilled.

Interiors

The most significant change as compared to older icebreakers was the arrangement of the superstructure. The reason for this was the great attention to noise problems caused by ice. All living quarters were placed on the superstructure and some floating floors were installed. The interior linings were made of double steel cassettes with superior sound insulation values. Also the fire protection was improved by using steel furniture. All artistical curvatures were leaved away to allow easy manufacturing.

Outfitting

For the first time, two rudders were installed on a Baltic icebreaker. After extensive testing in full scale and some modifications, there has not been problems and the steering cabability is excellent. The helicopter deck and hangar were also new features on a Baltic icebreaker.

All 19 Baltic icebreakers are still working, some of them have also been used in arctic conditions.

VOIMA, the first one, was in a complete refitting in 1978. Diesel generators were changed to Wärtsilä Vasa 16 V 22 type engines with elastic mountings. The electric transmission was converted to an AC-DC power station with thyristor rectifier.

The whole superstructure was redesigned and rebuilt. Now she has 14000 shp propulsion power and better and quieter living quarters than ever.

The smallest class KARHU is considered to be too small to assist today's cargo ships and they probably soon be replaced.

2. ARCTIC ICEBREAKERS

All arctic icebreakers made by Wärtsilä are deliveries to the Soviet Union. U.S and Canadian Governements have placed their orders to only domestic yards.

MOSKVA

The first arctic icebreaker from Wärtsilä was icebreaker MOSKVA in 1960. She has a displacement of 15340 t and 22000 shp. The main machinery layout, all three propellers at the stern and one rudder, have reminded unchanged in all Wärtsilä's Arctic icebreakers.

MOSKVA has four sister ships;
LENINGRAD, KIEV, MURMANSK, and VLADIVOSTOK.

ERMAK

The second Arctic icebreaker class was ERMAK, delivered 1974 with two sister ships ADMIRAL MAKAROV and KRASIN. With her 36000 shp she is still the most powerful diesel-electric icebreaker in the world. The displacement is 20241 t. Although the general arrangement is oldfashioned considering the delivery date, the ships are used successfully on the long routes of the Soviet Arctic.

Machinery

The ship has nine main engines Wärtsilä-Sulzer 12 ZL 40/48 with a power of 4600 bhp each. The electric transmission, delivered by Strömberg, is of DC-DC type. The propellers with bolted blades have a diameter of 5,4m. In addition to heeling, also air bubbling was installed.

KAPITAN SOROKIN

The third class KAPITAN SOROKIN with three sisters, KAPITAN NIKOLAEV, KAPITAN DRANITSYN, and KAPITAN KHLEBNIKOV of which the first one was delivered only three years later, in 1977, than ERMAK, has a more modern outlook. The influence of the URHO class is clearly seen. KAPITAN SOROKIN has 22000 shp and a displacement of 14900 t. She is working in Siberian river areas and estuaries, where the waters are too shallow for bigger icebreakers.

Machinery

Six main diesel engines are Wärtsilä-Sulzer 9 ZL 40/48 type with a power of 4140 bhp each. The main generators are of AC type and DC propulsion motors are fed by diode rectifiers. Both heeling and air bubbling are installed. The fuel which is used is about 300 SRI for main and auxillary engines

3. ANTARCTIC ICEBREAKER

ALMIRANTE IRIZAR

Wärtsilä has also delivered one icebreaker for Antarctic supply operations, the Argentinian icebreaker ALMIRANTE IRIZAR, delivered in 1978. She has a displacement of 14900 t and a power of 16200 shp. The main features compared to previous mentioned icebreakers are the bigger number of passengers on board, scientific laboratories and a capability to take cargo. The ship is sailing longer periods in open waters including heavy seas. Fin stabilizers are installed to reduce rolling in such cases.

Machinery

The main diesels are Wärtsilä-Pielstick 8 PC 2-5 L type, 5200 bhp each. The electric transmission AC-DC with separate auxillary diesel generators. The air bubbling is fed by the main generators

4. SOME ICEBREAKERS BUILT IN OTHER COUNTRIES

JAPAN

After bad experiences with the ~~nuclear~~
^{FUJI}
icebreaker ~~MITSUBISHI~~, Japan has made a diesel-electric
icebreaker for Antarctic supply. SHIRASE has a
displacement of 12000-17600 t and 30000 shp. The main
engines are six Mitsui-MAN 12 V 42 M. The ship was
delivered in 1982.

USA

The icebreakers POLAR-STAR and POLAR-SEA have a
displacement of 13190 t and a maximum power of 60000
shp. The machinery is CODOG type and with
diesel-electric mode the ship has a power of 18000
shp. POLAR-STAR was delivered in 1976.

*ICE PRESSURES ROUGHLY
2x Pile BATHIC ~ Pile ARTIC*

*just
purch*

CANADA

The Canadian Coast Guard's new icebreaker
PIERRE RADISSON has a displacement of 8180 t and a
power of 13600 shp. It was delivered in 1978 for
Arctic and Great Lakes service. She has a
diesel-electric machinery.

The private companies in Canada have made two interesting supply ship-icebreakers. Dome Petroleum's CANMAR KIGORIAK, delivered in 1979, has 16600 shp and Gulf Canada's new ship 22200 shp and 6190 t displacement. The later will be delivered in 1983. Both ships have geared diesel machinery with CP propellers.

FEDERAL REPUBLIC OF GERMANY

Germany's new research ship POLAR STERN has 19100 shp and is intended for use in the Antarctic. The machinery is geared diesels with CP propellers. She was delivered in 1982.

USSR

Since building the first nuclear icebreaker LENIN in 1960, the Soviet Union has used them for long Siberian routes. The icebreaker ARKTIKA was delivered in 1975 and the sister ship SIBIR in 1978. A third vessel of the same design is under construction. The displacement of ARKTIKA¹ is 23460 t and the power about 66600 shp, which makes her the most powerful icebreaker in the world.

* ЛЕВ И Д БИЛЕВ

5 SOME DESIGN QUESTIONS

Hydrodynamics

The icebreaker design has to consider many additional things compared to ships which are operating only in open waters. The hull form must be a compromise taking into account seaworthiness, hydrodynamics and icebreaking capability. The good icebreaking bow may easily lead to spraying which is harmful in icing conditions. Propellers and stern lines are causing problems with an increasing demand for lower draft and higher outputs. To achieve reasonable clearancies, good wake field, good icebreaking stern and low pressure pulses, extensive model testing in ice and in a conventional model basin are often needed. The increasing number of rudders will not make the design easier.

Noise and vibration

The question of noise and vibration has become more important in the last 15 years, when many countries have made rules and recommendations. When a ship is navigating in ice, the problem is still more complicated.

Noise and vibration are almost like alternative choices for a designer; A quiet, vibrating cabin in the superstructure or noisy in the hull. The better support the superstructure has, the easier the structure borne noise is proceeding there.

For estimating the ice noise, it may be considered as a structure borne noise source, affecting the bow region. All secondary noise sources become important when the propeller is milling ice.

For vibration estimations there is no specific excitation force and frequencys due to icebreaking. All possible frequencys will be present.

Others

When considering icebreaker design, the first thing is of course the strength of the hull, propellers, shafting and rudders. After many full scale tests and studies, the level of knowledge is now better than some years ago.

Many smaller item like isolation, ventilation, sea inlets and machineries on open decks need special attention for working properly in arctic conditions.

Future

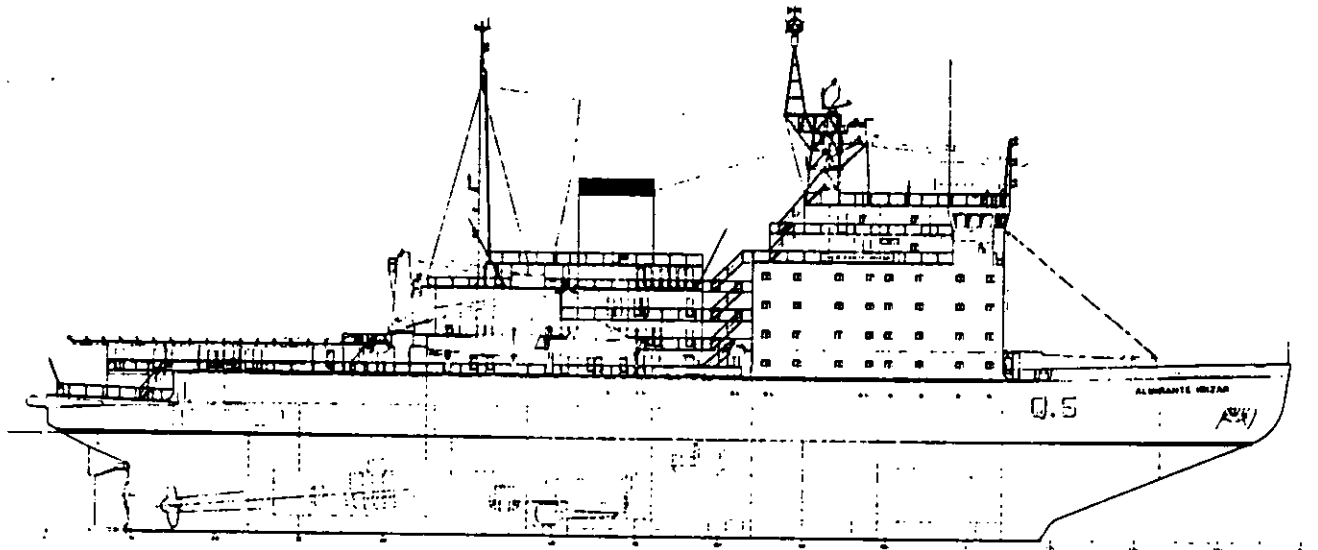
The rapid developement of medium speed diesels has made it possible to design more effective and compact machinery and they will keep their position as a main prime mover for icebreakers. The use of heavier fuel will be the practice also in icebreakers. For more demanding purposes electric transmission will be the main solution but in the future AC-AC type. The geared diesel machinery will for economic reasons also be made for a less demanding use.

The tremendous development in communication, navigation and alarm systems will lead to smaller crews and one-man operated bridge design. The number of icebreakers in the future will be increasing, how fast, will depend on oil prices, developments in the Antarctic and, like the whole shipbuilding industry, on the economical situation in the world.

C.B = .5 → .59 .7
 OLD NEW RIVER 18's

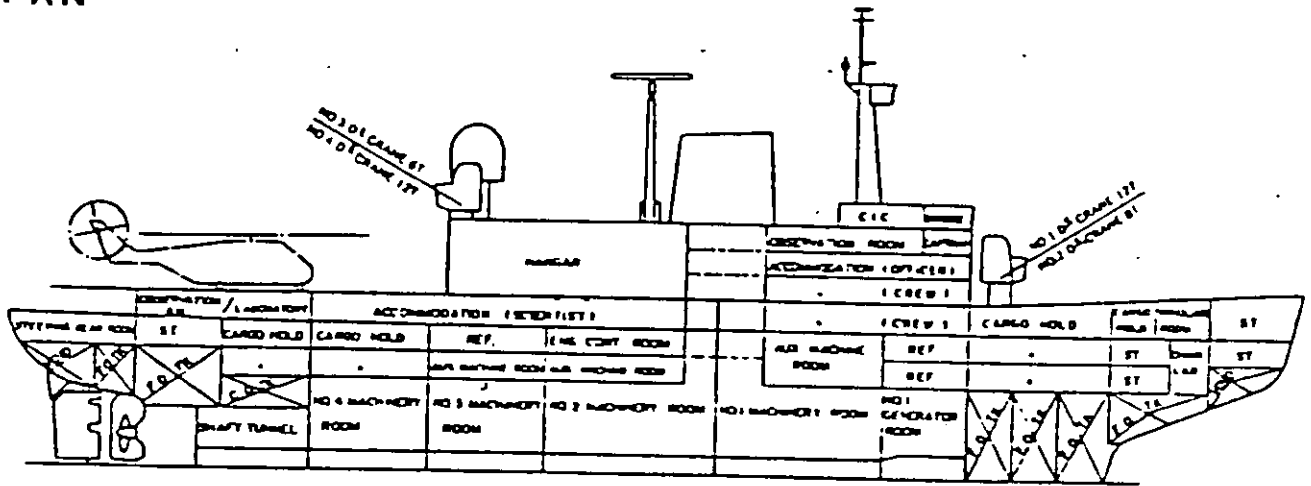
ANTARCTIC ICEBREAKER

WEGEMT 1983
13/XXX



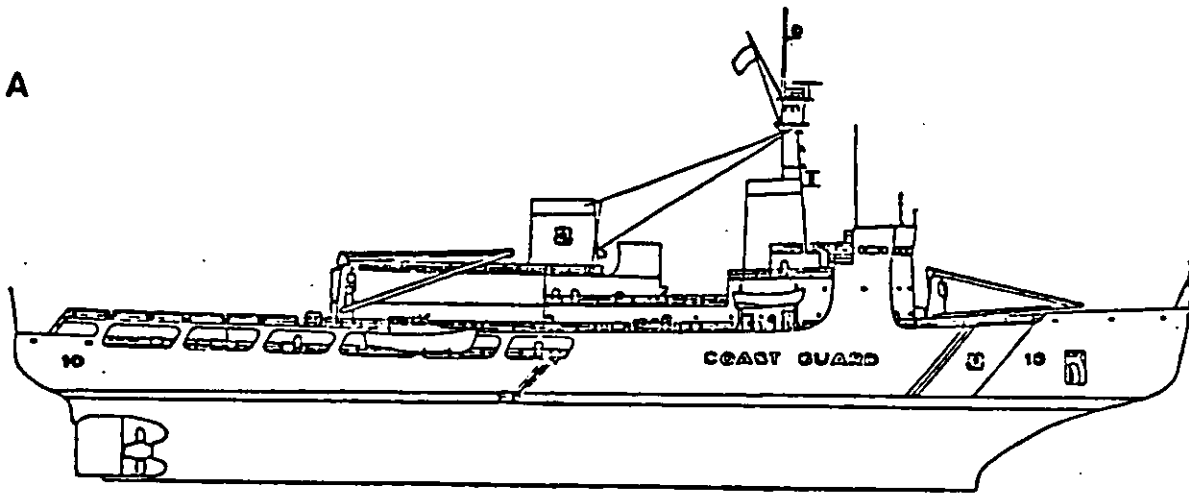
A.R.A. ALMIRANTE IRIZAR 1978 119.3 m

JAPAN



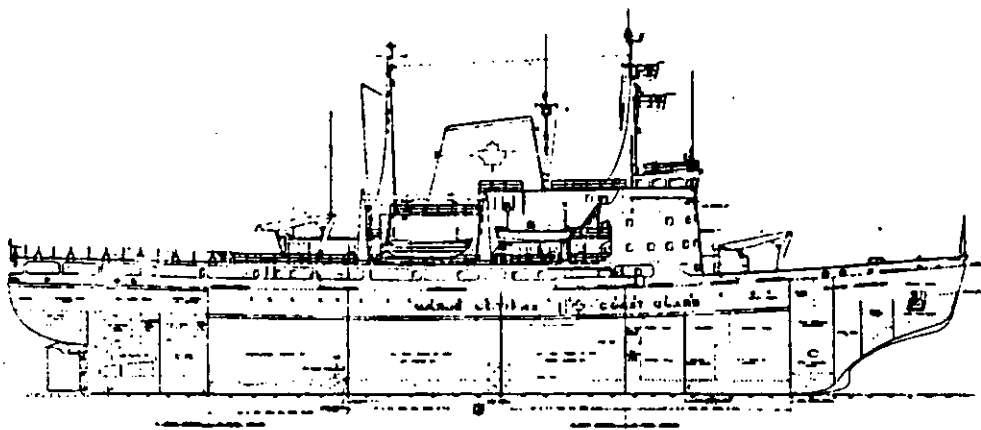
SHIRASE 1982 134 m

USA



POLAR STAR 1976 121.6 m

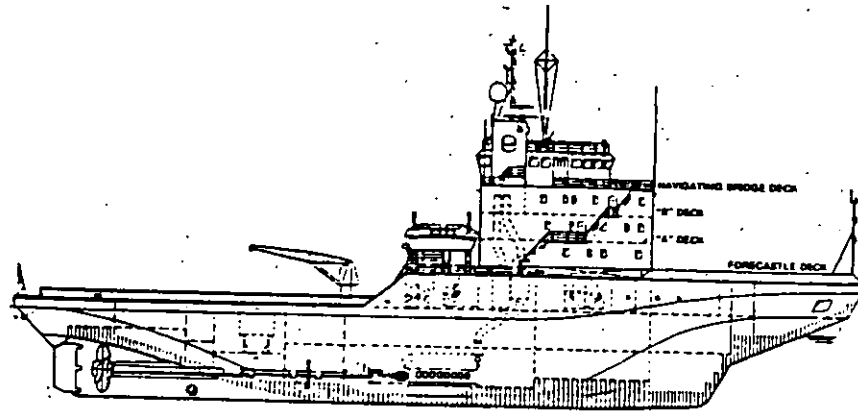
CANADA



PIERRE RADISSON 1978 98.2 m

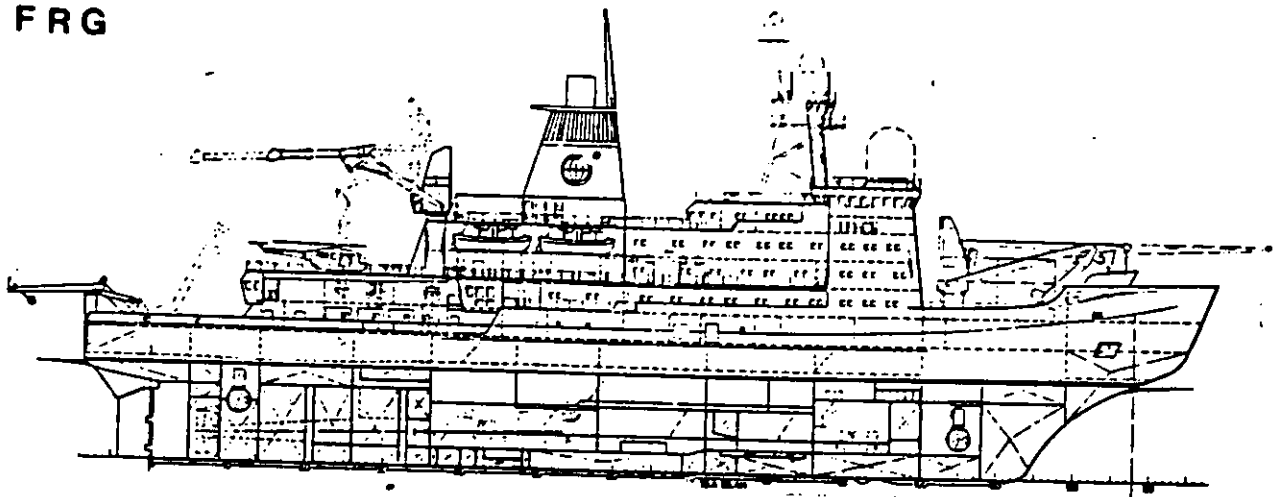
CANADA

WEGEMT 1983
15/XXX



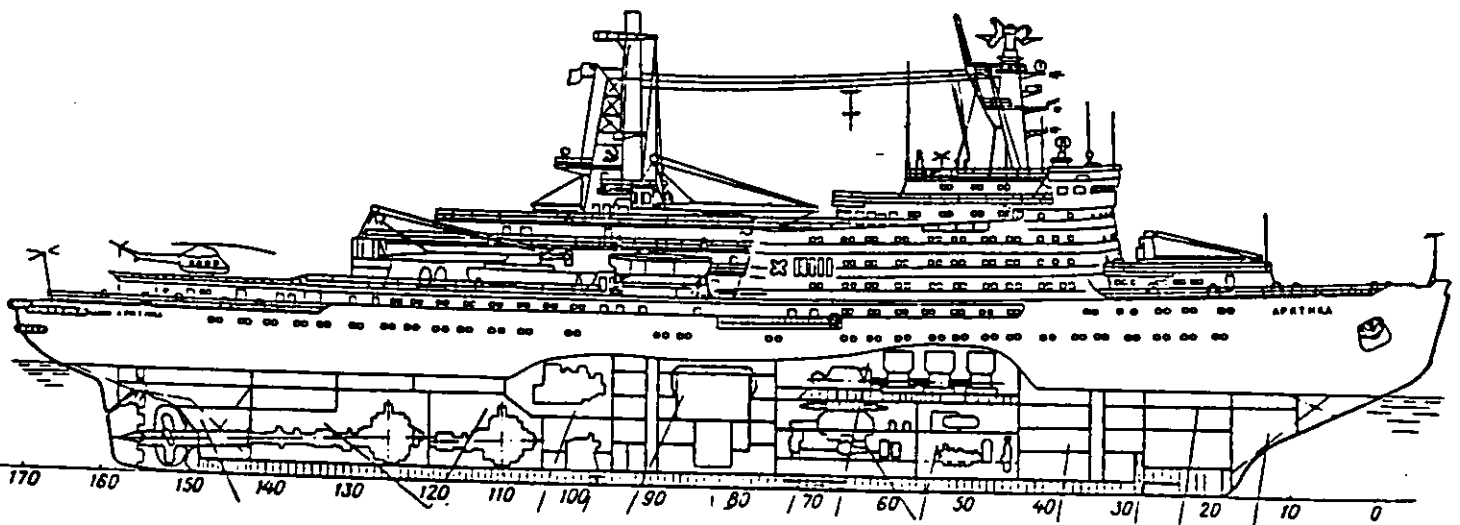
GULF CANADA 1983 88m

FRG



PÖLAR STERN 1982 118.0m

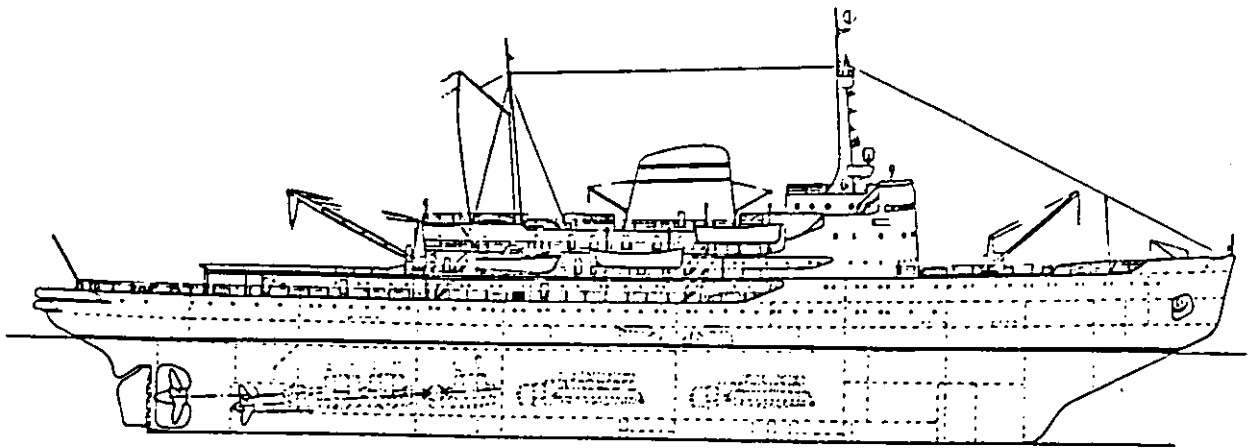
USSR



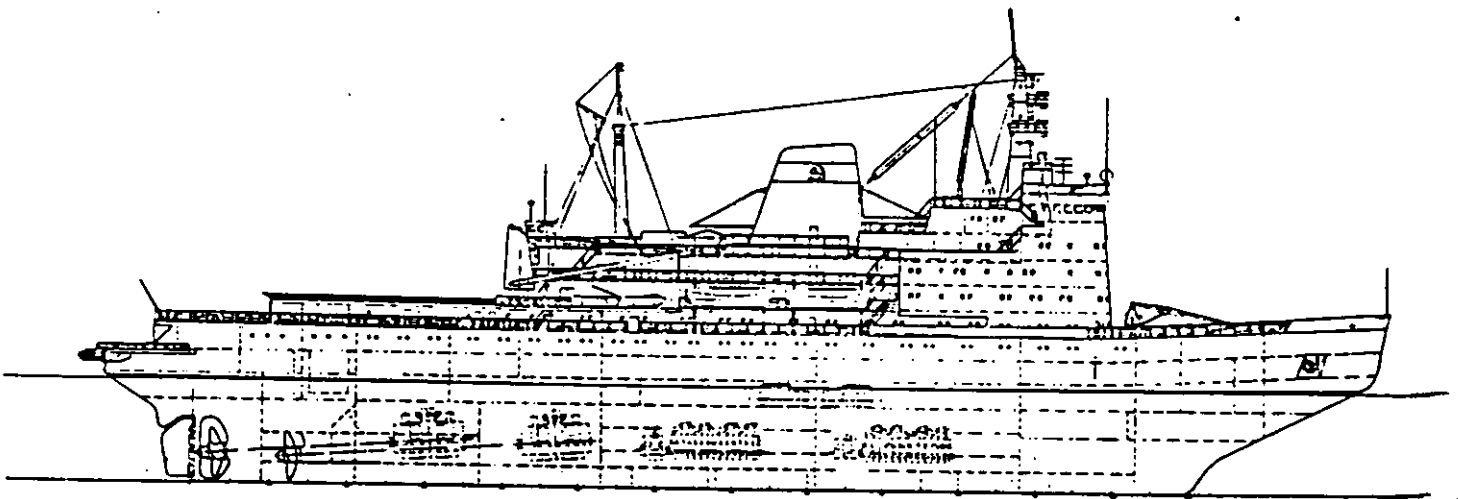
ARCTIKA 1975 147.0m

ARCTIC ICEBREAKERS

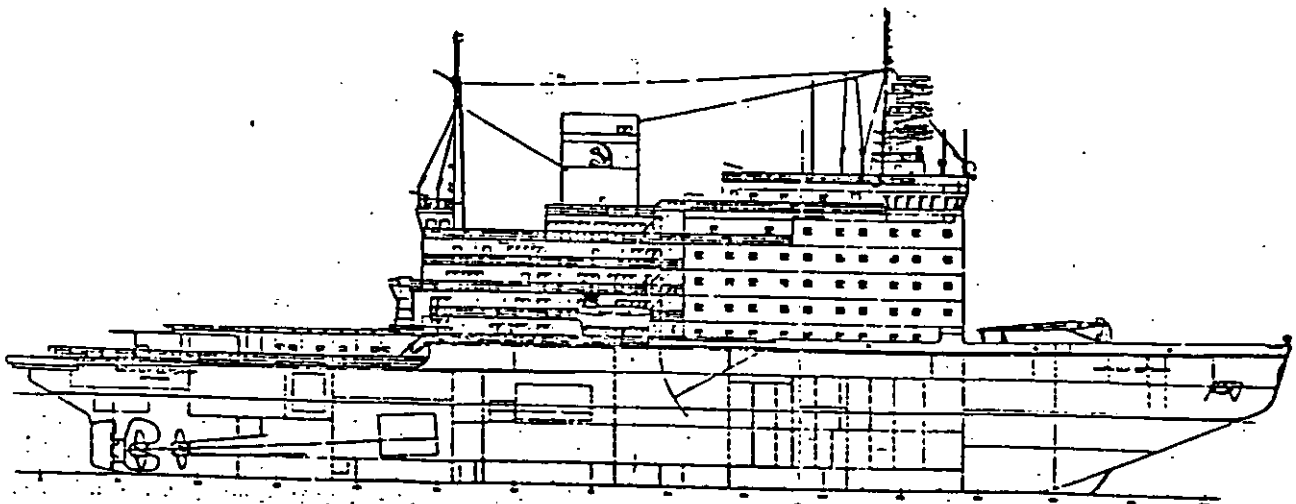
WEGEMT 1983
16/XXX



MOSKVA 1960 122.1 m



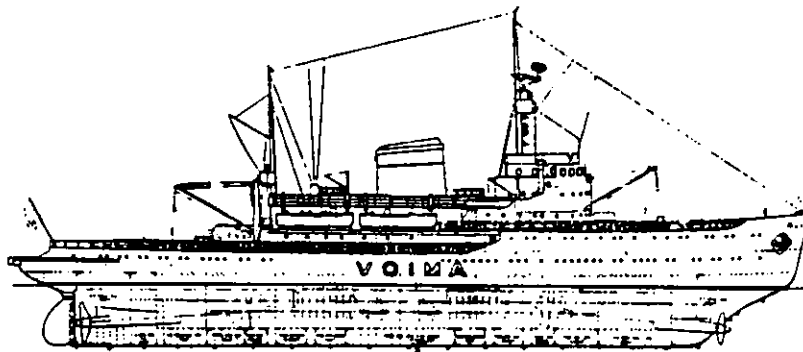
ERMAK 1974 135.0 m



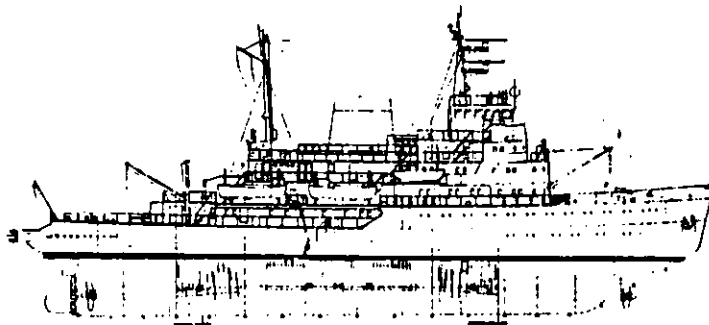
KAPITAN SOROKIN 1977 131.9 m

BALTIC ICEBREAKERS

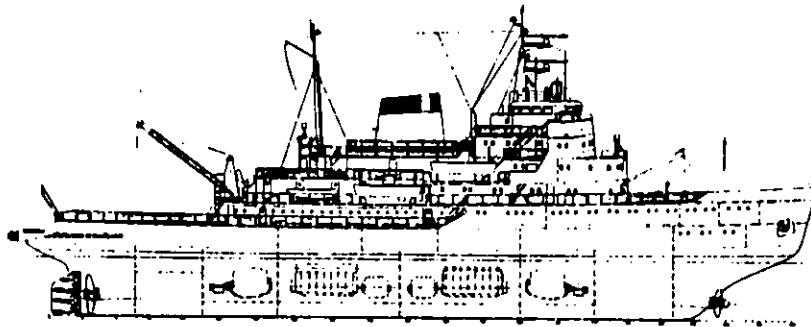
WEGEMT 1983
17/XXX



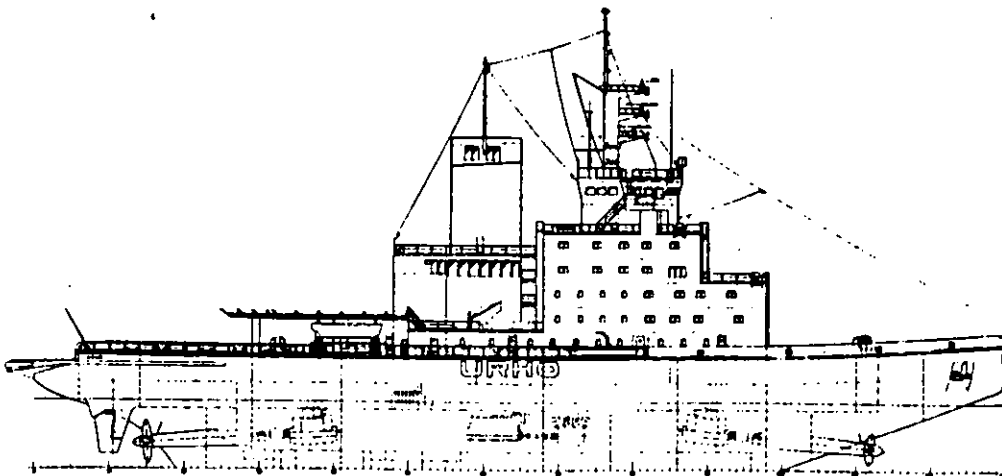
VOIMA 1954 83.5 m



KARHU 1958 74.2 m



TARMO 1963 84.5 m



URHO 1975 104.6 m



Mr Markku Kanerva

ICEBREAKING CARGO SHIPS

ABSTRACT

A case study of an arctic multipurpose cargo ship designed for Soviet arctic shipping is presented. Basic information for the project was data of the Soviet arctic traffic: amount and type of cargo, routes, existing vessels and icebreakers, experience of the traffic, environmental conditions (ice, snow, wind etc.) and harbours. Some information was also available concerning factories, mills and other production facilities in the Siberia and investments planned for the two next five years periods. The project started in 1975, contract for the first nine ships was signed in June 1980 and the first vessel was delivered in November 1982. Background of the project is described, simulation of the arctic operation and economical comparisons of some alternatives will be given. Design features and alternative propulsion systems are also discussed. Model testing procedure of various alternatives in ice, in open water, in cavitation tunnel and in rough seas was started already in 1978. Comparisons of model test and full scale measurements of open water trials indicate a good correlation and generally a very good behaviour of the vessel. Unfortunately full scale ice tests are going on during March and April of this year and the results are not yet available. A general description of the vessel is presented including propulsion system, cargo-handling etc. and also some ideas of an icebreaking cargo vessel in the future.

1
INTRODUCTION

Arctic shipping can be divided into two groups: scientific and merchant shipping. Scientific arctic shipping dates back 19th century and Nordenskiöld. Merchant shipping in the Soviet Arctic started in the beginning of this century but the development was quite slow and suffered from various problems until the end of sixties (lack of powerful icebreakers and cargo ships, cargo handling problems, environmental circumstances, lack of suitable materials and equipment etc.) But until the urge for raw materials (oil, minerals and wood) at the end of sixties made it profitable to start various kind of projects in the Arctic and thus also arctic shipping with specialized ships and equipment.

Earlier experience had proven that conventional icebreakers or merchant vessels with ice strengthening were not the solution for the Arctic shipping, because of multiyear ice, exceptional environmental conditions and lack of repair and maintenance possibilities. Specialized ships and equipment were needed.

This paper will give a brief overlook of the Soviet Arctic shipping and a case study of a special arctic multipurpose ship.

2
ARCTIC SHIPPING IN THE SOVIET UNION

The Arctic shipping in the Soviet Union can be divided into two parts:

- arctic river traffic
- arctic sea traffic

These two traffic modes are competing against each other, especially where railway traffic is connected to river traffic. Ships for sea traffic are usually larger and have higher ice class. Part of the river ships can also sail on sea.

Shipping of cargo to the Soviet Arctic can be performed in three ways:

- from river headwaters (if near to railway or road) along the river with river ships
- along sea and river delta with sea going ships
- along sea to river delta with sea going ships and from there with barges or river ships along the river

2.1
River traffic

Traffic on Siberian rivers (Ob, Enisei, Lena) has been limited up till now to the period between June and November. River traffic is mainly including shipping of equipment and raw materials with river sea going ships. Amount of cargo is remarkable, for example in 1979 2 milj.ton along Enisei to Norilsk via Dudinka or 2-3 milj.ton along Ob to river delta. Ob and Enisei are the most important routes, along Ob exists a large amount of gas resources and along Enisei exists a copper combine in Norilsk and sawmill in Igarka. River fleet is mainly including river ships, barges, tugs, ice-breakers, dredgers and floating power stations.

2.2
Sea traffic

The most important reason for shipping in the Soviet Arctic is the natural resources found in the Northern Siberia. The main traffic areas are the Yamal Peninsula, the Bay of Ob, delta of river Enisei (Dudinka, Igarka), delta of river Lena (Tiksi) and Pevek in the North-East Siberia. Egvekinot in the Bering Sea and Magadan in the Okhota Sea are also important.

The northern passage is being sailed mainly on summer time, from July to October. The year round traffic has been succeeded to maintain only to Dudinka (Enisei) from 1978 and Magadan (Okhota Sea). Figure 1 is presenting the shipping routes in 1978 and in 1980.

From the shipping point of view the northern passage has been divided into two parts: western and eastern. Main harbours for the western traffic are Murmansk and Arhangel and for the eastern Vladivostok, the frontier being east from the Cape of Taimyr.

Winter traffic in the eastern part has been limited south from the Strait of Bering. Summer traffic is mainly service of various kind of equipment. Main harbours are: Mys Shmidta, Pevek, Zelenyy Mys, Nizhneyansk and Tiksi. The traffic of Nizhenayansk (1,75 milj.ton in 1979) is being handled with barges which are loaded from sea-going ships at Tiksi.

The total amount of cargo shipped along Lena was in 1981 12 milj.tons, but on the other hand the amount of cargo from north to south was only 250.000 ton. 40.000 ton of various equipment goes through the harbour of Pevek. Most of the ships visiting Pevek come from east, in 1979 7 ships from west and 19 ships from east.

One major problem in the eastern route is the probability of early coming winter, for example in 1979 7 ships were forced to stay in Pevek for the whole winter.

The shipping traffic in the western Soviet Arctic is much more valued, first of all because there is much more two way cargo. The main harbours are: Dudinka and Igarka on Enisei, Novyy Port, Salekhard and Jamburg on Ob, Mys Kharasavey in Yamal Peninsula, Amderma and Pechora areas. Dudinka is the only harbour which is open year round (11 months). The annual amount of cargo through Dudinka is about 5,5 milj.ton, of which about 3 milj.ton is sea traffic. Most of the cargo is equipment for Norilsk and ore (about 2 milj.ton) from Norilsk. The amount of cargo shipped through Dudinka from 1970 up to 1981 is presented in fig. 2. Figure 3 shows the length of traffic period in the northern passage through years 1920-1981. The ore shipping from Dudinka was started in 1960 and the amount of ore was about 200.000 ton. The Wärtsilä built Sorokin-class icebreakers, which are capable to sail at the shallow waters of Enisei delta, have succeeded in lengthening the traffic period of Dudinka up to year round. During winter time about 10 ships (20.000 tdw) pay a visit to Dudinka.

Igarka is the Siberian harbout for sawmill products, figure 4 presents the amount of these products being shipped through years 1950-1981. Traffic period starts a little bit earlier than in Dudinka, because the river is already open in Igarka while it is still flooding in Dudinka. It is quite usual that part of the fleet is wintering in Igarka.

In the delta of Ob east from the Yamal Peninsula the main harbours are Novyy Port, Jamburg and Salekhard. Cargo is usually equipmet for gasfields, drilling equipment and pipes. Active period is only during summer, for example during summer 1980 50 sea going ships sailed on the Ob area.

In Novyy Port cargo is unloaded into barges which will be handled by tugs to Nadym- and Taz-rivers. There is no information available of return cargo. The amount of pipe cargo to Novyy Port was 80.000 ton in 1980.

Gas was founded in Yamal Peninsula at the beginning seventies. The first ship with equipment cargo arrived in 1976, figure 5 presents the amount of cargo to the Cape of Kharasavey in Yamal through years 1976-1980. This area is operated in winter time, icebreakers are pushing the cargo ships towards firm ice, cargo is then unloaded and delivered to shore by lorries. Various reasons forced to choose this system: water depth is very limited near Yamal, earlier the traffic was operated in summer time with barges that did not succeed, a lot of cargo lost because of heavy wind and seas.

2.3

The Soviet Fleet for Arctic Shipping

All the vessels which operate on the Northern Sea Route, are at least ice strengthened and most of them have an icebreaking bow. Generally and especially concerning multipurpose cargo ships the size of vessels and the amount of ice strengthening have increased. Table 1 shows the amount of vessels approved by the Soviet Register to sail on the Northern Sea Route in 1970 and 1977 (ice class UL and ULA), part of these vessels have never sailed on arctic regions. The amount of icebreakers and ULA-class vessels has increased. The share of timber carriers has remarkably dropped because of very old fleet and because of a change in the ice class into lower class.

The Soviet Arctic multipurpose cargo ship fleet (ULA-class) included 21 ships in 1977. After that at least 14 UL-class bulk/container carriers (so called Dimitri Donskoi-class) have been delivered to the Morflot shipowners.

There are orders for 14 ULA-class arctic multipurpose ships (so called SA-15 class), for one nuclear driven and for one diesel driven barge/container carrier. SA-15 class will be described later in details in this paper.

Building of special arctic (icebreaking) cargo vessels started in the Soviet Union in the fifties. Experience had shown that ordinary, conventional vessels, even if they had an ice-strengthened hull, could not cope with the problems in the arctic shipping.

Their speed in an icebreaker convoy is no more than a few knots and they could not manage even in light ice conditions without the assistance of an icebreaker.

The first specially built arctic cargo ships were the "Lena"-class ships which were built during the fifties. At the end of fifties - at the beginning of sixties the so called "Amguema"-class ships were built based on the experience of "Lena"-class ships. Table 2 shows the main dimensions of these two prototypes and figures 6 and 7 give the impression of "Amguema"-ships. Both series are Soviet built and have an ice class UL. At that time a direct-current diesel-electric propulsion system coupled to a fixed pitch propeller proved to be most suitable for operation in arctic ice conditions. A diesel-electric installation was designed with two main electric current circuits for both prototypes. Automatic control with electric motor transmission could better ensure that a constant power was maintained when the propeller torque varied. The reliability of operation was guaranteed in case of frequent starting and reversing without considerable energy recuperation and in case of a reduction of revolutions of the electric drive motor when there was a sharp increase in the propeller torque without overloading the diesels. The propulsion system is designed for a full use of the engine power at the speed with any number of generators cut in and also for operation in the case of two propeller blades were broken. During operation of varying ice conditions, when various engine loads and reversals are frequent, the diesel-electric propulsion system has shown great flexibility and reliability.

The maximum loads for the hull structure for these two prototypes were chosen as follows: bow, midship and stern sections 300, 150 and 250 ton/m accordingly at the beginning (without allowing for the work of the stringers) and 375, 200 and 300 ton/m for the outer plating. Insufficient strength of the framing especially in the midships has limited the attainable speed and operation in ice fields. But on the other hand good manoeuvring qualities at low speeds have allowed these ships to avoid very large ice obstacles thus increasing the mean passage speed.

Table 2 shows the dimensioning and maximum loads for the hull structure. Shell plating thickness in the ice belt is 28 mm in the bow, 20 mm in the midships and 24 mm at the stern; transverse framing has been used.

The presence of deep tanks fore and aft of the engine room allows the ships to be trimmed to an even keel when carrying any kind of cargo with full use of the stowage space and to adjust the stability when proceeding in ballast. The capacity of ballast tanks makes it possible to have the propeller tip 2 m below water level when sailing in ballast. Unsinkability of the ship is assured in case two adjacent compartments are flooded at an initial draught up to 7.60 m provided that ballast is taken on as the fuel is consumed.

The hull form of both prototypes is icebreaker like and their icebreaking capability was satisfactory for medium ice conditions (ice thickness is not known). But in close-packed ice fields with ordinary thickness of ice these ships have already had problems and the passage has been possible only by ramming. This gives an impression that either the installed power is too small or the hull form is not the best possible, or perhaps both.

The short description of the "Lena"- and "Amguema" type ships gives an idea of the background and experience of the Soviet Arctic cargo ships. We do not have any information available, if these ships are still in operation in the Arctic.

3

ENVIRONMENTAL CONDITIONS

The environmental conditions in the Soviet Arctic are very severe and special attention has to be paid for the reliability and independence of an arctic multipurpose cargo ship in order to not only withstand the environmental conditions but to successfully operate under them.

In the following some of the special environmental conditions are listed.

Ice conditions:

- ice thickness, level icefields from 10 cm up to 1,5 m and over
- packed ice, especially in the Kara Sea in the Strait of Novaya Zemlya with east winds
- natural channels may appear with north-west winds
- broken channels get back into ice very fast
- ice pressures are high, especially in the river deltas
- ice conditions are changing rapidly
- ice stream
- icening of ships.

Temperature can drop down to -50°C and will stay usually for a period of 1-2 months below -30°C . Wind is quite normal (0-20 m/s) during winters, during summer times higher wind speeds are reached. Rivers are flooding every spring for about one month. Water depth is very limited in river deltas and especially near the Yamal Peninsula.

Some of the technical problems involved in the environment are:

- lack of harbours
- ships are in much harder use and thus aging faster than in conventional traffic
- the supply of fuel is difficult to arrange.

The Northern Arctic Route from Murmansk to Vladivostok can be sailed only in summer time due to the insufficient amount of icebreakers and ice-breaking cargo ships. The worst places due to hardest ice conditions are the Strait of Novaya Zemlya and Viljkitski. There is also a route north of Novaya Zemlya, see figure 1, but the strait of Viljkitski is very hard to go around because north of Severnaya Zemlya is the area of multiyear ice.

OWNER'S SPECIFICATION FOR THE ARCTIC CARGO SHIP

A first indication of a new serie of arctic multi-purpose cargo ships to be designed and built for the Soviet shipowner Morflot was given in discussions with Sudoimport and Morflot in 1975. It was stated then that the "Amguema"- and "Lena"-class ships are too small.

The first idea was that two sizes of ships should be designed, 12500 ton dwt and 5000 ton dwt, but Morflot indicated that these figures are not binding and the optimum for the larger vessel is between 12500 ton dwt and 21000 ton dwt. The operational area is the Soviet Arctic, the Northern Arctic Route, both western and eastern areas. Because the ships will be specially designed for arctic conditions, cargo will be delivered to the nearest open harbours (Murmansk or Vladivostok) and the ships will operate from these harbours; but on the other hand the ships will be classified for world around traffic.

Ice class UL or ULA, was to be clarified thoroughly taking into account the effect of ice pressures. Maximum draught 9 m and breadth lower than with the existing arctic icebreakers. Container and ro-ro handling possibilities.

Various main propulsion systems were to be simulated, diesel-electric, direct coupled diesels (long stroke) or medium speed diesels coupled via reduction gear, and a fixed pitch propeller in all alternatives.

After two years period having made various simulations and designs the final owner's technical specification was received in April 1977. The project was named SA-12 (Sub Arctic 12.000 ton dwt).

The specification included among other things:

- deadweight should be about 14.000 ton dwt
- the ship is a general cargo carrier capable of taking long cargo (pipes), pallets, heavy cargo up to 80 ton (elements of drilling rigs, equipment and technical vehicles), reefer cargo, liquefied oil cargo, steel structures, vehicles, 1A and 1C containers including the height of 8.5 feet, fuels and lubricants, explosive cargo, flammable liquids and containerized chemicals
- operational area unlimited, operational radii 12.000 miles
- class USSR Register KM [⊙] UL 1 A1, hull, rudder and propeller to be dimensioned according to ULA ice class

- all the shipbuilding conventions and regulations to be fulfilled (SOLAS -74, IMCO -73, IMCO -72, various USSR regulations, US Coast Guard regulations, Suez and Panama regulations etc.)
- the ship will have 5 cargo holds, 2 decks, cargo hatches as broad as possible, a ro-ro deck, a stern-angle ramp, double skin. Hull material and deck machinery are chosen and designed to withstand -45°C temperature, living and working quarters are isolated according to -50°C temperature
- maximum draught 9 m, breadth about 24 m
- hatch covers in the upper deck are dimensioned for ISO 1C and 1A 20 ton containers or for 32 ton containers respectively
- loading or unloading the ship can happen in harbour, in anchor or directly on an icefield via stern ramp and/or using deck cranes (2x20 ton, 2x12,5 ton, 1 80 ton derrick)
- an air bubbling system and a roll stabilization system should be included
- in all loading conditions even keel must be reached
- when sailing in ballast the forward draught must be at least 3% of the length of the ship having the propeller immersed at the same time
- trial speed at the design draught and at the 90% of the maximum continuous rating of the main engine should be 17 knots
- icebreaking capability should be at least 0,80 m
- propulsion system includes two medium speed diesel engines having ice fly wheel and coupled to a single fixed pitch propeller. The main engine fuel can have viscosity highest 1500 sec R1
- cabins for 39 crew members, 10 for passenger and 1 for pilot

From the first indications the deadweight of the ship had increased already up to 14.000 ton dwt, but the name was still SA-12. Having received the technical specification traffic simulations were performed in order to find out the optimum size of the ship and roughly the amount of power to be installed. Within short after the simulations name of the project was changed into SA-15. Thorough simulations were performed also concerning various propulsion system alternatives.

TRAFFIC SIMULATIONS

A simulation study was performed in order to find out the effect ship size and installed power on transport costs of general cargo in the Soviet Arctic. Three various shipping routes have been studied in year round traffic

- Murmansk-Dikson
- Dikson-Tiksi
- Tiksi-Beringovskij

Ice conditions which have been used in the simulations are based on weather and ice statistics published concerning those areas. Icebreaker assistance of the existing Soviet icebreakers operating in the Arctic have been taken into account.

The ship is a general cargo vessel equipped ro-ro and lo-lo cargo handling possibilities. A deadweight range from 10.000 ton to 20.000 ton was varied. Maximum draught was 9 m, L/B-ratio was chosen according to resistance and strength requirements and a double skin was designed for the ship. The main alternative for the propulsion system was a diesel-electric-system, power ranging from 8.000 shaft kW up to 16.000 shaft kW coupled to a single fixed pitch propeller.

Following cost factors have been taken into consideration:

- capital costs, paying off time 10 years, annual interest 7%
- fuel costs
- crew costs
- repair costs, 1% of the purchase price

The assisting icebreaker is a 26.500 shaft kW polar icebreaker 'Ermak-type' and a loss of 12 hours for each voyage has been taken into account for waiting icebreaker etc.

Results of the simulation are presented in figures 8-13, figures 8-10 show the transport costs at various routes as a function of ship size and installed power. The optimum size for all three routes was a vessel with a deadweight of 12.000 - 14.000 ton dwt and a breadth of 23,5 - 25,5 m accordingly.

When the annual transport is taken into consideration, figures 11-13, a clear maximum is reached with breadth 25,5 m.

Figure 14 shows the effect of installed power during the worst winter month for ships with 23,5 m and 25,5 m breadth. The optimum installed powers seem to be 9 MW and 12 MW. The simulations show that an optimum ship has a deadweight of 12.000 - 14.000 dwt, a breadth of 23,5 - 25,5 m, and installed power of 9 - 12 MW respectively. The power figures do not include any safety margins.

6. CHOICE OF THE MAIN PROPULSION SYSTEM

Choice of the main propulsion system is one of the main design features for an arctic ship. The conventional icebreaker propulsion system, diesel-electric system with fixed pitch propeller, is not in every case the best possible system for an arctic multipurpose cargo ship when taking into consideration price, weight and room needed for the engine room.

In the following a short technical comparison of five various alternatives for a propulsion system will be presented. In every alternative the main engines are two medium speed diesel engines developing together 12,94 MW at 520 rpm. Propeller (fixed pitch or controllable pitch propeller) is a four bladed propeller having a diameter of 5,60 m and 135 rpm at maximum power.

Alternatives which have been studied:

1. A controllable pitch propeller coupled via a reduction gear and friction couplings
2. A fixed pitch propeller coupled into two DC electrical motors which are fed from AC generators via diod rectifiers
3. A fixed pitch propeller coupled via a reduction gear and hydraulic couplings
4. A fixed pitch propeller coupled via a two step reduction gear and hydraulic or friction couplings
5. A fixed pitch propeller coupled via a reduction gear and friction couplings or hydraulic torque exchanges.

These alternatives have been compared at three various conditions:

- open water, propulsion system is working at the best possible efficiency, ship's speed have been compared
- bollard pull, propulsion system is working at the gear ratio for ice conditions, bollard thrust have been compared
- working under ice load, ship's speed is 2 m/s, a constant ice torque is affecting to the propeller, propeller thrust have been compared.

6.1

C_{pp}, reduction gear, friction couplings

This alternative is presented in figure 15 and it does not include any new technics. There is a lot experience of similar systems both in open water and also in ice at least in milder ice conditions than in the Arctic. The propulsion system has been in use without any damage in firm ice up to ice thickness of 1 m and in broken ice up to thickness of 0,5 - 4,0 m and coverage 8/10 - 10/10.

The level of risk is low if correct dimensioning is used and the existing experience is being utilized. Weight and price are low compared to other alternatives. High efficiency for large power range means also low service costs without depending on the service profile.

6.2

F_{pp}, DC motors, AC generators

Figure 16 shows the principle of this alternative. A fixed pitch propeller is being powered by DC electrical motors which are fed by AC generators via diod rectifiers.

This is a very well-known alternative and it has been used as icebreaker propulsion system and thus it does not include any unknown risks. Disadvantages are quite high price and weight and on the other hand low efficiency.

6.3

F_{pp}, reduction gear, hydraulic coupling

In this alternative a fixed pitch propeller is powered via a reduction gear and hydraulic couplings, see figure 17.

The purpose of the hydraulic couplings is:

- to restrict the incoming torque of diesel engines up to the nominal torque of the engines in all operational conditions and thus a constant torque can be reached over the whole rpm range
- to make it possible to use lower propeller rpm than is possible according to main engine characteristics and gear ratio

Torque via the hydraulic couplings is depending on the rpm difference between the primary and secondary parts. In order to prevent torque increase when the rpm difference is increasing the filling of the hydraulic coupling has to be controlled and changed. The first two above mentioned features can be fulfilled only if it is possible to drive the couplings continuously with varying filling and the extra power is being absorbed via the coupling oil in oil coolers.

There was no experience available at that time of ships equipped with controllable hydraulic couplings which could be driven with part fillings, and a control system for ice operation was not even designed. A lot of risks existed concerning part fillings, cavitation at high powers and cooling system, and in order to withstand the torque peak coming from a suddenly stopped propeller a reliable and fast control system would be needed. This means that prototype risks were remarkable. Price and weight of the third alternative is between the first and the second. Efficiency is a little bit lower than with the first alternative.

6.4

Fpp, two step reduction gear,
hydraulic and friction couplings

In this alternative, see figure 18, a fixed pitch propeller is powered via a two step reduction gear and hydraulic or friction couplings. Friction couplings are used for the higher rpm range of the gear and hydraulic couplings for the lower range.

An advantage compared to alternative 3 is a good efficiency in open water and in principal a possibility for higher torque at low propeller revs in ice operations. The use of higher gear ratio in ice operations do have some restrictions; what should be the maximum propeller rpm: if it is too low the maximum power will be reached only at bollard pull, if it is too high the bollard pull will be restricted. In this comparison the gear ratio has been chosen in such a way that the propeller will absorb the maximum power at ship's speed 4 m/s. This means that only 11% higher torque can be reached by the ice gear ratio. To change the gear ratio a diesel reversal is needed (i.e. to stop the ship), which means that the system is by no means automatical.

Risks and disadvantages are the same as in alternative 3, but the more complicated reduction gear is heavier and the price is higher. Efficiency in ice operations is about the same as with the alternative 3, in open water the high efficiency (same as alternative 1) is reached only in one operational mode (point).

6.5

Fpp, reduction gear, friction couplings,
hydraulic torque exchangers

The fifth alternative is presented in figure 19, a fixed pitch propeller is powered via a reduction gear and friction couplings or hydraulic torque exchangers. The advantage of this system is compared to hydraulic coupling that a 2...3 times higher torque can be reached on propeller shaft at low rpm and still having constant torque in diesel engines. Disadvantages are: large and complicated reduction gear and high efficiency cooling system.

There are no experiences of torque exchangers of this size, problems and risks are about the same as with hydraulic couplings. Efficiency is about the same as with diesel-electric-alternative, price and weight are also about the same.

6.6

Results of the comparison

Results are presented in table 4. All the presented figures are results of simplified calculations, which means that the results should be considered relatively, the absolute values give just an indication of the speed or thrust level. In open water with all the alternatives same speed will be reached except with diesel-electric-system due to lower efficiency, difference is about 0.2 m/s.

Cop-alternative (1) has the highest bollard thrust and hydraulic coupling with single stop reduction gear the lowest. Difference between highest and lowest thrust value is 24%. In ice operation the differences are increasing, highest thrust will be reached with diesel-electric-system, with cop nearly the same (98%) and with torque exchange also quite high thrust (94% compared diesel-electric). Both alternatives with hydraulic couplings have quite low thrust values, alternative 4 53% and alternative 3 34% of the thrust of the cop alternative. Recommendation for a propulsion system for an arctic multipurpose cargo ship would be alternative 1 or 2.

The final chosen propulsion system was none of the above described alternatives but a combination alternative 1 and 3: a controllable pitch propeller powered via a reduction gear and friction couplings or hydraulic couplings. Friction couplings are for open water and light ice operations and hydraulic couplings for heavy ice operations. The final propulsion system will be described in more details in chapter 8.

7.

MODEL AND FULLSCALE TESTING

A thorough serie of model testing of this arctic multipurpose cargo ship was started about one and half year before contract in 1979. In between the name of the project had changed in SA-15 (sub arctic 15.000 ton dwt). Model tests were started with ice testing in WIMB (Wärtsilä Ice Model Basin, the old one), the total modeltesting sequence included: ice model tests, open water tests (resistance, propulsion etc.), cavitation tests and seakeeping tests. A large number of alternatives and conditions were tested.

- loss in bollard thrust about 4% compared to a conventional cp propeller, but greater margin against thrust breakdown which obviously brings back the losses in bollard thrust
- no remarkable air suctioning at low draughts

In spite of the good model test results it was decided to check the propeller performance also in the full scale by photographing and measuring the propeller induced pressures. Suction side cavitation was found to be less and more stable than in model scale, see figure 21. No pressure side cavitation occurred. The propeller induced pressure pulses were found to be on the same level as in model scale, blade frequency 2,5 kPa two engine mode, see figure 22. At the one engine mode the pressure was about 1 kPa. Both values can be considered to be low and indicates that the total vibration level of the vessel should be low. This was actually proved by the vibration measurements, see figure 23.

7.3

Seakeeping tests

Seakeeping capabilities of the SA-15 ships were modeltested at the Finnish Technical Research Centre, Shiplaboratory. Tests were performed in head and beam seas in moderate and heavy irregular waves using Pierson-Moskowitz seaspectra and also some regular waves were used. The results showed that the ship has good seakeeping capabilities:

- no shipping of green water occurred, which is extremely important for lowering the possibility of icing of weather deck and deck equipment
- no severe bottom slammings occurred
- accelerations were low for the deck cargo fastenings
- the ship motions were acceptable

DESCRIPTION OF THE PROPULSION SYSTEM

The main propulsion system includes two medium speed diesel engines, two hydraulic and two friction couplings, one double input, one output reduction gear box and a controllable pitch propeller. A schematic view of the system is presented in figure 24 and the engine room arrangement in figure 25.

Main engines are two Wärtsilä-Sulzer diesel engines, type 14 ZV 40/48, maximum power 7700 kW (10.500 bhp) at 560 rpm each intended for short period use only, maximum continuous rating is 6950 kW (9.450 bhp) = 90% of the maximum power. The reason for increasing the main engine power from the original 12.000 kW up to 13.900 kW is purely to increase reliability and independence of the ship. The main engines are four-stroke, single-acting, reversible, turbo-charged, trunk piston type marine engines with rotating pistons and direct fuel injection.

Reduction gear is a Renk made double input single output marine gear type Renk ASM 2x187,5. Two hydrodynamic or hydraulic couplings are included, type Voith 1660 TR, also elastic (or friction) and clutch couplings are included.

A thrust bearing, type RENK ST 71, is separately installed in the shaft line.

The propeller and intermediate shafts are hollow bored for the pitch setting mechanism and the oil distribution box is arranged at the forward end of the gear box. The shaft line is connected to a controllable pitch, four-bladed propeller type KaMeWa 235 XF 1/4. Material of the propeller is special stainless steel. Propeller diameter is 5,60 m, maximum revs 120 rpm and hub diameter 2,35 m. Propeller blades can be changed under water by divers.

8.1

Propulsion system operation

The propulsion system can be operated via friction (elastic) couplings or hydraulic couplings. Friction couplings are used in open water for one and two engine modes which both have own combinator (pitch/rpm-control system). Friction couplings can be utilized also in light ice conditions and the control can be arranged with a combinator or with a constant rpm program. The hydraulic (hydrodynamic) couplings are intended for heavy ice conditions, slip of the couplings is about 8% at the maximum continuous rating. Power control is stepless in the range from 0 to 100%. A constant rpm program is intended for the ice operations.

7.1
Ice model tests

The ice model tests were started at the beginning of 1979 in order to find out first of all the ice-breaking capability of the ship but also to see the propeller-rudder-action in various ice conditions. The basic hull form version had a conventional ice-breaker bow and a stern with open propeller. The specified icebreaking capability had increased up to ice thickness of one meter and twenty centimeter snow. The first test serie included resistance and propulsion tests forward and backward in even ice with ice thickness from 0.8 m to 1.8 m at various speeds, and same kind of tests in broken channels. The specified icebreaking capability could be reached in continous mode, and in broken channel a speed of about 4 m/s could be reached.

The second step was to test a newly developed special icebreaker bow and modified for a cargo ship.. The results were extremely good, icebreaking capability of being about 1.2 m thick ice in continous mode. But inspite of the good results the ship-owner was not willing to choose this hullform because the risk for higher slamming and course unsta-bility in heavy seas might be too pronounced.

The use of nozzle propeller in icegoing ships has been lately discussed and tested (in model- and fullscale) a lot. There are some icegoing ships which do have a nozzle propeller but the amount experience at the beginning of 1979 was quite limited. The amount of extra thrust of a nozzle propeller (some 30% at bollard condition) was really a facinating advantage if it would be really achiev-able in the reality and thus a nozzle propeller alternative was model tested as a third step in ice tests. Same ice conditions were tested as for the earlier versions and same speed were used. The propeller nozzle system worked very well at lower ice thicknesses in level ice and in channel for both directions. But when increasing the ice thickness the nozzle became full of ice and the propeller stopped both in level ice and channel. Propeller shaft torque and thrust varied a lot and were in some cases more than three times the respective open water values. Nozzle induced extra resistance was also remarkable.

Decision was quite clear : the nozzle propeller gave no benefit for this arctic multipurpose cargo ship in heavy ice operations, which are obvious operational circumstances for this kind of a ship.

The final step in ice model testing was performed with the final hull form and propeller model. The final form became as a result of open water (resistance, propulsion, wake etc.) and seakeeping tests. The aftship configuration was modified into a bulbous stern in order to achieve a good wakefield and to fit the huge hub of the cpp (diameter 2,35 m) into the hull form. The rudder is a semi-spade rudder with two lower bearings and without any solepiece. The idea behind the modifications was not only the open water performance but also the ice operations and to avoid ice blocks going into the propeller. Ice tests at various speeds proved this idea, the propeller was working nearly in ice free flow even with the highest tested ice thicknesses (about 2 m). This meant that the measured thrust and torque variations at the propeller shaft were really low.

The final hull form is presented in figure 20 in a perspective view. The hull form is very much different from that of conventional merchant ships. The stern form resembles that of efficient polar icebreakers, the hull form is designed to prevent any damage by the ice pressure without sacrificing too much displacement. The horn type rudder is specially designed for use in heavy ice conditions using icebreaker experience. It has two lower bearings in order to withstand high ice loads. As a summary of ice model tests can be stated: the SA-15 class ships are capable of breaking uniform level ice with a thickness in excess of one meter in a continuous mode of operation. As these ships are designed to cope with all the prevailing ice conditions in the Arctic including ridges, ice under pressure, shallow water etc., they will be able to perform independently in moderate, arctic ice conditions. The ice-going capability of SA-15-class is outstanding, it has no rivals in the class of arctic cargo ships. The Canadian MV Arctic gets to the closest, it is capable of breaking ice of around 2 ft thick and to operate in the Arctic during summer time only.

7.2

Open water and propeller tests

The hydrodynamical design parameters for an arctic multipurpose cargo ship differ a lot from those of a conventional cargo ship. Some of these parameters concerning hull form and propeller are listed below:

- maximum net thrust at low speeds for ice operation mode
- good icebreaking and manoeuvring capabilities in various ice conditions
- minimum propeller-ice interaction
- enough inertia to overcome high iceloads
- correct dimensioning of the propeller, shaft and pitch setting mechanism in order to avoid damages and on the other hand not to lose too much in the propeller efficiency with heavy dimensions
- low resistance and high propulsive efficiency in open water
- low cavitation and propeller induced pressure pulses against the hull
- low vibrations
- no pressure side cavitation at one engine mode at low pitch settings
- ship motions and accelerations to be low in rough seas
- no bottom slamming or shipping of green water in rough seas

7.2.1

Open water model tests

Ice model tests have been already described in chapter 7.1, and the propulsion system will be described in the next chapter (8). The open water tests for the hull form included resistance and propulsion tests, flow line and wake measurements and bollard pull measurements in still water.

Resistance and propulsion test results showed that the owner's specification could be fulfilled with a good margin, at 90% power of the maximum continuous rating (90% of 21.000 hp) at design draught of 8.5 m a speed of 18.1 knots could be reached.

The flow lines in the aftship and the wakefield would have a large effect on the propeller performance and propeller induced pressure pulses especially when the propeller diameter was limited (5.6 m) and a high power should be absorbed (21.000 hp).

Various alternatives were tested and in the final aft ship a bulbous stern was introduced in combination with a horn rudder. The measured wakefield with the final hull form is presented in figure 21. The open water tests were partly performed by the Finnish Technical Research Centre, Shiplaboratory, and partly by the Krylov Institute in Leningrad.

7.2.2 Propeller tests

According to the ice model tests an open propeller was selected as it had a much higher total efficiency in heavy ice conditions than a nozzle propeller. The propeller design conditions can be listed as follows:

- ice conditions, speed from backing to 10 knots, draught between 8-9 m, propeller to be operated via friction couplings or hydraulic couplings, maximum continuous engine power 18900 hp, maximum allowable engine power for short periods 21000 hp.
- open water condition with two main engines, speed about 18 knots, draught from ballast Gm up to 10 m, propeller to be operated via friction couplings, maximum continuous engine power 18900 hp
- open water condition with one main engine, speed about 15.7 knots, draught as above propeller to be used via friction couplings, maximum continuous engine power 9450 hp

Propeller diameter was limited into 5.60 m in order to have enough clearance above and also to baseline because of the risk of bottom contact. This means that regarding icebreaking ships the power output per propeller area (21.000 hp/5.60 m diameter) the SA-15 class ship is the second highest in the world and the highest with cp propeller. Only the Soviet Arctica-class nuclear icebreakers have a slightly higher rating.

Propeller model tests were performed at the KaMeWa Laboratory and the Krylov Institute. The following promising results were obtained:

- moderate cavitation on the suction side at two engine mode, open water, see figure 21
- no cavitation erosion
- low propeller induced pressure pulses, below 3 kPa just above the propeller at two engine mode, open water, blade frequency, see figure 22
- no pressure side cavitation at one engine mode
- loss in open water efficiency due to high dimensions and cavitation about 4%, two engine mode

Reversing of the propeller can be made either by reversing the pitch or by reversing the main engines. In the latter case it is possible to reach a higher astern thrust. Reversing time for the both alternatives has been optimized taking into account backpower, inertia and other dynamic features of the propulsion system. Reversing can be performed fluently and quick. Stepless power control makes it easy to operate in a convoy or to perform various manoeuvres.

The torque characteristics of the main engines can be improved by running the hydraulic couplings with part fillings, thus stopping of main engines in heavy ice conditions can be avoided. But using part fillings means that the efficiency goes down and part of the main engine power has to be absorbed by coolers. If the propeller is locked in ice the cooling system is dimensioned in such a way that the full power can be absorbed by the coolers. This was checked in the trials by running the main engines at full power towards each other and having the propeller clutched off.

8.2

Dimensioning of the propulsion system

The propulsion has been dimensioned according to the requirements of ULA ice class and the experience of icebreakers and ice strengthened cargo ships equipped with cp propellers. Dimensioning philosophy is to have propeller blade as the weakest link i.e. having a strength pyramid from propeller blade up to main engine. Strength requirements have led to a propeller hub diameter of 2,35 m and shaft diameter of about 1 m, in order to have adequate dimensions for the pitch changing mechanism. Various ice conditions and ice loads have been used in dimensioning, bending one blade horizontally, stopping propeller during one revolution, high frequency varying load etc. Dimensioning of the propeller have been finally checked by using finite element method with varying ice loads on the blade.

9

SHORT DESCRIPTION OF THE SA-15 SHIPS

9.1

General description

The Wärtsilä-designed SA-15 type icebreaking multi-purpose ship is intended for navigation in arctic ice-covered waters independently or behind an ice-breaker.

The Wärtsilä air bubbling system is arranged for the ship to improve her icebreaking performance and manoeuvrability.

Cargo containment system consists of five holds. All holds are fitted with tween decks. Lower holds Nos. 2, 3 and 4 are designed mainly for general cargo, bulk cargoes and containers. Tween decks Nos. 2, 3, 4 and 5 are designed mainly for general cargo, ro-ro cargo and containers. Hold No. 1 is designed for explosives, inflammable liquids and chemicals in packages. The double skin construction is reaching up to tween deck in holds Nos. 2, 3, 4 and 5 and up to upper deck in engine room.

Hydraulically operated folding type hatch covers are arranged on upper deck and crane operated non-water-tight hatch covers on tween decks except on tween deck no. 1 where the hatch cover is hydraulically operated.

The stern ramp arrangement feeds ro-ro cargo to tween decks via cargo doors.

The cargo gear consists of three single deck cranes and one twin deck crane.

Electricity is generated by three diesel driven alternators.

Pressure for air-bubbling system is generated by two diesel driven compressors, one of which is also coupled via disengaging coupling to a diesel-generator set.

General arrangement of the ship is presented in figure 26.

On the upper deck hatch cover No. 2 it is possible to place air-cushion vehicle for transportation or repair work. Air-cushion vehicle is accompanying each vessel.

Length max.	20.7 m
Breadth max.	9.9 m
Hovering height	0.6-0.7 m
Payload	38 tonnes
Output	625 kW

Appendix 1 presents a short list of equipment and features designed specially for arctic conditions.

9.2 Performance data

The ship can operate normally at the following temperature:

- seawater max. +32°C
- seawater min. -2°C
- air temp.max. +35°C
- air temp.min. -50°C

The sailing area is unrestricted.
Fuel oil capacity for a range of 12000/16000 nautical miles.
Provision stores sufficient for 60 days.

Water ballast capacity is sufficient for the ship to operate in pure ballast condition in arctic ice-covered waters.

The ship will obtain suitable trim and stability at the typical loading conditions and fulfils the subdivision and stability rules of the USSR Register as a two-compartment ship to the draught of 9.00 m.

9.3 Main dimensions

Length over all (stern notch excluded)	174.00 m
Length at design water line	164.00 m
Breadth max mld	24.50 m
Breadth at design water line mld	24.00 m
Depth mld to upper deck	15.20 m
Depth mld to tween deck	10.20 m
Draught design	8.50 m
Draught arctic subdivision load line	9.00 m
Draught maximum	10.50 m

9.4
Material

The hull is constructed for going in continuous arctic ice. Structural steel, including casting and forgings is all special steel and good uniform quality, which is suitable to arctic ice waters and -50°C temperature. Special consideration is paid to the ice zone, where special RAUTARUUKKI RAEX, grade E-32 Polar steel plates are used.

9.5
Hull equipment

The ship is equipped with a special towing notch for towing other ships or pushing by an icebreaker.

9.5.1
Stern ramp

The ship can be loaded and unloaded through the angled stern ramp, Navire make, which is at a 65° angle to the ship's center line. The maximum load from the ramp on the wharf is 2 t/m^2 . The loading of the ramp is same as on tween deck. The ramp can also be lowered down to ice-field, allowing for the max. sloping angle 17° .

Total length 14.5 + 3.5 m
Free driving breadth 5.0 m

The ramp is electro hydraulically operated.

9.5.2
Rudder

The ship equipped with one semi-balanced horn-type, streamlined, double plated rudder of welded construction.

There is a keyless conical coupling with a nut between stock and rudder blade.

The rudder has two lower bearings. The pintle bearing is of Tufnol in way of stainless steel bushing and welded on linings.

A rudder carrier bearing is fitted in the steering gear room at the upper end of the rudder trunk.

9.5.3
Air bubbling system

The ship is provided with the Wärtsilä airbubbling system to improve the ship's capability to penetrate through level icefields, broken channels and pressure ridges and to minimize the risk that the ship will get stuck into ice.

The air for the system is delivered by two radial type compressors, each capable of delivering 4.9 m³/s of free air to a pressure of 100 kPa (absolute). The power need for each compressor at ambient temperature 0° is approx. 650 kW. The compressors are provided with sufficient safety margin to the surge limit.

The main compressors are driven by two diesel engines.

The master panel, located in the engine control room, is equipped with all indicators needed by the engineers to maintain the system under safe conditions.

The control panel located on the bridge enables the officer in command to start and stop the system and to operate all the valves.

The air bubbling system works also as a bow thruster.

9.5.4 Cargo cranes

The cargo gear consists of three single electro hydraulic deck cranes and one twin electro hydraulic deck cranes and one twin electro hydraulic deck crane Hågglung & Söner make.

Single cranes type: G 2022-1

- lifting capacity 200 kN
- outreach max. 22 m

Twin crane type: G 4020-2

- lifting capacity 2 x 400 kN
- outreach max. 20 m

9.5.5 Insulation and lining in accommodation

Efficient thermal insulation is used due to ship's operation on polar regions.

Cabins are prefabricated units.

Walls are made of elements consisting of one (1) plastic film coated, min. 0.75 mm thick, galvanized steel plate with 25 mm thick rockwool on backside as thermal and sound insulation. Elements are connected together with galvanized steel jointing profile. Walls are connected to a bottom frame of painted steel pipe 30 x 30 x 2 mm.

The construction of ceiling is similar to the wall construction. The ceiling is self supported.

Cabins are without floor and mounted on ordinary steel deck.

9.5.6

Painting and surface treatment

All steel material with a thickness of 5 mm or over is blasted to the preparation grade Sa 2,5 and directly treated with a two-compartment iron epoxy primer 20-25 my.

Painting is INTERNATIONAL PAINTMARINE COATINGS make.

Shell below 6.5 m waterline has vinyl tar and antifouling.

Shell between 6.5-11.0 m water line (ice zone) has INERTA 160

Shell above 11.0 m waterline has alkyd paint.

9.6

Ventilation in accommodation

The heating and air conditioning plant, HI-Press make, is dimensioned for:

Cooling:	- outside temperature	+35°C
	relative humidity	70%
	- inside temperature	+29°C
	relative humidity	60%
Heating:	- outside temperature	-50°C
	- inside temperature	+20°C
	- relative humidity	40%

In addition to air conditioning plant there is hot water heating in all cabins and common spaces.

References:

1. Wilkman, G.: Neuvostoliiton arktinen liikenne (The Arctic Traffic of Soviet Union), in Finnish Wärtsilä Arctic Design and Marketing, report no. M5 September 1982, Wärtsilä internal report
2. Maklakov, N.T.: Icebreaking Cargo Vessels for Arctic Waters. Sudostroenie 27, No. 1, 1981 p. 4.
3. Juurmaa, K.: Selvitys aluksen koon ja konetehon vaikutuksesta kuljetuskustannuksiin Neuvostoliiton arktisilla alueilla. 13.10.1975 in Finnish, Wärtsilä internal report
4. Juurmaa, K., Laakso, J.: Arktisen lastilaivan koneistovaihtoehdoista. In Finnish. Wärtsilä Arctic Design and Marketing, report no. N11A, February 1979, Wärtsilä internal report
5. Resistance, propulsion, streamline, wakefield and bollard pull test for an icebreaking freighter. Technical Research Centre of Finland, Ship Laboratory. Model test reports LAI-0242 A/B/80, ordered by Wärtsilä Turku Shipyards
6. Model test results of an arctic freighter, P-2000. Report of Krylov Institute, Leningrad 1981, ordered by Wärtsilä Turku Shipyards
7. Cavitation and Pressure Pulse Test with KaMeWa Propeller Model no. 695-B, Report PR-707, Wärtsilä Abo 1956-61, January 1981
8. Seakeeping model tests for an arctic freighter. Technical Research Centre of Finland, Ship Laboratory, Model test reports LAI-244 A/B/C/D/E/81, ordered Wärtsilä Turku Shipyards

Ship type	1 9 7 0		1 9 7 7		Change
	Size dwt	Number of ships	Size dwt	Number of ships	
Icebreakers	873-5609	23	354-6147	30	+7
Cargo ships of ULA-class	6560-9573	12	310-9280	21	+9
Timber carriers	3300-6500	188	4454-6780	26	-162
Tankers	1340-11680	31	17200	10	-21
Fishing factories	1330-11086	48	790-1139	29	-19
Passanger ships	1350-1400	17	2427	5	-12
Tugs	46-570	157	71-605	143	-14
Others	100-9000	<u>266</u>	190-7430	<u>23</u>	<u>-243</u>
Total		737		287	-450

Table 1.

Ships registered in the Soviet Register
under ice class UL or ULA in 1970 and 1977

	"Lena"	"Amguema"
Maximum length, m	130.20	133.10
Maximum beam, m	18.90	18.90
Moulded depth, m	11.20	11.60
Weight of ship, tons	5110	4840
Normal draught, m:		
with general cargo	7.62	7.62
with bulk cargo	8.27	8.85
Design draught to load line, m	8.27	9.10
Cargo capacity, tons		
with general cargo	4810	5000
with bulk cargo	6100	7400
Deadweight, tons:		
with general cargo	6265	6300
with bulk cargo	7430	8700
Bale capacity of holds, m ³	8960	9700
Capacity of deep tank for cargo fuel	1200	None
Gross capacity, reg.tons	7500	7968
Nett capacity, reg.tons	4300	3435
Power of main diesels, e.h.p.	4x2050	4x1800
Trials speed at draught of 7.60 m, knots	15.4	15.0
Number of decks	3	2

Table 2.

Main parameters of the "Lena"- and "Amguema"-
class ships

Part of ship	Frame load without allowing for work of stringers		Maximum load of one frame allowing forward of stringers tons	Design load on shell plating, tons/m ²
	tons/m	per fr. tons		
Bows as far as fr. 33	200	80	385	390
Bows in the transition region fr. 33-54	150	60	Not checked	$\frac{290}{275}$
Cylindrical part of WL in region of fr. 54-117	110	43	" "	200
Stern in the transition region fr. 117-131	110	43	" "	240
Stern from fr. 131 aft	110	43	" "	250

Note: The loads taken by the external plating are obtained by calculating the plate as a rigidly fixed strip beam; the permissible stresses are taken to be equal to the material's proof stress.

Table 3. Calculated maximum and design loads for some hull structures of the "Amguema"-type ships.

Alternative	Open water		Bollard condition			Ice condition		
	Speed (m/s)	Thrust (kN)	Diesel engine (kW)	Propeller power (kW)	Thrust (kN)	Diesel engine (kW)	Propeller power (kW)	
1	9.7	1350	12 940	12 425	630	12 940	12 425	
2	9.5	1210	12 940	11 000	640	12 940	11 000	
3	9.7	1090	12 940	9 250	220	12 940	4 900	
4	9.7	1210	12 940	10 995	340	12 940	6 540	
5	9.7	1190	12 940	10 838	600	12 940	10 159	

Table 4. Results of a comparison of five various propulsion systems for an arctic multipurpose cargo ship

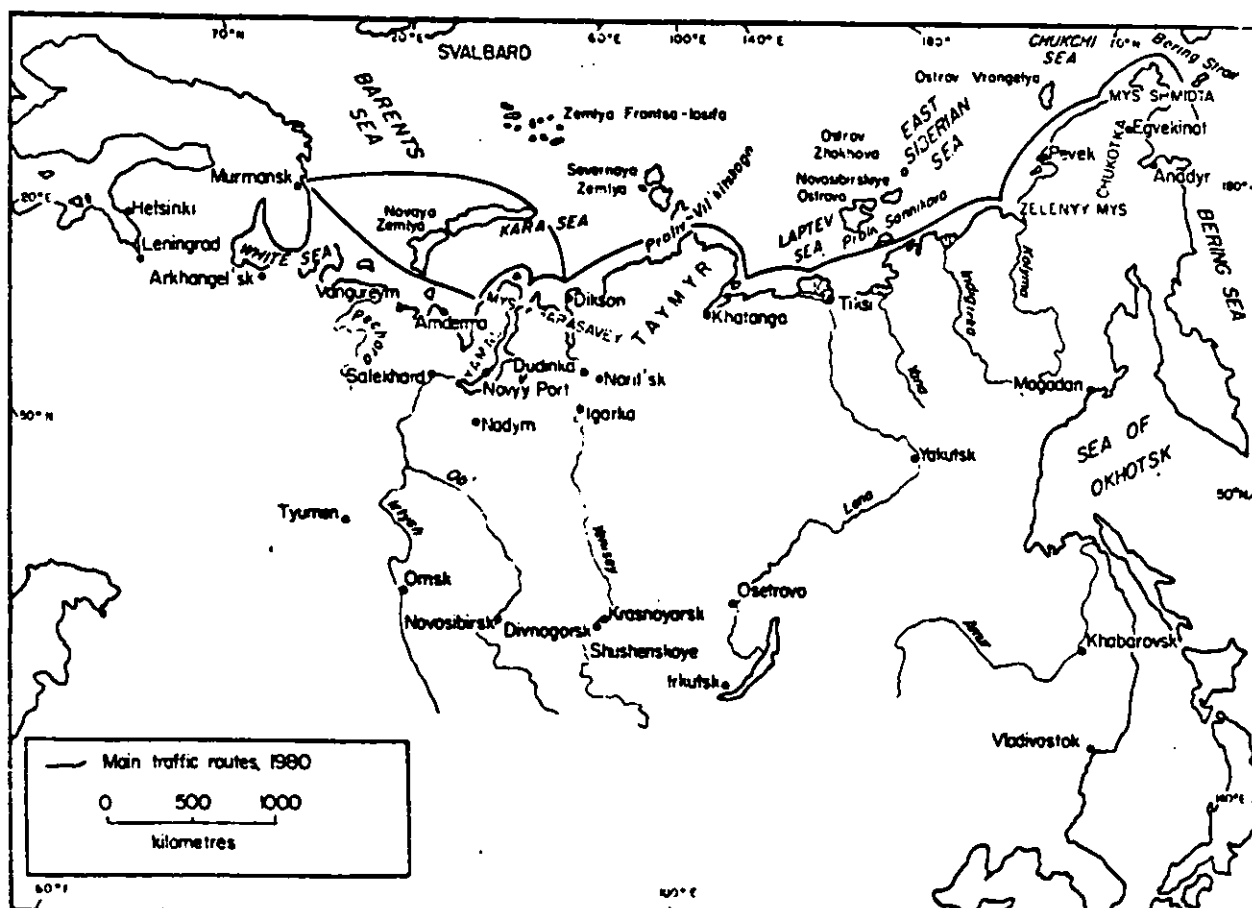
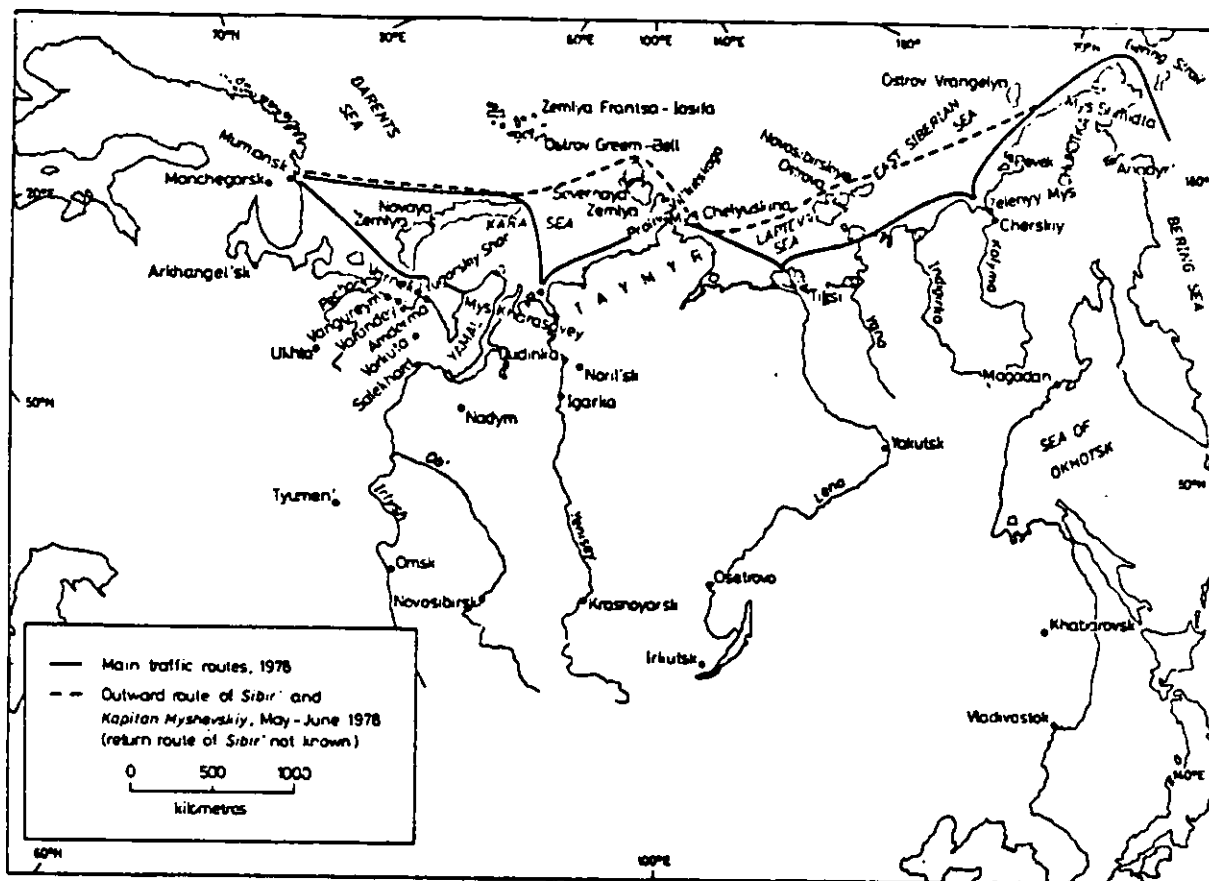
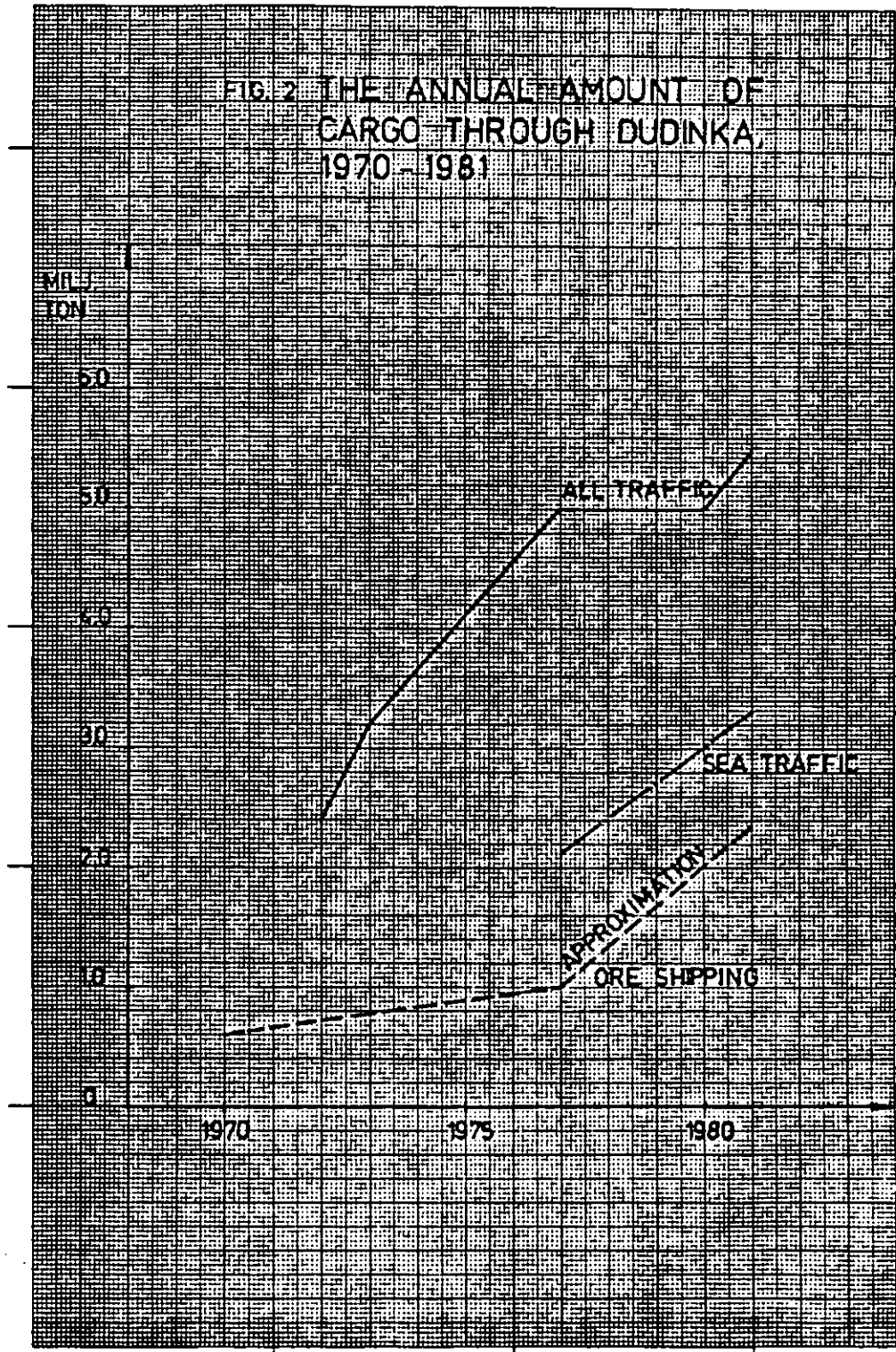
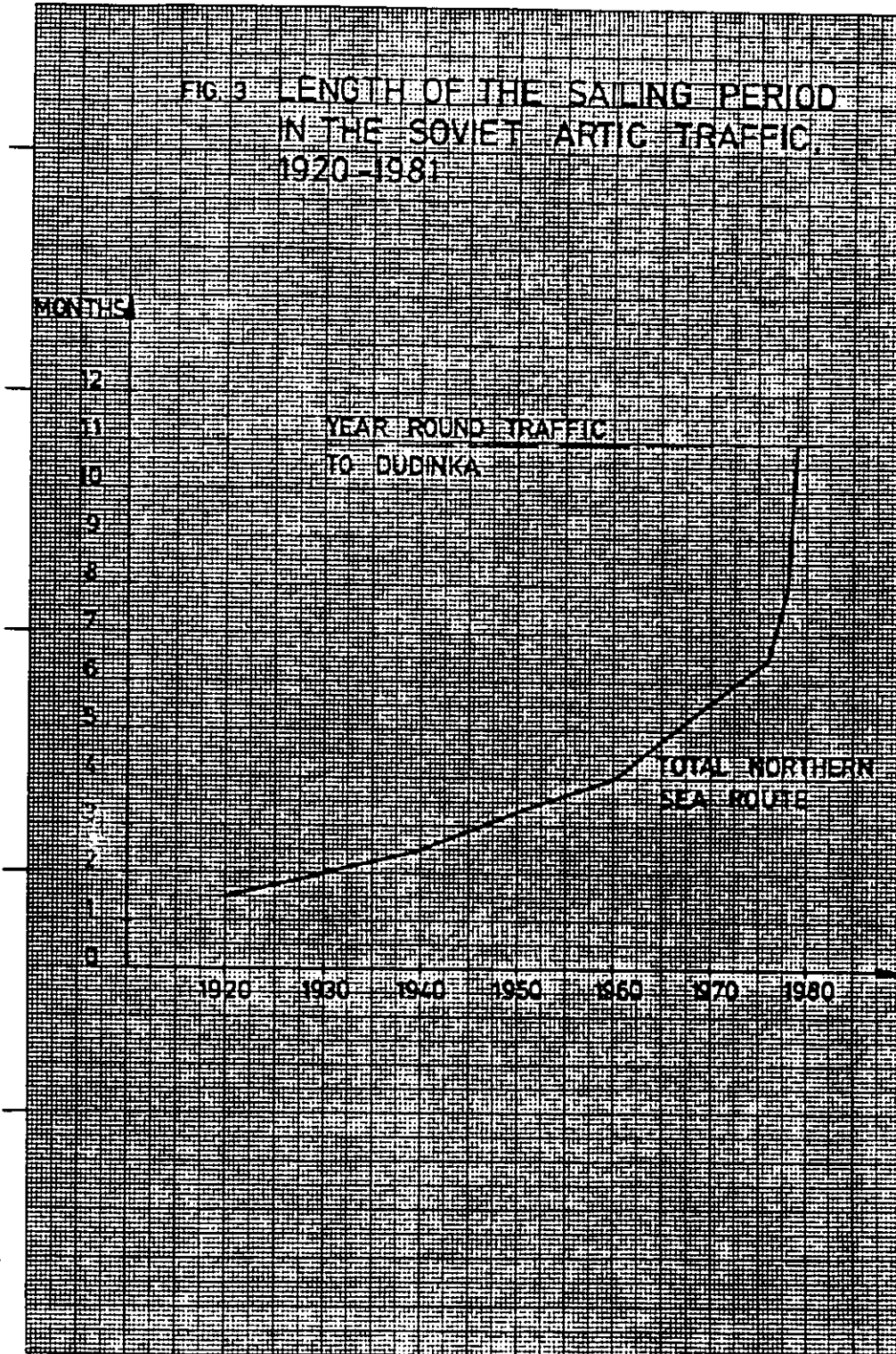
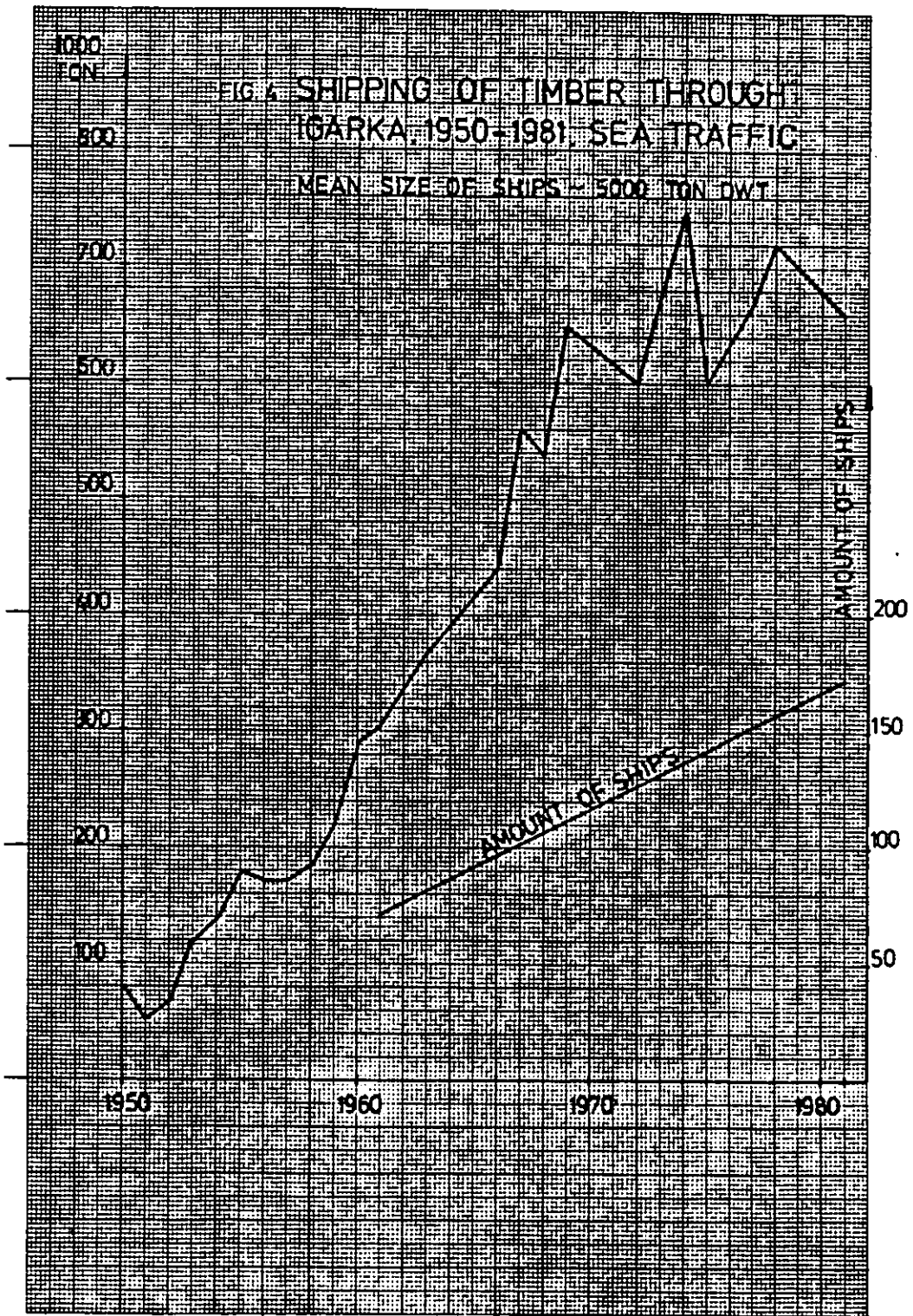
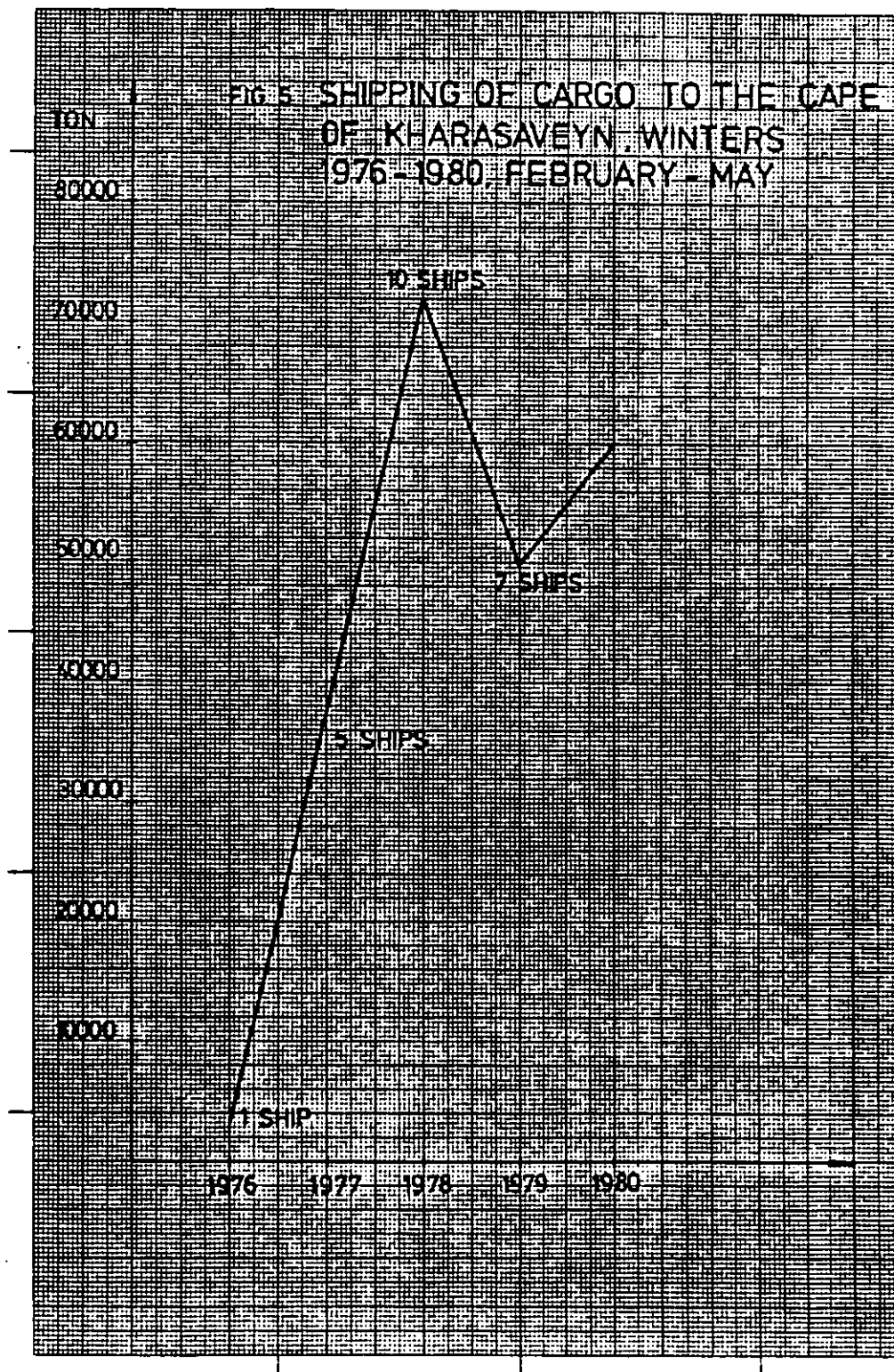


Figure 1. Main traffic routes through the Northern Sea Route, 1978 and 1980









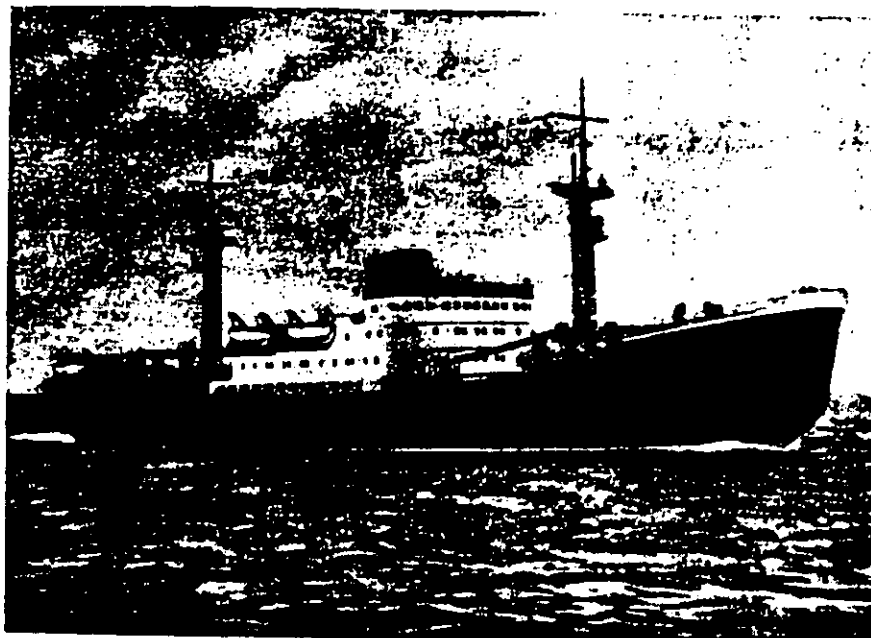


Fig. 6

A general view of the "Amguema"-class icebreaking cargo vessel.

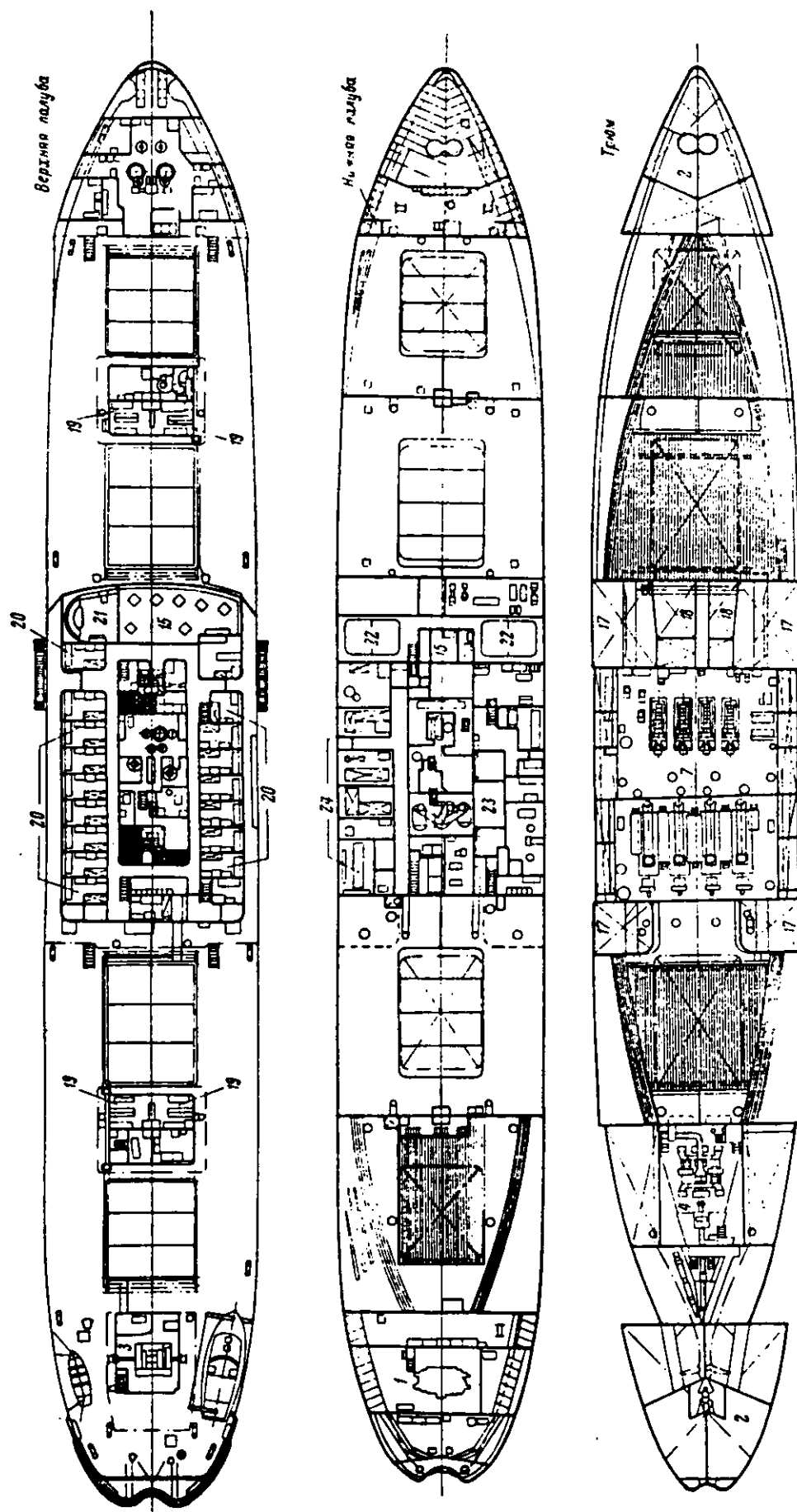


Fig. 7.

General arrangement of the "Amquema"-class ship.

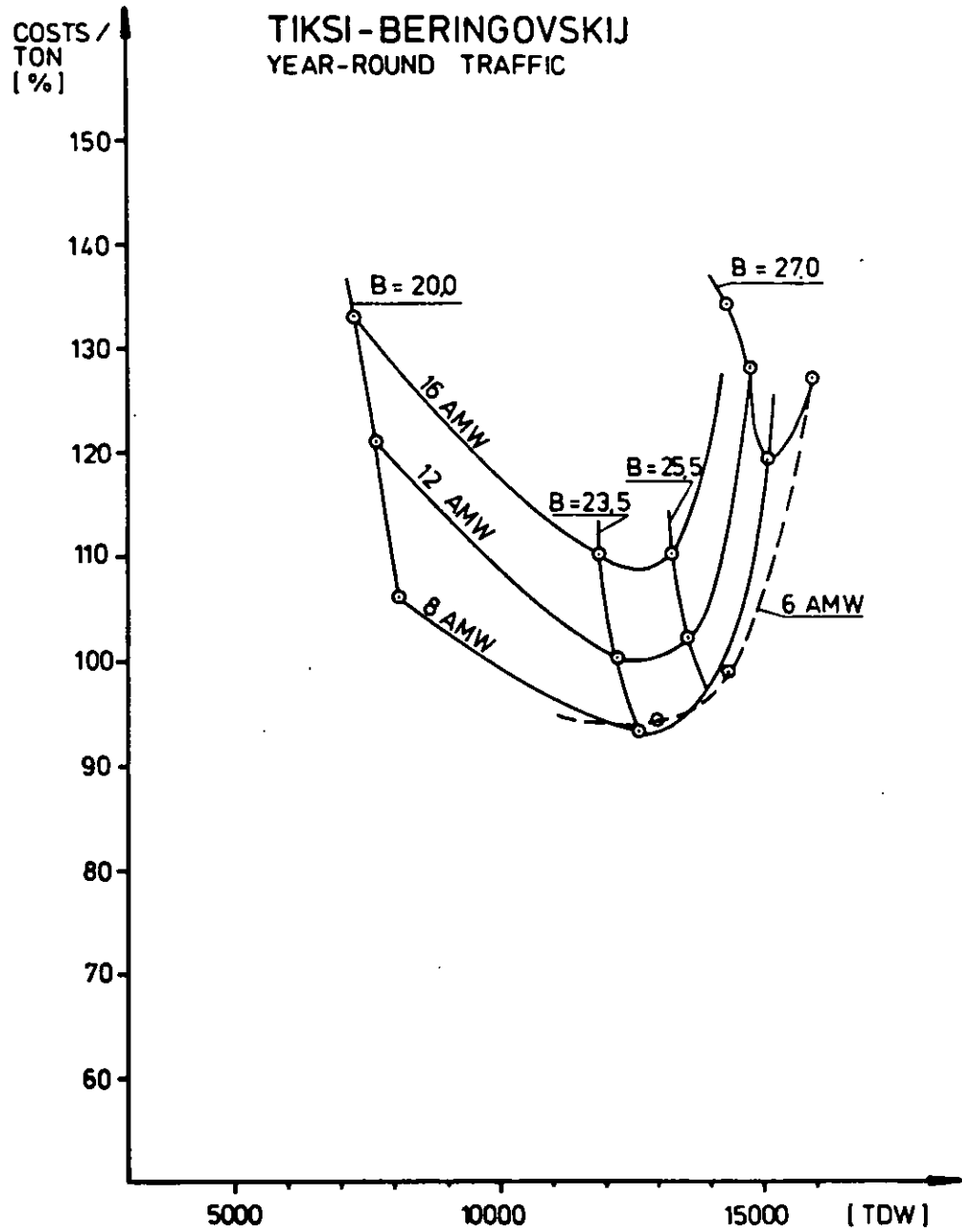


Fig. 8. Year round traffic simulation. Costs/ton as a function of deadweight, breadth and installed power for Tiksi-Beringovskij route.

MURMANSK - DIKSON
YEAR-ROUND TRAFFIC

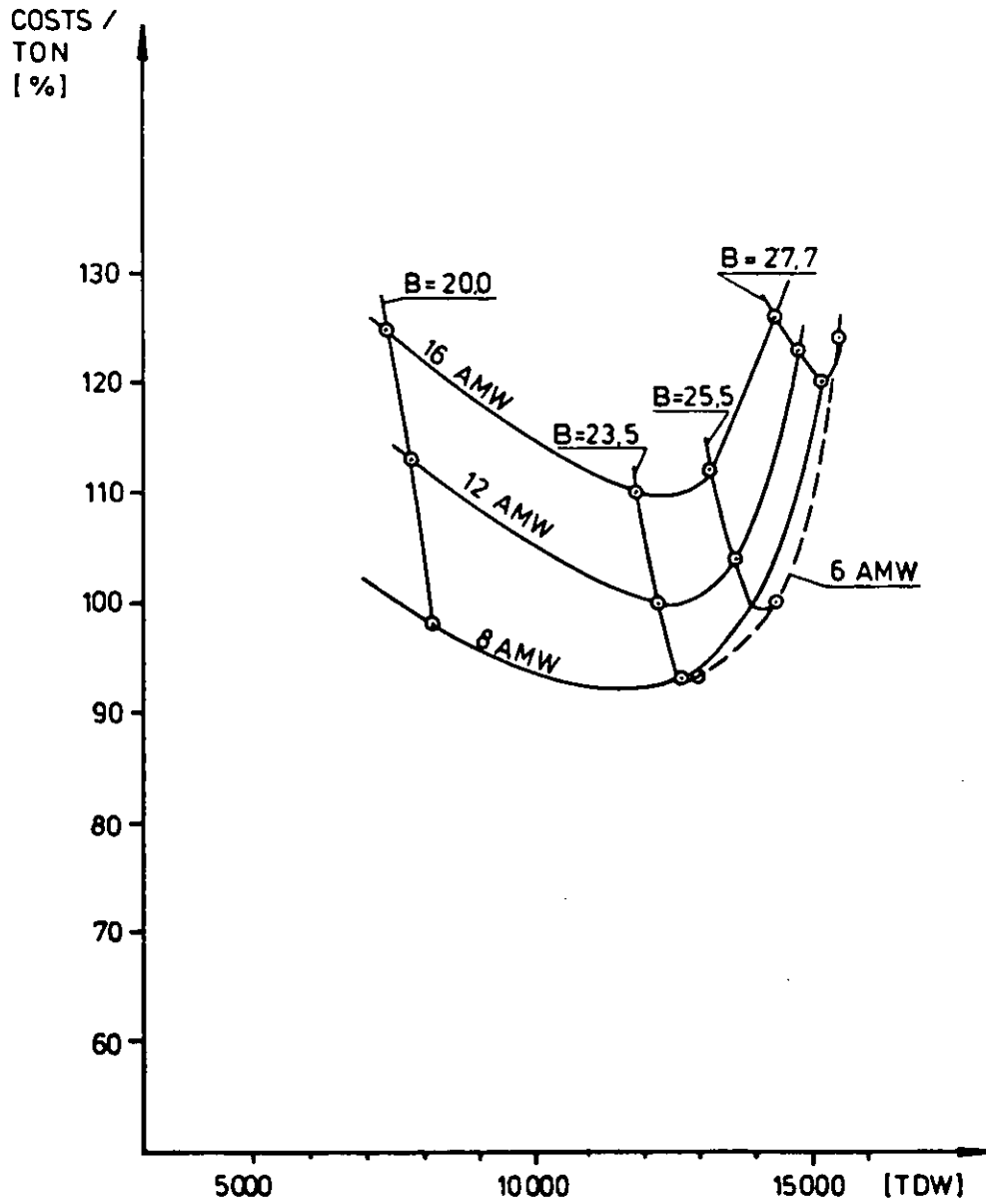


Fig. 9. Year round traffic simulation. Costs/ton as a function of deadweight, breadth and installed power for Murmansk - Dikson route.

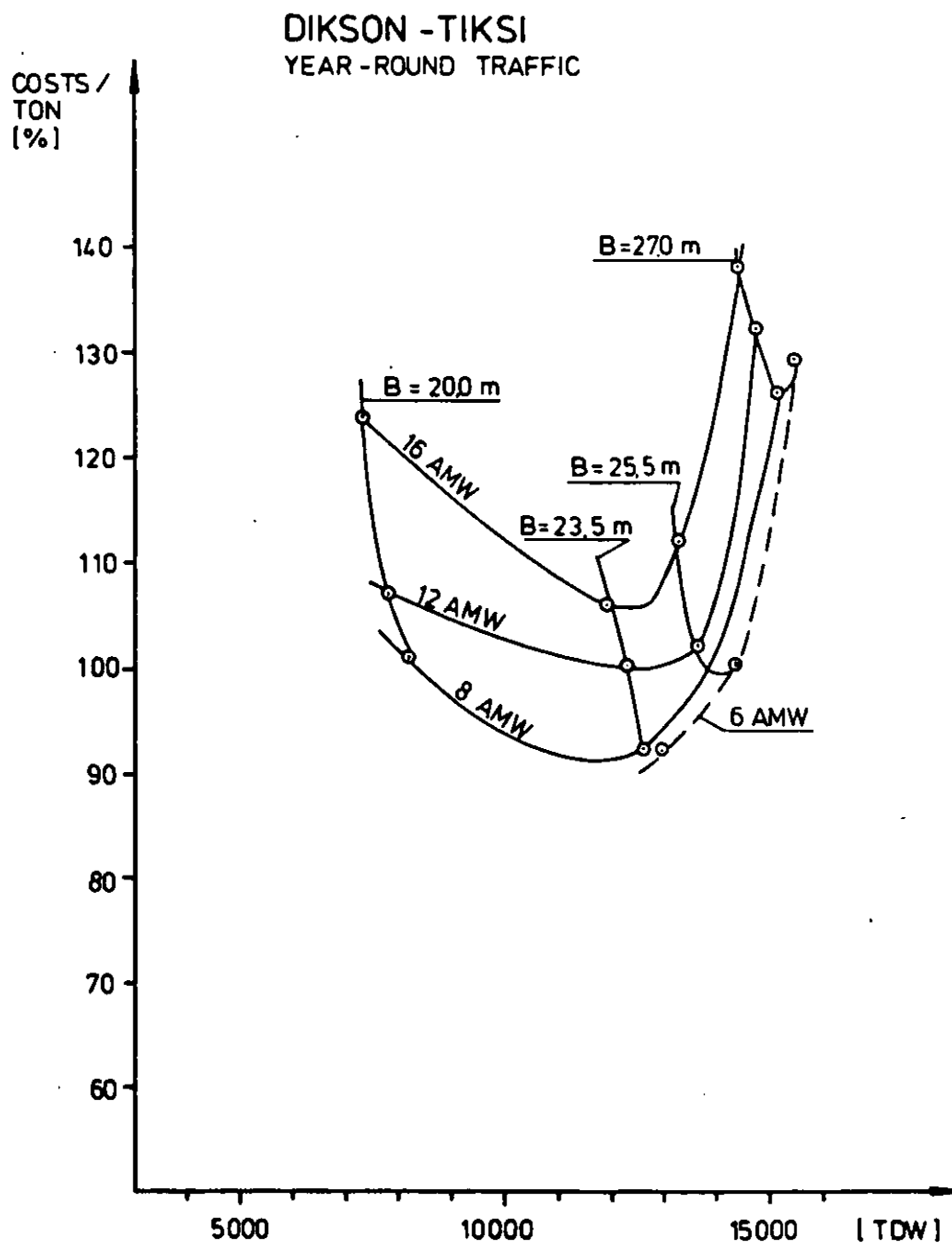


Fig. 10. Year round traffic simulation. Costs/ton as a function of deadweight, breadth and installed power for Dikson - Tiksi route.

TIKSI - BERINGOVSKIJ

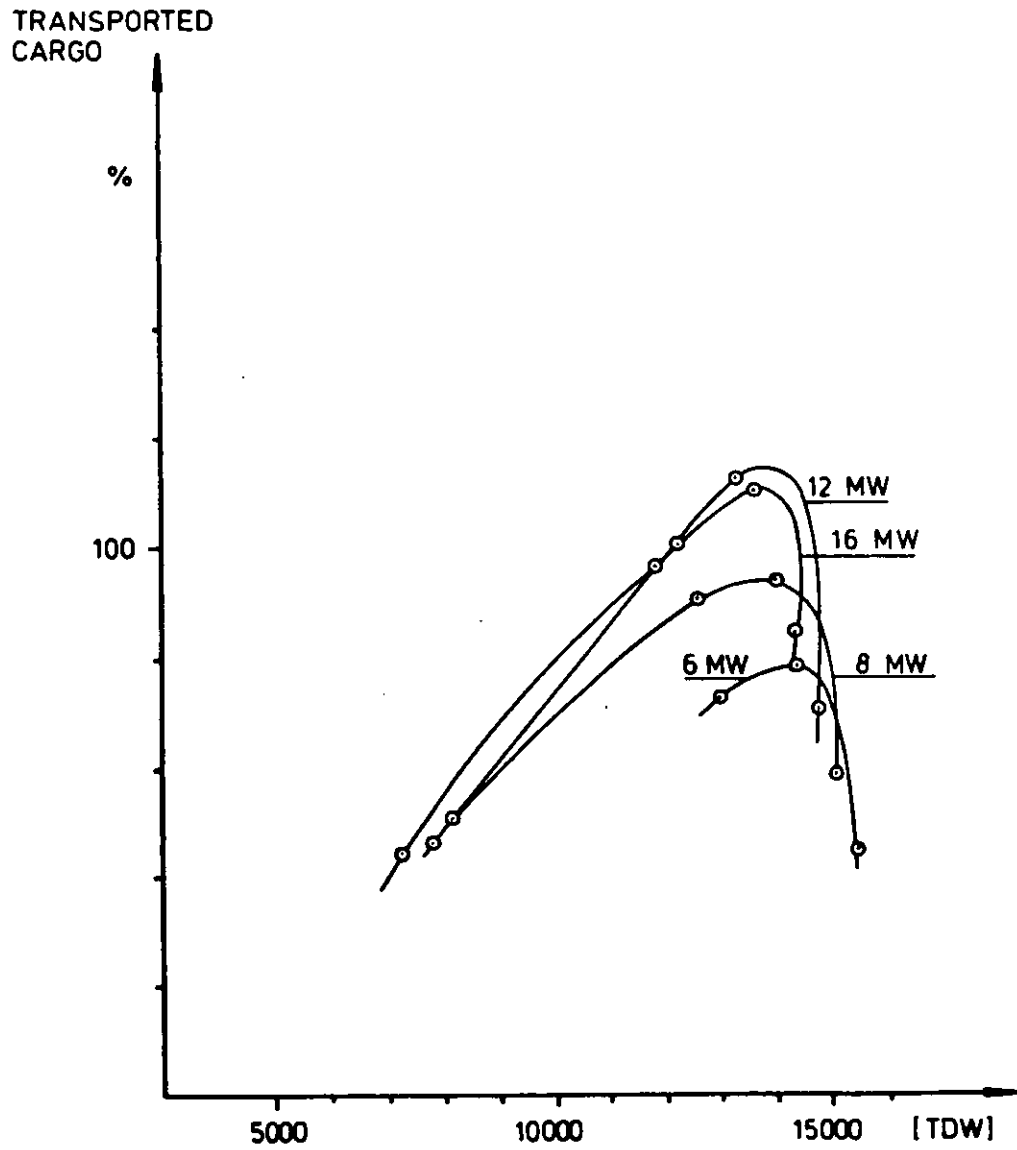


Fig. 11. Transported cargo in year round traffic as a function of deadweight and installed power for Tiksi - Beringovskij route.

MURMANSK - DIKSON

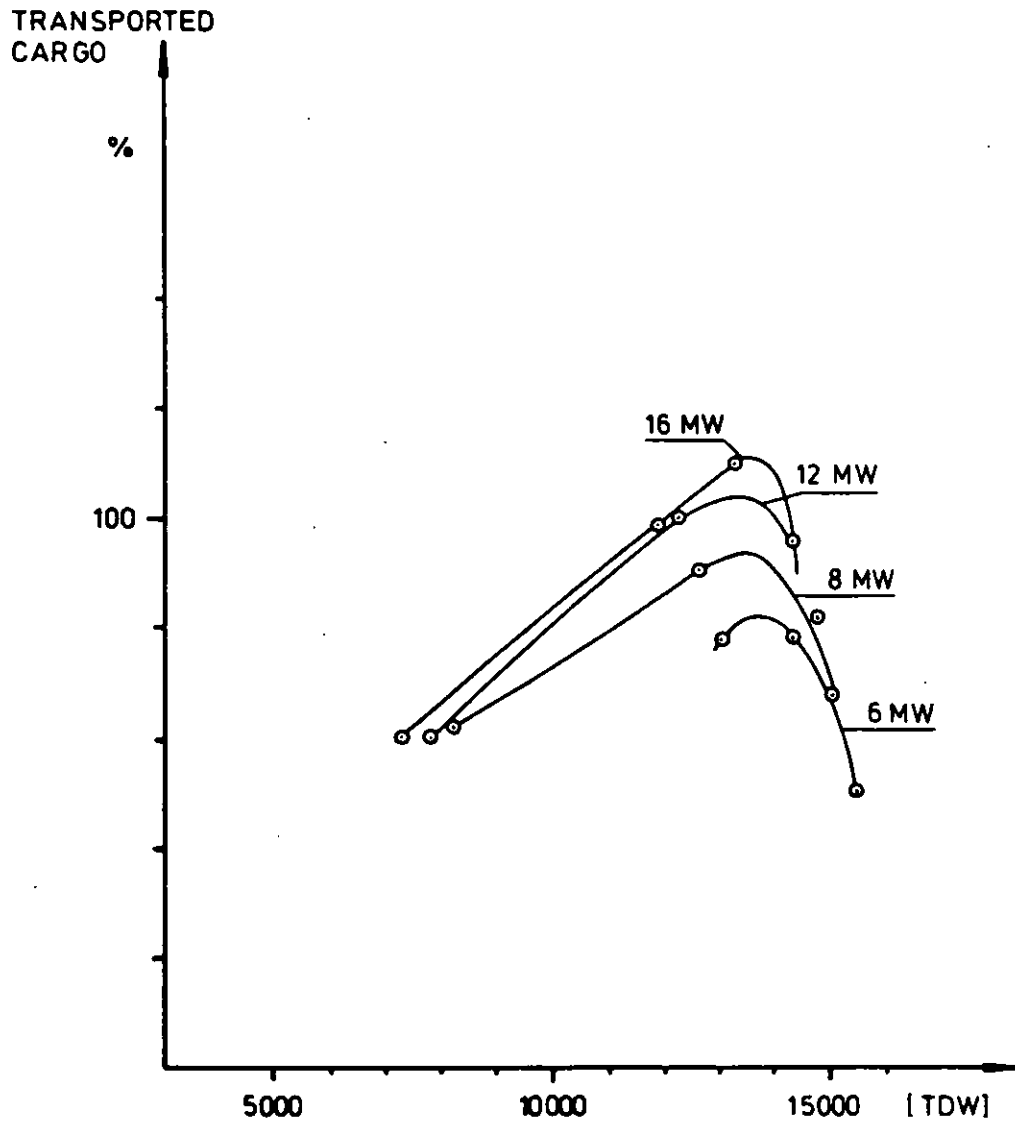


Fig. 12. Transported cargo in year round traffic as a function of deadweight and installed power for Murmansk - Dikso route.

DIKSON - TIKSI

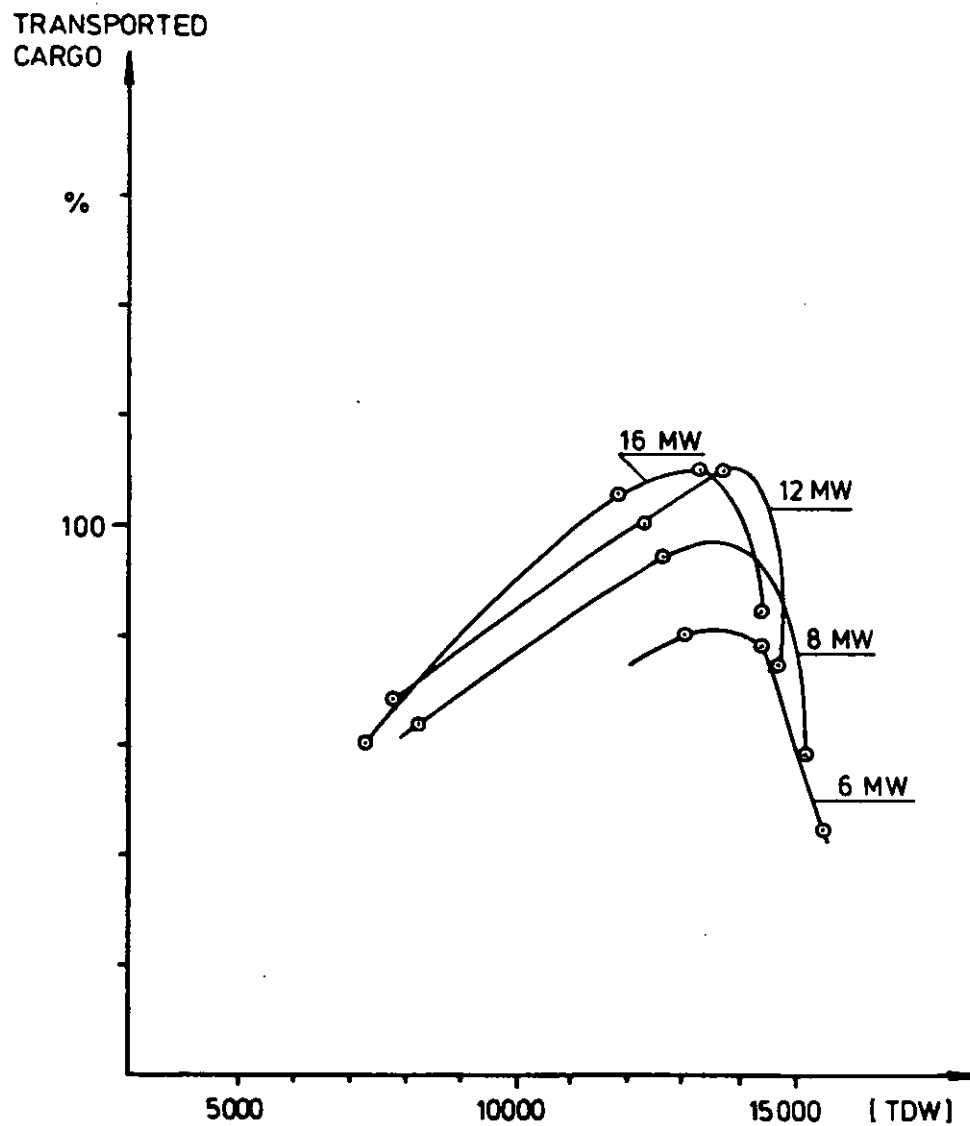


Fig. 13. Transported cargo in year round traffic as a function of deadweight and installed power for Dikson - Tiksi route.

TIKSI - BERINGOVSKIJ
WORST MONTH

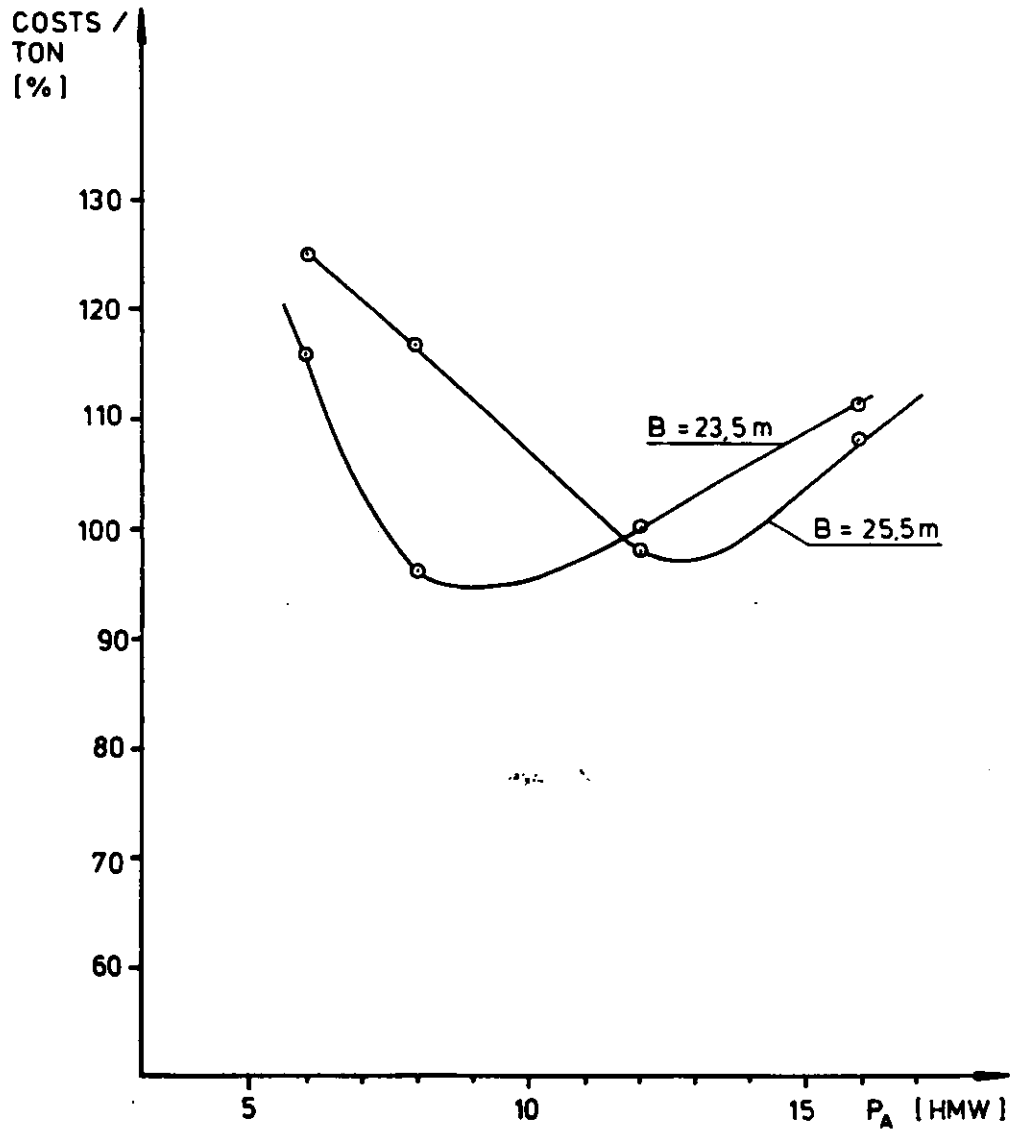


Fig. 14. Costs/ton for the worst month on Tiksi - Beringovskij route as a function of installed power for two breadths.

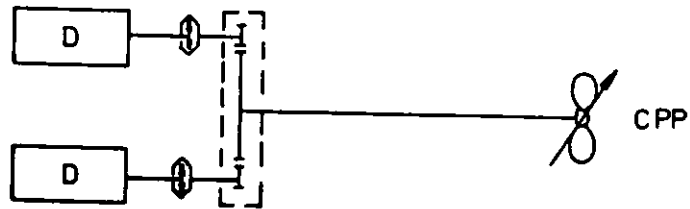


Fig. 15. Propulsion system alternative 1, cpp, reduction gear, friction couplings and main diesel engines.

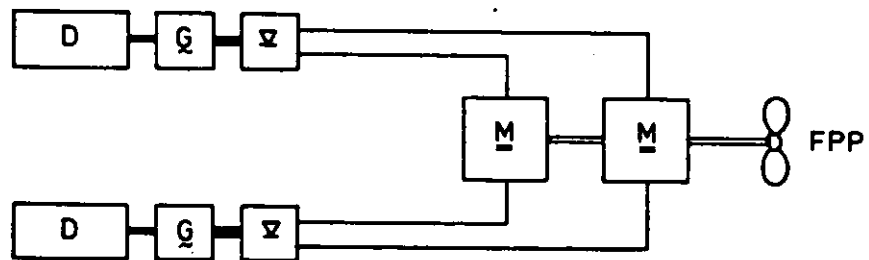


Fig. 16. Propulsion system alternative 2, fpp, DC electrical motors, diode rectifiers, AC generators and main diesel engines.

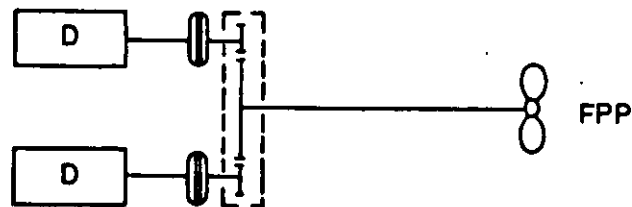


Fig. 17. Propulsion system alternative 3, fpp, reduction gear, hydraulic couplings and main diesel engines.

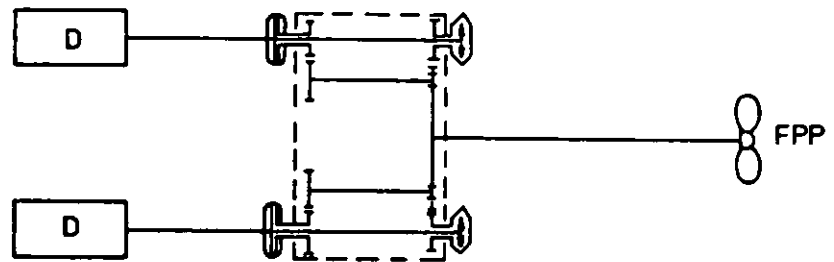


Fig. 18. Propulsion system alternative 4, fpp, two step reduction gear, hydraulic couplings and friction couplings.

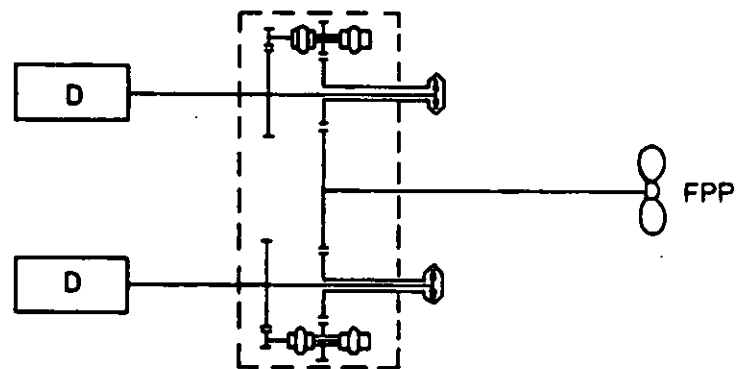


Fig. 19. Propulsion system alternative 5, fpp, reduction gear, friction couplings and hydraulic torque exchanger.

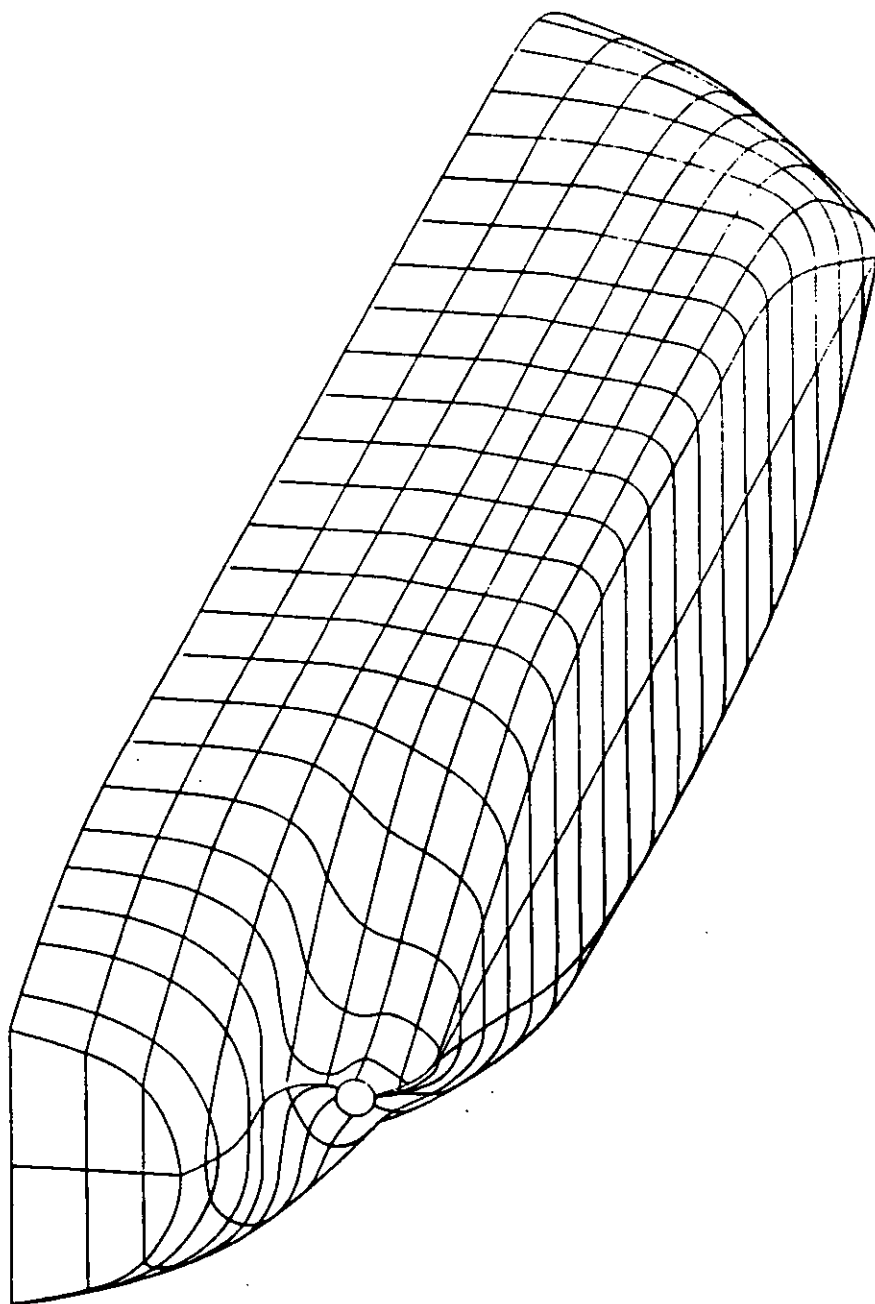


Fig. 20. Final hull form of the arctic multipurpose cargo ship, SA-15, built by Wärtsilä Turku Shipyards.

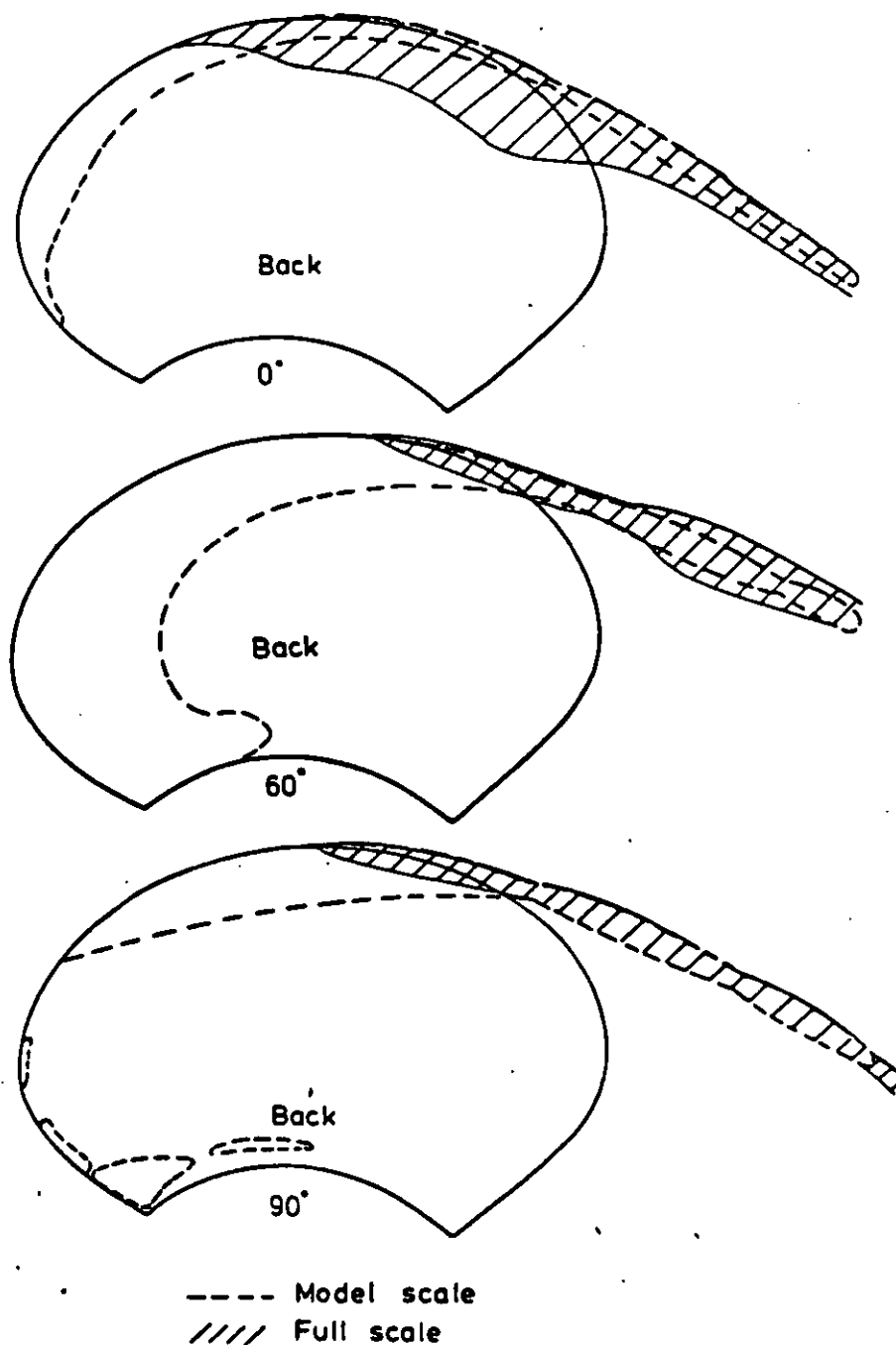


Fig. 21. Propeller cavitation observations of the arctic multipurpose cargo ships, SA-15, model scale and full scale, maximum continuous power, speed 18 knots, draught in model scale 8.5 m, in full scale 7.8 m.

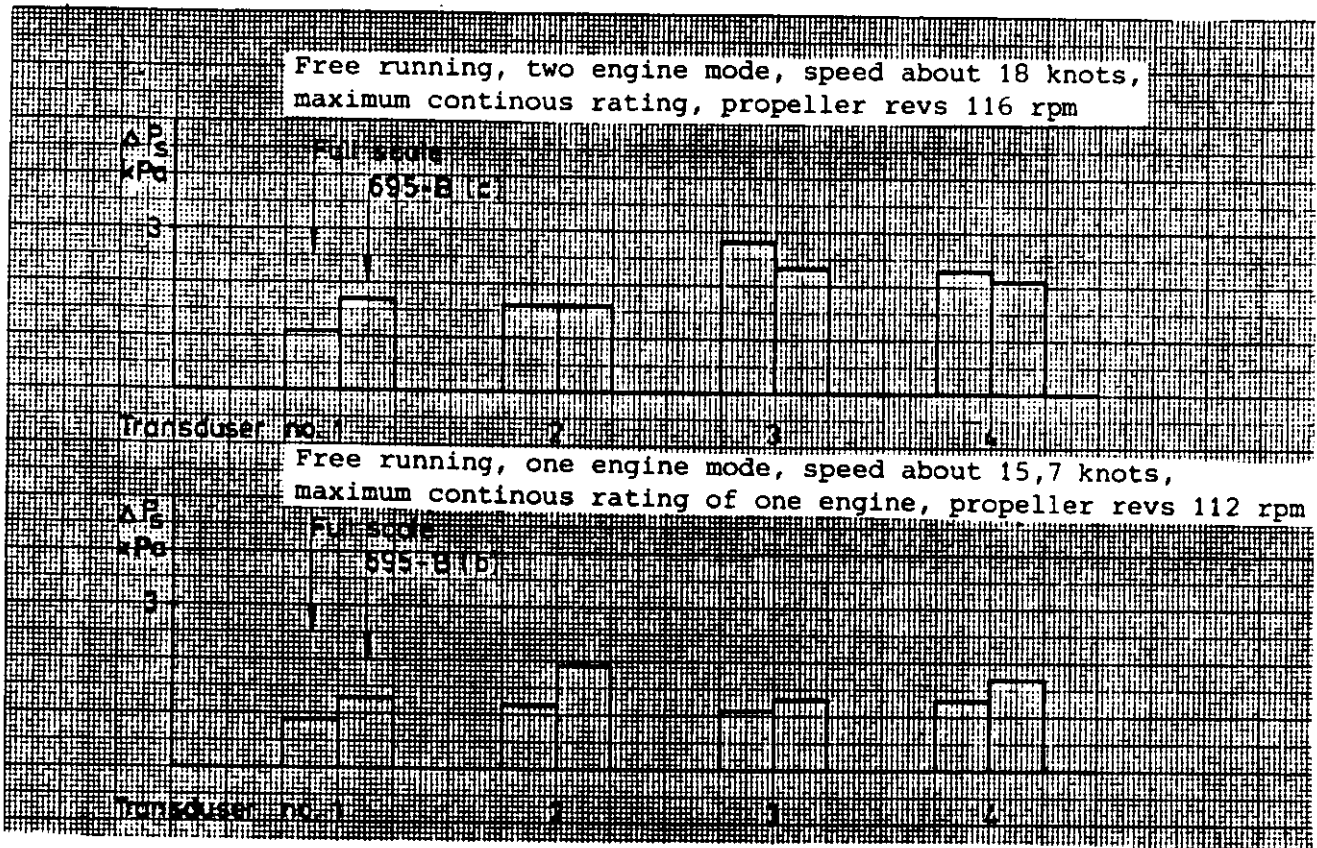


Fig. 22. Propeller induced pressure pulses of the arctic multipurpose cargo ship, SA-15. Model and full scale results, blade frequency, single amplitude. Transducer 3 is just above the propeller.

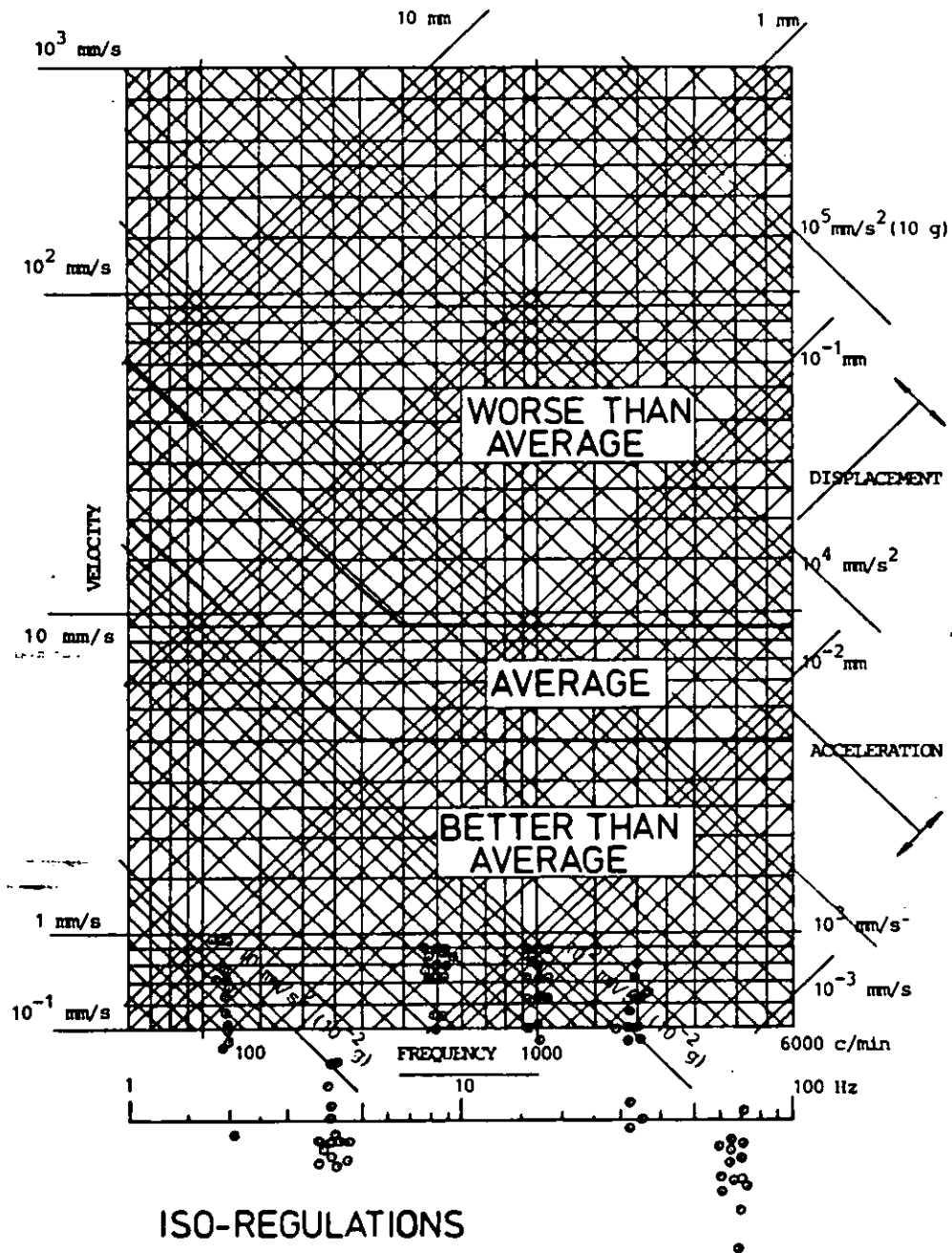


Fig. 23. Results of vibration measurements of the arctic multipurpose cargo ship, SA-15, \odot indicate measured points in super-structure, engine room and all over the hull.

SULZER 2 x 14ZV40
2 x 6930 kW / 540 rpm

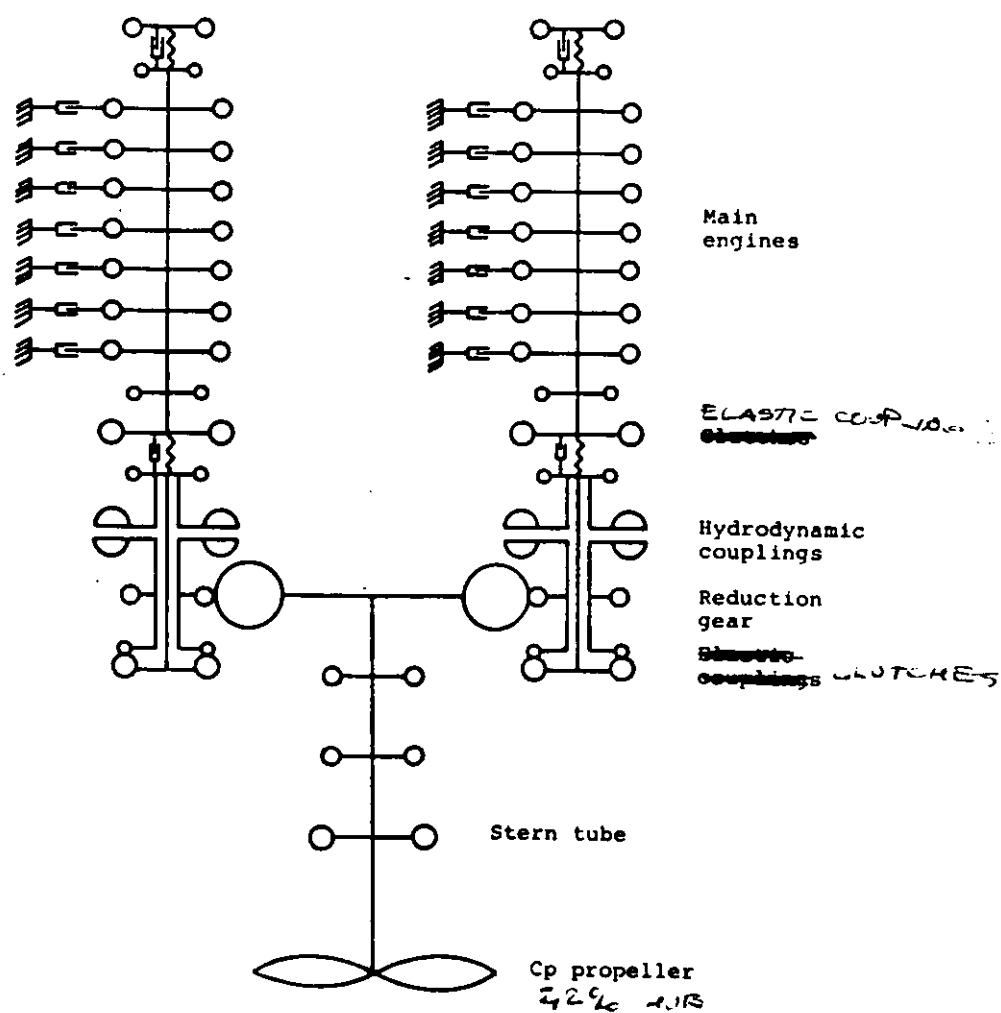


Fig. 24. Schematic presentation of the propulsion system of the arctic multipurpose cargo ship, SA-15.

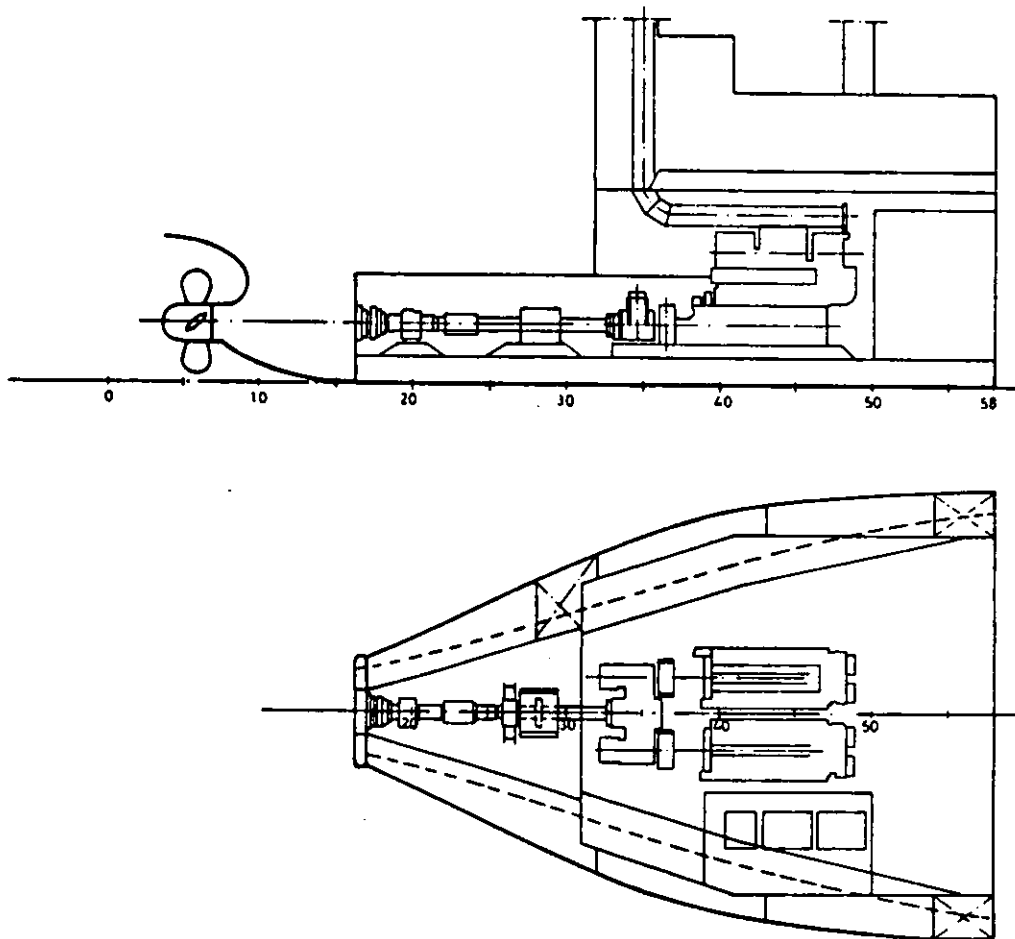


Fig. 25. Engine room general arrangement
of the arctic multipurpose cargo ship,
SA-15.

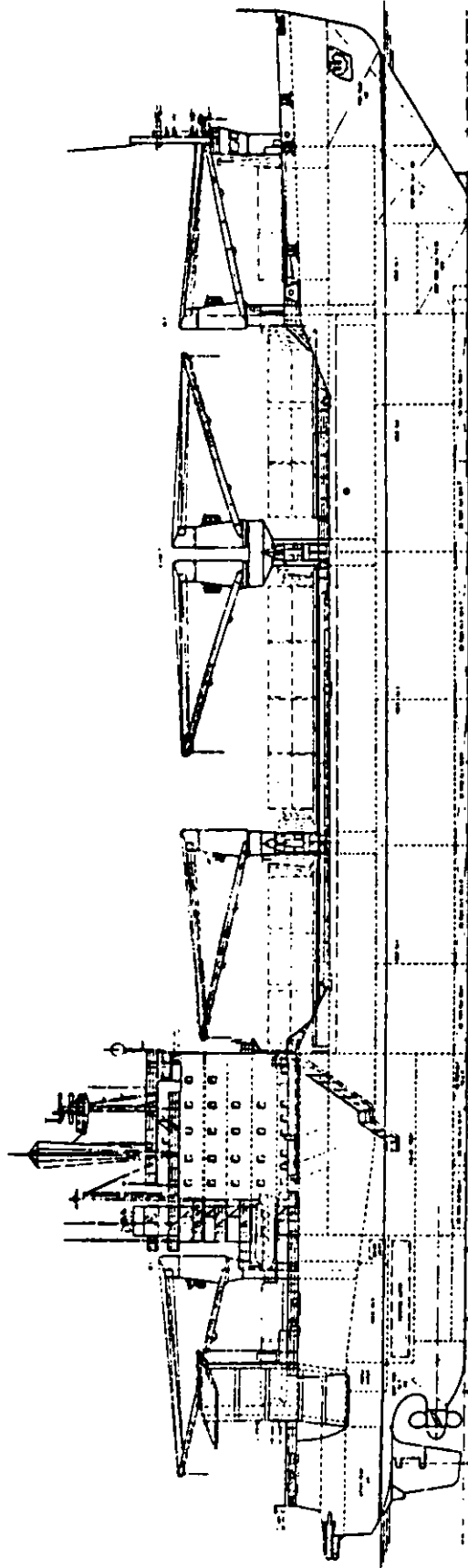


Fig. 26 General arrangement of the Wärtsilä built arctic multipurpose cargo ship, SA-15.

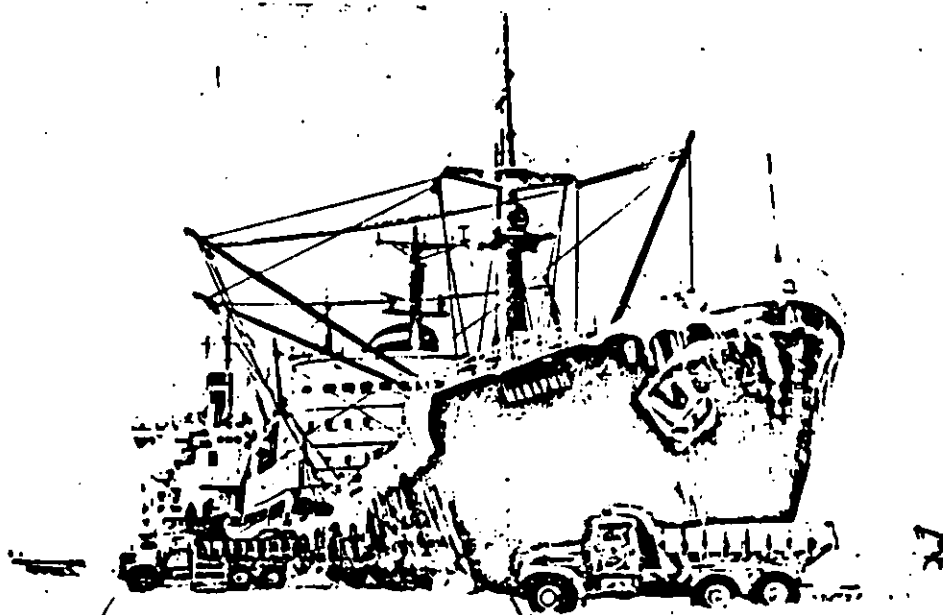
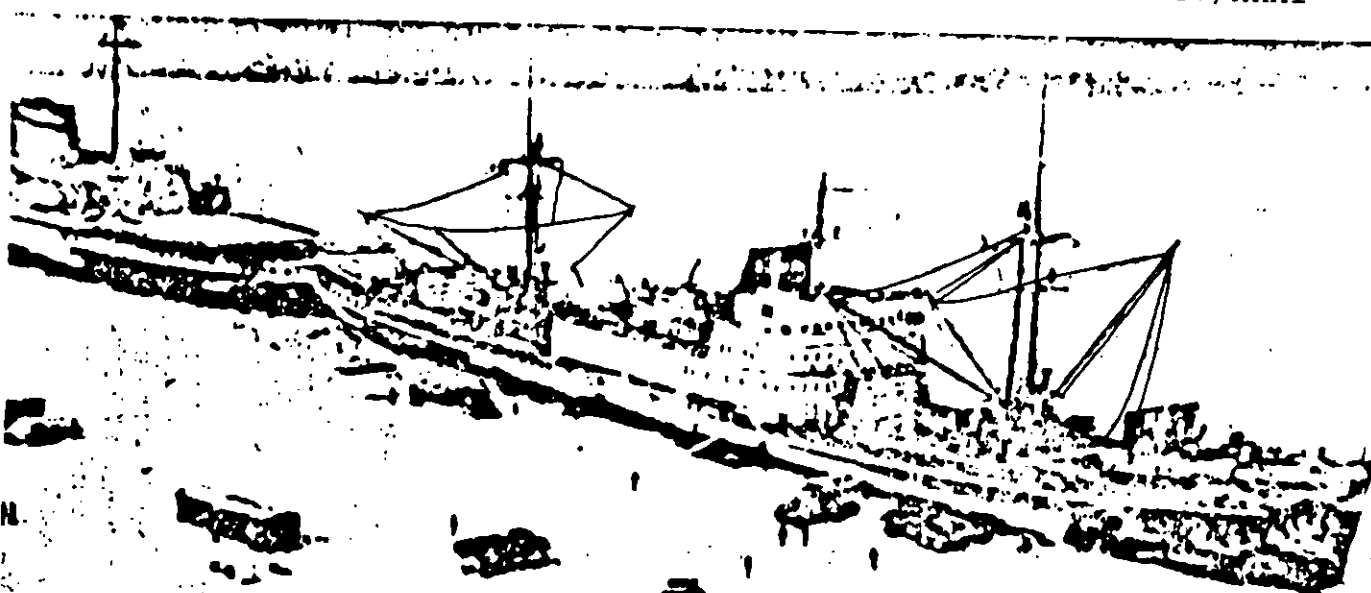


Figure 27

Unloading of an arctic freighter wedged into fast ice by an icebreaker near Yamal Peninsula as a resupply operation for a natural gas development project in early spring.

ARCTIC MULTIPURPOSE VESSEL

SA-15

SOME SPECIAL DESIGN FEATURES DUE TO ARCTIC ICE-
COVERED WATERS AND LOW TEMPERATURE

1. The ship can operate normally at the following temperatures:
 - sea water min. - 2°C
 - air temp. min. -50°C
2. According to ULA ice class the ship fulfils the subdivision and stability rules of the USSR Register as a two compartment ship.
3. Structural steel, including castings and forgings is all special steel and good uniform quality, which is suitable to arctic ice waters and -50°C temperature. Special consideration is paid to the ice zone, where special RAUTARUUKKI RAEX, grade E-32 Polar steel plates are used.
4. The ship is equipped with the special towing notch for towing other ships or pushing by an icebreaker.
5. The ice that forms on a ship's weatherdeck presents a special problem in the design of weatherdeck hatch covers. Removing the ice requires a great deal of hard work in very cold working conditions; the problems caused by the need to remove ice from the hatch covers have been overcome by the following measures:
 - wheel tracks and support pieces were placed in the watertight parts of the ship
 - the hatch covers were equipped with ice-breaking devices
 - container corner pieces are such that it is possible for a layer of ice to remain on the hatch covers,
 - all hydraulic pipes and hoses and the equipment needed for their operation were located in watertight parts of the ship

- the edges of the hatch covers were aligned as accurately as possible with the ship's exterior surfaces, i.e. the number of ice-collecting surfaces is minimized
- the sealing surfaces between the panels are as close as possible to the topplate; i.e. the number of ice-collecting depressions is minimized
- the sealing rubber remains elastic even at -60°C

The following principles were applied to the design of the hydraulic circuit:

- in order to keep the pipes in the main pipework as short as possible, several pump units are used
 - the pump units are placed in a heated space (minimum temperature -10°C)
 - the heating circulation of oil is arranged
 - greater than normal size pipes and valves were selected in order to minimize pressure losses
 - a thin hydraulic oil was selected with a solidification point below -60°C
 - hydraulic cylinders and hoses were placed in a watertight space protected from the weather.
6. Vertically mounted capstain type windlasses. Electric motors are situated under the deck.
 7. The ship is provided with the Wärtsilä airbubbling system to improve the ship's capability to penetrate through level icefields, broken channels and pressure ridges and to minimize the risk that the ship will get stuck.
 8. Deck cranes
- A deck crane to be operated at extremely low temperatures should have all machinery build-in into a closed heated crane housing. This is valid for both electric and hydraulic cranes.

If service has to be carried out on components placed outdoors, this is very difficult at low temperatures. In arctic crane all service work is carried out in the heated crane housing. This means that service work can be carried out also under extreme weather conditions. Service can also be carried out on the open sea. This is an essential feature of an arctic crane.

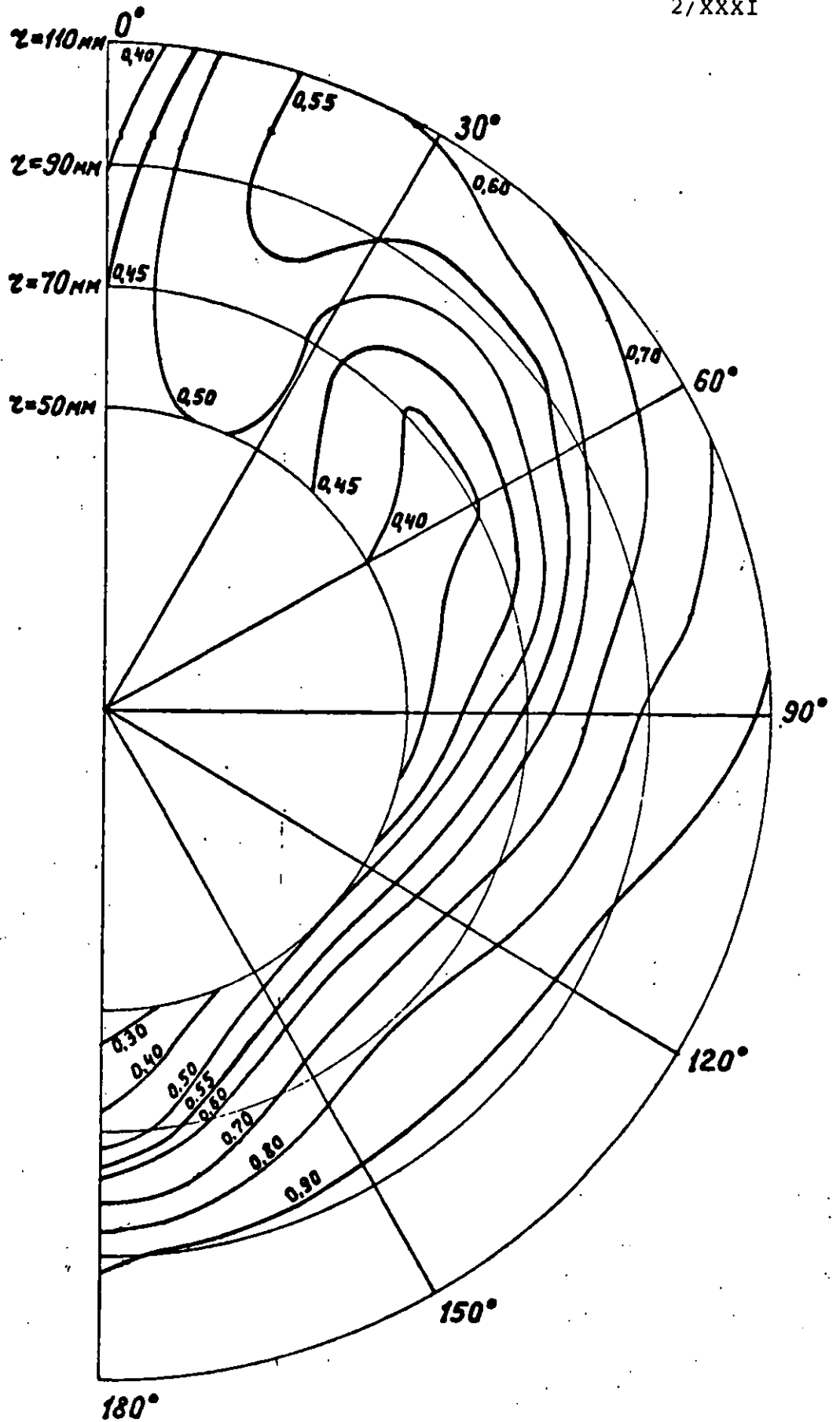


Fig. 21 a.

Axial wakefield of the arctic multipurpose cargo ship, SA-15, $T = 8.5$ m, speed 18 knots.

Subject: ICEBREAKING CARGO SHIPS

E R R A T A

page	chapter	line	corrected
5	2	1	Gas was found in the Yamal Peninsula at the beginning of seventies.
5	2	11	summer time with barges but that did not succeed, a lot of cargo was lost because of...
9	2	5	ro-ro cargo handling possibilities.
11	1	2	out the effect of ship size ...
11	3	1	The ship is a general cargo vessel equipped with ro-ro...
12	last word		exchangers.
15	3	5	compared to a hydraulic coupling system ...
16	2	2	...with single step reduction...
16	2	7	...with torque exchanger also...
16	3	2	...a combination of alternative 1 and 3...
16	4	4	...had changed into SA-15...
17	1	10	...and backward in level ice...
17	3	12	...same speeds were used...
18	3	4	The stem form...
19	2	6	...high iceloads and pressures
20	1	4	...presented in figure 21 a.
20	2	12	...from ballast 6 m up to 10 m,...
22	3	5	clutch couplings are included.
22	6	10	rating in open water.

Figure 21 a to be added.

The entrance to the driver's cab is entirely inside, via the foundation and through the bottom plate of the crane. The entrance, moreover, heated through fan heaters.

Certain components of the crane are placed outside and are not available for heating. E g wire sheaves, hook, shackle. These parts are made of steel with guaranteed impact strength down to 40° below zero or lower.

The material in the crane housing and foundation is heated from the inside, but is on the outside exposed to the outside air. Also here steel with guaranteed impact strength at low temperatures is used.

The oil used in the hydraulic crane should be suited for work at low temperatures.

9. Accommodation walls are made of elements consisting of one plastic film coated, min. 0,75 mm thick, galvanized steelplate with 25 mm thick rockwool on backside as thermal and sound insulation. Furthermore all cold bulkheads and cold decks are insulated with 120 mm rockwool.

In addition to air conditioning plant there is hot water heating in all cabins and common spaces.

10. Ice zone on shell is painted with INERTA 160 paint 1 x 500 my.
11. Navigation wings are covered and heated.
12. The passageway is arranged between accommodation and foreship under the deck.



Mr M. Edgecombe

OPERATING A FLEET IN THE CANADIAN ARCTIC - A REVIEW OF
DOME'S BEAUFORT SEA FLEET

ABSTRACT

In support of its Arctic offshore drilling operation, Canadian Marine Drilling Ltd. (Canmar), a wholly-owned subsidiary of Dome Petroleum Limited, Calgary, Canada, introduced its first icebreaking supply boat and some barges into the Canadian Beaufort Sea in the summer of 1975. Since that time, it has built up a Beaufort Sea fleet of forty ships ranging from barges and supply ships to drillships, a drydock and two icebreakers. The fleet is supported by two shore facilities, one at Tuktoyaktuk, and the other at McKinley Bay.

In this paper, the growth of both the fleet and the shorebase facilities are documented as they relate to the drilling activity in the Beaufort. General arrangements and principle particulars of the major fleet members are given. The McKinley harbour development is outlined and illustrated. The recent construction of two islands, Tarsiut and the SSDC, are discussed and general arrangements are also presented.

In total, this paper outlines the development and structure of the largest fleet operating in the Canadian Arctic at the present time.

1. BACKGROUND

Canmar was established by Dome Petroleum Limited in 1973 as a wholly-owned offshore drilling subsidiary. It began operations in the Canadian Beaufort Sea in 1975 with one icebreaking supply boat and some barges in preparation to commence drilling in 1976. In the seven years of operation (1976-1982), Canmar has drilled some 82,000 m of hole, with the deepest well penetrating to 5,000 m. The drilling up to date has confirmed the potential of the Beaufort Sea as a hydrocarbon producer since almost every hole has tested oil and gas in various quantities. So far, delineation drilling has not been carried out extensively enough to prove the commercial value of any particular structure.

2. ACCESS

Compared to other offshore operating areas, the Beaufort Sea is extraordinary because the drilling season from ships is considerably longer than the access windows, as shown in Fig. 1. Because of this, it is uneconomical to bring in a drillship or a dredge for only one season, which means that a large fleet has to winter in the Beaufort Sea every year. For the same reason, all repair and maintenance must be performed in the North since a trip South for repairs would take up most of a season's operating time.

3. SAFE WINTER HARBOUR

In 1975, there was only one established harbour - Tuktoyaktuk - in the Canadian Beaufort Sea. That harbour is excellent with deep water - 20 km - and well protected from every direction. The only problem is that the access is very shallow for 45 km, which excludes entry of ships with a draft greater than 4 m. Thus, only

the shallow draft supply ships could be wintered in Tuktoyaktuk, while the drillships with a draft of about 7 m, had to be stored elsewhere for the winter. For the winter of 76/77, it was decided to bring the three drillships to Cove Point at Hershel Island (Fig. 1). The experience of this winter was negative as the anchoring area was not well protected and considerable ice movement occurred. Luckily, the ships sustained only minor damage.

In the winter of 1977/78, a safe harbour was chosen at Summer Harbour (Fig. 2). This is an excellent deep water harbour with protection from all ice movements. The problem here, however, is the considerable distance from the operating area - 160 km - which proved to be especially cumbersome in the spring of 1978. When the ice moved away from the drillsites, there was still 100 km of shorefast ice between Summer Harbour and open water, and even after hard work by the four icebreaking supplyships, it took several weeks to reach the operating area. By that time, the ice between the wintering site and the drilling area had broken up anyway and so the whole exercise proved to be pretty much unnecessary.

To improve matters, Dome negotiated the lease of the 15000 shp Canadian Coast Guard icebreaker, John A. McDonald, but operations during the fall of 1978 showed only a marginal improvement. Thus, two important decisions were made:

1. To construct a 16,400 shp experimental icebreaker, Kigoriak, to replace the John A. McDonald; and,
2. to construct a winter harbour close to the operations area.

There are no natural deep water harbours closer than

Summer Harbour, and so Dome negotiated a lease for the cutter suction dredge Aquarius from Zanen Verstoep (Fig. 3) even before the final choice of the harbour location was made. After considerable study, McKinley Bay was chosen, the main reason being the possibility to finish the anchoring basin in one summer season (Fig. 2). In the fall of 1979, the proximity of McKinley Bay proved its value as the last drillship was brought in to the mooring basin in early December. In the middle of December, the landfast ice in McKinley Bay shifted about 30 m in a heavy storm with considerable damage to a supply ship and a barge. The next summer an inner basin and a protective island were dredged (Fig. 4) and thus, after five years, the fleet was finally in a safe winter harbour.

4. DRILLSHIPS

Canmar owns and operates four drillships in the Beaufort Sea (Figs. 5 to 8). Explorers I and II were modified to Arctic drillships from WWII surplus cargo ships. Explorer III, the former dynamically positioned Havdrill, was reinforced with ice strengthened sponsons along the ship's sides. Explorer IV is the former drillship Dalmahoy to which sponsons were added.

Because of the shallow water in the operating area - 20 to 100 m - dynamical positioning cannot be used and all four ships have mooring systems consisting of eight anchors on wires. Explorer IV has under hull fairleads and a Wärtsilä air bubbler system to reduce friction between ice and the hull. This makes it the most capable in ice of the four ships and thus, usually the last ship to reach harbour in the fall.

The drillships supported by icebreakers are able to continue working in much more difficult ice conditions than anticipated. They have been able to stay on

location and drilling in up to 60 cm ice with ridges.

The limiting factor is not the drillship but the capability of the icebreakers to break the oncoming ice fast enough. In 1983, Gulf Canada is bringing an improved drillship, the CDU (conical drilling unit) into the Beaufort Sea, with improved anchoring power and a unidirectional target for the ice, together with two 22,000 shp icebreakers. It will be very interesting to observe how much the season will be extended by this system.

Based on operating experience in the Arctic, considerable improvement have been made to the Canmar drillships, such as added insulation and protection from the elements.

In the case of Explorers I and II, so much topside weight was added that the reserve stability eventually was inadequate. Calculations showed that the addition of concrete into the double bottom would have eaten up most of the usable deadweight of the ships, and so, the only reasonable correction was to add a new pair of sponsors. It was not acceptable to take the two ships out of the Beaufort Sea to do this because they would have lost almost two drilling seasons each. As no dock was available, the sponsors had to be fitted while the drillships were floating. The sections of the sponsors were prefabricated in Vancouver, B.C. and trucked over the winter road to Tuktoyaktuk. There, the sponsors were welded into units each weighing approximately 200 tonnes. These were dragged over the ice to McKinley Bay where they were launched into a prepared opening in the ice and welded to the drillships. The work was completed on time and budget in spite of some unexpected incidents, for example, the partial loss of the ice road between Tuktoyaktuk to McKinley Bay.

5. ARTIFICIAL ISLANDS

In 1979, it was very likely that oil and gas production in the Beaufort Sea would take place from permanent structures. At that time, there was considerable experience with shallow water (up to 10m) islands with 1:15 slopes within the shorefast ice area. In deep waters, this method of construction would require excessive sand volumes. Model experiments showed that as long as you stayed away from the water penetration area, it would be possible to construct and maintain a slope of 1:5. Calculations indicated that permanent structures of this type could be competitive with drillships even in fairly deep water if the season lasted for about 200 days.

The first island of this type was designed and constructed by Canmar for Gulf Canada at Tarsiut in 21 m of water (Fig. 8). Tarsiut consists of a 1:5 slope between the -6.5 m and -21.0 m water level. The water penetration is made up of four independent concrete caissons. The caissons and the area inside the caissons are filled with sand to give a lateral resistance of about 80 000 tonnes.

Tarsiut Island was finished in November, 1981 with drilling commencing that same December and rig demobilization occurring in September, 1982.

The experience with Tarsiut showed several things:

1. The four independent caissons concept makes the startup difficult as the island has to be finished before equipment can be installed;
2. Moving of the island to another drilling location is not possible within one season; and,

3. The island is able to withstand all first-year ice conditions without damage.

The experience with Tarsiut Island led Carmar into the design and construction of the Single Steel Drilling Caisson (SSDC) (Figs. 9 and 10). This concept was conceived in December, 1981, the construction contract was signed in March, 1982 with Hitachi Zosen of Japan, and the unit was delivered into the Beaufort Sea in early September, 1982 and installed on the berm at Uviluk in 31 m water depth in October, 1982. To meet this tight schedule, a surplus VLCC was used. The stern was cut away and the bow part was heavily ice-strengthened using approximately 7,000 tonnes of steel and 14,000 tonnes of concrete.

In 1983, the SSDC will be moved to the Nerlerk location in 47 m of water depth. The SSDC is the first permanent structure to be tested outside the landfast zone and has already given some new insight into ice behaviour around such a structure.

The bulk of the island berm work was performed by two trailer suction hopper dredgers as shown in Table 1. These dredgers are the Geopotes X on contract from Volker Stevin (Fig. 11), and the Hendrik Zanen on contract from Zanen Verstoep (Fig. 12). As may be seen from Table 1, the dredger Aquarius also has been useful, especially in the deep suction mode employed at Nerlerk. This is a special case, however, as there is a deposit of good quality sand within pumping distance from the drilling location. The maximum operating depth of the Aquarius in this mode is 75 m.

The dredging and construction work is supported by two barges (Figs. 13 and 14). The Carmar workbarge is mainly used to accurately position the discharge pipe

while building the berm, while the Canmar Constructor is mainly used in mobilization and rigging work due to its considerable offshore crane capability.

6. DRYDOCK

In 1976, when drillship operations in the Beaufort Sea started there was a WWII floating dock in Tuktoyaktuk. It was large enough for the supply ships but much too small for the drillships. As the drillships did not have to be drydocked for five years, it was decided to take the risk and not spend the money for a large floating dock. In hindsight, that decision was proven correct as the drillships only had some minor incidents that could be repaired in the spring inside frozen boxes.

In 1980, the fleet that could not be docked had grown to eight including two travelling suction hopper dredgers with a large number of bottom doors as well as the icebreaker Kigoriak. Thus, it was decided to build a floating drydock in Japan (Fig. 15) which was delivered in the Beaufort Sea in September 1981. To increase the operational flexibility of the dock, it was build in two parts:

1. A submersible barge with four stability towers and a maximum lifting capability of 30 000 tonnes; and,
2. A separate workbarge with accommodation, cranes, workshops, stores, etc.

It is thus possible to use the floating dock part as a normal submersible barge to move heavy units, such as caissons, for large distances under tow.

The drydock had a busy year in 1982 with 180 operating days.

7. DRILLSHIP AND DREDGER SUPPORT

The drillships and dredgers need support in the form of suppliers, anchor handling, icebreaking, etc. To give this support, Canmar operates 10 major ships in addition to many smaller units that are used for survey, crew changes, etc.

The 10 major ships are as follows:

1. Supplier I - IV (Fig. 16), are used for anchor handling, supply transportation and secondary icebreaking.
2. Supplier V (Fig. 17), is used for coring, shallow seismic work, etc.
3. Supplier VI and VII (Fig. 18), are used for carrying supplies during the open water season.
4. Supplier VIII (Fig. 19), is the main carrier of bulk cargo and fuel in the open water season and in thin ice.
5. Robert LeMeur (Fig. 20), is also a large carrier of bulk cargo and fuel but in addition has year round icebreaking capability due to large power and good icebreaking hull form.
6. Kigoriak (Fig. 21), is an icebreaker and anchor handling ship with a limited supply capability. It has proven year round operating capability in the Canadian Beaufort Sea.

8. CONCLUSIONS

The Canmar fleet has been built during an eight year time frame starting in 1974. At that time, there was very limited understanding of the environmental conditions in the Beaufort Sea. Many people had even considered it impossible to operate in such a hostile environment.

Actual experience has shown that operating in ice-infested waters is easier than expected if you have the right equipment.

If a new fleet had to be built, major improvements could be made based on operating experience.

TABLE 1
VOLUMES DREDGED PER ISLAND
(cubic Meters)

<u>VESSEL</u>	<u>TARSIUT</u>	<u>ISLAND UVILUK</u>	<u>NERLERK</u>
"GEOPOTES X"	868,670	1,468,000	1,237,10
"HENDRIK ZANEN"	558,260	868,240	939,970
"AQUARIUS" USING A BARGE LOADING SYSTEM	459,940	-	-
"AQUARIUS" IN DEEP SUCTION MODE	-	-	1,284,660
"GEOPOTES IX"	71,960	86,310	-
TOTAL VOLUME	1,958,830	2,422,550	3,461,730
TOTAL NUMBER OF DREDGING DAYS	183*	160	147

*NOTE: The Tarsiut dredging days include 73 days for filling the caissons, storm damage, backfilling, etc.

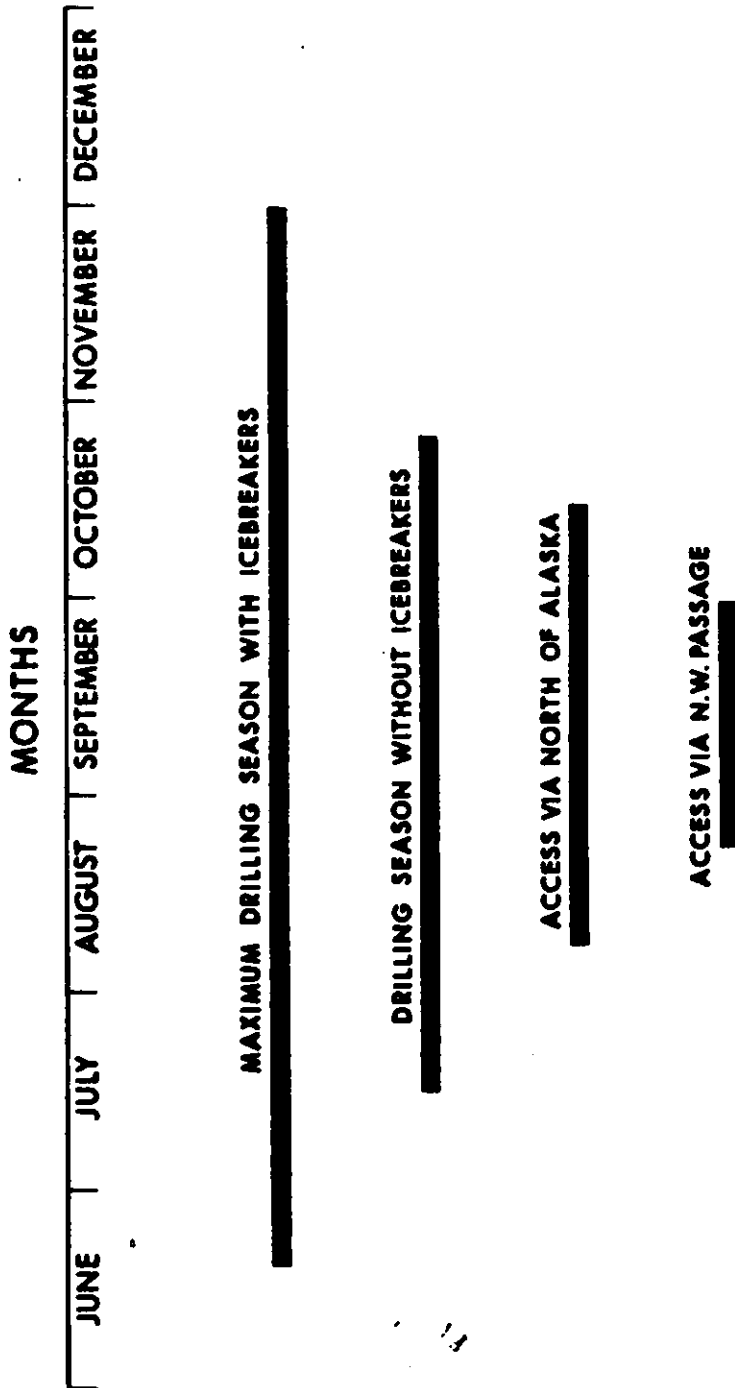


FIG. 1 DRILLING AND ACCESS SEASONS FOR THE BEAUFORT SEA

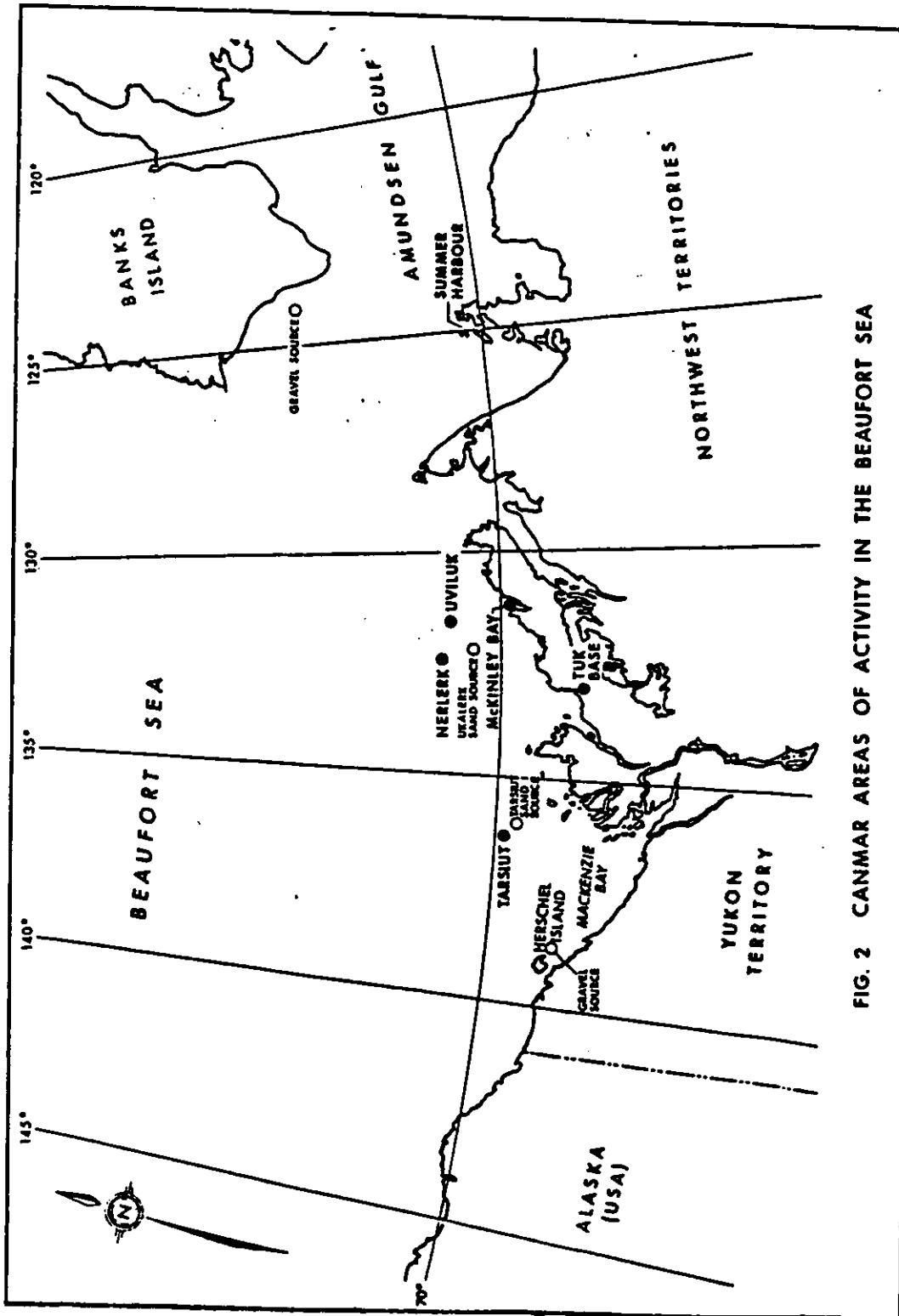


FIG. 2 CANMAR AREAS OF ACTIVITY IN THE BEAUFORT SEA

PRINCIPAL PARTICULARS

LENGTH (OVERALL)	107.00 m
WIDTH	19.00 m
MOULDED DEPTH	7.50 m
MAXIMUM DRAUGHT	4.9 m
POWER ON CUTTER	1,985 KW (2700 HP)
POWER ON UNDERWATER PUMP	1,764 KW (2400 HP)
POWER ON DISCHARGE PUMPS	2 × 2,793 KW (2 × 3800 HP)
MAXIMUM CUTTER DEPTH	29.00 m
POWER FOR PROPULSION	2 × 1,764 KW (2 × 2400 HP)
MAXIMUM SUCTION DEPTH	75.00 m
DIAMETER DISCHARGE PIPE	850 mm

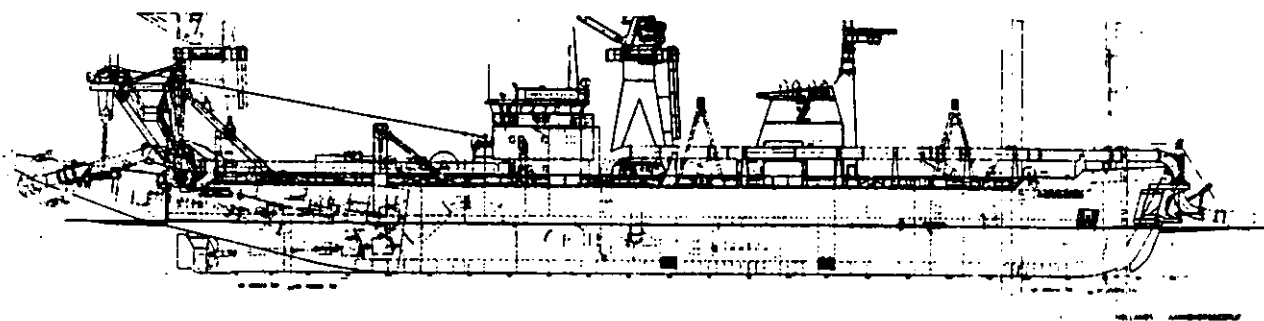


FIG. 3 CUTTER SUCTION DREDGER AQUARIUS

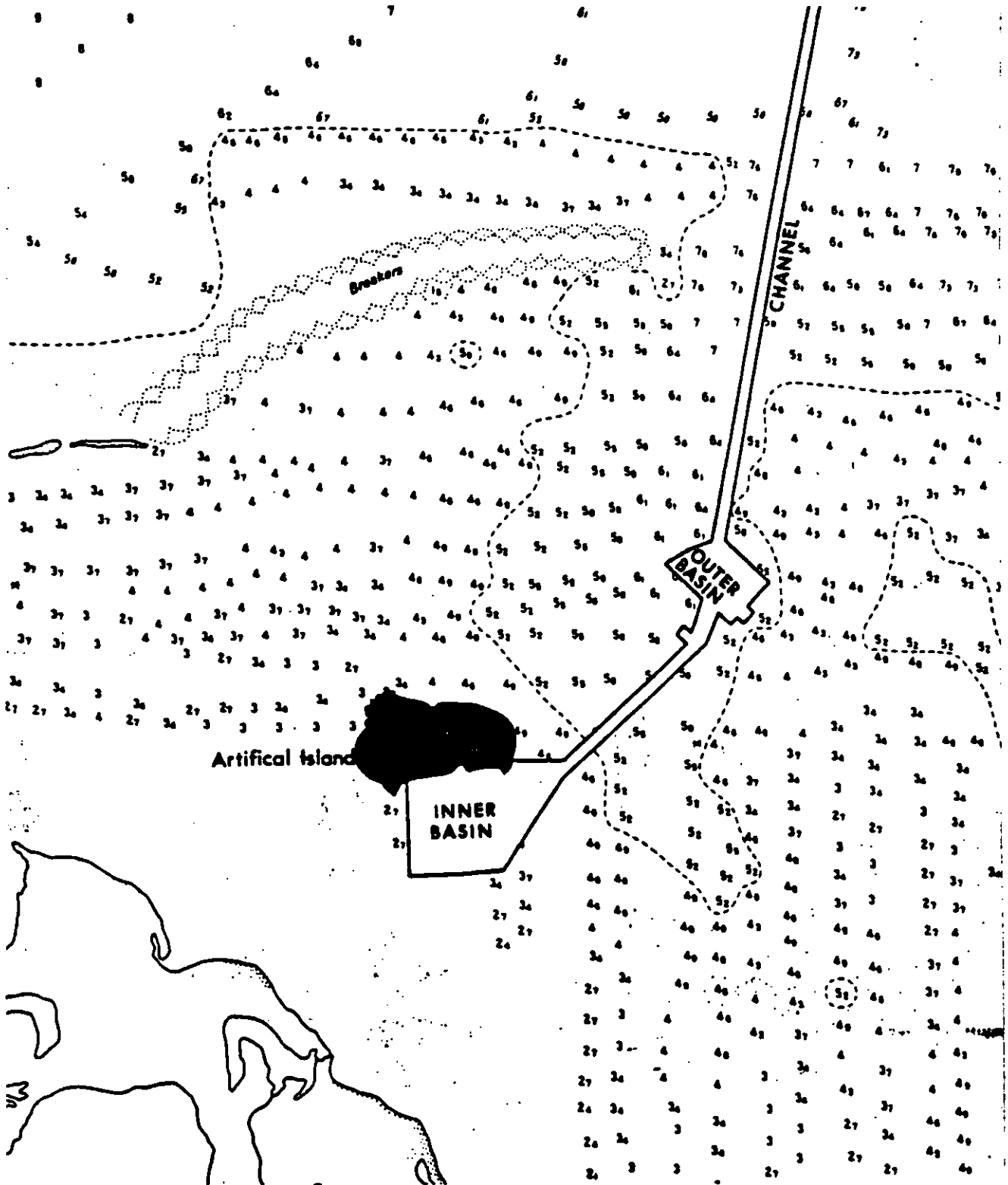


FIG. 4 (a) DREDGED IMPROVEMENTS TC MCKINLEY BAY

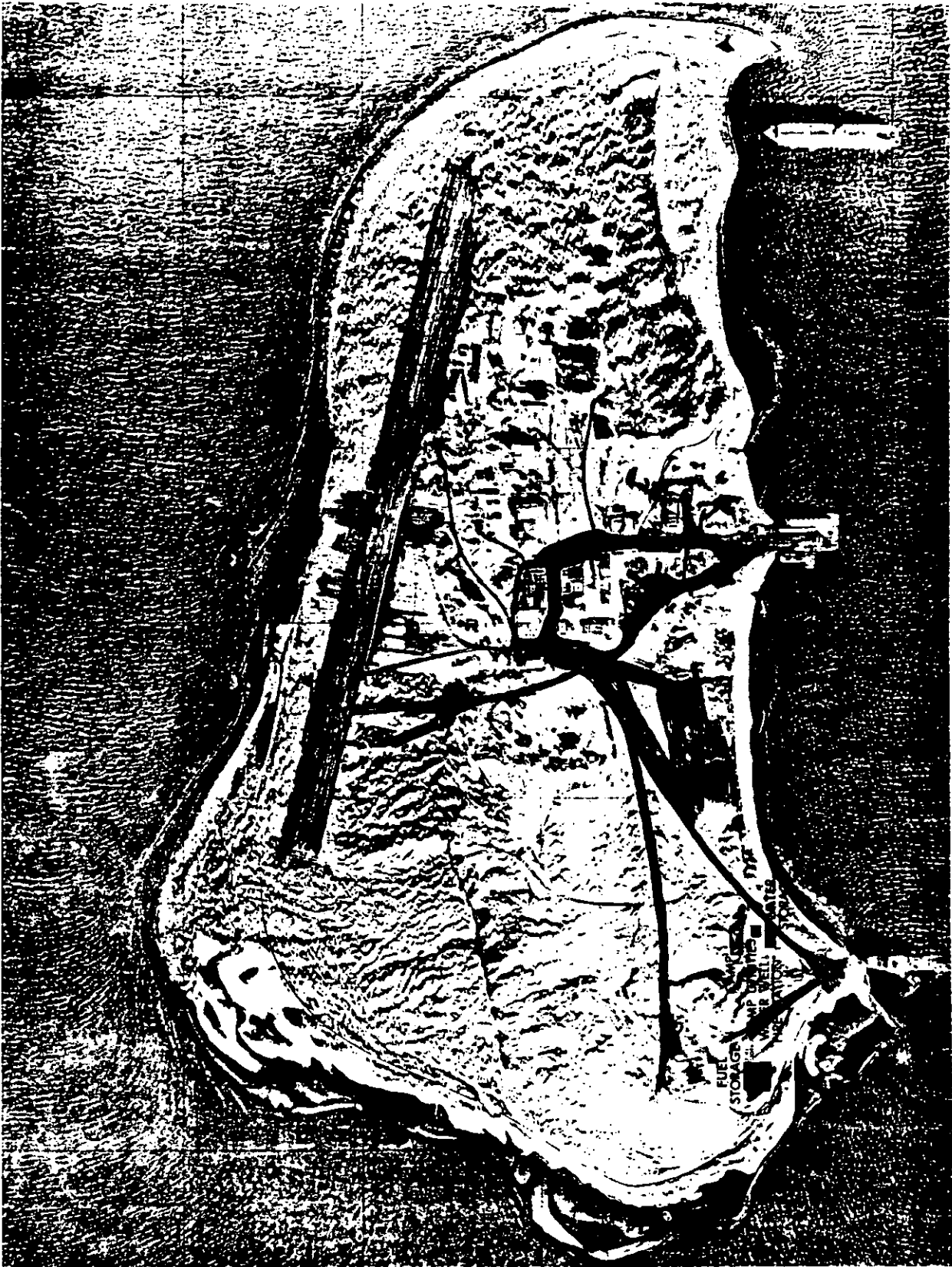


FIG. 4(b) DREDGED ISLAND FACILITY, MCKINLEY BAY

PRINCIPAL PARTICULARS

LENGTH O. A.	114.86 m
BEAM	30.48 m
DEPTH	8.72 m
LOADED DRAFT	6.76 m
LOADED DISP.	12,594 TONNES
LIGHT DISP.	6,496 TONNES
INSTALLED H.P.	7,875

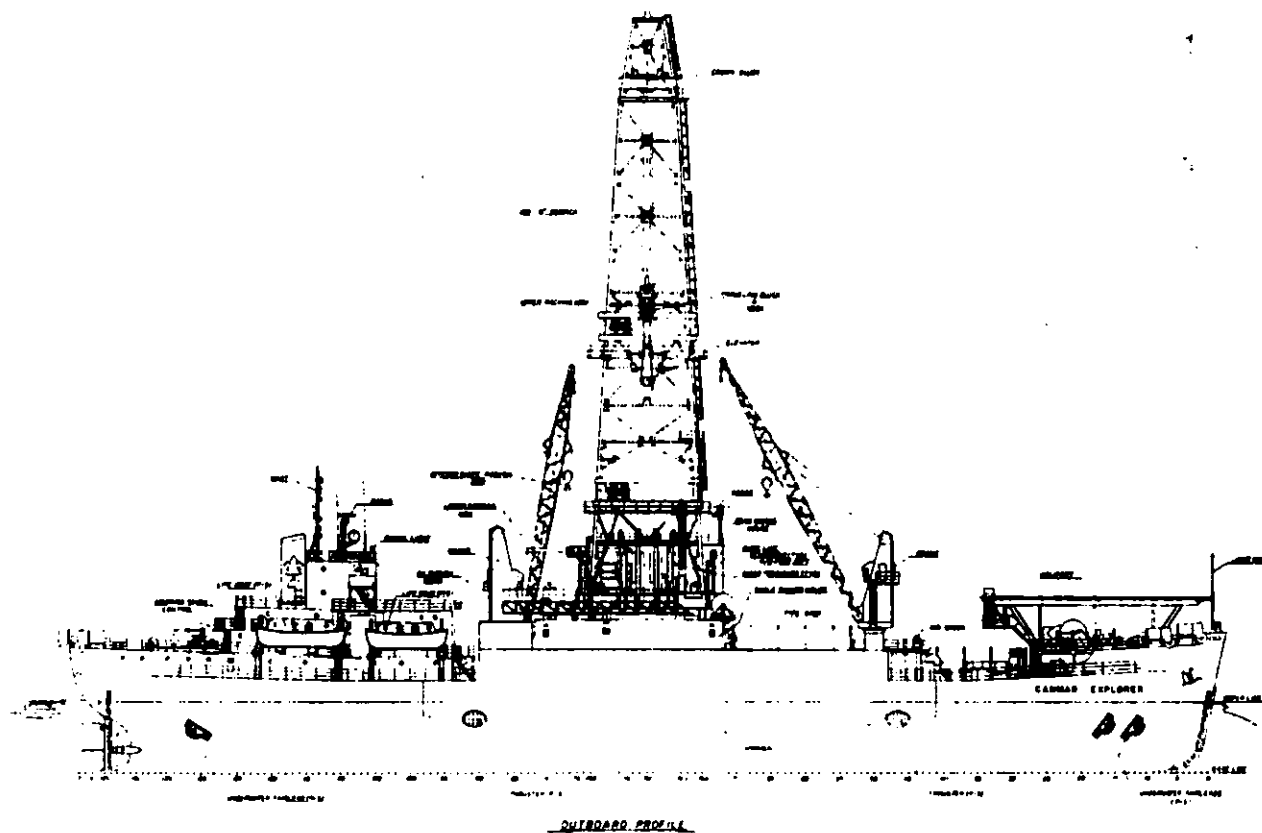


FIG. 5-6 CANMAR EXPLORER 1 & 2
(SAME DESIGN)

PRINCIPAL PARTICULARS

LENGTH O. A.	153.00 m
BEAM	23.79 m
DEPTH	12.5 m
LOADED DRAFT	7.5 m
LOADED DISP.	16,519 TONNES
LIGHT DISP.	9,083 TONNES
INSTALLED H. P.	17,000

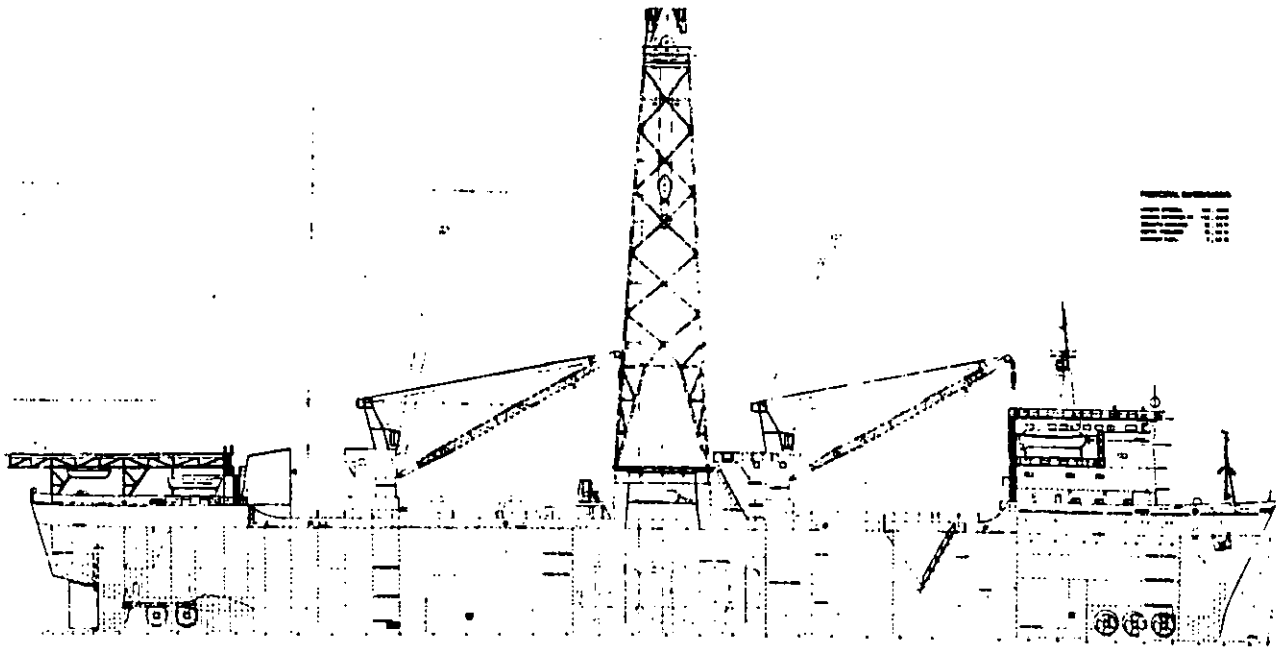


FIG. 7 CANMAR EXPLORER 3

PRINCIPAL PARTICULARS

LENGTH O. A.	118.6 m
BEAM	25.12 m
DEPTH	8.71 m
LOADED DRAFT	6.4 m
LOADED DISP.	12,105 TONNES
LIGHT DISP.	6,718 TONNES
INSTALLED H. P.	6,600

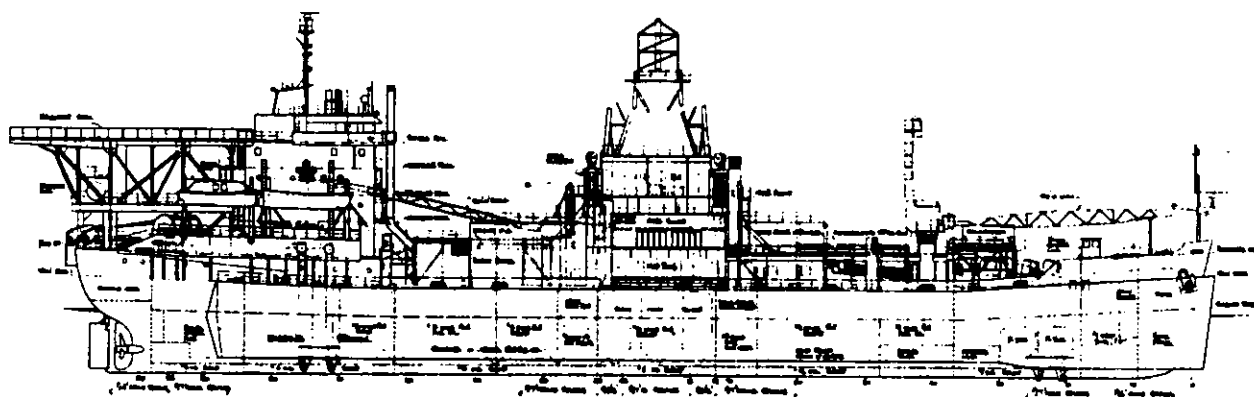


FIG. 8 CANMAR EXPLORER 4

PRINCIPAL PARTICULARS

LENGTH AT DECK	202.35 m
BREADTH	53.0 m
DEPTH	25.3 m
DRAFT ON BERM	9.0 m

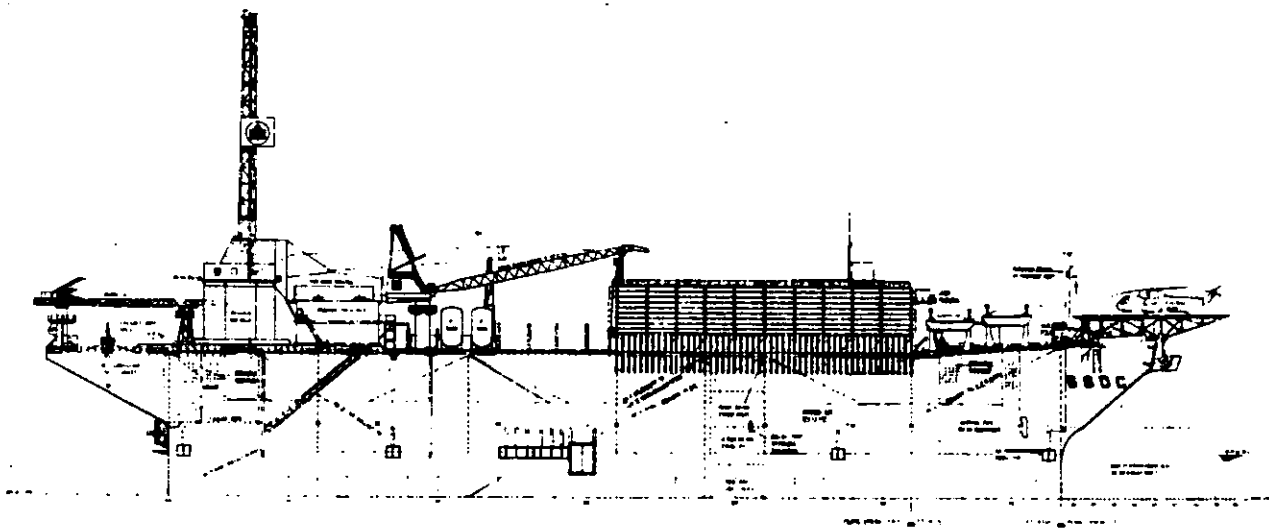
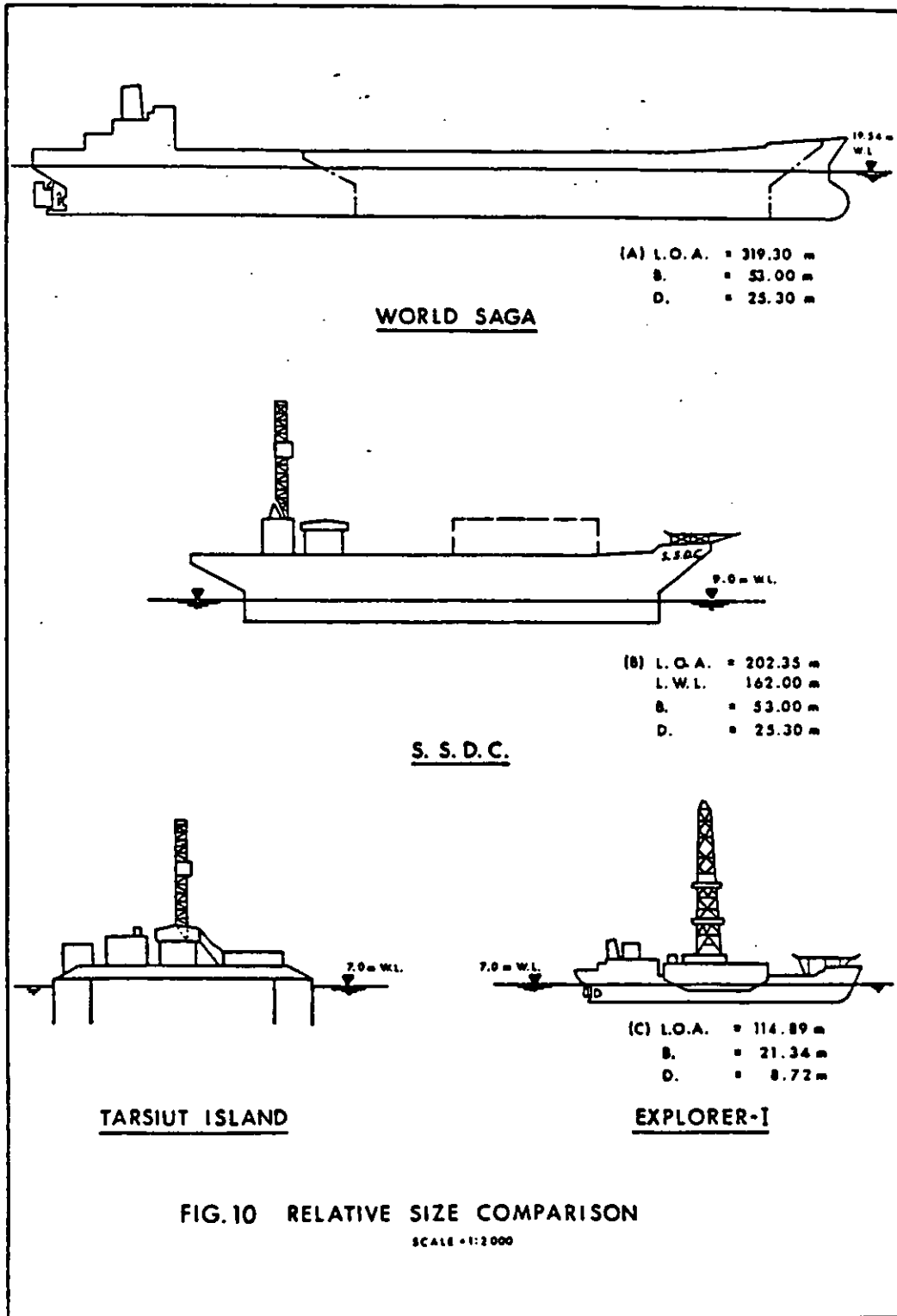


FIG. 9 CANMAR SSDC



PRINCIPAL PARTICULARS

LENGTH O. A.	136.02 m
WIDTH O. A.	21.6 m
MOULDED DEPTH	12.95 m
DRAUGHT LOADED MAXIMUM	12.01
HP FOR PUMPS	2 × 3000
DIAMETER SUCTION PIPES	2 × 1200 mm
HP FOR PROPULSION	2 × 6000
MAXIMUM DREDGING DEPTH	35 m
HOPPER CAPACITY	8645 m ³

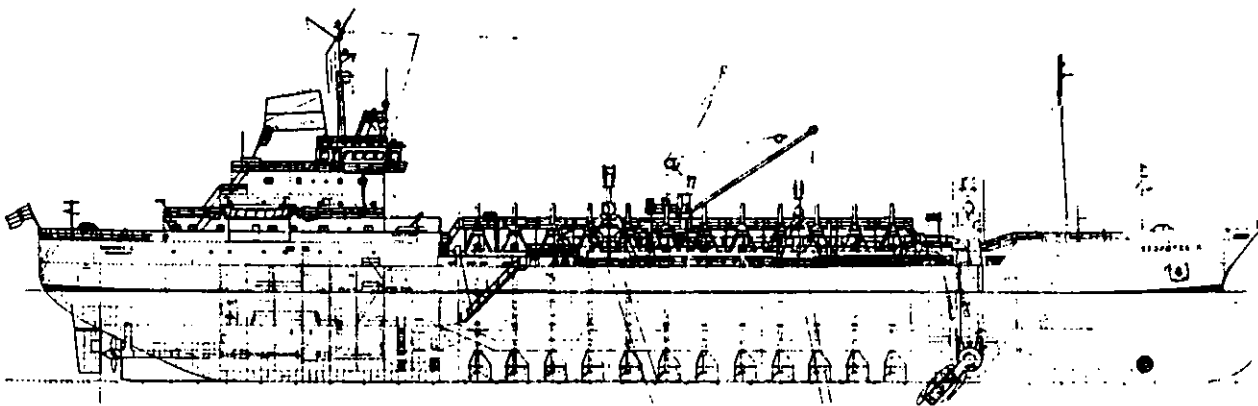


FIG. 11 TRAILER SUCTION HOPPER DREDGER GEOPOTES 10

PRINCIPAL PARTICULARS

LENGTH O. A.	119.50 m
WIDTH O. A.	18.50 m
MOULDED DEPTH	9.75 m
DRAUGHT LOADED	7.80 MAX.
POWER ON PUMPS	2 × 1,175 KW (2 × 1600 HP)
DIAMETER SUCTION PIPES	2 × 900 mm
POWER FOR PROPULSION	2 × 2,060 KW (2 × 2800 HP)
MAXIMUM DREDGING DEPTH	43 m
HOPPER CAPACITY	5760 m ³

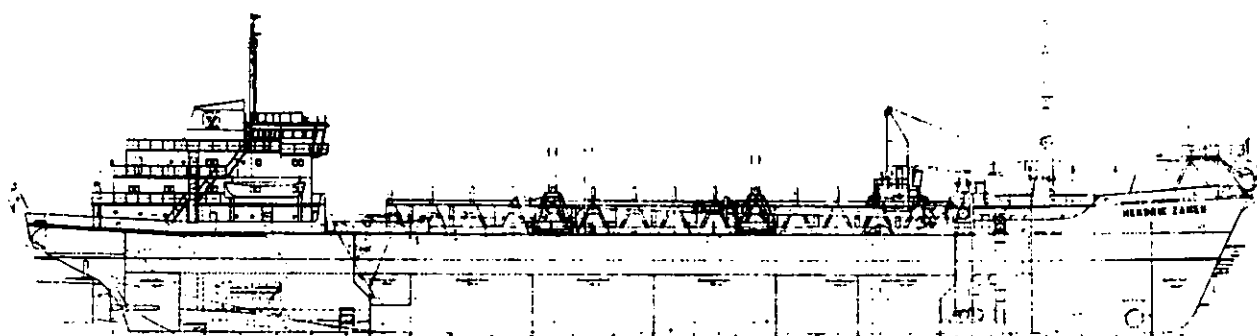


FIG. 12 HENDRIK ZANEN

PRINCIPAL PARTICULARS

LENGTH	68.3 m
WIDTH	19.0 m
MOULDED DEPTH	3.4 m
DRAUGHT	2.0 m
ACCOMMODATION FOR	36 MEN
MAXIMUM CRANE CAPACITY	80 TONNES
MAXIMUM DEPTH OF DISCHARGE PIPE	30 m
NUMBER OF ANCHORS	4-5 TONNE STEVIN ANCHORS
ANCHOR WINCHES	2 x 240 HP

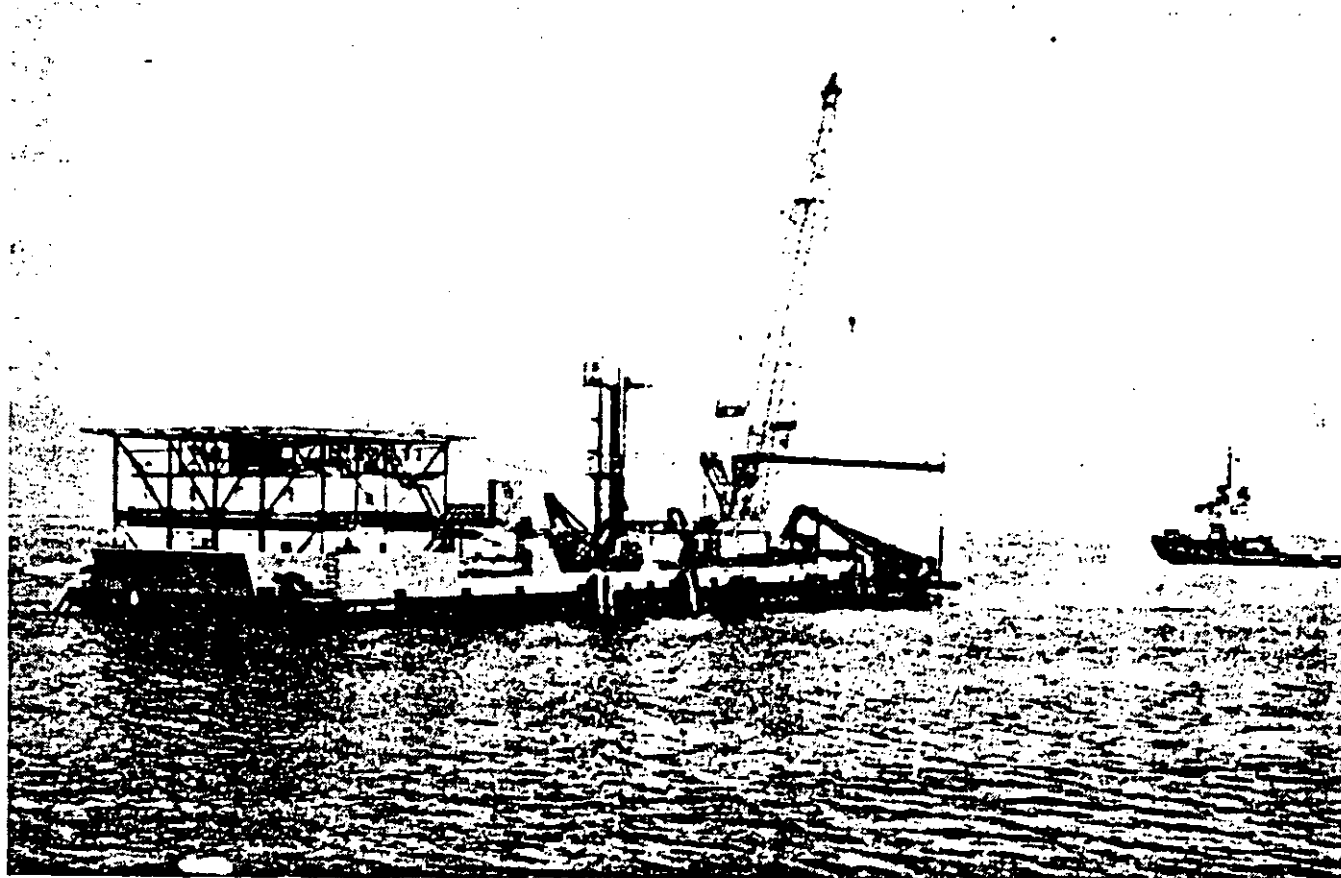


FIG. 13 CANMAR WORKBARGE

PRINCIPAL PARTICULARS

LENGTH	88.2 m
WIDTH	24.4 m
MOULDED DEPTH	6.0 m
DRAUGHT	4.07 m
ACCOMMODATION FOR	194 MEN
MAXIMUM CRANE CAPACITY	150 TONNES
MAXIMUM DEPTH OF DISCHARGE PIPE	45 m
NUMBER OF ANCHORS	8-7.5 TONNE STEVIN ANCHORS
ANCHOR WINCHES	MAX. 60 TONNES PULL PER WINCH

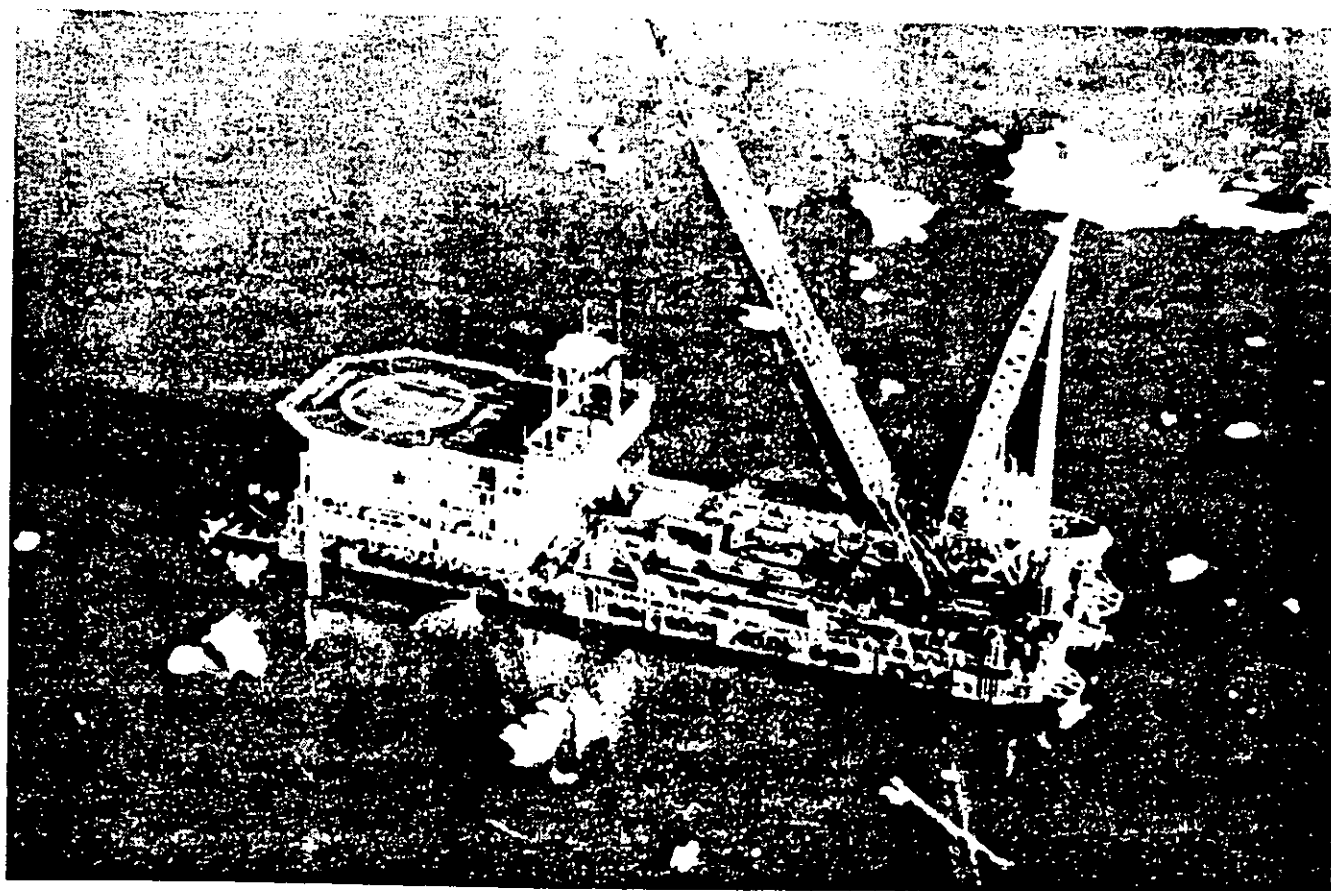


FIG. 14 CANMAR CONSTRUCTOR

PRINCIPAL PARTICULARS

LENGTH O. A.	131.06 m
BREADTH	48.77 m
LOADED DRAFT	5.67 m
BALLAST	52,032 TONNES

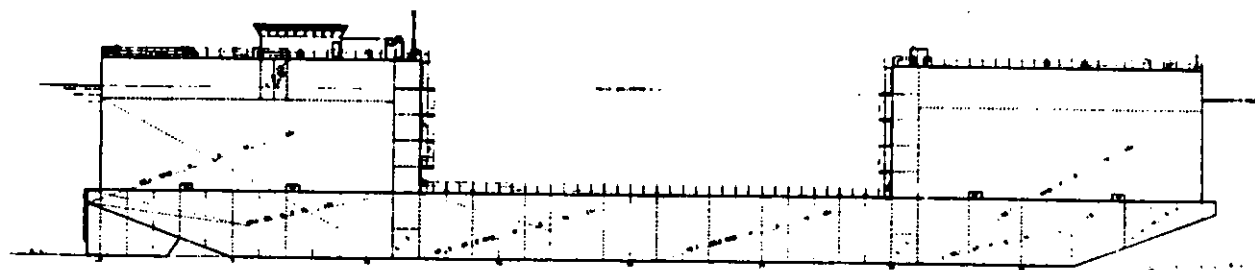


FIG. 15 CANMAR CAREEN

PRINCIPAL PARTICULARS

LENGTH O. A.	62.5 m
BEAM	13.7 m
DEPTH	5.6 m
LOADED DRAFT	4.3 m
LOADED DISP.	2,376 TONNES
LIGHT DISP.	1,335 TONNES
INSTALLED H.P.	7,700

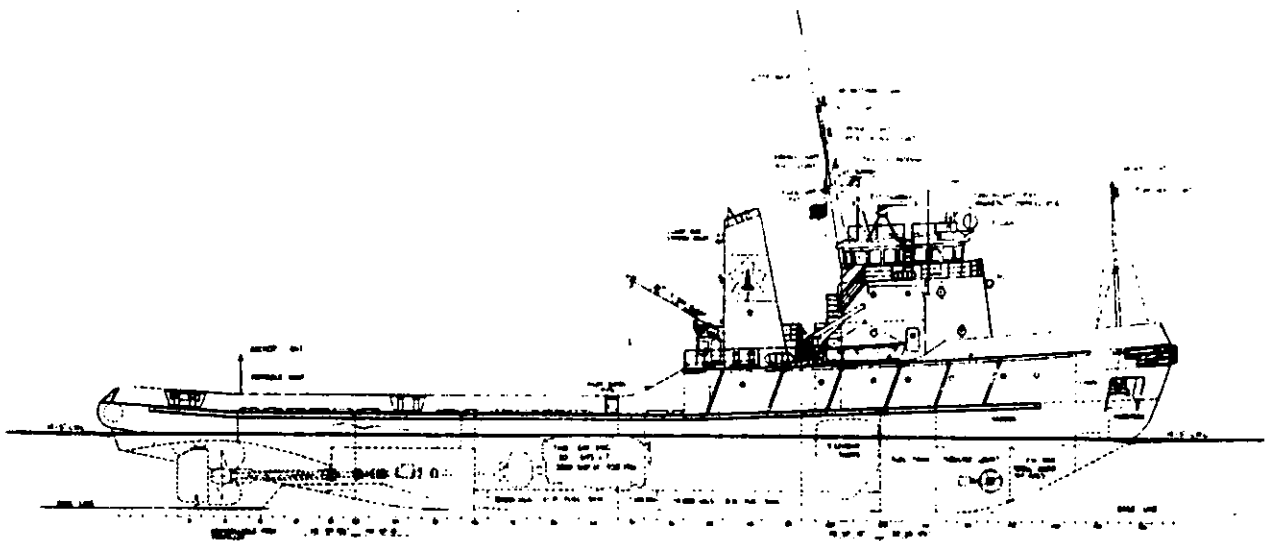


FIG. 16 CANMAR SUPPLIER 1 TO 4

PRINCIPAL PARTICULARS

LENGTH O. A.	39.6 m
BEAM	13.4 m
DEPTH	3.4 m
LOADED DRAFT	2.6 m
LOADED DISP.	1,117.5 TONNES
LIGHT DISP.	524 TONNES
INSTALLED H.P.	2,500

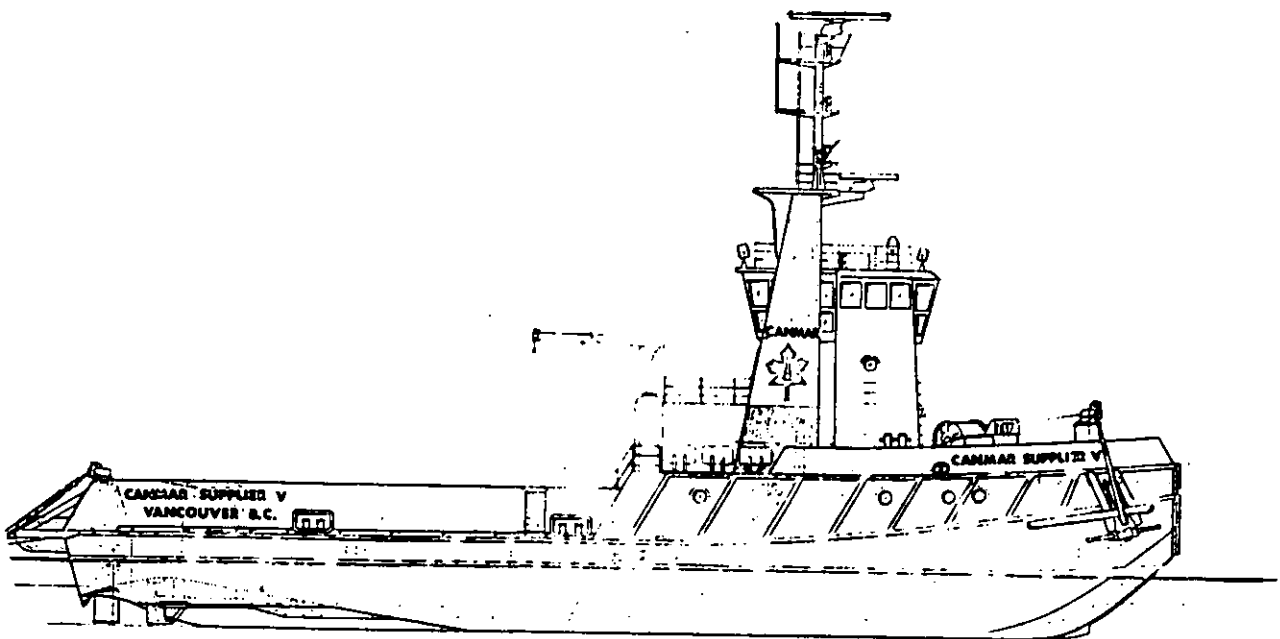


FIG. 17 CANMAR SUPPLIER 5

PRINCIPAL PARTICULARS

LENGTH O. A.	56.25 m
BEAM	11.75 m
DEPTH	5.1 m
LOADED DRAFT	4.7 m
LOADED DISP.	1,625.2 TONNES
LIGHT DISP.	1,035.5 TONNES
INSTALLED HP	7,260

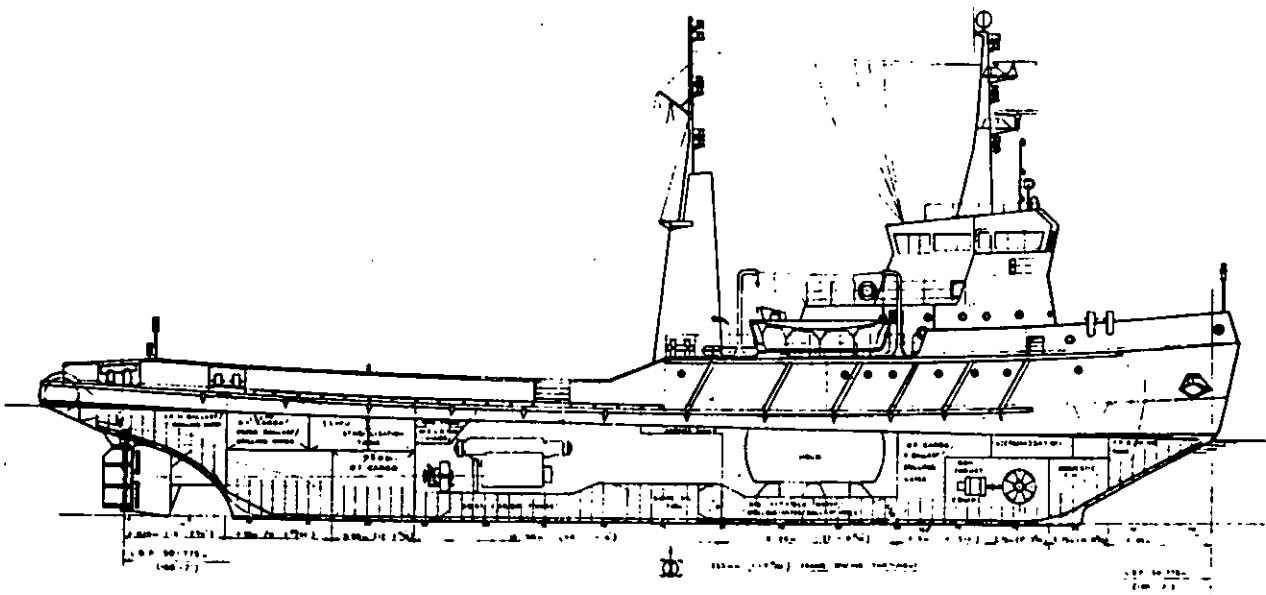


FIG. 18 CANMAR SUPPLIER 7

PRINCIPAL PARTICULARS

LENGTH O. A.	64.13 m
BEAM	15.67 m
DEPTH	4.75 m
LOADED DRAFT	3.5 m
LOADED DISP.	2,827.5 TONNES
LIGHT DISP.	1,153 TONNES
INSTALLED H.P.	3,085

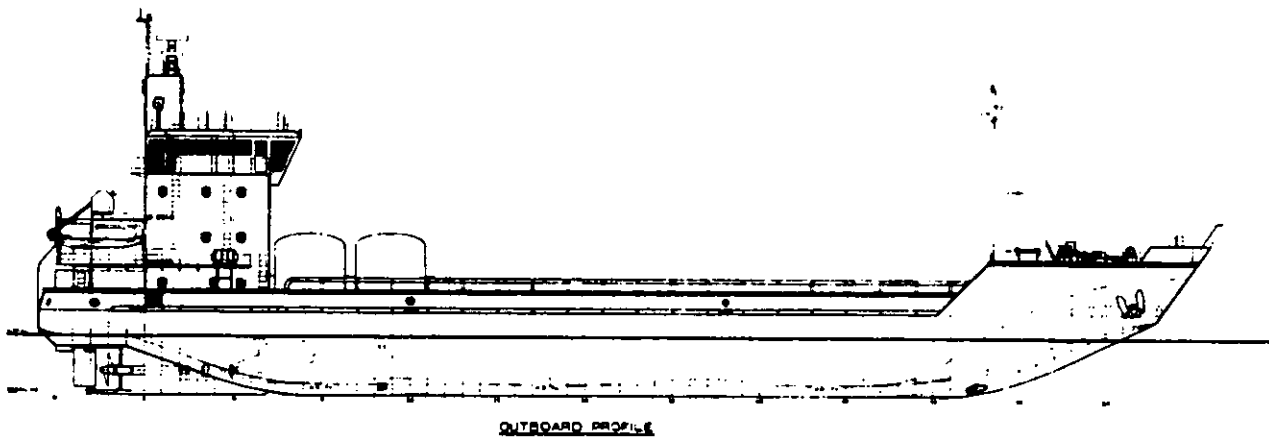


FIG. 19 CANMAR SUPPLIER 8

PRINCIPAL PARTICULARS

LENGTH O. A.	82.5 m
BEAM	18.0/19.0 m
DEPTH	7.5 m
LOADED DRAFT	5.5 m
LOADED DISP.	5,600 TONNES
LIGHT DISP.	3,162 TONNES
INSTALLED H. P.	9,800

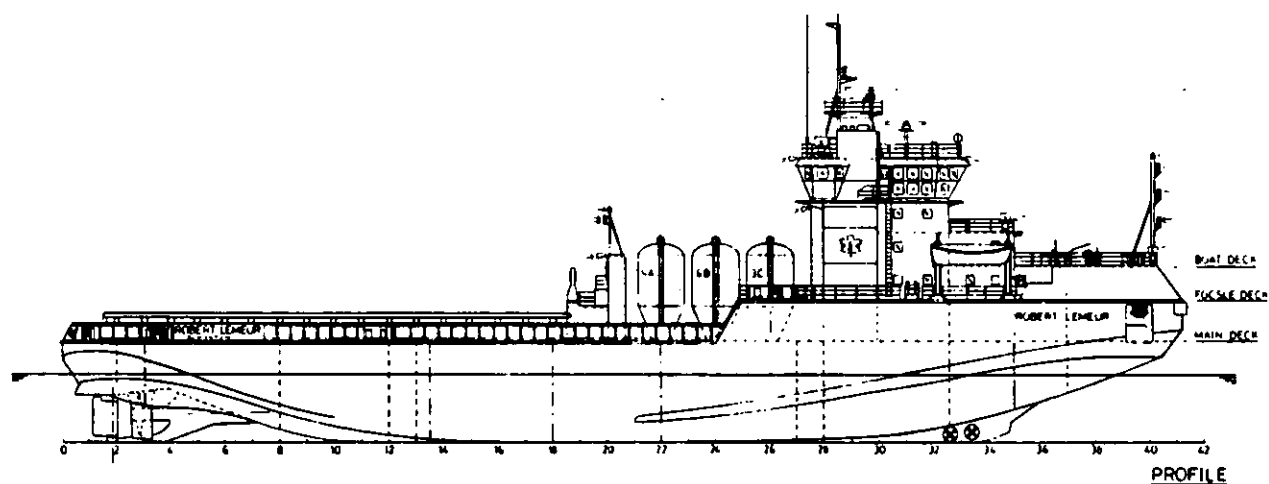


FIG. 20 M. V. ROBERT LEMEUR

PRINCIPAL PARTICULARS

LENGTH O. A.	90.72 m
BEAM	17.25/18.25 m
DEPTH	10.00 m.
LOADED DRAFT	8.35 m
LOADED DISP.	6,549 TONNES
LIGHT DISP.	4,483 TONNES
INSTALLED H. P.	17,300

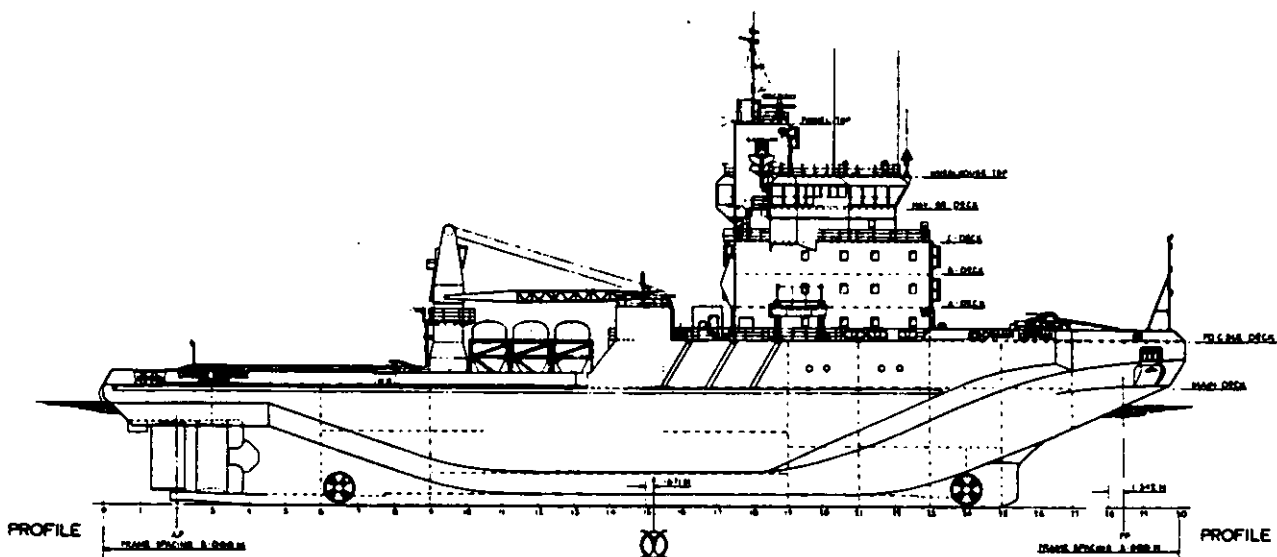
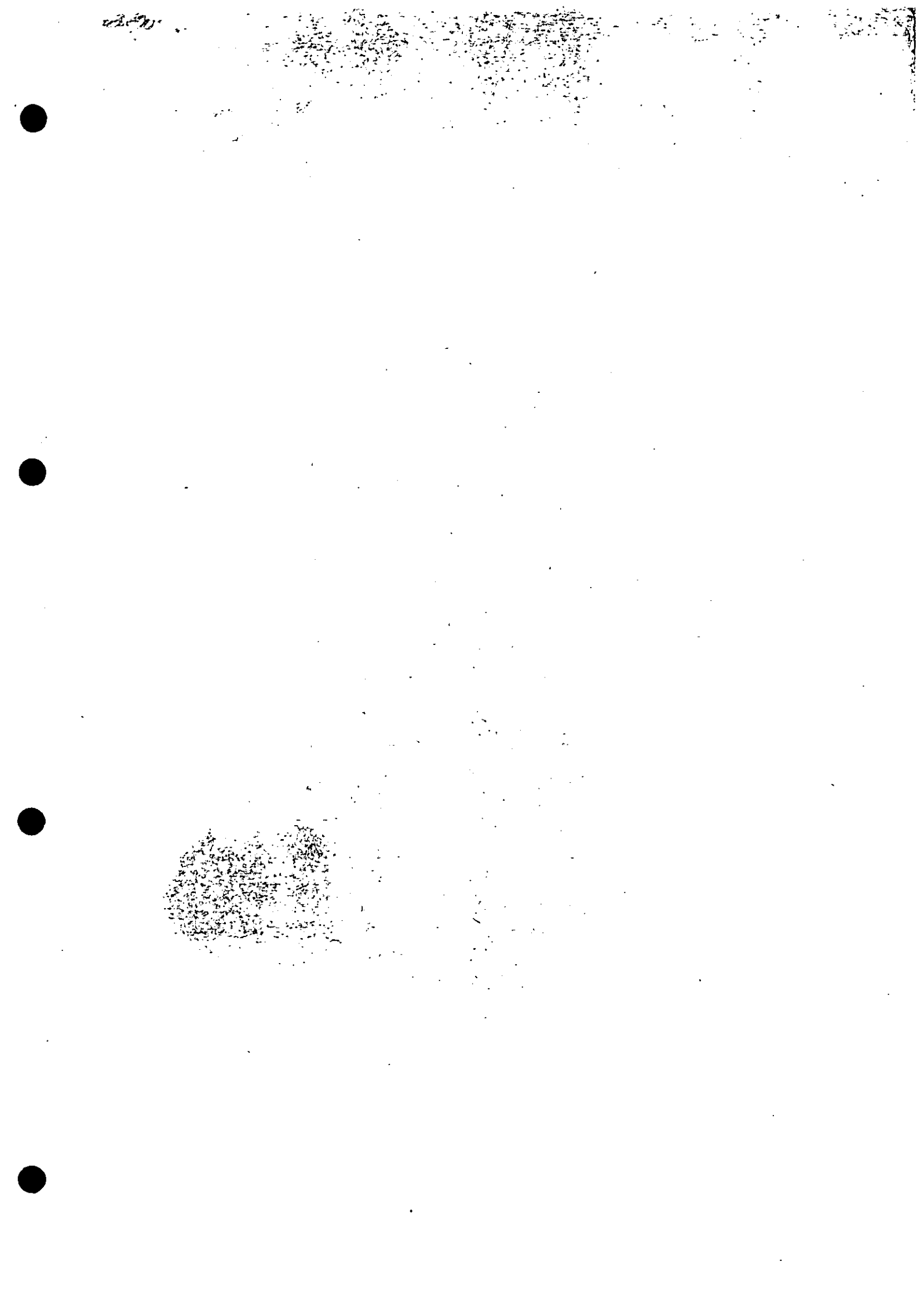


FIG. 21 M.V. CANMAR KIGORIAK



NOTES ON AIR CUSHION ICEBREAKING

by P. G. Noble

INTRODUCTION

For more than ten years, air cushion icebreaking has been under development in North America and more recently in Finland. The use of an air cushion vehicle as an icebreaking system was recognised in the winter of 1971-72 in Yellowknife, in the Canadian Northwest Territories when air cushion transporter ACT 100 broke ice while being towed at a relatively low speed across Great Slave Lake. The second trial at Tuktoyaktuk Harbour confirmed the observation found in earlier tests and provided a better understanding of the mode of ice failure and the cushion pressure-ice thickness relationship. Other tests followed in Montreal harbour and Toronto harbour with the Terracross H119 towed air cushion raft and the Hover Jack. During the experiments with the self-propelled air cushion vehicle, Voyageur, at Parry Sound, Ontario, two modes of icebreaking were observed. The first one occurred when the ACV was moving at low speed. This mode of failure breaks the ice by introducing an air cavity under the ice cover which causes the ice to fail due to its own weight and lack of buoyant support. A second failure mode occurs when the air cushion vehicle proceeds at critical or "hump" speed. At this point, the flexural wave induced in the ice surface is sufficient to break the ice into pieces.

The use of air cushion technology for breaking ice has now developed from the pure experimental stage to the point where useful operations are being performed.

One of the requirements for icebreaking is to assist shipping in ice covered waters. This has traditionally been accomplished by specifically

designed icebreaking ships which essentially operate on the principle of applying downward force on the ice in their bow area and require high horse power in order to accomplish this. With continuing expansion of ice area operations by both commercial and government agencies, new methods of icebreaking and ice transitting are continually being developed and air cushion icebreaking, with its effective use of power, has a role to play.

METHODOLOGY

As mentioned previously, it has been found that there are two distinct speed regimes where the air cushion icebreaking phenomenon occurs. For the sake of this lecture, these are defined as low speed and critical speed icebreaking.

The low speed method (Fig. 1) depends on being able to propagate the air bubble underneath the ice and is therefore dependent on having cracks or openings in the ice sheet in order to commence icebreaking. This type of air cushion icebreaking is also dependent on having a cushion pressure head somewhat in excess of the ice sheet thickness. As the platform approaches the edge of an ice sheet, the air pressure generated and contained within the platform's skirt system depresses the water level beneath the platform relative to the surrounding surface by an amount approximating the air cushion pressure head. As the platform moves onto the ice sheet, the skirt rides up over the ice still maintaining its air seal. The ice sheet penetrates the pressurized air cushion where the depressed water level allows an air cavity to form between the underside of the ice and the water

which extends forward and around the advancing platform being fed from the cushion. The ice sheet under the platform with the buoyant force of removed, becomes a cantilever plate which eventually fails due to its own weight when the cantilever section reaches a critical length. The overhanging ice section breaks away and the broken pieces fall into the water below to float at the depressed level created by the cushion pressure head, as shown on Figure 2. This phenomenon has been observed at and filmed from within the cushion of the ACVs on several occasions.

Several attempts have been to derive satisfactory theoretical approaches to determine the failure mechanisms of the failures involved in air cushion icebreaking but due to the many assumptions that must be made in order to solve this complex problem, the current state-of-the-art is such that the theoretically predicted results may vary considerably from one theory to another and none has proved totally satisfactory in giving results that are corroborated by full scale evidence.

Presently, the critical speed method is even less clearly defined as to a thorough understanding of the phenomenon and to its limiting parameters and limiting variables. This is due again to the lack of established theory and also the lack of model and full scale experimental data. Basically, any vehicle moving at a critical speed over floating ice sheet generates a wave pattern in the ice which can sufficiently amplify the stress in the ice to cause failure. The critical velocity depends on the various ice characteristics such as thickness and flexural strength and also on the water depth. Early experiments led to the assumption that the wave formation was developed at a critical velocity which was coincident with the crafts over-water hump speed but in more recent observations the ice wave has been developed at vessel speeds which do not correspond to the expected critical velocity.

Due to the success of this type of icebreaking for ice clearance and flood control work, opportunities to conduct extensive controlled experiments have not been available but, clearly, this very powerful method of icebreaking justifies continued development.

HISTORICAL VIEW OF AIR CUSHION ICEBREAKING

Since the birth of modern air cushion vehicles in 1959 in the U.K., a multitude of craft has been built and tested in various environmental conditions around the world. Tests in cold regions revealed that the amphibious air cushion vehicle has a good ability to break ice.

In operations on Lake Erie in the winter of 1969, Bell SK5s broke the ice cover over which they travelled. In tests in Vaxholm in Sweden in 1971, the Hovermarine Hover Cat II also broke the ice over which it travelled.

Recognition of the potential of air cushion icebreaking was probably first realised after the ACT 100 air cushion transporter trials were conducted at Yellowknife during the winter of 1971-72 when the craft was towed across Great Slave Lake on a winch system and broke through the ice. Officials of Transport Canada who had witnessed the tests became very interested in air cushion icebreaking as a concept and have, since 1971, initiated several full scale and model scale tests to better understand and evaluate this icebreaking method.

In 1972, Transport Canada trials with the ACT 100 at Tuktoyaktuk harbour in the Northwest Territories demonstrated icebreaking and air cushion ferrying potential. In the spring of 1973, tests with a Terracross H119 towed air cushion raft were conducted in Montreal. In February of 1974, tests were conducted in Toronto harbour when a tug pushed two different air cushion rafts, a Terracross H119 and a Hover Jack HJ15. Unseasonably warm weather curtailed testing but icebreaking capability was again demonstrated. In another series of tests in the spring of 1972, the

Canadian Coast Guard was evaluating the self-propelled Bell Aerospace Voyageur ACV's icebreaking capabilities at Parry Sound, Ontario. It was during these trials, as the craft was proceeding to the low speed test site, that it was observed, when accelerating to a velocity approaching hump speed, a large standing wave appeared in the ice about half a craft length astern. The ice sheet over the traversed area was continually failing on the wave crest. A hastily arranged, controlled experiment was organised where the craft speed was accurately measured and the wave and ice characteristics recorded. There was no further opportunity to exploit this discovery in Parry Sound but the potential was immediately recognised as being a breakthrough in icebreaking, at least for inland fresh water, first-year ice. Early 1974 was a significant turning point in the development of air cushion vehicle icebreaking in North America. Not only had the Voyageur convincingly shown the potential of critical speed icebreaking but also the air cushion vehicle icebreaking inter-departmental working group of the federal Canadian Government recommended that the Department of Transport should investigate the effect of attaching an air cushion platform to the bow of a ship. Model tests were conducted in synthetic ice and indicated a dramatic reduction in resistance of the ship when the ACV platform was attached. As a result of these trials, a design study was commissioned for a platform attached to the icebreaker CCGS Montcalm.

By mid 1975, Transport Canada had decided to set up a multi-year development program to enhance conventional icebreaking capabilities by using air cushion technology with particular regard to the approach of attaching an air cushion platform to the bow of a ship.

The first phase of this program culminated in a successful full scale trials of the CCGS Alexander Henry - ACT100 conducted on Lake Superior at Thunder Bay, Ontario through the winter of 1975-76. The second year of the program, 1976-77, was also carried out in Thunder Bay where the ACT 100 now renamed the ICEATER I was coupled to a commercial tug, an Ice Class tanker and the icebreaker CCGS Griffon.

RECENT DEVELOPMENTS

The data collected during the Thunder Bay trials so clearly indicated the advance made by improving icebreaking that the Canadian Coast Guard issued a design requirement for an air cushion bow-attachment to fit light to medium icebreakers. After some problems with the construction phase, this air cushion bow is now in service at Thunder Bay, Ontario.

The system consists of an air cushion icebreaking bow fitted in front of an icebreaker. The air cushion bow is a diamond-shaped platform with the aft corner notched to allow attachment to the ship. (Figure 3). Three 500KW diesel engines power the lifting fans and the system allows freedom to pitch and heave and at the same time provides a good seal against the pressure under the platform. The ACIB geometry is shown in Figure X and its performance is summarized in Table Y. The Alexander Henry light icebreaker was used as the first trial ship; the ship has a 3,300 ton displacement, is 64.1m long, 13.26 beam and a draft of 5.86m and is capable of developing a maximum thrust of 340 KN through two propellers. The two vehicles are attached using pretensioned cables to minimize sway and surge of the ACIB relative to the icebreaker.

The most recent tests were conducted in Thunder Bay harbour on Lake Superior between the months of January and April, 1982. The program consisted of hover over land and over water tests on the ACIB, followed by icebreaking tests using the CCGS Alexander Henry. The icebreaking tests with the ACIB - Alexander Henry system were conducted at the end of April 1982. Unfortunately, the ice was weak and disintegrating in some areas at this time. However, during the icebreaking tests, the resistance of the ACIB relative to the ship and the thrust of the system were measured so that comparison to previous experiments conducted with the Alexander Henry alone in the icebreaking mode and with the modified ACT ICEATER air cushion bow could be made.

The results plotted on Figure 4 show the dramatic improvement in non-dimensionalized resistance when the Alexander Henry has the addition of the air cushion icebreaking bow and its results such as these that have encouraged the continued development of low speed air cushion icebreaking.

FUTURE DEVELOPMENTS

Air cushion icebreaking so far has been mainly carried out in temperate ice regimes such as the St. Lawrence River, the Great Lakes and some limited areas of the Baltic. Attempts have been made to use air cushion vehicles as over-ice transport in Arctic areas but this has not been successful to date, primarily due to the poor ability of existing ACVs to navigate areas of rough ice which are found throughout the Arctic. A number of developments are, however, underway. In Northern Alaska, where there is continued expansion of offshore oil development in the Prudhoe Bay area, a number of air cushion vehicles are now in service, both as personnel and cargo carriers in the relatively smooth ice within the Barrier Islands. These ACVs have been used as transport vehicles and are not designed or intended to break the ice. In fact, in early season operations, when there is thin ice around, which does break, the operations of these vehicles is severely hampered due to the tearing of skirts when encountering broken ice pieces.

Another development that is progressing is the investigation of rigid side wall or semi-submerged air cushion vehicles as Arctic-transitting vehicles. To date, only analytical investigation of this concept has been carried out but it is hoped in the near future that model testing of such vessels will be undertaken in Canada.

CONCLUSIONS

The current state-of-the-art is such that it is possible to design reliable air cushion vehicle bow attachments for light icebreakers to

improve their performance in uniform, level, first-year ice. The main role for such equipment will be in ice management within harbours, ports, canals, etc. The use of free-flying air cushion vehicles at critical speed for ice jam control and flood control is also an accepted practice. This takes place mostly in areas where there is sufficient tidal or river current action to move the broken ice away after the vehicle has passed over and broken the ice. So far, the use of air cushion icebreakers in the Arctic has not reached a practical stage. Consideration is being given to a number of applications, both expanding the existing experience from more temperate ice regimes and also looking at different techniques and combinations of air cushion vehicles with other vessels such as catamarans or semi-submersibles to improve or enhance their ice-transitting performance.

Much work remains to be done in these developments. Some of the key areas are:

- ° a better theoretical understanding of both slow speed and critical speed icebreaking must be obtained
- ° better model testing techniques should be developed in order to more reliably predict full scale performance
- ° the performance of skirt systems under very high pressures and low temperatures still needs development, both with regard to the system design and to the material properties of the skirt
- ° more operational experience must be gained in order that the design circle may be closed and better full scale experimental and operating information can be fed back into the new designs that will be required for the next few years.

BIBLIOGRAPHY ON ACV ICEBREAKING

Turner, W.N., Urquhard, M.D., and Hill, W.L. "ADS Phase I Ice Tests with an Air Cushion Transporter". Paper presented at the 23rd Annual Technical Meeting of the Petroleum Society of the C.I.M., May 1972.

Nevel, D.E. "Moving Loads on a Floating Ice Sheet". CRREL Report, May 1968.

Nevel, D.E. "Bearing Capacity of Floating Ice Sheets". CRREL Report, December 1968.

Dickins, D.F. "Ice Conditions - CCG Voyager Icebreaking Trials" DOE Report, April 1974.

Lecourt, E.J. and Kim, J.K. "Mathematical Model of Icebreaking with an ACV", Arctec Canada Limited, Technical Note 39-2, 1974.

Poitras, R.H. "Pilot ACV Icebreaking Trials". Transportation Development Centre Report D500-174-1-6.

Kerr, A.D. "The Bearing Capacity of Floating Ice Plates Subjected to Static or Quasi-Static Loads - A Critical Survey". CRREL Research Report 333, March 1975.

Wade, R.G., Edwards, R.Y. and Kim, J.K. "Improvements in Icebreaking by Use of Air Cushion Technology". Paper presented at SNAME "ICE TECH 75" Symposium in Montreal, April 1975.

Canadian Coast Guard, Fleet Systems, ACV Evaluation & Development Unit Winter and Icebreaking Evaluation of CCG Voyager CH-CGA (Montreal) Transport Canada Report TP 297, Spring 1975.

Canadian Coast Guard, Fleet Systems, ACV Evaluation & Development Unit River Icebreaking for Flood Control Conducted by CCG Voyager CH-CGA (Quebec Region), Transport Canada Report TP 406, April 1976.

Ball, M.A. "Report on the Full-scale Icebreaking Tests of an Air Cushion Bow Platform Attached to the CCGS Alexander Henry, Thunder Bay, Ontario - January-April 1976." Canadian Coast Guard ACV Division Report to Transportation Development Centre, Transport Canada Report TP 903, November 1976.

Ball, M.A. "Continuous Advances with Air Cushion Icebreaking". Proceeding of Canadian Aeronautics and Space Institute 10th Air Cushion Technology Symposium, Calgary, Alberta, October 1976.

Robertson, B.W. "The High-Speed Method of Air Cushion Icebreaking". Proceeding of Canadian Aeronautics and Space Institute 10th Air Cushion Technology Symposium, Calgary, Alberta, October 1976.

Air Cushion Vehicle Division, Canadian Coast Guard. "The Application of Air Cushion Technology to Icebreaking - Canadian Experience". National Research Council of Canada, Associate Committee on Air Cushion Technology, Technical Report 1/77

Hearnshaw, J.D. "The ACV Icebreaking Bow Development Program - an Overview and Status Report". Presented to a joint meeting of CIME and SNAME Toronto, Transport Canada Report TP 818, March 1977.

Snyder, J.C. and Ball, M.A. "Iceater I - The Air Cushion Icebreaker". Paper OTC 3002, presented at the 9th Offshore Technology Conference, Houston, Texas, U.S.A. May 1977.

Ball, M.A. "Air Cushion Icebreaking - What is the Potential?" 11th Canadian Symposium on Air Cushion Technology, Vancouver, September 1977.

Edwards, R.Y., Nadreau, J.P and Dunnem M.A. "Results of Full Scale Field Trials of ACT-100 with CCGS Alexander Henry, Transport Canada, Arctec Canada Report 150C, October 1976.

Dunne, M.A. "Results of Tests Conducted using Ships of Two Different Breadths to push an Air Cushion Transporter in Ice". Transport Canada Research and Development Agency. Arctec Canada Report 207-2, June 1977.

Abdelnour, R., Noble, P. and Hope A. "Model Tests of Air Cushion Icebreakers". Presented at the 13th Canadian Symposium on Air Cushion Technology, Montreal, September 1979.

FIGURE 1

WEGEMT 1983
11/XXXIII

PRINCIPLE OF OPERATION OF
AN AIR CUSHION ICE BREAKING BOW

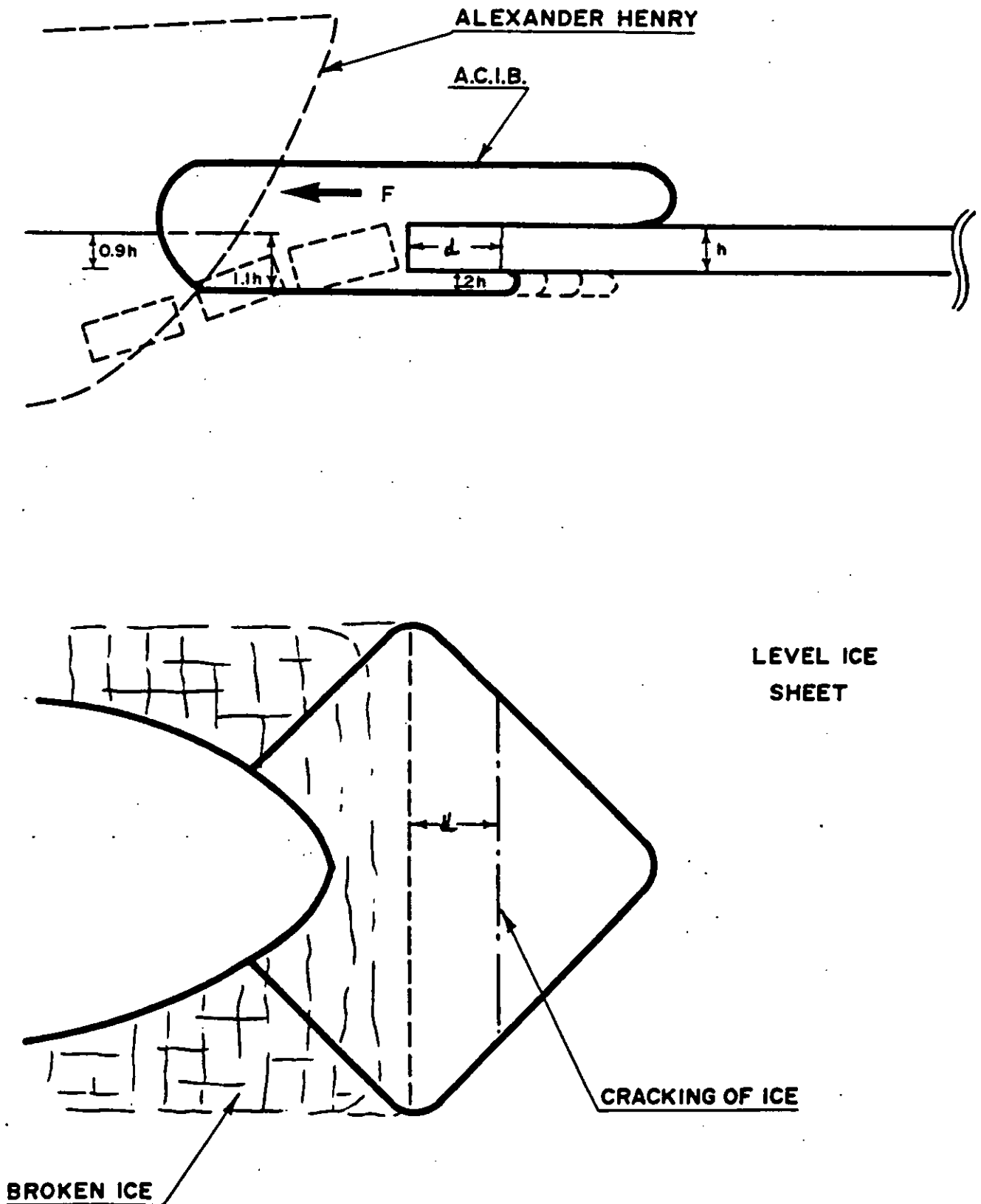
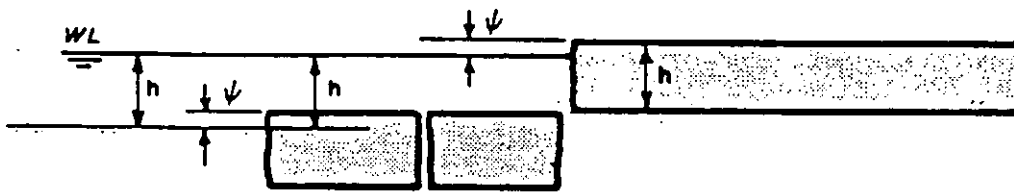


FIGURE 2

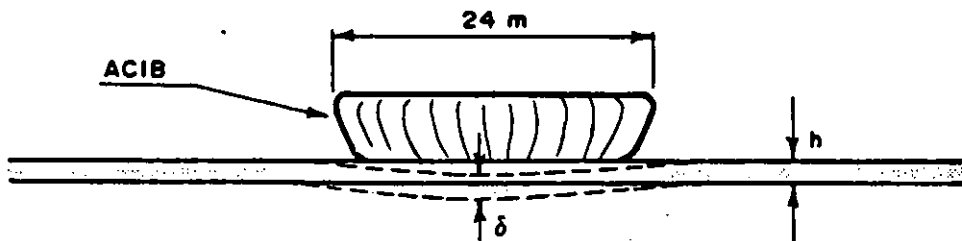
WEGEMT 1983
12/XXXIII

REQUIRED CUSHION PRESSURE

TO OVERCOME THE ICE THICKNESS (h)



TO OVERCOME THE ICE DEFLECTION (δ)



TO PROVIDE A GAP ϵ FOR AIR PROGRESSION UNDER ICE

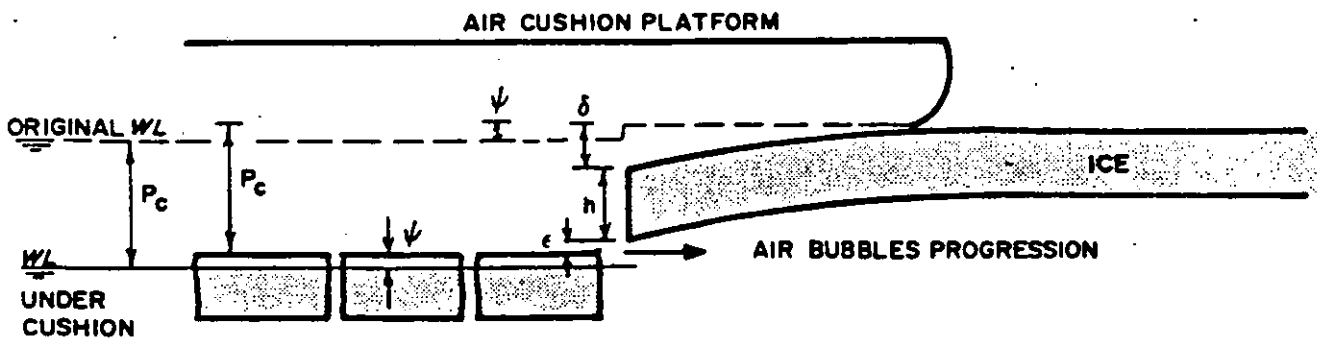
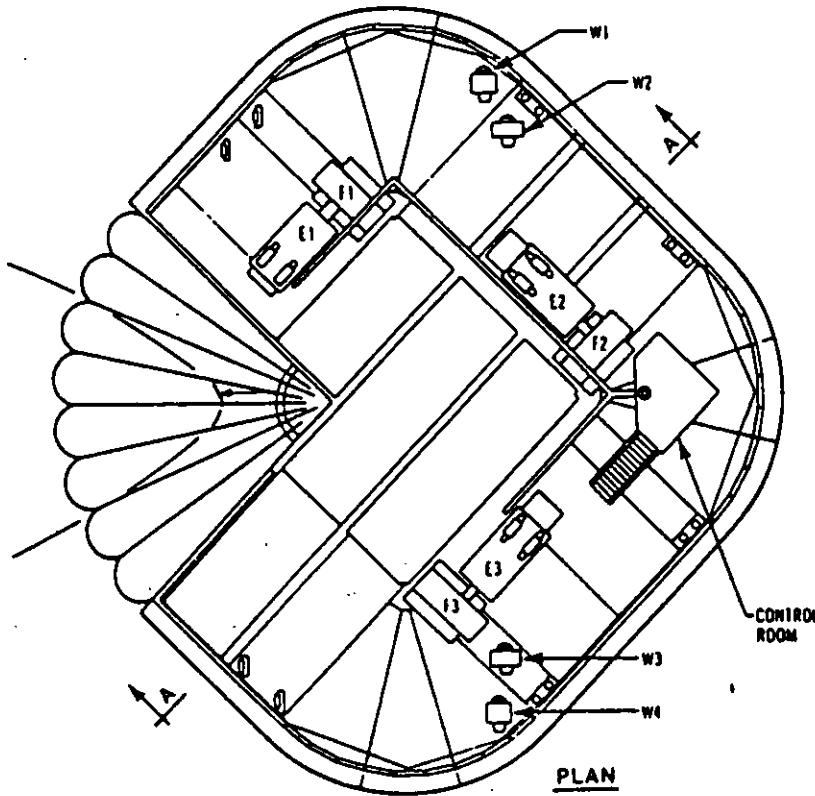


FIGURE 3

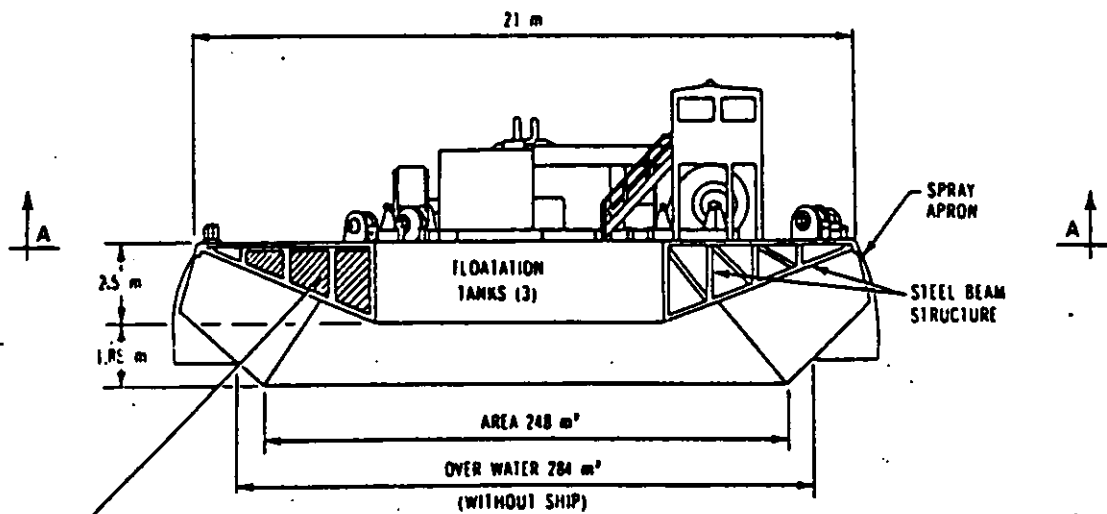
WEGEMT 1983
13/XXXIII



ACIB - HSL 533

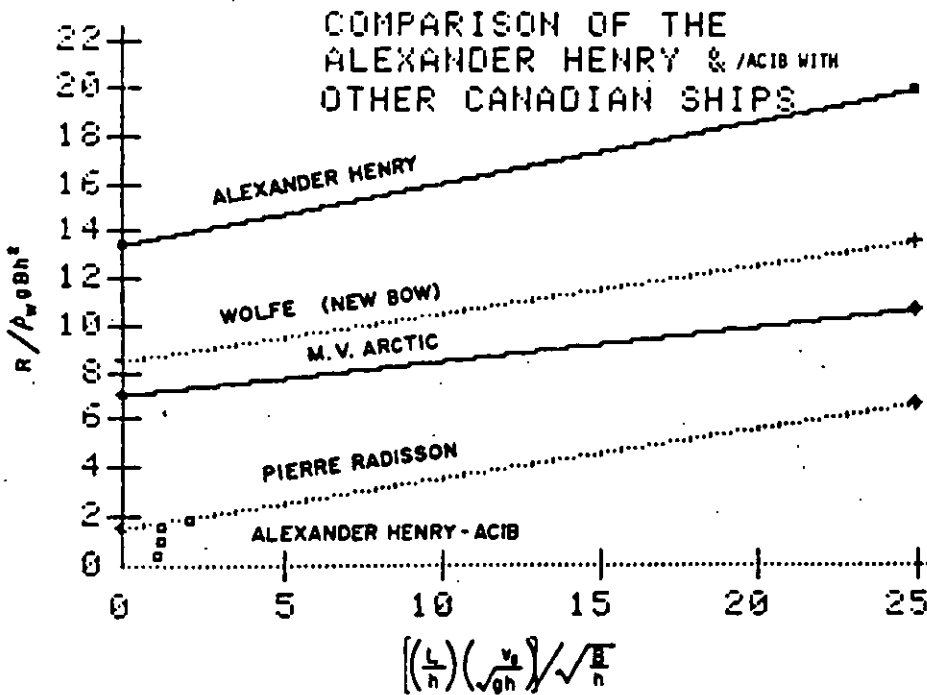
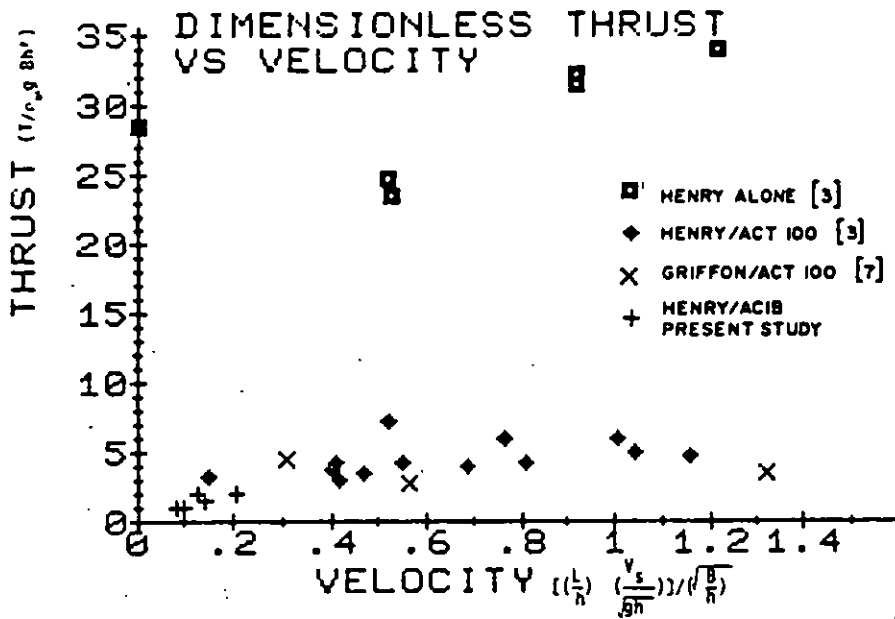
WEIGHT	CUSHION PRESSURE
MAX. 270 t	10 kPa
MIN. 180 t (166.2 md)	6 kPa
CUSHION AREA 284m ² (unnotched)	
OVERALL BEAM 24.7 m	
CUSHION BEAM AT 10 kPa = 22.6 m	
W1, W4 - NOTCHING WINCHES = 160 kW	
W2, W3 - TRANSIT WINCHES = 60 kW	
E: ENGINES (3), EACH 490 kW	
F: FANS (3), EACH 95 m ³ /s AT 10 kPa	

ACIB - HSL 533



FLOATATION TANKS - 166 m³
BUOYANCY BLOCKS - 156 m³

FIGURE 4





Mr Egon Wessels

ICE LOAD ON CYLINDRICAL AND CONICAL OFFSHORE
STRUCTURES

1.0 Introduction

Ice forces are the main concern when designing offshore structures such as drilling platforms, transloading points, bridge piers or light houses for ice infested areas. These forces are limited by the failure strength of the ice, which is a function of several parameters like temperature, salinity, crystal structure and thickness of the ice, width, inclination, shape and roughness of the structure and the velocity of the ice-structure interaction.

The goal of engineers is to find the functional relationship among these parameters for application in design work. So far, it is not possible to solve this problem by pure application of analytical methods because of different gaps in the knowledge about fracture mechanism and failure criterion of the anisotropic material ice.

Several investigators including PEYTON (1966), NEILL (1970, 1972), SCHWARZ (1970), CROASDALE (1974), NEVEL (1976), SAEKI et al (1977) and MAATANEN (1978) have performed large scale ice force measurements of relatively narrow structures - like single legs - directly in the field. The results of these field tests are limited to the specific ice conditions and structural dimensions prevailing for the individual tests. They have been used to develop empirical equations and to check the results of small scale model tests carried out by AFANASEV (1972), HIRAYAMA et al (1974), FREDERKING and GOLD (1975) and MICHEL and TOUSSAINT (1977).

Recently field measurements were performed of ice forces exerted on the rubble pile accumulation in front of wide structures, as e.g. artificial or natural islands, which act as an obstacle to the movement of ice. These very costly field experiments are mostly carried out as joint industry projects, the results of which are proprietary. As an example for a non-

industry field study of ice structure interaction I would like to mention the Adams Island Project being performed over a three years time span starting 1982. First results of this study will be reported during the POAC '83 conference to be held in Helsinki subsequent to the '83-WEGEMT-Course (FREDERKING et al, 1983).

The analytical computation of ice loads as presented in this lecture has to be based on a product which combines the results of field measurements, large scale tests and laboratory model tests with theoretical solutions.

Field measurements provide actual values for the ice load events that could occur annually. Design values, however, have to represent rare events, which are expected to occur irregularly or even not once during the foreseen life of a structure. As design ice loads are not likely to be measured during field tests, the common procedure is, to use laboratory model testing and theoretical methods for extrapolation of the available field data to more extreme conditions anticipated for design purposes.

The objective of this lecture is to present an elementary introduction into procedures for predicting ice forces on offshore structures. The type of structures regarded in this paper are vertical cylindrical columns, monocones as well as cylindrical legs outfitted with conical collars. Wide structures, as e.g. artificial islands, with their typical surrounding rubble pile up feature will only be considered briefly, because another lecture on this specific topic will be presented during the course.

Finally some practical estimations of ice load on exemplary fixed offshore structures will be given.

2.0 Design Ice Conditions

The ice forces exerted onto offshore structures are mainly influenced by the severity of the ice conditions which are considered to be decisive. Especially the thickness of level ice, pressure ridges and rubble accumulations can be regarded as controlling parameter of the ice structure interaction. Hence, a rough overview of extreme design ice conditions as to be expected in arctic regions, e.g. in the southern Beaufort Sea, will be given in the following to provide an idea of the ice conditions which have to be considered for the calculation of ice load as carried out later on during this lecture.

2.1 Level Ice

The annual sheet ice can be assumed to grow to a thickness of 2.1 m in the design case for first year level ice. Multiyear ice, however, is considerably thicker; multiyear floes are known to be quite irregular, but as an effective thickness 4.5 m is a reasonable assumption.

Table 2.1 and Table 2.2 show ice property design values associated with their return period which were determined by BERCHA & STENNING (1979) for the southern Beaufort Sea region at 45 m to 75 m water depth.

The following classification of level ice conditions in the southern Beaufort Sea was given by KOVACS & MELLOR (1974):

" The southern Beaufort Sea can be subdivided into three ice zones: (1) fast ice zone, (2) seasonal pack ice zone, and (3) polar pack ice zone.

The fast ice zone typically extends outward to the 20-m depth contour by winter's end. The undeformed ice normally reaches a thickness of 2.0 to 2.1 m, but on occasion it reaches 2.4 m in thickness.

The seasonal pack ice zone continues out 100 to 200 km to the toe of the continental shelf. The undeformed seasonal ice in this zone also reaches an average thickness of 2.0 to 2.1 m and has a salinity of 3 ‰ to 14 ‰.

The polar pack ice zone consists predominantly of thick multi-year floes which are surrounded in summer by open water or thin ice and in winter by first-year ice. The low-lying terrain of old multi-year floes varies in thickness from 2.1 to 4.5 m, and the ice has a salinity of 0 ‰ to 6 ‰.

Note that the polar pack ice is never far away from the first two zones and can be driven in toward the coast at any time by a strong onshore storm wind. Therefore, such terms as "average ice conditions" have no real significance, because these conditions are so variable and the data are rather sparse".

2.2. Pressure Ridges

Pressure ridges are of main concern for the determination of extreme ice loads on structures, because they are generally of much higher thickness than the surrounding level ice and partly of comparable strength.

One has to distinguish between first year ridges, which are composed of largely unconsolidated fragmented level ice pieces, and multi-year ridges which are solidly frozen together. The cross-section of an extremely thick first year ridge is shown in Fig. 2.1. Fig. 2.2. shows a similar cross-section of a multiyear ridge. Several authors have reported on the determination of the ridge sail height to keel depth ratio. An average value of about 1:4 can be stated (see e.g. HUDSON, 1980).

The known ratio of sail height to keel depth gives the opportunity to calculate total ridge thicknesses based on sail height measurements obtained e.g. by means of aerial photographic flights. Table 2.3 and Fig. 2.3 show the frequency distribution of measured ridge sail heights at different ice conditions and Fig. 2.4 the frequency of submarine measurements of ridge keel depths.

2.3 Rubble Piles

A region of heavily deformed, first-year ice may be referred to as a rubblepile, indicating a grounded feature, whereas rubble fields contain one or more rubble piles (API, 1982). The areal and thickness distributions and consolidation properties of rubble fields have to be considered as a potential design parameter. The available data, however, for determination of extreme design rubble pile conditions is only sparse at present.

Some recommendations for extreme grounded rubble pile features to be considered for design work are shown in the guidelines of the American Petroleum Institute (see Table 2.4). Table 2.4 also includes assumptions of extreme values for different ice features, like sheet ice, rafted ice, first and multiyear ridges.

3.0 Ice Forces on Vertical Structures

As the ice cover moves horizontally, forces are exerted on isolated vertical structures such as drilling platforms, lighthouses, bridge piers or artificial islands. Factors contributing to the horizontal ice cover motions are thermal deformations, the formation of cracks and deformations due to external forces acting on the ice cover. If the total movement of the ice cover is much larger than the deformation of the structure, which is the case for fixed rigid structures regarded here, the exerted force corresponds to compression failure of the ice cover at the maximum rate of ice movement. The key parameter for this type of ice structure interaction is the crushing or compressive strength σ_c of the ice.

3.1 Strain Rate Dependency

The uniaxial compressive strength of ice depends on strain rate, loading direction of structure and temperature of ice. Fig. 3.1 shows the well-known universal curve of MICHEL & TOUSSAINT (1977), where the compressive strength of ice determined during uniaxial crushing tests as well as during indentation tests of different investigators is plotted versus strain rate. The failure mode is divided into three parts: a ductile region at strain rates lower than $5 \cdot 10^{-4} \text{ sec}^{-1}$, where crushing strength depends on the strain rate at a power of 0.32, a brittle region with a strain rate greater than 10^{-2} sec^{-1} , where crushing strength is constant, and a transition zone between the ductile and brittle regions.

WU, CHANG & SCHWARZ (1976) performed laboratory uniaxial compression tests and achieved strength-strain rate dependencies as shown in Fig. 3.2. With decreasing ice temperature the transition from ductile to brittle mode occurs more abruptly and at lower strain rates. The transition to brittle was explained by means of a dislocation theory, according to which at high strain rates dislocation velocity is too low to allow ductile behaviour by plastic yielding and therefore cleavage fracture and linking of grain boundary cracks occur. This also explains well the more random crushing behaviour in the brittle region.

In order to convert indenter velocity respectively ice velocity to strain rate, the velocity must be divided by a length. This length is related to the size of the zone of ductile deformation in front of the indenter. HIRAYAMA et al (1974) use the concept of fracturing frequency, i.e. interaction velocity divided by crushing length per cycle or velocity divided by plastic zone width before indenter. The formula originally suggested by KORZHAVIN (1962)

$$\dot{\epsilon} = \frac{v}{2b} \quad (3.1)$$

may be used, where v is the indentation velocity and b is the width of the structure.

3.2 Crushing Failure

KORZHAVIN's (1962) well known formula may serve as a useful starting point for a discussion of the ice pressure exerted by crushing failure load. The effective ice pressure p_e is defined by the failure load F divided by the product of the width of structure b and the ice thickness h

$$p_e = \frac{F}{b \cdot h} \quad (3.2)$$

Korzhavin's formula for a vertical cylinder is

$$p_e = I \cdot m \cdot k \cdot \kappa \cdot \sigma_c \quad (3.3)$$

where I is indentation coefficient, m is a shape coefficient, k is a constant coefficient, κ is a strain rate function, σ_c is the uniaxial failure strength in crushing for the actual strain rate.

The indentation coefficient I is seen as a pure geometrical factor and a function of the width ratio B/b where B is the width of the ice sheet. Indentation tests with samples of warm natural river ice gave the result

$$I = \left(\frac{B}{b} \right)^{1/3} \quad \frac{B}{b} < 15 \quad (3.4)$$

$$I = 2.5 \quad \frac{B}{b} > 15$$

The results does not account for the dependence of I on the aspect ratio b/h, which has been the subject of many later investigations.

The shape coefficient m has the following values:

Indenter shape	m
flat	1.0
semicircular	0.90
wedge-shaped, $60^\circ < 2\alpha < 120^\circ$	$0.85 \sqrt{\sin \alpha}$

For wedge angle less than 60° no further reduction in m was observed. The contact coefficient k is given as a function of ice velocity and indenter width

Indenter width b (m)	Ice velocity (m/s)		
	0.5	1	2
3 - 6	0.7	0.6	0.5
6 - 10	0.6	0.5	0.4

The low value of k is a consequence of the high strain rates used in the tests.

The strain rate coefficient κ was found to be

$$\kappa = \left(\frac{\dot{\epsilon}_0}{\dot{\epsilon}} \right)^{1/3} = \left(\frac{V_0}{V} \right)^{1/3} \quad (3.5)$$

where $\dot{\epsilon}_0$ is the strain rate at the reference ice velocity $v_0 = 1.0$ m/s. The range of strain rates in the tests was from 10^{-3} to 10^{-20} s $^{-1}$, and for this range equation (3.5) agrees with later investigations.

AFANASEV's (1972) formula is based on model tests with saline ice

$$\frac{p_e}{\sigma_c} = m C \quad (3.6)$$

The shape coefficient m is given for flat and semicircular indentors and have the same values as in Korzhavin's formula, $m = 1.0$ and 0.9 , respectively. The coefficient C is given by

$$C = \left(5 \frac{h}{b} + 1\right)^{1/2} \quad \frac{b}{h} > 1 \quad (3.7)$$

$$C = 4 \quad \frac{b}{h} = 0.1$$

For $0.1 < b/h < 1$ a linear interpolation is recommended.

Korzhavin's and Afanasev's investigations have defined one indentation coefficient each: Korzhavin's I is a function of B/b while Afanasev's is a function of b/h . Nondimensional geometrical variables are frequently called aspect ratios. The aspect ratios B/b and b/h should not be confused, as the indentation pressure p_e increases with B/b and decreases with b/h . Each of these two parameters is a measure of confinement, which raises p_e above its unconfined values obtained in a uniaxial compression test.

The failure of ice in uniaxial compression tests does not correspond to the failure in nature where the ice is more or less laterally confined by the surrounding ice sheet. FREDERKING (1977) found that for columnar grained ice samples, the strength was 2 to 5 times stronger when lateral deformation was prevented than in normal uniaxial tests as shown in Figure 3.3 and Figure 3.4. The plain strain condition as referred to in these two figures is explained by sketches in Figure 3.5 compared with the plain stress condition. The criteria for these conditions are described by the equations

$$\text{plane strain: } \dot{\epsilon}_z = \dot{\epsilon}_{xz} = \dot{\epsilon}_{yz} = 0 \quad (3.8)$$

$$\text{plane stress: } \sigma_z = \tau_{xz} = \tau_{yz} = 0 \quad (3.9)$$

RALSTON (1978) predicted ice pressures at low aspect ratios $b/h < 1$ which are close to the experimental results of Michel and Toussaint (see Figure 3.6). While this may be a region of little practical interest, a more complete analysis reveals that the assumption of plane strain (Equ. 3.8) is very restrictive. In fact, it would only be valid for $b/h < 0.25$. For higher values the normalized ice pressure drops off as shown in Figure 3.6.

A more complete analysis was undertaken by REINICKE & REMER (1978) for the polycrystalline ice described in Figure 3.7. In addition to the Hill-failure mechanism shown in Fig. 3.8 which provides plane strain and plane stress upper bounds, they used a three dimensional mechanism to determine intermediate values. Their results are represented by the curve shown in Figure 3.9.

The dependency of the effective ice pressure on the aspect ratio, i.e. ice pressure decreases with increasing values of b/h , as predicted by laboratory tests and analytical approaches (see Fig. 3.6 and 3.9) is confirmed by different independent field measurements of ice indentation pressure on piles. Some of these full scale data are presented in Figure 3.10.

3.3 Cleavage Failure

Thorough investigations of the failure initiation of a horizontal level ice sheet acting against narrow vertical indentors showed that cleavage failure precedes one of the three crack patterns which are commonly stated as crushing, shear or buckling. The initial failure of the ice occurs by horizontal cleavage of the ice cover in front of the indenter due to tensile strain in the vertical direction.

The description of cleavage failure is difficult in respect to the dependence of the effective ice pressure p_e on the aspect ratio b/h as stated in chapter 3.2. The empirical formulas proposed so far can be written

$$p_e/\sigma_c = C \cdot b^a \cdot h^b \quad (3.10)$$

where C obviously must have the dimension $\lambda^{-(a+b)}$. The numerical values of C , a and b given by various authors are:

		C	a	b
Hamanaka ()	flat	6.8		
	circular	5.0	-0.32	0
	wedge	4.5		
Hirayama et al (1974)	circular	3.57	-0.5	0.1
	flat	6.8		
Saeki et al (1977)	circular	5.0	-0.5	0
	wedge	4.5		

Figure 3.11 shows the comparison of ice force prediction according to SAEKI et al (1977) and HIRAYAMA et al (1974) with field measurements of SCHWARZ (1970) and NEILL (1970).

The lack of knowledge of the governing physical lengths incorporated in the coefficient C makes the extrapolation of formulas of type (3.10) difficult. It is only within their tested range that these empirical equations can be fully trusted. It should be noted, however, that the field measurements of SCHWARZ (1970) are in good agreement with the empirical formula established by HIRAYAMA et al (1974) based on model test results (see Fig. 3.12).

The statement of low or negligible influence of ice thickness on the effective ice pressure compared to the strong influence of indenter width as proposed by the empirical formulae of this chapter is emphasized by the results of FREDERKING & GOLD (1975). Their experiments showed that p_e/σ_c is a function of b , but independent of h (see Fig. 3.13).

3.4 Buckling Failure

Buckling failure is the formation of one or more cracks at some distance from the structure by a combination of bending and compression.

The buckling mechanism is not sufficiently similar to crushing to permit a direct comparison. However, buckling in itself is well known, so that an independent computation of buckling pressure can be made. A comparison will then reveal which of the failure mechanisms will produce the lowest ice pressure and consequently govern the case. In general it is found that buckling is likely for thin ice sheets only, i.e. at high aspect ratios.

The classical theoretical work by HETENYI (1946) considered the uniformly loaded plate edge of the ice sheet which was treated as an elastic plate resting on an elastic foundation.

Indentation and other nonuniform load situations require numerical solutions. SODHI and HAMZA (1977) used a finite element method, while WANG (1978) used both finite differences and finite elements.

Hetenyi showed that for the two-dimensional case the buckling pressure is

$$\sigma_0 = \frac{\sqrt{kD}}{h} \quad (3.11)$$

where $k = \rho_w g$ is the foundation modulus = 1000 kg/m^3 ,

$$D = \frac{Eh^3}{12(1-\nu^2)} \quad (3.12)$$

is the flexural rigidity of the plate, E is Young's modulus, ν is Poisson's ratio, and h is ice thickness. The three-dimensional case gives an indentation pressure σ defined by

$$\sigma = \frac{F}{2Rh} = \frac{4q}{(2R/L)^2} \quad (3.13)$$

where

$$q = \frac{\sigma h R^2}{D} \quad (3.14)$$

is the traditionally used nondimensional buckling pressure. WANG (1978) introduced another nondimensional version

$$\frac{\sigma}{\sigma_0} = \frac{4q}{(2R/L)^2} \quad (3.15)$$

where

$$L = \left(\frac{D}{k}\right)^{1/4} = \left(\frac{Eh^3}{12k(1-\nu^2)}\right)^{1/4} \quad (3.16)$$

is the characteristic length of the ice sheet. It is related but not equal to the critical wave length of the ice sheet in buckling. The buckling condition can now be presented in a diagram of $2R/L$ versus σ/σ_0 .

The indenter pressure found by SODHI and HAMZA (1977) for a flat indenter is compared with Wang's result for a circular indenter in Figure 3.14. Both are solutions for a frictionless boundary, and the agreement is seen to be good except for small values of $2R/L$. According to Wang the case with a fixed boundary condition, i.e. with the ice sheet frozen to the indenter, gives much higher pressures (Fig. 3.15).

3.5 Ice Load by Failure of Pressure Ridges

Pressure ridges in drifting ice fields represent, in many cases, the most severe loading condition for the design of offshore structures. However, the knowledge of strength and failure characteristics of different types of ridges is very limited. The design load is usually given in the form of $F_r = AxP$, where P is the force corresponding to crushing of a uniform ice sheet and A the amplification factor for consideration of pressure ridge failure. Referring to ERANTI & LEE (1981), the value of the coefficient A for first year ridges ranges typically from 1.5 to 3.0 depending on local experience, ridge sizes and degree of ridge consolidation. Figure 3.16 shows a design ridge and appropriate pressure diagram used by Finnish Board of Navigation.

DOLGOPOLOV et al (1975) estimated the maximum force on a cylindrical structure penetrating through a first year pressure ridge by

$$F_r = F_{cr} + F_p \quad (3.17)$$

where F_{cr} corresponds to the force needed to crush the frozen upper part of the ridge. This force can be approximated by using Equation 3.3. One has to keep in mind that the thickness of the solid ice layer of the ridge usually is larger than of the surrounding ice sheet.

The force F_p is exerted by shearing of the loose underwater portion of the ice ridge. This force is estimated by the equation

$$F_p = \mu H_e D (0.5 H_e \mu \gamma_b + 2c) \left(1 + \frac{2H}{3D}\right) \quad (3.18)$$

where $\mu = \tan (45^\circ + \phi/2)$

ϕ = angle of internal friction in the mass of ice blocks

H_e = design thickness of the underwater portion of the ridge $H < H_e < H + D/2$

H = thickness of the underwater portion of the ridge

D = design structure width within the boundaries of the underwater portion of the ridge

γ_b = ice bouyancy

c = cohesion between ice blocks

The design thickness of the underwater portion of the ridge H_e is larger than the initial thickness value H because the ridge thickens during interaction with the structure.

3.6 Codes for Ice Load Determination

A review of the existing codes for the determination of ice loads on vertical structures is given in the following.

American Petroleum Institute (API). Recommended Practice

$$F_h = C b h \sigma_c \quad (3.19)$$

C depends on the shape of the structure and the relative velocity between structure and ice floe, i.e. C is a combined shape and strain rate coefficient. The range of C is

$$0.3 < C < 0.7.$$

The value of σ_c varies with temperature, salinity and other factor in the range

$$1.38 \text{ MPa} < \sigma_c < 3.45 \text{ MPa.}$$

Canadian Standard Association (CSA). Old Highway Code and American Association of State Highway Officials (AASHO):

$$F_h = p_e b h \quad (3.20)$$

This very simple formula allows only one value of the effective ice pressure

$$p_e = 2.76 \text{ MPa}$$

No limits of application are given.

1974 CSA Bridge Code

$$F_h = p_e b h$$

The change from the CSA Old Highway Code is that the ice strength is varied between

$$0.69 \text{ MPa} < p_e < 2.76 \text{ MPa}$$

The previous single value of p_e now is the upper bound

Canadian Light House Practice

$$F_h = m b h \sigma_c \quad (3.21)$$

m is a combined shape and contact coefficient with a range

$$0.4 < m < 0.9$$

The crushing strength σ_c should be chosen in the rather narrow range

$$1.38 \text{ MPa} < \sigma_c < 1.72 \text{ MPa}$$

USSR - SN - T6/66 Code

$$F_h = m A b h \sigma_c \quad (3.22)$$

The shape coefficient m has the following values

wedge 45°	0.54
flat 180°	1.0
semicircular	0.9

A is a regional climatic coefficient with range

$0.75 < A < 2.25$	spring breakup
$2 < A$	winter breakup

The USSR is divided into 5 regions with A increasing from southwest towards northeast. The crushing strength σ_c has two values

Winter (maximum water level)	0.75 MPa
Spring (breakup)	0.45 MPa

The low strength values must be seen in context with the regional climate coefficient A. If A did not appear in the formula, the range of ice strength necessary to give the same results would be

$$0.56 \text{ MPa} < \sigma_c < 1.69 \text{ Mpa}$$

Even so the ice strength is rather low compared with other formulae.

4.0 Ice Forces on Inclined Structures

It is well known that ice forces on structures can be reduced by providing a sloping plane instead of a vertical face. As the angle between structure and ice cover decreases the failure of the ice cover changes from compression to shear and bending and since the compressive strength of ice is much higher than the flexural strength and the shear strength, the ice forces decreases with declining angle from the vertical.

4.1 Bending Failure Mechanism

As the advancing ice sheet first encounters the sloping structure, local crushing occurs on the underside of the ice sheet. The local crushing causes an interaction force normal to the structure surface. In addition, because the ice is moving relative to the surface, a frictional force is also generated. The normal and tangential force can be divided into vertical and horizontal components V and H acting at the centre of the crushed area. In the simple two-dimensional model shown in Figure 4.1 the forces acting on the ice will be V , H , gravity and buoyancy forces; the latter can be considered as an elastic foundation. As the ice sheet continues to advance the crushed area will increase causing V and H to increase. Assuming an unlimited driving force, V and H will continue to increase until the ice fails in bending, if the sloping structure is properly designed.

Except for very steep structures the effect of H on the bending failure of the ice can be ignored. The ice sheet then behaves like a plate on an elastic foundation. The load V to fail the ice sheet governs the initial lateral load on the structure. Subsequent loads are generally higher because of the additional load required to push the ice pieces up the slope.

4.2 Inclined Planes

Considering the initial interaction between ice and the inclined plane the relationship between V , H , N and μ can be derived by resolving forces, that is;

$$H = N \sin \alpha + \mu N \cos \alpha \quad (4.1)$$

$$V = N \cos \alpha + \mu N \sin \alpha \quad (4.2)$$

therefore,

$$H = V \left(\frac{\sin \alpha + \mu \cos \alpha}{\cos \alpha - \mu \sin \alpha} \right) \quad (4.3)$$

The maximum value of V will be limited by the strength of the ice sheet with an edge loading. It is assumed that the ice sheet can be represented by a beam on an elastic foundation, the strength of which is limited by its bending moment capacity M_0 . Most beam strength tests on ice measure bending moment capacity but with the results converted to a flexural strength (σ_f) using simple bending theory, that is,

$$\sigma_f = \frac{6M_0}{bh^2} \quad (4.4)$$

where b is the width of the beam and h is the ice thickness. For a semi-infinite beam on an elastic foundation it can be shown (HETENYI, 1946) that the maximum bending moment M_0 due to an edge load V is given by

$$M_0 = \frac{V}{\beta e^{\pi/4}} \sin \left(\frac{\pi}{4} \right) \quad (4.5)$$

where $1/\beta$ is a characteristic length defined by

$$\beta = \left(\frac{K}{4EI} \right)^{1/4} \quad (4.6)$$

where K is the foundation constant equal to $\rho_w g b$ for a floating beam, ρ_w is the density of water, g is the gravitational constant, E is the elastic modulus, and I is the second moment of area of the cross section ($b \cdot h^3/12$).

For subsequent interactions after breaking the ice a force system is considered as shown in Figure 4.2. P is the force required to push the ice up the slope.

From these assumptions the following equation can be derived for the horizontal force on the structure per unit width

$$\frac{H}{b} = \sigma_f \left(\frac{\rho_w g h^5}{E} \right)^{1/4} C_1 + Z \rho_i g C_2 \quad (4.7)$$

where Z is the height reached by the ice on the slope and ρ_i is the density of the ice. The coefficients C_1 and C_2 are functions only of α and μ . Values for C_1 and C_2 are plotted in Figures 4.3 and 4.4 for typical values of α and μ .

In equation (4.7) the first term can be considered to be the force necessary to break the ice, and the second term can be considered to be the force necessary to push the ice pieces up the sloping structure. As a two-dimensional theory these assumptions might be considered accurate for a very wide structure, but as will be discussed later it is probably inaccurate for narrow structures. For structures which are narrow relative to the characteristic length, the zone of ice failure will be wider than the structure itself, also most of the ice pieces will not necessarily ride up the structure but go around it. Nevertheless it is useful to discuss the importance of some of the key parameters on the context of the simple 2-D theory.

4.3 Effect of Friction and Slope Angle

For a typical example of a structure with a freeboard of 5 m - i.e. $Z = 5$ m - subject to forces imposed by ice 1 m thick with a flexural strength of 700 kPa, the effect of friction and slope angle is shown in Figure 4.5. It can be seen that the effect of friction and slope angle becomes significant above an angle of 45° . For a structure with an angle of 55° the horizontal ice force increases from 125 kNm^{-1} $\mu = 0.1$, to 450 kNm^{-1} for $\mu = 0.5$. For steep angles and high friction the ice may fail in crushing rather than bending. Figure 4.5 emphasizes the need to maintain smooth surfaces on sloping structures so that ice forces are minimized. Even for very shallow angled structures high friction can increase the ice loads significantly.

4.4 Effect of Ice Thickness

Ice thickness is probably the most significant parameter affecting ice forces on sloping structures. In the simple 2-D analysis, the ice breaking component is proportional to $h^{1.25}$ and the ride-up force is directly proportional to h . The affect of thickness for a typical example is shown in Figure 4.6. It is interesting to note from Figure 4.7 that the ice ride-up force is larger than the ice breaking force. However, this observation can only be considered relevant to 2-D theory as might be applicable to a very wide structure. For a narrow structure, the ice breaking component will be larger and the ice ride-up component smaller.

4.5 Conical Structures

The different failure mode between ice acting on inclined planes respectively on conical structures is conceptually shown in Figure 4.7. Intuitively it will be appreciated that 3-D effects cause divergence from the simple theory more for narrow structures than for wide structures.

For the ice breaking component, the simple beam theory is replaced by a more complex plate theory for which elastic analyses have been made using theories developed for plates on elastic supports. NEVEL (1972) has proposed equations for the ultimate failure of ice plates which can be applied to this problem.

It is generally assumed that the essence of the ice force problem on a conical structure reduces to the prediction of the forces necessary to fail a series of ice wedge formed by radial cracking of the ice as it advances against the cone (see Fig. 4.7). Nevel's (1972) equation for the force to fail these wedges is given as;

$$\frac{6P}{b_0 \sigma h^2} = 1.05 + 2.00 \left(\frac{a}{l}\right) + 0.50 \left(\frac{a}{l}\right)^2 \quad (4.8)$$

where P is the failure force on the tip of the wedge, σ is the ice

flexural strength, h is the ice thickness, a is the distance from the tip of the wedge over which it is loaded, b_0 is a constant defining the width of the wedge b in the equation

$$b = b_0 \chi \quad (4.9)$$

where χ is the distance along the wedge, b_0 is a constant and ℓ is the characteristic length for the plate given by

$$\ell = \left(\frac{Eh^3}{12\rho_w g} \right)^{0.25} \quad (4.10)$$

BERCHA and DANYS (1975) have made use of the above theory to present an elastic analysis of the ice breaking component of the ice force on a conical structure. Their results are repeated here in Figures 4.8 and 4.9 for structures with waterline diameters up to 18.3 m (60 ft) subject to ice of 0.91 m (3 ft) thickness.

An approach for ice forces on a conical structure using plastic limit analysis has been proposed by RALSTON (1977). His results can be expressed in the form

$$H = A_4 \left[A_1 \sigma h^2 + A_2 \rho_w g h D^2 + A_3 \rho_w g h (D^2 - D_T^2) \right] \quad (4.11)$$

$$V = B_1 H + B_2 \rho_w g h (D^2 - D_T^2) \quad (4.12)$$

where D_T is the top diameter and D is the waterline diameter. A_1 and A_2 are coefficients dependent on $\rho_w g D^2 / \sigma h$, and A_3 , A_4 , B_1 and B_2 are coefficients dependent on the cone angle α and friction μ . Values for these coefficients are reproduced in Figure 4.10.

It should be noted that Ralston's analysis includes both the forces due to ice ride-up and ice breaking. In equation (4.11) the first two terms are due to ice breaking and the third term results from the ice pieces sliding over the surface of the cone. It is of interest to note that for narrow structures, Ralston's theory predicts the ride-up component to be small compared with ice breaking, see Figure 4.11.

For wide structures the ice ride-up component becomes a larger part of the total force, see Figure 4.12.

EDWARDS and CROASDALE (1976) used the theory of an infinite beam on elastic foundation to estimate the forces that a multi-year ridge exerts on a conical structure. At first stage of interaction a crack forms at the contact point with the structure. The vertical load necessary to cause the formation of this crack is given by

$$V_1 = \frac{4I\sigma_f}{yL} \quad (4.13)$$

$$L = \left(\frac{4EI}{kb}\right)^{0.25} \quad (4.14)$$

where I = moment of inertia of the ridge cross section

σ_f = the flexural strength of the ridge ice

y = distance from neutral axis to surface in tension (top surface)

L = characteristic length of the ridge

k = foundation constant, 9.81 kN/m^3

b = ridge width

The ice force can still increase after the formation of the initial crack until hinge cracks form. Considering a simultaneous failure of two semi-infinite beams we get

$$V_2 = \frac{6.17 I \sigma_f}{y L} \quad (4.15)$$

In this case, y is the distance from neutral axis to the bottom of ridge.

The horizontal forces depend on the cone angle α and friction coefficient between ice and the structure μ . They are given by

$$H = V \frac{\sin \alpha + \mu \cos \alpha}{\cos \alpha - \mu \sin \alpha} \quad (4.16)$$

A comparison of sheet ice failure on upward breaking and downward breaking cones has been undertaken by RALSTON (1979) using plastic limit analysis.

The calculated horizontal forces on an example cone versus cone angle are plotted for both cases in Figures 4.13 and 4.14 under application of two different yield criteria (Johansen and Tresca). The comparison of the upward- and downward breaking force curves show an obvious advantage for the downward breaking geometry. The calculated force for the inverted cone is about 1/2 of the force computed for the upward-breaking cone at all cone angles. However, some of the downward-breaking advantages may be lost if ice ridges and rubble accumulation between the conical surface and the sea floor occur in shallow water conditions. Adfreeze and friction effects, on the other hand, may be easier to deal with on a downward-breaking cone. The warmer temperatures on the submerged conical surface may increase the effectiveness of coatings and heating techniques applied to reduce the effect of friction and adfreeze.

Additional factors, however, such as the contribution of the vertical force to the overturning moment should also be considered when downward-breaking cones are of interest, because the vertical force component on a downward-breaking cone tends to lift the cone and adds to the overturning moment applied to the cone.

4.6 Experimental Data

At present only few data are available for laboratory experiments carried out to investigate the interaction between ice and conical structures.

In 1978 a series of model tests were carried out on downward breaking conical structures in the Hamburg Ice Model Basin (HSVA) using low salinity model ice and a warming technique to control the E/σ ratio (SCHWARZ et al, 1978). A scale factor of 20:1 was selected for the tests. Fixed cones of angles 15° , 30° , 45° and 60° were tested in 50 mm thick ice of 60 kPa flexural strength at velocities ranging from 0.01 to 0.05 m/s. A schematic of the test arrangement is shown

in Figure 4.15. The effect of the thickness and flexural strength variations were also investigated for the 45° structure. Vertical forces were observed to first increase rapidly and then decrease with increasing velocity, whereas the horizontal forces increased with increasing velocity. Cone angles of 15° and 30° showed the lowest horizontal force (see Figure 4.16). Ice thickness variation was observed to have a stronger influence on the vertical forces than on the horizontal force. Two test series were run with the 45° conical structure arranged so that it oscillated in the 1-2 Hz range. Horizontal force reduction of one third and two thirds of the corresponding fixed cone force were observed for the vertical and combined vertical and horizontal motion cases, respectively.

These results demonstrate that a potential exists for the design of offshore structures which, by either passive or active devices, would be subjected to substantially reduced ice forces.

In 1970, tests were conducted in the Arctec model basin on 45° angle cones up to 100 cm in diameter with ice up to 7 cm thick. Results from these tests have been reported by EDWARDS and CROASDALE (1976).

An empirical relationship derived by Edwards and Croasdale from their tests is given as

$$H = 1.6 \sigma h^2 + 6.0 \rho g D h^2 \quad (4.17)$$

(for a 45° angle cone with an ice to cone friction coefficient of 0.05). The investigators proposed that the first term represents the ice breaking portion of the ice force and the second term represents the ice clearing component.

In 1971, tests were conducted with cones up to 28 cm in diameter with ice up to 3.5 cm thick by AFANASEV et al (1971). From observations of their tests they proposed the following formula based on elastic plate theory

$$H = \frac{\sigma h^2 S_x \tan \alpha}{1.93 \rho} \quad (4.18)$$

where S_x is the length of the circumferential crack given as

$$S_x = 1.76 \left(r + \frac{\pi}{4} \ell \right) \quad (4.19)$$

r is the cone radius at ice level, and ℓ is the characteristic length given by

$$\ell = \left(\frac{Eh^3}{12 \rho g (1-\nu^2)} \right)^{0.25} \quad (4.20)$$

E is Young's modulus and ν is Poisson's ratio.

Measurements of ice forces on an inclined pier have been published by NEILL (1976). The pier was inclined at 23° to the vertical and forces up to 788 kNm^{-1} were measured for ice 0.75 m thick.

Experiments have been conducted in a large outdoor test basin in Calgary on a 45° angle cone with a 3.1 m (10 ft) waterline diameter with ice up to 0.6 m (2 ft) thick. Results from these experiments have not yet been published.

A very comprehensive model test program was carried out at Hamburg Ice Model Basin (HSVA) in 1980 to investigate the influence of several parameters of structural and ice conditions on the ice forces exerted on upward- and downward-breaking fixed as well as on downward-breaking floating cones (WESSELS, unpublished). The work was undertaken within the international joint venture COSMAR (Concrete Structures for Marine Production, Storage and Transportation of Hydrocarbons). The test results will be published 1984 at the IAHR-Symposium on Ice in Hamburg.

TRYDE (1977) has investigated ice acting on a narrow wedge-shaped pier by conducting model tests. He proposed the following empirical method for predicting ice forces on a narrow sloping wedge:

$$H = C_F \sigma_c hb \quad (4.21)$$

where σ_c is the ice compressive strength and C_F is a "reduction coefficient" expressed as,

$$C_F = \frac{5.2 \epsilon^{1/3}}{C^{1/2}} \quad (4.22)$$

where

$$C = 0.16 \left[\frac{E}{\rho V_c^2 \sin \beta} \right]^{1/2} \frac{C_1}{C_2} C_3^2 \quad (4.23)$$

where $\epsilon = \sigma/\sigma_c$, σ is the bending strength, σ_c is the compression strength of the ice, E is the Young's modulus, ρ is the ice density and V_c the velocity of the floe. The coefficients C_1 , C_2 and C_3 are given as

$$C_1 = 1 - \mu \frac{\tan \alpha}{\sin \beta} \quad (4.24)$$

$$C_2 = \mu + \frac{\tan \alpha}{\sin \beta} \quad (4.25)$$

$$C_3 = 6 \left(\frac{h}{b} \cos \beta + \frac{C_1}{C_2} \right) \quad (4.26)$$

where 2β is the included angle at the point of the wedge in the horizontal plane, α is the inclination of the slope of the wedge to the horizontal and μ the coefficient of friction. Tryde suggests that the value of C_F is most likely to be in the range 0.1 to 0.3, implying that ice failure in bending imposes forces which are 10 to 30% of the ice crushing forces. As far as can be determined Tryde's formula does not account for ice ride-up and is quite sensitive to modulus of elasticity. The formula is not strictly applicable to conical structures.

5.0 Ice Forces on Multilegged Structures

So far in this lecture only offshore structures supported by single leg substructures have been considered. From the construction point of view, however, the design of a multilegged platform introduces some substantial advantages in terms of stability of the platforms support.

The knowledge about ice load on multilegged structures is very sparse because of the complicated failure mechanism of the different legs interfering with each other. This problem seems to be better addressed by performance of model tests than by application of theoretical analysis, as for the analytical approach the assessment of ice failure interference is very difficult.

A model test program was carried out at Hamburg Ice Model Basin (HSVA) in 1982 to investigate the ice load on three and four legged offshore platforms (WESSELS & EVERS, unpublished). This test series was performed on behalf of the German joint venture COSMAR (Concrete Structures for Marine Production, Storage and Transportation of Hydrocarbons - Phase II). The results are confidential three years after completion of the project.

5.1 Failure Mechanism

Figure 5.1 schematically shows different conceivable failure modes of a pressure ridge incorporated in level ice interacting with a four legged structure. An assessment of different directions of ice attack against multilegged structures obviously results in the definition of most unfavourable cases, which are of main concern for design purposes. If for example two "front" legs of a four legged platform simultaneously penetrate into the ice, than the two other legs at the rear are situated in the "ice shadow" and thus will not catch any reasonable ice load. However, if the ice movement direction is changed by lets say 20° , all four legs will be attacked simultaneously by ice, i.e. the total horizontal load on the structure will be much higher in that case.

To achieve a reasonable design ice load on the total multilegged platform, it is not realistic to assume that the peak loads at each of the single legs would occur simultaneously. The maximum ice load on the total structure is much less than the sum of the maximum loads on the single legs. Additionally, the interference of failure mechanism of the single legs in some cases reduces the ice load on a single leg compared to the same leg interacting with ice independently of other structural members.

5.2 Effect of Leg Spacing

Leg spacing is the most sensitive parameter for the evaluation of ice interaction with multilegged structures. Figure 5.2 schematically shows the dependency of the total horizontal ice force on a structure versus leg spacing L/D . If the distance of the legs is sufficiently large, i.e. larger than $L/D_{critical}$, each of the individual legs will act as a single independent structure interacting with ice. Hence, for L/D -values larger than $L/D_{critical}$ the total horizontal force will be independent of the leg spacing.

If the leg spacing decreases from $L/D_{critical}$ the total horizontal ice force will also decrease until a minimum value is reached at $L/D_{optimum}$. This decrease of total force is caused by interference of the failure mechanism at the individual legs. When decreasing the leg spacing further more below $L/D_{optimum}$ until the imaginary limit $L/D = 1$ is reached, the total horizontal ice force will increase again due to the entrapping of broken ice pieces inbetween the narrow multilegged substructure. The characteristic values of leg spacing $L/D_{critical}$ and $L/D_{optimum}$ can be determined by means of model tests in ice.

6.0 Ice Induced Vibration of Structure

Interaction between drifting ice and a fixed structure can be classified by the four types in Table 6.1 in which $\dot{\delta}_i$ is the deflection rate of the ice and $\dot{\delta}_s$ is the deflection rate of the structure.

So far in this lecture the two first types of interaction were described, whereas in this chapter we shall deal with the two last classes.

The starting point for vibration analysis is an appropriate oscillator model. For our present purpose of illustration the structure is reduced to a simple oscillator with one degree of freedom. Its mechanical analog is shown in Figure 6.1, and the differential equation is

$$m\ddot{x} + r\dot{x} + kx = F(t) \quad (6.1)$$

where the m is the mass, r the damping coefficient and k the stiffness or restoring coefficient for the structure. The exciting or driving force $F(t)$ is the dynamic ice force.

Included in the mass is the so-called added hydrodynamic mass, or the mass of fluid oscillating with the structure. The added mass depends on the shape and for a circular cylinder it is about equal to the mass of the water displaced by the cylinder. The left side of equation 6.1 describes the structure and its foundations and is the same for all environmental loadings, i.e. wind, current, waves and ice.

6.1 Self-Excited Vibrations

The term self-excited vibration refers to a special condition of forcing in which the vibration is either caused or controlled by the motion of the structure itself (DEN HARTOG, 1956). The exciting force is a function of the velocity of vibration. By definition this type of force is known as a damping force. However, the velocity-dependent force is damping only when its direction is opposite to the velocity of the vibrating structure. When the force happens to have the same direction as the structure, it is not a damping force but an exciting force. To account for this the term "negative damping" was defined and has since proven useful as it implies both velocity-dependence and excitation. The velocity dependent driving force is $F(v_r)$ where v_r is given in Table 6.1.

For most civil engineering problems it is permissible to assume

$$\dot{\delta}_i \ll \dot{\delta}_s,$$

$$v_r = v_i - \dot{\delta}_s \quad (6.2)$$

$$F(v_r) = F(v_i - \dot{\delta}_s) = F(v_i) + \frac{\partial F(v_i)}{\partial v_r} (-\dot{\delta}_s) \quad (6.3)$$

Inserting (6.3) in an oscillator equation similar to (6.1) the total damping becomes

$$F(\dot{\delta}_s) = \left[r + \frac{\partial F(v_i)}{\partial v_r} \right] \dot{\delta}_s \quad (6.4)$$

The condition for negative damping obviously is

$$\frac{\partial F(v_i)}{\partial v_r} < -r \quad (6.5)$$

6.2 Vibration Frequencies

In the most cases of self-excited vibrations the driving force $F(t)$ is quasi-steady and has no frequency components near the frequency of the induced vibration. Unfortunately, no information exists for prediction of critical ice velocities which cause vibrations. Several authors have suggested a frequency range based on their own observations. Their findings are summarized in Table 5.2.

It is interesting to note that the observed range has increased by an order of magnitude in both directions since Peyton made his first tests in 1966. Further increase is unlikely, as the values already cover the range of natural frequencies for conceivable bottom-mounted flexible structures.

6.3 Periodic Ice Force on Rigid Structures

Even the most uniform indentation is in reality an unsteady process, producing a time varying indenter force. This time series is sometimes purely stochastic but has commonly periodic components and is often strongly periodic. The periodicity is related to the mode of failure and is most pronounced for brittle flexural and shear failure. The sudden failure causes a rapid unloading which is repeated only after a certain reloading time. The resulting force cycle is assymmetric with a slow build-up and a more rapid unloading as suggested in Figure 6.2 (IAHR, unpublished). For a rigid structure NEILL (1976) suggested that a purely stochastic loading is unlikely. The ice will tend to break into pieces with a certain preferred size distribution, and these sizes L_{ice} together with the ice velocity U_i determine a frequency distribution

$$f_{ice} = \frac{U_{ice}}{L_{ice}} \quad (6.6)$$

This is easy to accept as long as the broken pieces are of the same size as the width of the structure. When the ice fails and forms such a piece, a substantial unloading takes place. Thus f_{ice} from equ. (6.6) becomes the frequency of successive peak ice forces.

On the other hand, when $L/B \ll 1$ the unloading resulting from the formation of one small piece is only a small fraction of the total ice force. If the local failures, which produce pieces all along the width B , occurred simultaneously, the sum would add up to rather complete unloading. But it is not easy intuitively to see why local failures should be in phase. In fact, the local failure tend consistently to be out of phase: One failure leads to the next by a shifting of the points of contact between the ice and the structure. There is considerable evidence to support this view. Full scale ice force records published by NEILL et al (1980), show a small variance for high frequency oscillations for crushing failure, which produces small pieces, and large variance for lower frequency oscillations for bending failure, which produces larger pieces.

6.4 Periodic Ice Force on Flexible Structures

For resonant vibrations of flexible structure MAATANEN (1975) proposed the expression

$$f_c = \frac{kv_{ice}}{\sigma_c hd} \quad (6.7)$$

where k is the stiffness of the structure, d its diameter, v_{ice} is the velocity, h the thickness and σ_c the crushing strength of the ice. The formula is based on the assumption that the oscillation frequency is

$$f_c = \frac{v_{ice}}{\delta_{max}} \quad (6.8)$$

where $\delta_{max} = F/K$ is the static deflection under the maximum load. Thus both inertia and damping forces are neglected. The difference between equ. (6.6) and equ. (6.7) is that equ. (6.6) assumes the failure of the ice to be governed by deflection/deformation of the ice alone, whereas equ. (6.7) assumes deflection of the structure to be important.

Observations on vibrating structures reveal, not surprisingly, that their frequencies fall below the value given by equ. (6.7). From the oscillator equation (6.1) it is clear that crushing ice pressure will occur at less than full static deflection δ_{max} when the inertial force or the damping force is nonnegligible. Figure 6.3 shows MAATANEN's (1978) own findings. In general he expects a reduction of 20-30% below f_c due to damping, and he leaves the formula (6.7) for cases with large super-structure mass.

BLINKARN (1970) examined whether the idea of self-excitation by negative damping forces could explain observed vibrations of a test platform in Cook Inlet, Alaska. Using PEYTON's (1966) data on ice strength versus strain rate he showed that the structure would indeed vibrate.

A purely theoretical ice model was proposed earlier by MATLOCK (1971) who described its mechanical analog shown in Figure 6.4 as follows:

"The ice is replaced by a rigid base, on rollers, transporting a series of elastic brittle cantilever or teeth. When each tooth comes in contact

with the mass, force Q is proportional to the deformation δ of the tooth. This relation is elastic (reversible) up to the point of fracture. At a maximum deformation δ_{\max} the tooth fractures completely and is permanently discarded. The interaction force then remains at zero until the next tooth comes in contact with the mass. With this simple model remarkably good general agreement were obtained with Peyton's 1966 field and laboratory data.

7.0 Computation of Examples

In order to present some practical examples of ice load estimation, in the following computations of ice forces are performed for different ice conditions. The examples are based on those given by ERANTI & LEE (1981), but adjusted to the equations presented in this lecture.

7.1 Crushing against Vertical Cylindrical Structure

Ice movements of 0.04 m/sec are assumed in an area of landfast low salinity sea ice with design thickness 1 m and design temperature -3 °C. The problem is to estimate the ice force on a lighthouse with diameter 6 m under these circumstances.

The strain rate is according to equation 3.1

$$\dot{\epsilon} = \frac{0.04}{2 \times 6} = 3.3 \times 10^{-3} \text{ sec}^{-1}$$

The uniaxial compression strength for these conditions is about 1.5 MN/m², the indentation coefficient I is assumed to be 2.5 and the shape factor m = 0.9. Because ice is practically in continuous horizontal and vertical movement, frozen-in condition or even initial failure with perfect contact is not likely to occur. We select contact coefficient 0.6. With the strain rate coefficient κ = 2.9 equation 3.3 (Korzhasin) gives

$$F = 2.5 \times 0.9 \times 0.6 \times 2.9 \times 1.5 \times 6 \times 1 = 35 \text{ MN}$$

For the same example the horizontal force is calculated by means of other empirical formula given above:

a) Afanasev - equation (3.6)

The shape factor m is 0.9

The coefficient C is given by equ. (3.7): $C = \left(5 \cdot \frac{1}{6} + 1\right)^{1/2} = 1.35$

Equ. (3.6) then gives

$$F = 1.35 \times 0.9 \times 1.5 \times 6 \times 1 = 11 \text{ MN}$$

The reduction in force compared to the result using Korzhavin's formula is due to the account for the aspect ratio dependency in Afanasev's formula which Korzhavin neglected.

b) Hirayama et al - equation (3.10)

$$F = 3.57 \times 600^{1/2} \times 100^{1.1} \times 15 = 207,891 \text{ kp} \\ \cong 2.1 \text{ MN}$$

c) Saeki et al - equation (3.10)

$$F = 5.0 \times 600^{1/2} \times 100 \times 15 = 183,711 \text{ kp} \\ = 1.8 \text{ MN}$$

In order to calculate the buckling force we need the characteristic length of ice L . With Young's modulus $E = 4000 \text{ MN/m}^2$ equ.(3.16) gives

$$L = \left(\frac{4000 \times 1^3}{12 \times 0.0098 \times (1-0.33)} \right)^{1/4} = 13.9 \text{ m}$$

With $D/L = 0.43$ we get even for semi-infinite ice sheet with frictionless boundary using equ. (3.15) and Figure 3.15

$$F = 6 \times 6 \times 0.0098 \times 13.9^2 = 70 \text{ MN}$$

Buckling is thus not probable to occur and crushing failure governs the design.

7.2 Level Ice Failure against Conical Structure

The problem is to estimate the ice force against a conical light house with diameter at water line 16 m and at top 4 m with a cone angle $\alpha = 50^\circ$. The ice thickness is assumed to be 1 m, the flexural strength 0.8 MN/m^2 and the friction coefficient between ice and concrete $\mu = 0.25$.

$$\text{With } \frac{\rho_w g D^2}{\sigma_f h} = \frac{0.0098 \times 16^2}{0.8 \times 1.0} = 3.1 \text{ in Figure 4.10, we get } A_1 = 1.7$$

and $A_2 = 0.14$. The rest of the constants are $A_3 = 0.35$; $A_4 = 2.2$; $B_1 = 0.6$ and $B_2 = 0.031$. The horizontal component is given by equation 4.11:

$$H = [1.7 \times 0.8 \times 1.0^2 + 0.14 \times 0.0098 \times 1.0 \times 16^2 + 0.35 \times 0.0098 \times 1.0 (16^2 - 4^2)] \times 2.2 = 5.5 \text{ MN}$$

of which 3.8 MN arise from breaking the ice sheet and the rest from broken ice pieces sliding over the surface. The vertical component is according to equation 4.12

$$V = 0.6 \times 5.5 + 0.031 \times (-0.0098) \times 1.0 (16^2 - 4^2) = 3.4 \text{ MN}$$

The horizontal force is only about one-fifth of the force corresponding to crushing failure against a structure of same diameter at waterline.

7.3 Pressure Ridge Failure against Cylindrical Structure

The force is estimated that a pressure ridge with underwater portion thickness 12 m exerts on a cylindrical structure with diameter 8 m. The angle of friction during penetration is assumed to be 40°, the average cohesion between blocks is 10 kN/m² and uniform ice thickness is 1 m.

It is not probable that the ice sheet happens to have its maximum strength just at the position of the ridge. That is why the strength of the upper portion of the ridge is assumed to be 75% of design ice strength in crushing. With aspect ratio D/h = 8 we get from equation (3.6)

$$F_{cr} = 0.75 \times 0.9 \times \sqrt{5 \times 1/8 + 1} \times 2.0 \times 1.0 \times 8.0 = 14 \text{ MN}$$

The contribution of the underwater portion of the ridge is given by equation (3.18). Assuming that the effective height of the ridge is 14 m we get

$$F_p = \tan(65^\circ) \times 14 \times 8 (0.5 \times 14 \times \tan(65^\circ) \times 0.82 + 2 \times 10) \times \left(1 + \frac{2 \times 12}{3 \times 8}\right) = 16000 \text{ kN} = 16 \text{ MN.}$$

In this case, the ratio between ridge load and the load corresponding to crushing of a uniform ice sheet is 1.6. If the structure were narrower this ratio would have been larger.

7.4 Multi-Year Pressure Ridge Failure against Conical Structure

A failure mode is considered such that a center crack of the ridge first occurs in front of the cone and subsequently two hinge cracks symmetrically develop at both sides of the cone. Assuming that the shape of the ridge is rectangular with width 24 m and height 16 m and that the Young's modulus of ice is 5000 MN/m^2 and the bending strength 0.5 MN/m^2 , we get the characteristic length and the vertical forces from equations (4.13), (4.14), and (4.15)

$$L = \left(\frac{4 \times 5000 \times 24 \times 16^3}{0.0098 \times 24 \times 12} \right)^{0.25} = 162 \text{ m}$$

$$V_1 = \frac{4 \times 24 \times 16^3 \times 0.5}{8 \times 162 \times 12} = 13 \text{ MN}$$

$$V_2 = \frac{6.17 \times 24 \times 16^3 \times 0.5}{8 \times 162 \times 12} = 20 \text{ MN}$$

The corresponding horizontal forces assuming cone angle 50° and friction coefficient 0.25 are according to equation (4.16)

$$H_1 = 13 \left(\frac{\sin 50^\circ + 0.25 \cos 50^\circ}{\cos 50^\circ - 0.25 \sin 50^\circ} \right) = 27 \text{ MN}$$

$$H_2 = 20 \left(\frac{\sin 50^\circ + 0.25 \cos 50^\circ}{\cos 50^\circ - 0.25 \sin 50^\circ} \right) = 47 \text{ MN}$$

Small and loose pressure ridges that are typical in many sea areas with temperate climate, do not always represent the most severe loading condition on a structure. The large pressure ridge with total thickness up to 30 m and multi-year pressure ridges, however, represent a major hazard, on offshore structures. Experience of the degree of consolidation of ridges has to be gained in order to improve design accuracy.

8.0 Limitations

This lecture should be an elementary introduction to estimation of ice forces on structures. Therefore not all conceivable ice loads were addressed. The consideration was limited to loads exerted by level ice and first and multiyear pressure ridges. For the actual case of designing a structure against ice attack possibly additional types of ice load have to be considered, as e.g. ice bergs, grounded rubble pile up, uplifting forces due to tidal action and thermal expansion of ice.

REFERENCES

- Afanasev, V.P., Y.V. Dolgoplov and Z.J. Shveishtein (1972): Ice pressure on isolated structures in the sea. Trudy Leningrad, Arkt. i Antarkt. Inst., vol. 300, p. 61-80. U.S. Army Cold Regions Research and Engineering Laboratory, Draft Translation 346.
- Afanasev, V.P., Y.V. Dolgoplov and Z.J. Shveishtein (1971): Ice pressure on individual marine structures. In Ice Physics and Ice Engineering, Israel. Program for Scientific Translation, 1973, p. 50-68.
- American Petroleum Institute (1982): Planning, designing and constructing fixed offshore structures in ice environments. APJ-Bulletin 2N, Dallas, Texas.
- Bercha, F.G. and J.V. danys (1975): Prediction of ice forces on conical offshore structures. Marine Science Communication, p. 365-380.
- Bercha, F.G. and D.G. Stenning (1979): Arctic offshore deepwater ice-structure interactions. Offshore Technology Conference. OTC paper 3632. Houston, Texas.
- Blenkarn, K.A. (1970): Measurement and analysis of ice forces on Cook Inlet structures. Offshore Technology Conference. Dallas, Texas.
- Chen, W.F. (1975): Limit analysis and soil plasticity. Elsevier, Amsterdam.
- Croasdale, K.R. (1974): Crushing strength of Arctic ice. In Reed, J.C. and Sater, J.E., ed., The Coast and Shelf of the Beaufort Sea. Proceedings of a symposium on Beaufort Sea and shelf research. Arlington, Virginia, Arctic Institute of North America, p.p. 377-399.
- Dolgoplov, Y.V., V.P. Afanasev, V.A. Korenkov and D.F. Panfilov (1975): Effect of hummocked ice on piers of marine hydraulic structures. International Assoc. of Hydr. Res. Symposium on Ice Problems, Hanover, New Hampshire.
- Den Hartog, J.P. (1956): Mechanical vibrations. Mc Graw-Hill Book Co.
- Danys, J.V. and F.G. Bercha (1976): Investigations of ice forces on a conical offshore structure. Ocean Eng., Vol. 3, No. 5, p. 299-310.
- Eranti, E. and G.C. Lee (1981): Introduction to ice problems in civil engineering. State University of New York and Buffalo. Center for Cold Regions Engineering, Science and Technology (81-1).
- Edwards, R.Y. and K.R. Croasdale (1976): Model experiments to determine ice forces on conical structures. Preprint, Symp. Appl. Glaciol., Cambridge, England.

- Frederking, R. and L.W. Gold (1975): Experimental study of edge loading of ice plates. Can. Geotech. J., Vol. 12, p. 456-464.
- Frederking, R.N.W., (1977): Plain strain compressive strength of columnar-grained and granular-snow ice. J. of Glaciology, Vol. 18, No. 89, pp. 505-596.
- Frederking, R., J. Schwarz, E. Wessels and L. Hoffmann (1982): Model investigations of ice forces on cylindrical structures. Intermaritec Conference. IMT paper 82-203. Hamburg.
- Frederking, R., T. Sanderson, E. Wessels and M. Inoue (1983): Ice behaviour around a small arctic island. POAC 1983. Helsinki.
- Hetenyi, M. (1946): Beams on elastic foundations. The University of Michigan Press, Ann Arbor.
- Hirayama, K., J. Schwarz and H.C. Wu (1974): An investigation of ice forces on vertical structures. University of Iowa (IIHR Report No. 158).
- Hudson, R.D. (1980): Ridge statistics of the Beaufort sea shear zone. Proceedings of workshop on sea ice ridging and pile-up. National Research Council Canada. Technical Memorandum No. 134. Calgary. Alberta.
- JAHK: River and lake ice engineering. Chapter III: Ice mechanics. International Association of Hydraulic Research. Editor: E. Ashton. CRREL. Hanover. New Hampshire. To be published.
- Kopaigoradski, E.M. and Vershinin, S.A. (1974): Discussion of Construction Regulations; Investigation of ice loads on cylindrical supports during movements of ice floes. Hydrotechnical Construction (translation of *Gidrotekhnicheskoe Stroitel'stvo*, No. 9, pp. 40-42, Sept. 1973).
- Korzhasin, K.N. (1962): Action of ice on engineering structures. CRREL Translation 260. 1971.
- Kovacs, A. and M. Mellor (1974): Sea ice morphology and ice as a geologic agent in the southern Beaufort Sea, The Coast and Shelf of the Beaufort Sea. p. 113-161. Arctic Institute of North America. Editor: J.C. Reed and J.E. Sater.
- Määtänen, M. (1975): Experience of ice forces against a steel lighthouse mounted on the seabed, and proposed constructional refinements. POAC-75.
- Määtänen, M. (1978): On conditions for the rise of self-excited ice-induced autonomous oscillations in slender marine pile structures. Research Report No. 25, Winter Navigation Research Board. Finland.

- Matlock, H., W.P. Dawkins and J.J. Panak (1971): Analytical model for ice-structure interaction. *Journal of the Engineering Mechanics Div., ASCE*, Aug. 1971.
- Michel, B. and N. Toussaint (1977): Mechanisms and theory of indentation of ice plates. *J. Glaciol.*, Vol. 19, No. 81, p. 285-301.
- Neill, C.R. (1970): Ice pressure on bridge piers in Alberta, Canada. *IAHR Ice Symposium, Reykjavik*.
- Neill, C.R. (1976): Dynamic ice forces on piers and piles. *Can. J. Civ. Eng.*, Vol. 3, No. 2, p. 305-341.
- Neill, C.R. et al. (1980): Ice effects on bridges (draft). *Roads and Transportation Assoc. of Canada*.
- Nevel, D.E. (1972): The ultimate failure of floating ice sheets. *Proc. of IAHR Symposium, Leningrad*, pp 17-22.
- Nevel, D.E. and Haynes, D.F. (1976): Interpretation of the tensile strength of ice under triaxial stresses. *CRREL-report 76-5*.
- Peyton, H.R. (1966): Sea ice forces. *Conference on Ice Pressure Against Structures. NRC Technical Memorandum No. 92. Laval University, Quebec*.
- Ralston, T.D. (1977): Ice force design considerations for conical offshore structures. *Fourth POAC Conference, St. John's, Newfoundland*.
- Ralston, T.D. (1978): An analysis of ice sheet indentation. *Proc. Int. Ass. of Hydr. Res. Symposium on Ice Problems*, pp. 5-31, Lulea, Sweden.
- Ralston, T.D. (1979): Plastic limit analysis of sheet ice loads on conical structures. *JUTAM Symposium on the Physics and Mechanics of Ice. Copenhagen. Springer Verlag*.
- Reinicke, K.M. and Remer, R. (1978): A procedure for the determination of ice forces - illustrated for polycrystalline ice. *Proceedings 4th IAHR Symposium on Ice. Lulea, Sweden*.
- Saeki, H., Hamanaka, K. and Ozaki, A. (1977): Experimental study on ice force on a pile. *Fourth Int. Conf. on Port and Ocean Engineering under Arctic Conditions. St. John's, Newfoundland*.
- Sodhi, D.S. and Hamza, H.E. (1977): Buckling analysis of a semi-infinite ice sheet. In *Proceedings, 4th International Conference on Port and Ocean Engineering under Arctic Conditions (POAC 77)*, Memorial University of Newfoundland, St. John's Newfoundland, 26-30 Sept., 1977.

- Spedding, L.G. (1980): Rule of thumb ridge height distribution. Proceedings of workshop on sea ice ridging and pile-up. National Research Council Canada. Technical Memorandum No. 134. Calgary, Alberta.
- Schwarz, J. (1970): Treibeisdruck auf Pfähle. Mitt. Franzius-Institut für Grund- und Wasserbau, Techn. Universität Hannover, Heft 24.
- Schwarz, J., Frederking, R.F., Wessels, E. and Hoffmann, L. (1978): Theoretische Untersuchungen und Durchführung stützender Eistankmodellversuche zur Ermittlung der Eisdruckkräfte auf Rohrstützentragwerke von Offshore Plattformen. HSVA-Bericht Nr. 1512.
- Tryde, P. (1977): Ice forces. Journal of Glaciology, Vol. 19, No. 81.
- Wang, Y.S. (1978): Buckling analysis of a semi-infinite ice sheet moving against cylindrical structures. Proc. Int. Ass. Hydr. Res., Symposium on Ice Problems, Lulea, Sweden.
- Wessels, E. (1980): Model tests on fixed and floating conical structures in ice. COSMAR I-Report PP 4-3. To be published.
- Wessels, E. and Evers, K.U. (1982): Model tests on vertical multi-legged structures in ice. COSMAR II-Report, T 4-2. Unpublished.
- Wu, R.C., Chang, K.J. and Schwarz, J. (1976): Fracture in the compression of columnar-grained ice, Eng. Fracture Mechanics, 8: 365-372.
- Wright, B. and McGonical, D. (1980): Features of first and multi-year ridges. Proceedings of workshop on sea ice ridging and pile-up. National Research Council Canada. Technical Memorandum No. 134. Calgary, Alberta.

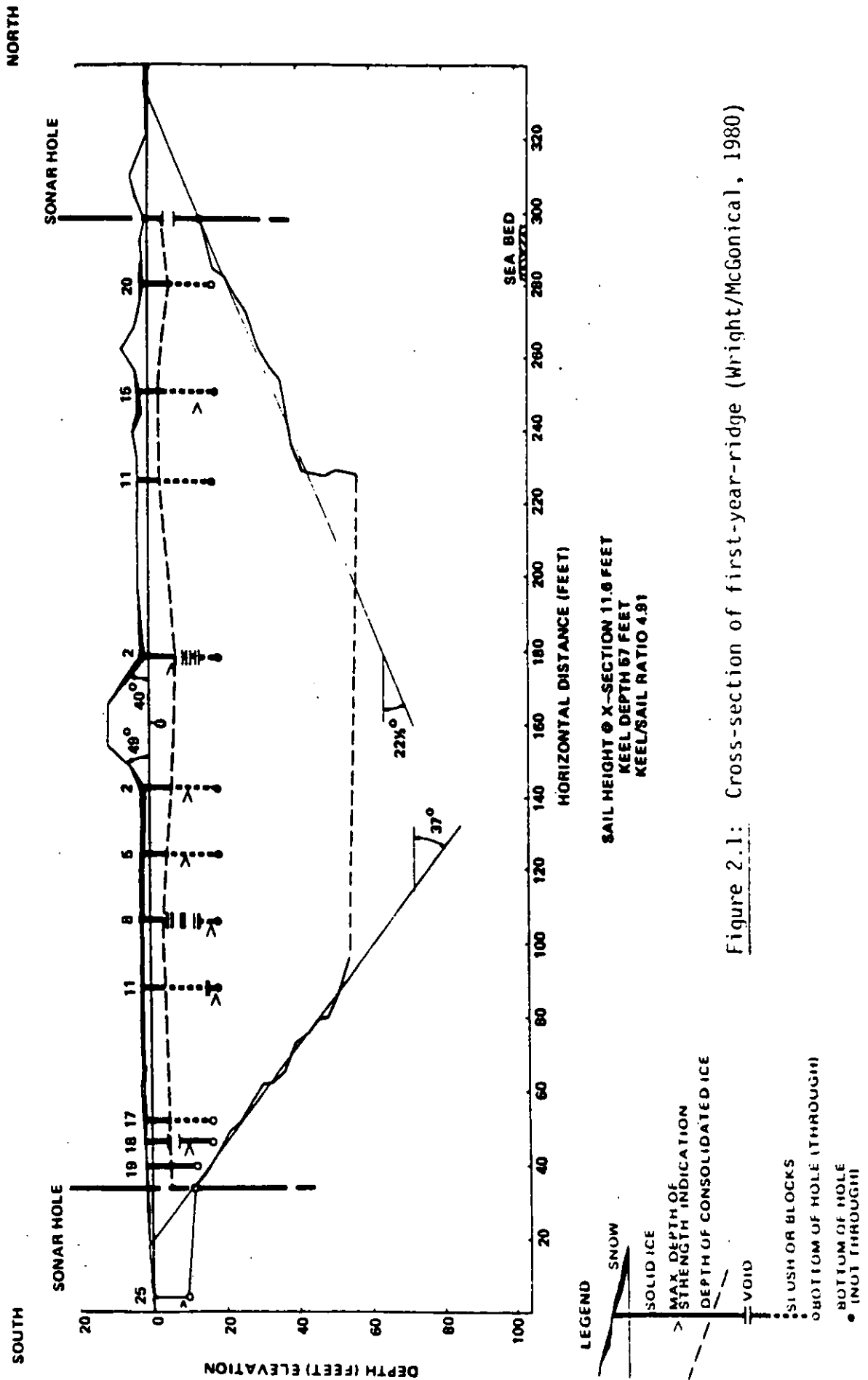


Figure 2.1: Cross-section of first-year-ridge (Wright/McGonical, 1980)

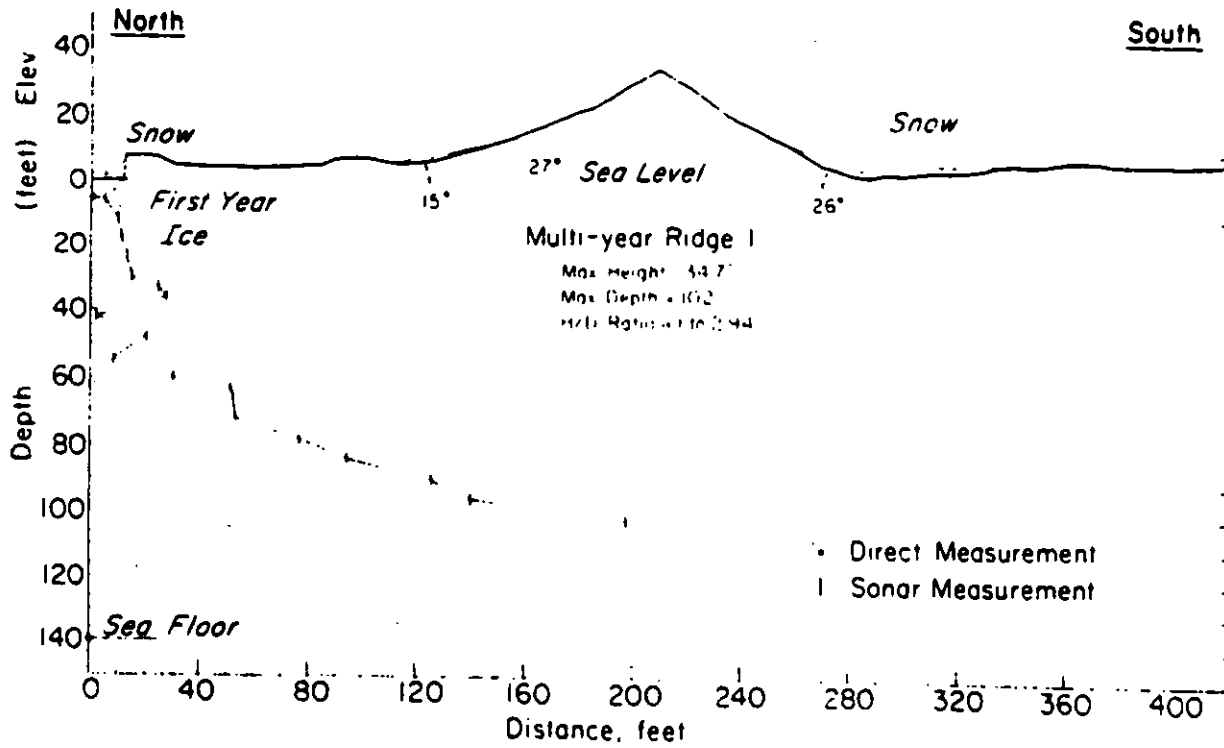


Figure 2.2: Partial cross-section of multi-year ridge (Wright/McGonical, 1980)

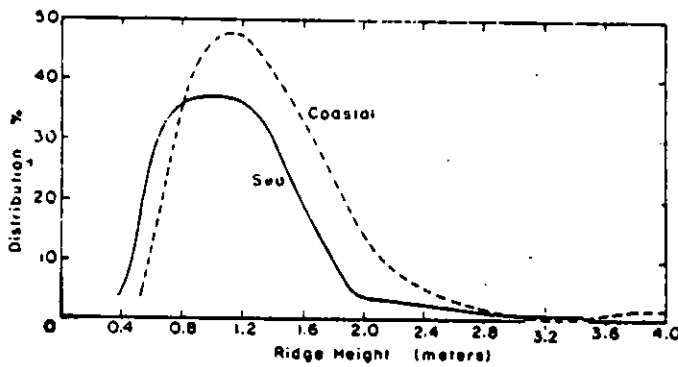


Figure 2.3: Pressure ridge height distribution in the first 5 km of the shear zone (coastal) versus that occurring farther seaward (Kovacs/Mellor, 1974)

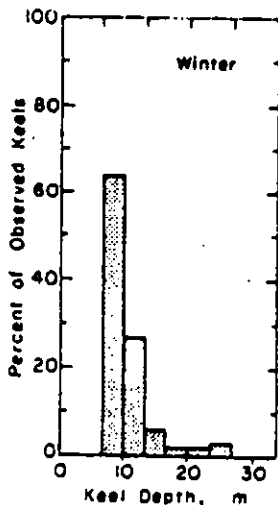


Figure 2.4: Percentage of keels deeper than 6 m along a 65-km submarine track in the polar pack ice zone. (Kovacs/Mellor, 1974)

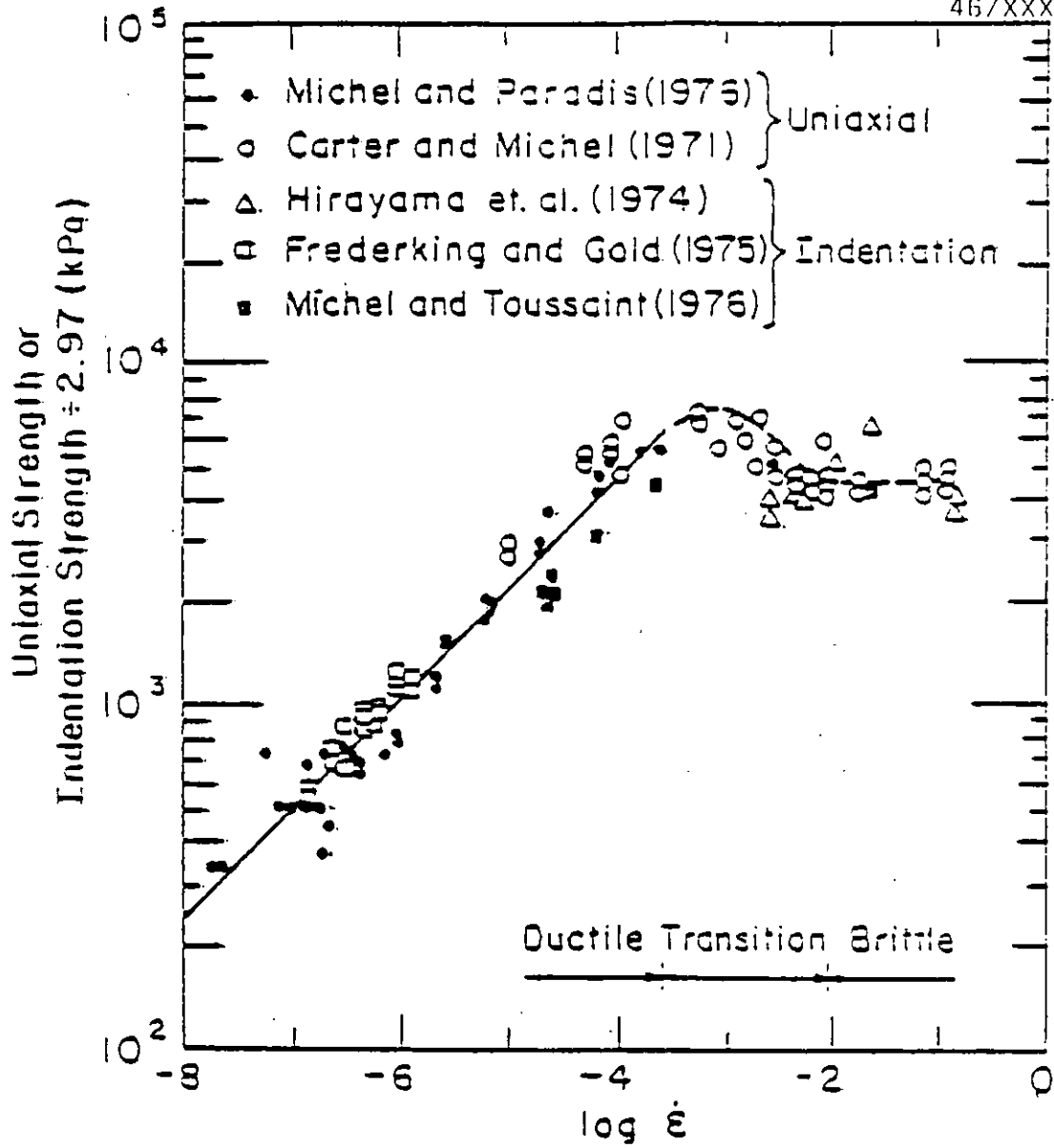


Figure 3.1: Uniaxial crushing and indentation strength of S-2 ice at -100°C (after Michel & Toussaint, 1977)

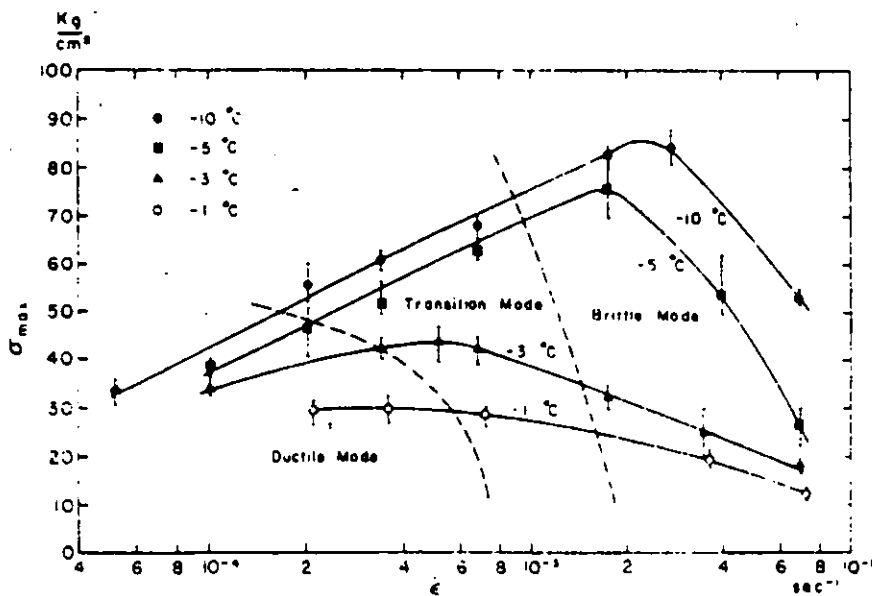


Figure 3.2: Ice crushing strength vs. strain rate and temperature (Wu, Chang & Schwarz, 1976)

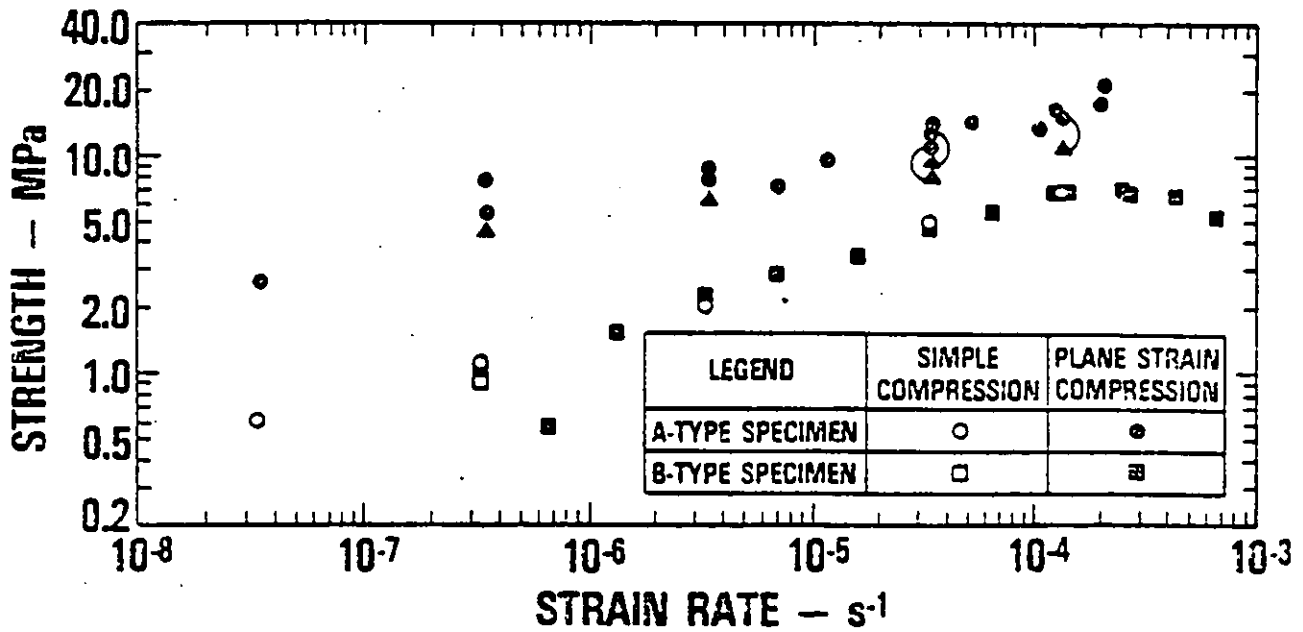


Figure 3.3: Strain rate dependence of confined and unconfined ice strength; S-2 columnar-grained ice, -10°C (After Frederking, 1977)

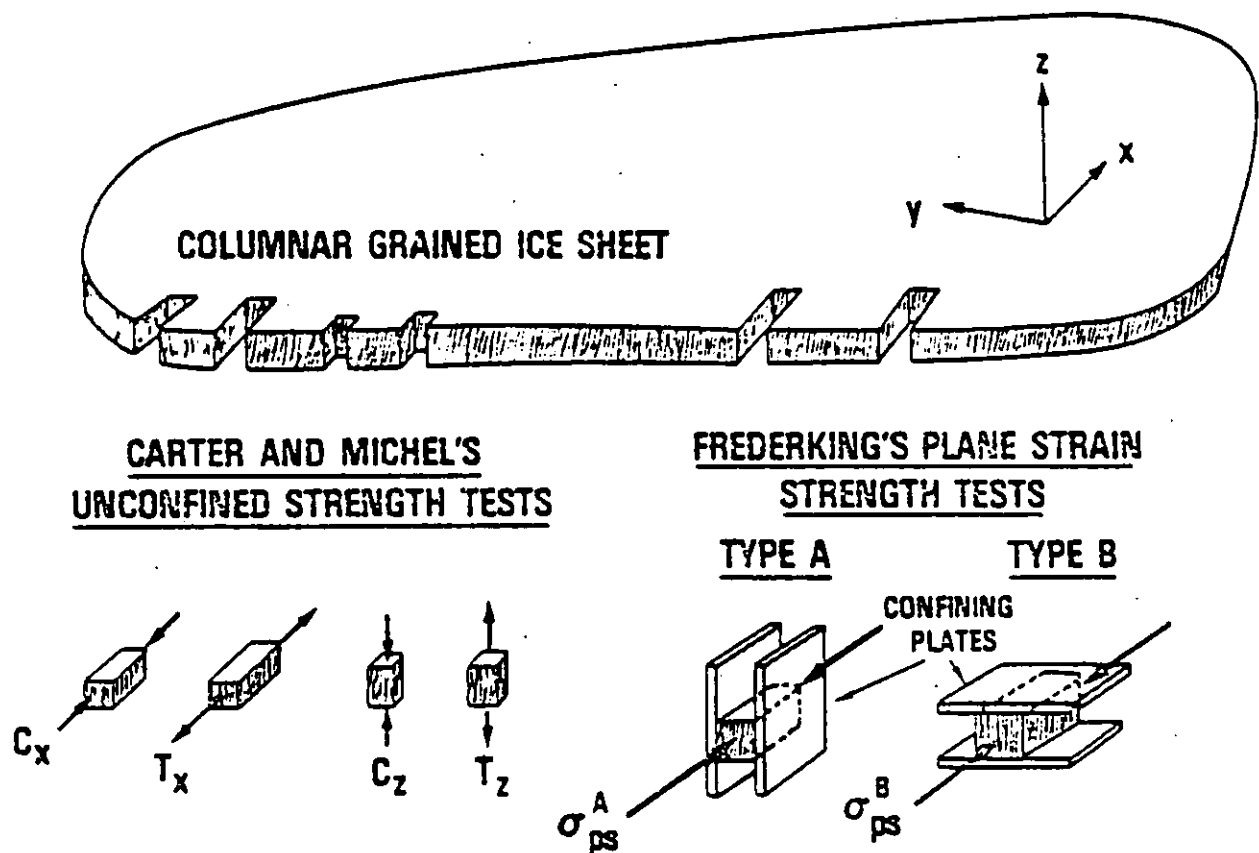


Figure 3.4: Unconfined and plane strain ice strength tests for columnar-grained ice (Ralston, 1978)

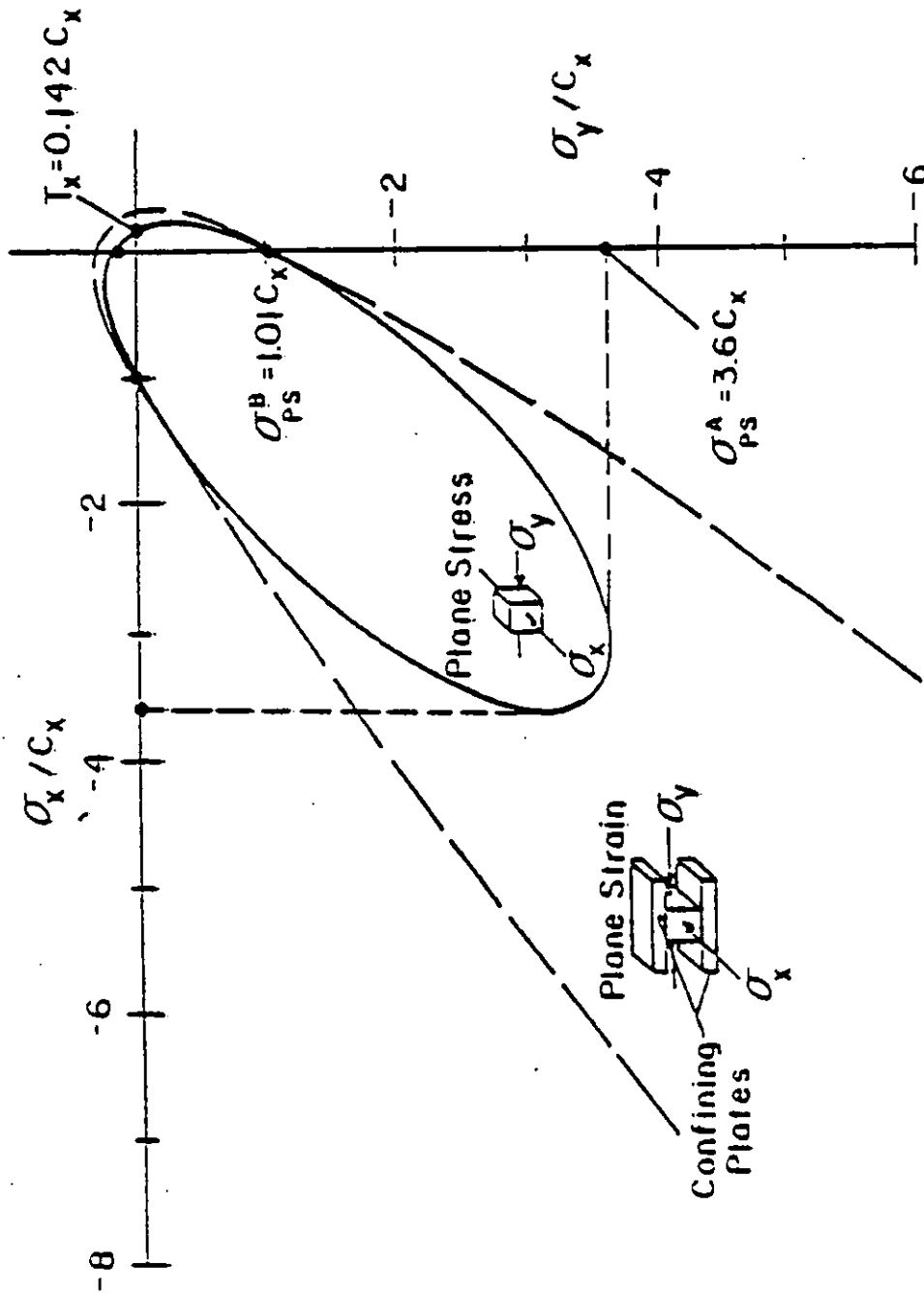


Figure 3.5: Plane stress and plane strain ice yield surface (After Ralston, 1978)

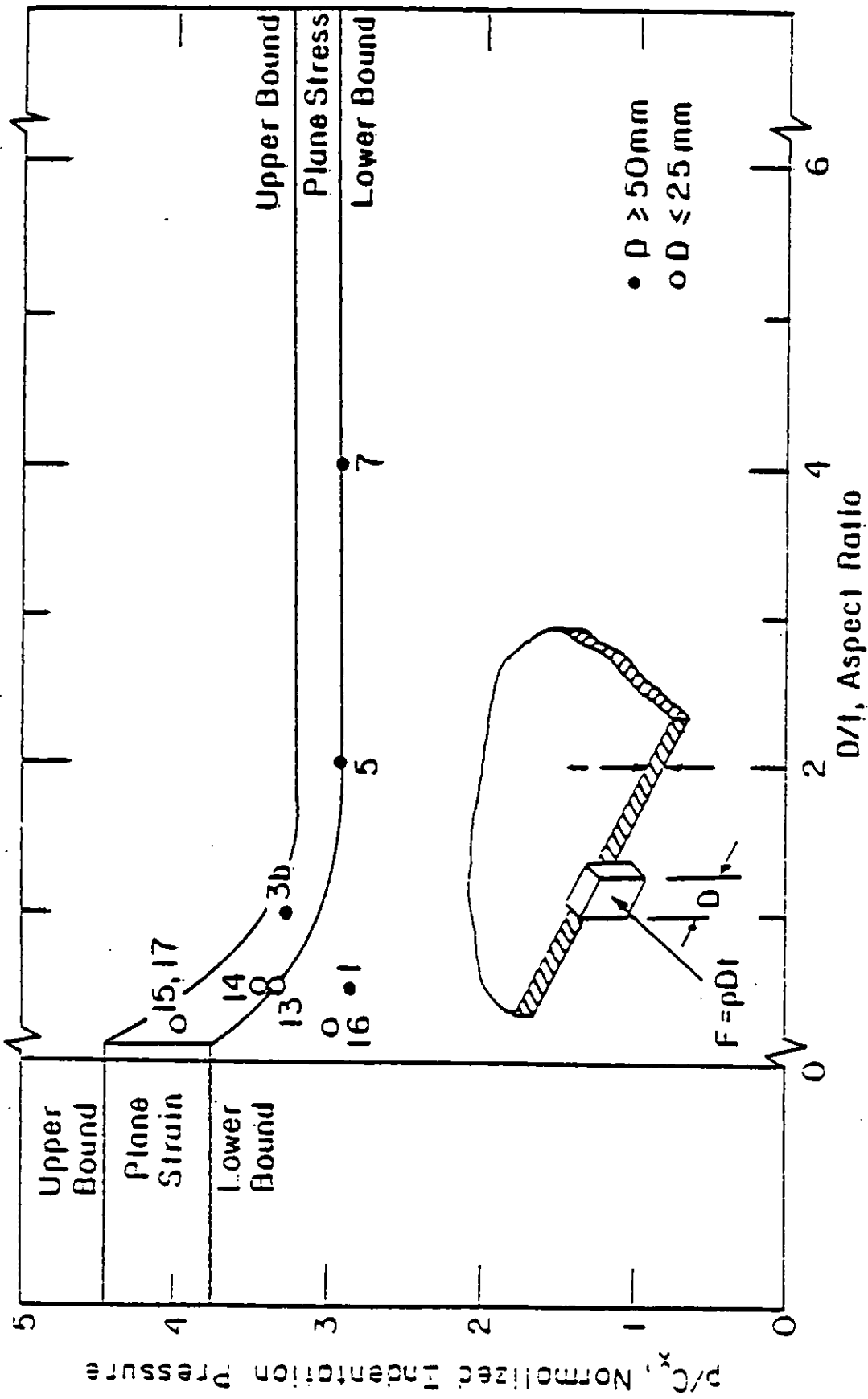


Figure 3.6: Comparison of computed bounds for indentation pressure with test data of Michel & Toussaint, 1976 (After Ralston, 1978)

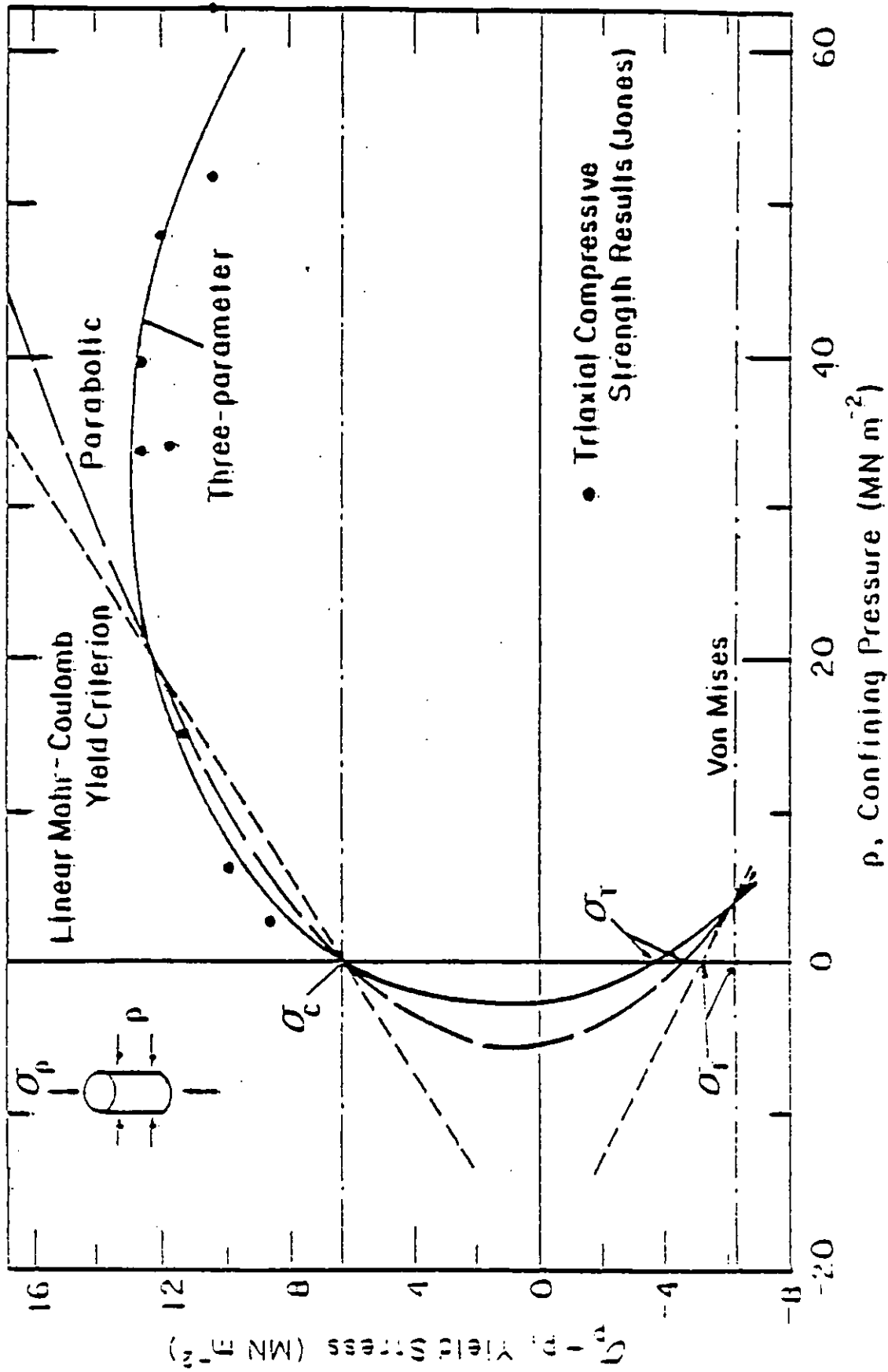


Figure 3.7: Triaxial compressive strength results for polycrystalline ice and approximating yield criteria (After Reinecke & Remer, 1978)

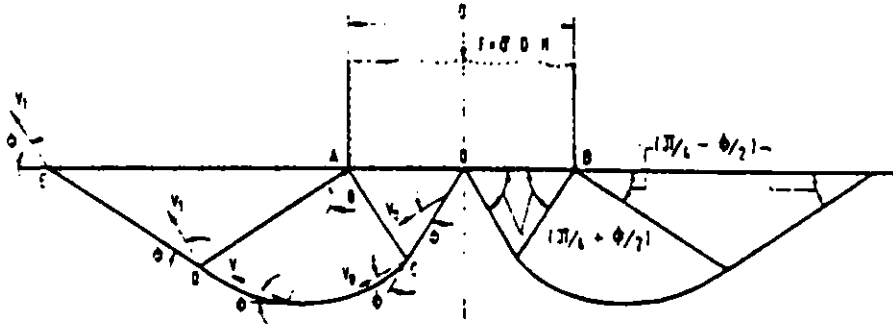


Figure 3.8: Hill failure mechanism (After Chen, 1975)

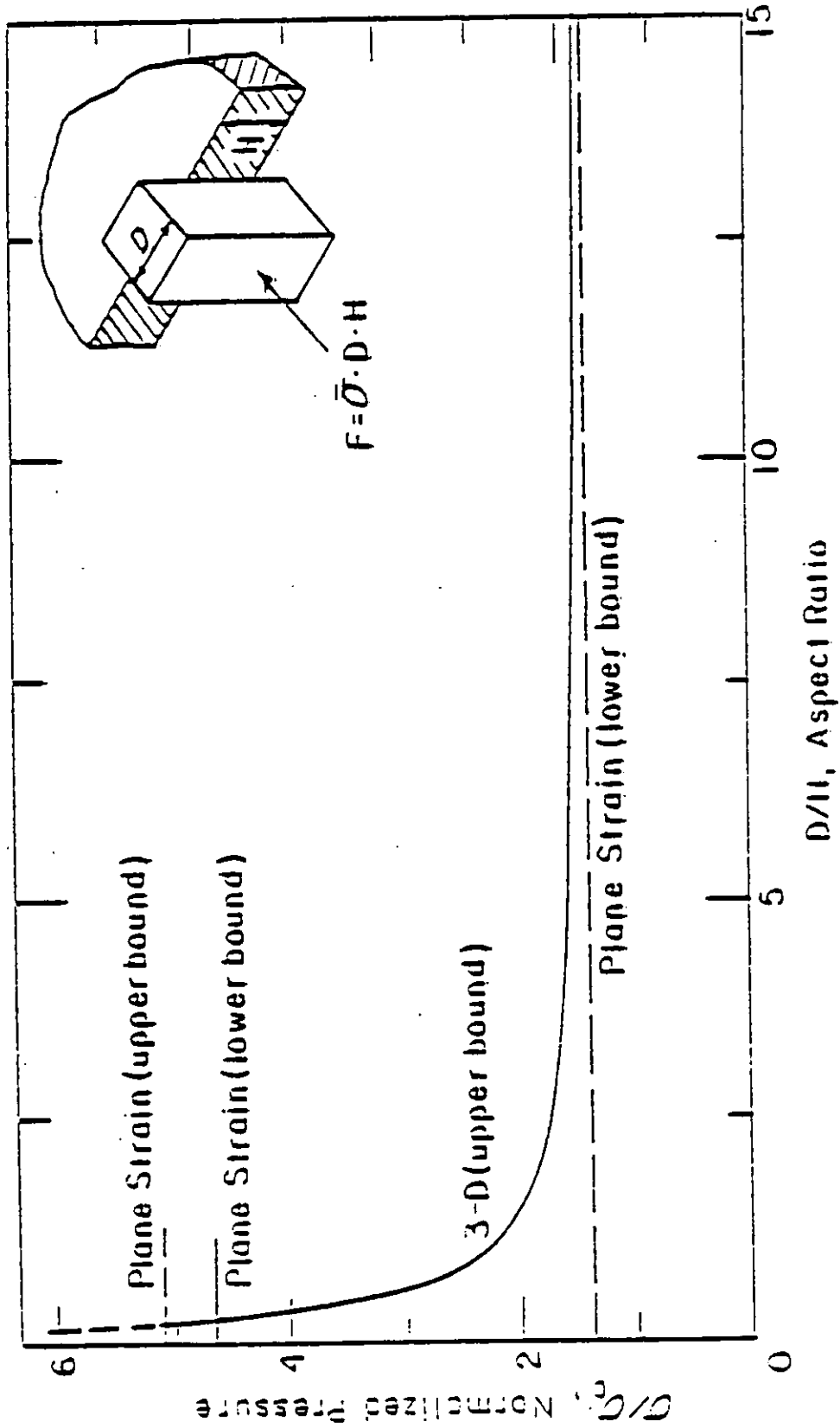


Figure 3.9: Bounds for indentation pressure derived for the three-parameter yield function
(After Reinecke & Remer, 1978)

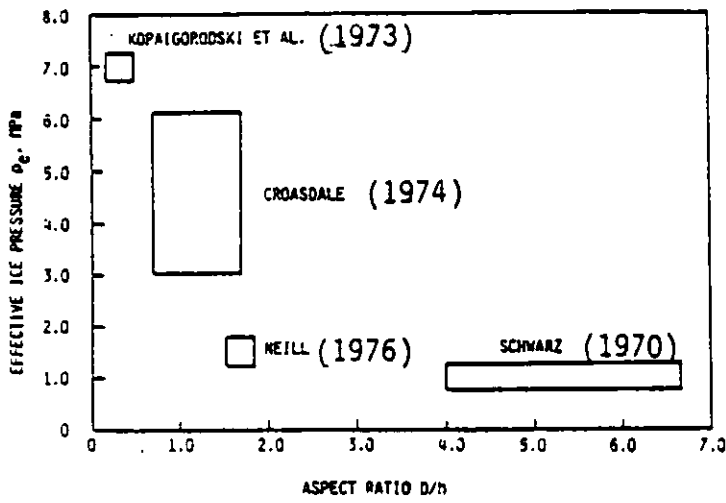


Figure 3.10: Effective ice pressure of different field tests versus aspect ratio. (Frederking et al, 1982)

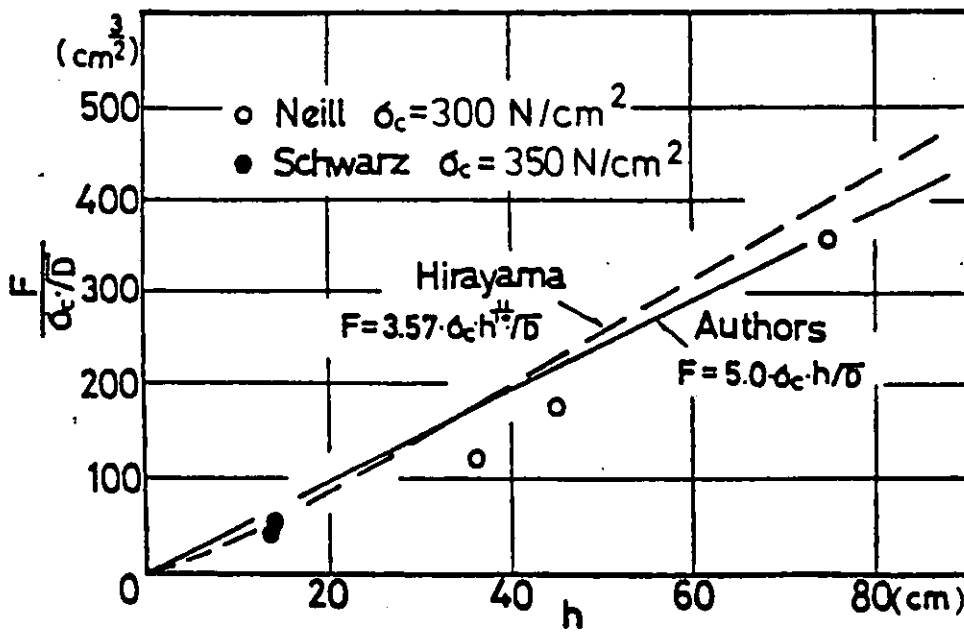


Figure 3.11: Comparison between several predictions of ice forces on vertical piles (Saeki et al, 1977)

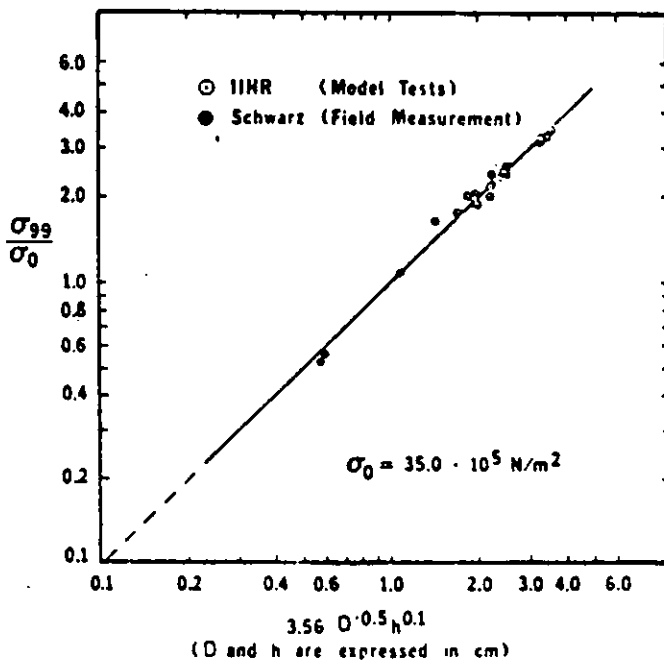


Figure 3.12: Effective ice stresses as a function of ice thickness and pile diameter. (Hirayama et al, 1974)

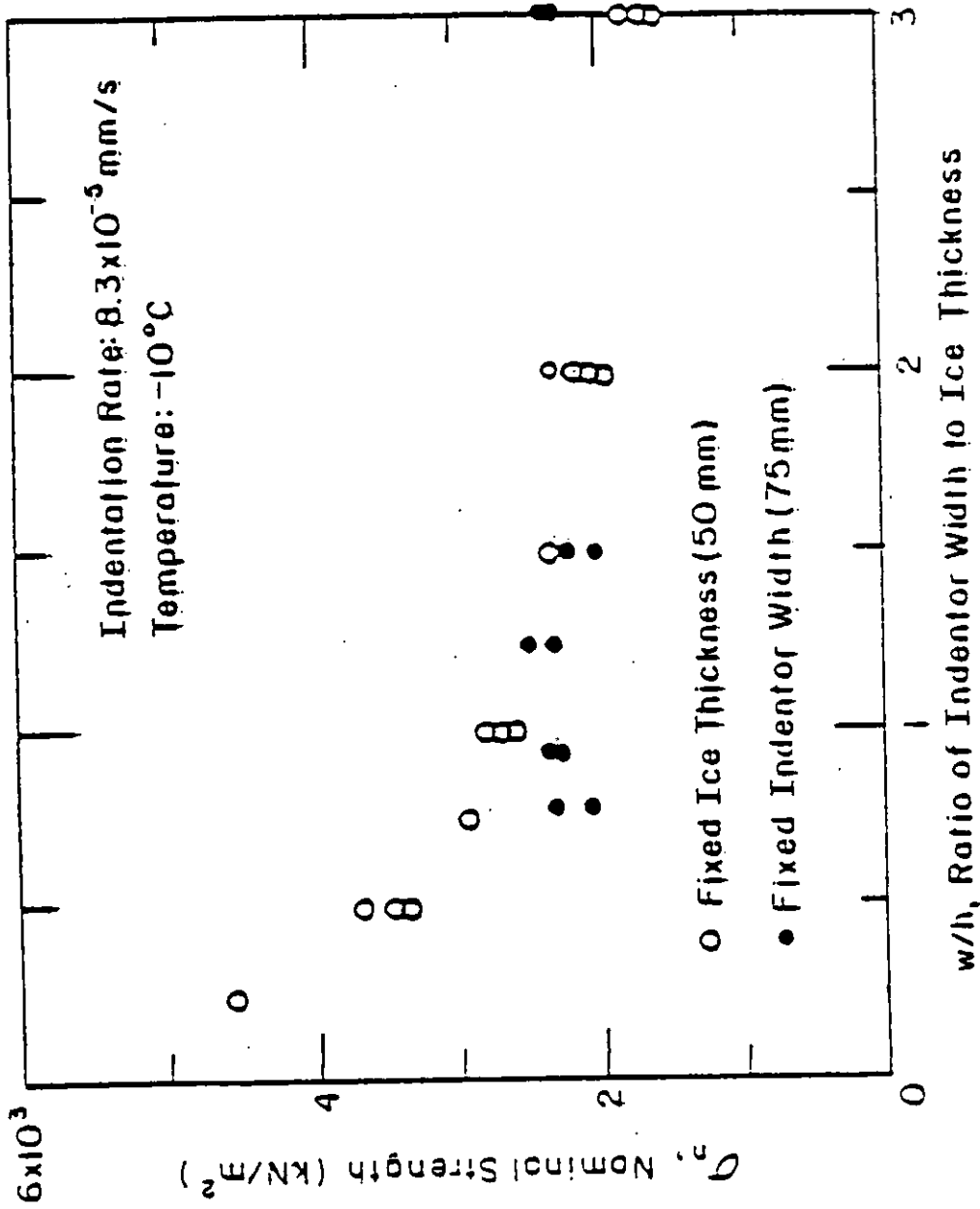


Figure 3.13: Evidence of weak dependence of σ_c on ice thickness.
(After Frederking & Gold, 1975)

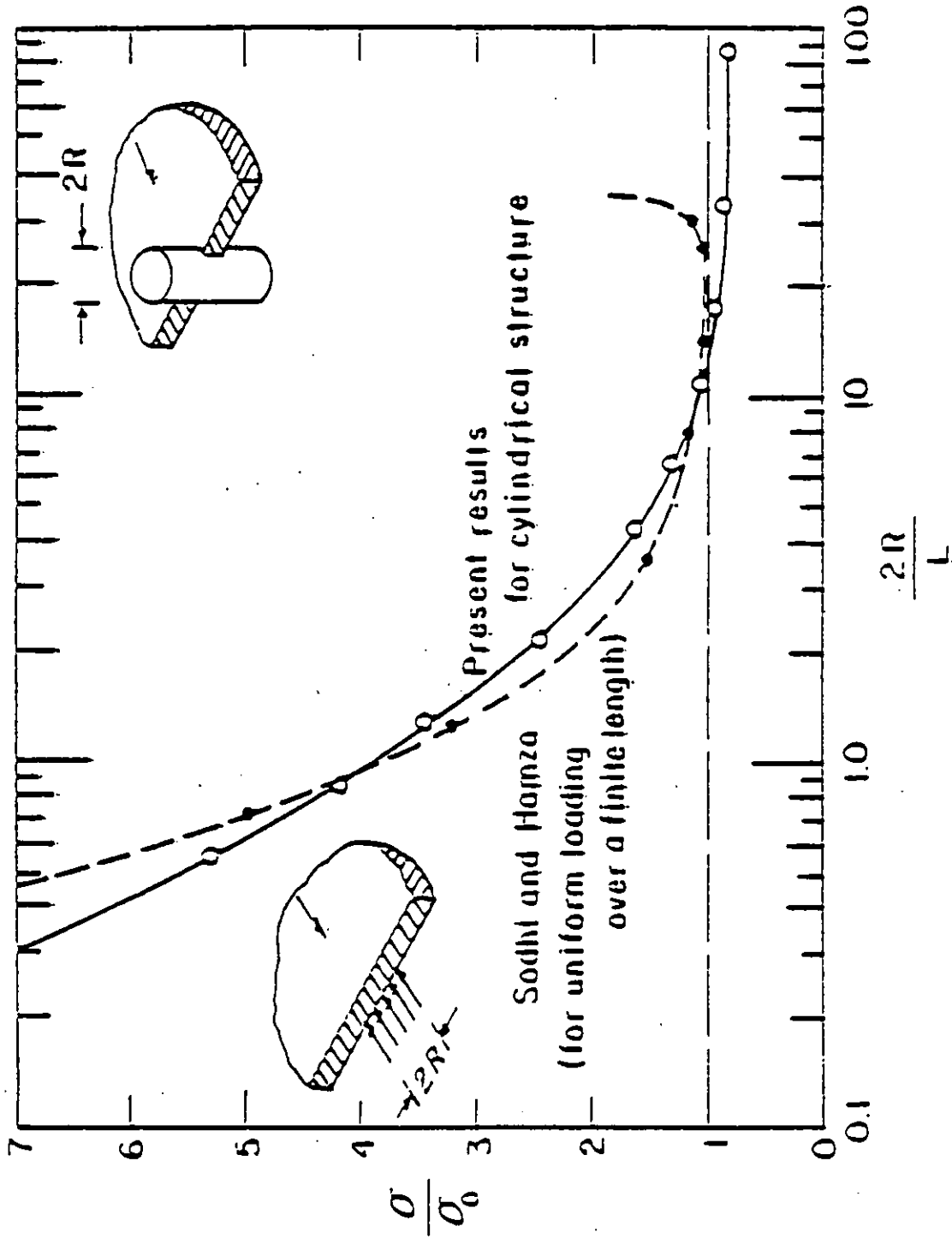


Figure 3.14: Buckling pressure - comparison of flat and cylindrical indentors. (After Wang, 1978)

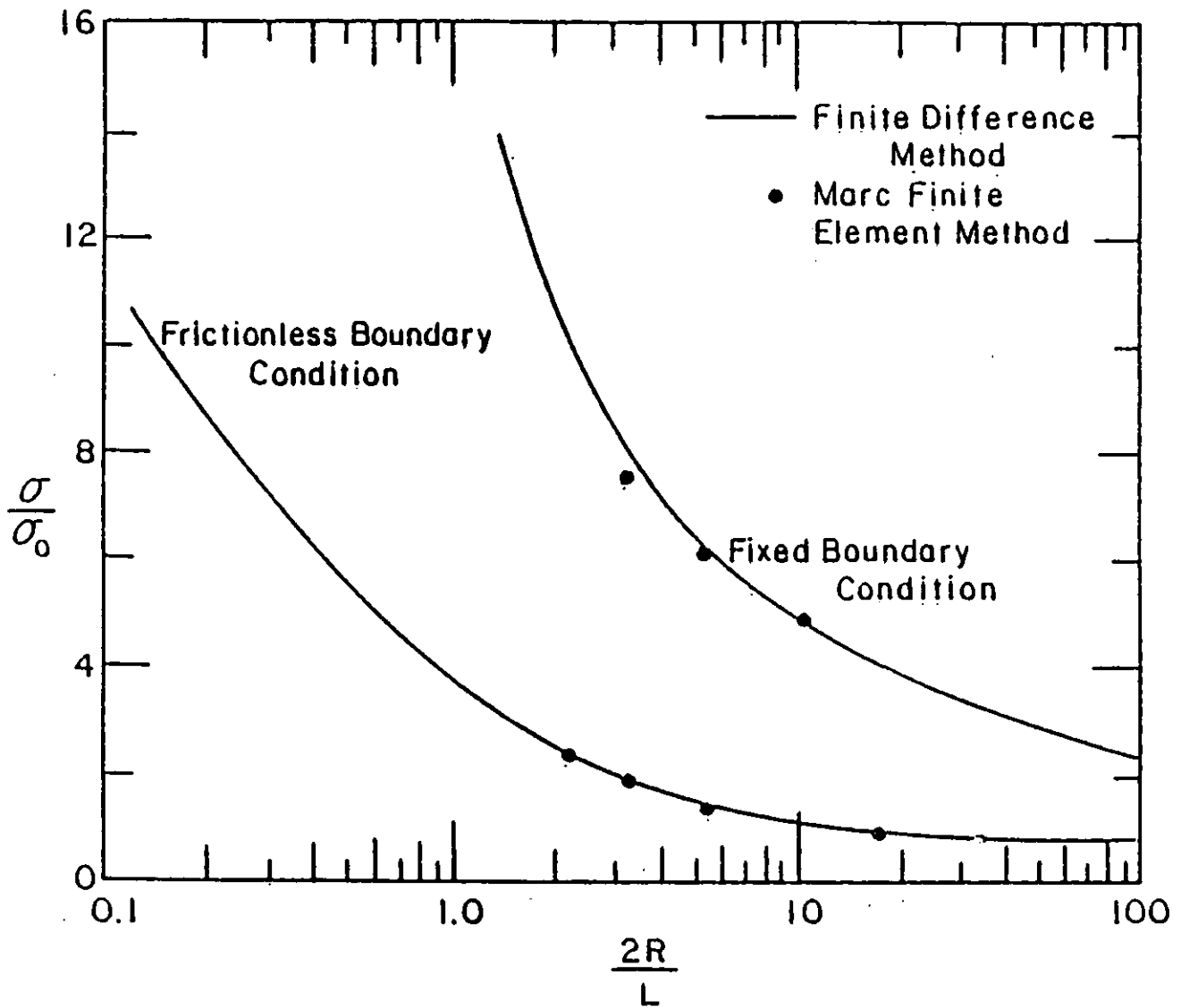


Figure 3.15: Solution of the buckling pressure for slipping and adfreeze condition (after Wang, 1978)

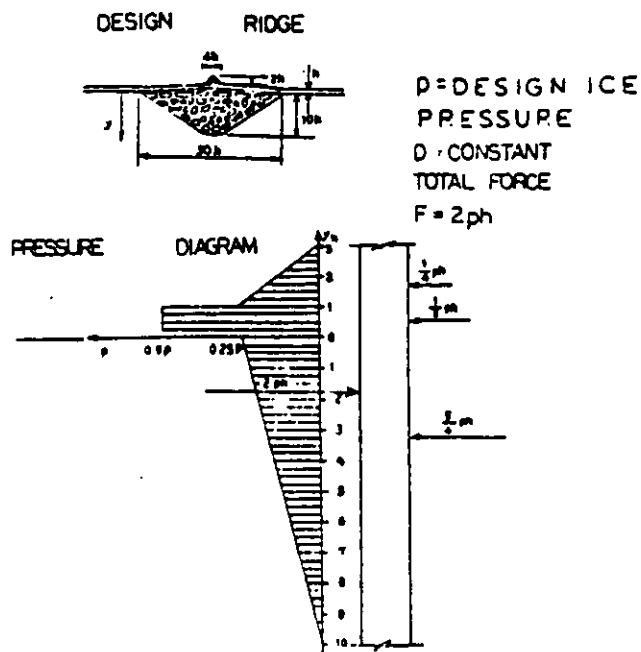
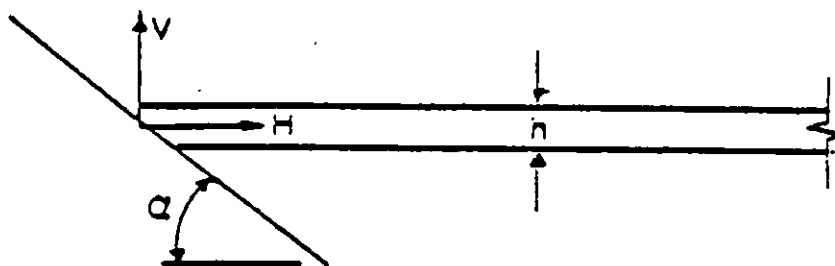
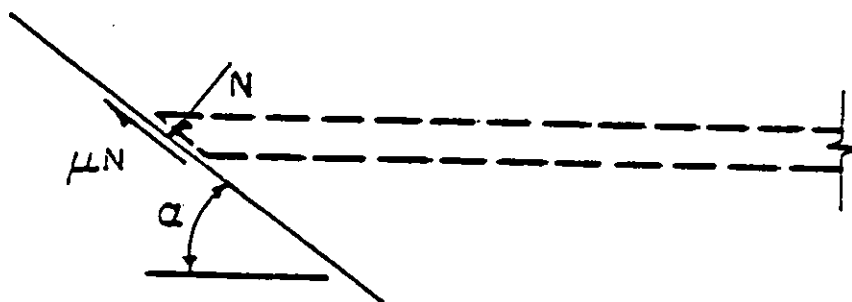


Figure 3.16:

A design ridge and pressure diagram used by Finnish Board of Navigation (Eranti/Lee, 1981)



a. Forces Acting on Ice



b. Forces on Structure

Figure 4.1: Initial interaction between ice and an inclined plane (IAHR, to be published)

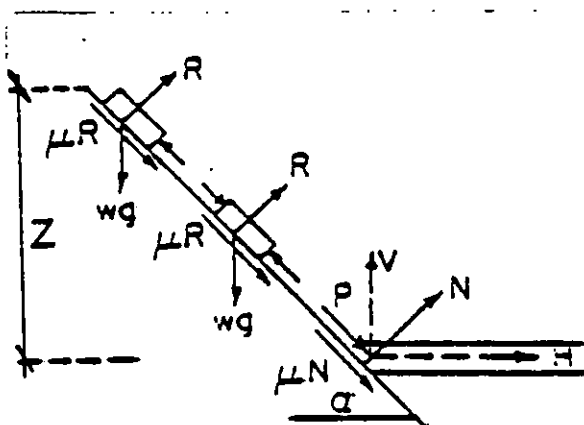


Figure 4.2: General interaction between ice and an inclined plane (IAHR, to be published)

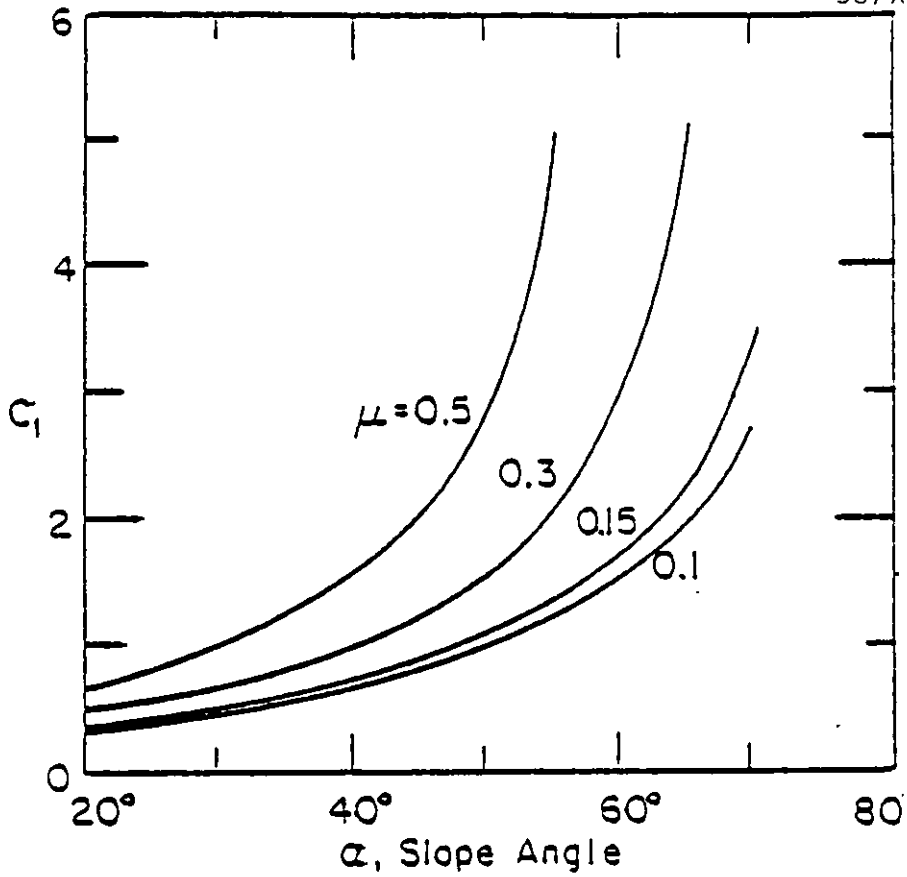


Figure 4.3: Coefficient C_1 as a function of slope angle α and friction factor μ (IAHR, to be published)

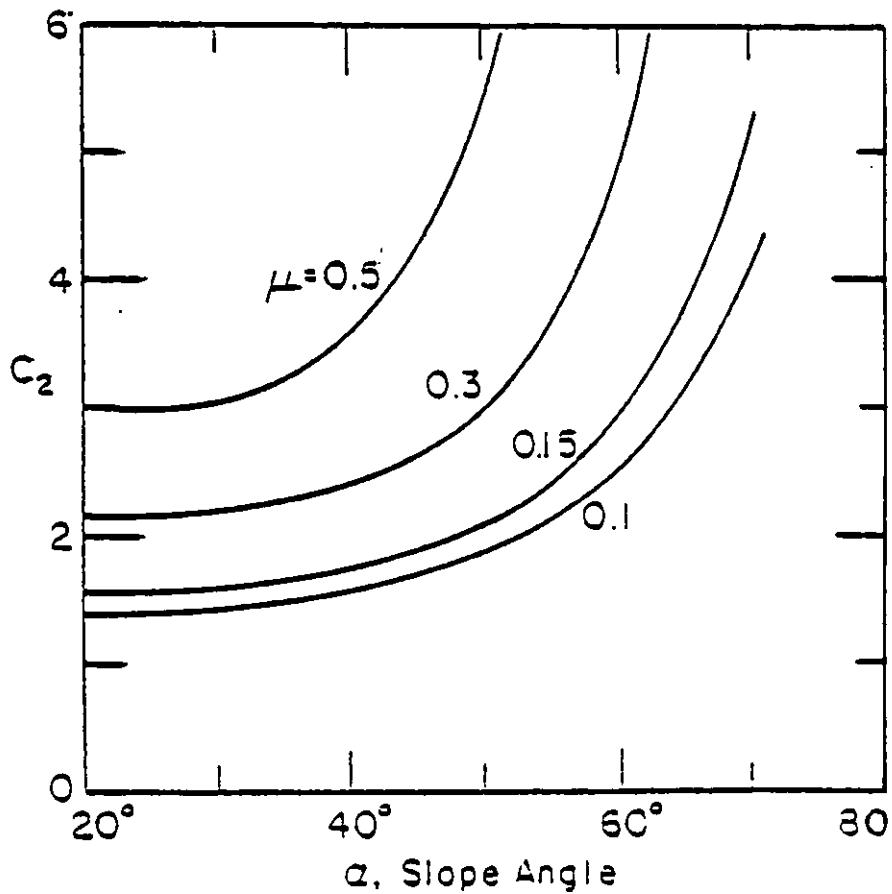


Figure 4.4: Coefficient C_2 as a function of slope angle α and friction factor μ (IAHR, to be published)

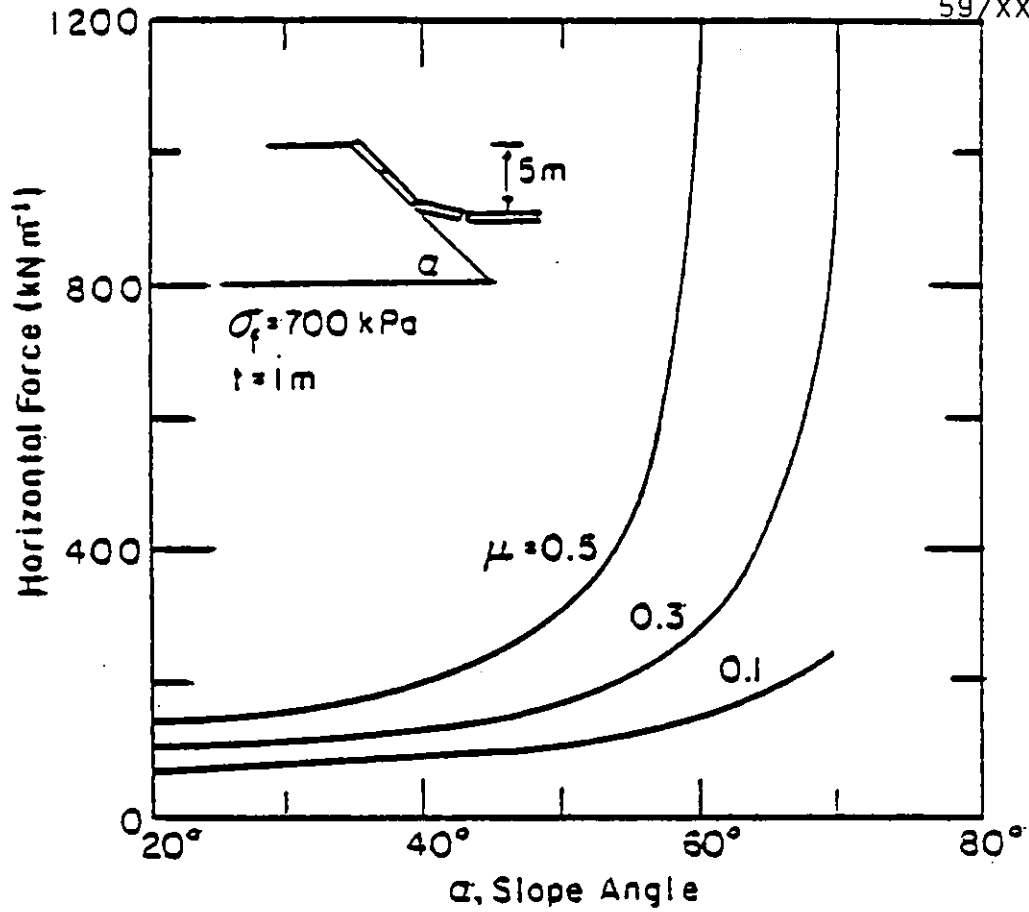


Figure 4.5: Horizontal force as a function of slope angle α and friction factor μ using simple 2-D theory (IAHR, to be published)

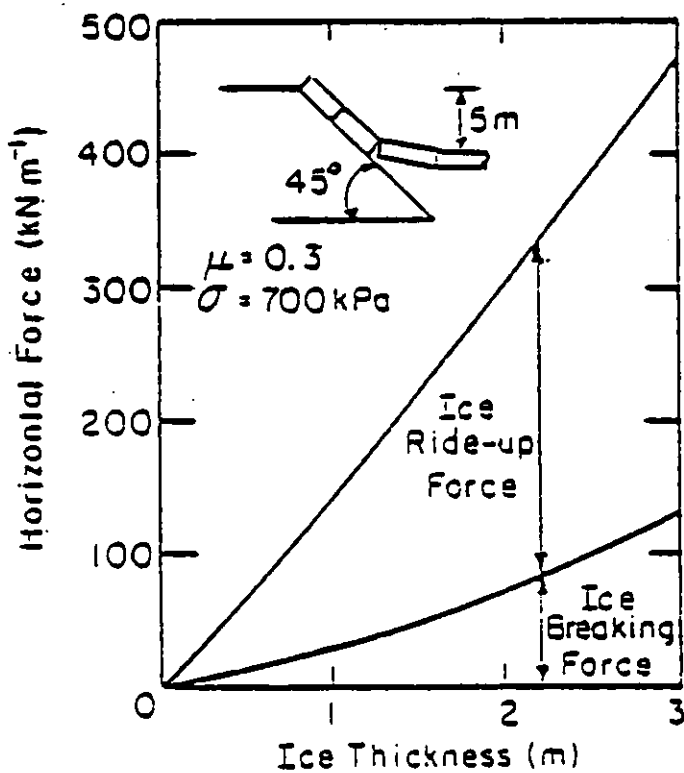
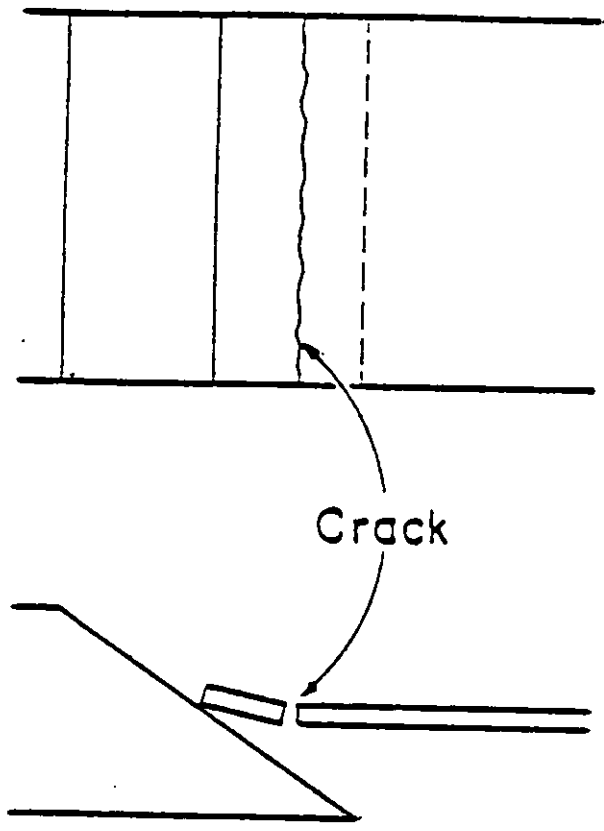
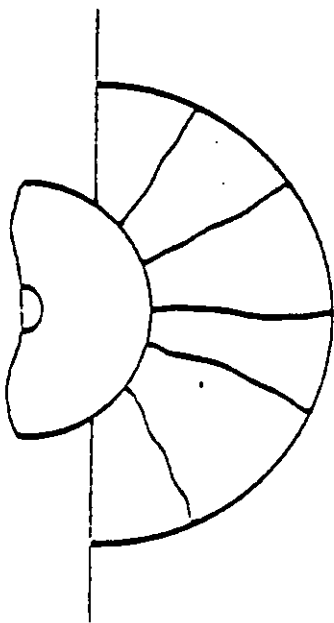


Figure 4.6: Horizontal force as a function of ice thickness using simple 2-D theory (IAHR, to be published)



Simple 2-D Theory



3-D Theory

Figure 4.7: Ice action on sloping structures: comparison between inclined plane and conical structure

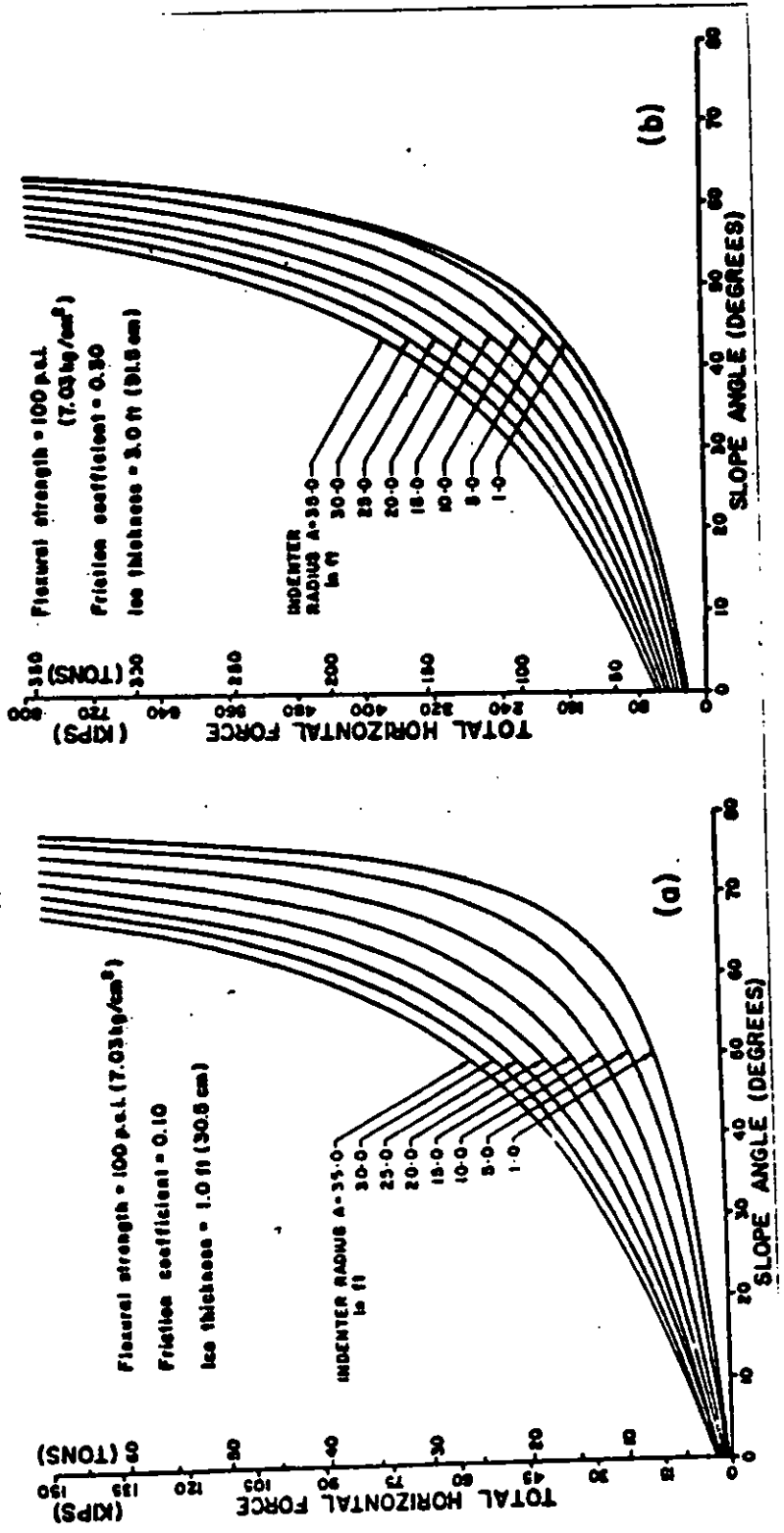


Figure 4.8: Horizontal force as function of slope angle and indenter radius for constant flexural strength, friction factor and ice thickness (after Danys and Bercha, 1976)

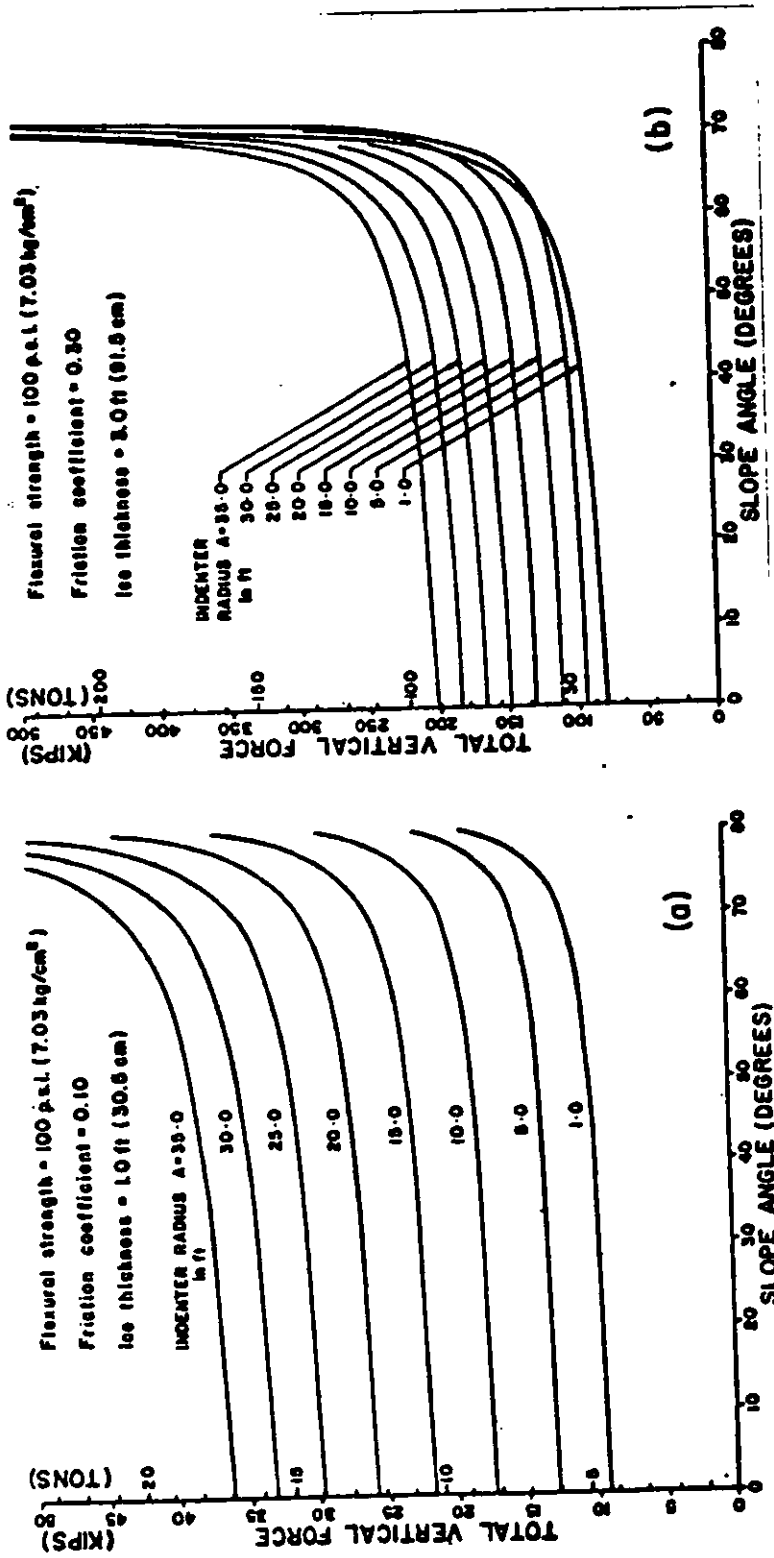


Figure 4.9: Vertical force as function of slope angle and indenter radius for constant flexural strength, friction factor and ice thickness (after Danys and Bercha, 1976)

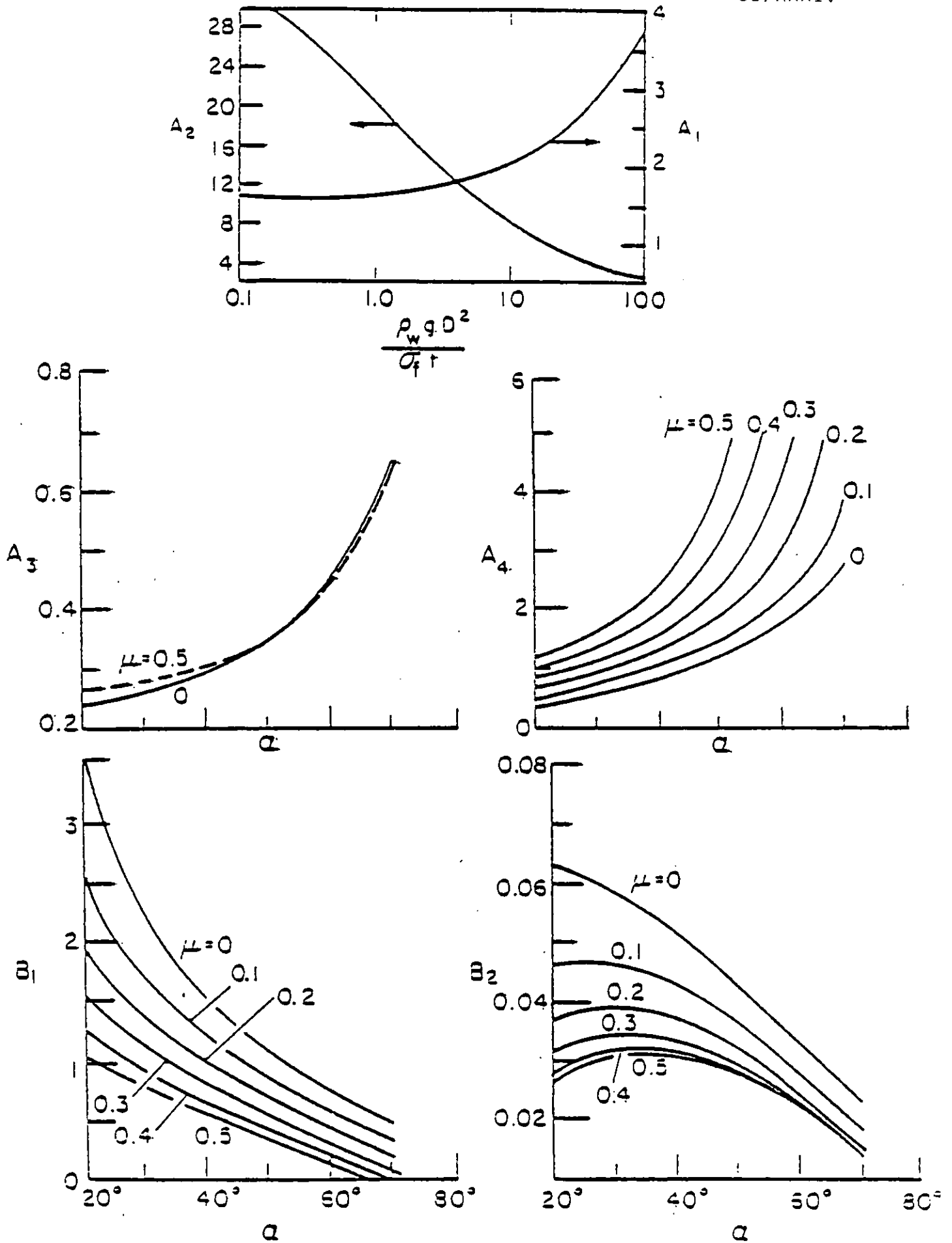


Figure 4.10: Ice force coefficients for plastic analysis (after Ralston, 1977)

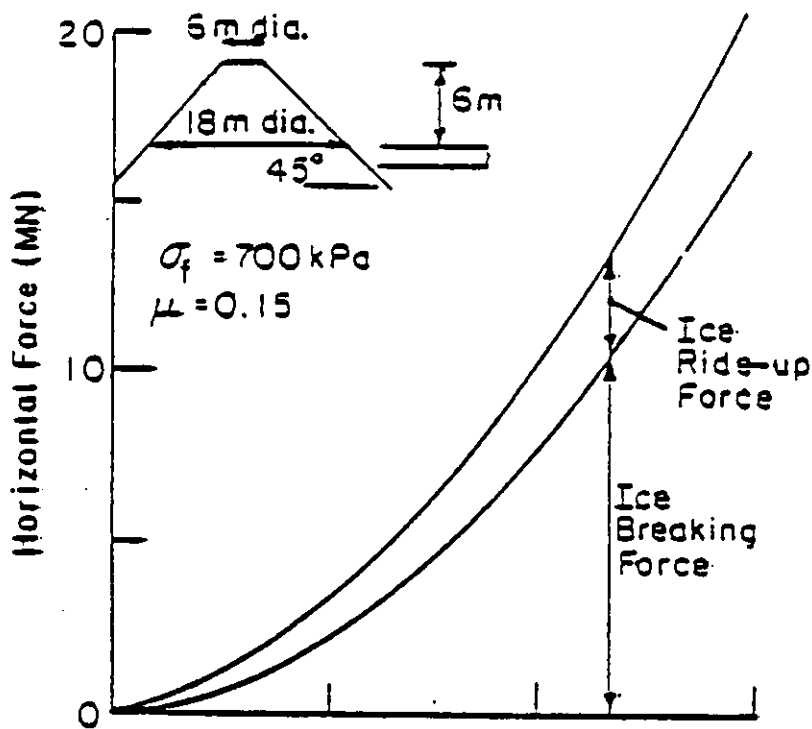


Figure 4.11: Horizontal force as a function of ice thickness for a narrow structure, using Ralston's (1977) theory (IAHR, to be published)

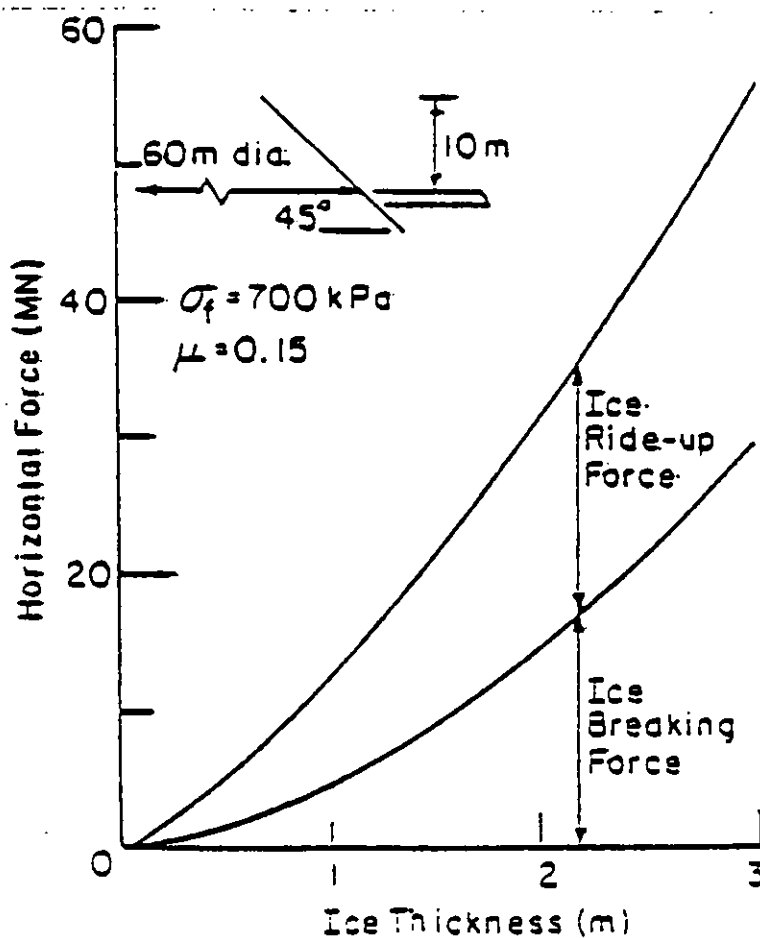


Figure 4.12: Horizontal force as a function of ice thickness for a wide structure, using Ralston's (1977) theory (IAHR, to be published)

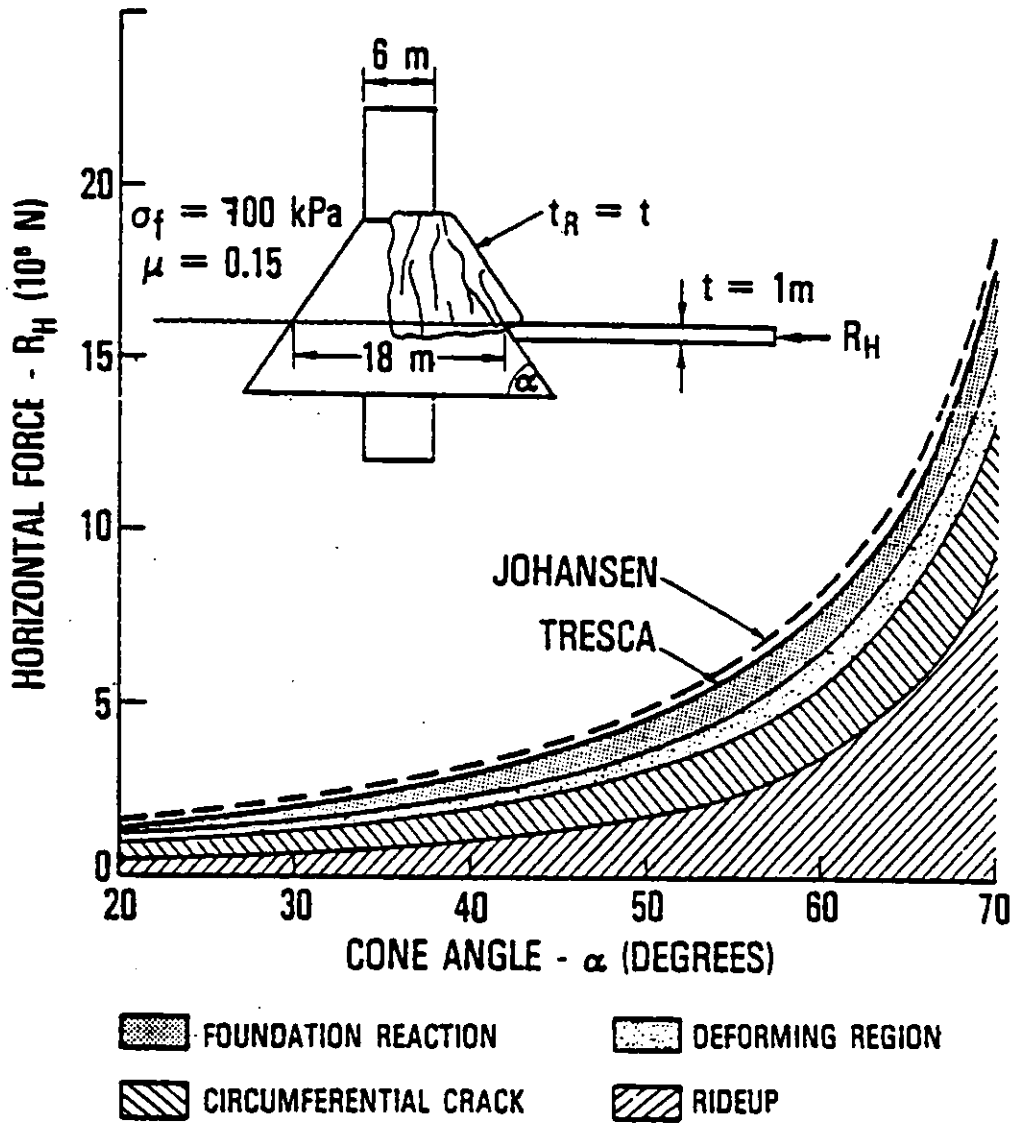


Figure 4.13: Ice forces on an upward-breaking cone (Ralston, 1979)

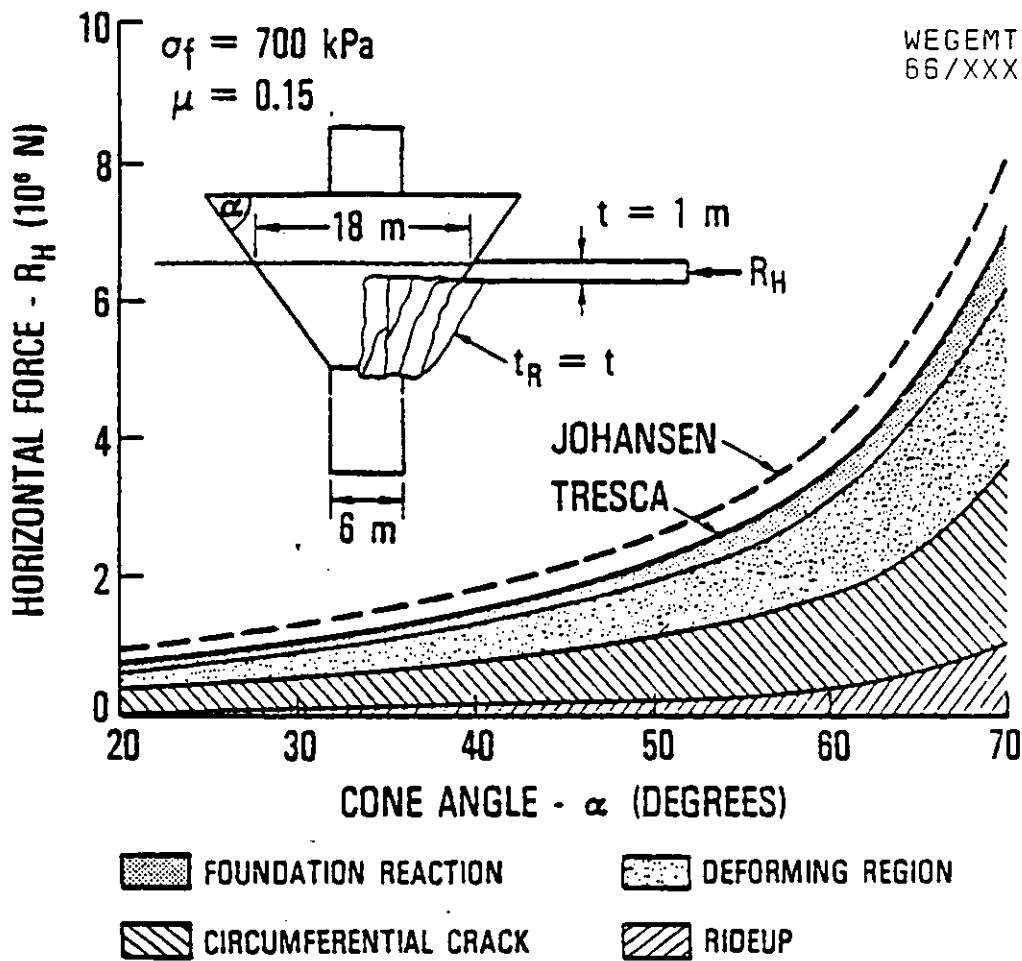


Figure 4.14: Ice forces on a downward-breaking cone (Ralston, 1979)

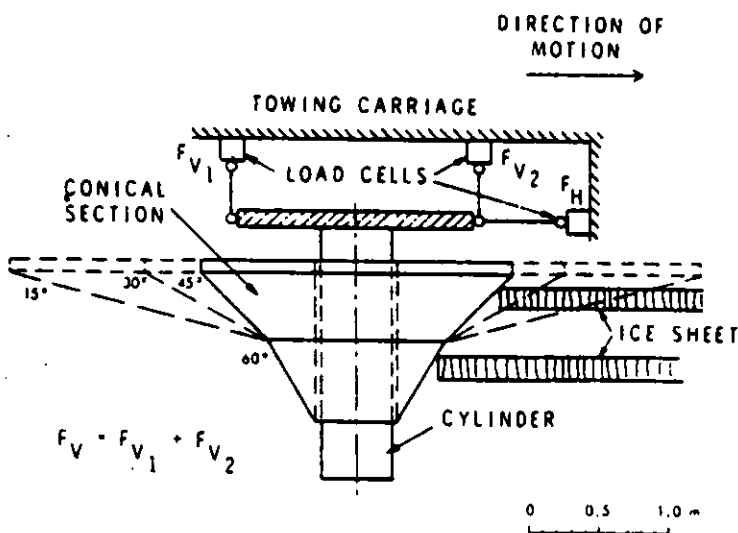


Figure 4.15: Schematic of fixed conical model structure (Schwarz et al, 1978)

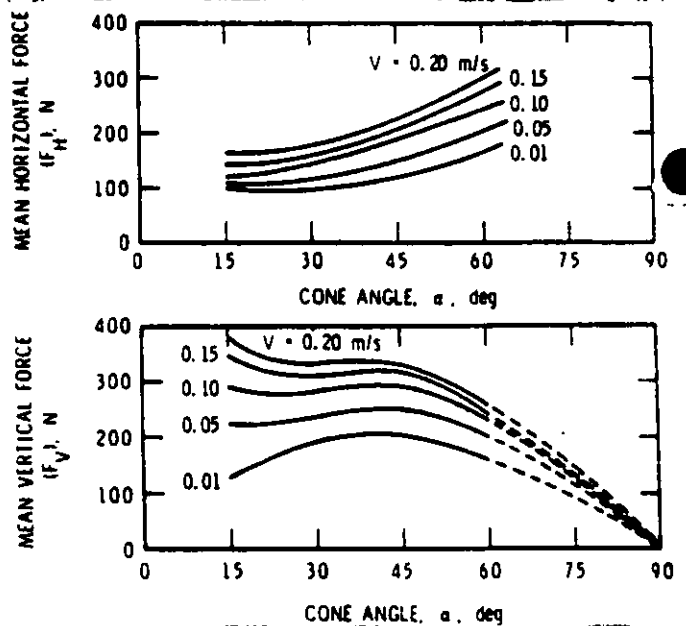


Figure 4.16: Influence of cone angle α on ice forces (Schwarz et al, 1978)

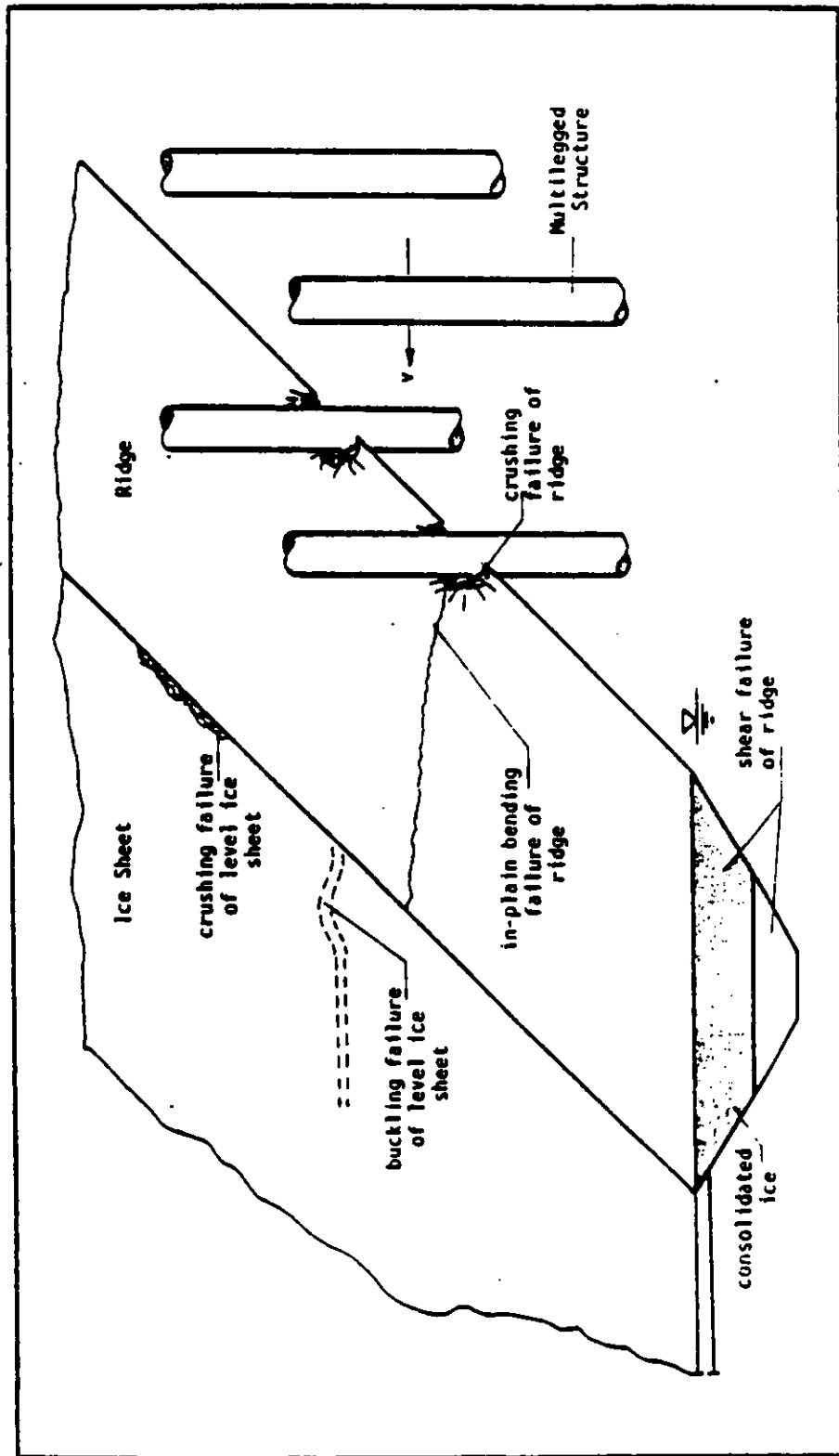
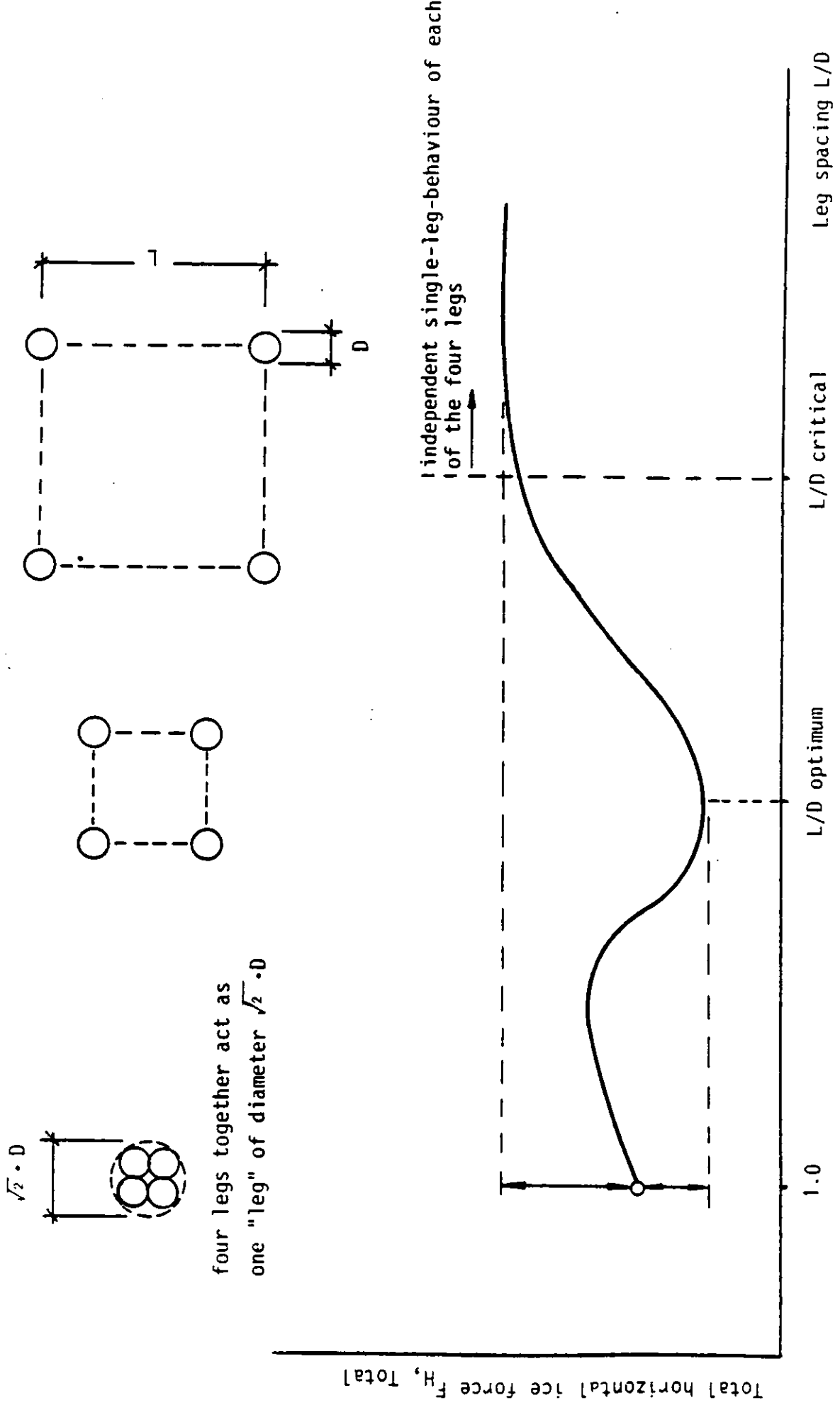


Figure 5.1: Failure modes of ridge and level ice sheet interacting with a multilegged structure



four legs together act as
one "leg" of diameter $\sqrt{2} \cdot D$

Figure 5.2: Total horizontal force on a four-legged platform versus leg spacing

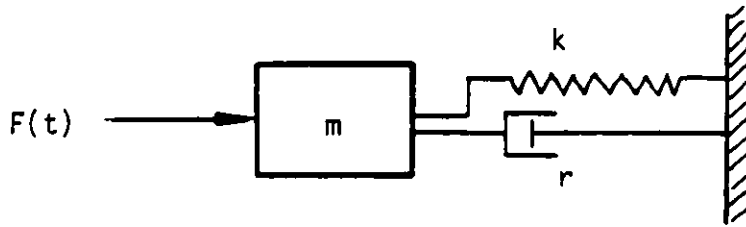


Figure 6.1: Mechanical analog for vibration analysis

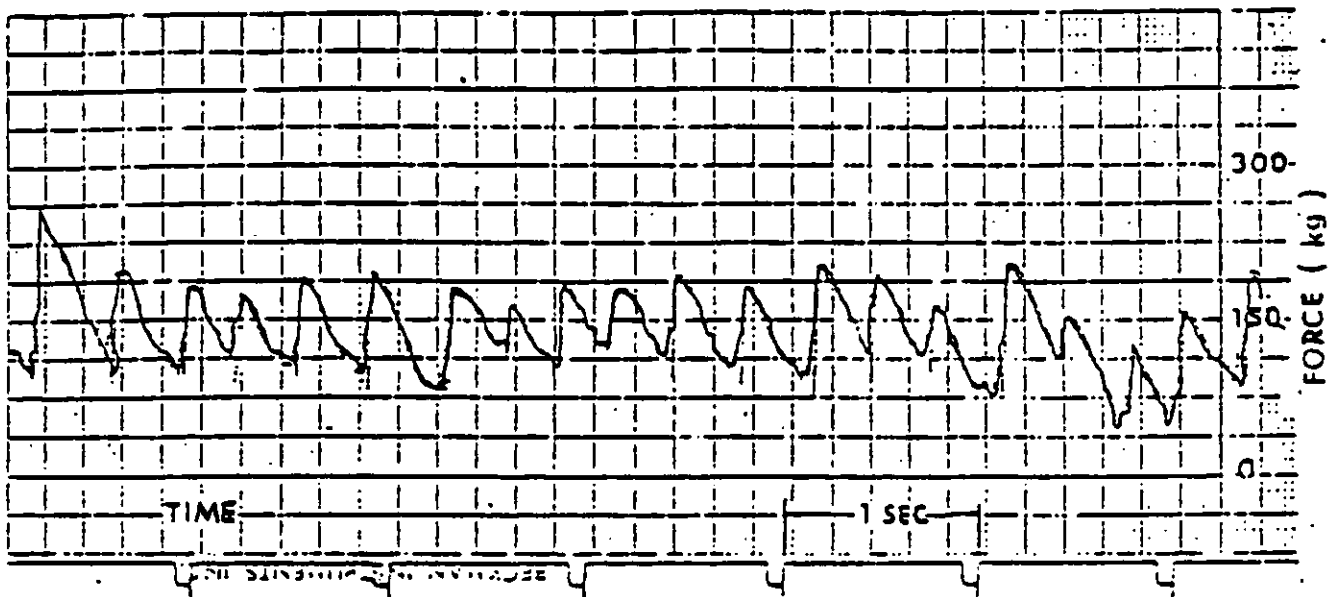


Figure 6.2: Periodic, asymmetric ice force record
(After Blenkarn, 1970)

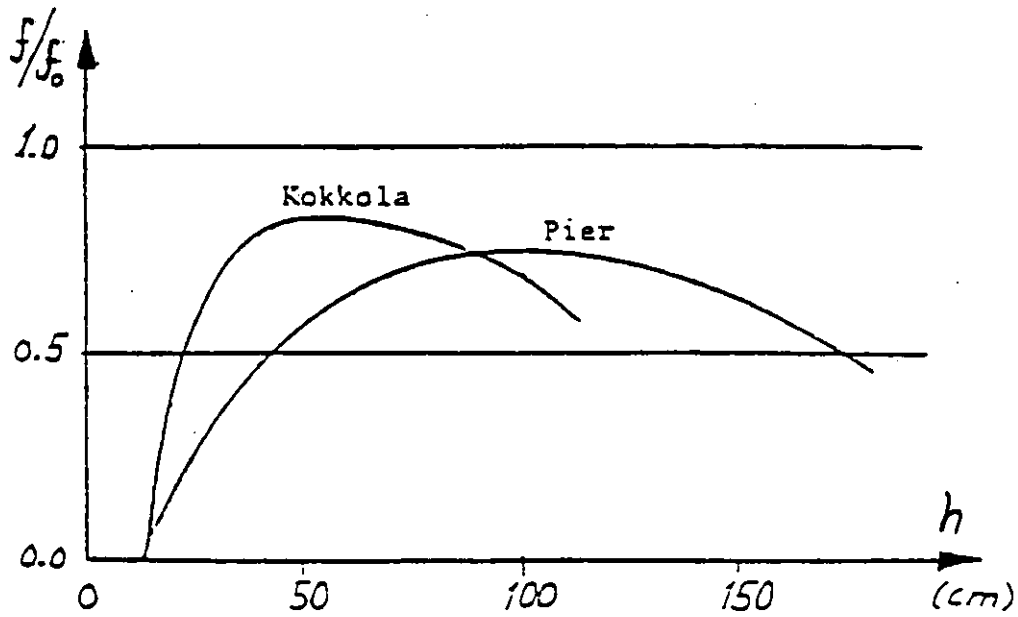


Figure 6.3: Observed oscillation frequencies as functions of ice thickness (after Määttänen, 1978)

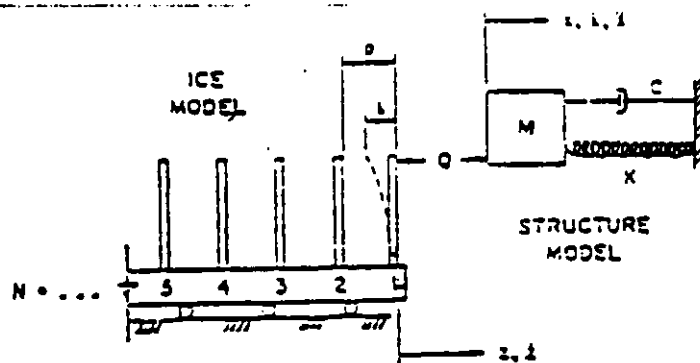


Figure 6.4: Matlock's mechanical analog for ice and structure interaction

Return Period	Depth (Ft.)	Width (Ft.)	Length (Ft.)	Sheet Thickness (Ft.)
90 day	45	155.9	∞	10
10 year	78.1	270.5	1000	10
100 year	115	398	500	15

Table 2.1: Ridge and sheet geometric properties (Bercha/Stenning, 1979)

Property	Significance	Sheet (Psi)	Ridge (psi)
Crushing Strength	U.B.	372	350
	Mean	240	230
	L.B.	108	180
Flexural Strength	U.B.	175	168
	Mean	100	95
	L.B.	0	0

Table 2.2: Mechanical properties of sheets and ridges (Bercha/Stenning, 1979)

Case No.	Ice Conditions to which Distribution Applies	Percent of Ridges in Each Height Category				
		0.75-1.5	1.5-3.0	3.0-4.5	4.5-7.0	6.0 + m
1	Landfast ice composed only of first year ice	73.0	25.2	1.3	0.5	
2	Landfast ice containing multi-year ice	68.3	28.6	2.5	0.3	
3	New ice cover on the shear zone during Nov. and Dec.	90.4	9.6			
4	Mackenzie mid-winter shear zone composed of first year ice only	64.9	32.0	2.7	0.4	
5	Alaskan mid-winter shear zone composed of first-year ice only	63.1	34.5	2.2	0.2	
6	Chuckchi mid-winter first year ice cover	77.0	21.8	1.1	0.1	
7	Alaskan and Mackenzie shear zone composed of multi-year ice	67.6	29.5	2.3	0.6	
8	Summer first-year ice conditions	77.1	20.5	1.9	0.5	
9	Summer ice composed of multi-year ice concentrations less than 5/10	81.8	15.2	2.7	0.3	0.001
10	Summer ice composed of multi-year ice concentrations greater than 5/10	84.8	14.0	1.1	0.1	0.001
11	All summer multi-year ice concentrations	84.1	14.0	1.7	0.2	0.01

Table 2.3: Recommended ridge height distribution for various ice conditions (HUDSON, 1982)

<u>Ice Feature</u>	<u>Inside Barrier Islands</u>	<u>Outside Barrier Islands</u>
Sheet Ice Thickness, ft.	7	7
Radtet Sheet Ice Thickness, ft.	7	15
First year Ridges keel depth, ft. sail height, ft. width at waterline, ft.	water depth AOGA Project #55 (1980) AOGA Project #55 (1980)	water depth AOGA Project #55 (1980) AOGA Project #55 (1980)
Multi year Ridges keel depth, ft. sail height, ft. width at waterline, ft.	water depth Wright (1978) Wright (1978)	water depth Wright (1978) Wright (1978)
Rubble Piles (grounded) width, ft. length, ft. sail height, ft.	300 1000 water depth	500 1000 water depth

Table 2.4: Guidelines for extreme ice features in the Alaskan Beaufort Sea (API, 1982)
(limited to 60 ft water depth)

structure	ice	relative velocity v_r
inelastic	inelastic	v_0
inelastic	elastic	$v_0 + \dot{\delta}_i$
elastic	inelastic	$v_0 - \dot{\delta}_s$
elastic	elastic	$v_0 + \dot{\delta}_i - \dot{\delta}_s$

Table 6.1 Types of ice-structure interaction models
(IAHR, unpublished)

Author	Year	f. Hz.	Remarks
Peyton	1966	1	Cook Inlet crushing failure
Kivisild	1969	0.1 - 0.5	No ice failure
Blenkarn	1970	0.1 - 1	Cook Inlet, failure and nonfailing
Neill	1976	0.5 - 5	Review, Canadian experience
Määttänen	1978	0.5 - 10	Gulf of Bothnia

Table 6.2 Observed ice force frequencies
(IAHR, unpublished)



Ice Action on Artificial
Islands and Wide Structures

BY

K. R. Croasdale

Notes for presentation at "Ships and Structures in Ice"; Seventh Graduate School of the West European Graduate Education - Marine Technology; Helsinki University, March 1983.

1.0 Introduction

Offshore drilling in the shallow waters of the Canadian Beaufort Sea commenced in 1973 from an artificial island. The main reason for using an island was because the presence of sea ice for nine months of the year prevented the use of more conventional methods.

At that time, industry had reviewed various alternatives for offshore drilling in the Arctic. These various concepts are shown conceptually in Figure 1. It is of interest to look back now (ten years later) and note that islands have been very effective out to about 20m, (with the newer retained islands now pushing 30m and beyond). Moreover, commencing in 1976, drillships have been used to drill wells in deeper water during the short summer season. (Figure 2)

Also, about a decade ago, we in the petroleum industry were considering various production concepts for the Arctic offshore regions. Some being considered at that time are shown conceptually in Figure 3.

Although no oil production has yet occurred from the Beaufort Sea, the production concept most favoured at this time is the artificial island. The recently compiled Environmental Impact Statement for the Canadian Beaufort Sea indicates that all three proponents (Dome Petroleum, Esso Resources Canada, and Gulf Canada Resources) see islands as the best form of production platform (at least initially).

This lecture will discuss the Canadian experience with artificial islands. However, islands for exploratory drilling are also being used off Alaska, but to date they have not been used in as deep water as off Canada.

Footnote on units:

The metric SI system has been used, however, some of the older material may contain Imperial units. In some places I have quoted both Kilopascals (KPa) and pounds per square inch (psi) for ice pressure. Newtons (N) have been used as much as possible for force units; in certain places I have also shown a tonnes (force) unit (not strictly correct).

2.0 History Of Canadian Beaufort Sea Islands

The summary description of the development of artificial islands provided in The Beaufort Sea - Mackenzie Delta Environmental Impact Statement (EIS) (Dome, Esso, Gulf - 1982) is quoted here

"The first offshore well in the Beaufort Sea was drilled by Imperial Oil in the winter of 1973 - 74. This well was drilled from the artificial island Immerk B-48, where construction had started using a stationary suction dredge in the summer of 1972. This island was constructed at a fairly sheltered location in the offshore delta in a water depth of 3 metres. The first winter demonstrated that the island could withstand the winter ice. After placing additional fill during the next summer, drilling commenced. Figure 4 illustrates drilling at Immerk B-48.

Up to the spring of 1982, industry has built and drilled from 20 artificial islands in the Arctic. Figure 5 shows the locations of these islands. Most have been built in the summer by dredging sand from the seafloor, but some have been constructed in winter by trucking gravel over the ice.

Construction efficiency has been gradually improved as working knowledge of the Arctic environment has increased. Table 2.1 summarizes basic information on artificial islands constructed and drilled from to date.

Most of the earlier islands used weighted slope protection materials such as sandbags to protect the relatively steep upper side slopes of the islands from wave and current erosion. The islands Netserk, Adgo and Kugmallit, were built this way.

Basic changes in building concepts were made as the water depth increased and as experience was gained. Sacrificial beach designs were introduced in 1976 with the construction of Arnak L-30. Arnak has been followed by Kannerk, Isserk, Issungnak and Alerk which are all of the sacrificial beach design. Figure 6 shows typical cross-section of sandbag retained islands and sacrificial beach islands.

As exploration from artificial islands moved into deeper-water, island designs have been refined and construction techniques improved; each new island being another step forward in the development of island building technology.

The Issungnak island completed in 1979, was built in 20 metres of water using material dredged near the site and supplemented with granular material hauled from Tuft Point. This deeper water island required 5 million cubic metres of material.

One problem with the conventional islands in deeper water is that although construction starts in the early summer, it cannot be completed until the fall. This time of year, though, is characterized by severe and frequent storms, which may interfere with the dredging operations and can result in erosion problems. At this time, the islands are particularly vulnerable to erosion until erosion protection measures are installed.

TABLE 2.1

BASIC INFORMATION ON ARTIFICIAL ISLANDS
(CANADIAN BEAUFORT SEA)

Island	Year Constructed	Water Depth m	Construction Season	Operator
Immerk B-48	1972-73	3	Summer	ESSO
Adgo F-28	1973	2	Summer	ESSO
Adgo P-25	1974	2	Summer	ESSO
Pullen E-17	1974	1.5	Summer	ESSO
Netserk B-44	1974	4.5	Summer	ESSO
Adgo C-15	1975	2	Summer	ESSO
Ikattok J-17	1975	2	Summer	ESSO
Netserk F-40	1975-76	7	Summer	ESSO
Unark L-24	1974-75	2	Winter	Sunoco et al.
Pelly D-35	1975	2	Winter	Sunoco et al.
Sarpik B-35	1976	3.5	Winter	ESSO
Kugamallit H-59	1976	5	Summer	ESSO
Adago J-27	1976	2	Summer	ESSO
Arnak L-30	1976	8.5	Summer	ESSO
Kannerk G-42	1976	8	Summer	ESSO
Isserk E-27	1977	13	Summer	ESSO
Issungnak O-61	1976-79	20	Summer	ESSO
Alerk P-23	1980-81	11.5	Summer	ESSO
West Atkinson	1981	7	Summer	ESSO
Tarsiut N-44	1981	22	Summer	Gulf Canada
Uviluk P-66	1982	31	Summer	DOME
Itiyok I-27	1982	15	Summer	ESSO

As islands were built in deeper water, economics necessitated changes in geometry to reduce fill volume requirements. Since the island is a cone, the volume of material required is very sensitive to water depth and side slope of the berm (Figure 7). Thus, it is apparent that steeper sides slopes minimize fill volume and reduce cost.

This rationale led to the design of the Tarsiut island which was built in 1981 (Figure 8) The sand berm does not extend to the surface and the side slopes of 1 in 5 to 1 in 7 are steeper than those at the Issungnak island, which are about 1 in 15. Concrete caissons are placed on top of the berm to penetrate the wave zone and once filled with sand, form a foundation for the drilling equipment.

The Tarsiut island required approximately 1.5 million cubic metres of fill material, which was obtained from subsea borrow areas approximately 65km and 10 km from the island.

The Tarsiut island is also a research platform, being heavily instrumented in order to continue measurement of ice forces. The data obtained from monitoring of ice forces and behaviour at Tarsiut will help to further refine the design of other deep water artificial islands. As more experience is obtained refinements are made to concepts and design details of islands and caissons currently under development.

The Esso caisson retained island (Figure 9) is already in the Beaufort. The Gulf Mobile Arctic Caisson (Figure 10) is being constructed. Dome's single steel drilling caisson is placed at Uviluk and drilling".

A summary of the related research is also provided in the EIS and this is also quoted here because it traces the development of our understanding of ice interaction which I shall be presenting later in this lecture.

"Canadian industry has been conducting research on ice interactions and island building technology in the Beaufort Sea for over a decade. Design have been developed that are capable of withstanding extreme ice conditions in water up to 60 metres deep. Figure 11 illustrates the major design criteria requirements and the corresponding types of research that have been conducted The successful construction and operation of over 20 exploration islands in water up to 22 metres deep has provided experience which contributes to the design of islands in deeper water.

Much of the research has been conducted through co-operative programs of the Arctic Petroleum Operators Association (APOA), an association of petroleum companies with interest in the Canadian Arctic. Due to the high costs of research in the Arctic, the association was formed to provide a vehicle for cost sharing. Research projects are proposed and operated by individual members. Other members can then voluntarily participate in any project, by sharing in the cost of the project in return for the data. This research has contributed significantly to an increased knowledge of ice and its interation with structures.

In 1969, research and data - gathering activities began with the purpose of providing technology for offshore drilling in the ice-infested waters of the Beaufort Sea. The approach was to consider bottom founded structures, which would have the ability to withstand the loads imposed by moving ice. This required knowledge of the ice environment, as well as the lateral forces exerted by ice as it failed against the structures.

At that time, available technology was inadequate to deal with the problem. Some experience had been gained in Cook Inlet, Alaska, in dealing with sub- Arctic ice, and bridge piers in ice-infested rivers had been standing up for centuries. Even so, the action of Arctic ice on fixed structures was considered to be a unique problem, owing to the greater strength, thickness and lower temperature of the ice.

Several study areas have been pursued, including general ice conditions and behaviour, extreme ice features, and ice strength and forces. Information on ice behaviour and ice conditions have been systematically collected each year since the early 1970's in the shallow waters of the Beaufort Sea (Spedding, 1974, 1981) and in the deeper water areas (McGonigal and Wright, 1980; Wright et al., 1981).

The first experimental Arctic offshore research project investigated the action of an Arctic ice sheet against a vertical pile-type structure (Croasdale, 1970, 1974). This "Nutcracker Project" was so called because of the special devices, resembling giant nutcrackers, which were used to measure the crushing strength of ice against circular piers. The Nutcracker tests provided valuable design data, but also indicated the presence of a size effect, which made it difficult to extrapolate the ice failure strengths to those relevant to large structures. It became obvious that an intensive research effort was required to more fully understand the importance of various ice and structure parameters on ice loading.

It was from this realization that the research effort into ice blossomed. There were many facets to subsequent studies. Experimental ice indentation tests were done on lake ice at intermediate scale with specially designed apparatus (Taylor, 1973; Miller 1974). Similar tests were conducted at smaller scale on thin ice sheets in a cold room. Field measurements of ice behaviour and ice properties continued (Kry, 1973; Gladwell, 1976). A large outdoor ice test basin was constructed to observe and record ice loading on structures (Verity, 1975). The following outlines some of this work.

The portable field test apparatus constructed for indentation measurements was used at Eagle Lake, a freshwater lake, near Calgary. It consisted of two steel load faces separated by powerful hydraulic cylinders supported in a gantry. The load faces were forced apart in the ice sheet and the failure loads recorded. Three consecutive years of measurements were taken to obtain data on the effect of various parameters. These included the dependence of aspect ratio (indenter width/ice thickness) on the crushing strength of ice, as well as the effect of indenter shape, indenter-ice bonding, temperature and loading rate. Follow-up experimental work using the same apparatus investigated the buckling characteristics of ice at large aspect ratios (Trofimenkoff, 1975). Field test results were correlated with the mechanical properties determined from cold room laboratory experiments.

These tests identified the ice failure modes for different loading rates and showed that they were an important factor in determining the ice failure strength. Furthermore, these tests, as well as observations of the crushing failure of ice against artificial islands (Gladwell, 1977) and cold room experiments, indicated that the ice did not fail simultaneously in the entire interaction region. Rather, at any one time, different local areas of the interaction region were in different stages of failure. In other words, it appeared appropriate to consider the failure region divided into a number of independent zones, with the number of zones increasing as the structure width increased.

These observations indicated that the design stress for a wide structure should be less than for a narrow structure (Kry, 1979, 1980). A stochastic model was developed, which quantified the decrease in design stress for wide structures, compared to narrow structures. This allowed prediction of ice stresses on artificial islands based on data obtained from tests on continuous crushing of lake ice and in the cold room.

Further direct measurements of ice pressures around islands (Strilchuk, 1977), the observation of ice failure modes around islands, additional continuous crushing measurements at Eagle Lake, and segmented indenter tests in the cold room, added to confidence in the stochastic model for predicting ice failure loads in the interaction zone at an island or other structure.

The presence of ice rubble fields around islands complicated the application of ice failure loads in the interaction zone to a load on the island (Kry, 1977). However, recent work in monitoring the formation, nature and stability of ice rubble fields has added to the knowledge of how they influence the stability of the structure which they surround.

Concurrent with the above studies, experimental data were being gathered on the interaction of ice with conical structures. The main reason for considering conical structures was the reduction in ice force one could expect through bending rather than crushing. This was of particular importance where impact with multi-year ridges could be expected.

To provide confirmation of earlier theoretical and small scale modelling, a large open air ice test basin was constructed in Calgary in 1973. Initially, this Canadian facility was used to test a 45° cone structure at approximately one tenth scale using sheet ice and ridges. The cone was instrumented to measure horizontal and vertical forces and record the ice failure modes. In subsequent years, tests were also conducted on model artificial islands (Semeniuk, 1976) a section of a caisson retained island (Rosenegger 1977) and recently on a 30° conical structure. Field programs to measure the flexural strength of Arctic ice complemented this work (Kry 1975). Of particular interest was the determination of the strength of multi-year ice ridges in the Beaufort Sea (Gladwell 1976).

More recently, research has been conducted at Hans Island, a natural island in the High Arctic, situated in the Kennedy Channel between Ellesmere Island and Greenland. Each summer when the ice breaks up, large multi-year ice floes move down the channel and collide with this rocky island. Measurements obtained here are the first compiled for the interaction between thick multi-year ice and a large structure, and simulate the interaction expected at a large Beaufort Sea platform. Finally, ice forces are being measured on the Tarsiut artificial island, which is considered a prototype of future deep water production platforms."

3.0 Summary Of Arctic Coastal Ice Features

In order to set the scene for the discussion on ice interaction, it is necessary to define the types of ice features which have to be considered in the design of structures for the southern Beaufort Sea.

What follows is only a brief summary as it is assumed that previous speakers at this school have covered this topic in some detail. This summary is given in the form of copies of the overheads (slides) which have been given by the author during previous talks on the topic. Slides showing ice features will also be shown as time permits. (Figure 12 to 17 are part of this section).

ARCTIC COASTAL ICE FEATURES

OVERVIEW

- ICE PRESENT OVER MOST OF ARCTIC OCEAN FOR MOST OF THE YEAR
- ICE CLEARS FROM THE COASTAL ZONE FOR ONLY ONE TO THREE MONTHS
- FREEZE-UP COMMENCES SEPTEMBER / OCTOBER
- BREAK-UP COMPLETE JULY / AUGUST
- FAST ICE GROWS OUT FROM SHORE TO REACH 20 - 25 M WATER DEPTH BY JANUARY
- EXCEPT CLOSE TO SHORE, ARCTIC ICE IS HEAVILY RIDGED
- POLAR PACK CONTAINS MULTI-YEAR ICE, RIDGES AND HUMMOCK FIELDS
- ICE ISLANDS CAN OCCUR BUT ARE RARE

FAST ICE

- SMOOTH NEAR SHORE (AND BETWEEN ISLANDS)
- SALINE ICE EXCEPT NEAR RIVER MOUTHS
- REACHES ABOUT 2 METRES THICK, NORMAL MAXIMUM (BUT CAN BE RAFTED AND RIDGED)
- MOVES UNDER ACTION OF THERMAL STRAIN, WIND STRESS AND PRESSURE FROM POLAR PACK
- MOVEMENTS GENERALLY AT A LOW RATE (LESS THAN 1 M / HR). USUALLY
THAN 3 METRE TOTAL MOVEMENT PER EXCURSION
- SOMETIMES MOVEMENTS OF SEVERAL 100 METRES OCCUR
(NEAR THE EDGE OF THE LANDFAST ICE)

FAST ICE

- EXTENT OF FAST ICE DEVELOPS FROM 5 - 6 METRES WATER DEPTH IN EARLY WINTER TO 20 - 25 METRES DEPTH BY JANUARY
- EXTENSIVE MOVEMENTS OUTSIDE THE 6 METRE DEPTH DURING NOVEMBER AND DECEMBER CAUSE CONSIDERABLE RIDGING (OFTEN GROUNDED)
- DURING BREAK-UP LARGE SHEETS OF PREVIOUSLY FAST-ICE, 10 to 15 km ACROSS, MOVE THROUGH THE AREA
- MULTI-YEAR ICE CAN BE PRESENT IN THE FAST-ICE FROM PREVIOUS FALL
- STATIONARY PERIODS COMBINED WITH SMALL TIDES CAN LEAD TO ADFREEZE OF ICE ON STRUCTURES

PACK ICE

(SOMETIMES CALLED POLAR ICE ON POLAR PACK)

- CAN BE FIRST-YEAR OR MULTI-YEAR ICE
- CHARACTERIZED BY LARGE "YEAR-ROUND" MOVEMENTS (UP TO SEVERAL KM/DAY)
- SHEAR ZONE SEPARATES FAST ICE AND PACK ICE
- SHEAR ZONE HEAVILY RIDGED: OPEN LEAD OFTEN PRESENT WHEN WINDS OFFSHORE
- IN THE CANADIAN BEAUFORT SEA, A TRANSITION ZONE OF MAINLY FIRST-YEAR ICE (BUT MOBILE) EXISTS BETWEEN FAST ICE AND POLAR PACK
- MULTI-YEAR RIDGES AND FLOES VERY COMMON
- ALWAYS A SMALL PERCENTAGE OF THIN ICE AND / OR OPEN WATER
- NORMAL MULTI-YEAR ICE THICKNESS IS ABOUT 3 TO 4 METRES
- TYPICAL MAXIMUM MULTI-YEAR RIDGE THICKNESS IS ABOUT 16 METRES
- EXTREME MULTI-YEAR FLOES CAN BE UP TO 50 METRES THICK
- PACK ICE CAN INVADE IN SUMMER (QUICKLY!)
- OCCASIONAL ICE ISLAND EXISTS IN PACK ICE (UP TO 55 METRES THICK)

WEGEMT 1983
11/XXXV

K.R. CROASDALE
1983

FIRST YEAR RIDGES

- USUALLY FORMED FROM RELATIVELY THIN ICE IN LEADS (AT SHEAR ZONE)
- INITIALLY AN ACCUMULATION OF ICE RUBBLE HELD TOGETHER BY BUOYANCY AND FRICTION
- SLOWLY REFREEZE
- ARE THE GENESIS OF MULTI-YEAR RIDGES
- OFTEN GROUNDED OUT TO 20 - 25 METRES OF WATER
- IN DEEPER WATER CAN BE 50 METRES THICK OR GREATER
- KEEL TO SAIL HEIGHT ABOUT 4.0
- SELDOM GOVERN ICE LOADS ON STRUCTURES
- INTERFERE WITH OVER-ICE TRANSPORTATION
- CAN CAUSE SEA FLOOR SCORING
- THEIR FORMATION IS A STRESS RELIEVING MECHANISM WHICH MAY HELP LIMIT FORCES ON LARGE STRUCTURES

MULTI-YEAR RIDGES AND HUMMOCK FIELDS

- FULLY CONSOLIDATED
- NEAR-FRESH ICE AND RANDOM STRUCTURE (TOUGH)
- 16 METRE THICKNESS NOT UNCOMMON
- MAXIMUM THICKNESS COULD BE UP TO 50 METRES
- MULTI-YEAR HUMMOCK FIELDS SEVERAL KM ACROSS AND WITH LOCAL THICKENINGS UP TO 50 METRES HAVE BEEN OBSERVED OFF THE CANADIAN ARCHIPELAGO
- EXTREME MULTI-YEAR HUMMOCK FIELD FOR DESIGN MAY BE ABOUT 10 KM x 10 KM IN AREA WITH EXTENSIVE (1 KM) LOCAL THICKENINGS 50 M THICK. SUCH A FEATURE WILL GOVERN THE DESIGN OF OFFSHORE STRUCTURES IN DEEPER WATER (50 M OR GREATER)

ICE ISLANDS

- ICE-SHELF ICE (FRESH)
- CALVE OFF THE NORTH WEST COAST OF ELLESMERE ISLAND
- 20 - 60 METRES THICK
- CAN BE SEVERAL KM ACROSS
- COMPARABLE TO EXTREME MULTI-YEAR HUMMOCK FIELD AS THE MOST HAZARDOUS ICE FEATURE TO CONTEND WITH
- LOW ICE-ISLAND POPULATION MAY JUSTIFY NOT DESIGNING FOR THEM (RETURN PERIOD FOR COLLISION FOR LARGE ICE ISLANDS MAY BE GREATER THAN 500 YEARS)

K.R. CROASDALE
1983

ARCTIC COASTAL ICE FEATURES - DESIGN IMPLICATIONS

WATER DEPTH

● 0 TO ABOUT 3 METRES

TYPICAL DESIGN CONSIDERATIONS

- DESIGN FOR SLOW MOVING SEA ICE UP TO 2 M THICK
- SEA ICE COULD BE FRESH NEAR RIVER MOUTHS
- CAN DEFEND

● 3 METRES TO ABOUT 20 METRES
(FAST ICE ZONE)

- DESIGN FOR FAST MOVING SHEET ICE UP TO 2M THICK
- DESIGN FOR FAST MOVING MULTI-YEAR RIDGES AND FLOES THICK AS WATER DEPTH PLUS STORM TIDE
- CONSIDER ADFREEZE
- CONSIDER ICE RIDE-UP

● 20 METRES PLUS

- DESIGN FOR MULTI-YEAR RIDGES & FLOES UP TO 50 METRES THICK (RISK ANALYSIS)
- SHEET ICE REFROZEN RUBBLE FIELDS UP TO 5 METRES THICK
- CONSIDER ADFREEZE
- CONSIDER ICE ISLANDS (RISK ANALYSIS OR DEFENCE)
- CONSIDER ICE RIDE-UP

4.0 General Logic For Ice Forces

An overall logic for ice forces as proposed by the author in 1980 (Croasdale, 1980) is shown in Figure 18.

The forces transmitted to a structure by the ice are generated by natural forces such as winds, currents or thermal strains. These natural forces can be concentrated on the structure by large ice sheets and represent an upper limit for the ice forces. The more usually addressed upper limit for the ice forces, is the force to fail the ice against the structure in the easiest mode of ice failure. Sometimes one can select the mode of failure which gives the lowest force but often one has to check several modes.

Another consideration relates to the clearance of ice around the structure; if ice rubble builds-up on the structure the mode of ice failure (and hence the force) can change.

Environmental driving forces can be calculated separately and compared with ice interaction forces to indicate the design force.

Environmental factors such as rate and magnitude of ice movement also input to other parts of the logic diagram as shown.

For the ice interaction force, the mode of ice failure is the most important factor to consider. Intuitively one can expect ice crushing against vertical structures. However it is well known that thin ice can buckle at lower forces than crushing. Furthermore ice rubble in front of a vertical structure can lead to bending failure in a similar way to the formation of first-year ridges. Bending failure will occur against a sloping structure, but the presence of re-frozen rubble or high friction due to ice freezing to the structure can lead to ice crushing at higher loads. All these possibilities may have to be considered.

The ice-type governs both the failure mode and the actual interaction force. Such factors as thickness, ridge shapes and sizes, crystal structure, salinity, and temperature are known to be important and will need to be specified.

Structure shape has already been discussed in terms of side angle. For sloping structures, the friction between the ice and the sides is also important in determining the horizontal force. In addition, the width of the structure will influence two things; first the way ice rubble clears around the structure; and second whether ice failure is simultaneous across the full width of the structure.

For certain low-freeboard structures the problem of ice encroaching onto the structure may have to be considered. As shown in the logic diagram, such factors as structure shape, extent of ice movement and characteristics such as strength or thickness will all have to be considered in determining the extent of ice ride-up or pile-up on the structure.

In a later publication (Croasdale and Marcellus, 1981), the concepts of "limit stress" and "limit force" were defined (Figure 19). The "limit stress" load being the force limited by local ice failure in front of the structure; the "limit-force" load being limited by the environmental driving forces. For very thick ice features, once the initial kinetic energy of the features, has been dissipated, then it appears as though "limit-force" loads apply. In this case they are governed by ridge-building in the surrounding pack ice plus wind and current drag (see Figure 20).

A more comprehensive logic involving the probabilities of extreme ice feature occurrences and ice velocity statistics is shown conceptually in Figure 21. This approach has been used in the work done recently for the Beaufort Sea EIS partners (Marcellus and Roth, 1982). A typical output is shown in Figure 22 for a hypothetical structure in 60m of water.

5.0 Ice Action On Wide Structures

Observations of ice action against artificial islands in the Beaufort Sea have given us insight into how ice fails against wide structures, particularly for first-year ice in the winter. Observations indicate that the advancing ice has difficulty clearing, and a rubble field of broken ice is formed on the front of the structure. (Croasdale and Marcellus, 1977; Garrett and Kry, 1977; Kry, 1980). See Figure 23.

The presence of the rubble field has a significant influence on the subsequent ice action.

5.1 Limit-stress loads (mixed-mode failure)

As itemized in Figure 23, the ice rubble will usually ground on the slopes of an artificial island and the active zone of ice failure moves to the outside of the grounded rubble. Observations indicate that the ice failure mode will depend on the thickness and constancy of ice motion but in general we see multi-zones of ice failure across the width. It is quite possible that in some zones ice crushing occurs whilst in others the ice may fail in flexure or by buckling. The net result being a lower average ice force across the width of the active zone than is usually the case for crushing against a narrow structure.

Kry, 1980 (Figure 24) gives some typical forces for various types of failure; ranging from 0.05 MNm for flexure in the early winter to a typical force of 3MNm for a zone of crushing which might occur later in the winter.

As illustrated conceptually in Figure 25, the rubble has two significant effects; it lowers the average force for mixed failure mode in the active zone; furthermore the actual shape of the structure at the water-line becomes irrelevant to the forces being generated.

In the copies of the overheads which follow, (Fig. 26 - 30) a short review of the mixed mode of ice failure against rubble is given. All the investigators who have considered this phenomenon have generally obtained results for average ice pressures which are below 50 psi (0.35 MPa). Such values have not yet been proven but seem to be compatible with observations of the stability of grounded rubble (which we will discuss later). For a more detailed review of mixed mode ice failure against ice rubble you should read Assur, 1971; Kry, 1977; Kry, 1980; Bercha and Ghoneim 1980, Berch et al 1980, Allyn and Wasilewski 1979, Allyn, 1980.

5.2 Limit-stress loads (crushing)

Despite the potentially lower forces which a rubble field may lead to (because of mixed-mode failure), there are still situations where pure crushing across a wide structure can occur and lead to higher forces. Two situations come to mind. The first is if the ice has been almost stationary for several months (land-fast ice); the ice thickens at the active zone so that when it does move, the likelihood of mixed mode failure is reduced. The second is if multi-year ice impacts against a vertically-faced structure during a polar ice invasion in the summer months or early autumn.

Ice crushing against a vertical-faced narrow structure has already been addressed by a previous lecturer. At sufficiently high strain rates brittle failure occurs. If there is initially a good fit (contact coefficient = 1.0) between structure and ice, then the highest ice pressure (force divided by structure width and ice thickness) occurs with the first failure.

Subsequent peaks (with a more random contact) are lower; this is illustrated in Figure 32. (Michel and Toussaint, 1979).

On a wide structure, that is one which is wider than about 4 to 5 thicknesses, field observations indicate that non-simultaneous crushing occurs across the structure. This observation led to the development by Kry (1980) of a model which accounts for this mode of failure. The basis for the model is illustrated in Figure 33. The interaction width is divided into a number of statistically independent zones. The effective ice pressure over the entire width is the average of the simultaneous local ice pressure values. Intuitively one can appreciate that this average effective ice pressure will be less than the maximum on any single zone. A design ice pressure can be estimated associated with a particular risk of exceedance based on expected ice movement (or penetration of the extreme multi-year ice event around the structure).

As illustrated in Figure 34 this theory yields results which show a lower effective design stress as the structure width increases.

Another phenomenon which tends to reduce effective ice loads across wide structures is the tendency for brittle materials to have lower strength as the volume of material under load increases. This so-called size effect is not yet well understood, but efforts are currently underway to develop an understanding using fracture mechanics and theories developed for rocks and coal. (Iyer, 1983).

5.3 Other aspects of limit-stress loads on shallow water islands

(Figure 35)

In very shallow water when the ice is landfast, a frozen-in ice condition can occur. Such a condition can theoretically lead to very high loads if the ice should suddenly start to move. Fortunately such movements in very shallow water are unlikely. Furthermore, defensive slots can be implemented to avoid the frozen-in condition (Croasdale and Marcellus, 1978).

Also, experience has shown that within the nearshore, landfast zones the rates of ice movement are generally very low, and under such conditions the ice forces will be limited by strain rate effects.

Using such a rationale Exxon (1979) proposed a design load for shallow islands in the landfast ice of about 270 kips per foot (about 250 psi). (1.7 MPa)

5.4 Ice rubble fields (Figure 36)

As already discussed, ice movement against wide structures leads to significant ice rubble formation. For structures with underwater berms, the rubble generally grounds out to a water depth of about 20m by the end of the winter.

A typical sequence of rubble formation is shown in Figure 37 for an island in the deeper parts of the landfast ice. In the case shown, when the ice eventually becomes landfast, the grounded rubble consolidates by freezing and forms a rigid annulus around the structure. In the landfast ice with limited ice movement the thick ice at the active zone eventually fails against the consolidated ice rubble in a non-simultaneous crushing mode.

For islands beyond the landfast ice the ice failure against the consolidated rubble is likely to be a mixed-mode type of failure involving continuous rubble and ridge building. Those rubble areas not grounded being wiped away as the ice movement direction changes.

Observations (Kry, 1977) indicate that the permanent rubble field around an island usually does consolidate and refreeze to effectively increase the diameter or width of the structure exposed to the moving ice.

It is usual to assume grounding out to about the 20m water depth on the berm (again based on observations). This distance determines the effective diameter (width) of the ice action. (Figure 38)

However, the rubble also has a beneficial effect, in that its own sliding resistance adds to the ultimate resistance of the island / rubble combination.

An upper bound for the sliding resistance of grounded rubble can be simply calculated by considering the weight of the rubble on the sea floor or berm and combining this with the coefficient of friction at the sea floor based on a granular material. (Croasdale and Marcellus, 1977; Kry, 1977).

The equation governing rubble sliding resistance is then:

$$R = A(1-c) \left[h_m \rho_i + y(\rho_i - \rho_w) \right] g \tan \phi$$

where A is the area of grounded rubble; c is the rubble porosity; h_m is the mean height above the water line; y is the mean water depth; ρ_i and ρ_w are ice and water densities, and ϕ is the friction angle of the material at the sliding plane. (Figure 39)

Typically, a grounded rubble field can double the ultimate sliding resistance of an island.

5.5 Extreme Ice Features ("Limit-Force" Loads)

(Figure 40)

As already discussed in section 3.0, structures which are placed in deeper water have to withstand the ice of the polar pack.

Large multi-year floes with extreme ice thickening and ice islands (although these are very rare) have to be considered. These are often driven by the surrounding pack ice.

The "limit-force" approach which will now be described was developed to consider these extreme interactions.

The concept of extreme ice feature interaction as governed by "limit-force" is illustrated in Figure 41. (repeat of Figure 20)

In stage (1) of ice interaction, the load is dominated by an interaction force which slows down the large ice feature and dissipates its kinetic energy. The level of force will depend on the type of interaction, plus the mass and velocity of the ice feature. If the ice acts against a dredged island then the kinetic energy dissipation will likely mainly be scouring of the lower berm of the island. If the structure has a 'hard' perimeter, then the interaction force is governed by deformation and failure of the ice locally against the structure (as well as by the mass and velocity of the ice).

Once the large ice feature has stopped moving relative to the structure, the surrounding pack-ice continues to move relative to the large ice feature, this is stage (2) of the interaction process shown in Figure 4. The average pack ice force on the ice feature (and hence the structure) will presumably be a function of the average ridge-building force in the pack ice across its width. If this integrated pack ice force (plus the wind stress on the ice island) is large enough then the ice will continue to fail locally around the structure in the thicker ice (limit-stress). Preliminary calculations indicate however that for very thick ice features (and wide structures) the limit to the ice force is the pack ice ridging-building force rather than that derived from the local ice failure stress. Hence the term 'limit-force' approach to ice structure interaction, and hence our interest in better defining average 'ridge-building' forces across a wide front.

The issues relating to the stopping of an extreme ice feature by an underwater berm are itemized in Figure 42.

Simple models for this interaction have been developed (Croasdale and Marcellus, 1981; Marcellus 1980).

They equate the initial kinetic energy of the ice and the work done by driving forces during interaction to the work done by soil forces and gain in potential energy of the ice as it rides up.

The work indicates that a very extreme ice feature such as one 10km by 10km and 50m thick moving at 0.5 ms⁻¹ can be stopped by a large berm (Figure 43).

Once the ice feature has been brought to rest a simple equation for the limit force is given by (Figure 44).

Limit force = wind drag + current drag + ridge building force

$$F = C_{10} \rho_a V_w^2 L^2 + C_c \rho_w V_c^2 L^2 + wL$$

where L is the length and width of the ice feature (assumed to be a square); ρ_a is the air density; ρ_w is the water density; C_{10} and C_c are drag coefficients; V_w is the wind speed; V_c is the current speed and w is the ridge building force (average over width L).

The above equation assumes that the wind, current and ice movement are all in the same direction.

For the purpose of this discussion, the current drag will be ignored. A value of $C_{10} = 3 \times 10^{-3}$ will be assumed, and a 33 ms⁻¹ extreme wind speed will be used. For ridge building, the force calculated by Parmerter and Coon for a 3 m thick sheet will be used, i.e. 4×10^4 Nm⁻¹. (See Figure 45)

On the basis of the above values and assumptions, Table 5.1 shows the results from equation (5) for various ice feature widths.

The total limit force is also plotted in Figure 46.

Inspection of the tabulated values is of interest; at the 10 km ice feature size, it will be noted that the ridge building and wind drag forces are about equal. Consequently, if the ridge building force actually turns out to be 10 times higher than the Parmerter and Coon model, then total force increases by about 5 times the tabulated value.

TABLE 5.1

DRIVING FORCES VERSUS ICE FEATURE SIZE

ICE FEATURE SIZE	WIND DRAG FORCE	PACK ICE FORCE	TOTAL FORCE	TOTAL FORCE
km	N	N	N	tonnes
1.0	4.22×10^6	40.02×10^6	44.42×10^6	4.50×10^3
2.0	1.67×10^7	7.99×10^7	9.66×10^7	9.85×10^3
5.0	1.06×10^8	2.00×10^8	3.06×10^8	3.12×10^4
10.0	4.22×10^8	4.00×10^8	8.22×10^8	8.38×10^4
20.0	1.69×10^9	0.08×10^9	2.49×10^9	2.54×10^5
30.0	3.80×10^9	1.20×10^9	5.00×10^9	5.10×10^5
40.0	6.75×10^9	1.60×10^9	8.35×10^9	8.51×10^5
50.0	1.05×10^{10}	0.20×10^{10}	1.25×10^{10}	1.27×10^6
100.0	4.20×10^{10}	0.40×10^{10}	4.60×10^{10}	4.70×10^6

The most interesting comparisons are shown in Figure 46 where typical 'limit-stress' loads (assuming the thick ice is failing locally against the structure) are also indicated. The 'limit-stress' loads are independent of the ice feature width but are of course a function of ice thickness and structure width.

Figure 46 indicates that for an extreme ice feature 50 m thick (i.e. a yet-to-be calved ice island or multi-year hummock field) crushing against a 200 m wide structure, the ice feature would have to be about 75 km across for the limit stress load to be reached. This size of extreme ice feature is not considered possible. For a realistic extreme ice feature size of say 10 km, the typical 'limit-force' is about 2.9×10^6 tonnes. This is about 30 times lower than the typical 'limit-stress' load.

It is the large difference between the two approaches which is stimulating the current research on ridge building forces. Furthermore, the load levels indicated by the limit-force approach suggest that offshore structures capable of resisting the worst possible ice features such as ice islands, can probably be built in the Arctic Ocean.

5.6 Ice Ride-up

Ice ride up is a concern for low freeboard structures, especially islands with sloping beaches. Croasdale et al (1978) reviewed ice ride-up mechanisms and developed theoretical models for the limits for ice ride-up. Concepts from that paper are reproduced here as Figures 47 to 54.

Kovacs and Sodhi (1980) reviewed natural occurrences of ice ride-up and pile-up for the period of 1879 to 1979. For 24 extreme cases of ride-up on sloping beaches, the mean maximum elevation gain was 9m above sea level. Of the 24 extreme cases of pile-up the maximum elevation gain has been about 11m above sea level.

Model tests have shown that vertical faced structures are very resistant to ice ride-up, although some ice encroachment may occur from an extreme pile-up against the vertical face.

Kovacs and Sodhi (1980) showed that a rubble pile is an effective barrier to ice ride-up. Using measurements from actual sites, they calculated that the minimum force required to slide rubble up a beach exceeds the force required to continue rubble building by a factor of 3 or 4.

6.0 Summary

Artificial islands and hybrid caisson/berm structures are being used in the shallow waters of the Arctic Ocean for petroleum exploration. To date, over 20 islands have been successfully built and used in water depths out to 30m.

It is envisaged that similar but larger structures can be used for petroleum production in even deeper water.

All the islands and structures placed to date have successfully withstood the ice. Ice action on wide structures involves mechanisms not normally seen in ice action on narrow structures. For example, ice failing against wide structures cannot clear easily, and piles of ice rubble develop which affect the ice interaction. Grounded rubble adds to the sliding resistance of the structure. Non-simultaneous ice failure also occurs across a wide structure giving lower average ice pressures than against a narrow structure.

Extreme ice features present in the Arctic Ocean may be considered in the design of permanent production structures. Island-type structures can be built to withstand these kinds of features although additional research is needed on the limits to the driving forces of the polar pack.

Ice ride-up and ice encroachment of pile-ups have to be considered in the design of islands. Work to date, indicates that designs can be conceived to eliminate this risk.

7.0 Acknowledgements

These notes have been based on work done over the past decade by the author and his colleagues in Canada. The imaginative activities of companies such as Esso Canada Resources (Imperial Oil), Dome Petroleum and Gulf Canada Resources have enabled the achievements and understanding discussed in this review to occur, and without them these notes and this lecture would not be possible. The author thanks Petro-Canada for giving me permission to present this talk.

8.0 References

- Allyn, N., Wasilewski (1979), "Some Influences of Ice Rubble Field Formation Around Artificial Islands", 5th POAC, 1979.
- Allyn, N. (1980), "Ice Pile-up Around Offshore Structures in the Beaufort Sea", NRC Workshop on Sea Ice Ridging and Pile-Up, October 1980, NRC Tech Memo 134.
- Assur, A. (1971), "Forces In Moving Ice Fields", Proceedings of 1st POAC Conference, Trondheim, Norway (1971).
- Bercha, F.G. & Ghoneim, G.A. (1980), "Evaluation Of Pile-Up Formation and Structure Interaction Forces", Presented at NRC Ice Ridging and Pile-Up Workshop, Calgary, Alberta 1980 (Proceedings to be published as National Research Technical Memorandum).
- Bercha, F.G. et al, "Effect Of Pile-Ups and Rubble Fields On Ice-Structure Interaction Forces". Offshore Technology Conference, 1980. (OTC 3884).
- Croasdale, K.R. (1980), "The Nutcracker Ice Strength Tester and its Operation in the Beaufort Sea", Proceedings of IAHR Ice Symposium, Reykjavik, Iceland.
- Croasdale, K.R. (1974), "Crushing Strength of Arctic Ice", J.C. Reed and J.E. Sater(eds). The Coast and Shelf of the Beaufort Sea. The Arctic Institute of North America.
- Croasdale, K.R. (1975), "Ice Forces on Marine Structures", IAHR Third International Symposium On Ice Problems, Hanover, New Hampshire.
- Croasdale, K.R. & R.W. Marcellus (1978), "Ice and Wave Action on Artificial Islands in the Beaufort Sea", Can. J. Civil Eng. 5. 1:98-113.
- Croasdale, K.R., M. Metge & P.H. Verity (1978), "Factors Governing Ice Ride-up on Sloping Beaches", Proceedings of IAHR Ice Symposium, Lulea, Sweden.
- Croasdale, K.R. (1980), "Ice Forces On Fixed Rigid Structures", (A state-of-the-art report for IAHR, 1978) CRREL Special Report 80-26. Editor, T. Carstens.
- Croasdale, K.R. & R.W. Marcellus (1981), "Ice Forces on Large Marine Structures", Proceeding of IAHR Ice Symposium, Quebec, City, Canada.
- Dome Petroleum Ltd, Esso Resources Canada Ltd., & Gulf Canada Resources Inc., (1982), "Beaufort Sea - Mackenzie Delta Environmental Impact Statement (EIS)", Calgary, Alberta.
- Exxon Production Research Co., (1979), "Technical Seminar on Alaskan Beaufort Sea Gravel Island Design", Houston, U.S.A.
- Garrett, D.H. & Kry, P.R. (1978), "Construction of Artificial Islands As Beaufort Sea Drilling Platforms", Journal of Canadian Petroleum Technology, April-June, pp 773-79.

- Gladwell, R.W. (1976), "Field Studies of Eight First-Year Sea-Ice Pressure Ridges in the Southern Beaufort Sea", Esso Resources Canada Limited, APOA Project 75.
- Gladwell, R.W. (1976), "Field Studies of the Strength and Physical Properties of a Multi-Year Ice Pressure Ridge in South Beaufort Sea", Esso Resources Canada Ltd., APOA Project 91.
- Gladwell, R.W. (1977), "Ice Conditions Around Artificial Islands 1975-76", Esso Resources Canada Limited, APOA Project 105.
- Hibler, W.D. III (1975), "Statistical Variations In Arctic Sea Ice Ridging and Deformation Rates", SNAME Ice Tech Symposium, Montreal.
- Jahns, H.O. (1979), "Production Islands", Technical Seminar on Alaskan Beaufort Sea Gravel Island Design. Exxon Production Research Company, Houston.
- Kovacs, A & D.S Sodhi (1980), "Shore Ice Pile-up and Ride-up Field Observations, Models, Theoretical analyses", Cold Regions Science and Technology, Elsevier Scientific Publishing, Amsterdam.
- Kry, P.R. (1975), "Flexural Strength and Youngs Modulus of Landfast Ice by the Mackenzie River Delta", Esso Resources Canada Limited, APOA Project 84.
- Kry, P.R. (1980), "Ice Forces on Wide Structures", Canadian Geotechnical Journal 17, 1:97-113.
- Kry, P.R. (1977), "Ice Rubble Fields in the Vicinity of Artificial Islands", Proceedings of the Fourth International Conference on Port and Ocean Engineering under Arctic Conditions, Memorial University of Nfld., St. John's.
- Kry, P.R. (1979), "Implications of Structure Width for Design Ice Forces", Proceedings of the IUTAM Symposium, Physics and Mechanics of Ice, Copenhagen.
- Marcellus, R.W. & T.B. Morrison (1982), "Ice Design Statistics for the Canadian Beaufort Sea", Prepared by Canada Marine Engineering Ltd., Report 1015, for the EIS partners.
- Marcellus, R.W. & D.R. Roth (1982), "An Initial Probabilistic Assessment of Ice Loading on Beaufort Sea Structures", Prepared by Canada Marine Engineering Ltd., Report 1016 to Dome Petroleum Limited.
- McGonigal & Wright (1980), "Ice Movement in the Canadian Beaufort Sea", Intermaritec, Hamburg, West Germany.
- Michel, B. & Toussaint, (1977), "Mechanisms and Theory of Indentation of Ice Plates", Journal of Glaciology, Vol. 19, No. 81.
- Miller, T.W. (1974), "Ice Crushing Test", Esso Resources Canada Limited, APOA Project 66.
- Parmeter, R.R. & M.D. Coon, (1972), "Model of Pressure Ridge Formation in Sea Ice", Journal Of Geophysical Research Vol. 77, No. 33:6565-6576.
- Pritchard, R.S (1976), "An Estimate of the Strength Of Arctic Pack Ice", AIDJEX Bulletin No. 34 .

Rosenegger, L.W. (1977), "Experimental Ridge CRI Interaction", Esso Resources Canada Limited, APOA Project 125.

Rothrock, D.A. (1975), "The Steady Drift Of An Incompressible Arctic Ice Cover", Journal Of Geophysical Research, Vol. 80, No. 3, pp 387-397.

Semeniuk, A. (1976), "Large Scale Ice Interaction Tests with an Artificial Island and with a Caisson Retained Island", Winter 1975 - 76. Esso Resources Canada Limited, Calgary, APOA Project 103.

Spedding, L.G. (1981), "Landfast Ice Motion Observed in the Mackenzie Delta Region of the Southern Beaufort Sea in the 1972-1973 Winter", Coastal Engineering Vol. 5:193.

Spedding, L.G. (1981), "1974-75 Landfast Ice Motion Observation For the Mackenzie Delta Region of the Beaufort Sea", ASME Energy Sources Conference, January, 1981.

Spedding, L.G. (1974), "The Extent and Growth Pattern of Landfast Ice in the Southern Beaufort Sea - Winter 1972-73", Esso Resources Report TPRT-2ME-76, APOA Project 54.

Strilchuk, A.R. (1977), "Ice Pressure Measurement", Netserk F-40 1975-76, Esso Resources Canada Limited, APOA Project 105.

Taylor, T.D. (1973), "Ice Crushing Test", Esso Resources Canada Limited, APOA Project 52.

Trofimenkoff, P.N. (1975), "Ice Strength Test", Esso Resources Canada Ltd.

Verity, P.H. (1975), "Small Prototype Cone Test", Winter 1973-74, Esso Resources Canada Limited, APOA Project 65.

Vittoratus, E.S. (1980), "Ice Conditions Around Isserk E-27", 1977-78, Esso Resources Canada Ltd. Report IPRT-3ME-80.

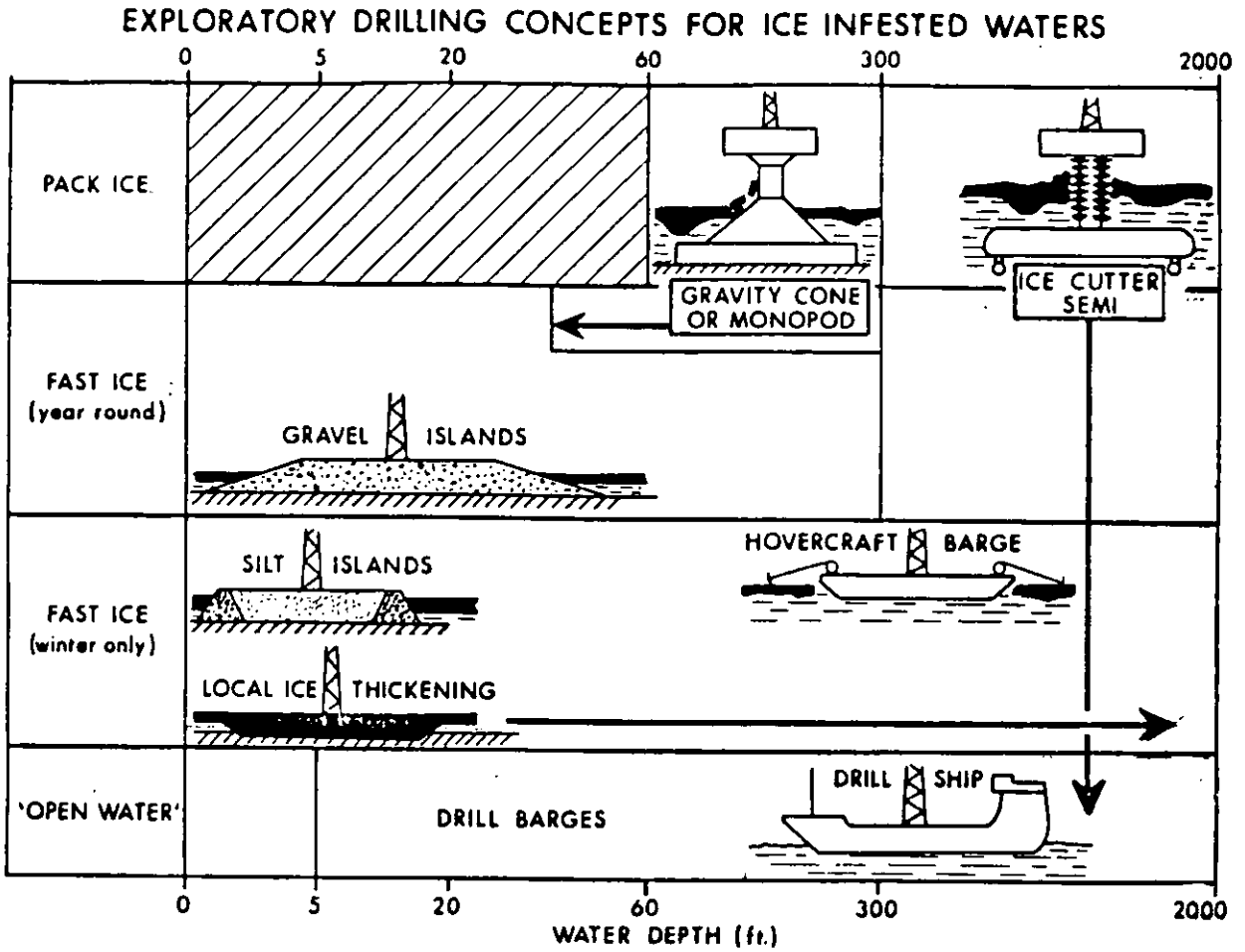


Fig. 1. Exploratory drilling concepts for ice infested waters.

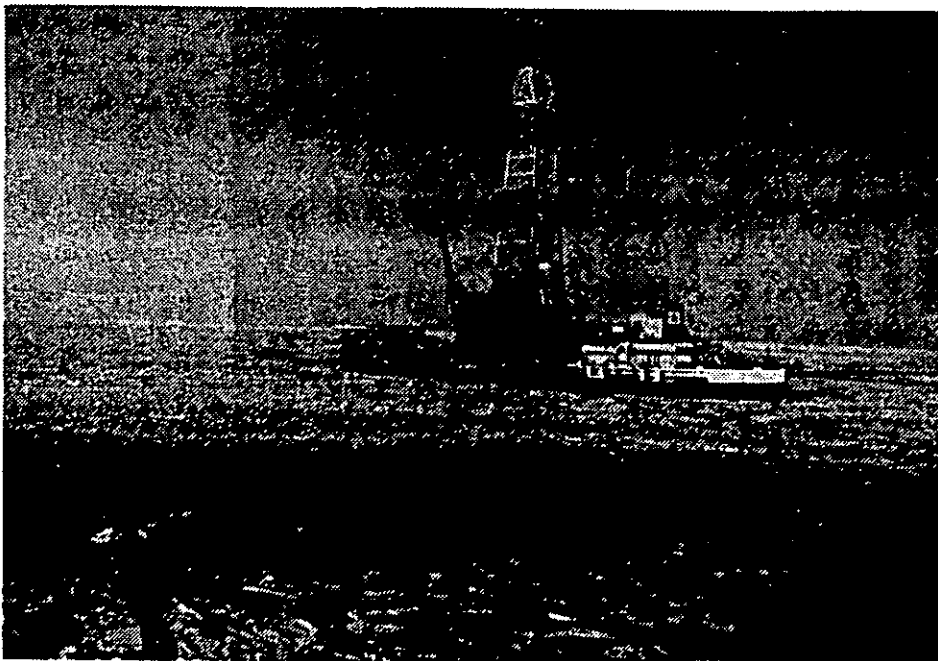


Fig. 2. Dome Drilling Ship in the Beaufort Sea.

PRODUCTION CONCEPTS FOR ICE INFESTED WATERS

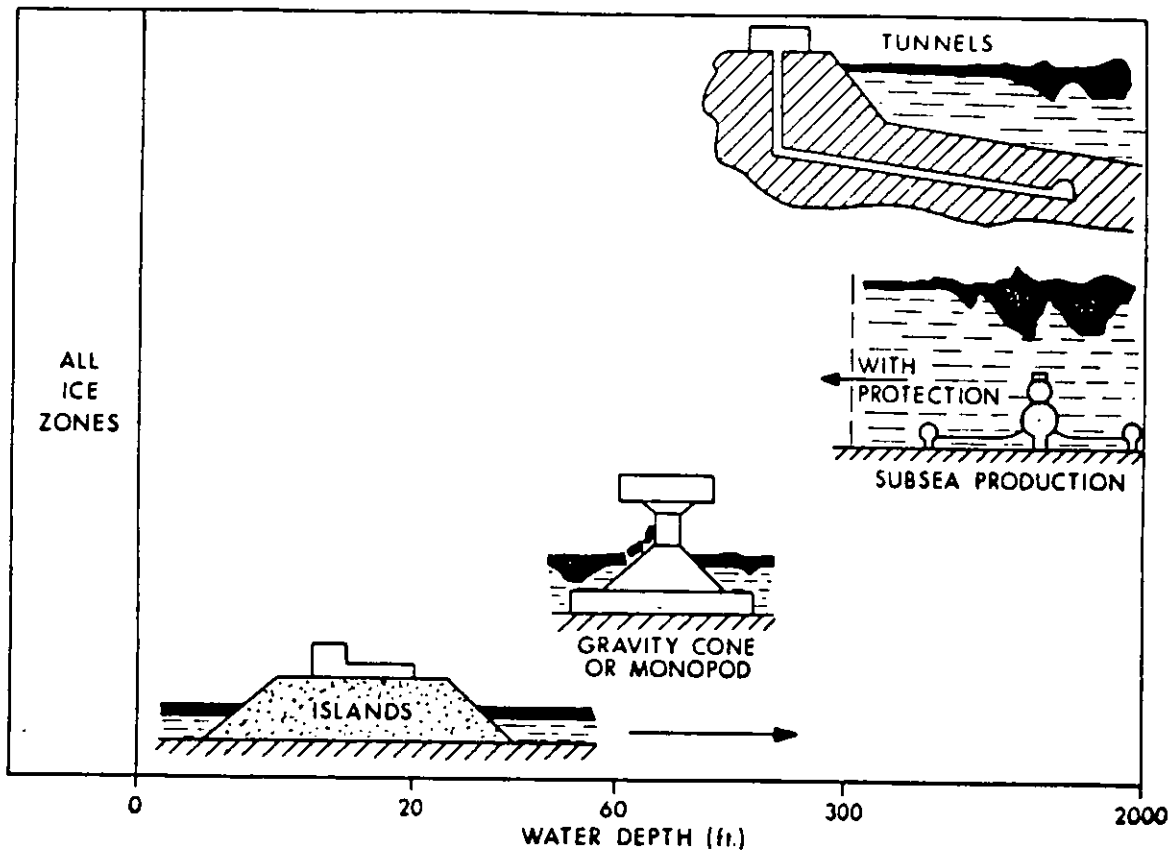


Fig. 3. Production concepts for ice infested waters.

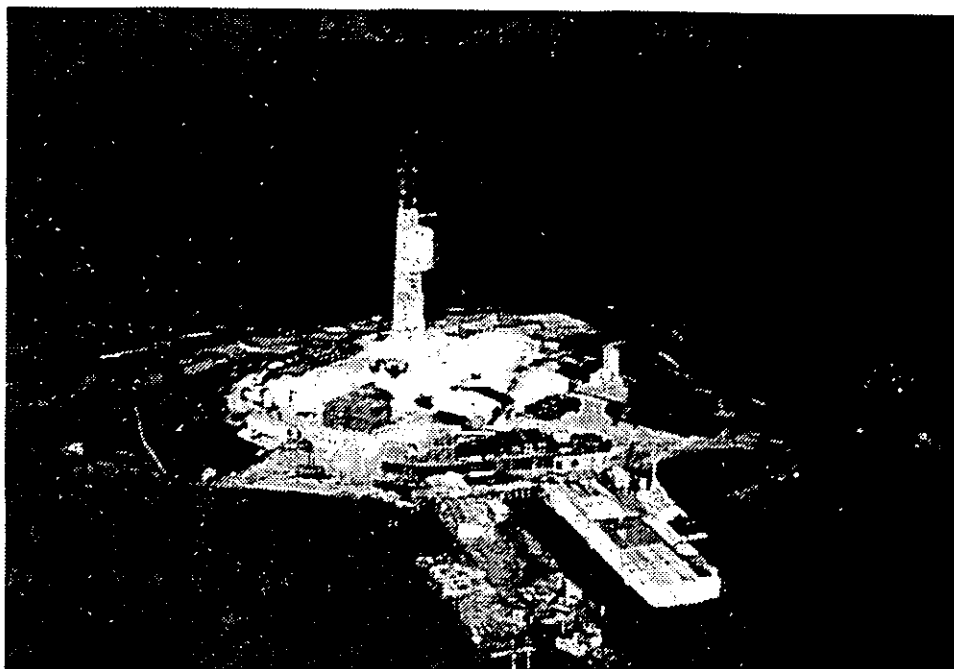


Fig. 4. Immerk artificial island.

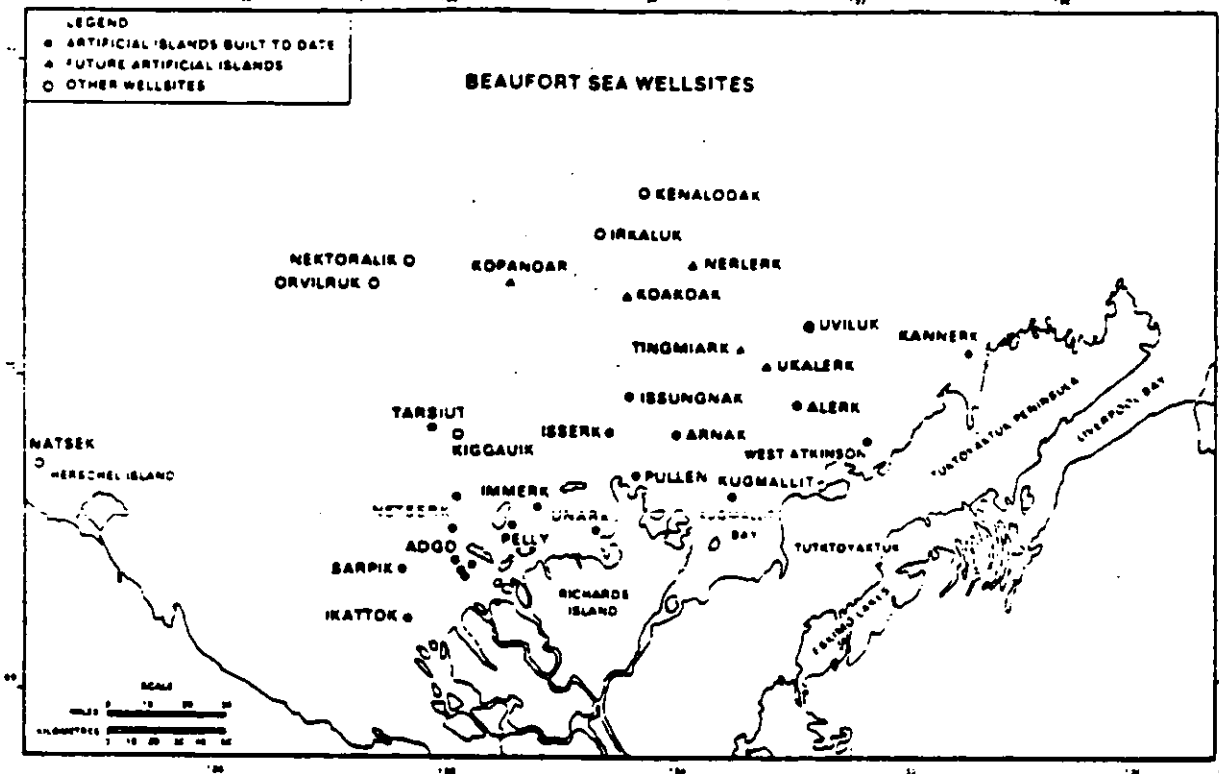


Fig. 5. Beaufort Sea Island Locations.

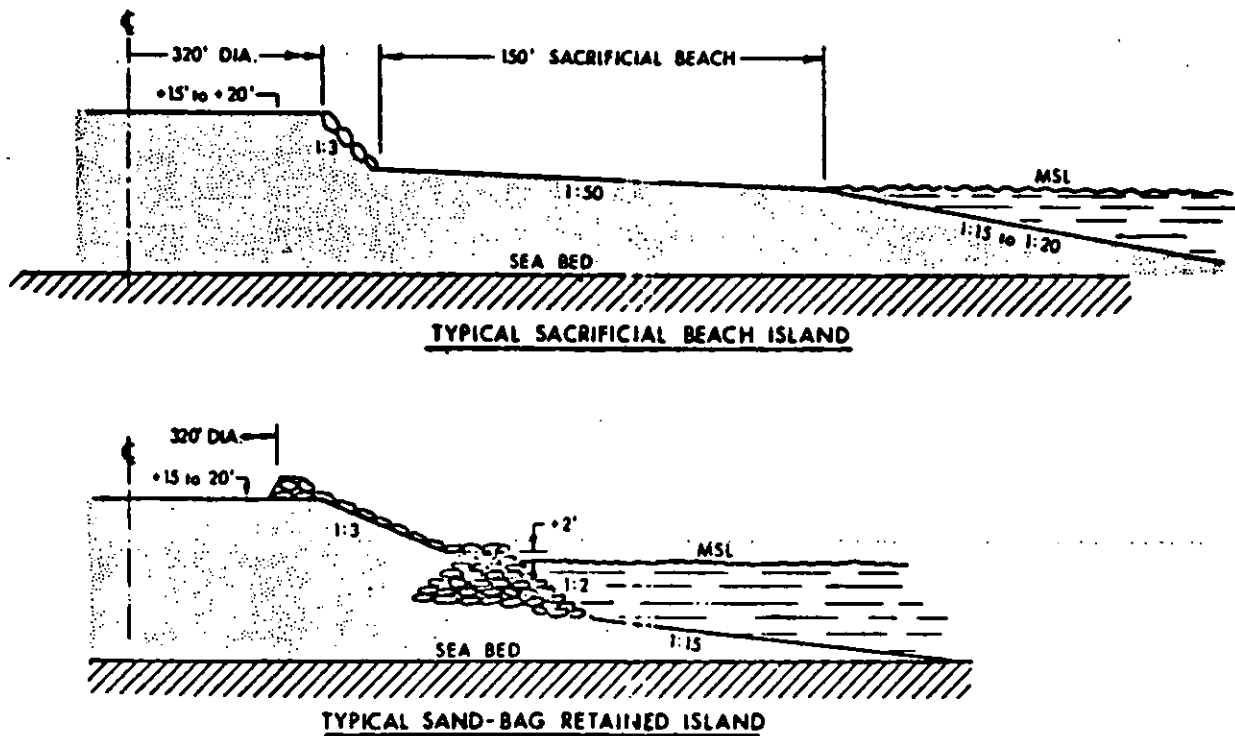


Fig. 6. Island beach cross-sections.

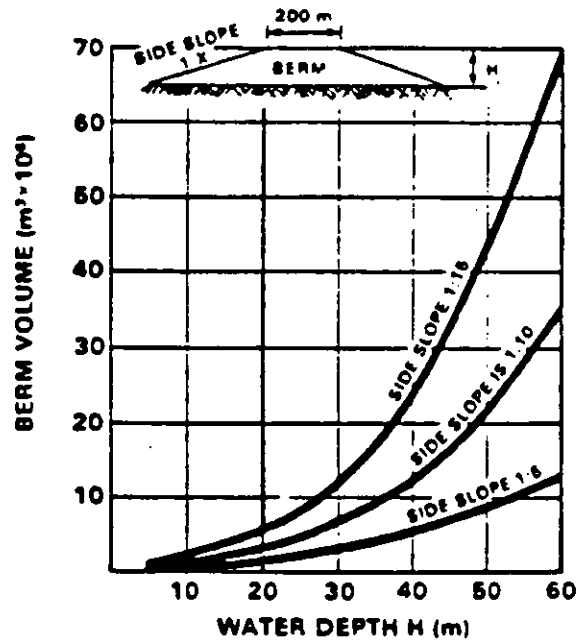


Fig. 7. Berm volume versus water depth (Beaufort Sea EIS 1982).

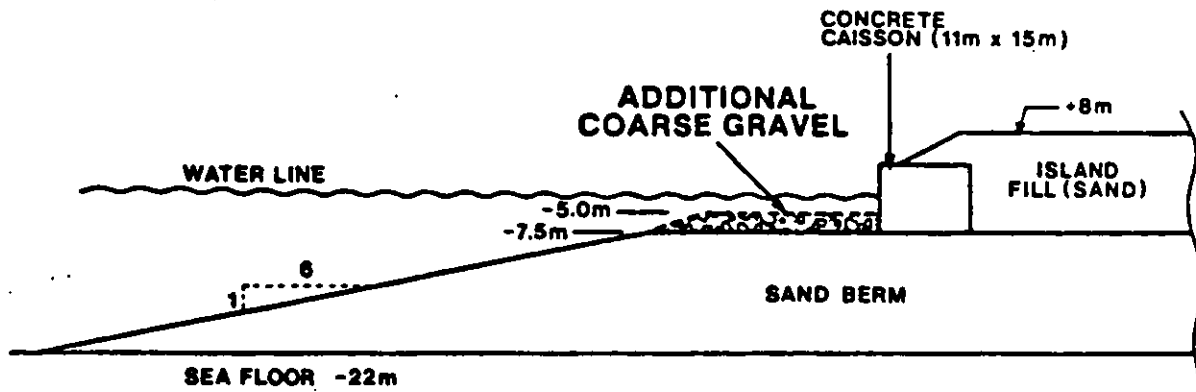


Fig. 8. Tarsiut island cross-section.

ISLAND DESIGN CRITERIA AND RESEARCH

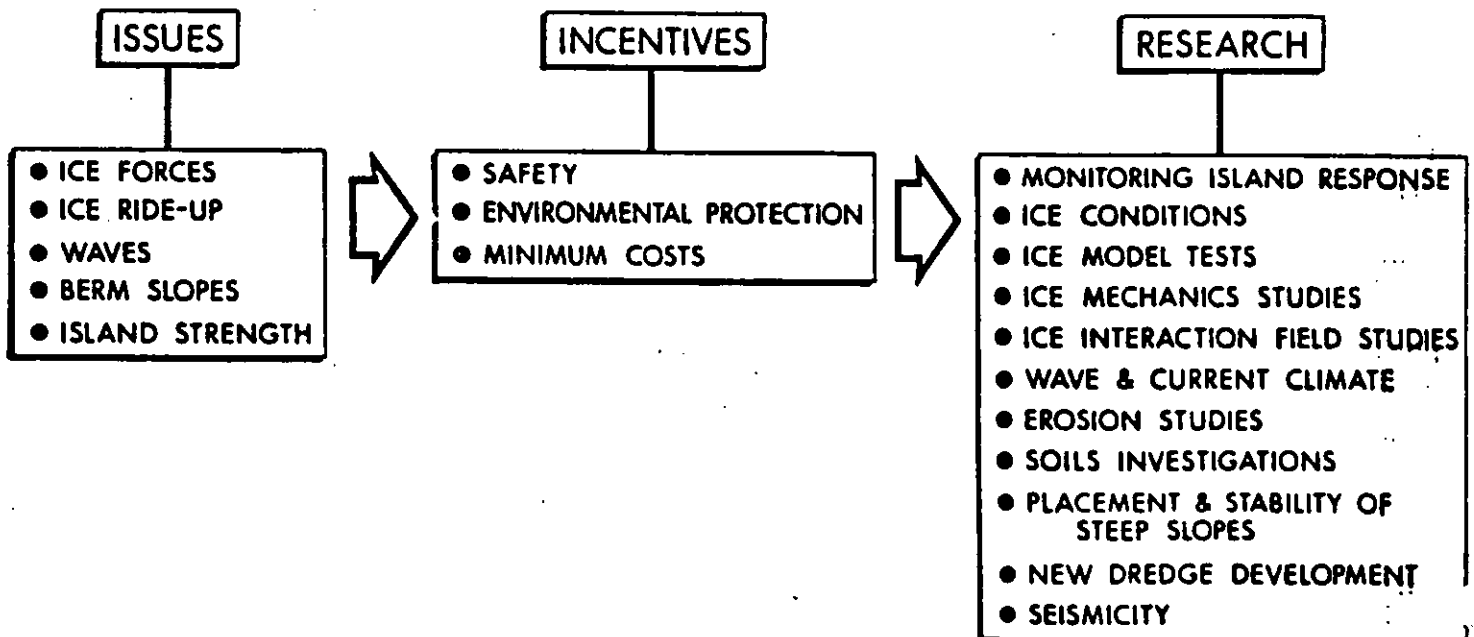
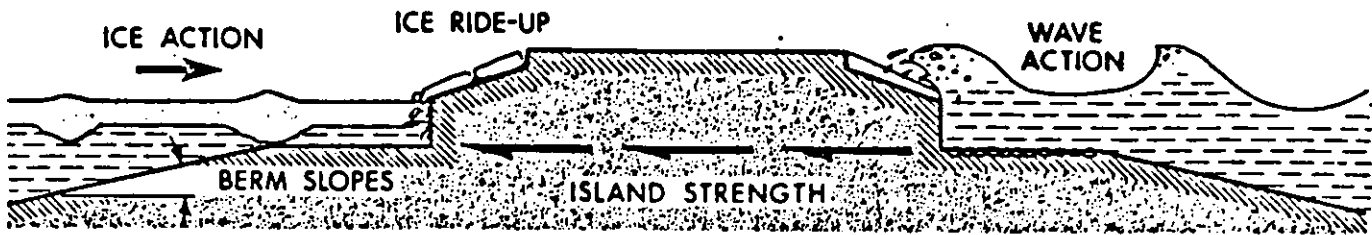
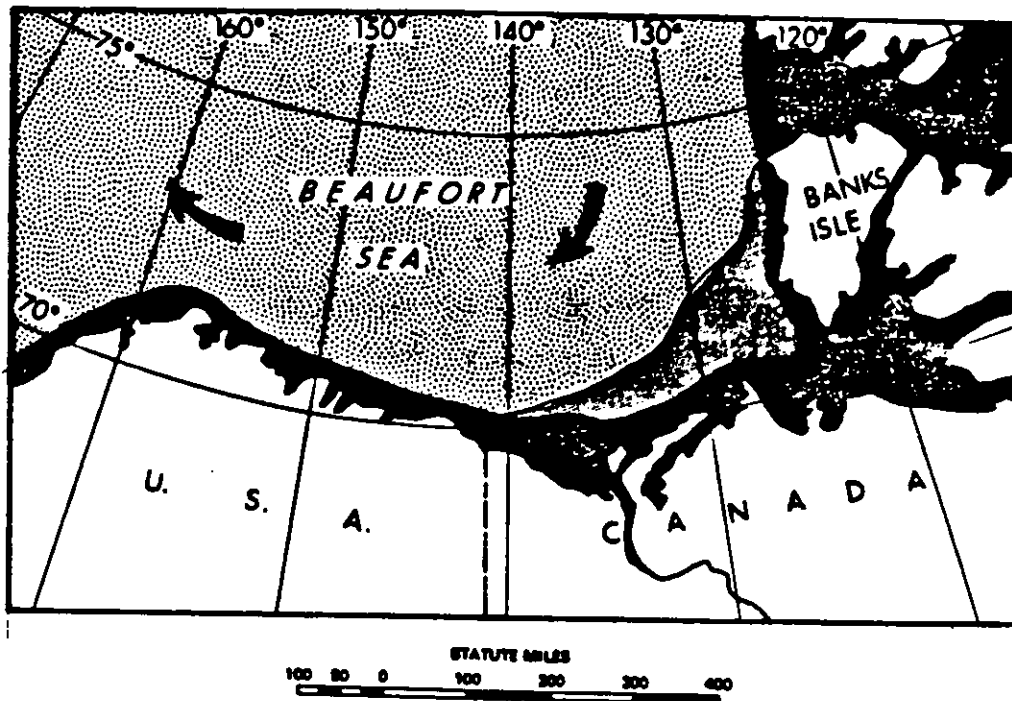


Fig. 11. Island design criteria and research.



ARCTIC PACK ICE



MAINLY OLD ICE 3-4 METERS THICK MOVING SLOWLY YEAR ROUND.

SOLID AND UNMOVING



OLD OR FIRST YEAR ICE OR A MIXTURE OF BOTH COMPLETELY COVERING THE WATERWAY.

MORE THAN 7/8ths



MAINLY FIRST YEAR ICE 1-2 METERS THICK IN INTERMITTENT RESTRICTED MOTION.

Fig. 12. Typical winter ice conditions in Beaufort sea area (february).

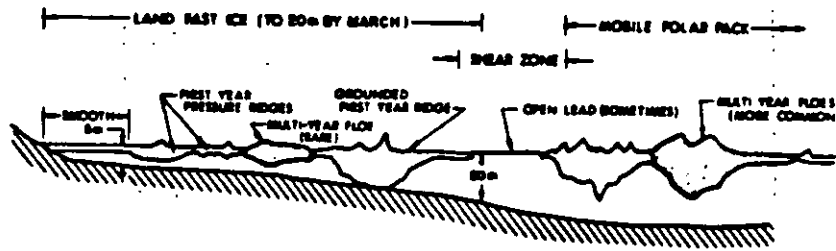


Fig. 13. Typical winter ice conditions, Beaufort Sea.

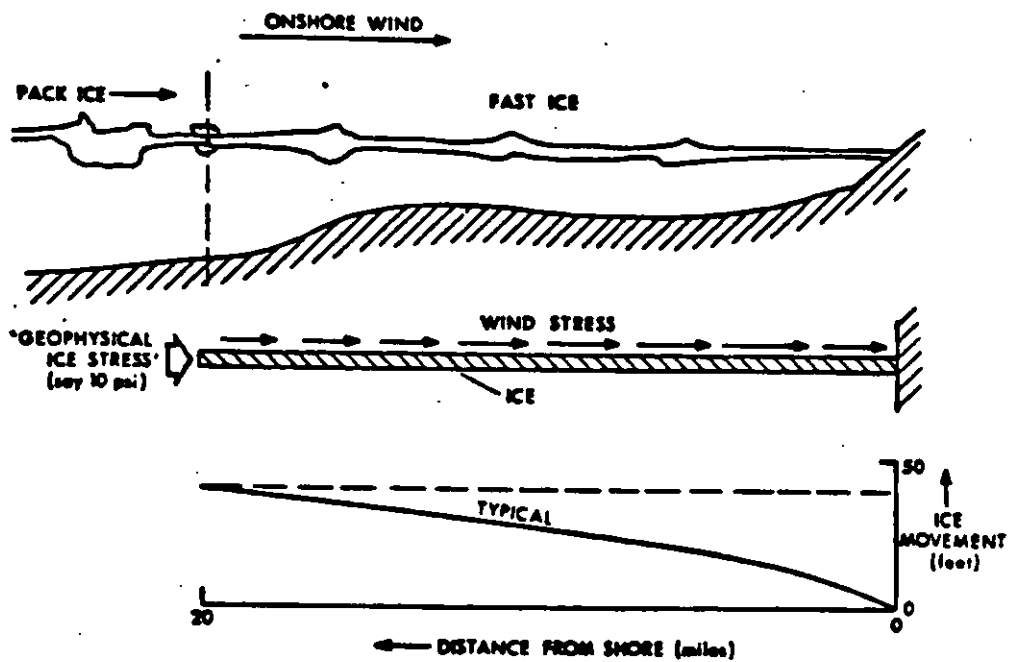


Fig. 14. Landfast ice movement model.

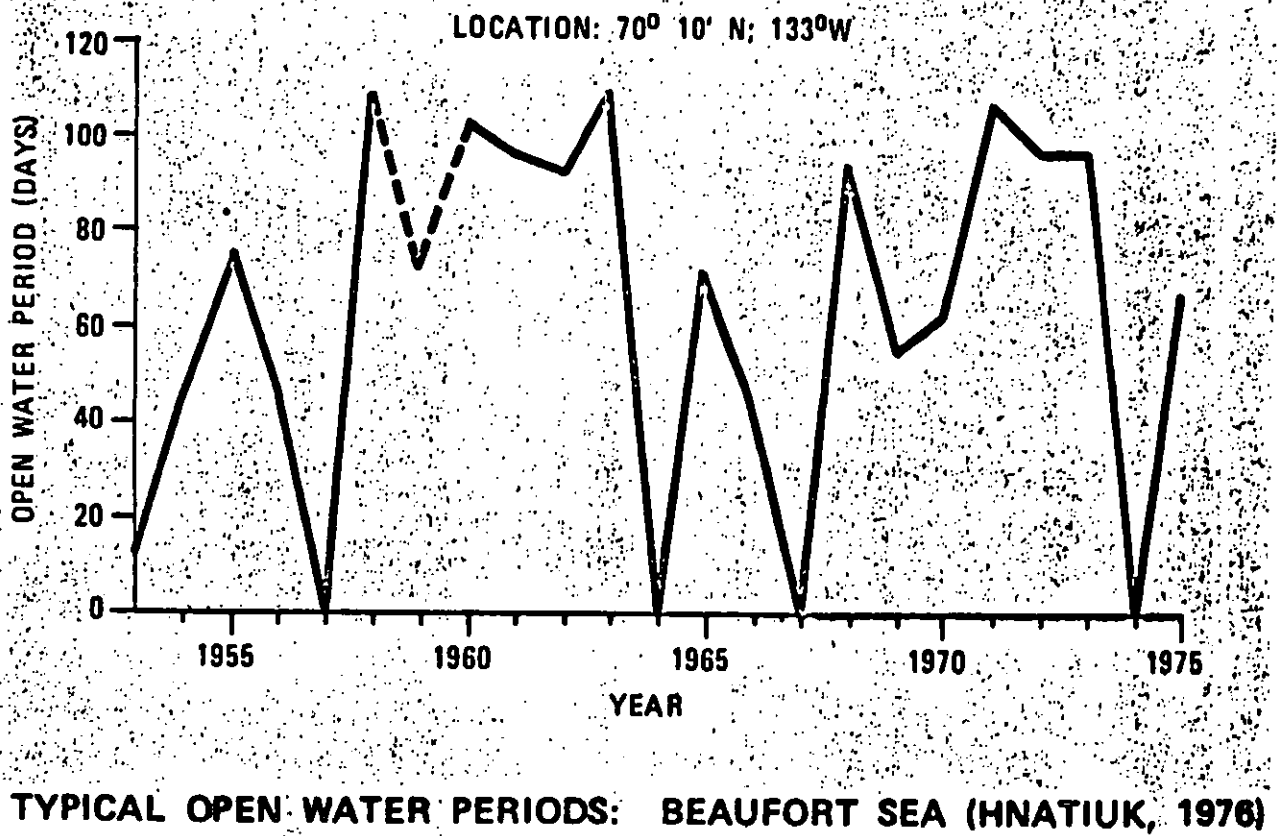


Fig. 15. Typical open water periods (Hnautiuk 1976).

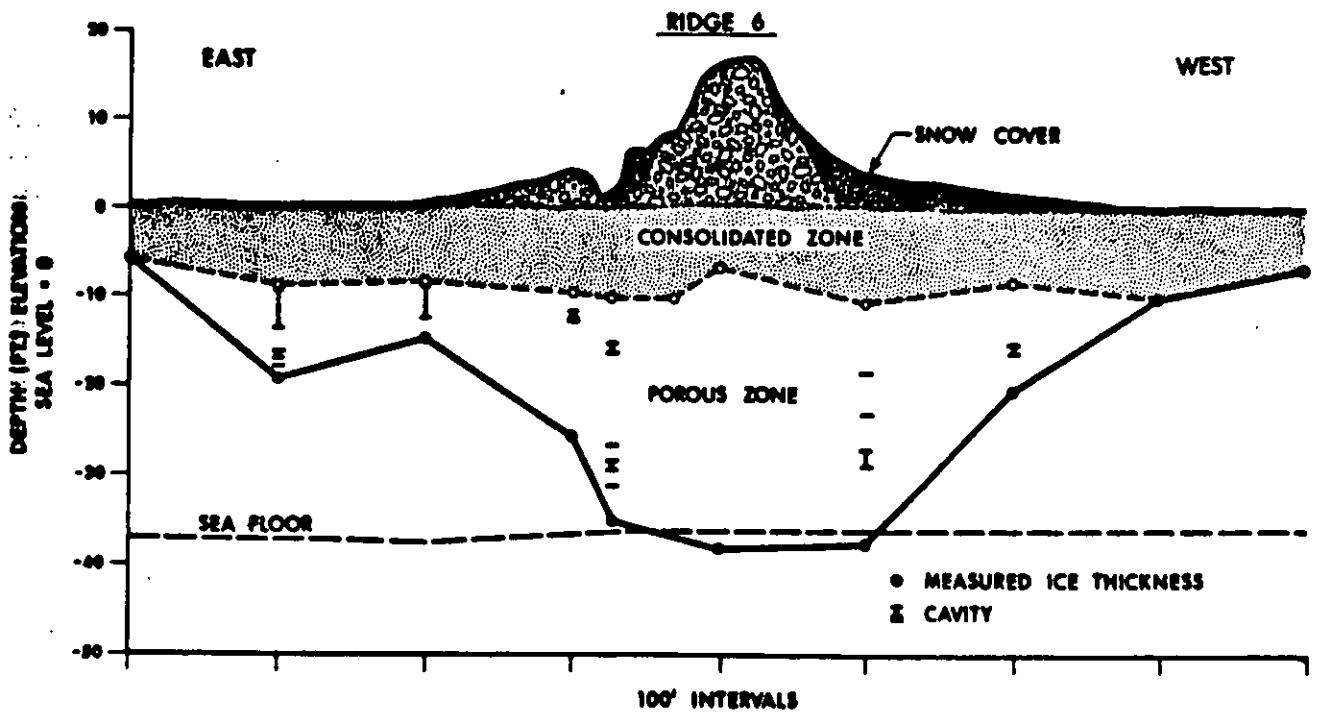


Fig. 16. Typical profile of a first-year ridge in the Beaufort Sea.

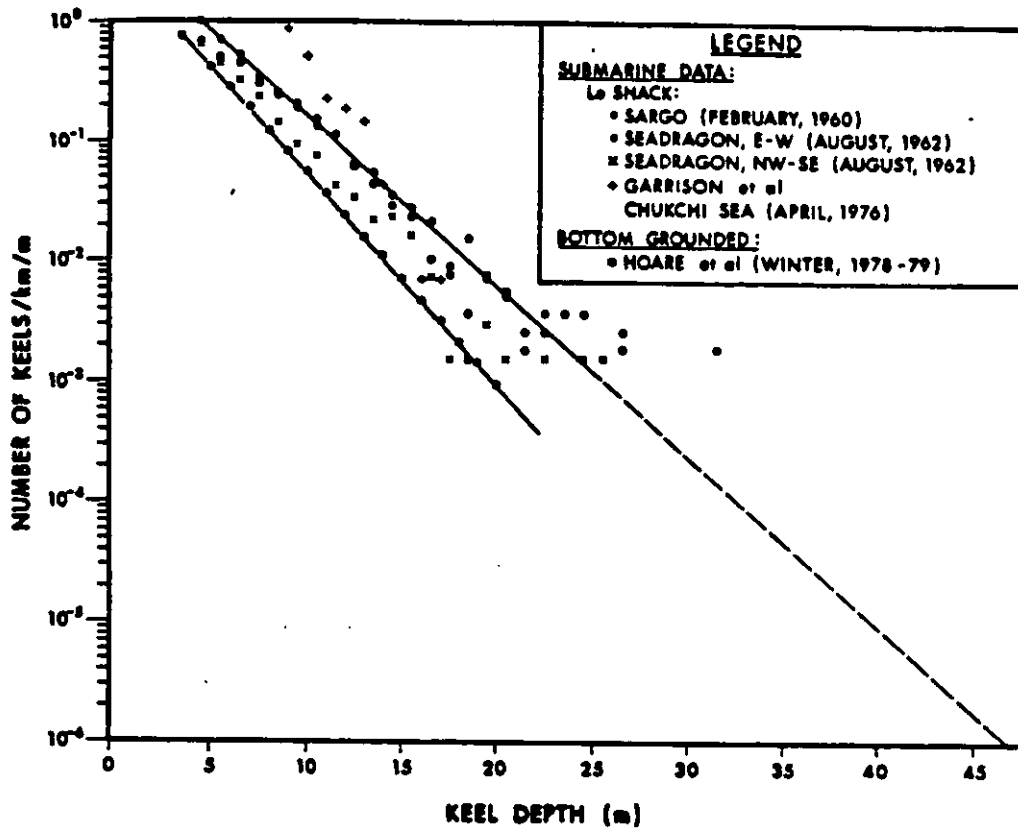


Fig. 17. Number of ice keels versus keel depth, Beaufort Sea.

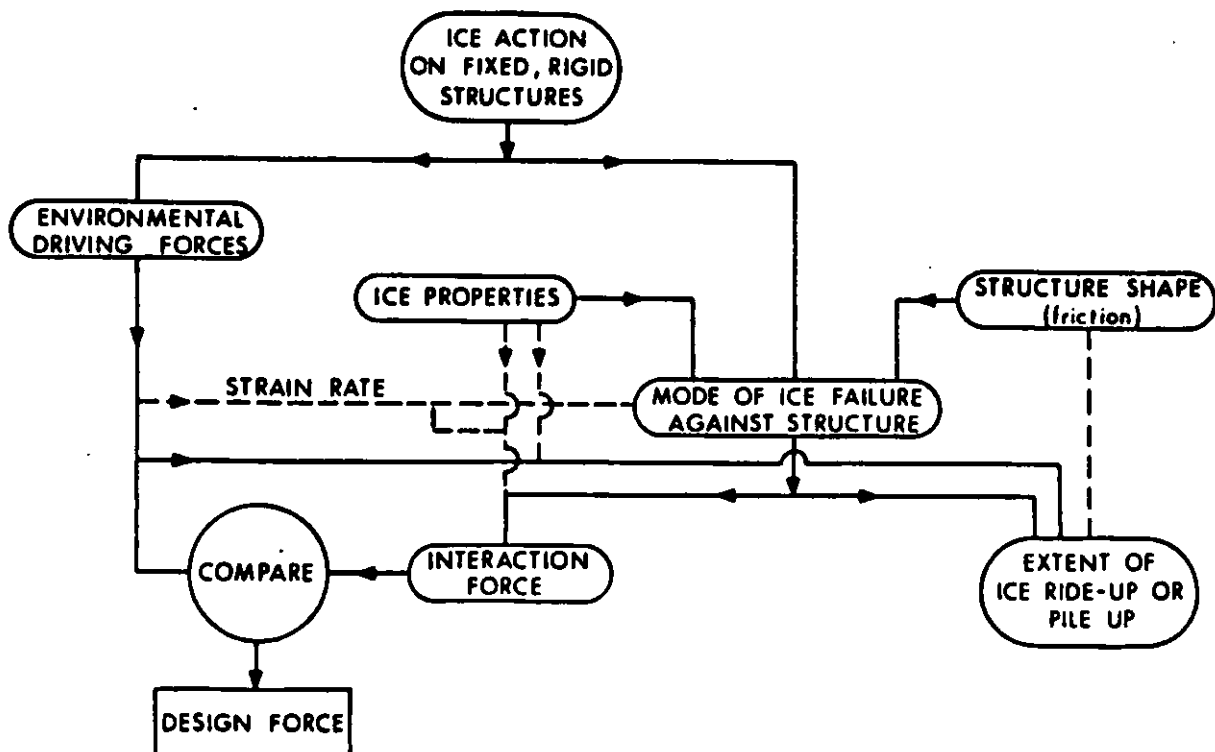


Fig. 18. Logic for considering action on fixed, rigid structures.

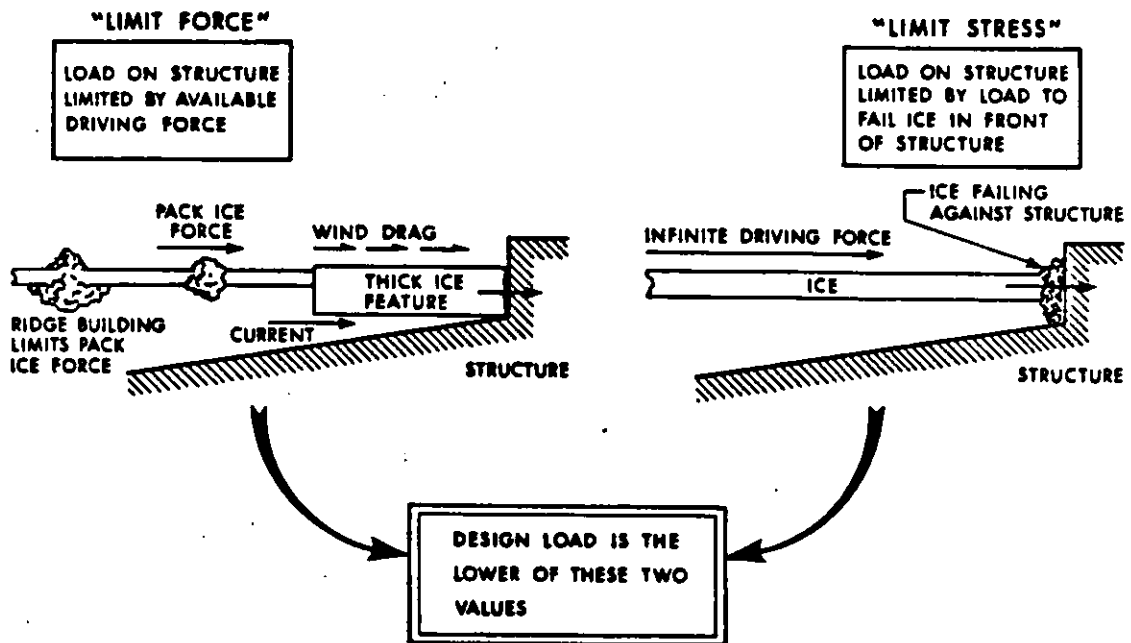


Fig. 19. Logic for design ice load.

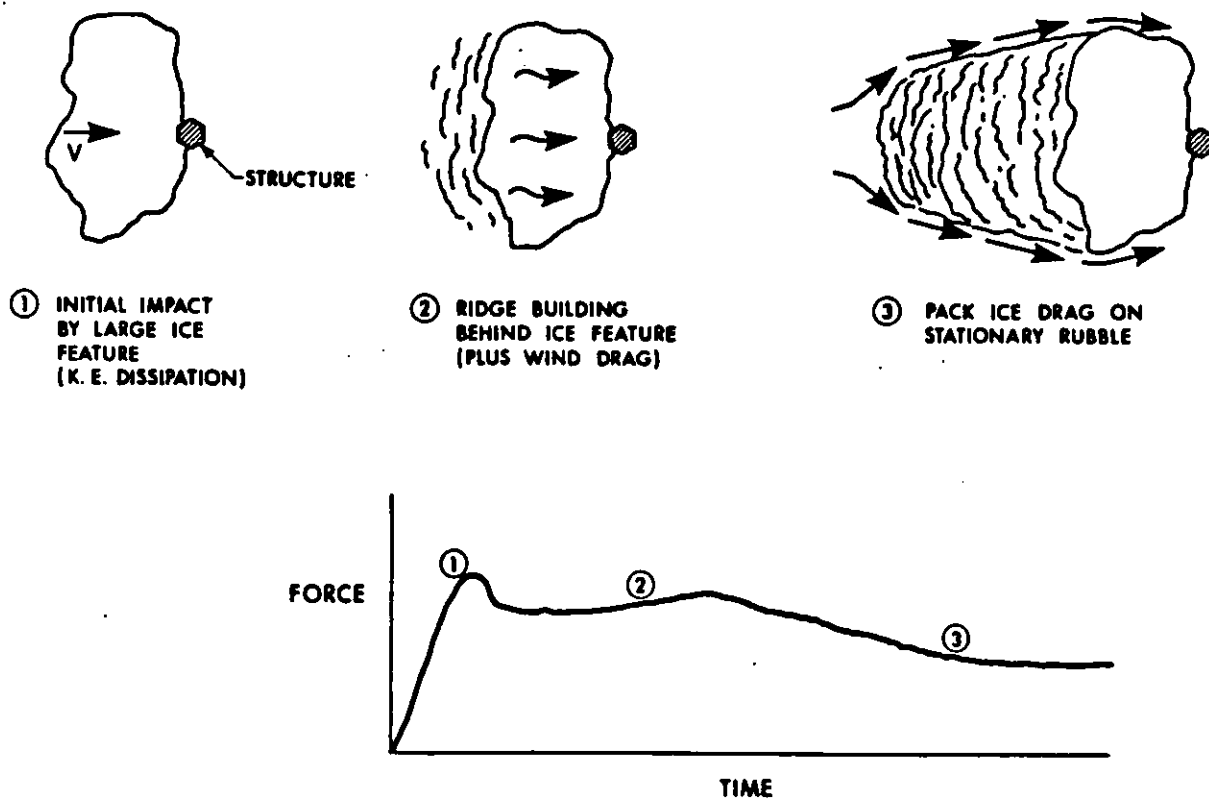


Fig. 20. Stages in ice-structure interaction.

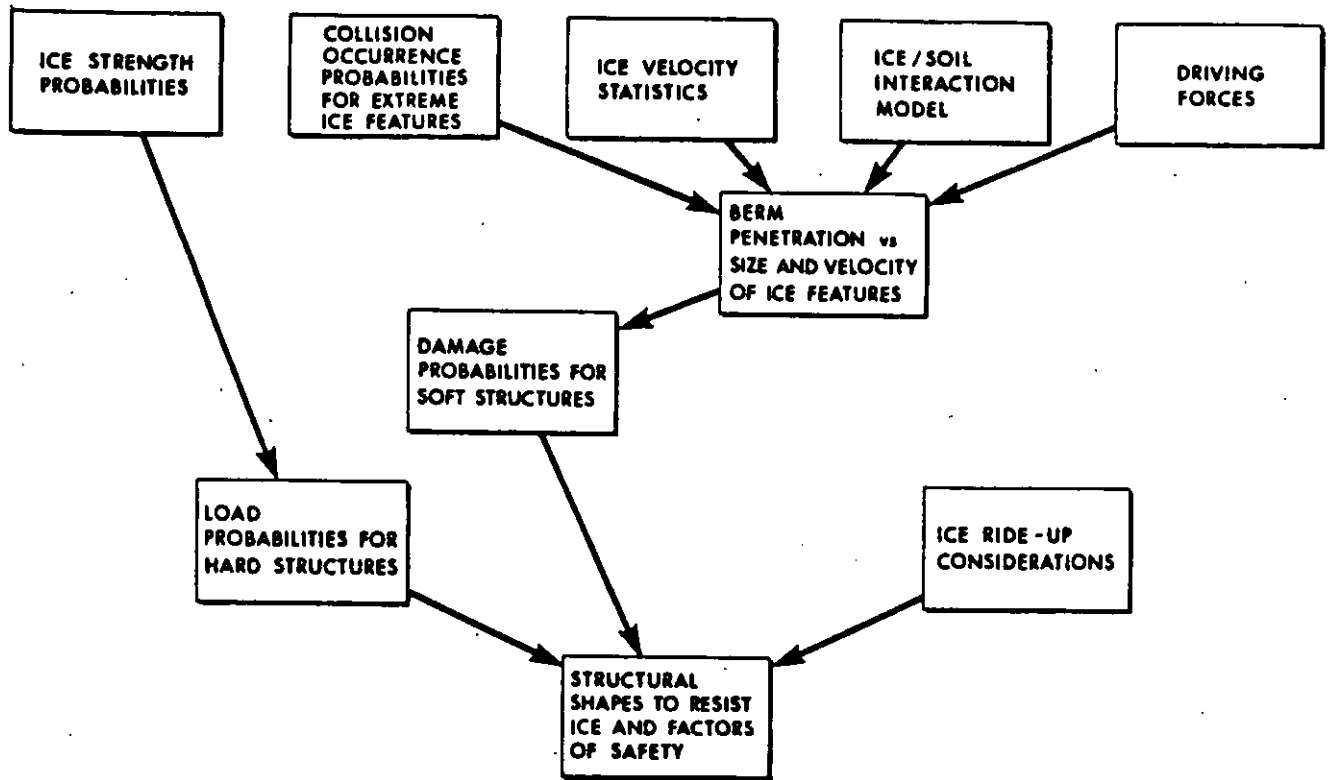
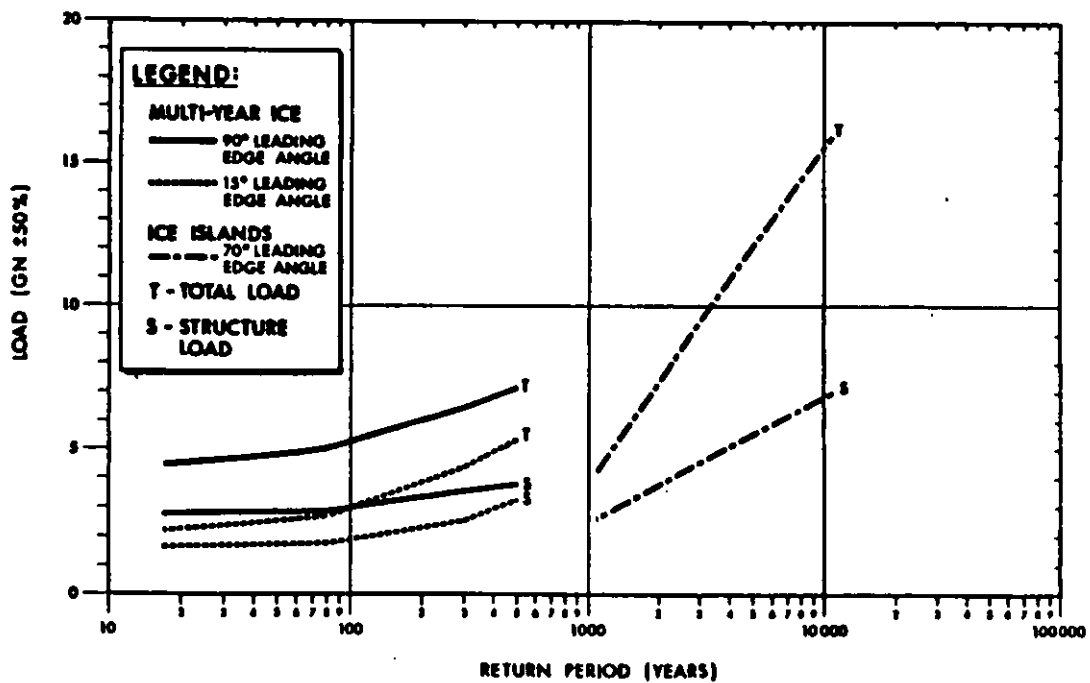
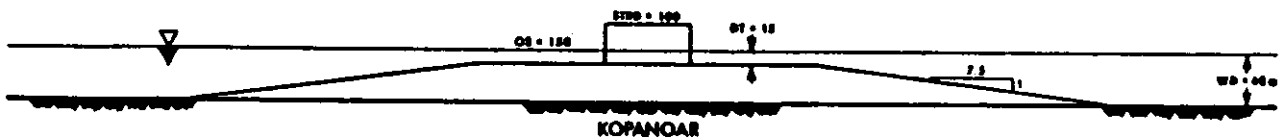


Fig. 21. Logic for designs to resist ice.



ESTIMATED LOADS VERSUS RETURN PERIOD AT KOPANOAR
(MARCILUS & RÖTH 1982)

Fig. 22. Typical Ice loads versus return period.

• ASPECTS OF WIDE STRUCTURE INTERACTION

- STRUCTURE TOO WIDE FOR ICE TO CLEAR (FOR CONSTANT DIRECTION OF MOTION)
- ICE RUBBLE FORMS
- ICE RUBBLE MAY GROUND AROUND SHALLOW STRUCTURES
- GROUNDED ICE RUBBLE CAN BE 'PERMANENT' FEATURE FOR REMAINDER OF WINTER
- ACTIVE ZONE MOVES TO OUTSIDE OF RUBBLE
- ICE FAILURE MODE WILL DEPEND ON THICKNESS AND CONSTANCY OF ICE MOTION
- MULTI-ZONES OF ICE FAILURE ACROSS WIDTH
- DIFFERENT MODES OF ICE FAILURE CAN OCCUR FROM ZONE TO ZONE

Fig. 23. Ice action on wide structures.

K.R. CROASDALE
1983

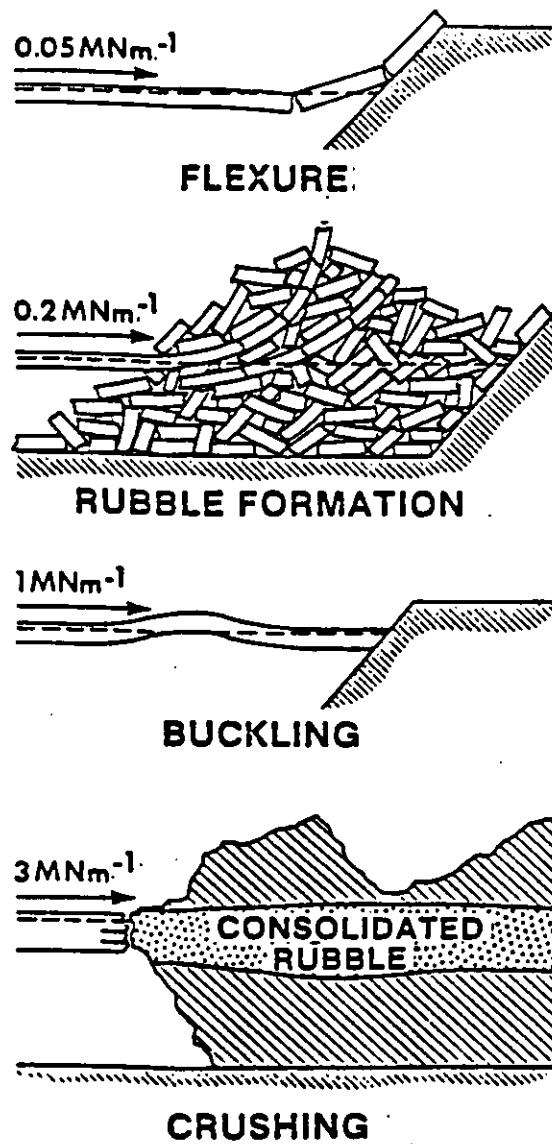
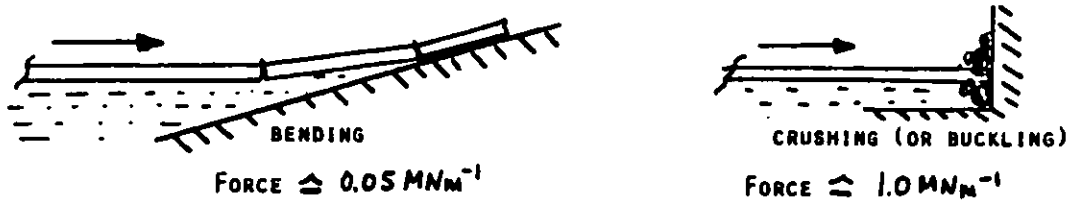


Fig. 24. Typical forces for ice on wide structures (Kry, 1980).

1) THIN ICE FAILS AGAINST BARE STRUCTURE IN EARLY WINTER



(2) THICKER ICE FAILS ON OUTSIDE OF RUBBLE

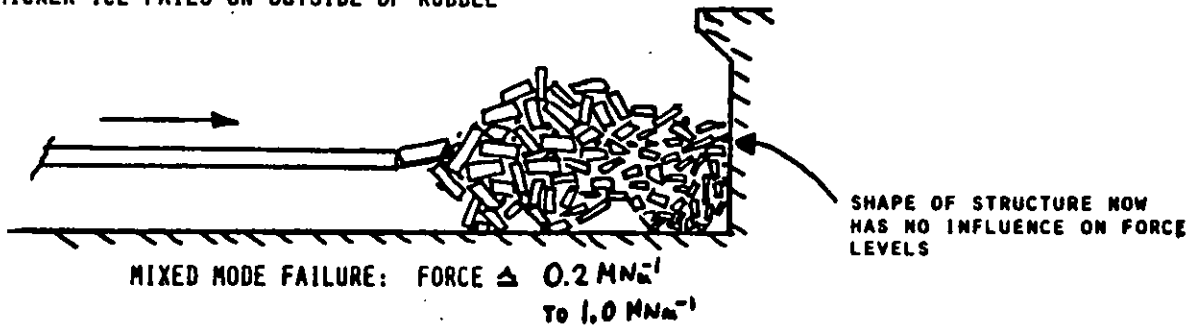


Fig. 25. Wide structures; typical winter scenario.

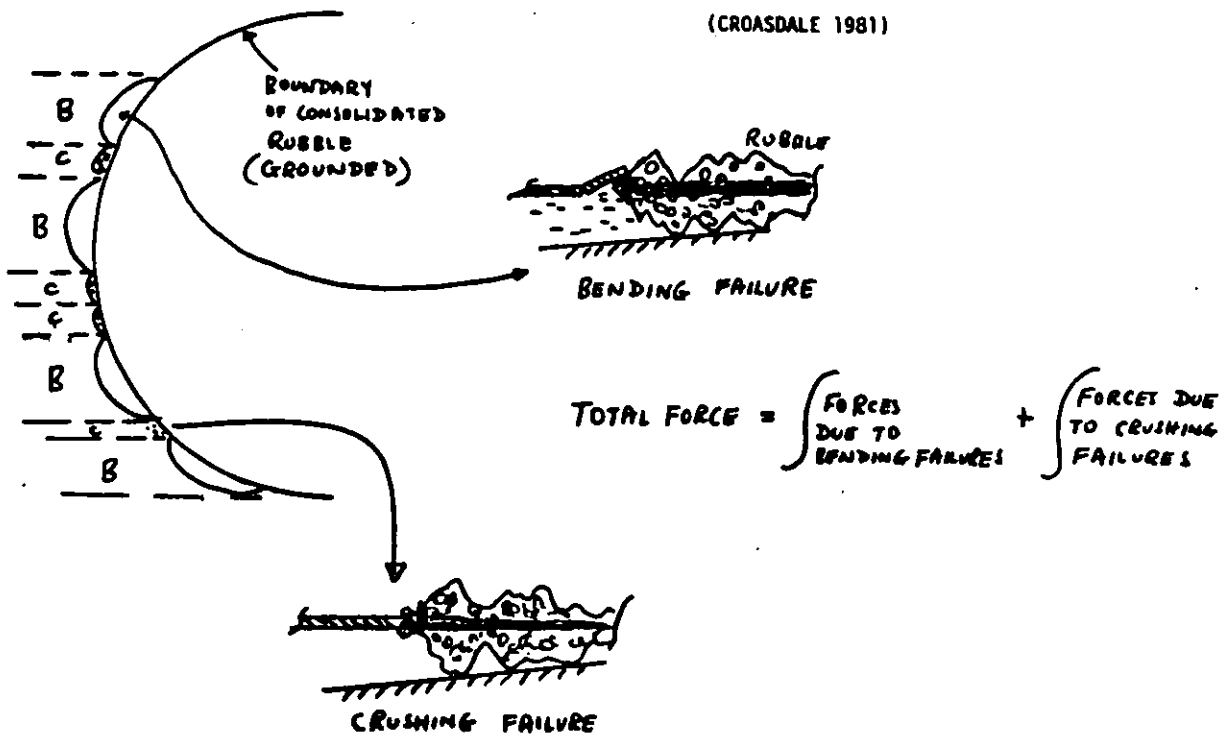


Fig. 26. Mixed mode failure on outside of rubble.

- ASSUR FIRST SUGGESTED APPROACH BASED ON RANDOM DISTRIBUTION OF ICE BLOCK ANGLES (1971)

- KRY (1980) DEVELOPED ASSUR'S APPROACH AND QUOTES APPROXIMATE RELATIONSHIP AS (FOR RANDOM BLOCK DISTRIBUTION)

$$\text{AVERAGE FORCE / UNIT WIDTH} = \frac{2\mu H_L}{\pi}$$

μ
 H_L IS COEFFICIENT OF FRICTION (LESS THAN 0.4, NEARER 0.2)
IS FORCE / UNIT WIDTH FOR PURE CRUSHING OR BUCKLING (SEE NEXT GRAPH)

- BERCHA AND GHONEIM (1980) DEVELOPED SIMILAR APPROACH WHICH GIVES SIMILAR RESULTS TO ABOVE

- KRY'S ENERGY APPROACH GIVES FORCE LEVELS 5-10 TIMES LESS THAN MIXED-MODAL APPROACH

K.R. CROASDALE
1983

Fig. 27. Mixed mode failure against rubble.

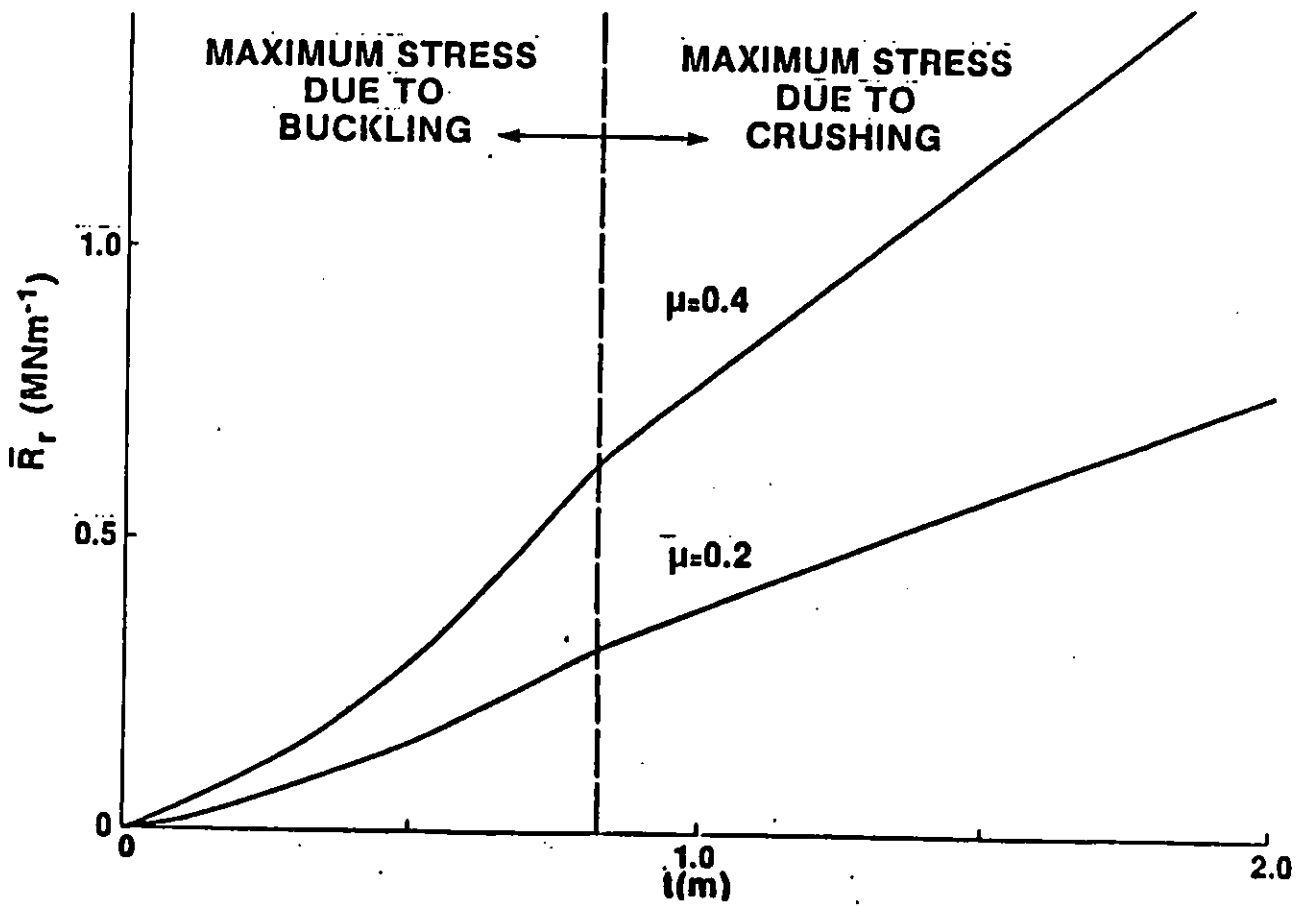


Fig. 28. Average force versus ice thickness (Kry 1980).

TABLE 2
Forces per unit width during
rubble formation (MNm^{-1})

Water Depth (m)	Sail Height (m)	Sheet ice thickness (m)		
		0.5	1.0	2.0
5	5	0.02	0.03	0.04
5	10	0.08	0.09	0.13
5	15	0.16	0.19	0.25
15	5	0.02	0.03	0.04
15	10	0.07	0.08	0.11
15	15	0.15	0.18	0.22

Figure 29. Forces per unit width during rubble formation
(Kry 1980).

IMPLICATIONS

- ENERGY APPROACH GIVES LOWEST AVERAGE FORCE VALUES - 0.25 MNm^{-1}
(18 PSI FOR 6 FEET OF ICE)
- FOR NOMINAL CRUSHING PRESSURE IN ONE ZONE OF 250 PSI (1.7 MPa)
MIXED MODAL APPROACH (WITH $= 0.2$) GIVES AVERAGE ICE
PRESSURE ACROSS FULL WIDTH OF 32 PSI (0.22 MPa)
- ABOVE VALUES ARE UNPROVEN, BUT OBSERVATIONS IN NATURE INDICATE
GROUNDED RUBBLE IS USUALLY STABLE, IMPLYING EITHER LOW ICE FORCES
OR HIGH RUBBLE SLIDING RESISTANCE
- IF RUBBLE FIELD IS IN LANDFAST ICE, REDUCED ICE MOTIONS AT
END OF WINTER MAY LEAD TO MORE EXTENSIVE CRUSHING AGAINST REFROZEN
RUBBLE

K.R. CROASDALE
1983

Fig. 30. Mixed mode failure against rubble - implications.

- APPLICABLE TO NON-FROZEN IN CONDITION
- OBSERVATIONS IN NATURE INDICATE SEPARATE ZONES OF FAILURE ABOUT
4-5 THICKNESSES WIDE
- MODEL DEVELOPED BY KRY (1978) TO COMBINE STATISTICALLY
THE FORCES VERSUS DISTANCE FOR EACH ZONE
- THE WIDER THE STRUCTURE, THE LOWER THE MEAN ICE STRESS

K.R. CROASDALE
1983

Fig. 31. Crushing across a wide structure.

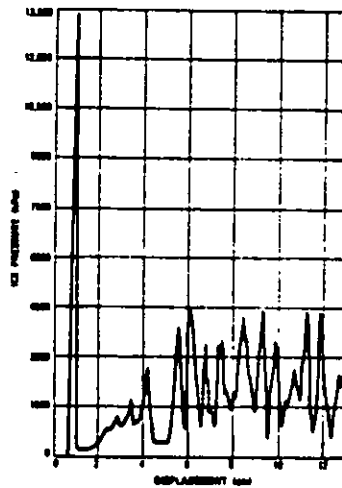


Fig. 32. Indentation pressure versus displacement (Michel & Toussaint 1976).

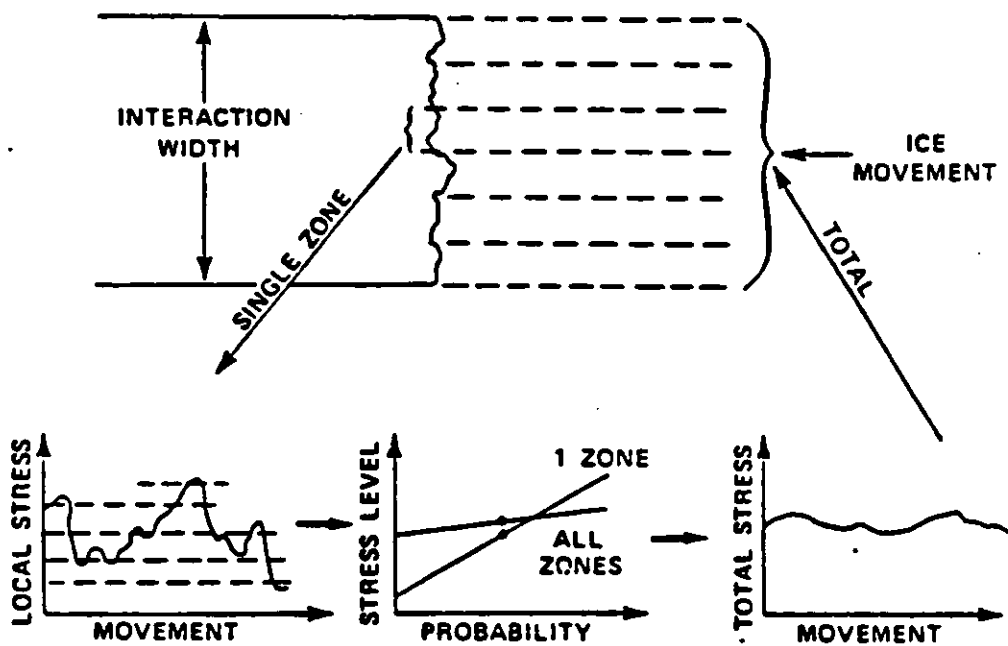


Fig. 33. Kry's stochastic model.

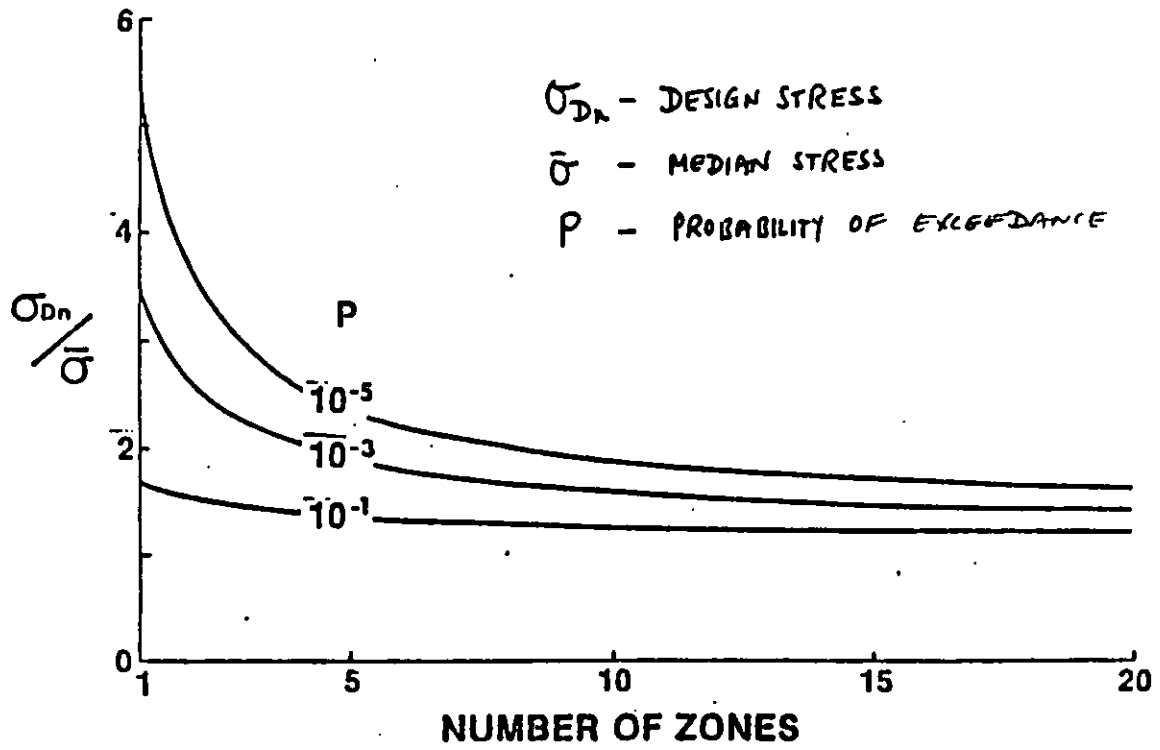


Fig. 34. Design stress versus number of zones.

- FROZEN-IN CONDITION MAY APPLY
- BUT THIS EFFECT CAN BE AVOIDED BY CUTTING SLOTS IN SURROUNDING ICE
- ICE MOVEMENT RATES IN LANDFAST ICE ARE LOW (< 10 FT/HR)
- ICE FORCES MAY BE LIMITED BY STRAIN RATE (2×10^{-6} SEC $^{-1}$)
(SEE EXXON SEMINAR)
- EXXON RECOMMENDED 270 KIPS/FT WIDTH WITH SLOT DEFENSE
(ABOUT 250 PSI)

Fig. 35. Other aspects of ice forces on islands in shallow water.

- ISLANDS BUILT IN BEAUFORT SEA INDICATE SIGNIFICANT ICE RUBBLE
GROUNDS AROUND THEM
- IN EARLY WINTER, RUBBLE HAS SLIDING RESISTANCE WHICH APPEARS TO
BE GREATER THAN ICE FORCES
- LATER IN WINTER, IT IS NOT CLEAR IF CONSOLIDATED RUBBLE TRANSMITS
HIGHER FORCES DUE TO THICKER ICE TO THE STRUCTURE
- RUBBLE FIELDS CAN INCREASE EFFECTIVE DIAMETER EXPOSED TO MOVING
ICE; BUT ADDITIONAL SLIDING RESISTANCE IS OBTAINED FROM GROUNDED
RUBBLE

Fig. 36. Ice rubble fields.

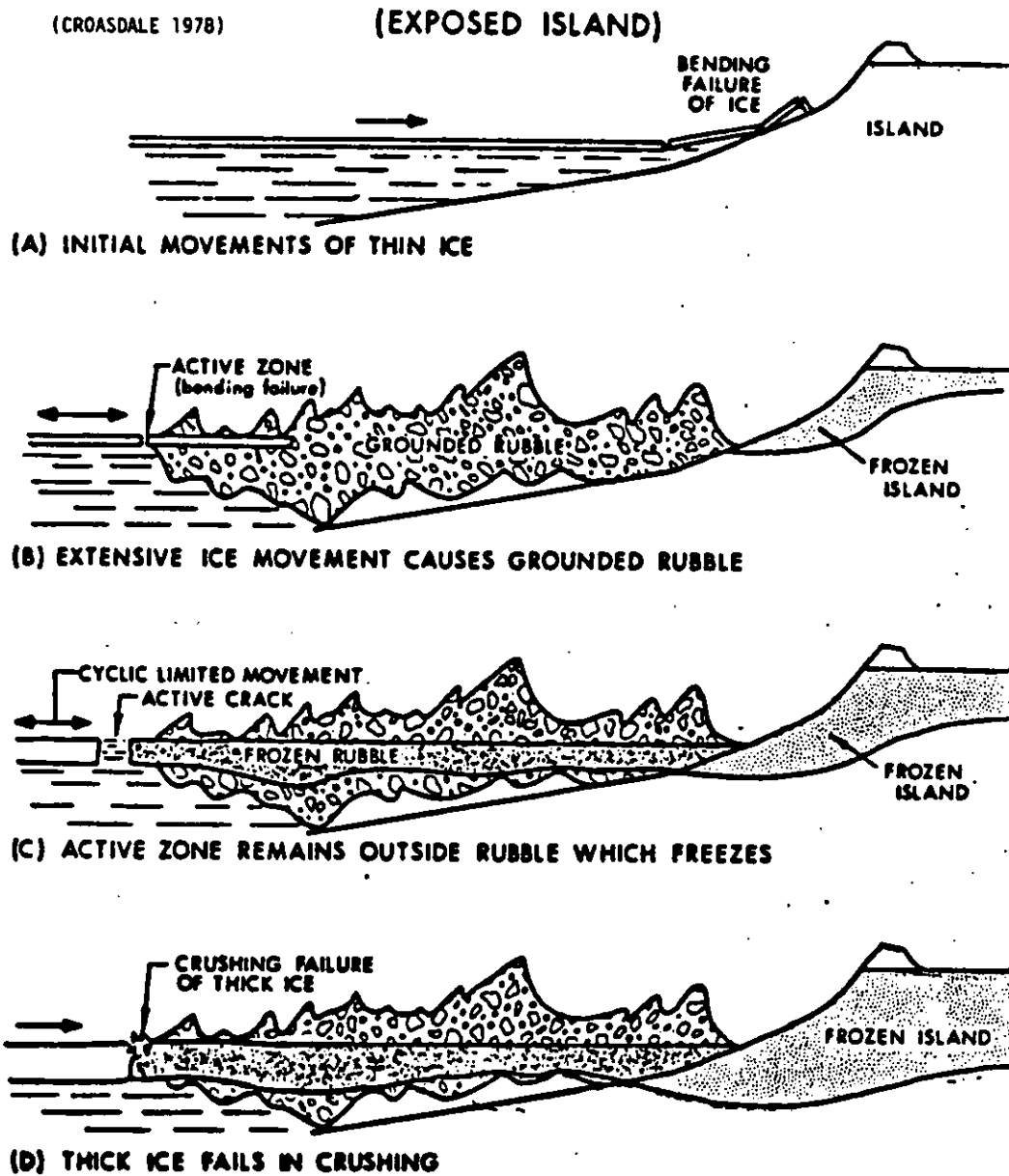


Fig. 37. Sequence of ice action on island beach.

(CROASDALE & MARCELLUS 1978)

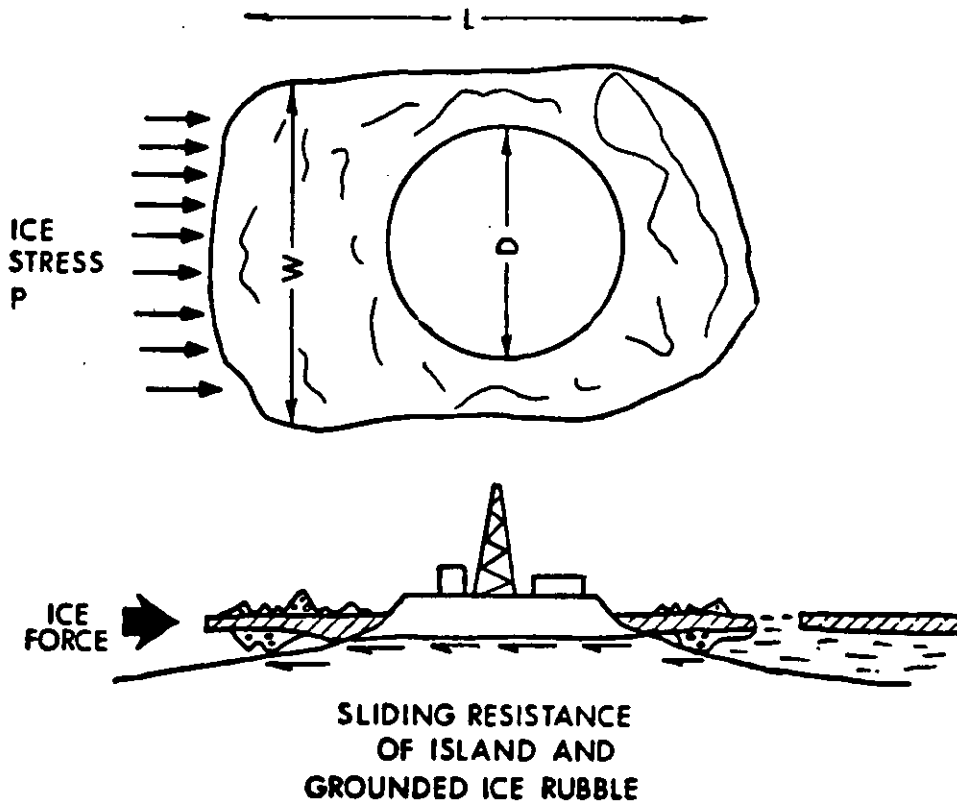


Fig. 38. Refrozen ice rubble.

(CROASDALE & MARCELLUS 1978)

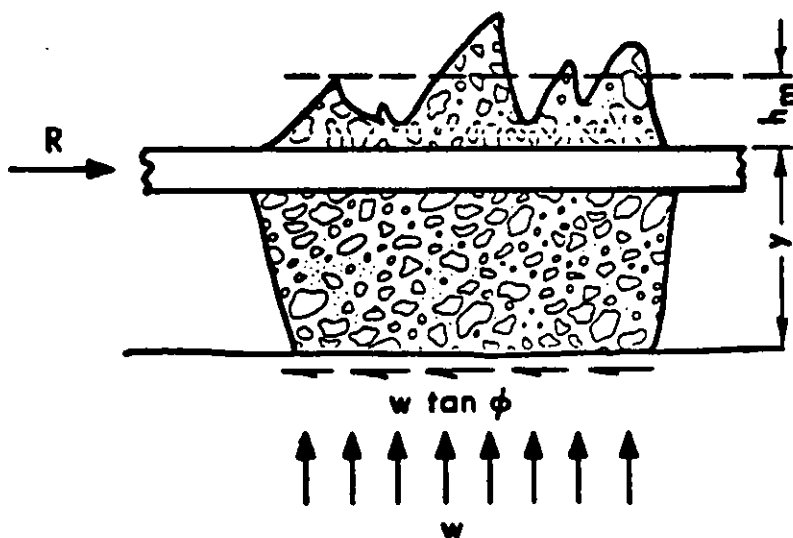


Fig. 39. Sliding resistance of ice rubble.

- STRUCTURES PLACED IN DEEPER WATER HAVE TO WITHSTAND ICE OF THE POLAR PACK
- WORST ICE FEATURES ARE ICE ISLANDS (VERY RARE) AND MULTI-YEAR HUMMOCK FIELDS
- THESE ICE FEATURES CAN BE UP TO 50 M THICK
- DIFFICULT TO DESIGN-FOR ON "LIMIT-STRESS" BASIS (ICE FAILING LOCAL TO STRUCTURE)
- ONE APPROACH IS TO USE A "SOFT STRUCTURE" TO ABSORB INITIAL KINETIC ENERGY
- STEADY LOADS AFTER IMPACT ARE GOVERNED BY PACK-ICE DRIVING FORCES ("LIMIT-FORCE")

Fig. 40. Extreme ice features.

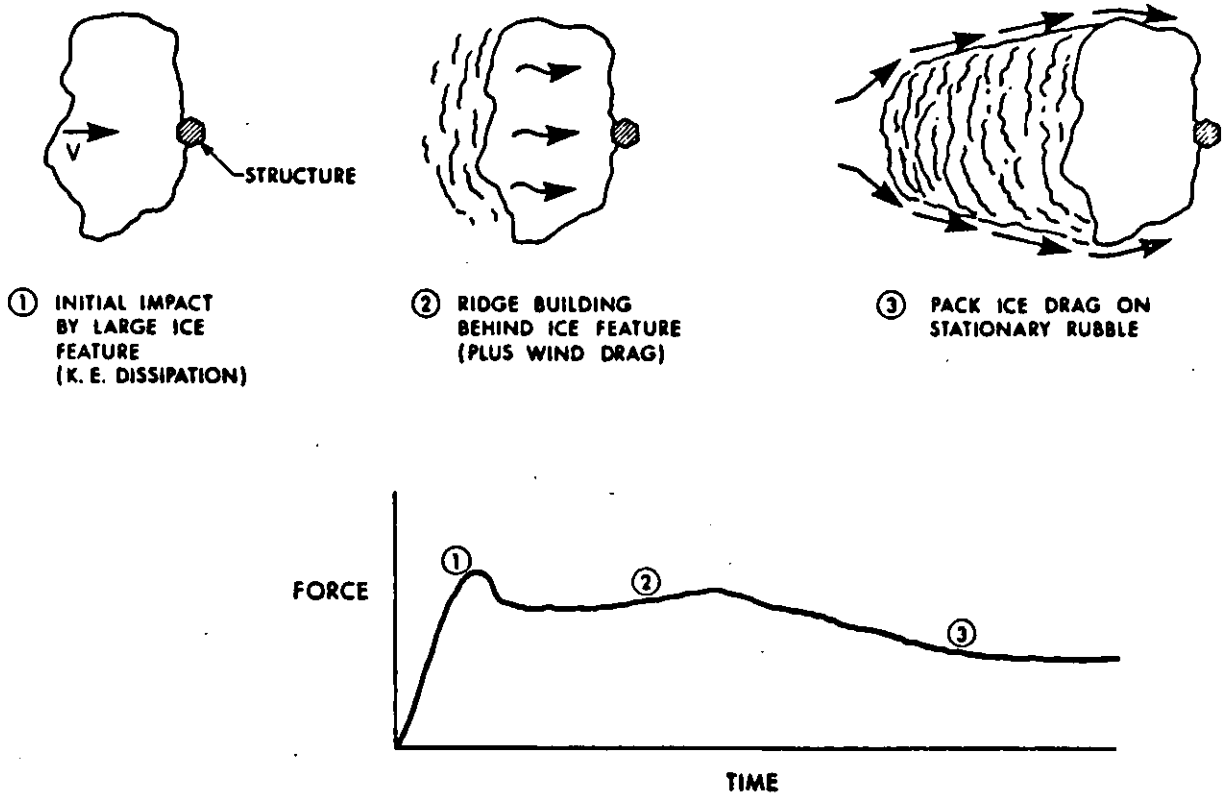
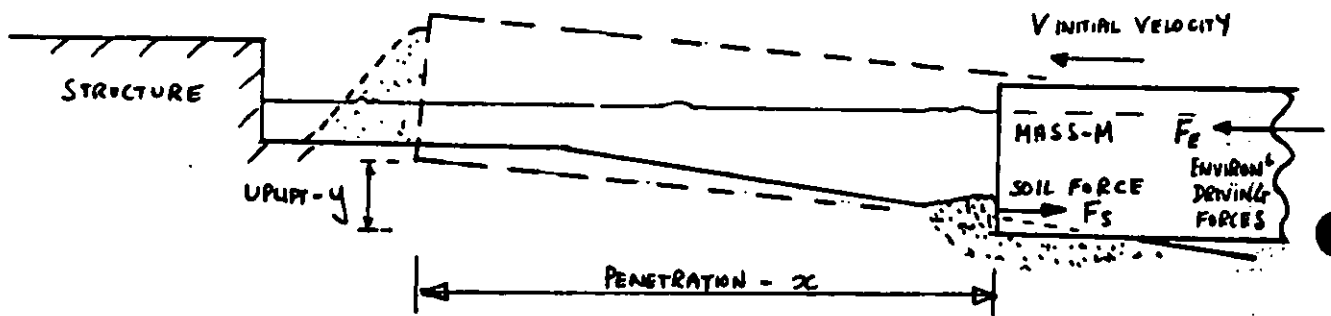


Fig. 41. Stages in ice structure interaction.



• BERM DESIGNED SO THAT EXTREME ICE FEATURE IS STOPPED BEFORE CONTACTING THE STRUCTURE

$$\begin{aligned}
 &\text{INITIAL KINETIC ENERGY OF ICE} + \text{WORK DONE BY ENVIRONMENTAL FORCES DURING PENETRATION} = \text{WORK DONE BY SOIL FORCES} + \text{GAIN IN POTENTIAL ENERGY OF ICE} \\
 &\frac{MV^2}{2} + \int F_e dx = \int F_s dx + Mgy
 \end{aligned}$$

Fig. 42. Initial kinetic energy dissipation against a soft structure.

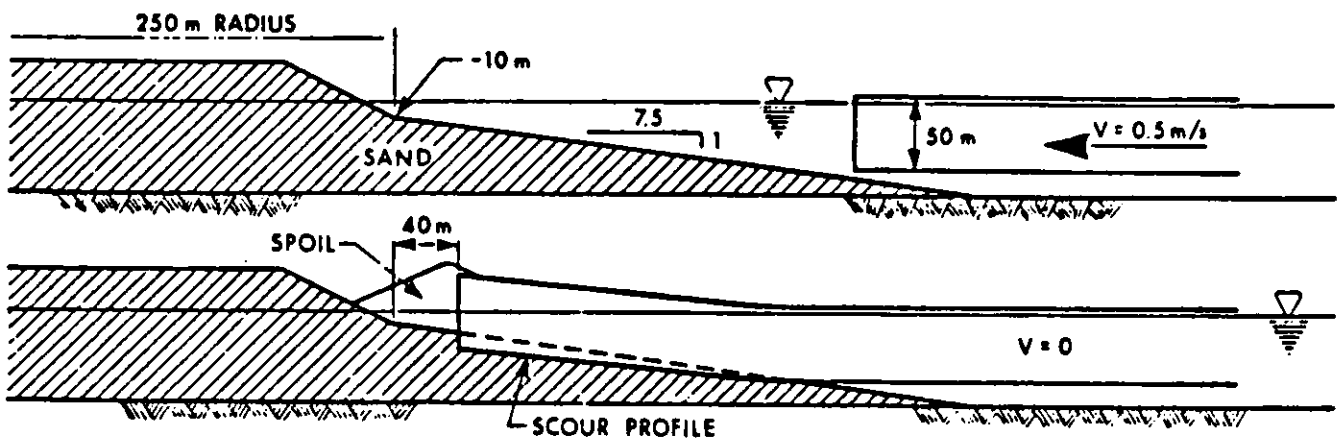
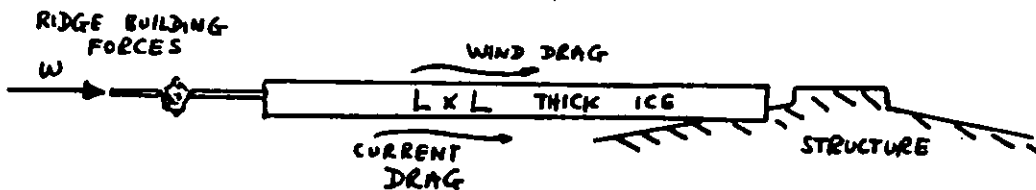


ILLUSTRATION OF THE INTERACTION BETWEEN A 50 m THICK ICE FEATURE AND A BERMED ISLAND

(CROASDALE & MARCELLUS 1981)

Fig. 43. Illustration of the interaction between a 50 m thick ice feature and a bermed island.



$$\text{LIMIT FORCE} = \text{WIND DRAG} + \text{CURRENT DRAG} + \text{PACK ICE FORCE}$$

$$\underline{F_L = C_{10} \rho_a V_w^2 L^2 + 0.5 C_c \rho_w V_c^2 L^2 + W L}$$

REFERENCE: CROASDALE K.R. MEO - ICE FORCES ON LARGE MARINE STRUCTURES, TO BE PUBLISHED AT IAHR [CO-AUTHORED WITH R.N. MARCELLUS]

Fig. 44. Steady limit forces.

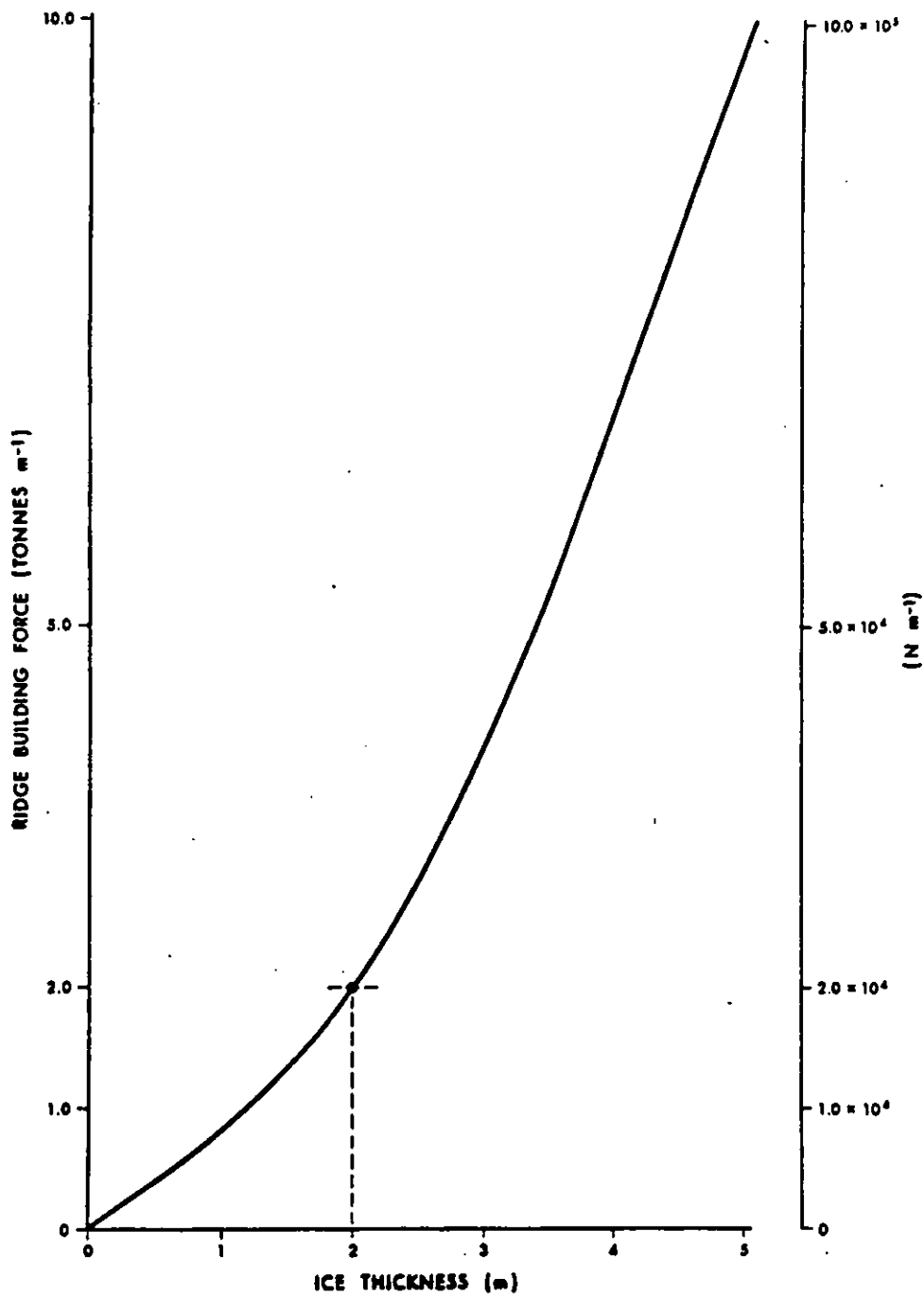
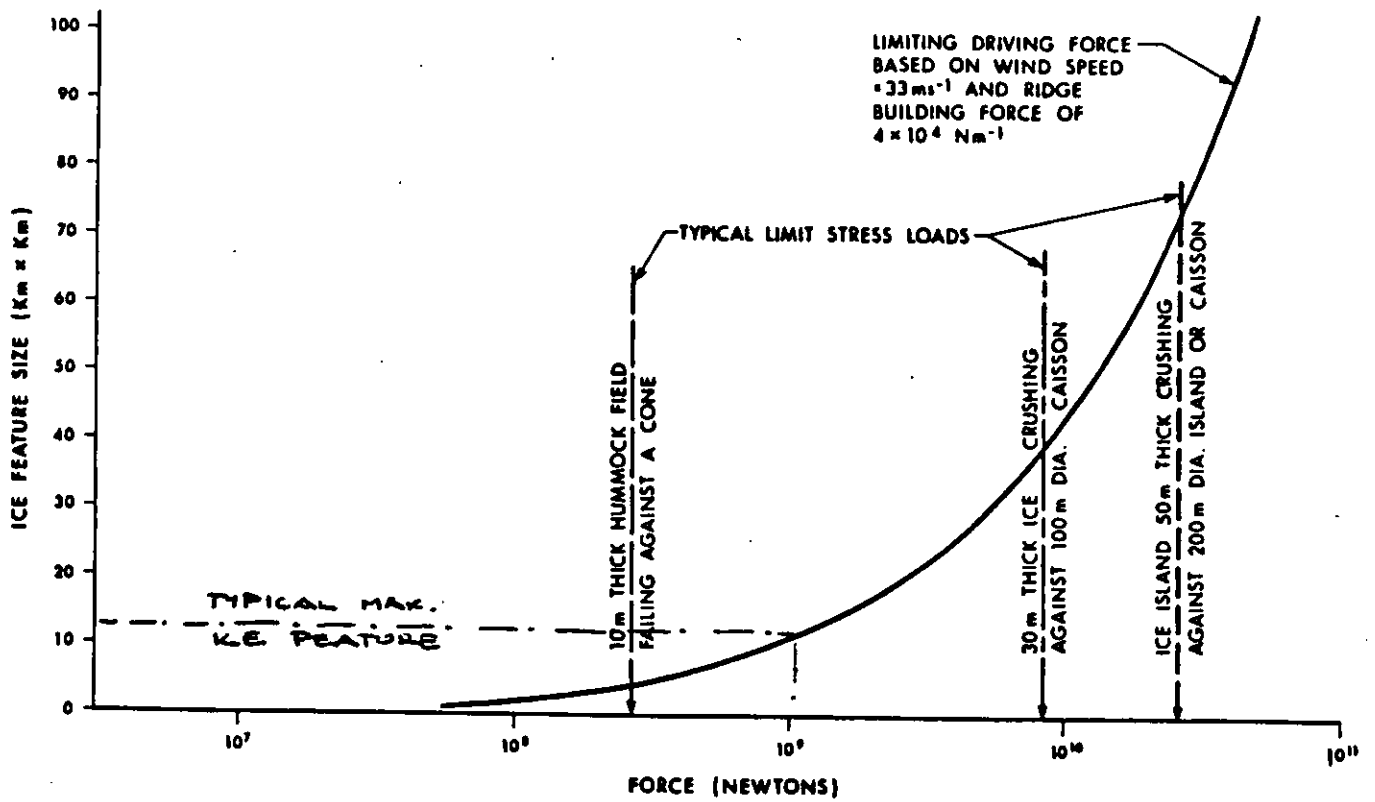


Fig. 45. Ridge building: average force vs ice thickness (Parameter and Coon, 1973).



(CROASDALE, 1980)

LIMITING FORCES
(AFTER INITIAL KINETIC ENERGY DISSIPATION)

Fig. 46. Limiting force (Croasdale 1980).

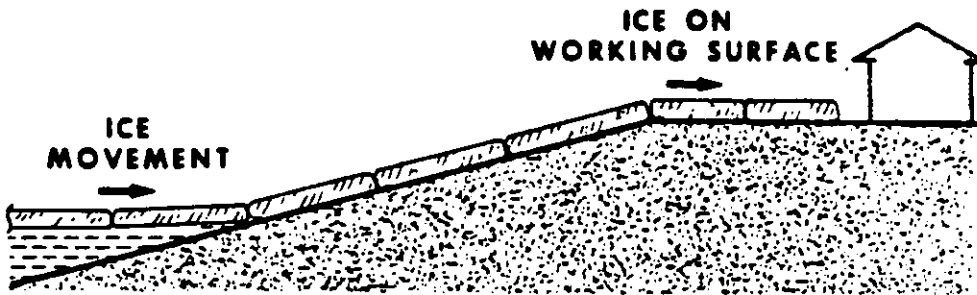


FIG. 47 SIMPLE ICE RIDE-UP

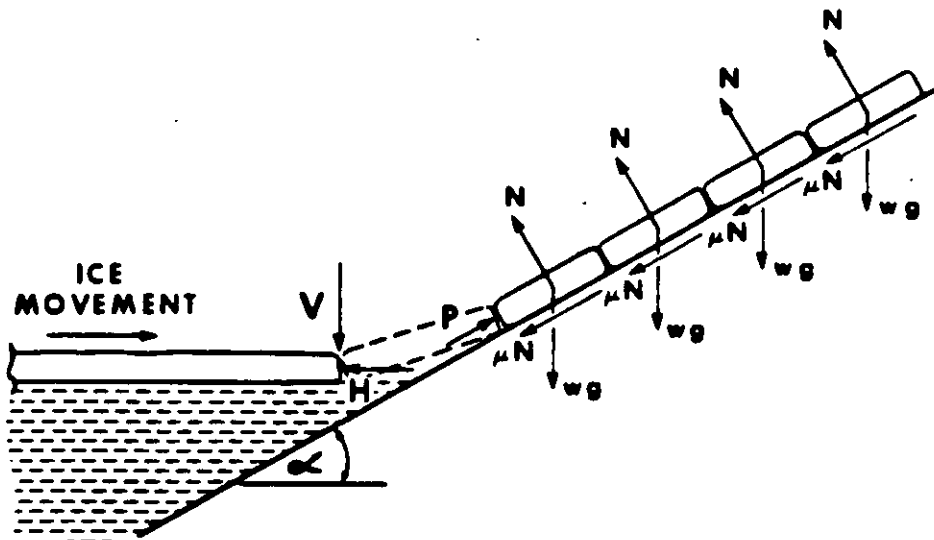


FIG. 48 FORCES FOR SIMPLE RIDE-UP

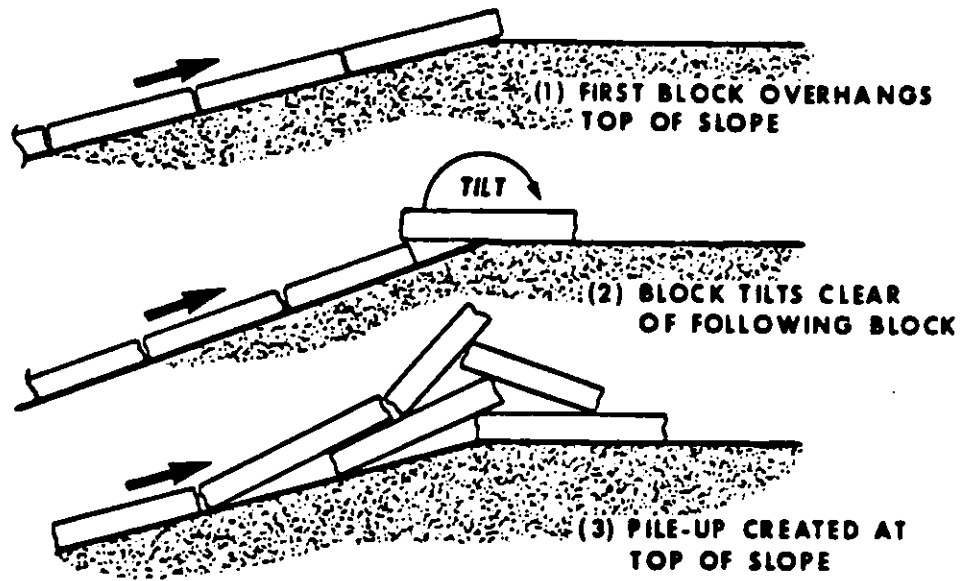


FIG. 49 KINEMATIC INSTABILITY
(PILE-UP AT TOP OF SLOPE)

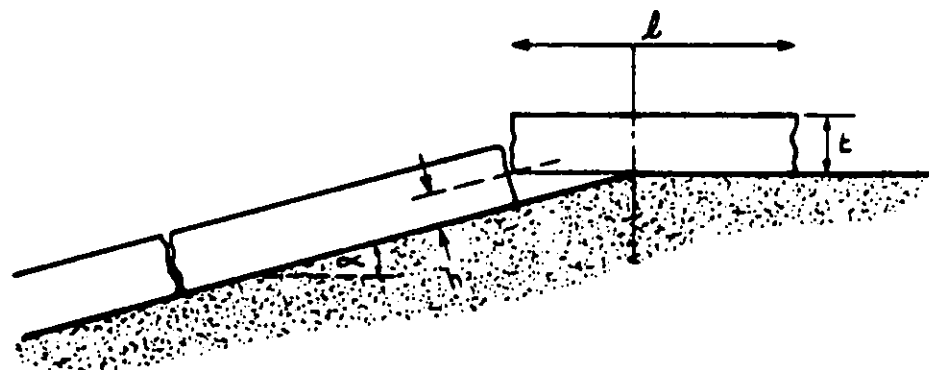


FIG. 50 CONFIGURATION FOR RIDE-UP PAST A SLOPE CHANGE

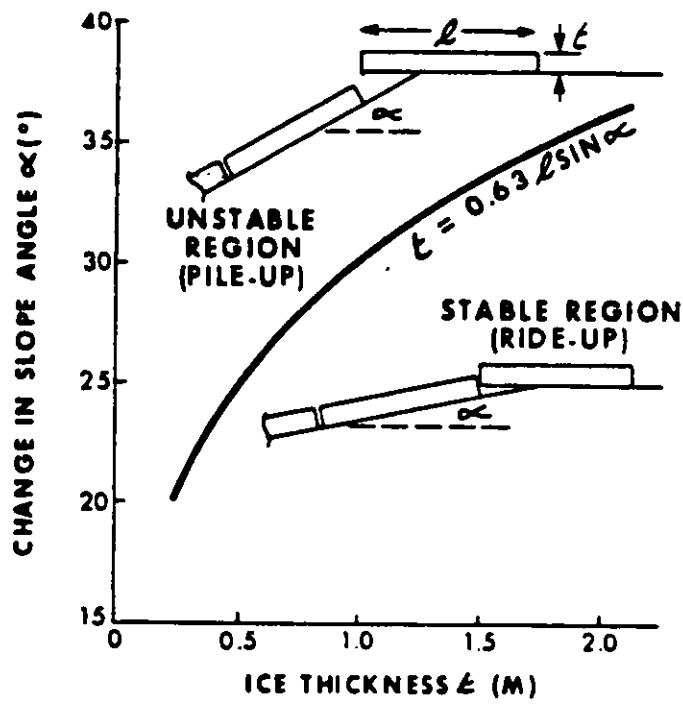


FIG. 51 CRITERION FOR RIDE-UP PAST A CHANGE IN SLOPE

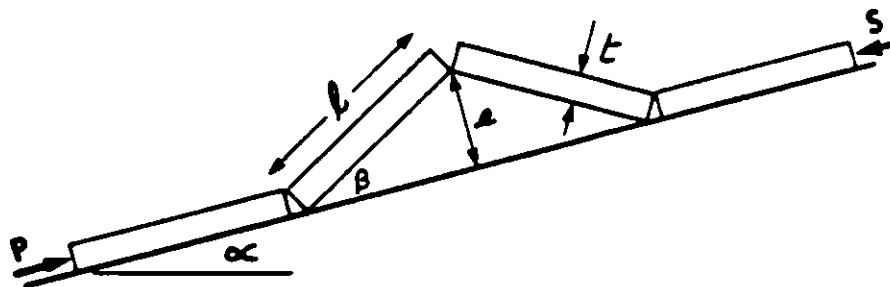


FIG. 52 COMPRESSION INSTABILITY

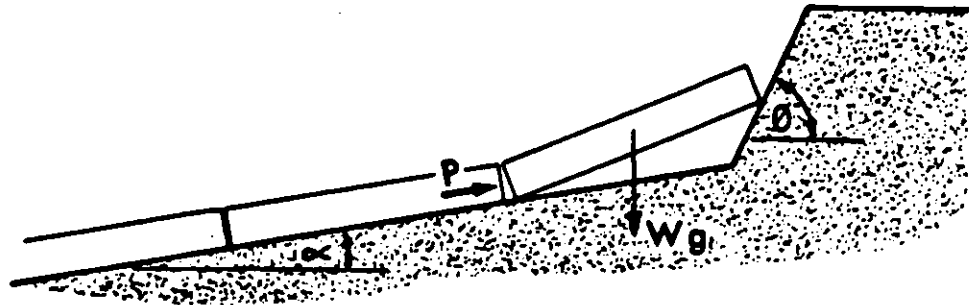


FIG. 53 POTENTIAL JAMMING OF FIRST ICE BLOCK
AT CHANGE OF SLOPE ANGLE

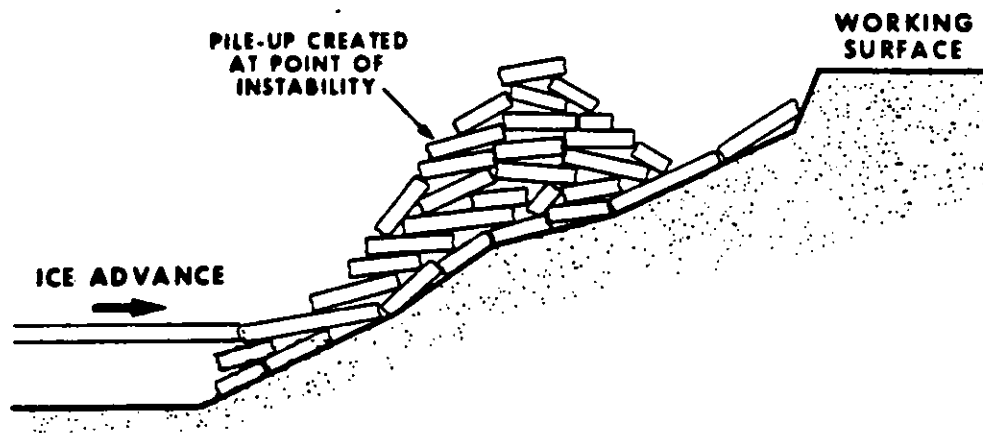
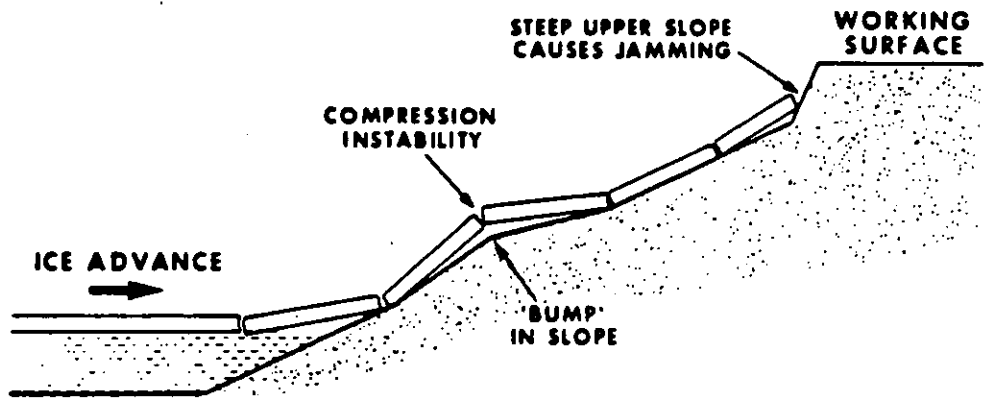


FIG.54 DESIGN TO RESIST ICE RIDE-UP



FLOATING AND SUBMERGED STRUCTURES IN ICE

by: Peter G. Noble.

INTRODUCTION

When a body of water, such as a river, lake or part of a sea freezes over, the ice cover so formed often interacts with a variety of submerged or floating structures such as water intakes, ice booms or ships moored or navigating in such waters. This interaction can be caused by a number of factors, including changes in water level, horizontal movement of water under or air over the ice, or by changes in the ambient temperature.

The problem of designing for ice loads has been around for many years, but it is only comparatively recently that any extensive work has been carried out. During the past ten years, the fields of ice mechanics and cold regions engineering have received impetus from the exploration for and discovery of hydrocarbon resources in northern regions. This recent upswing in cold regions activity has produced a considerable quantity of laboratory data on the properties of ice as measured from small samples and has included a number of projects where

ice load data have been acquired at both model and full scale. In addition, numerous mathematical models have been proposed, but with limited full scale data available for comparison, they do not as yet offer a complete solution. It can be said that, although valuable experience has been gained in the past few years, much work remains to be done before engineers can accurately predict ice loads on marine structures in general or submerged and floating structures in particular.

There are few established "rules of thumb" or "handbook formulations" which can be generally applied. With this in mind and in order to present information which will guide the neophyte "ice engineer" to successful design practices, five specific design studies will be presented, covering site specific applications of a floating plant barge for Arctic use, river ice retention booms, semi-submersible rig drilling design for temperate ice covered waters, water intake pipelines and submarine electrical power conduits.

FLOATING PLANT BARGE FROZEN-IN

This example takes into consideration the ice loads applied to a barge frozen into a pool or protected dock area. The ice loads applied to the vessel consist of the following:

- ° thermal pressure due to the abrupt changes in air temperature
- ° wind induced force of moving ice floes.

In order to predict the forces of stresses that might occur, it is necessary to have information not only on the properties of ice, but also on the actions between the ice and the barge.

Static thermal ice pressure exerted on the barge will develop due to a rise in temperature of the ice cover, when its free expansion is obstructed by the shores and the structures. This thermal ice action acquires maximum significance for the design of a barge of substantial extent under the climatic conditions typified by the abrupt fluctuation in air temperatures, and hence ice temperatures.

The deformation of ice is a complex dependence on a number of factors, including temperature and structure of ice, duration of the effect, nature of load and the state of stress in ice. In addition, the local conditions like the configuration and nature of the shoreline also have a tremendous influence.

Because of insufficient knowledge on this mechanism, there is no accurate method of determining the thermal pressure. However, empirical equations have been developed by various investigators in this regard.

Korzhasin [1] suggested an empirical equation of the form:

$$P = 3.1 \frac{(T_i + 1)^{1.67}}{T_i^{0.88}} \Phi^{0.33}$$

where P = thermal pressure in t/m²

$$T_i = 0.35 T_A$$

$$\Phi = 0.35 \Delta T_A / t$$

T_A = mean air temperature in °C

ΔT_A = rise in air temperature (°C) during time t (hrs.)

Values for the thermal ice pressure (P) were calculated for various initial ice temperatures and different rate of increase of air temperatures. The results are depicted in Figure 1'. The general design values used by Canadian engineers vary between 14.87 to 22.31 tons per linear metre for rigid structures, such as concrete dams, and for flexible structures it is 7.44 ton/lin.m. Korzhavin states that values between 5 to 30 ton/m² are used in the U.S.S.R; for a completely restrained condition, a value as high as 60 ton/m² is used. For ice cover of 2 metres in thickness, the design values vary between 2.5 to 30 ton/lin.m.

Wind blowing along the ice surface induces a force which tends to move the ice cover, which in turn exerts pressure on the barge. This wind induced ice force depends on a number of factors like wind speed, surface texture and the ice cover area. Danys [2] suggested an equation for the force exerted by the wind against ice cover in the following form:

$$F = 0.132 C U A \quad (\text{KG})$$

where C = drag coefficient (equals to 1.6×10^{-3} for normal snow covered ice)

U = wind speed in m/sec

A = surface area of ice cover in m^2

The pressure acting on the hull of the barge through the ice cover can then be expressed by:

$$P_w = F/Bh$$

where

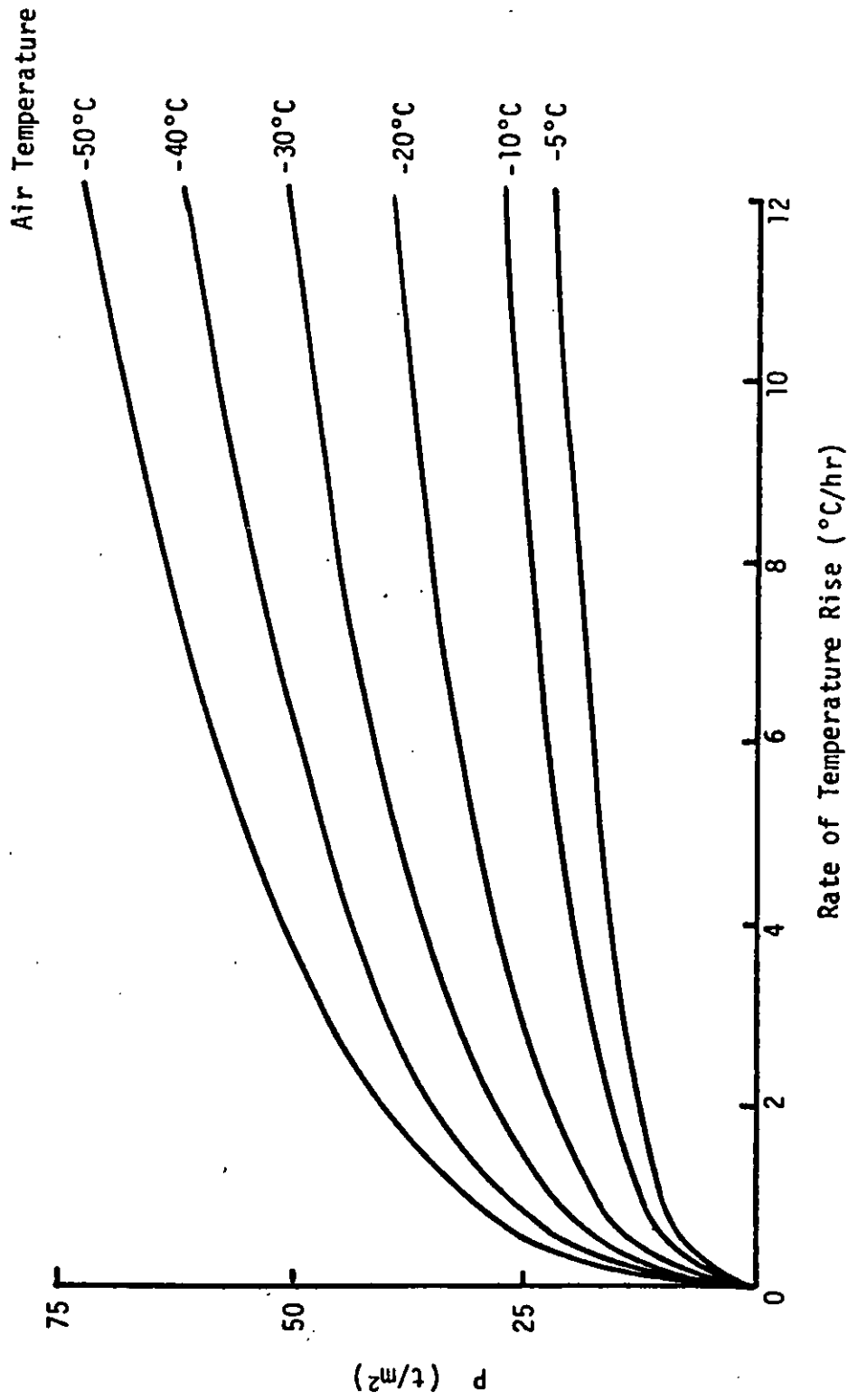
P_w = wind induced ice pressure in Kg/m^2

B = contact length in m

h = ice thickness in m

Values of wind induced ice pressure acting on a 148 m long barge have been calculated for various wind speeds and ice thickness, for a dock area of 40,000 sq. m. The computed results are plotted against the ice thickness as a function of wind pressure (Figure 2).

It can be seen that for restricted dock areas the thermal ice load dominates and conversely other estimates could be made to show that, when frozen into an extensive ice sheet, the wind induced loads would become more significant.

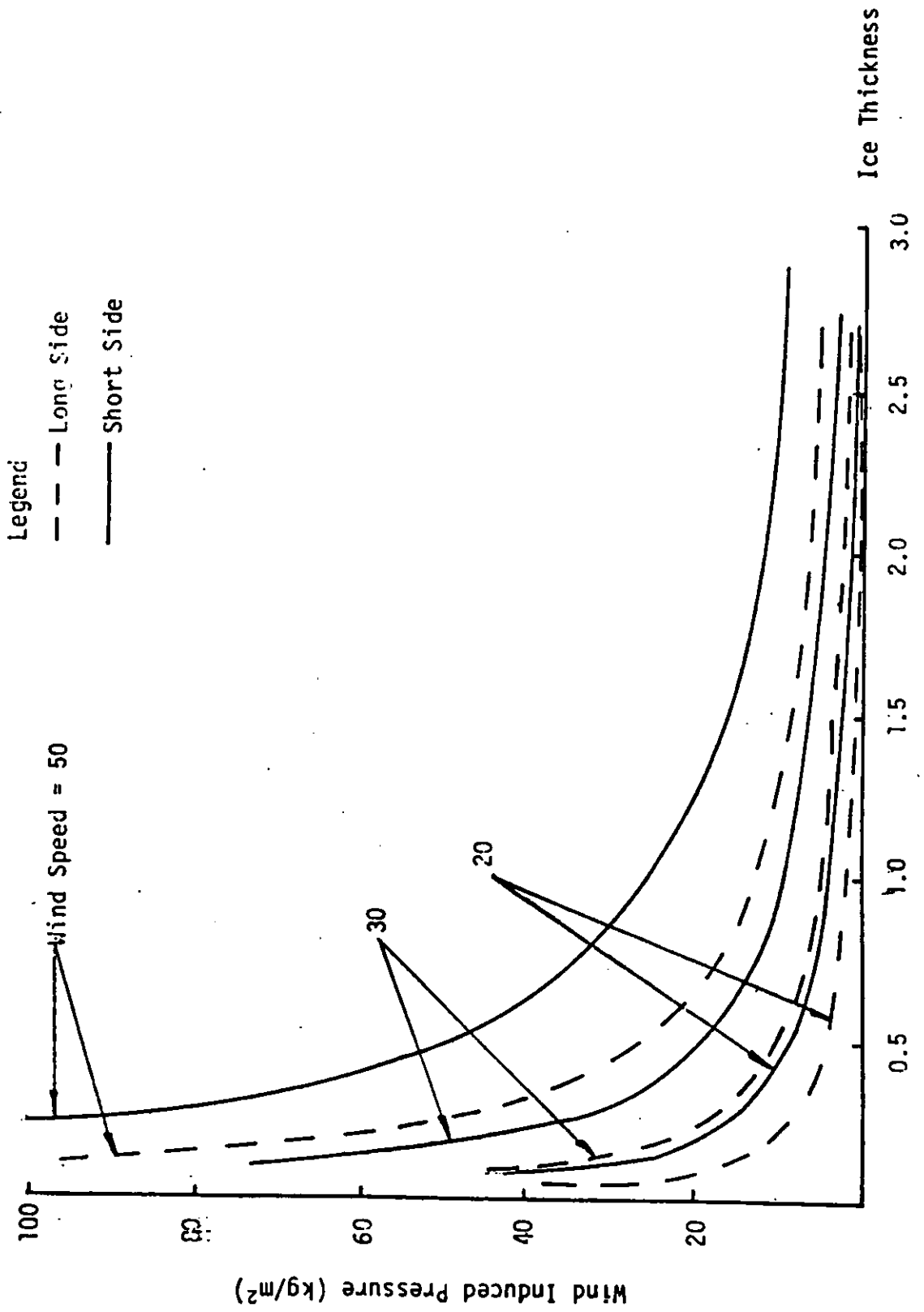


THERMAL ICE PRESSURE

FIGURE 1

FIGURE 2

WIND INDUCED ICE PRESSURE



FLOATING ICE BOOMS

In early winter, ice booms are used to assist nature in quickly forming a solid ice cover on rivers. The open water, insulated in this way, is no longer the source of frazil ice which, in the past, has caused ice jams, flooding, and the loss of electrical generating capacity. They function in other ways as well as strengthening the ice sheet edge against subsequent damage and restraining its movement.

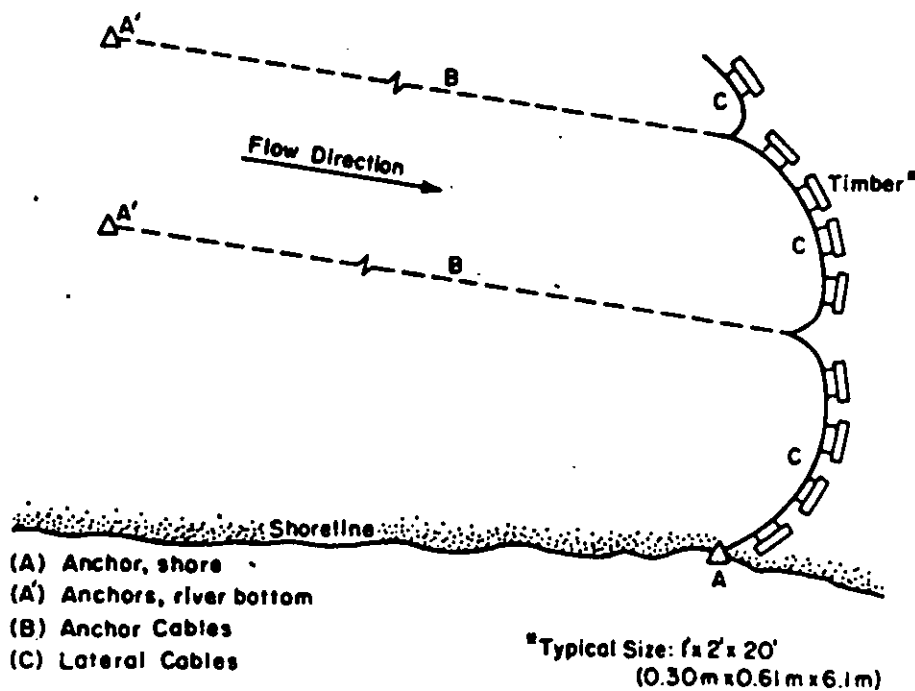
Ice booms are basically lines of floating timbers or pontoons held in place by heavy cable structures connected to buried anchors. They were developed and are used mainly by hydroelectric power groups but they also help facilitate ship navigation in winter. The general details of an ice boom are shown in Figure 3. In operation, the floating barrier restrains the ice floes and the resultant load is transferred to the cable structure and ultimately to the anchors. The anchor cables extend upstream and slope downwardly in that direction at a shallow angle. This lets the booms submerge if the ice forces become too great, as they often do during spring ice break-up.

The floating portion of the ice boom is designed to sag downstream a certain amount. The cable length is often twenty-five or thirty per cent greater than the span to reduce the load in the cable. A secondary benefit of this feature arises when an anchor is inadvertently displaced and the movement can be absorbed by the slack. Anchors used in mud and clay sometimes readjust their position under load.

The anchors used underwater are of three general types, rock anchors, clay or mud anchors and pile clusters. The piles are used in materials of intermediate strength between rock and mud or clay. The rock anchors are usually set in holes drilled deep into the bedrock. One type is a large chain that is suspended in the hole and then fixed in place with concrete. The chain links allow the direction of the anchor load to change without twisting the anchor. The shore anchors are usually of the buried "dead man" type.

FIGURE 3

TYPICAL ICE BOOM



High strength steel wire ropes are used for the structure. Bridge cable has been used in some locations, for example, on Lac St. Pierre in Canada, but generally the 6x19 construction wire rope is easier to handle with conventional equipment. The cables are interconnected by wire rope fittings and heavy steel junction plates. These structural components require that floats be added to keep them from sinking the booms.

Many of the booms, or floating barrier units, are made from Douglas Fir and are roughly 1x2x20' or 30 ft. in size. The general scarcity of large sizes of this wood has led to at least one case of making them from metal. Steel pontoons 1 1/3x2 1/2x20 ft. have been built for ice booms on the Riviere des Prairies north of Montreal. Sometimes two or more pieces are used in parallel.

Except for some ship and handling forces, the load P on an ice boom comes from the ice cover behind it which is continually acted upon by natural phenomena. In simplest terms, after Berdennikov [3]

$$P = Q + D + W + G + I + F$$

where Q = hydrodynamic force at the upstream edge of the ice cover
D = is frictional drag of water flowing beneath the ice cover
W = is frictional drag of air flowing above the ice cover
G = is downstream component of the weight of the ice cover
I = impact force of collecting ice flows
F = is the frictional force or the shearing force from the shore line.

Each of the above terms has significance according to the physical conditions applied and Q, G and I can often be neglected.

Wind can vary in intensity and direction and little is known about its effect on ice accumulations. Siefert and Langleben [4] evaluated a relationship for the shear or drag stress τ_a for wind.

$$\tau_a = C \rho_a U^2$$

where U = mean wind speed, 10m height

ρ_a = air density

and C = a drag coefficient.

They found median values for C of 1.7×10^{-3} and 2.2×10^{-3} over sea ice in the Gulf of St. Lawrence and that maximum C was probably 3.0×10^{-3} for the study.

With the latter value, a 60 mph (26.8 m/s) wind at 20°F (-6.7C) would give a drag stress

$$\tau_a = 0.051 \text{ lb/ft}^2 \text{ (2.44Pa)}$$

The force W is the product of the stress and the ice area.

The drag force D depends upon the roughness of the underside of the ice cover and upon the mean velocity of stream flow. The underside of the ice cover and the stream bed form a hydraulic conduit and the Manning roughness factor n is generally used to describe its roughness. Equations have been developed to distinguish between stream bed roughness and ice cover roughness although the two are sometimes the same. Michel[5] gives an approximate range of roughness values for ice cover of from 0.013 to 0.09 $\text{ft}^{1/6}$; generally ice is rougher in early winter and smoother later on.

The intensity of shear at the boundary of a conduit in uniform flow can be expressed as

$$\tau_o = \frac{f}{4} \frac{\rho V^2}{2}$$

where f is the Darcy-Weisbach coefficient, and V is the mean velocity relative to the boundary, ice cover in this case. The Manning n is related to f through flow considerations as

$$\frac{1}{\sqrt{f}} = \frac{1.49 R^{1/6}}{\sqrt{8g} n}$$

where R is the hydraulic radius of the conduit and the factor 1.49 has the dimension of \sqrt{g} . Combining the above equations yields

$$\tau_o = 0.45 n^2 R^{-1/3} \rho g V^2$$

For a median value of $n = 0.051 \text{ ft}^{1/6}$, $V = 2.25 \text{ ft/sec}$, $R = 17 \text{ ft}$ and $g\rho = 62.4 \text{ lb/ft}^3$

$$\tau_o = 0.14 \text{ lb/ft}^2 \text{ (6.9 Pa)}$$

The force D is the product of this stress and the ice area. Under the above conditions 1/2 square mile of ice would be loaded by nearly two million pounds.

The force F due to friction at the shoreline acts to hold the ice cover back. As the individual floes are restrained by the ice boom they push against each other in response to flow forces. Because of their irregular but generally rounded shape some of this push is exerted laterally. The floes are restrained from moving laterally by the river banks. There exists at this time of year a coefficient of friction between the cover and the bank and F is the product of this coefficient and the bank force.

Latyshenkov [6] conducted a test of ice boom forces in a small power canal with parallel sides. His results showed that these frictional forces were cumulative in an exponential manner such that after the cover length was greater than 2 1/2 to 3 times the canal width, the cover no longer needed support from the boom. The ice in effect is jamming but in a two dimensional manner only and, in the case of the ice booms, this is helpful.

Under average conditions the ice during spring break-up can act with much greater force on the boom. The broken ice pieces are much larger and responding to the added influence of meltwater they move with greater momentum and drag force. According to Pariset [7], the retarding effect of the shoreline (friction) which previously aided the ice boom now practically disappears. The ice boom generally will sink under excessive loads and let the ice slide over. Occasionally, the ice and boom and structure will entangle to the extent that very high loads are developed. Forces over 300,000 lbs have been measured in anchor ropes; it is not uncommon for 7/8 inch chains and large timbers to be broken.

Interesting information on the economics of ice booms in allowing efficient generation of hydro power along with general performance data are given by Perham [8].

ICE WORTHINESS CONSIDERATIONS FOR THE DESIGN OF SEMI-SUBMERSIBLE
RIGS OPERATING IN TEMPERATE ICE REGIMES

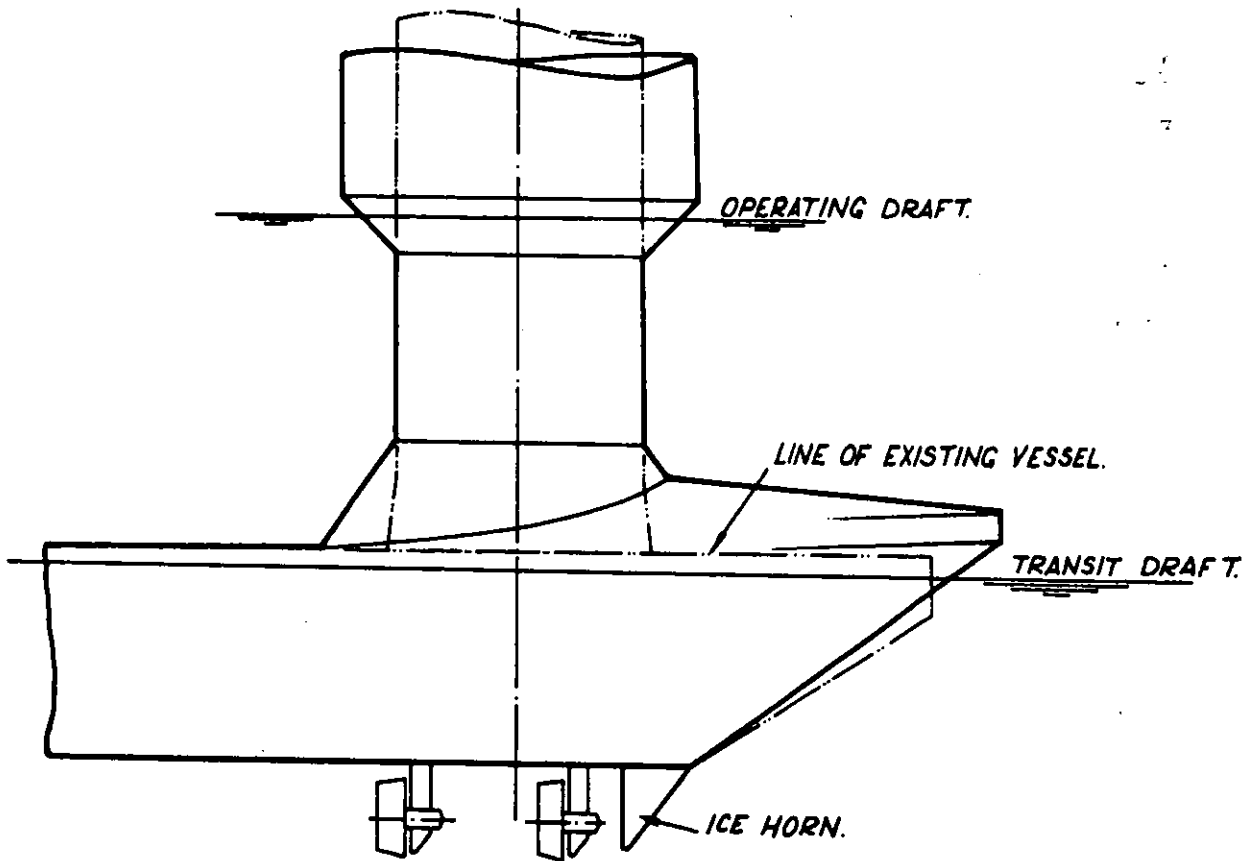
Increasing offshore drilling activities in more and more hostile environments such as the Bering, Barents and Labrador Seas, is creating a demand for floating drilling systems which are both sea-worthy and ice-worthy.

The design examples discussed here are based on proposed modifications to an existing design of semi-submersible to enhance its ice-worthiness while minimising the degradation of sea-worthiness.

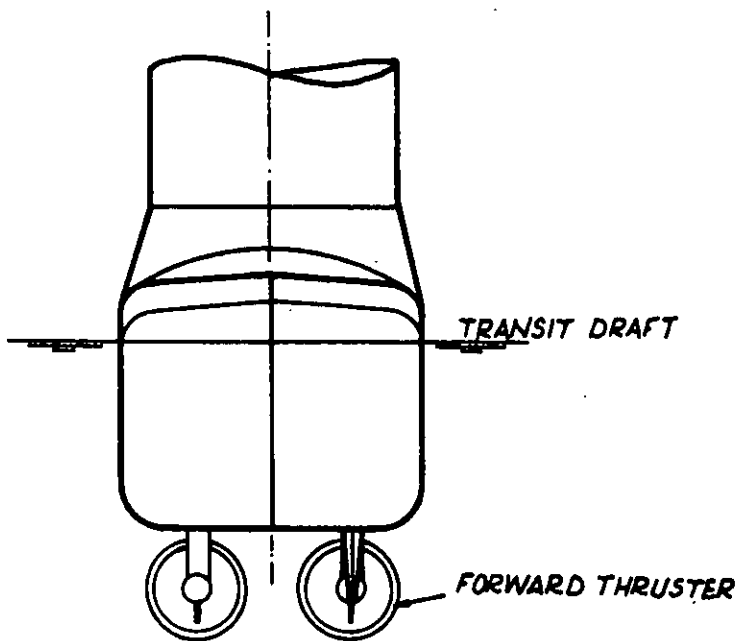
Figure 4 shows the proposed changes at the fore-end of the pontoons. The bow has been raised into a "whale back" to minimise the possibility of ice ride-over during transit in light ice and an ice horn has been added to protect the forward azimuthing thruster.

In addition, the lower columns have been reduced in diameter and the upper columns increased, with a downward conical transition piece fitted. This is intended to minimise ice loading while at drilling draft by causing the ice to fail in flexure rather than by crushing or bucking. All of the columns of the rig would be modified in this way.

In improving the ice worthiness of any vessel, attention to detail design is also important. In the case of the semi-sub, for example, the normal



SIDE ELEVATION



VIEW ON BOW

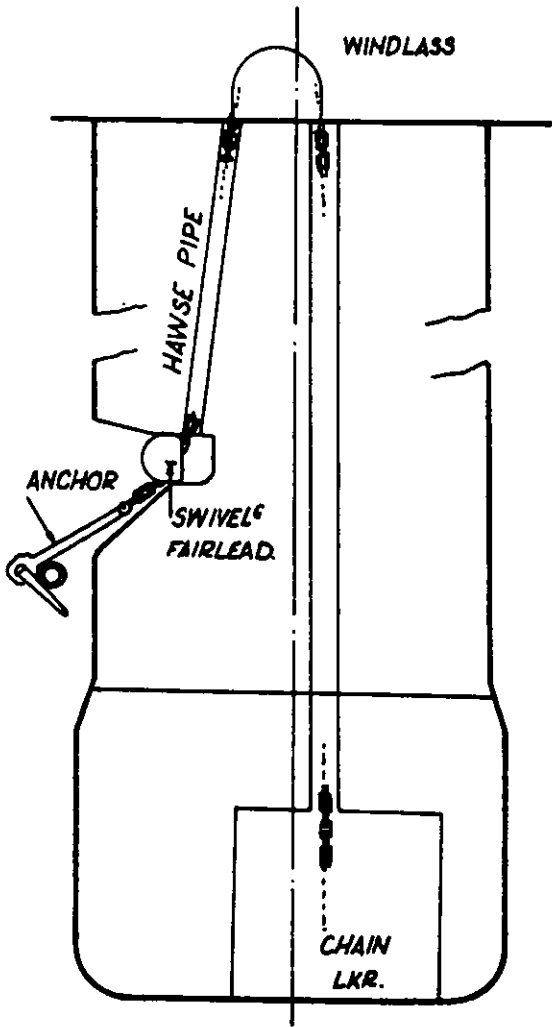
Figure 4

**CHANGES TO THE HULL OF A
SEMISUBMERSIBLE TO IMPROVE
ICE TRANSIT & CLEARING.**

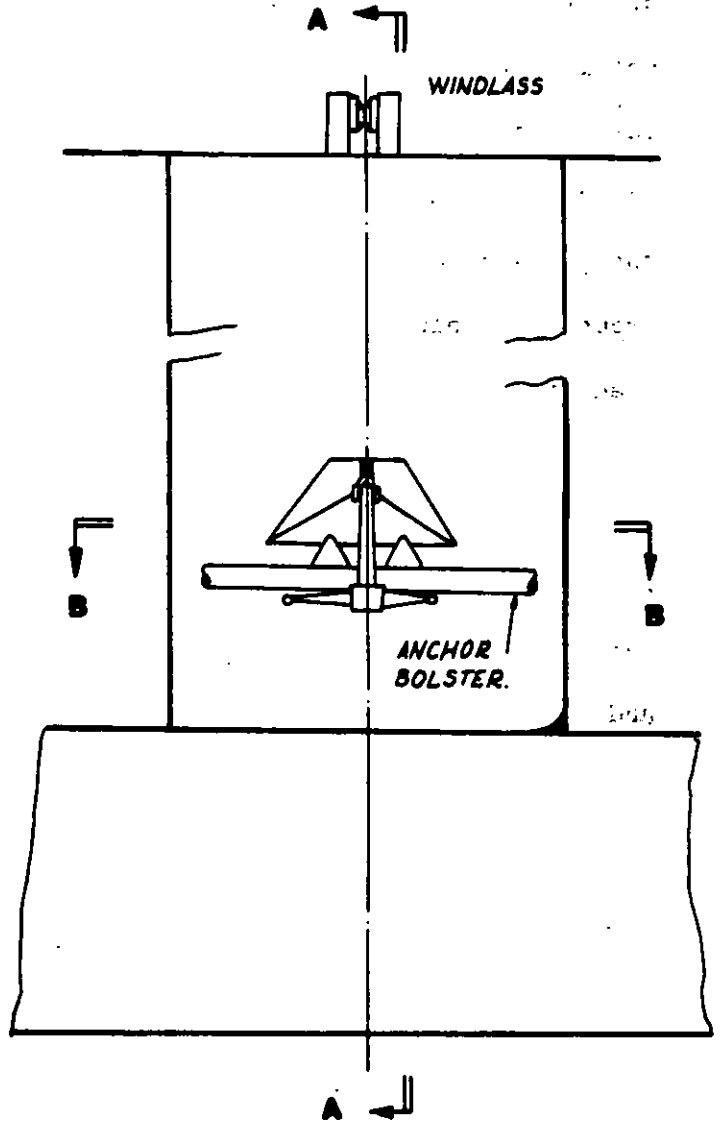
practice of running the main mooring lines up the outside of the columns from underwater fairleads, allows considerable interaction to take place between the mooring and the ice. This has two effects. The ice can "pluck" at the mooring while moving around the leg and, secondly, the pressure of the external mooring can interrupt the free flow of ice around the column causing a build-up of ice which will increase the total load in the mooring system. A suggested improvement is shown on Figure 5.

A further consideration in the basic design of semi-subs for ice-infested waters is whether to use a 4, 6 or 8 column configuration. Model tests carried out by Noble [9] indicate that for the same total waterplane area and waterplane inertia, a 4 column rig appears to give the lowest ice load due to lack of ice bridging between the legs.

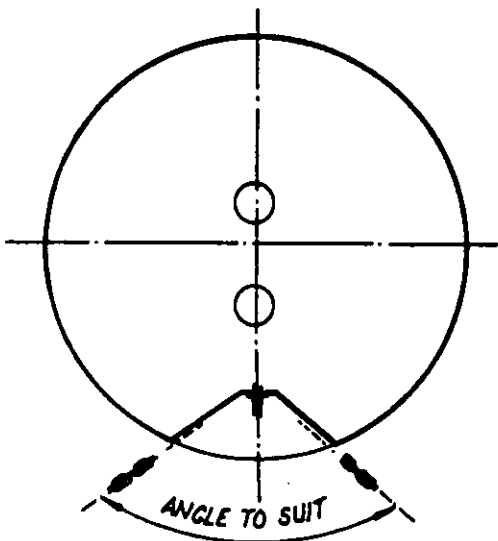
Much work remains to be done to produce effective designs of semi-submersible vessels which will be both ice and sea-worthy.



SECTION A-A



ELEVATION ON LEG



SECTION B-B

Figure 5

**IMPROVED MOORING ARRANGEMENT
-TO REDUCE ICE - MOORING SYSTEM
INTERACTION.**

WATER INTAKE PIPELINE

This case is concerned with a specific incident in which an underwater pipeline was damaged by ice, and as such, it is felt, gives valuable insight into this type of problem. It also illustrates some of the shortcomings of existing design and construction techniques in cold regions.

A 24 inch diameter water intake pipeline approximately 5 miles long was installed in Great Slave Lake in 1977/78 to meet increased water requirements for the town of Hay River, N.W.T. The line, with its associated intake structure and pumphouse, was put into service in January, 1979. By late spring, it became apparent that the line had failed and that water was being drawn into the system from near-shore.

After ice break-up, divers examined the line and found the line was broken at a point 7100 ft. from shore. This case study will review the work done to ascertain the possible mechanisms causing failure to the pipe and to suggest improvements which might minimise future damage from ice.




Figure 6 shows the general layout of the new pipeline (which was damaged) and an older, smaller bore pipeline to the east which had operated successfully for a number of years. Also shown on Figure 6 are the ice conditions prevailing prior to break-up in May, 1978.

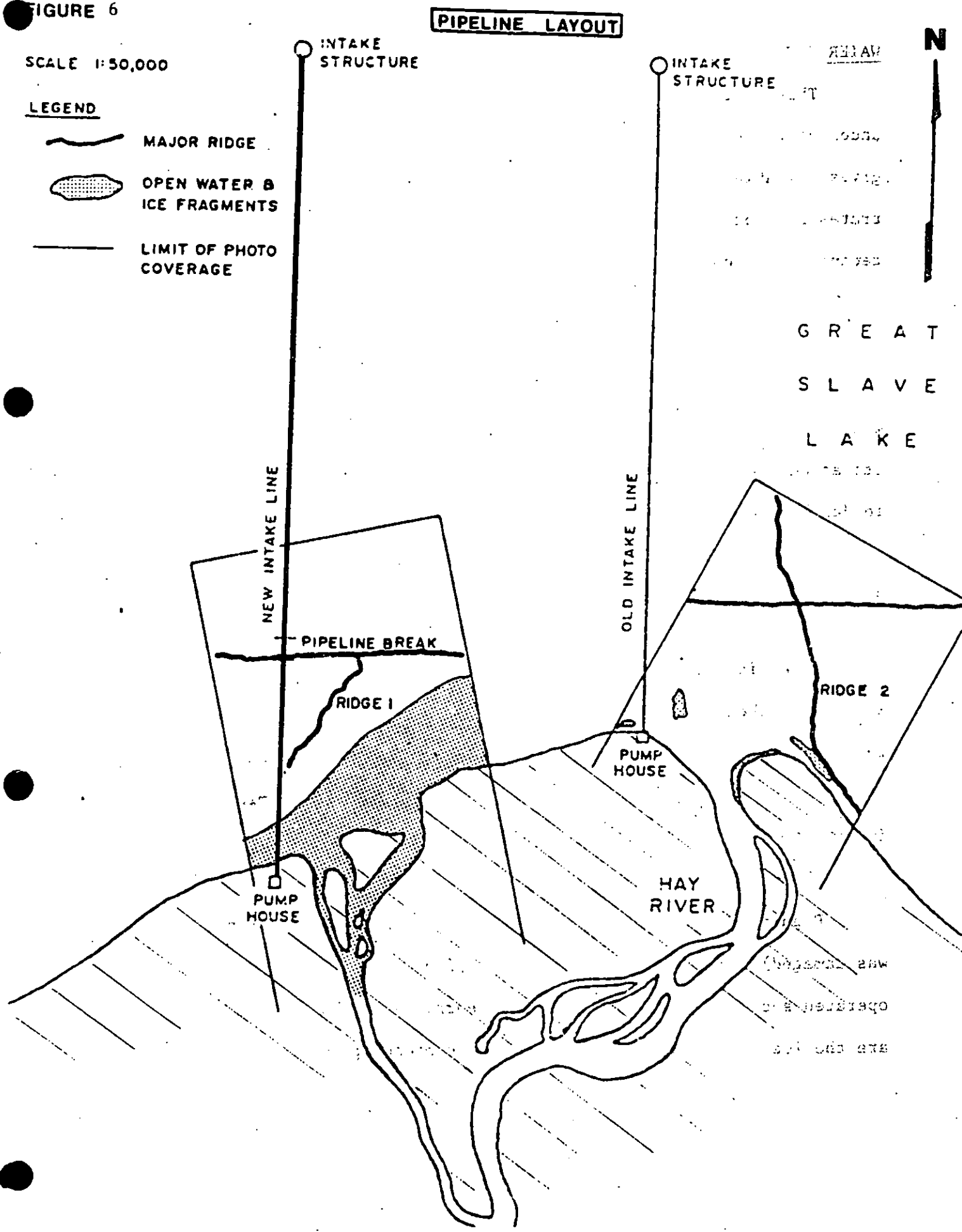
FIGURE 6

PIPELINE LAYOUT

SCALE 1:50,000

LEGEND

-  MAJOR RIDGE
-  OPEN WATER & ICE FRAGMENTS
-  LIMIT OF PHOTO COVERAGE



G R E A T
S L A V E
L A K E

was
operated
and

As can be seen, major pressure ridging was present in the vicinity

of the subsequently discovered pipe break. Figure 7 shows the broken pipe sections as sketched by divers in the summer of 1979 when the pipe damage was identified. Subsequent side scan sonar traces of the area shown in Figures 8 and 9 show large scours in the lake bottom in the vicinity of the pipe.

It is known that considerable forces were exerted on the intake pipe as evidenced by the depths of scours observed on the lake bottom. The magnitude of the forces required to have created the scours can be estimated using the following information:

- ° The maximum depth of scours observed was six ft.
- ° Although the width of the scour was not measured, visual observations by the diver suggest a typical value to be expected might be 20 ft. This is supported by the sonar data which gives scour widths of 8 to 32 ft.
- ° The soil material at the pipeline break is a highly consolidated clay. The following soil properties may be assumed as typical and can be used to provide an estimate of the shearing resistance of the soil:
 - soil unit weight (γ): 132 lb/ft³
 - effective cohesion (c): 2000 lb/ft²
 - effective angle of internal friction (ϕ): 0°

FIG. 7. **WATER INTAKE PIPE DAMAGE**

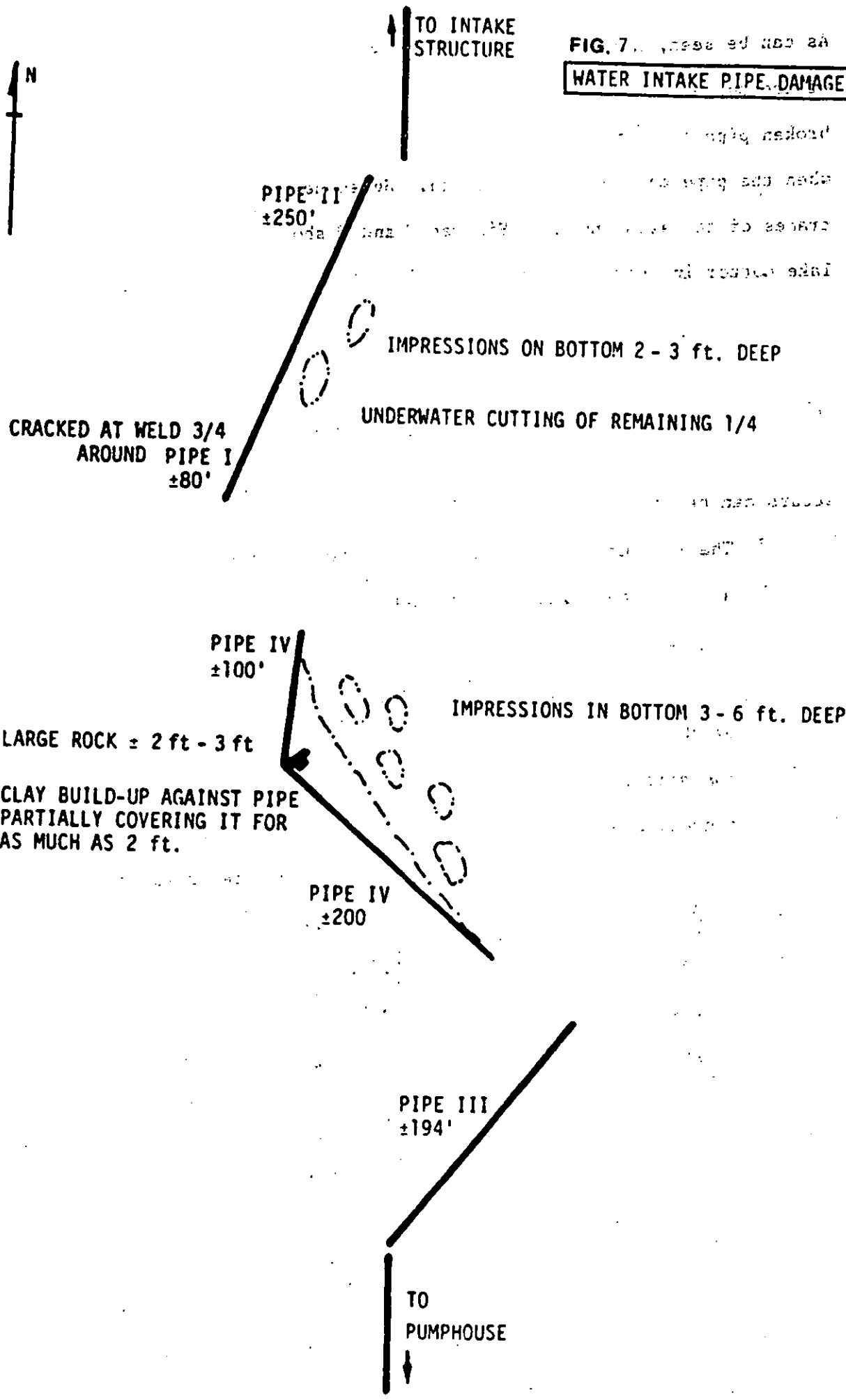
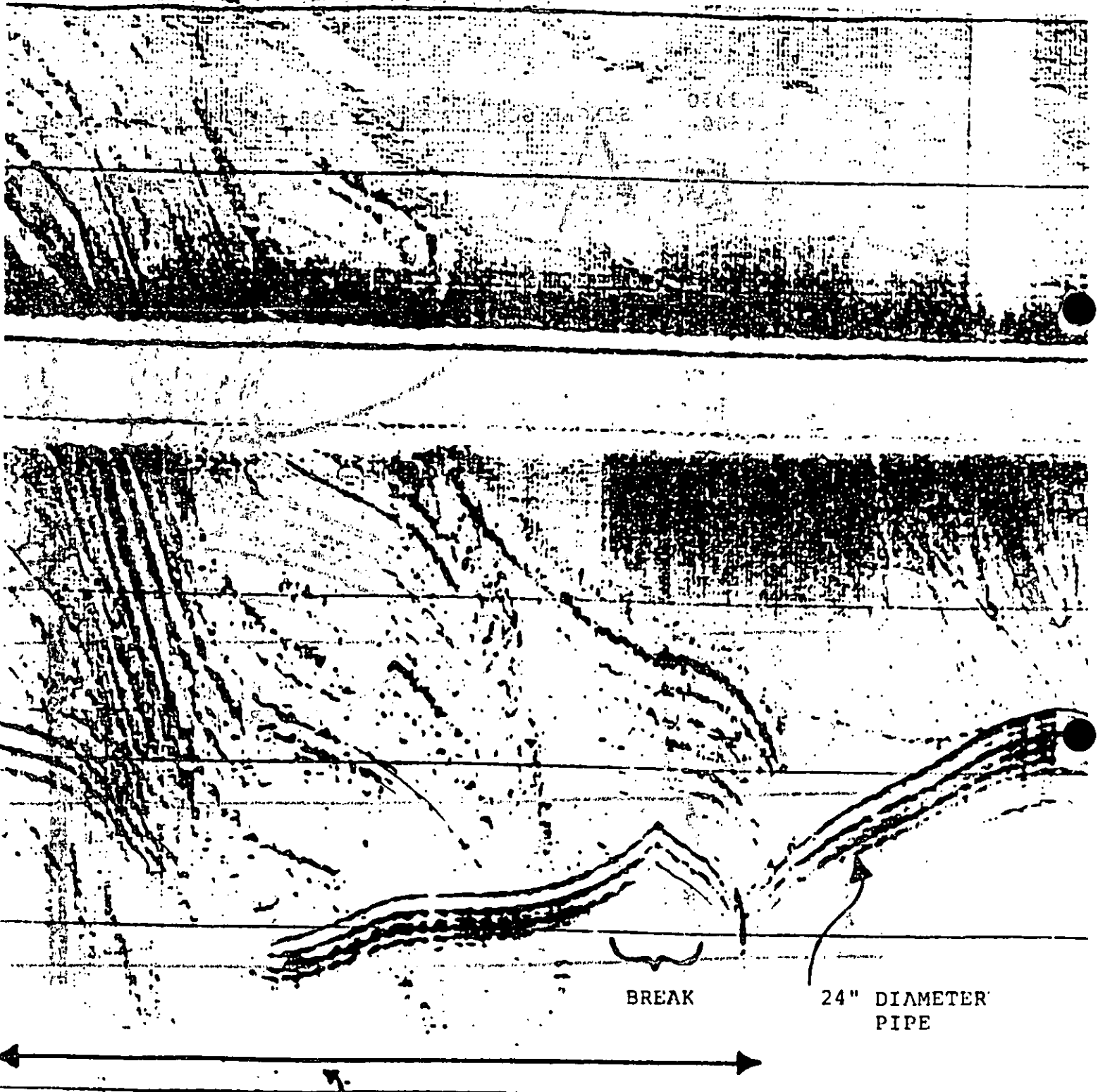


FIGURE 8
SIDE SCAN SONAR PROFILE -- MAIN BREAK

SCALE:
Longitudinal: 1:3350 Transverse: 1:500

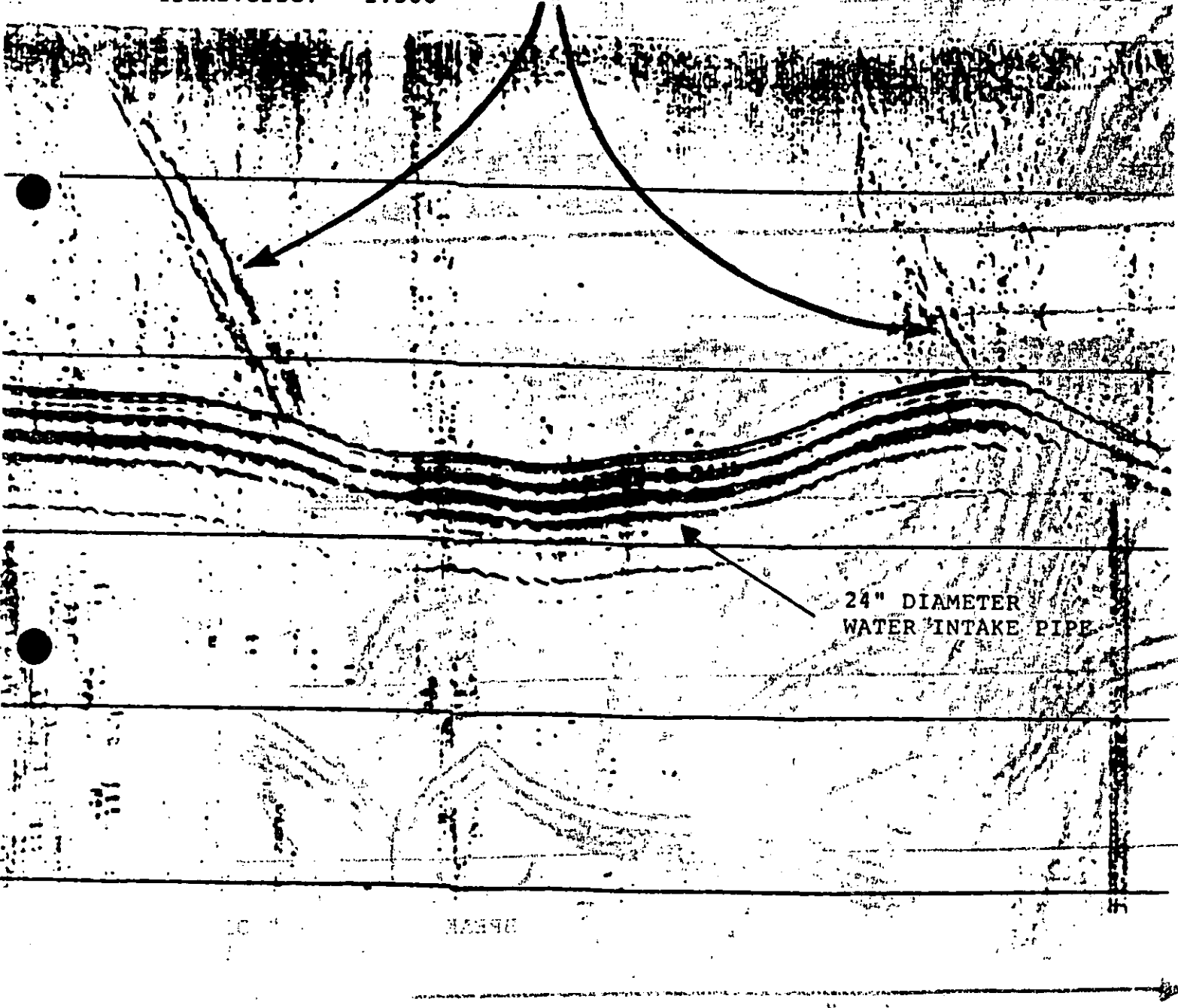


MULTIPLE SCOURS OVER 500 m LENGTH PIPE
INDIVIDUAL SCOURS 2.5 - 10 m WIDE

FIGURE 9
SIDE SCAN SONAR PROFILE
ADDITIONAL SCOURS

SCALE:
Longitudinal: 1:3350
Transverse: 1:500

SINGLE SCOUR APPROX. 100 m LONG & 10 m WIDE



INDIVIDUAL SCOURS ARE
AND THE LOCATIONS OVER THE

The frontal bulldozing resistance may be estimated by calculating the force created by passive earth pressure against a wide (width much greater than height) frictionless wall thrusting horizontally into a submerged sediment having cohesion. [10] From standard soil mechanics, this may be estimated as follows:

$$R = (1/2 \gamma^1 Z^2 N\phi + 2cZ \sqrt{N\phi}) W$$

where R = bulldozing resistance

γ^1 = submerged unit weight of sediment

Z = effective scour depth

$$N = (1 + \sin\phi) / (1 - \sin\phi)$$

This gives: R = 0.51 x 10⁶ lb, using a scour depth of six feet, a width of 20 ft. and the soil properties listed above.

Since this analysis does not include an allowance for friction, or for the pileup ahead of the keel or lateral displacement of the soil, this estimate is likely to be low. Other investigators (e.g.[10]) have felt that this type of analysis may be low, possibly by as much as by a factor of 2. However, it is felt that an understanding of the magnitude of the forces can be gained from this analysis.

It has been shown that large forces would have to have been generated in order to have created the scours. Wind action is the most likely agent. The wind stress on the ice surface can be as much as follows:

as follows:

as follows:

$$\gamma = C C_d V_w^2$$

where γ = wind shear stress

C = air density

C_d = drag coefficient of ice surface

V_w = wind velocity

$$W = \gamma A = C C_d V_w^2 A$$

A typical value for C_d is 0.0015 [11]. Using the above equation, a wind of 30 mph would produce an average shear stress of 0.51×10^4 psi on the ice surface. A northerly wind, blowing across Great Slave Lake from Lonely Bay would have a fetch of approximately 50 miles. Over a one mile wide strip of ice, this would produce a total force of 10.4×10^6 lbs. (approximately 2,000 lbs/ft.). Consequently, it is clear that wind action could have generated sufficient force on the ice sheet to have created the scours, with the wind generated force acting on a 200 - 300 foot strip.

The impact of pressure ridge keel with the intake line and the grounding of the pressure ridge over the intake line would impose both lateral and vertical stresses on the pipeline.

A grounded pressure ridge is usually uplifted from its isostatic equilibrium level. Since this mass of ice is supported by the pipe, vertical stresses are imposed. A ridge with a 13 foot sail and 100 foot breadth grounded transversely on the pipeline break would impose a vertical force of 3.18×10^5 pounds per foot of the ridge, using the Kovacs pressure ridge geometric model. If this force was distributed evenly

over the breadth of the keel, a vertical stress of 960 psi would be imposed on the pipe. However, it is doubtful that the ridge keel would have sufficient structural integrity to mobilize the full vertical load. The ice in the ridge keel may fail by crushing or shearing of the inter-ice block bonds, or of the blocks themselves. Relatively low values for these ice strengths are expected since the ice temperature will be relatively high due to presence of the water. The effects of confinement of the ice within the ridge keel may, however, serve to cause high local pressures to be exerted on the pipe. It is possible that pressures higher than 350 psi (the design stress used for the pipe) could be exerted locally. However, since local indentations were not observed in the salvaged pipe, it is likely that the pipe was not broken by the imposition of vertical stresses.

Horizontal stresses could be applied to the pipeline by the impact of a drifting pressure ridge keel or on ice floe accumulation. As was shown previously, a force of approximately 0.5×10^6 lba was required to cut the observed lake bottom scours. If we consider this force to be distributed over an area equal to the width of the trench by the diameter of the pipeline (i.e. 20 feet) by 2 feet, a structural integrity of the ridge keel of 89 psi would be required in order to mobilize the full energy of the keel into scouring.

This is not an excessive requirement given the confinement imposed by the grounding of the ridge keel and the consolidation of the ridge with time. Consequently, all ice accumulations capable of

impacting the pipeline, except possibly newly formed ridges, would likely have had sufficient structural integrity to have damaged the pipeline.

Pipeline failure occurred at the welded joints between individual pipe sections. Since the pipeline was laid directly on the lake bottom, it had little stiffness with which to withstand lateral horizontal stresses. The impact of a pressure ridge keel or ice floe accumulation would tend to displace the pipe along the lake bottom. This would build up shear and bending stresses in the pipe. The shear and bending capacity of the pipeline joints can be estimated as follows:

- Assume a typical weld strength of 30,000 psi in shear and bending; and
 - Assume a weld thickness of 1/4 inch between adjacent 3/8 inch wall pipe sections
- This gives shear capacity for each weld of 57×10^6 lbs and bending capacity of each weld of 202 tons ft. (neglecting the inner concrete liner due to cracking)

The impact of a pressure ridge would be applied over a relatively small length of the pipeline and would bend the pipeline around the ridge keel since frictional forces (and possibly some scouring) resisting lateral displacement would act over a greater length of the

pipe. It is difficult to estimate the magnitude of these forces resisting lateral displacement of the pipeline.

However, a conservative estimate of the pipe's capacity to withstand horizontal forces can be made by assuming the intake line to be a series of individual pipes each 400 feet in length, that are rigidly grounded at their end points. Assuming a friction factor between the pipe and the lake bottom of 1.0 and a typical pipe weight approximately 200 lb/ft would resist lateral displacement. Using simple beam theory, an ice thrust of approximately 17,000 lbs. concentrated as a point load at the centre of the pipe would exert a maximum bending moment of 202 tons ft. on the pipe section midpoint.

As shown previously, considerably greater forces must have been exerted on the lake bottom during the creation of the scours. Consequently, it is clear from the above estimate that the pipe did not have sufficient lateral support to withstand the horizontal stresses imposed on it by the impact of an ice mass.

CONCLUSION

Basically, lateral support was required for the pipe to prevent subsequent failures. This could be done in several ways, including trenching or the buildup of a berm over the exposed pipe. The extent of the lateral support required depended on several factors. It was recommended that its extent be based on the maximum ridge keel depth to be expected over a given project lifetime. In this case, the

maximum observed extent of ridging from air photo analysis was 8700 feet offshore and since ridges inshore will not have a keel depth greater than the water depth, structures offshore from the point where the ridge was grounded will not likely be impacted by the ridge.

The depth of protection required depends upon balancing the degree of lateral support required by the pipe against that provided by various depths of protection. In this case, a conservative approach was taken to recommend making the depth of protection equal to the depth of the maximum scour observed.

GREAT LAKES SUBMARINE POWER CABLE

A second practical area of ice engineering involving ice scouring is in the routing and protecting of underwater power cables. Figure 10 shows a proposed submarine cable corridor across Lake Erie where active ice scour zones exist on both the U.S. and Canadian sides. Measured scours on the Canadian side were up to 5 1/2 feet deep in water depths from 30 - 72 feet, while lesser scours (up to 2 feet) were found on the U.S. side.

COINTEGRATION

Analytical work done using techniques developed by Chari [12] and Pilkington [13] did not correlate well with the observed scours (i.e. these models gave much greater scour depths than observed in the field). The Chari and Pilkington models were developed for iceberg scours in soft sediments in which the indenting ice feature is assumed to remain unchanged in shape during the encounter. In the case of lake ice ridges

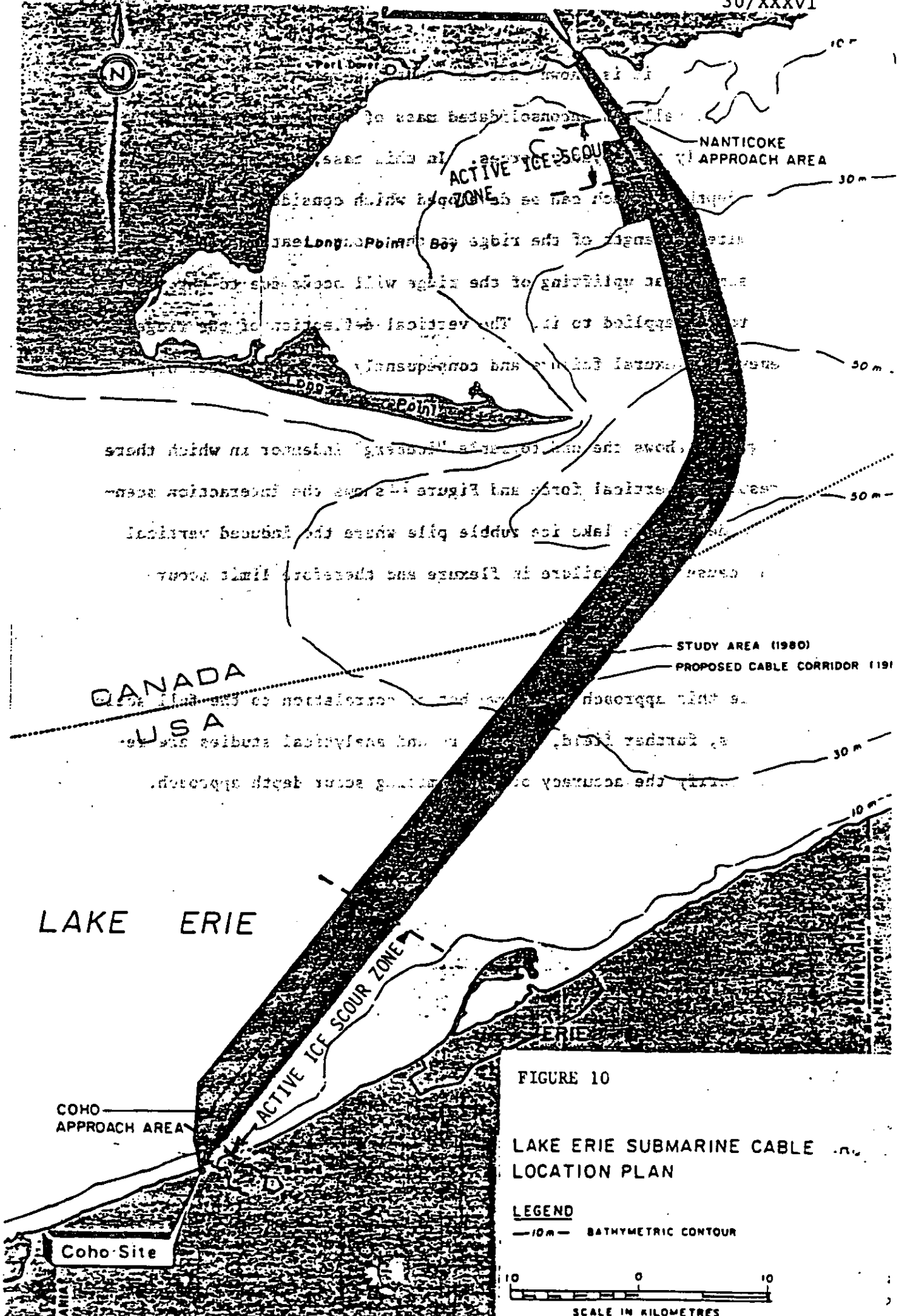


FIGURE 10

LAKE ERIE SUBMARINE CABLE
LOCATION PLAN

LEGEND

—10m— BATHYMETRIC CONTOUR



SCALE IN KILOMETRES

or rubble fields, it is known that the lower extremities of the features are usually an unconsolidated mass of ice blocks held together primarily by buoyancy forces. In this case, a simple limiting scour depth approach can be developed which considers the effect of the limited strength of the ridge on the scour created. This theory assumes that uplifting of the ridge will occur due to the vertical forces applied to it. The vertical deflection of the ridge will generate flexural failure and consequently limit the scour depth.

Figure 11 shows the undeformable "iceberg" indenter in which there is no resultant vertical force and Figure 12 shows the interaction scenario for a deformable lake ice rubble pile where the induced vertical force can cause ridge failure in flexure and therefore limit scour effects.

While this approach has shown better correlation to the full scale observations, further field, laboratory and analytical studies are required to verify the accuracy of the limiting scour depth approach.

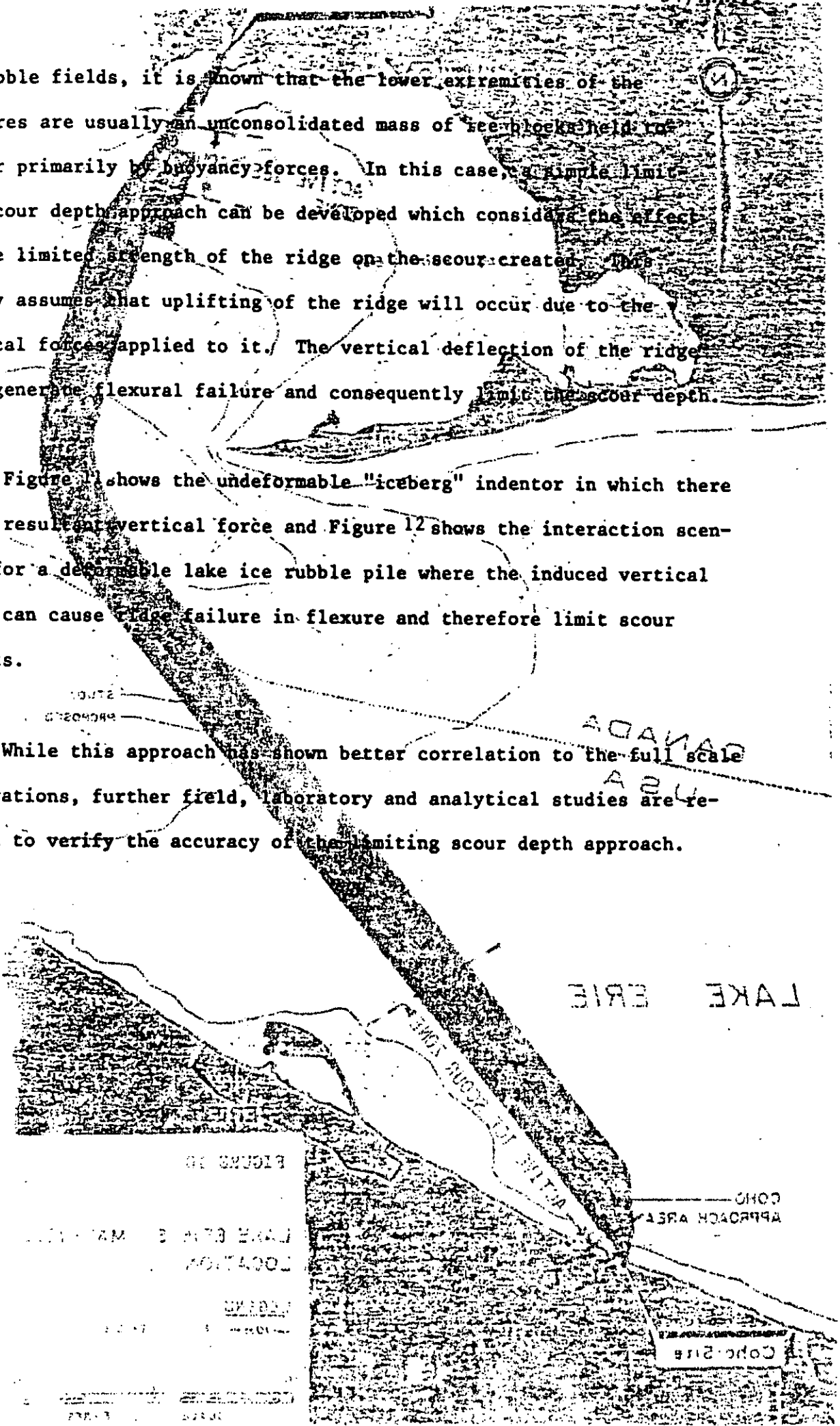


FIGURE 11
LAKE ERIE
LOCATION
SCALE
APPROACH AREA

FIGURE 11

ICEBERG SCOUR

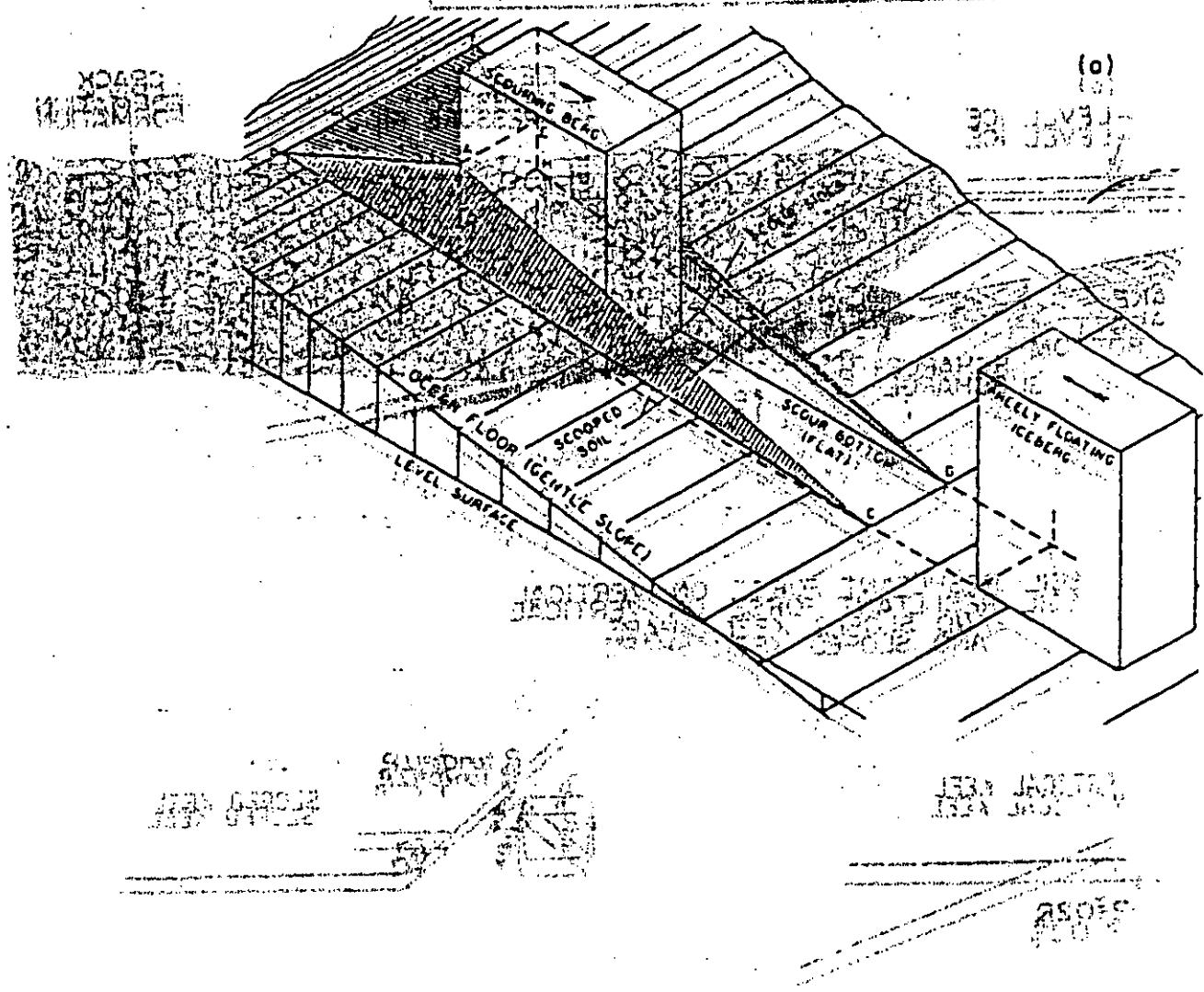
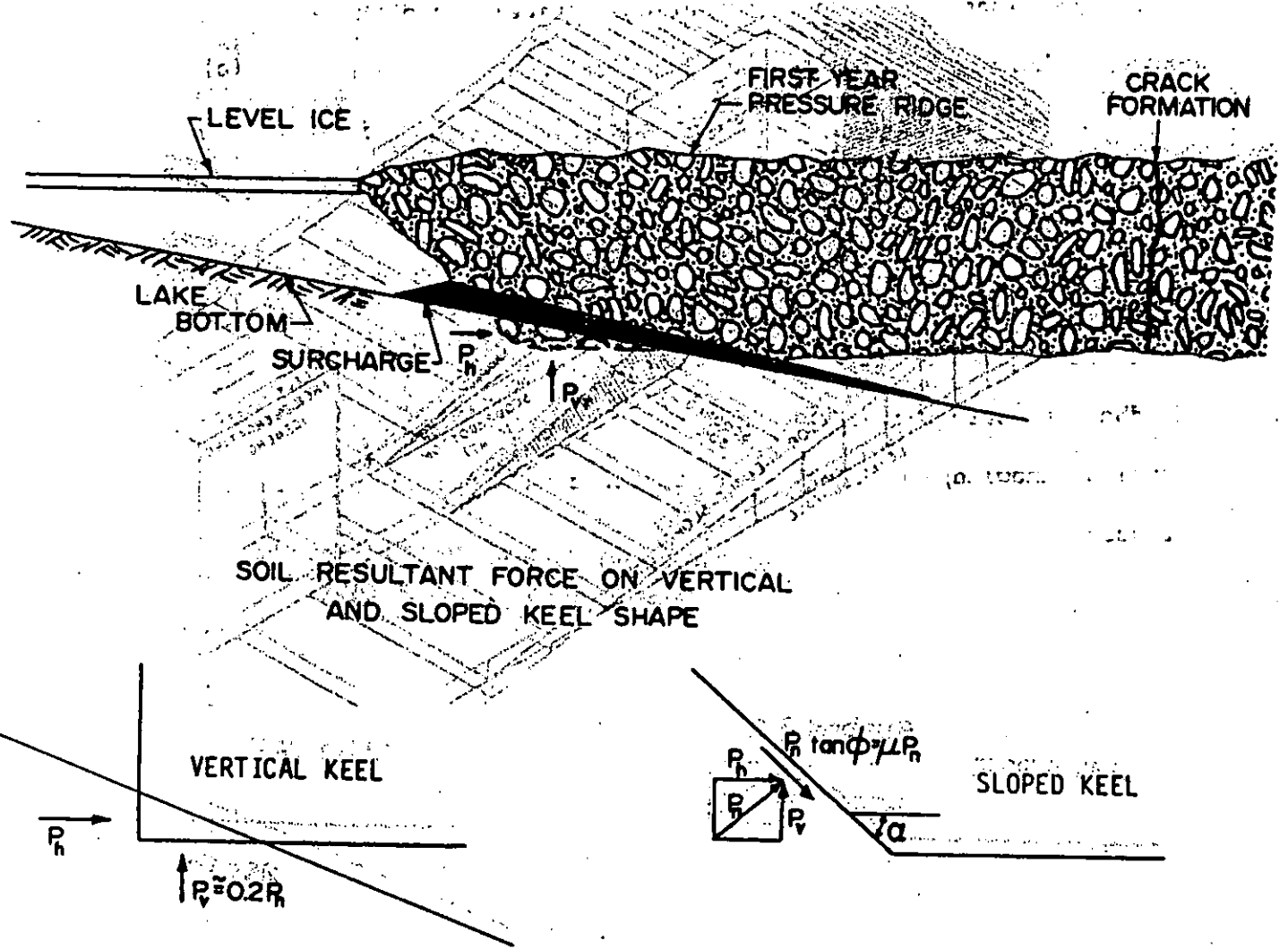


FIGURE 12
INTERACTION SCENARIO CONSIDERED



CONCLUSIONS

As stated in the introduction, the state-of-the-art of designing for ice forces on submerged and floating structures is such that, with some exceptions, few codes, regulations, guidelines or rules of thumb exist to help the engineer solve practical design problems. Fortunately, this is not a static situation, and significant effort is being directed towards solving ice interaction problems in a number of countries around the world. The next few years will see a considerable increase in the information available to engineers and designers and it is to be hoped that the increased interest in cold regions engineering will encourage feedback of both successful and unsuccessful approaches so that the level of knowledge of designing for such conditions continuously increases.

... Winter Regime of Rivers & Lakes, Cold Regions Science
 ... Monography III-2 ... Cold Regions Research
 ... Engineering Laboratory, Hanover, N.H.
 ... Design Factors for River Ice Spans Analyzed
 ... Soviet'ev in Russian Vol. 12, No. 4, 1946.
 ... E. & Haussler. Formation and Evolution of Ice Covers on
 ... Transactions of the Engineering Institute of Canada, Vol. 2,
 ... R.E. Some Economic Benefits of Ice Booms. In Inter-
 ... Symposium on Cold Regions Engineering, University of Alaska

24012010400

REFERENCES

1. Korzhavin, K.N., "Action of Ice on Engineering Structures", U.S. Army CRREL TL 260, 1971.
2. Danys, J.V., "On Wind Induced Static Ice Forces on Offshore Structures", POAC 77, 4th International Conference on Port & Ocean Engineering under Arctic Conditions, September 1977.
3. Berdennikov, V.P., "Dynamic Conditions of Formation of Ice Jams on Rivers, Soviet Hydrology-Selected Papers, English Translation by American Geophysical Union, 1964.
4. Siefert, W.J. & Langleben, M.P., "Air Drag Coefficient and Roughness Length of a cover of Sea Ice. Journal of Geophysical Research, Vol 77, No. 15, May, 1972.
5. Michel, B., Winter Regime of Rivers & Lakes. Cold Regions Science and Engineering Monography III-B 1a U.S. Army, Cold Regions Research and Engineering Laboratory, Hanover, N.H.
6. Latyshenkov, A.M.. Design Factors for River Ice Booms Analyzed. Gidrotekhnicheskoye Stroitel'stvo in Russian Vol.15, No.4, 1946.
7. Pariset, E. & Hausser. Formation and Evolution of Ice Covers on Rivers. Transactions of the Engineering Institute of Canada, Vol.5, No.1.
8. Perham, R.E. Some Economic Benefits of Ice Booms. 2nd International Symposium on Cold Regions Engineering, University of Alaska 1976.
9. Noble, P. and Singh, D., "Model Tests of Ice Action on Legs of Semi-Submersible Rig", Offshore Technology Conference, May 1982.

REFERENCES

10. Kovacs, A. & Mellor, M., "Sea Ice Morphology and Ice as a Geologic Agent in the Southern Beaufort Sea"; U.S. Army Corps of Engineering, Iceprint from the Coast and Shelf of the Beaufort Sea. AINA, 9174.
11. Michel, B., "Ice Mechanics", Laval University Press, Quebec City 1979.
12. Chari, T., Geotechnical Aspects of Iceberg Scours on Ocean Floors, Canadian Geotechnical Journal, Vol.16, 1979.
13. Pilkington, R. & Iyer, H., "An Analytical Study of Ice Scour on the Sea Bottom". APOA Project 69, 1975.